SINGLE ELECTRON TRANSFER IN ORGANIC SYNTHESIS TARGETED TOWARDS SUSTAINABLE MANUFACTURE

Joshua Philip Barham

A thesis presented in partial fulfilment of the requirements for the degree of Doctor of Philosophy

Department of Pure and Applied Chemistry, University of Strathclyde

API Chemistry, GlaxoSmithKline

March 2017

DECLARATION

This thesis is the result of the author's original research. It has been composed by the author and has not been previously submitted for examination which has led to the award of a degree.

Signed: Date:

ACKNOWLEDGEMENTS

First and foremost, I would like to thank my supervisors, Prof. John Murphy and Dr. Matthew John. Throughout my time at both GlaxoSmithKline and the University of Stathclyde, I was bombarded with optimism, encouragement and brilliant ideas. John and Matt are inspiring not only as chemists but as people; I have discovered a great deal about myself as a result of their guidance and behaviour and I intend to reflect some of the qualities they passed on to me in my future career.

I thank Professors Harry Kelly and William Kerr for granting me the opportunity of the Collaborative PhD Programme. I first met Harry in 2012 during the Residential Chemistry Training Experience where he introduced me to GlaxoSmithKline. As a constant source of support, Harry has provided endless development opportunities for my peers and for me. The most important lesson that Harry has taught me is to reflect on and be proud of successes and achievements. I will always remember or, will never be able to forget, Billy's stories; there is no man better equipped to preach the bizarre anecdotes of academia.

I thank Prof. Patrick Vallance (President, GSK Pharmaceuticals R&D) for funding my PhD and for granting me with the opportunity to present my work both to him, and externally at international conferences. I thank GSK Senior Leaders Dr. John Baldoni, Dr. David Allen, Prof. Vance Novack, Dr. Mike Anson, Dr. Vipulkumar Patel and Dr. Stephen Hermitage for accomodating me within their respective departments, and for providing inspiration and direction throughout my PhD. I thank Mike for financing chemicals, conferences and travel/accomodation during visits to, and my secondment in, the University of Strathclyde.

I thank the GSK staff who have provided me with valuable technical and administrative support; Andrew Shore, Rita Tailor, Alec Simpson, Dr. Andrew Edwards, Richard Jones, Andrew Roberts, Dr. Marco Smith, Thomas Atherton, Suhel Nagori, Benson Ampuko, Saito Gon, Dr. Simon Watson, Terri Davidson, Andrea Malley and Tricia Lucas-Clarke. I thank Dawn Peel; her administrative prowess and smooth, organisational execution has been crucial in the course of this PhD and is greatly appreciated. I thank Dr. Richard Horan, who relentlessly attends PhD group meetings bringing valuable expertise to the students. Moreover, I thank Richard as a first-aider for his swift and professional response to my left hand's unfortunate encounter with a shattered reaction vessel. I thank Dr. Phil Rushworth and Dr. Peter Scott for their guidance and mentoring in my first year. I thank Dr. Yuichi Tateno and Dr. Alistair Roberts for introducing me to process chemistry during the Residential Chemistry Training Experience (09) at GSK. I thank my industrial PhD peers (and friends) for engaging discussions and general frivolity, in and out of work.

I thank my collaborators (GSK and external), whose assistance and expertise proved essential in many of the investigations present. I thank Lee Edwards (GlaxoSmithKline) and Dr. Callum MacGregor (Chemistry, University of Cambridge) for their contributions to my research in photochemistry. Lee has 'taken me under his wing', acting almost as a third supervisor and he has invested a great deal of his time and influence in enabling my photochemical research. I thank Prof. David Birch and Dr. Philip Yip (Photophysics, University of Strathcyde), for engaging in a fruitful collaboration which has granted me a stronger understanding of photochemical and photophysical processes in my reactions. I thank Dr. Leonard Berlouis and Dr. Hardeep Farwaha (Chemistry, University of Strathclyde) for teaching me electrochemistry. I thank Prof. John Walton (Chemistry, University of St. Andrews) for running (and advising on interpretation of) EPR spectroscopy samples which directly contributed to this study. I thank Dr. Colin Edge (GlaxoSmithKline) and Dr. Tell Tuttle (University of Strathclyde) for training

me in computational chemistry. I thank the ESPRC UK Mass Spectrometry staff for their HRMS service the GSK Stevenage staff for their in-house HRMS service.

I thank the JAM group for accomodating me in their lab and for introducing me to all sorts of strange and wonderful chemistry. Namely, Dr. Graeme Coulthard, Dr. Eswararao Doni, Dr. Jonathan Chua, Dr. Anthony McDonagh, Dr. Greg Anderson and PhD students Katie Emery, Florimond Cumine, Mark Allison, Samuel Dalton, Jude Arokianathar, Giuseppe Nocera and Andrew Smith. In particular, Graeme, Doni, Katie and I worked closely together as '*t*(eam)-butoxide'. I thank Graeme and Sam for our work together uncovering the mysteries of alkali metal bases. Their experiments and analyses directly contributed to this study and are clearly indicated. I thank Katie for her luminescence quenching experiments, which directly contributed to this study and are clearly indicated. I thank the University of Strathclyde staff who have provided me with valuable technical and administrative support; Dr. Laura Paterson, Angela Anderson, Craig Irving, Alexander Clunie and Patricia Keating.

I thank my examiners, Prof. Burkhard König and Dr. Allan Watson for setting aside time to examine this Thesis. Allan has been a strong source of support and guidance throughout the PhD programme and I have thorougly enjoyed our discussions.

I thank Prof. Jim Anderson for all his teaching, mentoring and inspiration during my MSci Chemistry course at University College London and beyond; as he regularly delivered continuing education courses at GSK Stevenage. Jim taught me the importance of mechanism in organic chemistry; that understanding how things work is much more important than the observed result. As time has passed, I have come to realise that Jim's message extends beyond organic chemistry and into other aspects of life.

I thank my friends; Martijn den Ronden, Amar Karia, Wei Dai, Simon Batty, Glen Silvester, Rebecca Sharp, Dhiral Vaghelia, Philip Yip, Joanna Sadler,

Oscar Brown, Alex Leask, Lauren Hogg (and many more), for all the hikes, climbs, pubs, playful abuse and general hilarity and which ensued over the years. This helped make the challenges of a PhD that much more bearable.

I thank my parents, Melanie and Philip Barham, for all their love and everything they have sacrificed in the name of my education. I thank my grandparents, Rosemary and Derald Barham, for all the crumbles, baked beans, mountains and country walks.

Last, but certainly not least, I thank my darling Sarah Coutts for her unconditional love and support which made these last four years so special.

ABSTRACT

Single electron transfer technology has received considerable interest in organic synthesis in recent years. Single electron transfer gives rise to unconventional modes of reactivity and intermediates, thus serving as a platform for innovative bond constructions, deconstructions and functional group transformations. This is of key importance to the pharmaceutical industry, where the brevity of synthetic routes to small molecules both accelerates drug discovery and drives chemical efficiency in late-stage development. In many cases, single electron transfer chemistry unlocks reaction conditions which are milder, safer and more cost-effective than conventional chemistries. This Thesis investigates two fields of single electron transfer research and contributes new methodology and mechanistic understanding to both.

Volume 1 investigates the *N*-functionalisation of tertiary amines, which is an important method for the elaboration of naturally occuring raw materials into pharmaceutically useful compounds. Two complementary methodologies driven by single electron oxidation were developed. The first method, using visible-light photoredox catalysis, achieved selective benzylic *N*-C**H**$_2$ functionalisation of *N*-substituted tetrahydroisoquinolines. The second method, using stable radical cation salts, achieved selective *N*-C**H**$_3$ functionalisation of trialkylamines.

Volume 2 investigates transition metal-free C-H arylation reactions, which are of particular importance to the pharmaceutical industry, given the costly nature of transition metals typically used in catalysis and their long-term sustainability. These reactions are triggered by single electron reduction, effected by a combination of simple alkali metal alkoxide bases and cheap, readily available organic additives. The interplay of the alkoxide and the

different organic additives is not fully understood but is key to unlocking milder reaction conditions and broadening substrate scope in these reactions. Comprehensive mechanistic studies were undertaken in this regard.

PUBLICATIONS

1) *One-pot Functionalisation of N-Substituted Tetrahydroisoquinolines by Photooxidation and Tunable Organometallic Trapping of Iminium Intermediates*

J. P. Barham, M. P. John, J. A. Murphy

Beilstein Journal of Organic Chemistry **2014**, *10*, 2981.

2) *Double Deprotonation of Pyridinols generates Potent Organic Electron-donor Initiators for Haloarene-arene Coupling*

J. P. Barham, G. Coulthard, R. G. Kane, N. Delgado, M. P. John, J. A. Murphy

Angewandte Chemie International Edition **2016**, *55*, 4492.

3) *KOtBu: A Privileged Reagent for Electron Transfer Reactions?*

J. P. Barham, G. Coulthard, K. J. Emery, E. Doni, F. Cumine, G. Nocera, M. P. John, L. E. A. Berlouis, T. McGuire, T. Tuttle, J. A. Murphy

Journal of the American Chemical Society **2016**, *138*, 7402.

4) *Contra-thermodynamic Hydrogen Atom Abstraction in the Selective C-H Functionalization of Trialkylamine N-CH_3 Groups*

J. P. Barham, M. P. John, J. A. Murphy

Journal of the American Chemical Society **2016**, *138*, 15482.

ABBREVIATIONS

δ = (value)	chemical shift
ΔG	change in Gibbs free energy
$\Delta\Delta$G	difference between the change in Gibbs free energy
1,3-DNB	1,3-dinitrobenzene
4,7-dOMe-phen	4,7-dimethoxy-1,10-phenanthroline
Å	angstrom
A = (value)	amperes
abs	absorption
Ac	acetyl
acac	acetylacetonate
ACE-Cl	α-chloroethyl chloroformate
AG	activating group
APCI	Atmospheric-Pressure Chemical Ionisation
aq.	aqueous
Ar	aryl
atm = (value)	atmosphere
a.u. = (value)	arbitrary unit
Bac	*tert*-butylaminocarbonyl

BDE	bond dissociation energy
BHAS	Base-promoted Homolytic Aromatic Substitution
Bn	benzyl
Boc	*tert*-butoxycarbonyl
Bpin	pinacolborate
bpy	2,2′-bipyridine
bpz	2,2′-bipyrazine
*i*Bu	isobutyl
*n*Bu	*n*-butyl
*t*Bu	*tert*-butyl
^{o}C = (value)	celsius
ca.	circa (= approximately)
calcd.	calculated
CAN	ceric ammonium nitrate
cat.	catalyst
CDC	Cross-Dehydrogenative Coupling
CFL	compact fluorescent lightbulb
cm = (value)	centimetre
conPET	consecutive photoinduced electron transfer
COSY	Homonuclear Correlation Spectroscopy
CV	Cyclic Voltammetry

CYP	cytochrome P450 and derivatives thereof
DABCO	1,4-diazabicyclo[2.2.2]octane
dba	dibenzylideneacetone
DBU	1,8-diazabicyclo[5.4.0]undec-7-ene
DCA	9,10-dicyanoanthracene
DCE	1,2-dichloroethane
DCM	dichloromethane
DDQ	2,3-dichloro-5,6-dicyanobenzoquinone
DEPT	Distortionless Enhancement by Polarisation Transfer
dF(CF_3)ppy	2-(2,4-difluorophenyl)-5-trifluoromethylpyridine
DFT	Density Functional Theory
DIPEA	*N*,*N*-diisopropylethylamine
DMA	*N,N*-dimethylacetamide
DMAP	4-dimethylaminopyridine
DME	dimethoxyethane
DMF	*N,N*-dimethylformamide
DMSO	dimethyl sulfoxide
DNA	deoxyribonucleic acid
DoE	Design of Experiments
dppm	1,1-bis(diphenylphosphino)methane
dr	diastereomeric ratio

dtbpy	4,4′-di-*tert*-butyl-2,2′-dipyridyl
E^+	electrophile
EDA	electron donor/acceptor complex
EDTA	ethylenediaminetetraacetic acid
ee	enantiomeric excess
E^o	standard potential
$E_{1/2}$	half potential
E^p_{ox}	peak oxidation potential
E^p_{red}	peak reduction potential
EPR	Electron Paramagnetic Resonance
ESI	Electrospray Ionisation
Et	ethyl
eq.	equivalents of
F = (value)	quenching fraction
Fc	ferrocene
FTIR	Fourier Transform Infrared
fs	femtoseconds
g = (value)	gram
G = (value)	gauss
GSK	GlaxoSmithKline
h = (value)	hour

hABH	human alkB homologue and derivatives thereof
HAT	hydrogen atom transfer
HMBC	Heteronuclear Multiple Bond Correlation
HNESP	High Resolution Nano-Electrospray Ionisation
HOMO	highest occupied molecular orbital
HPLC	High Performance Liquid Chromatography
HRMS	High Resolution Mass Spectrometry
HSQC	Heteronuclear Single Quantum Correlation
Hz = (value)	hertz
I_{abs}	rate constant for absorption
IC	internal conversion
ICP-MS	Inductively Coupled Plasma Mass Spectrometry
ICP-OES	Inductively Coupled Plasma Optical Emission Spectroscopy
IPA	propan-2-ol
IR	infrared spectroscopy
ISC	intersystem crossing
J = (value)	coupling constant (Hz)
J = (value)	joule
kcal = (value)	kilocalorie
KIE	kinetic isotope effect

LCMS	Liquid Chromatography Mass Spectrometry
LED	light emitting diode
LG	leaving group
Lit.	literature
LOQ	limit of quantification
LUMO	lowest unoccupied molecular orbital
m = (value)	metre
m	*meta*
M = (value)	mole per litre (mol dm^{-3})
MB	methylene blue
m-CPBA	*meta*-chloroperoxybenzoic acid
MCS	Multi-Channel Scaling (time-correlated single photon counting)
MDAP	mass directed auto purification
Me	methyl
mes	mesityl
mg = (value)	milligram
2-MeTHF	2-methyltetrahydrofuran
min = (value)	Minute
MLCT	metal-to-ligand charge transfer
mL	millilitre

mmol	millimole
mol%	mole percentage
m.p. = (value)	melting point
MS	molecular sieves
Ms	mesyl
$NADP^+$	nicotinamide adenine dinucleotide phosphate (oxidised form)
NADPH	nicotinamide adenine dinucleotide phosphate (reduced form)
NBS	*N*-bromosuccinimide
N/A	not applicable
ND	not determined
NHE	Normal Hydrogen Electrode
nm	nanometre
NMR	Nuclear Magnetic Eesonance
n.r.	no reaction
ns	nanosecond
Nu	nucleophile
o	*ortho*
OFAT	One-Factor-at-a-Time
p	*para*
PCA	Principal Component Analysis

PDI	perylenediimide
PEG	polyethylene glycol
Ph	phenyl
phen	phenanthroline and derivatives thereof
Piv	pivaloyl
PMB	*para*-methoxybenzyl
ppm = (value)	parts per million
ppb = (value)	parts per billion
PPTS	pyridinium *para*-toluenesulfonate
ppy	2-phenylpyridinato-C^2,*N*
*i*Pr	isopropyl
*n*Pr	*n*-propyl
ps	picoseconds
PTFE	polytetrafluoroethylene
p-TSA	*para*-toluenesulfonic acid monohydrate
Q-phos	pentaphenyl(di-*tert*-butylphosphino)ferrocene
quant.	quantitative (100%) yield
Ra-Ni	Raney Nickel
t_R	residence time
RNA	ribonucleic acid
rt	room temperature

R_T	retention time
s = (value)	seconds
sat.	saturated
SCE	Saturated Calomel Electrode
SET	single electron transfer
SHE	Standard Hydrogen Electrode
SMD	surface mounted device (5050 SMD = 5.0 mm x 5.0 mm)
S_N1	unimolecular nucleophilic substitution
S_N2	bimolecular nucleophilic substitution
S_NAr	nucleophilic aromatic substitution
SOMO	singly occupied molecular orbital
SSA	Steady-State Approximation
SSCE	Sodium Saturated Calomel Electrode
TBME	*tert*-butyl methyl ether
TBPA	tris(*p*-bromophenyl)amine
TBPA-X	tris(*p*-bromophenyl)aminium (X = counterion)
TBHP	*tert*-butyl hydroperoxide
TCSPC	Time-Correlated Single Photon Counting
TEMPO	2,2,6,6-tetramethyl-1-piperidinyloxyl radical
TBME	*tert*-butylmethyl ether
Tf	trifluoromethylsulfonyl

TFA	trifluoroacetic acid
THF	tetrahydrofuran
THIQ	tetrahydroisoquinoline
TMEDA	tetramethylethylenediamine
TMS	trimethylsilyl
p-tol	*para*-tolyl
TPBPA	tris(*p*-biphenyl)amine
TPBPA-X	tris(*p*-biphenyl)aminium (X = counterion)
TPP	tetraphenylporphyrin
TPPS	5,10,15,20-tetrakis(4-sulfonatophenyl)porphyrin
TPTA	tris(*p*-tolyl)amine
TPTA-X	tris(*p*-tolyl)aminium (X = counterion)
t = (value)	time
Ts	*para*-toluenesulfonyl
T.S.	transition state
v	Cyclic Voltammetry scan rate
UV	ultraviolet (<400 nm)
UV-A	ultraviolet long wave (320 - 400 nm)
UV-vis	Ultraviolet-visible Spectroscopy (>320 nm to <800 nm)

VOLUME 1: SITE-SELECTIVE *N*-FUNCTIONALISATION OF TERTIARY AMINES UNDER SINGLE ELECTRON TRANSFER OXIDATION

Joshua Philip Barham

A thesis presented in partial fulfilment of the requirements
for the degree of Doctor of Philosophy

Department of Pure and Applied Chemistry, University of Strathclyde

API Chemistry, GlaxoSmithKline

March 2017

SUMMARY

N-Functionalisation is an unconventional yet powerful tool used for building complexity into tertiary amines. In the pharmaceutical industry, *N*-functionalisation is an important method for the elaboration of naturally occuring raw materials into pharmaceutically useful compounds. Historical approaches which involve *N*-dealkylation of tertiary amines typically require several chemical steps and can suffer poor yields, poor selectivities or the requirement for toxic and expensive reagents.

Recent approaches to *N*-functionalisation which avoid *N*-dealkylation are highlighted. Such approaches generally proceed through catalytic oxidation to an iminium salt which is intercepted by a nucleophile in a single step. A notable platform for the oxidation step is visible-light photoredox catalysis, a technology which has received an explosion of interest from the synthetic community over the last decade. Visible-light is used to excite a photocatalyst which performs a single electron oxidation of a tertiary amine to generate an amine radical cation. Further processes yield the iminium salt which is intercepted by a nucleophile.

Substrates employed in these novel approaches often contain structural features (for example, *N*-aryl substituents) which lend themselves to facile oxidation and regioselective iminium salt formation. Yet, application of such processes to more complicated substrates (such as trialkylamines, where several possible iminium salts could form) or those containing additional functional groups has been met with limited success to date. Herein, novel approaches toward a regio- and chemoselective *N*-functionalisation of trialkylamines are described.

Initially, the functionalisation of well precedented *N*-substituted tetrahydroisoquinoline substrates was explored in order to develop practical

experience in visible-light photoredox catalysis and photoreactor design at GSK. Novel photooxidation conditions were established applicable to *N*-alkyl as well as *N*-aryl tetrahydroquinolines, forming iminium salts exclusively at the benzylic *N*-C**H**$_2$ position. Reaction conditions permitted a wide range of organometallic nucleophilic additions to photogenerated iminium salt intermediates in a single pot, affording products in moderate to excellent (47 - 95%) yields. The methodology was applied in a concise synthesis of opioid analgesic methopholine. Scalability of visible-light photochemistry was successfully demonstrated at GSK; productivity was significantly increased by moving from a batch to a flow reactor. Productivity of 17 g/h (3 kilo/week) was achieved in flow.

However, when reaction conditions successfully employed for *N*-substituted tetrahydroisoquinolines were applied to trialkylamines, no reaction was observed. This was rationalised by a subtle mismatch in redox potentials between the excited state photocatalyst and the trialkylamine. Exhaustive photophysical studies were carried out which probed the interaction of the excited state photocatalyst with trialkylamines. Subsequently, a photocatalyst was identified which had an excited state that interacted strongly with trialkylamines. However, reactions stalled in the laboratory, presumably due to a mismatch in redox potentials elsewhere in the photocatalytic cycle.

Finally, a non-photochemical approach to the *N*-functionalisation of trialkylamines is disclosed. This approach utilises stable, rechargeable radical cation salts and DABCO to generate iminium salt equivalents with good chemoselectivity and notable regioselectivity (up to > 30 : 1 *N*-C**H**$_3$: *N*-C**H**$_2$ functionalisation). Iminium salt equivalents were then intercepted with organometallic reagents to afford *N*-C**H**$_3$ functionalised products in moderate to excellent (31 - 83%) yields. The mechanism is elucidated by a combination of radical cyclisation experiments, redox potentials, computation, rationalisation of by-products and spectroscopic detection of reaction intermediates.

Conclusions of the research and areas of future work are presented. General experimental details and specific details for physical chemistry/photophysical techniques are described. Detailed preparative methods and analytical data for key compounds and all novel compounds synthesised are given. A comprehensive list of references is provided.

TABLE OF CONTENTS

TABLE OF FIGURES

1. Introduction and Related Work

1.1. *N*-Functionalisation of Tertiary Amines: Pharmaceutical Significance

N-Functionalisation, the elaboration of a tertiary amine into a differentially-substituted tertiary amine, is an unconventional but powerful tool for building complexity into tertiary amines. This transformation is particularly valuable in the field of semi-synthetic opioids, where a simple structural change from an *N*-methyl group to other alkyl moieties drastically alters pharmacological activity.[1–3] Such alteration is exemplified by the opioids shown in Figure 1. Oxymorphone is used as an analgesic agent for the management of pain, and is a μ-opioid receptor agonist approximately 10 times more potent than morphine. In stark contrast, the structurally similar naltrexone is used to manage opiate dependence and to treat overdose, functioning as an antagonist for the same receptor. The reversal of pharmacological activity is attributed to the structural change at the tertiary amine, from the *N*-methyl group into a cyclopropylmethyl appendage.[4]

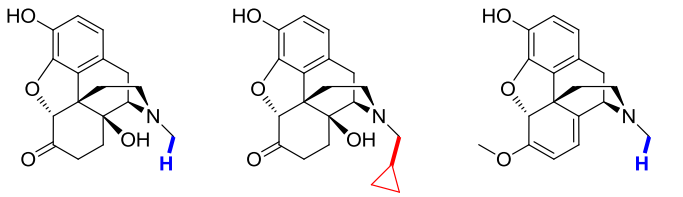

oxymorphone
μ-opioid agonist

naltrexone
μ-opioid antagonist

oripavine
natural opioid precursor

Figure 1: *Opioid molecules displaying different biological activities.*[1,4]

Rather than constructing the morphine skeleton *de novo*, industrial syntheses of semi-synthetic opioids utilise oripavine (Figure 1) as a starting material. In addition to other alkaloids, oripavine is extracted from *papaver somniferum* (poppies) on a kilotonne per annum scale.[5] Elaborating this readily available

material into pharmacologically active synthetic opioid medicines imparts significant value. In fact, a general approach to a number of semi-synthetic opiates has been *N*-dealkylation and *N*-alkylation; replacing the *N*-methyl group of a naturally occurring opiate with other alkyl substituents such as *N*-allyl and *N*-cyclopropylmethyl.[6,7,8] The following section highlights historical synthetic strategies relevant to this elaboration.

1.2. *N*-FUNCTIONALISATION OF TERTIARY AMINES: HISTORICAL APPROACHES

1.2.1. THE VON BRAUN REACTION

Historically, *N*-functionalisation has been accomplished through *N*-dealkylation (usually *N*-demethylation) followed by *N*-alkylation. One of the earliest reported chemical *N*-dealkylations was the von Braun reaction.[9,10] In the early 1900's, von Braun exposed *N*-methylpyrrolidine **1** to cyanogen bromide which yielded pyrrolidine **3** (Scheme 1). In the reaction mechanism (Scheme 2),[11] cyanogen bromide acts as an electrophile which is attacked by tertiary amine **4**, resulting in *N*-cyanoammonium salt **6a**.[12]

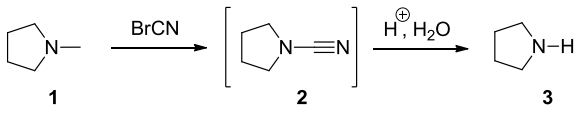

***Scheme 1**: The von Braun reaction of N-methylpyrrolidine followed by acid hydrolysis.*[10]

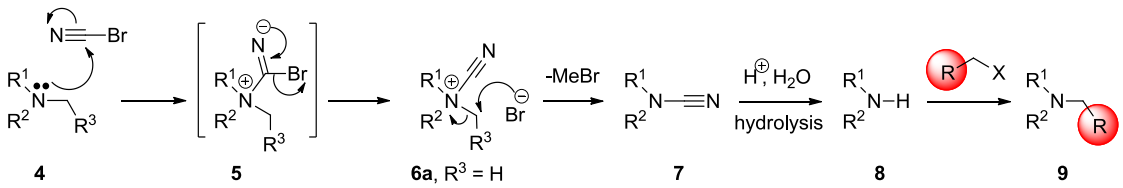

***Scheme 2**: Mechanism for the von Braun N-dealkylation reaction of tertiary amines.*[11]

Spontaneous decomposition of **6a** forms methyl bromide and cyanamide **7**. Acid hydrolysis of **7** affords secondary amine product **8**,[11] which might be further elaborated by alkylation to tertiary amine **9**.

1.2.2. THE USE OF CHLOROFORMATES

In the 1980's, *N*-dealkylation was accomplished by using chloroformates, which resulted in cleaner reaction profiles than the von Braun reaction.[12,13] In addition, the toxicity of cyanogen bromide and its necessary safety precautions and environmental considerations could be avoided.[7] Chloroformates facilitated *N*-dealkylation (Scheme 3), in substrates such as *N*-ethylpiperidine **10** and *N,N*-diethylaniline **11** to give their respective *nor*-salts (**12** and **13**) in excellent yields (99 and 87%, respectively).[13]

A commonly used chloroformate is α-chloroethyl chloroformate or, 'ACE-Cl' (Scheme 3).[14] Having observed *N*-demethylation and *N*-deethylation in simple substrates, Olofson successfully applied ACE-Cl to 6-acetylcodeine obtaining *nor*-product **14** in excellent (97%) yield.[14] However, the advantages of chloroformates in terms of yield and safety of the *N*-demethylation process are somewhat offset by the increased cost of these reagents and the generation of chlorinated waste. Furthermore, chloroformates are typically manufactured from phosgene,[14] a highly toxic colourless gas, such that necessary safety precautions and environmental considerations are simply shifted upstream in the supply chain.

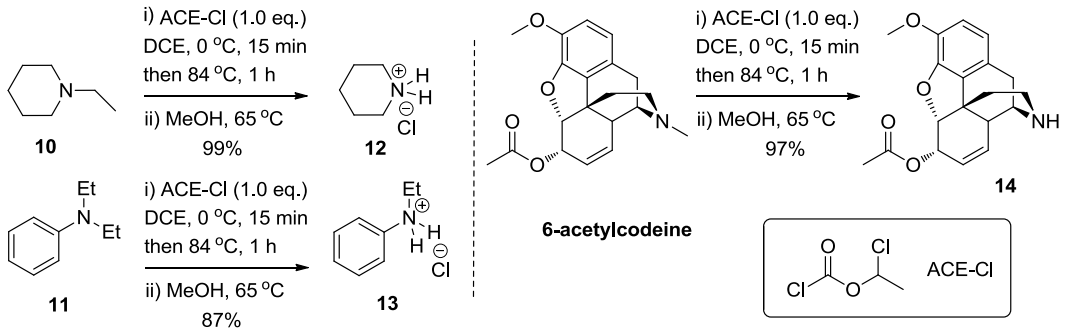

***Scheme 3**: N-Dealkylation of a selection of substrates using chloroformates reported by Olofson.*[14]

1.2.3. The Non-classical Polonovski Reaction

The classical Polonovski reaction (which will not be discussed in detail here) is that of an *N*-oxide with an activating agent (for example, an acid anhydride, an acid chloride and sulfur dioxide), which induces E2 elimination to afford iminium salts.[15] The non-classical Polonovski reaction is a variant which has been used to accomplish *N*-dealkylation under notably mild conditions. Although this reaction originated in 1927,[16] it was relatively underused until a surge of interest in the 21st century.[7,17] This was triggered by Guillou, who achieved *N*-demethylation of (-)-galanthamine to *nor*-product **16** by a non-classical Polonovski reaction, *via* N-oxide intermediate **15** (Scheme 4).[18]

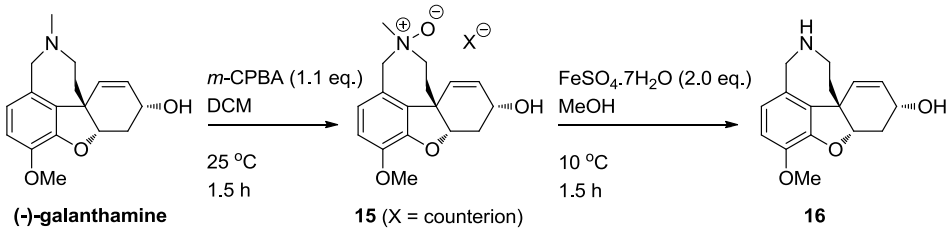

Scheme 4: *N-Demethylation of (-)-galanthamine via a non-classical Polonovski reaction.*[18]

The non-classical Polonovski reaction is a two-step process. *N*-Oxidation of tertiary amine **4** by an oxidant (for example, by H_2O_2 or *m*-CPBA), followed by acidification, results in a protonated N-oxide species **17** (Scheme 5). The mechanism of the Fe(II)-mediated *N*-dealkylation of N-oxides (**17**) was investigated by Gapski.[19] Treatment of **17** with Fe(II) salts facilitates single electron transfer (SET)-reduction to yield Fe(III), radical cation species **18** and hydroxide. There are two pathways available to **18**; pathway A sees a second SET reduction by Fe(II), returning starting material, and so is undesirable. Pathway B involves deprotonation, yielding α-amino radical **19**, which is oxidised to iminium salt **20** by Fe(III). Hydrolysis of **20** generates the secondary amine product **8**.

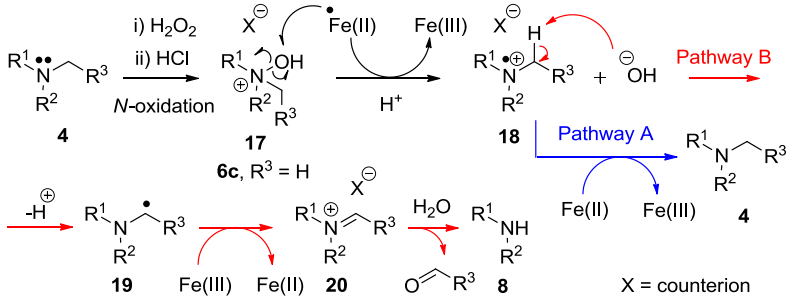

Scheme 5: *Mechanism for the Fe(II)-mediated N-demethylation of N-oxides.*[19]

Significant progress in the non-classical Polonovski reaction has been made by Scammells, who originally disclosed a simple and efficient protocol employing H_2O_2 to effect *N*-oxidation, followed by $FeSO_4.7H_2O$ to mediate *N*-dealkylation in moderate to very good yields (44 - 87% over the two steps).[7] Higher yields were disclosed in a modified protocol using *m*-CPBA for *N*-oxidation and Fe(0) powder in the *N*-dealkylation step.[20] However, selectivity is a limitation here, with the ratio of secondary : tertiary amine (**8** : **4**) depending highly on the substrate, from 97 : 1 to 2 : 1 (secondary : tertiary).[20]

Though several strategies for *N*-dealkylation exist, generally the industrially amenable strategy involves chloroformates, with previously mentioned advantages and disadvantages.[7] The non-classical Polonovski reaction uses less expensive reagents, milder and safer conditions but is not always industrially amenable due to the competing pathways in the mechanism (Scheme 5) resulting in mixtures of secondary and tertiary amine products.[19,20] Furthermore, the presence of iron salts can cause problems with purification, particularly with larger scale syntheses.

Use of iron chelating agents such as ETDA, citrate salts and tetraphenylporphyrin (TPP) can alleviate the problem in some cases.[8,19] Interestingly, Scammells employed these types of iron porphyrin complexes as catalysts in the non-classical Polonovski reaction (Figure 2).[8,21] Such complexes are key components of Nature's process for *N*-oxidation and *N*-dealkylation in the liver.[8,21]

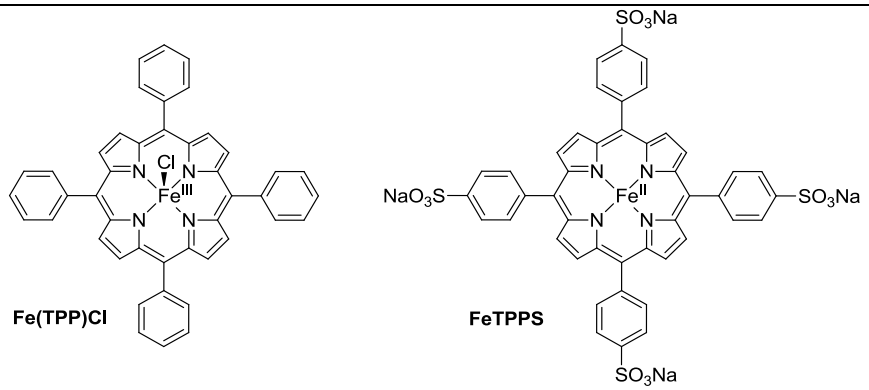

***Figure 2**: Iron porphyrin complexes reported in the non-classical Polonovski reaction.*[8]

1.3. *N*-FUNCTIONALISATION OF TERTIARY AMINES: NATURE'S APPROACHES

So far, focus has been placed on the *N*-dealkylation/*N*-demethylation of tertiary amines within the context of organic synthesis. However, *N*-demethylation of tertiary amines has been achieved in nature long before the efforts of the organic chemist. Nature's agents for *N*-demethylation have benefitted from millions of years of evolutionary optimisation, resulting in their execution of high chemo-, regio- and stereoselectivity in processes. Such agents are enzymes, specifically *N*-demethylases.

1.3.1. *N*-DEALKYLATION AS A METABOLIC PATHWAY

N-Demethylases play a key role in the metabolism of caffeine in humans and other mammals. It was found that caffeine is metabolised initially in the liver by cytochrome P450 (CYP) enzymes, which induce *N*1-, *N*3- and *N*7-demethylation to yield theobromine, paraxanthine and theophylline respectively (Scheme 6). In addition to caffeine, one of the main metabolic pathways of morphine involves *N*-demethylation to *nor*-morphine in the liver.[4,22] Ducharme found that two cytochrome P450 enzymes facilitate morphine *N*-demethylation in the liver, CYP3A4 and CYP2C8 (Scheme 7).[22] Cytochrome P450-mediated oxidations proceed as shown below (Scheme 8).[23] Considering formation of theobromine as an example, caffeine first

undergoes hydroxylation *via* the CYP enzyme system (which consists of Fe(II), cofactor NADPH, oxygen (O_2) and a proton source). Several mechanisms for oxidation could operate in the CYP enzyme active site (for example, direct insertion of oxygen into a C-H bond or *N*-oxidation and non-classical Polonovski-type demethylation). Direct insertion of oxygen into the *N*-CH_3 would form aminol intermediate **21**, cofactor $NADP^+$ and H_2O. The aminol intermediate then liberates formaldehyde to yield theobromine.

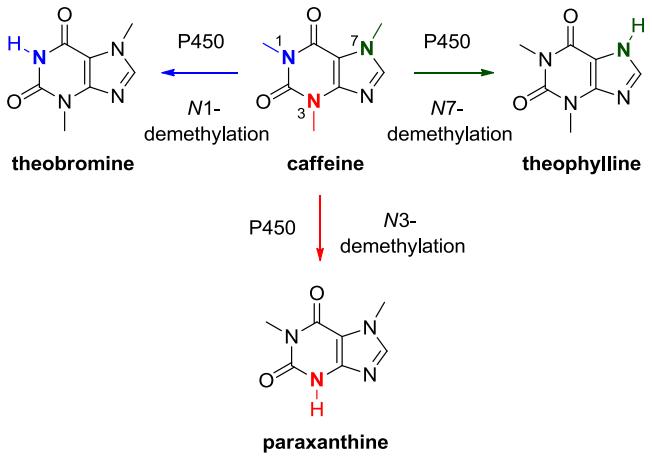

***Scheme 6**: Initial metabolism of caffeine in mammals by cytochrome P450.*[24]

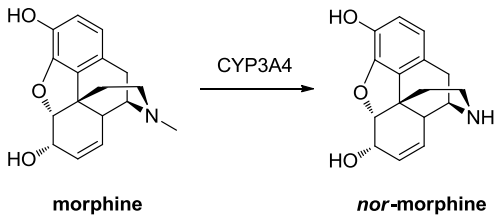

***Scheme 7**: N-Demethylation of morphine to nor-morphine, facilitated by CYP3A4.*[4,22]

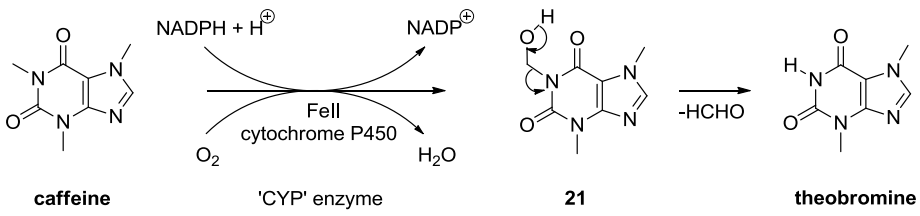

***Scheme 8:** Mechanism for N-demethylation of caffeine by CYP enzymes. Direct insertion of oxygen into a C-H bond is depicted.*[23]

Kinetic and inhibition studies have demonstrated a strong correlation between caffeine 3-demethylation (Scheme 5, pathway B) and *N*-oxidation of carcinogenic tertiary *N*-arylamines in human hepatic microsomal preparations (by cytochrome P450),[25] suggesting that the mechanism involved in the non-classical Polonovski chemistry could be implicated in effecting *N*-demethylation.

1.3.2. *N*-DEALKYLATION IN GENETIC MATERIAL REPAIR

It is known that the cytotoxic nature of alkylating agents can be attributed to their reaction with DNA and RNA at N and O atoms.[23,26] For example, in the case of RNA for example, if *N*1-alkylation occurs in adenine or *N*3-alkylation occurs in cytosine, this will modify the groups involved in base-pairing thereby affecting translation. However, mammals have cellular defence systems which respond by recruiting oxidative DNA dealkylases. It was reported that two 'human AlkB homologues' or, hABH's (hABH2 and hABH3) are Fe(II) oxidative dealkylases which repair alkylation damage in DNA *via O*- and *N*-demethylation (Scheme 9, *N*-demethylation shown).[26] Firstly, 1-methyladenine undergoes oxidation by the 'AlkB' system,[23] which comprises an Fe(II) oxygenase, O_2 and 2-oxoglutarate. This yields succinate, aminol intermediate **22** and evolves CO_2 (paralleling the *N*-demethylation mechanism shown in Scheme 8). The aminol intermediate **22** fragments to adenine and formaldehyde.

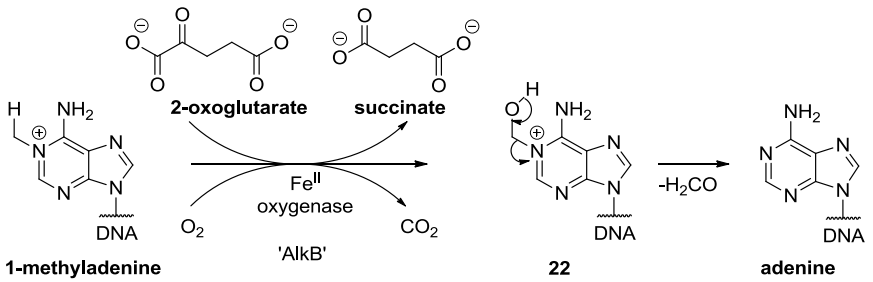

Scheme 9: *Mechanism for N-demethylation of 1-methyladenine by hABH's.*[23]

1.4. *N*-FUNCTIONALISATION OF TERTIARY AMINES: AVOIDING *N*-DEALKYLATION

Setting Mother Nature's contributions aside, the chemical strategies for *N*-dealkylation all possess a common theme; namely an activation step and a dealkylation step. Moreover, in order to capitalise on the alteration of pharmacological activity which is imparted by replacing (for example) the *N*-methyl group of an opiate with another alkyl moiety,[4] alkylation usually follows *N*-dealkylation. Thus in terms of synthetic chemistry, the overall '*N*-functionalisation' transformation comprises three steps i) activation, ii) demethylation and iii) alkylation (Scheme 10, *N*-demethylation shown).

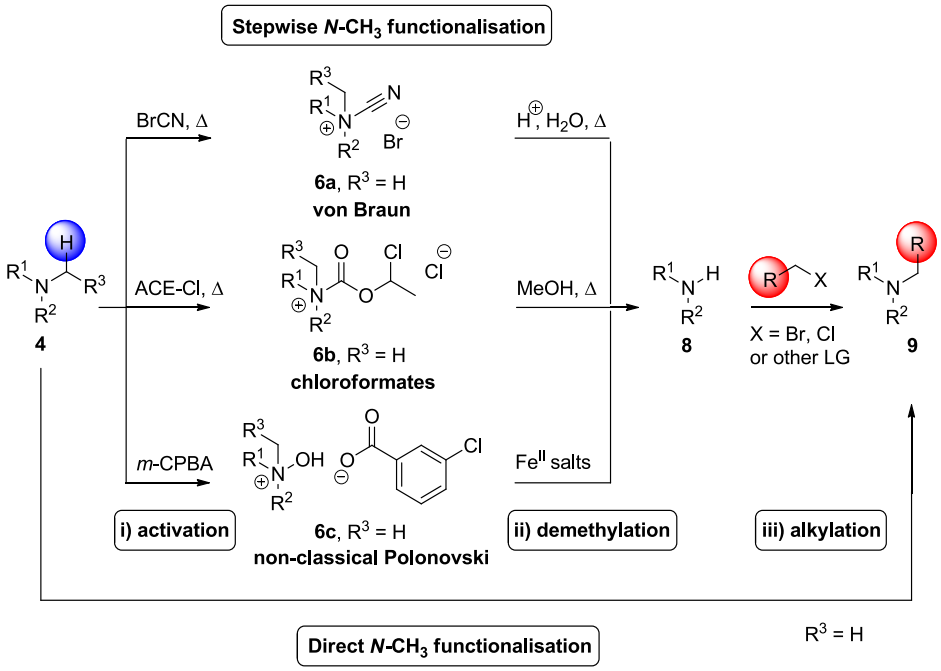

***Scheme 10**: N-Functionalisation of tertiary amines via N-dealkylation and N-alkylation.*

Conversely, recent developments have used oxidations to transform the tertiary amine into an electrophile (an iminium salt) *in situ* which has been intercepted with a nucleophile (Scheme 11, nucleophile depicted as R^-) in a direct *N*-functionalisation.[27] In theory, this approach increases efficiency as it

condenses the number of chemical operations to one step and preserves the carbon atom(s) derived from the original *N*-alkyl substituent.[28]

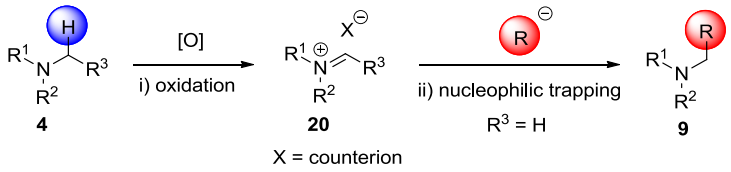

***Scheme 11**: Recent approaches to N-functionalisation via oxidation and nucleophilic trapping of iminium salts.*

1.4.1. Oxidative *N*-Functionalisations of *N*-Aryl Tertiary Amines

Popular substrates used to demonstrate this methodology are *N*-aryl-1,2,3,4-tetrahydroisoquinolines (*N*-aryl THIQs).[27] Presumably, this is due to facile oxidation of the aniline function of *N*-phenyl THIQ **23**, the stability of intermediates (such as **24** and **25** which result from SET oxidation mechanisms) en route to the iminium salt intermediate (**26**) and the stability of the highly conjugated **26** itself. Together, these structural and electronic features impart facile reaction and high regioselectivity to the process (Scheme 12). In 2005, Li reported a Cross-Dehydrogenative Coupling (CDC) reaction between **23** and $MeNO_2$ (Scheme 13) yielding the product (**27**) in good (65%) yield.[29]

Klussmann proposed a radical mechanism (Scheme 14) beginning with oxidation of Cu(I) by *tert*-butyl hydroperoxide (TBHP) (Scheme 14, equation 1).[27] The resulting Cu(II) species reacts with another molecule of TBHP resulting in a Cu(II) *tert*-butylperoxyl complex (Scheme 14, equation 2), whilst the resulting *tert*-butoxyl radical abstracts a hydrogen from either TBHP (Scheme 14, equation 3) or tertiary amine **4**. The α-amino radical **19** undergoes termination by reacting either with the *tert*-butyl hydroperoxyl complex or the *tert*-butyl hydroperoxyl radical to give species **28**. The equilibrium of species **28** with iminium **20** is assisted by a [Cu] species acting as a Lewis acid. Finally, iminium **26** undergoes a nitro-Mannich reaction to give β-nitroamine **29**.

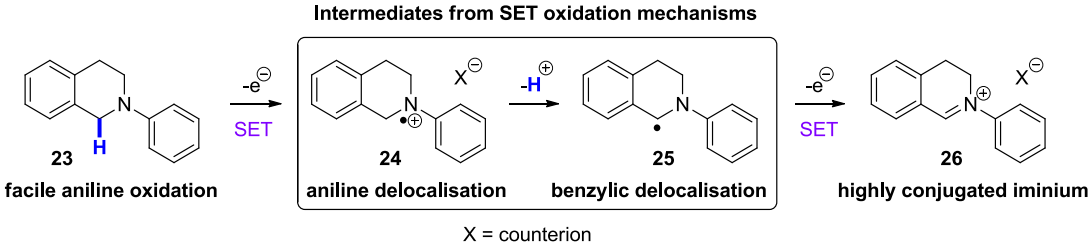

***Scheme 12**: Structural and electronic features of N-aryl THIQs and intermediates toward a highly conjugated iminium intermediate.*

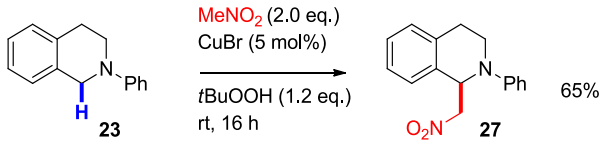

***Scheme 13:** Cu(I)-catalysed CDC reaction between N-phenyl THIQ and $MeNO_2$.*[29]

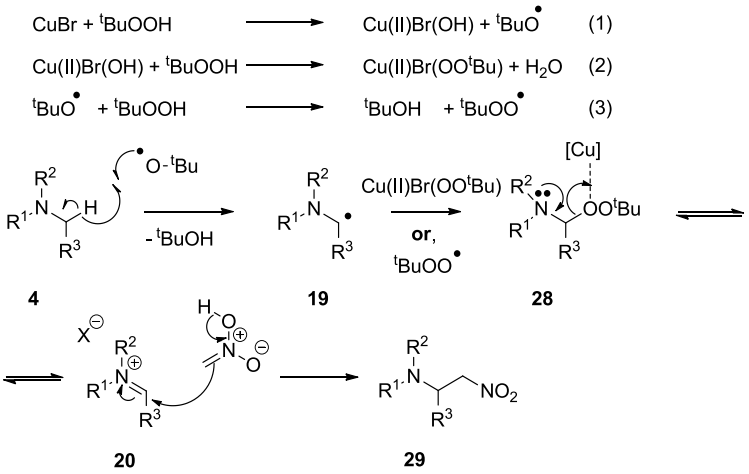

***Scheme 14**: Mechanism proposed for the Cu(I)-catalysed CDC reaction between N-aryl THIQs and $MeNO_2$.*[27]

Doyle employed Fe(III) as an alternate catalyst which enables use of O_2 as an oxidant.[30] Under aerobic conditions and using MeOH as a solvent, *N,N*-dimethylaniline **30** underwent oxidative functionalisation to give methoxy-substituted compound **31** in good (50%) yield (Scheme 15), which is a stable iminium salt reservoir susceptible to nucleophilic attack. Doyle proposed a mechanism involving direct oxidation of the aniline (**30**) to its radical cation

(**32**) by Fe(III). To arrive at the iminium salt intermediate (**33**), hydrogen atom transfer (HAT) from **32** to Fe(II)-bound dioxygen is proposed (Scheme 16).

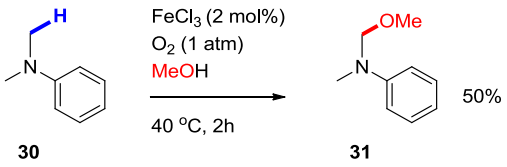

***Scheme 15**: Iron(III)-catalysed aerobic oxidative functionalisation of anilines.*[30]

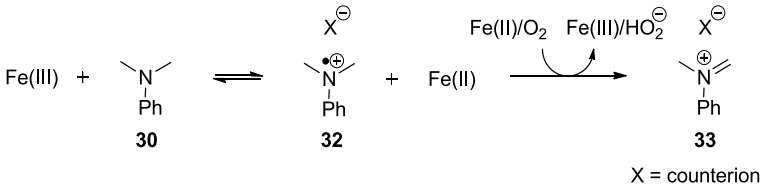

***Scheme 16**: Mechanism proposed for iron(III)-catalysed aerobic oxidation of anilines.*[30]

Doyle uses redox potentials† to rationalise this. According to Doyle, the small difference in oxidation potentials between Fe(III) [E^{o} (Fe^{III}/Fe^{II}) = +0.77 *vs.* NHE]‡,[30] and *N*,*N*-dimethylaniline [E^{p}_{ox} ($PhN^{\bullet+}Me_2/PhNMe_2$) = +0.97 *vs.* NHE]‡,[31] enables a good shuttle of electrons from Fe(III) to O_2,[30] compared to Cu(II) (E^{o} (Cu^{II}/Cu^{I}) = +0.15 *vs*. NHE).‡,[30] Presumably, the mismatch of redox potentials between *N*,*N*-dimethylaniline and Cu(II) explains the requirement for TBHP in Li's Cu(I)-catalysed CDC (Scheme 13).[29] It is worth noting that values for Fe(III) or Cu(II) quoted are standard redox potentials (E^{o}),† which are measured under standard conditions. Whilst an indication of ease of oxidation, standard redox potentials are not representative of the reaction conditions employed. For *N*,*N*-dimethylaniline, the value quoted (E^{p}_{ox}) is an oxidation peak potential,† measured in DCM solvent with $n$$Bu_4NPF_6$ electrolyte, which is different to both standard redox potential conditions and

†For definition, measurement and interpretation of redox potentials, see Appendix. Unless literature is cited, all redox potentials quoted herein have been measured and are *vs*. SCE in MeCN, unless otherwise stated. ‡The NHE is outmoded terminology for the SHE, see Appendix.

the reaction conditions.[31] To ensure valid conclusions, it is important to compare redox potentials that have been measured under the same conditions. Prabhu reported a versatile CDC reaction between *N*-aryl THIQs (such as **23**) and a host of stabilised nucleophiles, catalysed by molecular I_2 to give products in good to excellent (54 - 98%) yields (Scheme 17).[32] A very similar protocol was disclosed by Itoh which uses H_2O_2, rather than O_2, as the terminal oxidant.[33] Similar to Doyle's mechanistic proposal for Fe(III) catalysed oxidation (Scheme 16),[30] Prabhu proposed direct SET oxidation of the aniline function of **23** by I_2 (Scheme 18), followed by HAT from **24** to an iodine radical (presumably, deriving from collapse of the I_2 radical anion) to give iminium salt **26**. This exists in equilibrium with methoxy-substituted compound **34**.

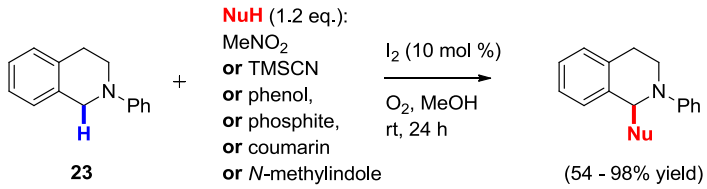

***Scheme 17**: Molecular iodine-catalysed CDC reaction reported by Prabhu.*[32]

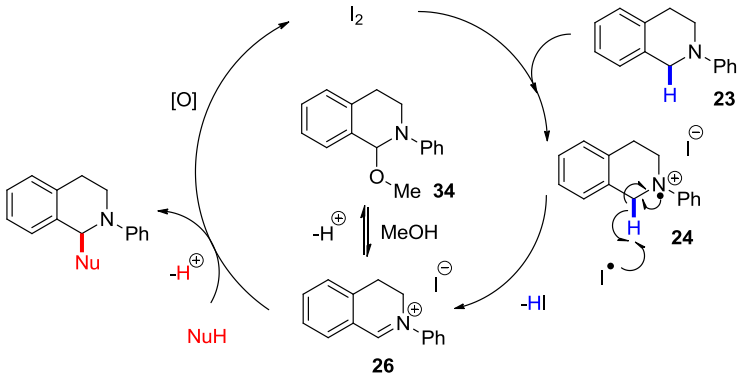

***Scheme 18**: Mechanism proposed for the iodine-catalysed CDC reaction of N-aryl THIQs.*[32]

Huo reported an aerobic oxidation catalysed by the commercially available tris(*p*-bromophenyl)aminium hexachloroantimonate (**TBPA**-$SbCl_6$) salt, followed by a Mannich reaction with various ketones to give the

functionalised products (for example, **35**, see Scheme 19). The proposed mechanism commenced with oxidation of *N*-phenyl THIQ (**23**) to its radical cation (**24**) by the **TBPA** radical cation (Scheme 20).[34]

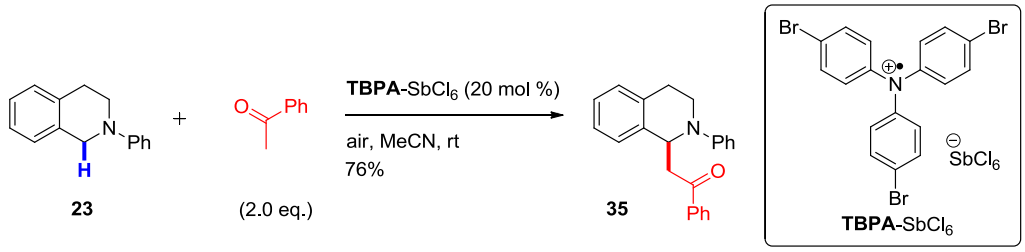

***Scheme 19**: **TBPA**-$SbCl_6$-catalysed aerobic oxidation of N-aryl THIQs.*[34]

Simultaneously, the **TBPA** salt reacts with O_2 to generate radical **36**, which undergoes HAT with the starting material (**23**) (yielding α-amino radical **25**). HAT from radical cation **24** to α-amino radical **25** regenerates starting material (**23**) and generates iminium salt **26**. Homolysis of species **37** regenerates a molecule of **TBPA** salt and a hydroperoxyl radical which regenerates a second molecule of **TBPA** salt through oxidation of the neutral triarylamine. The iminium salt (**26**) is then intercepted by a ketone pronucleophile in a Mannich reaction. An alternative, plausible mechanism could involve oxidation of the highly reducing α-amino radical [E^{p}_{ox} (Et_2N^{+}=$CHCH_3$/Et_2N−$^{\bullet}CHCH_3$) = -1.12 V *vs.* SCE][35] by O_2 [$E_{1/2}$ (O_2/$O_2^{\bullet-}$) = -0.75 V *vs*. SCE],[35] affording the iminium salt and superoxide. Superoxide (or peroxyl radical derived therefrom) could undergo HAT with the starting material (**23**), regenerating α-amino radical (**25**) and thus propagating a chain reaction.

The authors observe that no product was furnished under an Ar atmosphere, but there seems to be no direct evidence presented for the combination of oxygen with the **TBPA** radical cation to give **36**.[34] In a separate publication, the authors propose a different mechanism whereby α-amino radical **25** is oxidised directly by the hydroperoxyl radical to yield iminium salt **26**.[36] Other reports find that the commercially available **TBPA**-$SbCl_6$ is a latent source of

antimony pentachloride ($SbCl_5$) and it is this that serves as the active oxidant (the oxidation potential of $SbCl_5$ has not been reported).[37–40]

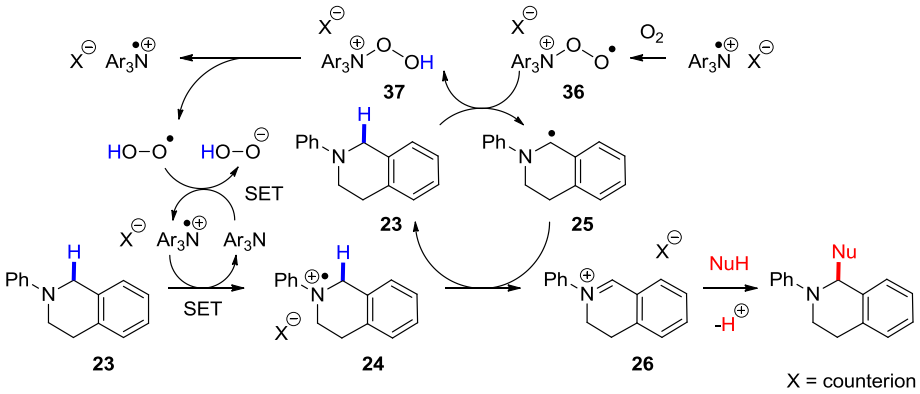

Scheme 20: *Proposed mechanism for aerobic catalytic TBPA salt oxidation of THIQs.*[34]

In addition to the examples discussed herein, many variations of oxidative CDC methodology exist using different oxidants (DDQ,[41] V(IV),[42] Ru(III),[43] hypervalent iodine reagents,[44] electrochemical oxidation[45]) and different nucleophiles (heteroaromatics,[27,46] cyanides,[43] arylboronic acids[47]). It is beyond the scope of this introductory chapter to cover them all. Suffice to say, *N*-substituted THIQs are predisposed to undergo facile and selective oxidation to iminium salts which are readily trapped with nucleophiles, as demonstrated by the plethora of chemistry in this field. Surprisingly, though *N*-aryl THIQs are common substrates in this type of oxidative chemistry, *N*-alkyl THIQs are scarcely used (some reports exist).[42,48,49]

1.4.2. *N*-Functionalisations of Trialkylamines: Challenges

In moving from *N*-aryl tertiary amines to trialkylamines, the first challenge is that trialkylamines are more difficult to oxidise on nitrogen (Figure 3). For example, compare *N*-phenyl THIQ **23** [E^p_{ox} ($N^{\bullet+}$-Ph THIQ/*N*-Ph THIQ) = +0.83 V *vs.* SCE] with *N*-methyl THIQ [E^p_{ox} ($N^{\bullet+}$-Me THIQ/*N*-Me THIQ) = +1.15 V *vs.* SCE] and triethylamine [E^p_{ox} ($Et_3N^{\bullet+}/Et_3N$) = +1.10 V *vs.* SCE] which do not have an aniline group. Although the two trialkylamines have more basic lone pairs than *N*-phenyl THIQ (**23**), the nitrogen radical cation

resulting from oxidation enjoys less stability and thus the oxidation potential is more positive.

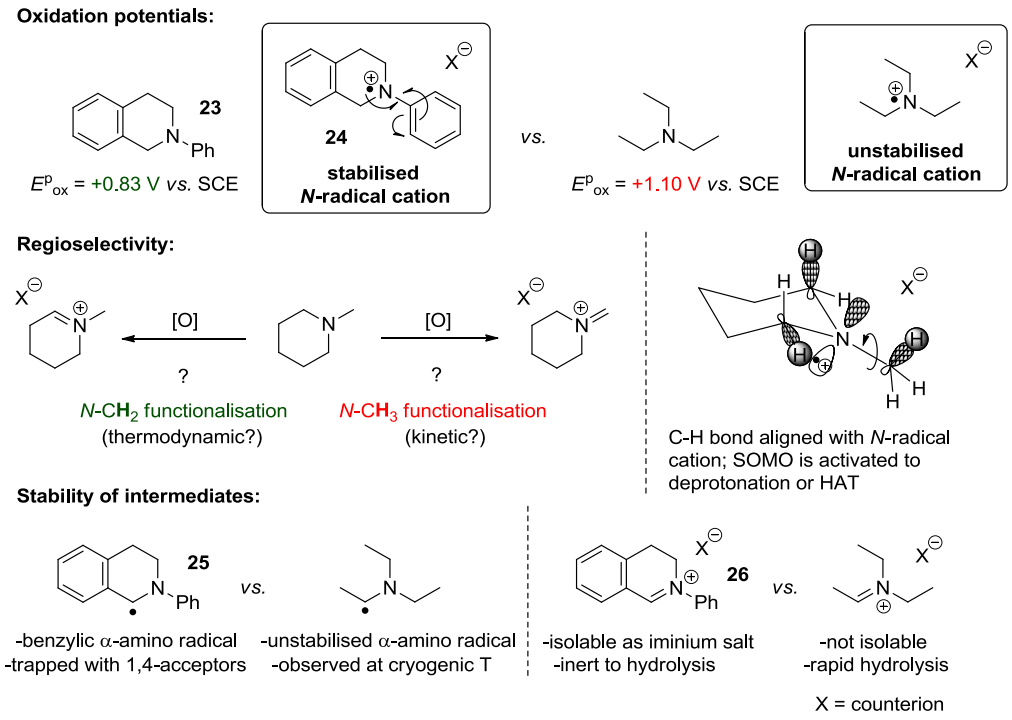

***Figure 3**: Challenges arising from the use of trialkylamines as substrates.*

The second challenge is regioselectivity. For iminium salts derived from *N*-aryl THIQs (such as **26**), regioselectivity is to be expected, since the α-amino radical derived from THIQs (such as **25**) is benzylic and the iminium salt (**26**) is highly conjugated. It is less clear how to achieve and rationalise (*a priori*) the regioselective functionalisation of trialkylamine substrates where more than one iminium salt could form (Figure 3). Considering *N*-methylpiperidine as an example, Whilst the endocyclic iminium salt might be the more substituted thermodynamic product,[50] the exocyclic iminium salt might be favoured by a stereoelectronic requirement for the breaking C-H σ bond. Once the radical cation is formed, the C-H σ orbital must lie eclipsed to the radical cation singly occupied molecular orbital (SOMO) for HAT to occur. Assuming the radical cation SOMO adopts sp^2 hybridisation,[51] neither the axial nor the equatorial C-H σ orbitals of the *N*-C**H**$_2$ overlap effectively. Conformational changes in the ring system are required to achieve overlap of

the endocyclic C-H σ orbitals, with associated energy penalties. On the other hand, the exocyclic CH_3 merely needs to rotate to achieve C-H σ orbital overlap, with minimal energy penalties. It is reported that this stereoelectronic effect would also apply to deprotonation.[52]

A third challenge is stability of intermediates. For example, whilst α-amino radicals derived from *N*-aryl THIQs (such as **25**) enjoy benzylic stabilisation and have been successfully intercepted by 1,4-acceptors,[53,54] trialkylamine α-amino radicals are highly transient (ca. 700 ns lifetime in 1 : 9 water/MeCN solvent)[55] and need cryogenic to sub-zero (*ca*. -50 ^{o}C to *ca*. -15 ^{o}C) temperatures to be observed by EPR.[56] Similarly, whilst iminium salts derived from *N*-aryl THIQs are moisture-stable and isolable,[57,58] iminium salts derived from trialkylamines suffer from rapid hydrolysis.[59] In accordance with these challenges, trialkylamine *N*-functionalisation is less precedented but some reports do exist (with α-cyanations and arylations being most common) and these will now be presented.

1.4.3. *N*-FUNCTIONALISATIONS OF TRIALKYLAMINES: CYANATIONS

Ofial reported TBHP-mediated α-cyanation of trialkylamines (such as **37**) using potassium thiocyanate as the cyanide source (Scheme 21).[60] The authors assume formation of radical cation **18**, which forms iminium **20** *via* the same pathway as the non-classical Polonovski reaction (see Scheme 5, pathway B, Section 1.2.3). At the same time, the excess of TBHP present oxidises KSCN to yield the cyanide nucleophile (thiocyanate oxidation by H_2O_2 to form cyanide is a well known reaction which has been studied in detail).[60,61] An Fe(II)-catalysed TBHP-mediated α-cyanation using TMSCN was reported earlier by the same group.[62] Lambert reported the use of tropylium cation salts, proposed to operate by hydride transfer from trialkylamine **39** (Scheme 22), but the authors could not rule out a pathway commencing with direct SET oxidation on the trialkylamine nitrogen atom.[63] Other examples of oxidative trialkylamine cyanations use chlorine dioxide,[64] manganese-based oxide catalysts[65] and PEGylated magnetic (iron)

nanoparticles (in combination with H_2O_2).[66] In all these methods, substrates containing an *N*,*N*-dimethyl unit undergo successful and selective reactions. However, for other substrates, reactions generally suffer from variable regioselectivity, elevated reaction temperatures and/or extended reaction times (days).

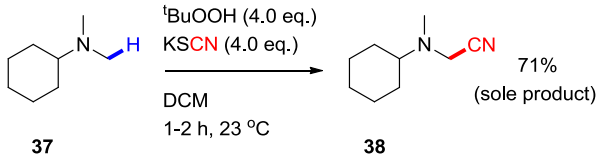

***Scheme 21**: TBHP-mediated α-cyanation of cyclohexyldimethylamine.*[60]

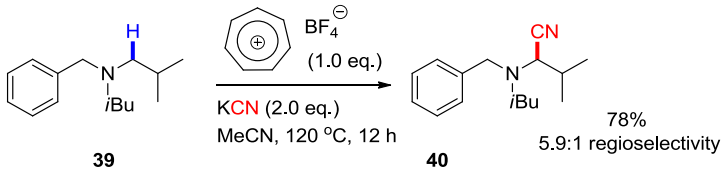

***Scheme 22**: Tropylium-mediated α-cyanation of N-benzyldiisobutylamine.*[63]

Though a direct *N*-oxidation (rather than an *N*-functionalisation *per se*), Jahn reported oxidative cyclisations of trialkylamines induced by **TBPA**-PF_6 (Scheme 23). This stable radical cation salt engages in SET oxidation of trialkylamine **41**, affording the trialkylamine radical cation **43**, corroborated by its rapid 5-*exo*-*trig* cyclisation onto the pendant alkene chain (Scheme 24). Oxidation of the resulting radical **44** by a second equivalent of radical **TBPA**-PF_6 forms dication **45**, which is susceptible to either deprotonation or nucleophilic attack at the carbocation (for example, attack of water affords the desired product, **42**).

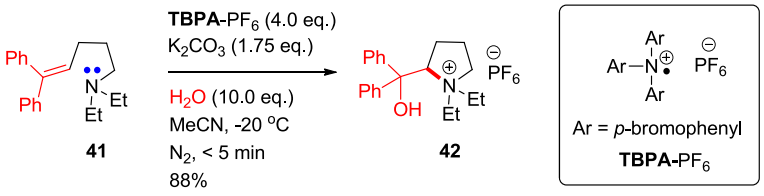

***Scheme 23**: TBPA salt-induced oxidative cyclisations of tertiary amines.*[67]

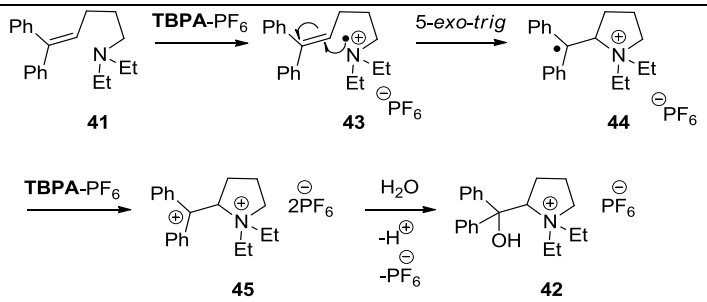

***Scheme 24**: Mechanism proposed by Jahn for oxidative cyclisation of tertiary amines.*[67]

Furthermore, mechanistic involvement of the counterion was avoided through use of the hexafluorophosphate counterion instead of the hexachloroantimonate counterion. Unfortunately, since this oxidation is stoichiometric in **TBPA**-PF_6, molar efficiency[68] is particularly poor; the reaction conditions require 4.0 eq. of **TBPA**-PF_6 to remove just two electrons in the reaction mechanism (in theory, only 2.0 eq. of **TBPA**-PF_6 is required).

1.4.4. *N*-FUNCTIONALISATIONS OF TRIALKYLAMINES: ARYLATIONS AND ALKYLATIONS

Recently, transition metal catalysis has made an advance in the site-selective functionalisation of trialkylamines. Generally, these methods have displayed selectivity for C-H functionalisation remote from the amine, but *N*-functionalisations can be achieved in some instances. Hartwig reported a powerful method for trialkylamine functionalisation (Scheme 25); regioselective C-H borylation and one-pot cross-coupling.[69]

The mechanism involved is a direct C-H insertion (σ-bond metathesis) rather than SET oxidation. As such, selectivity is not necessarily dictated by the amine. When only *N*-methyl groups were present, these could be successfully functionalised α- to the nitrogen atom. However, when *N*-ethyl systems were used (n = 2) borylation occurred β- to the nitrogen atom, and ethers were functionalised successfully with similar regioselectivity. Therefore, this chemistry cannot distinguish between tertiary amines and ethers but it

offers complementary regioselectivity to oxidative *N*-functionalisations (which functionalise a C-H bond α- to the nitrogen atom). It is important to note that yields were based on the aryl halide, and a large excess of trialkylamine was typically employed (12.0 eq.).

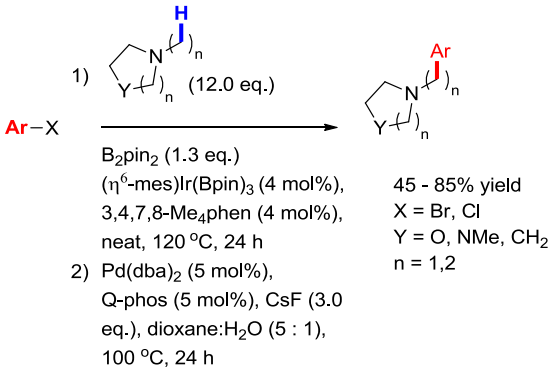

***Scheme 25**: Regioselective C-H functionalisation of trialkylamines.*[69]

Sanford reported the remote functionalisation of trialkylamines *via* a transannular approach (Scheme 26). For cyclic amines in 6-membered rings or for 3-azabicyclo[3.1.0]hexane cores, initial coordination of the nitrogen atom to palladium results in activation of a transannular C-H bond and formation of a palladacycle, which couples with aryl halides.[70] Interestingly, substrates were not immune to functionalisation α- to the nitrogen atom, since $NaBH_4$ was employed in the work up to react with aminals and other by-products derived from both starting materials and products. Substrates required a fluoroamide directing group, which had a geminal dimethyl unit. No *N*-methyl containing substrates were reported.

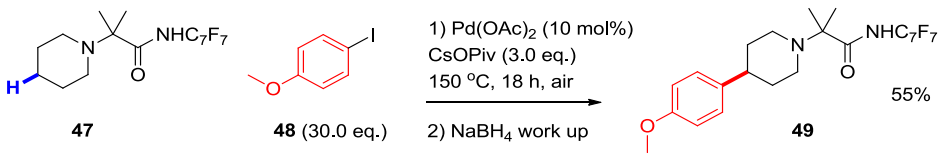

***Scheme 26**: Remote functionalisation of trialkylamines via transannular C-H activation.*[70]

Sanford was able to achieve the remote functionalisation of trialkylamines in another way; by use of *in situ* protonation (Scheme 27).[71] Trifluoroacetic acid

served to protonate the amine, causing an Fe(III)/*t*BuOOH oxidative system to target remote benzylic positions. Complex mixtures of products resulted from functionalisation α- to the nitrogen atom if the amine was not protonated.[71]

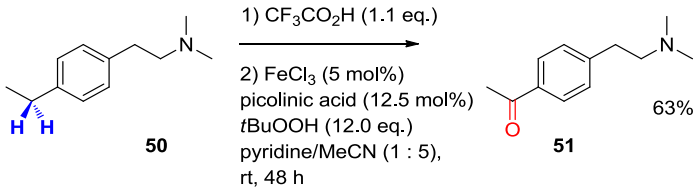

***Scheme 27**: Remote functionalisation of trialkylamines via in situ protonation.*[71]

Finally, Hou reported the hydroaminoalkylation of alkenes using trialkylamine reagents (Scheme 28).[72] Here, remarkable selectivity was achieved for the *N*-methyl group with no other functionalised products or regioisomers observed by ^{1}H NMR. The authors propose formation of a mono-cationic scandium species which initially binds tightly to the amine, resulting in deprotonation. Presumably, regioselectivity results from this deprotonation step, although the authors make no comment on the origins of the regioselectivity.

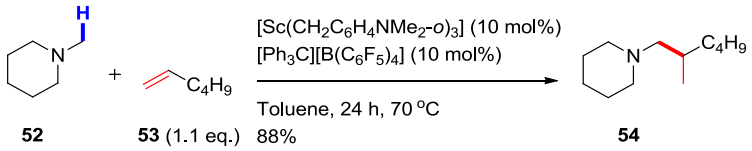

***Scheme 28**: Sc-catalysed hydroaminoalkylation of alkenes with trialkylamines.*[72]

The reaction performed well with a range of simple trialkylamines and alkenes/styrenes, but suffered severe limitations with substrate scope. Namely, oxygen-containing substrates are incompatible (due to oxophilicity of the cationic scandium) and conjugated dienes result in polymerisation. Interestingly, trialkylamines with too much steric bulk (such as *N*,*N*-dicyclohexylmethylamine) failed, whilst trialkylamines with too little steric bulk

(*N*,*N*-diethylmethylamine) also failed. Remarkably, *N*-ethylpiperidine gave no reaction, highlighting the selectivity for *N*-methyl over *N*-ethyl groups.

In summary, a variety of reported methods exist for the site-selective functionalisation of tertiary amines. Some methods employ an oxidative system followed by a nucleophile, whilst others rely on a directed C-H activation step. A notable method for site-selective functionalisation of tertiary amines is visible-light photoredox catalysis, which has achieved complementary chemistries under mild conditions. Before discussing these examples, a brief introduction to the relevant photophysics and photochemistry fundamentals will be presented.

1.5. VISIBLE-LIGHT PHOTOREDOX CATALYSIS: PHOTOPHYSICS AND PHOTOCHEMISTRY FUNDAMENTALS

Visible-light is one of the most abundant energy sources in the solar system. Chemists have long sought to use visible-light to power organic synthesis,[73,74] but have been hampered by the fact that most organic molecules absorb UV, not visible-light. Nature's solution is chlorophyll, a biomolecular pigment (or, 'photocatalyst') which absorbs visible-light to drive photosynthesis of glucose and oxygen from water and carbon dioxide (feedstocks which do not themselves absorb visible-light). Organic chemists soon established that this principle could be applied within the context of organic synthesis. Rather than directly transferring light energy to organic molecules *via* high energy UV photons, a visible-light activated 'photocatalyst' acts as a mediator for indirectly transferring the energy of visible-light photons to organic molecules (or, engages organic molecules in electron transfer).

In recent years, the field of visible-light photoredox catalysis has received much attention in synthetic organic chemistry.[75,76] Visible-light photochemistry is attractive to synthetic chemists for a number of reasons. Firstly, it is considered to be green chemistry.[76,77] Visible-light is a clean and

safe source of energy. Secondly, it is highly practical chemistry to perform. Notwithsanding solar abundance (typically too variable for reproducible chemistry), highly efficient artificial sources of visible-light (for example, fluorescent bulbs, LEDs) are readily available at every visible wavelength and reactions can be conducted with regular glassware. This contrasts with the specialist light sources, reactor designs, glassware and safety precautions implicated by UV photochemistry.

From a chemical efficiency perspective, since organic molecules typically do not absorb visible-light, high energy side pathways (for example, Norrish Type I cleavage; cleavage of C-C bond adjacent to a carbonyl resulting from UV excitation of that carbonyl)[78,79] as a consequence of direct excitation (and which plague UV photochemical processes) are avoided.[75,78,80] Higher product yields typically result and less waste/by-products are generated. Visible-light photoredox catalysis allows access to unconventional intermediates and modes of reactivity under exceptionally mild conditions,[75,77] thus arming the organic chemist with new opportunities for bond constructions/cleavages in synthetic routes. Furthermore, visible-light photochemistry can still generate complex molecular scaffolds which are normally the domain of UV photochemistry. Certain chemistries which are thermally forbidden (for example, [2+2]-cycloadditions to give cyclobutanes) are easily achieved under visible-light photoredox catalysis.[81,82]

Before setting visible-light photoredox catalysis in the context of tertiary amine functionalisation, it is useful to consider the photoelectronic properties of some prototypical visible-light photoredox catalysts. An introduction to the principles of classical (UV-mediated) photochemistry is beyond the scope of this introduction; readers are referred to some key publications and texts in this field.[78,79,83,84] Where applicable, basic photochemical principles will be introduced and considered within the context of visible-light photocatalysis.

1.5.1. PHOTOELECTRONIC PROPERTIES OF VISIBLE-LIGHT PHOTOREDOX CATALYSTS

Polypyridyl complexes of ruthenium and iridium have attracted significant attention as visible-light photocatalysts.[75] For example, tris(2,2′-bipyridine)ruthenium(II) $[Ru(bpy)_3]^{2+}$ has a prominent absorption band at 452 nm (blue light). This corresponds to electronic excitation from a metal-centred orbital π^M to a ligand-centred orbital π^{*L}.[85] Hence, the excited singlet state is termed a metal-to-ligand charge transfer ($^1MLCT_1$) state.[76] This $^1MLCT_1$ state undergoes ultrafast (*ca.* 15 fs)[86] intersystem crossing (ISC) to the corresponding lower energy triplet state ($^3MLCT_1$). Processes such as this are termed 'spin-forbidden' as they break the law of the conservation of angular momentum. Though ISC is formally a spin-forbidden process, it can readily occur due to overlap between the vibrational levels of the similar energy $^1MLCT_1$ and $^3MLCT_1$ electronic states. It is possible for $^3MLCT_1$ to return to the ground state ($^1A_1$) by phosphorescence or intersystem crossing.

However, these are both spin-forbidden processes and this time there is poor overlap between the vibrational levels of the two electronic states. This renders the lifetime of $^3MLCT_1$ relatively long (890 - 1100 ns in degassed MeCN)[87–89] such that it can engage in photochemistry. By engaging in photochemistry with molecules, the $^3MLCT_1$ state is able to relay energy to (or electrons to or from) these molecules to create reactive intermediates. If this occurs, $^3MLCT_1$ is said to be 'quenched' and molecules which interact with $^3MLCT_1$ are termed 'quenchers'. This $^3MLCT_1$ triplet state is the excited state formally referred to as $*[Ru(bpy)_3]^{2+}$ in the literature, and will be referred to in this way henceforth. A Jablonski diagram[76] shows transitions, rate constants and energy states of $[Ru(bpy)_3]^{2+}$ (Figure 4). A salient feature of $*[Ru(bpy)_3]^{2+}$ is that it is both more oxidising and more reducing than its corresponding ground state, rendering it a powerful mediator for redox chemistry.[75,90] It follows that two catalytic cycles can be accessed (Figure 5).[75,76] The first cycle begins with quencher **A** donating an electron to $*[Ru(bpy)_3]^{2+}$ (to the π^{*M} HOMO of $^3MLCT_1$) which affords $\mathbf{A}^{\bullet+}$ and $[Ru(bpy)_3]^{+}$.

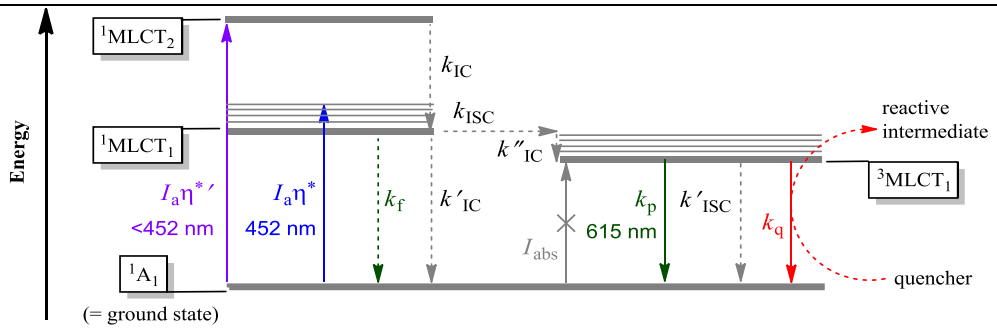

***Figure 4**: Simplified Jablonski diagram for $[Ru(bpy)_3]^{2+}$ as a prototypical photoredox catalyst. The rate constants k_f, k_{IC}, k_{ISC}, k_p and k_q represent fluorescence, internal conversion (IC), intersystem crossing (ISC), phosphorescence and chemical quenching, respectively. The rate constant for absorption is denoted by $I_a\eta^*$, where I_a is the rate at which light is absorbed by $^1A_1$ and η^* is the efficiency of population of excited state from the absorption of one photon at the excitation wavelength.*

This state of the catalyst is sometimes referred to as Ru^{I} in the literature, but formally the surplus electron resides in the ligands and the metal centre is still Ru^{II}. However, in line with convention and for simplicity, this thesis will use Ru^{I} and $*Ru^{II}$ to represent $[Ru(bpy)_3]^{+}$ and $*[Ru(bpy)_3]^{2+}$, respectively (and the appropriate convention for other Ru or Ir complexes when referring to redox potentials). Since $*[Ru(bpy)_3]^{2+}$ is quenched by reduction, this first step is termed *reductive quenching*. Stoichiometric oxidant **B** removes the surplus electron from $[Ru(bpy)_3]^{+}$, thereby regenerating $[Ru(bpy)_3]^{2+}$ and generating $\mathbf{B}^{\bullet-}$. The second cycle begins with quencher **C** removing an electron from $*[Ru(bpy)_3]^{2+}$ (from the π^{*L} LUMO of $^3MLCT_1$) to yield $\mathbf{C}^{\bullet-}$ and a $[Ru(bpy)_3]^{3+}$ species. This is known as *oxidative quenching*. Stoichiometric reductant **D** donates an electron to $[Ru(bpy)_3]^{3+}$, thereby regenerating $[Ru(bpy)_3]^{2+}$ and generating $\mathbf{D}^{\bullet+}$. By spatially separating the HOMO from the LUMO, variation of either the oxidation or the reduction potential can be achieved with only a small change in the other.[91]

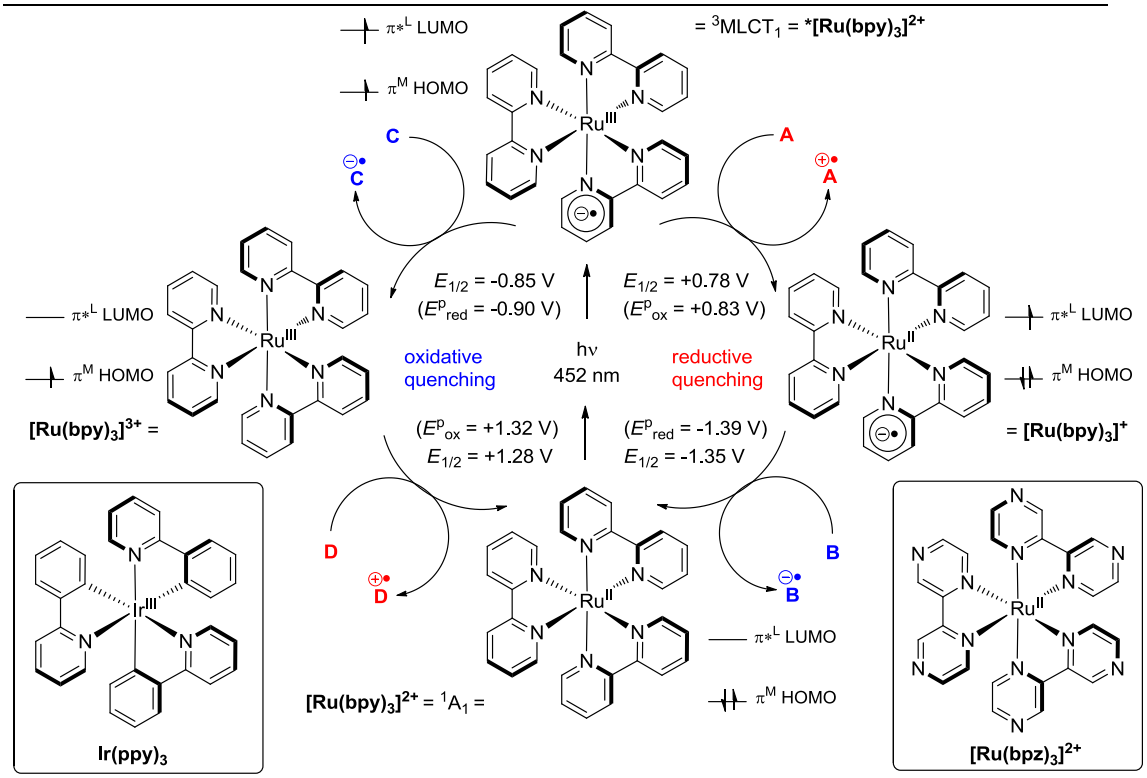

***Figure 5**: Reductive and oxidative quenching cycles and simplified molecular orbital diagrams for $[Ru(bpy)_3]^{2+}$. Structure of $[Ru(bpy)_3]^{2+}$. Redox potentials $E_{1/2}$ are given vs. the saturated calomel electrode (SCE).*[75]

For example, in comparing the excited states of $[Ru(bpz)_3]^{2+}$ to $[Ru(bpy)_3]^{2+}$, the presence of additional electron-withdrawing nitrogen atoms in the ligand framework results in the excited state, $*[Ru(bpz)_3]^{2+}$, being a more potent oxidant [$E_{1/2}$ ($*Ru^{II}/Ru^{I}$) = +1.41 V *vs.* SCE] than $*[Ru(bpy)_3]^{2+}$ [$E_{1/2}$ ($*Ru^{II}/Ru^{I}$) = +0.78 V *vs.* SCE]. Commonly used polypyridyl complexes of iridium operate similarly but between Ir(II), Ir(III) and Ir(IV) oxidation states.[75,80] The advantages of the iridium photocatalysts is that iridium, as a group 9 and period 6 element, is more electronegative and has more and larger orbitals than ruthenium. Therefore, iridium photocatalysts benefit from a greater HOMO-LUMO gap (370 - 410 nm) than their ruthenium counterparts (430 - 460 nm), meaning more photonic input.[76,91] An example is $Ir(ppy)_3$ (Figure 5), whose high photonic input (near-UV light, λ_{max} = 380 nm) and negatively charged ligands render its excited state $*Ir(ppy)_3$ a potent reductant [$E_{1/2}$

($Ir^{IV}/*Ir^{III}$) = -1.73 V *vs.* SCE].[75,92] Furthermore, iridium photocatalysts seem more amenable to tuning their redox potentials through the use of heteroleptic complexes, whereas ruthenium complexes tend to be homoleptic.[75,80,93]

Tertiary amines are commonly cited as reductive quenchers of $*[Ru(bpy)_3]^{2+}$, to give tertiary amine radical cations (as $\mathbf{A}^{\bullet+}$, Figure 5). Multiple fates have been proposed for the tertiary amine radical cation, outlined in Scheme 29. Firstly, the tertiary amine radical cation could undergo deprotonation to yield an α-amino radical (Scheme 29, pathway 1), which in turn could undergo SET oxidation to give an iminium salt. The α-amino radical has several other fates available to it, which are discussed subsequent to the fates of the tertiary amine radical cation.

The acidity of trialkylamine radical cations is a topic of debate in the literature. It is generally accepted that oxidation of trialkylamines to trialkylamine radical cations corresponds with a lowering of bond dissociation energy (BDE) and pK_a of the α-amino C-H bond, but the extent of acidification is unclear. Nelsen recognised a common assumption that trialkylamine radical cations were extremely acidic,[94] so much so that it had even been suggested that trifluoroacetate was a strong enough base to effect deprotonation.[95]

In one report by Stephenson, triethylamine [BDE (C-H) = 90.7 kcal mol^{-1}, pK_a = ≥ 40.0] is compared to triethylamine radical cation [BDE (C-H) = ~17 kcal mol^{-1}, pK_a = ~26.7][96] but a subsequent review by Stephenson reports different numbers for the triethylamine radical cation [BDE (C-H) = ~42 kcal mol^{-1}, pK_a = ~14.7].[97] Values quoted by MacMillan for BDEs triethylamine [BDE (C-H) = 80 kcal mol^{-1}] and triethylamine radical cation [BDE (C-H) = 47 kcal mol^{-1}] were different still, and pK_a values of 3 and 13 are quoted for trialkylamine radical cations.[75] Nelsen calculated that trialkylamine radical cation pK_a values were greater than 15.0,[94] concluding that deprotonation does not occur if bases no stronger than trialkylamines are the only ones present.

The second fate of the tertiary amine radical cation is reaction with a hydrogen atom transfer (HAT) agent to afford the iminium salt directly (Scheme 29, pathway 2).[75,96–98] The hydrogen atom transfer agent could be $\mathbf{B}^{\bullet-}$ formed in the photoredox cycle (Figure 5), or $\mathbf{B}^{\bullet-}$ might fragment to form an anion and a more stable radical which acts as the HAT agent.[96] Finally, the tertiary amine radical cation could itself act as a HAT agent[99,100] resulting in the protonated tertiary amine and generating other radical species (Scheme 29, pathway 3).

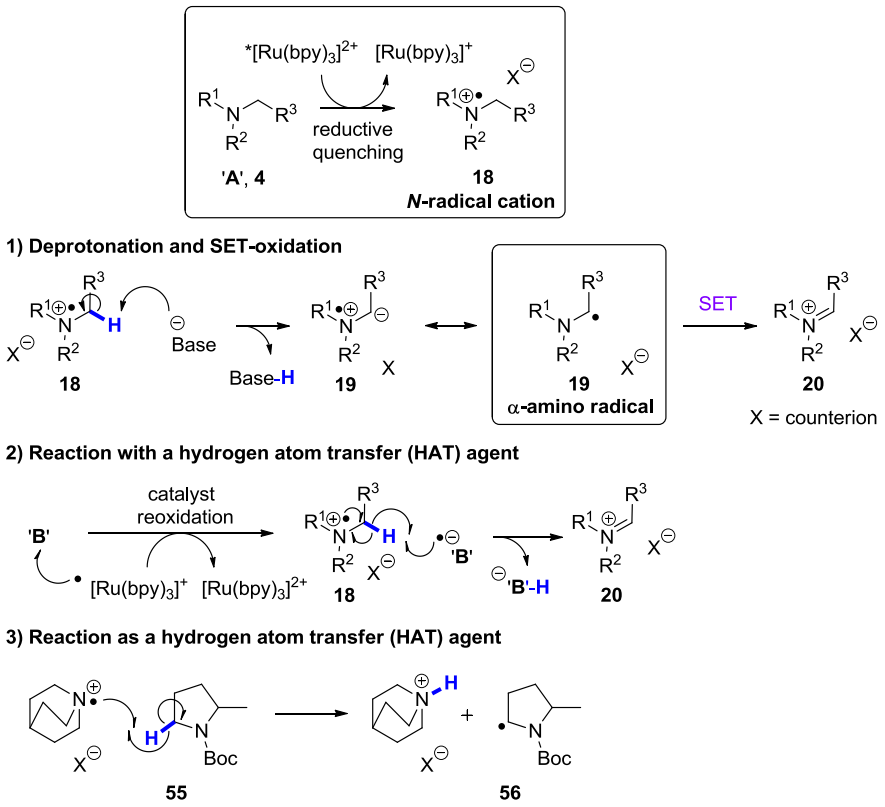

***Scheme 29**: Fates of tertiary amine radical cations generated by reductive quenching.*

The α-amino radical intermediate has several fates available to it (Scheme 30) besides oxidation. For example, α-amino radicals are nucleophilic radicals which can be captured with 1,4-acceptors such as methyl vinyl ketone, as reported by Reiser[53] and Yoon (Scheme 31).[54] Conjugate addition

affords **57**, which undergoes SET reduction and protonation to give **58**. Overall, this is a redox-neutral process.

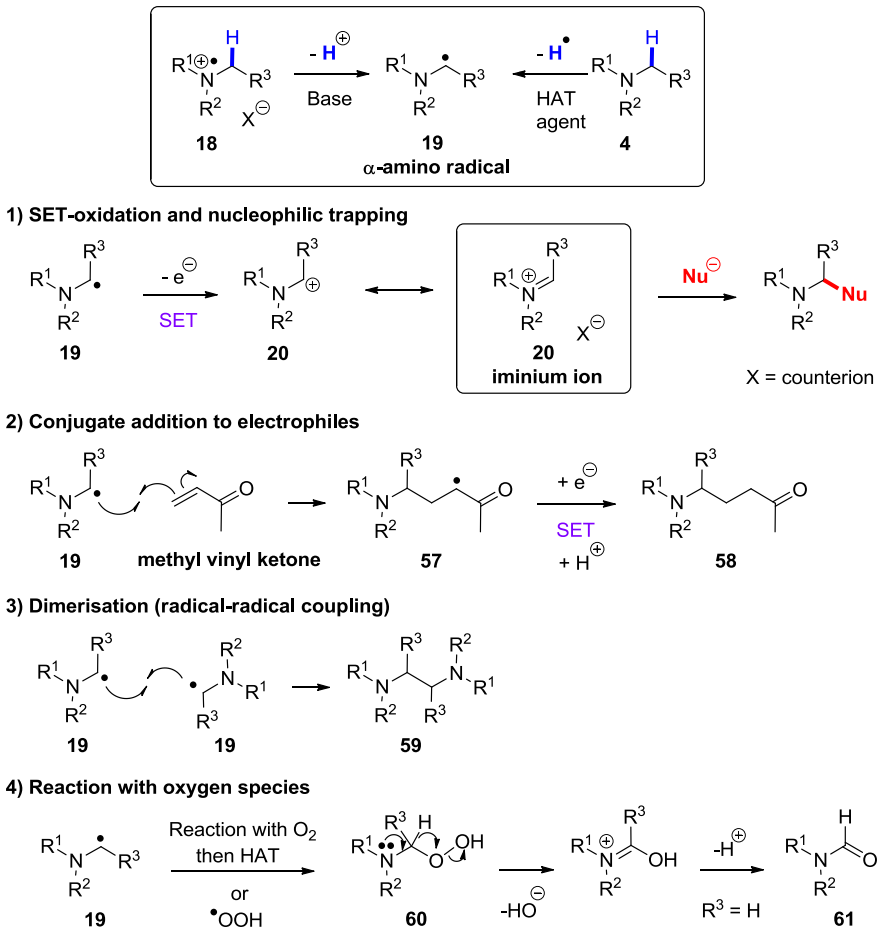

***Scheme 30**: Fates of α-amino radicals generated by deprotonation of tertiary amine radical cations or HAT reactions of tertiary amines.*

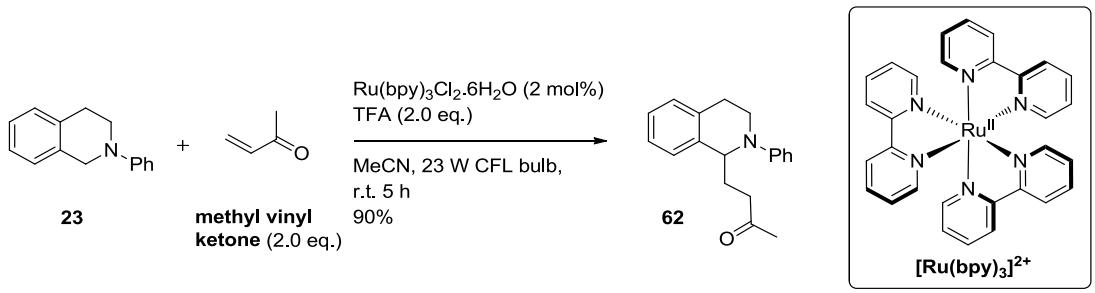

***Scheme 31**: Photoredox-catalysed radical addition of α-amino radicals to 1,4-acceptors.*

Alternatively, the α-amino radical can undergo radical-radical coupling; for example, dimerisation to give dimer **59** (Scheme 30, pathway 3).[35,53,96] This observation, and the observation of 1,4-addition reactions, corroborates the intermediacy of α-amino radicals in these transformations. Finally, combination with reactive oxygen species such as molecular oxygen (followed by HAT) or hydroperoxyl radical)[35,53,90,96,101] would result in intermediate **60** which loses H_2O to give α-oxidation products such as *N*-formyl compound **61** (Scheme 30, pathway 4). It is worth noting that if superoxide were to undergo HAT with **18**, this would directly afford iminium salt **20** and a peroxide anion which might attack **20** and ultimately generate *N*-formyl species **61** in the same manner.

1.5.2. Tertiary Amines in Net-reductive Photocatalytic Processes

Simple trialkylamines Et_3N, DIPEA and TMEDA have been commonly employed as reductive quenchers (**A**, Figure 5),[75] where they have served as terminal reductants in net-reductive processes. For example, Xiao employed DIPEA [E^p_{ox} (DIPEA$^{\bullet+}$/DIPEA) = +0.85 V *vs.* SCE] as a reductive quencher of *$[Ru(bpy)_3]^{2+}$ and net reductant in the photoredox-catalysed oxidation of boronic acids to phenols (Scheme 32).[102] Upon excitation of $[Ru(bpy)_3]^{2+}$ to *$[Ru(bpy)_3]^{2+}$ [E^p_{ox} (*Ru^{II}/Ru^{I}) = +0.83 V *vs.* SCE], reductive quenching would afford DIPEA$^{\bullet+}$ and $[Ru(bpy)_3]^{+}$ (although redox potentials are close here, it is noted that this electron transfer is marginally endergonic according to the redox potentials).

Since $[Ru(bpy)_3]^{+}$ is a potent reductant [$E_{1/2}$ (Ru^{II}/Ru^{I}) = -1.35 V *vs.* SCE], this species was proposed to reduce molecular oxygen [$E_{1/2}$ (O_2/$O_2^{\bullet-}$) = -0.75 V *vs*. SCE][35] to superoxide, which would react with the arylboronic acid substrate to give a peroxyl-type radical. This peroxyl-type radical was proposed to undergo HAT with DIPEA$^{\bullet+}$ to give a DIPEA-derived iminium salt and a peroxyborane species[102] which is primed to undergo 1,2-rearrangement to afford the phenol product and expel hydroxide anion.[103] Remarkably, no details on the light source wavelength were given in this

publication; only ‘visible-light’ was written.

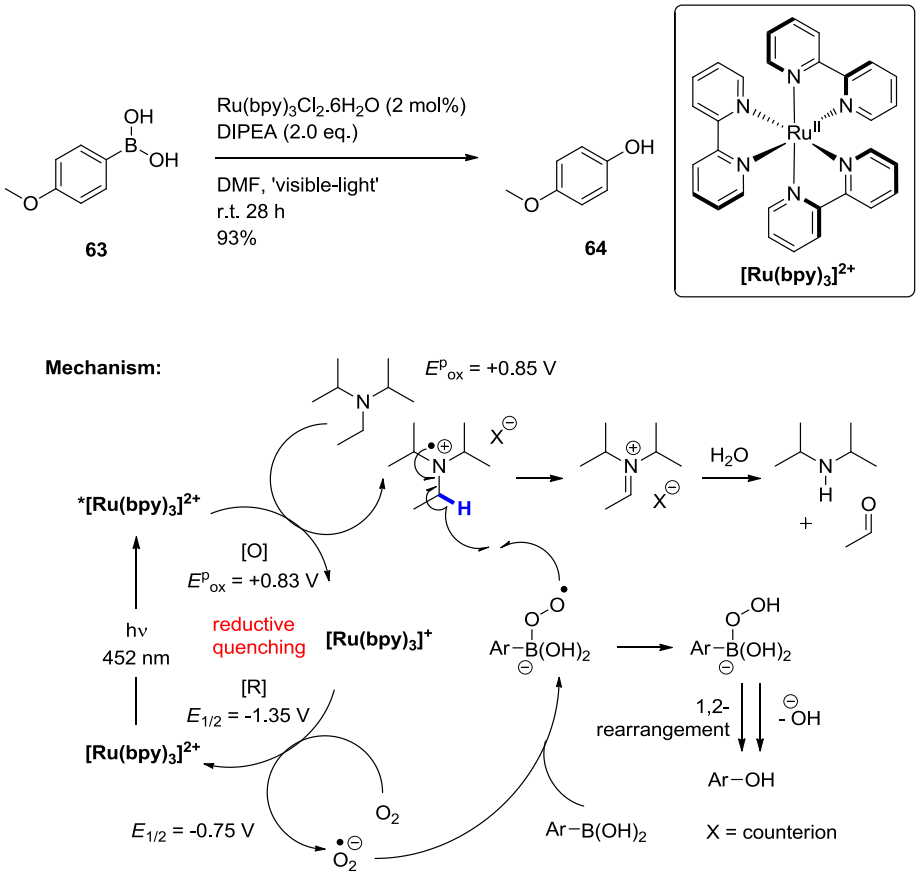

***Scheme 32**: Photoredox-catalysed oxidation of arylboronic acids to phenols.*

The photoredox oxidative hydroxylation of arylboronic acids was revisited by Scaiano, who reported a transition metal-free alternative using methylene blue. In addition, the kinetics of photocatalyst quenching and implications of singlet oxygen were thoroughly investigated using laser flash photolysis studies for both methylene blue and $[Ru(bpy)_3]^{2+}$ photocatalysts, which will be discussed in Section 2.2.[104]

DIPEA was also implicated as a reductive quencher by Stephenson, in the photocatalysed dehalogenation of alkyl halides (Scheme 33).[105] Following SET reduction, alkyl radicals are generated which are proposed to undergo HAT (with one of DIPEA, $DIPEA^{\bullet+}$ or formic acid) to furnish the dehalogenated product. Interestingly, even alkyl chlorides could be reductively dehalogenated in this chemistry (reactions of alkyl chlorides

required Hantzsch ester as an additive, see Scheme 33), however substrates possessed 'activated' C-X bonds which ensured highly stabilised (benzylic, α- to an ester) radicals in all cases (for example, bromide **65a** and chloride **66a**).

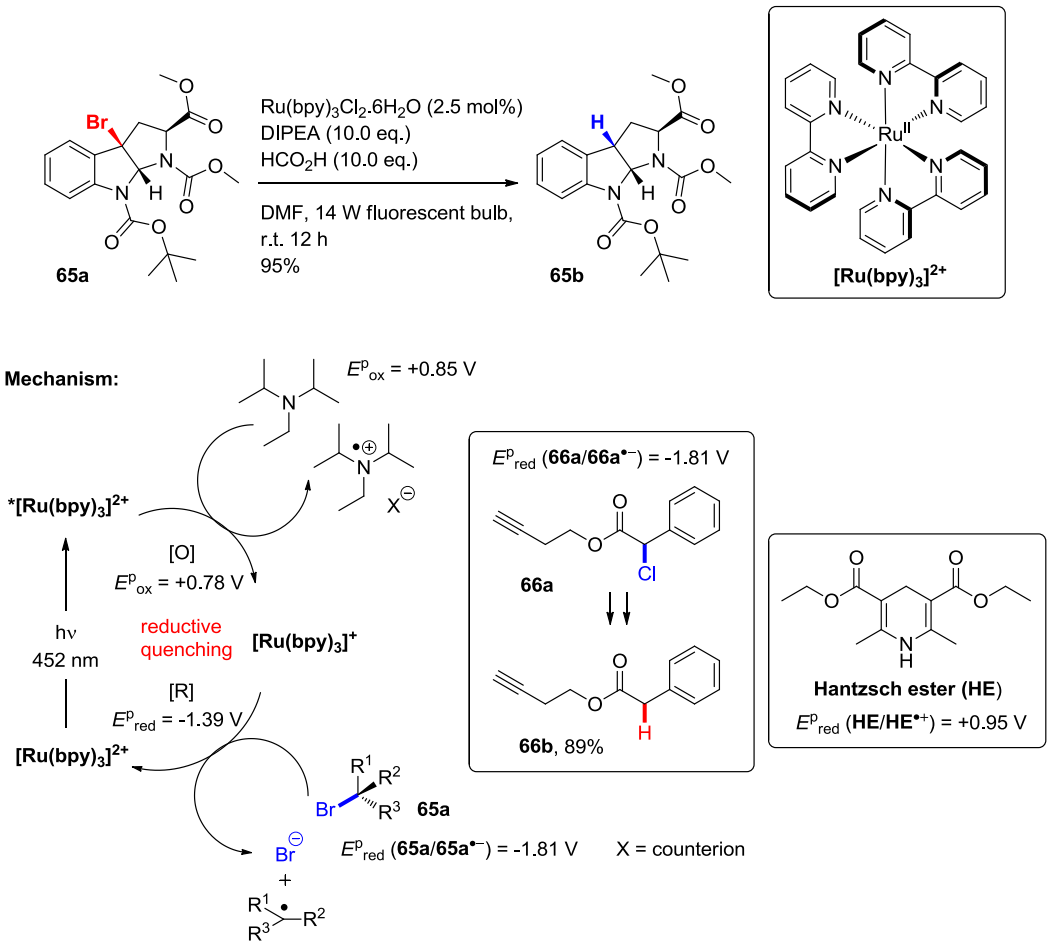

***Scheme 33**: Photoredox-catalysed reductive dehalogenation of alkyl halides.*

In a subsequent report, 'unactivated' aryl (and alkyl) iodides were successfully dehalogenated by Stephenson,[92] but aryl bromides and aryl chlorides remained unreactive. Related to this is the maximum available energy from the visible-light photon. The energy of a photon of 440 nm (blue light) is 2.8 eV, and in the case of Ru photocatalysts, *ca*. 0.6 eV is lost in nonradiative photophysical processes to reach the triplet state ($^3MLCT_1$).[106] The available energy of typical photocatalysts just reaches the reduction

potential of aryl iodides [E^{p}_{red} (PhI/PhI$^{\bullet-}$) = -1.59 V[107] or -2.24 V[108] *vs.* SCE and for *fac*-*Ir(ppy)$_3$, $E_{1/2}$ (Ir^{IV}/*Ir^{III})= -1.73 V *vs.* SCE,[75] noting that E^{p}_{red}, the reduction peak potential, will be slightly more negative than $E_{1/2}$], but not aryl bromides [E^{p}_{red} (PhBr/PhBr$^{\bullet-}$) = -2.44 V *vs.* SCE][108] or aryl chlorides [E^{p}_{red} (PhCl/PhCl$^{\bullet-}$) = -2.78 V *vs.* SCE].[108] This limitation was partially tackled by König, who reported the reductive dehalogenation of aryl bromides and aryl chlorides (substituted with electron-withdrawing groups) using an organophotocatalyst (**PDI**) and triethylamine as a reductive quencher (Scheme 34).[106]

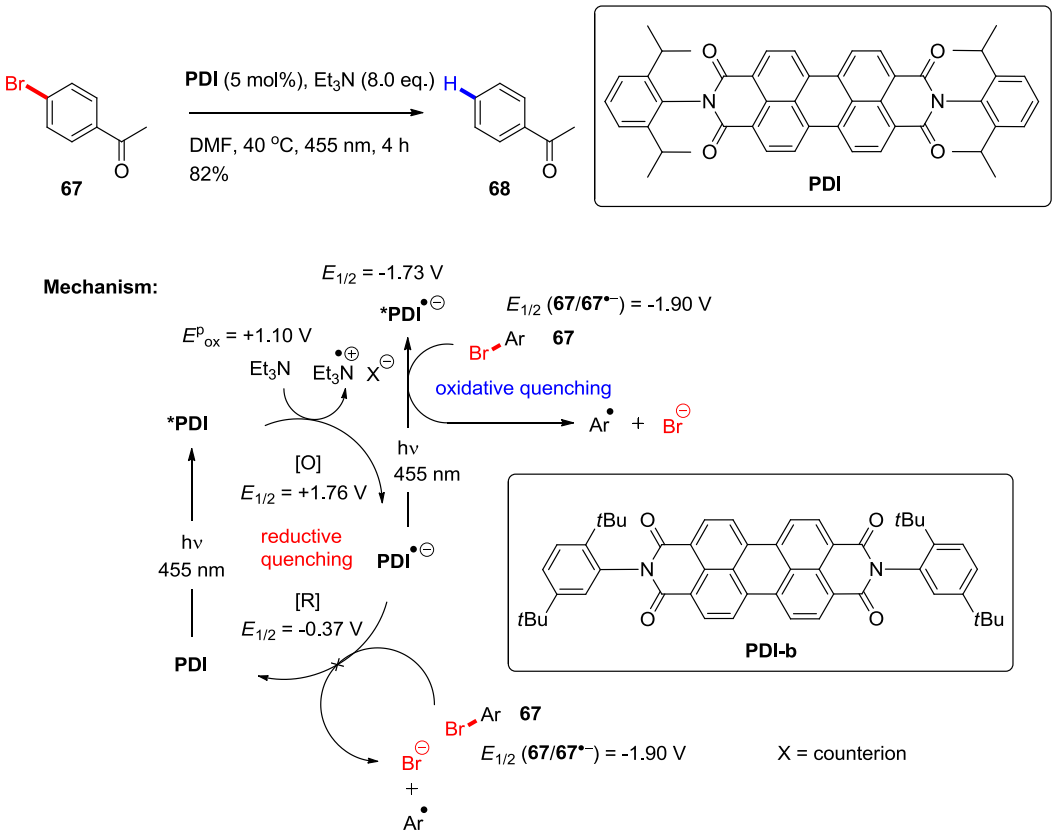

***Scheme 34**: Organophotoredox-catalysed reductive dehalogenation of aryl halides.*[106]

Here, redox potentials of related compound **PDI-b**[109] are used to explain the mechanism.[110] Following excitation of **PDI**, reductive quenching with Et_3N [E^{p}_{ox} ($Et_3N^{\bullet+}$/Et_3N) = +1.10 V *vs.* SCE] occurs, which is favourable according

to redox potentials [$E_{1/2}$ (**PDI**-**b**/**PDI**-**b**$^{\bullet-}$) = -0.43 *vs*. SCE,[109] therefore $E_{1/2}$ (***PDI**-**b**/**PDI**-**b**$^{\bullet-}$) = +1.76 V *vs*. SCE, assuming $E_{0,0}$ transition energy = 2.13 eV consistent with the emission peak of ***PDI** at 582 nm].[†,106] The ground state radical anion **PDI**$^{\bullet-}$ is not a potent enough reductant to reduce aryl bromides (for example, **67**). However, **PDI**$^{\bullet-}$ itself absorbs visible-light and can absorb a second photon to gain more energy, [$E_{1/2}$ (**PDI**-**b**/***PDI**-**b**$^{\bullet-}$) = -1.73 V *vs*. SCE based on the $E_{0,0}$ transition energy = 1.30 eV][109,110] bringing it within range of aryl bromides and chlorides [substituted by electron-withdrawing groups, for example $E_{1/2}$ (**67**/**67**$^{\bullet-}$) = -1.90 V *vs.* SCE].[109,110]

Highly reactive aryl radicals are generated, which can abstract hydrogen atoms from the solvent or can be captured with electron-rich heterocycles in a net C-C bond forming process.[106] In this discovery, König showed the potential of harnessing consecutive visible-light photons (consecutive photoelectron transfer = conPET) to boost the maximum available energy to photoredox catalysts. Based on this principle, König found that the mechanism (regular PET *vs*. conPET) could be altered by changing the irradiation wavelength.[111] Presumably, conPET could equally apply to oxidations using organic dyes if the radical cation (following oxidative quenching) absorbs visible-light. Here, the secondary amine derived from the reductive quencher (**A**, Figure 5) was detected (diethylamine from the use of triethylamine as a reductive quencher).[106] The secondary amine would result from hydrolysis of an iminium salt, thus corroborating the generation of iminium salts in these photocatalytic processes.

1.5.3. TERTIARY AMINES IN NET-OXIDATIVE PHOTOCATALYTIC *N*-FUNCTIONALISATIONS

The process of generating iminium salts from tertiary amines by reductive quenching was utilised in a synthetic sense by Stephenson. Using *N*-phenyl-1,2,3,4-tetrahydroisoquinoline (**23**) as a reductive quencher under

[†]Redox potentials compared here are slightly different; one is a half potential $E_{1/2}$ (*vs*. SCE) and one is an oxidation peak potential E^{p}_{ox} (*vs*. SCE). However, ΔE is so large that this subtle difference can be ignored.

$[Ru(bpy)_3]^{2+}$ photoredox catalysis led to iminium salt **26** which was trapped in a nitro-Mannich reaction to yield **27** (Scheme 35).[98] Here, nitromethane was used as the reaction solvent, no additional base (triethylamine) was required and the overall reaction took 20 h.

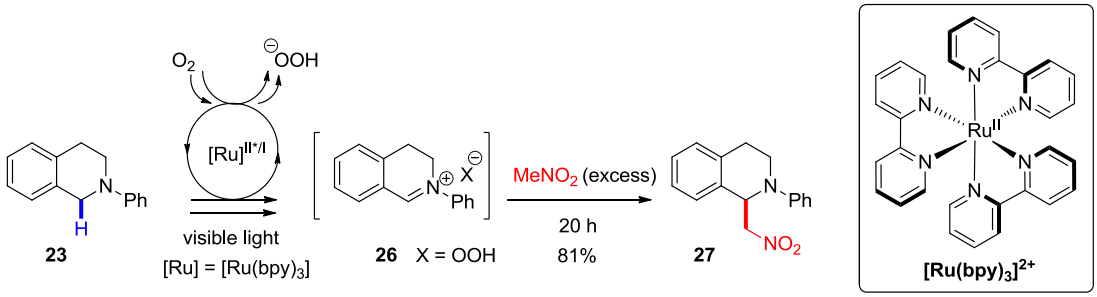

***Scheme 35**: Visible-light catalysed oxidative iminium generation and nitro-Mannich trapping.*[98]

Following this seminal work, *N*-aryl THIQ substrates now represent a popular choice for photocatalytic oxidation (Scheme 36). Iminium salt **26** was trapped by Stephenson using classical nucleophiles such as nitronates,[98] silyl enol ethers and enolates of 1,3-ketoesters.[96] At the same time, Rueping coupled photocatalytic generation of iminium salt **26** with an L-proline-catalysed Mannich reaction [very low (8%) ee's were reported].[90]

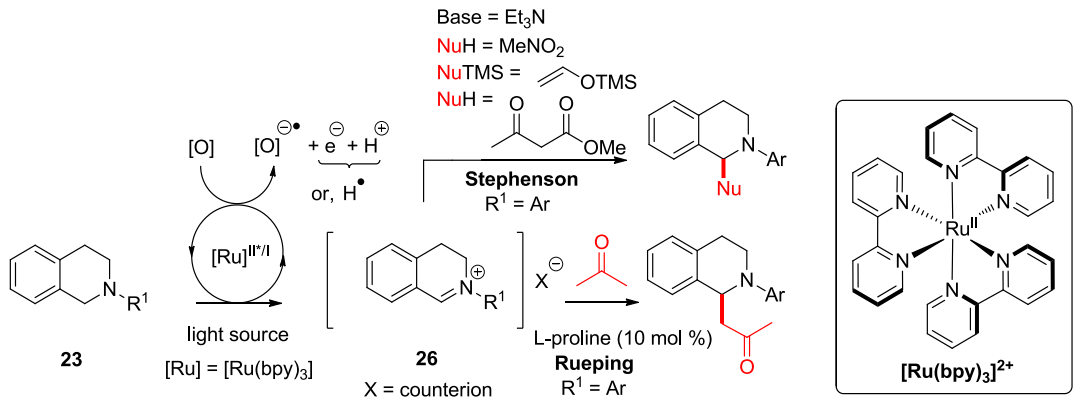

***Scheme 36:** Nucleophiles previously employed to trap N-aryl THIQ iminium salts.*[90,96]

The use of other photocatalysts to generate, and stabilised carbon nucleophiles to intercept, iminium salts has been explored,[57,90,98,112] as well as photocatalysis requiring no sacrificial oxidant.[113] Using chiral thiourea catalysis, Stephenson and Jacobsen disclosed asymmetric nucleophilic additions, yielding products in modest to excellent (42 - 99%) ee's.[114] The opportunity for scale-up (and enhancement) available to these visible-light photochemical processes *via* continous flow processing has been demonstrated in the literature.[115,116]

The use of O_2 as a catalyst reoxidant (**B**, Figure 5) is disputed within the literature.[53,90,96,98] Rueping claims that O_2 is key in obtaining high catalytic turnover *via* catalyst reoxidation.[90] In one report, Stephenson reported a 76% conversion in 20 h for a degassed reaction, compared to 100% conversion (81% isolated yield, Scheme 35) in 20 h for a non-degassed reaction.[98] However, in a subsequent report, Stephenson claimed that 'slow catalyst turnover with oxygen' was the reason for pursuing stoichiometric oxidant driven transformations which biased formation of the iminium salt.[96] Several divergent pathways can operate in the aerobic mechanism (Scheme 30),[53,90,96] and a thorough investigation of these pathways was recently reported by König.[35] Following on from investigations under aerobic conditions, Stephenson reported that use of stoichiometric oxidant $BrCCl_3$ [E^p_{red} ($BrCCl_3/BrCCl_3^{\bullet-}$) = -1.36 V *vs.* SCE] under anaerobic conditions gave formation of iminium salt **26** in < 3 h (Scheme 37).[77,96]

Following reductive quenching, HAT from the N-radical cation to the trichloromethyl radical was proposed as the predominant mechanism (Scheme 29, pathway 2). It was suggested that if any α-amino radical was formed, its oxidation pathway (Scheme 30, pathway 1) would be accelerated by excess oxidant.[96] In this chemistry, once the iminium salt had formed, addition of nitromethane (5.0 eq.) only gave very slow conversion of iminium salt **26** to product. Therefore, addition of triethylamine (5.0 eq.) was required (4 h for nitro-Mannich reaction completion), in contrast to the aerobic conditions which did not require an additional base. Excellent isolated yields

(95%) for nitro-Mannich products are reported using these anaerobic reaction conditions.[96]

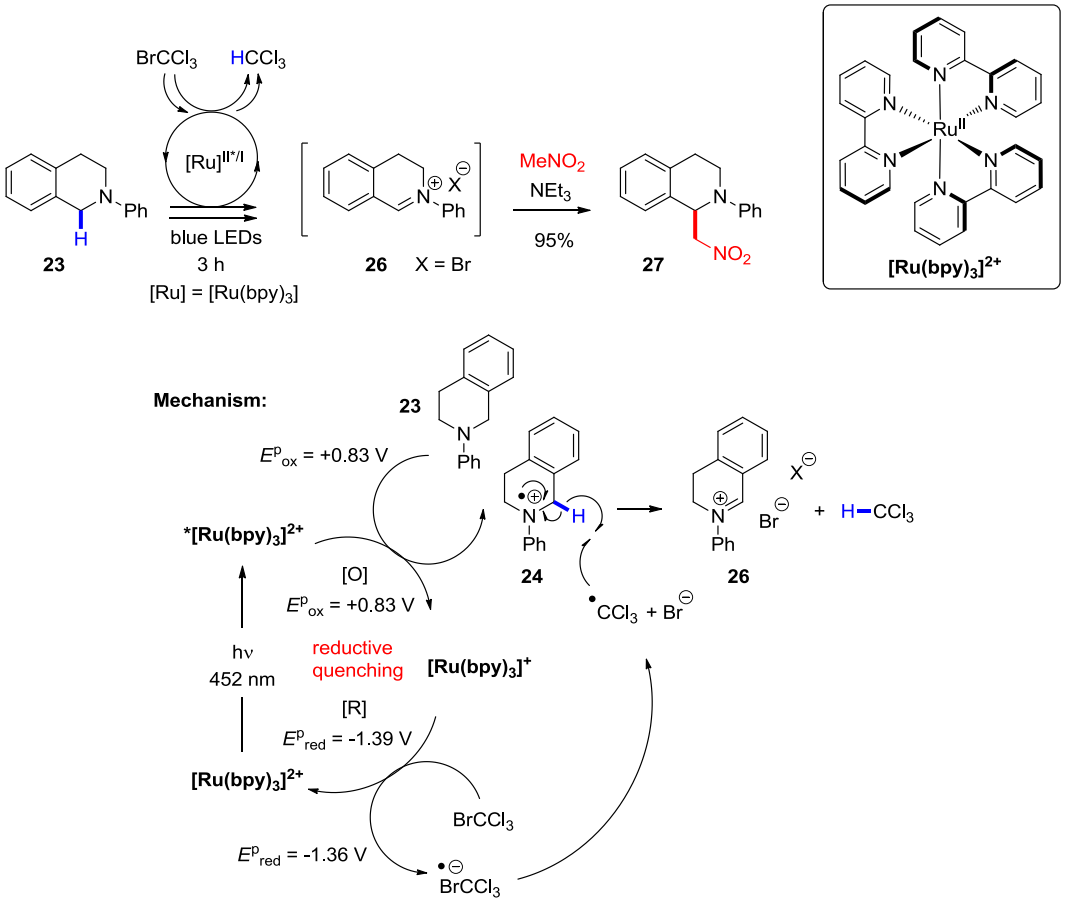

***Scheme 37**: Photoredox-catalysed anaerobic iminium salt formation and nitro-Mannich trapping.*[96]

Interestingly, Zeitler found that the anaerobic conditions employing $BrCCl_3$ oxidant proceeded just as effectively *in the absence of* $[Ru(bpy)_3]^{2+}$ (Scheme 38).[58] The presence of light proved to be essential to the success of the transformation. A radical chain mechanism was proposed, initiated by excitation and electron transfer reaction of an electron donor/acceptor (**EDA**) complex **69** (Scheme 38) to give **24**, trichloromethyl radical and bromide. Deprotonation of **24** affords the highly reducing α-amino radical **25** [E^{p}_{ox} (Et_2N^{+}=$CHCH_3$/Et_2N−$^{\bullet}CHCH_3$/) = -1.12 V vs. SCE][35] which can enter the propagation step.

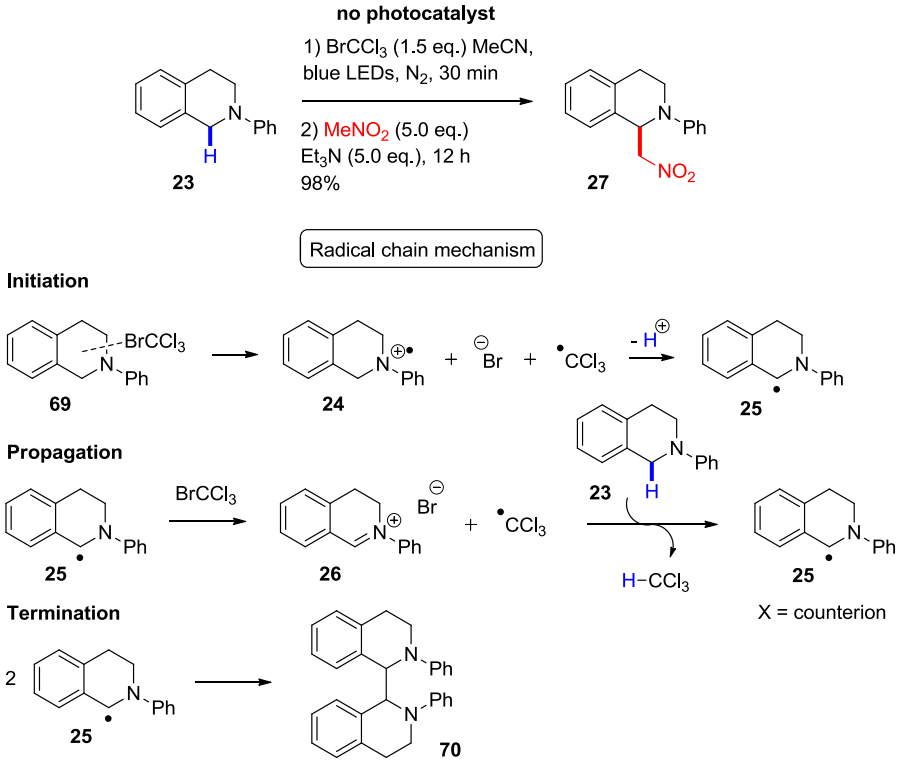

***Scheme 38**: Photoredox catalyst-free anaerobic radical chain iminium salt formation mechanism for $BrCCl_3$ oxidant, proposed by Zeitler.*[58]

The α-amino radical **25** is oxidised by $BrCCl_3$ generating iminium salt **26**, trichloromethyl radical and bromide anion. The resulting trichloromethyl radical can undergo HAT with the starting THIQ **23**, affording $CHCl_3$ and regenerating α-amino radical **25**, thereby propagating the chain (Zietler demonstrates that initiation by homolysis of $BrCCl_3$ and propagation by atom-transfer radical addition is another plausible mechanism, and photochemical homolysis of $BrCCl_3$ has been previously reported).[58,117] Although a radical chain mechanism was proposed, light on/off reactions were performed to investigate conversion during dark periods and reaction progress was only significant during irradiation periods. A similar radical chain mechanism was proposed by Yoon in the photoredox-catalysed radical addition of α-amino radicals to 1,4-acceptors (Scheme 31), where HAT from the starting THIQ is rate-limiting.[54] Recent studies from the Yoon group have demonstrated radical chain mechanisms in multiple photoredox chemistries (characterised

by quantum yields of $\Phi > 1.0$).[118]

Evidence for Zeitler's radical chain propagation mechanism manifests from the ability to oxidise *N*-alkyl THIQs. So far, all the net-oxidative photoredox-catalysed examples cited have used *N*-aryl THIQs as substrates. The aniline moiety of *N*-aryl THIQs renders their facile oxidation [E^{p}_{ox} ($N^{\bullet+}$-Ph THIQ/*N*-Ph THIQ) = +0.83 V *vs*. SCE], with the oxidation potential falling within range of *$[Ru(bpy)_3]^{2+}$ [E^{p}_{ox} (*Ru^{II}/Ru^{I}) = +0.83 V *vs.* SCE]. Since the stabilising aniline moiety is not present in *N*-alkyl THIQs, their oxidation potential is higher [E^{p}_{ox} ($N^{\bullet+}$-methyl THIQ/*N*-methyl THIQ) = +1.15 V *vs*. SCE]. Turnover of a closed photocatalytic cycle (Figure 5) depends on electron transfer to *$[Ru(bpy)_3]^{2+}$, which is now significantly endergonic. On the other hand, the radical chain mechanism propagates *via* HAT, whose success will be most influenced by the stability of the α-amino radical (**25**). Chain propagation proceeds through HAT, is independent of the redox potential of the *N*-substituted THIQ and thus should operate similarly well for both *N*-aryl THIQs and *N*-alkyl THIQs (the BDE of the α-amino C-H bond will be important, of course).

1.5.4. *N*-FUNCTIONALISATION OF TRIALKYLAMINES UNDER PHOTOREDOX CATALYSIS

Given there are many photoredox processes reported using trialkylamines (Et_3N or DIPEA) as sacrificial reductive quenchers, it is surprising that there are few photoredox processes optimised for the *N*-functionalisation of the trialkylamine as a substrate. As mentioned in Section 1.4.2, trialkylamines are challenging to oxidise, suffer from regioselectivity issues and unstable intermediates in their reactions.

Stephenson reported regioselective functionalisation of the *N*-C**H**$_3$ group of *N*-methylmorpholine using heterocyclic partner **71** (Scheme 39).[119] Here, oxidative quenching (Figure 5) of excited *$Ir(ppy)_3$ [$E_{1/2}$ (Ir^{IV}/*Ir^{III}) = -1.73 V *vs.* SCE][119] by molecular oxygen [$E_{1/2}$ (O_2/$O_2^{\bullet-}$) = -0.75 V *vs.* SCE][35] generates an Ir(IV) species [$E_{1/2}$ (Ir^{IV}/Ir^{III})= +0.77 V *vs.* SCE][119] which is proposed to be reduced by *N*-methylmorpholine [E^{p}_{ox} ($N^{\bullet+}$-methylmorpholine/*N*-

methylmorpholine) = +1.10 V *vs.* SCE] and in doing so the ground state catalyst is regenerated (the authors acknowledge that electron transfer from *N*-methylmorpholine to the Ir(IV) species is significantly endergonic). Deprotonation of the resulting radical cation at the *N*-C**H**$_3$ group yields an α-amino radical which adds to the heterocyclic partner.

Whilst the origins of regioselectivity are unclear, it was reported that excess *N*-methylmorpholine favoured *N*-C**H**$_3$ functionalisation. Details of rearomatisation are not discussed (presumably, HAT with solvent/trialkylamine or oxidation/deprotonation). The reaction was optimised for **71** and a very large excess of *N*-methylmorpholine (20.0 eq.) was required. Optimal conditions gave 75% conversion of **71**, a 12 : 1 *exo*:*endo* ratio and 56% isolated yield of **72**. The scope of trialkylamine was explored; generally 20.0 eq. of amine is required, a 10 : 1 *exo*:*endo* ratio is observed and modest to good isolated yields (20 - 54%) are reported.

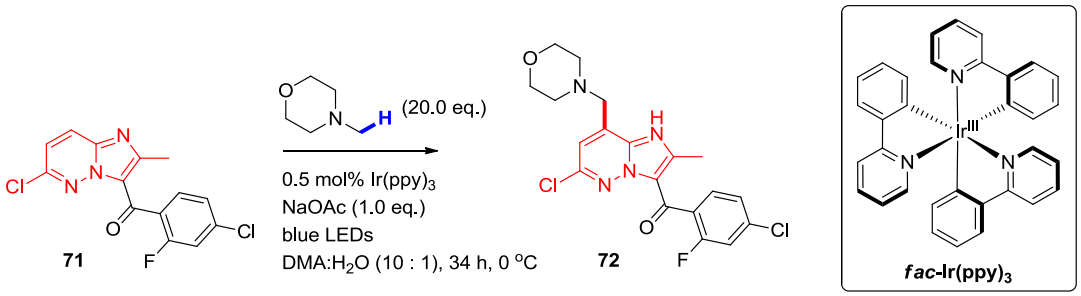

***Scheme 39**: Regioselective activation of N-methylmorpholine under photoredox catalysis coupling with a heterocyclic partner.*[119]

Santamaria reported selective *N*-demethylation of the *N*-C**H**$_3$ group of dextromethorphan (**73**) using 9,10-dicyanoanthracene (DCA) as an organic photocatalyst and air as the terminal oxidant (Scheme 40).[52] Variable amounts of an *N*-formyl species (**75**) were initially observed (40 - 60% 'product ratio'), however adding $LiClO_4$ (0.5 eq.) gave secondary amine (**74**) as the major product (80 - 100% 'product ratio'). There is no mention of an *N*-C**H**$_2$-derived iminium (or products derived therefrom). Santamaria proposes that *DCA^1 initially oxidises dextromethorphan (**73**) to its N-radical cation.

Deprotonation then follows a stereoelectronic effect (preferred deprotonation of the *N*-C**H**$_3$ group which can freely rotate to align a C-H bond with the N-radical cation SOMO, see Figure 3) to afford the least stable 1^o α-amino radical. Santamaria claims that addition of $LiClO_4$ disfavours the combination of α-amino radical intermediates with reactive oxygen species which leads to the *N*-formyl species (Scheme 30, pathway 4).[52] Interestingly, in a separate report and using a similar photocatalytic system, Santamaria discloses *N*-C**H**$_2$ selective cyanation of *N*-alkyl-3-piperideines (such as **36**) *via* the thermodynamic iminium salt (Scheme 41).[50]

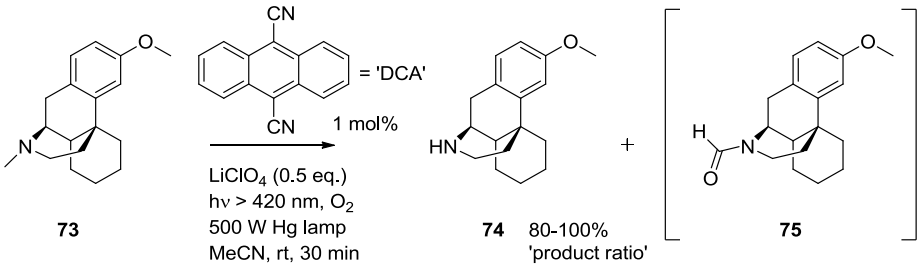

Scheme 40: *Selective oxidation of the N-C**H**$_3$ position of dextromethorphan.*[52]

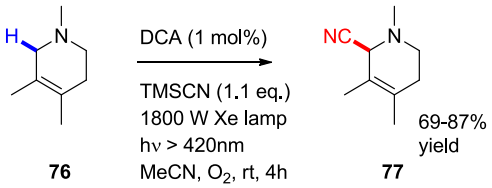

Scheme 41: *Selective cyanation of N-C**H**$_2$ position of N-alkyl-3-piperideines.*[50]

Hashmi reported the *N*-functionalisation of various trialkylamines using 1-iodoalkynes under photoredox catalysis (Scheme 42). Here, a gold photoredox catalyst $[Au_2(\mu\text{-dppm})_2]^{2+}$ was employed which was activated by sunlight or UVA light (λ = 315 - 400 nm). Due to the $^*Au_2^{2+}$ complex being a powerful reductant [E^o ($[Au_2(dppm)_2^{3+}]/^{2+*}$) = -1.55 V *vs*. SSCE],[120] the 1-iodoalkyne species **79** [$E_{1/2}$ ((iodoethynyl)benzene/(iodoethynyl)benzene radical anion) = -0.89 V *vs.* SCE][121] was proposed as an oxidative quencher

(**C**, Figure 5),† affording an alkynyl radical (**81**). The trialkylamine substrate would serve as the terminal reductant (**D**, Figure 5) to regenerate the ground state $[Au_2(\mu\text{-dppm})_2]^{2+}$ and the trialkylamine-derived radical cation. Deprotonation would afford an α-amino radical, primed to couple with the alkynyl radical (**81**) to afford the desired product (**82**) and this is in line with the 'persistent radical effect' (the favourable combination of a relatively long-lived radical with a relatively short-lived radical).[122,123] The lifetimes of an α-aminoalkyl radical and a phenylethynyl radical are 700 ns (in 1 : 9 water/MeCN solvent)[55] and 2 ns (computed from electronic structure calculations and vibrational frequencies), respectively.[55,124]

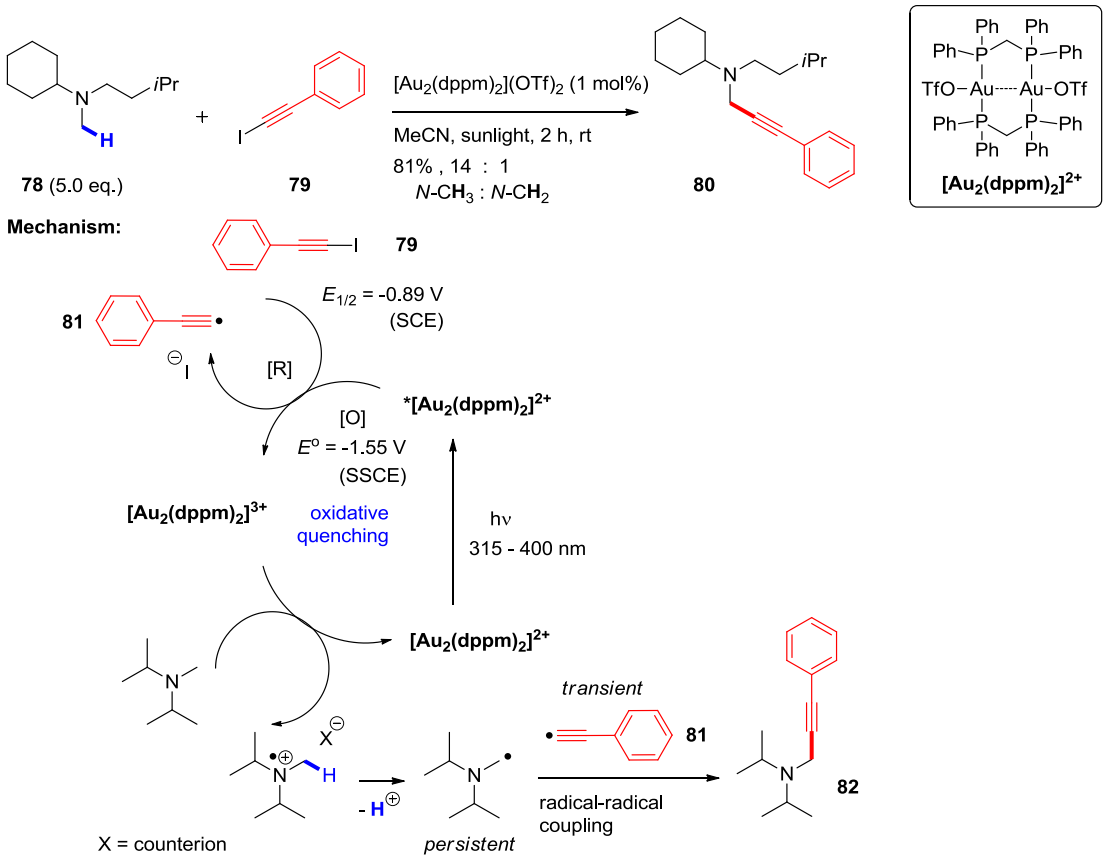

***Scheme 42**: Photoredox-catalysed alkynylation of trialkylamines with 1-iodoalkynes.*[121]

†Redox potentials quoted here give an indication of the ease of reduction but are not directly comparable; one is a standard potential E^o (*vs*. SSCE) and one is a half-wave potential $E_{1/2}$ (*vs*. SCE).

Through the use of a different photocatalytic system, Hashmi reported the *N*-functionalisation of various trialkylamines using tetrasubstituted *gem*-difluoroalkenes (Scheme 43).[125] In both of Hashmi's *N*-functionalisation reports, high regioselectivity was observed for *N*-methyl groups over other *N*-alkyl groups. This delivered sole products in many cases (most examples are statistically biased by the *N*,*N*-dimethyl unit being present, but the example in Scheme 42 proceeded with 14 : 1 regioselectivity). However, the excess of trialkylamine (3.0 - 5.0 eq.) is a limitation, certainly if the trialkylamine scaffold is valuable.

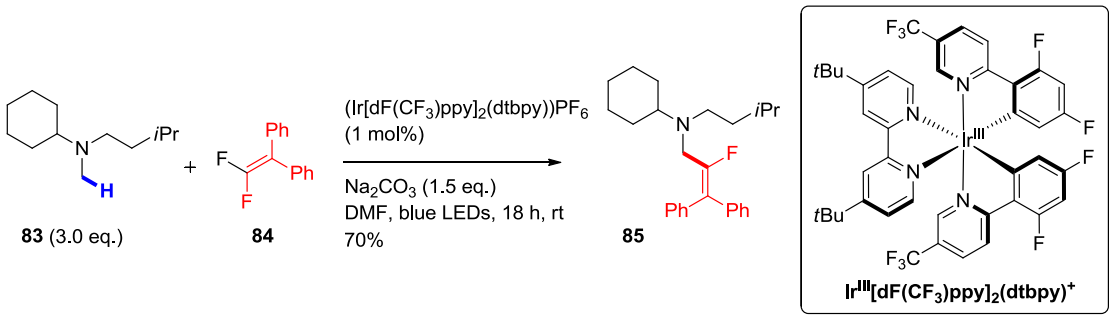

***Scheme 43**: Photoredox-catalysed monofluoroalkenylation of trialkylamines.*[125]

Though not trialkylamines *per se*, MacMillan reported the site-selective functionalisation of *N*-Boc and *N*-Bac protected secondary amines under photoredox catalysis (Scheme 44). This is important because *N*-Boc protected amines (for example, *N*-Boc-1,2,3,4-tetrahydroisoquinoline; E^{p}_{ox} ($N^{\bullet+}$-Boc-1,2,3,4-tetrahydroisoquinoline/*N*-Boc-1,2,3,4-tetrahydroisoquinoline) = +2.14 V *vs.* SCE) are markedly more difficult to oxidise than trialkylamines and previous attempts to functionalise *N*-Boc protected amines under photoredox catalysis have proved unsuccessful.[48,57] MacMillan's chemistry circumvented the issue of the nitrogen atom's high oxidation potential, instead using HAT chemistry to directly transform the *N*-C**H**$_2$ position of the protected amine (for example, **86**) into an α-amino radical.

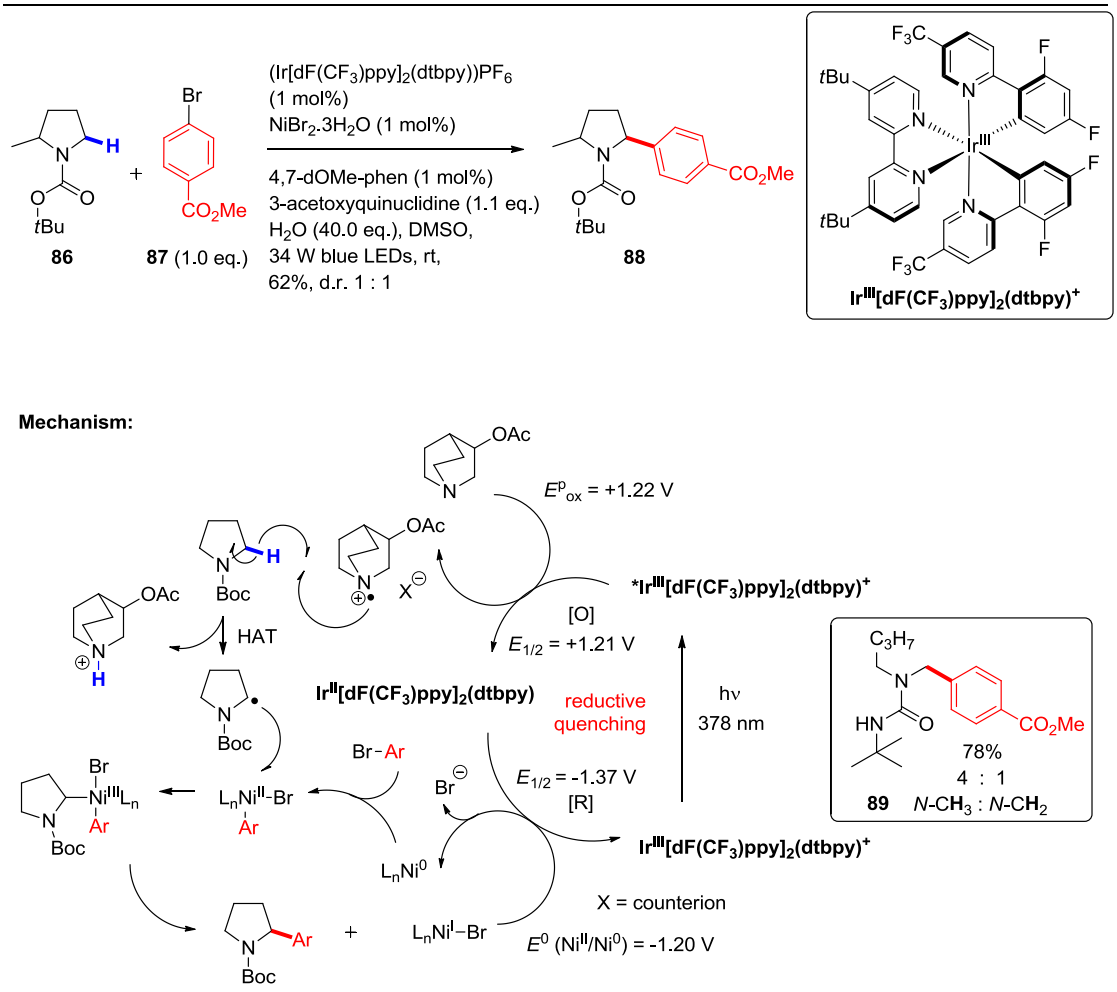

***Scheme 44**: Site-selective N-functionalisation of N-protected secondary amines under dual photoredox/nickel catalysis via HAT.*[†,‡]

Upon excitation of the photocatalyst, 3-acetoxyquinuclidine [E^{p}_{ox} (3-acetoxyquinuclidine radical cation/3-acetoxyquinuclidine) = +1.22 V *vs*. SCE in MeCN][100] acts as a reductive quencher of the excited $*Ir^{III}$ species [$E_{1/2}$ ($*Ir^{III}/Ir^{II}$) = +1.21 V *vs*. SCE][100] in line with the matching redox potentials, generating the 3-acetoxyquinuclidine radical cation. This undergoes HAT selectively with the *N*-C**H**$_2$ position of the N-protected secondary amine to afford an α-amino-type radical. Meanwhile, a Ni^0 species undergoes oxidative addition into the aryl bromide partner. The resulting Ni^{II} complex

[†]Redox potentials compared here are slightly different; one is a half potential $E_{1/2}$ (*vs*. SCE) and one is an oxidation peak potential E^{p}_{ox} (*vs*. SCE). [‡]Redox potentials are different; a half-wave potential $E_{1/2}$ (in MeCN) is being compared with a standard potential E^0 (in DMF).

captures the α-amino-type radical, then reductive elimination yields the desired product and regenerates the Ni^{I} species [$E_{1/2}$ (Ni^{II}/Ni^{0}) = -1.20 V *vs*. SCE in DMF][100] to complete the photoredox cycle by accepting an electron from the Ir^{II} species [$E_{1/2}$ (Ir^{III}/Ir^{II}) = -1.37 V *vs*. SCE in MeCN].[†,‡,100] When unsymmetrical amine substrates was employed, interesting regioselectivity patterns started to emerge, for example *N*-C**H**$_3$: *N*-C**H**$_2$ selectivity in the formation of **89** was 4 : 1. Following this work, Molander reported a computational investigation which found that instead of oxidative addition, the Ni^{0} species first captures the α-amino radical to form a Ni^{I} complex which then undergoes oxidative addition.[126,127]

[†]Redox potentials compared here are slightly different; one is a half potential $E_{1/2}$ (*vs*. SCE) and one is an oxidation peak potential E^{p}_{ox} (*vs*. SCE). [‡]Redox potentials are different; a half-wave potential $E_{1/2}$ (in MeCN) is being compared with a standard potential E^{0} (in DMF).

1.6. Primary Aim: Development of Regio- and Chemoselective *N*-Functionalisations of Tertiary amines

The site-selective *N*-functionalisation of trialkylamines is of interest to the pharmaceutical industry. Multiple pharmaceuticals and biologically active natural products contain a 1,2-disubstituted THIQ motif with alkyl or aryl substituents at the 1-position (Figure 6). For example, (-)-carnegine (a monoamine oxidase A inhibitor),[128] (+)-solifenacin (a bladder-selective muscarinic M_3 receptor antagonist and active ingredient of a top 200 selling pharmaceutical in 2008)[129,130] and (±)-methopholine (an opioid analgesic).[131,132]

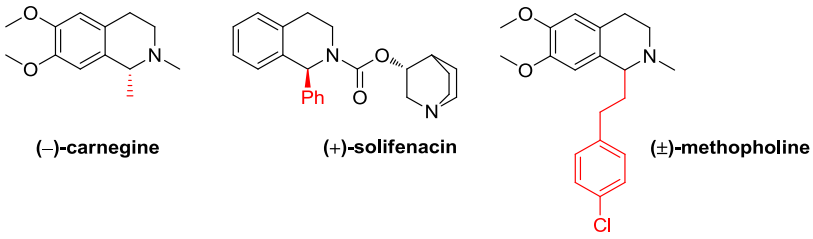

***Figure 6**: Examples of biologically active 1,2-disubstituted THIQs.*

Rather then *de novo* synthesis of the THIQ scaffold and subsequent chemistry, direct *N*-C**H**$_2$ functionalisation of the benzylic *N*-C**H**$_2$ position of a THIQ core could offer an alternative, rapid and efficient route to these types of molecules (Scheme 45). The 1-substituted THIQ core starting material can be prepared in a single step from commercial 1,2,3,4-tetrahydroisoquinoline or 6,7-dimethoxy-1,2,3,4-tetrahydroisoquinoline (available as its hydrochloride salt) by reductive amination[42] or Buchwald-Hartwig coupling[133] as well as other chemistries (see Chapter 5.8). Oxidation to the benzylic iminium salt is readily achieved and a wide range of nucleophiles can be employed to generate the product. Generally, highly stabilised organometallic reagents have been used: Cu-acetylides,[90,96,134,135] boronic acids[47] and various allylic species (silanes,[96] stannanes and Bpin esters[136]). By extending this methodology to unstabilised organometallic nucleophiles

(Grignards, organozinc reagents), the diversity of substituents that could be installed at the *N*-C**H**$_2$ position would be significantly increased (potentially allowing access to all three biologically active molecules in Figure 6).

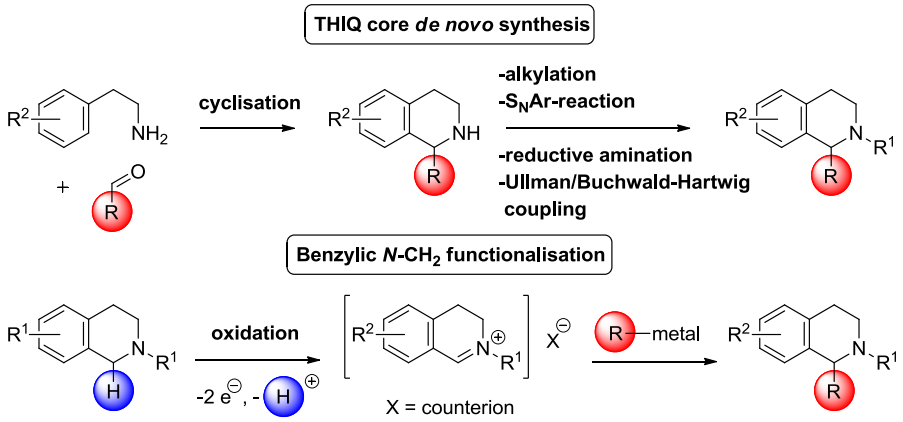

***Scheme 45**: THIQ core de novo synthesis vs. benzylic N-C**H**$_2$ functionalisation strategies.*

Of particular interest to the pharmaceutical industry is site-selective *N*-C**H**$_3$ functionalisation of trialkylamines. For example, stepwise *N*-C**H**$_3$ functionalisation has been utilised at GSK in the synthesis of buprenorphine **96** (Scheme 46). Following a Diels-Alder reaction of oripavine, a phenol protection of **90** and addition of a Grignard reagent to **91**, intermediate **92** is oxidised to its N-oxide salt (a mixture of diastereomers) by *m*-CPBA. Fe(II)-catalysed *N*-demethylation of N-oxide salt **93** (the non-classical Polonovski reaction) affords secondary amine **94**, which is alkylated to give intermediate **95**.

Overall, three chemical steps were required to transform the *N*-C**H**$_3$ compound **92** into differentially substituted *N*-alkyl compound **95** (Scheme 47). This provides scope for direct *N*-C**H**$_3$ functionalisation to decrease the number of chemical steps, enhancing efficiency in terms of yield and time. Furthermore, the strategy allows the original carbon atom of the *N*-C**H**$_3$ group to be retained and avoids the need for noxious alkylating agents, thus embedding the principles of green chemistry and molar efficiency.[68,137]

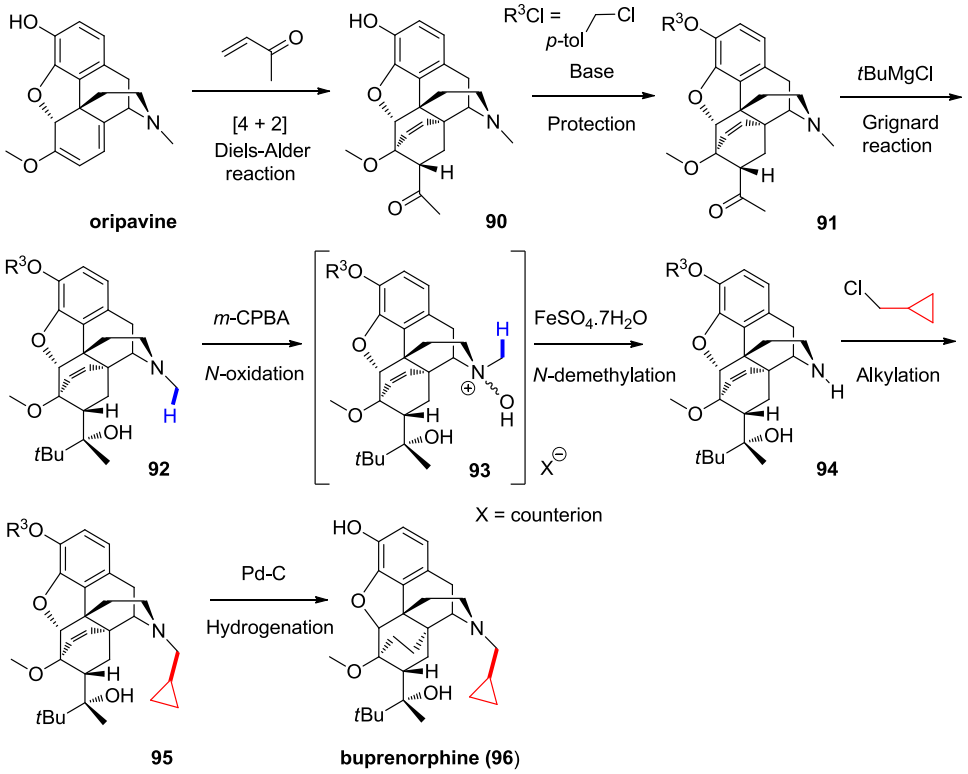

Scheme 46: *Synthesis of buprenorphine via a non-classical Polonovski reaction.*

Based on the literature presented in the introduction (Sections 1.4 and 1.5), a viable strategy for direct *N*-C**H**$_3$ functionalisation seems to be radical cation activation of the substrate by SET oxidation. Downstream chemical steps (deprotonation and SET oxidation, or HAT) would afford the iminium salt, primed to be intercepted by organometallic nucleophiles.

The primary aim of this research project is to develop technologies which oxidatively convert tertiary amines into iminium salts with high regio- and chemoselectivity and capture these iminium salts with organometallic nucleophiles; *ergo*, tertiary amines are directly converted into differentially substituted tertiary amines in a single-pot transformation. Photoredox catalysis was selected *a priori* as a vehicle for radical cation activation (Scheme 47), based on the principle that the redox potentials of photocatalyst excited states can be tuned to the organic substrate molecules

(by structural modifications of the photocatalyst architecture or by choosing a different class of photocatalyst).

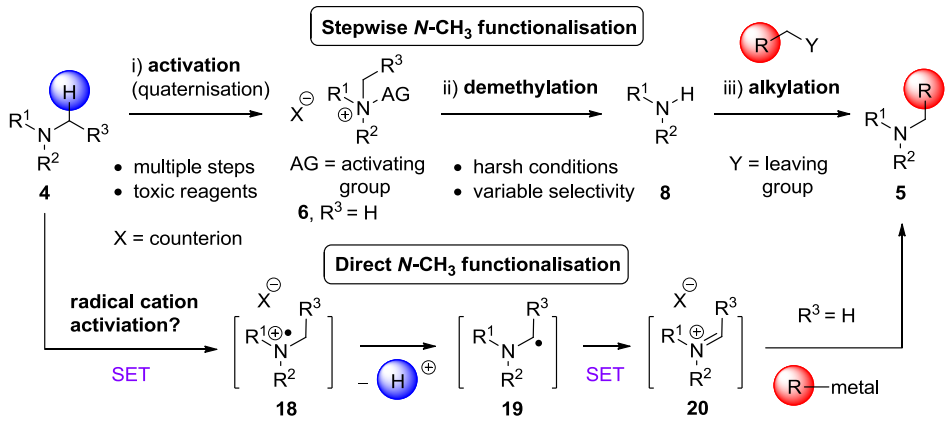

***Scheme 47**: Stepwise vs. direct N-C**H**$_3$ functionalisation strategies.*

1.7. Secondary Aim: The Application of Visible-Light Photoredox Catalysis Towards Sustainable Pharmaceutical Manufacture

Visible-light-mediated photocatalysis has evolved into a defined research field with a phenomenal increase in both the number and diversity of reported transformations.[138] Notwithstanding its prevalence in academia, the technology is rapidly gaining interest within the pharmaceutical industry with numerous efforts demonstrating the applicability of photocatalysis within a pharmaceutical setting. One reason for this could be that photocatalysis has been demonstrated as an efficient strategy for the synthesis and functionalisation of biologically relevant heterocycles[119,139,140] and for the late-stage functionalisation of molecules in general. Rapid derivatisation is of high importance to early stage discovery chemistry, where time is the key focus in synthetic routes. In the late-stage development of medicines, industry shifts its focus to efficiency, sustainability and scalability of synthetic routes.[119] It is well known that photochemistry is difficult to translate into large-scale batch processes, which is due to the large path lengths involved.[84] Photocatalyst (or in the case of UV photochemistry, substrate) absorption decays rapidly with increasing distance from the light source according to the Beer-Lambert law: $A = \epsilon c l$, where A is the absorption, c is the molar concentration and l is the path length. The absorption A is expressed as a logarithmic function of the ratio of transmitted light (I) to incident light (I_0) in equation 4.

$$A = -\log_{10} \frac{I}{I_0} \quad (4)$$

Assuming a modest 50.0 mM concentration for a typical reaction[84] and catalyst loading of 1 mol%, the catalyst concentration would be 0.5 mM. For A = 1 (i.e. 90% of the light is absorbed, I = 0.1 I_0) and an extinction coefficient (ε) of 11 280 M^{-1} cm^{-1} (as is the case for the 452 nm absorption band of $Ru(bpy)_3Cl_2$ in the visible-light region),[86] the path length required will

be around 0.2 cm. Effectively a thin film (2 mm) of reaction mixture closest to the light source absorbs 90% of the light and shields the bulk of the mixture. One can appreciate how difficult it would be to drive this reaction to completion in a 500 L batch reactor. Furthermore, the scales of batch photochemical processes are constrained by their reactor size, resulting in a large capital cost associated with construction of industrial-scale reactors.[74]

An alternative manifold for running large-scale photochemical reactions is flow chemistry. Flow reactors are typically thinner and benefit from large surface area-to-volume ratios than batch reactors. Thus, in the context of photochemistry, flow reactors have shorter path lengths for light transmission. Indeed, scalability of visible-light photochemisty has been demonstrated in flow.[78,80,92,115,116,141–143] One industrial process (Sanofi-Aventis) produces a third of the world's supply of Artemisinin (60 tons in 2014, 370 kg batches isolated).[144] Flow processes can be scaled by increasing flow rate, which does not necessarily correspond with an increase in reactor size. GSK have identified flow chemistry as a valuable future manufacturing technology and initiatives are currently underway applying it to synthetic routes where beneficial.

In a similar way, the second aim of this research project is to demonstrate the power of and help to embed visible-light photoredox catalysis technology within GSK, towards sustainable pharmaceutical manufacture. In-house capability will be established, reaction diagnostics will be developed and scalability will be demonstrated where appropriate. In order to address both primary and secondary aims, the well-established photoredox chemistry of *N*-substituted THIQs was chosen to provide a starting platform on which to base initial investigations, prior to exploring the *N*-functionalisation of trialkylamines. In the Results and Discussion, efforts to realise these two aims are reported and results are discussed.

2. Results and Discussion

Volume 1 reports and discusses efforts toward site-selective oxidative *N*-functionalisation of tertiary amines. In Chapter 2.1., the *N*-C**H**$_2$ functionalisation of *N*-substituted THIQs *via* Ru-based photoredox catalysis is explored. Attempts at *N*-functionalisation of trialkylamines under photoredox catalysis are disclosed and relevant electrochemical and luminescence quenching data are discussed in Chapter 2.2. Finally, a novel, non-photochemical approach to trialkylamine *N*-C**H**$_3$ functionalisation is discovered and discussed in Chapter 2.3.

2.1. Regioselective *N*-Functionalisation of *N*-Substituted Tetrahydroisoquinolines using Photoredox Catalysis

2.1.1. Photochemical Reactor Design and Validation

At the start of this project, the lack of experience and equipment in visible-light photochemistry at GSK Stevenage directed attention to the well-established chemistry of *N*-substituted THIQs, which was chosen as a model in order to design appropriate photoreactors. Firstly, *N*-functionalisation of *N*-phenyl-1,2,3,4-tetrahydroisoquinoline (**23**) was explored.[98,96] Stephenson's conditions[96] were employed with $[Ru(bpy)_3]^{2+}$ [E^p_{ox} ($*Ru^{II}/Ru^{I}$) = +0.83 V *vs.* SCE], $BrCCl_3$ [E^p_{red} ($BrCCl_3/BrCCl_3^{\bullet-}$) = -1.36 V *vs.* SCE] and a 30 W white LED floodlamp [λ_{max} = 449 nm, matching the visible absorption band of photocatalyst $[Ru(bpy)_3]^{2+}$ (λ_{max} = 452 nm)] for a single batch reaction setup (Figure 7, left). Iminium salt **26** was successfully generated in batch after 1 h and trapped with a nitronate to give nitro-Mannich product **27** in good yield (72%) (Scheme 48). However, the white LED floodlamp was deemed impractical for carrying out multiple or parallel reactions, due to non-uniform

distribution of light when reaction vessels were placed together. A more appropriate setup consisted of a 24 W blue LED strip (λ_{max} = 458 nm) combined with a Radley's carousel to fashion a parallel reactor (Figure 7, middle). In the $[Ru(bpy)_3]^{2+}$-photocatalysed oxidation of **23**, the blue LED strip in a parallel reaction setup was found to perform similarly to the LED floodlamp in single reaction setup (Figure 7, left), as evidenced below (Table 1, entries 1-2). A flow reactor (Vapourtec UV-150 R-series 10 mL coil) fitted with a 60 W blue LED flow bank (λ_{max} = 449 nm) was explored (Figure 7, right). At a flow rate of 10 mL/min (1 min residence time), full conversion was observed under the same conditions (Table 1, entry 3). Scalability in flow is discussed subsequently (see Section 2.1.6). Transmission spectra of light sources are given in the Appendix.

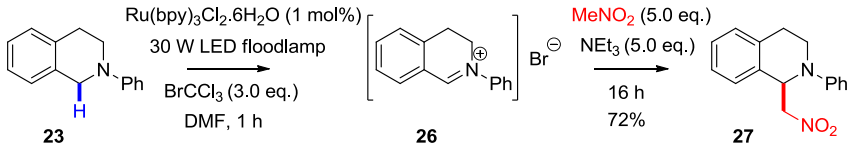

Scheme 48: *Visible-light photocatalysed N-functionalisation and nitro-Mannich trapping of N-phenyl THIQ.*

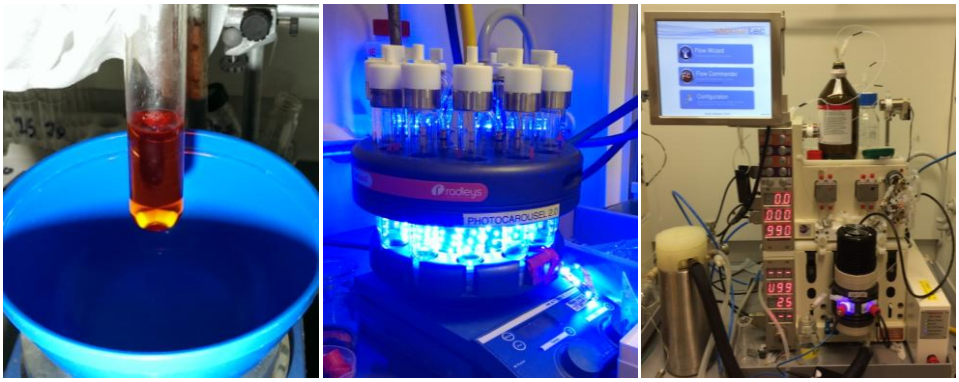

Figure 7*: Left: Single batch reactor irradiated with a white LED floodlamp from a distance of ca. 10 cm. Middle: Parallel batch reactor irradiating with a blue LED strip from a distance of ca. 5 cm. Right: Flow reactor irradiating the coil with a blue LED flow bank from a distance of 2.5 cm.*

Table 1: *Survey of photochemical reactors, solvent systems and oxidants.*

Entry	Light source	Catalyst[a]	Solvent	Time	Conversion[b]
1	LED floodlamp	$Ru(bpy)_3Cl_2$	DMF	< 5 min	60:40[c,d]
				1 h[e]	100:0
2	LED strip	$Ru(bpy)_3Cl_2$	DMF	< 5 min	70:30[c,f]
				1 h[e]	100:0
3	LED flow bank	$Ru(bpy)_3Cl_2$	DMF	2 min[e]	100:0[g,h]
4	LED strip	$Ru(bpy)_3Cl_2$	MeCN/ H_2O[i]	< 5 min	45:55[c,f]
				2 h[e]	100:0
5	LED strip	$Ru(bpy)_3Cl_2$	DMF	2 h	ND[j,f,k]
6	LED strip	$Ru(bpy)_3Cl_2$	MeCN/ H_2O[i]	2 h	10:90[l,f]
				16 h	25:75
7	LED strip	$Ru(bpy)_3(PF_6)_2$	MeCN (dry)	2 h	70:30[c,f]
				16 h[e]	100:0
8	LED strip	$Ru(bpy)_3Cl_2$	MeCN (dry)	2 h	ND[f,m,n]
9	LED strip	$Ru(bpy)_3Cl_2$	MeCN (dry)	2 h	80:20[f,o]
				3 h[e]	80:20
10	LED strip	$Ru(bpy)_3(PF_6)_2$	MeCN (dry)	2 h	80:20[f,p]
				3 h[e]	80:20

[a]catalyst loading is 1 mol%, $Ru(bpy)_3Cl_2$ refers to its hexahydrate salt. [b]Ratio of **26** : **23** by HPLC peak area (220 nm) at the time specified (corrected for relative absorbances of **26** and

23 at 220 nm, see Appendix). [c]$BrCCl_3$ (3.0 eq.) used as oxidant. [d]Single reaction setup (reaction degassed by freeze/pump/thaw). [e]time at which reaction was deemed complete (for the flow reactor, this is t_R). [f]Parallel reaction setup (reactions were degassed by freeze/pump/thaw). [g]Flow reaction setup using 10 mL/min flow rate (reactions were degassed by N_2 sparging for 20 min). [h]Catalyst loading is 0.05 mol%. [i]Ratio = 4 : 1. [j]reaction was left open to air. [k]A complex mixture of products was observed. [l]oxidant is TEMPO (2.0 eq.). [m]oxidant is $ClCH_2CN$ (3.0 eq.). [n]No reaction was observed. [o]oxidant is $BrCH_2CN$ (3.0 eq.). [p]oxidant is $BrCH_2CN$ (2.0 eq.). ND = not determined.

Reactions in MeCN:H_2O (4 : 1) achieved full conversion after 2 h (Table 1, entry 4), which was a more practical solvent system than DMF, in terms of its removal. When the reaction was conducted under air instead of using $BrCCl_3$ (Table 1, entry 5), a complex mixture of products was observed after 2 h. Using TEMPO (2.0 eq.) in place of $BrCCl_3$ gave sluggish conversion (Table 1, entry 6). Reactions slowed significantly when using anhydrous MeCN solvent, presumably due to the poor solubility of $Ru(bpy)_3Cl_2$ observed. Even when the more soluble $Ru(bpy)_3(PF_6)_2$ was employed (Table 1, entry 7), reactions took 16 h to complete (consistent with observations made by Stephenson and Jacobsen).[114] Interestingly, although no reaction occurred using $ClCH_2CN$ (E^p_{red} = -2.17 V *vs.* SCE) as an oxidant (Table 1, entry 8), high conversion (80%) was observed when $BrCH_2CN$ (E^p_{red} = -1.86 V *vs.* SCE) was employed as an oxidant (Table 1, entries 9 and 10),[145] which was surprising as it falls out of range of the redox potential of $[Ru(bpy)_3]^+$ [E^p_{red} (Ru^{II}/Ru^I) = -1.39 V *vs.* SCE].[75]

2.1.2. Organometallic Trapping of Photogenerated Iminium Salt Intermediates

Whilst nucleophilic trappings of iminium salts such as **26** with highly stabilised carbon nucleophiles are well represented in the literature, reports of organometallic additions in this context are limited to aryl[47,49,146] and alkynyl[48,90,96,134] nucleophiles and substrate scope is generally limited to *N*-aryl THIQs. However, Li reported a stoichiometric hypervalent iodine-mediated *N*-aryl THIQ oxidation which tolerated a wide range of

organometallic nucleophiles[44] and Yu developed methodology for THIQ alkynylation which does not require *N*-aryl motifs (starting from the secondary amine).[147]

Yet, there seemed to be no general procedure for organometallic trapping of iminium salts generated by oxidative functionalisation (a methodology amenable to a range of tertiary amine substrates and unstabilised carbon nucleophiles). An important feature of photoredox catalysis is that different photocatalysts have different redox potentials upon accessing the excited state.[57,75,76,148] Therefore, it was envisaged that more oxidising photoredox catalysts might be appropriate for exploring trialkylamines, particularly substrates resembling opioids. Use of $Ru(bpy)_3(PF_6)_2$ in the photocatalytic step (instead of $Ru(bpy)_3Cl_2$) circumvented the requirement for water in the solvent,[114] which was thought to promote reaction compatibility with reactive organometallic reagents. Using $Ru(bpy)_3(PF_6)_2$ catalyst and $BrCCl_3$ oxidant in anhydrous MeCN under the parallel reaction setup (Table 1, entry 7), full conversion of **23** to **26** was attained after 16 h. However, a complex mixture of products was observed as soon as vinylmagnesium bromide was added. Generation of radical intermediates or carbenes upon reacting Grignard reagents or magnesium turnings with $BrCCl_3$ or $CHCl_3$ are evidenced in the literature.[149,150]

Initially, the volatilities of $BrCCl_3$ and $CHCl_3$ were taken advantage of by removing them under vacuum and replacing the solvent. A solvent switch was similarly required by Jacobsen and Stephenson in their optimal conditions;[114] after photoactivation of **24** the MeCN solvent was switched to TBME for a thiourea-catalysed enantioselective alkylation step. With the requirement for a solvent switch, MeCN : H_2O (4 : 1) and $Ru(bpy)_3Cl_2$ were employed in photoactivations to facilitate full conversion of **23** to **26** in 2 h. Since MeCN forms an azeotrope with water, switching solvent was easily achieved by concentration under vacuum. After dissolving crude **26** in anhydrous MeCN and shielding from ambient light, alkyl, aryl and vinyl

Grignard reagents added rapidly (< 5 min) to **26**, affording products in good to excellent (62 - 90%) yields (Table 2).[57] Grignard reagents were chosen due to high reactivity, commercial availability and operational simplicity (as solutions in THF, 2-MeTHF or Et_2O). The enhanced electrophilicity of **26** *vs*. MeCN results in faster reaction of the Grignard reagent with **26** despite the solvent (MeCN) being present in vast excess.

Table 2: *Addition of a variety of organometallic reagents to photogenerated iminium salts.*

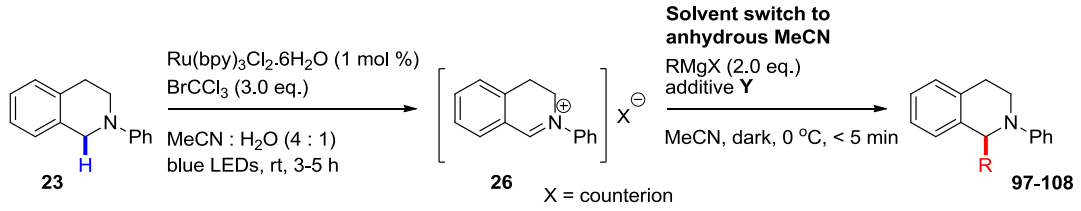

Entry	R-Metal	Additive Y	R[a]	Yield[b]
1	RMgBr[c]	-	vinyl (**97**)	80
2	RMgBr[c]	-	Me (**98**)	78
3	RMgCl[c]	-	Et (**99**)	75
4	RMgCl[c]	-	*i*Pr (**100**)	78
5	RMgBr[c]	-	cyclopropyl (**101**)	66
6	RMgBr[c,d]	-	Bn (**102**)	69
7	RMgBr[c]	-	Ph (**103**)	90
8	RMgBr[c]	CuBr[e]	Ph (**103**)	77
9	RMgBr[c]	-	4-FC_6H_4 (**104**)	72
10	RMgBr[c]	-	4-$MeOC_6H_4$ (**105**)	62

Entry	R-Metal	Additive Y	R[a]	Yield[b]
11	RMgBr[c]	-	allyl (**106**)	ND[f]
12	RTMS	-	allyl (**106**)	ND[g]
13	RMgBr[c]	$ZnCl_2$[h]	allyl (**106**)	37, 88[i]
14	RI	In[j]	allyl (**106**)	92, 68[k]
15	RMgBr[c]	-	2-methylallyl (**107**)	ND[f]
16	RMgBr[c]	$ZnCl_2$[h]	2-methylallyl (**107**)	90
17	RMgCl[c]	$ZnCl_2$[h]	2-butenyl (**108**)	92[l]

[a]Product numbers in parenthesis. [b]Isolated (%) yields after chromatography. [c]Commercially available solutions in THF, 2-MeTHF or Et_2O. [d]6.0 eq. used. [e]Grignard (2.0 eq.) premixed with CuBr (2.6 eq.). [f]A complex mixture of products was observed. [g]No reaction was observed. [h]Grignard (2.0 eq.) premixed with a solution of $ZnCl_2$ (2.6 eq.). [i]Solvent switched to THF before the addition of the organometallic reagent. [j]allyl iodide (3.0 eq.) premixed with In powder (2.0 eq.). [k]Direct addition of the allylindium reagent without a solvent switch. [l]Product is a 1 : 1 mixture of diastereomers where R = 1-methyl-2-propenyl. ND = not determined.

Notably, allyl and 2-methylallyl Grignard additions (Table 2, entries 11 and 15) were exceptions and resulted in complex mixtures of products. We reasoned that use of a less reactive organometallic would suppress undesirable pathways. However, allyltrimethylsilane did not react with **26**, consistent with literature observations (Table 2, entry 12).[96,136] As organometallics of intermediate reactivity, allylzinc halides were explored. Pleasingly, 2-methylallylzinc and 2-butenylzinc reagents added to **26** to afford their products in 90% and 92% isolated yields, respectively (Table 2, entries 16 and 17). Conversely, addition of the allylzinc reagent to **26** afforded by-products as well as the desired product (Table 2, entry 13).[57] To temper reactivity even further, an allylindium reagent[151] was employed. Allylindium reagents have attracted attention for their tolerance to water[152] and have

mediated reactions where allyl Grignards and allylzinc reagents have failed.[153] Gratifyingly, the allylindium reagent did not afford the by-products seen with the allylzinc reagent, instead affording desired product **106** in 92% isolated yield (Table 2, entry 14). Strikingly, the same reagent was added without a solvent switch and tolerated $BrCCl_3$, $CHCl_3$ and H_2O, affording the product albeit in lower yield (68%).

2.1.3. Substrate Scope and Application in the Synthesis of Methopholine

Regarding substrate scope, iminium salts derived from a range of electronically diverse *N*-aryl substituted THIQs (**109**-**113**) were trapped with PhMgBr to afford products (**117**-**121**) in fair to excellent (47-95%) yields (Table 3, entries 2-6). Although $Ru(bpy)_3Cl_2$ was ineffective at oxidising *N*-Boc protected THIQ **116** (Table 3, entry 9), subjecting *N*-alkyl THIQs **114** and **115** to the reaction conditions for 16 h furnished in both cases their corresponding benzylic *endo*-iminium salts, which were trapped by PhMgBr to afford products **122** and **123** in 58% and 81% yield, respectively (Table 3, entries 7 and 8). Prior to this work, photocatalytic oxidation of *N*-methyl THIQs by $[Ru(bpy)_3]^{2+}$ had only been reported once in the literature.[48]

***Table 3**: Substrate scope of organometallic additions to iminium salts generated via visible-light photoredox catalysis.*

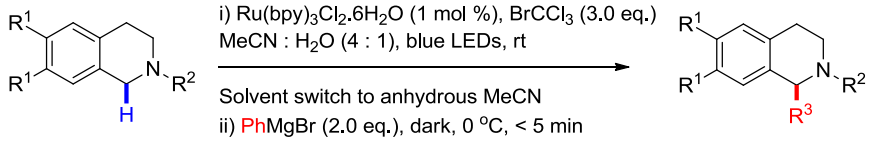

Entry	R^1/R^2 [a]	Yield[b,c]
1	H/Ph (**23**)	90 (**103**)[d,e]
2	H/2-naphthyl (**109**)	47 (**117**)[f]
3	OMe/Ph (**110**)	95 (**118**)[e]

Entry	R^1/R^2 [a]	Yield[b,c]
4	H/4-$MeOC_6H_4$ (**111**)	52 (**119**)[e]
5	H/4-BrC_6H_4 (**112**)	53 (**120**)[e]
6	H/4-$NO_2C_6H_4$ (**113**)	77 (**121**)[e]
7	H/Me (**114**)	58 (**122**)[g]
8	OMe/Me (**115**)	81 (**123**)[g]
9	H/CO_2tBu (**116**)	ND[h]

[a]Starting material numbers in parenthesis. [b]Isolated (%) yields after chromatography. [c]Product numbers in parenthesis. [d]Entry 7, Table 1 given for comparison. [e]Photoactivation time of 2 h. [f]Photoactivation time of 4 h. [g]Photoactivation time of 16 h. [h]No photoactivation reaction observed. ND = not determined.

Previous syntheses of methopholine from **115** have involved (4-chloro)phenylacetylene as a pronucleophile.[42,154] However, isolation and hydrogenation of the resulting THIQ intermediate are required to access methopholine. Photoactivation of **115** and trapping the resultant benzylic *endo*-iminium salt with Grignard **124** resulted in a 56% yield of methopholine (Scheme 49). This concise synthesis is higher yielding than previously reported syntheses (based on **115** as a starting material)[42,154,155] with no intermediate isolations required.[57]

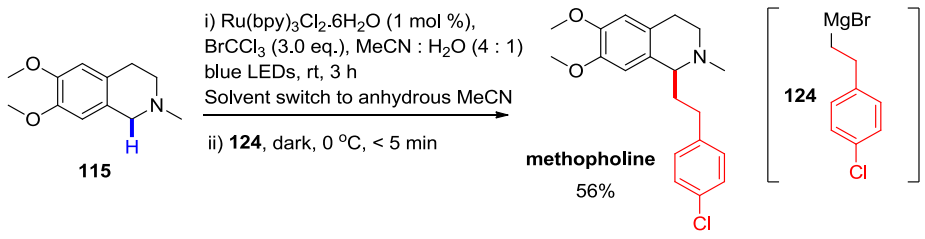

***Scheme 49**: A concise synthesis of methopholine.*

2.1.4. ONE-POT PHOTOOXIDATION AND DIRECT ORGANOMETALLIC ADDITIONS

Revisiting the concept of direct organometallic addition after photoactivation (thus far precluded by the use of $BrCCl_3$), compatibility might be accomplished in two ways. Firstly, moderate the reactivity of the organometallic to tolerate $BrCCl_3$ or secondly, find alternative oxidants which tolerate the organometallic. Whilst the former looked promising with the allylindium example, the latter approach was thought to be more general in terms of increasing nucleophile scope. Stephenson reported diethyl bromomalonate as an effective oxidant to regenerate $[Ru(bpy)_3]^{2+}$, but general application of this alkyl halide oxidant was ruled out due to potential side-reactions of the malonyl radical and diethyl malonate.[96] The use of alternative alkyl halide oxidants that would form inert by-products was envisaged.

Promising conversion with $BrCH_2CN$ resulted in its selection as an alkyl halide oxidant because (according to the mechanism proposed by Stephenson)[96] it would form MeCN as an 'inert' product (Scheme 50). Grignard additions were unaffected by traces of residual $BrCH_2CN$ and a selection of substrates (**23**, **110**-**112**) and Grignard reagents were employed, affording the products (**97**-**98**, **103**, **118**-**120**) in encouraging (50 - 77%) yields (Table 4). Recently, this use of unstabilised carbon nucleophiles (organometallics) to intercept iminium salts in a one-pot reaction was disclosed and it was demonstrated that *N*-alkyl THIQ substrates could undergo photoactivation.[57]

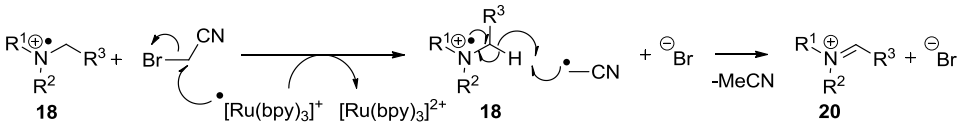

Scheme 50: *Inert by-product MeCN formed by $BrCH_2CN$ during the photoredox cycle.*

Table 4: *Direct one-pot organometallic additions to photogenerated iminium salts.*

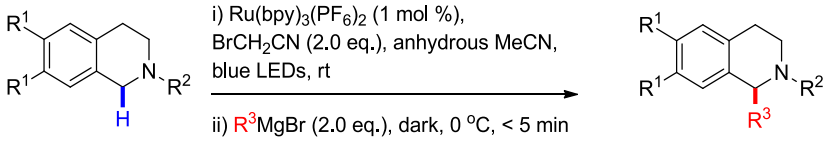

Entry	$R^1/R^2/R^3$ [a]	Yield[b,c]
1	H/Ph/vinyl (**23**)	77 (**97**)[d]
2	H/Ph/Me (**23**)	73 (**98**)[d]
3	H/Ph/Ph (**23**)	61 (**103**)[d]
4	OMe/Ph/Ph (**110**)	72 (**118**)[d]
5	H/4-MeOC$_6$H$_4$/Ph (**111**)	73 (**119**)[d]
6	H/4-BrC$_6$H$_4$/Ph (**112**)	50 (**120**)[e,f]

[a]Starting material numbers in parenthesis. [b]Isolated (%) yields after chromatography. [c]Product numbers in parenthesis. [d]Photoactivation time of 3 h. [e]Photoactivation time of 5 h. [f]Heating required to solubilise substrate.

However, the one-pot method using $BrCH_2CN$ appears to be limited to *N*-aryl THIQs since $BrCH_2CN$ acted as a very efficient alkylating agent of *N*-methyl THIQ **115** (Scheme 51) to give **125**. The more hindered oxidant 2-bromopropionitrile similarly led to alkylation of **115** to give **126**. It was clear that an alternate, more general oxidation methodology was required for trialkylamines.

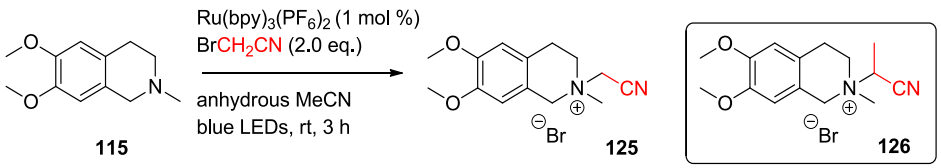

Scheme 51*: Alkylation of N-alkyl THIQs in the presence of bromoacetonitrile.*

2.1.5. MECHANISTIC STUDIES ON THE PHOTOGENERATION OF IMINIUM SALTS

Mechanistic studies on the visible-light photoredox iminium formation step were initially not deemed necessary due to the general acceptance of Stephenson's proposed mechanisms for reactions involving O_2 or $BrCCl_3$ as terminal oxidants.[96,98] Detailed investigations of the mechanism were later reported,[35,58] which prompted further studies on $BrCH_2CN$ to be carried out (control reactions) as part of this project.

A control reaction in the dark ruled out any background, non-photochemical oxidation (or alkylation) of **23** by $BrCH_2CN$ (Table 5, entry 1). Interestingly, in the presence of light but *without any photoredox catalyst*, the $BrCH_2CN$ reaction proceeded with identical conversion to the standard reaction conditions where $Ru(bpy)_3(PF_6)_2$ was present (Table 5, entries 2-3). The iminium salt intermediate was observed in 79% yield, and addition of PhMgBr gave the *N*-C**H**$_2$ functionalised product **103** in 60% yield. This result parallels the result in Table 4, entry 3 (the one-pot conditions where $Ru(bpy)_3(PF_6)_2$ was present), where addition of PhMgBr gave the *N*-C**H**$_2$ functionalised product **103** in 61% yield. It is thus very likely that the iminium salt (**26**) formed with the same chemical efficiency (79%) under the standard conditions, consistent with the limited product yields of 50 - 77% in the one-pot process (Table 4).

When *N*-methyl THIQ substrate **114** was treated under Zeitler's photocatalyst-free conditions with $BrCCl_3$, full conversion to the corresponding iminium salt **127** (detected in 89% yield) was observed after 16 h, consistent with that reported by Zeitler (Table 5, entry 4). This is comparable to the reaction where $Ru(bpy)_3(PF_6)_2$ was present (Table 3, entry 7), which similarly gave full conversion of **114** after 16 h (trapping with PhMgBr afforded a 58% yield of **122,** see Table 5, entry 5). That the reaction does not require the photoredox catalyst but does require light corroborates an **EDA** complex between *N*-phenyl THIQ and $BrCH_2CN$ as the visible-light active species (complex **128**, Scheme 52). Photoexcitation of the **EDA**

complex (**128**), SET and deprotonation of *N*-phenyl THIQ radical cation **24** could serve as the initiation of a radical chain propagation mechanism involving $BrCH_2CN$ (Scheme 52) which mirrors that proposed by Zietler for $BrCCl_3$ (Scheme 38, Section 1.5.4.).[58] Initiation by homolysis of $BrCH_2CN$ and propagation by atom-transfer radical addition is another plausible mechanism[58] (the acetonitrile radical could undergo HAT[77] with **24**, but this would not be a chain mechanism; or this pathway could serve as a termination step).

***Table 5**: Control reactions in the absence of light and photocatalyst.*

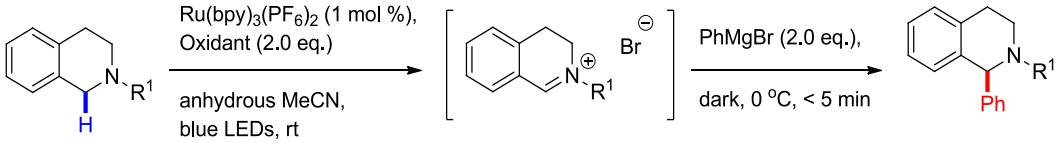

23, R^1 = Ph
114, R^1 = Me

26, R^1 = Ph
127, R^1 = Me

103, R^1 = Ph
122, R^1 = Me

Entry	Oxidant	Catalyst[a]	R^1	Time[b]	Conversion
1	$BrCH_2CN$	-	Ph	2 h	ND[c,d]
2	$BrCH_2CN$	-	Ph	2 h	80:20[d,e] (79%[f], 60%[g])
3	$BrCH_2CN$	$Ru(bpy)_3(PF_6)_2$	Ph	2 h	80:20[d]
4	$BrCCl_3$[h]	-	Me	16 h	100:0[e,i] (89%[j])
5	$BrCCl_3$[h]	$Ru(bpy)_3Cl_2.6H_2O$	Me	16 h	100:0[i,k] (58%[g])

The parallel reaction setup was used (reactions were degassed by freeze/pump/thaw). [a]Catalyst loading (if added) is 1 mol%. [b]time at which reaction was deemed complete. [c]Reaction conducted in the dark, no reaction was observed. [d]Ratio of **26** : **23** by HPLC peak area (220 nm) at the time specified (corrected for relative absorbances of **26** and **23** at 200 nm). [e]No photocatalyst added. [f]Yield of **26** determined by ^{1}H NMR. [g]Isolated yield of trapped product, **103** or **122**, after PhMgBr (2.0 eq.) was added. [h]3 eq. of $BrCCl_3$ used. [i]Ratio of **127** : **114** by HPLC (220 nm) at the time specified. [j]Yield of **26** determined by ^{1}H NMR. [k]Reaction from Table 3, entry 7 shown for comparison. ND = not determined.

Mechanistic experiments employed by Zeitler in the invesigation of reactions involving $BrCCl_3$ could equally investigate reactions involving $BrCH_2CN$ (see Chapter 4.1). Although use of $BrCH_2CN$ does permit the one-pot photogeneration of iminium salts/addition of organometallic nucleophiles, it presents drawbacks in applications (formation of iminium salts in limited efficiency, alkylation of *N*-alkyl THIQs) compared to $BrCCl_3$ and no clear advantages in terms of cost, safety or efficiency. A full mechanistic investigation was deemed inappropriate and instead efforts were directed at investigating scalability of visible-light photochemistry in flow and at enabling *N*-functionalisation reactions of trialkylamines.

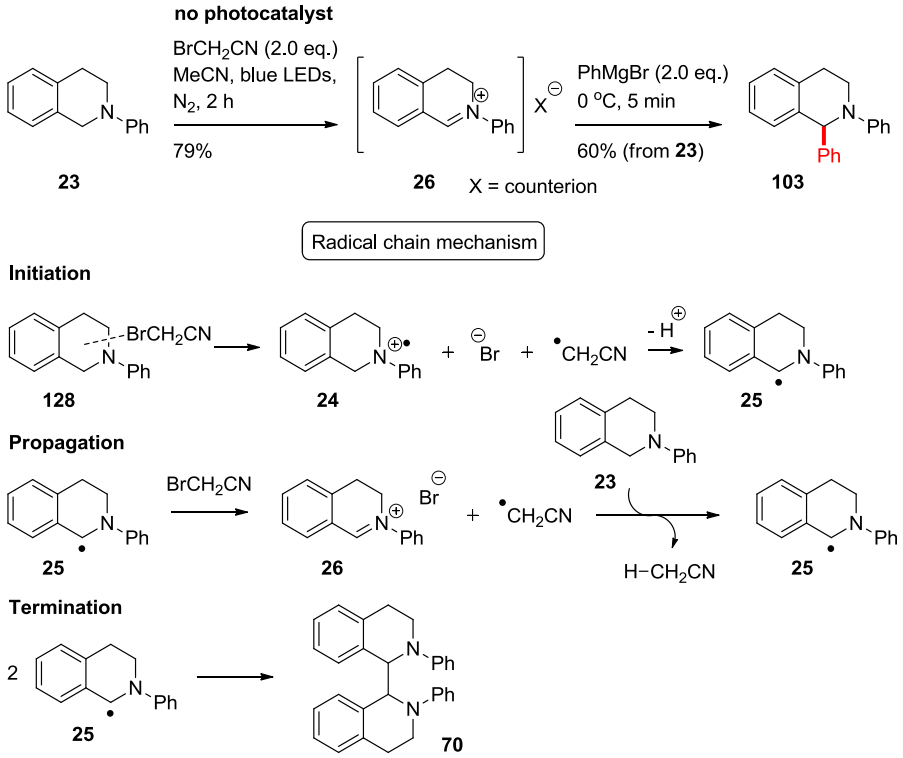

***Scheme 52**: Photoredox catalyst-free radical chain anaerobic iminium salt formation mechanism for $BrCH_2CN$ oxidant.*

2.1.6. Scalability of Visible-Light Photochemistry in Flow

For purposes of evaluating scalability of iminium salt formation *via* visible-light photoredox catalysis in flow, $BrCCl_3$ was selected as oxidant in iminium

salt photogeneration reactions. Initial flow conditions aimed to mimic those reported by Stephenson (t_R = 0.5 min).[115] The maximum flow rate available using the Vapourtec UV-150 (a 10 mL PTFE coil) was 16 mL/min (t_R = 0.6 min), which fell short of full conversion (Table 6, entry 1).

***Table 6**: Investigation of flow rate on conversion in the photogeneration of iminium salts.*

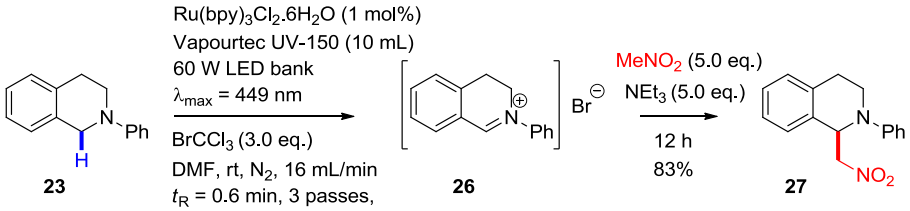

Entry	Catalyst Loading (mol %)	Flow rate[a] (mL/min)	t_R (min)	Conversion[b]
1	0.5	16.0	0.6	70 : 30
2	0.5	16.0	0.6 (x2)	80 : 20[c]
3	0.5	16.0	0.6 (x3)	100 : 0 (83%)[d,e]
4	0.05	16.0	0.6	80 : 20
5	0.05	14.0	0.7	90 : 10
6	0.05	10.0	1.0	100 : 0
7	0.05	4.0	2.5	100 : 0
8	0.05	2.0	5.0	100 : 0
9	0.05	1.0	10.0	100 : 0
10	0.05 (no $BrCCl_3$)	4.0	2.5	5 : 95[f]
11	0.05 ($BrCCl_3$)	4.0	2.5	5 : 95[f]

Entry	Catalyst Loading (mol %)	Flow rate[a] (mL/min)	t_R (min)	Conversion[b]
12	-	14.0	0.7	80 : 20 (70%)[g,h]

Reactions were degassed by N_2 sparging for 20 min. Unless otherwise stated, conversions were measured after a single pass (1 residence time, t_R) through the coil upon reaching steady state. [a]Pump flow rates were confirmed by solvent collection prior to experiments. [b]Ratio of **26** : **23** by HPLC peak area (220 nm) after a single pass (corrected for relative absorbances of **26** and **23** at 220 nm). [c]Conversion recorded after two passes. [d]Conversion recorded after three passes. [e]Following the completion of the photoactivation step, addition of nitromethane (5.0 eq.) and Et_3N (5.0 eq.) in the dark gave an isolated yield of nitro-Mannich product **27** shown in parenthesis. [f]Reaction conducted in the dark. [g]No photocatalyst added. [h]Yield of iminium salt **26**, determined by ^{1}H NMR, shown in parenthesis.

After 3 passes at 16 mL/min, full conversion to **26** by HPLC was observed and an 83% yield of nitro-Mannich product resulted (thus inferring that the minimum yield of iminium salt must be 83%). Interestingly, the catalyst loading could be lowered to 0.05 mol% with minimal effect on conversion (Table 6, entry 4). Increasing residence time by decreasing flow rate identified 10 mL/min as the threshold flow rate for full conversion (Faster flow rates start to reveal traces of starting material, slower flow rates give full conversion but lower productivity of material). Control reactions demonstrated no reaction of *N*-phenyl THIQ (**23**) with $BrCCl_3$ in the dark (after 12 h), and a flow reaction in the absence of $[Ru(bpy)_3]^{2+}$ at 14 mL/min gave high conversion and a 70% yield of **26** (Table 6, entry 12), fully according with Zeitler's observation[58] and consistent with observations in $BrCH_2CN$-mediated photocatayst-free reactions. This explains why conversion was unaffected by lowering the catalyst loading (Table 6, entry 1 *vs*. entry 4).

For the photocatalyst-free example, which reached high conversion at 14 mL/min flow rate (Table 6, entry 12), the calculated quantum yield (Φ = 0.8) indicated an unusually high quantum efficiency of this system (for determination of quantum yields, see Appendix). A radical chain mechanism

cannot be conclusively identified on the basis of this quantum yield which is below unity ($\Phi > 1.0$ is unequivocal evidence of radical chain mechanisms),[118] although a combination of short chain lengths and efficient non-radiative relaxation pathways could still arrive at this quantum yield. Of more interest was the chemical efficiency of the iminium salt formation, which, under these photocatalyst-free conditions and operating at 14 mL/min (a 70% yield of iminium salt **26**) gave a productivity of 16.8 g/h (58.3 mmol/h), or 2.8 kilo/week. This is likely approaching the full capacity for the Vapourtec UV-150 in this chemical system (near-full conversion was observed even at 16 mL/min, the reactor's highest capable flow rate). Even higher productivities should be accessible through a combination of engineering controls and chemistry optimisation. However, such investigations were deemed beyond the scope of this project and the established conditions sufficed to demonstrate proof of concept; that visible-light photochemistry could be successfully scaled within GSK (aligned with the secondary aim of the project).

It is quite clear that *N*-substituted THIQs are privileged scaffolds which undergo facile oxidation, even in the absence of a photoredox catalyst *via* radical chain reactions (initiated by excitation of **EDA** complexes or homolysis). However, the reported reactions of trialkylamines under photoredox catalysis do require the photocatalyst to see conversion.[119,121,125]

2.1.7. Regioselective *N*-Functionalisation of Trialkylamines using Photoredox Catalysis

A generally accepted theme in the field of photoredox catalysis is that trialkylamines (for example Et_3N and DIPEA) participate in reductive quenching of $*[Ru(bpy)_3]^{2+}$.[75,77,80,97,102,105] Thereby, trialkylamines are oxidised to N-radical cations which can be used synthetically. Based on this precedent, one would expect successful photooxidation of dextromethorphan (**73**), which is a trialkylamine resembling an opioid scaffold.

Surprisingly, no reaction was observed even after 16 h (Scheme 53). Use of $BrCH_2CN$ as oxidant led to alkylation as observed for *N*-methyl THIQs (Scheme 53). In order to investigate the thermodynamics of **SET** between the excited state of a photoredox catalyst and substrate, redox potentials obtained from CV experiments can be compared.†

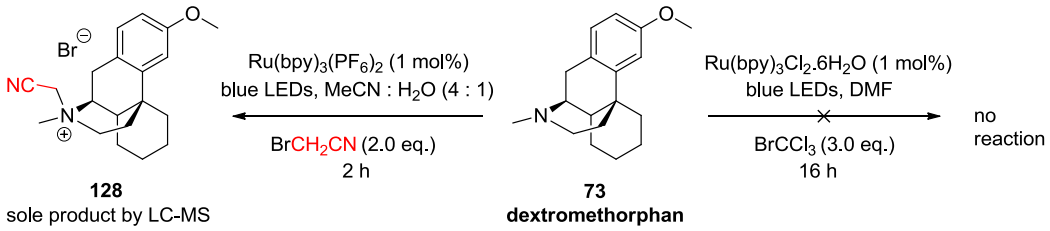

***Scheme 53**: No productive reaction of dextromethorphan under $[Ru(bpy)_3]^{2+}$ reductive quenching conditions.*

Comparison of $*[Ru(bpy)_3]^{2+}$ [E^p_{ox} ($*Ru^{II}/Ru^{I}$) = +0.83 V *vs.* SCE] and trialkylamines DIPEA [E^p_{ox} ($R_3N^{\bullet+}/R_3N$) = +0.85 V *vs.* SCE], dextromethorphan **73** [E^p_{ox} ($R_3N^{\bullet+}/R_3N$) = +0.90 V *vs.* SCE], triethylamine and *N*-methylmorpholine [E^p_{ox} ($R_3N^{\bullet+}/R_3N$) = +1.10 V *vs.* SCE for both] revealed a slight mismatch in redox potentials. Oxidation would be endergonic, but redox potentials were still close enough to expect electron transfer and thus reactivity in the lab. Furthermore, cyclic voltammograms of *N*-phenyl THIQ **23** and dextromethorphan **73** (compared to ferrocene as an external standard) both revealed irreversible one-electron oxidations, which is important if back electron transfer is an efficient pathway.

Notwithstanding the power of redox potentials in making thermodynamic predictions, the conditions under which CV is run are inevitably different to the reaction conditions, and redox potentials can vary.† Furthermore, redox potentials do not offer any insight into kinetic barriers.‡ To this end, attention

†How comparisons of redox potentials translate to themodynamic predictions, and a discussion around the factors which can affect redox potentials, see Appendix. ‡Although cyclic voltammetry cannot provide data on reaction kinetics, it can be used to obtain other useful kinetic data (diffusion coefficients) by variation of scan rates, see Appendix for details and examples.

was directed toward luminescence quenching experiments.[75] It was envisaged that luminescence data obtained from treating $*[Ru(bpy)_3]^{2+}$ with various tertiary amine quenchers could account for their variable reactivity in the lab.

2.2. Luminescence Quenching of Ru-based Photoredox Catalysts

Luminescence quenching experiments directly measure the interaction between the excited state of a photoredox catalyst and a substrate (quencher). Considering $[Ru(bpy)_3]^{2+}$ in the context of a simplified Jablonski diagram (Figure 8), it can be seen that $*[Ru(bpy)_3]^{2+}$ is deactivated by competing pathways; luminescence (phosphorescence), quenching and non-radiative pathways. Thus, if the rate of quenching (the quenching rate constant k_q) approaches or is greater than the rate of luminescence (the phosphorescence rate constant k_p), this manifests as a decrease in luminescence intensity (I) or excited state lifetime (τ), which are measurable quantities. Luminescence intensity (I) is measured by steady-state emission spectroscopy and the Stern-Volmer equation (equation 5) can be used to extract quenching rate constants (k_q),[156] see Appendix for derivations and details.

$$I^0/I = \tau^0/\tau = 1 + (k_q/k_0)[Q] = 1 + k_q\tau^0[Q] \quad (5)$$

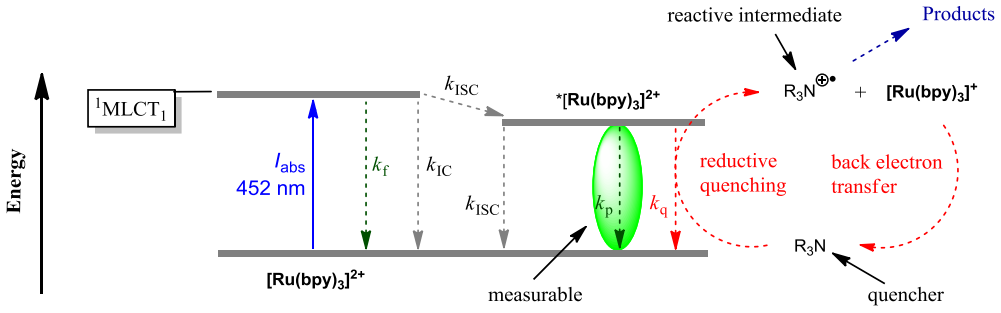

***Figure 8**: Simplified Jablonski diagram for $[Ru(bpy)_3]^{2+}$ showing competing luminescence and quenching pathways of $*[Ru(bpy)_3]^{2+}$.*

Alternatively, excited state lifetimes (τ) are directly measured by time-correlated single photon counting (TCSPC) or similar methods.[157] These techniques are complementary and can be used to extract information about

the kinetics and photophysics of quenching. Note that neither technique can decipher the photochemical nature of the quenching mechanism (electron transfer *vs*. energy transfer), nor do they provide insight into any subsequent downstream chemical pathways. The rate determining step of the chemical reaction may not involve *$[Ru(bpy)_3]^{2+}$. For example, initial electron transfer from R_3N to *$[Ru(bpy)_3]^{2+}$ yielding a change in luminescence indicates successful quenching, but could be followed by rapid back electron transfer[76] from $[Ru(bpy)_3]^{+}$ to $R_3N^{\bullet+}$ which is not detectable and may result in no chemical reaction in the laboratory despite observation of successful quenching. The key difference between luminescence quenching experiments and reaction conditions is the concentration of photocatalyst (luminescence quenching experiments are more dilute in photocatalyst, the consequences of this are discussed in the Appendix). Initial efforts treated *$[Ru(bpy)_3]^{2+}$ with different concentrations of *N*-phenyl THIQ **23** in order to detect differences in luminescence intensity (for Stern-Volmer analysis). Efforts were thwarted by a combination of two factors: i) low intensity associated with phosphorescence (a fundamentally 'forbidden' decay pathway) and ii) the substantial extent to which the *$[Ru(bpy)_3]^{2+}$ was quenched by O_2. Aerated samples containing different concentrations of $[Q]$ (*N*-phenyl THIQ - **23**) gave no difference in intensity for each $[Q]$ (Figure 9, left).

When samples were degassed by gently bubbling an inert gas (N_2 or Ar) into the sample at a constant gas flow rate and for a fixed time, differences in intensity for each $[Q]$ were resolved (Figure 9, right). A linear Stern-Volmer plot of (I_0/I)-1 *vs.* $[Q]$ was obtained for *$[Ru(bpy)_3]^{2+}$ using *N*-phenyl THIQ as a quencher (Figure 10, left). It was subsequently found that optimal degassing was observed with Ar rather than N_2 (see Appendix for optimisation of degassing methods). Saturating solutions of $[Ru(bpy)_3]^{2+}$ with Ar, air and pure O_2 gases allowed a Stern-Volmer plot to be obtained for oxygen as a quencher (Figure 10, right), which revealed a quenching rate constant *ca.* 50x greater than the quenching rate constant for *N*-phenyl THIQ

(**23**). The maximum quencher concentration employed in these Stern-Volmer quenching experiments was 7.5 mM. The concentration of dissolved oxygen in oxygen-saturated MeCN is 8.1 mM[158] which is almost a direct comparison. The concentration of dissolved oxygen in air-saturated MeCN is 1.7 mM.[159,160]

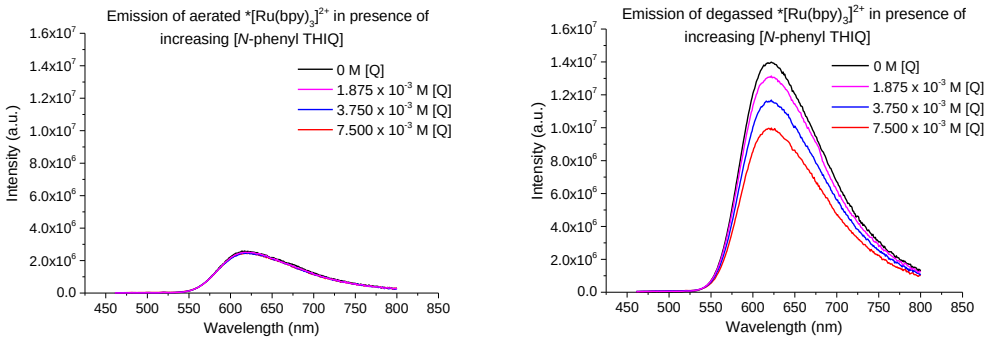

***Figure 9**: Left: Steady-state luminescence of aerated $[Ru(bpy)_3]^{2+}$ samples with increasing concentrations of N-phenyl THIQ (**23**). Right: Steady-state luminescence analysis of degassed $[Ru(bpy)_3]^{2+}$ samples with increasing concentrations of N-phenyl THIQ (**23**).*

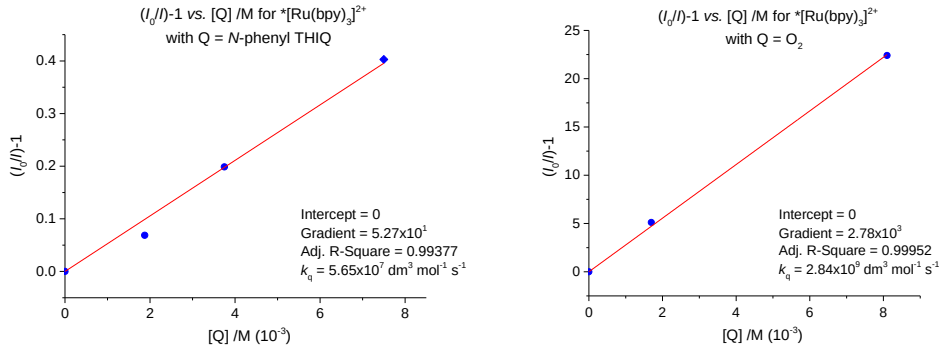

***Figure 10**: Left: Stern-Volmer plot for N-phenyl THIQ (**23**) as a quencher. Right: Stern-Volmer plot for oxygen as a quencher.*

Steady-state luminescence intensities and Stern-Volmer plots were obtained for key photocatalyst/quencher combinations to extract $\boldsymbol{k_q}$. Revisiting the photocatalytic oxidative functionalisation of *N*-phenyl THIQ (Scheme 48), the lifetime of $*[Ru(bpy)_3]^{2+}$ is significantly decreased in the presence of *N*-phenyl

THIQ (F = 13%) but not so by $BrCCl_3$ (F = 2%), nor $BrCH_2CN$ (F = 2%), nor $ClCH_2CN$ (F = 3%). In the first instance, this would imply that ***reductive quenching*** is the dominant reactive pathway. However, given that the reaction proceeded without $[Ru(bpy)_3]^{2+}$ in identical efficiency, it is most likely that the dominant mechanism does not involve $*[Ru(bpy)_3]^{2+}$ at all.

Table 7*: Lifetime of $*[Ru(bpy)_3]^{2+}$ in the presence of quenchers under N_2.*

Entry	τ (ns)[a]	F (%)[b]	Atmosphere	Quencher[c]	$E^p_{ox/red}$
1	933[d]	0	N_2	-	N/A
2	801[d]	13	N_2	*N*-phenyl THIQ (**23**), k_q = 5.65 x 10^7	+0.83
3	902[d]	3	N_2	$BrCCl_3$	-1.36
4	915[d]	2	N_2	$BrCH_2CN$	-1.86
5	909[d]	3	N_2	$ClCH_2CN$	-2.17
6	977[e]	0	Ar	-	N/A
7	237[f]	76	Air	-	-0.75 ($E_{1/2}$)[35]
8	112[f]	89	O_2	O_2, k_q = 2.84 x 10^9	-0.75 ($E_{1/2}$)[35]

[a]Lifetimes are calibrated to $*[Ru(bpy)_3]^{2+}$ as an external standard, run before and after a set of samples to ensure consistency. For comparisons to literature lifetimes of $*[Ru(bpy)_3]^{2+}$ under N_2 or Ar (τ^0), see Appendix. [b]The quenching fraction $F(\%) = ((\tau^0 - \tau)/\tau^0) \times 100$, under the same inert gas for both measurements. [c]Where applicable, Stern-Volmer plots were obtained and k_q is given in units of M^{-1} s^{-1}. [d]Average of nine measurements. [e]Average of six measurements. [f]Average of two measurements. N/A = not applicable.

2.2.1. On the Interactions of Ru-based Photoredox Catalysts with Trialkylamines

A core principle in the photoredox catalysis field is the notion that *$[Ru(bpy)_3]^{2+}$ is reductively quenched by trialkylamines (triethylamine, DIPEA) and this mechanism is depicted in many publications[102,105] and review articles.[75,77,80,97] The trialkylamine is generally present in excess, allegedly serving as a sacrificial reductant of *$[Ru(bpy)_3]^{2+}$ to generate $[Ru(bpy)_3]^{+}$, which in turn acts as a reductant to the substrate of interest (Figure 11).

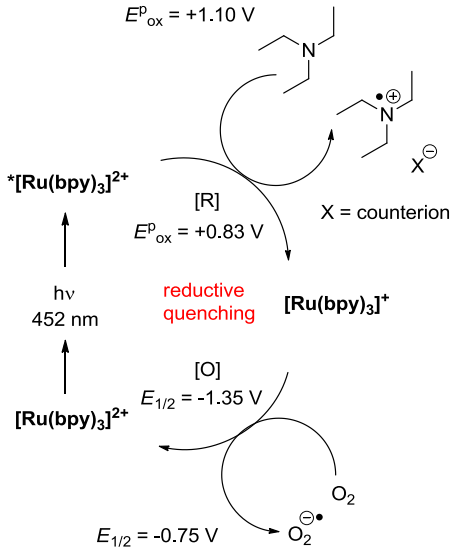

***Figure 11**: Generally accepted reductive quenching of *$[Ru(bpy)_3]^{2+}$ by trialkylamines.*

Given the oxidation power of *$[Ru(bpy)_3]^{2+}$ [E^p_{ox} ($*Ru^{II}/Ru^{I}$) = +0.83 V *vs.* SCE] and the oxidation potential of triethylamine [E^p_{ox} ($Et_3N^{\bullet+}/Et_3N$) = +1.10 V *vs.* SCE, which matches the +1.00 V *vs.* SCE reported by MacMillan[75] but is different to the +0.78 V *vs.* SCE quoted by Stephenson],[97] potentials are close enough that one might expect electron transfer to be plausible, albeit thermodynamically uphill. However, photophysical studies have shown that trialkylamines are very poor quenchers of *$[Ru(bpy)_3]^{2+}$. A very large excess in trialkylamine concentration relative to $[Ru(bpy)_3]^{2+}$ (> 3 M triethylamine and 10^{-4} M concentration of $[Ru(bpy)_3]^{2+}$ was required to observe near-

complete luminscence quenching (here, $[Et_3N]$ is > 30,000x [{$Ru(bpy)_3^{2+}$}]).[104,161] Quenching of $*[Ru(bpy)_3]^{2+}$ with Et_3N has a reported k_q = 3.90 x 10^6 M^{-1} s^{-1} (DIPEA gives k_q = 6.21 x 10^6 M^{-1} s^{-1}).[104] Where trialkylamines have been employed in $[Ru(bpy)_3]^{2+}$ photoredox catalysis and cited as reductive quenchers, smaller concentration differences in trialkylamine and $[Ru(bpy)_3]^{2+}$ are found (for example, [trialkylamine] is *ca.* 40 - 400x [{$Ru(bpy)_3^{2+}$}]).[102,105,162]

A related point is that formal photocatalytic functionalisations of trialkylamines (as substrates, not simply sacrificial reductants) using $*[Ru(bpy)_3]^{2+}$ are not reported. To achieve this transformation, one approach is to use photocatalysts which give more potent oxidising excited states, for example $Ir[dF(CF_3)ppy]_2(dtbbpy)PF_6$ [$E_{1/2}$ ($*Ir^{IV}/Ir^{III}$) = +1.21 V *vs.* SCE].[125] Another approach is to oxidatively quench a photocatalyst which is a potent reductant in its excited state, such as $[Au_2(\mu\text{-dppm})_2]Cl_2$ [E^0 ($Au_2^{3+}/*Au_2^{2+}$) = -1.60 V *vs.* SCE][121] or *fac*-$Ir(ppy)_3$, [$E_{1/2}$ ($Ir^{IV}/*Ir^{III}$) = -1.73 V *vs.* SCE].[75,92,119] This generates an oxidising, non-excited state of the catalyst (mechanistic details are shown in the introduction) which persists and can perform endergonic oxidations (provided these oxidations are irreversible). Intrigued by the reported photophysical data and lack of trialkylamine functionalisation examples using $*[Ru(bpy)_3]^{2+}$, a decision was made to measure the lifetime of $*[Ru(bpy)_3]^{2+}$ in the presence of various tertiary amines (Table 8) to confirm the plausibility of published mechanisms.

***Table 8**: Lifetime of $*[Ru(bpy)_3]^{2+}$ in the presence of quenchers under Ar.*

Entry	τ (ns)[a]	F (%)[b]	Atmosphere	Quencher[c]	$E^p_{ox/red}$[d]
1	977[e]	0.0	Ar	-	N/A
2	237[f]	76	Air	-	-0.75 ($E_{1/2}$)[35]
3	112[f]	89	O_2	O_2, k_q = 2.84 x 10^9	-0.75 ($E_{1/2}$)[35]

Entry	τ (ns)[a]	F (%)[b]	Atmosphere	Quencher[c]	$E^{p}_{ox/red}$[d]
4	972	1	Ar	*N*-Boc THIQ (**116**)	+2.14
5	955[f]	2	Ar	Et_3N	+1.10
6	972[f,g]	1	Ar	Hantzsch ester	+0.95
7	981[f,g,h]	-1	Ar	Hantzsch ester	+0.95
8	956[f]	2	Ar	DIPEA	+0.85
9	733[g,i,j]	25	Ar	DIPEA	+0.85
10	650[g,h,j]	34	Ar	DIPEA, k_q = 7.15 x 10^6	+0.85
11	965[g,j]	1	Ar	DIPEA:formic acid 1 : 1	ND
12	467[f,h]	52	Ar	DIPEA:formic acid 1 : 1	ND
13	946	3	Ar	dextromethorphan (**73**)	+0.90
14	889[f,g,i]	9	Ar	dextromethorphan (**73**)	+0.90
15	853	20	Ar	*N*-phenyl THIQ (**23**)	+0.83
16	205[h]	79	Ar	*N*-phenyl THIQ (**23**)	+0.83
17	269[g,j]	73	Ar	4-$MeOC_6H_4NPh_2$, k_q = 3.48 x 10^8	+0.83
18	571[f,g]	42	Ar	*N*,*N*-dimethylaniline, k_q = 1.13 x 10^8	+0.78
19	447	54	Ar	DABCO, k_q = 1.43 x 10^8	+0.69
20	228	77	Ar	tri-*p*-tolylamine, k_q = 5.57 x 10^8	+0.82

Entry	τ (ns)[a]	F (%)[b]	Atmosphere	Quencher[c]	$E^{p}_{ox/red}$[d]
21	970[g,j]	1	Ar	chloride **66a**	-2.14
22	979[f,g]	0	Ar	bromide **65a**	-1.81
23	936[h]	4	Ar	bromide **65a**	-1.81
24	989[g,j]	-1	Ar	diethyl bromomalonate	-1.96
25	974[e,h]	0	Ar	diethyl bromomalonate	-1.96
26	958[g,j]	2	Ar	*trans*-1-phenyl-2-buten-1-one	-1.77
27	957[g,h,j]	2	Ar	*trans*-1-phenyl-2-buten-1-one	-1.77
28	982[g,j]	-1	Ar	$LiBF_4$	ND
29	963[g,h,j]	1	Ar	$LiBF_4$	ND
30	952[g,j]	3	Ar	$LiBF_4$: *trans*-1-phenyl-2-buten-1-one 1 : 1	-1.56
31	926[g,h]	5	Ar	$LiBF_4$: *trans*-1-phenyl-2-buten-1-one 1 : 1	-1.56
32	929[g,j]	5	Ar	$LiBF_4$: *trans*-1-phenyl-2-buten-1-one : DIPEA 1 : 1 : 1	ND
33	675[g,h,j]	31	Ar	$LiBF_4$: *trans*-1-phenyl-2-buten-1-one : DIPEA 1 : 1 : 1	ND

The concentration of $Ru(bpy)_3(PF_6)_2$ was 10.0 μM. Unless otherwise stated, the quencher solutions were 7.5 mM. [a]Lifetimes are calibrated to $*[Ru(bpy)_3]^{2+}$ as an external standard, run before and after a set of samples to ensure consistency. For comparisons to literature

lifetimes of *[Ru(bpy)$_3$]$^{2+}$ under Ar (τ^0), see Appendix. [b]The quenching fraction $F(\%) = ((\tau^0 - \tau)/\tau^0) \times 100$, under the same inert gas for both measurements. [c]Where applicable, Stern-Volmer plots were obtained *via* steady-state luminescence quenching and k_q is given in units of M^{-1} s^{-1}. [d]Unless otherwise stated, measured oxidation or reduction peak potentials are given *vs*. SCE. [e]Average of six samples. [f]Average of two samples. [g]Measurement was conducted by Katie Emery at the University of Strathclyde. [h]The quencher solution was 75.0 mM. [i]The quencher solution was 37.5 mM. [j]Average of three samples. N/A = not applicable. ND = not determined.

Naturally, the observed lifetime τ for *[Ru(bpy)$_3$]$^{2+}$ in the presence of a given quencher ($[Q]$ = 7.5 mM) is related to the *rate of quenching* for that quencher, which is related to the quenching rate constant k_q (see Appendix). Using a sample of observed lifetimes (τ) and the corresponding k_q (calculated from Stern-Volmer plots) for a given quencher allowed a calibration curve to be plotted, which could be used to predict k_q from τ (Figure 12, left). For example, DIPEA (at 75.0 mM) gives τ = 650 ns and a value of 8.95 x 10^7 is obtained from the calibration curve. Given that concentration had to be increased by an order of magnitude ($[Q]$ = 75.0 mM) to observe a similar lifetime as the other quenchers (τ = 650 ns, and hence similar rate of quenching), the corresponding rate constant must be an order of magnitude smaller. Thus the quenching rate constant is k_q (predicted from Figure 12) = 8.95 x 10^6 M^{-1} s^{-1} which compares well with the measured and literature values (k_q (measured) = 7.15 x 10^6 M^{-1} s^{-1} and k_q (literature)[118] = 7.90 x 10^6 M^{-1} s^{-1}). Alternatively, using τ^0 = 977 ns for *[Ru(bpy)$_3$]$^{2+}$, $[Q]$ = 75.0 mM for DIPEA and k_q = 7.90 x 10^6 M^{-1} s^{-1}, the Stern-Volmer equation (equation 5) predicted τ = 641 ns, in very good agreement with the measured τ = 650 ns (see Appendix for the agreement of predicted and measured τ).

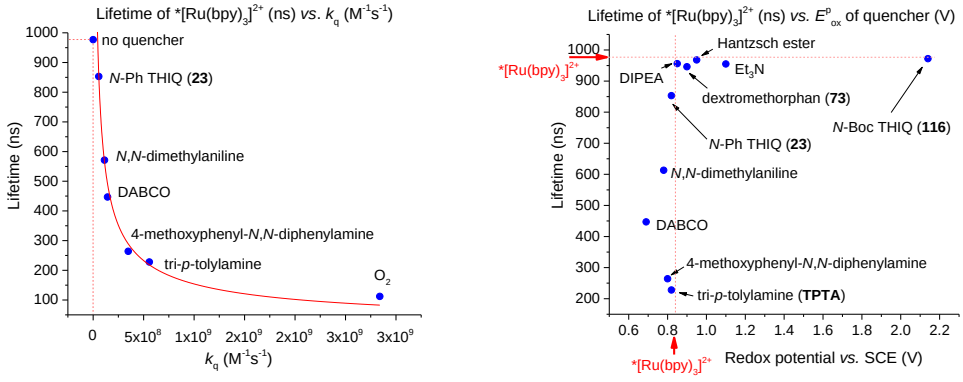

***Figure 12**: Left: Relationship between *Ru(bpy)$_3^{2+}$ lifetime and quenching rate constant k_q. Right: Relationship between *[Ru(bpy)$_3$]$^{2+}$ lifetime and redox potential of the tertiary amine quencher.*

Of greater interest is the relationship between the lifetime of *[Ru(bpy)$_3$]$^{2+}$ and the oxidation potential of the tertiary amine (E^p_{ox}). For E^p_{ox} ($R_3N^{\bullet+}/R_3N$) = > 0.9 V, the lifetime of *[Ru(bpy)$_3$]$^{2+}$ is unchanged, but as E^p_{ox} ($R_3N^{\bullet+}/R_3N$) falls into close proximity of (or below) E^p_{red} (*[Ru(bpy)$_3$]$^{2+}$), the lifetime of *[Ru(bpy)$_3$]$^{2+}$ decreases drastically (Figure 12, right). *[Ru(bpy)$_3$]$^{2+}$, though relatively long lived, is still on the nanosecond scale, such that thermodynamically uphill redox processes become difficult. Other redox-active species accessible through the catalytic cycle ([Ru(bpy)$_3$]$^{+}$ and [Ru(bpy)$_3$]$^{3+}$) are not excited states and so can persist to perform uphill redox processes.

The lifetime of *[Ru(bpy)$_3$]$^{2+}$ is almost unchanged in the presence of trialkylamines Et_3N, DIPEA and dextromethorphan. Furthermore, the intensity of *[Ru(bpy)$_3$]$^{2+}$ emission was unaffected by increasing concentrations of Et_3N (Figure 13, left) when taken as a direct comparison to *N*-phenyl THIQ (Bard did not observe quenching for this system because it is too slow, consistent with the endergonic driving force according to redox potentials).[163] In order to observe significant quenching (Figure 13, right), a much higher difference in concentration was required (here, [DIPEA] was 7,500x [{Ru(bpy)$_3^{2+}$}] and gave k_q = 7.15 x 10^6 M^{-1} s^{-1}). These observations could

reflect the non-reaction of dextromethorphan in the laboratory (in the reaction (Scheme 53, Section 2.1.7.), [trialkylamine] is 200x [{$Ru(bpy)_3^{2+}$}]). The results obtained raise questions over the generally accepted dogma that trialkylamines are efficient reductive quenchers of $*[Ru(bpy)_3]^{2+}$ (Figure 11), and some literature examples are now investigated with luminescence quenching experiments.

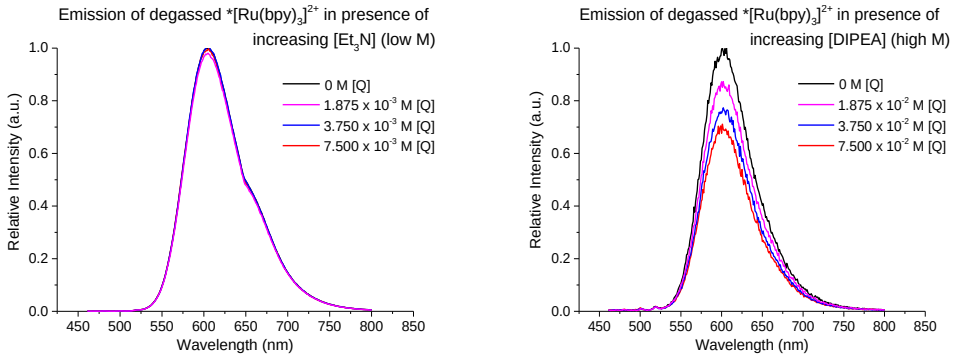

Figure 13: *Left: Steady-state emission intensity of $*[Ru(bpy)_3]^{2+}$ in the presence of increasing concentrations of R_3N. Right: Steady-state emission intensity of $*[Ru(bpy)_3]^{2+}$ using R_3N concentrations an order of magnitude higher, to detect quenching.*

2.2.2. The Role of Ru-based Photoredox Catalysts in the Oxidation of Arylboronic Acids

Xiao reported the photoredox oxidation of arylboronic acids to phenols, proposing DIPEA as a reductive quencher of $*[Ru(bpy)_3]^{2+}$ and molecular oxygen as the terminal oxidant (Scheme 32, Section 1.5.2.). However, when compared at the same concentration, it is clear that $*[Ru(bpy)_3]^{2+}$ preferentially undergoes oxygen quenching (here, [DIPEA] ≈ $[O_2]$ ≈ 750x higher concentration than [$Ru(bpy)_3^{2+}$]). Stern-Volmer analysis gave quenching rate constants which accord with the literature[104] and the rate constant for quenching of $*[Ru(bpy)_3]_2^{+}$ by O_2 (k_q = 2.84 x 10^9 M^{-1} s^{-1}) was 500x greater than by DIPEA (k_q = 7.15 x 10^6 M^{-1} s^{-1}). Two possibilities arise. Firstly, *oxidative quenching* could give rise to superoxide and $[Ru(bpy)_3]^{3+}$,

which is a potent oxidant [E^{p}_{ox} (Ru^{III}/Ru^{II}) = +1.32 V *vs.* SCE], capable of oxidising DIPEA [E^{p}_{ox} ($DIPEA^{\bullet+}$/DIPEA) = +0.85 V *vs.* SCE] which, in turn, effectively acts as the terminal reductant in the process (Figure 14).

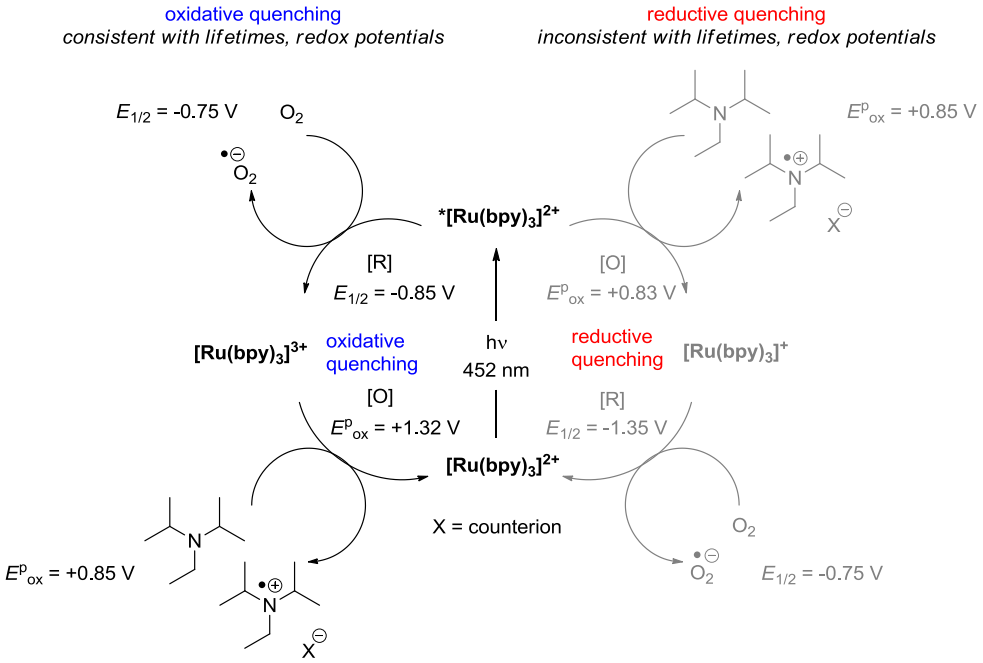

***Figure 14**: Arylboronic acid oxidation: unlikely reductive quenching proposed by Xiao vs. oxidative quenching validated by luminescence quenching and redox potentials.*[102]

Alternatively, $*[Ru(bpy)_3]^{2+}$ is a known sensitiser of singlet oxygen and so this pathway is likely in operation.[104,142,164] Indeed, $[Ru(bpy)_3]^{2+}$ and related complexes had witnessed applications in photodynamic therapy (singlet oxygen sensitisers)[165–167] and as oxygen sensors[168,169] long before their renaissance in organic synthesis. Singlet oxygen generated by $*[Ru(bpy)_3]^{2+}$ has been utilised in formation of endoperoxides.[142,164]

In order to probe the mechanism of action in Xiao's chemistry, Scaiano examined both $*[Ru(bpy)_3]^{2+}$ and excited state methylene blue (*MB), comparing DIPEA and O_2 as quenchers. Although the quenching rate constant for *MB being quenched by O_2 [k_q (literature)[104] = 2.46 x 10^9 M^{-1} s^{-1}] was *ca*. 10x larger than the quenching rate constant for DIPEA [k_q

(literature)[104] = 2.44 x 10^8 mol^{-1} M^{-1} s^{-1}], the concentration of DIPEA (0.3 M) was *ca.* 40x higher than O_2 (8.1 mM) in reactions. Scaiano calculates that 71% of *MB triplets are quenched by DIPEA. Therefore, the dominant pathway at the reaction concentration will be quenching by DIPEA. For *$[Ru(bpy)_3]^{2+}$ on the other hand, the concentration of DIPEA was *ca.* 40x higher than O_2 in reactions but the quenching rate constant for *$[Ru(bpy)_3]^{2+}$ being quenched by O_2 is 500x greater [k_q (literature)[104] = 2.97 x 10^9 M^{-1} s^{-1}] than the rate constant for quenching by DIPEA [k_q (literature)[104] = 6.21 x 10^6 M^{-1} s^{-1}]. Scaiano calculates that only 6% of *$[Ru(bpy)_3]^{2+}$ triplets are quenched by DIPEA. Lifetime measurements and rate constants obtained herein are consistent with Scaiano's values[104] and strongly support the notion that quenching of *$[Ru(bpy)_3]^{2+}$ by O_2 [k_q (measured) = 2.84 x 10^9 M^{-1} s^{-1}] overwhelms any quenching by DIPEA [k_q (measured) = 7.15 x 10^6 M^{-1} s^{-1}]. Therefore, the dominant pathway at the reaction concentration will be quenching by O_2 (Figure 14).

Scaiano examined the quenching of singlet oxygen phosphorescence and found that singlet oxygen is 5000x more likely to be quenched by DIPEA than by phenylboronic acid.[104] Therefore, Scaiano concludes that singlet oxygen does not itself play a significant role in product formation in Xiao's chemistry. Furthermore, superoxide generated *via* ***oxidative quenching*** cannot be ruled out as the reactive pathway to product. Unfortunately, it is not possible to delineate between energy transfer quenching *vs.* oxidative quenching solely on the basis of luminescence quenching measurements. In conclusion, although quenching of *$[Ru(bpy)_3]^{2+}$ by DIPEA is unlikely to be the reactive pathway, further data would be required to conclusively rule it out.

2.2.3. The Role of Ru-based Photoredox Catalysts in Reductive Dehalogenations

Stephenson reported an elegent dehalogenation of alkyl halides such as alkyl bromide **65a**, proposing DIPEA as a reductive quencher of *$[Ru(bpy)_3]^{2+}$

(Scheme 33, Section 1.5.2.). Under the reaction conditions, $[Ru(bpy)_3]^{2+}$ was irradiated in the presence of alkyl halide and DIPEA, with formic acid or Hantzsch ester acting as a terminal H atom source (here, [DIPEA] = 10x [alkyl halide] and [alkyl halide] = 40x $[\{Ru(bpy)_3\}^{2+}]$). Reductive quenching of $*[Ru(bpy)_3]^{2+}$ was proposed, but no photophysical studies were disclosed by Stephenson. Whitten's study was referred to where 'trialkylamines were found to disproportionate to the corresponding trialkylammonium salts and enamines upon visible-light irradiation in the presence of $Ru(bpy)_3Cl_2$'.[105] In fact, Whitten only made this observation when an additional PtO_2 catalyst was involved, and no reaction was observed between Et_3N and $[Ru(bpy)_3]^{2+}$ only.[161] Therefore, lifetime studies were undertaken to investigate the photocatalytic cycle.

As mentioned previously, $*[Ru(bpy)_3]^{2+}$ undergoes slow but definite quenching with DIPEA. Stephenson specifically reported the combination of DIPEA and formic acid as the reductive quencher. Using DIPEA:formic acid 1 : 1 gave unnoticeable quenching (F = 1%). Employing a much larger concentration of DIPEA:formic acid 1 : 1 relative to $[Ru(bpy)_3]^{2+}$ allowed a significant decrease in the lifetime to be observed (F = 52%). The lifetime of $*[Ru(bpy)_3]^{2+}$ did not significantly decrease in the presence of alkyl bromide **65a** (F = 0%) or alkyl chloride **66a** (F = 1%). The lifetime of $[Ru(bpy)_3]^{2+}$ did not decrease in the presence of Hantzsch ester (F = -1%), which was an additional component of reactions involving the alkyl chloride **66a**.[105]

Therefore, although reductive quenching of $[Ru(bpy)_3]^{2+}$ by DIPEA is very slow, these results force the conclusion that ***reductive quenching*** is in operation as suggested by Stephenson,[105] and accords with redox potentials, which show that oxidative quenching is more endergonic than reductive quenching (Figure 15). Following reductive quenching, $[Ru(bpy)_3]^{+}$ reduces the alkyl bromide (or alkyl chloride) to close the catalytic cycle (although this is thermodynamically uphill, $[Ru(bpy)_3]^{+}$ is a persistent ground state species and reduction of alkyl halides is irreversible).

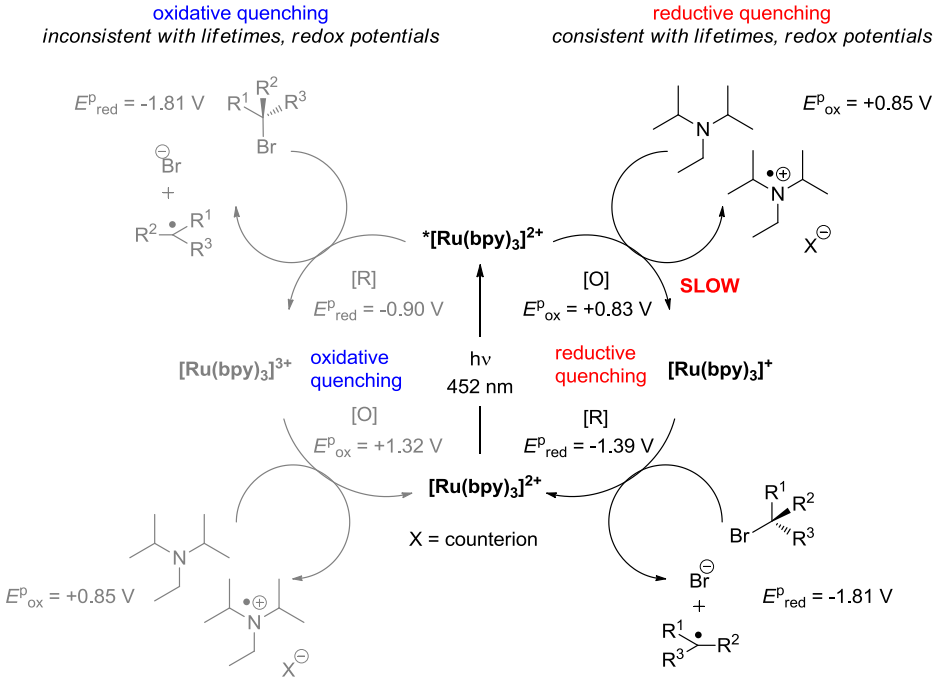

***Figure 15**: Reductive dehalogenation: reductive quenching proposed by Stephenson,[105] validated by luminescence quenching and redox potentials vs. unlikely oxidative quenching.*

2.2.4. The Role of Ru-based Photoredox Catalysts in [2+2]-Cycloadditions

Yoon reported intramolecular [2+2]-cycloadditions of bis(enones) under $[Ru(bpy)_3]^{2+}$ photoredox catalysis (Scheme 54).[162] Reductive quenching of $*[Ru(bpy)_3]^{2+}$ by DIPEA is proposed to give $[Ru(bpy)_3]^{+}$. This reduces the enone **129**, which is complexed with $LiBF_4$ as a Lewis acid. Stepwise radical [2+2]-cycloaddition furnishes **132**, which can either engage in SET reduction of either enone **129** (thereby propagating a radical chain) or $DIPEA^{\bullet+}$ (termination).

In a subsequent study, Yoon's mechanistic studies provided clear evidence for a radical chain process.[118] Here, reductive quenching of $*[Ru(bpy)_3]^{+}$ with DIPEA was proposed to initiate the reaction. Yoon's luminescence quenching studies found k_q = 7.80 x 10^6 M^{-1} s^{-1} (this value was derived from the Stern-Volmer plot in the paper using a value of τ = 977 ns for $*[Ru(bpy)_3]^{2+}$) for the

quenching of *[Ru(bpy)$_3$]$^{2+}$ by DIPEA,[118] consistent with rate constants determined by Scaiano[104] and herein.

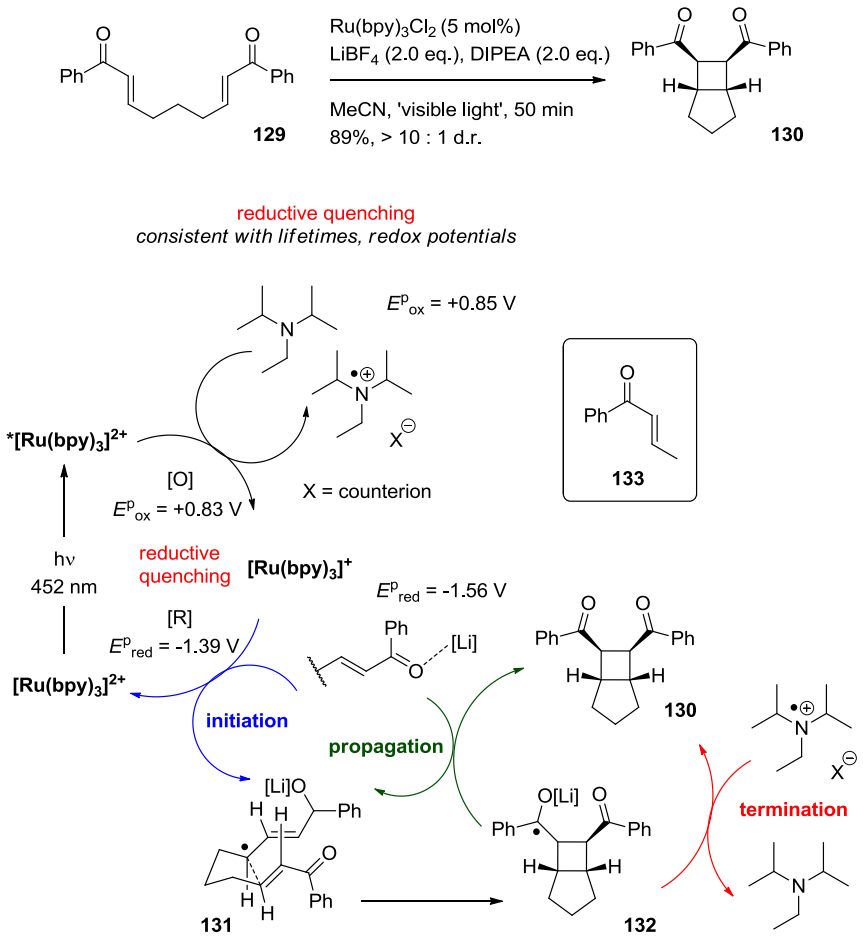

***Scheme 54**: [2+2]-Cycloaddition of a bis(enone) under Ru(bpy)$_3$Cl$_2$ photoredox catalysis.*[162]

No quenching of *[Ru(bpy)$_3$]$^{2+}$ by LiBF$_4$ or by the (bis)enone was observed by Yoon.[118] This accords with redox potentials (reported herein), which show that the enone [E^p_{red} (*trans*-CH$_3$CH=CHCOPh/CH$_3$CH=CHCOPh$^{\bullet-}$) = -1.77 V *vs*. SCE] is out of range of *[Ru(bpy)$_3$]$^{2+}$ [E^p_{red} = (Ru^{III}/*Ru^{II}) = -0.90 V *vs.* SCE]. Here, *trans*-1-phenylbuten-2-one (**133**) is taken as a surrogate for the bis(enone), which is reported to undergo crossed intermolecular [2+2]-photocycloadditions in the presence of *[Ru(bpy)$_3$]$^{2+}$, LiBF$_4$ and DIPEA.[170]

However, complexing the enone with $LiBF_4$ decreases E^p_{red} of the enone (a 1 : 1 mixture of *trans*-1-phenylbuten-2-one : $LiBF_4$ gave E^p_{red} (*trans*-$CH_3CH{=}CHCOPh/CH_3CH{=}CHCOPh^{\bullet-}$) = -1.56 V *vs.* SCE); and a 1 : 1 mixture of enone : $LiBF_4$ was not reported as a quencher. Consistent with Yoon's findings, the lifetime of $*[Ru(bpy)_3]^{2+}$ did not significantly decrease in the presence of $LiBF_4$ (F = 1%) or *trans*-1-phenylbuten-2-one (F = 2%) only. In the presence of a 1 : 1 mixture of $LiBF_4$: enone and at 75.0 mM concentration, a very small decrease (F = 5%) in $*[Ru(bpy)_3]^{2+}$ lifetime was observed compared to a significant lifetime decrease (F = 34%) in the presence of DIPEA (75.0 mM) as a quencher [comparable to a 1 : 1 : 1 mixture of $LiBF_4$: enone : DIPEA (F = 31%)]. These results confirm that ***reductive quenching*** (although slow) is in operation, and accords with redox potentials, which show that oxidative quenching is more endergonic than reductive quenching (Figure 16).

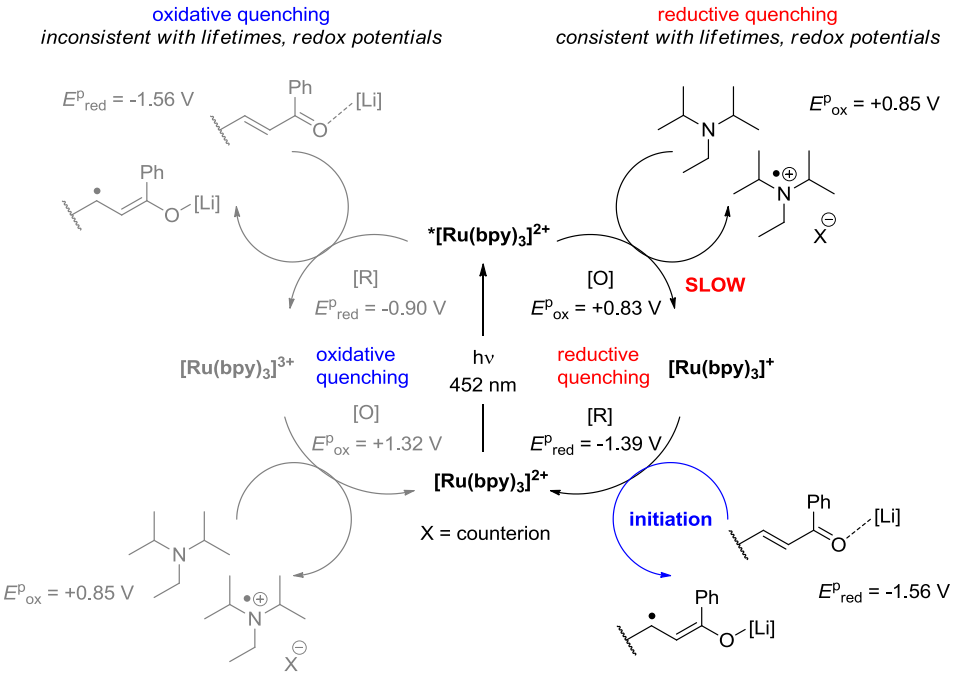

Figure 16*: [2+2]-Cycloadditions: reductive quenching pathway proposed by Yoon,*[118] *validated by luminescence quenching and redox potentials vs. unlikely oxidative quenching.*

Following reductive quenching, $[Ru(bpy)_3]^+$ reduces the Li-complexed enone to close the photocatalytic cycle (although this is endergonic, $[Ru(bpy)_3]^+$ is a persistent ground state species). Reduction of the Li-complexed enone initiates a radical chain mechanism where the product is generated overwhelmingly from the chain propagation step.[118]

Given that DIPEA and dextromethorphan can both engage in reductive quenching with $*[Ru(bpy)_3]^{2+}$ (albeit slowly), this raises the question of why dextromethorphan does not react in the laboratory [DIPEA and dextromethorphan have E^p_{ox} ($R_3N^{\bullet+}/R_3N$) = +0.85 V and +0.90 V *vs*. SCE, respectively]. One possibility is that back electron transfer might be more pronounced in the case of dextromethorphan. Dextromethorphan has smaller diffusion coefficient (D = 6.20 x 10^{-6} cm^2 s^{-1}) than DIPEA (D = 1.17 x 10^{-5} cm^2 s^{-1}), consistent with its higher molecular weight, such that it takes longer for the charge separated species to escape the solvent cage. This renders the dextromethorphan system more susceptible to undergo charge recombination (D, the diffusion coefficient, was measured by a CV scan rate dependence study, see Appendix). Another possibility is that the slow reductive quenching of $*[Ru(bpy)_3]^{2+}$ only manifests itself in successful reaction if it leads to a radical chain mechanism (as characterised by Yoon).[118]

2.2.5. The Role of Ru-based Photoredox Catalysts in Arene Alkylations

Stephenson reported the coupling of 2-bromomalonates with electron-rich heterocycles under $[Ru(bpy)_3]^{2+}$ photoredox catalysis (Scheme 55).[171] Reductive quenching of $*[Ru(bpy)_3]^{2+}$ by 4-methoxyphenyl-*N*,*N*-diphenylamine [E^p_{ox} ($4\text{-}MeOC_6H_4N^{\bullet+}Ph_2/4\text{-}MeOC_6H_4NPh_2$) = +0.83 V *vs*. SCE] is proposed, to give $[Ru(bpy)_3]^+$ and the 4-methoxyphenyl-*N*,*N*-diphenylammonium radical cation, which cannot serve as a H atom donor. Therefore, when $[Ru(bpy)_3]^+$ reduces diethyl bromomalonate to the corresponding malonyl radical (regenerating $[Ru(bpy)_3]^{2+}$), this radical is readily intercepted by *N*-methylindole instead of undergoing HAT. Further

chemistry gives rise to the desired product, **133**. Stephenson's luminescence quenching experiments identified 4-methoxyphenyl-*N*,*N*-diphenylamine as a quencher of *$[Ru(bpy)_3]^{2+}$ but data were not presented for other reaction mixture components. Herein, a notable decrease in the lifetime of *$[Ru(bpy)_3]^{2+}$ was observed in the presence of 4-methoxyphenyl-*N*,*N*-diphenylamine (F = 73%) and a rate constant measured by Stern-Volmer analysis (k_q = 3.48 x 10^8 M^{-1} s^{-1}). The lifetime of *$[Ru(bpy)_3]^{2+}$ did not decrease in the presence of diethyl bromomalonate (F = -1%).

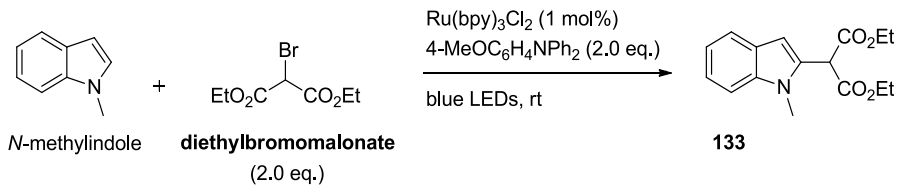

***Scheme 55**: Photoredox-catalysed coupling of electron-rich heterocycles with malonates.*[171]

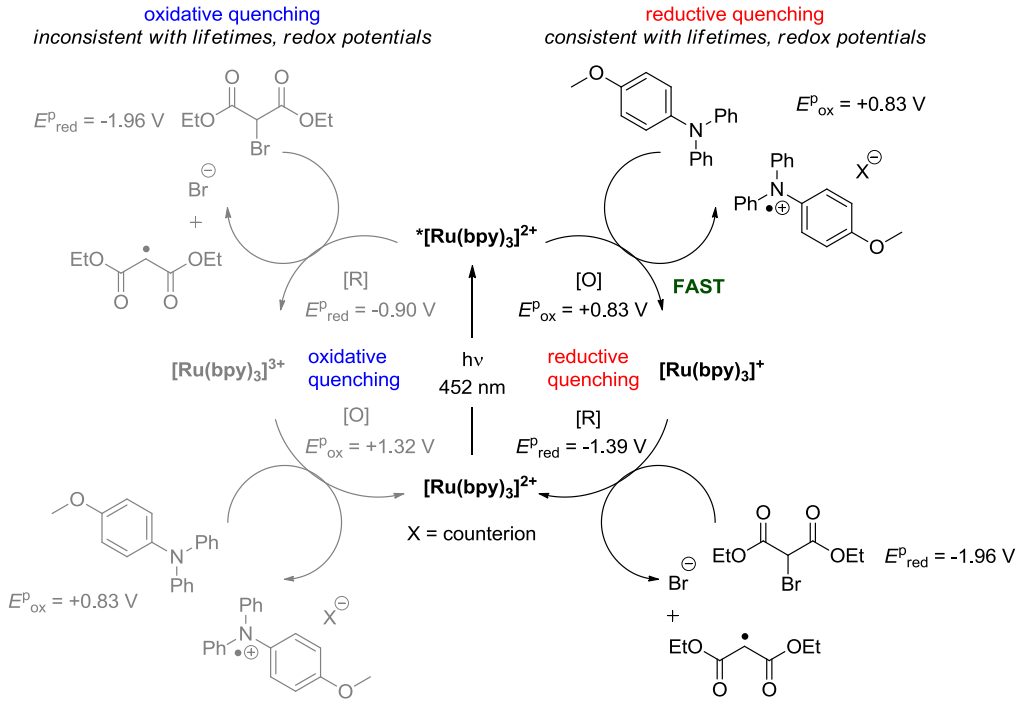

***Figure 17**: Arene alkylations: reductive quenching proposed by Stephenson,*[171] *validated by luminescence quenching and redox potentials vs. unlikely oxidative quenching.*

These results confirm that ***reductive quenching*** is in operation as suggested by Stephenson, and accord with redox potentials, which show that reductive quenching is thermodynamically favourable, whereas oxidative quenching is thermodynamically uphill (Figure 17). Following reductive quenching, $[Ru(bpy)_3]^+$ reduces diethyl bromomalonate to close the catalytic cycle.

2.2.6. On the Interactions of Highly Oxidising Ru-based Photoredox Catalysts with Trialkylamines

Although it is found that trialkylamines are very poor quenchers of $*[Ru(bpy)_3]^{2+}$, Whitten found that by rendering the ligands more electron-deficient (for example, in complex **134**, Figure 18) the ground state reduction potential of $\{RuL_3\}$ and hence oxidation potential of $*\{RuL_3\}$ becomes 0.4 - 0.6 V more positive (for **134**, $E_{1/2}$ ($*Ru^{II}/Ru^{I}$) = +1.23 V *vs*. SCE) and so triethylamine [E^{p}_{ox} ($Et_3N^{\bullet+}/Et_3N$) = +1.10 V *vs*. SCE] now falls within range of the oxidising $*\{RuL_3\}$. This is reflected by drastically enhanced quenching (for **134**, even for [Et_3N] = 10x [$\{RuL_3\}$], quenching of $*\{RuL_3\}$ can be detected). A decision was made to study the lifetime of $*[Ru(bpz)_3]^{2+}$ (Figure 18) using a selection of amine quenchers (Table 9). $[Ru(bpz)_3]^{2+}$ is readily available (as its hexafluorophosphate salt) and is a more potent oxidant in its excited state [$E_{1/2}$ ($*Ru^{II}/Ru^{I}$) = +1.41 V *vs*. SCE] than $*[Ru(bpy)_3]^{2+}$.

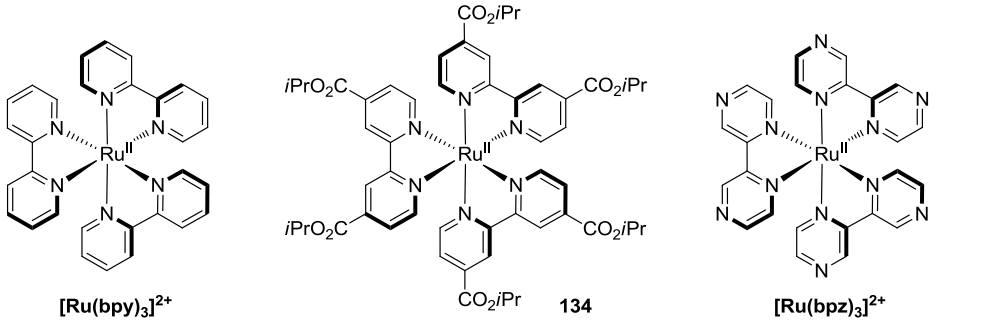

$[Ru(bpy)_3]^{2+}$
$E_{1/2}$ (Ru^{II}/Ru^{I}) = -1.35 V *vs*. SCE
$E_{1/2}$ ($*Ru^{II}/Ru^{I}$) = +0.77 V *vs*. SCE

134
$E_{1/2}$ (Ru^{II}/Ru^{I}) = -0.92 V *vs*. SCE
$E_{1/2}$ ($*Ru^{II}/Ru^{I}$) = +1.23 V *vs*. SCE

$[Ru(bpz)_3]^{2+}$
$E_{1/2}$ (Ru^{II}/Ru^{I}) = -0.71 V *vs*. SCE
$E_{1/2}$ ($*Ru^{II}/Ru^{I}$) = +1.41 V *vs*. SCE

Figure 18: *Effect of electron-withdrawing ligands on redox potentials of Ru complexes.*[161]

***Table 9**: Lifetime of *[Ru(bpz)$_3$]$^{2+}$ in the presence of quenchers under Ar.*

Entry	τ (ns)[a]	F (%)[b]	Atmosphere	Quencher[c]	$E^p_{ox/red}$
1	720[d]	0	Ar	-	-
2	518	28	Air	-	-0.75 ($E_{1/2}$)[35]
3	294	59	O_2	-	-0.75 ($E_{1/2}$)[35]
4	691	4	Ar	*N*-Boc THIQ	+2.14
5	316	56	Ar	Et_3N, k_q= 2.18 x 10^9	+1.10
6	299	58	Ar	DIPEA	+0.85
7	198	73	Ar	dextromethorphan (**73**)	+0.90
8	120	83	Ar	tri-*p*-tolylamine	+0.82
9	98	86	Ar	DABCO	+0.69

[a]Values are calibrated to [Ru(bpz)$_3$]$^{2+}$ as an external standard, run before and after a set of samples to ensure consistency. For comparisons to literature lifetimes of *[Ru(bpz)$_3$]$^{2+}$ under Ar (τ^0), see Appendix. [b]The quenching fraction $F(\%) = ((\tau^0 - \tau)/\tau^0) \times 100$, under the same inert gas for both measurements. [c]Where applicable, Stern-Volmer plots were obtained and k_q is given in units of M^{-1} s^{-1}. [d]Average of two measurements.

Strong quenching of *[Ru(bpz)$_3$]$^{2+}$ was observed for Et_3N, DIPEA and dextromethorphan, with lifetime decreases paralleling or exceeding that in the presence of O_2. Stern-Volmer analysis was conducted for quenching of *[Ru(bpz)$_3$]$^{2+}$ with Et_3N, revealing a rate constant k_q = 2.18 x 10^9 M^{-1} s^{-1}. This strong interaction between *[Ru(bpz)$_3$]$^{2+}$ and dextromethorphan (**73**) demanded attention in the laboratory (Scheme 56)! Traces of secondary amine (**74**) were observed immediately upon irradiation. However, the conversion of **73** to **74** stalls after this initial reaction (ratio **74** : **73** = 10 : 90[†] after 16 h). Stalling was observed when either the 24 W blue LED strip (λ_{max} = 458 nm) or the 30 W LED floodlamp (λ_{max} = 449 nm) were used, [†]By HPLC peak area (220 nm), uncorrected for relative responses.

and when anaerobic conditions employing either $BrCCl_3$, or diethyl bromomalonate were used. Although $*[Ru(bpz)_3]^{2+}$ [$E_{1/2}$ ($*Ru^{II}/Ru^{I}$) = +1.41 V *vs.* SCE][75] is almost twice as oxidising as $*[Ru(bpy)_3]^{2+}$ [$E_{1/2}$ ($*Ru^{II}/Ru^{I}$) = +0.78 V *vs.* SCE], reoxidation of $[Ru(bpz)_3]^{+}$ is twice as difficult [$E_{1/2}$ (Ru^{II}/Ru^{I}) = -0.71 V *vs.* SCE][75] as it is for $[Ru(bpy)_3]^{+}$ [$E_{1/2}$ (Ru^{II}/Ru^{I}) = -1.35 V *vs.* SCE].[75] Therefore, reoxidation of $[Ru(bpz)_3]^{+}$ using $BrCCl_3$ (E^{p}_{red} = -1.36 V *vs.* SCE) is now significantly endergonic. If catalyst reoxidation becomes too slow, rapid back electron transfer could predominate and prohibit the reactive pathway. Use of O_2 as the terminal oxidant is only slightly endergonic and should promote reoxidation [$E_{1/2}$ ($O_2/O_2^{\bullet-}$) = -0.75 V *vs.* SCE]. Consistent with this, aerobic conditions gave higher conversion after the same time period (ratio **74** : **73** = 20 : 80[†]), but a longer reaction time gave complex mixtures.

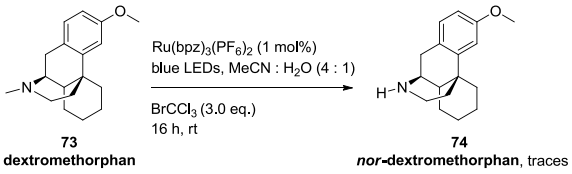

73
dextromethorphan

74
***nor*-dextromethorphan**, traces

***Scheme 56**: N-Demethylation of dextromethorphan under $Ru(bpz)_3Cl_2$ photocatalysis giving trace amounts of nor-dextromethorphan.*

Overall, the direct measurement of excited photocatalyst lifetime serves as a valuable platform for reporting mechanistic information. The data herein only concerns $*[Ru(bpy)_3]^{2+}$ and $*[Ru(bpz)_3]^{2+}$, but the combination of redox potentials and luminescence quenching can and should be used to routinely study photocatalyst and quencher combinations in order to establish the mechanism of reaction. For example, König used lifetime measurements to rule out reductive quenching and determine an oxidative quenching photocatalytic cycle in a photocatalysed sulfonylation reaction of alkenes.[172]

Since this investigation, examples of trialkylamine functionalisation under photoredox catalysis have emerged.[119,121,125] Yet at the time, a decision was made to investigate alternative modes of oxidation to achieve trialkylamine *N*-

C**H**$_3$ functionalisation that did not rely on the complexity of a photocatalytic cycle with compatible redox potentials and carefully balanced kinetics. Therefore, triarylaminium radical cation salts were investigated which had been demonstrated oxidants of both *N*-aryl THIQs[34,36] and trialkylamines[67] in the literature. We envisaged that the oxidising power of these agents could be harnessed to access iminium salts. Furthermore, triarylaminium salts are intensely coloured and we envisaged that colour changes during the reaction might give clues to the mechanism.

2.3. REGIOSELECTIVE *N*-FUNCTIONALISATION OF TRIALKYLAMINES USING RADICAL CATION SALTS

2.3.1. RADICAL CATION SALT-MEDIATED AEROBIC *N*-FUNCTIONALISATION OF TERTIARY AMINES

Attention was first directed to Huo's chemistry,[34] where *N*-C**H**$_2$ functionalisation of *N*-aryl THIQs was accomplished in air using **TBPA**-$SbCl_6$ as a catalyst. A decision was made to repeat the literature conditions using acetophenone as a reported pronucleophile (Table 10).[34] Concerns over the non-innocence of the counterion[37,38,40] prompted studying both **TBPA**-$SbCl_6$ and **TBPA**-PF_6 salts as catalysts. Herein, **TBPA** will refer to the neutral triarylamine and **TBPA**-X will refer to the triarylaminium salt. Using 20 mol% **TBPA**-$SbCl_6$ gave near-full conversion of **23** to iminium salt **26** and over-oxidised product **135** (Table 10), but no desired product **136** or **35** when either acetone or acetophenone (2.0 eq.) were employed as pronucleophiles, respectively (Table 10, entries 2-3). Using 20 mol% **TBPA**-PF_6 on the other hand, gave no reaction (Table 10, entries 4-5).

***Table 10**: Aerobic catalytic oxidation of N-phenyl THIQ under various conditions.*

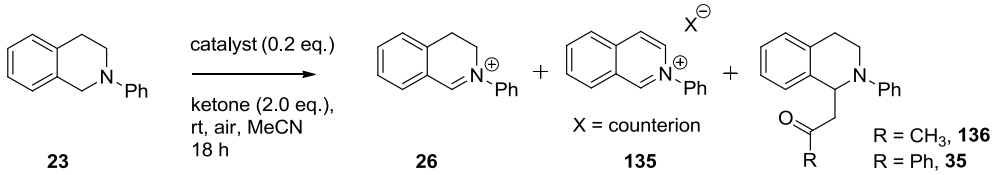

23 **26** **135**

Entry	Catalyst[a]	Ketone	Ratio 23 : 26 : 135[b]
1[c]	-	acetophenone	-
2	**TBPA**-$SbCl_6$	acetophenone	1 : 6.4 : 4.8
3	**TBPA**-$SbCl_6$	acetone	1 : 6.0 : 4.8

Entry	Catalyst[a]	Ketone	Ratio 23 : 26 : 135[b]
4[c]	**TBPA**-PF_6	acetophenone	-
5[c]	**TBPA**-PF_6	acetone	-
6	$SbCl_5$	acetophenone	1 : 2.0 : 1.1

[a]Catalyst loading (if added) is 20 mol%. [b]Ratio of **23** : **26** : **135** by HPLC peak area (220 nm, uncorrected) at the time specified. [c]No reaction observed.

As a control reaction, using $SbCl_5$ (20 mol%) as a catalyst gave iminium salt **26** as the major product (Table 10, entry 6). Results conclusively identify the hexachloroantimonate anion as non-innocent (oxidations have previously been reported using tropylium hexachloroantimonate whereas the corresponding tetrafluoroborate or perchlorate gave no reaction).[40] The breakdown of hexachloroantimonate to $SbCl_5$ is known,[37,38] and $SbCl_5$ is shown here to be an active catalyst in the aerobic oxidation, albeit in slightly lower conversion than when **TBPA**-$SbCl_6$ was used. Huo's conditions were applied to dextromethorphan in the presence of water (instead of ketone pronucleophile) to test for *N*-demethylation. However, no reaction was observed employing either **TBPA**-$SbCl_6$ or **TBPA**-PF_6 as catalyst (Scheme 57). These findings rule out any **TBPA**-catalysed or $SbCl_5$-catalysed reactions of trialkylamines in air.

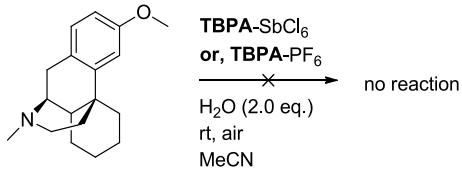

73
dextromethorphan

Scheme 57*: Aerobic oxidation of dextromethorphan using* ***TBPA****-$SbCl_6$ as a catalyst.*

A mechanistically simple situation would be that of a stoichiometric single electron oxidation (Scheme 58), based on the work of Jahn who

demonstrated oxidation of trialkylamines using **TBPA**-PF_6 (Scheme 23, Section 1.4.3.).[67] After an initial SET oxidation to yield radical cation **18** (and without a pendant radical trap in the substrate as reported by Jahn)[67] it was envisaged that deprotonation would afford α-amino radical **19** which could undergo a second SET oxidation to furnish iminium **20** (H atom abstraction from **18** by **19** could also occur). As mentioned previously, Nelsen found that R_3N is not sufficiently basic to deprotonate its own radical cation (pK_a > 15).[94]

Therefore, in theory (in the absence of base), the moment an excess of 1.0 eq. oxidant is added, the blue colour should persist (as the trialkylamine is completely oxidised to radical cation **18**). After addition of base (to deprotonate the radical cation), addition of a further 1.0 eq. oxidant should furnish iminium **20**. Therefore, 2.0 eq. oxidant and 1.0 eq. base should furnish 1.0 eq. of iminium **20**. One added mechanistic complexity is that α-amino radical **19** could abstract a hydrogen atom from its radical cation precursor **18** but in this case, the net result of 2.0 eq. oxidant and 1.0 eq. base would still be 0.5 eq. of iminium **20** (and 0.5 eq. returned starting material). In practice, it was necessary for Jahn to use up to 3.5 eq. oxidant to achieve full conversion.[67] Jahn's conditions were selected as a good starting point for demethylation of dextromethorphan.

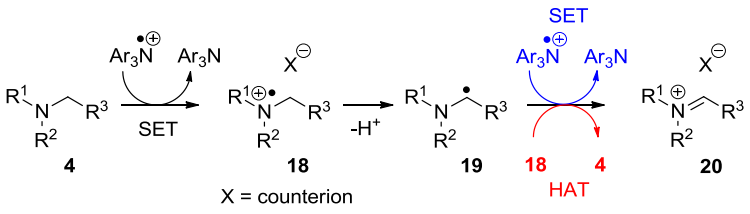

Scheme 58: *Mechanism for radical cation induced demethylation of trialkylamines (based on a general mechanism proposed in the literature).*[173]

2.3.2. Reported Syntheses of Stable Radical Cation Salts

The synthesis of a series of tri-*para*-substituted arylaminium radical cation salts was reported by Walter in 1955.[174] Whilst the triphenylaminium salt is unstable in air, a selection of tri-*para*-substituted arylaminium salts was

stable in air. For example, tri-*p*-tolylaminium perchlorate (**TPTA**-ClO_4) solid was reported to be stable for 'several days' and Walter claimed that tri-*p*-biphenyl perchlorate (**TPBPA**-ClO_4) was 'stable indefinitely', having kept it in a refrigerator for at least a year.[174] Here, **TPTA and TPBPA** will refer to the neutral triarylamines, whilst **TPTA**-X and **TPBPA**-X will refer to the triarylaminium salts. In order to prepare some tri-*para*-substituted arylaminium radical cation salts, synthesis of some tri-*para*-substituted arylamines was necessary. Although **TBPA**-$SbCl_6$ is commercially available, a decision was made to prepare the hexafluorophosphate salt due to the non-innocence of the hexachloroantimonate anion found in Section 2.3.1. Tris-*p*-bromophenylamine (**TBPA**) is commercially available.

2.3.3. Synthesis of Radical Cation Salt Precursors

Preparation of tri-*p*-biphenylamine (**TPBPA**) from **TBPA** was achieved in 35% yield *via* a triple Suzuki reaction (Scheme 59).[175] The modest yield results from poor solubility of **TPBPA** which results in crystallisation during column chromatography which interferes with separation. Impurities which are more polar than **TPBPA** are observed to elute first, and using more polar eluent systems results in co-elution (purification by recrystallisation might be superior for future investigations). To achieve even this modest yield, a high $Pd(PPh_3)_4$ loading is required (10 mol%) rendering the reaction rather cost-intensive.[175] Tri-*p*-tolylamine (**TPTA**) is commercially available, or can be synthesised by a double Buchwald-Hartwig reaction in good (77%) yield (Scheme 60).[176]

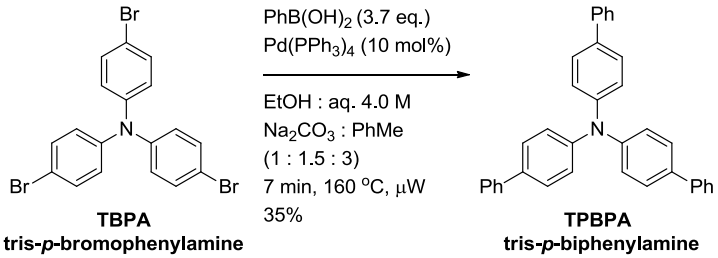

***Scheme 59**: Microwave-assisted triple Suzuki reaction to synthesise tri-p-biphenylamine.*[175]

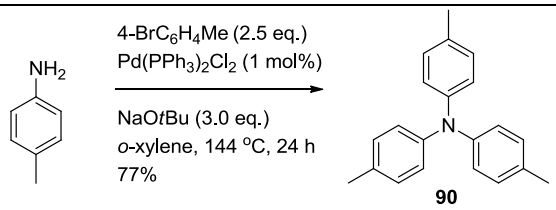

***Scheme 60**: Double Buchwald-Hartwig reaction to synthesise tri-p-tolylamine.*[176]

2.3.4. Synthesis and Characterisation of Radical Cation Salts

With **TBPA**, **TPBPA** and **TPTA** in hand and using a modification of Jahn's preparation,[67] tris(*p*-bromophenyl)aminium hexafluorophosphate (**TBPA**), tri-*p*-biphenylaminium hexafluorophosphate (**TPBPA**) and tri-*p*-tolylaminium hexafluorophosphate (**TPTA**) were rapidly synthesised in high (79 - 90%) yield (Scheme 61) as dark blue, dark green and dark purple microcrystalline solids, respectively.

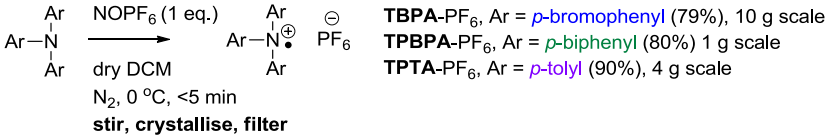

***Scheme 61**: Synthesis of triarylaminium radical salta with various para-substituents.*

2.3.5. Characterisation of Radical Cation Salts

Whilst the hexafluorophosphate anion could be observed by ^{19}F and ^{31}P NMR (single peak), the organic radical cations of **TBPA**, **TPBPA** and **TPTA** could not be observed by ^{1}H or ^{13}C NMR. The rapid relaxation time of free radical species during NMR spectroscopy leads to extremely broad signals and a very low signal-to-noise ratio.[177] Despite their single peak and apparent purities by LCMS (> 95%), mass spectrometry cannot distinguish between the radical salts (**TBPA**, **TPBPA** and **TPTA**) and the corresponding neutral triarylamines from which they were derived. By UV-visible absorption spectroscopy **TBPA**-PF_6 gave consistent peaks with the literature (Figure

19).[67] Similar peaks were observed for **TPTA**-PF_6 and different peaks were observed for **TPBPA**-PF_6 (see Appendix). Electron paramagnetic resonance (EPR) spectroscopy identified salts **TBPA**-PF_6, **TPBPA**-PF_6 and **TPTA**-PF_6 as radical species (Figure 20). For **TBPA**-PF_6, the signal shape, linewidth (70 G) and full-width half-maximum (12 G) correspond well with the literature (albeit with different counter anions present).[178] Salts **TPBPA**-PF_6 and **TPTA**-PF_6 showed similar EPR signals, with indications of hyperfine coupling observed for **TPBPA**-PF_6 (see Appendix).

Cyclic voltammetry characterised the oxidising power of salts **TBPA**-PF_6, **TPBPA**-PF_6 and **TPTA**-PF_6. Triarylamines **TBPA** and **TPTA** clearly showed reversible, one-electron oxidations by comparison with ferrocene as an external standard and potentials were consistent with reported values (Figure 21).[38,179] Poor solubility of **TPBPA** in the electrolyte solution (0.1 M *n*Bu_4NPF_6/MeCN) resulted in a weak, poorly resolved voltammogram whose current cannot be compared with ferrocene although an estimation of redox potentials can be made (see Appendix). The oxidation potential of **TBPA** [$E_{1/2}$ (**TBPA**$^{\bullet+}$/**TBPA**) = +1.10 V *vs.* SCE] being more positive than **TPTA** [$E_{1/2}$ (**TPTA**$^{\bullet+}$/**TPTA**)= +0.78 V *vs.* SCE] accords with inductive electronic effects (electron-withdrawing *para*-Br substituents *vs.* electron-donating *para*-CH_3 substituents). Whilst it is difficult to determine accurate information from the weak voltammogram of **TPBPA**, the oxidation potential appears to sit between **TBPA** and **TPTA** [$E_{1/2}$ (**TPBPA**$^{\bullet+}$/**TPBPA**) = +0.89 V *vs.* SCE].

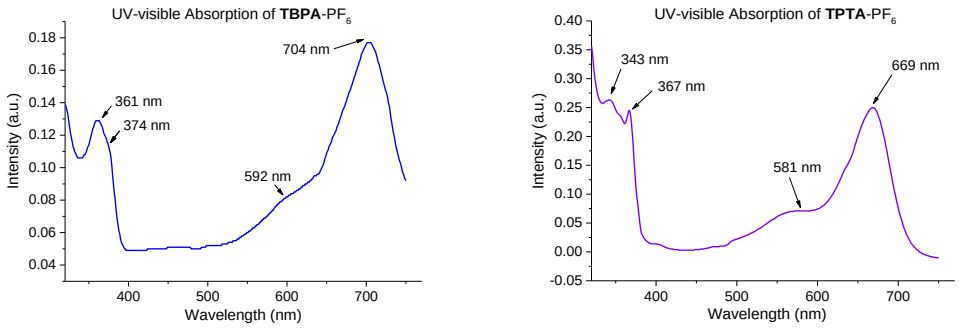

***Figure 19**: Ultraviolet-visible absorption spectra of **TBPA**-PF_6 and **TPTA**-PF_6.*

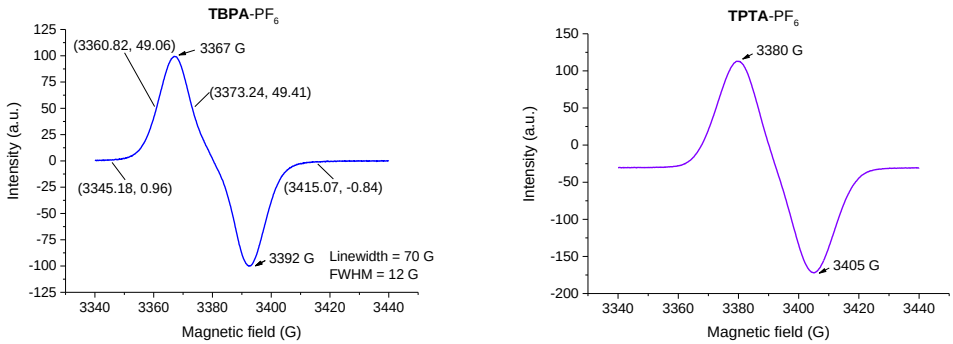

***Figure 20**: Electron Paramagnetic Resonance spectra of **TBPA**-PF_6 and **TPTA**-PF_6.*

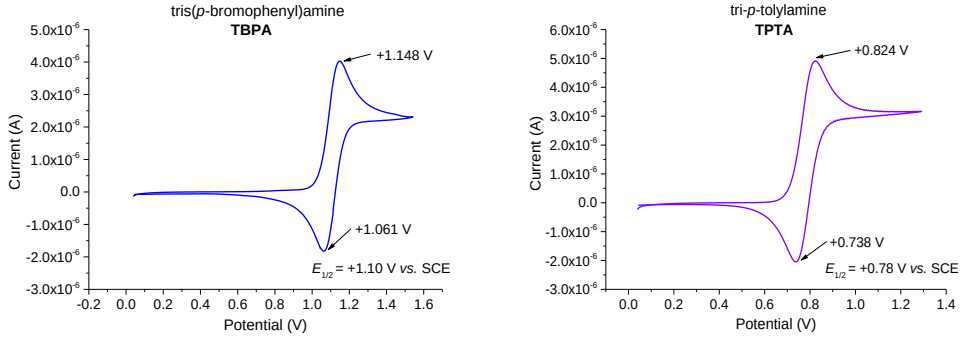

***Figure 21**: Cyclic voltammograms of **TBPA** and **TPTA**.*

2.3.6. Employment of Radical Cation Salts which are Susceptible to Nucleophiles

Initially, Jahn's conditions were applied to dextromethorphan (**73**) as a substrate, monitoring for *N*-demethylation (Table 11, see Section 5.19.1, Table 15, for the comprehensive data set). Pleasingly, operating under Jahn's conditions with K_2CO_3 as a base (alternating addition of **TBPA**-PF_6 and base, see Section 5.19.1 for details) revealed *nor*-dextromethorphan (**74**) by LCMS, but conversion was limited and an *N*-formyl by-product (**137**) resulted (Table 11, entry 3). A variation of Jahn's conditions employed 2,6-di-*tert*-butylpyridine (2.0 eq.), which Jahn added before starting the reaction and found higher selectivity for the deprotonation pathway.[67] Employing the analogous base 2,6-lutidine did not seem to alter the selectivity of reaction

with the *N*-formyl by-product (**137**) still observed (Table 11, entry 5). Interestingly, quinuclidine and DABCO markedly improved the selectivity in favour of *nor*-dextromethorphan **74** (Table 11, entries 6 and 7).

***Table 11**: Oxidation of dextromethorphan (**73**) by **TBPA**-PF_6 under various conditions.*

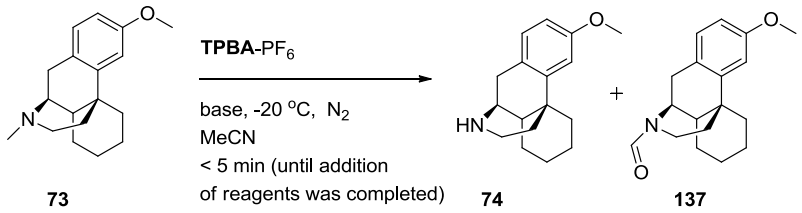

Entry	Base	Temperature, °C	Solvent	TBPA-PF_6, eq.	Ratio[a] 73 : 74 : 137
1	-	-20	MeCN, 10.0 eq. H_2O	2.5	1.0 : 0.2 : < 0.1
2	NaOAc	-20	MeCN, 10.0 eq. H_2O	2.5	1.0 : 0.1 : < 0.1[b]
3	K_2CO_3	-20	MeCN, 10.0 eq. H_2O	2.5	1.0 : 0.6 : 0.4[b]
4	-	0	dry MeCN	2	1.0 : 0.1 : < 0.1
5	2,6-lutidine	0	dry MeCN	2	1.0 : 0.5 : 0.4[c]
6	quinuclidine	0	dry MeCN	2	1.0 : 1.5 : 0.1[c,d]
7	DABCO	0	dry MeCN	2	1.0 : 0.5 : < 0.1[c,d]

[a]Ratio of **73** : **74** : **137** by LCMS (220 nm) at the time specified. [b]Portionwise addition of oxidant until colour is dark blue, then portionwise addition of base until colour is brown. [c]All base present at start, portionwise addition of oxidant. [d]base-oxidant adduct observed by LCMS.

Although quinuclidine supressed *N*-formyl product **137**, a new peak was detected by LCMS (M^+ = 515). Similarly, when DABCO was used, a new peak was detected (M^+ = 514). Masses are consistent with the cations of a quinuclidine or DABCO oxidant adduct (**138** or **139,** respectively), which form through nucleophilic attack on **TBPA**-PF_6 and loss of a bromine radical (Scheme 62). This was confirmed by a control reaction of DABCO with **TBPA**-PF_6, giving **139** as the sole product which was isolated as its trifluoroacetate salt (see Section 5.19.3 for details). Nucleophilic aromatic substitution reactions on tris(*p*-bromophenyl)aminium cations have been documented in the literature, with acetate ion or 2,3-diazabicyclo[2.2.2]oct-2-ene as nucleophiles.[180,181]

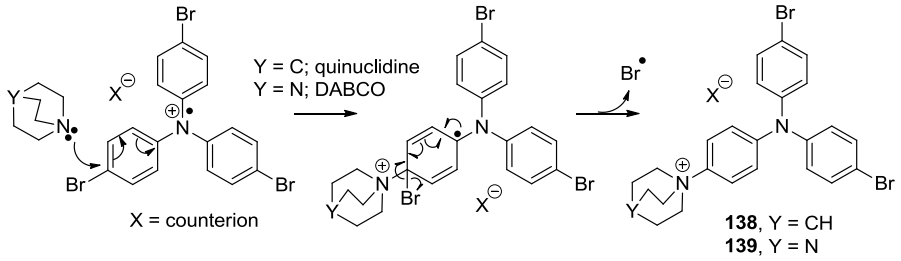

***Scheme 62**: S_NAr-type mechanism for nucleophilic addition to tris(p-bromophenyl)aminium radical cation.*

2.3.7. Employment of Radical Cation Salts which are Inert to Nucleophiles

Nucleophilic addition to both **TPBPA**-PF_6 and **TPTA**-PF_6 would be reversible due to the absence of a *para*-leaving group. Compared to **TPBPA**-PF_6, *para*-nucleophilic attack on **TPTA**-PF_6 might be disfavoured by inductive donation from the *para*-CH_3 group. In addition, solubility of **TPBPA** was poor and its synthesis was low yielding. Therefore, **TPTA**-PF_6 was selected as the oxidant, which effected smooth conversion of dextromethorphan (**73**) to *nor*-dextromethorphan (**74**) by LCMS. Comprehensive reaction optimisation was carried out to identify optimal conditions for this transformation. Investigations looked at the impact of order of addition, temperature, concentration, solvent,

oxygen, water, equivalents of **TPTA**-PF_6/DABCO and different nucleophiles (see Chapter 5.20). The optimum conditions were **TPTA**-PF_6 (3.4 eq.), DABCO (4.5 eq.), -5 ^oC temperature and anhydrous MeCN solvent. It is important to note that whilst *nor*-dextromethorphan is observed by LCMS, this is due to the aqueous conditions of the LCMS column effecting hydrolysis of a reactive intermediate (initially proposed to be iminium salt **140**).

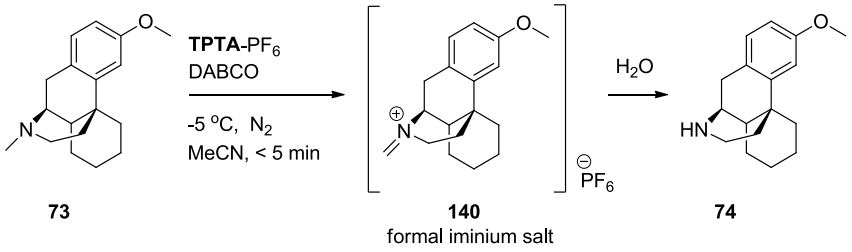

***Scheme 63**: N-Demethylation of dextromethorphan via initially proposed formal iminium salt.*

Since the reaction solvent is anhydrous MeCN, the reaction must proceed *via* an 'iminium'-type intermediate which undergoes hydrolysis during the aqueous conditions of the LCMS to give *nor*-dextromethorphan. It was initially proposed that this intermediate was a formal iminium salt (**140**), which could be trapped by organometallic nucleophiles and the latter was found to be the case (see Section 5.20.8). The optimal conditions were addition of organometallic (5.0 eq.) at 0 ^oC under N_2.

2.3.8. Regioselective C-H Functionalisation of Dextromethorphan using Grignard Reagents

Under the optimal conditions identified, a variety of Grignard reagents underwent successful addition to the stable iminium reservoir to give products **142** - **148** in good to excellent isolated yields (48 - 83%) over two steps (Table 12).

***Table 12**: Exocyclic C-H functionalisation of dextromethorphan (**73**) with a variety of organometallic nucleophiles.*[a]

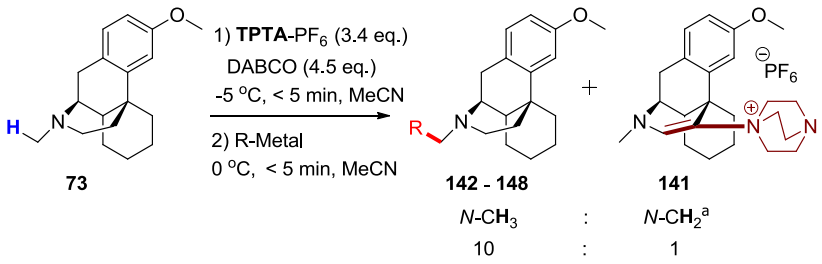

Entry	R-Metal	Product	Product Yield, %[b]	Recovered TPTA, %[b]
1	Et-MgBr	**142**	81	99
2	allyl-I/In[c]	**143**	71	99
3	cyclopropyl-MgBr	**144**	74	99
4	vinyl-MgBr	**145**	75	99
5	Ph-MgBr	**146**	83	99
6	4-pentenyl-MgBr	**147**	57	99
7	3-butenyl-MgBr	**148**	48	ND

[a]Aqueous work up instead of organometallic addition gave *nor*-dextromethorphan **74** (83%) and **141** (8%); thus selectivity was 10 : 1 in the oxidation step (see Scheme 64); [b]Isolated yields (%) after chromatography. [c]allyl iodide (3.0 eq.) premixed with In powder (2.0 eq.). ND = not determined.

Aware of the enhanced reactivity of allyl Grignards and allylzinc halides resulting in their reaction with MeCN (as identified in the previously mentioned study of *N*-aryl THIQs),[57] it was speculated that their high reactivity might not differentiate between the 'iminium' intermediate and MeCN. Therefore, allylindium sesquihalide was automatically selected as a nucleophile which underwent successful reaction to give desired product **143** in 71% yield. When the organometallic reagent was not added after the

oxidation reaction, aqueous work up and purification gave *nor*-dextromethorphan (**74**) in 83% yield (Scheme 64). This result corroborates an intermediate in the reaction, following *N*-C**H**$_3$ functionalisation, which is unstable to hydrolysis.

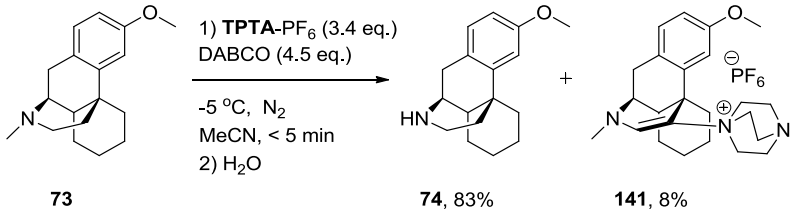

***Scheme 64**: Isolation of nor-dextromethorphan and a DABCO-enamine adduct following aqueous work up of the oxidation reaction of dextromethorphan.*

Interestingly, *N*-C**H**$_2$ functionalisation operated as a minor pathway giving rise ultimately to a DABCO-enamine by-product **141**, in 8% yield (therefore, *N*-C**H**$_3$ *vs. N*-C**H**$_2$ selectivity for dextromethorphan was deemed 10 : 1). Another feature of the reaction is the ability to easily recover **TPTA** in almost quantitative (99%) yield (> 95% purity) through a silica plug. Using aforementioned chemistry, **TPTA** can be easily and rapidly recharged into **TPTA**-PF_6 thereby demonstrating reagent recyclability which offsets the reagent-intensive oxidation.

2.3.9. Regioselective C-H Functionalisation of Trialkylamines using Grignard Reagents

Substrate scope of the **TPTA**-PF_6/DABCO mediated C-H functionalisation of trialkylamines is demonstrated in Table 13. In the trialkylamine scope, chemo- and highly regioselective functionalisation occurred in fair to high yields (48 - 81%) with the exception of **157** and **159**. Remarkably, *N*-methylmorpholine and benzyl-protected 1-methylpiperidin-4-ol gave exclusive regioselectivity for the *N*-C**H**$_3$ group (> 30 : 1),[†] affording products **155** and

[†]For selectivities > 30 : 1, the minor component could not be detected in the ^{1}H NMR spectrum of the crude reaction products.

156 in 77% and 77% yield. The secondary alcohol in tropine was tolerated in the synthesis of **154**. This contrasts with the KSCN/*t*BuOOH-mediated α-cyanation of trialkylamines reported by Ofial which gave oxidation to the ketone.[60] Esters α- and β- to the trialkylamine were tolerated; in the synthesis of **152**, no *N*-C**H**$_2$ functionalisation was observed despite the stabilising α-ester. Moving to substrates featuring highly electron-rich arenes, PMB-protected 1-methylpiperidin-4-ol gave exclusive *N*-C**H**$_3$ selectivity (> 30 : 1) at the trialkylamine for *N*-C**H**$_3$ functionalisation, but competing PMB cleavage resulted in an 18% yield of PMB-OH, in addition to 23% of the desired product (**157**) (starting material was recovered in 37% yield).

***Table 13**: Regioselective C-H functionalisation of trialkylamines.*[a]

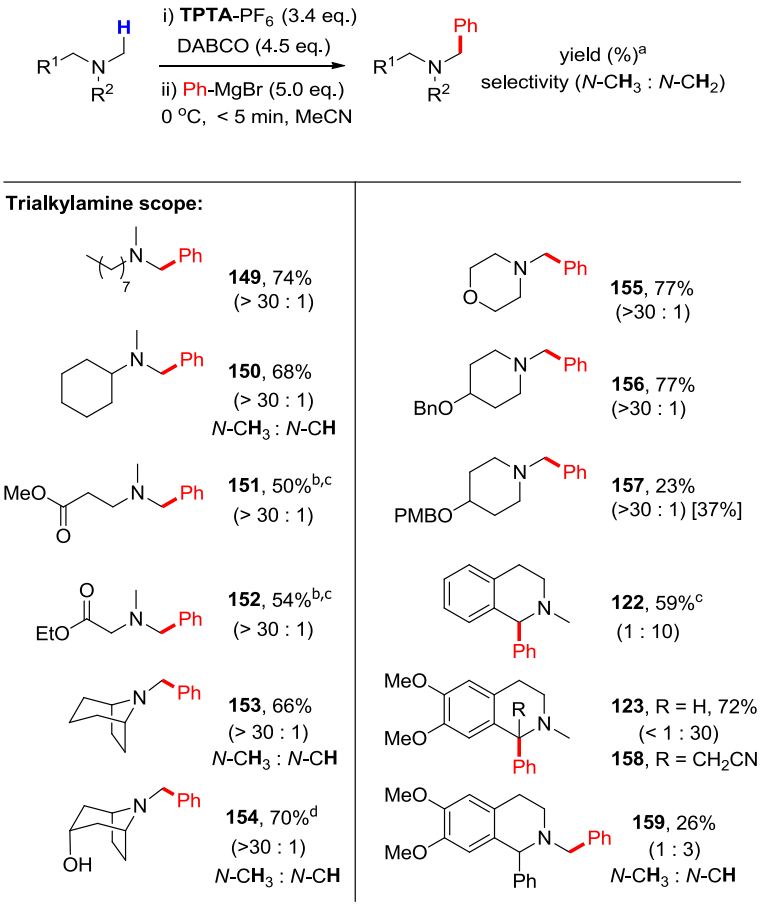

[†]For selectivities > 30 : 1, the minor component could not be detected in the ^{1}H NMR spectrum of the crude reaction products.

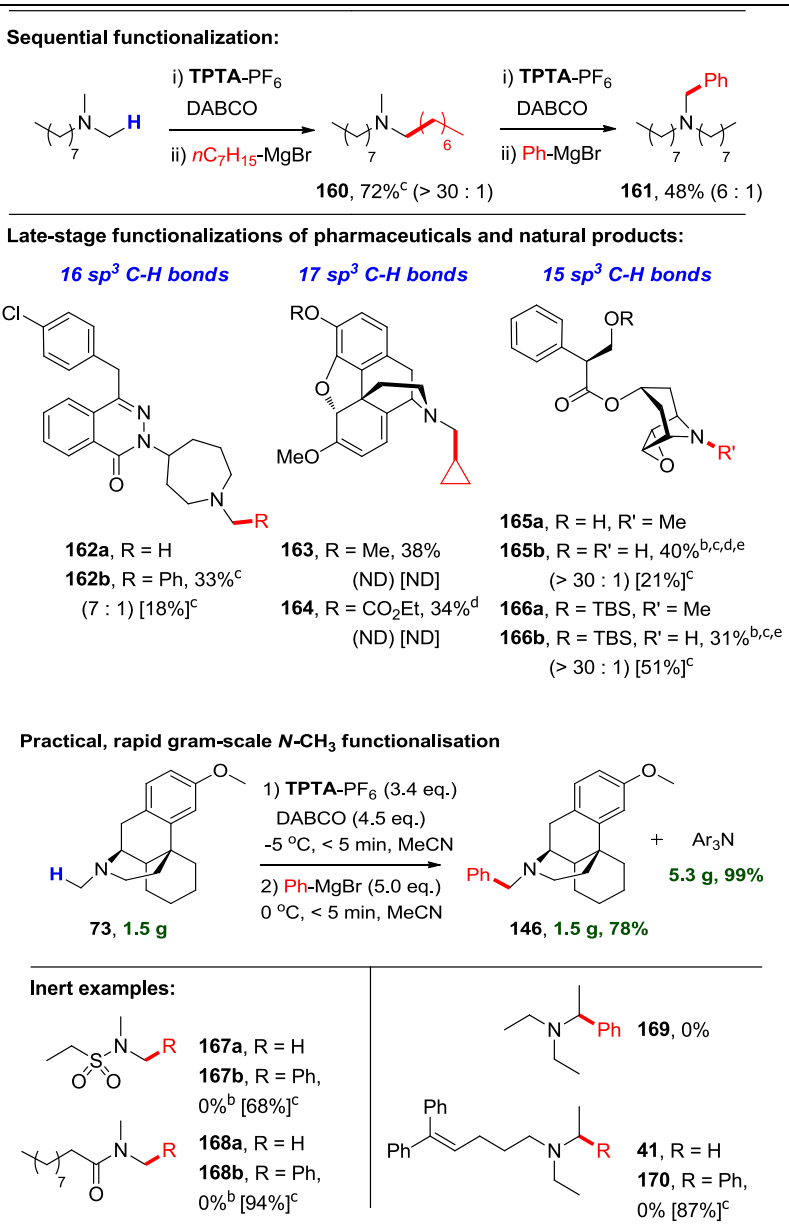

[a]Unless otherwise stated, isolated yields (%) after chromatography are given. Selectivities represent the ratio of *N*-C**H**$_3$: *N*-C**H**$_2$ functionalised products as determined by ^{1}H NMR. Yield of returned starting material, if detected, is determined by ^{1}H NMR and given in square brackets. Phenylmagnesium bromide is used unless otherwise shown. [b]An extra 1.0 eq. of sacrificial organometallic reagent used due to the free alcohol [c]Phenylzinc halide used due to sensitive functional groups. [d]Yield determined by ^{1}H NMR. [e]*N*-demethylation was observed. ND = not determined.

[†]For selectivities > 30 : 1, the minor component could not be detected in the ^{1}H NMR spectrum of the crude reaction products.

Isolation of PMB-OH rather than the expected aldehyde suggests formation of piperidin-4-one. Interestingly, for *N*-methyl THIQ derivatives **114** and **115**, complete reversal of regioselectivity occurred, resulting in functionalisation of the benzylic *N*-C**H**$_2$ to afford **122** and **123** in 59% and 72% yield respectively, contrasting with the other trialkylamines. However, functionalisation at the benzylic position is expected and is readily achieved in these cores.[42,49,57,155,182]

Subjecting the product **123** to the reaction conditions resulted in N-CH functionalisation (*N*-C**H**$_3$: *N*-C**H** selectivity = 1 : 3) to give an MeCN-adduct **158**, in addition to the *N*-C**H**$_3$ functionalised product (**159**). Sequential functionalisation of *N*,*N*-dimethyloctylamine was achieved, giving initially *N*-methyldioctylamine (**160**) in 72% yield (60% isolated yield) when the *n*-heptyl Grignard was employed. Functionalisation of the remaining *N*-C**H**$_3$ group of *N*-methyldioctylamine (**160**) with the phenyl Grignard gave **161** in 48% yield. In this second reaction, the selectivity was noteworthy at 6 : 1 selectivity in favour of *N*-C**H**$_3$ functionalisation, despite the statistical bias (1x *N*-C**H**$_3$ *vs*. 2x *N*-C**H**$_2$ positions). As examples of late-stage functionalisation, azelastine (**162a**), thebaine (featuring an *N*-C**H**$_3$ group) and thebaine's carbonate derivative (featuring an *N*-C**H**$_3$ group), were subjected to the reaction conditions and underwent successful *N*-C**H**$_3$ functionalisation to give **162b**, **163** and **164**, albeit in moderate yields (33 - 38%).

Interestingly, scopolamine (**165a**) and its protected analogue (**166a**) were also activated at the *N*-C**H**$_3$ group, but gave *N*-demethylation products **165b** and **166b** in 40% and 31% yields, respectively. It is proposed that the epoxide group might sterically deactivate the *N*-C**H**$_3$ group to HAT. The sulfonamide and amide *N*-C**H**$_3$ groups of **167a** and **168a** were untouched by the reaction conditions, highlighting the selectivity of the chemistry and its tolerance to electronically deactivated *N*-C**H**$_3$ groups. What was very striking was that trialkylamines containing only *N*-C**H**$_2$R positions gave no reaction under the conditions employed. Strikingly, triethylamine gave no successful reaction but recovery and quantification of starting material was not possible.

Therefore, non-volatile *N*,*N*-diethyl analogue **41** was employed and similarly gave no reaction. This observation markedly contrasts with previously reported trialkylamine functionalisations, which offered scope to engage trialkylamine *N*-C**H**$_2$R positions.[60,63,121,125] A second observation is that, in general, excellent to exclusive selectivity (6 : 1 to > 30 : 1) was observed for the *N*-C**H**$_3$ position over *N*-C**H**$_2$R or *N*-C**H**R$_2$ positions, with the highest levels of *N*-C**H**$_3$: *N*-C**H**$_2$ selectivity reported here competing with or exceeding those reported elsewhere. Even for non-cyclic trialkylamines such as *N*,*N*-dimethyloctylamine and the most testing *N*-methyldioctylamine (**160**); selectivities were > 30 : 1 and 6 : 1 in favour of *N*-C**H**$_3$ functionalisation, respectively.

These two observations indicated that the transformation proceeds through a different mechanism to that shown in Scheme 58, Section 2.3.1. (*via* the N-radical cation of the substrate). This led us to propose that successful reactivity and *N*-C**H**$_3$ selectivity derives from DABCO radical cation engaging in direct *H atom transfer* (HAT) with the trialkylamine substrate (Figure 22). Consistent with polarity matching expectations,[99,100] the electron-poor DABCO radical cation engages with the electron-poor α-amino C-H bond of trialkylamine **4**.

Following HAT, it is proposed that the intermediate α-amino radical **19** undergoes rapid trapping by a second molecule of DABCO$^{\bullet+}$ to yield metastable intermediate **171**.[†] This aligns with the known ability of trialkylamine radical cations to participate in HAT.[99,100,161,183] The relatively long lifetime of DABCO radical cation[183–185] renders it a likely partner for coupling with transient α-amino radicals,[161] according to the persistent radical effect.[122,123,184,186] The metastable intermediate **171** then undergoes an S_N2 reaction with an organometallic nucleophile to afford the *N*-C**H**$_3$ functionalised product. Experimental and computational evidence supporting this HAT mechanism are now outlined.

[†]Rapid oxidation of α-amino radical to an iminium salt which is intercepted by DABCO as a nucleophile cannot be ruled out as a pathway to **171**.

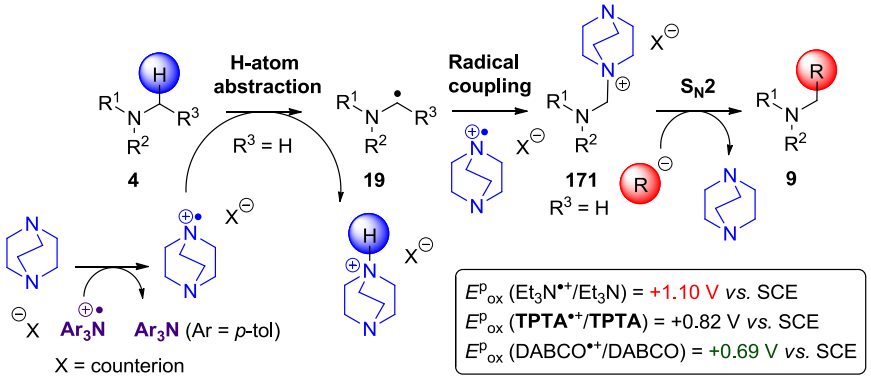

***Figure 22**: Proposed mechanism for the radical cation salt/DABCO-mediated C-H functionalisation of trialkylamines.*

2.3.10. Mechanistic Studies on the Regioselective C-H Functionalisation of Trialkylamines

Firstly, the identity of the metastable intermediate was elucidated. Following the oxidation reaction of dextromethorphan **73**, a range of soft nucleophiles was added (nitronates, silyl enol ethers, Cu-acetylides and potassium trifluoroborates) but no reaction was observed in any case. The non-reaction of soft nucleophiles was inconsistent with a formal iminium salt (**140**) as an intermediate, since formal iminium salts such as **140** are anticipated to be highly reactive (more reactive than the stable iminium salts derived from *N*-substituted THIQs, such as **26**, which do react with soft nucleophiles). Therefore, intermediate **172** (Figure 23) was proposed which underwent an S_N2 reaction (rather than an S_N1 reaction proceeding through formal iminium salt **140**). Though unstable to isolation, intermediate **172** was tentatively identified by ^{1}H NMR studies of a reaction in MeCN-d_3 (see Chapter 5.27). Adducts of this type have been reported when treating iminium salts with quinuclidine.[187,188]

In order to investigate whether the reaction mechanism involved oxidation of trialkylamine substrates to their N-radical cations, Jahn's oxidative cyclisation

[†]If DABCO is absent at the start and **TPTA**-PF_6 (3.4 eq.) and DABCO (4.5 eq.) are added portionwise, **42** is observed in 28% yield.

chemistry was revisited; where the intermediacy of N-radical cations is demonstrated *via* their rapid 5-*exo*-trig radical cyclisations.[67]

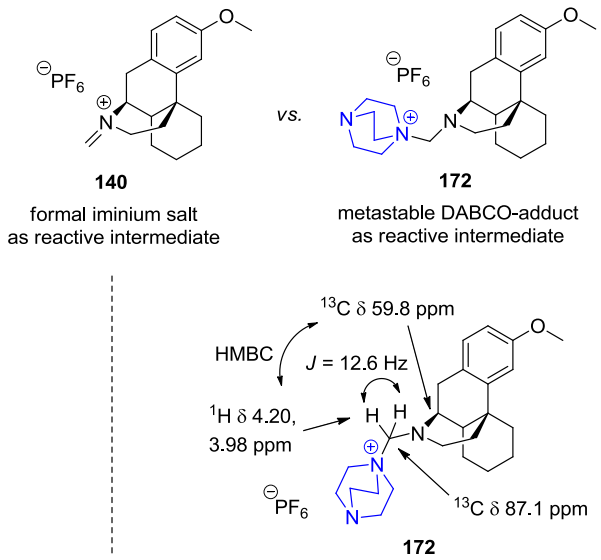

***Figure 23**: Left: Initially proposed formal iminium salt as the reactive intermediate vs. ultimately proposed identity of the reactive intermediate iminium equivalent. Right: Key NMR assignments and long range coupling observed.*

Using **TPTA**-PF_6 as oxidant under Jahn's conditions,[67] cyclisation of **41** occurred to afford **42** in 80% yield by ^{1}H NMR (Scheme 65) which is directly comparable with Jahn's **TBPA**-PF_6 result (Scheme 23, Section 1.4.3.). This confirms that **TPTA**-PF_6 [E^p_{ox} (**TPTA**$^{\bullet+}$/ **TPTA**) = +0.82 V *vs.* SCE] is capable of oxidising trialkylamines [E^p_{ox} ($Et_3N^{\bullet+}$/Et_3N) = +1.10 V *vs.* SCE] to N-radical cations despite this being thermodynamically uphill. This was rationalised by an irreversible driving force which manifests from precipitation; as **TPTA**-PF_6 is added to the reaction a white precipitate is observed (**TPTA**).

However, under the *N*-C**H**$_3$ functionalisation conditions where DABCO was present, substrate **41** gave no reaction and an 87% yield of starting material was observed by ^{1}H NMR.[†] Therefore, under these conditions the reaction does not proceed *via* the N-radical cation of the substrate. Therefore,

[†]If DABCO is absent at the start and **TPTA**-PF_6 (3.4 eq.) and DABCO (4.5 eq.) are added portionwise, **42** is observed in 28% yield.

DABCO is oxidised more rapidly than **41**, which accords with redox potentials, showing that DABCO [E^{p}_{ox} ($DABCO^{\bullet+}$/DABCO) = +0.69 V *vs.* SCE] undergoes more facile oxidation than triethylamine [E^{p}_{ox} ($Et_3N^{\bullet+}$/Et_3N) = +1.10 V *vs.* SCE]. Interestingly, when the analogous *N*,*N*-dimethyl-containing substrate **173** (using Jahn's conditions,[67] this did cyclise to give **174**) was employed, *N*-C**H**$_3$ functionalisation occurred to give **175** in 38% yield by ^{1}H NMR;[†] no 5-*exo* (N-radical cation) or 6-*exo* (α-amino radical) cyclisation was observed. When *N*,*N*-dimethyl-containing substrate **176** was employed in order to probe for α-amino radical intermediates, *N*-C**H**$_3$ functionalisation again occurred to give **177a** in 48% yield by ^{1}H NMR;[‡] no 5-*exo* (α-amino radical) cyclisation was observed.

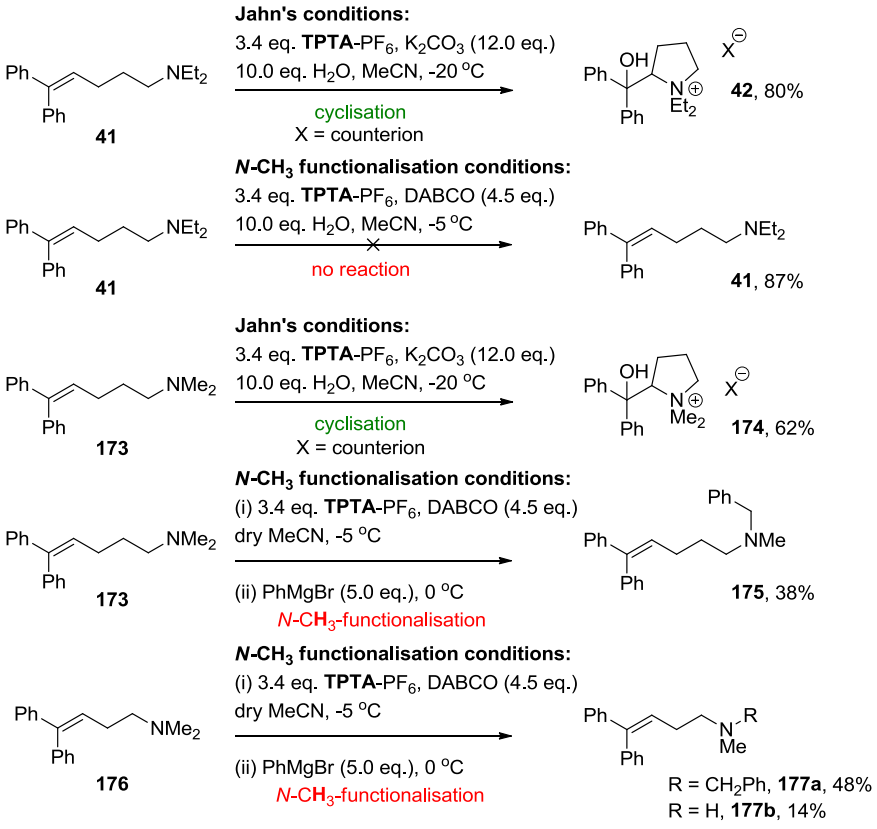

Scheme 65: *Reactions of radical cation and α-amino radical reporter substrates.*

[†]Despite the diminished yield, **175** was observed as the sole substrate-derived component in the ^{1}H NMR spectrum of the crude reaction products. [‡]*N*-demethylation also occurred, affording **177b** in 14% yield.

Though unexpected, the α-amino radical could still be an intermediate in the reaction mechanism if faster pathways were available than 5-*exo*-trig cyclisation. For example, if the coupling reaction of the α-amino radical and DABCO radical cation were to be very rapid. Alternatively, rapid oxidation to the formal iminium salt could occur, followed by nucleophilic addition of DABCO. In light of the established mechanism, the super-stoichiometric amounts of DABCO (4.5 eq.) and **TPTA**-PF_6 (3.4 eq.) required for full conversion in the oxidation step are now justified, in order to generate a sufficient concentration of $DABCO^{\bullet+}$ for HAT (and potentially for combination with the α-amino radical to give **171**). Computation was used to probe selectivity (*N*-C**H**$_3$: *N*-C**H**$_2$) in the HAT step, and the overall thermodynamic reaction profile (Figure 24).

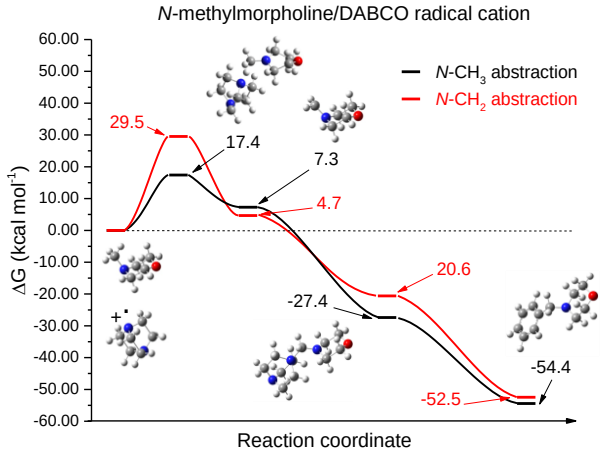

***Figure 24**: Reaction free energy (ΔG) profile for N-C**H**$_3$ vs. N-C**H**$_2$ H atom abstraction from N-methylmorpholine, formation of the N-C**H**$_3$-derived DABCO adduct intermediate and respective N-benzyl product. All starting materials, products and transition states were calculated using density functional theory (DFT) calculations using an unrestricted B3LYP functional with a 6-31+G(d,p) basis set and C-PCM implicit solvent model (acetonitrile) as implemented in Gaussian09.*

For *N*-methylmorpholine, the product radical of HAT from *N*-C**H**$_2$ (secondary radical) was more stable than that of HAT from *N*-C**H**$_3$ (primary radical) by 2.6 kcal mol^{-1}, as expected for the difference in energy between primary and secondary radicals (Table 14, entry 1).[185] Interestingly, however, the transition state for HAT from the *N*-C**H**$_3$ to DABCO radical cation is a staggering 12.1 kcal mol^{-1} lower in energy than the corresponding transition state for HAT from the *N*-C**H**$_2$. This accounts for the experimental selectivity observed (> 30 : 1). The resulting primary radical then follows a barrierless pathway to the *N*-methylmorpholine *N*-C**H**$_3$ DABCO-adduct. Overall, *N*-C**H**$_3$ functionalisation of *N*-methylmorpholine to give **155** is exergonic (ΔG = -54.4 kcal mol^{-1}) with a 17.4 kcal mol^{-1} barrier (sufficiently accessible through the Boltzmann distribution at -5 ^{o}C).† Similar selectivity was predicted for trimethylammonium radical cation as an HAT agent ($\Delta\Delta$G (T.S.) = 12.7 kcal mol^{-1}, Table 14, entry 2). Computing *N*-methylmorpholine with methyl radical (a smaller HAT agent) resulted in less pronounced *N*-C**H**$_3$ selectivity ($\Delta\Delta$G (T.S.) = 1.3 kcal mol^{-1}, Table 14, entry 3).

Substrates *N*-methyldiethylamine, *N*-methyldioctylamine (**160**), *N*-methyl-1,2,3,4-tetrahydroisoquinoline (**114**), 6,7-dimethoxy-*N*-methyl-1,2,3,4-tetrahydroisoquinoline (**115**) and dextromethorphan (**73**) were studied computationally to probe *N*-C**H**$_3$: *N*-C**H**$_2$ selectivity with the DABCO radical cation, trimethylammonium radical cation and methyl radical as abstractors. Smaller $\Delta\Delta$G (T.S.) was observed for DABCO radical cation abstracting from *N*-methyldioctylamine ($\Delta\Delta$G (T.S.) = 3.3 kcal mol^{-1}), with *N*-C**H**$_3$ abstraction giving the lower energy transition state, but higher energy primary radical product (Table 14, entry 5). It is worth noting that calculated $\Delta\Delta$G values are significantly larger than expected. In theory, a $\Delta\Delta$G = 1.4 kcal mol^{-1} predicts a selectivity of 10 : 1 and, for every additional 1.4 kcal mol^{-1}, selectivity should increase by an order of magnitude. However, this model

†Reactions with a 20 kcal mol^{-1} barrier proceed spontaneously at rt. At 25 ^{o}C, a fraction of 2.21 x 10^{-15} molecules have energies exceeding the activation energy according to the Boltzmann distribution. This translates to a barrier of 18 kcal mol^{-1} leading to a spontaneous reactions at -5 ^{o}C.

finds $\Delta\Delta G$ = 2.7 kcal mol^{-1} for the HAT reaction of dextromethorphan (**73**) with DABCO$^{\bullet+}$, which gives 10 : 1 *N*-C**H**$_3$: *N*-C**H**$_2$ selectivity experimentally. This highlightes the simplicity of the model used, which does not account for solvent effects in the transition state, computes at zero kelvin in the gas phase and assumes infinite dilution.[189] Importantly, though the absolute numbers are not reflective, a strong trend is observed between calculations and experiment as can be seen by comparing Table 14, entries 4 and 7.

***Table 14**: Difference in ΔG(T.S.) for a range of trialkylamine substrates and HAT agents.*

Entry	HAT reaction	ΔΔG(T.S.), kcal mol^{-1}	*N*-CH$_3$: *N*-CH$_2$[a]
1	*N*-methylmorpholine/DABCO$^{+\bullet}$	12.1[b]	> 30 : 1
2	*N*-methylmorpholine/Me$_3$N$^{+\bullet}$	12.7[b]	-
3	*N*-methylmorpholine/Me$^{\bullet}$	1.3[b]	-
4	dextromethorphan (**73**)/DABCO$^{+\bullet}$	2.7[b]	10 : 1
5	*N*-methyldioctylamine (**160**)/DABCO$^{+\bullet}$	3.3[b]	6 : 1
6	*N*-methyldioctylamine (**160**)/Me$^{\bullet}$	1.8[b]	-
7	*N*-methyl-1,2,3,4-tetrahydroisoquinoline (**114**)/DABCO$^{+\bullet}$	-2.6[c]	1 : 10
8	6,7-dimethoxy-*N*-methyl-1,2,3,4-tetrahydroisoquinoline (**115**)/DABCO$^{+\bullet}$	-3.8[c]	< 1 : 30

All starting materials, products and transition states were calculated using density functional theory (DFT) calculations using an unrestricted B3LYP functional with a 6-31+G(d,p) basis set and C-PCM implicit solvent model (acetonitrile) as implemented in Gaussian09. [a]Experimental selectivity *N*-C**H**$_3$: *N*-C**H**$_2$ determined by ^{1}H NMR of the crude reaction products. [b]The transition state for *N*-C**H**$_2$R HAT was is lower in energy than *N*-C**H**$_3$ HAT. [c]The transition state for *N*-C**H**R′R″ HAT is lower in energy than *N*-C**H**$_3$ HAT.

The computed barrier for *N*,*N*-dimethyldecanamide reinforces the notion that an electronic component to the HAT pathway is present which manifests in the non-reactivity of **167a** and **168a**, as well as the difference in selectivity in the formation of **122** and **123**. More intruguing is that computational results and experimental observations suggest that *steric factors* are heavily implicated in the success and selectivity of the HAT reaction. One steric factor is the hindrance around the trialkylamine substrate *N*-C**H**$_3$ and *N*-C**H**$_2$ positions. For *N*-methyl trialkylamines with more congested *N*-C**H**$_3$ groups, *N*-C**H**$_3$ *vs*. *N*-C**H**$_2$ selectivity is diminished. Whilst *N*-methylmorpholine gave product **155** in exclusive (> 30 : 1) *N*-C**H**$_3$: *N*-C**H**$_2$ selectivity, *N*-methyldioctylamine (**160**, which is more congested due to freely rotating alkyl groups) gave product **161** in less (6 : 1) *N*-C**H**$_3$: *N*-C**H**$_2$ selectivity.

On the other hand, for *N*-methyl THIQs with more congested benzylic positions, *N*-C**H**$_3$ *vs*. benzylic (*N*-C**H**$_2$ or *N*-C**H**) selectivity increases. Considering the syntheses of **123** and **159**, *N*-C**H**$_3$: benzylic position selectivity increases from almost none (1 : > 30) to 1 : 3 due to hindrance around the benzylic position when **123** is used as a substrate. For the late-stage functionalisation of azelastine (**162a**) to **162b**, flexibility in the 7-membered ring may explain the diminished *N*-C**H**$_3$: *N*-C**H**$_2$ selectivity (7 : 1). Steric interference of the neighbouring epoxide in **165a** and **166a** may hinder HAT and/or subsequent steps in the mechanism, leading to *N*-demethylation (although electronic effects likely play an additional role here).

Another steric factor is the hindrance of the HAT agent. Significantly diminished selectivity was observed computationally for the uncongested methyl radical, whereas notable selectivity was observed for trimethylammonium radical cation or DABCO$^{+\bullet}$, presumably due to the steric environment around the radical cation. An important steric factor is the structure of DABCO$^{+\bullet}$,[190] which sees the radical cation delocalised between the two nitrogen p-orbitals. As well as imparting stability to enhance lifetime,[183,184] this results in a steric 'cage' around the radical cation element, allowing DABCO$^{+\bullet}$ to be uniquely selective in its reactions.

The stabilisation of the radical cation serves to lower the oxidation potential of the N atom below that of an ordinary trialkylamine, such that $DABCO^{+\bullet}$ can be selectively generated in the presence of the trialkylamine substrate.

In summary, $DABCO^{+\bullet}$, generated *in situ* through the use of stable, rechargeable radical cation salts, engages in contra-thermodynamic HAT with trialkylamines with remarkable regioselectivity for *N*-C**H**$_3$ groups. Experimental observations and computational studies indicate the importance of steric and electronic effects to the *N*-C**H**$_3$: *N*-C**H**$_2$ selectivity of the reaction. The least stable, primary α-amino radicals are captured within metastable DABCO-adduct intermediates which can be readily intercepted with hard nucleophiles (organometallics or water), facilitating *N*-functionalisation in a single pot. The transformation is rapid, scalable and benefits from recyclable **TPTA**-PF_6. This *direct* *N*-functionalisation methodology has potential applications in medicinal chemistry. For example, the late-stage functionalisation of molecules or the investigation of structure-activity relationships, where changing a *N*-C**H**$_3$ to another *N*-alkyl group could drastically alter pharmacological activity of a molecule.

3. CONCLUSIONS

Volume 1 of this Thesis presents novel approaches toward *N*-functionalisation of trialkylamines with organometallic reagents. In Chapter 2.1., building on the work of Stephenson, novel photooxidation conditions were established with $[Ru(bpy)_3]^{2+}$, applicable to *N*-alkyl as well as *N*-aryl THIQs. Iminium salt intermediates (formed with exclusive selectivity for the benzylic *N*-C**H**$_2$ position) are intercepted by a wide range of organometallic nucleophiles in a single pot, affording products in good to excellent (62 - 95%) yields. The methodology is applied in a concise synthesis of the pharmaceutical, methopholine, which is of comparable efficiency to previous approaches. The chemistry served to exemplify application of visible-light photoredox catalysis towards sustainable manufacture at GSK. Scalability was successfully demonstrated in flow, where productivity reached 16.7 g / h (2.8 kilo / week).

Mechanistic studies, control reactions and observations in the literature revealed that *N*-substituted THIQs were highly privileged cores, undergoing facile oxidation to form stable intermediates. It was found that the photoredox reaction conditions which successfully oxidised *N*-substituted THIQs were unsuccessful with dextromethorphan (a trialkylamine mimicking a synthetic opioid). Redox potentials indicated slightly unfavourable themodynamics, backed by luminescence quenching experiments which revealed the poor interaction of $*[Ru(bpy)_3]^{2+}$ with trialkylamines. A number of photoredox processes in the literature had been proposed to function *via* reductive quenching of $*[Ru(bpy)_3]^{2+}$ by trialkylamines yet did not disclose photophysical data to support this, and so these were explored using luminescence quenching experiments in Chapter 2.2. Results dictated that the slow quenching of $*[Ru(bpy)_3]^{2+}$ by trialkylamines must indeed be the reactive pathway, since other components were poorer quenchers. However,

*$[Ru(bpy)_3]^{2+}$ was quenched very strongly by O_2 thus contesting the reductive quenching mechanism originally proposed by Xiao.[102] By employing the more oxidising *$[Ru(bpz)_3]^{2+}$, pronounced reductive quenching was observed in the presence of trialkylamines yet reactions did not proceed in the laboratory.

Finally, a non-photochemical approach to the *N*-functionalisation of trialkylamines was established in Chapter 2.3. Stable, rechargeable radical cation salts are used as oxidants which generate masked iminium salts with generally high regioselectivity for the *N*-C**H**$_3$ position. These masked iminium salts were trapped with organometallic reagents to afford products in good to excellent (48 - 83%) yields with notable chemoselectivity. The methodology was successfully applied to functionalise dextromethorphan on gram-scale. Sequential functionalisation of *N*,*N*-dimethyl-containing trialkylamines was demonstrated, and late-stage functionalisation of some pharmaceuticals and natural products was achieved in modest (31 - 40%) yields. Computational studies, redox potentials and radical cyclisation experiments corroborate the *in situ* formation of DABCO radical cation, a simple organic molecule which acts as a highly selective HAT agent in this unique transformation. Overall, Volume 1 of this Thesis describes how single electron oxidation has been harnessed to develop two complementary methods for *N*-functionalisation of tertiary amines with organometallic reagents.

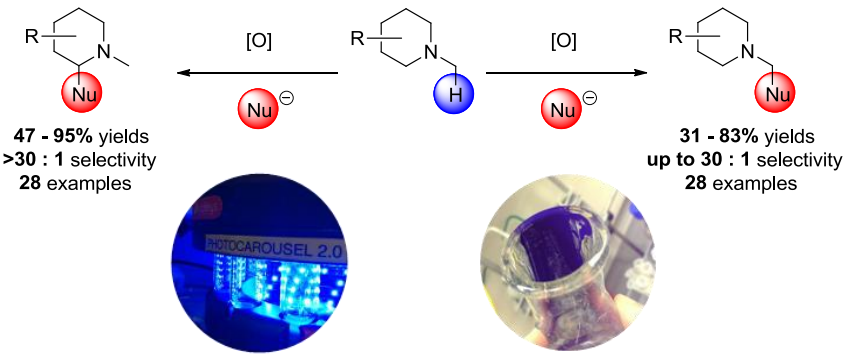

***Scheme 66**: Summary of work: Complementary methods for N-functionalisation of tertiary amines under single electron oxidation.*

4. Future Work

4.1. Identify the Mechanism of the Photocatalyst-free Visible-light Photogeneration of Iminium Salts from *N*-Substituted Tetrahydroisoquinolines using Bromoacetonitrile

Control reactions identified that visible-light powered oxidation of *N*-aryl THIQs with $BrCH_2CN$ proceeded in the absence of a photoredox catalyst, analogous to Zeitler's findings for reactions involving $BrCCl_3$.[58] A radical chain mechanism is suggested for reactions involving $BrCH_2CN$, consistent with that proposed by Zeitler for reactions involving $BrCCl_3$. However, further mechanistic studies are required to fully elucidate the mechanism. Future work to further elucidate the mechanism could include light on/off experiments and quantum yield measurements (to determine whether radical chains are operating), investigations of iminium salt formation mass balance (identification of impurities which compose the remaining mass balance and their structures which could inform a mechanistic proposal) and application of $BrCH_2CN$ in a Kharasch reaction[58] with an alkene (Scheme 67). As reported by Zeitler,[58] successful Kharasch reaction would demonstrate that initiation by homolysis and propagation by atom-transfer radical addition could operate. The formation of a visible-light active **EDA** complex between the *N*-aryl THIQ and $BrCH_2CN$ could be investigated by UV-visible spectroscopy, based on investigations of photocatalyst-free transformations reported by Melchiorre[191] and Zeitler.[58]

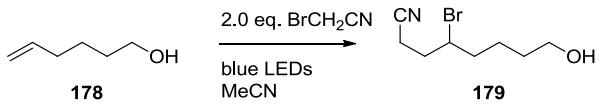

***Scheme 67**: Kharasch reaction to test homolytic cleavage of bromoacetonitrile by visible-light as an initiation pathway.*

4.2. To Increase Further Productivity of the Visible-Light Powered Oxidation of *N*-Substituted Tetrahydroisoquinolines in Flow

Visible-light powered oxidation of *N*-phenyl THIQ was scaled to a productivity of 16.7 g/h (2.8 kilo/week) in continuous flow, approaching the maximum capacity for the flow reactor setup. This result sufficed to establish proof of concept; that visible-light photochemistry could be successfully scaled at GSK. Due to time constraints, lack of available equipment and changing priorities, further optimisation either in terms of chemistry or engineering was deemed beyond the scope of the project and was not undertaken. Even higher productivities should be accessible through a combination of engineering controls and chemistry optimisation. Engineering controls could include: higher flow rates (higher capacity pumps), more intense light sources and shorter path lengths for light transmission. Chemistry optimisation in flow could investigate factors such as: light intensity, wavelength, solvent, concentration, temperature, flow rate and number of reagent equivalents. Optimisation could involve one factor at a time (OFAT) or statistical software such as Design of Experiments (DoE) could be employed.[192] By using DoE, interactions between factors can be identified. Chemistry optimisation could be conducted in batch, using photochemical screening plates for high-throughput analysis, then translated back to flow for scaling up.

4.3. Alternative Approaches to Generating DABCO Radical Cation

It was discovered that $DABCO^{\bullet+}$ functions as a highly selective HAT agent, yet it is currently generated *in situ* through the use or super-stoichiometric amounts of triarylaminium salts.[193] Literature precedent from the MacMillan group has demonstrated the generation of quinuclidinium radical cations in photoredox processes.[99,100] Herein, luminescence quenching studies revealed that DABCO is an excellent reductive quencher of $*[Ru(bpy)_3]^{2+}$.

Therefore, one could envisage generating DABCO$^{\bullet+}$ in this way to be used in a net-oxidative *N*-C**H**$_3$ functionalisation process (Scheme 68). Examples of terminal oxidants could include O_2 or $BrCCl_3$, where redox potentials indicate these species are sufficient to oxidise both the resulting $[Ru(bpy)_3]^+$ and (following HAT) the α-amino radical. Pioneering work by Molander, Fensterbank, Doyle and MacMillan has demonstrated coupling of alkyl radicals (generated *via* photoredox catalysis from silanes,[194,195] trifluoroborate salts,[126,127] carboxylate salts[196] thiols,[197] ethers[198] or *N*-Boc-protected amines[100]) to aryl halides *via* nickel catalysis (Johannes has found that oxygen can be crucial for the activation of the Ni(II) precatalyst and the reproducibility of these reactions).[199] On this basis, α-amino radicals could potentially be intercepted in a nickel catalytic cycle in order to directly couple trialkylamines to aryl halides in a catalytic fashion and without the need for preformed organometallic reagents (Scheme 69).

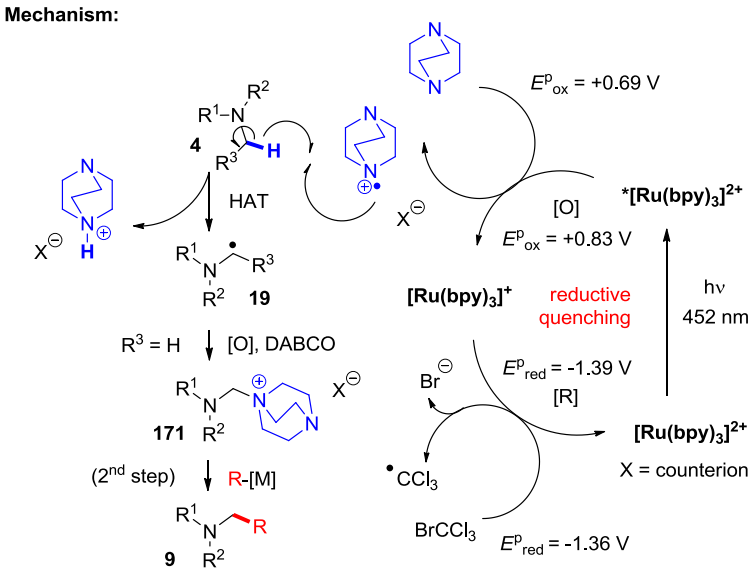

***Scheme 68**: Net-oxidative N-functionalisation of trialkylamines using photoredox catalysis to generate DABCO radical cation as a HAT agent.*

[†]Redox potentials are different here; a half-wave potential $E_{1/2}$ (in MeCN) is being compared with a standard potential E^0 (in DMF).

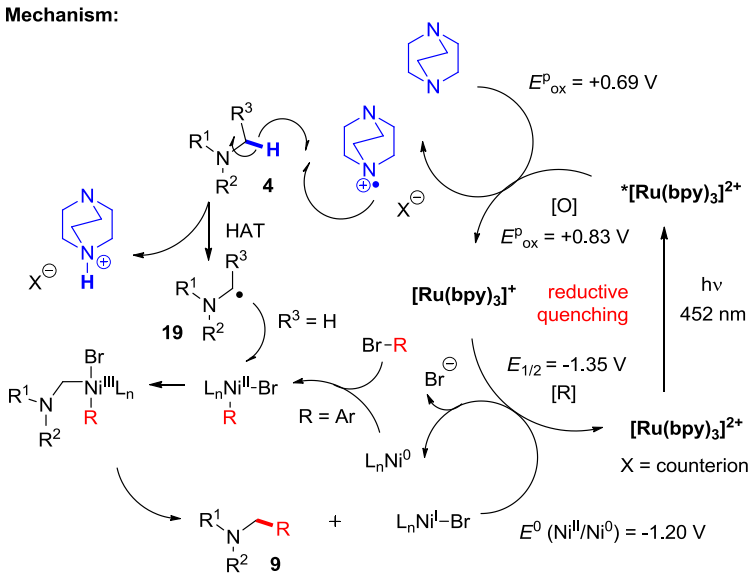

***Scheme 69**: Redox-neutral N-functionalisation of trialkylamines via merging photoredox catalysis with Ni-catalysis, using DABCO radical cation as a HAT agent.*[†]

Furthermore, due to the ease of oxidation of DABCO and because $[Ru(bpy)_3]^+$ is a potent reductant [the redox potential matches that of the corresponding $[Ir^{III}[dF(CF_3)ppy]_2(dtbpy)]^-$ species derived from the $Ir[dF(CF_3)ppy]_2(dtbpy)(PF_6)$ complex], $[Ru(bpy)_3]^{2+}$ could be used in place of expensive Ir-based complexes commonly used in these dual catalytic cycles. Potential issues could arise, depending on the rates of α-amino radical coupling to DABCO$^{\bullet+}$ *vs*. the nickel complex, or competing addition of DABCO$^{\bullet+}$ to the nickel complex.[193]

An alternative way to conduct the net-oxidative process would be electrochemical oxidation. Since DABCO undergoes more facile oxidation than trialkylamine substrates during CV,[193] it follows that aniodic oxidation could selectively generate DABCO$^{\bullet+}$ in the presence of the trialkylamine (Figure 25). Following HAT, the α-amino radical could either couple to DABCO$^{\bullet+}$ or donate an electron to the electrode surface (to afford a formal iminium salt primed to nucleophilic addition of DABCO).

[†]Redox potentials are different here; a half-wave potential $E_{1/2}$ (in MeCN) is being compared with a standard potential E^0 (in DMF).

Electrochemical oxidation would strip away the complexity of using triarylaminium salts, photocatalytic cycles and light sources and could be conducted and scaled in flow. An issue could be the requisite reaction at the cathode (protons are not present in the reaction mixture and are only generated during the reaction which may not be sufficient to complete the circuit). Typically, the cathode reaction involves reduction of a protic solvent such as H_2O, but the metastable DABCO-adduct will not tolerate aqueous conditions.[193] Therefore, use of a split cell configuration (which separates the cathodic and anodic reactions) could overcome this issue.

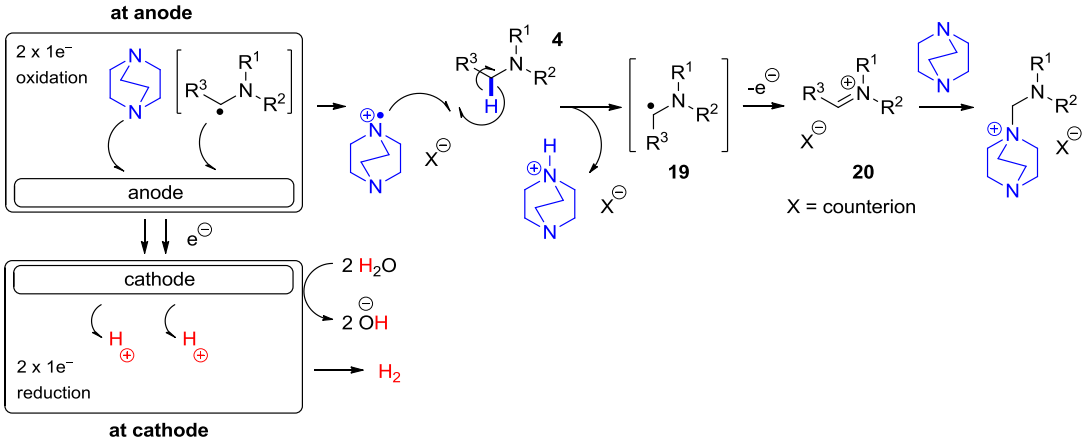

***Figure 25**: Generation of DABCO radical cation by anodic oxidation.*

Another issue could be achieving selective oxidation of DABCO if a potential is continuously applied between the electrodes. Photoredox catalysis may offer an advantage since the oxidant is an excited state which (although continuously generated) has a relatively short lifetime such that it might be more selective. Finally, the vast excess of electrolyte (normally a surfactant such as nBu$_4$NPF$_6$) required for electrochemical synthesis could be problematic to separate from the desired product.

4.4. Triarylaminium Radical Cation Salts as Super-Oxidising Photocatalysts

Herein, **TPBPA**-PF_6 was synthesised and identified as a stable and rechargeable radical cation salt which is a reasonably powerful oxidant [$E_{1/2}$ (**TPBPA**$^{\bullet+}$/**TPBPA**) = +0.89 V *vs.* SCE].[193] Since photoexcitation of a radical anion affords a super-reducing agent (as demonstrated by König),[106] it is conceived that photoexcitation of a radical cation (**TPBPA**-PF_6, λ_{max} = 412 nm) would afford a super-oxidising agent. Looking beyond trialkylamines, ***TPBPA**-PF_6 might be capable of oxidising arenes, alkenes or amides to radical cations. For example, a radical cation Diels-Alder cycloaddition reaction could be initiated by ***TPBPA**-PF_6 oxidising styrene **180**. The resulting radical cation undergoes stepwise [4+2]-cycloaddition to afford **181**, which can either close the photoredox cycle by oxidising **TPBPA**, or can oxidise **180** to propagate a radical chain reaction (Figure 26). The emission spectrum of ***TPBPA**-PF_6 is needed to predict its oxidation potential.

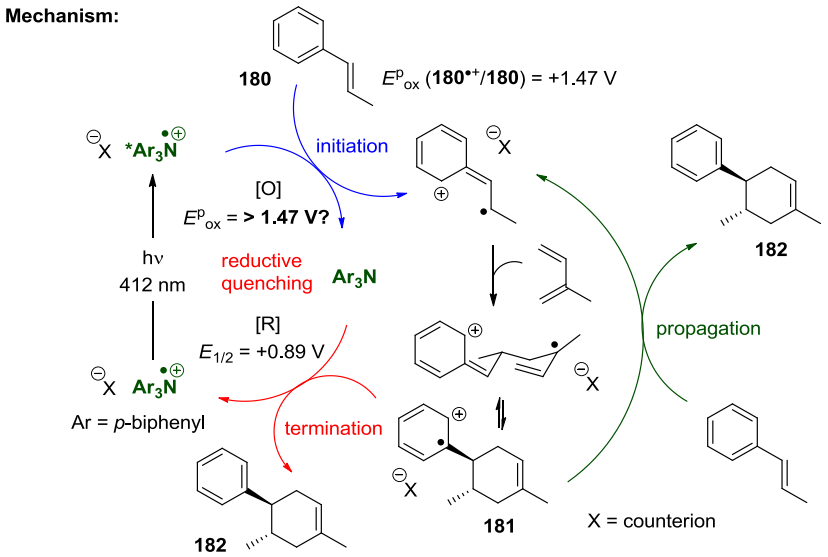

***Figure 26**: Photoexcited triarylaminium salt as a potent oxidant initiating a radical cation Diels-Alder cycloaddition.*

This proposal is inspired by Yoon's report of radical cation Diels-Alder cycloaddition of electron-rich styrene **183** with isoprene in the presence of

*[Ru(bpz)$_3$]$^{2+}$ [E^p_{ox} (*Ru^{II}/Ru^{I})= +1.45 V *vs*. SCE], which gave a 98% yield of **184** (Scheme 70).[200] A radical chain mechanism was subsequently identified by the quantum yield (Φ = 44.0), which directly compares to the chain length of the reaction if initiated by **TBPA**-SbF_6 (chain length = 41.0).[118] Taking advantage of the radical chain mechanism, an electrocatalytic 'redox tag' method was subsequently published following Yoon's work.[201] However, a limitation of Yoon's method is the necessity for electron-rich dienophiles; for example, styrene **180** (an unsubstituted phenyl ring) gave no reaction with isoprene, presumably due to its oxidation potential falling marginally out of range of *[Ru(bpz)$_3$]$^{2+}$ [E^p_{ox} (**180**$^{\bullet+}$/**180**) = +1.47 V *vs.* SCE].[200] The electrocatalytic method similarly gave no reaction of **180**.[201]

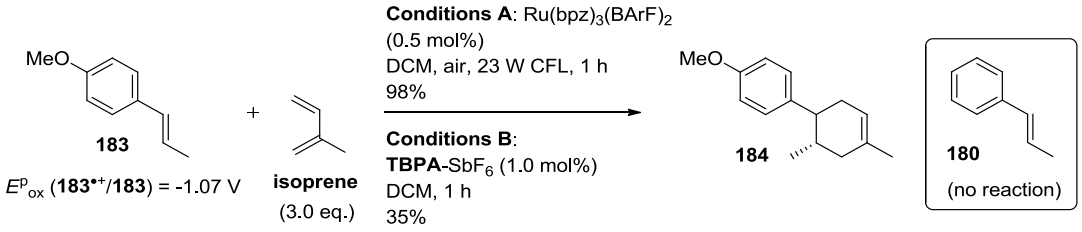

***Scheme 70**: Radical cation Diels-Alder cycloaddition initiated by *[Ru(bpz)$_3$]$^{2+}$ vs. triarylaminium salt.*[200]

Currently, acridinium-type salts developed by Fukuzumi[202] and popularised by Nicewicz[110,203] are the most oxidising and generally applied type of photoredox catalyst activated by visible-light ($E_{1/2}$ = +2.18 V to +2.32 V *vs.* SCE).[110] Nicewicz has demonstrated oxidation of alkenes, achieving overall anti-Markovnikov-selective alkene hydrofunctionalisation reactions.[204] In addition, oxidation of arenes has been demonstrated in a site-selective C-H amination reaction.[205] Super-oxidising photoexcited triarylaminium radical cation salts could be able to effect similar transformations. Given that the benzylic positions of **TPTA**-PF_6 are prone to reaction under certain conditions (for example, deprotonation or HAT), **TPBPA**-PF_6 could be the photocatalyst of choice here, or the triarylaminium salt derived from 4-methoxyphenyl-*N*,*N*-diphenylamine could be used [where E^p_{ox} ($Ar_3N^{\bullet+}$/Ar_3N) = +0.79 V *vs*. SCE].

5. EXPERIMENTAL

5.1. GENERAL EXPERIMENTAL DETAILS

Unless specified otherwise, reactions were carried out under an inert (N_2) atmosphere. Cryogenic conditions (-78 ^{o}C) were achieved using dry ice/acetone baths. Temperatures of 0 ^{o}C were obtained by means of an ice bath. 'Room temperature' (rt) indicates temperatures in the range of 20 - 25 ^{o}C. HPLC was conducted using an Agilent Technologies instrument (either 1100, 1200, 1260 or 1290 series) fitted with a Phenomenex Kinetex C18 column (8 minute method), or a Waters CsH C18 column (5 minute method), or a Agilent Zorbax SB C18 column (3 minute method), using a gradient of MeCN/H_2O with 0.05%(v/v) trifluoroacetic acid. HPLC product ratios are determined from the UV trace (220 nm).

LCMS was conducted using a Waters ZQ 2000 instrument fitted with either a Phenomenex Luna C18 column (low pH, 8 minute method) or a Waters XBridge C18 column (high pH, 5 minute method), using as eluent either a gradient of MeCN/10.0 mM ammonium bicarbonate in H_2O (High pH) or a gradient of MeCN/H_2O with 0.05%(v/v) trifluoroacetic acid (Low pH). Unless otherwise stated, LCMS product ratios were determined from the UV trace (220 nm). For purposes of thin layer chromatography (TLC), POLYGRAM SIL G/$_{UV254}$ silica plates were used, with UV light ($\lambda = 254$ nm) and potassium permanganate (in H_2O solution) or phosphomolybdic acid (in EtOH solution) used for visualisation.

Purification was generally achieved by normal phase column chromatography, either manually using Fluka analytical grade silica gel or, using a BIOTAGE SP4 purification instrument with BIOTAGE SNAP HP-Sil cartridges 25g, 50g, 100g and 300g. In some cases, crude material was dry-loaded onto celite prior to normal phase column chromatography. In some

cases, purification was achieved by reverse phase preparative LCMS using a Waters ZQ micromass ZQ 2000 instrument or, 'Mass Directed Autoprep' (MDAP), fitted with a Waters XBridge C18 column (or a Waters XSelect CSH C18 column) and using as eluent either a gradient of MeCN/10.0 mM ammonium bicarbonate in H_2O (High pH) or a gradient of MeCN/H_2O with 0.05%(v/v) trifluoroacetic acid (Low pH). In some cases, normal phase column chromatography gave some pure material and MDAP purification was used to recover further pure material from any contaminated column fractions.

All NMR data were collected using a Bruker Avance 400 Ultrashield instrument using 400 MHz, 376.5 MHz and 101 MHz for ^{1}H, ^{19}F and ^{13}C NMR, respectively. Data were manipulated using ACD/SpecManager version 12.5. Reference values for residual solvents were taken as δ = 7.27 ($CDCl_3$) and 2.50 ppm (DMSO-d_6) for ^{1}H NMR; δ = 77.00 ppm ($CDCl_3$) for ^{13}C NMR. Multiplicities for coupled signals were denoted as: s = singlet, d = doublet, t = triplet, q = quartet, m = multiplet, br. = broad, apt. = apparent and dd = double doublet *etc.* Coupling constants (*J*) are given in Hz. Where appropriate, COSY, DEPT, HSQC and HMBC experiments were carried out to aid assignment. Melting points were recorded using a Stuart Scientific SMP40 system. In this Volume, UV-visible absorption measurements were performed using a Merck Pharo 100 Spectroquant spectrophotometer. All samples were prepared at 1.0 x 10^{-5} M. For UV-visible spectra of photocatalysts and triarylaminium salts, see Appendix.

In this Volume, infrared data were collected using a Perkin-Elmer Spectrum 100 FTIR spectrometer as a thin film unless otherwise stated. High Resolution Mass spectral analyses were carried out at ESPRC National Mass Spectrometry Service Centre in Swansea on a LTQ Orbitrap XL instrument, or using an in-house service on either a Thermo Fisher Exactive instrument or a Bruker maXis impact instrument. Instruments used a quadrupole time-of-flight (Q-TOF) technique with Atmospheric Pressure Chemical Ionisation (APCI), Electrospray Ionisation (ESI) or High Resolution

Nano-Electrospray Ionisation (HNESP), and masses observed are accurate to within 5 ppm. All solvents and reagents were purchased from reputable suppliers (for example, Sigma-Aldrich, Alfa Aesar, Fluorochem) and were generally used as supplied or, in some cases, purified using standard techniques.[206] Prior to use, all reaction vessels involved in the synthesis of organometallic reagents were dried overnight in a vacuum oven (> 50 ^{o}C); all manipulations were performed under N_2. All novel compounds (structures for which literature data could not be found) are denoted with italic and bold numbers.

5.2. PHOTOCHEMICAL REACTORS

Visible-light photochemical reactions were initially carried out using a Professional LED 30 W floodlight (model no. A65KN) with λ_{max} = 449 nm, positioned *ca*. 10 cm from the reaction (Figure 7, left, Section 2.1.1.). Ultimately, batch reactions were performed in Radleys (RR91080 quick-thread glass reaction tube and RR91088 quick-thread decreased volume) reaction vessels with lids (PTFE quick-thread) fitted with a gas tap and rubber septum (Figure 7, middle, Section 2.1.1.). These reaction vessels were placed in a Radleys parallel reactor which had a blue LED 24 W strip (λ_{max} = 458 nm) wrapped around the central reservation (2 m length used, 6x coils), such that the distance between the LED strip and reaction vessels was *ca*. 2 cm. Degassing was achieved using 3 x freeze/pump/thaw cycles. Reaction vessels were triple evacuated/N_2 filled after sample taking. Flow photochemistry was performed using a Vapourtec Ltd. UV-150 Photochemical Reactor (R-Series) 10 mL coil, equipped with a fibre-optic emission probe and a 60 W blue LED (λ_{max} = 449 nm) or violet LED (λ_{max} = 424 nm) bank (Figure 7, right, Section 2.1.1.). Degassing was achieved with N_2 sparging for 20 min.

5.3. CYCLIC VOLTAMMETRY

For general experimental details pertaining to cyclic voltammetry, see Appendix. In this Volume, all solutions were prepared at 10.0 mM concentration (in 0.1 M nBu$_4$NPF$_6$/MeCN as solvent) using anhydrous, degassed MeCN. Ru(bpz)$_3$(PF$_6$)$_2$ was analysed at 1.0 mM concentration. Peak heights are given in amps (A); ferrocene was used as an external standard to ensure consistency throughout the study and whose peak height corresponds to a one-electron oxidation. All samples were completely soluble in the electrolyte solution, with the exception of tri-*p*-biphenylamine which was sparingly soluble. Except tri-*p*-biphenylamine, all tertiary amines gave similar peak heights to ferrocene, corresponding to a one-electron oxidation. Potentials are given relative to the saturated calomel electrode (*vs.* SCE).

5.4. STEADY-STATE LUMINESCENCE MEASUREMENTS

Steady-state luminescence measurements were performed using a HORIBA Jobin Yvon Fluorolog 3-22, which comprised an Ushio UXL 450S-O 450 W xenon short arc lamp as an excitation source, 200 - 900 nm double grating excitation and emission monochromators and a R928 Hamamatsu photomultiplier tube. The integration time was set to 0.1 s and the slit widths were 5 nm for both excitation and emission. The excitation monochromator was set to 450 nm and emission set to measure 460 - 800 nm. A signal detector (S1) was enabled to measure the intensity signal (counts s^{-1}) and a reference detector (R1) was enabled to compensate for light source fluctuations (μA). Therefore, 'Intensity' refers to S1/R1 with the unit: counts s^{-1}/μA but is given arbitrary units (a.u.) for simplicity.

All photocatalyst solutions were prepared at 2.0 x 10^{-5} M concentration in MeCN. Quencher solutions were generally prepared at 1.5 x 10^{-2} M in MeCN. In some cases, more concentrated (0.15 M in MeCN) solutions were prepared. The catalyst solution (1 mL) was diluted with different volumes of quencher solutions and different volumes of MeCN to achieve 1.0 x 10^{-5} M

catalyst together with the desired quencher concentration in a total volume of 2 mL. For example, 1 mL of a solution of $Ru(bpy)_3(PF_6)_2$ (2.0×10^{-5} M in MeCN) was combined with 0.5 mL of a solution of *N*,*N*-dimethylaniline (1.5×10^{-2} M in MeCN) and 0.5 mL of MeCN to give a sample containing $Ru(bpy)_3(PF_6)_2$ (1.0×10^{-5} M) and *N*,*N*-dimethylaniline (3.75×10^{-3} M) in 2 mL MeCN.

Sample degassing was achieved by bubbling sealed cuvettes through a needle with Ar/N_2 for 5 min and measuring immediately. Care was taken to ensure a constant gas flow rate for a given set of samples from the N_2/Ar cylinder, and control samples containing photocatalyst only were run at intervals and used to calibrate data accordingly. For details and comparisons of degassing methods, see Appendix.

5.5. TIME-RESOLVED LUMINESCENCE MEASUREMENTS

Time-resolved luminescence measurements and lifetime measurements were performed using the time-correlated single photon counting technique (TCSPC) with or without Multi-Channel Scaling (MCS) on a HORIBA Jobin Yvon FluoroCube. Excitation was performed using either pulsed LEDs operating at 1 MHz repetition rate (excitation at 471 nm for $[Ru(bpy)_3]^{2+}$ and $[Ru(bpz)_3]^{2+}$, monitoring phosphorescence emission at 606 nm and collecting data in the 340 μs measurement range). Low absorption was maintained at the excitation wavelength (A = 0.1) and lifetimes were measured at the magic angle (54.7°). Lifetimes were obtained using HORIBA DAS6 decay analysis software where decays were fitted to one exponential.

Lifetime and Stern-Volmer data pertaining to Table 8, entry 2 (one of the two replicates) entries 6-7, 9-10, 14-15, 18-19, 21 and 23-32 were obtained by Katie Emery at the University of Strathclyde.

5.6. ELECTRON PARAMAGNETIC RESONANCE MEASUREMENTS

All EPR solutions were prepared at 1.0 x 10^{-2} M concentration in MeCN. EPR spectra were recorded on a Bruker EMX 10/12 spectrometer operating at 9.5 GHz with 100 kHz modulation. All samples were prepared in NMR tubes inside a glovebox under N_2. EPR data were processed using WinSIM Public EPR Software Tools (P.E.S.T.) software (MS-Windows 9x, NT, Version 0.98) from the National Institute of Environmental Health Sciences. All EPR samples were analysed by Prof. John C. Walton at the University of St. Andrews.

5.7. PREPARATION OF *N*-SUBSTITUTED TETRAHYDROISOQUINOLINES

N-Phenyl-1,2,3,4-tetrahydroisoquinoline (**23**)

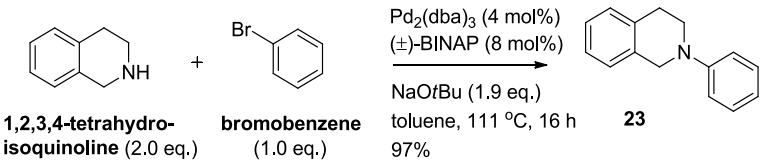

Prepared according to a literature procedure.[133] A flask was charged with tris(dibenzylideneacetone)dipalladium(0) (1.28 g, 1.40 mmol, 4 mol%), (±)-2,2′-bis(diphenylphosphino)-1,1′-binaphthalene (1.74 g, 2.79 mmol, 8 mol%) and toluene (100 mL). The reaction was degassed for 10 min before stirring at reflux (111 °C) for 15 min. The reaction mixture was allowed to cool to rt before sodium *tert*-butoxide (6.41 g, 66.6 mmol, 1.9 eq.), bromobenzene (3.7 mL, 35.1 mmol, 1.0 eq.) and 1,2,3,4-tetrahydroisoquinoline (8.8 mL, 70.3 mmol, 2.0 eq.) were added. The reaction mixture was stirred at reflux (111 °C) for 16 h, before being cooled to rt and filtered through celite. The filtrate was concentrated in vacuo to yield a black oil, which was purified by column chromatography (a gradient of 1 - 5% EtOAc/heptane) to afford **23** as a pale yellow microcrystalline solid (7.1 g, 97%), m.p. 46 - 48 °C (lit. 45 - 46 °C[41]); IR ν_{max} (neat) 3039 - 2825 (C-H), 1660 (Ar), 1597 (Ar), 1500 (Ar), 1448, 1432, 1387, 1337, 1292, 1268, 1227, 1209 cm^{-1}; ^1H NMR (400 MHz, $CDCl_3$) δ 7.33

- 7.28 (2H, m, C*H*), 7.16 (4H, m, C*H*), 6.99 (2H, d, *J* = 7.9 Hz, C*H*), 6.82 (1H, t, *J* = 7.4 Hz, C*H*), 4.41 (2H, s, CH_2), 3.56 (2H, t, *J* = 5.9 Hz, CH_2), 2.98 (2H, t, *J* = 5.9 Hz, CH_2); ^{13}C NMR (101 MHz, $CDCl_3$) δ 150.6 (*C*), 134.9 (*C*), 134.5 (*C*), 129.2 (*C*H), 128.5 (*C*H), 126.5 (*C*H), 126.3 (*C*H), 126.0 (*C*H), 118.7 (*C*H), 115.1 (*C*H), 50.8 (*C*H_2), 46.5 (*C*H_2), 29.1 (*C*H_2); HRMS (+ESI) *m/z* calculated for $C_{15}H_{16}N$ [M+H$^+$] 210.1283; Found 210.1277. Data are consistent with the literature.[41,46]

N-Naphthyl-1,2,3,4-tetrahydroisoquinoline (109)

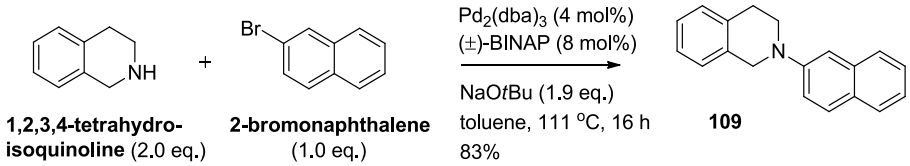

1,2,3,4-tetrahydro-isoquinoline (2.0 eq.) | **2-bromonaphthalene** (1.0 eq.) | **109**

Prepared according to a literature procedure.[133] Following reaction of 1,2,3,4-tetrahydroisoquinoline (1.8 mL, 14.4 mmol, 2.0 eq.), 2-bromonaphthalene (1.50 g, 7.20 mmol, 1.0 eq.), sodium *tert*-butoxide (1.31 g, 13.6 mmol, 1.9 eq.), tris(dibenzylideneacetone)dipalladium(0) (0.28 g, 0.31 mmol, 4 mol%), (±)-2,2′-bis(diphenylphosphino)-1,1′-binaphthalene (0.36 g, 0.58 mmol, 8 mol%) in refluxing (111 °C) toluene (25 mL) for 16 h, filtration through celite and concentration *in vacuo* yielded a black oil, which was purified by column chromatography (a gradient of 5 - 20% toluene/heptane (1% Et_3N)) to afford **109** as a white microcrystalline solid (1.56 g, 83%); m.p. 88 - 90 °C; IR ν_{max} (neat) 3056 - 2803 (C-H), 1627 (Ar), 1592 (Ar), 1508 (Ar), 1456 (Ar), 1376, 1344, 1273, 1252, 1220 cm^{-1}; ^{1}H NMR (400 MHz, $CDCl_3$) δ 7.79 - 7.69 (3H, m, C*H*), 7.41 (1H, td, *J* = 6.9 Hz, 1.2 Hz, C*H*), 7.38 (1H, dd, *J* = 9.0 Hz, 2.5 Hz, C*H*), 7.29 (1H, td, *J* = 8.0 Hz, 1.1 Hz, C*H*), 7.24-7.18 (5H, m, C*H*), 4.54 (2H, s, CH_2), 3.69 (2H, t, *J* = 5.9 Hz, CH_2), 3.06 (2H, t, *J* = 5.8 Hz, CH_2). Data are consistent with literature.[133]

6,7-Dimethoxy-1,2,3,4-tetrahydroisoquinoline (110)

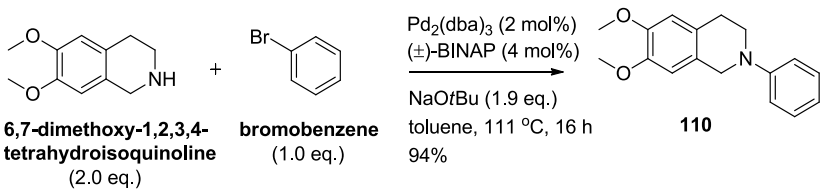

6,7-dimethoxy-1,2,3,4-tetrahydroisoquinoline (2.0 eq.)

bromobenzene (1.0 eq.)

Prepared according to a literature procedure.[133] Following reaction of 6,7-dimethoxy-1,2,3,4-tetrahydroisoquinoline (1.83 mL, 9.47 mmol, 2.0 eq.), bromobenzene (0.50 mL, 4.74 mmol, 1.0 eq.), sodium *tert*-butoxide (0.87 g, 9.02 mmol, 1.9 eq.), tris(dibenzylideneacetone)dipalladium(0) (0.18 g, 0.19 mmol, 4 mol%), (±)-2,2′-bis(diphenylphosphino)-1,1′-binaphthalene (0.23 g, 0.37 mmol, 8 mol%) in refluxing (111 °C) toluene (20 mL) for 16 h, filtration through celite and concentration *in vacuo* yielded a black oil, which was purified by column chromatography (a gradient of 5 - 20% EtOAc/heptane (1% Et_3N)) to afford **110** as a white microcrystalline solid (1.20 g, 94%); m.p. 97 - 99 °C (lit. 92 - 94 °C[207]); IR ν_{max} (neat) 3001 - 2808 (C-H), 1600 (Ar), 1577 (Ar), 1518 (Ar), 1504 (Ar), 1463 (Ar), 1448, 1416, 1379, 1338, 1321, 1269, 1252, 1236, 1211 cm^{-1}; ^1H NMR (400 MHz, $CDCl_3$) δ 7.27 (2H, apt. t, *J* = 7.8 Hz, C*H*), 6.98 (2H, apt. d, *J* = 8.4 Hz, C*H*), 6.82 (1H, apt. t, *J* = 7.3 Hz, C*H*), 6.64 (1H, s, C*H*), 6.63 (1H, s, C*H*), 4.32 (2H, s, CH_2), 3.86 (3H, s, CH_3), 3.85 (3H, s, CH_3) 3.53 (2H, apt. t, *J* = 5.8 Hz, CH_2), 2.88 (2H, apt. t, *J* = 5.7 Hz, CH_2); ^{13}C NMR (101 MHz, $CDCl_3$) δ 150.6 (*C*), 147.6 (*C*), 147.5 (*C*), 129.2 (*C*H) 126.7 (*C*), 126.2 (*C*), 118.7 (*C*H), 115.3 (*C*H), 111.4 (*C*H), 109.4 (*C*H), 56.0 (CH_3), 55.9 (CH_3), 50.5 (CH_2), 46.7 (CH_2), 28.5 (CH_2); HRMS (+APCI) *m/z* calculated for $C_{17}H_{20}NO_2$ $[M+H^+]$ 270.1494; Found 270.1490. ^1H and ^{13}C NMR data are consistent with the literature.[207] There is a discrepancy between the literature and observed melting point.

N-(*p*-Methoxyphenyl)-1,2,3,4-tetrahydroisoquinoline (111)

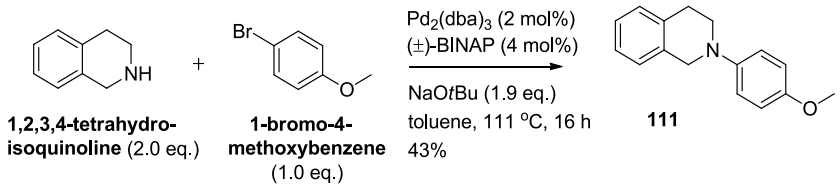

1,2,3,4-tetrahydro-isoquinoline (2.0 eq.) + **1-bromo-4-methoxybenzene** (1.0 eq.)

Prepared according to a literature procedure.[133] Following reaction of 1,2,3,4-tetrahydroisoquinoline (2.0 mL, 16.0 mmol), 1-bromo-4-methoxybenzene (1.0 mL, 8.0 mmol), sodium *tert*-butoxide (1.46 g, 15.2 mmol, 1.9 eq.), tris(dibenzylideneacetone)dipalladium(0) (0.29 g, 0.32 mmol), (±)-2,2′-bis(diphenylphosphino)-1,1′-binaphthalene (0.40 g, 0.64 mmol) in refluxing (111 ^{o}C) toluene (25 mL) for 16 h, filtration through celite and concentration *in vacuo* yielded a brown oil, which was purified by column chromatography (a gradient of 1 - 5% EtOAc/heptane) to afford **111** as a white microcrystalline solid (0.82 g, 43%); m.p. 88 - 90 ^{o}C (lit. 92 - 94 ^{o}C[208]); IR ν_{max} (neat) 2997 - 2751 (C-H), 1584 (Ar), 1509 (Ar), 1459 (Ar), 1442, 1384, 1349, 1331, 1301, 1273, 1206 cm^{-1}; ^{1}H NMR (400 MHz, $CDCl_3$) δ 7.19 - 7.09 (4H, m, C*H*), 6.99 (2H, d, *J* = 9.1 Hz, C*H*), 6.88 (2H, d, *J* = 9.0 Hz, C*H*), 4.29 (2H, s, CH_2), 3.77 (3H, s, CH_3), 3.44 (2H, apt. t, *J* = 5.8 Hz, CH_2), 2.98 (2H, apt. t, *J* = 5.8 Hz, CH_2); ^{13}C NMR (101 MHz, $CDCl_3$) δ 153.5 (*C*), 145.4 (*C*), 134.6 (2 x *C*), 128.7 (*C*H), 126.5 (*C*H), 126.3 (*C*H), 125.9 (*C*H), 118.0 (*C*H), 114.6 (*C*H), 55.6 (*C*H_3), 52.7 (*C*H_2), 48.4 (*C*H_2), 29.1 (*C*H_2); HRMS (+APCI) *m/z* calculated for $C_{18}H_{24}NO$ [M+H^{+}] 240.1388; Found 240.1382. ^{1}H and ^{13}C NMR data are consistent with the literature.[208] There is a discrepancy between the literature and observed melting point.

N-(*p*-Bromophenyl)-1,2,3,4-tetrahydroisoquinoline (112)

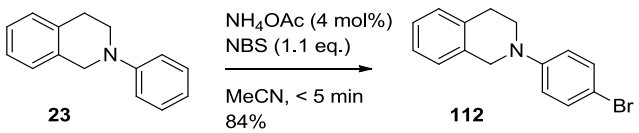

23 **112**

Prepared according to a literature procedure.[209] A reaction vessel was charged with *N*-phenyl-1,2,3,4-tetrahydroisoquinoline (**23**) (415.0 mg, 2.0

mmol), ammonium acetate (6.0 mg, 77.8 μmol), MeCN (10 mL) and then *N*-bromosuccinimide (380.0 mg, 2.1 mmol) was added. A colour change from clear to pale brown solution was immediately observed. The reaction mixture was stirred for 5 min before concentrating to dryness. The resultant mixture was added to a separatory funnel with EtOAc (20 mL) and water (20 mL). The layers were separated and aqueous layer extracted with further EtOAc (2 x 20 mL). The combined organic layers were dried ($MgSO_4$), filtered and concentrated *in vacuo* to yield a pale yellow glassy solid, which was purified by column chromatography (10% EtOAc/heptane) to yield **112** as a white microcrystalline solid (485.9 mg, 84%); m.p. 80 - 82 ^oC (lit. 71 - 72 ^oC[207]); IR ν_{max} (neat) 3033 - 2840 (C-H), 1585 (Ar), 1492 (Ar), 1458 (Ar), 1431, 1383, 1339, 1300, 1270, 1225 cm^{-1}; ^1H NMR (400 MHz, $CDCl_3$) δ 7.38 (2H, d, *J* = 8.8 Hz, C*H*), 7.25 - 7.13 (4H, m, C*H*), 6.86 (2H, d, *J* = 8.8 Hz, C*H*), 4.39 (2H, s, CH_2), 3.55 (2H, apt. t, *J* = 5.9 Hz, CH_2), 2.99 (2H, apt. t, *J* = 5.7 Hz, CH_2); ^{13}C NMR (101 MHz, $CDCl_3$) δ 149.4 (*C*), 134.7 (*C*), 134.0 (*C*), 131.9 (*C*H), 128.5 (*C*H), 126.5 (2 x *C*H), 126.2 (*C*H), 116.5 (*C*H), 110.5 (*C*), 50.4 (CH_2), 46.3 (CH_2), 28.9 (CH_2); HRMS (+APCI) *m/z* calculated for $C_{15}H_{15}{}^{79}BrN$ $[M+H^+]$ 288.0388; Found 288.0387. ^1H and ^{13}C NMR data are consistent with the literature.[207] There is a discrepancy between the literature and observed melting point.

N-(*p*-Nitrophenyl)-1,2,3,4-tetrahydroisoquinoline (113)

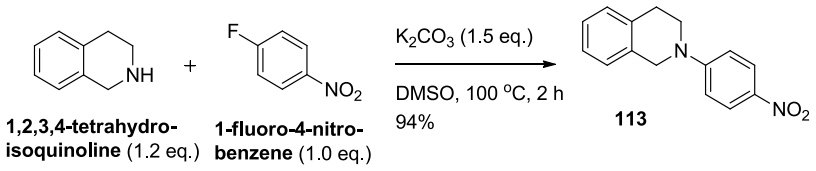

Prepared according to a literature procedure.[210] A mixture of 1,2,3,4-tetrahydroisoquinoline (1.50 mL, 12.0 mmol), 1-fluoro-4-nitrobenzene (1.06 mL, 10.0 mmol), K_2CO_3 (2.09 g, 15.1 mmol) and DMSO (10 mL) was triple evacuated/N_2 filled and stirred at 100 ^oC for 2 h. After cooling to rt, ice water (20 mL) was added and a yellow precipitate was observed. After collection by filtration and drying *in vacuo*, **113** was obtained as a bright yellow

microcrystalline solid (2.39 g, 94%); m.p. 154 - 156 ^{o}C (lit. 152 - 154 ^{o}C[211]); IR ν_{max} (neat) 2912 - 2858 (C-H), 1599 (Ar), 1580 (Ar), 1508 (Ar), 1479 (N-O), 1464 (Ar), 1390, 1312 (N-O), 1222, 1202 cm^{-1}; ^{1}H NMR (400 MHz, $CDCl_3$) δ 8.18 (2H, d, *J* = 9.4 Hz, C*H*), 7.28 - 7.17 (4H, m, C*H*), 6.84 (2H, d, *J* = 9.4 Hz, C*H*), 4.58 (2H, s, CH_2), 3.70 (2H, t, *J* = 5.9 Hz, CH_2), 3.03 (2H, t, *J* = 5.9 Hz, CH_2); ^{13}C NMR (101 MHz, $CDCl_3$) δ 153.8 (*C*), 137.7 (*C*), 134.9 (*C*), 133.1 (*C*), 128.1 (*C*H), 127.2 (*C*H), 126.7 (*C*H), 126.5 (*C*H), 126.2 (2 x *C*H), 111.2 (2 x *C*H), 48.8 (*C*H_2), 44.8 (*C*H_2), 29.0 (*C*H_2). Data are consistent with the literature.[211,212]

tert-Butyl-3,4-dihydroisoquinoline-2(1*H*)-carboxylate (116)

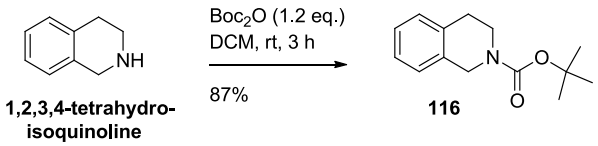

Prepared according to a modified literature procedure.[213] To a round-bottomed flask charged with di-*tert*-butyl dicarbonate (10.1 g, 46.2 mmol) and DCM (5 mL) was added 1,2,3,4-tetrahydroisoquinoline (5.05 g, 37.9 mmol) by syringe, over 10 min. Gas evolved and a colour change from yellow to green solution was observed. After 3 h, the reaction mixture was concentrated *in vacuo* to yield a pale brown oil (11.97 g). In order to destroy unreacted di-*tert*-butyl dicarbonate, a modified literature procedure was used.[214] The oil was redissolved in DCM (10 mL) and solid imidazole (2.57 g, 37.9 mmol) was added gradually until effervescence ceased. The reaction mixture was stirred for 15 min before washing with a solution of 1% HCl (2 x 100 mL) previously cooled to 0 - 5 ^{o}C. The organic layer was washed with $NaHCO_3$ (50 mL), dried ($MgSO_4$) and concentrated *in vacuo* to yield analytically pure **116** as a pale brown oil (7.73 g, 87%); IR ν_{max} (neat) 2976 - 2931 (C-H), 1690 (C=O), 1454 (Ar), 1418, 1392, 1364, 1342, 1296, 1234 cm^{-1}; ^{1}H NMR (400 MHz, $CDCl_3$) δ 7.23 - 7.08 (4H, m, C*H*), 4.59 (2H, s, CH_2), 3.72 - 3.61 (2H, m, CH_2), 2.85 (2H, t, *J* = 5.7 Hz, CH_2), 1.50 (9H, s, CH_3), ^{13}C NMR (101 MHz, $CDCl_3$) δ 154.9 (*C*=O), 134.8 (*C*), 133.7 (*C*), 128.7 (*C*H),

126.3 (2 x *C*H), 126.2 (*C*H), 79.7 (*C*), 46.0 (*C*H_2), 40.6 (*C*H_2), 29.0 (*C*H_2), 28.5 (*C*H_3); HRMS (+ESI) *m/z* calculated for $C_{10}H_{12}NO_2$ [M-(-{$C(CH_3)_2$=CH_2})H^+] 178.0868; Found 178.0861. Data are consistent with the literature.[213]

N-Methyl-1,2,3,4-tetrahydroisoquinoline (114)

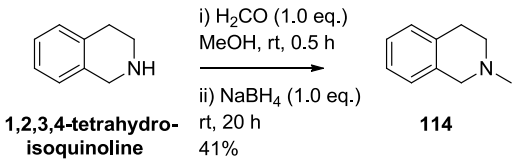

1,2,3,4-tetrahydro-isoquinoline **114**

Prepared according to a literature procedure.[42] A flask was charged with MeOH (50 mL) and 1,2,3,4-tetrahydroisoquinoline (5.0 mL, 39.9 mmol), before formaldehyde (37% w/w in water with 10-15% MeOH stabiliser, 3.30 mL, 39.9 mmol) was added dropwise over 5 min. The reaction was stirred for 30 min before sodium borohydride (1.50 g, 40.1 mmol) was added portionwise over 5 min. The reaction was stirred for 20 h before concentrating to dryness. EtOAc (20 mL) and water (20 mL) were added, the resultant mixture was poured into a separatory funnel and the layers were separated. The aqueous layer was extracted with EtOAc (2 x 20 mL). The combined organic layers were dried ($MgSO_4$), filtered and concentrated *in vacuo* to yield a pale brown residue, which was purified by column chromatography (a gradient of 50 - 70% EtOAc (1% Et_3N)/heptane) to yield **114** as a pale brown oil (2.41 g, 41%); IR ν_{max} (neat) 2920 - 2779 (C-H), 1498 (Ar), 1455 (Ar), 1378, 1290, 1270, 1253, 1222 cm^{-1}; ^{1}H NMR (400 MHz, $CDCl_3$) δ 7.20 - 7.09 (3H, m, C*H*), 7.07 - 7.00 (1H, m, C*H*), 3.60 (2H, s, CH_2), 2.98 - 2.90 (2H, m, CH_2), 2.74 - 2.67 (2H, m, CH_2), 2.47 (3H, s, CH_3), ^{13}C NMR (101 MHz, $CDCl_3$) δ 134.8 (*C*), 133.8 (*C*), 128.6 (*C*H), 126.4 (*C*H), 126.1 (*C*H), 125.5 (*C*H), 58.0 (*C*H_2), 52.9 (*C*H_2), 46.1 (*C*H_3), 29.2 (*C*H_2). HRMS (+ESI) *m/z* calculated for $C_{10}H_{14}N$ [M+H^+] 148.1121; Found 148.1114. Data are consistent with literature.[42]

6,7-Dimethoxy-*N*-methyl-1,2,3,4-tetrahydroisoquinoline (115)

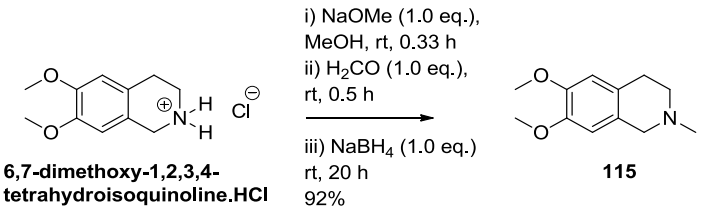

Prepared according to a literature procedure.[42] A flask was charged with MeOH (50 mL) and 6,7-dimethoxy-1,2,3,4-tetrahydroisoquinoline hydrochloride (5.03 g, 21.9 mmol), before NaOMe (25% w/w in MeOH) (5.00 mL, 22.0 mmol) was added. The reaction was stirred for 20 min and formaldehyde (37% w/w in water with 10-15% MeOH stabiliser, 1.70 mL, 22.8 mmol) was added dropwise over 5 min. The reaction was stirred for 30 min before sodium borohydride (0.83 g, 21.9 mmol) was added portionwise over 5 min. The reaction was stirred for 20 h before concentrating to dryness. EtOAc (30 mL) and water (30 mL) were added. The resultant mixture was poured into a separatory funnel and the layers were separated. The aqueous layer was extracted with EtOAc (2 x 30 mL) The combined organic layers were dried ($MgSO_4$), filtered and concentrated *in vacuo* to yield a white solid, which was purified by column chromatography (a gradient of 80 - 100% EtOAc (1% Et_3N)/heptane) to yield **115** as a colourless solid (4.18 g, 92%) m.p. 80 -82 ^oC (lit. 79 - 81 ^oC[215]); IR ν_{max} (neat) 3253 - 2724 (C-H), 1661 (Ar), 1610 (Ar), 1519 (Ar), 1454 (Ar), 1371, 1344, 1323, 1289, 1255, 1226, 1213 cm^{-1}; ^1H NMR (400 MHz, $CDCl_3$) δ 6.60 (1H, s, C*H*), 6.52 (1H, s, C*H*), 3.85 (3H, s, CH_3), 3.84 (3H, s, CH_3), 3.51 (2H, s, CH_2), 2.85 (2H, apt. t, J = 5.7 Hz, CH_2), 2.67 (2H, apt. t, J = 5.9 Hz, CH_2), 2.45 (3H, s, CH_3), ^{13}C NMR (101 MHz, $CDCl_3$) δ 149.5 (*C*), 147.2 (*C*), 126.7 (*C*), 125.8 (*C*), 111.4 (*C*H), 109.4 (*C*H), 57.6 (*C*H_2), 55.9 (2 x *C*H_3), 53.0 (*C*H_2), 48.1 (*C*H_3), 28.9 (*C*H_2); HRMS (+ESI) *m/z* calculated for $C_{12}H_{18}NO_2$ [M+H^+] 208.1332; Found 208.1322. Data are consistent with literature.[42,215]

1-(Nitromethyl)-*N*-phenyl-1,2,3,4-tetrahydroisoquinoline (**27**)

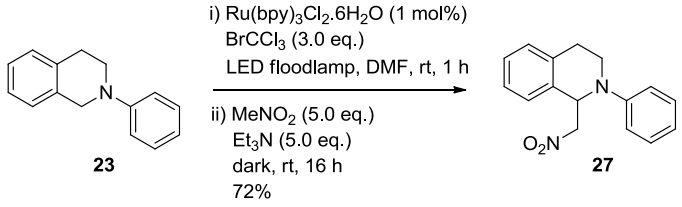

Prepared according to a literature procedure.[96] A reaction vessel was equipped with a magnetic stirrer bar and was charged with *N*-phenyl-1,2,3,4-tetrahydroisoquinoline (**23**) (0.51 g, 2.39 mmol), $Ru(bpy)_3Cl_2.6H_2O$ (20.2 mg, 27.0 μmol, 1 mol%) and DMF (10 mL). The flask was degassed (3x freeze/pump/thaw) before degassed (3x freeze/pump/thaw) $BrCCl_3$ (0.71 ml, 7.20 mmol) was added at rt. The mixture was then irradiated by a 30 W LED floodlamp at a distance of *ca.* 10 cm under N_2. After 1 h, when starting material was fully consumed by HPLC (see Table 1, entry 1), the LED floodlamp was removed. The reaction vessel was covered in aluminium foil before addition of nitromethane (0.65 mL, 11.95 mmol) and triethylamine (1.70 mL, 12.20 mmol). After 16 h, the reaction mixture was poured into a separatory funnel containing sat. aq. $NaHCO_3$ (150 mL) and Et_2O (50 mL). The layers were separated and aqueous layer extracted with Et_2O (2 x 50 mL). The combined organic layers were washed with brine (50 mL), dried ($MgSO_4$), filtered and concentrated *in vacuo* to yield the crude product as a red oil, which was purified by flash column chromatography (10 - 40% EtOAc/heptane) gave **27** as a yellow oil, which crystallised overnight to give a bright yellow powder (0.46 g, 72%); m.p. 92 - 94 ^oC (lit. 89 - 90 ^oC[29]); IR ν_{max} (neat) 3058 - 2919 (C-H), 1596 (Ar), 1547 (N-O), 1493 (Ar), 1497 (Ar), 1429, 1382 (N-O), 1351, 1312, 1291, 1279, 1251, 1210 cm^{-1}; ^1H NMR (400 MHz, $CDCl_3$) δ 7.30 - 7.25 (2H, m, C*H*), 7.25 - 7.15 (3H, m, C*H*), 7.15 (1H, d, *J* = 7.3 Hz, C*H*), 6.99 (2H, d, *J* = 8.3 Hz, C*H*), 6.85 (1H, t, *J* = 7.3 Hz, C*H*), 5.55 (1H, apt. t, *J* = 7.3 Hz, C*H*), 4.87 (1H, dd, *J* = 12.2, 7.8 Hz, CH_2), 4.56 (1H, dd, *J* = 12.2, 6.4 Hz, CH_2), 3.71 - 3.58 (2H, m, CH_2), 3.09 (1H, ddd, *J* = 16.6, 8.8, 5.9 Hz, CH_2), 2.82 (1H, ddd, *J* = 16.6, 5.9, 4.9 Hz, CH_2); ^{13}C NMR (101 MHz, $CDCl_3$) δ 148.4 (*C*), 135.3 (*C*), 132.9 (*C*), 129.5 (*C*H), 129.2 (*C*H), 128.1 (*C*H),

127.0 (*C*H), 126.7 (*C*H), 119.4 (*C*H), 115.1 (*C*H), 78.8 (CH_2), 58.2 (*C*H), 42.1 (CH_2), 26.5 (CH_2); HRMS (+ESI) *m/z* calculated for $C_{16}H_{17}N_2O_2$ $[M+H^+]$ 269.1290; Found 269.1285. Data are consistent with the literature.[29,216]

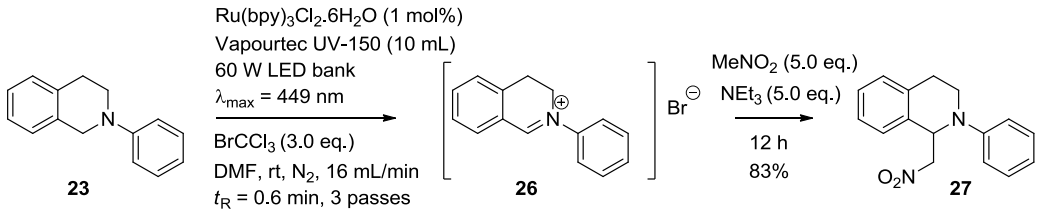

Alternatively, the Vapourtec UV-150 photochemical flow reactor (10 mL coil) was employed and reaction conditions were based on conditions reported in the literature.[115] A reaction vessel was equipped with *N*-phenyl-1,2,3,4-tetrahydroisoquinoline (**23**) (1.00 g, 4.70 mmol), $Ru(bpy)_3Cl_2.6H_2O$ (17.0 mg, 24.0 μmol, 0.5 mol%) and DMF (47 mL). The mixture was sparged with N_2 for 20 min before $BrCCl_3$ (1.40 ml, 14.0 mmol) was added at rt. The mixture was sparged with N_2 for 20 min, then passed through a photochemical flow reactor at 16 mL/min (0.6 min residence time), irradiating at 449 nm. The reaction mixture was sparged with N_2 for 15 min, then reexposed to the reaction conditions for a further two passes (a total of three passes, *ca*. 2 min overall residence time) to achieve full conversion. The reaction was sampled for HPLC after each pass (see Table 6, entries 1-3, Section 2.1.6.). The reaction mixture was covered in foil and placed under N_2. Triethylamine (3.3 mL, 24.0 mmol) and nitromethane (1.3 mL, 24.0 mmol) were added dropwise and the reaction mixture allowed to stir at rt for 16 h. Work up and purification gave **27** as a microcrystalline pale yellow solid (1.07 g, 83%), ^{1}H NMR data are consistent with the data listed above.

5.8. General Procedure 1: Photoactivation of *N*-Substituted Tetrahydroisoquinolines

A reaction vessel was charged with *N*-substituted tetrahydroisoquinoline (1.0 eq.), photocatalyst (0.01 eq.) and solvent (7.5 mL) (as specified in Table 1). The flask was degassed (3x freeze/pump/thaw) before the degassed (3x

freeze/pump/thaw) oxidant (as specified in Table 1, Section 2.1.1.) was added at rt. The mixture was then irradiated within the specified photoreactor (as specified in Table 1) whilst under N_2. At the specified time (Table 1), the ratio of iminium salt : *N*-substituted tetrahydroisoquinoline (for example, **26** : **23**) was determined by HPLC. Unless they had completed earlier (as deemed by HPLC), reactions were deemed complete after 16 h. This step is termed 'photoactivation', and isolation of the crude iminium salt is described overleaf. Photoactivation was generally conducted on 1.00 mmol scale in the parallel LED strip photoreactor using $Ru(bpy)_3Cl_2.6H_2O$ (10.0 μmol, 1 mol%) as photocatalyst, $BrCCl_3$ (3.00 mmol, 3.0 eq.) as oxidant and MeCN : H_2O (4 : 1, 7.5 mL) as solvent.

Alternatively, **General Procedure 1** photoactivation was conducted open to air, using $Ru(bpy)_3Cl_2.6H_2O$ (1 mol%) as the catalyst and DMF as the solvent (Table 1, entry 5).

Alternatively, **General Procedure 1** photoactivation was conducted using TEMPO (2.0 eq.) as the oxidant, $Ru(bpy)_3Cl_2.6H_2O$ (1 mol%) as the catalyst and MeCN : H_2O (4 : 1) as the solvent (Table 1, entry 6).

Alternatively, **General Procedure 1** photoactivation was conducted using $ClCH_2CN$ (2.0 eq.) as the oxidant, $Ru(bpy)_3Cl_2.6H_2O$ (1 mol%) as the catalyst and MeCN : H_2O (4 : 1) as the solvent. No reaction occurred (Table 1, entry 8).

Alternatively, **General Procedure 1** photoactivation was conducted using $BrCH_2CN$ (2.0 eq.) as the oxidant, $Ru(bpy)_3(PF_6)_2$ (1 mol%) as the catalyst and anhydrous MeCN as the solvent (Table 1, entry 10).

***N*-Phenyl-3,4-dihydroisoquinolinium bromide** (**26**)

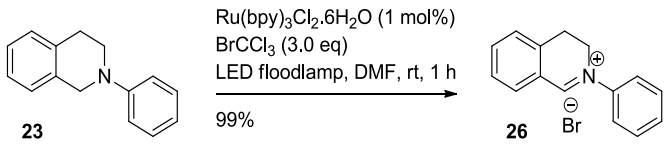

After photoactivation of *N*-phenyl-1,2,3,4-tetrahydroisoquinoline **23** (0.95 g, 4.54 mmol) using the LED floodlamp photoreactor according to **General Procedure 1**, the reaction mixture was concentrated to dryness and redissolved in the minimal amount of MeCN. Toluene (10 mL) was added and the reaction mixture was concentrated to dryness. DCM (10 mL) was added and the reaction mixture concentrated *in vacuo* to yield crude **26** as a brown solid (1.22 g, 99%),† which was used without further purification; m.p. 158 - 162 ^{o}C (lit. 164 - 165[217]); IR ν_{max} (neat) 3402 - 3028 (C-H), 1628 (C=N^{+}), 1602 (Ar), 1567 (Ar), 1490 (Ar), 1455 (Ar), 1387, 1321, 1274, 1228, cm^{-1}; ^{1}H NMR (400 MHz, $CDCl_3$) δ 10.38 (1H, s, C*H*), 8.52 (1H, d, *J* = 7.9 Hz, C*H*), 8.04 (2H, d, *J* = 7.9 Hz, C*H*), 7.76 (1H, t, *J* = 7.6 Hz, C*H*), 7.62 - 7.47 (4H, m, C*H*), 7.39 (1H, d, *J* = 7.9 Hz, C*H*), 4.59 (2H, t, *J* = 7.9 Hz, CH_2), 3.52 (2H, t, *J* = 7.9 Hz, CH_2); ^{13}C NMR (101 MHz, $CDCl_3$) δ 166.0 (*C*H), 142.4 (*C*), 138.8 (*C*H), 136.9 (*C*H), 135.9 (*C*), 131.3 (*C*H), 130.5 (*C*H), 129.0 (*C*H), 127.9 (*C*H), 125.8 (*C*), 122.6 (*C*H), 51.6 (CH_2), 26.0 (*C*H$_2$); HRMS (+ESI) *m/z* calculated for $C_{15}H_{14}N$ [M] 208.1121; Found 208.1116; ^{1}H and ^{13}C data are consistent with the literature for the chloride salt.[58]

_N_-Methyl-3,4-dihydroisoquinolinium bromide (**127**)

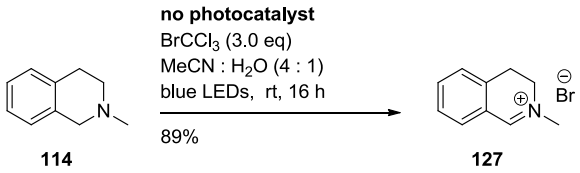

114 **127**

After photoactivation of *N*-methyl-1,2,3,4-tetrahydroisoquinoline **114** (147.2 mg, 1.00 mmol) using the blue LED parallel reactor according to **General Procedure 1** (no photocatalyst was added), the reaction mixture was concentrated to dryness and redissolved in the minimal amount of MeCN. Toluene (2 mL) was added and the reaction mixture was concentrated to dryness. DCM (1 mL) was added and the reaction mixture was concentrated *in vacuo* to yield crude **127** as a pale brown solid (221.2 mg, 98%); IR ν_{max} (neat) 3410 - 2594 (C-H), 1668 (C=N^{+}), 1601 (Ar), 1576 (Ar), 1491 (Ar), 1455

†Corrected for the mass of $Ru(bpy)_3Cl_2.6H_2O$ present.

(Ar), 1408, 1361, 1320, 1291, 1265, 1233, 1206 cm^{-1}; ^{1}H NMR (400 MHz, $CDCl_3$) δ 10.18 (1H, s, C*H*), 8.09 (1H, d, *J* = 7.3 Hz, C*H*), 7.77 (1H, d, *J* = 7.6 Hz, C*H*), 7.51 (1H, t, *J* = 7.7 Hz, C*H*), 7.45 (1H, d, *J* = 7.6 Hz, C*H*), 4.30 (2H, t, *J* = 8.1 Hz, CH_2), 4.14 (3H, s, CH_3), 3.45 (2H, t, *J* = 8.2 Hz, CH_2); ^{13}C NMR (101 MHz, $CDCl_3$) δ 166.7 (*C*H), 137.4 (*C*), 135.3 (*C*), 133.8 (*C*H), 128.0 (*C*H), 127.8 (*C*H), 124.1 (*C*), 50.2 (CH_2), 47.8 (CH_3), 24.9 (*C*H_2); HRMS (+ESI) *m/z* calculated for $C_{15}H_{14}N$ [M] 146.0964; Found 146.0968; ^{1}H and ^{13}C data are consistent with the literature.[58] To the brown solid was added 1,3,5-trimethoxybenzene (16.8 mg, 0.10 mmol, 10 mol%) and the yield of **127** determined by ^{1}H NMR analysis (89%, see Table 5, entry 4).†

5.9. General Procedure 2: Organometallic Trapping of Iminium Salt Intermediates

Following photoactivation of *N*-substituted-1,2,3,4-tetrahydroisoquinoline (1.0 eq.) according to **General Procedure 1** and concentration of the reaction mixture, the crude iminium salt (for example, *N*-phenyl-3,4-dihydroisoquinolinium bromide **26**) was dissolved in anhydrous MeCN (5 mL) and the reaction vessel was covered in foil. After cooling to 0 ^{o}C, the organometallic reagent (2.0 eq.) was added dropwise over 15 min under N_2. After allowing to warm to rt, sat. aq. NH_4Cl (10 mL) was carefully added and the resulting mixture filtered through celite into a separatory funnel containing EtOAc (50 mL) and water (100 mL). The layers were separated and the aqueous layer was extracted with further EtOAc (2 x 50 mL). The combined organic layers were dried ($MgSO_4$), filtered and concentrated *in vacuo* to yield the crude product, which was purified by silica gel chromatography in the solvent mixture indicated to afford the desired product. Alternatively, for photoactivations according to **General Procedure 1** using $BrCH_2CN$ and anhydrous MeCN, reactions were cooled to 0 ^{o}C and organometallic reagents added directly without concentration of the reaction mixture.

†10% of an unknown impurity was present by ^{1}H NMR comparing to the internal standard. Further purification of this reactive intermediate was not deemed practical and it was decided not to obtain a m.p.

_N_-Phenyl-1-vinyl-1,2,3,4-tetrahydroisoquinoline (*97*)

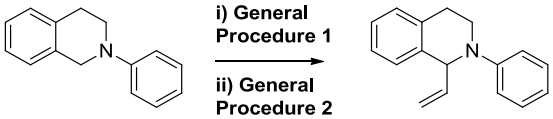

23 97

Conducted according to **General Procedure 2**. Following photoactivation of **23** (197.0 mg, 0.94 mmol) according to **General Procedure 1**, crude **26** was dissolved in anhydrous MeCN (5 mL). After cooling to 0 ^{o}C, vinylmagnesium bromide (1.90 mL, 1.0 M in THF, 1.90 mmol) was added dropwise over 15 min. Work up gave the crude product as a brown oil. Purification by flash column chromatography (a gradient of 10 - 20% DCM (1% Et_3N)/heptane) gave ***97*** as a yellow oil (176.2 mg, 80%); IR ν_{max} (neat) 3023 - 2908 (C-H), 1596 (Ar), 1502 (Ar), 1474 (Ar), 1455 (Ar), 1431, 1383, 1358, 1344, 1326, 1300, 1259, 1226 cm^{-1}; ^{1}H NMR (400 MHz, $CDCl_3$) δ 7.26 (2H, apt. t, *J* = 7.1 Hz, C*H*), 7.22 - 7.14 (4H, m, C*H*), 6.94 (2H, d, *J* = 8.1 Hz, C*H*), 6.77 (1H, t, *J* = 7.3 Hz, C*H*), 6.03 (1H, ddd, *J* = 17.0, 10.3, 5.1 Hz, C*H*), 5.26 (1H, d, *J* = 4.9 Hz, C*H*), 5.19 - 5.08 (2H, m, CH_2), 3.62 (2H, apt. t, *J* = 6.0 Hz, CH_2), 3.08 - 2.98 (1H, m, CH_2), 2.97 - 2.87 (1H, m, CH_2); ^{13}C NMR (101 MHz, $CDCl_3$) δ 149.8 (*C*), 138.9 (*C*H), 136.7 (*C*), 135.6 (*C*), 129.2 (*C*H), 128.4 (*C*H), 127.7 (*C*H), 126.8 (*C*H), 126.1 (*C*H), 117.9 (*C*H), 115.4 (*C*H_2), 114.7 (*C*H), 61.9 (*C*H), 43.0 (*C*H_2), 28.4 (*C*H_2); HRMS (+ESI) *m/z* calculated for $C_{17}H_{20}N$ [M+H^{+}] 236.1428; Found 236.1434.

Alternatively, following photoactivation of **23** (205.0 mg, 0.98 mmol) according to **General Procedure 1** with $BrCH_2CN$ (0.14 mL, 2.00 mmol) and $Ru(bpy)_3(PF_6)_2$ (8.4 mg, 9.8 μmol) in anhydrous MeCN (7.5 mL), the reaction mixture was cooled to 0 ^{o}C. To the reaction mixture was added vinylmagnesium bromide (2.00 mL, 1.0 M in THF, 2.00 mmol) dropwise over 15 min. Work up† and purification as above gave ***97*** as a colourless oil (178.5 mg, 77%); ^{1}H NMR (400 MHz, $CDCl_3$) δ 7.27 (2H, apt. t, *J* = 8.1 Hz, C*H*),

†Here, work up was performed without celite filtration and extraction used H_2O (10 mL) and EtOAc (3 x 30 mL).

7.24 - 7.16 (4H, m, C*H*), 6.93 (2H, d, *J* = 7.9 Hz, C*H*), 6.77 (1H, t, *J* = 7.3 Hz, C*H*), 6.01 (1H, ddd, *J* = 16.7, 10.5, 4.9 Hz, C*H*), 5.24 (1H, d, *J* = 4.8 Hz, C*H*), 5.18 - 5.10 (2H, m, CH_2), 3.67 - 3.55 (2H, m, CH_2), 3.06 - 2.98 (1H, m, CH_2), 2.97 - 2.89 (1H, m, CH_2); ^{1}H NMR data are consistent with the data listed above.

1-Methyl-*N*-phenyl-1,2,3,4-tetrahydroisoquinoline (*98*)

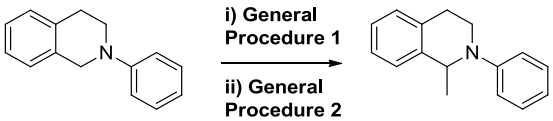

23 **98**

Conducted according to **General Procedure 2**. Following photoactivation of **23** (197.0 mg, 0.94 mmol) according to **General Procedure 1**, crude **26** was dissolved in anhydrous MeCN (5 mL). After cooling to 0 ^{o}C, methylmagnesium bromide (3.2 M in 2-MeTHF) (0.60 mL, 1.92 mmol) was added dropwise over 15 min. Work up gave the crude product as a brown oil. Purification by flash column chromatography (a gradient of 5 - 20% DCM (1% Et_3N)/heptane) gave ***98*** as a pale yellow oil (164.5 mg, 78%); IR ν_{max} (neat) 3022 - 2922 (C-H), 1597 (Ar), 1502 (Ar), 1447, 1386, 1328, 1287, 1266, 1228 cm^{-1}; ^{1}H NMR (400 MHz, $CDCl_3$) δ 7.27 (2H, apt. t, *J* = 7.9 Hz, C*H*), 7.23 - 7.12 (4H, m, C*H*), 6.96 (2H, d, *J* = 8.2 Hz, C*H*), 6.78 (1H, t, *J* = 7.3 Hz, C*H*), 4.95 (1H, q, *J* = 6.6 Hz, C*H*), 3.71 - 3.62 (1H, m, CH_2), 3.59 - 3.49 (1H, m, CH_2), 3.11 - 3.01 (1H, m, CH_2), 2.95 - 2.85 (1H, m, CH_2), 1.48 (3H, d, *J* = 6.8 Hz, CH_3), ^{13}C NMR (101 MHz, $CDCl_3$) δ 149.9 (*C*), 140.3 (*C*), 134.6 (*C*), 129.3 (*C*H), 128.7 (*C*H), 126.9 (*C*H), 126.3 (*C*H), 126.1 (*C*H), 118.0 (*C*H), 115.1 (*C*H), 54.6 (*C*H), 41.5 (*C*H_2), 28.6 (*C*H_2), 20.9 (*C*H_3); HRMS (+APCI) *m/z* calculated for $C_{16}H_{18}N$ [M+H$^+$] 224.1434; Found 224.1431.

Alternatively, following photoactivation of **23** (207.0 mg, 0.99 mmol) according to **General Procedure 1** with $BrCH_2CN$ (0.14 mL, 2.00 mmol) and $Ru(bpy)_3(PF_6)_2$ (8.1 mg, 9.4 μmol) in anhydrous MeCN (7.5 mL), the reaction mixture was cooled to 0 ^{o}C. To the reaction mixture was added methylmagnesium bromide (3.2 M in 2-MeTHF) (0.62 mL, 1.98 mmol)

dropwise over 15 min. Work up† and purification as above gave ***98*** as a colourless oil (161.2 mg, 73%); ^{1}H NMR (400 MHz, $CDCl_3$) δ 7.27 (2H, apt. t, *J* = 7.9 Hz, C*H*), 7.22 - 7.11 (4H, m, C*H*), 6.96 (2H, d, *J* = 8.1 Hz,C*H*), 6.77 (1H, t, *J* = 7.2 Hz, C*H*), 4.94 (1H, q, *J* = 6.7 Hz, C*H*), 3.68 - 3.60 (1H, m, CH_2), 3.56 - 3.47 (1H, m, CH_2), 3.10 - 2.99 (1H, m, CH_2), 2.94 - 2.85 (1H, m, CH_2), 1.45 (3H, d, *J* = 6.9 Hz, CH_3); ^{1}H NMR data are consistent with the data listed above.

1-Ethyl-*N*-phenyl-1,2,3,4-tetrahydroisoquinoline (*99*)

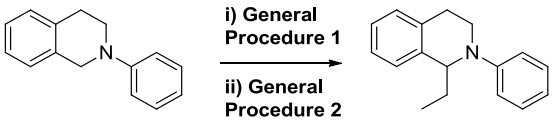

23 **99**

Conducted according to **General Procedure 2**. Following photoactivation of **23** (197.0 mg, 0.94 mmol) according to **General Procedure 1**, crude **26** was dissolved in anhydrous MeCN (5 mL). After cooling to 0 ^{o}C, ethylmagnesium chloride (0.95 mL, 2.0 M in THF, 1.90 mmol) was added dropwise over 15 min. Work up gave the product as a brown oil. Purification by flash column chromatography (a gradient of 5 - 20% DCM (1% Et_3N)/heptane) gave ***99*** as a pale yellow oil (166.3 mg, 75%); IR ν_{max} (neat) 3023 - 2929 (C-H), 1597 (Ar), 1502 (Ar), 1473 (Ar), 1456 (Ar), 1390, 1331, 1294, 1266, 1221 cm^{-1}; ^{1}H NMR (400 MHz, $CDCl_3$) δ 7.25 (2H, td, *J* = 8.7, 1.5 Hz, C*H*), 7.21 - 7.10 (4H, m, C*H*), 6.90 (2H, d, *J* = 8.2 Hz, C*H*), 6.73 (1H, t, *J* = 7.3 Hz, C*H*), 4.57 (1H, apt. t, *J* = 7.0 Hz, C*H*), 3.69 - 3.54 (2H, m, CH_2), 3.07 - 2.99 (1H, m, CH_2), 2.93 - 2.83 (1H, m, CH_2), 2.07 - 1.94 (1H, m, CH_2) 1.83 - 1.70 (1H, m, CH_2) 1.02 (3H, t, *J* = 7.4 Hz, CH_3); ^{13}C NMR (101 MHz, $CDCl_3$) δ 149.7 (*C*), 138.9 (*C*), 135.1 (*C*), 129.2 (*C*H), 128.4 (*C*H), 127.4 (*C*H), 126.4 (*C*H), 125.7 (*C*H), 116.9 (*C*H), 113.6 (*C*H), 60.7 (*C*H), 42.0 (*C*H_2), 29.5 (*C*H_2), 27.3 (*C*H_2), 11.4 (*C*H_3); HRMS (+APCI) *m/z* calculated for $C_{17}H_{20}N$ [M+H^{+}] 238.1596; Found 238.1589.

†Here, work up was performed without celite filtration and extraction used H_2O (10 mL) and EtOAc (3 x 30 mL).

1-Isopropyl-*N*-phenyl-1,2,3,4-tetrahydroisoquinoline (*100*)

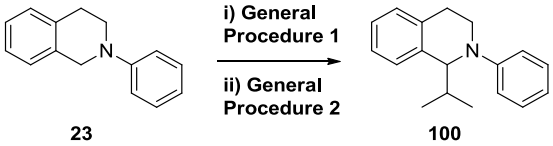

Conducted according to **General Procedure 2**. Following photoactivation of **23** (197.0 mg, 0.94 mmol) according to **General Procedure 1**, crude **26** was dissolved in anhydrous MeCN (5 mL). After cooling to 0 ^{o}C, isopropylmagnesium chloride (0.95 mL, 2.0 M in THF, 1.90 mmol) was added dropwise over 15 min. Work up† gave the product as a brown oil. Purification by flash column chromatography (a gradient of 5 - 20% DCM (1% Et_3N)/heptane) gave ***100*** as a pale yellow oil (184.7 mg, 78%); IR ν_{max} (neat) 3100 - 2957 (C-H), 1596 (Ar), 1502 (Ar), 1472 (Ar), 1392, 1365, 1344, 1323, 1297, 1278, 1221 cm^{-1}; ^{1}H NMR (400 MHz, $CDCl_3$) δ 7.27 - 7.09 (6H, m, C*H*), 6.92 (2H, d, *J* = 8.1 Hz, C*H*), 6.72 (1H, t, *J* = 7.2 Hz, C*H*), 4.45 (1H, d, *J* = 7.9 Hz, C*H*), 3.82 - 3.71 (1H, m, CH_2), 3.60 - 3.51 (1H, m, CH_2), 3.02 (2H, apt. t, *J* = 6.4 Hz, CH_2), 2.25 - 2.11 (1H, m, C*H*), 1.12 (3H, d, *J* = 6.8 Hz, CH_3) 0.98 (3H, d, *J* = 6.6 Hz, CH_3); ^{13}C NMR (101 MHz, $CDCl_3$) δ 150.5 (*C*), 138.1 (*C*), 135.4 (*C*), 129.1 (*C*H), 128.4 (*C*H), 128.3 (*C*H), 126.6 (*C*H), 125.3 (*C*H), 117.0 (*C*H), 114.0 (*C*H), 64.9 (*C*H), 43.3 (*C*H_2), 34.6 (*C*H), 27.5 (*C*H_2), 20.7 (*C*H_3), 20.2 (*C*H_3); HRMS (+APCI) *m/z* calculated for $C_{18}H_{22}N$ [M+H$^+$] 252.1752; Found 252.1743.

1-Cyclopropyl-*N*-phenyl-1,2,3,4-tetrahydroisoquinoline (*101*)

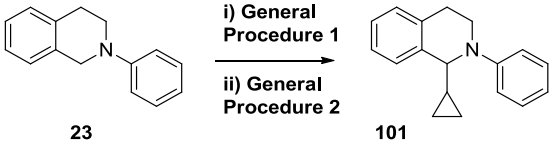

Conducted according to **General Procedure 2**. Following photoactivation of **23** (192.0 mg, 0.92 mmol) according to **General Procedure 1**, crude **26** was dissolved in anhydrous MeCN (5 mL). After cooling to 0 ^{o}C,

†Here, work up was performed without celite filtration.

cyclopropylmagnesium bromide (1 M in 2-MeTHF) was added dropwise over 15 min. Work up gave the product as a brown oil. Purification by flash column chromatography (a gradient of 10 - 20% DCM(1% Et_3N)/heptane) gave ***101*** as an orange microcrystalline solid (151.1 mg, 66%); m.p. 56 - 58 ^oC; IR ν_{max} (neat) 3052 - 2834 (C-H), 1592 (Ar), 1496 (Ar), 1463 (Ar), 1451 (Ar), 1427, 1385, 1352, 1315, 1259, 1226, 1211 cm^{-1}; ^1H NMR (400 MHz, $CDCl_3$) δ 7.32 - 7.22 (2H, apt. t, *J* = 8.0 Hz, C*H*), 7.22 - 7.12 (4H, m, C*H*), 6.98 (2H, d, *J* = 7.9 Hz, C*H*), 6.79 (1H, apt. t, *J* = 7.3 Hz, C*H*), 4.47 (1H, d, *J* = 5.3 Hz, C*H*), 3.85 - 3.73 (1H, m, CH_2), 3.70 - 3.60 (1H, m, CH_2), 3.11 - 2.99 (1H, m, CH_2), 2.96 - 2.85 (1H, m, CH_2), 1.39 - 1.27 (1H, m, C*H*), 0.60 - 0.43 (2H, m, CH_2), 0.39 - 0.25 (2H, m, CH_2); ^{13}C NMR (101 MHz, $CDCl_3$) δ 150.0 (*C*), 137.4 (*C*), 135.1 (*C*), 129.1 (*C*H), 128.4 (*C*H), 127.4 (*C*H), 126.6 (*C*H), 125.6 (*C*H), 117.7 (*C*H), 114.9 (*C*H), 61.8 (*C*H), 42.3 (*C*H_2), 27.4 (*C*H_2), 16.5 (*C*H), 3.8 (*C*H_2), 2.9 (*C*H_2); HRMS (+APCI) *m/z* calculated for $C_{18}H_{20}N$ [$M+H^+$] 250.1596; Found 250.1591.

1-Benzyl-*N*-phenyl-1,2,3,4-tetrahydroisoquinoline (*102*)

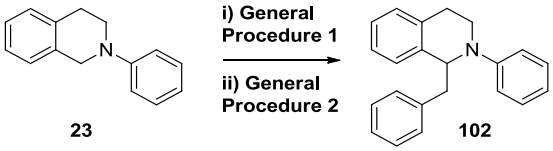

Conducted according to **General Procedure 2**. Following photoactivation of **23** (198.0 mg, 0.95 mmol) according to **General Procedure 1**, crude **26** was dissolved in anhydrous MeCN (5 mL). After cooling to 0 ^oC, benzylmagnesium bromide (5.70 mL, 1.0 M in THF, 5.70 mmol)† was added dropwise over 15 min. Work up gave the crude product as a brown oil. MDAP purification gave ***102*** as a yellow oil (194.9 mg, 69%); IR ν_{max} (neat) 3061 - 2919 (C-H), 1596 (Ar), 1502 (Ar), 1494 (Ar), 1473 (Ar), 1452 (Ar), 1391, 1328, 1275, 1230 cm^{-1}; ^1H NMR (400 MHz, $CDCl_3$) δ 7.31 - 7.14 (7H, m, C*H*), 7.11 - 7.01 (3H, m, C*H*), 6.89 (2H, d, *J* = 7.9 Hz, C*H*), 6.81 - 6.73 (2H, m, C*H*), 4.94 (1H, apt. t, *J* = 6.4 Hz, C*H*), 3.72 - 3.63 (1H, m, CH_2CH_2N), 3.61 - 3.54 (1H,

†6.0 eq. of reagent were required for full conversion.

m, CH_2), 3.33 - 3.25 (1H, m, CH_2), 3.09 - 2.97 (2H, m, CH_2, CH_2), 2.83 - 2.73 (1H, m, CH_2); ^{13}C NMR (101 MHz, $CDCl_3$) δ 149.3 (*C*), 138.9 (*C*), 137.6 (*C*), 135.1 (*C*), 129.8 (*C*H), 129.2 (*C*H), 128.2 (*C*H), 128.1 (*C*H), 127.6 (*C*H), 126.6 (*C*H), 126.2 (*C*H), 125.5 (*C*H), 117.2 (*C*H), 113.7 (*C*H), 61.5 (*C*H), 42.4 (*C*H_2), 42.1, (*C*H_2), 27.5 (*C*H_2); HRMS (+APCI) *m/z* calculated for $C_{22}H_{22}N$ [M+H^+] 300.1752; Found 300.1745.

1,2-Diphenyl-1,2,3,4-tetrahydroisoquinoline (**103**)[47]

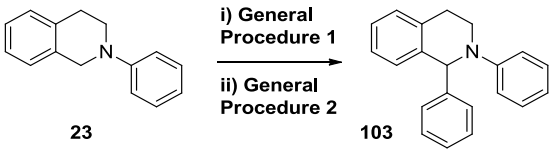

Conducted according to **General Procedure 2**. Following photoactivation of **23** (197.0 mg, 0.94 mmol) according to **General Procedure 1**, crude **26** was dissolved in anhydrous MeCN (5 mL). After cooling to 0 ^{o}C, phenylmagnesium bromide (1.90 mL, 1.0 M in THF 1.90 mmol) was added dropwise over 15 min. Work up gave the crude product as a brown oil. Purification by flash column chromatography (a gradient of 5 - 10% DCM (1% Et_3N)/heptane) gave a yellow oil, which crystallised overnight to yield **103** as a microcrystalline orange solid (241.4 mg, 90%); m.p. 68 - 71 ^{o}C (lit. 62 - 64 ^{o}C[44]); IR ν_{max} (neat) 3022 - 2854 (C-H), 1593 (Ar), 1573 (Ar), 1504 (Ar), 1491 (Ar), 1472 (Ar), 1457 (Ar), 1445, 1432, 1382, 1360, 1342, 1326, 1300, 1268, 1251, 1227, 1209 cm^{-1}; ^{1}H NMR (400 MHz, $CDCl_3$) δ 7.32 - 7.14 (11H, m, C*H*), 6.94 (2H, d, *J* = 8.0 Hz, C*H*), 6.79 (1H, t, *J* = 7.1 Hz, C*H*), 5.88 (1H, s, C*H*), 3.78 - 3.68 (1H, m, CH_2), 3.63 - 3.53 (1H, m, CH_2), 3.07 - 2.88 (2H, m, CH_2); ^{13}C NMR (101 MHz, $CDCl_3$) δ 149.5 (*C*), 143.1 (*C*), 137.9 (*C*), 135.7 (*C*), 129.1 (*C*H), 128.2 (*C*H), 128.1 (*C*H), 127.8 (*C*H), 127.3 (*C*H), 127.0 (*C*H), 126.8 (*C*H), 126.1 (*C*H), 117.5 (*C*H), 113.9 (*C*H), 62.8 (*C*H), 43.8 (*C*H_2), 28.0 (*C*H_2); HRMS (+APCI) *m/z* calculated for $C_{21}H_{20}N$ [M+H^+] 286.1596; Found 286.1593. ^{1}H NMR and IR data are consistent with the literature.[47] Alternatively, following photoactivation of **23** (198.0 mg, 0.95 mmol) according to **General Procedure 1**, crude **26** was dissolved in MeCN (5 mL).

Separately, phenylmagnesium bromide (1.90 mL, 1.0 M in THF, 1.90 mmol, 2.0 eq.) was added to a suspension of copper(I) bromide (0.35 g, 2.44 mmol, 2.6 eq.) in anhydrous THF (2 mL) at -78 ^{o}C. After stirring for 30 min at -78 ^{o}C, then stirring for 30 min at rt, the resultant suspension was removed by syringe and added dropwise to the crude **26** in MeCN over 15 min at 0 ^{o}C. Work up and purification as before gave **103** as a microcrystalline orange solid (208.9 mg, 77%); ^{1}H NMR (400 MHz, $CDCl_3$) δ 7.34 - 7.15 (11H, m, C*H*), 6.88 (2H, d, *J* = 8.2 Hz, C*H*), 6.77 (1H, t, *J* = 7.3 Hz, C*H*), 5.85 (1H, s, C*H*), 3.79 - 3.70 (1H, m, CH_2), 3.58 - 3.49 (1H, m, CH_2), 3.03 - 2.87 (2H, m, CH_2); ^{1}H NMR data are consistent with the data listed above.

Alternatively, following photoactivation of **23** (204.0 mg, 0.98 mmol) according to **General Procedure 1** with $BrCH_2CN$ (0.14 mL, 2.00 mmol) and $Ru(bpy)_3(PF_6)_2$ (8.8 mg, 10.2 μmol) in anhydrous MeCN (7.5 mL), the reaction mixture was cooled to 0 ^{o}C. To the reaction mixture was added phenylmagnesium bromide (2.00 mL, 1.0 M in THF, 2.00 mmol) dropwise over 15 min. Work up and purification as above gave **103** as a microcrystalline orange solid (170.4 mg, 61%); ^{1}H NMR (400 MHz, $CDCl_3$) δ 7.34 - 7.16 (11H, m, C*H*), 6.88 (2H, d, *J* = 8.0 Hz, C*H*), 6.77 (1H, t, *J* = 7.3 Hz, C*H*), 5.85 (1H, s, C*H*), 3.79 - 3.70 (1H, m, CH_2), 3.57 - 3.48 (1H, m, CH_2), 3.02 - 2.88 (2H, m, CH_2); ^{1}H NMR data are consistent with the data listed above. Alternatively, to the crude product was added 1,3,5-trimethoxybenzene (10 mol%) and the yield of **103** was determined by ^{1}H NMR analysis (see Appendix for example calculations).

1-(4-Fluorophenyl)-*N*-phenyl-1,2,3,4-tetrahydroisoquinoline (104)[218]

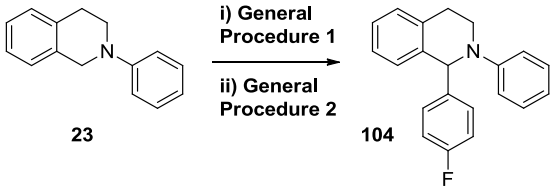

23 **104**

Conducted according to **General Procedure 2**. Following photoactivation of **23** (192.0 mg, 0.92 mmol) according to **General Procedure 1**, crude **26** was dissolved in anhydrous MeCN (5 mL). After cooling to 0 ^{o}C, 4-fluorophenylmagnesium bromide (1.85 mL, 1.0 M in THF, 1.85 mmol) was added dropwise over 15 min. Work up† gave the crude product as a brown oil. Purification by flash column chromatography (a gradient of 5 - 10% DCM (1% Et_3N)/heptane) gave **104** as a yellow oil (199.6 mg, 72%); IR ν_{max} (neat) 3027 - 2916 (C-H), 1596 (Ar), 1503 (Ar), 1475 (Ar), 1457 (Ar), 1410, 1382, 1359, 1346, 1327, 1300, 1253, 1219 cm^{-1}; ^{1}H NMR (400 MHz, $CDCl_3$) δ 7.28 - 7.15 (8H, m, C*H*), 6.93 (2H, apt. t, *J* = 8.7 Hz, C*H*), 6.88 (2H, d, *J* = 8.1 Hz, C*H*), 6.79 (1H, t, *J* = 7.3 Hz, C*H*), 5.82 (1H, s, C*H*), 3.72 - 3.64 (1H, m, CH_2), 3.56 - 3.46 (1H, m, CH_2), 3.03 - 2.94 (1H, m, CH_2), 2.93 - 2.84 (1H, m, CH_2); ^{13}C NMR (101 MHz, $CDCl_3$) δ 161.8 (d, $J_{C\text{-}F}$ = 245.3 Hz, *C*), 149.5 (*C*), 138.8 (d, $J_{C\text{-}F}$ = 3.2 Hz, *C*), 137.6 (*C*), 135.7 (*C*), 129.2 (*C*H), 129.0 (d, $J_{C\text{-}F}$ = 8.0 Hz, *C*H), 128.2 (*C*H), 127.8 (*C*H), 127.1 (*C*H), 126.2 (*C*H), 117.9 (*C*H), 115.0 (d, $J_{C\text{-}F}$ = 21.4 Hz, *C*H), 114.2 (*C*H), 62.3 (*C*H), 43.7 (*C*H_2), 28.0 (*C*H_2); HRMS (+APCI) *m/z* calculated for $C_{21}H_{19}FN$ [M+H^{+}] 304.1496; Found 304.1500. Data are consistent with literature.[218]

1-(4-Methoxyphenyl)-*N*-phenyl-1,2,3,4-tetrahydroisoquinoline (105)[47]

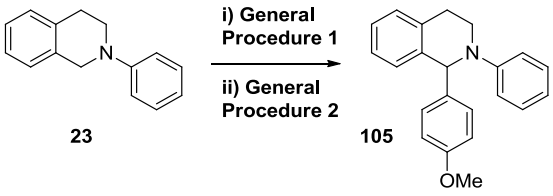

23 105

Conducted according to **General Procedure 2**. Following photoactivation of **23** (192.0 mg, 0.92 mmol) according to **General Procedure 1**, crude **26** was dissolved in anhydrous MeCN (5 mL). After cooling to 0 ^{o}C, 4-methoxyphenylmagnesium bromide (3.70 mL, 0.5 M in THF, 1.85 mmol) was added dropwise over 15 min. Work up gave the crude product as a brown oil. Purification by flash column chromatography (a gradient of 20 - 30% DCM (1% Et_3N)/heptane) gave **105** as a pale yellow oil (179.9 mg, 62%);

†Here, work up was performed without celite filtration.

IR ν_{max} (neat) 2908 - 2835 (C-H), 1596 (Ar), 1504 (Ar), 1474 (Ar), 1463 (Ar), 1441, 1383, 1360, 1345, 1328, 1301, 1246 cm^{-1}; ^{1}H NMR (400 MHz, $CDCl_3$) δ 7.30 - 7.11 (8H, m, C*H*), 6.90 (2H, d, *J* = 8.0 Hz, C*H*), 6.82 - 6.74 (3H, m, C*H*), 5.82 (1H, s, C*H*), 3.77 (3H, s, CH_3), 3.74 - 3.67 (1H, m, CH_2), 3.58 - 3.48 (1H, m, CH_2), 3.05 - 2.85 (2H, m, CH_2); ^{13}C NMR (101 MHz, $CDCl_3$) δ 158.5 (*C*), 149.6 (*C*), 138.1 (*C*), 135.7 (*C*), 135.2 (*C*), 129.1 (*C*H), 128.5 (*C*H), 128.2 (*C*H), 127.8 (*C*H), 126.9 (*C*H), 126.1 (*C*H), 117.5 (*C*H), 114.1 (*C*H), 113.5 (*C*H), 62.3 (*C*H), 55.2 (*C*H_3), 43.5 (*C*H_2), 28.0 (*C*H_2); HRMS (+APCI) *m/z* calculated for $C_{22}H_{22}NO$ [$M+H^+$] 316.1701; Found 316.1701. Data are consistent with literature.[47]

N-Phenyl-1-allyl-1,2,3,4-tetrahydroisoquinoline (106)[219]

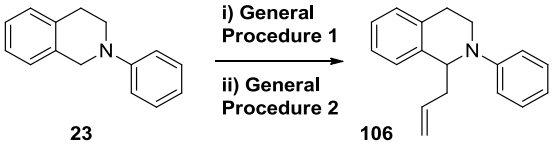

23 106

Conducted according to **General Procedure 2**. Following photoactivation of **23** (198.0 mg, 0.95 mmol) according to **General Procedure 1**, crude **26** was dissolved in anhydrous MeCN (5 mL). The allyl indium sesquihalide reagent (1.0 M in DMF) was prepared by a literature procedure[151] using indium powder (-100 mesh) (210 mg, 1.8 mmol, 2.0 eq.) in DMF (2 mL) and adding allyl iodide (0.35 mL, 3.83 mmol, 3.8 eq.). The resultant milky white suspension was removed by syringe (2.3 mL, 1.2 M in DMF) and added dropwise to crude **26** in MeCN over 15 min at 0 ^{o}C. Work up gave the crude product as a brown oil. Purification by column chromatography (10 - 20% DCM (1% Et_3N)/heptane) gave **106** as a pale yellow oil (217.6 mg, 92%); ^{1}H NMR (400 MHz, $CDCl_3$) δ 7.28 (2H, apt. t, *J* = 7.6 Hz, C*H*), 7.23 - 7.12 (4H, m, C*H*), 6.94 (2H, d, *J* = 8.0 Hz, C*H*), 6.77 (1H, apt. t, *J* = 7.3 Hz, C*H*), 5.95 - 5.83 (1H, m, C*H*), 5.15 - 5.05 (2H, m, CH_2), 4.78 (1H, t, *J* = 6.8 Hz, C*H*), 3.71 - 3.59 (2H, m, CH_2), 3.11 - 3.01 (1H, m, CH_2), 2.96 - 2.87 (1H, m, CH_2), 2.82 - 2.73 (1H, m, CH_2), 2.58 - 2.48 (1H, m, CH_2). ^{1}H NMR data are consistent with the data listed on the subsequent page.

Alternatively, following photoactivation of **23** (201.0 mg, 0.96 mmol) according to **General Procedure 1**, the reaction mixture was cooled to 0 ^{o}C. The allylindium reagent derived from reaction of allyl iodide (0.35 mL, 3.83 mmol, 3.8 eq.) and indium powder (0.22 g, 1.92 mmol, 2.0 eq.) in DMF (2.0 mL) was added directly to the reaction mixture dropwise over 15 min at 0 ^{o}C. Work up[†] and purification gave **106** as a pale yellow oil (162.5 mg, 68%); ^{1}H NMR (400 MHz, $CDCl_3$) δ 7.27 (2H, apt. t, *J* = 7.9 Hz, C*H*), 7.21 - 7.10 (4H, m, C*H*), 6.91 (2H, d, *J* = 8.2 Hz, C*H*), 6.77 (1H, apt. t, *J* = 7.3, C*H*), 5.93 - 5.80 (1H, m, C*H*), 5.11 - 5.03 (2H, m, CH_2), 4.76 (1H, t, *J* = 6.8 Hz, C*H*), 3.70 - 3.56 (2H, m, CH_2), 3.11 - 2.99 (1H, m, CH_2), 2.94 - 2.85 (1H, m, CH_2), 2.79 - 2.70 (1H, m, CH_2), 2.56 - 2.45 (1H, m, CH_2); ^{1}H NMR data are consistent with the data listed on the subsequent page.

Alternatively, following photoactivation of **23** (196.0 mg, 0.94 mmol) according to **General Procedure 1**, crude **26** was suspended in anhydrous THF (5 mL). Separately, allylmagnesium bromide (1.0 M in Et_2O) (1.90 mL, 1.90 mmol, 2.0 eq.) was added to zinc chloride (1.30 mL, 1.9 M in THF, 2.5 mmol, 2.6 eq.) in THF (2 mL) at -78 ^{o}C. After stirring for 30 min at -78 ^{o}C and then 30 min at rt, the resultant milky white suspension was removed by syringe and added dropwise to the crude **26** in THF over 15 min at 0 ^{o}C. Work up[‡] and purification gave **106** as a pale yellow oil (205.5 mg, 88%); ^{1}H NMR (400 MHz, $CDCl_3$) δ 7.25 (2H, apt. t, *J* = 8.2 Hz, C*H*), 7.21 - 7.10 (4H, m, C*H*), 6.91 (2H, d, *J* = 8.1 Hz, C*H*), 6.75 (1H, apt. t, *J* = 7.2, C*H*), 5.94 - 5.81 (1H, m, C*H*), 5.12 - 5.02 (2H, m, CH_2), 4.78 (1H, t, *J* = 6.7 Hz, C*H*), 3.70 - 3.56 (2H, m, CH_2), 3.09 - 2.99 (1H, m, CH_2), 2.94 - 2.85 (1H, m, CH_2), 2.80 - 2.69 (1H, m, CH_2), 2.55 - 2.46 (1H, m, CH_2); ^{1}H NMR data are consistent with the data listed on the subsequent page.

Alternatively, following photoactivation of **23** (198.0 mg, 0.95 mmol) according to **General Procedure 1**, crude **26** was dissolved in anhydrous MeCN (5 mL). Separately, allylmagnesium bromide (1.0 M in Et_2O) (1.90 mL,

[†]Here, work up was performed without celite filtration. [‡]Here, work up was performed without celite filtration and extraction used H_2O (10 mL) and EtOAc (3 x 30 mL).

1.90 mmol, 2.0 eq.) was added to zinc chloride (1.30 mL, 1.9 M in THF, 2.5 mmol, 2.6 eq.) in THF (2 mL) at -78 ^{o}C. After stirring for 30 min at -78 ^{o}C and then 30 min at rt, the resultant milky white suspension was removed by syringe and added dropwise to the crude **26** in MeCN over 15 min at 0 ^{o}C. Work up and purification gave **106** as a colourless oil (86.9 mg, 37%); IR ν_{max} (neat) 3023 - 2835 (C-H), 1638 (C=C) 1596 (Ar), 1502 (Ar), 1473 (Ar), 1451 (Ar), 1390, 1344, 1327, 1297, 1267, 1222 cm^{-1}; ^{1}H NMR (400 MHz, $CDCl_3$) δ 7.27 (2H, apt. t, *J* = 8.1 Hz, C*H*), 7.22 - 7.11 (4H, m, C*H*), 6.93 (2H, d, *J* = 8.0 Hz, C*H*), 6.77 (1H, td, *J* = 7.3, 0.9 Hz, C*H*), 5.94 - 5.82 (1H, m, C*H*), 5.13 - 5.03 (2H, m, CH_2), 4.78 (1H, t, *J* = 6.8 Hz, C*H*), 3.71 - 3.58 (2H, m, CH_2), 3.11 - 3.00 (1H, m, CH_2), 2.95 - 2.85 (1H, m, CH_2), 2.81 - 2.71 (1H, m, CH_2), 2.56 - 2.47 (1H, m, CH_2); ^{13}C NMR (101 MHz, $CDCl_3$) δ 149.4 (*C*), 138.1 (*C*), 135.6 (*C*H), 134.9 (*C*), 129.2 (*C*H), 128.5 (*C*H), 127.3 (*C*H), 126.5 (*C*H), 125.7 (*C*H), 117.3 (*C*H), 117.0 (*C*H_2), 114.0 (*C*H), 59.4 (*C*H), 42.0 (*C*H_2), 40.9 (*C*H_2), 27.4 (*C*H_2); HRMS (+APCI) *m/z* calculated for $C_{18}H_{20}N$ [M+H^{+}] 250.1596; Found 250.1587. Data are consistent with the literature.[219]

1-(2-Methylallyl)-*N*-phenyl-1,2,3,4-tetrahydroisoquinoline (107)[96]

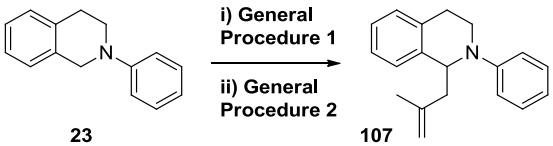

23 **107**

Conducted according to **General Procedure 2**. Following photoactivation of **23** (198.0 mg, 0.95 mmol) according to **General Procedure 1**, crude **26** was dissolved in anhydrous MeCN (5 mL). Separately, 2-methylallylmagnesium bromide (0.5 M in Et_2O) (3.80 mL, 1.90 mmol, 2.0 eq.) was added to zinc chloride (1.30 mL, 1.9 M in THF, 2.5 mmol, 2.6 eq.) in THF (2 mL) at -78 ^{o}C. After stirring for 30 min at -78 ^{o}C and then 30 min at rt, the resultant milky white suspension was removed by syringe and added dropwise to the crude **26** in MeCN over 15 min at 0 ^{o}C. Work up gave the crude product as a brown oil. Purification by column chromatography (0 - 5% toluene/heptane (1% Et_3N)) gave **107** as a yellow oil (224.8 mg, 90%); IR ν_{max} (neat) 3024 - 2914

(C-H), 1646 (C=C), 1597 (Ar), 1502 (Ar), 1474 (Ar), 1451 (Ar), 1390, 1330, 1291, 1268, 1210 cm^{-1}; ^{1}H NMR (400 MHz, $CDCl_3$) δ 7.28 (3H, apt. t, *J* = 7.2 Hz, C*H*), 7.22 - 7.08 (4H, m, C*H*), 6.97 (1H, d, *J* = 8.0 Hz, C*H*), 6.78 (1H, t, *J* = 7.3 Hz, C*H*), 4.90 (1H, apt. t, *J* = 7.0 Hz, C*H*), 4.86 (1H, br. s, CH_2), 4.72 (1H, br. s, CH_2), 3.68 (2H, apt. t, *J* = 6.2 Hz, CH_2), 3.13 - 3.00 (1H, m, CH_2), 2.93 - 2.83 (1H, m, CH_2), 2.78 - 2.70 (1H, m, CH_2), 2.50 - 2.40 (1H, m, CH_2), 1.84 (3H, s, CH_3); ^{13}C NMR (101 MHz, $CDCl_3$) δ 149.5 (*C*), 142.9 (*C*), 138.5 (*C*), 134.7 (*C*), 129.2 (*C*H), 128.5 (*C*H), 127.4(*C*H), 126.4 (*C*H), 125.5 (*C*H), 117.4 (*C*H), 114.2 (*C*H), 113.5 (*C*H_2), 58.2 (*C*H), 44.6 (*C*H_2), 41.7 (*C*H_2), 26.9 (*C*H_2), 22.9 (CH_3); HRMS (+APCI) *m/z* calculated for $C_{19}H_{22}N$ [M+H^+] 264.1752; Found 264.1747. Data are consistent with literature.[96]

1-(But-3-en-2-yl)-*N*-phenyl-1,2,3,4-tetrahydroisoquinoline (*108*)

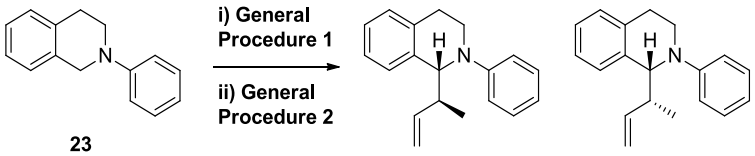

Conducted according to **General Procedure 2**. Following photoactivation of **23** (198.0 mg, 0.95 mmol) according to **General Procedure 1**, crude **26** was dissolved in anhydrous MeCN (5 mL). Separately, 2-butenylmagnesium bromide (0.5 M in THF) (4.00 mL, 2.00 mmol, 2.1 eq.) was added to zinc chloride (1.30 mL, 1.9 M in THF, 2.5 mmol, 2.6 eq.) in THF (2 mL) at -78 ^{o}C. After stirring for 30 min at -78 ^{o}C and then 30 min at rt, the resultant milky white suspension was removed by syringe and added dropwise to the crude **26** in MeCN over 15 min at 0 ^{o}C. Work up† gave the crude product as a brown oil. Purification by column chromatography (2 - 5% toluene/heptane (1% Et_3N)) gave ***108*** as a yellow oil (229.1 mg, 92%) and as a 1 : 1 mixture of diastereomers; IR ν_{max} (neat) 3023 - 2923 (C-H), 1638 (C=C), 1574 (Ar), 1597 (Ar), 1502 (Ar), 1474 (Ar), 1456 (Ar), 1418, 1392, 1371, 1299, 1269, 1218 cm^{-1}; ^{1}H NMR (400 MHz, $CDCl_3$) <u>diastereomer 1:</u> δ 7.30 - 7.08 (6H, m,

†Here, work up was performed without celite filtration.

C*H*), 6.90 (2H, apt. d, *J* = 6.8 Hz, C*H*), 6.77 - 6.70 (1H, m, C*H*), 6.03 - 5.92 (1H, m, C*H*), 5.11 - 4.89 (2H, m, C*H*), 4.60 (1H, d, *J* = 7.4 Hz, C*H*), 3.82 - 3.71 (1H, m, CH_2), 3.54 - 3.44 (1H, m, CH_2), 3.13 - 2.93 (2H, m, CH_2), 2.83 - 2.71 (1H, m, C*H*), 1.11 (3H, d, *J* = 6.6, CH_3); diastereomer 2: δ 7.30 - 7.08 (6H, m, C*H*), 6.90 (2H, apt. d, *J* = 6.8 Hz, C*H*), 6.77 - 6.70 (1H, m, C*H*), 5.76 - 5.64 (1H, m, C*H*), 5.11 - 4.89 (2H, m, C*H*), 4.54 (1H, d, *J* = 6.8 Hz, C*H*), 3.82 - 3.71 (1H, m, CH_2), 3.54 - 3.44 (1H, m, CH_2), 3.13 - 2.93 (2H, m, CH_2), 2.83 - 2.71 (1H, m, C*H*), 1.21 (3H, d, *J* = 7.0, CH_3); ^{13}C NMR (101 MHz, $CDCl_3$) diastereomer 1 and diastereomer 2: δ 149.8 (*C*), 149.7 (*C*), 141.9 (*C*H), 141.4 (*C*H), 137.2 (*C*), 136.6 (*C*), 135.5 (2 x *C*), 129.2 (*C*H), 129.1 (*C*H), 128.4 (*C*H), 128.3 (*C*H), 128.1 (*C*H), 128.0 (*C*H), 126.7 (*C*H), 126.6 (*C*H), 125.4 (*C*H), 125.1 (*C*H), 116.8 (*C*H), 116.7 (*C*H), 115.1 (*C*H_2), 113.9 (*C*H_2), 113.5 (*C*H), 113.1 (*C*H), 63.7 (*C*H), 63.6 (*C*H), 44.6 (*C*H), 43.8 (*C*H), 43.0 (*C*H_2), 42.9 (*C*H_2), 27.6 (*C*H_2), 27.3 (*C*H_2), 18.2 (*C*H_3), 16.8 (*C*H_3); HRMS (+ESI) *m/z* calculated for $C_{19}H_{22}N$ [M+H$^+$] 264.1747; Found 264.1747.

_N_-(Naphthalen-2-yl)-1-phenyl-1,2,3,4-tetrahydroisoquinoline (117)

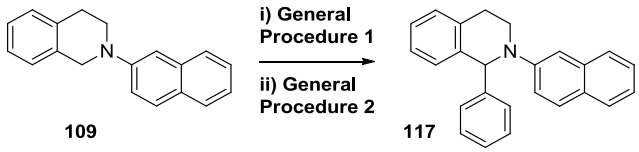

Conducted according to **General Procedure 2**. Following photoactivation of **109** (251.0 mg, 0.97 mmol) according to **General Procedure 1**, the crude iminium salt was dissolved in anhydrous MeCN (10 mL). After cooling to 0 ^{o}C, phenylmagnesium bromide (2.1 mL, 1.0 M in THF, 2.1 mmol) was added dropwise over 15 min. Work up gave the crude product. MDAP purification (high pH) gave ***117*** as a pale brown oil (153.1 mg, 47%); IR ν_{max} (neat) 3025 - 2917 (C-H), 1626 (Ar), 1597 (Ar), 1509 (Ar), 1492 (Ar), 1470 (Ar), 1446, 1386, 1356, 1319, 1300, 1259, 1217 cm^{-1}; ^{1}H NMR (400 MHz, $CDCl_3$) δ 7.71 (2H, t, *J* = 7.8 Hz, C*H*), 7.64 (1H, d, *J* = 8.2 Hz, C*H*), 7.39 - 7.17 (12H, m, C*H*), 7.08 (1H, d, *J* = 2.5 Hz, C*H*), 6.03 (1H, s, C*H*), 3.84 - 3.76 (1H, m, CH_2), 3.71 - 3.63 (1H, m, CH_2), 3.08 - 2.90 (2H, m, CH_2); ^{13}C NMR (101 MHz,

$CDCl_3$) δ 147.4 (*C*), 142.9 (*C*), 137.6 (*C*), 135.7 (*C*), 134.9 (*C*), 128.8 (*C*H), 128.2 (2 x *C*H), 127.9 (*C*H), 127.5 (2 x *C*H), 127.4 (*C*H, *C*), 127.1 (*C*H), 126.9 (*C*H), 126.3 (*C*H), 126.2 (*C*H), 122.4 (*C*H), 117.4 (*C*H), 108.2 (*C*H), 62.8 (*C*H), 43.8 (CH_2), 28.0 (CH_2); HRMS (+APCI) *m/z* calculated for $C_{25}H_{22}N$ [$M+H^+$] 336.1752; Found 336.1745.

6,7-Dimethoxy-1,2-diphenyl-1,2,3,4-tetrahydroisoquinoline (*118*)

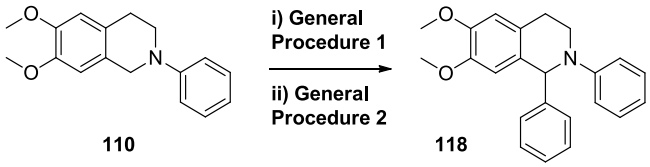

Conducted according to **General Procedure 2**. Following photoactivation of **110** (266.0 mg, 0.99 mmol) according to **General Procedure 1**, the crude iminium salt was dissolved in anhydrous MeCN (5 mL). After cooling to 0 ^oC, phenylmagnesium bromide (2.0 mL, 1.0 M in THF, 2.0 mmol) was added dropwise over 15 min. Work up gave the crude product as a brown oil. Purification by column chromatography (a gradient of 70 - 100% toluene/heptane (1% Et_3N)) gave a yellow oil, which crystallised overnight to yield ***118*** as a microcrystalline yellow solid (323.3 mg, 95%); m.p. 103 - 105 ^oC; IR ν_{max} 3021 - 2835 (C-H), 1598 (Ar), 1512, 1503 (Ar), 1483, 1383, 1354, 1336, 1274, 1241, 1221, 1206 cm^{-1}; ^1H NMR (400 MHz, $CDCl_3$) δ 7.30 - 7.17 (7H, m, C*H*), 6.92 (2H, d, *J* = 8.4 Hz, C*H*), 6.78 (1H, t, *J* = 7.3 Hz, C*H*), 6.75 (1H, s, C*H*), 6.68 (1H, s, C*H*), 5.79 (1H, s, C*H*), 3.88 (3H, s, CH_3), 3.86 (3H, s, CH_3), 3.65 - 3.50 (2H, m, CH_2), 2.98 - 2.88 (1H, m, CH_2), 2.83 - 2.74 (1H, m, CH_2); ^{13}C NMR (101 MHz, $CDCl_3$) δ 149.8 (*C*), 148.0 (*C*), 147.3 (*C*), 143.3 (*C*), 129.2 (*C*), 129.1 (*C*H), 128.1 (*C*H), 127.8 (*C*), 127.6 (*C*H), 126.8 (*C*H), 117.9 (*C*H), 114.7 (*C*H), 111.3 (*C*H), 111.2 (*C*H), 62.4 (*C*H), 56.1 (CH_3), 55.9 (CH_3), 43.2 (CH_2), 27.1 (CH_2); HRMS (+APCI) *m/z* calculated for $C_{23}H_{24}NO_2$ [$M+H^+$] 346.1807; Found 346.1800.

Alternatively, following photoactivation of **110** (257.0 mg, 0.97 mmol) according to **General Procedure 1** with $BrCH_2CN$ (0.14 mL, 2.00 mmol) and

$Ru(bpy)_3(PF_6)_2$ (8.4 mg, 9.8 μmol) in anhydrous MeCN (7.5 mL), the reaction mixture was cooled to 0 °C. To the reaction mixture was added phenylmagnesium bromide (2.00 mL, 1.0 M in THF, 2.00 mmol) dropwise over 15 min. Work up† and purification as above gave ***118*** as a microcystalline yellow solid (170.4 mg, 72%); ^{1}H NMR (400 MHz, $CDCl_3$) δ 7.25 - 7.16 (7H, m, C*H*), 6.91 (2H, d, *J* = 8.1 Hz, C*H*), 6.77 (1H, t, *J* = 7.3 Hz, C*H*), 6.74 (1H, s, C*H*), 6.67 (1H, s, C*H*), 5.78 (1H, s, C*H*), 3.87 (3H, s, CH_3), 3.86 (3H, s, CH_3), 3.65 - 3.49 (2H, m, CH_2), 2.97 - 2.87 (1H, m, CH_2), 2.82 - 2.73 (1H, m, CH_2). ^{1}H NMR data are consistent with the data listed on the previous page.

N-(*p*-Methoxyphenyl)-1-phenyl-1,2,3,4-tetrahydroisoquinoline (119)[47]

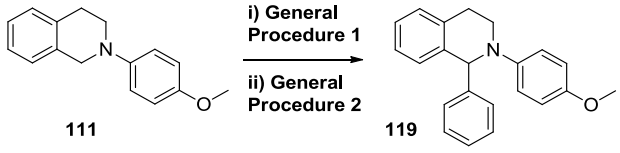

Conducted according to **General Procedure 2**. Following photoactivation of **111** (223.0 mg, 0.93 mmol) according to **General Procedure 1**, the crude iminium salt was dissolved in anhydrous MeCN (5 mL). After cooling to 0 °C, phenylmagnesium bromide (1.90 mL, 1.0 M in THF, 1.90 mmol) was added dropwise over 15 min. Work up gave the crude product. Purification by flash column chromatography (a gradient of 50 - 70% toluene/heptane (1% Et_3N)) gave a yellow oil, which crystallised overnight. The yellow solid was recrystallised from MeCN to yield **119** as a microcrystalline yellow solid (152.5 mg, 52%); m.p. 129 - 131 °C (lit. 128 - 129 °C[44]); IR ν_{max} (neat) 3023 - 2823 (C-H), 1508 (Ar), 1493 (Ar), 1464 (Ar), 1451 (Ar), 1440, 1370, 1293, 1264, 1242, 1216, 1204 cm^{-1}; ^{1}H NMR (400 MHz, $CDCl_3$) δ 7.25 - 7.14 (9H, m, C*H*), 6.83 (2H, d, *J* = 9.4 Hz, C*H*), 6.81 (2H, d, *J* = 9.4 Hz, C*H*), 5.67 (1H, s, C*H*), 3.76 (3H, s, CH_3), 3.63 - 3.55 (1H, m, CH_2), 3.47 - 3.38 (1H, m, CH_2), 3.04 - 2.89 (2H, m, CH_2); ^{13}C NMR (101 MHz, $CDCl_3$) δ 152.9 (*C*), 144.5 (*C*), 143.3 (*C*), 137.7 (*C*), 135.5 (*C*), 128.4 (*C*H), 128.1 (2 x *C*H), 128.0 (*C*H),

†Here, work up was performed without celite filtration and extraction used H_2O (10 mL) and EtOAc (3 x 30 mL).

126.8 (*C*H), 126.7 (*C*H), 126.0 (*C*H), 117.8 (*C*H), 114.5 (*C*H), 64.4 (*C*H), 55.6 (CH_3), 44.6 (CH_2), 28.2 (CH_2); HRMS (+APCI) *m/z* calculated for $C_{22}H_{22}NO$ $[M+H^+]$ 316.1701; Found 316.1697. Data are consistent with the literature.[47]

Alternatively, following photoactivation of **111** (238.9 mg, 1.00 mmol) according to **General Procedure 1** with $BrCH_2CN$ (0.14 mL, 2.00 mmol) and $Ru(bpy)_3(PF_6)_2$ (8.6 mg, 10.0 μmol) in anhydrous MeCN (7.5 mL), the reaction mixture was cooled to 0 °C. To the reaction mixture was added phenylmagnesium bromide (2.00 mL, 1.0 M in THF, 2.00 mmol) dropwise over 15 min. Work up† and purification as above gave **119** as a microcrystalline yellow solid (231.3 mg, 73%); ^{1}H NMR (400 MHz, $CDCl_3$) δ 7.25 - 7.14 (9H, m, C*H*), 6.82 (2H, d, *J* = 9.1 Hz, C*H*), 6.81 (2H, d, *J* = 9.3 Hz, C*H*), 5.67 (1H, s, C*H*), 3.75 (3H, s, CH_3), 3.62 - 3.54 (1H, m, CH_2), 3.46 - 3.38 (1H, m, CH_2), 3.03 - 2.89 (2H, m, CH_2). ^{1}H NMR data are consistent with the data listed above.

N-(*p*-Bromophenyl)-1-phenyl-1,2,3,4-tetrahydroisoquinoline (*120*)

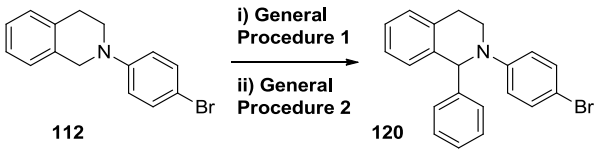

Conducted according to **General Procedure 2**. Following photoactivation of **112** (278.0 mg, 0.95 mmol) according to **General Procedure 1**, the crude iminium salt was dissolved in dry MeCN (10 mL). After cooling to 0 °C, phenylmagnesium bromide (2.0 mL, 1.0 M in THF, 2.0 mmol) was added dropwise over 15 min. Work up‡ gave the crude product as a yellow brown oil. MDAP purification gave ***120*** as a colourless oil (181.6 mg, 53%); IR ν_{max} (neat) 3025 - 2841 (C-H), 1587 (Ar), 1490 (Ar), 1473 (Ar), 1456 (Ar), 1447, 1382, 1361, 1331, 1299, 1250, 1227 cm^{-1}; ^{1}H NMR (400 MHz, $CDCl_3$) δ 7.36-7.16 (11H, m, C*H*), 6.74 (2H, d, *J* = 9.1 Hz, C*H*), 5.79 (1H, s, C*H*),

†Here, work up was performed without celite filtration and extraction used H_2O (10 mL) and EtOAc (3 x 30 mL). ‡Work up was performed without celite filtration and extraction used H_2O (50 mL) and toluene (3 x 50 mL).

3.77 - 3.68 (1H, m, CH_2), 3.54 - 3.44 (1H, m, CH_2), 3.01 - 2.89 (2H, m, CH_2); ^{13}C NMR (101 MHz, $CDCl_3$) δ 148.5 (*C*), 142.5 (*C*), 137.6 (*C*), 135.5 (*C*), 131.8 (*C*H), 128.3 (*C*H), 128.1 (*C*H), 127.7 (*C*H), 127.2 (*C*H), 127.1 (*C*H), 127.0 (*C*H), 126.3 (*C*H), 115.3 (*C*H), 109.4 (*C*), 62.8 (*C*H), 44.0 (*C*H_2), 28.0 (*C*H_2); HRMS (+APCI) *m/z* calculated for $C_{21}H_{19}{}^{79}BrN$ [M+H$^+$] 364.0701; Found 364.0696.

Alternatively, following photoactivation of **112** (185.9 mg, 0.65 mmol) according to **General Procedure 1** with $BrCH_2CN$ (90.0 μL, 1.29 mmol) and $Ru(bpy)_3(PF_6)_2$ (5.6 mg, 6.5 μmol) in anhydrous MeCN (6 mL) and anhydrous THF (3 mL) (every 1 h, the reaction mixture was heated gently until the precipitate dissolved for a total reaction time of 5 h), the reaction mixture was cooled to 0 ^{o}C. To the reaction mixture was added phenylmagnesium bromide (1.30 mL, 1.0 M in THF, 1.30 mmol) dropwise over 15 min. Work up[†] and purification as above gave ***120*** as a yellow oil (117.3 mg, 50%); ^{1}H NMR (400 MHz, $CDCl_3$) δ 7.37 -7.19 (11H, m, C*H*), 6.75 (2H, d, *J* = 9.1 Hz, C*H*), 5.80 (1H, s, C*H*), 3.79 - 3.69 (1H, m, CH_2), 3.55 - 3.46 (1H, m, CH_2), 3.04 - 2.90 (2H, m, CH_2). ^{1}H NMR data are consistent with the data listed above.

N-(*p*-Nitrophenyl)-1-phenyl-1,2,3,4-tetrahydroisoquinoline (121)[220]

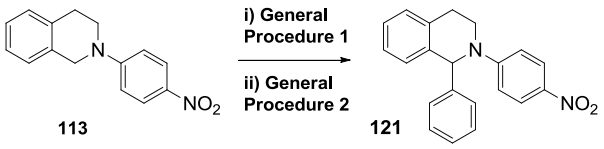

Conducted according to **General Procedure 2**. Following photoactivation of **113** (245.0 mg, 0.97 mmol) according to **General Procedure 1**, the crude iminium salt was dissolved in anhydrous MeCN (10 mL). After cooling to 0 ^{o}C, phenylmagnesium bromide (2.0 mL, 1.0 M in THF, 2.0 mmol) was added dropwise over 15 min. Work up gave the crude product, which was purified by flash column chromatography (a gradient of 70 - 100% toluene/heptane (1% Et_3N)) to afford **121** as a yellow microcrystalline solid (244.9 mg, 77%);

[†]Here, work up was performed without celite filtration and extraction used H_2O (10 mL) and EtOAc (3 x 30 mL).

m.p. 141 - 143 ^{o}C (lit. 145 - 147 ^{o}C[220]); IR ν_{max} (neat) 3075 - 2947 (C-H), 1598 (Ar), 1584 (N-O), 1506 (Ar), 1482 (Ar), 1466 (Ar), 1446, 1436, 1389, 1359, 1313 (N-O), 1299, 1257, 1231, 1219, 1207 cm^{-1}; ^{1}H NMR (400 MHz, $CDCl_3$) δ 8.16 (2H, d, *J* = 9.5 Hz, C*H*), 7.42 (1H, dd, *J* = 6.8, 2.0 Hz, C*H*), 7.35 - 7.19 (8H, m, C*H*), 6.81 (2H, d, *J* = 9.5 Hz, C*H*), 5.99 (1H, s, C*H*), 3.91 (1H, dt, *J* = 11.2, 4.8 Hz, CH_2), 3.67 - 3.58 (1H, m, CH_2), 2.98 (2H, dd, *J* = 7.8, 4.7 Hz, CH_2); ^{13}C NMR (101 MHz, $CDCl_3$) δ 153.6 (*C*), 140.8 (*C*), 137.7 (*C*), 137.1 (*C*), 135.1 (*C*), 128.7 (*C*H), 128.0 (*C*H), 127.9 (*C*H), 127.6 (*C*H), 127.4 (*C*H), 126.8 (*C*H), 126.4 (*C*H), 126.2 (*C*H), 111.1 (*C*H), 62.3 (*C*H), 44.8 (*C*H_2), 27.9 (*C*H_2); HRMS (+APCI) *m/z* calculated for $C_{21}H_{19}N_2O_2$ [M+H$^+$] 331.1447; Found 331.1442. Data are consistent with the literature.[220]

N-Methyl-1-phenyl-1,2,3,4-tetrahydroisoquinoline (122)[221]

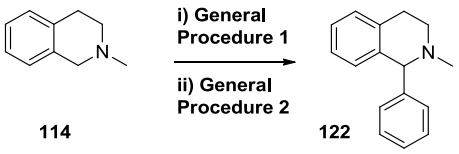

114 122

Conducted according to **General Procedure 2**. Following photoactivation of **114** (147.2 mg, 1.00 mmol) according to **General Procedure 1**, the crude iminium salt was dissolved in dry MeCN (5 mL). After cooling to 0 ^{o}C, phenylmagnesium bromide (2.00 mL, 1.0 M in THF, 2.00 mmol) was added dropwise over 15 min. Work up† gave the crude product, which was purified by flash column chromatography (a gradient of 20 - 40% EtOAc (1% Et_3N)/heptane) to afford **122** as a yellow oil (129.8 mg, 58%); IR ν_{max} (neat) 3061 - 2701 (C-H), 1601 (Ar), 1492 (Ar), 1450 (Ar), 1426, 1366, 1345, 1315, 1289, 1248, 1218 cm^{-1}; ^{1}H NMR (400 MHz, $CDCl_3$) δ 7.34 - 7.23 (5H, m, C*H*), 7.14 - 7.05 (2H, m, C*H*), 6.97 (1H, apt. t, *J* = 7.2 Hz, C*H*), 6.64 (1H, d, *J* = 7.8 Hz, C*H*), 4.23 (1H, s, C*H*), 3.32 - 3.21 (1H, m, CH_2), 3.16 - 3.08 (1H, m, CH_2), 2.87 - 2.78 (1H, m, CH_2), 2.67 - 2.59 (1H, m, CH_2), 2.23 (3H, s, CH_3); ^{13}C NMR (101 MHz, $CDCl_3$) δ 144.0 (*C*), 138.6 (*C*), 134.3 (*C*), 129.6 (*C*H), 128.5

†Here, work up was performed without celite filtration and extraction used H_2O (40 mL) and EtOAc (3 x 40 mL).

(*C*H), 128.3 (2 x *C*H), 127.3 (*C*H), 125.9 (*C*H), 125.6 (*C*H), 71.6 (*C*H), 52.4 (CH_2), 44.4 (CH_3), 29.6 (CH_2). Data are consistent with literature.[221]

6,7-Dimethoxy-*N*-methyl-1-phenyl-1,2,3,4-tetrahydroisoquinoline (123)[222]

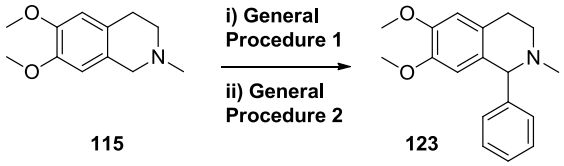

115 123

Conducted according to **General Procedure 2**. Following photoactivation of **115** (201.2 mg, 0.97 mmol) according to **General Procedure 1**, the crude iminium salt was dissolved in dry MeCN (5 mL). After cooling to 0 ^{o}C, phenylmagnesium bromide (1.95 mL, 1.0 M in THF, 1.95 mmol) was added dropwise over 15 min. Work up† gave the crude product as a brown oil. Purification by flash column chromatography (a gradient of 40 - 50% EtOAc (1% Et_3N)/heptane) gave **123** as a pale yellow oil, which crystallised overnight to yield an off-white microcrystalline solid (222.4 mg, 81%); m.p. 82 - 84 ^{o}C, IR ν_{max} (neat) 2950 - 2789 (C-H), 1610 (Ar), 1515 (Ar), 1467 (Ar), 1453 (Ar), 1404, 1366, 1332, 1307, 1252, 1216 cm^{-1}; ^{1}H NMR (400 MHz, $CDCl_3$) δ 7.35 - 7.22 (5H, m, C*H*), 6.61 (1H, s, C*H*), 6.10 (1H, s, C*H*), 4.19 (1H, s, C*H*), 3.85 (3H, s, CH_3) 3.56 (3H, s, CH_3), 3.25 - 3.06 (2H, m, CH_2), 2.76 - 2.70 (1H, m, CH_2), 2.66 - 2.57 (1H, m, CH_2), 2.24 (3H, s, CH_3), ^{13}C NMR (101 MHz, $CDCl_3$) δ 147.0 (2 x *C*), 143.8 (*C*), 130.3 (*C*), 129.5 (*C*H), 128.2 (*C*H), 127.3 (*C*H), 126.5 (*C*), 111.4 (*C*H), 110.6 (*C*H), 71.0 (*C*H), 55.8 (CH_3), 55.7 (CH_3), 52.2 (CH_2), 44.3 (CH_3), 28.9 (CH_2); HRMS (+APCI) *m/z* calculated for $C_{18}H_{22}NO_2$ [M+H$^+$] 284.1651; Found 284.1648. Data are consistent with literature.[222]

†Here, work up was performed without celite filtration and extraction used H_2O (40 mL) and EtOAc (3 x 40 mL).

(±)-Methopholine[155]

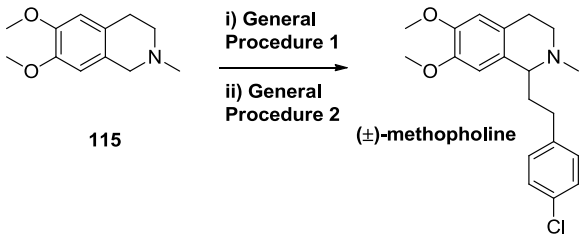

Conducted according to **General Procedure 2**. Following photoactivation of **115** (199.0 mg, 0.96 mmol) according to **General Procedure 1**, the crude iminium salt was dissolved in dry MeCN (5 mL). Separately, a solution of (4-chlorophenethyl)magnesium bromide **124** (1.5 M in THF) was prepared by charging a reaction vessel with magnesium turnings (238.0 mg, 10.0 mmol), anhydrous THF (8.0 mL) and a small crystal of I_2 before adding 4-chlorophenethyl bromide (1.12 mL, 7.70 mmol) dropwise under N_2. A color change from pale brown to colourless was apparent. After refluxing (66 ^oC) for 10 min under N_2 and cooling to rt, the resultant turbid solution was removed by syringe (5.25 mL, 1.5 M in THF) and added dropwise to the crude iminium salt in MeCN over 15 min at 0 ^oC. Work up† gave the crude product as a pale red oil. Purification by flash column chromatography (a gradient of 20 - 100% EtOAc/heptane) gave **(±)-methopholine** as an off-white powder (185.3 mg, 56%); m.p. 111 - 113 ^oC (lit. 109 - 110 ^oC[223]), IR ν_{max} (neat) 2937 - 2786 (C-H), 1611 (Ar), 1518 (Ar), 1491 (Ar), 1467 (Ar), 1448, 1418, 1405, 1372, 1357, 1338, 1320, 1254, 1212 cm^{-1}; ^1H NMR (400 MHz, $CDCl_3$) δ 7.24 (2H, d, *J* = 8.1 Hz, C*H*), 7.12 (2H, d, *J* = 8.3 Hz, C*H*), 6.58 (1H, s, C*H*), 6.53 (1H, s, C*H*), 3.86 (3H, s, CH_3), 3.84 (3H, s, CH_3), 3.41 (1H, apt. t, *J* = 5.0 Hz, C*H*), 3.18 - 3.08 (1H, m, CH_2), 2.82 - 2.65 (4H, m, CH_2), 2.58 - 2.48 (1H, m, CH_2), 2.47 (3H, s, CH_3), 2.08 - 1.97 (2H, m, CH_2); ^{13}C NMR (101 MHz, $CDCl_3$) δ 147.3 (2 x *C*), 141.4 (*C*), 131.2 (*C*), 129.8 (*C*H), 129.6 (*C*), 128.3 (*C*H), 126.8 (*C*), 111.3 (*C*H), 109.9 (*C*H), 62.6 (*C*H), 56.0 (*C*H_3), 55.8 (*C*H_3), 48.2 (*C*H_2), 42.7 (*C*H_3), 36.8 (*C*H_2), 30.8 (*C*H_2), 25.5 (*C*H_2); HRMS (+APCI) *m/z* calculated for $C_{20}H_{25}ClNO_2$ $[M+H^+]$ 346.1568;

†Here, work up was performed without celite filtration and extraction used H_2O (40 mL) and EtOAc (3 x 40 mL).

Found 346.1571. ^{1}H NMR and IR data are consistent with literature.[155]

5.10. PHOTOACTIVATION OF *N*-ARYL TETRAHYDROISOQUINOLINES IN FLOW

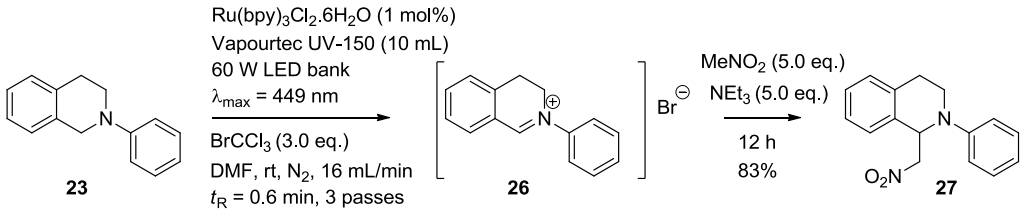

The Vapourtec UV-150 Photochemical Flow Reactor (10 mL coil) was employed and reaction conditions were based on conditions reported in the literature (Table 6, entries 4 - 6, Section 2.1.6.).[115] A reaction vessel was equipped with *N*-phenyl-1,2,3,4-tetrahydroisoquinoline (**23**) (2.00 g, 4.70 mmol), $Ru(bpy)_3Cl_2.6H_2O$ (3.4 mg, 4.80 μmol, 0.05 mol%) and DMF (94 mL). The mixture was sparged with N_2 for 20 min before $BrCCl_3$ (2.80 ml, 14.0 mmol) was added at rt. The mixture was sparged with N_2 for 20 min, then passed through a photochemical flow reactor at the specified flow rate (Table 6, entries 4 - 9), irradiating at 450 nm. The system was assumed to reach steady state after 1.5 residence times and the reaction was sampled for HPLC. For the reaction with no photocatalyst (Table 6, entry 12), a known volume of reaction mixture was collected after reaching steady state, 1,3,5-trimethoxybenzene (10 mol%) was added and the yield was determined by ^{1}H NMR.

5.11. PHOTOACTIVATION OF *N*-ALKYL TETRAHYDROISOQUINOLINES USING BROMOACETONITRILE

N-(Cyanomethyl)-6,7-dimethoxy-*N*-methyl-1,2,3,4-tetrahydroisoquinolin-2-ium bromide (125)

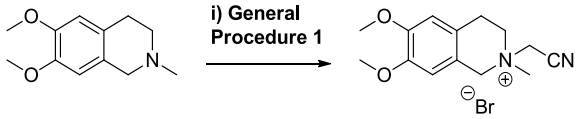

115 125

Following photoactivation of **115** (199.0 mg, 0.96 mmol) according to **General Procedure 1** with $BrCH_2CN$ (0.14 mL, 2.00 mmol) and $Ru(bpy)_3(PF_6)_2$ (8.4 mg, 9.8 μmol) in anhydrous MeCN (7.5 mL) for 3 h, a yellow/orange precipitate was observed and no starting material was observed by HPLC or LCMS. LCMS (Low pH, 8 min gradient) revealed a new peak: R_T = 2.0 min, [M] = 247. A sample of the reaction mixture was filtered to obtain the orange precipitate which was tentatively assigned as **125** by ^{1}H NMR (400 MHz, CD_3OD) δ 6.93 (1H, s, C*H*), 6.84 (1H, s, C*H*), 3.97 (2H, t, *J* = 6.5 Hz, CH_2), 3.87 (3H, s, CH_3), 3.85 (3H, s, CH_3), 3.43 (3H, s, NCH_3);[†]

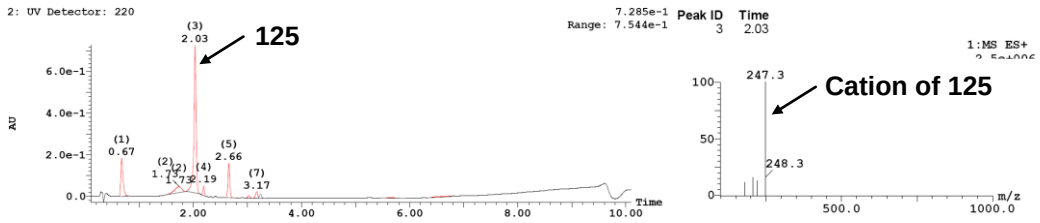

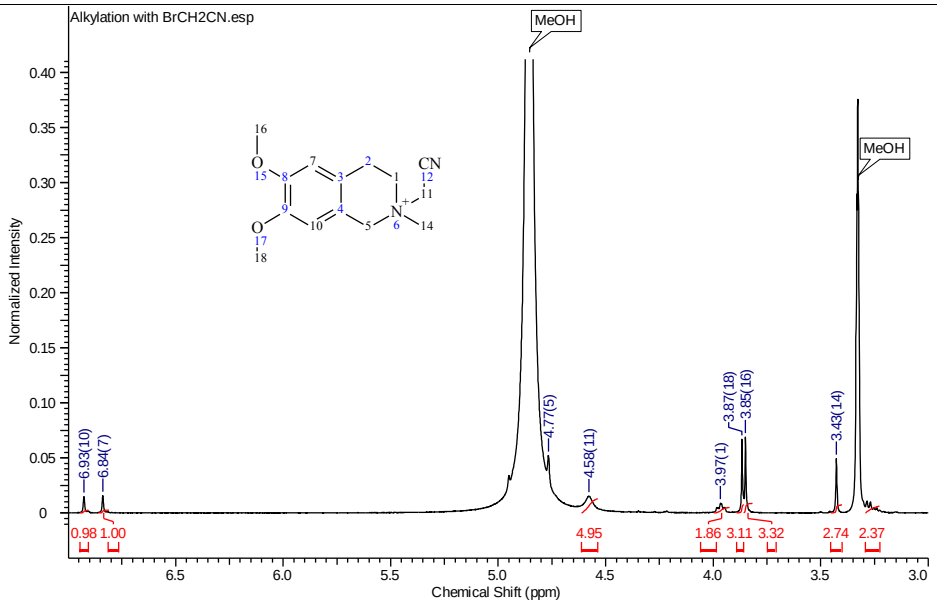

***Figure 27**: LCMS and ^{1}H NMR evidence of alkylation of 6,7-dimethoxy-N-methyl THIQ with bromoacetonitrile.*

_N_-(Cyanomethyl)-6,7-dimethoxy-_N_-methyl-1,2,3,4-tetrahydroisoquinolin-2-ium bromide (**126**)

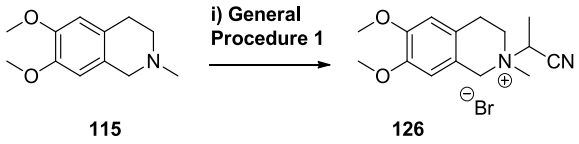

115 **126**

Following photoactivation of **115** (106.0 mg, 0.51 mmol) according to **General Procedure 1** with $BrCH_2CN$ (0.14 mL, 2.00 mmol) and $Ru(bpy)_3(PF_6)_2$ (4.4 mg, 5.1 μmol) in anhydrous MeCN (4.0 mL) for 24 h, a yellow/orange precipitate was observed. LCMS (High pH, 5 min gradient) revealed a new peak (Figure 28): R_T = 1.18 min, [M] = 261 (Figure 28), tentatively assigned as **126**. Also detected was unreacted **115**: R_T = 1.92 min, $[M+H^+]$ = 208.

†The remaining ^{1}H NMR signals were obscured by MeOH and H_2O solvent peaks

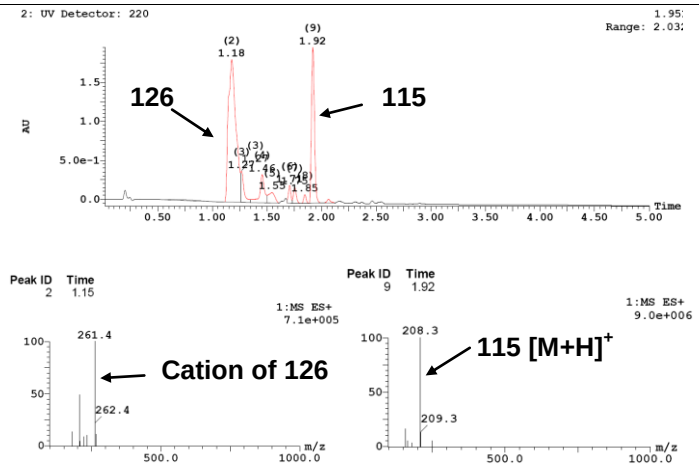

***Figure 28**: LCMS evidence of alkylation of 6,7-dimethoxy-N-methyl THIQ with 2-bromopropionitrile.*

5.12. PREPARATION OF DEXTROMETHORPHAN AND RELATED COMPOUNDS

(4b*S*,9*S*)-3-Methoxy-11-methyl-6,7,8,8a,9,10-hexahydro-5*H*-9,4b-(epimin-oethano)phenanthrene (dextromethorphan, 73)

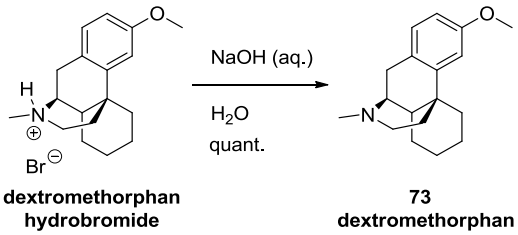

Dextromethorphan hydrobromide (9.48 g, 25.4 mmol) was dissolved in H_2O (600 mL). NaOH (1 M) was added to basify the solution until pH 10, as indicated by pH paper, then TBME (100 mL) was added. The layers were separated and the aqueous layer was extracted with TBME (2 x 100 mL). The combined organic layers were dried ($MgSO_4$), filtered and concentrated *in vacuo* to yield **73** as a white microcrystalline solid (6.90 g, 100%); m.p. 109 - 111 ^{o}C (lit. 109 - 111 ^{o}C[224]); IR ν_{max} (neat) 2923 - 2798 (C-H), 1607 (Ar), 1505 (Ar), 1465 (Ar), 1447, 1431, 1380, 1328, 1317, 1298 cm^{-1}; ^{1}H NMR

(400 MHz, $CDCl_3$) δ 7.02 (1H, d, *J* = 8.3 Hz, C*H*), 6.81 (1H, d, *J* = 2.5 Hz, C*H*), 6.71 (1H, dd, *J* = 8.3, 2.7 Hz, C*H*), 3.79 (3H, s, CH_3), 2.97 (1H, d, *J* = 18.1 Hz, CH_2), 2.80 (1H, dd, *J* = 5.4, 3.2 Hz, C*H*), 2.62 (1H, dd, *J* = 18.1, 5.6 Hz, CH_2), 2.47 - 2.32 (5H, m, CH_3, 2 x CH_2), 2.08 (1H, td, *J* = 12.2, 3.2 Hz, CH_2), 1.81 (1H, dt, *J* = 12.7, 2.9 Hz, C*H*), 1.73 (1H, td, *J* = 12.7, 4.9 Hz, CH_2), 1.68 - 1.61 (1H, m, CH_2), 1.56 - 1.48 (1H, m, CH_2), 1.45 - 1.29 (5H, m, CH_2), 1.21 - 1.07 (1H, m, CH_2); ^{13}C NMR (101 MHz, $CDCl_3$) δ 158.2 (*C*), 141.8 (*C*), 130.0 (*C*), 128.5 (*C*H), 111.1 (*C*H), 110.7 (*C*H), 58.0 (*C*H), 55.2 (*C*H_3), 47.3 (*C*H_2), 45.5 (*C*H), 42.9 (*C*H_3), 42.2 (*C*H_2), 37.3 (*C*), 36.7 (*C*H_2), 26.8 (*C*H_2), 26.6 (*C*H_2), 23.3 (*C*H_2), 22.3 (*C*H_2); HRMS (+ESI) *m/z* calculated for $C_{18}H_{26}NO$ [M+H$^+$] 272.2014; Found 272.2009. Data are consistent with the literature.[225] NMR Assignments assisted by a literature study.[226]

3-Methoxy-6,7,8,8a,9,10-hexahydro-5*H*-9,4b-(epiminoethano)phenanthre-ne (**74**)

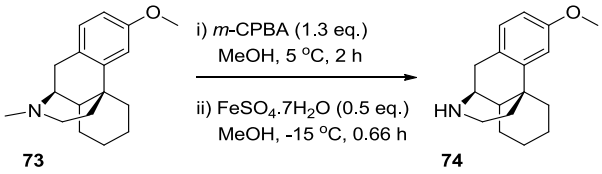

73 **74**

Prepared according to a modified literature procedure.[7] A reaction vessel was charged with **73** (264 mg, 0.97 mmol) and MeOH (2.4 mL) before cooling to 5 °C. 3-Chloroperbenzoic acid (282 mg, 1.26 mmol) in MeOH (1 mL) was added dropwise over 5 min. The reaction was stirred for 2 h, before cooling to -15 °C. $FeSO_4.7H_2O$ (138.0 mg, 0.50 eq.) in MeOH (2 mL) was added over 40 min. The resultant mixture was stirred at -15 °C until the reaction was deemed complete by LCMS (2 h). The reaction mixture was poured onto a solution of potassium citrate (1 M) (10 mL) and TBME (10 mL). TBME (10 mL) was added, the layers were separated and the aqueous layer was extracted with TBME (3 x 10 mL). The combined organic layers were washed with sat. aq. K_2CO_3 (3 x 20 mL). The combined aqueous layers were extracted with TBME (4 x 10 mL), then concentrated to dryness, then redissolved in TBME (20 mL) and extracted with sat. aq. K_2CO_3 : H_2O (1 : 1)

(2 x 20 mL). The combined organic layers were dried ($MgSO_4$), filtered and concentrated to give an off-white microcrystalline solid (153.9 mg). MDAP purification (High pH) afforded **74** as an off-white residue (11.3 mg, 5%);† IR ν_{max} (neat) 2928 - 2856 (C-H), 1674 (Ar), 1610 (Ar), 1576 (Ar), 1495 (Ar), 1454 (Ar), 1432, 1319, 1270, 1240, 1200 cm^{-1}; ^1H NMR (400 MHz, $CDCl_3$) δ 7.05 (1H, d, *J* = 8.3 Hz, C*H*), 6.81 (1H, d, *J* = 2.6 Hz, C*H*), 6.70 (1H, dd, *J* = 8.4, 2.6 Hz, C*H*), 3.80 (3H, s, CH_3), 3.16 - 3.08 (1H, d, *J* = 17.5, 6.2 Hz, CH_2), 3.08 - 3.03 (1H, m, C*H*), 2.71 (1H, d, *J* = 17.6 Hz, CH_2), 2.69 - 2.55 (2H, m, CH_2), 2.35 - 2.24 (1H, m, CH_2), 1.89 (1H, br. s, N*H*), 1.74 (1H, dt, *J* = 12.7, 2.8 Hz, C*H*), 1.69 - 1.47 (3H, m, CH_2), 1.44 - 1.24 (5H, m, CH_2), 1.12 - 0.98 (1H, m, CH_2); ^{13}C NMR (101 MHz, $CDCl_3$) δ 158.2 (*C*), 141.7 (*C*), 130.0 (*C*), 128.5 (*C*H), 111.2 (*C*H), 110.7 (*C*H), 55.2 (*C*H_3), 51.2 (C*H*), 46.0 (C*H*), 42.7 (*C*H_2), 39.2 (*C*H_2), 38.3 (*C*), 37.0 (*C*H_2), 33.6 (*C*H_2), 26.9 (*C*H_2), 26.7 (*C*H_2), 22.1 (*C*H_2); HRMS (+ESI) *m/z* calculated for $C_{17}H_{24}NO$ [$M+H^+$] 258.1852; Found 258.1851. Data are consistent with the literature.[8]

3-Methoxy-6,7,8,8a,9,10-hexahydro-5*H*-9,4b- (epiminoethano)phenanthre -ne-11-carbaldehyde (**137**)

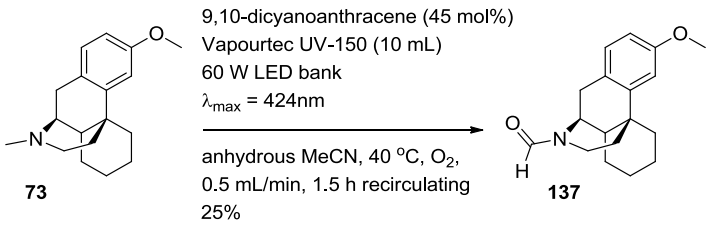

Prepared according to a modified literature procedure.[101] An oven-dried reaction vessel was charged with **73** (165.0 mg, 0.61 mmol), 9,10-dicyanoanthracene (62.0 mg, 0.27 mmol, 0.45 eq.), $LiClO_4$ (65.0 mg, 0.62 mmol, 1.0 eq.) and anhydrous MeCN (40 mL). The mixture was stirred with gentle heating until in solution and allowed to cool to rt, before it was fed through a needle (fitted with a filter) into a Vapourtec UV-150 Photochemical Flow Reactor (10 mL coil) (0.5 mL/min) which had been pre-flushed with

†Although the isolated yield was very poor, the crude product was obtained in 61% yield, 92% purity by HPLC peak area (220 nm).

anhydrous MeCN (20 mL). The reaction mixture was irradiated with 424 nm LEDs at 40 ^{o}C recirculating at 0.5 mL/min for 1.5 h whilst bubbling with an O_2 balloon. The reactor was flushed with MeCN (20 mL) to collect the solution of crude product which was concentrated *in vacuo*. 1,3,5-Trimethoxybenzene (10.3 mg, 61.0 μmol, 10 mol%) was added and the yield of **137** determined by ^{1}H NMR analysis (25%). MDAP purification (High pH) gave **137** as a yellow oil (14.6 mg, 8%) as a 1 : 1 mixture of two rotamers; IR ν_{max} (neat) 2929 - 2856 (C-H), 1667 (C=O), 1610 (Ar), 1496 (Ar), 1454 (Ar), 1429, 1296, 1269, 1241 cm^{-1}; ^{1}H NMR (400 MHz, $CDCl_3$) rotamer 1 and rotamer 2 (it is not possible to distinguish between the individual rotamers, so their combined data is reported. In the assignment, 1H corresponds to 1H of an individual rotamer): δ 8.16 (1H, s, C*H*O), 8.00 (1H, s, C*H*O), 7.03 (2H, t, *J* = 7.7 Hz, C*H*), 6.85 (2H, d, *J* = 2.6 Hz, C*H*), 6.76 (2H, dd, *J* = 8.4, 2.7 Hz, C*H*), 4.67 - 4.62 (1H, m, C*H*), 4.16 (1H, dd, *J* = 13.8, 5.0 Hz, CH_2), 3.80 (6H, s, CH_3), 3.71 - 3.67 (1H, m, C*H*), 3.31 - 3.12 (3H, m, CH_2), 2.97 (1H, td, *J* = 13.2, 3.6 Hz, CH_2), 2.73 - 2.62 (2H, m, CH_2), 2.48 (1H, td, *J* = 13.2, 4.2 Hz, CH_2), 2.43 - 2.35 (2H, m, CH_2), 1.75 - 1.42 (12H, m, CH_2, C*H*), 1.41 - 1.28 (6H, m, CH_2), 1.19 - 1.08 (2H, m); ^{13}C NMR (101 MHz, $CDCl_3$) rotamer 1 and rotamer 2 (it is not possible to distinguish between the individual rotamers, so their combined data is reported. In the assignment, all observed ^{13}C peaks are listed): δ 160.7 (*C*HO), 160.6 (*C*HO), 158.7 (*C*), 158.6 (*C*), 140.2 (2 x *C*), 129.1 (*C*H), 129.0 (*C*H), 128.2 (*C*), 127.6 (*C*), 111.5 (*C*H), 111.4 (2 x *C*H), 111.3 (*C*H), 55.2 (2 x *C*H_3), 53.8 (*C*H), 46.4 (*C*H), 45.0 (*C*H), 43.8 (*C*H), 42.1 (*C*H_2), 41.2 (*C*H_2), 40.9 (*C*H_2), 38.9 (*C*), 38.7 (*C*), 36.6 (*C*H_2), 36.5 (*C*H_2), 35.0 (*C*H_2), 32.3 (*C*H_2), 30.8 (*C*H_2), 26.4 (*C*H_2), 26.2 (3 x *C*H_2), 22.0 (*C*H_2), 21.9 (*C*H_2); HRMS (+ESI) *m/z* calculated for $C_{18}H_{24}NO_2$ [M+H^{+}] 286.1807; Found 286.1803. ^{1}H and ^{13}C NMR data are consistent with the literature.[101]

5.13. PHOTOACTIVATION OF DEXTROMETHORPHAN

Photoactivation of dextromethorphan (**73**) according to **General Procedure 1**, using $Ru(bpy)_3Cl_2.6H_2O$ as the catalyst, $BrCCl_3$ (3.0 eq.) as the oxidant, DMF

as the solvent and using the LED floodlamp gave no reaction after 16 h (Figure 29). Photoactivation of dextromethorphan (**73**) according to **General Procedure 1**, using $Ru(bpy)_3(PF_6)_2$ as the catalyst, $BrCH_2CN$ (2.0 eq.) as the oxidant, MeCN : H_2O (4 : 1) as the solvent and using the blue LED strip instead gave rise to alkylation to afford **128** as the sole product by LCMS after 2 h (Figure 30), R_T = 2.15 min, $[M^+]$ = 311 (Figure 30), tentatively assigned as the cation of **128**. Photoactivation of dextromethorphan (**73**) according to **General Procedure 1**, using $Ru(bpz)_3(PF_6)_2$ as the catalyst, $BrCCl_3$ (3.0 eq.) as the oxidant in MeCN : H_2O (4 : 1) using the blue LED strip gave rise to traces of *nor*-dextromethorphan (**74**) by LCMS after 16 h (Figure 31), R_T = 2.39 min, $[M+H^+]$ = 258 (Figure 31), assigned as **74** by comparison with the LCMS of an authentic standard.

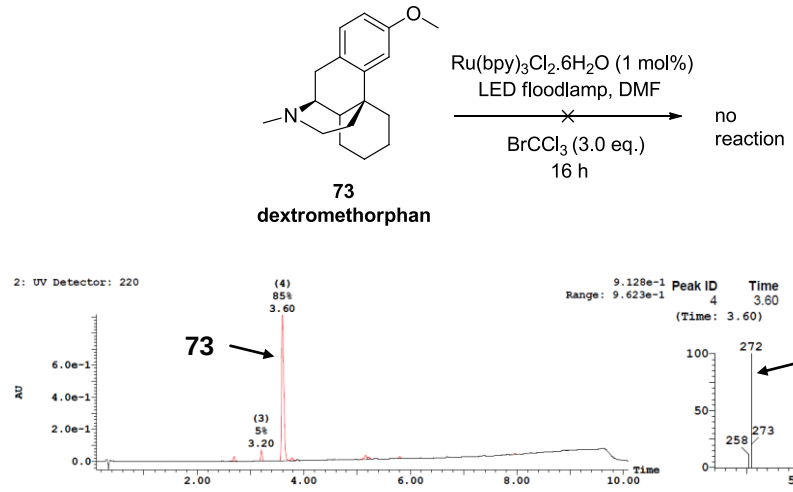

***Figure 29**: [Ru(bpy)$_3$]$^{2+}$-catalysed anaerobic demethylation of dextromethorphan irradiating with a LED floodlamp with $BrCCl_3$ as the oxidant in DMF. No reaction after 16 h.*

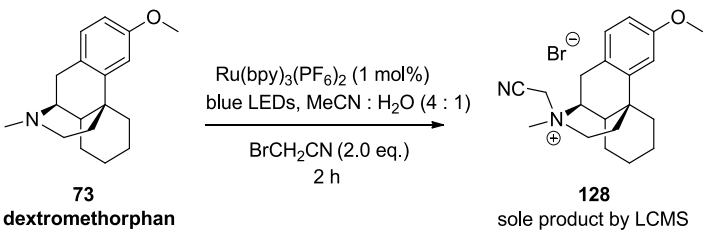

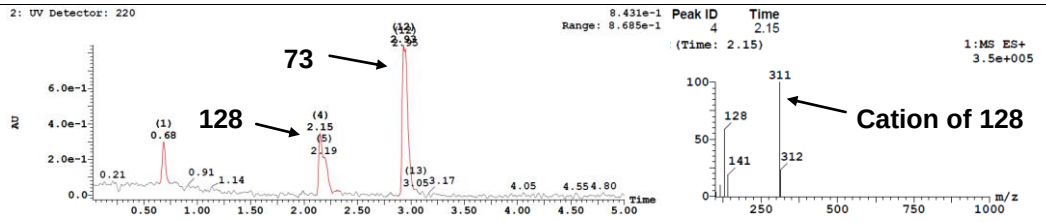

***Figure 30**: [Ru(bpy)$_3$]$^{2+}$-catalysed anaerobic demethylation of dextromethorphan irradiating with blue LEDs with BrCH$_2$CN in MeCN : H$_2$O (4 : 1). Alkylation was observed.*

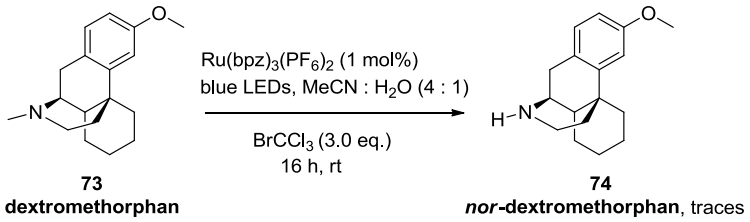

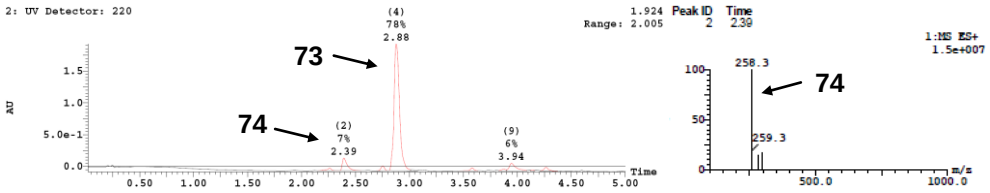

***Figure 31:** [Ru(bpz)$_3$]$^{2+}$-catalysed demethylation of dextromethorphan irradiating with blue LEDs with BrCCl$_3$ as the oxidant in MeCN : H$_2$O (4 : 1). Traces of nor-product **74** after 16 h.*

5.14. Preparation of Substrates for Luminescence Quenching Experiments

(*S*)-*tert*-Butyl 3-(3-methoxy-2-((methoxycarbonyl)amino)-3-oxopropyl)-1*H*-indole-1-carboxylate (186)

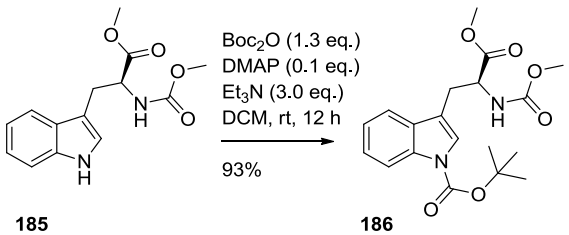

Prepared according to a literature procedure. To a solution of (*S*)-methyl-3-(1*H*-indol-3-yl)-2-((methoxycarbonyl)amino)propanoate (**185**) (1.20 g, 4.34 mmol) in DCM (20 mL) was added di-*tert*-butyl dicarbonate (1.00 g, 5.74 mmol, 1.3 eq.) and DMAP (60.0 mg, 0.49 mmol, 0.1 eq.) and triethylamine (1.8 mL, 12.9 mmol, 3 eq.) at rt. After stirring for 12 h at rt, the reaction mixture was diluted with DCM (50 mL) and washed with H_2O (50 mL) followed by brine (50 mL). The organic layer was dried (Na_2SO_4), filtered and concentrated before loading onto celite. Purification by column chromatography (7 - 30% EtOAc/heptane) gave **186** as a colourless amorphous solid (1.55 g, 93%); $[\alpha_D]^{25\ °C}_{\lambda}$ (c 0.73, $CHCl_3$): +43.9 º (lit.:[105] +42.4 º (c 0.73, $CHCl_3$)); IR ν_{max} (neat) 3354 (N-H), 2979 - 2954 (C-H), 1727 (C=O), 1523 (Ar), 1453 (Ar), 1370, 1309, 1256, 1226 cm^{-1}; ^1H NMR (400 MHz, $CDCl_3$) δ 8.11 (1H, br. s, C*H*), 7.49 (1H, d, *J* = 7.4 Hz, C*H*), 7.41 (1H, s, C*H*), 7.36 - 7.29 (1H, m, C*H*), 7.29 - 7.22 (1H, m, C*H*), 5.28 (1H, br. s, N*H*), 4.78 - 4.67 (1H, m, C*H*), 3.70 (6H, br. s, CH_3), 3.31 - 3.18 (2H, m, CH_2), 1.68 (9H, s, CH_3); ^{13}C NMR (101 MHz, $CDCl_3$) δ 172.1 (*C*), 156.3 (*C*), 149.6 (*C*), 135.4 (*C*), 130.4 (*C*), 124.6 (*C*H), 124.1 (*C*H), 122.6 (*C*H), 118.8 (*C*H), 115.3 (*C*H), 114.8 (*C*), 83.8 (*C*), 54.0 (*C*H, *C*H_3), 52.4 (*C*H_3), 28.2 (*C*H_3), 27.8 (*C*H_2); HRMS (+ESI) *m/z* calculated for $C_{19}H_{25}N_2O_6$ $[M+H^+]$ 377.1707; Found 377.1690. Data are consistent with the literature.[105]

(2*S*,3a*R*,8a*R*)-8-*tert*-Butyl 1,2-dimethyl 3a-bromo-3,3a-dihydropyrrolo-[2,3-*b*]indole-1,2,8(2*H*,8a*H*)-tricarboxylate (**65a**)

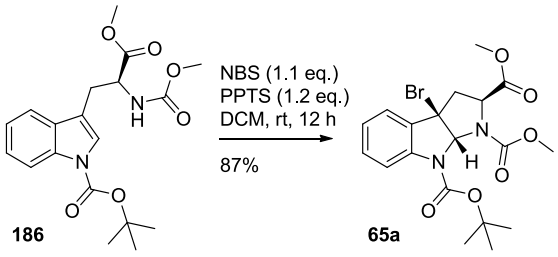

Prepared according to a literature procedure. To a solution of (*S*)-*tert*-butyl 3-(3-methoxy-2-((methoxycarbonyl)amino)-3-oxopropyl)-1*H*-indole-1-carboxyl

-ate (**186**) (1.55 g, 4.4 mmol) in DCM (45 mL) was added PPTS (1.20 g, 4.78 mmol, 1.2 eq.) and NBS (0.84 g, 4.72 mmol, 1.1 eq.) at rt. The colourless reaction mixture turned a pale yellow solution after NBS was added. After stirring for 12 h at rt, the reaction mixture was diluted with DCM (30 mL) and washed with sat. aq. $NaHCO_3$ (50 mL). The aqueous layer was extracted with DCM (2 x 30 mL). The combined organic layers were dried (Na_2SO_4), filtered and concentrated *in vacuo* before loading onto celite. Purification by column chromatography (7 - 30% EtOAc/heptane) gave **65a** as a colourless gum (1.76 g, 87%); $[\alpha_D]^{25\ °C}_{\lambda}$ (c 0.89, $CHCl_3$): -166.1 º (lit.:[105] -162.9 º (c 0.89, $CHCl_3$)); IR ν_{max} (neat) 2979 - 2955 (C-H), 1752 (C=O), 1716 (C=O), 1604 (Ar), 1479 (Ar), 1447, 1392, 1368, 1333, 1288, 1258, 1205 cm^{-1}; ^1H NMR (400 MHz, $CDCl_3$) δ 7.61 (1H, br. s, C*H*), 7.40 - 7.31 (2H, m, C*H*), 7.14 (1H, apt. t, *J* = 7.1 Hz, C*H*), 6.39 (1H, s, C*H*), 4.00 - 3.94 (1H, m, C*H*), 3.78 (3H, s, CH_3), 3.71 (3H, s, CH_3), 3.31 - 3.23 (1H, m, CH_2), 2.91 - 2.83 (1H, m, CH_2), 1.62 (9H, s, CH_3); ^{13}C NMR (101 MHz, $CDCl_3$)† δ 171.2 (*C*), 152.0 (*C*), 141.2 (*C*), 132.4 (*C*), 130.8 (*C*H), 124.5 (*C*H), 123.3 (*C*H), 118.2 (*C*H), 83.8 (*C*), 82.3 (*C*H), 59.7 (*C*H), 59.5 (*C*H_3), 52.9 (*C*), 52.6 (*C*H_3), 41.9 (*C*H_2), 28.3 (*C*H_3); HRMS (+ESI) *m/z* calculated for $C_{19}H_{24}{}^{79}BrN_2O_6$ [M+H^+] 455.0812; Found 455.0818. Data are consistent with the literature.[105]

But-3-yn-1-yl 2-chloro-2-phenylacetate (**66a**)

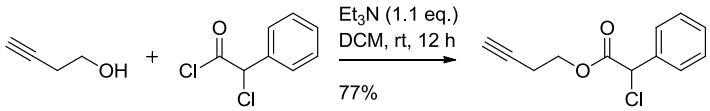

187 (1.0 eq.) **188** (1.0 eq.) **66a**

Prepared according to a literature procedure. A 25 mL round-bottomed flask equipped with a stirrer bar and septum was dried under vacuum with a heatgun (600 ^oC), placed under N_2, and allowed to cool to rt before but-3-yn-1-ol (**187**) (0.25 g, 3.60 mmol) and DCM (36 mL) were added. Et_3N (0.55 mL, 4.00 mmol, 1.1 eq.) and α-chloro-2-phenylacetyl chloride (**188**) (0.57 mL, 3.60 mmol, 1.0 eq.) were added dropwise at rt. Gas evolution was observed

†The remaining quaternary carbon could not be observed.

and the reaction mixture appeared as a colourless solution. After stirring for 12 h at rt, the reaction mixture was diluted with Et_2O (50 mL) and water (50 mL). The layers were separated and the aqueous layer was extracted with Et_2O (2 x 50 mL). The combined organic layers were dried (Na_2SO_4), filtered and concentrated loading onto celite. Purification by column chromatography (3 - 20% EtOAc/heptane) gave **66a** as a pale brown oil (0.61 g, 77%); IR ν_{max} (neat) 3297 (C≡C-H), 3066 - 2968 (C-H), 2349 (C≡C), 1754 (C=O), 1587 (Ar), 1542 (Ar), 1497 (Ar), 1456 (Ar), 1423, 1386, 1339, 1314, 1281, 1229 cm^{-1}; ^1H NMR (400 MHz, $CDCl_3$) δ 7.54 - 7.49 (2H, m, C*H*), 7.43 - 7.35 (3H, m, C*H*), 5.39 (1H, s, C*H*), 4.35 - 4.22 (2H, m, CH_2), 2.53 (2H, dt, *J* = 6.9, 2.7 Hz, CH_2), 1.96 (1H, t, *J* = 2.7 Hz, C*H*); ^{13}C NMR (101 MHz, $CDCl_3$) δ 168.1 (*C*), 135.6 (*C*), 129.3 (*C*H), 128.9 (*C*H), 128.0 (*C*H), 79.2 (*C*), 70.2 (*C*H), 63.8 (*C*H), 58.9 (*C*H_2), 18.8 (*C*H_2); HRMS (+ESI) *m/z* calculated for $C_{12}H_{12}{}^{35}ClO_2$ $[M+H^+]$ 233.0520; Found 233.0513. Data are consistent with the literature.[105]

5.15. PREPARATION OF TRIARYLAMINES

Tri-*p*-tolylamine (TPTA)

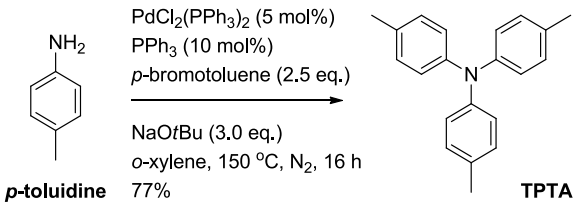

Prepared according to a literature procedure.[176] An oven-dried reaction vessel equipped with a magnetic stirrer was charged with NaO*t*Bu (5.77 g, 60.0 mmol), $PdCl_2(PPh_3)_2$ (70.0 mg, 0.10 mmol), PPh_3 (52.0 mg, 0.20 mmol), *p*-toluidine (2.14 g, 20.0 mmol), *p*-bromotoluene (8.55 g, 50.0 mmol) and *o*-xylene (160 mL). The mixture was stirred at reflux (144 ^oC) for 16 h under N_2. The reaction mixture was allowed to cool to rt and further $PdCl_2(PPh_3)_2$ (70.0 mg, 0.10 mmol) and PPh_3 (52.0 mg, 0.20 mmol) were added before stirring at reflux (144 ^oC) for 6 h under N_2. The reaction was allowed to cool to rt,

filtered through celite and concentrated *in vacuo* loading onto celite. Purification by column chromatography (heptane) gave tri-*p*-tolylamine (**TPTA**) as a white microcrystalline solid (4.44 g, 77%); m.p. 114 - 116 ^{o}C (lit. 112 - 115 ^{o}C[176]); IR ν_{max} (neat) 3025 - 2858 (C-H), 1608 (Ar), 1580 (Ar), 1504 (Ar), 1318, 1291, 1272 cm^{-1}; ^{1}H NMR (400 MHz, $CDCl_3$) δ 7.03 (6H, d, *J* = 8.3 Hz, C*H*), 6.97 (6H, d, *J* = 8.6 Hz, C*H*), 2.30 (9H, s, CH_3); ^{13}C NMR (101 MHz, $CDCl_3$) δ 145.7 (*C*), 131.7 (*C*), 129.7 (*C*H), 123.9 (*C*H), 20.7 (*C*H_3); LCMS (High pH, 5 min gradient): R_T = 4.3 min, [M+H$^+$] = 288. Data are consistent with the literature.[176]

Tris(*p*-biphenyl)amine (TPBPA)

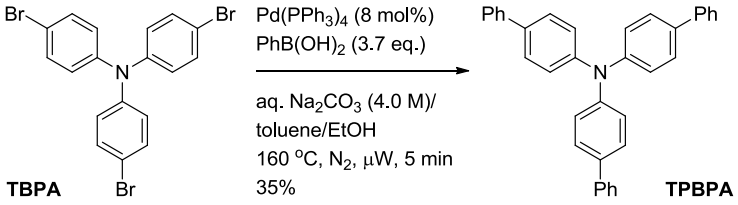

Prepared according to a modified literature procedure.[175] Eight mixtures of tris(*p*-bromophenyl)amine (**TBPA**) (0.72 g, 1.49 mmol), $Pd(PPh_3)_4$ (150.0 mg, 0.13 mmol) and phenylboronic acid (0.68 g, 5.58 mmol, 3.7 eq.) in aqueous Na_2CO_3 (4.0 M, 3.8 mL), toluene (7.5 mL) and EtOH (2.5 mL) were prepared and triple evacuated/N_2 filled, before stirring above reflux (160 ^{o}C) for 5 min under microwave conditions. The mixtures were each quenched with H_2O (2 mL) before they were combined and filtered through celite into a separatory funnel containing H_2O (100 mL) and DCM (100 mL). The layers were separated and the aqueous layer was extracted with DCM (2 x 100 mL). The combined organic layers were dried ($MgSO_4$), filtered and concentrated *in vacuo* before loading onto celite. Purification by column chromatography (10 - 90% toluene/heptane) gave tris(*p*-biphenyl)amine (**TPBPA**) as a white microcrystalline solid (1.97 g, 35%); m.p. 251 - 253 ^{o}C (lit. 261 ^{o}C[227]); IR ν_{max} (neat) 3028 (C-H), 1596 (Ar), 1514 (Ar), 1482 (Ar), 1448, 1316, 1293, 1280, 1263 cm^{-1}; ^{1}H NMR (400 MHz, $CDCl_3$) δ 7.60 (6H, d, *J* = 7.1, C*H*), 7.53 (6H, d, *J* = 8.6, C*H*), 7.45 (6H, t, *J* = 7.6 Hz, C*H*), 7.34 (3H, t, *J* = 7.5 Hz, C*H*), 7.27

(6H, d, *J* = 8.6 Hz, C*H*), ^{13}C NMR (101 MHz, $CDCl_3$) δ 146.8 (*C*), 140.6 (*C*), 135.7 (*C*), 128.8 (*C*H), 127.9 (*C*H), 126.9 (*C*H), 126.7 (*C*H), 124.4 (*C*H), LCMS (High pH, 5 min gradient): R_T = 4.6 min, [M+H$^+$] = 474. Data are consistent with the literature.[227]

5.16. PREPARATION OF TRIARYLAMINIUM RADICAL CATION SALTS

Tris(*p*-bromophenyl)aminium hexafluorophosphate (**TBPA**-PF_6)

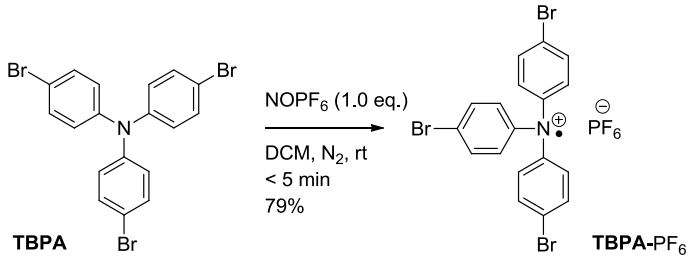

Prepared according to a literature procedure.[67] A solution of nitrosonium hexafluorophosphate (3.2 g, 18.3 mmol) in DCM (30 mL) was bubbled vigorously with N_2. A solution of tris(*p*-bromophenyl)amine (**TBPA**) (8.8 g, 18.3 mmol) in DCM (30 mL) was slowly added at rt during N_2 bubbling. An immediate colour change was observed from colourless to dark blue/black. Once addition was complete, the mixture was bubbled for 15 min with N_2, before Et_2O (150 mL) was added to generate a precipitate, which was collected by filtration and dried under vacuum to yield **TBPA**-PF_6 as a dark blue/black microcrystalline solid (9.04 g, 79%); m.p. = 136 - 138 ^oC (decomp.); IR ν_{max} (neat) 1602, 1546 (Ar), 1477 (Ar), 1417, 1312, 1254 cm^{-1}; UV-vis (MeCN): λ_{max} = 364, 374, 592, 704 nm; ^{19}F NMR (376.5 MHz, MeCN-d_3) δ -72.9 (d, 706 Hz, PF_6^-); LCMS (High pH, 5 min gradient): R_T = 4.4 min, [M+H$^+$] = 482.0; HRMS (+ESI) *m/z* calculated for $C_{18}H_{12}{}^{79}Br_3N$ [M] 478.8520; not detected. Data are consistent with the literature.[67] No signals observed by ^{1}H or ^{13}C NMR. Compound not detected by +ESI HRMS. An EPR signal was observed confirming the presence of a radical species (see Section 2.3.5, Figure 20), consistent with the literature EPR spectrum.[178]

Tris(*p*-biphenyl)aminium hexafluorophosphate (**TPBPA**-PF_6)

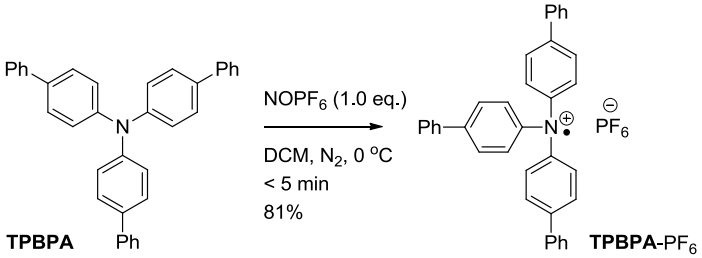

Prepared according to a modified literature procedure,[67] using tris(*p*-biphenyl)amine (**TPBPA**) as a substrate. A solution of nitrosonium hexafluorophosphate (0.99 g, 5.28 mmol) in DCM (50 mL) was bubbled vigorously with N_2. A suspension of tris(*p*-biphenyl)amine (**TPBPA**) (2.67 g, 5.64 mmol) in DCM (100 mL) was slowly added at rt during N_2 bubbling. An immediate colour change was observed from colourless to dark green/black. Once addition was complete the mixture was bubbled for 15 min with N_2. After most of the solvent was removed *in vacuo* the mixture was poured onto ice cold TBME (100 mL) to generate a precipitate, which was collected by filtration and dried under vacuum to yield **TPBPA**-PF_6 as a dark green/black microcrystalline solid (2.84 g, 81%); m.p. = 257 - 259 °C; IR ν_{max} (neat) 1564 (Ar), 1417, 1322, 1267 cm^{-1}; UV-vis (MeCN): λ_{max} = 340, 412 nm; ^{19}F NMR (376.5 MHz, MeCN-d_3) δ -72.9 (d, 706 Hz, PF_6^-); LCMS (High pH, 5 min gradient): R_T = 4.6 min, $[M+H^+]$ = 474.0; HRMS (+ESI) *m/z* calculated for $C_{36}H_{27}N$ [M] 473.2143; not detected. No signals observed by ^1H or ^{13}C NMR. Compound not detected by +ESI HRMS. An EPR signal was observed confirming the presence of a radical species (see Appendix).

Tri-*p*-tolylaminium hexafluorophosphate (**TPTA**-PF_6)

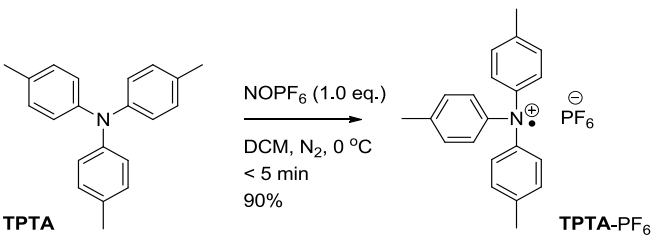

Prepared according to a modified literature procedure,[67] using tri-*p*-tolylamine (**TPTA**) as a substrate. A solution of nitrosonium hexafluorophosphate (1.84 g, 10.5 mmol) in DCM (110 mL) was bubbled vigorously with N_2. A solution of tri-*p*-tolylamine (**TPTA**) (3.02 g, 10.5 mmol) in DCM (50 mL) was slowly added at 0 ^{o}C during N_2 bubbling. An immediate colour change was observed from colourless to dark blue/black. Once addition was complete the mixture was bubbled for 15 min with N_2. After most of the solvent was removed *in vacuo* the mixture was poured onto ice cold (1 : 1) TBME : heptane (200 mL) to generate a precipitate, which was collected by filtration and dried under vacuum to yield **TPTA**-PF_6 as a purple microcrystalline solid (4.08 g, 90%); m.p. = 151 - 153 ^{o}C; IR ν_{max} (neat) 1580 (Ar), 1428, 1257 cm^{-1}; UV-vis (MeCN): λ_{max} = 343, 367, 581, 669 nm; ^{19}F NMR (376.5 MHz, MeCN-d_3) δ -72.9 (d, 706 Hz, PF_6^-); LCMS (High pH, 5 min gradient): R_T = 4.2 min, [M+H$^+$] = 288; HRMS (+ESI) *m/z* calculated for $C_{21}H_{21}N$ [M] 288.1752; Found 288.1746. No signals were observed by ^{1}H or ^{13}C NMR. An EPR signal confirmed the presence of a radical species (see Section 2.3.5, Figure 20).

5.17. PREPARATION OF TRIALKYLAMINES

Ethyl ((7a*R*,12b*S*)-7-methoxy-3-methyl-2,3,4,7a-tetrahydro-1*H*-4,12-methanobenzofuro[3,2-*e*]isoquinolin-9-yl) carbonate (*189*)

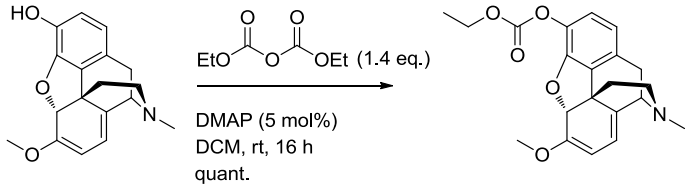

oripavine **189 thebaine carbonate derivative**

Prepared according to a literature procedure.[228] A reaction vessel was charged with oripavine (1.25 g, 4.20 mmol) and DCM (30 mL). Diethyl pyrocarbonate (0.811 g, 5.00 mmol), followed by DMAP (24.0 mg, 0.20 mmol, 5 mol%) were added at rt. A vigorous evolution of gas was observed upon

addition of DMAP with concomitant dissolution of oripavine. The reaction mixture was stirred at rt for 16 h. Diethyl pyrocarbonate (0.162 g, 1.00 mmol) was added at rt and the resultant mixture stirred at rt for 1 h. The reaction mixture was diluted with DCM (100 mL), washed with aq. HCl (1 M, 30 mL) and basified with sat. aq. $NaHCO_3$ (30 mL). The organic layer was separated and dried over Na_2SO_4, filtered and concentrated to dryness before loading onto celite. Purification by column chromatography (8% MeOH/DCM) afforded **189** as a pale brown gum (1.55 g, 100%); IR ν_{max} (neat) 2931 - 2840 (C-H), 1761 (C=O), 1671 (C=C), 1607 (Ar), 1493 (Ar), 1445, 1369, 1338, 1238 cm^{-1}; ^1H NMR (400 MHz, $CDCl_3$) δ 6.84 (1H, d, *J* = 8.3 Hz, C*H*), 6.65 (1H, d, *J* = 8.3 Hz, C*H*), 5.59 (1H, d, *J* = 6.6 Hz, C*H*), 5.34 (1H, s, C*H*), 5.07 (1H, d, *J* = 6.4 Hz, C*H*), 4.37 - 4.25 (2H, m, CH_2), 3.65 (1H, d, *J* = 6.9 Hz, C*H*), 3.62 (3H, s, CH_3), 3.32 (1H, d, *J* = 18.1 Hz, CH_2), 2.81 (1H, dt, *J* = 12.8, 3.4 Hz, CH_2), 2.74 - 2.62 (2H, m, CH_2), 2.47 (3H, s, CH_3), 2.22 (1H, dt, *J* = 12.6, 5.1 Hz, CH_2), 1.78 (1H, dd, *J* = 12.7, 2.2 Hz, CH_2), 1.37 (3H, t, *J* = 7.1 Hz, CH_3); ^{13}C NMR (101 MHz, $CDCl_3$)† δ 153.2 (*C*=O), 152.3 (*C*), 147.6 (*C*), 134.5 (*C*), 133.3 (*C*), 132.8 (*C*), 121.5 (*C*H), 119.3 (*C*H), 111.9 (*C*H), 96.3 (C*H*), 89.9 (C*H*), 64.9 (CH_2), 60.6 (*C*H), 55.1 (*C*H_3), 45.9 (*C*H_2), 42.4 (*C*H_3), 36.8 (*C*H_2), 29.8 (*C*H_2), 14.1 (*C*H_3); LCMS (High pH, 5 min gradient): R_T = 2.7 min, [M+H^+] = 370. Data are consistent with the literature.[228]

(2*S*)-(1*S*,2*S*,7*R*)-9-Methyl-3-oxa-9-azatricyclo[3.3.1.$0^{2,4}$]nonan-7-yl 3-((*tert*-butyldimethylsilyl)oxy)-2-phenylpropanoate (*166a*)

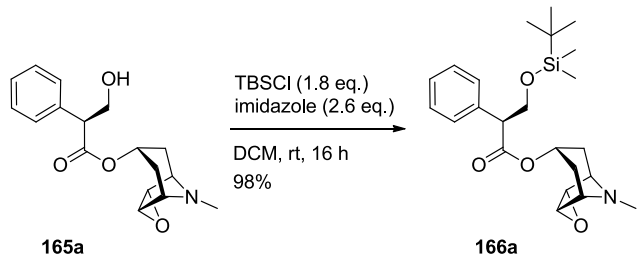

165a
scopolamine

166a

Scopolamine free base was prepared from the hydrobromide salt in the same manner as for dextromethorphan (**73**) from dextromethorphan hydrobromide

†The remaining two quaternary carbons could not be observed.

(see Chapter 5.13). To a solution of scopolamine free base (**165a**) (182.3 mg, 0.60 mmol) in DCM (8.0 mL) was added *tert*-butyldimethylsilyl chloride (81.0 mg, 0.54 mmol, 0.9 eq.) and imidazole (52.0 mg, 0.76 mmol, 1.3 eq.) and the solution stirred at rt for 16 h. Water (10 mL) was added and the reaction mixture was basified with sat. aq. $NaHCO_3$ (5 mL). The layers were separated and the aqueous layer was extracted with DCM (2 x 10 mL). The combined organic layers were dried ($MgSO_4$), filtered and concentrated to give the crude product as a colourless amorphous solid. The crude product was re-subjected to the reaction conditions exactly as outlined above. After stirring for 16 h, work up gave **166a** as a colourless amorphous solid (246.9 mg, 98%); IR ν_{max} (neat) 2929 - 2856 (N-H, C-H), 1730 (C=O), 1495 (Ar), 1472 (Ar), 1421, 1361, 1329, 1256 cm^{-1}; ^1H NMR (400 MHz, $CDCl_3$) δ 7.36 - 7.27 (5H, m, C*H*), 5.00 (1H, apt. t, *J* = 5.5 Hz, C*H*), 4.20 (1H, apt. t, *J* = 9.4 Hz, C*H*), 3.83 - 3.76 (1H, m, CH_2), 3.75 - 3.67 (1H, m, CH_2), 3.50 (1H, d, *J* = 2.8 Hz, C*H*), 3.15 - 3.12 (1H, m, C*H*), 3.12 (1H, d, *J* = 3.0 Hz, C*H*), 3.06 - 3.02 (1H, m, C*H*), 2.50 (3H, s, CH_3), 2.16 - 2.08 (1H, m, CH_2), 2.08 - 2.00 (1H, m, CH_2), 1.63 (1H, d, *J* = 14.9 Hz, CH_2), 1.45 (1H, d, *J* = 14.9 Hz, CH_2); 0.87 (9H, s, CH_3), 0.04 (3H, s, CH_3), 0.02 (3H, s, CH_3); HRMS (+ESI) *m/z* calculated for $C_{23}H_{36}NO_4Si$ [$M+H^+$] 418.2408; Found 418.2396. Data are consistent with the literature.[229]

N,*N*-Diethyl-5,5-diphenylpent-4-en-1-amine (41)

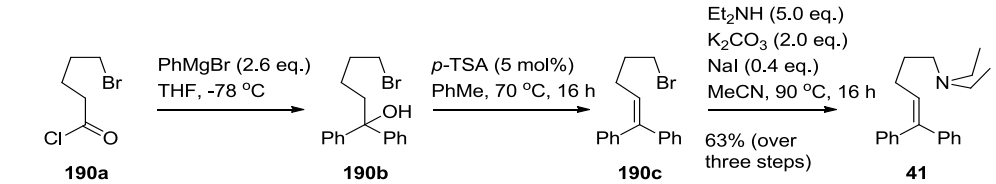

190a 5-bromopentanoyl chloride — **190b** — **190c** — **41**

Prepared according to a literature procedure.[230] An oven-dried vessel was charged with 5-bromopentanoyl chloride (**190a**) (1.20 g, 6.00 mmol) and anhydrous THF (6 mL) and triple evacuated/N_2 filled. After cooling to -78 °C, phenylmagnesium bromide (15.6 mL, 1.0 M in THF, 2.6 eq.) was added dropwise under N_2. The reaction mixture was allowed to warm to rt. The

reaction was quenched by dropwise addition of MeOH (3 mL) at 0 ^{o}C, before adding sat. aq. NH_4Cl (9 mL). The reaction mixture was filtered through celite and diluted with DCM (30 mL), water (30 mL) and brine (10 mL). The aqueous layer was extracted (2 x 30 mL DCM), dried ($MgSO_4$), filtered and concentrated *in vacuo* to give the crude 5-bromo-1,1-diphenylpentan-1-ol (**190b**) as a colourless oil (2.14 g); ^{1}H NMR (400 MHz, $CDCl_3$) δ 7.43 - 7.38 (4H, m, C*H*), 7.33 (4H, apt. t, *J* = 7.6 Hz, C*H*), 7.26 - 7.21 (2H, m, C*H*), 3.37 (2H, t, *J* = 6.9 Hz, CH_2), 2.34 - 2.27 (2H, m, CH_2), 2.09 (1H, s, O*H*), 1.95 - 1.84 (2H, m, CH_2), 1.50 - 1.41 (2H, m, CH_2); which was used without further purification.

An oven-dried vessel equipped with a condenser and stirrer bar was charged with the crude 5-bromo-1,1-diphenylpentan-1-ol (**190b**) and anhydrous toluene (6 mL). *p*-Toluenesulfonic acid monohydrate (64.0 mg, 5 mol%) was added and the reaction mixture was triple evacuated/N_2 filled and stirred at 70 ^{o}C for 16 h under N_2. Upon cooling to rt, the reaction was basified with sat. aq. $NaHCO_3$ (10 mL) to pH 8 - 9. The reaction mixture was diluted with DCM (30 mL), water (30 mL) and brine (10 mL). The aqueous layer was extracted (2 x 30 mL DCM), dried ($MgSO_4$), filtered and concentrated *in vacuo* to give crude 5-bromo-1,1-diphenylpent-1-ene (**190c**) as a brown oil (1.95 g); ^{1}H NMR (400 MHz, $CDCl_3$) δ 7.40 - 7.14 (10H, m, C*H*), 6.04 (1H, t, *J* = 7.5 Hz, C*H*), 3.38 (2H, t, *J* = 6.8 Hz, CH_2), 2.31 - 2.21 (2H, m, CH_2), 2.05 - 1.95 (2H, m, CH_2); which was used without further purification.

An oven-dried vessel equipped with a condenser and stirrer bar was charged with the crude 5-bromo-1,1-diphenylpent-1-ene (**190c**) (1.95 g), K_2CO_3 (1.79 g, 2.0 eq.), diethylamine (3.38 mL, 5.0 eq.), sodium iodide (388.0 mg, 0.4 eq.) and anhydrous MeCN (100 mL). The reaction mixture was triple evacuated/N_2 filled and stirred at reflux (90 ^{o}C) for 16 h under N_2. After cooling to rt, the reaction mixture was diluted with TBME (30 mL), water (30 mL) and brine (10 mL). The aqueous layer was extracted (2 x 30 mL TBME), dried (a ~1 : 1 mixture of K_2CO_3 and $MgSO_4$), filtered and concentrated *in vacuo* before loading onto celite. Purification by column chromatography (10

- 60% EtOAc/heptane) gave the product **41** as a pale brown oil (1.11 g, 70% over three steps, based on 6.00 mmol of 5-bromopentanoyl chloride **190a**); IR ν_{max} (neat) 2968 - 2797 (C-H), 1598 (Ar), 1495 (Ar), 1444, 1369, 1295, 1200 cm^{-1}; ^{1}H NMR (400 MHz, $CDCl_3$) δ 7.41 - 7.16 (10H, m, C*H*), 6.10 (1H, t, *J* = 7.5, C*H*), 2.50 (4H, q, *J* = 7.2 Hz, CH_2), 2.44 - 2.37 (2H, m, CH_2), 2.11 (2H, q, *J* = 7.5 Hz, CH_2), 1.60 (2H, quint., *J* = 7.6 Hz, CH_2), 1.01 (6H, t, *J* = 7.1 Hz, CH_3), ^{13}C NMR (101 MHz, $CDCl_3$) δ 142.8 (*C*), 141.8 (*C*), 140.2 (*C*), 129.9 (*C*H), 129.7 (*C*H), 128.1 (2 x *C*H), 127.2 (*C*H), 126.9 (*C*H), 126.8 (*C*H), 52.6 (*C*H_2), 46.9 (*C*H_2), 27.9 (*C*H_2), 27.4 (*C*H_2), 11.7 (*C*H_3), HRMS (+ESI) *m/z* calculated for $C_{21}H_{28}N$ $[M+H^+]$ 294.2216; Found 294.2214. Data are consistent with the literature.[67]

N,*N*-Dimethyl-5,5-diphenylpent-4-en-1-amine (173)

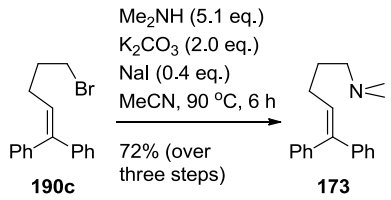

The synthesis of crude 5-bromo-1,1-diphenylpent-1-ene (**190c**) was carried out as described above. An oven-dried vessel equipped with a condenser and stirrer bar was charged with the crude 5-bromo-1,1-diphenylpent-1-ene (**190c**) (1.84 g), K_2CO_3 (1.69 g, 2.0 eq.), dimethylamine (15.6 mL, 2.0 M in THF, 5.1 eq.), sodium iodide (366.0 mg, 0.4 eq.) and anhydrous MeCN (60 mL). The reaction mixture was triple evacuated/N_2 filled and stirred at reflux (90 ^{o}C) for 6 h under N_2. After cooling to rt, the reaction mixture was diluted with TBME (30 mL), water (30 mL) and brine (10 mL). The aqueous layer was extracted (2 x 30 mL TBME), dried (a ~1 : 1 mixture of K_2CO_3 and $MgSO_4$), filtered and concentrated *in vacuo* before loading onto celite. Purification by column chromatography [(20 - 60% EtOAc/heptane, then 2 - 10% MeOH/EtOAc (1% Et_3N)] gave the product **173** as a pale brown oil (1.14 g, 72% over three steps, based on 6.00 mmol of 5-bromopentanoyl chloride **190a**); IR ν_{max} (neat) 2940 - 2763 (C-H), 1494 (Ar), 1443, 1444, 1264 cm^{-1}; ^{1}H

NMR (400 MHz, $CDCl_3$) δ 7.40 - 7.15 (10H, m, C*H*), 6.10 (1H, t, *J* = 7.5, C*H*), 2.27 - 2.22 (2H, m, CH_2), 2.20 (6H, s, CH_3), 2.13 (2H, q, *J* = 7.5 Hz, CH_2), 1.63 (2H, quint., *J* = 7.6 Hz, CH_2), ^{13}C NMR (101 MHz, $CDCl_3$) δ 142.7 (*C*), 141.8 (*C*), 140.2 (*C*), 129.9 (*C*H), 129.5 (*C*H), 128.2 (*C*H), 128.1 (*C*H), 127.2 (*C*H), 126.9 (*C*H), 126.8 (*C*H), 59.5 (*C*H_2), 45.5 (*C*H_3), 28.2 (*C*H_2), 27.7 (*C*H_2), HRMS (+ESI) *m/z* calculated for $C_{19}H_{24}N$ [M+H^+] 266.1903; Found 266.1895. There are discrepencies between the ^{1}H and ^{13}C NMR shifts observed and those reported in the literature.[231] The identity of compound **173** was confirmed by IR and HRMS analyses.

N,*N*-Dimethyl-4,4-diphenylbut-3-en-1-amine (176)

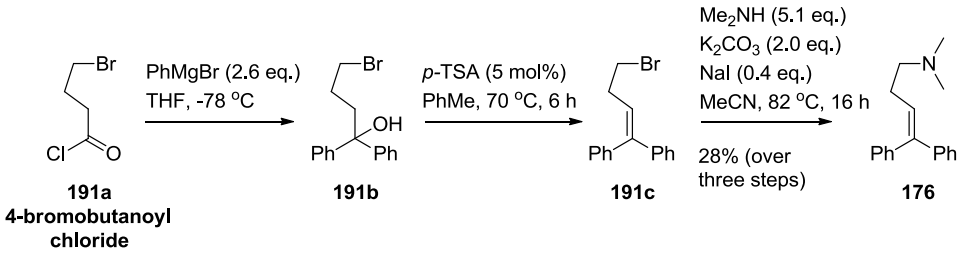

191a 4-bromobutanoyl chloride | **191b** | **191c** | **176**

An oven-dried vessel was charged with 4-bromobutanoyl chloride (**191a**) (1.11 g, 6.00 mmol) and anhydrous THF (6 mL) and triple evacuated/N_2 filled. After cooling to -78 °C, phenylmagnesium bromide (15.6 mL, 1.0 M in THF, 2.6 eq.) was added dropwise under N_2. The reaction mixture was allowed to warm to rt. The reaction was quenched by dropwise addition of MeOH (3 mL) at 0 °C, before adding sat. aq. NH_4Cl (9 mL). The reaction mixture was filtered through celite and diluted with DCM (30 mL), water (30 mL) and brine (10 mL). The aqueous layer was extracted (2 x 30 mL DCM), dried ($MgSO_4$), filtered and concentrated *in vacuo* to give a colourless oil, which was purified by column chromatography (10 - 30% EtOAc/heptane) to afford 4-bromo-1,1-diphenylbutan-1-ol (**191b**) as an amorphous colourless solid (0.98 g); ^{1}H NMR (400 MHz, $CDCl_3$) δ 7.44 - 7.39 (4H, m, C*H*), 7.33 (4H, apt. t, *J* = 7.5 Hz, C*H*), 7.27 - 7.24 (2H, m, C*H*), 3.44 (2H, t, *J* = 6.5 Hz, CH_2), 2.49 - 2.42 (2H, m, CH_2), 2.08 (1H, br. s, O*H*), 1.93 - 1.84 (2H, m, CH_2); which was used without further purification.

An oven-dried vessel equipped with a condenser and stirrer bar was charged with the crude 4-bromo-1,1-diphenylbutan-1-ol (**191b**) and anhydrous toluene (3 mL). *p*-Toluenesulfonic acid monohydrate (31.0 mg, 5 mol%) was added and the reaction mixture was triple evacuated/N_2 filled and stirred at 70 ^{o}C for 16 h under N_2. Upon cooling to rt, the reaction was basified with sat. aq. $NaHCO_3$ (10 mL) to pH 8 - 9. The reaction mixture was diluted with DCM (15 mL), water (10 mL) and brine (5 mL). The aqueous layer was extracted (2 x 15 mL DCM), dried ($MgSO_4$), filtered and concentrated *in vacuo* to give crude 4-bromo-1,1-diphenylbut-1-ene (**191c**) as a brown oil (0.85 g); ^{1}H NMR (400 MHz, $CDCl_3$) δ 7.43 - 7.16 (10H, m, C*H*), 6.10 (1H, t, *J* = 7.2 Hz, C*H*), 3.44 (2H, t, *J* = 7.0 Hz, CH_2), 2.71 (2H, q, *J* = 7.0 Hz, CH_2); which was used without further purification.

An oven-dried vessel equipped with a condenser and stirrer bar was charged with the crude 4-bromo-1,1-diphenylbut-1-ene (**191c**), K_2CO_3 (0.82 g, 2.0 eq.), dimethylamine (7.56 mL, 2.0 M in THF, 5.1 eq.), sodium iodide (177.0 mg, 0.4 eq.) and anhydrous MeCN (50 mL). The reaction mixture was triple evacuated/N_2 filled and stirred at reflux (82 ^{o}C) for 16 h under N_2. After cooling to rt, the reaction mixture was diluted with TBME (30 mL), water (30 mL) and brine (10 mL). The aqueous layer was extracted (2 x 30 mL TBME), dried (a ~1 : 1 mixture of K_2CO_3 and $MgSO_4$), filtered and concentrated *in vacuo* before loading onto celite. Purification by column chromatography (10 - 100% EtOAc/heptane, then 5 - 10% MeOH/EtOAc) gave the product **176** as a pale brown oil (426.0 mg, 28% over three steps, based on 6.00 mmol of 4-bromobutanoyl chloride **191a**); IR ν_{max} (neat) 3023 - 2764 (C-H), 1598 (Ar), 1494 (Ar), 1459, 1443, 1371, 1265 cm^{-1}; ^{1}H NMR (400 MHz, $CDCl_3$) δ 7.38 - 7.10 (10H, m, C*H*), 6.06 (1H, t, *J* = 7.3, C*H*), 2.38 (2H, t, *J* = 7.6 Hz, CH_2), 2.27 (2H, q, *J* = 7.3 Hz, CH_2), 2.17 (6H, s, CH_3); ^{13}C NMR (101 MHz, $CDCl_3$) δ 142.7 (*C*), 142.5 (*C*), 140.1 (*C*), 129.8 (*C*H), 128.2 (*C*H), 128.0 (*C*H), 127.2 (*C*H), 127.1 (*C*H), 127.0 (*C*H), 126.9 (*C*H), 59.6 (*C*H_2), 45.3 (*C*H_3), 28.1 (*C*H_2); HRMS (+ESI) *m/z* calculated for $C_{18}H_{22}N$ [M+H^{+}] 252.1747; Found 252.1728. Data are consistent with the literature.[232]

4-(Benzyloxy)-1-methylpiperidine (*193*)

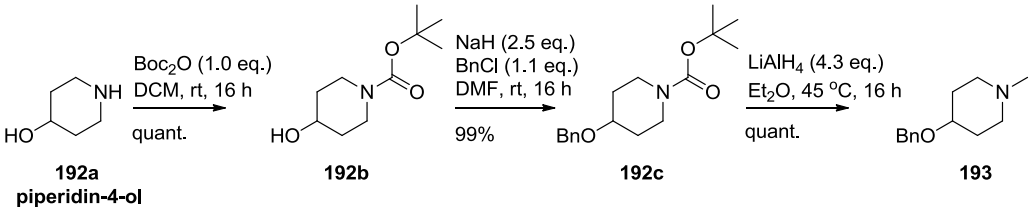

A reaction vessel was charged with di-*tert*-butyl dicarbonate (6.49 g, 29.7 mmol) and DCM (10 mL) and was triple evacuated/N_2 filled. A solution of piperidin-4-ol (**192a**) (3.69 g, 36.5 mmol) in DCM (10 mL) was added dropwise over 15 min. A gas was evolved. The reaction was stirred for 16 h under N_2. In order to destroy unreacted di-*tert*-butyl dicarbonate, a modified literature procedure was used.[214] DCM (10 mL) and imidazole (2.79 g, 41.0 mmol) were added. A gas was evolved. The reaction was stirred for 15 min before washing with cold (0 - 5 ^oC) 1% HCl (100 mL). The layers were separated and the aqueous layer was extracted with DCM (2 x 25 mL). The combined organic layers were washed with cold (0 - 5 ^oC) 1% HCl (100 mL) and the aqueous layer was extracted with DCM (2 x 50 mL). The combined organic layers were dried ($MgSO_4$), filtered and concentrated *in vacuo* to yield the crude *tert*-butyl 4-hydroxypiperidine-1-carboxylate **192b** as a colourless oil (6.35 g); ^1H NMR (400 MHz, $CDCl_3$) δ 3.91 - 3.79 (3H, m, CH_2 and C*H*), 3.08 - 3.00 (2H, m, CH_2), 1.90 - 1.81 (2H, m, CH_2), 1.51 - 1.41 (11H, m, 3 x CH_3 and CH_2); which was used without further purification.

To a solution of crude *tert*-butyl 4-hydroxypiperidine-1-carboxylate **192b** (3.46 g, 17.2 mmol) in dry DMF (70 mL) was added NaH (60% dispersion in mineral oil, 1.75 g, 44.0 mmol) and the reaction was triple evacuated/N_2 filled. The reaction was stirred for 2 h at rt, before dropwise addition of benzyl chloride (2.22 mL, 19.3 mmol). The reaction was stirred for 16 h at rt, before adding brine (70 mL) and EtOAc (70 mL). The organic layer was separated and aqueous layer extracted with EtOAc (2 x 70 mL). The combined organic layers were dried ($MgSO_4$), filtered and concentrated *in vacuo* to yield the crude *tert*-butyl 4-(benzyloxy)piperidine-1-carboxylate **192c** as a yellow oil

(5.09 g); ^{1}H NMR (400 MHz, $CDCl_3$) δ 7.39 - 7.28 (5H, m, C*H*), 4.57 (2H, s, CH_2), 3.84 - 3.74 (2H, m, CH_2), 3.62 - 3.54 (1H, m, C*H*), 3.16 - 3.07 (2H, m, CH_2), 1.91 - 1.81 (2H, m, CH_2), 1.65 - 1.55 (2H, m, CH_2), 1.47 (9H, s, CH_3); which was used without further purification.

According to a literature procedure,[233] *tert*-butyl 4-(benzyloxy)piperidine-1-carboxylate **192c** (1.17 g, 4.0 mmol) in Et_2O (20 mL) was added dropwise under an N_2 atmosphere to a flask containing $LiAlH_4$ (17.2 mL, 1.0 M in THF) in Et_2O (50 mL) at rt. The solution was stirred at reflux (35 ^{o}C) for 16 h, before cooling to 0 ^{o}C and carefully quenching with successive addition of 655 μL of water, 655 μL of 15% NaOH and 1.85 mL of water. The reaction mixture was filtered through celite, the solids were washed heavily with Et_2O and the filtrate was dried over $MgSO_4$, filtered and concentrated *in vacuo* to yield 4-(benzyloxy)-1-methylpiperidine (***193***) as a yellow oil (0.82 g, 100%) which was analytically pure; IR ν_{max} (neat) 2926 - 2781 (C-H), 1497 (Ar), 1453 (Ar), 1360, 1277, 1204 cm^{-1}; ^{1}H NMR (400 MHz, $CDCl_3$) δ 7.39 - 7.28 (5H, m, C*H*), 4.55 (2H, s, CH_2), 3.47 - 3.37 (1H, m, C*H*), 2.77 - 2.66 (2H, m, CH_2), 2.27 (3H, s, CH_3), 2.17 - 2.07 (2H, m, CH_2), 1.99 - 1.88 (2H, m, CH_2), 1.76 - 1.66 (2H, m, CH_2); ^{13}C NMR (101 MHz, $CDCl_3$) δ 138.9 (*C*), 128.3 (*C*H), 127.5 (*C*H), 127.4 (*C*H), 73.9 (*C*H), 69.7 (*C*H_2), 53.3 (*C*H_2), 46.2 (*C*H_3), 31.3 (*C*H_2), HRMS (+ESI) *m/z* calculated for $C_{13}H_{20}NO$ [M+H^{+}] 206.1539; Found 206.1532.

4-((4-Methoxybenzyl)oxy)-1-methylpiperidine (*195*)

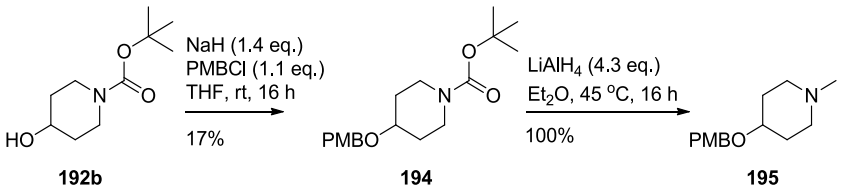

A slurry of NaH powder (1.15 g, 47.9 mmol) in dry THF (15 mL) was triple evacuated/N_2 filled. A solution of crude *tert*-butyl 4-hydroxypiperidine-1-carboxylate **192b** (6.62 g, 32.9 mmol) in dry THF (15 mL) was added dropwise over 15 min. The reaction was stirred for 30 min before dropwise

addition of *p*-methoxybenzyl chloride (4.90 mL, 36.2 mmol). The reaction was stirred for 16 h at rt, before quenching at rt by careful addition of acetic acid (5.7 mL) and water (10 mL). When all gas had been evolved, the reaction was basified with sat. aq. $NaHCO_3$ (to pH = 8) before adding EtOAc (50 mL) and water (50 mL). The layers were separated and the aqueous layer was extracted with EtOAc (2 x 50 mL). The combined organic layers were dried ($MgSO_4$), filtered and concentrated *in vacuo* to yield a yellow oil, which was purified by column chromatography (10 - 20% TBME/heptane(1% Et_3N)) to afford *tert*-butyl 4-((4-methoxybenzyl)oxy)piperidine-1-carboxylate ***194*** as a colourless oil (1.78 g, 17%); IR ν_{max} (neat) 2932 - 2862 (C-H), 1688 (C=O), 1613 (Ar), 1587 (Ar), 1513 (Ar), 1420, 1364, 1302, 1274, 1235 cm^{-1}; ^1H NMR (400 MHz, $CDCl_3$) δ 7.26 (2H, d, *J* = 8.6 Hz, C*H*), 6.90 (2H, d, *J* = 8.6 Hz, C*H*), 4.49 (2H, s, CH_2), 3.81 (3H, s, CH_3), 3.80 - 3.72 (2H, m, CH_2), 3.58 - 3.51 (2H, m, CH_2), 3.13 - 3.05 (2H, m, CH_2), 1.89 - 1.81 (2H, m, CH_2), 1.62 - 1.57 (2H, m, CH_2), 1.46 (9H, s, CH_3); ^{13}C NMR (101 MHz, $CDCl_3$) δ 159.1 (*C*), 154.9 (*C*=O), 130.8 (*C*), 129.0 (*C*H), 113.9 (*C*H), 79.4 (*C*), 73.7 (*C*H), 69.5 (CH_2), 55.3 (CH_3), 41.3 (CH_2), 31.1 (CH_2), 28.4 (CH_3), HRMS (+ESI) *m/z* calculated for $C_{18}H_{28}NO_4$ $[M+H^+]$ 322.2013; Found 322.2015.

According to a literature procedure,[233] *tert*-butyl 4-((4-methoxybenzyl)oxy) piperidine-1-carboxylate **194** (1.29 g, 4.0 mmol) in Et_2O (20 mL) was added dropwise under an N_2 atmosphere to a flask containing $LiAlH_4$ (17.2 mL, 1.0 M in THF) in Et_2O (50 mL) at rt. The solution was stirred at (35 ^oC) for 16 h, before cooling to 0 ^oC and carefully quenching with successive addition of 655 μL of water, 655 μL of 15% NaOH and 1.85 mL of water. The reaction mixture was filtered through celite, the solids were washed heavily with Et_2O, the filtrate was dried over $MgSO_4$, filtered and concentrated *in vacuo* to yield a yellow oil, which was purified by column chromatography (5% MeOH/DCM (1% Et_3N)) to give a pale brown oil, which was washed with DCM (20 mL) and aq. 1% K_2CO_3 (20 mL). The layers were separated and the aqueous layer extracted with DCM (2 x 20 mL). The combined organic layers were dried ($MgSO_4$), filtered and concentrated *in vacuo* to yield 4-((4-

methoxybenzyl)oxy)-1-methylpiperidine ***195*** as a pale brown oil (684.0 mg, 73%); IR ν_{max} (neat) 2939 - 2781 (C-H), 1613 (Ar), 1587 (Ar), 1513 (Ar), 1466 (Ar), 1359, 1301, 1277, 1246 cm^{-1}; ^{1}H NMR (400 MHz, $CDCl_3$) δ 7.26 (2H, d, *J* = 8.7 Hz, C*H*), 6.89 (2H, d, *J* = 8.7 Hz, C*H*), 4.48 (2H, s, CH_2), 3.81 (3H, s, CH_3), 3.44 - 3.36 (1H, m, C*H*), 2.76 - 2.67 (2H, m, CH_2), 2.27 (3H, s, CH_3), 2.16 - 2.08 (2H, m, CH_2), 1.95 - 1.87 (2H, m, CH_2), 1.76 - 1.64 (2H, m, CH_2); ^{13}C NMR (101 MHz, $CDCl_3$) δ 159.1 (*C*), 131.0 (*C*), 129.0 (*C*H), 113.8 (*C*H), 73.6 (*C*H), 69.4 (*C*H_2), 55.3 (*C*H_3), 53.4 (*C*H_2), 46.2 (*C*H_3), 31.4 (*C*H_2), HRMS (+ESI) *m/z* calculated for $C_{14}H_{22}NO_2$ $[M+H^+]$ 236.1645; Found 236.1643.

5.18. Initial Studies: Oxidation of dextromethorphan using TBPA-PF_6

5.18.1. Applying Jahn's Conditions in an Oxidation of dextromethorphan

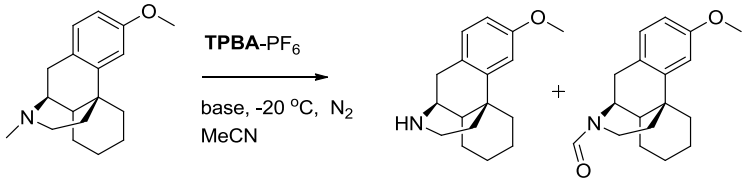

This experiment was conducted according to Jahn's procedure,[67] using the colour changes as indicators for the addition of reagents. A reaction vessel was charged with **73** (50.0 mg, 0.18 mmol) and MeCN (3.5 mL). H_2O (33.0 μL, 10.0 eq.) was added and the solution cooled to -20 °C (dry ice/IPA bath) and placed under an N_2 funnel. **TBPA**-PF_6 (145.0 mg, 0.23 mmol, 1.25 eq.) was added as a solid under an atmosphere of N_2 and the colour of the mixture changed to blue. K_2CO_3 (25 mg, 0.18 eq., 1.0 eq.) or another base (Table 15, see overleaf) was added and the colour of the mixture changed to brown. **TBPA**-PF_6 (145.0 mg, 0.23 mmol, 1.25 eq.) was added and the colour of the mixture changed to blue. K_2CO_3 (25 mg, 0.18 eq., 1.0 eq.) was added and the colour of the mixture changed to brown. The reaction was sampled for LCMS and ratio of **73** : **74** : **137** was determined by LCMS peak area

(Table 15, entry 3). A control reaction was conducted without base (Table 15, entry 1). Alternatively, NaOAc was used as a base (Table 15, entry 2).

***Table 15**: Oxidation of dextromethorphan (**73**) by **TBPA**-PF_6 under various conditions.*

Entry	Base	T, ^oC	Solvent	TBPA-PF_6, eq.	Ratio **73 : 74 : 137**[a]
1	-	-20	MeCN (10.0 eq. H_2O)	2.5	1.0 : 0.2 : < 0.1
2	NaOAc	-20	MeCN (10.0 eq. H_2O)	2.5	1.0 : 0.1 : < 0.1[b]
3	K_2CO_3	-20	MeCN (10.0 eq. H_2O)	2.5	1.0 : 0.6 : 0.4[b]
4	K_2CO_3	-20	dry MeCN	2.5	1.0 : 0.6 : 0.3[b]
5	K_2CO_3	-20	dry MeCN	2	1.0 : 0.2 : < 0.1[b]
6	K_2CO_3	0	dry MeCN	2	1.0 : 0.2 : < 0.1[b]
7	-	0	dry MeCN	2	1.0 : 0.1 : < 0.1
8	2,6-lutidine	0	dry MeCN	2	1.0 : 0.5 : 0.4[c]
9	2,6-lutidine	0	dry MeCN	3	1.0 : 1.4 : 1.3[c]
10	2,6-lutidine	0	dry MeCN	4	1.0 : 5.0 : 7.5[c]
11	2,6-lutidine	0	dry DMF	2	1.0 : 0.4 : 0.5[c]
12	2,6-lutidine	0	dry MeOH	2	1.0 : 0.9 : < 0.1[c]
13	quinuclidine	0	dry MeCN	2	1.0 : 1.5 : 0.1[c,d]
14	DABCO	0	dry MeCN	2	1.0 : 0.5 : < 0.1[c,d]

[a]Ratio of **73** : **74** : **137** by LCMS peak area (220 nm, uncorrected) at the time specified. [b]Portionwise addition of oxidant until colour is dark blue, then portionwise addition of base

until colour is brown. [c]All base present at start, portionwise addition of oxidant. [d]base-oxidant adduct observed by LCMS.

5.18.2. APPLYING MODIFIED LITERATURE CONDITIONS IN AN OXIDATION OF DEXTROMETHORPHAN

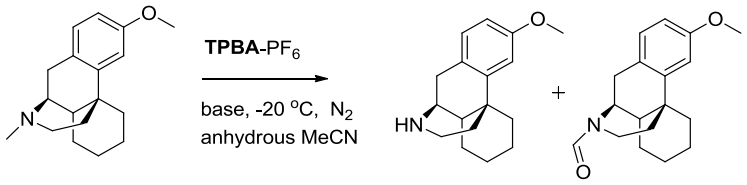

73 **74** **137**

This experiment was conducted according to a modified literature procedure.[67] A predried reaction vessel was charged with **73** (50.0 mg, 0.18 mmol) and anhydrous MeCN (3.5 mL). The solution cooled to -20 °C (dry ice/IPA bath) and placed under an N_2 funnel. **TBPA**-PF_6 (145.0 mg, 0.23 mmol, 1.25 eq.) was added as a solid under an atmosphere of N_2 and the colour of the mixture changed to blue. K_2CO_3 (25 mg, 0.18 eq., 1.0 eq.) was added and the colour of the mixture changed to brown. **TBPA**-PF_6 (145.0 mg, 0.23 mmol, 1.25 eq.) was added and the colour of the mixture changed to blue. K_2CO_3 (25 mg, 0.18 eq., 1.0 eq.) was added and the colour of the mixture changed to brown. The reaction was sampled for LCMS (Table 15, entry 4) and ratio of **73** : **74** : **137** was determined from the integration area.

Alternatively, anhydrous MeCN was used as solvent (Table 15, entry 4) [higher conversion than entry 1]. Alternatively, **TBPA**-PF_6 (2.0 eq.) was added in total and anhydrous MeCN was used as solvent (Table 15, entry 5) [lower conversion than entry 4]. Alternatively, **TBPA**-PF_6 (2.0 eq.) was added in total, anhydrous MeCN was used as solvent and the reaction was conducted at 0 °C (Table 15, entry 6) [same conversion as entry 5]. Alternatively, the reaction was conducted in the absence of base, **TBPA**-PF_6 (2.0 eq.) was added in total, anhydrous MeCN was used as solvent and the reaction was conducted at 0 °C (Table 15, entry 7) [similar conversion to entry 1]. Alternatively, 2,6-lutidine was used as a base (Table 15, entry 8) under the conditions employed in Table 15, entry 8 [higher conversion than

entry 7, see Figure 32]. Further portions of **TBPA**-PF_6 were added (3.0 eq., 4.0 eq. in total) and the conversion followed by LCMS (Table 15, entries 9 and 10) [increasing conversion with added oxidant]. Alternatively, the reaction was run in DMF or MeOH as solvent (Table 15, entries 11 and 12) under the conditions employed in Table 15, entry 8 [DMF gave same conversion as entry 8 and similar selectivity for **74**, MeOH gave same conversion as entry 8 but higher selectivity for **74**].

Alternatively, quinuclidine (2.0 eq.) was used as the base (Table 15, entry 13) under the conditions employed in Table 15, entry 8 [increased selectivity for **74** and higher conversion]. After addition of **TBPA**-PF_6 (2.0 eq.) the *N*-formyl product **137** was suppressed (Figure 33, top), but a new peak (**138**) appeared at 3.7 min (high pH LCMS, M^+ = 515).

Alternatively, DABCO (2.0 eq.) was used as the base (Table 15, entry 14). After addition of **TBPA**-PF_6 (2.0 eq.) the *N*-formyl product **137** was suppressed (Figure 33, bottom), but a new peak (**139**) appeared at 3.2 min (high pH LCMS, M^+ = 514).

Alternatively, the reaction was conducted according to a literature procedure which had been successfully applied to the oxidation of *N*-aryl-1,2,3,4-tetrahydroisoquinolines,[34] using catalytic **TBPA**-$SbCl_6$ (0.2 eq.), with H_2O (2.0 eq.) present in place of the ketone pronucleophile, stirring under air for 16 h at rt (Table 15, entry 15) [trace product observed].

Alternatively, the catalytic literature procedure[34] was conducted using **TBPA**-PF_6 (0.2 eq.), with H_2O (2.0 eq.) present in place of the ketone pronucleophile, stirring under air for 16 h at rt (Table 15, entry 16) [no conversion observed]. These findings rule out an aerobic catalytic mechanism in reactions of trialkylamines.

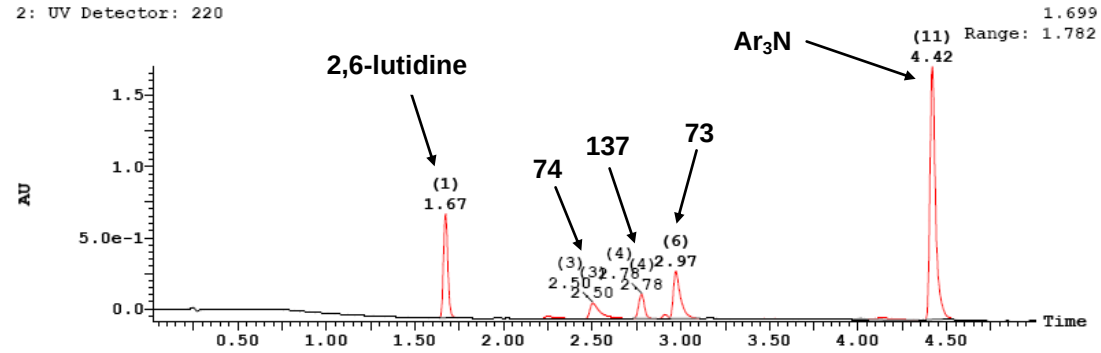

Figure 32: *Example LCMS trace (high pH) for oxidation of dextromethorphan using 2,6-lutidine (2.0 eq.) as the base, at 0 °C.*

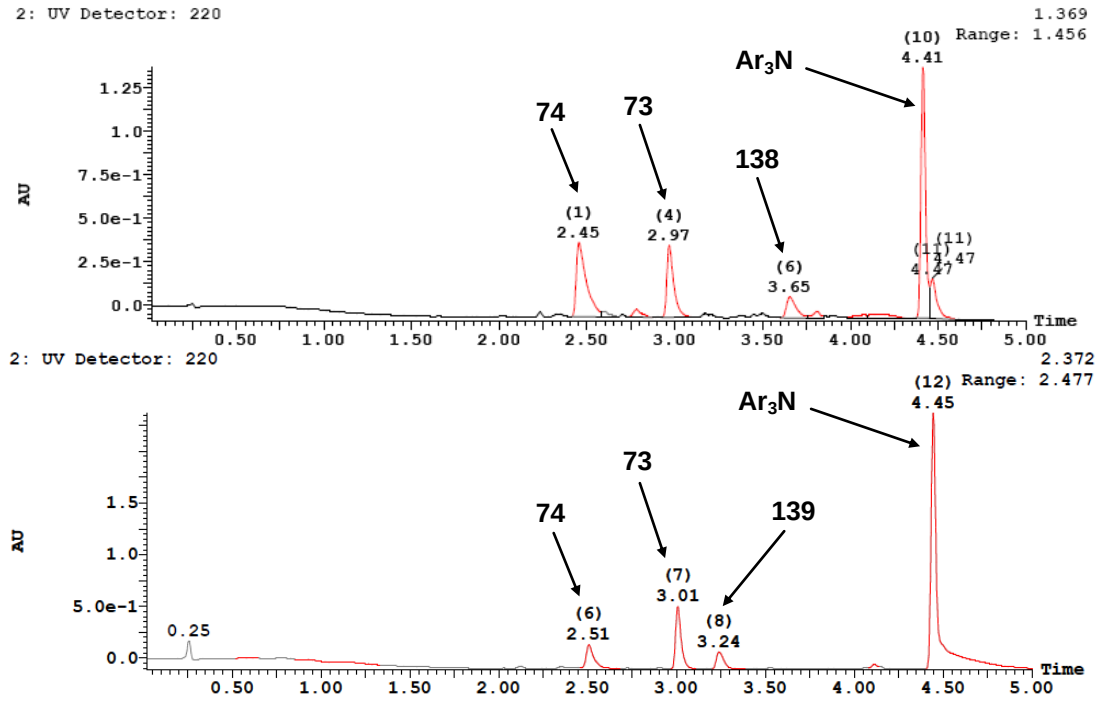

Figure 33*: Example LCMS traces (high pH) for oxidation of dextromethorphan* ***73*** *using quinuclidine (2.0 eq.) as the base (top) or DABCO (2.0 eq.) as the base (bottom), at 0 °C.*

5.18.3. Evidence for TBPA-PF_6 Undergoing Nucleophilic Aromatic Substitution

When using quinuclidine (2.0 eq.) as base with **TBPA**-PF_6 (2.0 eq.) as oxidant, a new peak appeared at 3.7 min (high pH LCMS, M^+ = 515). Use of

DABCO (2.0 eq.) led to a new peak at 3.2 min (high pH LCMS, M+ = 514). The mass ions observed are consistent with adducts **138** and **139**; an S_NAr-type mechanism is proposed for their formation (Scheme 71). To confirm this proposal, DABCO was treated with **TBPA**-PF_6 in the absence of any other trialkylamine substrate and adduct **139** was observed as the sole product by LCMS (peak at 3.2 min, high pH LCMS, M^+ = 514) besides tris(*p*-bromophenyl)amine (Figure 34). An aromatic substitution reaction has been previously observed, upon treating **TBPA**-PF_6 with acetate ion[180] or 2,3-diazabicyclo[2.2.2]oct-2-ene[181] as nucleophiles. Given the susceptibility of **TBPA**-PF_6 to the aromatic substitution reaction, a decision was made to employ **TPTA**-PF_6 as the oxidant, which is blocked to nucleophilic substitution.

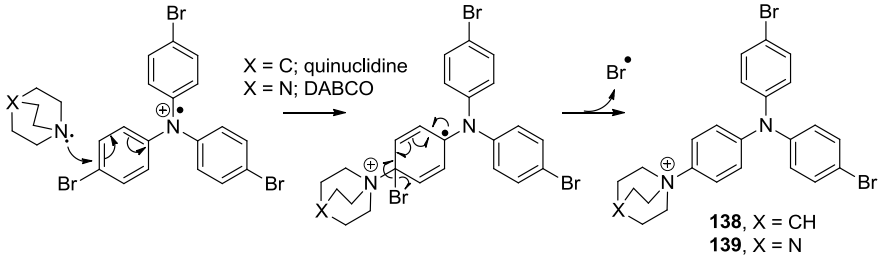

***Scheme 71**: S_NAr-type mechanism for DABCO reacting with tris(p-bromophenyl)aminium radical cation.*

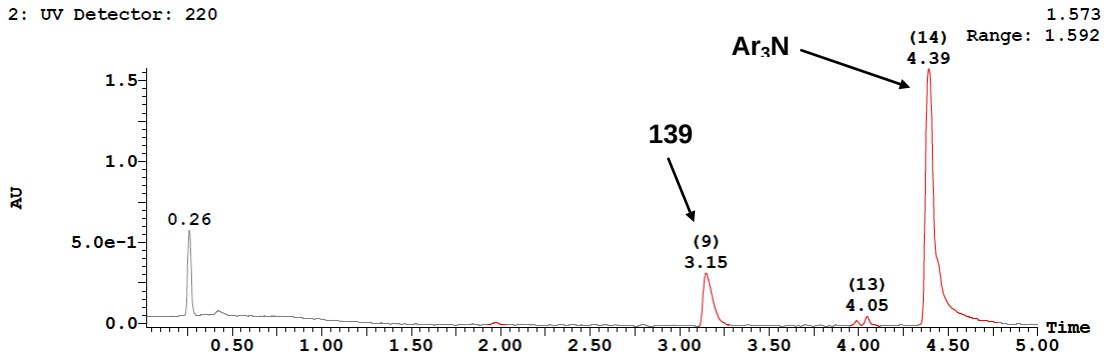

***Figure 34**: LCMS trace (high pH) for treatment of **TBPA**-PF_6 (0.8 eq.) with DABCO (1.0 eq.) in the absence of any other trialkylamine substrate.*

1-(4-(Bis(4-bromophenyl)amino)phenyl)-1,4-diazabicyclo[2.2.2]octan-1-ium trifluoroacetate (***139***)

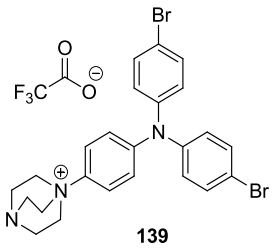

139

A reaction vessel was charged with DABCO (278 mg, 2.48 mmol) and anhydrous MeCN (15 mL) before cooling to -5 ^{o}C and placing under an N_2 funnel. **TBPA**-PF_6 (345.0 mg, 0.55 mmol) was added as a solid under an atmosphere of N_2. Further portions (8x) of **TBPA**-PF_6 (103.0 mg, 0.17 mmol) were added. The reaction mixture was a pale brown slurry. MeOH (1.0 mL) was added, the reaction mixture filtered through celite and DCM (100 mL) and H_2O (100 mL) were added. The layers were separated and the aqueous layer was extracted with DCM (2 x 100 mL). The combined organic layers were dried ($MgSO_4$), filtered and concentrated *in vacuo* before loading onto celite. The crude product was loaded onto a silica plug and eluted with warm (40 ^{o}C) heptane to remove tri-*p*-tolylamine. The plug was then eluted with TBME/heptane (50%) (4 x 100 mL), then MeOH/DCM (5%) (4 x 100 mL). The MeOH/DCM fractions were combined and concentrated *in vacuo* to afford a brown oil. MDAP purification (Low pH) afforded ***139*** as a pale yellow gum (16.7 mg, 2%);[†] IR ν_{max} (neat) 3416, 3065 - 2894 (C-H), 1685 (C=O), 1579 (Ar), 1509 (Ar), 1486 (Ar), 1317, 1272 cm^{-1}; ^{1}H NMR (400 MHz, $CDCl_3$) δ 7.72 (2H, d, *J* = 9.4 Hz, C*H*), 7.42 (4H, d, *J* = 8.7 Hz, C*H*), 7.10 (2H, d, *J* = 9.4 Hz, C*H*), 6.98 (4H, d, *J* = 8.7 Hz, C*H*), 3.95 (6H, apt. t, *J* = 7.3 Hz, CH_2), 3.39 (6H, apt. t, *J* = 7.3 Hz, CH_2); ^{13}C NMR (101 MHz, $CDCl_3$) δ 148.8 (*C*),

[†]Although product **139** appears stable to reverse phase chromatography, significant product decomposition was observed upon purification through a silica plug, resulting in a very low yield obtained for analysis. The trifluoroacetic acid in the chromatography eluant and the presence of a peak in the ^{19}F NMR indicated the trifluoroacetate anion was present, but ^{13}C NMR peaks for the anion could not be detected. The IR stretch at 1685 cm^{-1} cannot be used to distinguish between trifluoroacetate and bicarbonate anions.

145.0 (*C*), 138.8 (*C*), 133.0 (*C*H), 127.0 (*C*H), 122.2 (*C*H), 121.9 (*C*H), 117.9 (*C*), 56.2 (CH_2), 45.9 (CH_2); ^{19}F NMR (376.5 MHz, $CDCl_3$) δ -74.9 (s, CF_3); HRMS (+ESI) *m/z* calculated for $C_{24}H_{24}{}^{79}Br_2N_3^+$ [M^+] 512.0330; Found 512.0331.

^{1}H NMR (400 MHz, $CDCl_3$) – **139**

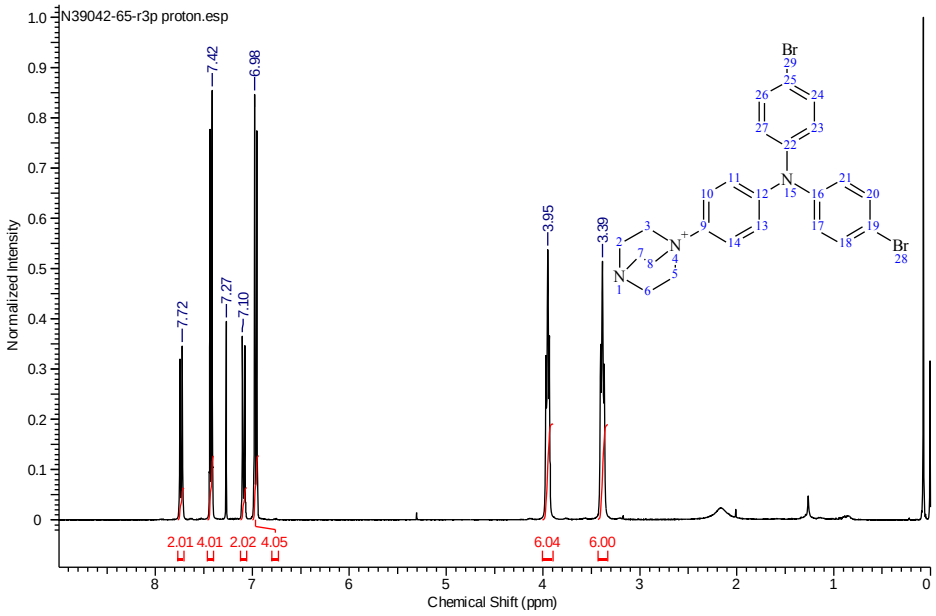

^{13}C NMR (101 MHz, $CDCl_3$) – **139**

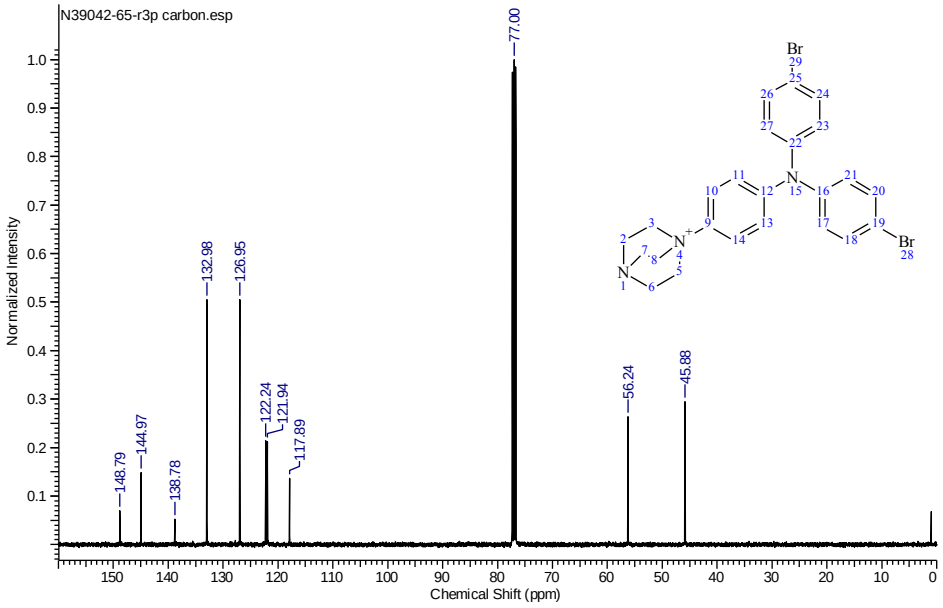

***Figure 35**: ^{1}H and ^{13}C NMR spectra for DABCO-adduct **139**.*

5.19. REACTION OPTIMISATION OF THE TPTA-PF_6-MEDIATED OXIDATION OF DEXTROMETHORPHAN

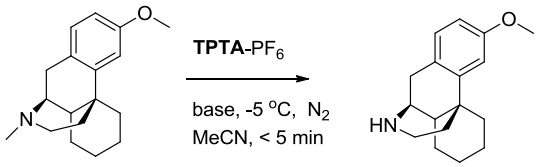

73 **74**

Oxidation Procedure 1: A predried reaction vessel was charged with dextromethorphan **73** (12.5 mg, 50.0 μmol), and anhydrous MeCN (1.5 mL, 33 mM) before cooling to 0 °C and placing under an N_2 funnel. **TPTA**-PF_6 (20.0 mg, 50.0 μmol, 1.0 eq.) was added portionwise as a solid. **TPTA**-PF_6 (6.0 mg, 15.0 μmol, 0.3 eq.) was added portionwise as a solid and the colour turned blue. Quinuclidine (5.1 mg, 50.0 μmol, 1.0 eq.) was added as a solid and the colour turned orange. Further portions (3x) of **TPTA**-PF_6 (6.0 mg, 15.0 μmol, 0.3 eq.) were added. Quinuclidine (5.1 mg, 50.0 μmol, 1.0 eq.) was added as a solid and the colour turned orange. Further portions (3x) of **TPTA**-PF_6 (6.0 mg, 15.0 μmol, 0.3 eq.) were added. Quinuclidine (5.1 mg, 50.0 μmol, 1.0 eq.) was added as a solid and the colour turned orange. The reaction was sampled for LCMS and ratio of **73** : **74** : **137** was determined (Table 16, entry 1). Alternatively, DABCO was used as a base (portions added were 1.0 eq.) and the reaction was sampled for LCMS after 3.1 eq. and 3.4 eq. **TPTA**-PF_6 were added in total (Table 16, entries 2,3).

Oxidation Procedure 2: Alternatively, the portions of DABCO added were 1.5 eq. (total added = 4.5 eq.) and the reaction was sampled for LCMS after 3.1 eq. of **TPTA**-PF_6 were added in total (Table 16, entry 4). Alternatively, the portions of DABCO added were 0.5 eq. (total added = 3.0 eq.) and the reaction was sampled for LCMS after 3.1 eq. of **TPTA**-PF_6 were added in total (Table 16, entry 5).

Oxidation Procedure 3: Alternatively, the total amount of DABCO (4.5 eq.) was present at the start of the reaction and the reaction was sampled for

LCMS after 3.4 eq. of **TPTA**-PF_6 were added in total (Table 16, entry 6). Alternatively, DABCO (4.5 eq., 3x 1.5 eq. portions) was added after the total amount of **TPTA**-PF_6 (3.4 eq.) had been added (Table 16, entry 7). Alternatively, the total amount of DABCO (4.5 eq.) was present at the start of a reaction where dextromethorphan was absent, then the total amount of **TPTA**-PF_6 (3.4 eq.) was added, then dextromethorphan (**73**) (1.0 eq.) was added (Table 16, entry 8).

5.19.1. Effect of Stoichiometry and Order of Addition on the Oxidation Reaction

Table 16: *Oxidation of dextromethorphan (**73**) using **TPTA**-PF_6.*

Entry	Base	Total Base, eq. (portion eq.)	TPTA-PF_6, eq.	Ratio 73 : 74 : 137[a]
1	quinuclidine	4.0 (1.0)	3.1	ND : 10.6 : 1.7[b]
2	DABCO	4.0 (1.0)	3.1	1.0 : 8.1 : 0.7[b]
3	DABCO	4.0 (1.0)	3.4	ND : 11.0 : 1.0[b]
4	DABCO	4.5 (1.5)	3.1	ND : 11.3 : 1.0[c]
5	DABCO	3.0 (0.5)	3.1	1.0 : 3.1 : ND[c]
6	DABCO	4.5 (at start)	3.4	ND : 10.3 : 1.0[d,e]
7	DABCO	4.5	3.4 (at start)	1.0 : 4.1 : 0.3[c,f]
8	DABCO	4.5 (at start)	3.4 (at start)	1.0 : 0.2 : ND[c,g]

[a]By LCMS peak area (220 nm, uncorrected). [b]Oxidation procedure 1. [c]Oxidation procedure 2. [d]Oxidation procedure 3. [e]Average of 3 runs (these were taken as the optimum conditions). [f]Premixing dextromethorphan (**73**) and **TPTA**-PF_6 before adding DABCO. [g]Premixing DABCO and **TPTA**-PF_6 before adding dextromethorphan (**73**). ND = not determined (not detected).

5.19.2. Reacting TPTA-PF_6 with DABCO as a Control Reaction to Isolate TPTA/DABCO-derived By-products

In order to establish whether any baseline impurities were derived from dextromethorphan (**73**), a control reaction was conducted omitting **73**. It revealed that **TPTA**-PF_6 and DABCO were not an innocent combination, even with the absence of a formal leaving group in **TPTA**-PF_6. In the absence of dextromethorphan, **TPTA**-PF_6 and DABCO reacted to afford some interesting products (Figure 36), ***196***, ***197*** and ***198*** as the three major components by LCMS. By comparison of the LCMS traces of reactions with and without **73** (Figure 37), it is clear that these products derive from **TPTA**-PF_6 and DABCO but not from **73**, and thus do not compromise product yields.

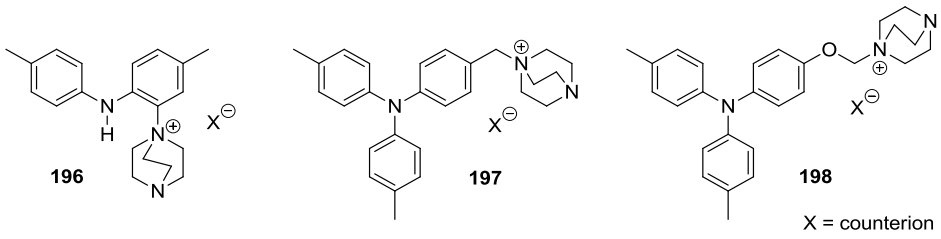

Figure 36*: Products derived from treatment of* ***TPTA****-PF_6 with DABCO only.*

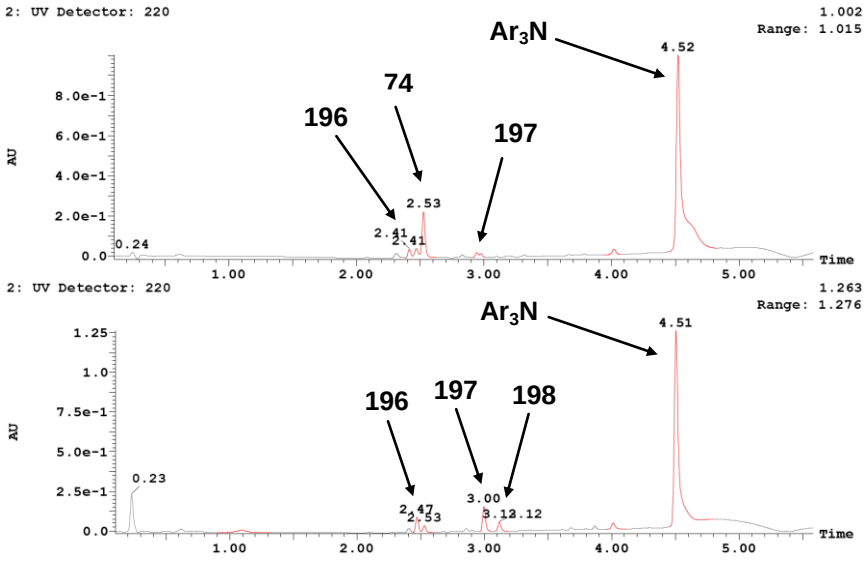

Figure 37: *LCMS traces (low pH) for oxidation reaction profile with dextromethorphan* ***73*** *(top) and without (bottom).*

Conducted according to **Oxidation Procedure 3**. A predried reaction vessel was charged with DABCO (287.0 mg, 2.48 mmol, 4.5 eq.) and anhydrous MeCN (15 mL) before cooling to -5 ^{o}C and placing under an N_2 funnel. **TPTA**-PF_6 (234.0 mg, 1.65 mmol, 1.0 eq.) was added under an atmosphere of N_2. Further **TPTA**-PF_6 8 x (71.0 mg, 0.17 mmol, 0.3 eq.) was added. The reaction mixture was a yellow slurry. The precipitate was allowed to settle. The supernatant was purified by Mass Directed Autoprep (MDAP, low pH or high pH). Where low pH MDAP methods were used, product-containing fractions were basified with 1% K_2CO_3 (10 mL), extracted with DCM (3 x 10 mL), dried ($MgSO_4$), filtered and concentrated *in vacuo* to yield DABCO/**TPTA**-PF_6 derived by-products ***196***, ***197*** and ***198***,[†] tentatively assigned as their bicarbonate salts due to no ^{19}F or ^{31}P signals being observed.

1-(5-Methyl-2-(*p*-tolylamino)phenyl)-1,4-diazabicyclo[2.2.2]octan-1-ium bicarbonate (***196***)

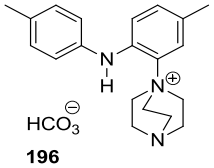

196

This compound was isolated as a pale brown oil;[‡] IR ν_{max} (neat) 3201 - 2906 (C-H), 1659 (Ar), 1467 (Ar), 1435 cm^{-1}; ^{1}H NMR (400 MHz, DMSO-d_6) δ 7.67 (1H, br. s, C*H*), 7.41 (1H, d, *J* = 8.0 Hz, C*H*), 7.34 (1H, s, N*H*), 7.23 (1H, d, *J* = 7.9 Hz, C*H*), 7.02 (2H, d, *J* = 8.1 Hz, C*H*), 6.57 (2H, d, *J* = 8.4 Hz, C*H*), 3.39 (6H, apt. t, *J* = 7.3 Hz, CH_2), 3.18 (6H, apt. t, *J* = 7.4 Hz, CH_2), 2.41 (3H, s, CH_3), 2.20 (3H, s, CH_3); ^{13}C NMR (101 MHz, DMSO-d_6)[§] δ 141.7 (*C*), 136.0 (*C*), 133.1 (*C*H), 132.1 (*C*H), 129.7 (*C*H), 123.1 (*C*H), 116.3 (*C*H),

[†]The by-products were isolated for identification purposes only, and were not quantified. [‡]Tentatively assigned as the bicarbonate salt based on the sodium bicarbonate present in the reverse-phase chromatography eluant, the K_2CO_3 used to basify fractions and the absence of ^{19}F and ^{31}P NMR signals (IR stretches for the bicarbonate anion were not detected). [§]The other three quaternary carbons could not be observed, the ^{13}C signal for the bicarbonate anion could not be observed.

54.1 (CH_2), 45.1 (CH_2), 20.7 (CH_3), 20.1 (CH_3); HRMS (+ESI) *m/z* calculated for $C_{20}H_{26}N_3$ [M] 308.2121; Found 308.2130. A partial mechanism is proposed for formation of **196**, *via* addition of the DABCO radical cation to **TPTA**-PF_6 followed by C-N bond cleavage (Figure 38). The nature of the C-N bond cleavage is unknown.

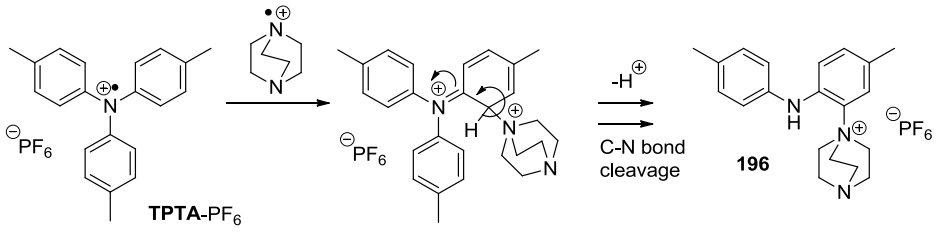

***Figure 38**: Mechanism proposed for the formation of **196**.*

^{1}H NMR (400 MHz, DMSO-d_6) – **196**

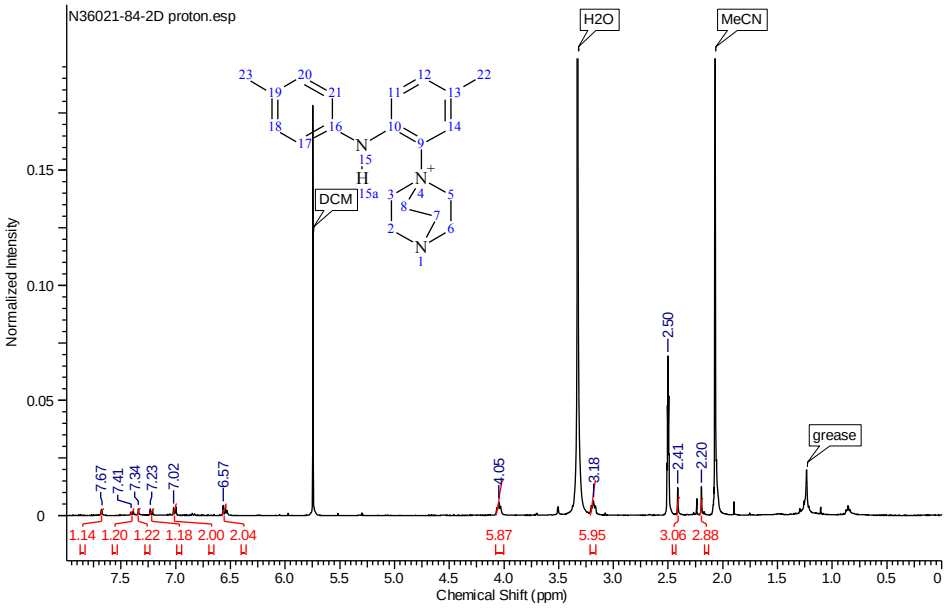

^{13}C NMR (101 MHz, DMSO-d$_6$) – **196**

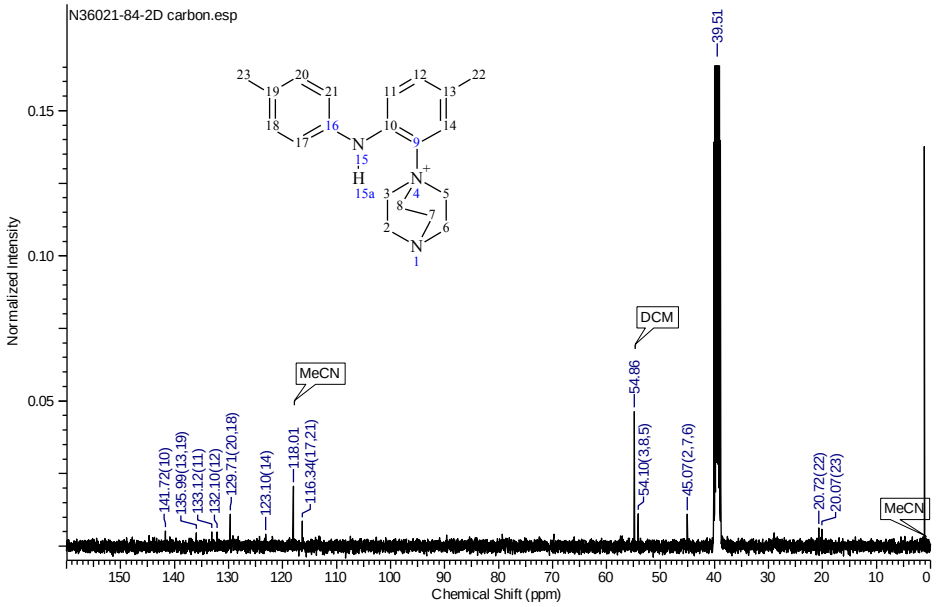

***Figure 39**: ^{1}H and ^{13}C NMR spectra for DABCO-adduct **196**.*

1-(4-(Di-*p*-tolylamino)benzyl)-1,4-diazabicyclo[2.2.2]octan-1-ium bicarbonate (***197***)

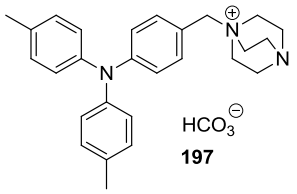

This compound was isolated as a pale brown oil;[†] IR ν_{max} (neat) 3390, 2943 (C-H), 1605 (Ar), 1508 (Ar), 1464 (Ar), 1322, 1295 cm^{-1}; ^{1}H NMR (400 MHz, DMSO-d$_6$) δ 7.28 (2H, d, *J* = 8.6 Hz, C*H*), 7.18 (4H, d, *J* = 8.2 Hz, C*H*), 7.00 (4H, d, *J* = 8.4 Hz, C*H*), 6.88 (2H, d, *J* = 8.6 Hz, C*H*), 4.37 (2H, s, CH_2), 3.25 (6H, apt. t, *J* = 7.3 Hz, CH_2), 3.02 (6H, apt. t, *J* = 7.3 Hz, CH_2), 2.28 (6H, s, CH_3); ^{13}C NMR (101 MHz, DMSO-d$_6$)[‡] δ 149.2 (*C*), 143.9 (*C*), 133.9 (*C*H), 133.6 (*C*), 130.3 (*C*H), 125.4 (*C*H), 119.4 (*C*H), 118.3 (*C*), 66.4 (*C*H$_2$), 51.4

[†]Tentatively assigned as the bicarbonate salt based on the sodium bicarbonate present in the reverse-phase chromatography eluant, the K_2CO_3 used to basify fractions and the absence of ^{19}F and ^{31}P NMR signals (IR stretches for the bicarbonate anion were not detected). [‡]The ^{13}C signal for the bicarbonate anion could not be observed.

(CH_2), 44.7 (CH_2), 20.4 (CH_3); HRMS (+ESI) *m/z* calculated for $C_{27}H_{32}N_3$ [M] 398.2591; Found 398.2589. A mechanism is proposed for formation of **197**, *via* deprotonation of a **TPTA**-PF_6 methyl group and radical-radical coupling of the resultant radical with $DABCO^{\bullet+}$ (Figure 40). Another plausible mechanism is H atom transfer between the **TPTA**-PF_6 methyl group and DABCO radical cation, followed by addition of DABCO as a nucleophile into the iminium-type species (not shown).

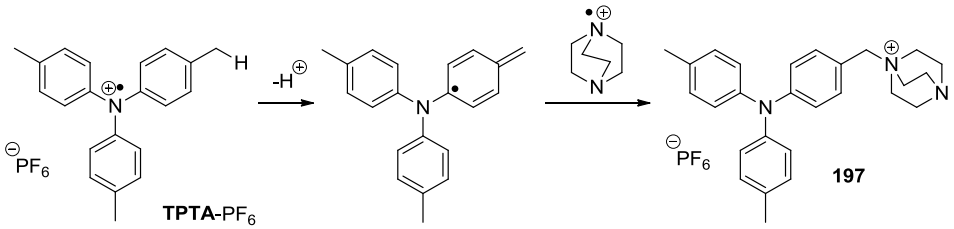

***Figure 40**: Mechanism proposed for the formation of **197**.*

^{1}H NMR (400 MHz, DMSO-d_6) – **197**

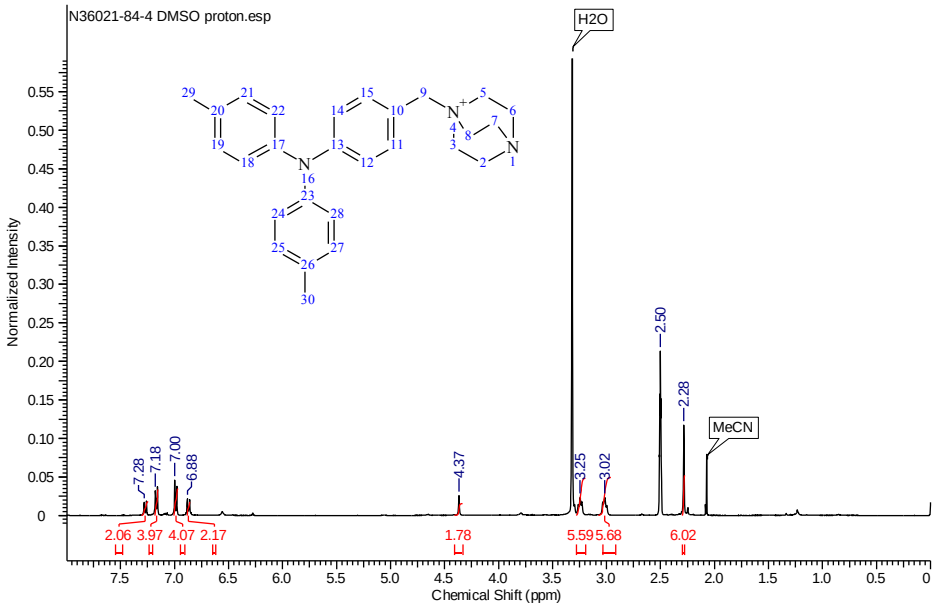

^{13}C NMR (101 MHz, DMSO-d$_6$) – **197**

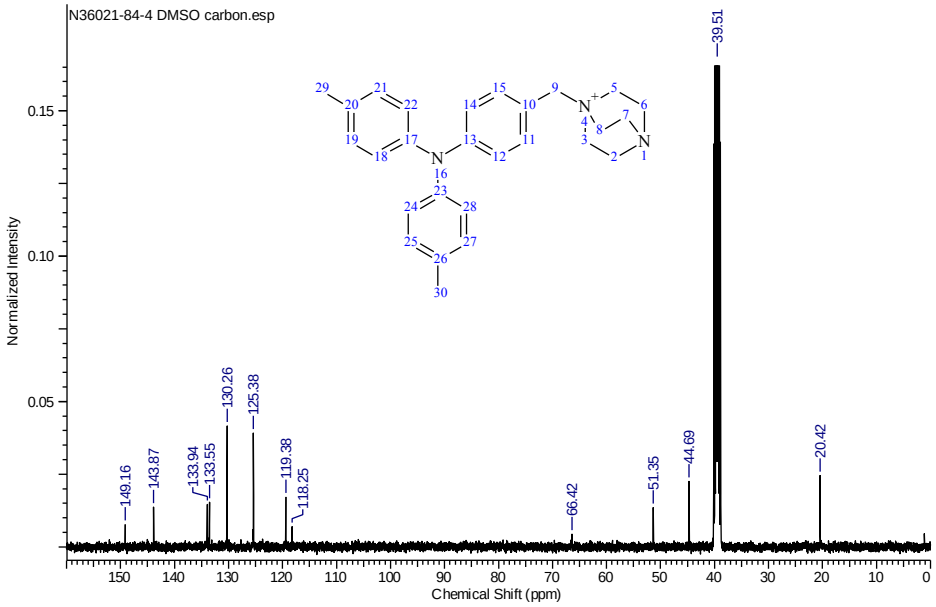

***Figure 41**: ^{1}H and ^{13}C NMR spectra for DABCO-adduct **197**.*

1-((4-(Di-p-tolylamino)phenoxy)methyl)-1,4-diazabicyclo[2.2.2]octan-1-ium bicarbonate (198)

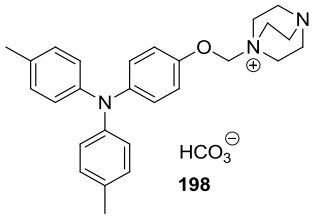

This compound was isolated as a pale brown oil;[†] IR ν_{max} (neat) 3200 - 3050 (C-H), 1659 (Ar), 1437 cm^{-1}; ^{1}H NMR (400 MHz, DMSO-d$_6$) δ 7.11 (2H, d, *J* = 9.0 Hz, C*H*), 7.07 (4H, d, *J* = 8.1 Hz, C*H*), 6.99 (2H, d, *J* = 9.0 Hz, C*H*), 6.85 (4H, d, *J* = 8.6 Hz, C*H*), 5.23 (2H, s, C*H*$_2$), 3.39 (6H, apt. t, *J* = 7.4 Hz, C*H*$_2$), 3.09 (6H, apt. t, *J* = 7.4 Hz, C*H*$_2$), 2.25 (6H, s, C*H*$_3$); ^{13}C NMR (101 MHz, DMSO-d$_6$)[‡] δ 151.4 (*C*), 145.0 (*C*), 143.3 (*C*), 131.7 (*C*), 130.0 (*C*H), 124.9 (*C*H), 123.3 (*C*H), 117.3 (*C*H), 86.9 (*C*H$_2$), 49.5 (*C*H$_2$), 44.3 (*C*H$_2$), 20.3

[†]Tentatively assigned as the bicarbonate salt based on the sodium bicarbonate present in the reverse-phase chromatography eluant, the K_2CO_3 used to basify fractions and the absence of ^{19}F and ^{31}P NMR signals (IR stretches for the bicarbonate anion were not detected). [‡]The ^{13}C signal for the bicarbonate anion could not be observed.

(CH_3); HRMS (+ESI) *m/z* calculated for $C_{27}H_{32}N_3O$ [M] 414.2540; Found 414.2549. It is tentatively proposed (Figure 42) that deprotonation of **TBPA**-PF_6 and combination of the resulting stabilised α-amino radical with molecular oxygen could give rise to a tetroxide intermediate (a known intermediate class in the aerobic degradation of DNA).[234] Breakdown of this tetroxide intermediate would afford a reactive alkoxyl radical, which could undergo a neophyl-type rearrangment and undergo radical-radical combination with DABCO radical cation to afford **198**.

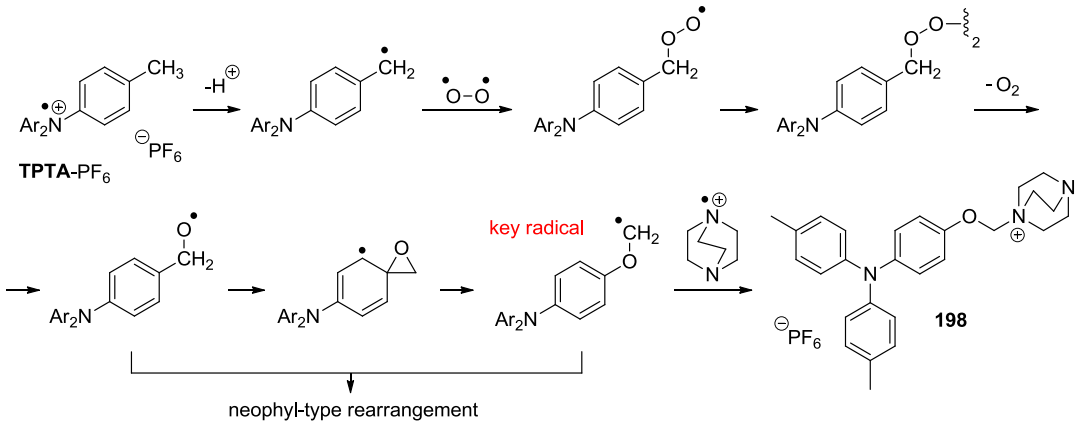

***Figure 42**: Mechanism proposed for the formation of **198**.*

^{1}H NMR (400 MHz, DMSO-d_6) – **198**

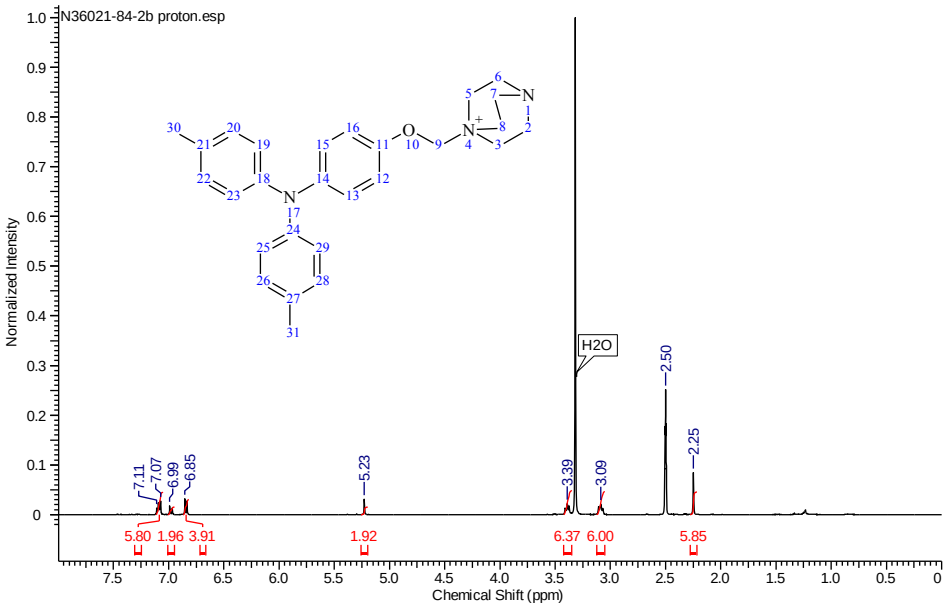

^{13}C NMR (101 MHz, DMSO-d_6) – **198**

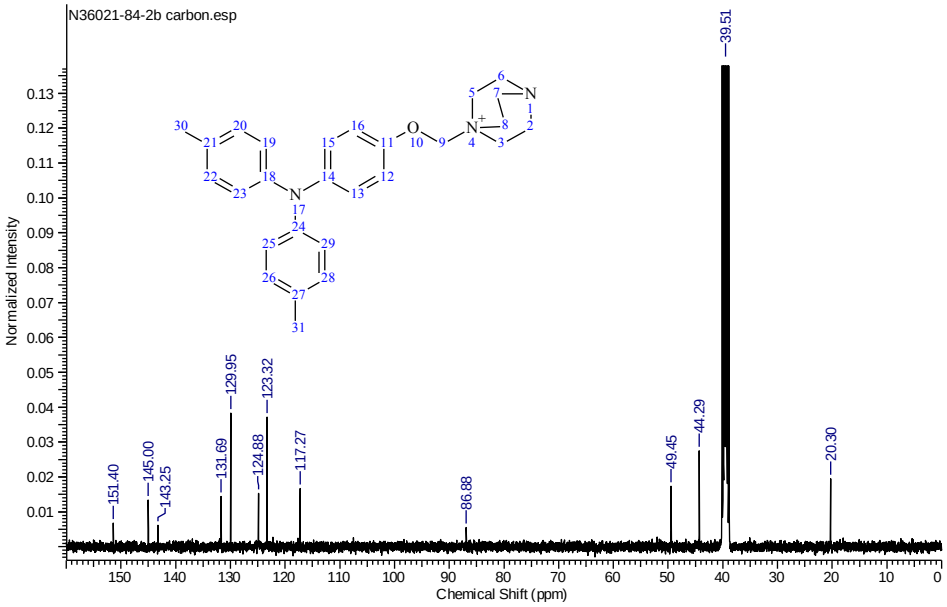

***Figure 43**: ^{1}H and ^{13}C NMR spectra for DABCO-adduct **198**.*

5.19.3. Effect of Solvent on the Oxidation Reaction

In order to logically select solvents which had different physical properties, a principal component analysis (PCA) was employed. The influence of solvent on the mechanism of a given chemical process is highly complex, and different solvents have a multitude of different physical and chemical properties. The PCA model is a mathematical treatment of a set of solvents using chosen descriptors (for example, boiling point, density, dielectric constant, lipophilicity), in order to generate a set of principal components which more accurately reflect the intrinsic molecular properties of solvents. A PCA solvent model was used to select eight different solvents which lay within different octants of the sphere (MeCN, DMF, DCM, THF (unstabilised), TBME, PhCl, $PhCH_2OH$ and MeOH) and these solvents were investigated in the oxidation reaction of dextromethorphan (**73**) using **TPTA**-PF_6, using conversion (LCMS peak area at 220 nm, uncorrected) as a response. The PCA model found that polar, aprotic solvents gave the highest conversion. No solvent tested imparted higher conversion than MeCN, and a solvent with

similar physical properties identified by the PCA model (1,4-dioxane) gave similar conversion to THF (unstabilised).

Oxidation Procedure 2 was used, with naphthalene (1.0 eq.) present at the start of the reaction as an internal standard. The relative ratio of **73** : **74** (dextromethorphan : *nor*-dextromethorphan) was used as a response after **TBPA**-PF_6 (3.1 eq.) had been added. Conversion to **74** was determined by the LCMS peak area corresponding to **74** (*nor*-dextromethorphan) expressed as a percentage of the sum of **73** and **74**'s LCMS peak areas.

Table 17*: Solvent screen using a principal component analysis solvent model using the ratio of* ***73*** *:* ***74*** *as a response.*

Solvent	Ratio 73 : 74 (conversion of 73)	Conversion
MeCN	1 : 3.6 (84%)	1 : > 2.8
DMF	1 : 2.4 (77%)	1 : 2.2 → 1 : 2.8
THF (unstabilised)	1 : 2.1 (74%)	1 : 1.6 → 1 : 2.2
1,4-dioxane	1 : 2.0 (73%)	1 : 1.6 → 1 : 2.2
DCM	1 : 1.7 (69%)	1 : 1.6 → 1 : 2.2
MeOH	1 : 1.6 (67%)	1 : 1.1 → 1 : 1.6
PhCl	1 : 0.8 (44%)	1 : < 1.0
BnOH	1 : 0.4 (17%)	1 : < 1.0
TBME	1 : 0.4 (17%)	1 : < 1.0

5.19.4. Effect of Temperature on the Oxidation Reaction

To investigate the effect of temperature, **Oxidation Procedure 3** was conducted at -15 ^{o}C, -5 ^{o}C and at rt. The oxidation reaction profile was identical for each temperature by LCMS (Figure 44).

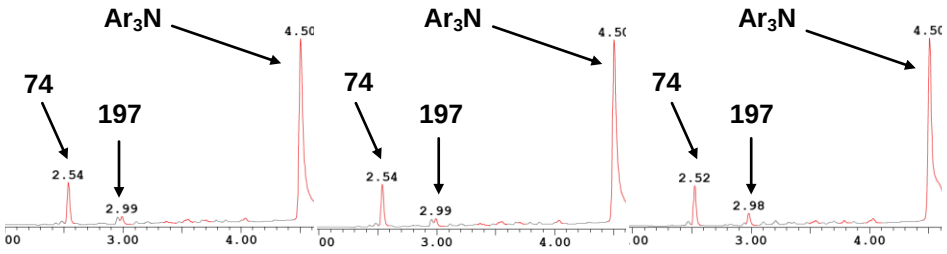

***Figure 44**: Left: Oxidation LCMS reaction profile at -15 °C. Middle: Oxidation LCMS reaction profile at -5 °C. Right: Oxidation LCMS reaction profile at rt (all low pH LCMS).*

5.19.5. Effect of Concentration on the Oxidation Reaction

Running **Oxidation Procedure 3** at higher concentration (110.0 mM) gave a complex mixture of products and poor conversion. Running **Oxidation Procedure 3** at lower concentration (11.0 mM) gave full conversion, but higher levels of **196**, **197** and **198**.

5.19.6. Isolation of *nor*-Dextromethorphan 74 and DABCO-Enamine Adduct 138 Following Aqueous Work Up

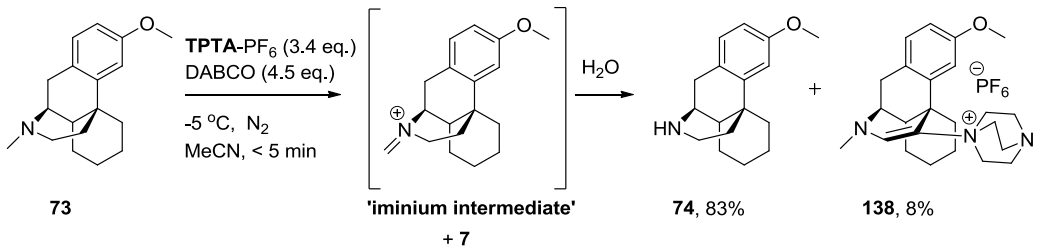

Conducted using **Oxidation Procedure 3.** After the oxidation reaction of dextromethorphan **73** (149.0 mg, 0.55 mmol), the reaction mixture was filtered through celite, and DCM (30 mL), H_2O (20 mL) and brine (10 mL) were added. The layers were separated and the aqueous layer was extracted with DCM (2 x 30 mL). The combined organic layers were dried ($MgSO_4$), filtered and concentrated *in vacuo* before loading onto celite. The crude product was loaded onto a silica plug and eluted with warm (40 °C) heptane to remove tri-*p*-tolylamine. The plug was flushed heavily with MeOH/DCM

(5%) and the fractions concentrated *in vacuo*. DCM (50 mL) and sat. aq. $NaHCO_3$ (50 mL) were added. The layers were separated and the aqueous layer was extracted with DCM (2 x 50 mL). The combined organic layers were dried ($MgSO_4$), filtered and concentrated *in vacuo*. MDAP purification (low pH) gave (after basification using sat. aq. $NaHCO_3$ and extraction with DCM as described above) *nor*-dextromethorphan **74** as a pale brown oil (117.6 mg, 83%);

***Nor*-dextromethorphan (74)**

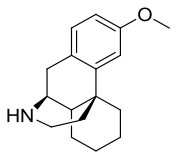

IR ν_{max} (neat) 2928 - 2856 (C-H), 1674, 1610 (Ar), 1576 (Ar), 1495 (Ar), 1454, 1432, 1320, 1270, 1240, 1200 cm^{-1}; ^1H NMR (400 MHz, $CDCl_3$) δ 7.04 (1H, d, *J* = 8.6 Hz, C*H*), 6.81 (1H, d, *J* = 2.7 Hz, C*H*), 6.72 (1H, dd, *J* = 8.3, 2.7 Hz, C*H*), 5.36 (1H, br. s, N*H*), 3.79 (3H, s, CH_3), 3.29 - 3.24 (1H, m, C*H*), 3.13 (1H, dd, *J* = 18.3, 6.1 Hz, CH_2), 2.88 - 2.80 (2H, m, CH_2), 2.72 - 2.62 (1H, m, CH_2), 2.34 (1H, d, *J* = 13.0 Hz, CH_2), 1.89 - 1.81 (1H, m, C*H*), 1.75 - 1.62 (2H, m, CH_2), 1.56 - 1.49 (1H, m, CH_2), 1.45 - 1.24 (5H, m, CH_2), 1.00 - 1.12 (1H, m, CH_2); ^{13}C NMR (101 MHz, $CDCl_3$) δ 158.2 (*C*), 141.7 (*C*), 130.0 (*C*), 128.5 (*C*H), 111.2 (*C*H), 110.7 (*C*H), 55.2 (*C*H_3), 51.2 (*C*H), 46.0 (*C*H), 42.7 (*C*H_2), 39.2 (*C*H_2), 38.3 (*C*), 37.0 (*C*H_2), 33.6 (*C*H_2), 26.9 (*C*H_2), 26.7 (*C*H_2), 22.1 (*C*H_2); HRMS (+ESI) *m/z* calculated for $C_{17}H_{24}NO$ [$M+H^+$] 258.1852; Found 258.1851. Data are consistent with the literature.[8]

1-(3-Methoxy-11-methyl-6,7,8,8a,9,10-hexahydro-5*H*-9,4b-(epiminoethen-o)phenanthren-13-yl)-1,4-diazabicyclo[2.2.2]octan-1-ium bicarbonate (*141*)

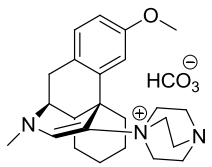

141

MDAP purification (low pH) also gave (after basification using sat. aq. $NaHCO_3$ and extraction with DCM as described above) **141** (below) as a pale yellow oil[†] (19.4 mg, 8%), IR ν_{max} (neat) 3404 - 2860 (br., O-H, C-H), 1687 (C=C), 1636 (C=O), 1608 (Ar), 1576 (Ar), 1497 (Ar), 1464 (Ar), 1414, 1321, 1291, 1259, 1237 cm^{-1}; ^{1}H NMR (400 MHz, $CDCl_3$) δ 7.21 (1H, s, C*H*), 7.13 (1H, d, *J* = 8.4 Hz, C*H*), 6.81 (1H, d, *J* = 2.3 Hz, C*H*), 6.72 (1H, dd, *J* = 8.5, 2.5 Hz, C*H*), 3.78 (3H, s, CH_3), 3.77 - 3.60 (6H, m, CH_2), 3.25 - 3.12 (6H, m, CH_2), 3.12 - 3.07 (1H, m, C*H*), 3.00 (3H, s, CH_3), 3.02 - 2.90 (3H, m, CH_2), 2.01 - 1.95 (1H, m, C*H*), 1.92 - 1.86 (1H, m, CH_2), 1.78 - 1.70 (1H, m, CH_2), 1.68 - 1.59 (1H, m, CH_2), 1.57 - 1.50 (1H, m, CH_2), 1.49 - 1.43 (1H, m, CH_2), 1.37 - 1.31 (1H, m, CH_2), 1.05 - 0.91 (1H, m, CH_2); ^{13}C NMR[‡] (101 MHz, $CDCl_3$) δ 157.5 (*C*), 140.6 (*C*), 136.0 (*C*H), 131.1 (*C*H), 126.6 (*C*), 121.4 (*C*), 113.6 (*C*H), 109.8 (*C*H), 57.1 (*C*H_2), 55.4 (*C*H_3), 54.4 (*C*H), 46.1 (*C*H_2), 43.4 (*C*H), 41.7 (*C*), 40.7 (*C*H_3), 35.3 (*C*H_2), 32.3 (*C*H_2), 26.0 (*C*H_2), 25.3 (*C*H_2), 21.8 (*C*H_2); HRMS (+ESI) *m/z* calculated for $C_{24}H_{34}N_3O$ [M] 380.2696; Found 380.2696.

Therefore, *N*-C**H**$_3$ *vs.* *N*-C**H**$_2$ selectivity for dextromethorphan is 10 : 1.

[†]Tentatively assigned as the bicarbonate salt based on the sodium bicarbonate present in the reverse-phase chromatography eluant, the K_2CO_3 used to basify fractions, the absence of ^{19}F and ^{31}P NMR signals and the IR stretch at 1687 cm^{-1}. [‡]The ^{13}C signal for the bicarbonate anion could not be observed.

5.19.7. NON-REACTION OF THE IMINIUM EQUIVALENT WITH SOFT NUCLEOPHILES

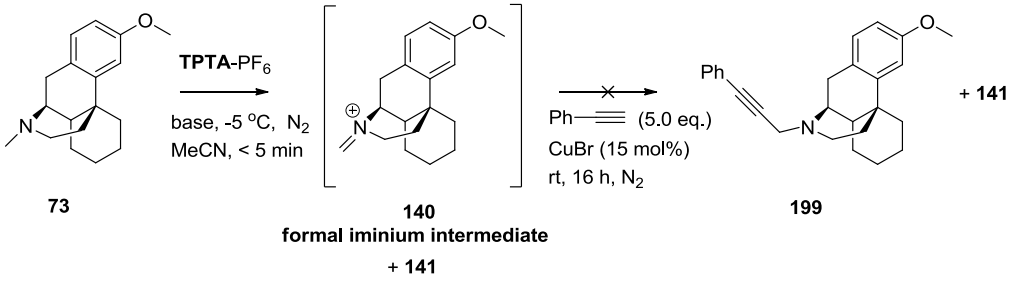

It was originally postulated that the oxidation reaction of dextromethorphan (**73**) gave formal iminium intermediate **140** following *N*-C**H**$_3$ functionalisation (as well as the *N*-C**H**$_2$ functionalised product **141**), and that **140** hydrolysed upon aqueous work up/purification (or LCMS) to afford *nor*-dextromethorphan **74** observed by LCMS (Figure 44). In an attempt to intercept this iminium intermediate, stabilised carbon nucleophiles were added after the oxidation step.

Conducted using **Oxidation Procedure 2** and a literature procedure for the nucleophilic addition.[96] After the oxidation reaction of dextromethorphan **73** (12.5 mg, 50.0 μmol), phenylacetylene (24.0 mg, 0.25 mmol, 5.0 eq.) and CuBr (1.0 mg, 7.50 μmol, 0.15 eq.) were washed in to the reaction using MeCN (0.5 mL) at rt. The reaction was stirred for 2 h before triethylamine (32.0 μL, 0.25 mmol, 5.0 eq.) was added. The reaction was stirred for 16 h at rt, then sampled for LCMS (Figure 45, top, no reaction observed). The reaction was cooled to 0 °C, placed under N_2 and PhMgBr (1.0 M in THF, 0.9 mL, 20.0 eq.) was added dropwise over 5 min, then sampled for LCMS (Figure 45, bottom, trace of phenylated product **146** observed amongst a complex mixture of products). Alternatively, following the oxidation reaction, i) $MeNO_2$ (5.0 eq.) and Et_3N (5.0 eq.), or ii) cyclohexenyltrimethylsilyl ether (5.0 eq.) or iii) potassium phenyltrifluoroborate (5.0 eq.) were added at rt. No reaction was observed in any case after 16 h at rt.

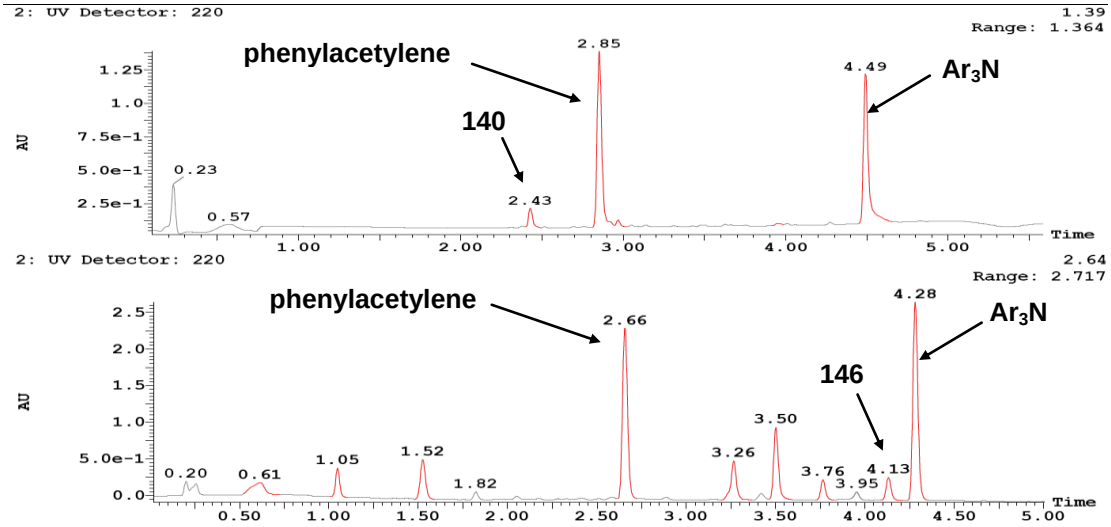

***Figure 45**: LCMS trace following **Oxidation Procedure 2**, after addition of phenylacetylene (5.0 eq.), CuI (cat.) and Et_3N (5.0 eq.) and 16 h stirring at rt (top, low pH). LCMS trace after addition of PhMgBr (20.0 eq.) after non-reaction of the Cu-acetylide (bottom, high pH).*

5.19.8. Successful Reaction of the Iminium Equivalent with a Grignard Reagent

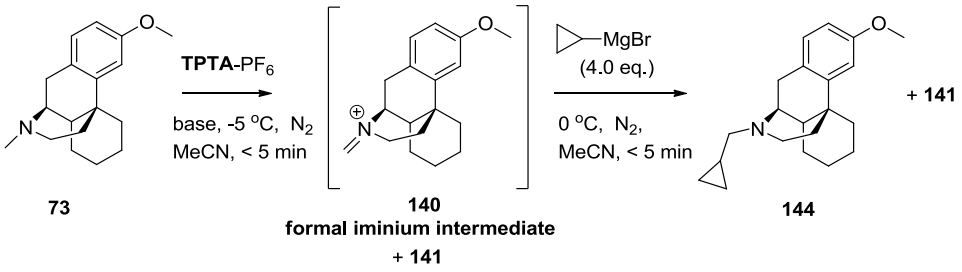

Conducted using **Oxidation Procedure 2**. After the oxidation reaction of dextromethorphan **73** (12.5 mg, 50.0 μmol), cyclopropylmagnesium bromide (1.0 M in 2-MeTHF, 4.0 eq.) was added at 0 °C under N_2. The reaction was sampled for LCMS (Figure 46, bottom, desired product **144** was observed).

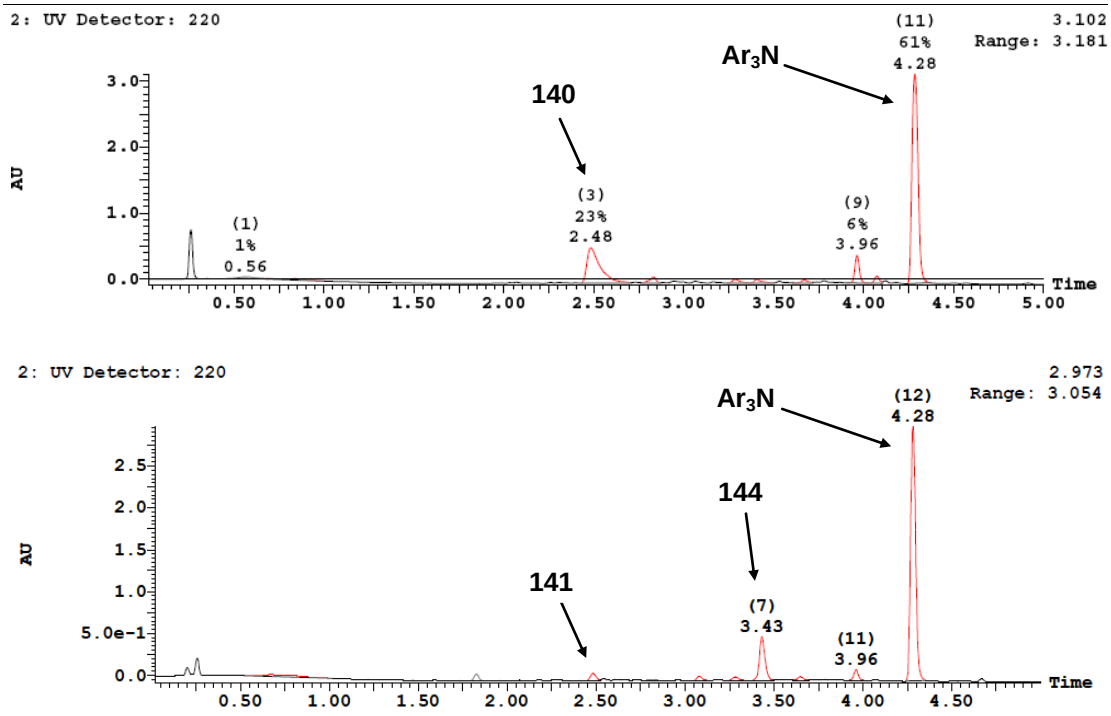

***Figure 46**: LCMS traces for oxidation of dextromethorphan using **TPTA**-PF_6 (3.4 eq.) as the oxidant under **Oxidation Procedure 3** (top). Subsequent addition of cyclopropylmagnesium bromide (4.0 eq.) following oxidation (bottom).*

5.19.9. Selection of Optimal Reaction Conditions

The optimal reaction conditions identified were **Oxidation Procedure 3**, using MeCN as solvent, -5 ^{o}C temperature, 33.0 mM concentration, 3.4 eq. **TPTA**-PF_6 and 4.5 eq. DABCO for the oxidation reaction, followed by the addition of organometallic reagents (5.0 eq.) at 0 ^{o}C under N_2. Although the oxidation reaction could be run open to air with a similar profile by LCMS, the optimal profile was found under an atmosphere of N_2. Although a lower concentration (11.0 mM) was beneficial to the oxidation reaction, it was deemed suboptimal for organometallic additions. The optimal reaction conditions are summarised in **General Procedure 3**.

5.20. General Procedure 3: Regioselective C-H Functionalisation of Trialkylamines and Organometallic Trapping of Iminium Equivalents

11-Benzyl-3-methoxy-6,7,8,8a,9,10-hexahydro-5*H*-9,4b-(epiminoethano)-phenanthrene (*146*)

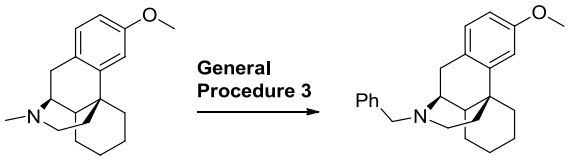

73 146

General Procedure 3: A predried reaction vessel was charged with dextromethorphan (149.0 mg, 0.55 mmol), DABCO (278 mg, 2.48 mmol, 4.5 eq.) and anhydrous MeCN (15 mL, 37.0 mM) before cooling to -5 ^{o}C and placing under an N_2 funnel. **TPTA**-PF_6 (234.0 mg, 0.55 mmol, 1.0 eq.) was added as a solid under an atmosphere of N_2. Further portions (8x) of **TPTA**-PF_6 (71.0 mg, 0.17 mmol, 0.3 eq.) were added. The reaction mixture was a yellow slurry. Phenylmagnesium bromide (1.0 M in THF) (2.75 mL, 2.75 mmol, 5.0 eq.) was added dropwise at 0 ^{o}C before the reaction was quenched with MeOH (1.0 mL) at 0 ^{o}C. The reaction mixture was filtered through celite and DCM (30 mL), H_2O (20 mL) and sat. aq. NH_4Cl (10 mL) were added. The layers were separated and the aqueous layer was extracted with DCM (2 x 30 mL). The combined organic layers were dried ($MgSO_4$), filtered and concentrated *in vacuo* before loading onto celite. The crude product was loaded onto a silica plug and eluted with warm (40 ^{o}C) heptane to yield tri-*p*-tolylamine (**TPTA**) as a white microcrystalline solid (530.0 mg, 99%); see Chapter 5.16 for data.

The plug was flushed heavily with MeOH/DCM (5%) and the fractions concentrated *in vacuo* before loading onto celite. Column chromatography (0 - 10% TBME/heptane (0.2% Et_3N)) gave ***146*** as a pale brown oil (158.6 mg, 83%); IR ν_{max} (neat) 2926 - 2835 (C-H), 1608 (Ar), 1576 (Ar), 1494 (Ar),

1453 (Ar), 1431, 1356, 1273, 1236 cm^{-1}; ^{1}H NMR (400 MHz, $CDCl_3$) δ 7.36 (2H, d, *J* = 7.1 Hz, C*H*), 7.31 (2H, t, *J* = 7.5 Hz, C*H*), 7.24 (1H, t, *J* = 7.2 Hz, C*H*), 7.06 (1H, d, *J* = 8.6 Hz, C*H*), 6.82 (1H, d, *J* = 2.7 Hz, C*H*), 6.73 (1H, dd, *J* = 8.4, 2.7 Hz, C*H*), 3.80 (3H, s, CH_3), 3.72 (1H, d, *J* = 13.5 Hz, CH_2), 3.62 (1H, d, *J* = 13.5 Hz, CH_2), 3.02 (1H, d, *J* = 18.1 Hz, CH_2), 2.88 - 2.83 (1H, m, C*H*), 2.63 (1H, dd, *J* = 18.1, 5.9 Hz, CH_2), 2.49 - 2.41 (1H, m, CH_2), 2.39 - 2.31 (1H, m, CH_2), 2.12 (1H, td, *J* = 12.1, 3.2 Hz, CH_2), 1.91 - 1.82 (1H, m, C*H*), 1.71 (1H, td, *J* = 12.5, 4.9 Hz, CH_2), 1.67 - 1.60 (1H, m, CH_2), 1.55 - 1.47 (1H, m, CH_2), 1.42 - 1.25 (5H, m, CH_2), 1.17 - 1.05 (1H, m, CH_2); ^{13}C NMR (101 MHz, $CDCl_3$) δ 158.1 (*C*), 142.1 (*C*), 139.8 (*C*), 130.1 (*C*), 128.7 (*C*H), 128.5 (*C*H), 128.2 (*C*H), 126.7 (*C*H), 111.1 (*C*H), 110.6 (*C*H), 59.4 (*C*H_2), 56.0 (*C*H), 55.2 (*C*H_3), 45.4 (*C*H_2), 45.3 (*C*H), 42.1 (*C*H_2), 37.9 (*C*), 36.7 (*C*H_2), 26.8 (*C*H_2), 26.6 (*C*H_2), 24.5 (*C*H_2), 22.3 (*C*H_2); HRMS (+ESI) *m/z* calculated for $C_{24}H_{30}NO$ $[M+H^+]$ 348.2322; Found 348.2325.

Alternatively, for reactions that did not use dextromethorphan **73** as a substrate, reactions were quenched using MeOH (1 mL) followed by sat. aq. NH_4Cl (3 mL) at 0 ^{o}C. Where products were quantified by internal standard, removal of tri-*p*-tolylamine through the silica plug was first achieved, then crude products were basified with sat. aq. $NaHCO_3$ (5 mL). Water (5 mL) was added, and organics were extracted with DCM (3 x 10 mL). The combined organic layers were dried ($MgSO_4$), filtered and concentrated *in vacuo*, then 1,3,5-trimethoxybenzene (10 mol%) was added and quantification achieved by ^{1}H NMR.

Alternatively, for reactions employing phenylzinc halide reagent, reactions were quenched using MeOH (1 mL) at 0 ^{o}C. DCM (100 mL) and aq. HCl (pH = 4) (50 mL) and water (50 mL) were added, the layers were separated and the aqueous layer was extracted with DCM (2 x 50 mL). The phenylzinc halide reagent (0.5 M) was prepared by addition of phenylmagnesium bromide (1.0 M in THF) (5.50 mL, 5.50 mmol, 10.0 eq.) to zinc chloride (1.9 M in THF, 3.8 mL, 7.2 mmol, 13.0 eq.) in THF (2 mL) at -78 ^{o}C, then stirring for 30 min at -78 ^{o}C, then stirring for 30 min at rt. The resultant milky white

suspension was removed by syringe (11.3 mL, 0.5 M) and used as necessary (half the volume, 5.0 eq. was used).

Alternatively, this reaction was conducted according to **General Procedure 3**† on gram-scale, using dextromethorphan (**73**) (1.49 g, 5.5 mmol), DABCO (2.78 g, 4.5 eq.) and anhydrous MeCN (150 mL, 37.0 mM). Addition of oxidant **TPTA**-PF_6 (8.06 g, 3.4 eq.) and phenylmagnesium bromide (1.0 M in THF, 27.5 mL, 5.0 eq.) followed by purificaton gave recovered tri-*p*-tolylamine (5.3 g, 99%); ^{1}H NMR (400 MHz, $CDCl_3$) δ 7.03 (6H, d, *J* = 8.4 Hz, C*H*), 6.98 (6H, d, *J* = 8.5 Hz, C*H*), 2.31 (9H, s, CH_3); and gave ***146*** (1.49 g, 78%); ^{1}H NMR (400 MHz, $CDCl_3$) δ 7.38 (2H, d, *J* = 7.3 Hz, C*H*), 7.34 (2H, t, *J* = 7.5 Hz, C*H*), 7.26 (1H, t, *J* = 7.1 Hz, C*H*), 7.08 (1H, d, *J* = 8.3 Hz, C*H*), 6.84 (1H, d, *J* = 2.5 Hz, C*H*), 6.75 (1H, dd, *J* = 8.3, 2.5 Hz, C*H*), 3.82 (3H, s, CH_3), 3.74 (1H, d, *J* = 13.5 Hz, CH_2), 3.65 (1H, d, *J* = 13.5 Hz, CH_2), 3.05 (1H, d, *J* = 18.1 Hz, CH_2), 2.90 - 2.85 (1H, m, C*H*), 2.62 (1H, dd, *J* = 18.1, 5.9 Hz, CH_2), 2.51 - 2.44 (1H, m, CH_2), 2.42 - 2.34 (1H, m, CH_2), 2.14 (1H, td, *J* = 12.2, 2.9 Hz, CH_2), 1.92 - 1.86 (1H, m, C*H*), 1.73 (1H, td, *J* = 12.5, 4.9 Hz, CH_2), 1.69 - 1.62 (1H, m, CH_2), 1.58 - 1.50 (1H, m, CH_2), 1.42 - 1.29 (5H, m, CH_2), 1.19 - 1.07 (1H, m, CH_2). ^{1}H NMR data of **146** obtained here are consistent with the data listed for **146** above (^{1}H NMR data of tri-*p*-tolylamine obtained here are consistent with the data listed for tri-*p*-tolylamine in Chapter 5.16).

3-Methoxy-11-propyl-6,7,8,8a,9,10-hexahydro-5*H*-9,4b-(epiminoethano)-phenanthrene (*142*)

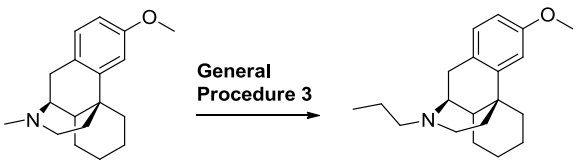

73 **142**

Prepared according to **General Procedure 3** using ethylmagnesium bromide (3.0 M in Et_2O). Column chromatography (0 - 80% TBME/heptane (1% Et_3N))

†Here, the reaction quench was performed adding MeOH (10 mL) at 0 °C, then NH_4Cl (30 mL)

gave ***142*** as a pale yellow oil (133.7 mg, 81%); IR ν_{max} (neat) 2926 - 2855 (C-H), 1609 (Ar), 1576 (Ar), 1495 (Ar), 1463 (Ar), 1431, 1376, 1271 cm^{-1}; ^{1}H NMR (400 MHz, $CDCl_3$) δ 7.01 (1H, d, *J* = 8.4 Hz, C*H*), 6.81 (1H, d, *J* = 2.6 Hz, C*H*), 6.71 (1H, dd, *J* = 8.4, 2.7 Hz, C*H*), 3.79 (3H, s, CH_3), 2.92 (1H, d, *J* = 18.1 Hz, CH_2), 2.89 - 2.87 (1H, m, C*H*), 2.60 (1H, dd, *J* = 18.1, 5.9 Hz, CH_2), 2.54 - 2.30 (3H, m, CH_2), 2.03 (1H, td, *J* = 12.3, 3.2 Hz, CH_2), 1.96 - 1.85 (1H, m, CH_2), 1.84 - 1.79 (1H, m, C*H*), 1.73 (1H, td, *J* = 12.7, 4.8 Hz, CH_2), 1.67 - 1.61 (1H, m, CH_2), 1.52 (2H, sext, *J* = 7.5 Hz, CH_2), 1.43 - 1.26 (6H, m, CH_2), 1.19 - 1.07 (1H, m, CH_2), 0.92 (3H, t, *J* = 7.3 Hz, CH_3); ^{13}C NMR (101 MHz, $CDCl_3$) δ 158.1 (*C*), 142.0 (*C*), 130.1 (*C*) 128.4 (*C*H), 111.1 (*C*H), 110.6 (*C*H), 57.1 (*C*H_2), 55.8 (*C*H), 55.2 (*C*H_3), 45.7 (*C*H_2), 45.2 (*C*H), 42.1 (*C*H_2), 37.9 (*C*), 36.7 (*C*H_2), 26.9 (*C*H_2), 26.6 (*C*H_2), 23.9 (*C*H_2), 22.3 (*C*H_2), 21.0 (*C*H_2), 12.1 (*C*H_3); HRMS (+ESI) *m/z* calculated for $C_{21}H_{30}NO$ $[M+H^+]$ 300.2327; Found 300.2326.

11-(But-3-en-1-yl)-3-methoxy-6,7,8,8a,9,10-hexahydro-5*H*-9,4b-(epimino-ethano)phenanthrene (*143*)

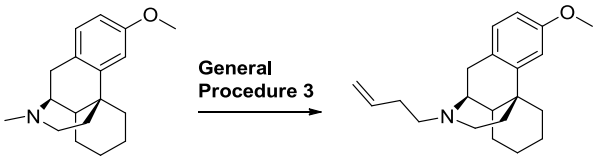

73 143

Prepared according to **General Procedure 3** using an allylindium reagent. The allyl indium sesquihalide reagent (1.0 M in DMF) was prepared by a literature procedure[151] using indium powder (-100 mesh) (631.0 mg, 5.5 mmol, 10.0 eq.) in DMF (5 mL) and adding allyl iodide (0.76 mL, 15.0 mmol, 15.0 eq.). The resultant milky white suspension was removed by syringe (5.8 mL, 1.0 M in DMF) and used as necessary (half the volume, 5.0 eq. were used). MDAP purification (low pH) followed by basification with 1 mol% aq. K_2CO_3 (30 mL), extraction with DCM (3 x 30 mL), drying ($MgSO_4$), filtration and concentration *in vacuo* gave ***143*** as a colourless oil (121.4 mg, 71%); IR ν_{max} (neat) 2925 - 2854 (C-H), 1610 (C=C), 1576 (Ar), 1495 (Ar), 1432, 1267,

1237 cm^{-1}; ^{1}H NMR (400 MHz, $CDCl_3$) δ 7.01 (1H, d, *J* = 8.4 Hz, C*H*), 6.81 (1H, d, *J* = 2.7 Hz, C*H*), 6.70 (1H, dd, *J* = 8.4, 2.7 Hz, C*H*), 5.91 - 5.78 (1H, m, C*H*), 5.11 - 4.98 (1H, m, CH_2), 4.99 (1H, *d*, *J* = 10.2 Hz, CH_2), 3.79 (3H, s, CH_3), 2.98 - 2.88 (2H, m, C*H*, CH_2), 2.66 - 2.49 (4H, m, CH_2), 2.34 (1H, d, *J* = 12.2 Hz, CH_2), 2.28 (2H, apt. q, *J* = 7.4 Hz, CH_2), 2.07 (1H, td, *J* = 12.3, 3.2 Hz, CH_2), 1.84 (1H, apt. d, *J* = 12.7 Hz, C*H*), 1.74 (1H, td, *J* = 12.7, 4.7 Hz, CH_2), 1.68 - 1.61 (1H, m, CH_2), 1.55 - 1.48 (1H, m, CH_2), 1.46 - 1.25 (5H, m, CH_2); 1.19 - 1.07 (1H, m, CH_2); ^{13}C NMR (101 MHz, $CDCl_3$) δ 158.2 (*C*), 141.8 (*C*), 136.8 (*C*H), 129.8 (*C*), 128.4 (*C*H), 115.4 (*C*H_2), 111.0 (*C*H), 110.6 (*C*H), 56.0 (*C*H), 55.1 (*C*H_3), 54.5 (*C*H_2), 45.6 (*C*H_2), 45.1 (*C*H), 42.0 (*C*H_2), 37.8 (*C*), 36.6 (*C*H_2), 32.4 (*C*H_2), 26.9 (*C*H_2), 26.6 (*C*H_2), 24.0 (*C*H_2), 22.2 (*C*H_2); HRMS (+ESI) *m/z* calculated for $C_{21}H_{30}NO$ [$M+H^+$] 312.2327; Found 312.2328.

11-(Cyclopropylmethyl)-3-methoxy-6,7,8,8a,9,10-hexahydro-5*H*-9,4b-(epiminoethano)phenanthrene (*144*)

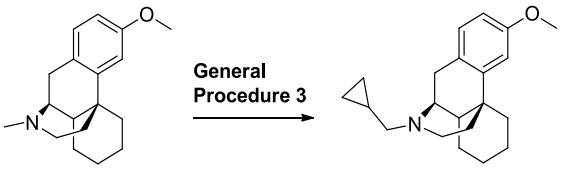

73 144

Prepared according to **General Procedure 3** using cyclopropylmagnesium bromide (1.0 M in 2-MeTHF). Column chromatography (0 - 60% TBME/heptane (1% Et_3N)) gave ***144*** as a pale brown oil (126.5 mg, 74%); IR ν_{max} (neat) 2925 - 2850 (C-H), 1609 (Ar), 1496 (Ar), 1463 (Ar), 1377, 1267, 1237 cm^{-1}; ^{1}H NMR (400 MHz, $CDCl_3$) δ 7.01 (1H, d, *J* = 8.5 Hz, C*H*), 6.81 (1H, d, *J* = 2.7 Hz, C*H*), 6.72 (1H, dd, *J* = 8.4, 2.6 Hz, C*H*), 3.79 (3H, s, CH_3), 3.24 - 3.14 (1H, m, C*H*), 2.88 (1H, d, *J* = 18.2 Hz, CH_2), 2.77 (1H, d, *J* = 10.7 Hz, CH_2), 2.68 (1H, dd, *J* = 18.2, 5.7 Hz, CH_2), 2.60 - 2.52 (1H, m, CH_2), 2.46 - 2.33 (2H, m, CH_2), 2.09 (1H, apt. t, *J* = 11.3 Hz, CH_2), 2.01 - 1.92 (1H, m, C*H*), 1.92 - 1.81 (1H, m, CH_2), 1.64 (1H, d, *J* = 13.2 Hz, CH_2), 1.52 (1H, d, *J* = 12.3 Hz, CH_2), 1.47 - 1.28 (5H, m, CH_2), 1.19 - 1.08 (1H, m, CH_2), 0.88 -

0.80 (1H, m, C*H*), 0.54 (2H, apt. d, *J* = 7.3 Hz, CH_2), 0.18 (2H, apt. d, *J* = 4.7 Hz, CH_2); ^{13}C NMR (101 MHz, $CDCl_3$) δ 158.1 (*C*), 142.0 (*C*), 130.0 (*C*), 128.4 (*C*H), 111.1 (*C*H), 110.6 (*C*H), 60.0 (*C*H_2), 55.8 (*C*H), 55.2 (*C*H_3), 45.8 (*C*H_2), 45.2 (*C*H), 42.0 (*C*H_2), 37.9 (*C*), 36.7 (*C*H_2), 26.9 (*C*H_2), 26.6 (*C*H_2), 23.9 (*C*H_2), 22.3 (*C*H_2), 9.5 (*C*H) 4.1 (*C*H_2), 3.6 (*C*H_2); HRMS (+ESI) *m/z* calculated for $C_{21}H_{30}NO$ [M+H$^+$] 312.2327; Found 312.2322.

11-Allyl-3-methoxy-6,7,8,8a,9,10-hexahydro-5*H*-9,4b-(epiminoethano)phenanthrene (*145*)

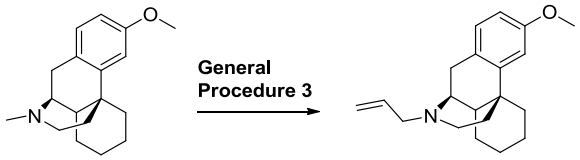

73 145

Prepared according to **General Procedure 3** using vinylmagnesium bromide (1.0 M in THF). Column chromatography (0 - 50% TBME/heptane (1% Et_3N)) gave ***145*** as a pale brown oil (143.1 mg, 75%); IR ν_{max} (neat) 2925 - 2854 (C-H), 1609 (C=C), 1576 (Ar), 1494 (Ar), 1463 (Ar), 1265, 1236 cm^{-1}; ^{1}H NMR (400 MHz, $CDCl_3$) δ 7.04 (1H, d, *J* = 8.4 Hz, C*H*), 6.81 (1H, d, *J* = 2.6 Hz, C*H*), 6.72 (1H, dd, *J* = 8.4, 2.7 Hz, C*H*), 5.96 - 5.84 (1H, m, C*H*), 5.23 - 5.09 (2H, m, CH_2), 3.79 (3H, s, CH_3), 3.28 - 3.10 (2H, m, CH_2), 2.99 - 2.88 (2H, m, C*H*, CH_2), 2.65 - 2.51 (2H, m, CH_2), 2.39 - 2.32 (1H, m, CH_2), 2.06 (1H, td, *J* = 12.4, 3.2 Hz, CH_2), 1.89 - 1.81 (1H, m, C*H*), 1.74 (1H, td, *J* = 12.7, 4.8 Hz, CH_2), 1.69 - 1.59 (1H, m, CH_2), 1.55 - 1.47 (1H, m, CH_2), 1.45 - 1.25 (5H, m, CH_2), 1.19 - 1.06 (1H, m, CH_2); ^{13}C NMR (101 MHz, $CDCl_3$) δ 158.2 (*C*), 141.8 (*C*), 135.9 (*C*H), 129.7 (*C*), 128.4 (*C*H), 117.4 (*C*H_2), 111.1 (*C*H), 110.7 (*C*H), 58.3 (*C*HN), 55.9 (*C*H_2), 55.2 (*C*H_3), 45.5 (*C*H_2), 45.0 (*C*H), 41.8 (*C*H_2), 37.8 (*C*), 36.6 (*C*H_2), 26.8 (*C*H_2), 26.6 (*C*H_2), 23.9 (*C*H_2), 22.2 (*C*H_2); HRMS (+ESI) *m/z* calculated for $C_{20}H_{28}NO$ [M+H$^+$] 298.2171; Found 298.2164.

11-(Hex-5-en-1-yl)-3-methoxy-6,7,8,8a,9,10-hexahydro-5*H*-9,4b-(epimino-ethano)phenanthrene (*147*)

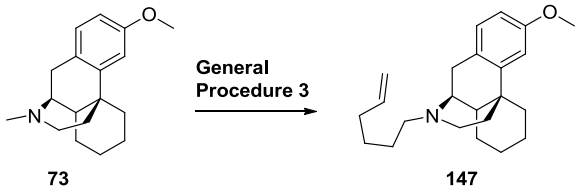

73 147

Prepared according to **General Procedure 3** using pent-4-en-1-ylmagnesium bromide. A solution of pent-4-en-1-ylmagnesium bromide (1.0 M in THF) was prepared by charging a reaction vessel with magnesium turnings (238.0 mg, 10.0 mmol), anhydrous THF (8.0 mL) and a small crystal of I_2 before adding 5-bromopent-1-ene (0.91 mL, 7.70 mmol) dropwise under N_2. A colour change from pale brown to colourless was apparent. After stirring at reflux (66 ^{o}C) for 10 min under N_2 and cooling to rt, the resultant turbid solution was removed by syringe (7.50 mL, 1.0 M in THF) and used as necessary (3.30 mL, 6.0 eq. were added). MDAP purification (low pH) followed by basification with 1 mol% aq. K_2CO_3 (30 mL), extraction with DCM (3 x 30 mL), drying ($MgSO_4$), filtration and concentration *in vacuo* gave ***147*** as a pale yellow oil (107.0 mg, 57%); IR ν_{max} (neat) 2926 - 2855 (C-H), 1640 (C=C), 1609 (Ar), 1576 (Ar), 1495 (Ar), 1463 (Ar), 1432, 1269, 1235 cm^{-1}; ^{1}H NMR (400 MHz, $CDCl_3$) δ 7.01 (1H, d, *J* = 8.6 Hz, C*H*), 6.80 (1H, d, *J* = 2.7 Hz, C*H*), 6.69 (1H, dd, *J* = 8.6, 2.7 Hz, C*H*), 5.88 - 5.76 (1H, m, C*H*), 5.05 - 4.90 (2H, m, CH_2), 3.79 (3H, s, CH_3), 2.97 - 2.88 (2H, m, C*H*, CH_2), 2.66 - 2.43 (4H, m, CH_2), 2.33 (1H, d, *J* = 13.0 Hz, CH_2), 2.13 - 2.01 (3H, m, CH_2), 1.88 - 1.81 (1H, m, C*H*), 1.75 (1H, td, *J* = 12.7, 4.7 Hz, CH_2), 1.68 - 1.61 (1H, m, CH_2), 1.57 - 1.48 (3H, m, CH_2), 1.47 - 1.26 (7H, m, CH_2), 1.19 - 1.06 (1H, m, CH_2); ^{13}C NMR (101 MHz, $CDCl_3$) δ 158.2 (*C*), 141.8 (*C*), 138.8 (*C*H), 129.7 (*C*), 128.4 (*C*H), 114.4 (*C*H_2), 111.0 (*C*H), 110.7 (*C*H), 55.9 (*C*H), 55.1 (*C*H_3), 54.9 (*C*H_2), 45.8 (*C*H_2), 45.0 (*C*H), 41.8 (*C*H_2), 37.8 (*C*), 36.6 (*C*H_2), 33.6 (*C*H_2), 27.1 (*C*H_2), 27.0 (*C*H_2), 26.8 (*C*H_2), 26.5 (*C*H_2), 23.9 (*C*H_2), 22.2 (*C*H_2); HRMS (+ESI) *m/z* calculated for $C_{23}H_{34}NO$ [M+H^{+}] 340.2635; Found 340.2638.

3-Methoxy-11-(pent-4-en-1-yl)-6,7,8,8a,9,10-hexahydro-5*H*-9,4b-(epimin-oethano)phenanthrene (*148*)

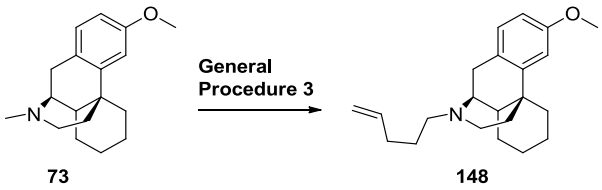

73 148

Prepared according to **General Procedure 3** using but-3-en-1-ylmagnesium bromide. A solution of but-3-en-1-ylmagnesium bromide (1.0 M in THF) was prepared by charging a reaction vessel with magnesium turnings (238.0 mg, 10.0 mmol), anhydrous THF (8.0 mL) and a small crystal of I_2 before adding 4-bromobut-1-ene (0.78 mL, 7.70 mmol) dropwise under N_2. A colour change from pale brown to colourless was apparent. After stirring at reflux (66 ^{o}C) for 10 min under N_2 and cooling to rt, the resultant turbid solution was removed by syringe (7.50 mL, 1.0 M in THF) and used as necessary (3.30 mL, 6.0 eq. were added). MDAP purification (low pH) followed by basification with 1 mol% aq. K_2CO_3 (30 mL), extraction with DCM (3 x 30 mL), drying ($MgSO_4$), filtration and concentration *in vacuo* gave ***148*** as a pale yellow oil (86.4 mg, 48%); IR ν_{max} (neat) 2928 - 2856 (C-H), 1610 (C=C), 1576 (Ar), 1496 (Ar), 1432, 1392, 1261, 1240 cm^{-1}; ^{1}H NMR (400 MHz, $CDCl_3$) δ 7.04 (1H, d, *J* = 8.3 Hz, C*H*), 6.81 (1H, d, *J* = 2.5 Hz, C*H*), 6.75 (1H, dd, *J* = 8.3, 2.7 Hz, C*H*), 5.86 - 5.74 (1H, m, C*H*), 5.10 - 4.98 (2H, m, CH_2), 3.79 (3H, s, CH_3), 3.18 - 3.09 (1H, m, C*H*), 2.93 (1H, d, *J* = 18.3 Hz, CH_2), 2.86 - 2.61 (4H, m, CH_2), 2.36 (1H, d, *J* = 13.0 Hz, CH_2), 2.11 (2H, q, *J* = 7.1 Hz, CH_2), 1.95 (1H, d, *J* = 12.7 Hz, C*H*), 1.84 (1H, td, *J* = 13.0, 4.7 Hz, CH_2), 1.76 - 1.63 (3H, m, CH_2), 1.54 (1H, d, *J* = 11.8 Hz, CH_2), 1.49 - 1.22 (6H, m, CH_2), 1.19 - 1.06 (1H, m, CH_2); ^{13}C NMR (101 MHz, $CDCl_3$)† δ 158.7 (*C*), 140.7 (*C*), 137.5 (*C*H), 128.6 (*C*H), 115.5 (*C*H), 111.3 (*C*H_2), 111.2 (*C*H), 56.7 (*C*H), 55.2 (*C*H_3), 54.1 (*C*H_2), 46.1 (*C*H_2), 43.7 (*C*H), 40.7 (*C*H_2), 37.4 (*C*), 36.2 (*C*H_2), 31.4 (*C*H_2), 26.6 (*C*H_2), 26.3 (*C*H_2), 25.5 (*C*H_2), 24.1 (*C*H_2), 22.0 (*C*H_2); HRMS (+ESI) *m/z* calculated for $C_{22}H_{32}NO$ [M+H^{+}] 326.2478; Found 326.2471.

†The remaining quaternary carbon could not be observed.

N-Benzyl-*N*-methyloctan-1-amine (149)

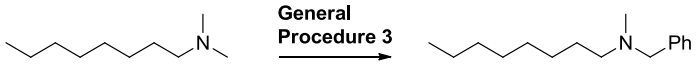

N,*N*-dimethyloctylamine 149

N,*N*-dimethyloctylamine (0.55 mmol) was subjected to **General Procedure 3** using phenylmagnesium bromide (1.0 M in THF) as a nucleophile. Column chromatography (3 - 25% EtOAc/heptane (1% Et_3N)) gave **149** as a pale brown oil (95.6 mg, 74%); IR ν_{max} (neat) 3028 - 2787 (C-H), 1495 (Ar), 1454 (Ar), 1365 cm^{-1}; ^1H NMR (400 MHz, $CDCl_3$) δ 7.36 - 7.21 (5H, m, C*H*), 3.48 (2H, s, CH_2), 2.36 (2H, t, *J* = 7.5 Hz, CH_2), 2.19 (3H, s, CH_3), 1.57 - 1.47 (2H, m, CH_2), 1.35 - 1.23 (10H, m, CH_2), 0.89 (3H, t, *J* = 6.7 Hz, CH_3); ^{13}C NMR (101 MHz, $CDCl_3$) δ 139.3 (*C*), 129.1 (*C*H), 128.1 (*C*H), 126.8 (*C*H), 62.3 (*C*H_2), 57.6 (*C*H_2), 42.3 (*C*H_3), 31.9 (*C*H_2), 29.6 (*C*H_2), 29.3 (*C*H_2), 27.5 (*C*H_2), 27.4 (*C*H_2), 22.7 (*C*H_2), 14.1 (*C*H_3); HRMS (+ESI) *m/z* calculated for $C_{16}H_{28}N$ [$M+H^+$] 234.2216; Found 234.2216. Data are consistent with the literature.[235]

N-Benzyl-*N*-methylcyclohexanamine (150)

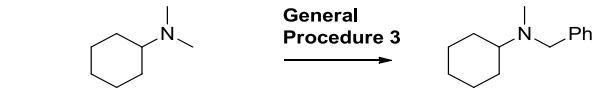

N,*N*-dimethylcyclohexylamine 150

Compound *N*,*N*-dimethylcyclohexylamine (0.55 mmol) was subjected to **General Procedure 3** using phenylmagnesium bromide (1.0 M in THF) as a nucleophile. Column chromatography (3 - 25% EtOAc/heptane (1% Et_3N)) gave **150** as a brown oil (75.8 mg, 68%); IR ν_{max} (neat) 3028 - 2787 (C-H), 1604 (Ar), 1495 (Ar), 1451 (Ar), 1361, 1262 cm^{-1}; ^1H NMR (400 MHz, $CDCl_3$) δ 7.36 - 7.20 (5H, m, C*H*), 3.58 (2H, s, CH_2), 2.49 - 2.40 (1H, m, C*H*), 2.20 (3H, s, CH_3), 1.94 - 1.78 (4H, m, CH_2), 1.68 - 1.61 (1H, m, CH_2), 1.37 - 1.07 (5H, m, CH_2); ^{13}C NMR (101 MHz, $CDCl_3$) δ 140.4 (*C*), 128.8 (*C*H), 128.1 (*C*H) 126.6 (*C*H), 62.5 (*C*H), 57.9 (*C*H_2), 37.7 (*C*H_3), 28.7 (*C*H_2), 26.5 (*C*H_2), 26.0 (*C*H_2); HRMS (+ESI) *m/z* calculated for $C_{14}H_{22}N$ [$M+H^+$] 204.1747; Found 204.1739. Data are consistent with the literature.[235]

Methyl-3-(benzyl(methyl)amino)propanoate (151)

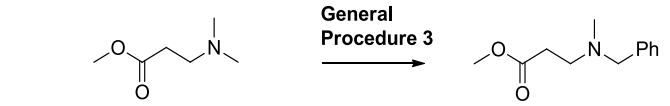

methyl 3-(dimethylamino)propanoate — 151

Methyl 3-(dimethylamino)propanoate (0.55 mmol) was subjected to **General Procedure 3** using phenylzinc halide (5.0 eq.) as a nucleophile. ^{1}H NMR of the crude reaction mixture (the concentrated DCM/MeOH fractions after the silica plug) revealed a 50% yield of **151** by comparison with an added internal standard (1,3,5-trimethoxybenzene, 9.2 mg, 55.0 μmol, 10 mol%). Column chromatography (a gradient of 0 - 6% MeOH/DCM) gave **151** as a brown oil (49.8 mg, 44%); IR ν_{max} (neat) 2951 - 2796 (C-H), 1733 (C=O), 1603 (Ar), 1507 (Ar), 1495 (Ar), 1453 (Ar), 1437, 1358, 1319, 1252, 1202 cm^{-1}; ^{1}H NMR (400 MHz, $CDCl_3$) δ 7.37 - 7.22 (5H, m, C*H*), 3.68 (3H, s, CH_3), 3.52 (2H, s, CH_2), 2.75 (2H, t, *J* = 7.3 Hz, CH_2), 2.54 (2H, t, *J* = 7.2 Hz, CH_2), 2.22 (3H, s, CH_3); ^{13}C NMR (101 MHz, $CDCl_3$) δ 173.0 (*C*), 138.6 (*C*), 128.9 (*C*H) 128.2 (*C*H), 127.0 (*C*H), 62.0 (*C*H_2), 52.6 (*C*H_2), 51.6 (*C*H_3), 41.8 (*C*H_3) 32.6 (*C*H_2); HRMS (+ESI) *m/z* calculated for $C_{12}H_{18}NO_2$ [M+H$^+$] 208.1332; Found 208.1335. Data are consistent with the literature.[236]

Ethyl 2-(benzyl(methyl)amino)acetate (152)

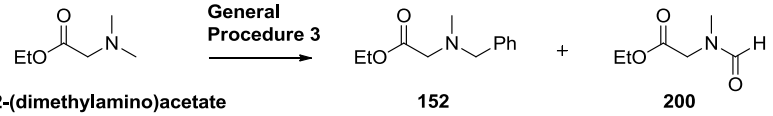

ethyl 2-(dimethylamino)acetate — 152 — 200

Ethyl 2-(dimethylamino)acetate (0.55 mmol) was subjected to **General Procedure 3** using phenylzinc halide (5.0 eq.) as a nucleophile. ^{1}H NMR of the crude reaction mixture (the concentrated DCM/MeOH fractions after the silica plug) revealed a 54% yield of **152** and a 5% yield of **200** by comparison with an added internal standard (1,3,5-trimethoxybenzene, 9.2 mg, 55.0 μmol, 10 mol%). Column chromatography (0 - 6% MeOH/DCM) gave an inseparable mixture of **152** and **ethyl 2-(*N*-methylformamido)acetate** (**200**) as a brown oil (57.6 mg); IR ν_{max} (neat) of the mixture: 2936 - 2809 (C-H),

1743 (C=O), 1672 (NC=O), 1603 (Ar), 1494 (Ar), 1454 (Ar), 1372, 1347, 1286; ^{1}H NMR (400 MHz, $CDCl_3$) of **152**: δ 7.36 - 7.16 (5H, m, C*H*), 4.16 (2H, q, *J* = 7.1 Hz, CH_2), 3.68 (2H, s, CH_2), 3.22 (2H, s, CH_2), 2.36 (2H, s, CH_3), 1.25 (3H, t, *J* = 7.1 Hz, CH_3); ^{13}C NMR (101 MHz, $CDCl_3$) of **152**: δ 170.9 (*C*), 137.8 (*C*H), 129.1 (*C*H) 128.1 (*C*H), 127.0 (*C*H), 61.1 (*C*H_2), 60.3 (*C*H_2), 57.6 (*C*H_2), 42.2 (*C*H_3), 14.2 (*C*H_3); HRMS (+ESI) of the mixture: *m/z* calculated for $C_{12}H_{18}NO_2$ [M+H^+] 208.1332; Found 208.1331. Data are consistent with the literature.[237]

Alternatively, compound ethyl 2-(dimethylamino)acetate (0.55 mmol) was subjected to **General Procedure 3** using **TPBPA**-PF_6 as oxidant and using phenylzinc halide (5.0 eq.) as a nucleophile. ^{1}H NMR of the crude reaction mixture (the concentrated DCM/MeOH fractions after the silica plug) revealed a 29% yield of **152** and a 12% yield of **200** by comparison with an added internal standard (1,3,5-trimethoxybenzene, 9.2 mg, 55.0 μmol, 10 mol%).

Interestingly, the use of **TPBPA**-PF_6 led to increased formation of **200**, which could form through direct *N*-oxidation.

Ethyl 2-(*N*-methylformamido)acetate (200)

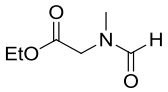

200

^{1}H NMR (400 MHz, $CDCl_3$) of **200** rotamer 1 and rotamer 2 (a 2 : 1 mixture of two rotamers, it is not possible to distinguish between the individual rotamers, so their combined data is reported. In the assignment, 1H corresponds to 1H of an individual rotamer) δ 8.08 (1H, s, C*H*O), 8.00 (1H, s, C*H*O), 4.19, (1H, q, *J* = 7.1 Hz, CH_2), 4.16 (1H, q, *J* = 7.1 Hz, CH_2), 4.05 (1H, s, CH_2), 3.93 (1H, CH_2), 3.00 (3H, s, CH_3), 2.90 (3H, s, CH_3), 1.26 (3H, t, *J* = 7.1 Hz, CH_3), 1.24 (3H, t, *J* = 7.1 Hz, CH_3); ^{13}C NMR (101 MHz, $CDCl_3$) of **200** rotamer 1 and rotamer 2 (it is not possible to distinguish between the individual rotamers, so their combined data is reported. In the assignment, all observed ^{13}C peaks are listed): δ 163.2 (*C*HO), 163.1 (*C*HO), 162.9 (2 x *C*=O), 61.6 (*C*H_2), 61.3

(CH_2), 50.8 (CH_2), 45.5 (CH_2), 35.2 (CH_3), 30.8 (CH_3), 14.1 (2 x CH_3). Data are consistent with the literature.[238]

The use of **TPBPA**-PF_6 led to increased formation of **200**, suggesting that direct *N*-oxidation may be the mechanistic pathway to **200** in that case, which is consistent with the higher oxidation potential of **TPBPA**-PF_6 (E^p_{ox} = +0.93 *vs.* SCE) compared to **TPTA**-PF_6 (E^p_{ox} = +0.82 *vs.* SCE). Similar behaviour was observed in the oxidation of **73** by **TPBPA**-PF_6, giving rise to detectable levels of *N*-formyl compound **137** (see Chapter 5.27).

8-Benzyl-8-azabicyclo[3.2.1]octane (153)

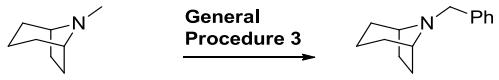

tropane **153**

Tropane (0.55 mmol) was subjected to **General Procedure 3** using phenylmagnesium bromide (1.0 M in THF) as a nucleophile. Column chromatography [a gradient of 1 : 9 TBME/heptane (no Et_3N) to 1 : 9 TBME/heptane (1% Et_3N)] gave **153** as a pale yellow oil (73.2 mg, 66%); IR ν_{max} (neat) 2928 - 2870 (C-H), 1495 (Ar), 1474 (Ar), 1451 (Ar), 1341, 1218 cm^{-1}; ^1H NMR (400 MHz, $CDCl_3$) δ 7.39 (2H, d, *J* = 7.5 Hz, C*H*), 7.32 (2H, t, *J* = 7.4 Hz, C*H*), 7.24 (1H, t, *J* = 7.3 Hz, C*H*), 3.54 (2H, s, CH_2), 3.20 - 3.13 (2H, m, C*H*), 2.07 - 1.97 (2H, m, CH_2), 1.85 - 1.72 (2H, m, CH_2), 1.65 - 1.43 (4H, m, CH_2), 1.38 - 1.29 (2H, m, CH_2); ^{13}C NMR (101 MHz, $CDCl_3$) δ 140.4 (*C*), 128.6 (*C*H), 128.1 (*C*H) 126.5 (*C*H), 59.5 (*C*H), 57.0 (CH_2), 31.4 (CH_2), 26.4 (CH_2), 16.8 (CH_2); LCMS (High pH, 5 min gradient): R_T = 2.8 min, $[M+H^+]$ = 202.0. Data are consistent with the literature.[239]

8-Benzyl-8-azabicyclo[3.2.1]octan-3-ol (154)

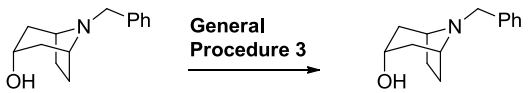

tropine **154**

Tropine (0.55 mmol) was subjected to **General Procedure 3** using phenylmagnesium bromide (1.0 M in THF, 3.30 mL, 6.0 eq. were required for this reaction) as a nucleophile. Column chromatography [a gradient of 30% TBME/heptane (no Et_3N) to 80% TBME/heptane (1% Et_3N)] gave **154** as a white microcrystalline solid (83.2 mg, 70%); m.p. 88 - 89 ^oC (lit. 92 ^oC[240]); IR ν_{max} (neat) 3274 (O-H), 2936 - 2871 (C-H), 1493 (Ar), 1455 (Ar), 1424, 1376, 1326, 1259, 1237, 1217 cm^{-1}; ^1H NMR (400 MHz, $CDCl_3$) δ 7.37 (2H, d, *J* = 7.4 Hz, C*H*), 7.30 (2H, t, *J* = 7.4 Hz, C*H*), 7.22 (1H, t, *J* = 7.2 Hz, C*H*), 4.08 (1H, t, *J* = 5.1 Hz, C*H*), 3.53 (2H, s, CH_2), 3.17 - 3.13 (2H, m, C*H*), 2.15 - 2.02 (6H, m, CH_2), 1.67 (2H, d, *J* = 13.9 Hz, CH_2); ^{13}C NMR (101 MHz, $CDCl_3$) δ 140.2 (*C*), 128.5 (*C*H), 128.1 (*C*H) 126.6 (*C*H), 65.3 (*C*H), 58.0 (*C*H_2), 56.8 (*C*H), 39.9 (*C*H_2), 26.3 (*C*H_2); HRMS (+ESI) *m/z* calculated for $C_{14}H_{20}NO$ $[M+H^+]$ 218.1545; Found 218.1539. ^1H NMR data are consistent with the literature.[241]

N-Benzylmorpholine (155)

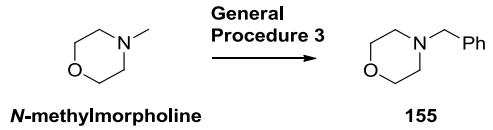

***N*-methylmorpholine** **155**

N-methylmorpholine (0.55 mmol) was subjected to **General Procedure 3**† using phenylmagnesium bromide (1.0 M in THF). Column chromatography (5 - 25% EtOAc/heptane (1% Et_3N)) gave **155** as a pale brown oil (75.2 mg, 77%); IR ν_{max} (neat) 3028 - 2808 (C-H), 1607 (Ar), 1495 (Ar), 1455 (Ar), 1352, 1286, 1264, 1206 cm^1; ^1H NMR (400 MHz, $CDCl_3$) δ 7.36 - 7.24 (5H, m, C*H*), 3.72 (4H, t, *J* = 4.7 Hz, CH_2), 3.51 (2H, s, CH_2), 2.46 (4H, t, *J* = 4.5 Hz, CH_2); ^{13}C NMR (101 MHz, $CDCl_3$) δ 137.7 (*C*), 129.2 (*C*H), 128.2 (*C*H), 127.1 (*C*H), 67.0 (*C*H_2), 63.5 (*C*H_2), 53.6 (*C*H_2); HRMS (+ESI) *m/z* calculated for $C_{11}H_{16}NO$ $[M+H^+]$ 178.1226; Found 178.1223. Data are consistent with the literature.[242]

Alternatively, compound *N*-methylmorpholine (0.55 mmol) was subjected to

†Here, the reaction quench was performed using NH_4Cl (5 mL) only at 0 ^oC.

General Procedure 3 using DMF as solvent and phenylzinc halide (5.0 eq.) as a nucleophile. Product **155** was not detected in the ^{1}H NMR of the crude reaction mixture, nor were substrate-derived materials identified. It was concluded that no reaction occurred in DMF.

1-Benzyl-4-(benzyloxy)piperidine (156)

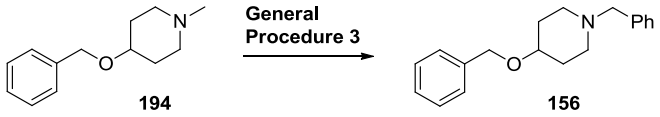

194 156

Compound **194** (0.52 mmol) was subjected to **General Procedure 3** using phenylmagnesium bromide (1.0 M in THF) as a nucleophile. Column chromatography (0 - 15% MeOH/DCM) gave ***156*** as a yellow oil (119.2 mg, 77%); IR ν_{max} (neat) 3028 - 2802 (C-H), 1495 (Ar), 1454 (Ar), 1360, 1205 cm^{-1}; ^{1}H NMR (400 MHz, $CDCl_3$) δ 7.39 - 7.24 (10H, m, C*H*), 4.56 (2H, s, CH_2), 3.53 (2H, s, CH_2), 3.49 - 3.41 (1H, m, C*H*), 2.83 - 2.74 (2H, m, CH_2), 2.25 - 2.13 (2H, m, CH_2), 2.00 - 1.89 (2H, m, CH_2), 1.77 - 1.65 (2H, m, CH_2); ^{13}C NMR (101 MHz, $CDCl_3$) δ 139.0 (*C*), 138.4 (*C*), 129.1 (*C*H), 128.3 (*C*H), 128.2 (*C*H), 127.4 (2 x *C*H), 127.0 (*C*H), 74.4 (*C*H), 69.7 (*C*H_2), 63.0 (*C*H_2), 51.0 (*C*H_2), 31.2 (*C*H_2); HRMS (+ESI) *m/z* calculated for $C_{19}H_{24}NO$ [M+H^{+}] 282.1852; Found 282.1844.

1-Benzyl-4-((4-methoxybenzyl)oxy)piperidine (157)

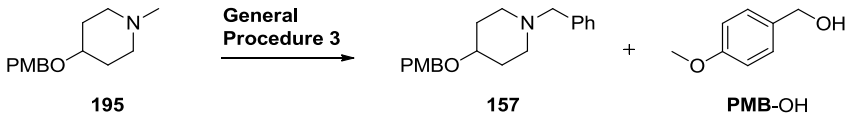

195 157 **PMB**-OH

Compound **195** (0.55 mmol) was subjected to **General Procedure 3** using phenylmagnesium bromide (1.0 M in THF). Column chromatography (1 - 5% MeOH/DCM) gave ***157*** as a pale lilac oil (38.9 mg, 23%); IR ν_{max} (neat) 3028 - 2804 (C-H), 1612 (Ar), 1586 (Ar), 1512 (Ar), 1495 (Ar), 1465 (Ar), 1454 (Ar), 1357, 1301, 1245 cm^{-1}; ^{1}H NMR (400 MHz, $CDCl_3$) δ 7.35 - 7.22 (7H, m, C*H*), 6.89 (2H, d, *J* = 8.8 Hz, C*H*), 4.48 (2H, s, CH_2), 3.81 (3H, s, CH_3), 3.52 (2H, s, CH_2), 3.46 - 3.38 (1H, m, C*H*), 2.82 - 2.73 (2H, m, CH_2), 2.24 - 2.09 (2H, m,

CH_2), 1.97 - 1.87 (2H, m, CH_2), 1.74 - 1.64 (2H, m, CH_2); ^{13}C NMR (101 MHz, $CDCl_3$) δ 159.1 (*C*), 131.1 (*C*), 129.1 (2 x *C*H), 129.0 (*C*H), 128.2 (*C*H), 127.0 (*C*H), 113.8 (*C*H), 74.1 (*C*H), 69.3 (*C*H_2), 63.0 (*C*H_2), 55.3 (*C*H_3), 51.1 (*C*H_2), 31.2 (*C*H_2); HRMS (+ESI) *m/z* calculated for $C_{20}H_{26}NO_2$ [M+H^+] 312.1958; Found 312.1943.

Column chromatography also yielded *p*-methoxybenzyl alcohol (**PMB**-OH) as a brown oil (14.0 mg, 18%); IR ν_{max} (neat) 3371 (O-H), 2932 (C-H), 1612 (Ar), 1586 (Ar), 1513 (Ar), 1454 (Ar), 1302, 1247 cm^{-1}; ^{1}H NMR (400 MHz, $CDCl_3$) δ 7.30 (2H, d, *J* = 8.6 Hz, C*H*), 6.92 (2H, d, *J* = 8.6 Hz, C*H*), 4.63 (2H, s, CH_2), 3.82 (3H, s, CH_3); ^{13}C NMR (101 MHz, $CDCl_3$) δ 159.3 (*C*), 133.1 (*C*), 128.6 (*C*H), 114.0 (*C*H), 65.1 (*C*H_2), 55.3 (*C*H_3); HRMS (+ESI) *m/z* calculated for $C_8H_{11}O$ [M+H^+] 139.0754; Found 139.0755. Data are consistent with the literature.[243]

Column chromatography also yielded returned starting material (**195**) as a brown oil (47.6 mg, 37%). ^{1}H NMR (400 MHz, $CDCl_3$) δ 7.26 (2H, d, *J* = 8.7 Hz, C*H*), 6.89 (2H, d, *J* = 8.7 Hz, C*H*), 4.48 (2H, s, CH_2), 3.81 (3H, s, CH_3), 3.48 - 3.37 (1H, m, C*H*), 2.81 - 2.71 (2H, m, CH_2), 2.31 (3H, s, CH_3), 2.27 - 2.18 (2H, m, CH_2), 1.99 - 1.89 (2H, m, CH_2), 1.78 - 1.66 (2H, m, CH_2); ^{1}H NMR data obtained here for **195** are consistent with the data obtained for **195** previously, see Chapter 5.18.

2-Methyl-1-phenyl-1,2,3,4-tetrahydroisoquinoline (122)

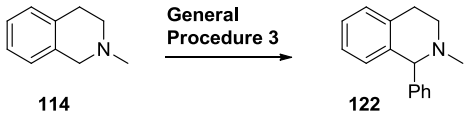

114 **122**

Compound **114** (0.55 mmol) was subjected to **General Procedure 3** using phenylmagnesium bromide (1.0 M in THF) as a nucleophile. ^{1}H NMR of the crude reaction mixture (the concentrated DCM/MeOH fractions after the silica plug) revealed a 59% yield of **122** by comparison with an added internal standard (1,3,5-trimethoxybenzene, 9.2 mg, 55.0 μmol, 10 mol%). MDAP

purification (high pH) gave **122** as a yellow oil (59.2 mg, 48%); IR ν_{max} (neat) 3025 - 2783 (C-H), 1493 (Ar), 1451 (Ar), 1366, 1290, 1140, 1125, 1099, 1067, 1028 cm^{-1}; ^{1}H NMR (400 MHz, $CDCl_3$) δ 7.33 - 7.22 (5H, m, C*H*), 7.14 - 7.05 (2H, m, C*H*), 6.97 (1H, apt. t, *J* = 7.3 Hz, C*H*), 6.61 (1H, d, *J* = 7.9 Hz, C*H*), 4.24 (1H, s, C*H*), 3.32 - 3.21 (1H, m, CH_2), 3.15 - 3.09 (1H, m, CH_2), 2.86 - 2.78 (1H, m, CH_2), 2.68 - 2.59 (1H, m, CH_2), 2.23 (3H, s, CH_3); ^{13}C NMR (101 MHz, $CDCl_3$) δ 144.0 (*C*), 138.6 (*C*), 134.3 (*C*), 129.6 (*C*H), 128.5 (*C*H), 128.3 (2 x *C*H), 127.3 (*C*H), 125.9 (*C*H), 125.6 (*C*H), 71.5 (*C*H), 52.4 (*C*H_2), 44.3 (*C*H_3), 29.5 (*C*H_2). HRMS (+ESI) *m/z* calculated for $C_{16}H_{18}N$ $[M+H^+]$ 224.1434; Found 224.1427. Data are consistent with the literature.[57]

6,7-Dimethoxy-2-methyl-1-phenyl-1,2,3,4-tetrahydroisoquinoline (123)

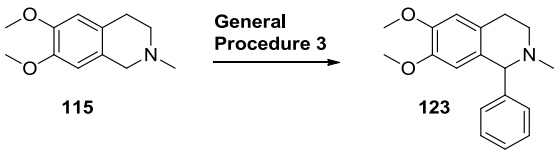

115 123

Compound **115** (0.55 mmol) was subjected to **General Procedure 3** using phenylmagnesium bromide (1.0 M in THF) as a nucleophile. Column chromatography (40 - 60% EtOAc/heptane (1% Et_3N)) gave **123** as an off-white microcrystalline solid (112.1 mg, 72%); m.p. 77 - 79 ^{o}C (lit. 77 - 79 ^{o}C[222]); IR ν_{max} (neat) 2950 - 2789 (C-H), 1610 (Ar), 1515 (Ar), 1467 (Ar), 1454 (Ar), 1404, 1366, 1332, 1307, 1252, 1216 cm^{-1}; ^{1}H NMR (400 MHz, $CDCl_3$) δ 7.36 - 7.24 (5H, m, C*H*), 6.62 (1H, s, C*H*), 6.11 (1H, s, C*H*), 4.21 (1H, s, C*H*), 3.86 (3H, s, CH_3), 3.57 (3H, s, CH_3), 3.25 - 3.07 (2H, m, CH_2), 2.82 - 2.72 (1H, m, CH_2), 2.68 - 2.59 (1H, m, CH_2), 2.26 (3H, s, CH_3). Data are consistent with the literature.[57]

2-Benzyl-6,7-dimethoxy-1-phenyl-1,2,3,4-tetrahydroisoquinoline (159)

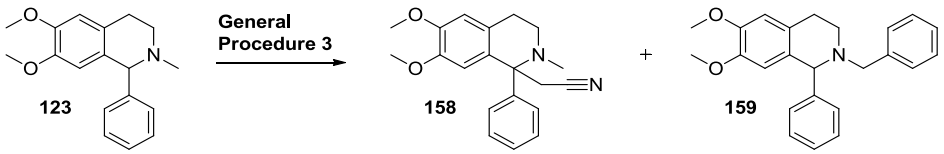

123 158 159

Compound **123** (0.42 mmol) was subjected to **General Procedure 3** using phenylmagnesium bromide (1.0 M in THF) as a nucleophile. Column chromatography (0 - 10% MeOH/DCM (1% Et_3N)) gave ***159*** as an amorphous colourless solid (39.7 mg, 26%); IR ν_{max} (neat) 3027 - 2832 (C-H), 1611 (Ar), 1513 (Ar), 1494 (Ar), 1464 (Ar), 1452 (Ar), 1407, 1367, 1333, 1295, 1253, 1222 cm^{-1}; ^1H NMR (400 MHz, $CDCl_3$) δ 7.40 - 7.20 (10H, m, C*H*), 6.62 (1H, s, C*H*), 6.22 (1H, s, C*H*), 4.56 (1H, s, C*H*), 3.86 (3H, s, CH_3), 3.80 (1H, d, *J* = 13.5 Hz, CH_2), 3.62 (3H, s, CH_3), 3.32 (1H, d, *J* = 13.5 Hz, CH_2), 3.14 - 3.14 (1H, m, CH_2), 3.02 - 2.91 (1H, m, CH_2), 2.76 - 2.68 (1H, m, CH_2), 2.57 - 2.49 (1H, m, CH_2); ^{13}C NMR (101 MHz, $CDCl_3$) δ 147.4 (*C*), 147.1 (*C*), 144.3 (*C*), 139.6 (*C*), 130.2 (*C*), 129.5 (*C*H), 128.7 (*C*H), 128.2 (*C*H), 128.1 (*C*H), 127.2 (*C*H), 127.0 (*C*), 126.8 (*C*H), 111.8 (*C*H), 110.9 (*C*H), 68.1 (*C*H), 58.7 (*C*H_2), 55.8 (2 x *C*H_3), 47.0 (*C*H_2), 28.4 (*C*H_2); HRMS (+ESI) *m/z* calculated for $C_{24}H_{26}NO_2$ $[M+H^+]$ 360.1970; Found 360.1958. Data are consistent with the literature.[244]

2-(6,7-Dimethoxy-2-methyl-1-phenyl-1,2,3,4-tetrahydroisoquinolin-1-yl)-acetonitrile (*158*)

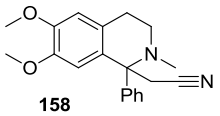

158

Compound (**158**) was isolated from the previous reaction as an amorphous colourless solid (74.2 mg, 54%); IR ν_{max} (neat) 2937 - 2835 (C-H), 2250 (C≡N), 1674, 1612 (Ar), 1515 (Ar), 1464 (Ar), 1446 (Ar), 1405, 1372, 1355, 1333, 1256, 1218 cm^{-1}; ^1H NMR (400 MHz, $CDCl_3$) δ 7.35 - 7.19 (5H, m, C*H*), 6.63 (1H, s, C*H*), 6.30 (1H, s, C*H*), 3.88 (3H, s, CH_3), 3.64 (3H, s, CH_3), 3.32 (1H, d, *J* = 16.4 Hz, CH_2), 3.18 (1H, d, *J* = 16.4 Hz, CH_2), 3.07 - 2.97 (1H, m, CH_2), 2.97 - 2.85 (3H, m, CH_2), 2.14 (3H, s, CH_3); ^{13}C NMR (101 MHz, $CDCl_3$) δ 148.1 (*C*), 147.3 (*C*), 142.6 (*C*), 130.8 (*C*), 127.9 (2 x *C*H, 1 x *C*), 127.4 (*C*H), 118.7 (*C*≡N), 111.7 (*C*H), 110.7 (*C*H), 65.2 (*C*), 56.0 (*C*H_3), 55.7 (*C*H_3), 47.1 (*C*H_2), 38.9 (*C*H_3), 28.9 (*C*H_2), 25.7 (*C*H_2); HRMS (+ESI) *m/z*

calculated for $C_{20}H_{23}N_2O_2$ [M+H$^+$] 323.1754; Found 323.1743.

N-Methyl-*N*-octyloctan-1-amine (160)

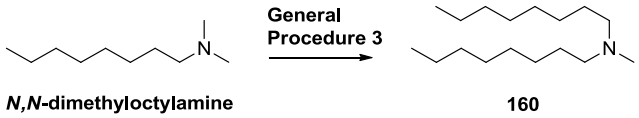

N,N-dimethyloctylamine **160**

N,*N*-Dimethyloctylamine was subjected to **General Procedure 3** using *n*-heptylmagnesium bromide (1.0 M in Et_2O) as a nucleophile. ^{1}H NMR of the crude reaction mixture (the concentrated DCM/MeOH fractions after the silica plug) revealed a 72% yield of **160** by comparison with an added internal standard (1,3,5-trimethoxybenzene, 9.2 mg, 55.0 μmol, 10 mol%). MDAP purification (low pH) gave (after basification using sat. aq. $NaHCO_3$ and extraction with DCM as described above) gave **160** as a colourless oil (84.7 mg, 60%); IR ν_{max} (neat) 2926 - 2856 (C-H), 1673, 1467, 1379, 1203 cm^{-1}; ^{1}H NMR (400 MHz, $CDCl_3$) δ 2.44 (4H, apt. t, *J* = 7.8 Hz, C*H*$_2$), 2.32 (3H, s, C*H*$_3$), 1.55 - 1.45 (4H, m, C*H*$_2$), 1.36 - 1.20 (20H, m, C*H*$_3$), 0.88 (6H, apt. t, *J* = 6.8 Hz, C*H*$_3$); ^{13}C NMR (101 MHz, $CDCl_3$) δ 57.7 (*C*H$_2$), 42.0 (*C*H$_3$), 31.8 (*C*H$_2$), 29.5 (*C*H$_2$), 29.2 (*C*H$_2$), 27.4 (*C*H$_2$), 26.6 (*C*H$_2$), 22.6 (*C*H$_2$), 14.1 (*C*H$_3$). HRMS (+ESI) *m/z* calculated for $C_{17}H_{38}N$ [M+H$^+$] 256.3004; Found 256.2999. Data are consistent with the literature.[245]

N-Benzyl-*N*-octyloctan-1-amine (161)

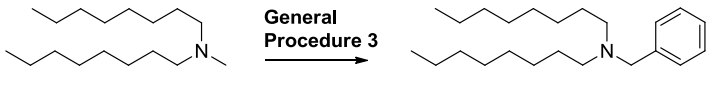

160 **161**

Compound **160** was subjected to **General Procedure 3** using phenylmagnesium bromide (1.0 M in THF) as a nucleophile.[†] Column chromatography (7 - 40% EtOAc/heptane) gave **161** as a colourless oil (88.1 mg, 48%); IR ν_{max} (neat) 2924 - 2795 (C-H), 1495 (Ar), 1454 (Ar), 1367 cm^{-1}; ^{1}H NMR (400 MHz, $CDCl_3$) δ 7.36 - 7.20 (5H, m, C*H*), 3.55 (2H, s, C*H*$_2$),

[†]^{1}H NMR of the crude reaction mixture revealed **161** : dioctylamine : an *N*-C**H**$_2$ functionalised product in a 1.0 : 0.27 : 0.20 ratio. The overall *N*-C**H**$_3$ *vs*. *N*-C**H**$_2$ selectivity was thus 6 : 1.

2.40 (4H, t, *J* = 7.4 Hz, C*H*$_2$), 1.52 - 1.42 (4H, m, C*H*$_2$), 1.35 - 1.20 (20H, m, C*H*$_2$), 0.90 (6H, t, *J* = 6.8 Hz, C*H*$_3$); ^{13}C NMR (101 MHz, $CDCl_3$) δ 140.4 (*C*), 128.8 (*C*H), 128.0 (*C*H), 126.5 (*C*H), 58.7 (*C*H$_2$), 53.9 (*C*H$_2$), 31.9 (*C*H$_3$), 29.6 (*C*H$_2$), 29.3 (*C*H$_2$), 27.5 (*C*H$_2$), 27.1 (*C*H$_2$), 22.7 (*C*H$_2$), 14.1 (*C*H$_3$); HRMS (+ESI) *m/z* calculated for $C_{23}H_{42}N$ [M+H$^+$] 332.3312; Found 332.3305. Data are consistent with the literature.[246]

5.21. LATE-STAGE FUNCTIONALISATION OF COMPLEX MOLECULES

2-(1-Benzylazepan-4-yl)-4-(4-chlorobenzyl)phthalazin-1(2*H*)-one (162b)

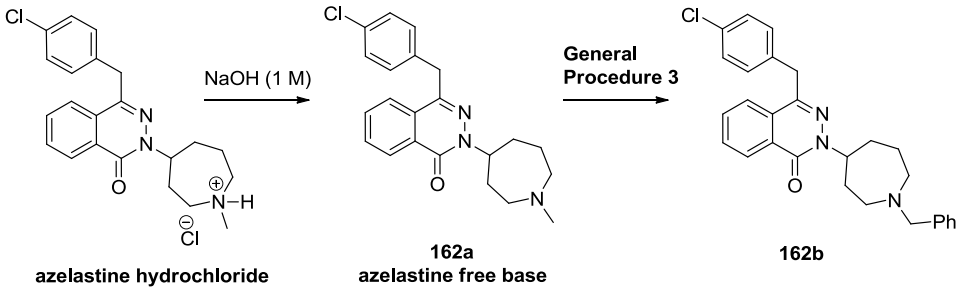

Azelastine free base (**162a**) was prepared from its hydrochloride salt in the same manner as dextromethorphan (**73**) (see Chapter 5.13). Azelastine free base (**162a**) (0.53 mmol) was subjected to **General Procedure 3** using phenylmagnesium bromide (1.0 M in THF) as a nucleophile. ^{1}H NMR of the crude reaction mixture† (the concentrated DCM/MeOH fractions after the silica plug) revealed a 33% yield of **162b** by comparison with an added internal standard (1,3,5-trimethoxybenzene, 8.9 mg, 53.0 μmol, 10 mol%). MDAP purification (high pH) gave **162b** as a pale brown oil (61.1 mg, 25%) which crystallised on standing to an off-white solid; m.p. 141 - 142 ^{o}C (lit. 140 - 141 ^{o}C[247]); IR ν_{max} (neat) 3063 - 2812 (C-H), 1646 (br., C=O, C=N), 1610 (Ar), 1586 (Ar), 1490 (Ar), 1452 (Ar), 1407, 1322 cm^{-1}; ^{1}H NMR (400 MHz, $CDCl_3$) δ 8.49 - 8.44 (1H, m, C*H*), 7.74 - 7.65 (3H, m, C*H*), 7.39 (2H, d, *J* = 7.1 Hz, C*H*), 7.34 (2H, t, *J* = 7.5 Hz, C*H*), 7.30 - 7.23 (3H, m, C*H*), 7.22 (2H,

†By comparison to the internal standard, an 18% yield of returned starting material (azelastine free base, **162a**) was observed, and a 5% yield of an *N*-C**H**$_2$ functionalised product. Therefore, *N*-C**H**$_3$ *vs*. *N*-C**H**$_2$ selectivity was deemed 7 : 1.

d, *J* = 8.3 Hz, C*H*), 5.43 - 5.34 (1H, m, C*H*), 4.28 (2H, s, CH_2), 3.68 (2H, s, CH_2), 2.85 - 2.65 (4H, m, CH_2), 2.25 - 2.09 (2H, m, CH_2), 2.08 - 1.97 (2H, m, CH_2), 1.96 - 1.84 (1H, m, CH_2), 1.82 - 1.72 (1H, m, CH_2); ^{13}C NMR (101 MHz, $CDCl_3$)† δ 158.4 (*C*=O), 144.3 (*C*), 139.7 (*C*), 136.4 (*C*), 132.7 (*CH*), 132.5 (*C*), 131.1 (*C*H), 129.9 (*C*H), 128.8 (2 x *C*H), 128.6 (*C*), 128.2 (C*H*), 127.5 (C*H*), 126.8 (C*H*), 124.4 (C*H*), 62.8 (*C*H_2), 56.4 (*C*H), 56.2 (*C*H_2), 51.9 (*C*H_2), 38.3 (*C*H_2), 33.6 (*C*H_2), 32.6 (*C*H_2), 25.3 (*C*H_2); HRMS (+ESI) *m/z* calculated for $C_{28}H_{29}{}^{35}ClN_3O$ [M+H$^+$] 458.1994; Found 458.1996. The m.p. is consistent with the literature (other data is not available for comparison).[247]

(7a*R*,12b*S*)-3-(Cyclopropylmethyl)-7,9-dimethoxy-2,3,4,7a-tetrahydro-1*H*-4,12-methanobenzofuro[3,2-*e*]isoquinoline (*163*)

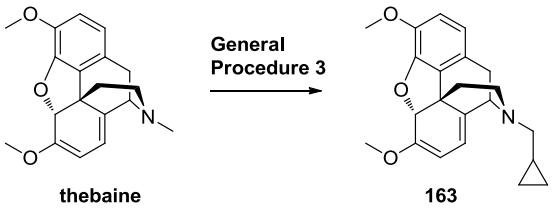

thebaine 163

Thebaine (0.55 mmol) was subjected to **General Procedure 3** using cyclopropylmagnesium bromide (1.0 M in 2-MeTHF) as a nucleophile. MDAP purification (high pH) gave ***163*** as a brown oil (73.5 mg, 38%); IR ν_{max} (neat) 2918 - 2835 (C-H), 1606 (Ar), 1505 (Ar), 1439 (Ar), 1371, 1329, 1281, 1258, 1232 cm^{-1}; ^{1}H NMR (400 MHz, $CDCl_3$) δ 6.64 (1H, d, *J* = 8.3 Hz, C*H*), 6.60 (1H, d, *J* = 8.1 Hz, C*H*), 5.55 (1H, d, *J* = 6.4 Hz, C*H*), 5.29 (1H, s, C*H*), 5.05 (1H, d, *J* = 6.4 Hz, C*H*), 3.92 (1H, d, *J* = 7.1 Hz, C*H*), 3.84 (3H, s, CH_3), 3.59 (3H, s, CH_3), 3.23 (1H, d, *J* = 18.1 Hz, CH_2), 2.89 (1H, dd, *J* = 13.0, 4.9 Hz, CH_2), 2.80 (1H, dd, *J* = 12.8, 3.4 Hz, CH_2), 2.72 (1H, dd, *J* = 17.9, 7.1 Hz, CH_2), 2.47 (2H, d, *J* = 6.4 Hz, CH_2), 2.21 (1H, dt, *J* = 12.5, 5.4 Hz, CH_2), 1.73 (1H, d, *J* = 12.5 Hz, CH_2), 0.95 - 0.85 (1H, m, C*H*), 0.58 - 0.52 (2H, m, CH_2), 0.18 - 0.12 (2H, m, CH_2); ^{13}C NMR (101 MHz, $CDCl_3$) δ 152.4 (*C*), 144.6 (*C*), 142.7 (*C*), 133.6 (*C*), 132.6 (*C*), 127.8 (*C*), 119.1 (*C*H), 112.7 (*C*H), 111.7 (*C*H), 95.9 (C*H*), 89.2 (C*H*), 59.1 (*C*H_2), 58.5 (*C*H), 56.3 (*C*H_3), 54.9 (*C*H_3),

†The remaining quaternary carbon could not be observed.

46.5 (*C*), 44.2 (*C*H_2), 36.8 (*C*H_2), 30.5 (*C*H_2), 9.5 (*C*H), 3.9 (*C*H_2), 3.7 (*C*H_2); HRMS (+ESI) *m/z* calculated for $C_{22}H_{26}NO_3$ [M+H^+] 352.1907; Found 352.1895.

(7a*R*,12b*S*)-3-(Cyclopropylmethyl)-7-methoxy-2,3,4,7a-tetrahydro-1*H*-4, 12-methanobenzofuro[3,2-*e*]isoquinolin-9-yl ethyl carbonate (*164*)

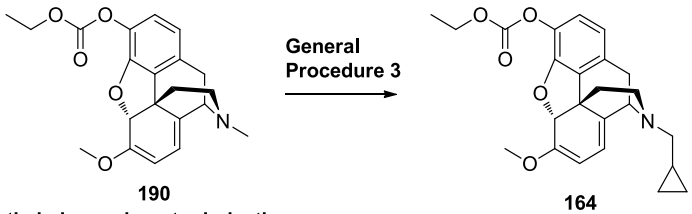

190
thebaine carbonate-derivative

164

Thebaine's carbonate derivative (**190**) (0.55 mmol) was subjected to **General Procedure 3** using cyclopropylmagnesium bromide (1.0 M in 2-MeTHF) as a nucleophile. ^{1}H NMR of the crude reaction mixture (the concentrated DCM/MeOH fractions after the silica plug) revealed a 34% yield of ***164*** by comparison with an added internal standard (1,3,5-trimethoxybenzene, 9.2 mg, 55.0 μmol, 10 mol%). MDAP purification (high pH) gave ***164*** as a brown oil (64.9 mg, 29%); IR ν_{max} (neat) 2921 - 2837 (C-H), 1762 (C=O), 1687 (C=C), 1607 (Ar), 1494 (Ar), 1445, 1369, 1335, 1238, 1204 cm^{-1}; ^{1}H NMR (400 MHz, $CDCl_3$) δ 6.83 (1H, d, *J* = 8.3 Hz, C*H*), 6.63 (1H, d, *J* = 8.1 Hz, C*H*), 5.58 (1H, d, *J* = 6.6 Hz, C*H*), 5.32 (1H, s, C*H*), 5.04 (1H, d, *J* = 6.4 Hz, C*H*), 4.35 - 4.24 (2H, m, CH_2), 3.94 (1H, d, *J* = 7.1 Hz, C*H*), 3.60 (3H, s, CH_3), 3.25 (1H, d, *J* = 18.1 Hz, CH_2), 2.91 (1H, dd, *J* = 13.0, 4.7 Hz, CH_2), 2.79 (1H, dd, *J* = 13.0, 3.4 Hz, CH_2), 2.76 (1H, dd, *J* = 18.3, 7.1 Hz, CH_2), 2.49 (2H, d, *J* = 6.4 Hz, CH_2), 2.21 (1H, dt, *J* = 12.5, 5.1 Hz, CH_2), 1.77 (1H, d, *J* = 12.5 Hz, CH_2), 1.36 (3H, t, *J* = 7.1 Hz, CH_3), 0.97 - 0.86 (1H, m, C*H*), 0.59 - 0.52 (2H, m, CH_2), 0.19 - 0.12 (2H, m, CH_2); ^{13}C NMR (101 MHz, $CDCl_3$) δ 153.2 (*C*=O), 152.2 (*C*), 147.4 (*C*), 134.8 (*C*), 133.4 (*C*), 132.7 (*C*), 129.8 (*C*), 121.4 (*C*H), 119.2 (*C*H), 112.0 (*C*H), 96.3 (C*H*), 90.0 (C*H*), 64.8 (CH_2), 59.0 (*C*H_2), 58.3 (*C*H), 55.0 (*C*H_3), 46.4 (*C*), 44.0 (*C*H_2), 36.5 (*C*H_2), 30.9 (*C*H_2), 14.1 (*C*H_3), 9.4 (*C*H), 3.9 (*C*H_2), 3.7 (*C*H_2); HRMS (+ESI) *m/z* calculated for

$C_{24}H_{28}NO_5$ [M+H$^+$] 410.1962; Found 410.1967.

Nor-scopolamine (165b)

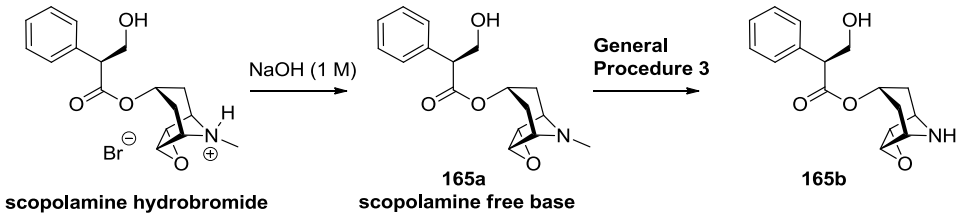

scopolamine hydrobromide — 165a scopolamine free base — 165b

Scopolamine free base (**165a**) was prepared from the hydrobromide salt in the same manner as dextromethorphan (**73**) from dextromethorphan hydrobromide (see Chapter 5.13). Scopolamine (0.45 mmol) was subjected to **General Procedure 3** using phenylzinc halide (6.0 eq.) as a nucleophile. ^{1}H NMR of the crude reaction mixture (the concentrated DCM/MeOH fractions after the silica plug) revealed a 40% yield of **165b** by comparison with an added internal standard (1,3,5-trimethoxybenzene, 7.6 mg, 45.0 μmol, 10 mol%).[†] MDAP purification (high pH) gave **165b** as an off-white solid (47.4 mg, 36%); m.p. 111 - 112 ^{o}C (lit. 110 - 112 ^{o}C[248]); IR ν_{max} (neat) 3311 - 2949 (br., O-H, N-H, C-H), 1723 (C=O), 1602 (Ar), 1494 (Ar), 1455 (Ar), 1421, 1394, 1333, 1270, 1231 cm^{-1}; ^{1}H NMR (400 MHz, $CDCl_3$) δ 7.40 - 7.29 (3H, m, C*H*), 7.24 (2H, d, *J* = 8.1 Hz, C*H*), 5.03 (1H, t, *J* = 5.1 Hz, C*H*), 4.21 - 4.14 (1H, m, CH_2), 3.85 - 3.73 (2H, m, CH_2, C*H*), 3.25 (1H, d, *J* = 2.9 Hz, C*H*), 3.22 - 3.17 (1H, m, C*H*), 3.08 - 3.03 (1H, m, C*H*), 2.62 (1H, s, N*H*), 2.50 (1H, d, *J* = 2.9 Hz, C*H*), 2.25 (1H, br. s, O*H*), 2.16 - 2.08 (1H, m, CH_2), 2.07 - 1.99 (1H, m, CH_2), 1.68 (1H, d, *J* = 15.1 Hz, CH_2), 1.45 (1H, d, *J* = 14.9 Hz, CH_2); ^{13}C NMR (101 MHz, $CDCl_3$) δ 171.8 (*C*=O), 135.7 (*C*), 129.0 (*C*H), 128.1 (*C*H), 128.0 (*C*H), 66.9 (*C*H), 64.0 (*C*H_2), 54.2 (*C*H), 53.9 (*C*H), 53.4 (*C*H), 51.8 (*C*H), 51.7 (*C*H), 31.4 (*C*H_2), 31.2 (*C*H_2); HRMS (+ESI) *m/z* calculated for $C_{16}H_{20}NO_4$ [M+H$^+$] 290.1387; Found 290.1383. Data are consistent with the literature.[248,249]

[†]A 22% yield of returned starting material (scopolamine free base, **165a**) was observed.

(2*S*)-(1*S*,2*S*,7*R*)-3-Oxa-9-azatricyclo[3.3.1.0^{2,4}]nonan-7-yl 3-((*tert*-butyldimethylsilyl)ox-y)-2-phenylpropanoate (*166b*)

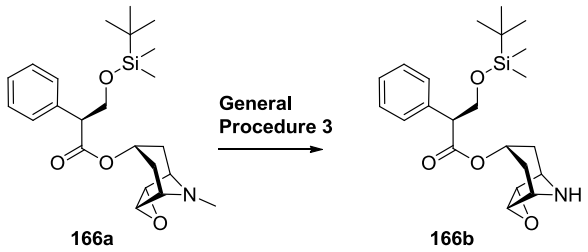

166a 166b

Compound **166a** (0.54 mmol) was subjected to **General Procedure 3** using phenylzinc halide (6.0 eq.) as a nucleophile. ^{1}H NMR of the crude reaction mixture (the concentrated DCM/MeOH fractions after the silica plug) revealed a 31% yield of ***166b*** by comparison with an added internal standard (1,3,5-trimethoxybenzene, 9.1 mg, 54.0 μmol, 10 mol%).[†] MDAP purification (high pH) gave ***166b*** as a pale brown oil (21.8 mg, 12%); IR ν_{max} (neat) 2952 - 2856 (N-H, C-H), 1730 (C=O), 1495 (Ar), 1472 (Ar), 1421, 1393, 1361, 1333, 1257, 1224 cm^{-1}; ^{1}H NMR (400 MHz, $CDCl_3$) δ 7.35 - 7.23 (5H, m, C*H*), 4.98 (1H, t, *J* = 5.1 Hz, C*H*), 4.18 (1H, t, *J* = 9.4 Hz, C*H*), 3.82 - 3.76 (1H, m, CH_2), 3.72 - 3.67 (1H, m, CH_2), 3.34 (1H, d, *J* = 3.0 Hz, C*H*), 3.22 - 3.18 (1H, m, C*H*), 3.11 - 3.08 (1H, m, C*H*), 2.92 (1H, d, *J* = 3.0 Hz, C*H*), 2.15 - 2.06 (1H, m, CH_2), 2.06 - 1.98 (2H, m, N*H*, CH_2), 1.68 (1H, d, *J* = 15.1 Hz, CH_2), 1.47 (1H, d, *J* = 15.1 Hz, CH_2), 0.85 (9H, s, CH_3), 0.02 (3H, s, CH_3), 0.00 (3H, s, CH_3); ^{13}C NMR (101 MHz, $CDCl_3$) δ 171.1 (*C*=O), 135.9 (*C*), 128.7 (*C*H), 128.1 (*C*H), 127.7 (*C*H), 66.6 (*C*H), 65.0 (*C*H_2), 55.0 (*C*H), 54.1 (*C*H), 53.7 (*C*H), 52.0 (*C*H), 51.9 (*C*H), 31.5 (*C*H_2), 31.3 (*C*H_2), 25.8 (*C*H_3), 18.2 (*C*), -5.5 (2 x *C*H_3); HRMS (+ESI) *m/z* calculated for $C_{22}H_{34}NO_4Si$ [M+H$^+$] 404.2252; Found 404.2249.

[†]A 51% yield of returned starting material (compound **166a**) was observed.

5.22. SUBSTRATES WHICH GAVE NO REACTION

N,*N*-Dimethylethanesulfonamide (167a)

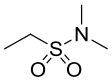

Compound **167a** (0.55 mmol) was subjected to **General Procedure 3**, using phenylmagnesium bromide (1.0 M in THF) as a nucleophile. ^{1}H NMR of the crude reaction mixture (the concentrated DCM/MeOH fractions after the silica plug) revealed no reaction; a 68% yield† of starting material (**167a**) was observed by comparison with an added internal standard (1,3,5-trimethoxybenzene, 9.2 mg, 55.0 μmol, 10 mol%).

N,*N*-Dimethyldecanamide (168a)

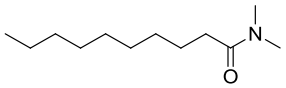

168a

Compound **168a** (0.55 mmol) was subjected to **General Procedure 3**, using phenylmagnesium bromide (1.0 M in THF) as a nucleophile. ^{1}H NMR of the crude reaction mixture (the concentrated DCM/MeOH fractions after the silica plug) revealed no reaction; a 94% yield† of starting material (**168a**) was observed by comparison with an added internal standard (1,3,5-trimethoxybenzene, 9.2 mg, 55.0 μmol, 10 mol%).

N,*N*-Diethyl-5,5-diphenyl-pent-4-en-1-amine (41)

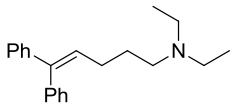

41

Compound **41** (0.35 mmol) was subjected to **General Procedure 3**, but running at 50.0 mM and using H_2O (10.0 eq.) additive (phenylmagnesium bromide was not added) in line with Jahn's conditions for trialkylamine N-

†No other substrate-derived products were observed in the crude ^{1}H NMR.

radical cation cyclisation (50.0 mM). ^{1}H NMR of the crude reaction mixture (the concentrated DCM/MeOH fractions after the silica plug) revealed no reaction; a 87% yield† of starting material (**41**) by comparison with an added internal standard (1,3,5-trimethoxybenzene, 5.6 mg, 35.0 μmol, 10 mol%).

5.23. Reactions of Radical Clock Substrates

1,1-Diethyl-2-(hydroxydiphenylmethyl)pyrrolidin-1-ium trifluoroacetate (42)

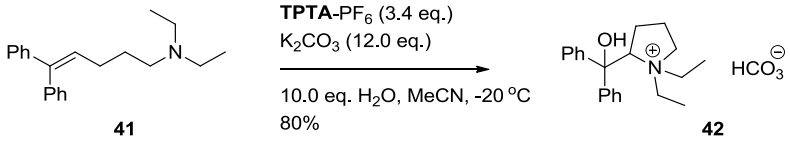

Prepared according to a modified literature procedure,[67] using **41** as a reagent, **TPTA**-PF_6 as oxidant and the colour changes as indicators for the addition of reagents. A reaction vessel was charged with **41** (103.0 mg, 0.35 mmol) and MeCN (7 mL). H_2O (60.0 μL, 10.0 eq.) was added and the solution cooled to -20 °C (dry ice/IPA bath) and placed under an N_2 funnel. **TPTA**-PF_6 (151.0 mg, 0.35 mmol, 1.0 eq.) was added as a solid under an N_2 atmosphere. A second portion of **TPTA**-PF_6 (45.0 mg, 0.11 mmol, 0.3 eq.) was added and the colour of the mixture changed to blue. Portions (2x) of K_2CO_3 (48.0 mg, 0.35 mmol, 1.0 eq.) were added; the colour of the mixture changed to brown. Further portions (3x) of **TPTA**-PF_6 (45.0 mg, 0.11 mmol, 0.3 eq.) were added; the colour of the mixture changed to blue. Further portions (2x) of K_2CO_3 (48.0 mg, 0.35 mmol, 1.0 eq.) were added; the colour of the mixture changed to brown. Further portions (3x) of **TPTA**-PF_6 (45.0 mg, 0.11 mmol, 0.3 eq.) were added; the colour of the mixture changed to blue. Further portions (8x) of K_2CO_3 (48.0 mg, 0.35 mmol, 1.0 eq.) were added but the colour did not change to brown, indicating reaction completion. A final portion of **TPTA**-PF_6 (45.0 mg, 0.11 mmol, 0.3 eq.) was added (3.4 eq. oxidant added in total). MeOH (1 mL) was added, followed by DCM (30 mL)

†No other substrate-derived products were observed in the crude ^{1}H NMR.

and water (30 mL). The layers were separated and the aqueous layer was extracted with DCM (2 x 30 mL). The combined organic layers were dried ($MgSO_4$), filtered and concentrated *in vacuo* before loading onto celite. The crude product was loaded onto a silica plug and eluted with warm (40 ^oC) heptane to remove tri-*p*-tolylamine. The plug was flushed heavily with MeOH/DCM (5%) and the fractions concentrated *in vacuo*. DCM (50 mL) and sat. aq. $NaHCO_3$ (50 mL) were added. The layers were separated and the aqueous layer was extracted with DCM (2 x 50 mL). The combined organic layers were dried ($MgSO_4$), filtered and concentrated *in vacuo*. Addition of 1,3,5-trimethoxybenzene (5.60 mg, 35.0 μmol, 10 mol%) revealed an 80% yield of **42**. MDAP purification (high pH) gave **42** as an amorphous colourless solid (91.7 mg, 71%);[†] IR ν_{max} (neat) 3228 (O-H), 3063 - 2850 (C-H), 1689 (C=O), 1598 (Ar), 1494 (Ar), 1450 (Ar), 1397, 1305, 1250, 1201 cm^{-1}; ^1H NMR (400 MHz, acetone-d_6) δ 7.86 (2H, d, *J* = 7.8 Hz, C*H*), 7.74 (2H, d, *J* = 8.1 Hz, C*H*), 7.36 (2H, t, *J* = 7.8 Hz, C*H*), 7.29 (2H, t, *J* = 7.8 Hz, C*H*), 7.25 - 7.14 (2H, m, C*H*), 5.53 (1H, dd, *J* = 9.1, 6.1 Hz, C*H*), 3.98 - 3.88 (1H, m, CH_2), 3.88 - 3.75 (2H, m, CH_2), 3.65 - 3.55 (1H, m, CH_2), 3.26 - 3.15 (1H, m, CH_2), 2.87 - 2.79 (1H, m, CH_2), 2.65 - 2.54 (1H, m, CH_2), 2.52 - 2.40 (1H, m, CH_2), 2.33 - 2.12 (2H, m, CH_2), 1.41 (3H, t, *J* = 7.1 Hz, CH_3), 1.20 (3H, t, *J* = 7.2 Hz, CH_3); ^{13}C NMR (101 MHz, acetone-d_6)[‡,§] δ 148.3 (*C*), 148.3 (*C*), 146.6 (*C*), 146.5 (*C*), 129.7 (*C*H), 129.4 (*C*H), 128.0 (*C*H), 127.9, (*C*H), 126.1 (*C*H), 125.9 (*C*H), 80.8 (*C*), 80.7 (*C*), 77.7 (*C*H), 64.1 (*C*H_2), 55.9 (*C*H_2), 53.5 (*C*H_2), 27.6 (*C*H_2), 20.7 (*C*H_2), 9.8 (*C*H_3), 9.2 (*C*H_3); HRMS (+ESI) *m/z* calculated for $C_{21}H_{28}NO$ [M] 310.2165; Found 310.2154. Data are consistent with the literature.[67]

^1H NMR data in $CDCl_3$ solvent are given for reference: ^1H NMR (400 MHz, $CDCl_3$) δ 7.69 (2H, d, *J* = 7.6 Hz, C*H*), 7.57 (1H, d, *J* = 7.8 Hz, C*H*), 7.34 -

[†]Tentatively assigned as the bicarbonate salt based on the sodium bicarbonate present in the reverse-phase chromatography eluant and the IR stretch at 1689 cm^{-1}. [‡]The ^{13}C signal for the bicarbonate anion could not be observed. [§]Six quaternary carbons observed (or three quaternary doublets with *J* = 9.2 Hz), possibly to due rotamers, making assignment non-trivial. All observed ^{13}C NMR peaks are listed.

7.20 (5H, m, C*H*), 7.16 (1H, t, *J* = 7.3 Hz, C*H*), 7.10 (1H, t, *J* = 7.3 Hz, C*H*), 6.91 (1H, br. s, OH), 5.09 (1H, t, *J* = 7.5 Hz, C*H*), 3.85 - 3.69 (2H, m, CH_2), 3.44 - 3.27 (2H, m, CH_2), 2.96 - 2.82 (1H, m, CH_2), 2.70 - 2.58 (1H, m, CH_2), 2.52 - 2.38 (2H, m, CH_2), 2.23 - 2.10 (1H, m, CH_2), 2.00 - 1.86 (1H, m, CH_2), 1.28 (3H, t, *J* = 7.2 Hz, CH_3), 1.04 (3H, t, *J* = 7.2 Hz, CH_3).

1,1-Dimethyl-2-(hydroxydiphenylmethyl)pyrrolidin-1-ium trifluoroacetate (*174*)

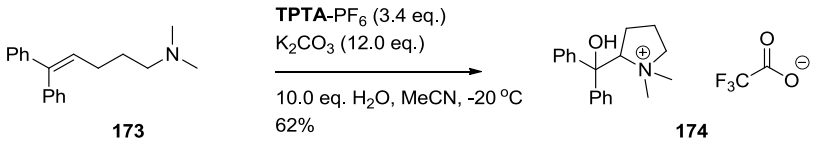

Prepared according to a modified literature procedure,[67] using **TPTA**-PF_6 as oxidant and using the colour changes as indicators for the addition of reagents to **173** (13.3 mg, 50.0 μmol) as substrate. ^{1}H NMR of the crude reaction mixture (the concentrated DCM/MeOH fractions after the silica plug) revealed a 62% yield of ***174*** by comparison with an added internal standard (1,3,5-trimethoxybenzene, 8.4 mg, 50.0 μmol, 100 mol%). The reaction was repeated on a larger scale for isolation, using **173** (151.0 mg, 0.35 mmol). MDAP purification (low pH) gave ***174*** as an amorphous colourless solid (53.8 mg, 39%);[†] IR ν_{max} (neat) 3283 (O-H), 3063 - 2978 (C-H), 1684 (C=O), 1475 (Ar), 1450 (Ar) cm^{-1}; ^{1}H NMR (400 MHz, $CDCl_3$) δ 7.68 (2H, d, *J* = 7.5 Hz, C*H*), 7.56 (2H, d, *J* = 7.8 Hz, C*H*), 7.38 - 7.28 (4H, m, C*H*), 7.27 - 7.17 (2H, m, C*H*), 5.55 (1H, br. s, OH), 5.10 (1H, t, *J* = 9.1 Hz, C*H*), 3.79 - 3.68 (1H, m, CH_2), 3.51 - 3.41 (1H, m, CH_2), 3.03 (3H, s, CH_3), 2.63 (3H, s, CH_3), 2.53 - 2.36 (2H, m, CH_2), 2.16 - 2.03 (2H, m, CH_2); ^{13}C NMR (101 MHz, $CDCl_3$)[‡] δ 145.4 (*C*), 142.8 (*C*), 129.1 (*C*H), 129.0 (*C*H), 128.0 (*C*H), 127.8 (*C*H), 125.5 (*C*H), 124.7 (*C*H), 80.4 (*C*H), 77.9 (*C*), 70.3 (*C*H_2), 54.7 (*C*H_3), 49.0 (*C*H_3), 25.2 (*C*H_2), 19.1 (*C*H_2); ^{19}F NMR (376.5 MHz, $CDCl_3$) δ -75.5 (s, CF_3); HRMS (+ESI) *m/z* calculated for $C_{19}H_{24}NO$ [M] 282.1852; Found 282.1852.

[†]Tentatively assigned as the trifluoroacetate salt based on the trifluoroacetic acid present in the reverse-phase chromatography eluant and the I.R. stretch at 1684 cm^{-1}. [‡]^{13}C signals for the trifluoroacetate anion could not be observed.

_N_-Benzyl-_N_-methyl-5,5-diphenylpent-4-en-1-amine (*175*)

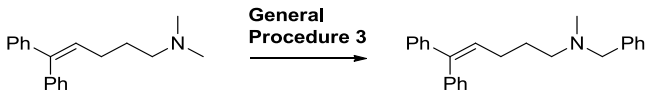

41 175

Compound **176** (0.35 mmol) was subjected to **General Procedure 3**, using phenylmagnesium bromide (1.0 M in THF) as a nucleophile. ^{1}H NMR of the crude reaction mixture (the concentrated DCM/MeOH fractions after the silica plug) revealed a 39% yield[†] of ***175*** by comparison with an added internal standard (1,3,5-trimethoxybenzene, 9.2 mg, 55.0 μmol, 10 mol%). MDAP purification (high pH) gave ***175*** as an brown oil (43.7 mg, 37%); IR ν_{max} (neat) 3025 - 2786 (C-H), 1598 (Ar), 1494 (Ar), 1444, 1364 cm^{-1}; ^{1}H NMR (400 MHz, $CDCl_3$) δ 7.40 - 7.13 (15H, m, C*H*), 6.08 (1H, t, *J* = 7.5 Hz, C*H*), 3.45 (2H, s, CH_2), 2.36 (2H, t, *J* = 7.3 Hz, CH_2), 2.21 - 2.10 (5H, m, CH_2, CH_3), 1.66 (2H, quintet, *J* = 7.3 Hz, CH_2); ^{13}C NMR (101 MHz, $CDCl_3$) δ 142.7 (*C*), 141.7 (*C*), 140.1 (*C*), 139.2 (*C*), 129.9 (*C*H), 129.7 (*C*H), 129.0 (*C*H), 128.1 (2 x *C*H), 128.0 (*C*H), 127.2 (*C*H), 126.8 (2 x *C*H), 126.7 (*C*H), 62.1 (*C*H_2), 56.9 (*C*H_2), 42.2 (*C*H_3), 27.7 (*C*H_2), 27.6 (*C*H_2); HRMS (+ESI) *m/z* calculated for $C_{25}H_{28}N$ [M+H$^+$] 342.2216; Found 342.2212.

_N_-Benzyl-_N_-methyl-4,4-diphenylbut-3-en-1-amine (*177a*)

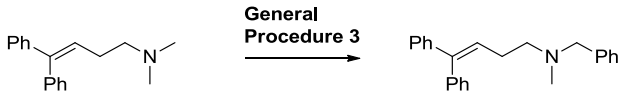

176 177a

Compound **176** (0.35 mmol) was subjected to **General Procedure 3**, using phenylmagnesium bromide (1.0 M in THF) as a nucleophile. ^{1}H NMR of the crude reaction mixture (the concentrated DCM/MeOH fractions after the silica plug) revealed a 48% yield of ***177a*** by comparison with an added internal standard (1,3,5-trimethoxybenzene, 5.9 mg, 35.0 μmol, 10 mol%). MDAP purification (low pH) gave (after basification using sat. aq. $NaHCO_3$ and extraction with DCM as described above) ***177a*** as a pale brown oil (48.3 mg,

[†]No other substrate-derived products were observed in the crude ^{1}H NMR.

42%); IR ν_{max} (neat) 3057 - 2787 (C-H), 1599 (Ar), 1494 (Ar), 1444, 1365, 1259 cm^{-1}; ^{1}H NMR (400 MHz, $CDCl_3$) δ 7.38 - 7.11 (15H, m, C*H*), 6.08 (1H, t, *J* = 7.3 Hz, C*H*), 3.45 (2H, s, CH_2), 2.49 (2H, t, *J* = 7.4 Hz, CH_2), 2.33 (2H, q, *J* = 7.4 Hz, CH_2), 2.15 (3H, s, CH_3); ^{13}C NMR (101 MHz, $CDCl_3$)† δ 142.6 (*C*), 142.4 (*C*), 140.1 (*C*), 139.0 (*C*), 129.8 (*C*H), 129.0 (*C*H), 128.2 (2 x *C*H), 128.0 (*C*H), 127.5 (*C*H), 127.2 (*C*H), 126.9 (*C*H), 126.8 (*C*H), 62.0 (CH_2), 57.0 (CH_2), 42.1 (CH_3), 27.7 (CH_2); HRMS (+ESI) *m/z* calculated for $C_{24}H_{26}N$ [M+H^+] 328.2052; Found 328.2060. In addition, a 14% yield of **177b** was observed in the ^{1}H NMR of the crude reaction mixture, which was isolated in the reaction described below.

_N_-methyl-4,4-diphenylbut-3-en-1-amine (*177b*)

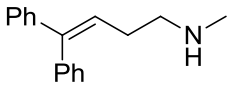

177b

Compound **176** (0.35 mmol) was subjected to **General Procedure 3** , but running at 50 mM and using H_2O (10.0 eq.) additive (phenylmagnesium bromide was not added as a nucleophile) in line with Jahn's conditions for trialkylamine N-radical cation cyclisation (50 mM). After addition of all reagents, stirring was ceased and the precipitate allowed to settle. The supernatent was collected and MDAP purification (high pH) gave **177b** as a colourless oil (14.9 mg, 18%); IR ν_{max} (neat) 3350 (br., N-H), 3023 - 2927 (C-H), 1599 (Ar), 1494 (Ar), 1444, 1363 cm^{-1}; ^{1}H NMR (400 MHz, $CDCl_3$)‡ δ 7.41 - 7.17 (10H, m, C*H*), 6.09 (1H, t, *J* = 7.4 Hz, C*H*), 2.70 (2H, t, *J* = 7.1 Hz, CH_2), 2.40 (3H, s, CH_3), 2.33 (2H, apt. q, *J* = 7.2 Hz, CH_2); ^{13}C NMR (101 MHz, $CDCl_3$) δ 143.2 (*C*), 142.5 (*C*), 140.0 (*C*), 129.8 (*C*H), 128.2 (*C*H), 128.1 (*C*H), 127.2 (*C*H), 127.1 (*C*H), 127.0 (*C*H), 126.9 (*C*H), 52.0 (CH_2), 36.4 (CH_3), 30.3 (CH_2); HRMS (+ESI) *m/z* calculated for $C_{24}H_{26}N$ [M+H^+] 238.1590; Found 238.1575.§

†The remaining aromatic CH could not be observed. ‡The NH proton was not observed. §The error between measured and calculated HRMS data found for **177b** is 6.9 ppm (> 5.0 ppm). The combination of spectral data as a whole determined **177b** as the correct structure.

5.24. COMPETITION EXPERIMENTS WITH TWO TRIALKYLAMINE SUBSTRATES

5.24.1. RADICAL CLOCK SUBSTRATE COMPETITION EXPERIMENT

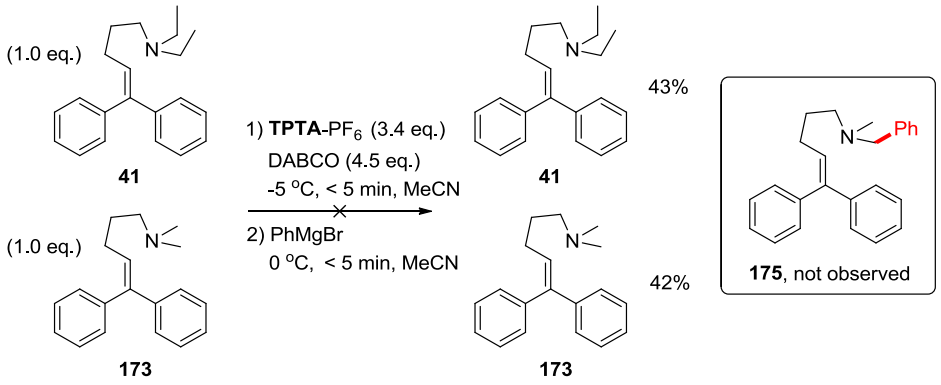

Reaction conducted according to **General Procedure 3**, using a 1 : 1 mixture of **41** (0.54 mmol) and **173** (0.54 mmol) as starting material and phenylmagnesium bromide (1.0 M in THF) as a nucleophile. DABCO (2.48 mmol, 4.5 eq.) and **TPTA**-PF_6 (1.87 mmol, 3.4 eq.) [relative to a single substrate (**173**), assuming that **41** would act as a dummy substrate and not interfere with the reaction of **173**]. ^{1}H NMR of the crude reaction mixture (the concentrated DCM/MeOH fractions after the silica plug) revealed a 43% yield of **41** and 42% yield of **173** by comparison with an added internal standard (1,3,5-trimethoxybenzene, 9.1 mg, 54.0 μmol, 10 mol%). Product **175** was not observed.

This reaction indicates interference of a normally non-reactive substrate (**41**) in the reaction of a normally reactive substrate (**173**). See the next page for a proposed rationale for this.

5.24.2. DEXTROMETHORPHAN-DERIVED SUBSTRATE COMPETITION EXPERIMENT

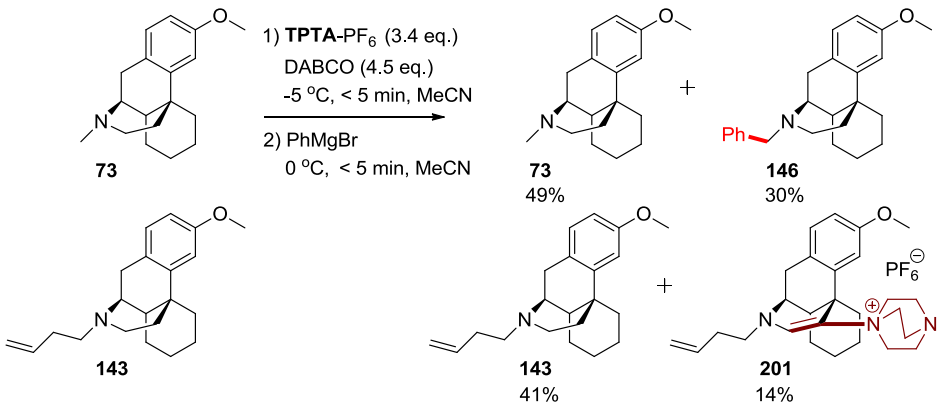

Reaction conducted according to **General Procedure 3**, using a 1 : 1 mixture of **73** (0.46 mmol) and **143** (0.46 mmol) as starting material and phenylmagnesium bromide (1.0 M in THF) as a nucleophile. DABCO (2.06 mmol, 4.5 eq.) and **TPTA**-PF_6 (1.56 mmol, 3.4 eq.) [relative to a single substrate (**73**), assuming that **143** would act as a dummy substrate and not interfere with the reaction of **73**]. ^{1}H NMR of the crude reaction mixture (the concentrated DCM/MeOH fractions after the silica plug) revealed a 49% yield of **73** and 41% yield of **143** by comparison with an added internal standard (1,3,5-trimethoxybenzene, 7.7 mg, 46.0 μmol, 10 mol%). Product **146** was observed in 30% yield. In addition, DABCO-enamine adduct **201** was observed in 14% yield.

This reaction indicates interference of substrate (**143**) in the normally successful reaction of substrate (**73**). The results of the these competition experiments point to interference of the 'dummy' substrate on the reaction of the normally successful substrate. Stephenson reported that increasing the equivalents of *N*-methylmorpholine led to erosion of *N*-C**H**$_3$ selectivity in his reported coupling of the *N*-methylmorpholine α-amino radical with arenes.[119] It was proposed that the primary α-amino radical could undergo HAT with the starting material to give the more stable secondary α-amino radical, serving to divert the normal reaction pathway. A similar pathway might operate in these competition experiments.

1-((4B*S*,9*S*)-11-(But-3-en-1-yl)-3-methoxy-6,7,8,8a,9,10-hexahydro-5*H*-9,4b-(epiminoetheno)phenanthren-13-yl)-1,4-diazabicyclo[2.2.2]octan-1-ium bicarbonate (*201*)

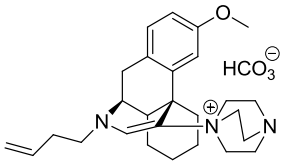

201

From the experiment on the previous page: MDAP purification (low pH) gave (after basification using sat. aq. $NaHCO_3$ and extraction with DCM as described above) ***201*** as a pale brown residue (21.4 mg, 10%);[†] IR ν_{max} (neat) 3404 - 2860 (br., O-H, C-H), 1686 (C=C), 1634 (C=O), 1608 (Ar), 1576 (Ar), 1497 (Ar), 1463 (Ar), 1426, 1341, 1319, 1290, 1238 cm^{-1}; ^1H NMR (400 MHz, $CDCl_3$) δ 7.19 (1H, s, C*H*), 7.08 (1H, d, *J* = 8.4 Hz, C*H*), 6.78 (1H, d, *J* = 2.5 Hz, C*H*), 6.67 (1H, dd, *J* = 8.5, 2.3 Hz, C*H*), 5.87 - 5.76 (1H, m, C*H*), 5.15 - 5.04 (2H, m, CH_2), 3.78 (3H, s, CH_3), 3.78 - 3.63 (6H, m, CH_2), 3.38 - 3.28 (1H, m, CH_2) 3.28 - 3.12 (8H, m, CH_2, C*H*), 3.07 - 2.94 (2H, m, CH_2), 2.89 (1H, d, *J* = 18.1 Hz, CH_3), 2.48 (1H, br. s, C*H*),[‡] 2.35 (2H, q, *J* = 7.0 Hz, CH_2), 1.92 - 1.83 (1H, m, CH_2), 1.78 - 1.70 (1H, m, CH_2), 1.67 - 1.60 (1H, m, CH_2), 1.57 - 1.50 (1H, m, CH_2), 1.50 - 1.43 (1H, m, CH_2), 1.43 - 1.24 (2H, m, CH_2), 1.05 - 0.91 (1H, m, CH_2); ^{13}C NMR (101 MHz, $CDCl_3$)[§] δ 157.4 (*C*), 140.4 (*C*), 135.4 (*C*H), 135.2 (*C*H_2), 131.0 (*C*H), 126.7 (*C*), 121.6 (*C*), 117.1 (*C*H), 113.7 (*C*H), 109.9 (*C*H), 57.1 (*C*H_2), 55.4 (*C*H_3), 53.2 (*C*H_2), 52.4 (*C*H), 46.0 (*C*H_2), 43.8 (*C*H), 41.9 (*C*), 35.3 (*C*H_2), 34.0 (*C*H_2), 33.6 (*C*H_2), 26.2 (*C*H_2), 25.4 (C*H*$_2$), 21.8 (C*H*$_2$); HRMS (+ESI) *m/z* calculated for $C_{27}H_{38}N_3O$ [M] 420.2997; Found 420.3009.

[†]Tentatively assigned as the bicarbonate salt based on the sodium bicarbonate present in the reverse-phase chromatography eluant and the IR stretch at 1689 cm^{-1}, [‡]Tentatively assigned to *H*CO_3^-; the broadening of the singlet made integration inaccurate. [§]The ^{13}C signal for the bicarbonate anion could not be observed.

5.25. REACTION OF AN *N*-BENZYL-*N*-METHYL-*N*-ALKYL TRIALKYLAMINE

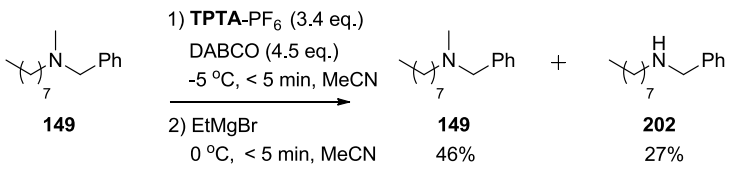

This reaction was conducted according to **General Procedure 3**, using **149** (0.17 mmol) as starting material and ethylmagnesium bromide (3.0 M in Et_2O) as a nucleophile. ^{1}H NMR of the crude reaction mixture (the concentrated DCM/MeOH fractions after the silica plug) revealed a 46% yield of returned starting material **149** and 27% yield of secondary amine **202** by comparison with an added internal standard (1,3,5-trimethoxybenzene, 2.9 mg, 17.0 μmol, 10 mol%). No *N*-C**H**$_2$ or *N*-C**H**$_3$ functionalised products were observed.

This reaction indicates preferential functionalisation of *N*-C**H**$_3$ to *N*-C**H**$_2$ in an open-chain system, but suffers from poor conversion and *N*-demethylation occurs rather than *N*-C**H**$_3$ functionalisation (*N*-C**H**$_2$ functionalisation was not observed at either the benzylic *N*-C**H**$_2$ or the octyl *N*-C**H**$_2$ position). This observation is consistent with that observed in the synthesis of **161** from *N*-methyldioctylamine (**160**), as well as the *N*-demethylation observed in the syntheses of **165b** and **166b** from scopolamine derivatives, alluding to steric deactivation of the *N*-C**H**$_3$ group in these molecules.

N-Benzyloctan-1-amine (202)

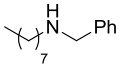

From the experiment on the previous page: MDAP purification (high pH) gave **202** as a pale brown oil (8.8 mg, 23%); IR ν_{max} (neat) 2925 - 2855 (C-H), 1497 (Ar), 1456 (Ar), cm^{-1}; ^{1}H NMR (400 MHz, $CDCl_3$) δ 7.37 - 7.22 (5H, s, C*H*), 3.79 (2H, s, CH_2), 2.63 (2H, t, *J* = 7.2 Hz, CH_2), 1.55 - 1.46 (2H, m, CH_2), 1.36 - 1.19 (10H, m, CH_2), 0.88 (3H, t, *J* = 7.0 Hz, CH_3); ^{13}C NMR (101

MHz, $CDCl_3$) δ 140.5 (*C*), 128.4 (*C*H), 128.1 (*C*H), 126.8 (*C*H), 54.1 (*C*H_2), 49.5 (*C*H_2), 31.8 (*C*H_2), 30.1 (*C*H_2), 29.5 (*C*H_2), 29.3 (*C*H_2), 27.4 (*C*H_2), 22.7 (*C*H_2), 14.1 (*C*H_3); HRMS (+ESI) *m/z* calculated for $C_{15}H_{26}N$ [$M+H^+$] 220.2060; Found 220.2055. Data are consistent with the literature.[250]

5.26. Reaction of dextromethorphan in Deuterated Solvent with TPBPA-PF_6 Oxidant to Detect the Intermediate Iminium Equivalent

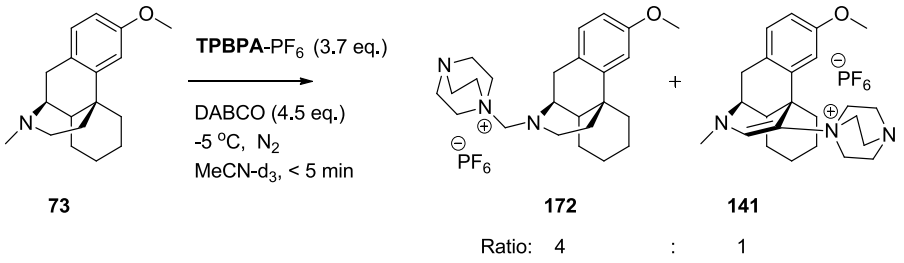

A reaction vessel was charged with dextromethorphan **73** (14.0 mg, 50.0 μmol), DABCO (11.6 mg, 0.1 mmol, 2.0 eq.) and MeCN-d_3 (1.5 mL) and was stirred at -5 °C under a funnel of N_2. **TPBPA**-PF_6 (32.0 mg, 50.0 μmol, 1.0 eq.) was added as a solid under an atmosphere of N_2. Further portions (3x) of **TPBPA**-PF_6 (9.3 mg, 0.3 eq.) were added. A brown slurry was observed. DABCO (5.8 mg, 1.0 eq.) was added as a solid. Further portions (3x) of **TPBPA**-PF_6 (9.3 mg, 0.3 eq.) were added. DABCO (5.8 mg, 1.0 eq.) was added. Further portions (3x) of **TPBPA**-PF_6 (9.3 mg, 0.3 eq.) were added. DABCO (5.8 mg, 1.0 eq.) was added. Further portions (2x) of **TPBPA**-PF_6 (9.3 mg, 0.3 eq.) were added. Full conversion was observed by LCMS (Figure 47). Stirring was ceased and the precipitate allowed to settle. The reaction mixture was pale red in colour, and the supernatant was taken for NMR analysis (Figure 48-50). By ^{1}H NMR, no iminium salt N^+=C***H***$_2$ was detected (Figure 48).

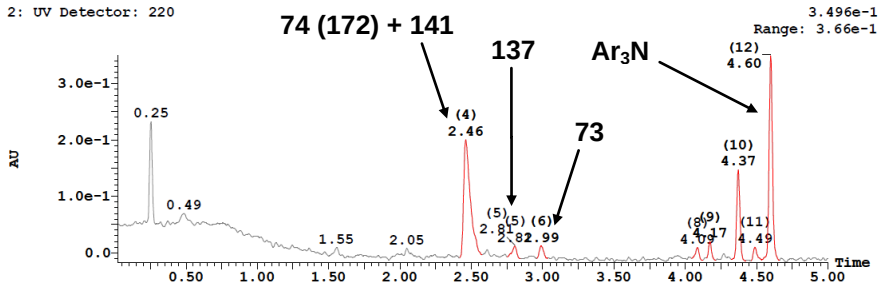

***Figure 47**: LCMS trace (high pH) for oxidation of dextromethorphan using **TPBPA**-PF_6 (4.3 eq.) as oxidant and DABCO (5.0 eq.) as base, in MeCN-d_3.*

The ^{1}H doublets at δ 4.20 ppm and δ 3.89 ppm were tentatively assigned as N-C***H***$_2$-N$^+$ [the coupling constant is consistent with geminal coupling (*J* = 12.4 Hz)]. The ^{13}C peak at δ 87.1 ppm was tentatively assigned as the bridging N-***C***H$_2$-N$^+$ due to downfield chemical shift (Figure 49). The ^{1}H doublets at δ 4.20 ppm and δ 3.89 ppm are coupling by COSY, assigned as N-C***H***$_2$-N$^+$ (Figure 50). The ^{1}H doublets at δ 4.20 ppm and δ 3.89 ppm are coupling to the ^{13}C peak at δ 87.1 ppm by HSQC. This carbon was assigned as N-***C***H$_2$-N$^+$. Coupling was observed between the ^{1}H doublet at δ 4.20 ppm (N-C***H***$_2$-N$^+$) and the ^{13}C peak at δ 59.8 ppm *N*-***C***HR′R″ by HMBC.

^{1}H NMR (400 MHz, MeCN-d_3) - crude reaction mixture

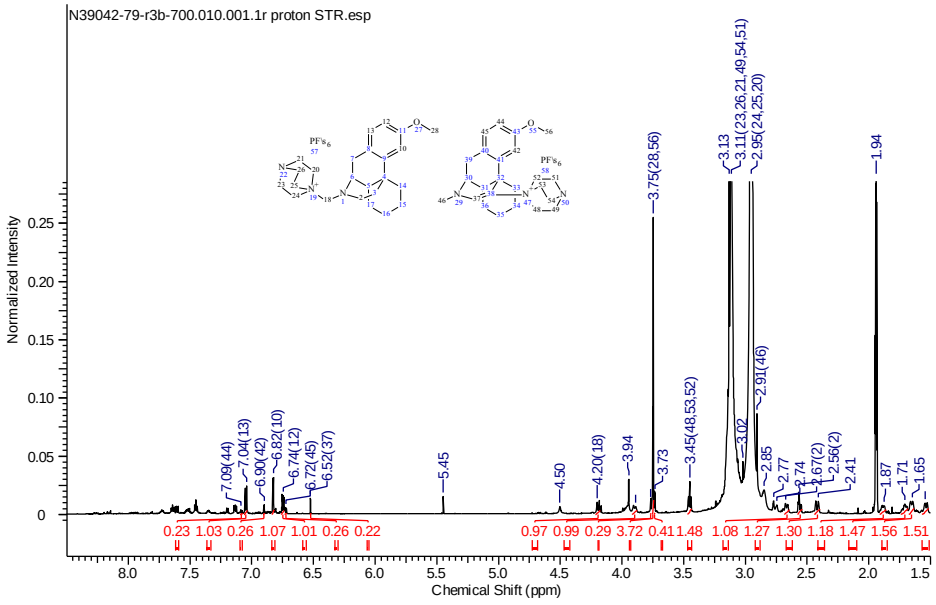

^{1}H NMR (400 MHz, MeCN-d_3) - crude reaction mixture expanded

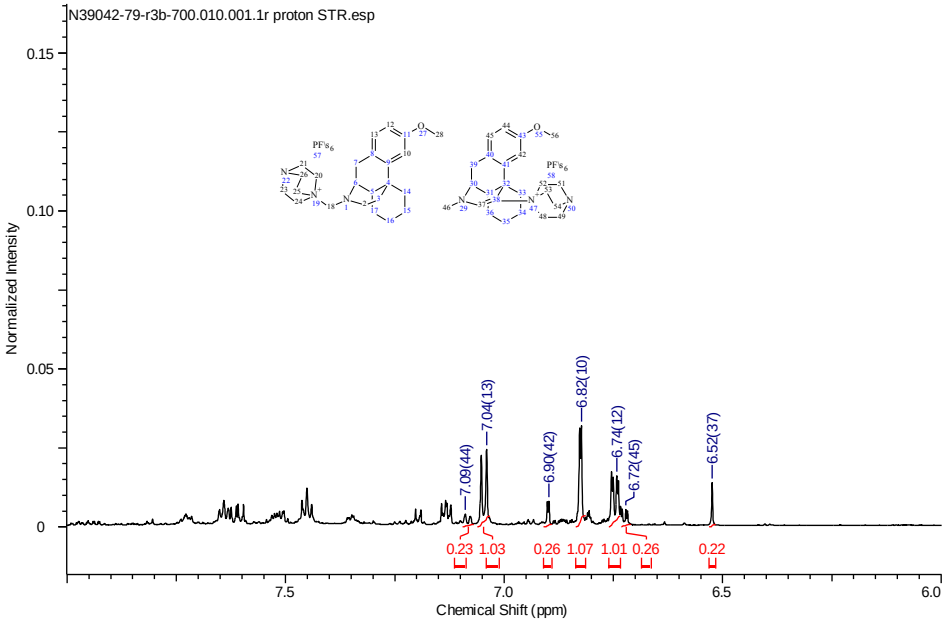

^{1}H NMR (400 MHz, MeCN-d_3) - crude reaction mixture expanded

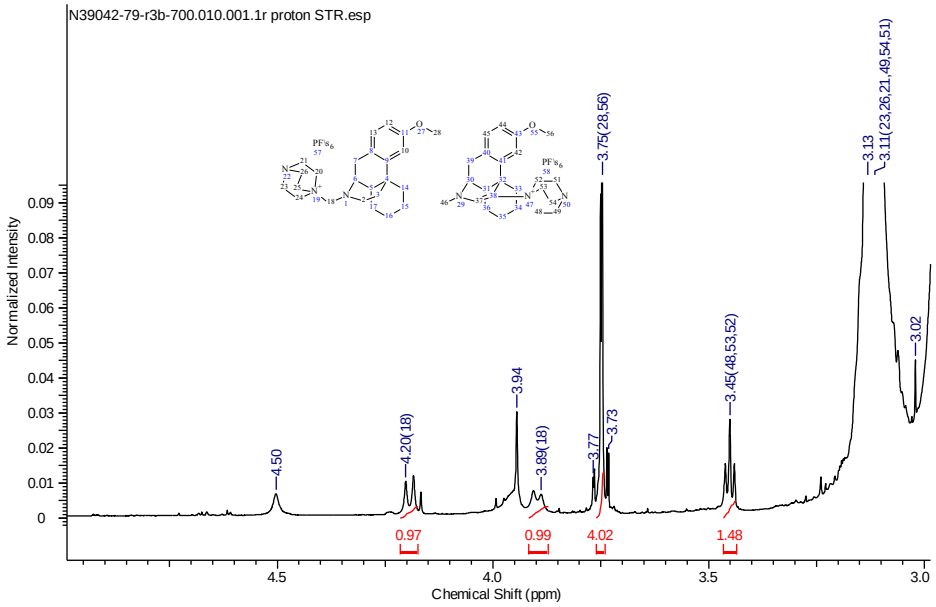

***Figure 48**: ^{1}H NMR of **TPBPA**-PF_6/DABCO-mediated oxidation of **73**.*

^{13}C NMR (101 MHz, MeCN-d_3) - crude reaction mixture expanded

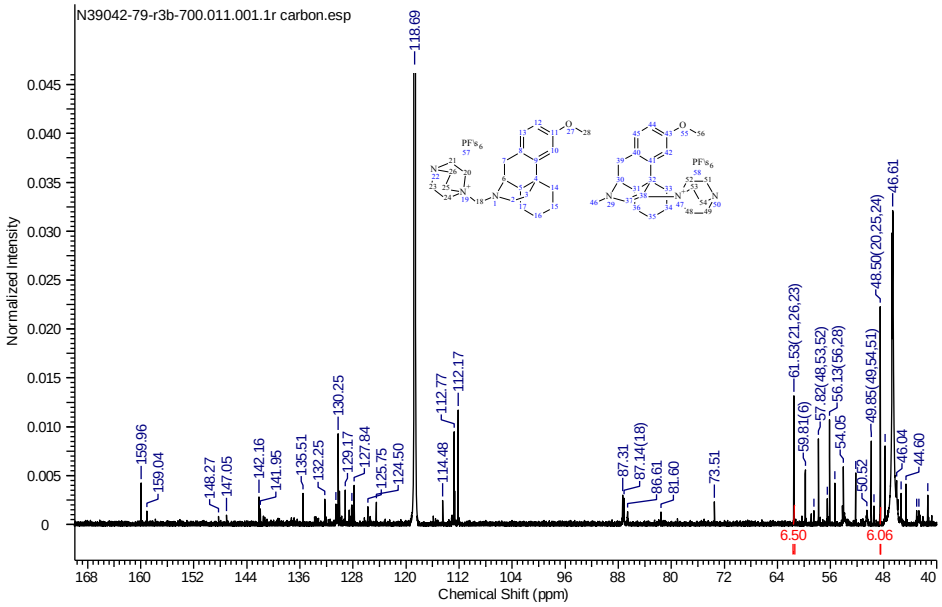

DEPT NMR (101 MHz, MeCN-d_3) - crude reaction mixture expanded

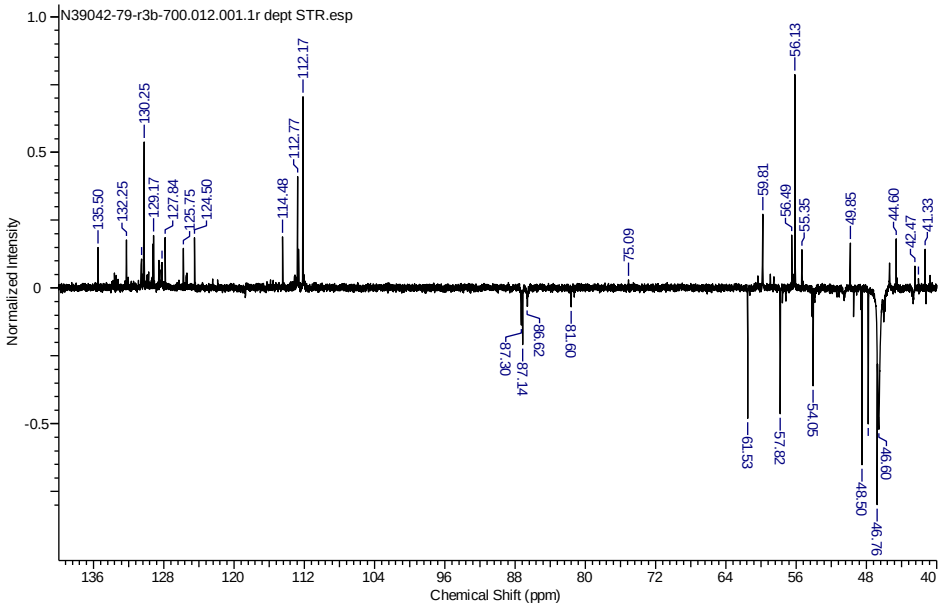

***Figure 49**: ^{13}C and DEPT-135 NMR of the crude reaction mixture from **TPBPA**-PF_6/DABCO-mediated oxidation of **73**.*

COSY NMR (MeCN-d_3) - crude reaction mixture expanded

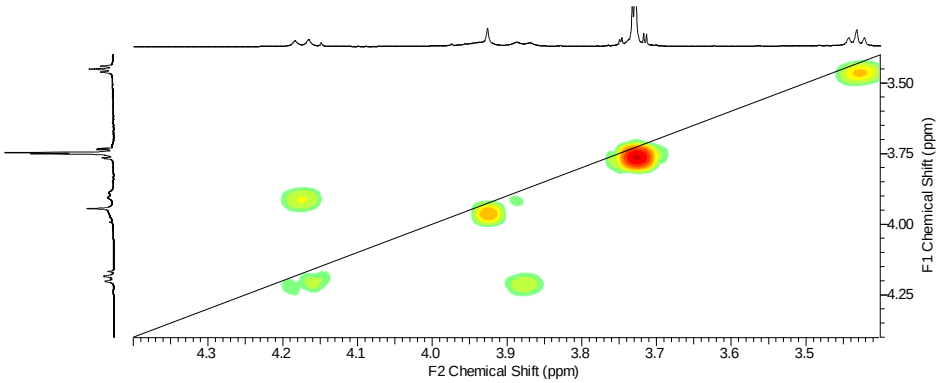

HSQC NMR (MeCN-d_3) - crude reaction mixture expanded

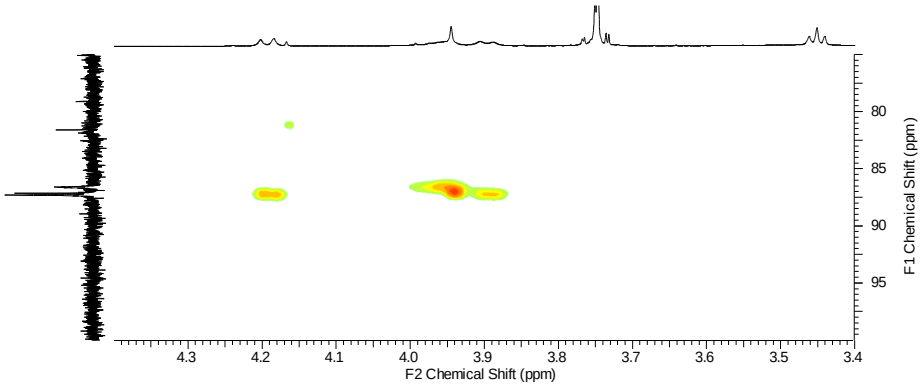

HMBC NMR (MeCN-d_3) - crude reaction mixture expanded

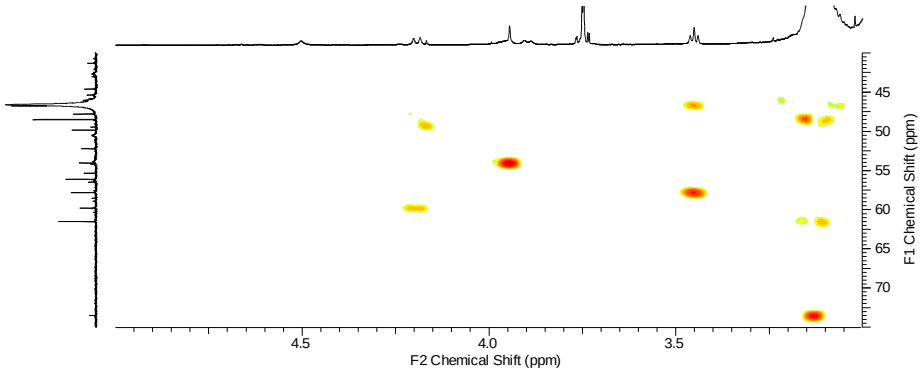

***Figure 50**: COSY, HSQC and HMBC NMR of the crude reaction mixture from **TPBPA**-PF_6/DABCO-mediated oxidation of **73** with revealing **172** and **141** with key couplings.*

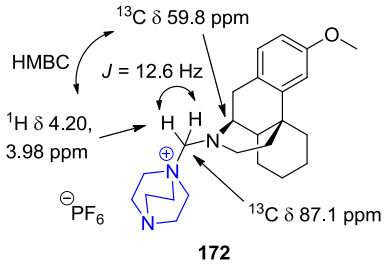

172

***Figure 50**: Key NMR shifts and couplings identifying **172**.*

HMBC couplings were observed between the ^{13}C peaks at δ 61.5 ppm, δ 48.5 ppm and the large, broad ^{1}H singlets at δ 3.1 and δ 3.0 ppm (from DABCO-derived species) but the DABCO-fragment C***H***$_2$'s of **172** could not be resolved and long-range coupling could not be conclusively verified.

5.27. COMPUTATIONAL INVESTIGATIONS

All calculations were performed using Density Functional Theory (DFT)[251,252] using the Gaussian09 software package.[189] All minima (reactants, intermediates, products) and maxima (transition states) were optimised using the UB3LYP functional with a 6-31+G(d,p) basis set on all atoms,[253] paralleling a study on hydrogen atom abstraction from tertiary amines using the cumyloxyl radical.[254] Solvation was modelled implicitly using the Conductor-like Polarisable Continuum Model (C-PCM)[255,256] for acetonitrile solvent. Frequency calculations were performed on all optimised structures in order to characterise minima (zero imaginary frequencies) and maxima (single imaginary frequency). All profiles are plotted using the Gibbs free energy values. GaussView 5.0.9 was used for the visualisation of structures. Computational data, reaction profiles and XYZ co-ordinates are contained within the Appendix.

6. REFERENCES

(1) Endoma-Arias, M. A. A.; Cox, D. P.; Hudlicky, T. *Adv. Synth. Catal.* **2013**, *355*, 1869–1873.

(2) Prommer, E. *Supp. Care Cancer* **2006**, *14*, 109–115.

(3) Deer, T. R.; Leong, M. S.; Buvanendran, A.; Gordin, V.; Kim, P. S.; Panchal, S. J.; Ray, A. L. *Comprehensive Treatment of Chronic Pain by Medical, Interventional, and Integrative Approaches*, 1st ed.; Springer: New York, 2013.

(4) Pasternak, G. W. *The Opiate Receptors*, 2nd Ed.; Humana Press, New York, 2011.

(5) *International Narcotics Control Board. Narcotic Drugs, Estimated world requirements for 2000, Statistics for 1998.*; United Nations, New York, 2000.

(6) Werner, L.; Machara, A.; Adams, D. R.; Cox, D. P.; Hudlicky, T. *J. Org. Chem.* **2011**, *76*, 4628–4634.

(7) McCamley, K.; Ripper, J. A.; Singer, R. D.; Scammells, P. J. *J. Org. Chem.* **2003**, *68*, 9847–9850.

(8) Dong, Z.; Scammells, P. J. *J. Org. Chem.* **2007**, *72*, 9881–9885.

(9) von Braun, J. *Chem. Ber.* **1909**, *42*, 2035–2057.

(10) von Braun, J. *Chem. Ber.* **1911**, *44*, 1252–1260.

(11) Hageman, H. A.; Elderfield, R. C. *J. Org. Chem.* **1949**, *14*, 605–637.

(12) Evain, E. J.; Cooley, J. H. *Synthesis* **1989**, *1*, 1–7.

(13) Olofson, R. A.; Schnur, R. C.; Bunes, L.; Pepe, J. P. *Tetrahedron Lett.* **1977**, *18*, 1567–1570.

(14) Olofson, R. A.; Martz, J. T. *J. Org. Chem.* **1984**, *49*, 2081–2082.

(15) Grierson, D. *The Polonovski Reaction. Organic Reactions*; John Wiley & Sons, 2004.

(16) Polonovski, M.; Polonovski, M. *Bull. Soc. Chim. Fr.* **1927**, *41*, 1190–1208.

(17) Singh, G.; Koerner, T. B.; Godefroy, S. B.; Armand, C. *Bioorg. Med. Chem. Lett.* **2012**, *22*, 2160–2162.

(18) Mary, A.; Renko, D. Z.; Guillou, C.; Thal, C. *Tetrahedron Lett.* **1997**, *38*, 5151–5152.

(19) Ferris, J. P.; Gerwe, R. D.; Gapski, G. R. *J. Am. Chem. Soc.* **1967**, *89*, 5270–5275.

(20) Kok, G. B.; Pye, C. C.; Singer, R. D.; Scammells, P. J. *J. Org. Chem.*

2010, *75*, 4806–4811.

(21) Kawano, Y.; Otsubo, K.; Matsubara, J.; Kitano, K.; Ohtano, T.; Morita, S.; Uchida, M. *Heterocycles* **1999**, *50*, 17–20.

(22) Projean, D.; Morin, P.-E.; Tu, T. M.; Ducharme, J. *Xenobiotica.* **2003**, *33*, 841–854.

(23) Falnes, P.; Johansen, R. F.; Seeberg, E. *Nature* **2002**, *419*, 2860–2863.

(24) Huq, F. *Asian J. Biochem.* **2006**, *1*, 276–286.

(25) Ann, M.; Iwasakit, M.; Guengericht, F. P.; Kadlubar, F. F. *Proc. Natl. Acad. Sci. U. S. A.* **1989**, *86*, 7696–7700.

(26) Aas, P. A.; Otterlei, M.; Falnes, P.; Vagbe, C. B.; Skorpen, F.; Akbari, M.; Sundhelm, O.; Bjoras, M.; Slupphaug, G.; Seeberg, E.; Krokan, H. E. *Nature* **2003**, *421*, 859–863.

(27) Boess, E.; Schmitz, C.; Klussmann, M. *J. Am. Chem. Soc.* **2012**, *134*, 5317–5325.

(28) Chaudhary, V.; Leisch, H.; Moudra, A.; Allen, B.; De Luca, V.; Cox, D. P.; Hudlicky, T. *Collect. Czech. Chem. C.* **2009**, *74*, 1179–1193.

(29) Li, Z.; Li, C.-J. *J. Am. Chem. Soc.* **2005**, *127*, 3672–3673.

(30) Ratnikov, M. O.; Xu, X.; Doyle, M. P. *J. Am. Chem. Soc.* **2013**, *135*, 9475–9479.

(31) Goto, Y.; Watanabe, Y.; Fukuzumi, S.; Jones, J. P.; Dinnocenzo, J. P. *J. Am. Chem. Soc.* **1998**, *120*, 10762–10763.

(32) Dhineshkumar, J.; Lamani, M.; Alagiri, K.; Prabhu, K. R. *Org. Lett.* **2013**, *15*, 1092–1095.

(33) Nobuta, T.; Tada, N.; Fujiya, A.; Kariya, A.; Miura, T.; Itoh, A. *Org. Lett.* **2013**, *15*, 547–577.

(34) Huo, C.; Wu, M.; Jia, X.; Xie, H.; Yuan, Y.; Tang, J. *J. Org. Chem.* **2014**, *79*, 9860–9864.

(35) Bartling, H.; Eisenhofer, A.; König, B.; Gschwind, R. M. *J. Am. Chem. Soc.* **2016**, *138*, 11860–11871.

(36) Huo, C.; Wang, C.; Wu, M.; Jia, X.; Wang, X.; Yuan, Y.; Xie, H. *Org. Biomol. Chem.* **2014**, *12*, 3123–3128.

(37) Ciminale, F.; Lopez, L.; Farinola, G. M.; Sportelli, S. *Tetrahedron Lett.* **2001**, *42*, 5685–5687.

(38) Ciminale, F.; Lopez, L.; Nacci, A.; D'Accolti, L.; Vitale, F. *Eur. J. Org. Chem.* **2005**, 1597–1603.

(39) Todres, Z. V. *Ion Radical Organic Chemistry: Principles and Applications*, 2nd ed.; CRC Press, 2008.

(40) Cowell, G. W.; Ledwith, A.; White, A. C.; Woods, H. J. *J. Chem. Soc. B* **1970**, 227–231.

(41) Tsang, A. S.-K.; Jensen, P.; Hook, J. M.; Hashmi, A. S. K.; Todd, M. H. *Pure Appl. Chem.* **2011**, *83*, 655–665.

(42) Jones, K. M.; Karier, P.; Klussmann, M. *ChemCatChem* **2012**, *4*, 51–54.

(43) Murahashi, S.-I.; Komiya, N.; Terai, H.; Nakae, T. *J. Am. Chem. Soc.* **2003**, *125*, 15312–15313.

(44) Muramatsu, W.; Nakano, K.; Li, C.-J. *Org. Biomol. Chem.* **2014**, *12*, 2189–2192.

(45) Chiba, T.; Takata, Y. *J. Org. Chem.* **1977**, *42*, 2974–2977.

(46) Li, Z.; Li, C.-J. *J. Am. Chem. Soc.* **2005**, *127*, 6968–6969.

(47) Baslé, O.; Li, C.-J. *Org. Lett.* **2008**, *10*, 3661–3663.

(48) Fu, W.; Guo, W.; Zou, G.; Xu, C. *J. Fluor. Chem.* **2012**, *140*, 88–94.

(49) Singh, K. N.; Kessar, S. V.; Singh, P.; Singh, P.; Kaur, M.; Batra, A. *Synthesis* **2014**, *46*, 2644–2650.

(50) Santamaria, J.; Kaddachi, M. T. *Synlett* **1991**, 739–740.

(51) Brouwer, A. M.; Zwier, J. M.; Svendsen, C.; Mortensen, O. S.; Langkilde, F. W.; Wilbrandt, R. *J. Am. Chem. Soc.* **1998**, *120*, 3748–3757.

(52) Santamaria, J. *Pure Appl. Chem.* **1995**, *67*, 141–147.

(53) Kohls, P.; Jadhav, D.; Pandey, G.; Reiser, O. *Org. Lett.* **2012**, *14*, 672–675.

(54) Espelt, L. R.; Wiensch, E. M.; Yoon, T. P. *J. Org. Chem.* **2013**, *78*, 4107–4114.

(55) Scaiano, J. C. *J. Phys. Chem.* **1981**, *85*, 2851–2855.

(56) Walton, J. C.; Nonhebel, D. C. *J. Chem. Soc. Perkin Trans. 2* **1987**, 1789–1794.

(57) Barham, J. P.; John, M. P.; Murphy, J. A. *Beilstein J. Org. Chem.* **2014**, *10*, 2981–2988.

(58) Franz, J. F.; Kraus, B.; Zeitler, K. *Chem. Commun.* **2015**, *51*, 8280–8283.

(59) Cesario, C.; Miller, M. J. *Tetrahedron Lett.* **2010**, *51*, 3050–3052.

(60) Wagner, A.; Ofial, A. R. *J. Org. Chem.* **2015**, *80*, 2848–2854.

(61) Wilson, I. R.; Harris, G. M. *J. Am. Chem. Soc.* **1960**, *82*, 4515–4517.

(62) Wagner, A.; Han, W.; Mayer, P.; Ofial, A. R. *Adv. Synth. Catal.* **2013**, *355*, 3058–3070.

(63) Allen, J. M.; Lambert, T. H. *J. Am. Chem. Soc.* **2011**, *133*, 1260–1262.

(64) Chen, C.-K.; Hortmann, A. G.; Marzabadi, M. R. *J. Am. Chem. Soc.* **1988**, *110*, 4829–4831.

(65) Yamaguchi, K.; Wang, Y.; Mizuno, N. *ChemCatChem* **2013**, *5*, 2835–

2838.

(66) Panwar, V.; Kumar, P.; Bansal, A.; Ray, S. S.; Jain, S. L. *Appl. Catal. A. Gen.* **2015**, *498*, 25–31.

(67) Jahn, U.; Aussieker, S. *Org. Lett.* **1999**, *1*, 849–852.

(68) McGonagle, F. I.; Sneddon, H. F.; Jamieson, C.; Watson, A. J. B. *ACS Sustain. Chem. Eng.* **2014**, *2*, 523–532.

(69) Li, Q.; Liskey, C. W.; Hartwig, J. F. *J. Am. Chem. Soc.* **2014**, *136*, 8755–8765.

(70) Topczewski, J. J.; Cabrera, P. J.; Saper, N. I.; Sanford, M. S. *Nature* **2016**, *531*, 220–224.

(71) Mbofana, C. T.; Chong, E.; Lawniczak, J.; Sanford, M. S. *Org. Lett.* **2016**, *18*, 4258–4261.

(72) Nako, A. E.; Oyamada, J.; Nishiura, M.; Hou, Z. *Chem. Sci.* **2016**, *7*, 6429–6434.

(73) Ciamician, G. *Science* **1912**, *36*, 385–394.

(74) Yoon, T. P.; Ischay, M. A.; Du, J. *Nat. Chem.* **2010**, *2*, 527–532.

(75) Prier, C. K.; Rankic, D. A.; MacMillan, D. W. C. *Chem. Rev.* **2013**, *113*, 5322–5363.

(76) Tucker, J. W.; Stephenson, C. R. J. *J. Org. Chem.* **2012**, *77*, 1617–1622.

(77) Hu, J.; Wang, J.; Nguyen, T. H.; Zheng, N. *Beilstein J. Org. Chem.* **2013**, *9*, 1977–2001.

(78) Kärkäs, M. D.; Porco Jr., J. A.; Stephenson, C. R. J. *Chem. Rev.* **2016**, *116*, 9683–9747.

(79) Coyle, J. D. *Photochemistry in organic synthesis*; The Royal Society of Chemistry: London, 1986.

(80) Shaw, M. H.; Twilton, J.; Macmillan, D. W. C. *J. Org. Chem.* **2016**, *81*, 6898–6926.

(81) Brimioulle, R.; Lenhart, D.; Maturi, M. M.; Bach, T. *Angew. Chem. Int. Ed.* **2015**, *54*, 3872–3890.

(82) Hurtley, A. E.; Lu, Z.; Yoon, T. P. *Angew. Chem. Int. Ed.* **2014**, *53*, 8991–8994.

(83) Barltrop, J. A.; Coyle, J. D. *Principles of photochemistry*; Wiley: Chichester, 1978.

(84) Knowles, J. P.; Elliott, L. D.; Booker-Milburn, K. I. *Beilstein J. Org. Chem.* **2012**, *8*, 2025–2052.

(85) Xi, Y.; Yi, H.; Lei, A. *Org. Biomol. Chem.* **2013**, *11*, 2387–2403.

(86) Muller, P.; Brettel, K. *Photochem. Photobiol. Sci.* **2012**, *11*, 632–636.

(87) Juris, A.; Balzani, V. *Helv. Chim. Acta* **1981**, *64*, 2175–2182.

(88) Lombard, J.; Boulaouche, R.; Amilan Jose, D.; Chauvin, J.; Collomb, M.-N.; Deronzier, A. *Inorg. Chim. Acta* **2010**, *363*, 234–242.

(89) Nakamaru, K. *Bull. Chem. Soc. Jpn.* **1982**, *55*, 2697–2705.

(90) Rueping, M.; Vila, C.; Koenigs, R. M.; Poscharny, K.; Fabry, D. C. *Chem. Commun.* **2011**, *47*, 2360–2362.

(91) Dixon, I. M.; Collin, J.-P.; Sauvage, J.-P.; Flamigni, L.; Encinas, S.; Barigelletti, F. *Chem. Soc. Rev.* **2000**, *29*, 385–391.

(92) Nguyen, J. D.; D'Amato, E. M.; Narayanam, J. M. R.; Stephenson, C. R. J. *Nat. Chem.* **2012**, *4*, 854–859.

(93) Teegardin, K.; Day, J. I.; Chan, J.; Weaver, J. *Org. Process Res. Dev.* **2016**, *20*, 1156–1163.

(94) Nelsen, S. F.; Ippoliti, J. T. *J. Am. Chem. Soc.* **1986**, *108*, 4879–4881.

(95) Lindsay Smith, J. P.; Kelly, R. P. *J. Chem. Soc., Chem. Commun.* **1978**, 329–330.

(96) Freeman, D. B.; Furst, L.; Condie, A. G.; Stephenson, C. R. J. *Org. Lett.* **2012**, *14*, 94–97.

(97) Beatty, J. W.; Stephenson, C. R. J. *Acc. Chem. Res.* **2015**, *48*, 1474–1484.

(98) Condie, A. G.; González-Gómez, J. C.; Stephenson, C. R. J. *J. Am. Chem. Soc.* **2010**, *132*, 1464–1465.

(99) Jeffrey, J. L.; Terrett, J. A.; MacMillan, D. W. C. *Science* **2015**, *349*, 1532–1536.

(100) Shaw, M. H.; Shurtleff, V. W.; Terrett, J. A.; Cuthbertson, J. D.; Macmillan, D. W. C. *Science* **2016**, *352*, 1304–1308.

(101) Santamaria, J.; Ouchabane, R.; Rigaudy, J. *Tetrahedron Lett.* **1989**, *30*, 3977–3980.

(102) Zou, Y.-Q.; Chen, J.-R.; Liu, X.-P.; Lu, L.-Q.; Davis, R. L.; Jørgensen, K. A.; Xiao, W.-J. *Angew. Chem. Int. Ed.* **2012**, *51*, 784–788.

(103) Davies, A. G. *J. Chem. Res.* **2008**, *7*, 361–375.

(104) Pitre, S. P.; McTiernan, C. D.; Ismaili, H.; Scaiano, J. C. *J. Am. Chem. Soc.* **2013**, *135*, 13286–13289.

(105) Narayanam, J. M. R.; Tucker, J. W.; Stephenson, C. R. J. *J. Am. Chem. Soc.* **2009**, *131*, 8756–8757.

(106) Ghosh, I.; Ghosh, T.; Bardagi, J. I.; König, B. *Science* **2014**, *346*, 725–728.

(107) Fry, A. J.; Krieger, R. L. *J. Org. Chem.* **1976**, *41*, 54–57.

(108) Pause, L.; Robert, M.; Savéant, J.-M. *J. Am. Chem. Soc.* **1999**, *121*, 7158–7159.

(109) Gosztola, D.; Niemczyk, M. P.; Svec, W.; Lukas, A. S.; Wasielewski, M.

R. *J. Phys. Chem. A* **2000**, *104*, 6545–6551.

(110) Romero, N. A.; Nicewicz, D. A. *Chem. Rev.* **2016**, *116*, 10075–10166.

(111) Ghosh, I.; König, B. *Angew. Chem. Int. Ed.* **2016**, *55*, 7676–7679.

(112) König, B.; Hari, D. P. *Org. Lett.* **2011**, *13*, 3852–3855.

(113) Zhong, J.-J.; Meng, Q.-Y.; Liu, B.; Li, X.-B.; Gao, X.-W.; Lei, T.; Wu, C.-J.; Li, Z.-J.; Tung, C.-H.; Wu, L.-Z. *Org. Lett.* **2014**, *16*, 1988–1991.

(114) Bergonzini, G.; Schindler, C. S.; Wallentin, C.; Jacobsen, E. N.; Stephenson, C. R. J. *Chem. Sci.* **2014**, *5*, 112–116.

(115) Tucker, J. W.; Zhang, Y.; Jamison, T. F.; Stephenson, C. R. J. *Angew. Chem. Int. Ed.* **2012**, *51*, 4144–4147.

(116) Rueping, M.; Vila, C.; Bootwicha, T. *ACS Catal.* **2013**, *3*, 1676–1680.

(117) Huyser, E. S. *J. Am. Chem. Soc.* **1960**, *82*, 391–393.

(118) Cismesia, M. A.; Yoon, T. P. *Chem. Sci.* **2015**, *6*, 5426–5434.

(119) Douglas, J. J.; Cole, K. P.; Stephenson, C. R. J. *J. Org. Chem.* **2014**, *79*, 11631–11643.

(120) Che, C.-M.; Kwong, H.-L.; Poon, C.-K.; Yam, V. W.-W. *J. Chem. Soc. Dalton Trans.* **1990**, 3215–3219.

(121) Xie, J.; Shi, S.; Zhang, T.; Mehrkens, N.; Rudolph, M.; Hashmi, A. S. K. *Angew. Chem. Int. Ed.* **2015**, *54*, 6046–6050.

(122) Fischer, H. *Chem. Rev.* **2001**, *101*, 3581–3610.

(123) Studer, A. *Chem.-Eur. J.* **2001**, *7*, 1159–1164.

(124) Gu, X.; Guo, Y.; Zhang, F.; Mebel, A. M.; Kaiser, R. I. *Chem. Phys. Lett.* **2007**, *436*, 7–14.

(125) Xie, J.; Yu, J.; Rudolph, M.; Rominger, F.; Hashmi, A. S. K. *Angew. Chem. Int. Ed.* **2016**, *55*, 9416–9421.

(126) Primer, D. N.; Karakaya, I.; Tellis, J. C.; Molander, G. A. *J. Am. Chem. Soc.* **2015**, *137*, 2195–2198.

(127) Gutierrez, O.; Tellis, J. C.; Primer, D. N.; Molander, G. A.; Kozlowski, M. C. *J. Am. Chem. Soc.* **2015**, *137*, 4896–4899.

(128) Bembenek, M. E.; Abell, C. W.; Chrisey, L. A.; Rozwadowska, M. D.; Gessner, W.; Brossi, A. *J. Med. Chem.* **1990**, *33*, 147–152.

(129) Naito, R.; Yonetoku, Y.; Okamoto, Y.; Toyoshima, A.; Ikeda, K.; Takeuchi, M. *J. Med. Chem.* **2005**, *48*, 6597–6606.

(130) Mack, D. J.; Weinrich, M. L.; Vitaku, E.; Njardarson, J. T. Top 200 Pharmaceutical Products by Worldwide Sales in 2008 http://njardarson.lab.arizona.edu/sites/njardarson.lab.arizona.edu/files/Top200PharmaceuticalProductsbyWordlwideSalesin2008v4.pdf (accessed Jan 20, 2016).

(131) Cass, L.; Frederik, W. S. *Am. J. Med. Sci.* **1963**, *246*, 550–557.

(132) Wanner, K. T.; Praschak, I.; Höfner, G.; Beer, H. *Arch. Pharm. Pharm. Med. Chem.* **1996**, *329*, 11–22.

(133) Buckley, B. R.; Christie, S. D. R.; Elsegood, M. R. J.; Gillings, C. M.; Bulman Page, P. C.; Pardoe, W. J. M. *Synlett* **2010**, 939–943.

(134) Li, Z.; Li, C.-J. *Org. Lett.* **2004**, *6*, 4997–4999.

(135) Li, Z.; MacLeod, P. D.; Li, C.-J. *Tetrahedron: Asymmetry* **2006**, *17*, 590–597.

(136) Möhlmann, L.; Blechert, S. *Adv. Synth. Catal.* **2014**, *356*, 2825–2829.

(137) Anastas, P. T.; Warner, J. C. *Green Chemistry: Theory and Practice*; Oxford University Press: New York, 2000.

(138) Gemmeren, M. V.; Lay, F.; List, B.; Douglas, J. J.; Nguyen, J. D.; Cole, K. P.; Stephenson, C. R. J. *Aldrichim. Acta* **2014**, *47*, 1–25.

(139) Nagib, D. A.; MacMillan, D. W. C. *Nature* **2011**, *480*, 224–228.

(140) Dirocco, D. A.; Dykstra, K.; Krska, S.; Vachal, P.; Conway, D. V; Tudge, M. *Angew. Chem. Int. Ed.* **2014**, *53*, 4802–4806.

(141) Beatty, J. W.; Douglas, J. J.; Miller, R.; McAtee, R. C.; Cole, K. P.; Stephenson, C. R. J. *Chem* **2016**, *1*, 456–472.

(142) Amara, Z.; Bellamy, J. F. B.; Horvath, R.; Miller, S. J.; Beeby, A.; Burgard, A.; Rossen, K.; Poliakoff, M.; George, M. W. *Nat. Chem.* **2015**, *7*, 489–495.

(143) Cambié, D.; Bottecchia, C.; Straathof, N. J. W.; Hessel, V.; Noël, T. *Chem. Rev.* **2016**, *116*, 10276–10341.

(144) Turconi, J.; Griolet, F.; Guevel, R.; Oddon, G.; Villa, R.; Geatti, A.; Hvala, M.; Rossen, K.; Göller, R.; Burgard, A. *Org. Process Res. Dev.* **2014**, *18*, 417–422.

(145) Isse, A. A.; Lin, C. Y.; Coote, M. L.; Gennaro, A. *J. Phys. Chem. B* **2011**, *115*, 678–684.

(146) Muramatsu, W.; Nakano, K.; Li, C.-J. *Org. Lett.* **2013**, *15*, 3650–3653.

(147) Zheng, Q.; Meng, W.; Jiang, G.; Yu, Z. *Org. Lett.* **2013**, *15*, 5928–5931.

(148) Ravelli, D.; Fagnoni, M.; Albini, A. *Chem. Soc. Rev.* **2013**, *42*, 97–113.

(149) Kharasch, M. S.; Reinmuth, O.; Urry, W. H. *J. Am. Chem. Soc.* **1947**, *69*, 1105–1110.

(150) Davis, M.; Deady, L. W.; Finch, A. J.; Smith, J. F. *Tetrahedron* **1973**, *29*, 349–352.

(151) Araki, S.; Shimizu, T.; Johar, P. S.; Jin, S.-J.; Butsugan, Y. *J. Org. Chem.* **1991**, *56*, 2538–2542.

(152) Shen, Z.-L.; Wang, S.-Y.; Chok, Y.-K.; Xu, Y.-H.; Loh, T.-P. *Chem. Rev.* **2013**, *113*, 271–401.

(153) Lee, K.; Lee, P. H. *Org. Lett.* **2008**, *10*, 2441–2444.

(154) Singh, K.; Singh, P.; Kaur, A.; Singh, P. *Synlett* **2012**, *23*, 760–764.

(155) Richter, H.; Fröhlich, R.; Daniliuc, C.-G.; García Mancheño, O. *Angew. Chem. Int. Ed.* **2012**, *51*, 8656–8660.

(156) Hoffman, M. Z.; Bolletta, F.; Moggi, L.; Hug, G. *J. Phys. Chem. Ref. Data* **1989**, *18*, 219–544.

(157) Blanc, S.; Pigot, T.; Cugnet, C.; Brown, R.; Lacombe, S. *Phys. Chem. Chem. Phys.* **2010**, *12*, 11280–11290.

(158) Achord, J. M.; Hussey, C. L. *Anal. Chem.* **1980**, *52*, 601–602.

(159) Stracke, F.; Heupel, M.; Thiel, E. *J. Photochem. Photobiol. A Chem.* **1999**, *126*, 51–58.

(160) Franco, C.; Olmsted III, J. *Talanta* **1990**, *37*, 905–909.

(161) DeLaive, P. J.; Foreman, T. K.; Giannotti, C.; Whitten, D. G. *J. Am. Chem. Soc.* **1980**, *102*, 5627–5631.

(162) Ischay, M. A.; Anzovino, M. E.; Du, J.; Yoon, T. P. *J. Am. Chem. Soc.* **2008**, *130*, 12886–12887.

(163) Kanoufi, F.; Zu, Y.; Bard, A. J. *J. Phys. Chem. B* **2001**, *105*, 210–216.

(164) Ghogare, A. A.; Greer, A. *Chem. Rev.* **2016**, *116*, 9994–10034.

(165) Kelly, J. M.; Tossi, A. B.; McConnell, D. J.; OhUigin, C. *Nucleic Acids Res.* **1985**, *13*, 6017–6034.

(166) Tossi, A. B.; Kelly, J. M. *Photochem. Photobiol.* **1989**, *49*, 545–556.

(167) DeRosa, M. C.; Crutchley, R. J. *Coord. Chem. Rev.* **2002**, *233-234*, 351–371.

(168) Kneas, K. A.; Xu, W.; Demas, J. N. *J. Chem. Educ.* **1997**, *74*, 696.

(169) Mills, A.; Thomas, M. D. *Analyst* **1998**, *123*, 1135–1140.

(170) Du, J.; Yoon, T. P. *J. Am. Chem. Soc.* **2009**, *131*, 14604–14605.

(171) Furst, L.; Matsuura, B. S.; Narayanam, J. M. R.; Tucker, J. W.; Stephenson, C. R. J. *Org. Lett.* **2010**, *12*, 3104–3107.

(172) Meyer, A. U.; Straková, K.; Slanina, T.; König, B. *Chem.-Eur. J.* **2016**, *22*, 8694–8699.

(173) Su, Z.; Mariano, P. S.; Falvey, D. E.; Yoon, U. C.; Oh, S. W. *J. Am. Chem. Soc.* **1998**, *120*, 10676–10686.

(174) Walter, R. I. *J. Am. Chem. Soc.* **1955**, *77*, 5999–6002.

(175) Li, Z.; Wu, Z.; Fu, W.; Liu, P.; Jiao, B.; Wang, D.; Zhou, G.; Hou, X. *J. Phys. Chem. C* **2012**, *116*, 20504–20512.

(176) Cai, L.; Qian, X.; Song, W.; Liu, T.; Tao, X.; Li, W.; Xie, X. *Tetrahedron* **2014**, *70*, 4754–4759.

(177) Richards, S. A.; Hollerton, J. C. *Essential Practical NMR for Organic Chemistry*; John Wiley & Sons, 2011.

(178) Waller, A. M.; Northing, R. J.; Compton, R. G. *J. Chem. Soc., Faraday Trans.* **1990**, *86*, 335–339.

(179) Eberson, L.; Olofsson, B.; Svensson, J.-O. *Acta Chem. Scand.* **1992**, *46*, 1005–1015.

(180) Eberson, L.; Olofsson, B. *Acta Chem. Scand.* **1989**, *43*, 698–701.

(181) Engel, P. S.; Hoque, A. K. M. M.; Scholz, J. N.; Shine, H. J.; Whitmire, K. H. *J. Am. Chem. Soc.* **1988**, *110*, 7880–7882.

(182) Rueping, M.; Koenigs, R. M.; Poscharny, K.; Fabry, D. C.; Leonori, D.; Vila, C. *Chem.-Eur. J.* **2012**, *18*, 5170–5174.

(183) Zheng, Z.-R.; Evans, D. H.; Nelsen, S. F. *J. Org. Chem.* **2000**, *65*, 1793–1798.

(184) Kim, D.; Scranton, A. B.; Stansbury, J. W. *J. Appl. Polym. Sci.* **2009**, *114*, 1535–1542.

(185) Smith Jr., J. O.; Taylor, H. S. *J. Chem. Phys.* **1939**, *7*, 390–396.

(186) Jeffrey, J. L.; Petronijević, F. R.; MacMillan, D. W. C. *J. Am. Chem. Soc.* **2015**, *137*, 8404–8407.

(187) Haake, M.; Böhme, von H. *Leibigs Ann. Chem.* **1967**, *705*, 147–153.

(188) Dinnocenzo, J. P.; Banach, T. E. *J. Am. Chem. Soc.* **1989**, *111*, 8646–8653.

(189) Frisch, M. J.; Trucks, G. W.; Schlegel, H. B.; Scuseria, G. E.; Robb, M. A.; Cheeseman, J. R.; Scalmani, G.; Barone, V.; Mennucci, B.; Petersson, G. A.; Nakatsuji, H.; Caricato, M.; Li, X.; Hratchian, H. P.; Izmaylov, A. F.; Bloino, J.; Zheng, G.; Sonnenberg, J. L.; Hada, M.; Ehara, M.; Toyota, K.; Fukada, R.; Hasegawa, J.; Ishida, M.; Nakajima, T.; Honda, Y.; Kitao, O.; Nakai, H.; Vreven, T.; Montgomery Jr, J. A.; Peralta, J. E.; Ogliaro, F.; Bearpark, M. J.; Heyd, J.; Brothers, E. N.; Kudin, K. N.; Staroverov, V. N. .; Kobayashi, R.; Normand, J.; Raghavachari, K.; Rendell, A. P.; Burant, J. C.; Iyengar, S. S.; Tomasi, J.; Cossi, M.; Rega, N.; Millam, N. J.; Klene, M.; Knox, J. E.; Cross, J. B.; Bakken, V.; Adamo, C.; Jaramillo, J.; Gomperts, R.; Stratmann, R. E.; Yazyev, O.; Austin, A. J.; Cammi, R.; Pomelli, C.; Ochterski, J. W.; Martin, R. L.; Morokuma, K.; Zakrzewski, V. G.; Voth, G. A.; Salvador, P.; Dannenberg, J. J.; Dapprich, S.; Daniels, A. D.; Farkas, Ö.; Foresman, J. B.; Ortiz, J. V.; Cioslowski, J.; Fox, D. J. Wallingford, CT, USA 2009.

(190) McKinney, T. M.; Geske, D. H. *J. Am. Chem. Soc.* **1965**, *87*, 3013–3014.

(191) Arceo, E.; Jurberg, I. D.; Álvarez-Fernández, A.; Melchiorre, P. *Nat. Chem.* **2013**, *5*, 750–756.

(192) Weissman, S. A.; Anderson, N. G. *Org. Process Res. Dev.* **2015**, *19*, 1605–1633.

(193) Barham, J. P.; John, M. P.; Murphy, J. A. *J. Am. Chem. Soc.* **2016**, *138*, 15482–15487.

(194) Corcé, V.; Chamoreau, L.-M.; Derat, E.; Goddard, J.-P.; Ollivier, C.; Fensterbank, L. *Angew. Chem. Int. Ed.* **2015**, *54*, 11414–11418.

(195) Jouffroy, M.; Primer, D. N.; Molander, G. A. *J. Am. Chem. Soc.* **2016**, *138*, 475–478.

(196) Zuo, Z.; Ahneman, D. T.; Chu, L.; Terrett, J. A.; Doyle, A. G.; MacMillan, D. W. C. *Science* **2014**, *345*, 437–440.

(197) Oderinde, M. S.; Frenette, M.; Robbins, D. W.; Aquila, B.; Johannes, J. W. *J. Am. Chem. Soc.* **2016**, *138*, 1760–1763.

(198) Shields, B. J.; Doyle, A. G. *J. Am. Chem. Soc.* **2016**, *138*, 12719–12722.

(199) Oderinde, M. S.; Varela-Alvarez, A.; Aquila, B.; Robbins, D. W.; Johannes, J. W. *J. Org. Chem.* **2015**, *80*, 7642–7651.

(200) Lin, S.; Ischay, M. A.; Fry, C. G.; Yoon, T. P. *J. Am. Chem. Soc.* **2011**, 19350–19353.

(201) Okada, Y.; Yamaguchi, Y.; Ozaki, A.; Chiba, K. *Chem. Sci.* **2016**, *7*, 6387–6393.

(202) Fukuzumi, S.; Kotani, H.; Ohkubo, K.; Ogo, S.; Tkachenko, N. V; Lemmetyinen, H. *J. Am. Chem. Soc.* **2004**, *126*, 1600–1601.

(203) Hamilton, D. S.; Nicewicz, D. A. *J. Am. Chem. Soc.* **2012**, *134*, 18577–18580.

(204) Margrey, K. A.; Nicewicz, D. A. *Acc. Chem. Res.* **2016**, *49*, 1997–2006.

(205) Romero, N. A.; Margrey, K. A.; Tay, N. E.; Nicewicz, D. A. *Science* **2015**, *349*, 1326–1330.

(206) Perrin, D. D.; Armarego, L. F. *Purification of Laboratory Compounds*, 3rd Ed.; Pergamon Press, New York, 1992.

(207) Brzozowski, M.; Forni, J. A.; Savage, G. P.; Polyzos, A. *Chem. Commun.* **2015**, *51*, 334–337.

(208) Marset, X.; Pérez, J. M.; Ramón, D. J. *Green Chem.* **2016**, *18*, 826–833.

(209) Das, B.; Venkateswarlu, K.; Majhi, A.; Siddaiah, V.; Reddy, K. R. *J. Mol. Catal. A Chem.* **2007**, *267*, 30–33.

(210) Shawcross, A. P.; Stanforth, S. P. *J. Heterocycl. Chem.* **1990**, *27*, 367–369.

(211) Holliman, G. F.; Mann, G. F. *J. Chem. Soc.* **1945**, 34–37.

(212) Toma, G.; Yamaguchi, R. *European J. Org. Chem.* **2010**, 6404–6408.

(213) Schrittwieser, J. H.; Resch, V.; Wallner, S.; Lienhart, W.-D.; Sattler, J. H.; Resch, J.; Macheroux, P.; Kroutil, W. *J. Org. Chem.* **2011**, *76*,

6703–6714.

(214) Basel, Y.; Hassner, A. *Synthesis* **2001**, 550–552.

(215) Yadav, J. S.; Reddy, B. V. S.; Reddy, M. M. *Tetrahedron Lett.* **2000**, *41*, 2663–2665.

(216) Neumann, M.; Zeitler, K. *Org. Lett.* **2012**, *14*, 2658–2661.

(217) Gross, H.; Ozegowski, S. *J. Prakt. Chem.* **1983**, *325*, 437–445.

(218) Zhang, Y.; Kindelin, P.; DeSchepper, D.; Zheng, C.; Klumpp, D. *Synthesis* **2006**, *11*, 1775–1780.

(219) Kumaraswamy, G.; Murthy, A. N.; Pitchaiah, A. *J. Org. Chem.* **2010**, *75*, 3916–3919.

(220) Hedley, K. A.; Stanforth, S. P. *Tetrahedron* **1992**, *48*, 743–750.

(221) Gray, N. M.; Cheng, B. K.; Mick, S. J.; Lair, C. M.; Contreras, P. C. *J. Med. Chem.* **1989**, *32*, 1242–1248.

(222) Valpuesta, M.; Ariza, M.; Díaz, A.; Suau, R. *Eur. J. Org. Chem.* **2010**, 4393–4401.

(223) Brossi, A.; Besendorf, H.; Pellmont, B.; Walter, M.; Schnider, O. *Helv. Chim. Acta* **1960**, *43*, 1459–1472.

(224) Schnider, O.; Grüssner, A. *Helv. Chim. Acta* **1951**, *34*, 2211–2217.

(225) Tung, R. Morphinan compounds. WO 2008/137474 A1, 2011.

(226) Swarbrick, J. D.; Ashton, T. D. *Chirality* **2010**, *22*, 42–49.

(227) Vamvounis, G.; Shaw, P. E.; Burn, P. L. *J. Mater. Chem. C* **2013**, *1*, 1322–1329.

(228) Machara, A.; Werner, L.; Endoma-Arias, M. A.; Cox, D. P.; Hudlicky, T. *Adv. Synth. Catal.* **2012**, *354*, 613–626.

(229) Nocquet, P.-A.; Opatz, T. *Eur. J. Org. Chem.* **2016**, 1156–1164.

(230) Newcomb, M.; Homer, J. H.; Shahin, H. *Tetrahedron Lett.* **1993**, *34*, 5523–5526.

(231) Hudgens, D. P.; Taylor, C.; Batts, T. W.; Patel, M. K.; Brown, M. L. *Bioorg. Med. Chem.* **2006**, *14*, 8366–8378.

(232) Duque-Benítez, S.; Ríos-Vásquez, L.; Ocampo-Cardona, R.; Cedeño, D.; Jones, M.; Vélez, I.; Robledo, S. *Molecules* **2016**, *21*, 381–396.

(233) Pouliquen, M.; Blanchet, J.; De Paolis, M.; Rema Devi, B.; Rouden, J.; Lasne, M.-C.; Maddaluno, J. *Tetrahedron Asymmetry* **2010**, *21*, 1511–1521.

(234) Breen, A. P.; Murphy, J. A. *Free Radic. Biol. Med.* **1995**, *18*, 1033–1077.

(235) Fujita, K.; Enoki, Y.; Yamaguchi, R. *Tetrahedron* **2008**, *64*, 1943–1954.

(236) de Rosales, R. T. M.; Tavaré, R.; Paul, R. L.; Jauregui-Osoro, M.; Protti,

A.; Glaria, A.; Varma, G.; Szanda, I.; Blower, P. J. *Angew. Chem. Int. Ed.* **2011**, *50*, 5509–5513.

(237) Poindexter, G. S.; Owens, D. A.; Dolan, P. L.; Woo, E. *J. Org. Chem.* **1992**, *57*, 6257–6265.

(238) Hay, M. P.; Wilson, W. R.; Denny, W. A. *Tetrahedron* **2000**, *56*, 645–657.

(239) Naylor, A.; Howarth, N.; Malpass, J. R. *Tetrahedron* **1993**, *49*, 451–468.

(240) Nádor, K.; György, L.; Doda, M. M. *J. Med. Chem.* **1961**, *3*, 183–185.

(241) Thotapally, R.; Pathak, A. B.; Kardile, B. S.; Sindhedkar, M. D.; Palle, V. P.; Kamboj, R. K. Indolylpyrimidines As Modulators of Gpr119. WO 2012/025811 A1, 2012.

(242) Zhou, S.; Junge, K.; Addis, D.; Das, S.; Beller, M. *Angew. Chem. Int. Ed.* **2009**, *48*, 9507–9510.

(243) Jia, Z.; Zhou, F.; Liu, M.; Li, X.; Chan, A. S. C.; Li, C.-J. *Angew. Chem. Int. Ed.* **2013**, *52*, 11871–11874.

(244) Tiwari, R. K.; Singh, D.; Singh, J.; Chhillar, A. K.; Chandra, R.; Verma, A. K. *Eur. J. Med. Chem.* **2006**, *41*, 40–49.

(245) Zheng, J.; Darcel, C.; Sortais, J.-B. *Chem. Commun.* **2014**, *50*, 14229–14232.

(246) Cui, X.; Dai, X.; Deng, Y.; Shi, F. *Chem.-Eur. J.* **2013**, *19*, 3665–3675.

(247) Engel, J.; Scheffler, G. N-benzyl, phenethyl, methoxyethyl or allyl substituted benzylphthalazinones having antiallergic and antihistamine action. US 4704387 A, 1987.

(248) Bertholdt, H.; Pfleger, R. *Arch. Pharm. Ber. Dtsch. Pharm. Ges.* **1968**, *301*, 934–940.

(249) Maksay, G.; Nemes, P.; Vincze, Z.; Bíró, T. *Bioorg. Med. Chem.* **2008**, *16*, 2086–2092.

(250) Nişancı, B.; Ganjehyan, K.; Metin, Ö.; Daştan, A.; Török, B. *J. Mol. Catal. A Chem.* **2015**, *409*, 191–197.

(251) Hohenberg, P.; Kohn, W. *Phys. Rev.* **1964**, *36*, 864–871.

(252) Kohn, W.; Sham, L. J. *Phys. Rev.* **1965**, *140*, 1133–1138.

(253) Becke, A. D. *J. Chem. Phys.* **1993**, *98*, 5648–5652.

(254) Salamone, M.; Dilabio, G. A.; Bietti, M. *J. Org. Chem.* **2011**, *76*, 6264–6270.

(255) Barone, V.; Cossi, M. *J. Phys. Chem. A.* **1998**, *102*, 1995–2001.

(256) Cossi, M.; Rega, N.; Scalmani, G.; Barone, V. *J. Comput. Chem.* **2003**, *24*, 669–681.

VOLUME 2: TRANSITION METAL-FREE C-H ARYLATIONS AND DEHALOGENATIONS USING SINGLE ELECTRON REDUCTION

Joshua Philip Barham

A thesis presented in partial fulfilment of the requirements
for the degree of Doctor of Philosophy

Department of Pure and Applied Chemistry, University of Strathclyde

API Chemistry, GlaxoSmithKline

March 2017

SUMMARY

Transition metal-free processes have attracted significant attention within the academic community in recent years. This topic is of particular importance to the pharmaceutical industry, given the costly nature of transition metals typically used in catalysis and the long-term sustainability of these metals. One class of transition metal-free process gaining popularity is transition metal-free C-H arylation. Rather than using transition metal catalysis, reactions are chain reactions triggered by a combination of alkali metal alkoxide bases (such as potassium *tert*-butoxide) and cheap, readily available organic additives (such as 1,10-phenanthroline). However, methods generally require high temperatures and extended reaction times, are limited to reactive haloarenes (generally iodoarenes and sometimes bromoarenes) and, whilst they are regiospecific on the haloarene, they display poor regioselectivity on the arene partner.

The continued development of mechanistic understanding is the key to addressing these issues. Whilst there are generally accepted mechanisms proposed for the propagation step of these chain reactions, the initiation step is the bottleneck for reactivity and is highly contested within the literature. Many authors propose that potassium *tert*-butoxide, either alone or as part of a complex with the organic additive, donates a single electron to the haloarene to initiate the reaction. Others propose that the combination of potassium *tert*-butoxide and the organic additive generates an organic electron donor *in situ* to initiate the reaction.

Herein, the ‘evidence’ attributed to potassium *tert*-butoxide, or a complex of 1,10-phenanthroline/potassium *tert*-butoxide, as the electron donor initiator in transition metal-free C-H arylations was critically examined and rationalised.

It was concluded that to date, there is no evidence for potassium *tert*-butoxide donating single electrons to haloarenes in these transition metal-free C-H arylation reactions. New mechanistic information contests the proposed role of potassium *tert*-butoxide in these reactions and instead supports the *in situ* formation of organic electron donors.

Next, the structural features of organic additives which allow successful C-H arylation with bromoarenes were elucidated. 2-Pyridinecarbinol, which was recently reported to effect successful C-H arylation with a range of bromoarenes under relatively mild conditions, was investigated and compared with a range of derivatives under the same conditions. Structure-activity relationships revealed the mechanism by which electron-deficient pyridinecarbinols and analogues are transformed into potent organic electron donor initiators. The organic electron donor derived from 2-pyridinecarbinol was compared with other reported electron donors revealing structural features which are key to engaging bromoarenes.

Another class of transition metal-free process of interest both within academia and industry is transition metal-free reductive cleavage, particularly, dehalogenation. Dehalogenations are typically conducted by using Pd-catalysed hydrogenation or by using tributyltin hydride chemistry. However, organotin reagents are associated with toxicity and purification issues. During the investigation of transition metal-free C-H arylations, control reactions revealed a surprising result. Potassium hydride mediates the dehalogenation of a variety of haloarenes *via* a radical mechanism, even *ortho*-disubstituted haloarenes which are generally considered inert to all mechanisms except single electron transfer. Upon inspection of the literature, limited reports suggest that alkali metal hydrides or main group metal hydrides can effect dehalogenation in the absence of transition metals, yet the mechanism of action is unclear. Experimental and computational studies shed light on the mechanism of this curious transformation.

TABLE OF CONTENTS

TABLE OF FIGURES

1. Introduction and Related Work

1.1 Transition Metal-free C-H Arylations and Reductive Cleavages: Pharmaceutical Significance

The discovery that certain reactions, once thought to be the domain of transition metal catalysis (C-H activations,[1,2] biaryl couplings,[3,4] Heck[5,6] and Sonogashira reactions[7,8]), can proceed in absence of transition metals marks one of the most prominent advances in organic chemistry of the 21st Century. This is of particular importance to the pharmaceutical industry, given the costly nature of prototypical transition metals used in catalysis (palladium, platinium, iridium, rhodium)[9,10] and the long-term sustainability of these metals which is an area of considerable concern.[11] Often overlooked is the cost of ligands, which can in some cases exceed that of the transition metal.[12] On the other hand, transition metal-free C-H arylation reactions are typically mediated by an alkali metal alkoxide base (commonly, potassium *tert*-butoxide) and an organic additive.[1,3-5,13,14] Whilst organic additives are not always required,[13,15,16] they significantly enhance reaction efficiency in terms of yield and time, simultaneously allowing reactions to be conducted at lower temperature. Although some reports have been explained by trace transition metal contaminants in reagents,[17] many other reports rule out this possibility (by interpretation of ICP-AES or ICP-MS analyses and spiking experiments) and propose a radical mechanism.[1,4,18]

Reductive dehalogenations are of global importance due to the high environmental toxicity of a large number of halogenated organics and their oxidised combustion products.[19,20] As such, the transformation is common within chemical waste treatment industries, but is less common in the pharmaceutical industry, or in organic synthesis. However, halogens have been utilised as directing groups in synthesis;[21] for example, in Diels-Alder

reactions[22,23] and in the Bartoli indole synthesis,[24] prior to dehalogenation. On laboratory scale, dehalogenations are typically achieved by palladium-catalysed hydrogenation, tributyltin hydride radical chemistry or lithiation/protic quench.[21,24–27] Whilst tin is a more sustainable metal than palladium, organotin reagents are highly toxic and can present problems with purification.[28] Some pharmaceutical syntheses have capitalised on the halogen's steric or electronic properties, and on large (kilo) scale, dehalogenation reactions have been achieved by means of palladium-catalysed hydrogenation.[20,29,30] Transition metal catalysis (group 8-10) in conjunction with phosphine or *N*-heterocyclic carbene ligands is another area which has received significant attention.[19] However, methods for reductive cleavage which avoid transition metal catalysts are attractive; especially the use of alkali metal hydrides or organic electron donors.

1.2 TRANSITION METAL-FREE C-H ARYLATION: HISTORICAL PERSPECTIVE

1.2.1. DISCOVERY OF TRANSITION METAL-FREE C-H ARYLATIONS

In 2008, Itami reported the coupling of iodoarenes to pyridine in the presence of KO*t*Bu and an Ir-based catalyst (Scheme 1).[18] A range of Ir complexes were tested, with $IrCl(CO)(PPh_3)_2$ giving the highest yield of coupled product **1** (41%). However, the control reaction gave a surprising result; the reaction proceeded in almost identical yield with KO*t*Bu only. Moving to pyrazine as a coupling partner, reactions of **1**,**3** and **4** proceeded under milder conditions to give coupled products **5**-**7** in good to excellent (64 - 98%) yields. Through trace metal analysis (ICP-AES) of the KO*t*Bu, Itami found that levels of Pd (< 0.06 ppm), Ru (< 0.20 ppm) and Rh (< 0.30 ppm) were below the detection limits, such that if transition metal catalysis were to be in operation, the catalyst would need to be sufficiently active at below parts-per-million levels to afford high yields of products. Whilst the mechanism remained elusive, addition of radical scavengers (TEMPO, galvinoxyl radical) completely shut

down the reaction.[18] This led Itami to suggest a radical mechanism.

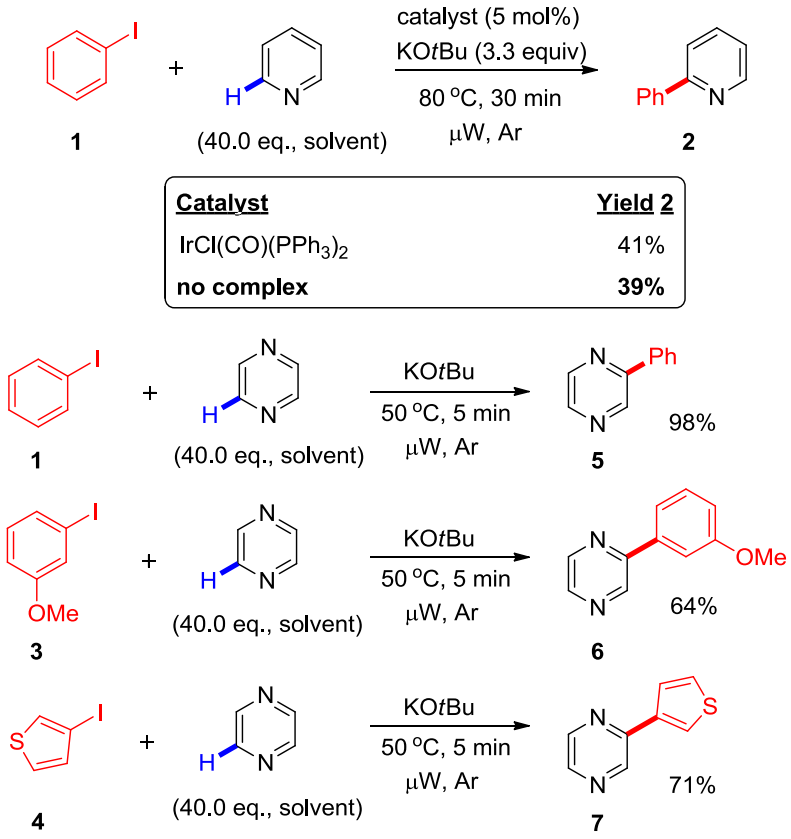

***Scheme 1**: Seminal report of coupling electron-deficient N-heterocycles to iodoarenes.*

Another observation was that coupling was only observed on the iodine-bearing carbon atom of the iodoarene.[18] Arynes were ruled out as intermediates (which have been evidenced to form under similar conditions at higher temperatures),[31] since regioisomers of coupled products (with respect to the iodoarene) would be expected. Finally, an interesting observation was made around the nature of the base required. Whilst KO*t*Bu promoted the reaction efficiently, NaO*t*Bu and LiO*t*Bu gave no reaction (although reaction was observed with NaO*t*Bu at higher temperature; 80 °C), highlighting the importance of the potassium cation. However, KOMe and KOH gave no reaction, highlighting the importance of the *tert*-butoxide anion. Therefore, KO*t*Bu appears to be a privileged reagent in these reactions.

1.2.2. Ruling Out Trace Transition Metals and Establishment of a Radical Mechanism

Following Itami's seminal work, Hayashi[3] and Shi[1] published the coupling of haloarenes (**8**) to arenes (**9**, benzene derivatives) using KO*t*Bu as a base and 1,10-phenanthroline (**phen**) derivatives as organic additives, generally at 100 ^{o}C. (Scheme 2). Whilst initial studies examined $Co(acac)_3$ as a catalyst, Shi found that the control reaction gave desired products (**10**) in similar efficiency (mirroring Itami's discovery).[1] Similarly concerned around impurities in the KO*t*Bu (10 ppb - 10 ppm of Pd, Cu and Fe were detected), Shi undertook studies monitoring the conversion of 4-bromoanisole (**11**) to desired product 4-methoxybiphenyl (**12**) in the presence of various added metal salts (10 - 1,000x the amounts detected by ICP-MS/ICP-AES). No significant enhancement of the reaction rate was observed (in some cases reaction rate was decreased). For experimental rigour, different commercial batches of KO*t*Bu, sublimed KO*t*Bu and **phen** from different suppliers were tested and did not dramatically affect the reaction outcome.

Hayashi reported couplings at higher temperature (155 ^{o}C) and found NaO*t*Bu and KO*t*Bu to be equally effective promoters at this temperature.[3] Mechanistic studies suggested the intermediacy of aryl radicals. When the reaction was conducted in THF-d_8 solvent (no arene coupling partner was present, which is normally employed as solvent) dehalogenation and deuteration occurred at exclusively the iodine-bearing carbon to give toluene-d_1 (**14**) (Scheme 3). Running the reaction in a 1 : 1 mixture of C_6D_6 : C_6H_6 as solvent gave coupled products **15** and **15-**d_5; k_H/k_D = 1.07 (Scheme 3), leading Hayashi to conclude that the rate-determining step of the mechanism does not involve cleavage of a C-H bond. Hayashi proposed that the role of the **phen** derivative (such as **Ph**-**phen**), as a highly conjugated species with a low-lying LUMO, was to act as a mediator for SET from the *tert*-butoxide anion to the haloarene.[3]

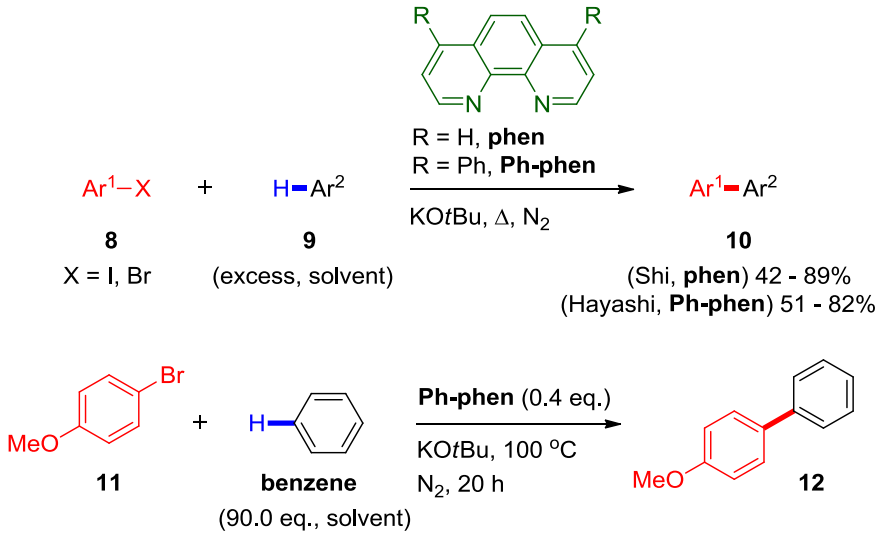

***Scheme 2**: Coupling of haloarenes to arenes in the presence of **phen**-type additives.*

The proposed mechanism begins with complexation of NaO*t*Bu and the phenanthroline derivative to afford **16** (Scheme 3, phenanthroline is shown). Following SET, the radical anion of the haloarene (**17**) fragments to iodide and aryl radical **18**. Aryl radical **18** adds to benzene to afford arylcyclohexadienyl radical **19**, which engages in SET with complex **20a**. Deprotonation of biaryl cation **21** affords desired product **15** and *t*BuOH; complex **16** can be regenerated from complex **20b** *via* complexation of NaO*t*Bu. The inactivity of structurally similar 2,2′-bipyridine (**bpy**) and the enhanced activity of **Ph-phen** compared to **phen** is rationalised on the stability of the respective radical anions (*via* conjugation); descriptive of their ability to act as SET mediators.[3] In this transition metal-free C-H arylation reaction mechanism (Scheme 3), a single electron is donated into an antibonding orbital of **13**. The electron could be donated into the π* to form radical anion **17**, which fragments to yield an aryl radical (**23**) and a halide.[3,32–34] In some instances (for example, electrochemical reduction of iodobenzene) the electron is injected into the σ* which results in concerted C-X bond cleavage.[35–38] In many proposed mechanisms in the literature, the SET event itself is generally not discussed and is simplified by either of the

reaction schemes shown in Scheme 4 (top); which will similarly be used as descriptors herein.

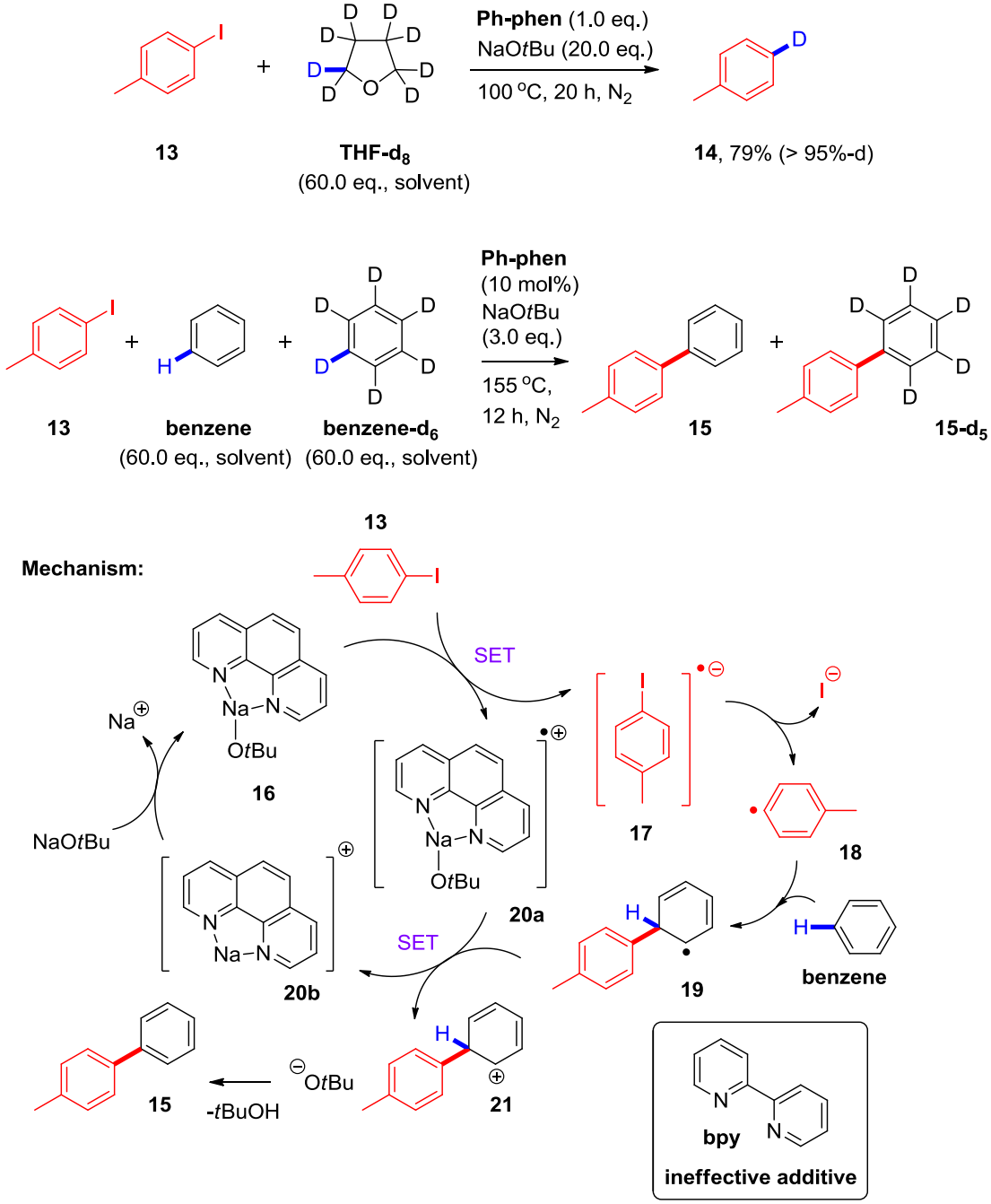

***Scheme 3**: Mechanistic experiments using deuterium labelling and proposed mechanism.*

It is noted that the mechanism chosen and the subtleties of the SET event depend on the system; complexation of the haloarene and the electron donor, solvent interactions and cationic/anionic interactions can all have influence.[39–41] The aryl radical (**23**) has several possible fates other than coupling to arenes; it is useful to consider these fates (Scheme 4). Firstly, the aryl radical (**23**) could undergo further SET reduction to an aryl anion (**24**) under reductive conditions,[33,42] followed by protonation to afford the formally reduced product, **25** (Scheme 4, pathway 1). Secondly, the aryl radical (**23**) could be intercepted in HAT, affording the formally reduced product (**25**) and another radical intermediate (Scheme 4, pathway 2).[43–45]

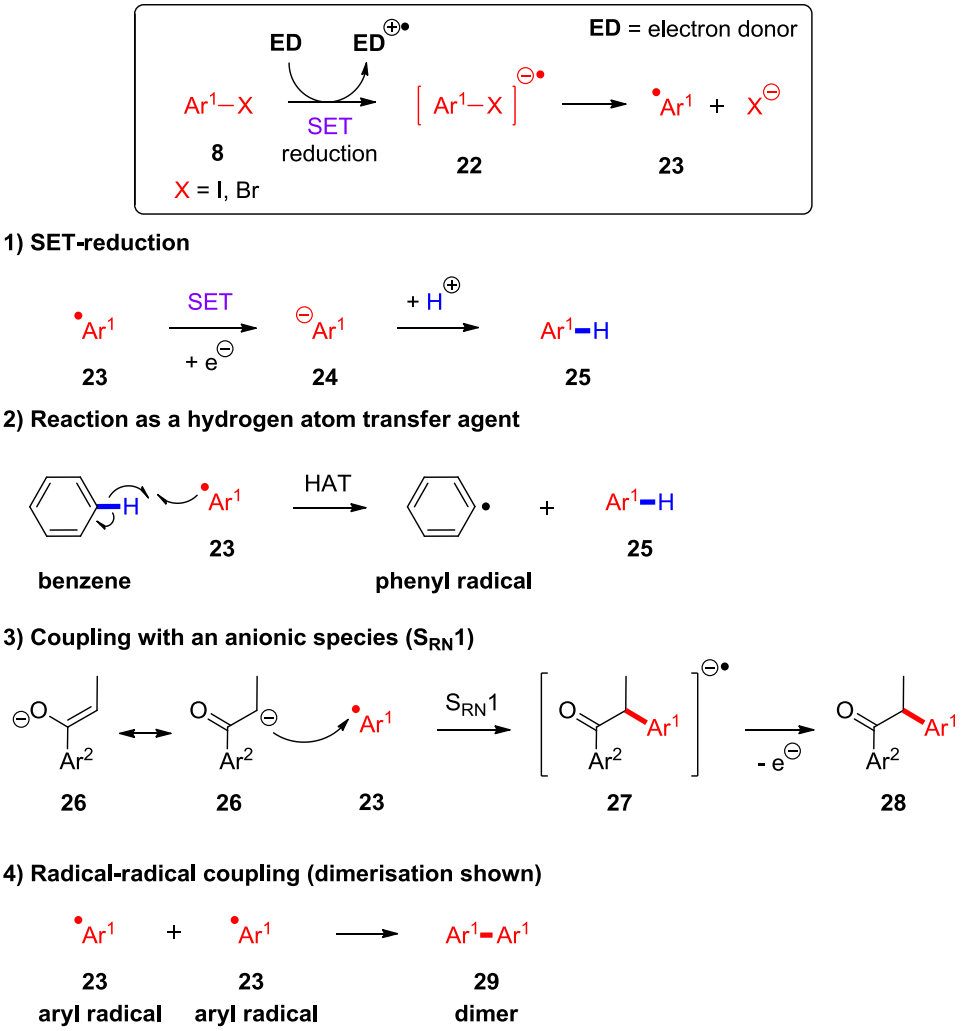

***Scheme 4**: Fates of aryl radicals generated under SET reduction conditions.*

Thirdly, the aryl radical (**23**) could be intercepted by an anionic species (for example, enolate **26**) to afford a radical anion (**27**) in an $S_{RN}1$-type reaction (Scheme 4, pathway 3).[38,46,47] Finally, the radical intermediate could be intercepted by another radical intermediate; for example, radical dimerisation (of **23**, to give **29**) may occur marking a termination event (Scheme 4, pathway 4). Different pathways are available to radical intermediates under air or oxidative conditions, and these are demonstrated for an α-amino radical as an example in Volume 1 (see Section 1.5.1., Scheme 30).

However, in the reactions reported by Shi[1] and Hayashi,[3] products arose overwhelmingly from the propagation step which involves addition of aryl radicals to arenes rather than HAT or radical-radical coupling. Charette disclosed the intramolecular cyclisation of haloarenes tethered to an arene *via* an ether, alkyl or amine linkage (Scheme 5).[34] A radical mechanism was proposed due to termination of the reaction upon addition of radical scavengers (TEMPO, galvinoxyl radical) together with inspection of the product distribution. When substrates such as **33** were employed (with *para*-substituents on the arene fragment), the regioselectivity was 10 : 1 in favour of regioisomer **34a** (a rearranged product where the new C-C bond is *para*- to the arene's original *para*-substituent).

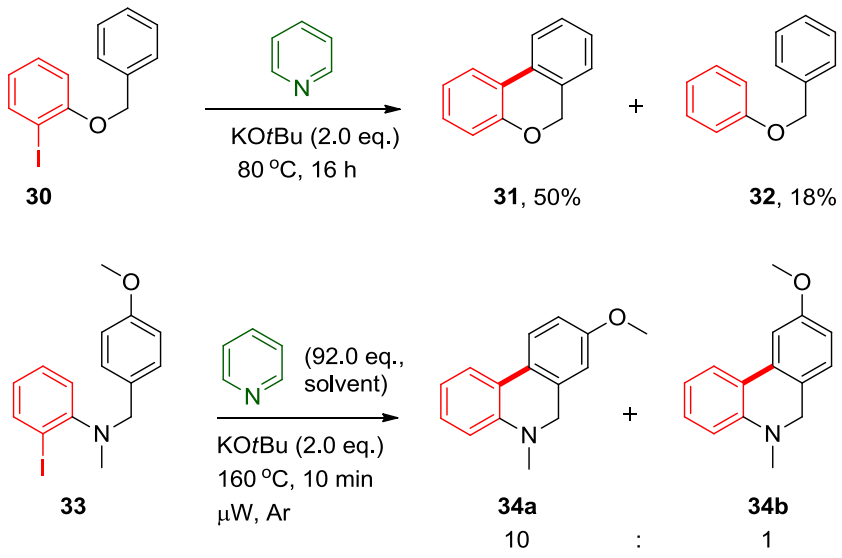

***Scheme 5**: Intramolecular arylations via a radical pathway.*

Charette rationalised the regioselectivity on the basis of stability of intermediates in a radical mechanism (Figure 1). Iodoarene **30** was treated with KO*t*Bu in pyridine at 80 ^{o}C affording cyclised product **31** and dehalogenated product **32**. The mechanism proposed is exemplified with substrate **33**, beginning with SET reduction of the C-I bond to generate (upon fragmentation of the iodoarene radical anion) an aryl radical, **35a** (Figure 1).

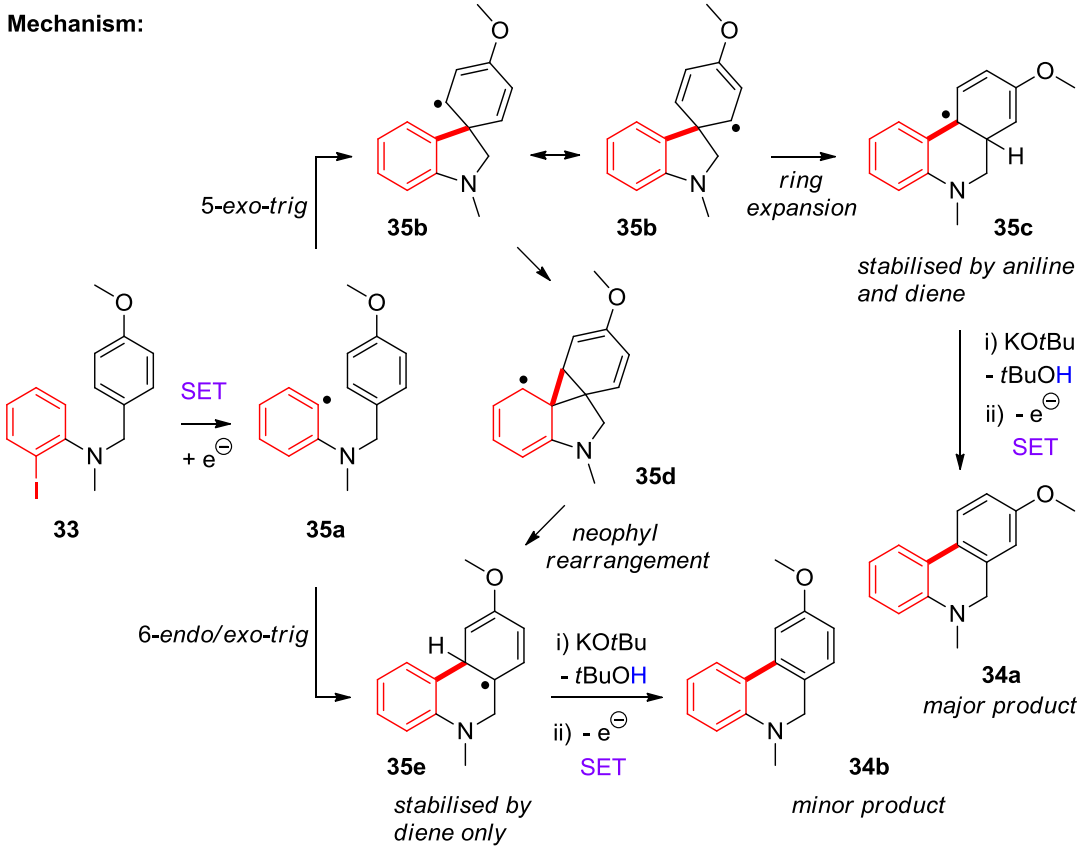

***Figure 1**: Proposed radical mechanism for intramolecular arylations.*

Aryl radical **35a** undergoes 5-*exo-trig* cyclisation onto the *ipso*- position of the tethered arene fragment to give **35b**, which undergoes ring expansion to **35c**,[†] where the radical is stabilised through resonance with the aniline and diene moieties. Deprotonation affords a radical anion, which is oxidised *via* SET to afford **34a** as the major product.

[†]From **35b**, a concerted ring expansion is proposed by Charette, but a more feasible mechanism is rearomatisation to form the α-amino radical, which then adds to the adjacent carbon to give **35c**.

Alternatively, aryl radical **35a** undergoes 6-*endo*/*exo*-trig cyclisation to afford **35e** (neophyl rearrangment of **35b** *via* **35d** is another route envisaged to **35e**), where the radical is stabilised through resonance with the diene but not with the aniline moeity. Deprotonation and SET oxidation affords **34b** as the minor product. In the absence of any phenanthroline mediator, Charette hypothesised that the pairing of pyridine with KO*t*Bu must give rise to an electron donor species which performs SET reduction of the C-I bond. Rather than the closed cycle mechanism proposed by Hayashi, Charette proposed that this initial SET (to **33**, for example) would initiate a radical chain reaction, where intermediates (radical anions derived from **35c** or from **35e**, for example) effect propagation by undergoing SET with the starting material (**33**). Lei and Kwong found that a range of organic additives could facilitate the same coupling reaction (under similar conditions).[4] For example, L-proline (**36**) furnished the product (**15**) in 34% yield, whilst 1,2-ethylenediamine (**37**) and DMEDA (**38**) furnished the product (**15**) in 81% and 84% yields, respectively (Scheme 6). In contrast, TMEDA (**39**) gave no reaction, suggesting that amine H atoms were essential. The *cis*-diol (*cis*-**40**) was an efficient promoter whilst the *trans*-diol (*trans*-**40**) was less effective.

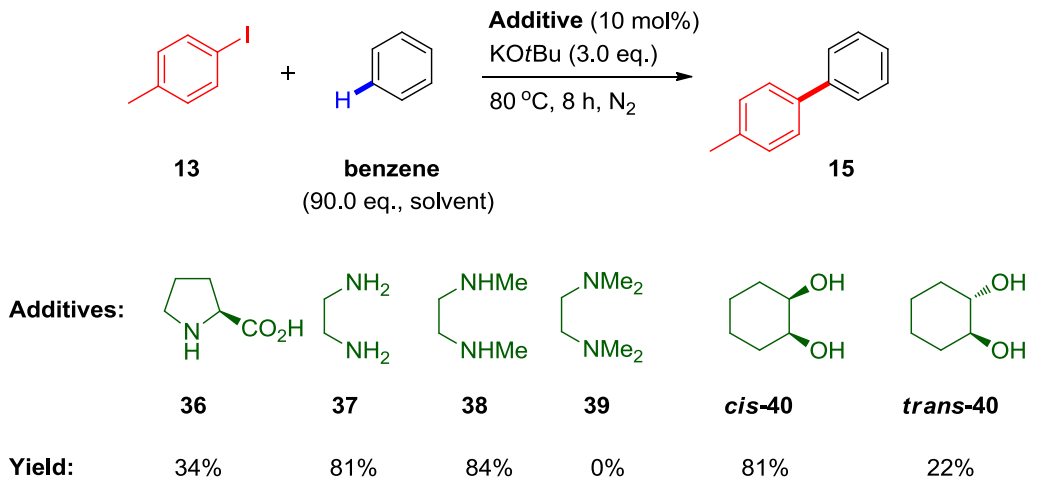

***Scheme 6**: Haloarene to arene coupling mediated by a number of organic additives.*

Similarly to Hayashi, no reaction was observed with other bases (NaH, KOH, Na_2CO_3, KOAc, NaO*t*Bu and LiO*t*Bu). A host of organic additives have since been reported to effect the C-H arylation reaction with haloarenes under transition metal-free conditions. Reports of additives include alcohols (such as ethanol[48]), diols,[4,48,49] diamines,[4,49,50] amino acids,[4,15] pyridinols,[14] arylhydrazines[51] and N-heterocyclic carbenes.[52] Other, more exotic examples of additives have been reported.[53–57] Murphy captured the range of organic additives employed in these reactions in a recent report.[58]

1.2.3. BASE-PROMOTED HOMOLYTIC AROMATIC SUBSTITUTION

Shortly after Charette's work, Studer and Curran disclosed a review of the transition metal-free C-H arylation research area and proposed a general mechanism which summarised the case for a radical chain mechanism.[37] The mechanism is referred to as Base-promoted Homolytic Aromatic Substitution (**BHAS**, Figure 2). Here, the aryl radical (**23**), generated by an initial electron donation to **8**, adds to arene coupling partner **9** (for example, PhH) to give **41**. Deprotonation gives the electron-rich radical anion **42**, which propagates the cycle by donating an electron to **8**, simultaneously affording biaryl product **10**. In addition to the evidence for a radical mechanism presented by Itami,[18] Hayashi,[3] Charette[34] and others, the intermediacy of radical anions was conclusively evidenced by Lei and Kwong,[4] who reported the transition metal-free C-H *bis*-arylation of 1-chloro-4-iodobenzene (**43**) with benzene. The reaction proceeded directly to give terphenyl (**45**), with only traces of *mono*-arylated product (**44**) observed. As reported originally by Bunnett and Creary,[32] radical anions such as $\mathbf{44}^{\bullet-}$ will preferentially undergo intramolecular SET (dissociating to aryl radical **46** and halide) than undergo intermolecular SET (to generate *mono*-arylated product **44**). Lei and Kwong observed similar behaviour for other dihalobenzenes and kinetic studies showed that **43** was consumed faster than **44**.[4] This rules out the possibility that the experimental result could be explained by **43** reacting to give the *mono*-arylated product (**44**) which then reacts faster than **43**.

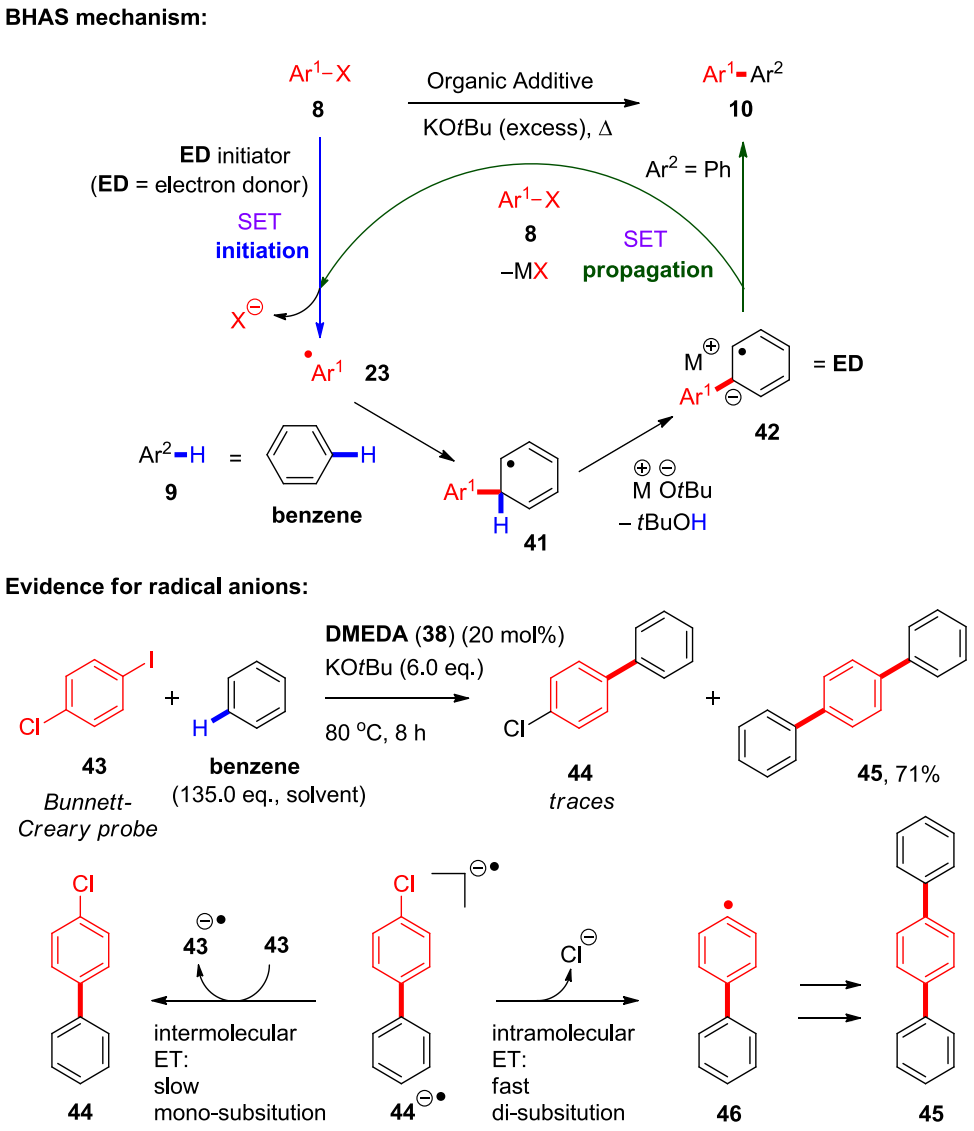

***Figure 2**: Base-promoted Homolytic Aromatic Substitution (**BHAS**) mechanism (top) and evidence for radical anions as intermediates (bottom).*

1.2.4. Elusive Nature of the Initiation Step and the Role of Organic Additives

Whilst the **BHAS** mechanism was generally accepted by the synthetic community, the initiation event (whereby aryl radical **23** is generated) was elusive and disputed in the literature.[44,58] Chain reaction initiation is possible with very low concentrations of active species, such that mechanisms and

intermediates which would be considered unlikely in a stoichiometric pathway must be considered. Unfortunately and as a consequence, it is generally not possible to isolate the products from initiation and other approaches (spectroscopy, structure activity relationships between initiators and stoichiometric transformations of initiators) are often used to decipher the mechanism of initiation.

On the basis of electron paramagnetic resonance (EPR) and cyclic voltammetry (CV) studies, Jutand and Lei claimed that **phen** and KO*t*Bu form complex **47**, which undergoes inner-sphere SET to generate *tert*-butoxyl radical and phenanthroline radical anion (**48**),[59] which in turn initiates the **BHAS** mechanism *via* SET to the haloarene **8** (Scheme 7, top). Wilden's findings appeared to be in support of this,[13] but Wilden also reported that when **phen** was absent and under high temperature (160 ^{o}C) conditions, the reaction still proceeded. Wilden proposed that the *tert*-butoxide anion of KO*t*Bu participates in *direct* SET to haloarenes (Scheme 7, bottom). In Section 1.2.5., Wilden's reactions (where **phen** is absent) and mechanistic proposal will be discussed. Firstly, the observations and interpretations presented by Jutand, Lei and Wilden for SET between KO*t*Bu and **phen** will be discussed. When **phen** was treated with KO*t*Bu in DMF at 100 ^{o}C, an EPR signal with hyperfine coupling was detected, attributed to the **phen** radical anion (**48**) by Jutand and Lei (a control experiment without **phen** gave no EPR signal).[59]

The second piece of evidence, as interpreted by Jutand and Lei, was based on CV.[59] The oxidation potential of KO*t*Bu was E^{p}_{ox} ($^{\bullet}$O*t*Bu/$^{-}$O*t*Bu) = +0.10 V *vs.* SCE in DMF. The CV of **phen** showed two successive reduction peaks at E^{p1}_{red} (**phen**/**phen**$^{\bullet-}$) = -2.06 V *vs*. SCE and E^{p2}_{red} (**phen**$^{\bullet-}$/**phen**$^{2-}$) = -2.23 V *vs.* SCE, corresponding to reduction of **phen** to the **phen** radical anion (**48**) and the **phen** dianion (**49**), respectively (Scheme 8). The potential difference between *tert*-butoxide and **phen** is so large (ΔE = > 2 V *vs*. SCE) that SET between these species is completely unfeasible thermodynamically. Jutand

and Lei demonstrated that direct SET from KO*t*Bu to haloarenes [E^{p}_{red} (PhBr/PhBr$^{\bullet-}$) = -2.67 V *vs*. SCE] is even less feasible.[59] It was proposed that complexation of **phen** by K^{+} might effect a shift to a more positive redox potential allowing reduction of **phen** by $^{-}$O*t*Bu. Apart from the interpretation of the observed EPR signal, no evidence is provided to corroborate this.

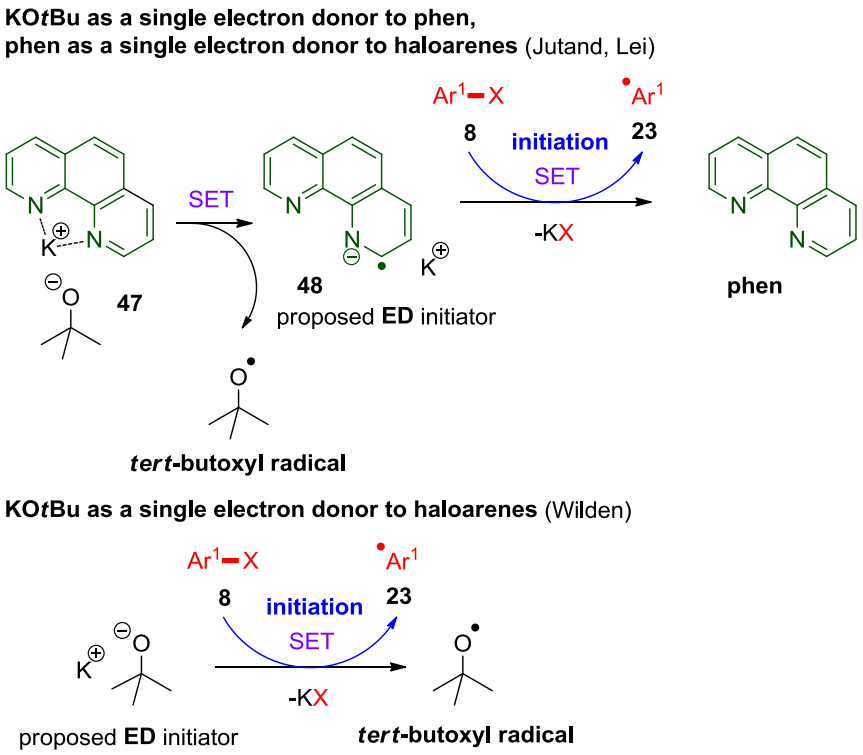

Scheme 7: *Proposed interaction between KOtBu and* ***phen*** *resulting in inner-sphere SET. Proposed direct SET between KOtBu and haloarenes.*

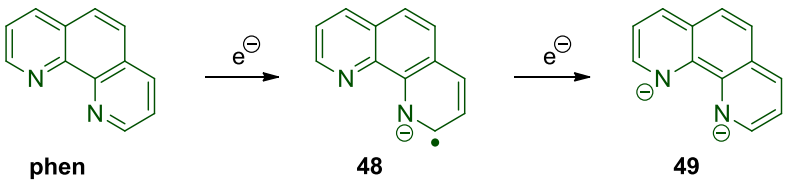

Scheme 8*: Sequential transfer of single electrons to* ***phen****.*

Evidence was shown for reduction of bromobenzene by the **phen** radical anion (**48**). When the CV of **phen** was conducted in the presence of increasing concentrations of bromobenzene, an increase in peak current was

observed for the second reduction peak [E^{p2}_{red} (**phen**$^{\bullet-}$/**phen**$^{2-}$) = -2.23 V *vs.* SCE] corresponding to dianion **49**.[59] Therefore, the **phen** dianion (**49**) reduces bromobenzene to generate PhBr$^{\bullet-}$ and **phen** radical anion (**48**) in the diffusion layer around the cathode. This would increase the effective concentration of **phen** radical anion (**48**) which would result in more current being drawn from the cathode as **phen** dianion (**49**) was regenerated.

At even higher concentrations of added bromobenzene, an increase in peak current was detectable for the first reduction peak [E^{p1}_{red} (**phen**/**phen**$^{\bullet-}$) = -2.06 V *vs*. SCE] corresponding to the **phen** radical anion (**48**). Therefore, **phen** radical anion (**48**) reduces bromobenzene to generate PhBr$^{\bullet-}$ and **phen**. Finally, the EPR signal observed from treating **phen** with KO*t*Bu in DMF at 100 ^{o}C [interpreted as the **phen** radical anion (**48**)] disappeared upon addition of bromobenzene. This is in line with Hayashi's proposal, and appears to confirm the generation of **phen** radical anion (**48**) in the reaction.

Wilden advocated SET between tertiary alkoxides and **phen** on the basis of mass spectrometry, ^{1}H NMR and a colour test for ketones.[13] Firstly, when potassium *tert*-pentoxide was mixed with **phen** in THF at rt and the mixture analysed by mass spectrometry, detection of butanone 'as a major component of the reaction mixture' was claimed (Scheme 9). However, since the reaction mixture is in THF solvent (which is identical in M.W. to butanone), reassurance would be needed over this experiment. Fragmentation of alkoxyl radicals by β-scission, to give ketones and alkyl radicals, is a known pathway (HAT to yield the corresponding alcohol is another plausible fate, in the presence of a H atom donor).[60]

Although Wilden proposed that β-scission of the *tert*-pentoxyl radical gave methyl radical and butanone, the fragmentation pathway to form ethyl radical and acetone is thermodynamically more favourable.[60] Furthermore, DiRocco experimentally demonstrated that fragmentation of *tert*-pentoxyl radical does not afford butanone together with methyl radical in significant amounts, but

rather gives rise to acetone and (the more stable) ethyl radical (Scheme 9).[61]

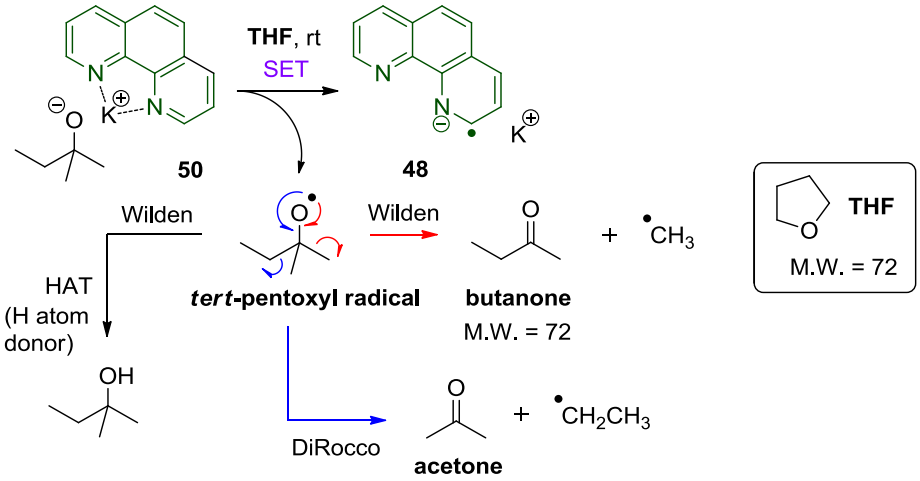

***Scheme 9**: Reaction between **phen** and potassium tert-pentoxide in THF giving rise to butanone and methyl radical. Alternative fragmentation to give acetone and ethyl radical. Comparison of butanone to THF.*

Upon mixing **phen** and KO*t*Bu in an equimolar ratio and analysing by ^{1}H NMR, Wilden observed a collapse of the *tert*-butyl peak from 9H to < 1H, suggesting the consumption of KO*t*Bu as it reacts with **phen**. However, although no experimental details were given for this experiment, the ^{1}H NMR spectrum here appears to have been recorded in $CDCl_3$ (singlet at δ 7.27 ppm). Again, reassurance would be needed over this experiment due to concerns about reaction of KO*t*Bu with $CDCl_3$ (reaction of $CHCl_3$ and KO*t*Bu giving rise to dichlorocarbenes is known).[62]

The final evidence disclosed by Wilden was that addition of 1,3-dinitrobenzene (1,3-DNB, **51**) to the reaction mixture derived from equimolar **phen** and potassium *tert*-pentoxide resulted in an intense purple colour.[13] This was regarded as a positive Janovsky test, which reports the presence of an enolisable ketone or aldehyde.[63,64] The Janovsky test was first reported in 1886,[65] as a test for enolisable aldehydes and ketones (which possess an α–hydrogen atom).[63] Wilden proposed that under high pH conditions, the enolate of butanone would add to 1,3-DNB (**51**) to afford adduct **52a**

(Scheme 10).[†,13] However, it is noted that the addition of the enolate of butanone to 1,3-dinitrobenzene would initially afford Meisenheimer adduct **53a**, which would require oxidation to **54a** and deprotonation to afford **52a**. The purple coloration could be associated with initial Meisenheimer adduct **53a** or proposed adduct **52a**. Another possibility, which was not mentioned by Wilden, was adduct **55a** resulting from the direct addition of potassium *tert*-pentoxide to 1,3-DNB (**51**).

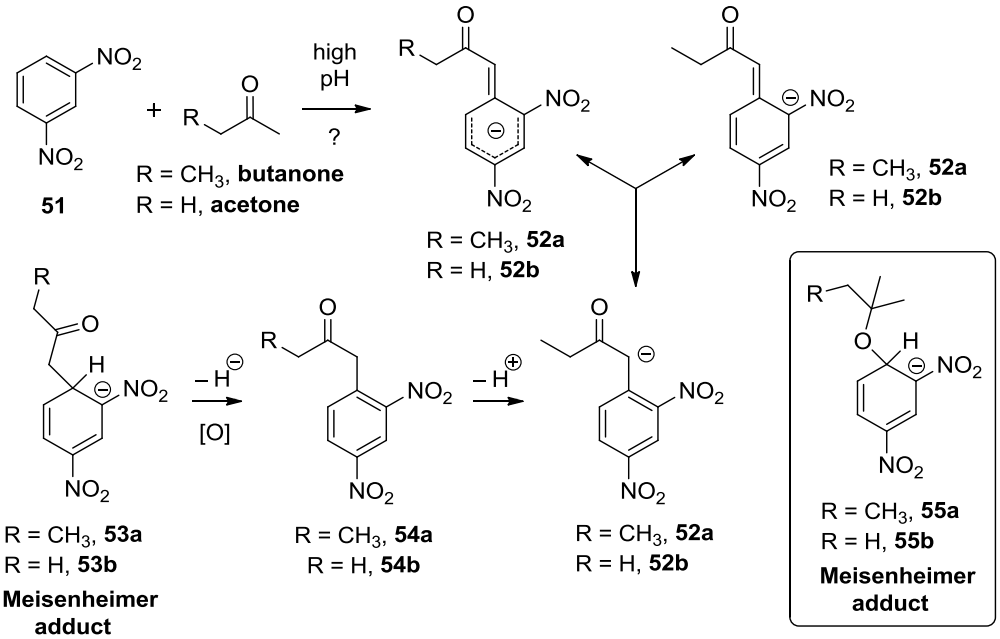

Scheme 10: *Mechanistic considerations in the formation of Janovsky adducts.*

1.2.5. ORGANIC ADDITIVE-FREE C-H ARYLATIONS AT HIGH TEMPERATURE

Many reports of transition metal-free C-H arylation reactions found that reactions did not proceed in the absence of the organic additive.[3,4,14,48] However, Bisai and Kumar reported that intramolecular C-H arylations took place *in the absence of any organic additive*.[16,66] Following this, Wilden reported the additive-free intermolecular C-H arylations with iodoarenes (with

[†]Although 'low pH' is written in the paper, a personal communication from Dr. Wilden to Prof. Murphy confirmed that the Janovsky test was carried out under high pH conditions.

ortho-H atoms) at elevated reaction temperature (160 ^{o}C). By heating iodoarenes in benzene with KO*t*Bu only, biaryl products are obtained in modest to high yields (Scheme 11, top).[13] This led Wilden to propose direct SET between KO*t*Bu and the iodoarene is feasible (no reaction of bromoarenes or chloroarenes was observed). Under the same conditions, NaO*t*Bu and LiO*t*Bu gave no reaction (NaO*t*Bu gave successful reaction when **phen** was used as an additive).

The rationalisation given was that metal alkoxides are in dynamic equilibrium between the covalent and charge-separated species (Scheme 11, bottom).[13] In the charge-separated form, Wilden proposed that the alkoxide can be considered in equilibrium with a species that bears a loosely bound electron (which, at elevated temperatures, can be transferred to the haloarene to initiate the reaction). It was proposed that the reducing power of group 1 metal alkoxides is increased moving down the group from LiO*t*Bu < NaO*t*Bu < KO*t*Bu as the degree of dissociation increases. This was in line with the absence of reaction when LiO*t*Bu and NaO*t*Bu are used in place of KO*t*Bu under additive-free conditions.

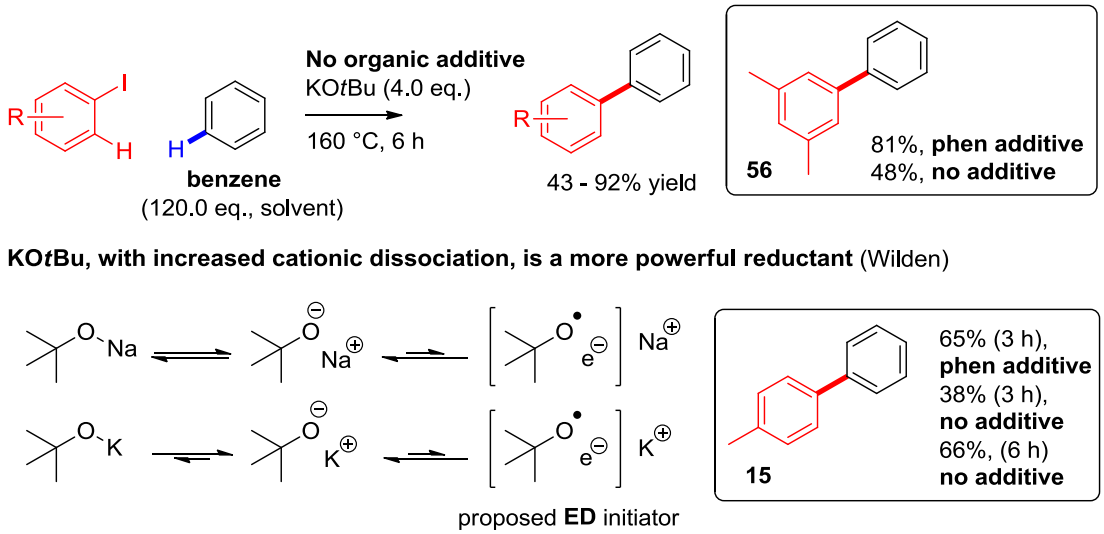

Scheme 11: *Transition metal-free and organic additive-free coupling at elevated temperature. Rationalisation of group 1 metal alkoxides as single electron donors.*

Despite the extreme difference in redox potentials between iodoarenes [E^{p}_{red} (PhI/PhI$^{\bullet-}$) = -2.24 *vs*. SCE in DMF][36] and *tert*-butoxide [E^{p}_{ox} ($^{\bullet}$O*t*Bu/$^{-}$O*t*Bu) = +0.10 V *vs.* SCE in DMF],[59] KO*t*Bu was presented as a single electron donor by Wilden. Although additives (**phen** or DMEDA) are not necessary to couple iodoarenes to arenes, Wilden's results indicate that reactions with organic additives are more efficient.[13] Biaryl product **56** was formed in almost double the yield when **phen** was used as an additive under the same conditions. The coupling of *p*-iodotoluene (**13**) to benzene to afford biaryl product **15** proceeded whether **phen** was used as an additive or not; however additive-free conditions required double the reaction time (6 h) to reach the same yield of **15**. In addition, additive-free coupling was not observed at 85 ^{o}C or 110 ^{o}C, whereas DMEDA effected coupling of *p*-iodotoluene (**13**) affording **15** in good (53%) yield at 85 ^{o}C after 6 h.[13] This is consistent with Lei and Kwong's results where exactly the same coupling reaction gave **15** in 83% yield after 8 h at 80 ^{o}C.[4]

Murphy reported the coupling reaction of 2,6-dimethyliodobenzene (**57a**) which, upon SET reduction affords the 2,6-dimethylbenzene aryl radical, **61** (Scheme 12). Addition to benzene (ultimately affording coupled product **58** *via* the **BHAS** mechanism, Figure 2) is more challenging for this hindered aryl radical (**61**), such that HAT with benzene becomes a competitive pathway. HAT affords the volatile *m*-xylene (**60**) and a phenyl radical. The phenyl radical adds to benzene ultimately affording biphenyl (**59**) *via* the **BHAS** mechanism. The relative rates of HAT *vs*. coupling to benzene are fixed, no matter the organic additive, giving rise to a characteristic ~3.5 : 1 ratio of biphenyl **59** : product **58** in these reactions. In the absence of **phen** the reaction does not proceed at all. In the presence of **phen**, an 18% combined yield of **58** and **59** (inseparable by chromatography) results. This observation is inconsistent with KO*t*Bu as an electron donor. A question arises around how KO*t*Bu gives rise to coupling in Wilden's case[13] when substrates are used which have *ortho*-H atoms.

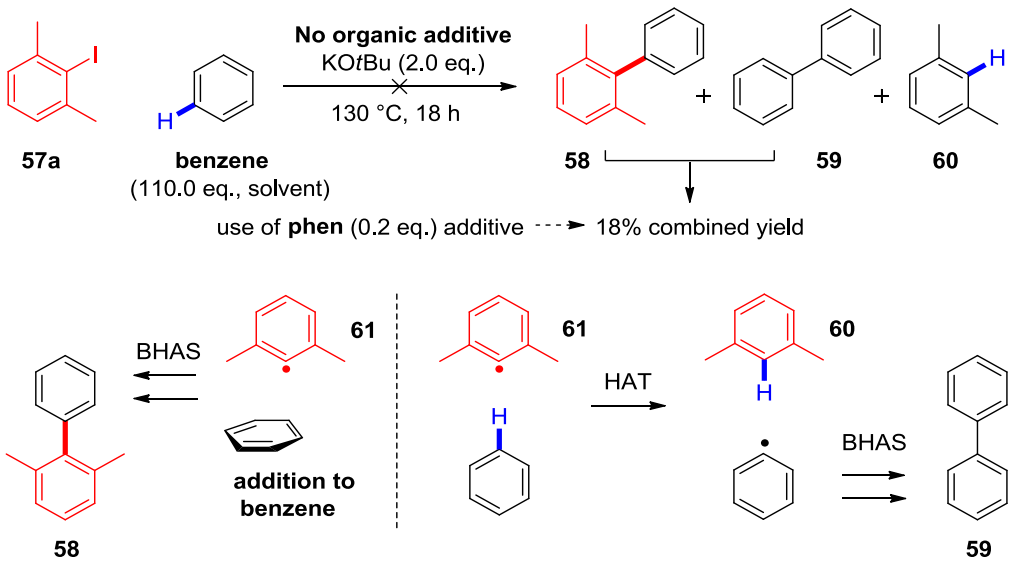

***Scheme 12**: No reaction of 2-iodo-m-xylene under additive-free conditions and successful coupling using **phen** as an organic additive. Mechanisms explaining product distribution.*

Literature shows that iodobenzene can be converted to benzyne by KO*t*Bu.[31] However, benzyne formation is ruled out by many publications on transition metal-free haloarene-arene coupling because regioisomers are not observed, suggesting that biaryl products do not derive from benzynes in any appreciable measure.[3,57,38] Murphy proposed that a very small concentration of a benzyne could be formed *as part of an initiation pathway solely* (Scheme 13). As a diradical, the benzyne could function in a similar way to aryl radical **23** (Figure 2, Section 1.2.3.). Addition to benzene and subsequent deprotonation would afford electron donor **62** (analogous to **42** in Figure 2), thereby triggering the **BHAS** mechanism. Since the product is delivered overwhelmingly by the propagation step and not the initiation step, a single regioisomer of the product (coupling to the halogen-bearing carbon) would still be expected (Figure 2).[44] The absence of reaction with **57a** supports this benzyne initiation hypothesis. With no *ortho*-H atoms, **57a** is blocked to benzyne formation and so it is claimed to function as a sole reporter of SET processes, Scheme 12.[44]

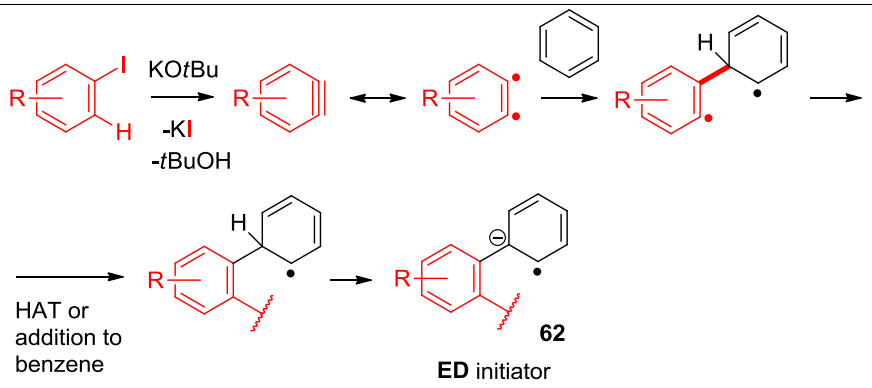

***Scheme 13**: Pathway from arynes to electron donors in the absence of **phen**.*

1.2.6. Organic Additives Form Organic Electron Donor Initiators

Murphy and Tuttle investigated the common proposal that **phen** acted as a mediator for SET from KO*t*Bu to haloarenes. By use of computation, it was found that electron transfer from a complex of NaO*t*Bu/**phen** to iodobenzene was significantly endergonic (+63.9 kcal mol^{-1}; +59.5 kcal mol^{-1} for the corresponding analogous potassium case), raising grave concerns about the feasibility of this mechanism (a subsequent computational study by Patil supported this).[40] In the laboratory, when **phen** was heated with KO*t*Bu only in benzene a deep-green solid material was produced (the same solid was observed in reactions with substrate). When removed from the glovebox and exposed to air, the solid was pyrophoric, reminiscent of the behaviour of previously synthesised organic electron donors.[42] Quenching the material with I_2 as an electron acceptor gave rise to **65** as almost a pure single compound (Scheme 14). This strongly implicates species **64** as an electron donor formed *in situ*, which presumably forms through deprotonation at the 2-position of **47**, addition to **phen** to give **63** and then, deprotonation. Murphy and Tuttle proposed that **64** was the electron donor responsible for initiating the **BHAS** reaction mechanism, not KO*t*Bu (either alone or *via* **phen** as a mediator).[44] Computational work by Patil supported **64** as the likely electron donor (although the subtleties of the electron transfer event are more complex than direct SET from **64** to the haloarene).[40]

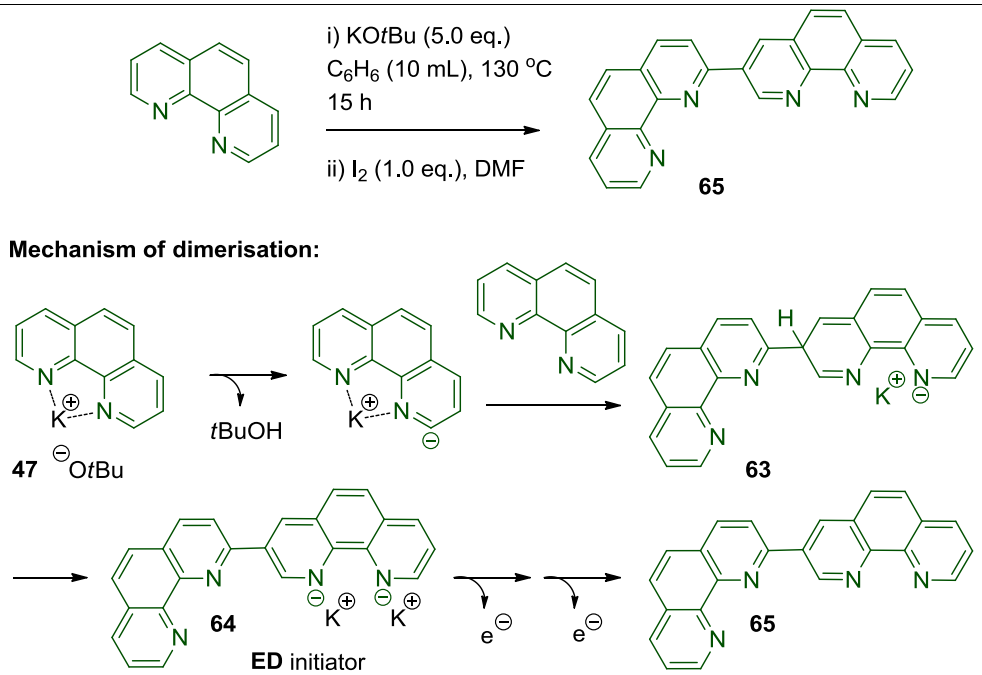

***Scheme 14**: Isolation and rationalisation of dimer **65** upon treating **phen** with KOtBu.*

The concept that organic additives formed electron donor initiators *in situ* was extended to rationalise how amino acids, alcohols and 1,2-diamines functioned in coupling reactions.[58] Known organic electron donors possess a common structural feature; an alkene substituted by electron-donating groups (Figure 3).[67] Of the electron donors shown, tetrathiafulvalene [**66**, $E^1_{1/2}$ = +0.36 V, $E^2_{1/2}$ = +0.15 V *vs*. SCE in DMF][68] is the least reducing but is able to reduce aryldiazonium salts to aryl radicals.[69,70] A computational study suggested that a redox potential of *ca*. -1.0 V *vs.* SCE was required to reduce aryl radicals to aryl anions,[71,72] which is significantly less facile than previously reported.[33,42] Tetrakis(dimethylamino)ethene [**67**, $E^1_{1/2}$ = -0.78 V, $E^2_{1/2}$ = -0.61 V *vs.* SCE in MeCN, or $E^1_{1/2}$ = -0.62 *vs*. SCE in DMF][73] can convert electron-deficient aryl bromides to anions[74] and CF_3I to the CF_3 anion,[75] but cannot reduce haloarenes without electron-withdrawing groups. More reducing still is imidazole-derived donor **68** (this exhibits a 2-electron wave at $E^1_{1/2}$ = -1.20 V *vs*. DMF) which reacts with iodoarenes to afford aryl

anions.[76] Moreover, dianion **69** is a potent electron donor with $E^1_{1/2}$ = -0.95 V, $E^2_{1/2}$ = -1.95 V *vs*. SCE in DMF, which can effect reductive cleavage of electron-rich iodoarenes, sulfones, Weinreb amides and aniline-derived sulfonamides (but not dialkyl arenesulfonamides).[77] Electron donor **70** was recently coined by Dyker and Murphy as 'the most reducing ground state organic electron donor' [$E^1_{1/2}$ (**70**$^{2+}$/**70**) = -1.70 V *vs*. SCE in DMF], which can cleave dialkyl arenesulfonamides and malononitriles without photoexcitation.[72] In the context of the transition metal-free C-H arylation reactions, organic additives could be converted into electron-rich alkene-containing species which resemble known organic electron donors.[67]

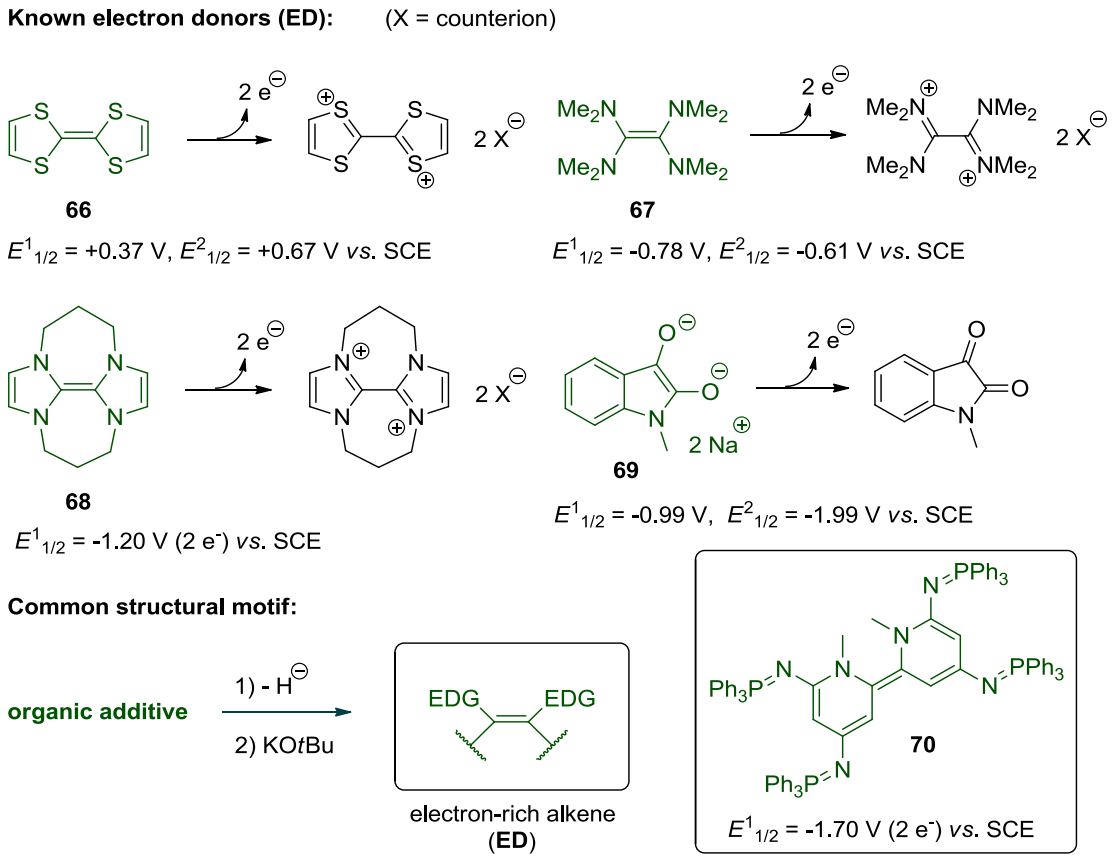

***Figure 3**: Known organic electron donors and common structural features. Proposed formation of organic electron donors in situ from treating organic additives with KOtBu.*

Murphy proposed a unifying mechanism for many of the reported additives: formation of an electron-rich enolate analogue (Figure 4).[58] Expulsion of hydride from cyclohexane-1,2-diol (**40**) followed by deprotonation of the resulting α-hydroxyketone (**71**) would give rise to electron-rich enolate analogue **72**. Enolate **72** could be the electron donor initiator itself or deprotonation on the hydroxyl group would afford an enediolate (**73**) as the electron donor initiator (that cyclohexane-1,2-diol (**40**) was more effective at promoting the coupling reaction of 2,6-dimethyliodobenzene **57a** than alcohol **77** suggests enediolate formation is important). Traces of DNP-adduct **74** were observed[58] thus confirming the occurance of Oppenauer-type oxidation of cyclohexane-1,2-diol (**40**) to α-hydroxyketone (**71**) under the reaction conditions (this was modelled computationally[58] and Woodward reported Oppenauer-type oxidation triggered by KO*t*Bu in toluene[78]).

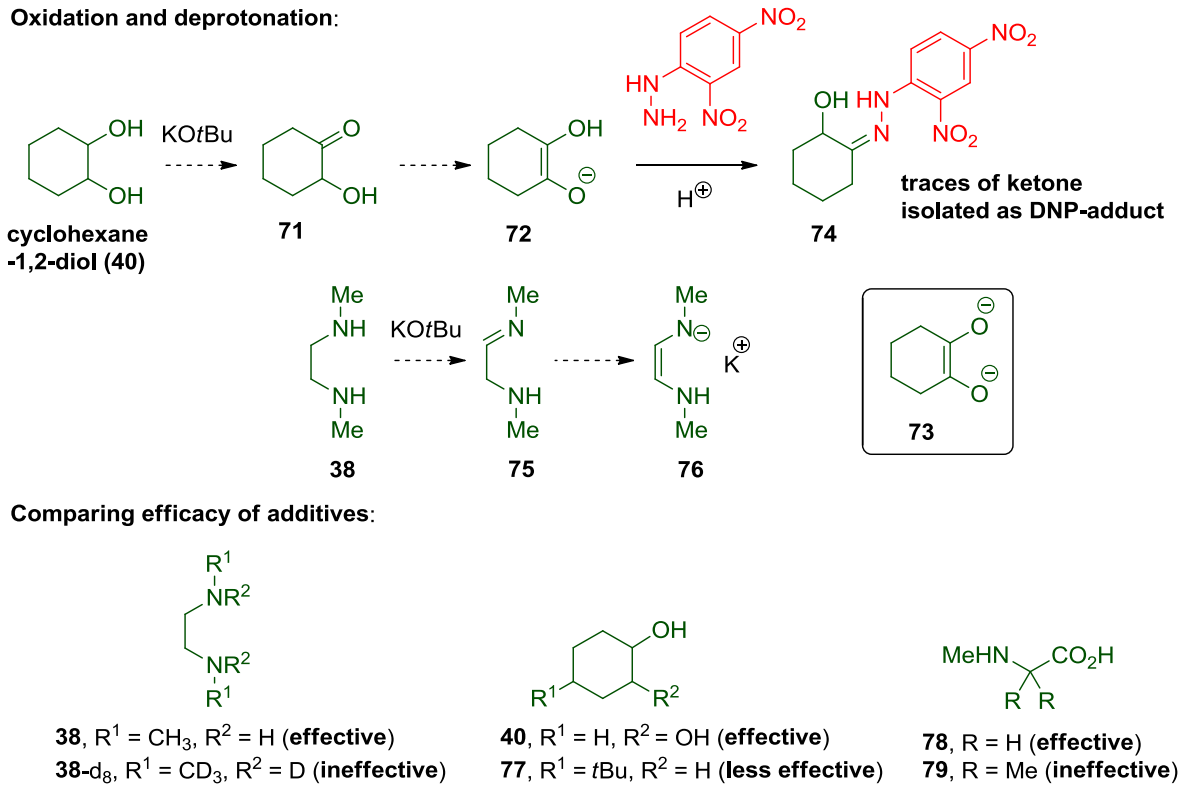

***Figure 4**: Comparison of organic additives and proposed mechanisms of activation.*

For DMEDA (**38**), oxidation and deprotonation would give electron-rich enamine **76** (which could be the electron donor initiator itself, or undergo a second deprotonation). This was demonstrated by comparing DMEDA (**38**) with its perdeuterated analogue (**38**-d_8) as additives in the coupling reaction of 2,6-dimethyliodobenzene **57a** (Scheme 12). Whilst DMEDA was an effective additive, the perdeuterated analogue DMEDA-d_8 was completely ineffective, presumably due to a KIE. Finally, whilst sarcosine (**78**) was an effective additive in the coupling reaction of **57a**, the analogous C,C-dimethylamino acid **79** (blocked to deprotonation at the CH_2) was completely ineffective.

1.2.7. Engaging Bromoarenes in Transition Metal-free C-H Arylations

Reported organic additives are extensively applied to iodoarenes with generally high success. Interestingly, whilst some organic additives effect couplings of bromoarenes [for example, **phen**, **Ph**-**phen**, pyridine (as solvent) and ethylene glycol],[1,3,34,49,53,54,57] others are not effective (for example, DMEDA (**38**), *n*BuOH, L-proline (**36**) and phenylhydrazine).[4,15,48,51,55,56] Apart from **phen** and **Ph**-**phen**, additives that successfully effected coupling of bromoarenes required temperatures exceeding 110 ^{o}C for extended reaction periods (up to 48 h).[34,53,54,57] That some additives promote coupling of bromoarenes and others do not (or do so less efficiently) suggests that the bottleneck is the initiation of the **BHAS** mechanism, rather than the propagation step (Figure 2). Indeed, the biaryl radical anion is highly reducing and should readily undergo SET with haloarenes [E^{p}_{red} (biphenyl/biphenyl$^{\bullet-}$) = -2.69 V *vs*. SCE in DMF].[79]

Kwong made an intriguing report that 2-pyridinecarbinol (**80**) efficiently promoted the transition metal-free C-H arylation with bromoarenes to give biaryl products in moderate to high (43 - 88%) yields at 80 ^{o}C (Scheme 15).[14] In one example, the reaction proceeded at rt to give a 68% yield of product (albeit with 0.4 eq. additive and after 72 h), the first report of a transition

metal-free C-H arylation at rt. The authors hesitate to comment on the mechanism for the coupling but make reference to the **BHAS** radical chain mechanism in their introduction section. Interestingly, at these milder conditions, no reaction was observed in the absence of 2-pyridinecarbinol (**80**), ruling out benzyne initiation.[44,58] Therefore, the electron-deficient 2-pyridinecarbinol (**80**) must be transformed under the reaction conditions into an electron donor initiator.

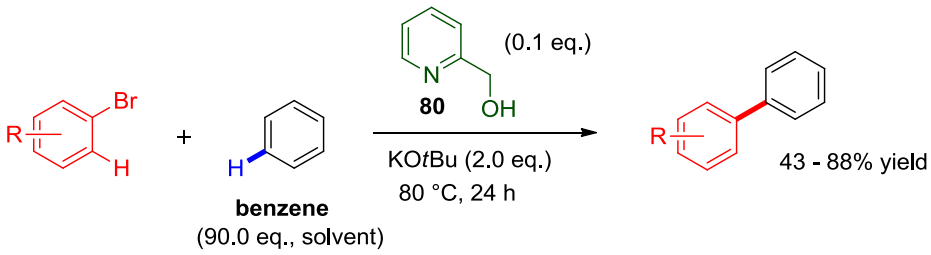

***Scheme 15**: C-H arylation with bromoarenes using 2-pyridinecarbinol as an additive.*

1.3 Transition Metal-free Dehalogenations

1.3.1. Reductive Dehalogenations using Lithium Aluminium Hydride

Beckwith reported a tin-free transition metal-free reductive dehalogenation of haloarenes using lithium aluminium hydride (**LAH**), di-*tert*-butyl peroxide (**DTBP**) and photochemical irradiation (Scheme 16).[80] Interestingly, iodo-, bromo-, chloro- and even fluoroarenes could be dehalogenated under these conditions. In the journey toward optimal reaction conditions, bromoarene substrate **83** was explored under a variety of conditions (Scheme 17).

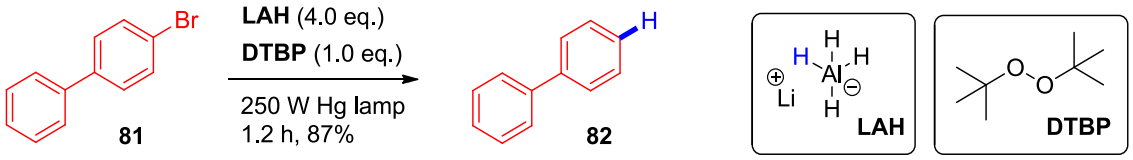

***Scheme 16**: Photochemical LAH-mediated dehalogenation.*

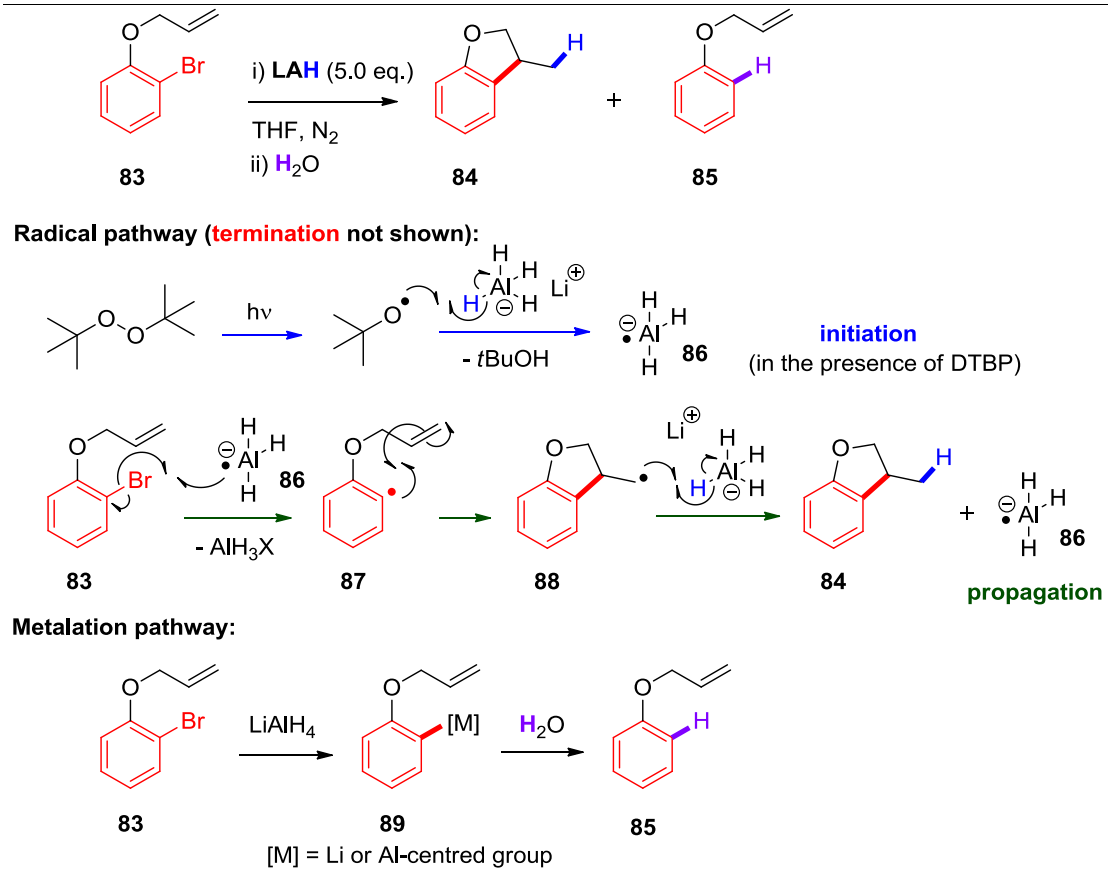

***Scheme 17**: Radical and metalation pathways for LAH-mediated dehalogenation.*

When bromoarene **83** was treated with LAH only under N_2 and quenched with D_2O after 28 h (18% reduction), dehalogenated product **85** was observed as the sole product with 91% D-incorporation.[81] Application of LAD under the same conditions for 64 h (17% reduction) gave a 10 : 1 mixture of **85** : **84**. Quenching with H_2O saw only 19% D-incorporation in **85** whereas quenching with D_2O saw 91% D-incorporation, suggesting D-incorporation in **85** came from D_2O. Interestingly, D-incorporation was pronounced in **84** regardless of whether the reaction was quenched with H_2O (71%) or D_2O (76%), suggesting D-incorporation in **84** came from LAD. Leaking air into the reaction mixture resulted in full conversion (100% reduction) after 22 h and the ratio of **85** : **84** was then 1 : 2.6. These results corroborate two distinct competing processes, the relative importance of which determine the rate

and outcome of the reaction.[81] One is a radical pathway; a radical chain mechanism is proposed (Scheme 17).[81]

An aluminium hydride complex **86** abstracts the bromine atom from **83** to afford aryl radical **87**, which undergoes rapid 5-*exo*-*trig* cyclisation to afford alkyl radical **88**. Alkyl radical **88** undergoes HAT with LAH to generate product **84** and regenerate the chain carrier (**86**). For reaction conditions involving **DTBP** and UV-light, homolysis of **DTBP** and HAT between the *tert*-butoxyl radical and LAH could serve as the initiation step to generate **86** (Scheme 17).[81] For reaction conditions in the absence of **DTBP** and UV-light which still give rise to product **84**,[81] the initiation step is unclear. The second pathway converts the haloarene to an arylmetal species (**89**) which is deuterated upon quenching by D_2O, in a non-radical mechanism. The identity and formation of the arylmetal species (**89**) is unclear. Instead of the radical mechanism proposed, intramolecular carboalumination of the pendant alkene by the arylmetal species could be envisaged. However, uncatalysed carboalumination of alkenes are generally reported under severe conditions which afford low regioselectivity, formation of by-products and polymerisation (although some selective homologations have been reported using trialkyl- and triarylaluminium reagents).[82–84]

Ultimately, addition of **DTBP** and ultraviolet irradiation favoured the radical mechanism and these conditions were applied as the optimal conditions for dehalogenation of a range of haloarenes, exemplified in Scheme 16.[80] Elsewhere, Jefford and Ashby reported that LAH can achieve challenging dehalogenations (for example, bridgehead and cyclopropyl haloalkanes, haloalkenes and haloarenes).[85–87] Ashby found evidence for radical intermediates and proposed single electron reduction of haloalkanes by LAH as the dominant mechanism.[86,87]

1.3.2. Reductive Dehalogenations and Decyanations using Alkali Metal Hydrides

Interestingly, Pierre reported the dehalogenation of iodo-, bromo- and chlorobenzene with potassium hydride (KH) under mild conditions (Scheme 18).[88] It was reported that treating iodobenzene with KH (5.0 eq.) in THF for 3 h at rt gave quantitative conversion of the starting material to benzene. Pierre excluded benzyne formation and an $S_{RN}1$-type mechanism due to the absence of evolved hydrogen gas (for a 5 mmol scale reaction, 0.11 L of hydrogen is expected at rt, 1 atm) and of biphenyl (**59**). Pierre acknowledged the possibility of an SET process, but found no evidence for radical intermediates by EPR spectroscopy during the reaction. The order of reactivity observed was ArI > ArBr >> ArCl, which ruled out an S_NAr mechanism. Therefore, Pierre proposed a non-radical mechanism involving concerted delivery of the hydride to the arene (and halide to the potassium) on the KH surface (Scheme 18). However, no evidence was provided for this mechanism.

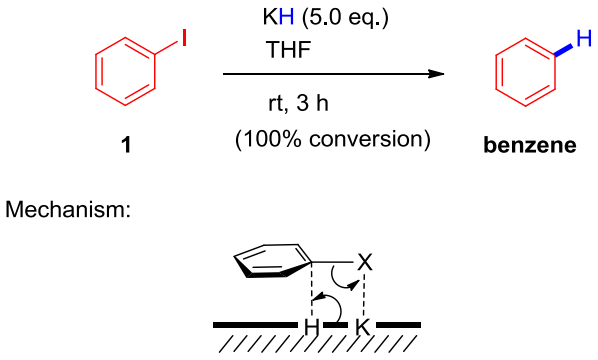

***Scheme 18**: Reductive dehalogenation of iodobenzene by KH, reported by Pierre.*[88]

Interestingly, Chiba reported a NaH/LiI composite-mediated decyanation reaction (Scheme 19).[89] Here, use of the potassium counterion (KI as the additive) gave poor conversion compared to LiI which gave near-quantitative conversion of **90** to reduced product **91**. Non-cyclisation of radical clock

substrates (such as **92**), together with deuterium labelling experiments (using THF-d_8 and D_2O) conclusively ruled out a radical mechanism.

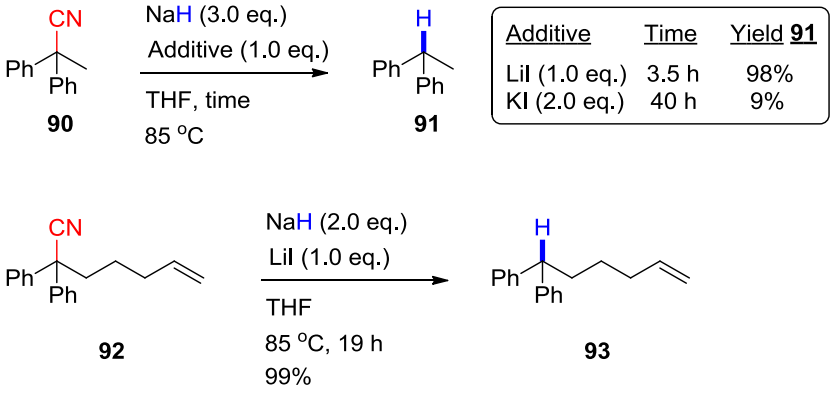

***Scheme 19**: NaH/LiI composite-mediated reductive decyanation reaction reported by Chiba.*[89]

1.3.3. Reductive Cleavage of Dithianes Mediated by Potassium *tert*-butoxide in DMSO

Moving to a different theme, Peñéñory reported a photochemical, KO*t*Bu-mediated reductive cleavage of dithianes in DMSO (Scheme 20).[90] It was reported that mixing dithiane **94** and KO*t*Bu in DMSO gave rise to a coloured electron donor/acceptor (**EDA**) complex (**96**). This **EDA** complex, upon photoexcitation, was proposed to undergo charge transfer to afford radical anion **97** and *tert*-butoxyl radical (which presumably decomposes according to pathways outlined in Scheme 9). Radical anion **97** undergoes C-S bond cleavage to afford open chain radical anion **98**, which undergoes HAT with 1,4-cyclohexadiene to afford **99** and the cyclohexadienyl radical. The second C-S bond cleavage could be triggered by formation of an **EDA** complex between **99** and KO*t*Bu, or deprotonation of the cyclohexadienyl radical to benzene radical anion (**100**), envisaged as a strong reductant. Reductive cleavage of **99** affords radical **101** and 1,3-propyldisulfide. Radical **101** engages in HAT with 1,4-cyclohexadiene to afford desired product **95** and the cyclohexadienyl radical.

It was envisaged that benzene radical anion (formed via deprotonation of the cyclohexadienyl radical) propagates a radical chain reaction by donating an electron to dithiane **94**. A quantum yield (Φ = 4.0) was calculated for the process (Φ > 1 is unequivocal evidence of radical chain mechanisms, see Volume 1 and Appendix for further details). Interestingly, this report implicates KO*t*Bu as a single electron donor initiator in a similar manner to that presented by Wilden, Jutand and Lei.[13,59,90]

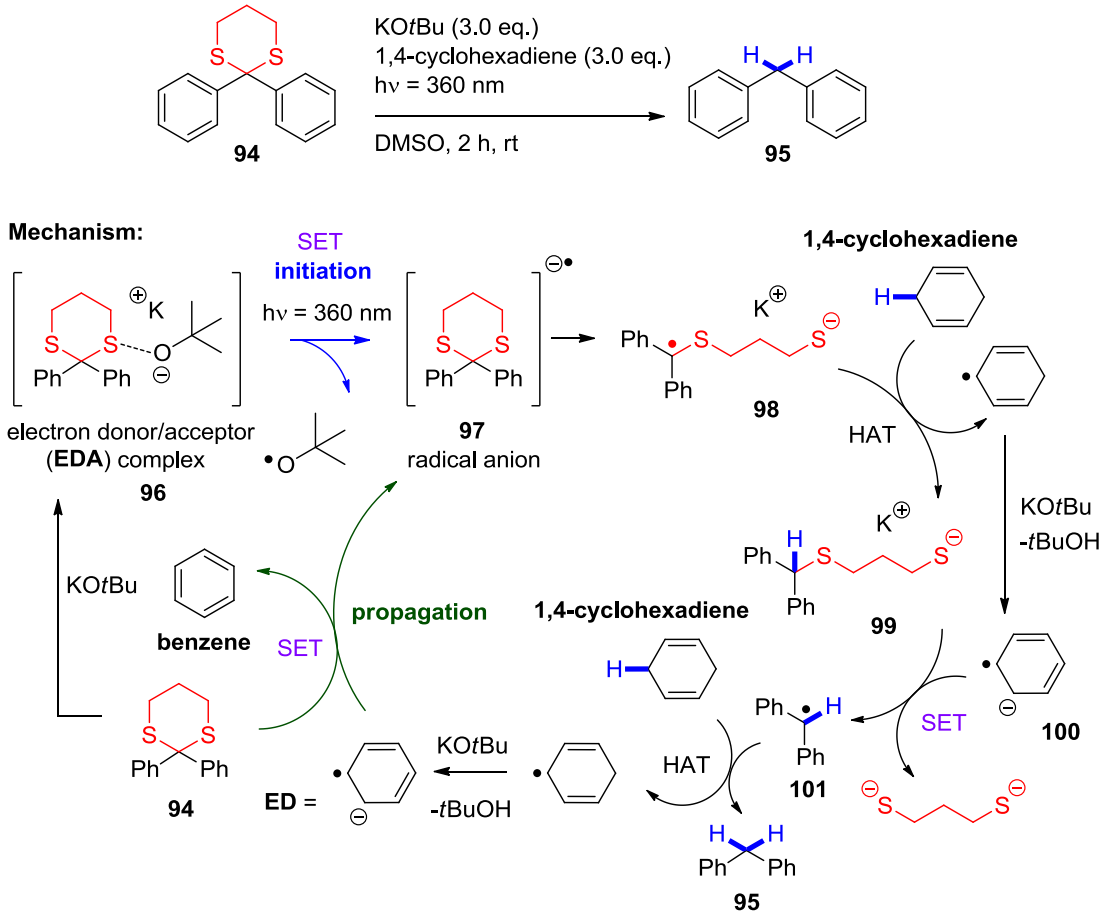

***Scheme 20*:** *Photochemical KOtBu-mediated reductive cleavage of dithianes in DMSO.*

1.4 PRIMARY AIM: TO DEVELOP FURTHER MECHANISTIC UNDERSTANDING IN TRANSITION METAL-FREE C-H ARYLATIONS AND REDUCTIVE CLEAVAGES

The primary aim of this research project is to develop further mechanistic understanding in transition metal-free C-H arylations and reductive cleavages; transformations which have attracted significant attention in recent years. Reactions generally proceed *via* radical pathways (commonly radical chain mechanisms). For example, transition metal-free C-H arylation is generally accepted to proceed *via* the Base-promoted Homolytic Aromatic Substitution (**BHAS**) radical chain reaction. However, the initiation step of these radical chain mechanisms is a topic of debate, with many reports claiming that potassium *tert*-butoxide (KO*t*Bu) donates single electrons (either directly or indirectly *via* a complex with an organic additive) to effect reductive cleavages. Computational studies and the difference in redox potentials raise grave concerns about the feasibility of this pathway.[44] Whilst KO*t*Bu appears to be a privileged reagent in these reactions (generally, other bases such as NaO*t*Bu, KOH and KOMe give no reaction), organic additives are generally necessary for reactivity and evidence has been presented for *in situ* transformation of these organic additives into organic electron donors which initiate **BHAS** reactions. The evidence presented for SET from KO*t*Bu will be critically examined in order to further mechanistic understanding in this evolving field.

Elsewhere, simple (non-transition) metal hydrides ($LiAlH_4$, NaH, KH) have been reported in reductive cleavage reactions (dehalogenations of haloarenes and haloalkanes), with hydride being the conceptually simplest reducing agent (besides the electron itself). However, the mechanism of these reactions remains unclear and so will form a subject of investigation.

1.5 Secondary Aim: To Elucidate the Role of Organic Additives which Allow Successful Coupling of Bromoarenes

Whilst iodoarenes are ubiquitous coupling partners in the field of transition metal-free C-H arylations, bromoarenes are less common. Successful coupling of bromoarenes depends on the reaction conditions employed and crucially on the nature of the organic additive. The secondary aim of this research project is to develop understanding in the behaviour of organic additives under C-H arylation reaction conditions. Kwong reported the transition metal-free C-H arylation with bromoarenes under relatively mild conditions using 2-pyridinecarbinol as an organic additive.[14] Is it intriguing that the electron-deficient 2-pyridinecarbinol should form an electron-rich organic electron donor under the reaction conditions, so this will represent the starting point for the investigation. The organic electron donor derived from 2-pyridinecarbinol, once identified, will be compared with other organic electron donors that enable coupling of bromoarenes. This should shed light on the features of organic electron donors which enable coupling to the challenging bromoarenes, thus allowing targeted design of novel organic additives which may allow coupling of chloroarenes in the future.

2. Results and Discussion

Volume 2 reports and discusses efforts toward developing mechanistic understanding in transition metal-free C-H arylation reactions and reductive cleavages. Firstly, in Chapter 2.1., evidence in the literature pertaining to KO*t*Bu as a single electron donor was critically examined and alternative interpretations are presented. Next, in Chapter 2.2., 2-pyridinecarbinol and analogues were investigated to gain insight into features of organic additives which lead to the initiation of transition metal-free C-H arylation reactions with bromoarenes. Finally, in Chapter 2.3., control reactions revealed an intriguing result; KH-mediated dehalogenation of haloarenes *via* a radical mechanism. Even *ortho*-disubstituted haloarenes were dehalogenated; these substrates are generally considered sole reporters of SET. Mechanistic studies on this transformation are disclosed.

2.1. The Role of potassium *tert*-butoxide in Transition Metal Free C-H Arylations with Haloarenes and in Reductive Cleavages

The work described in Chapter 2.1. was carried out as part of a collaborative project during a secondment to the University of Strathclyde, and includes contributions from Dr. Graeme Coulthard, Dr. Eswararao Doni and Florimond Cumine for completeness of the story. Dr. Graeme Coulthard and Joshua Barham contributed equally to Section 2.1.1., Dr Graeme Coulthard and Florimond Cumine were the sole contributors to Sections 2.1.3. and 2.1.5, respectively. Dr. Eswararao Doni prepared EPR samples for Section 2.1.7., which were analysed by Prof. John Walton at the University of St. Andrews. Joshua Barham was the sole contributor to Sections 2.1.2., 2.1.6. and 2.1.8.

(Dr. Graeme Coulthard prepared dimer **65** for Sections 2.1.6.). Unless otherwise stated, all work was conducted by Joshua Barham.

2.1.1. UV-VISIBLE SPECTROSCOPY INVESTIGATION OF THE JANOVSKY TEST

A positive Janovsky test (an intense purple coloration)[63] was presented by Wilden as evidence for the presence of butanone resulting from the breakdown of a *tert*-pentoxyl radical, which itself was proposed to arise from SET from potassium pentoxide to **phen** (Scheme 9).[13] It was reported that treating a few drops of a 1 : 1 mixture of **phen** and potassium *tert*-pentoxide in THF with 1,3-DNB (**51**) in a NaOH solution gave rise to a purple colour, attributed to species **52a** (Scheme 10, Section 1.2.5.). According to this rationale, mixing potassium *tert*-butoxide with **phen** and 1,3-DNB (**51**) should give **52b**. Aware of the dangers of drawing conclusions from a colour test, this Janovsky test was then investigated by UV-visible spectroscopy. If adduct **52a** (Scheme 10, which mirrors **52b**) was giving rise to the purple colour in Wilden's Janovsky test, deprotonation of ketone **54b** (prepared from chloroacetone and 1,3-dinitrobenzene using DBU as a base) should give **52b** and the same colour (Figure 5).

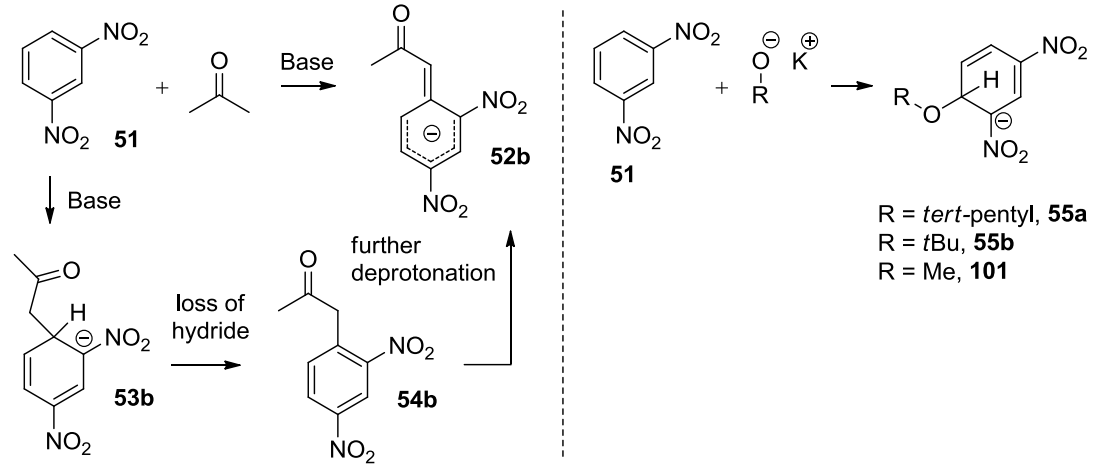

***Figure 5**: Left: Mechanistic considerations when treating 1,3-DNB with ketones under basic conditions. Right: Direct nucleophilic addition of tert-butoxide to 1,3-DNB.*

When **54b** was dissolved in THF and treated with KO*t*Bu (1.0 eq.), an intense red/purple colour was observed (Figure 6, right, **A**) and an intense UV-visible absorption at 490 nm was observed, corresponding to **52b** (Figure 6, left, red trace). Although full experimental details were not provided for Wilden's Janovsky test,[13] it was decided to investigate the test with KO*t*Bu and **phen**, proposed to generate acetone in the coupling reactions. Thus, **phen** (1.0 eq.) and KO*t*Bu (1.0 eq.) were dissolved in THF and stirred at room temperature for 2 h. When 1,3-DNB (**51**) was added, the purple colour observed was different (Figure 6, right, **B**) and the solution gave a UV-visible absorption peak at 554 nm (Figure 6, left, green trace). Therefore, this purple colour did not correspond to **52b** but another species, likely to be either **53b** or **55b**.

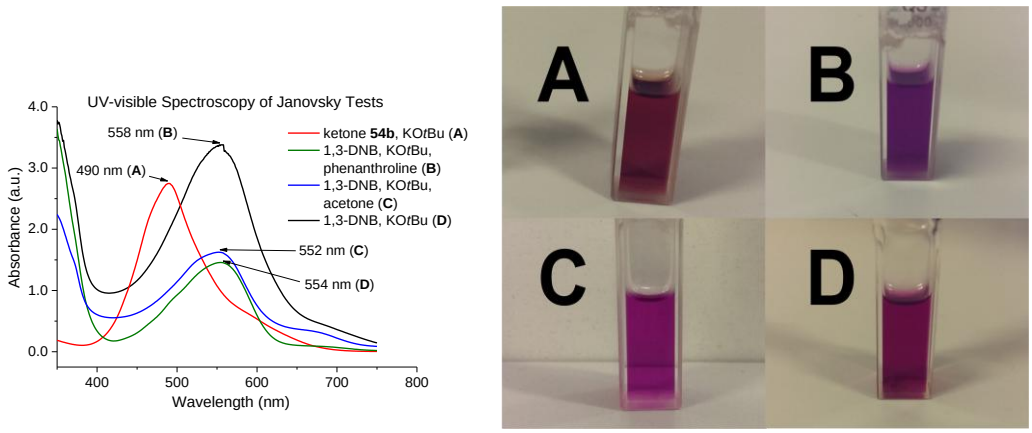

***Figure 6**: Left: UV-visible spectroscopy of Janovsky tests. Right: Purple colours observed.*

To probe further, KO*t*Bu (1.0 eq.), acetone (1.0 eq.) and 1,3-DNB (**51**) were combined in THF. The result was the same regardless of the order of addition; a similar purple colour was observed (Figure 6, right, **C**) with a UV-visible absorption at 552 nm (Figure 6, left, blue trace). This result gave the same absorption as a comparison sample using NaOH as base, consistent with that reported by Pollitt and Saunders.[63] Finally, the test was conducted in the absence of any added acetone. Thus, KO*t*Bu (1.0 eq.) was dissolved in THF and 1.0 eq. of 1,3-DNB (**51**) was added. The result was striking; a

similar purple colour was observed (Figure 6, right, **D**) with a UV-vis absorption at 558 nm (Figure 6, left, black trace). The result was *indistinguishable from that when a ketone was present in the mixture*, *indicating that a purple colour in the Janovsky test is not confirmation of the presence of a ketone*. The similarity of purple colours observed (Figure 6, right) indicate the dangers of drawing conclusions from a visual colour test. The results demonstrate that the species giving rise to a purple colour in Wilden's Janovsky test is not adduct **52b**, but is likely to be adduct **53b** or **55b**. To probe further, Janovsky tests were analysed by ^{1}H NMR.

2.1.2. ^{1}H NMR Spectroscopy Investigation of the Janovsky Test

Remarkably, Meisenheimer adducts to 1,3-DNB in the Janovsky test are stable enough to be observed by ^{1}H NMR. The addition of acetone to 1,3-DNB (**51**) under alkali conditions to give **53b** was observed by Fyfe and Foster.[64] Upon repeating their study, **53b** was successfully detected in DMSO-d_6 (Figure 7) with consistent peak multiplicities and consistent chemical shift differences between peaks to those reported (Fyfe and Foster quote chemical shifts in τ, ppm).[64] Since the UV-visible study could not distinguish between Meisenheimer adducts **53b** and **55b** as responsible for the purple colour, it was hypothesised that ^{1}H NMR might allow identification of **53b** or **55b** in Janovsky tests without added acetone. The poor solubility and potential reactivity[62] of metal alkoxides in $CDCl_3$ ruled out this NMR solvent. Residual DMSO and H_2O signals in DMSO-d_6 obscured signals of interest. Ultimately, DMF-d_7 was identified as a suitable solvent for the investigation.

Firstly, 1,3-DNB (**51**) was dissolved in DMF-d_7 and analysed by ^{1}H NMR (Figure 8), revealing three aromatic C*H* signals [^{1}H NMR (400 MHz, DMF-d_7) δ 8.94 (1H, t, *J* = 2.0 Hz, C*H*), 8.74 (2H, dd, *J* = 8.2, 2.1 Hz, C*H*), 8.09 (2H, t, *J* = 8.2, C*H*)] as expected. Addition of NaOMe (1.0 eq.) to 1,3-DNB (1.0 eq) dissolved in DMF-d_7 : acetone (1 : 1) immediately gave a dark purple solution

which was analysed by ^{1}H NMR. The spectrum observed (Figure 9) was broadly similar to that observed by Fyfe and Foster in DMSO-d$_6$ for **53b**,[64] [^{1}H NMR (400 MHz, DMF-d$_7$) discernable signals: δ 8.48 (1H, d, *J* = 2.0 Hz, C*H*), 6.72 - 6.66 (1H, m, C*H*), 5.43 (1H, dt, *J* = 10.3, 5.0, C*H*), 3.86 (1H, apt. q, *J* = 5.3, C*H*), 3.86 (1H, dt, *J* = 10.3, 5.0, C*H*)] identifying adduct **53b** (the C*H*$_3$ singlet and one of the C*H*$_2$ protons were masked by solvent signals, two unidentified signals were observed at δ 2.59 and 4.35 ppm).

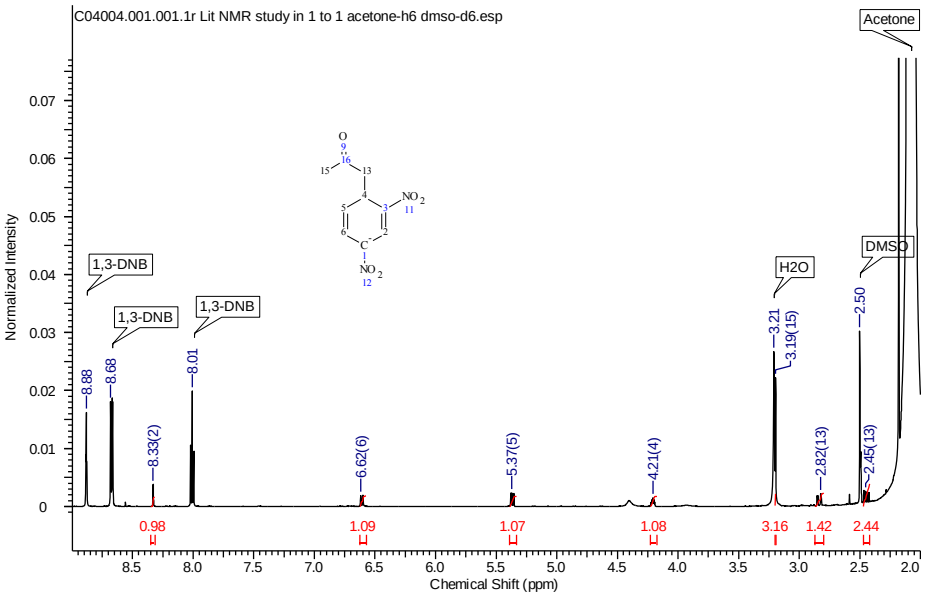

***Figure 7**: ^{1}H NMR spectrum of adduct **53b** in DMSO-d$_6$.*

Addition of NaOMe (1.0 eq.) to 1,3-DNB (**51**) (1.0 eq.) in DMF-d$_7$ (no acetone present) gave a dark purple solution which was analysed by ^{1}H NMR. The spectrum observed (Figure 10) now contained more deshielded peaks and an OC*H*$_3$ singlet [^{1}H NMR (400 MHz, DMF-d$_7$) discernable signals: δ 8.65 (1H, dd, *J* = 2.3, 1.0 Hz, C*H*), 7.15 (1H, dd, *J* = 9.4, 2.1 Hz, C*H*), 5.57 - 5.51 (2H, m, C*H*), 2.85 (3H, s, C*H*$_3$)] data which were consistent with the structure of **101** (an unidentified, minor component was also observed with discernable peaks at δ 8.52 ppm, 6.93 ppm and 5.58 ppm).

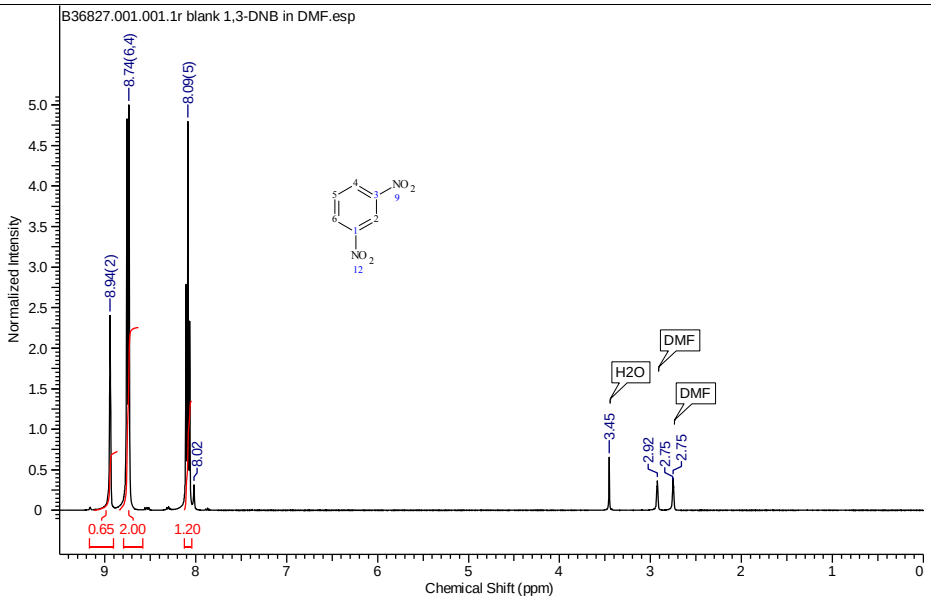

***Figure 8**: ^{1}H NMR spectrum of 1,3-dinitrobenzene (**51**) in DMF-d_7.*

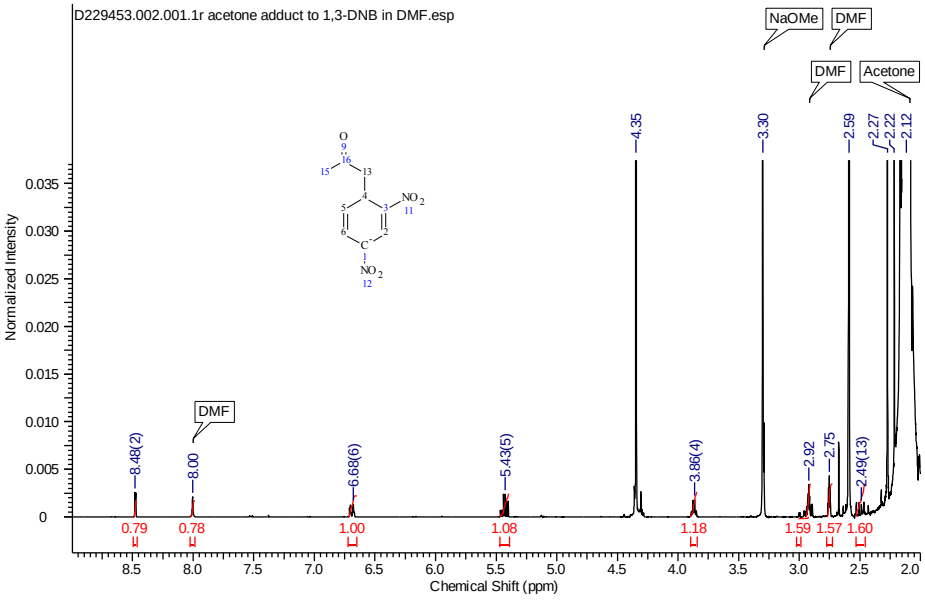

***Figure 9**: ^{1}H NMR spectrum of adduct **53b** in DMF-d_7.*

Unfortunately, the equivalent experiment using KO*t*Bu instead of NaOMe gave a complex mixture by ^{1}H NMR, potentially due to the stronger base (KO*t*Bu) facilitating further deprotonations at the higher concentrations employed here (compared to the UV-visible spectroscopy study of the Janovsky test). However, the study demonstrates the ability of alkoxides to form Meisenheimer adducts with 1,3-DNB (**51**) and therefore Meisenheimer

adduct **55b** is a likely candidate for causing the the purple coloration (since Wilden used potassium *tert*-pentoxide, the corresponding species would be **55a**, see Section 1.2.4.).

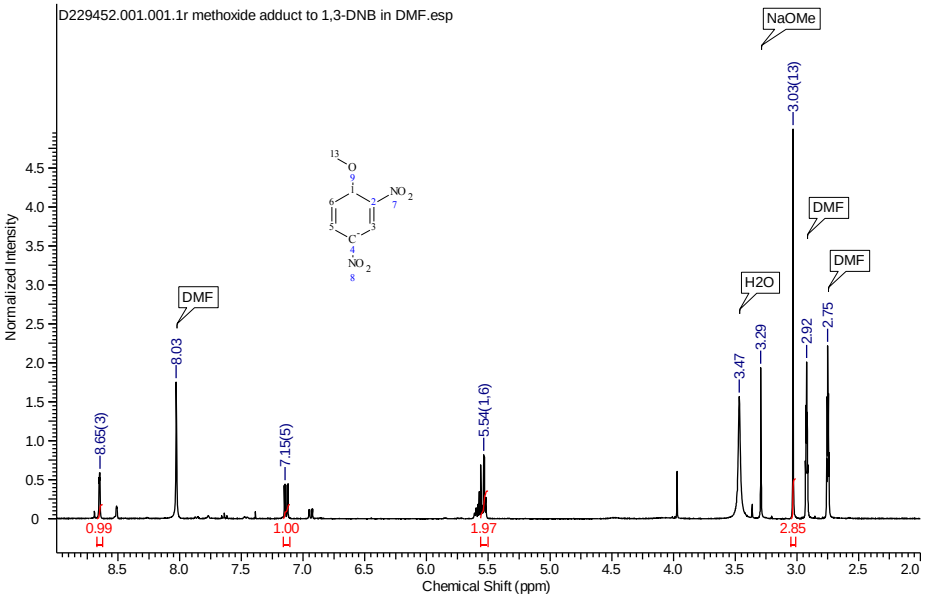

***Figure 10**: [1]H NMR spectrum of adduct **101** in DMF-d_7.*

2.1.3. ^{1}H NMR Spectroscopy Investigation of the Interaction Between Potassium *tert*-Butoxide and 1,10-Phenanthroline

Wilden reported that an equimolar mixture of **phen** and KO*t*Bu in THF gave rise to a 'black tar' immediately (here, the concentration used was unspecified).[13] When **phen** (1.0 eq.) and KO*t*Bu (1.0 eq.) were mixed in THF-d_8 under an inert atmosphere a blue/green colour resulted, but no black tar or precipitate was observed (here, the concentration used was 0.4 M). After 2 h at rt the mixture was analysed by ^{1}H NMR (Figure 11). In contrast to the observations of Wilden, no collapse of the *tert*-butyl signal [^{1}H NMR (400 MHz, THF-d_8) δ 1.16 (9H, s, CH_3)] was observed relative to the **phen** aromatic C*H* signals [^{1}H NMR (400 MHz, THF-d_8) δ 9.18 (2H, dd, *J* = 4.3, 1.5 Hz, C*H*), 8.30 (2H, dd, *J* = 8.3, 1.8 Hz, C*H*), 7.84 (2H, s, C*H*), 7.62 (2H, dd, *J* = 8.0, 4.3 Hz, C*H*)]. Despite mixing the two reagents in THF, it appears likely that Wilden's ^{1}H NMR spectrum[13] was recorded in $CDCl_3$ (a singlet is

seen at δ 7.27 ppm) raising our concerns over the solubility and reactivity of KO*t*Bu in this solvent.

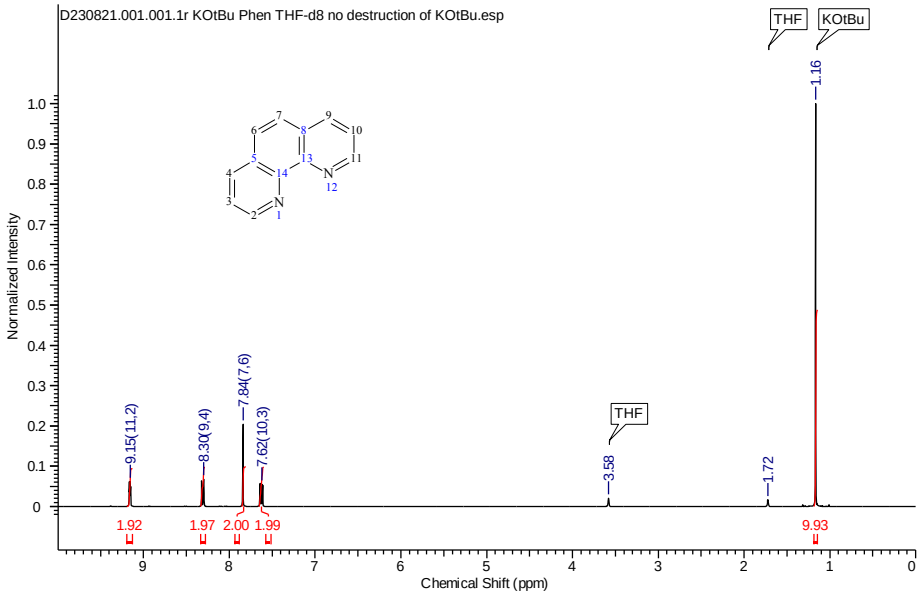

***Figure 11**: [1]H NMR spectrum of an equimolar mixture of **phen** and KOtBu in THF-d_8.†*

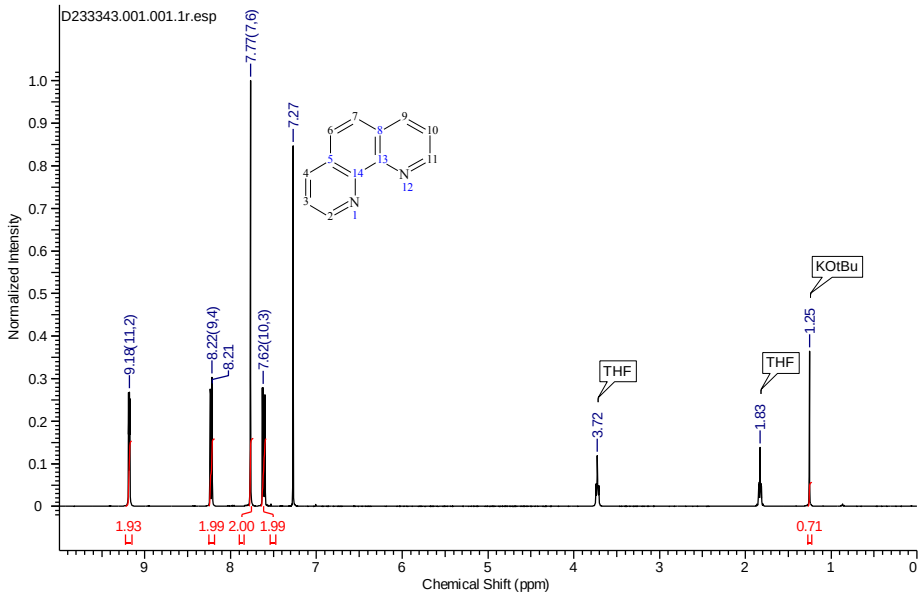

***Figure 12**: [1]H NMR spectrum of an equimolar mixture of **phen** and KOtBu in $CDCl_3$.†*

†Samples prepared and analysed by Dr. Graeme Coulthard at the University of Strathclyde.

When the experiment was then repeated in $CDCl_3$ solvent (Figure 12), collapse of the *tert*-butyl signal [^{1}H NMR (400 MHz, $CDCl_3$) δ 1.16 (0.7H, s, CH_3)] was observed relative to the **phen** aromatic C*H* signals [^{1}H NMR (400 MHz, $CDCl_3$) δ 9.18 (2H, dd, *J* = 4.3, 1.8 Hz, C*H*), 8.22 (2H, dd, *J* = 8.3, 1.8 Hz, C*H*), 7.77 (2H, s, C*H*), 7.62 (2H, dd, *J* = 8.2, 4.4 Hz, C*H*)] consistent with Wilden's observation. The comparison of scenarios in THF-d_8 and $CDCl_3$ suggest that KO*t*Bu exhibits poor solubility in, or background reactivity[†] with,[62] $CDCl_3$.

2.1.4. Initiation *via* Dimerisation of 1,10-phenanthroline to Generate an Electron Donor *in situ*

As highlighted in Chapter 1.2., additive-free conditions gave no reaction of 2,6-dimethyliodobenzene (**57a**), inconsistent with KO*t*Bu's proposed role as a single electron donor. In the presence of **phen**, the reaction afforded biaryl **58** and biphenyl **59** in a combined yield of 18% (35% of **57a** remained), with a 3.4 : 1 ratio of **58** : **59** (Table 1). In the presence of **phen** and substituting KO*t*Bu (pK_a (*t*BuOH) = 17 in H_2O) for the stronger base KH (pK_a (H_2) = 35 in H_2O),[91,92] the reaction afforded biaryl **58** and biphenyl **59** in a combined yield of 15%. A 3.9 : 1 ratio of **58** : **59** was observed in the KH/**phen** reaction.

The ratios of **58** : **59** being similar for KO*t*Bu and KH suggested that biaryls **58** and **59** were formed through the same mechanism in both cases. That the reaction proceeds in this way with KH as a surrogate base suggests that KO*t*Bu is not a privileged reagent and that dimerisation of **phen** to electron donor **64** is the likely mode of initiation. An interesting observation was that only traces of **57a** remained in the KH/**phen** reaction; this will be revisited and discussed in Section 2.3.1.

[†]If KO*t*Bu reacted with $CDCl_3$ to give *t*BuOD, this could have been lost to evaporation, see Section 5.2.4.

Table 1: *Coupling reactions of 2,6-dimethyliodobenzene with benzene in the presence of* ***phen****. Comparison of KOtBu and KH.*

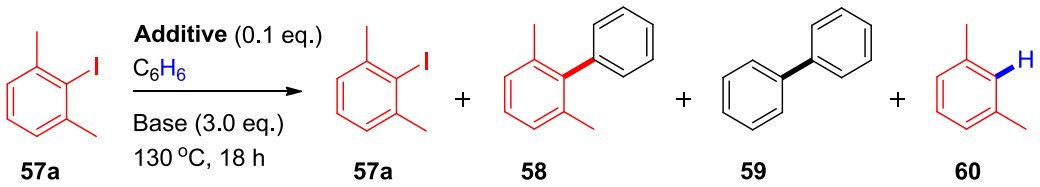

Entry	Additive/Base	57a[a] :	58[a] :	59[a] :	60[a]	Biaryl yield, mg[b] [recovered 57a (%)]
1	None/KO*t*Bu	1 :	< 0.01 :	< 0.01 :	< 0.01	0.3 [72]
2	**phen**/KO*t*Bu	1 :	0.12 :	0.41 :	0.15	15.5 [34][c]
3	**phen**/KH	1 :	5.32 :	21.0 :	15.9	13.0 [< 1][c]

[a]Ratios of products were determined by ^{1}H NMR of the reaction mixture at the end of the reaction, relative to the amount of **57a** which was arbitrarily set to 1. [b]Yield (mg) of combined biaryls (**58** and **59**), determined by ^{1}H NMR using 1,3,5-trimethoxybenzene (10 mol%) as an internal standard, yield (%) of returned **57a** shown in parenthesis (see Appendix for example calculations). [c]Reactions were conducted side-by-side.

2.1.5. Evidence of Aryne Formation Under Additive-free Conditions

When the additive-free conditions reported by Wilden were then applied to 4-iodotoluene (a 66% isolated yield of product **15** was reported) biaryl product **15** was isolated in only 27% yield, along with an inseparable mixture of products **102a** and **102b** in a 1 : 1 ratio, 40% combined yield (such products were not reported by Wilden).[†,13] This result demonstrates the formation of arynes under the reaction conditions, which lends weight to the proposal that arynes are involved in *initiating* the **BHAS** mechanism (product **15** is a single regioisomer, delivered overwhelmingly from the propagation step of the **BHAS** mechanism).

[†]This reaction was conducted by Florimond Cumine at the University of Strathclyde.

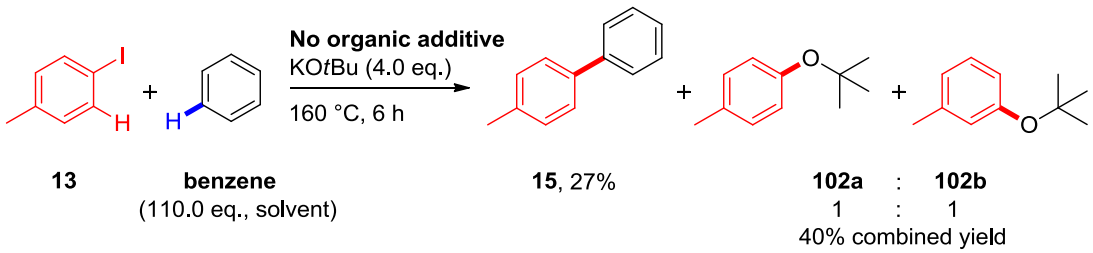

***Scheme 21**: Reaction of 4-iodotoluene under additive-free conditions.*

2.1.6. Cyclic Voltammetry Investigation into Electron Donors Derived from 1,10-phenanthroline and potassium *tert*-butoxide

Jutand and Lei had proposed a **phen**/KO*t*Bu complex initiated the **BHAS** mechanism on the basis of CV and EPR data.[59] On the other hand, Murphy had treated **phen** with KO*t*Bu under the reaction conditions and observed formation of dimer **65** (upon quenching the reaction with I_2 as an electron acceptor)[44] which implicated **64** as the electron donor initiator (Section 1.2.6.). To investigate further, **phen** and dimer **65**† were compared by CV (Figure 13). Operating under Jutand and Lei's CV conditions (0.3 M nBu$_4$NBF$_4$ in DMF, 0.5 V s^{-1} scan rate, rt, Pt wire working electrode and SCE reference electrode), the two reduction peaks observed for **phen** [E^{p1}_{red} (**phen**/**phen**$^{\bullet-}$) = -2.05 V, E^{p2}_{red} (**phen**$^{\bullet-}$/**phen**$^{2-}$) = -2.24 V *vs*. SCE] were consistent with those reported by Jutand and Lei [E^{p1}_{red} (**phen**/**phen**$^{\bullet-}$) = -2.03 V, E^{p2}_{red} (**phen**$^{\bullet-}$/**phen**$^{2-}$) = -2.23 V *vs*. SCE].[59]

By comparison with ferrocene peak currents (Figure 13, right, red trace), both peaks correspond to single electron transfers. Three peaks were observed for dimer **65**, [E^{p1}_{red} (**dimer**(**65**)/**dimer**$^{\bullet-}$(**103**)) = -1.70, E^{p2}_{red} (**dimer**$^{\bullet-}$(**103**)/**dimer**$^{2-}$(**64**)) = -1.94, E^{p3}_{red} (**dimer**$^{2-}$(**64**)/**dimer**$^{4-}$(**104**)) = -2.19 V *vs*. SCE]. The first two peaks correspond to one-electron transfers, forming **103** and **64**, respectively (Scheme 22). Due to the greater delocalisation

†Dimer **65** was synthesised by Dr. Graeme Coulthard at the University of Strathclyde.

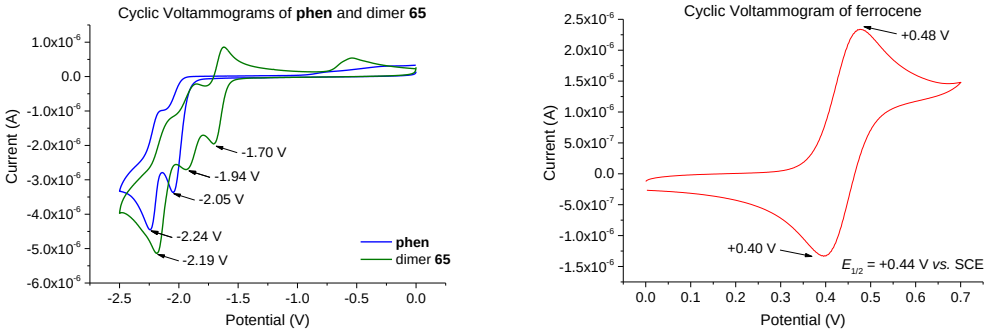

***Figure 13**: Left: Cyclic voltammograms of **phen** and dimer **65**. Right: Cyclic voltammogram of ferrocene as an external standard.*

afforded by the π-system of dimer **65**, it is reasonable to expect that cathodic voltages required to achieve reduction of dimer **65** and radical anion **103** are lower than those required to achieve reduction of **phen** and **phen**$^{\bullet-}$. The third peak corresponds to a two electron transfer to dianion **64** affording tetra-anion **104** [E^{p3}_{red} (**dimer**$^{2-}$(**64**)/**dimer**$^{4-}$(**104**)) = -2.19 V *vs*. SCE]. For a full discussion of this phenomenon, see Experimental, Section 5.2.7.

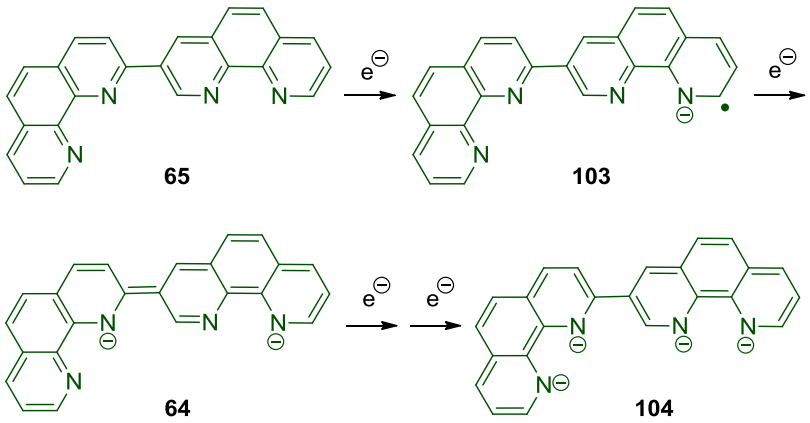

***Scheme 22**: Sequential transfer of single electrons to dimer **65**.*

Whilst the reduction potential of the dimer dianion **64** [E^{p2}_{red} (**dimer**$^{\bullet-}$(**103**)/**dimer**$^{2-}$(**64**)) = -1.94 V *vs*. SCE] is less negative than the reduction potential of **phen**$^{\bullet-}$ [E^{p1}_{red} (**phen**/**phen**$^{\bullet-}$) = -2.05 V *vs*. SCE, proposed to be the electron donor by Wilden, Jutand and Lei],[13,59] *it is reducing enough to undergo SET with haloarenes* (by comparison with a

neutral organic electron donor with E^{p1}_{red} = -1.70 V *vs*. SCE which reduces alkoxy-substituted iodoarenes).[72] Since dianion **64** can be formed from **phen** without electron donation from KO*t*Bu, this represents a strong alternative case for **64**, rather than KO*t*Bu, as the electron donor initiator in reactions involving **phen**. Attention was next directed to Jutand and Lei's EPR spectroscopy findings.

2.1.7. EPR Spectroscopy Investigation into Radical Species Derived from 1,10-phenanthroline and potassium *tert*-butoxide

In addition to their CV study, Jutand and Lei disclosed EPR spectra interpreted as evidence for SET from KO*t*Bu to **phen** and from **phen**$^{\bullet-}$ to haloarenes.[59] However, close inspection of their spectrum (Figure 2 within that publication)[59] revealed that the signal is not a symmetrical signal, indicating that more than one phenanthroline-type radical species was present. When **phen** was treated with KO*t*Bu and the mixture analysed by EPR in the study disclosed herein, the spectrum obtained was similar to the literature, although what appeared to be signs of hyperfine coupling or multiple radicals were observed (Figure 14, left). A second derivative spectrum revealed a large central reservation atop a smaller signal displaying hyperfine coupling, indicating multiple (possibly two) radical species (Figure 14, right).

Treating **phen** with KO*t*Bu yields dianion **64** which, due to matching redox potentials, could donate an electron to unreacted **phen** to yield **phen**$^{\bullet-}$ and dimer radical anion **103**. We note that this process appears thermodynamically unfavourable by cyclic voltammetry (Figure 13), but acknowledge the overlap of reduction waves as well as the sensitivity of EPR spectroscopy to minute concentrations of radicals. In the absence of hyperfine coupling and with the broad nature of the EPR signals observed, it is difficult to rely on this method to provide insight into the interaction between KO*t*Bu and **phen**.

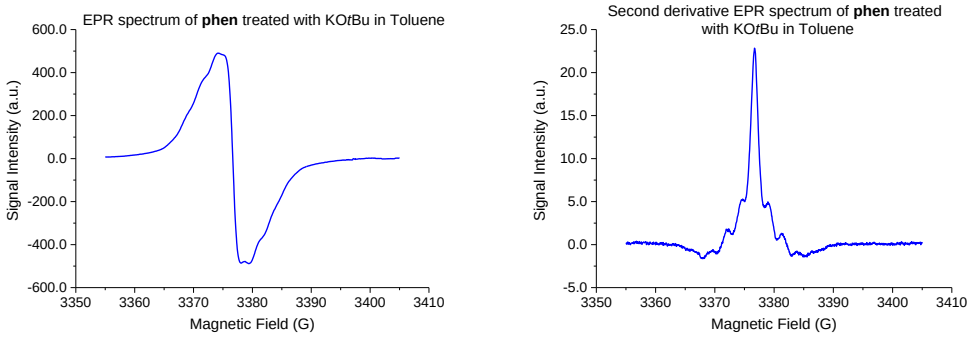

***Figure 14**: Left: EPR spectrum of **phen** treated with KOtBu in toluene. Right: Second derivative EPR spectrum.*[†]

2.1.8. UV-VISIBLE SPECTROSCOPY INVESTIGATION OF THE PHOTOCHEMICAL POTASSIUM *tert*-BUTOXIDE-MEDIATED REDUCTIVE CLEAVAGE OF DITHIANES

Dithiane **94** was synthesised from benzophenone and 1,3-propanedithiol in 40% yield, and appeared colourless in DMSO solution (Figure 15, right, A). No absorption in the visible was observed by UV-visible spectroscopy (Figure 15, **A**, black trace). Operating under Peñéñory's conditions, treating dithiane **94** (1.2×10^{-5} M) with KO*t*Bu (0.05 M) in DMSO gave rise to a yellow colour (Figure 15, right, **B**). UV-visible spectroscopy identified an absorption (466 nm) consistent with that observed by Peñéñory (Figure 15, left, red trace).

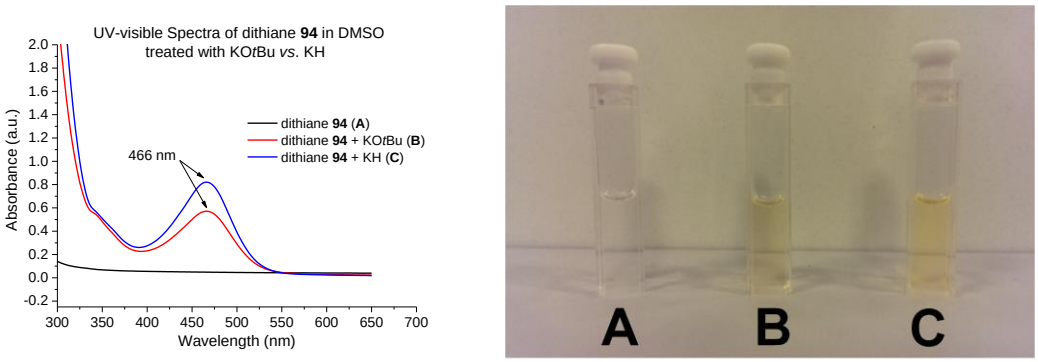

***Figure 15**: Left: UV-visible spectra of dithiane **94** in the presence of KOtBu and KH in DMSO. Right: Sample colours observed.*

[†]Sample prepared by Dr. Eswararao Doni and analysed by Prof. John Walton at the University of St. Andrews.

Interestingly, treating dithiane **94** (1.2 x 10^{-5} M) with KH (0.05 M) in DMSO gave an identical but more intense yellow colour (Figure 15, right, **C**) and UV-visible absorption (466 nm) (Figure 15, left, blue trace). When the photochemical cleavage reaction mediated by KO*t*Bu was performed under Peñéñory's conditions, a 50% yield of diphenylmethane (**95**) was determined by NMR of the crude reaction mixture (1,3,5-trimethoxybenzene was added as an internal standard) and an isolated yield of 45% resulted (Scheme 23). Interestingly, the reaction still proceeded when mediated by KH (albeit less cleanly) to give a 16% yield of **95** by NMR (13% isolated yield) amongst other products. In the absence of base, no reaction occurred. During the preparation of the reaction mixture for the photochemical cleavage reaction mediated by KH, evolution of gas was observed. Deprotonation of DMSO by KH to evolve H_2 gas is well precedented within the literature.[93] As such, we postulated whether the **EDA** complex giving rise to the colour was actually **105**, a complex of the *dimsyl anion and dithiane* **94** (Scheme 23).

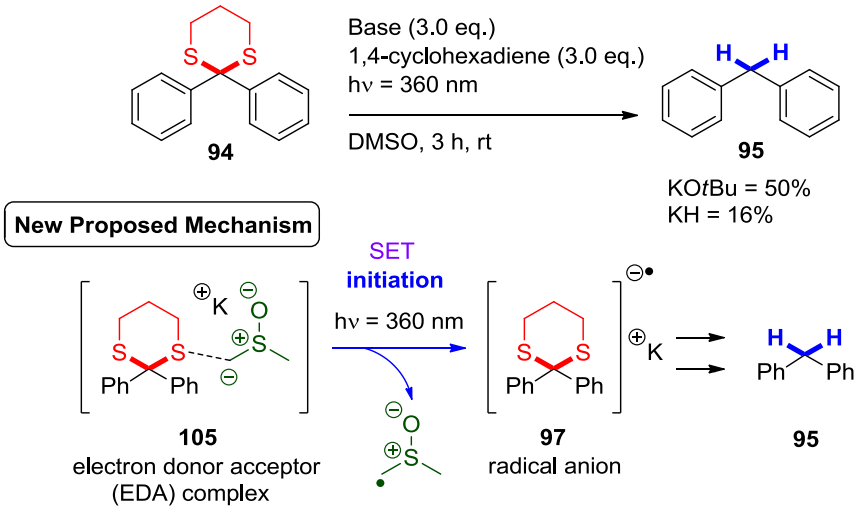

***Scheme 23**: Photochemical reductive cleavage of dithianes in DMSO mediated by KOtBu vs. mediated by KH and new proposed mechanism.*

This hypothesis was confirmed when Peñéñory's UV-visible study was conducted substituting DMSO for DMF. In DMF, neither dithiane **94** (Figure 16, **A**, red trace) nor its treatment with KO*t*Bu (Figure 16, **B**, blue trace)

resulted in a colour or UV-vis absorption. The only peak observed was the absorption of DMF at 330 nm (Figure 16, black trace).

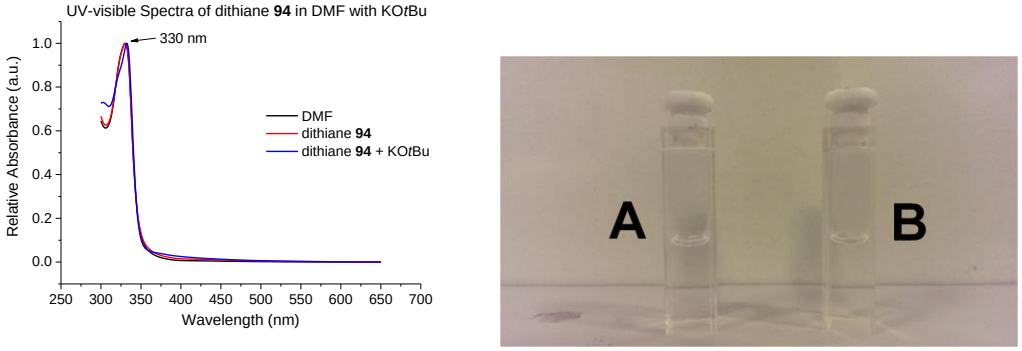

***Figure 16**: Left: UV-visible spectra of dithiane **94** in the presence of KOtBu in DMF. Right: Sample colours observed.*

In summary, a number of reports have advocated that KO*t*Bu functions as a single electron donor whilst providing little experimental evidence for this. In the transition metal-free C-H arylations with haloarenes, it is found herein that to date, there is no evidence to support KO*t*Bu acting directly as a single electron donor to haloarenes. This accords with a large mismatch in the redox potentials of KO*t*Bu [E^{p}_{ox} ($^{\bullet}$O*t*Bu/$^{-}$O*t*Bu) = +0.10 V *vs.* SCE in DMF[59]] and haloarenes [E^{p}_{red} (PhI/PhI$^{\bullet-}$) = -2.24 *vs*. SCE in DMF[36]], as well as computational studies by Murphy and Tuttle,[44,58] Taillefer[38] and Patil,[40] which raise grave concerns over the thermodynamic feasibility of this process. Instead, experimental and computational evidence supports the *in situ* formation of organic electron donors.

Another reaction where KO*t*Bu was proposed as a single electron donor was the photochemical KO*t*Bu-mediated reductive cleavage of 1,3-dithianes, reported by Peñéñory. Instead, herein evidence is presented for the reaction of KO*t*Bu with DMSO to afford the dimsyl anion, which forms an **EDA** complex with 1,3-dithianes. This **EDA** undergoes SET upon photoactivation to ultimately effect reductive cleavage.

2.2. Investigating the Function of 2-Pyridinecarbinol as an Additive in Transition Metal-free C-H Arylations with Bromoarenes

The work described in Chapter 2.2. was carried out as part of a collaborative project during a secondment to the University of Strathclyde, and includes contributions from Dr. Graeme Coulthard. Dr. Graeme Coulthard conducted reactions depicted in Table 2 (entries 25 and 26) and measured redox potentials of species **57b**, **140** and **111** by cyclic voltammetry. Unless otherwise stated, all other work was conducted by Joshua Barham.

Having clarified the role of KO*t*Bu in transition metal-free C-H arylation reactions, an explanation was still needed for why certain organic additives were more effective than others in couplings of bromoarenes. As mentioned in Section 1.2.7., whilst transition metal-free C-H arylations have routinely used iodoarenes, bromoarenes have been coupled with variable degrees of success depending on the organic additive used. Two examples of organic additives which have successfully effected C-H arylations with bromoarenes are **phen**[1] and 2-pyridinecarbinol (**80**).[14] Having established that **phen** forms dimer dianion **64** *in situ* as the organic electron donor, efforts were directed at identifying the organic electron donor formed *in situ* from **80**. It was postulated that comparing dimer dianion **64** with the electron donor derived from **80** might reveal the features of organic electron donors which enable successful initiation of C-H arylation reactions with bromoarenes.

2.2.1. Repeating the Literature and Proposals for Mechanisms of Initiation

Operating under Kwong's conditions, the reported coupling of *p*-bromotoluene (using 2-pyridinecarbinol as an additive) works as stated and a 60% isolated yield of **15** resulted (Scheme 24, top), which is identical to Kwong's yield (60%).[14] With this result in hand, a decision was made to

probe the mechanism of action of **80**. Although initiation of the **BHAS** mechanism routinely occurs through formation of an organic electron donor,[44,58] a second, more sluggish route of initiation can occur when the substrate can form arynes (see Section 1.2.5.), and this mechanism can cloud the picture. Kwong observed no coupling of *p*-bromotoluene to benzene in the absence of **80**,[14] thus suggesting that initiation *via* arynes was not occurring under these conditions. However, mechanistic studies would benefit from freedom to explore a range of conditions, and to guard against side-reactions with arynes, 2,6-dimethylhalobenzene coupling substrates (**57a/b/c**) were chosen. These substrates completely rule out aryne formation, thus allowing organic additives to be compared and focus to be placed solely on their ability to form electron donors *in situ* (Scheme 24, bottom).[44,58] Competent electron donors convert substrates **57a/b/c** into the corresponding aryl radicals, which undergo their competing signature reactions to afford 2,6-dimethylbiphenyl (**58**), biphenyl (**59**), *m*-xylene (**60**) and recovered **57a/b/c**.

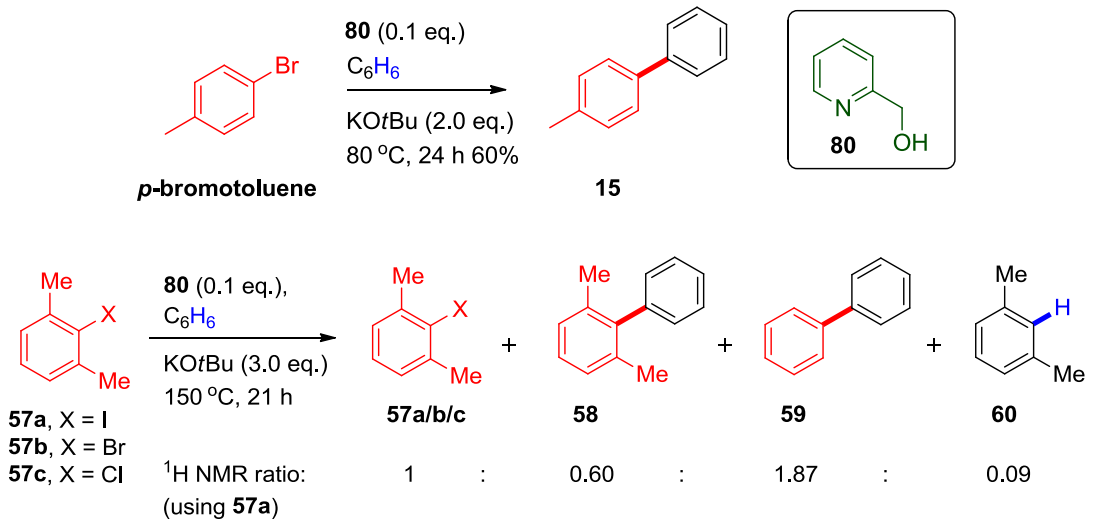

***Scheme 24**: KOtBu-mediated C-H arylation with bromoarenes using 2-pyridinecarbinol **80** as an additive.*

Because of the inefficient reactivity of **57** and the steric and electronic properties of the derived aryl radical, the yields from 2,6-

dimethylhalobenzenes (for example, **57a**) are always lower than for simple substrates (such as *p*-iodotoluene, **13**). To compensate for this, harsher reaction conditions (3.0 eq. KO*t*Bu, 0.1 eq. **80**, 150 ^{o}C for 21 h in benzene solvent) were utilised (relative to previous conditions).[58] Whilst bromoarene **57b** gave rise to coupling, the iodoarene **57a** reacted more efficiently, affording the combined biaryls (**58** and **59**) as the major component, and so **57a** was adopted as the routine substrate.

Reflecting on observations in the literature that oxidisable alcohols can initiate such coupling reactions,[4,53,48,16] together with previous work from the Murphy group which explores the mechanism for that process,[58] modes of activation were proposed for how KO*t*Bu reacted with 2-pyridinecarbinol **80** to form an electron donor. A noteworthy point is that *pyridinecarbinol analogues cannot form enolate analogues through the same mechanism as previously reported alcohol additives* (Figure 4, Section 1.2.6.). One mechanism (proposed by Murphy but not experimentally verified)[58] could involve double deprotonation by KO*t*Bu; firstly at the alcohol (to afford **107**) and secondly at the benzylic position (Figure 17, green pathway), to afford electron donor **109**. Here, pK_a of the benzylic C**H**$_2$ and the ability of the aromatic function to accept an electron would be important.

An alternative mechanism could involve oxidation of the pyridinol anion **107** *via* hydride loss. Hydride loss from primary and secondary alcohols has been demonstrated under the reaction conditions of the coupling reactions.[58] The resulting pyridinecarboxaldehyde (**111**) would not be an electron donor, but it could be susceptible to nucleophilic attack either at the aldehyde function (Figure 17, blue pathway) to give **113**, or at the aromatic ring, presumably at the *ortho*- or *para*-positions (*para*-attack is shown in Figure 17, red pathway to give **117**). Deprotonation of **113** and **117**, respectively, would give rise to likely electron donors **115** and **119**. Here, steric and electronic differences in the additive would influence nucleophilic attack by KO*t*Bu and would be important.

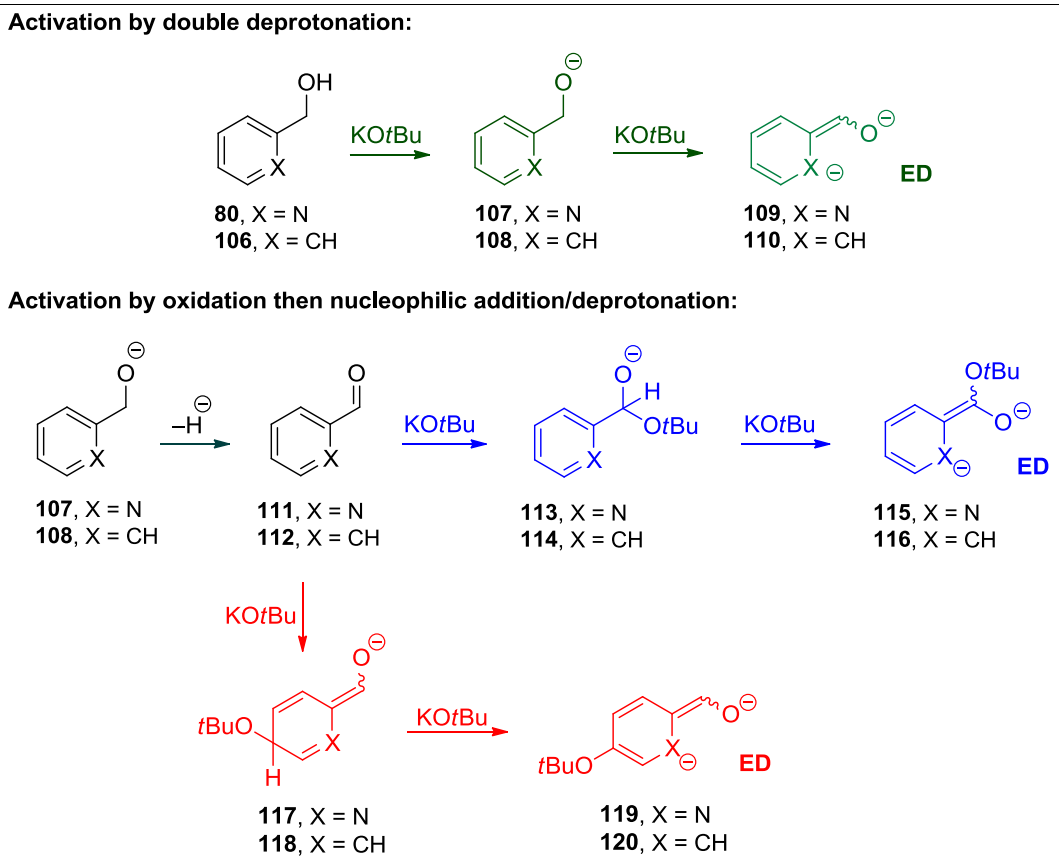

***Figure 17**: Proposed pathways for activation of 2-pyridinecarbinol-type scaffolds.*

To investigate which pathways were in operation, we postulated that if **111** was an intermediate *en route* to the electron donor initiator, differences in reactivity would become apparent through i) blocking the aldehyde group, ii) blocking the *ortho*- or *para*-positions, iii) deuteration and iv) varying the electronics of the additive. A selection of organic additives was chosen to investigate these factors (Figure 18).

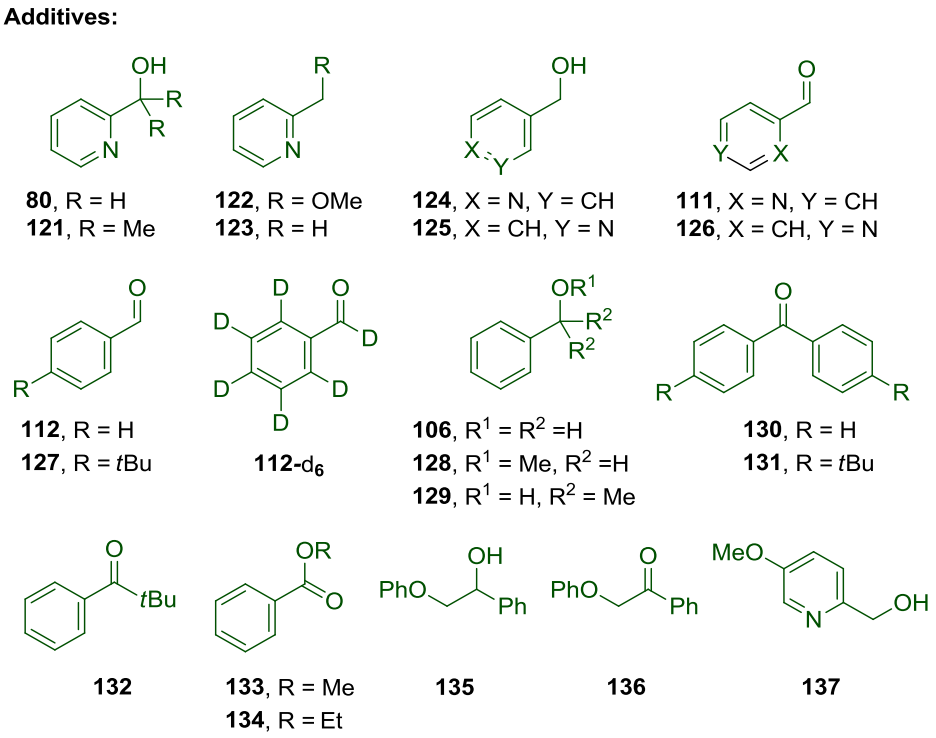

***Figure 18**: Selection of organic additives applied in C-H arylation reactions with 2,6-dimethylhalobenzenes.*

2.2.2. Investigation of 2-Pyridinecarbinol and Analogues

As mentioned, heating **57a** in benzene as solvent with KO*t*Bu (3.0 eq.) and additive (0.1 eq.) gave rise to **58**, **59** and **60**, with biaryls **58** and **59** as the major components. Products are clearly visible in the ^{1}H NMR spectrum of the crude reaction mixture, allowing facile determination of the ratio of **57a** : **58** : **59** : **60**. In key cases, the combined biaryls **58** and **59** were isolated by chromatography (as an inseparable mixture of **58** and **59**) and the yields determined or, alternatively, quantified by the use of ^{1}H NMR spectroscopy using an internal standard. All reactions were performed using the same amount of **57a** (116.0 mg, 0.5 mmol) under identical reaction conditions, that is, temperature, number of reagent equivalents, solvent volumes and time. For key comparisons of additives, a pair of reactions was run side-by-side and the reaction pair repeated. In the results shown (Table 2), the characteristic ratio of **58** : **59** (1 : ~3.5) was consistently observed,

determined by the relative rates of aryl radical addition to, *vs*. HAT from, benzene.

A blank reaction without an additive (Table 2, entry 1) gave no reaction of **57a**, confirming the inability of KO*t*Bu to act as an electron donor to haloarenes, as evidenced previously both in the literature and in Chapter 1.2.[44,58,38] To investigate the effect of blocking the benzylic position of 2-pyridinecarbinol (**80**), the *gem*-dimethyl additive **121** was tested under the reaction conditions side-by-side with **80** (the reaction pair was repeated to confirm reproducibility, Table 2, entries 3 and 4). It is clearly seen that the *gem*-dimethyl additive (**121**) is not capable of effecting the coupling, consistent with an important role for deprotonation at the benzylic position of **80**. Blocking the hydroxy proton as its methyl ether as in additive **122** halted the reaction, and removing the hydroxy group as in additive **123** resulted in significant loss of reactivity (entries 5 and 6).

***Table 2**: Coupling reactions of 2,6-dimethyliodobenzene with benzene, facilitated by a range of organic additives.*

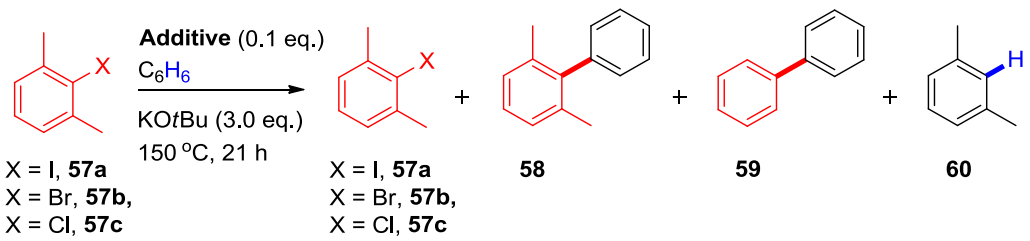

Entry	Additive	57a[a] :	58[a] :	59[a] :	60[a]	Biaryl yield, mg[b] [recovered 57 (%)]
1	-	1 :	< 0.01 :	0.02 :	< 0.01	1.5 [75]
2	**80**	1 :	0.24 :	0.55 :	0.06	ND[c]
3	**80**	1 :	0.60 :	1.87 :	0.09	35.0 (isolated) [ND][d,e]
		1 :	0.63 :	1.92 :	0.22	34.0 (isolated) [ND][d]

Entry	Additive	57a[a] :	58[a] :	59[a] :	60[a]	Biaryl yield, mg[b] [recovered 57 (%)]
4	**121**	1 :	0.02 :	0.06 :	< 0.01	4.0 (isolated) [ND][d,e]
		1 :	0.02 :	0.05 :	< 0.01	3.0 (isolated) [ND][d]
5	**122**	1 :	0.02 :	0.04 :	< 0.01	3.1 [65]
6	**123**	1 :	0.03 :	0.09 :	< 0.01	6.0 [61]
7	**124**	1 :	0.42 :	1.34 :	0.36	ND
8	**125**	1 :	0.28 :	0.82 :	0.04	ND
9	**111**	1 :	0.16 :	0.53 :	0.10	ND
10	**126**	1 :	0.15 :	0.45 :	0.04	ND
11	**112**	1 :	0.17 :	0.50 :	0.04	ND[f]
		1 :	0.17 :	0.50 :	0.04	ND
12	**127**	1 :	0.09 :	0.27 :	0.03	ND[f]
		1 :	0.09 :	0.27 :	0.03	ND
13	**112**[g]	1 :	0.13 :	0.39 :	0.04	ND[h]
14	**112**-d_6[g]	1 :	0.07 :	0.23 :	0.04	ND[h]
15	**106**	1 :	0.06 :	0.19 :	0.09	ND
16	**128**	1 :	0.01 :	0.03 :	0.01	2.1 [73]
17	**129**	1 :	0.01 :	0.03 :	< 0.01	2.6 [73]
18	**130**	1 :	0.07 :	0.25 :	0.05	8.3 [41]
19	**131**	1 :	0.03 :	0.08 :	< 0.01	4.4 [62]

Entry	Additive	57a[a] :	58[a] :	59[a] :	60[a]	Biaryl yield, mg[b] [recovered 57 (%)]
20	**132**	1 :	0.02 :	0.04 :	< 0.01	2.9 [72]
21	**133**	1 :	0.02 :	0.06 :	0.07	3.0 (isolated) [ND][d,k]
22	**134**	1 :	0.11 :	0.37 :	0.38	9.0 (isolated) [ND][d,k]
23	**135**	1 :	0.08 :	0.28 :	0.05	ND[l]
24	**136**	1 :	0.10 :	0.33 :	0.08	ND[l]
25	-	1 :	< 0.01 :	< 0.01 :	0.09	ND [60][m,n,o]
26	**80**	1 :	< 0.01 :	0.01 :	0.09	0.8 [60][m,n]

[a]2,6-Dimethyliodobenzene **57a** was used as substrate unless otherwise stated. Ratios of products were determined by ^{1}H NMR of the reaction mixture at the end of the reaction, relative to the amount of **57a** which was arbitrarily set to 1 (see Experimental, Section 5.3.2., for example calculations). [b]Combined yield (mg) of biaryls (**58** and **59**), determined by NMR spectroscopy using 1,3,5-trimethoxybenzene (10 mol%) as an internal standard (see Appendix for example calculations). The yield (%) of returned **57a** shown in [parenthesis]. [c]**57b** was used as a substrate. [d]Combined yield (mg) of the isolated biaryls **58** and **59**, which are inseparable by chromatography. [e,f]Reactions were conducted side-by-side under identical reaction conditions and the reaction pair was repeated. [g]Prepared side-by-side by CAN oxidation of toluene of toluene-d_6 (see Experimental).[h,i,k,l,n] The two reactions were conducted side-by-side under identical reaction conditions. [j]Average of three runs. [m]**57c** was used as a substrate and the reaction was conducted by Dr. Graeme Coulthard. [o]Biaryls were not detected by ^{1}H NMR spectroscopy. ND = not determined.

Next, 4-pyridinecarbinol (**124**) and 3-pyridinecarbinol (**125**) (Table 2, entries 7 and 8) were investigated and displayed a decrease in reactivity in that order (**80** > **124** > **125** in terms of observed reactivity). Additives **80** and **124** can, upon benzylic deprotonation, delocalise the negative charge onto the pyridine N whereas **125** cannot. Deprotonation at the benzylic position was confirmed when **80** was treated (in the absence of **57a**) with KO*t*Bu (2.0 eq.) in PhH/D_2O (1 : 1) at 130 ^oC for 18 hours, thus resulting in deuteration at the

benzylic position to afford **80** : **80**-d_1 : **80**-d_2 in a ratio of 1.0 : 0.7 : 0.2 (Scheme 25, see Appendix for details).

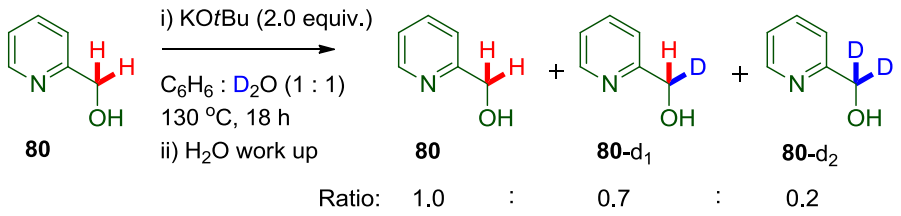

***Scheme 25**: KOtBu-mediated benzylic deuteration of 2-pyridinecarbinol (**80**) in the presence of D_2O.*

Next, 2-pyridinecarboxaldehyde (**111**) and 4-pyridinecarboxaldehyde (**126**) were tested (Table 2, Entries 9 and 10) and resulted in appreciably lower reactivity than the corresponding pyridinecarbinols **80** and **124**. If the pyridinecarbinols underwent hydride loss (as evidenced for other alcohol additives)[58] as the main pathway for generating single electron donors, then the pyridinecarboxaldehyde additives (**111** and **126**) should be more potent initiators than pyridinecarbinol additives (**80** and **124**). Therefore, these results strongly suggest that double deprotonation (Figure 17, green pathway) is the major pathway for electron donor formation from **80**.

2.2.3. Investigation of Benzaldehyde and Analogues

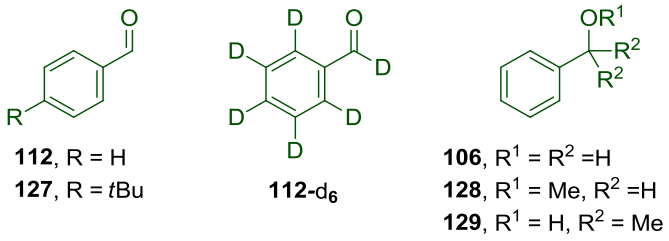

***Figure 19**: Benzaldehyde and analogues used as additives in the coupling reaction.*

Interestingly, pyridinecarboxaldehydes **111** and **126** did effect initiation (albeit less efficiently than the pyridinecarbinols **80** and **124**), suggesting that

hydride loss followed by nucleophilic addition/deprotonation could operate as an alternate pathway to form electron donors (Figure 17, red pathway and blue pathway). To probe further, benzaldehyde (**112**) was tested side-by-side with substituted analogue **127** and the reaction pair repeated to confirm reproducibility (Table 2, entries 11 and 12). Blocking the *para*-position halved the reaction conversion observed with **112**. To investigate the effect of deuteration, benzaldehyde-d_6 (**112**-d_6), synthesised from toluene-d_8, was compared side-by-side (Table 2, entries 13 and 14) with benzaldehyde-h_6 (**112**) (synthesised in exactly the same way from toluene-h_8, see Experimental, Section 5.3.1.).[94] Deuteration halved the conversion observed with **112**, indicating that formation of the initiator may include breaking of a C-H/C-D bond in the rate determining step. A primary kinetic isotope effect (KIE) is tentatively attributed to the initiation step, however the mechanism of termination is unknown and kinetic studies need to be performed prior to drawing firm conclusions.

An interesting observation is that benzyl alcohol (**106**) gave rise to lower reactivity than **112** (Table 2, entry 15), thus contrasting with the difference in reactivity between pyridinecarbinols (**80** and **124**) and their corresponding pyridinecarboxaldehydes (**111** and **126**). The electron deficiency of **80** and **124** renders them more susceptible to the double deprotonation mechanism (Figure 17, green pathway) than **106**. Oxidation followed by nucleophilic addition/deprotonation (Figure 17, blue pathway or red pathway) may be the preferred mechanism for electron donor formation from **106**, hence reactivity is enhanced with **112**, which is already an oxidation state higher. This proposal was confirmed through the use of the additives **128** and **129** (entries 16 and 17), which are blocked to both double deprotonation and oxidation and which gave no reaction. To investigate whether the aldehyde function was important, benzophenone (**130**) was tested side-by-side with substituted analogue (**131**) (Table 2, Entries 18-19).

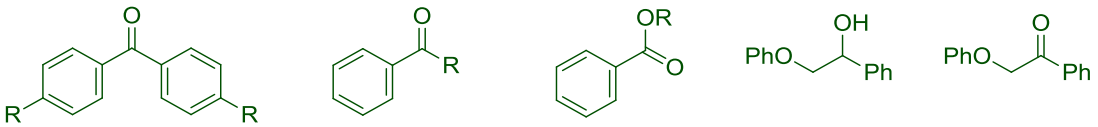

130, R = H
131, R = *t*Bu

132, R = *t*Bu
acetophenone, R = Me

133, R = Me
134, R = Et

135

136

***Figure 20**: Additives tested in the coupling reaction where the aldehyde function is blocked.*

Reactivity with **130** was similar to **106**, and the fact that coupling was observed supports the proposal for the pathway involving nucleophilic addition to the arene followed by deprotonation (Figure 17, red pathway). Furthermore, blocking the *para*-positions to nucleophilic attack in the form of additive **131** halved the reactivity, thus mirroring the difference in reactivity between additives **112** and **127**. Whilst the decrease in reactivity associated with blocking the *para*-positions lends support to the nucleophilic addition/deprotonation mechanism (Figure 17, blue pathway and red pathway), the fact that **127** and **131** still showed some reactivity (over the blank reaction, Table 2, entry 1) suggests that attack at the aldehyde function or *ortho*-positions are important.

To explore further, pivalophenone (**132**) was employed. Studies by ^{1}H NMR spectroscopy revealed that **132** experiences diminished conjugation between the carbonyl and the arene relative to acetophenone (see Experimental). Hence, it was predicted that the nucleophilic addition/deprotonation mechanism (Figure 17, red pathway) would be less available to **132**. In line with this, when **132** was applied in the coupling reaction of **57a**, no more reactivity than the blank reaction was observed (Table 2, entry 20). Overall, the benzophenone-type additives **130** and **131** were less effective than the benzaldehyde-type additives **112** and **127**, where the aldehyde function was available to react. To further probe the role of benzoyl groups, methyl benzoate (**133**) and ethyl benzoate (**134**) were studied side-by-side (Table 2, entries 21 and 22). Whilst ester **133** provided results similar to the blank

reaction, surprisingly, ester **134** gave appreciably higher reactivity. It was rationalised that transesterification under the reaction conditions would liberate ethoxide (Scheme 26) and Bi reported ethanol as an efficient promoter of KO*t*Bu-mediated C-H arylations.[48]

Through the previously reported mechanism (hydride loss, then deprotonation),[58] ethoxide would form the enolate of acetaldehyde, which can act as an electron donor. When ester **134** was subjected at room temperature to the reaction conditions in the absence of **57a**, full conversion of **134** occurred forming *tert*-butyl benzoate (**138**) as the sole product (see Appendix for the NMR spectra of the reaction mixture). This corroborates the liberation of ethoxide under the reaction conditions and is consistent with a literature report that transesterification of **134** with KO*t*Bu reportedly occurs in minutes at room temperature in Et_2O to give *tert*-butyl benzoate (**138**) in 79% yield.[95] Additives **135** and **136** were employed in the coupling reaction of **57a** (Table 2, entries 23 and 24). The alcohol **135** initiated the reaction (with similar efficacy to additives **106** and **130**), and was thought to proceed *via* oxidation to **136**. This proposal was supported when **136** gave similar activity.

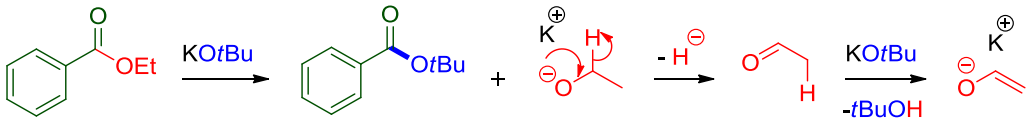

134 **138**

***Scheme 26**: Mode of activation for ethyl benzoate.*

2.2.4. Characterising the Reductive Power of Pyridinol-derived Electron Donors

Of the additives studied in Chapter 2.2., overall, it is the double deprotonation of **80** that forms the most potent class of electron donor (for example, dianion **109**), which can initiate reactions of bromoarenes. However, **109** is ineffective in reactions of chloroarenes. When 2,6-dimethylchlorobenzene

(**57c**) was treated with **80** under the standard reaction conditions, only trace amounts of biaryls were observed. The reaction was run side-by-side with a blank reaction where **80** was omitted (Table 2, entries 25 and 26). Compared to the successful reaction of *p*-bromotoluene (Scheme 24, Section 2.2.1.), Kwong reported that *p*-chlorotoluene gave a very low (8%) yield of biaryl **15** despite using more forcing conditions (120 ^{o}C, 24 h, 40 mol% of **80**). This result was successfully reproduced; *p*-chlorotoluene gave an 7% yield of **15** (Scheme 27).[†] In order to characterise the reducing power of pyridinol-derived dianions, attention was directed to cyclic voltammetry. The first reduction peak of 2-pyridinecarboxaldehyde (**111**)[†] at E^{p1}_{red} = -1.56 V *vs*. SCE was clearly visible and corresponded to a one-electron transfer (to give radical anion **141**) by comparison with ferrocene under the same conditions. The second peak appeared to be E^{p2}_{red} = < -2.50 V *vs.* SCE (at such negative potentials, solvent reduction partially masked the peak), indicating that dianion **109** is a highly potent organic electron donor, with reducing power in range of bromoarenes and chloroarenes (Table 3, see entries 2, 3 and 4). Electron donating groups present on the aromatic or carbonyl function (**139** and **140**) resulted in more negative potentials for E^{p1}_{red} (as expected), leading to the identification of pyridinecarbinol-type additive **137** (which mimics dianion **109** upon double deprotonation but would afford an even more electron-rich donor).

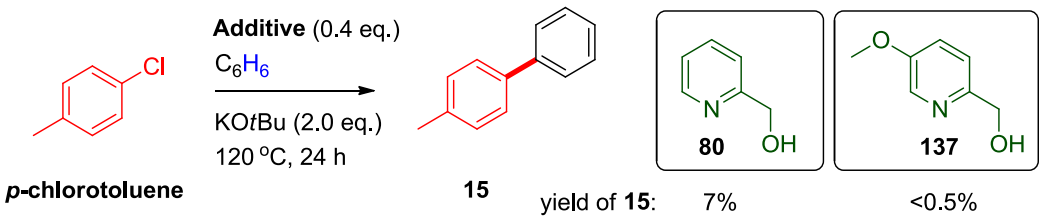

***Scheme 27**: KOtBu-mediated C-H arylation with p-chlorotoluene using a high loading of 2-pyridinecarbinol **80** as an additive.[†]*

[†]The reactions in Scheme 27, the syntheses of compounds **137** and **140** and CV measurements of **57b**, **111** and **140** were carried out by Dr. Graeme Coulthard at the University of Strathclyde.

***Table 3**: Redox potentials of pyridinecarboxaldehydes, picolinate esters and haloarenes.†*

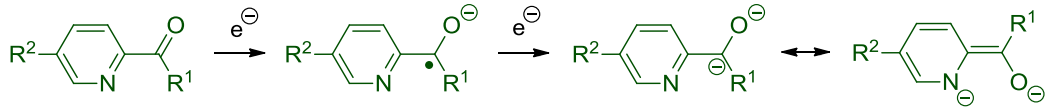

R^1 = H, R^2 = H, **111**
R^1 = OEt, R^2 = H, **139**
R^1, R^2 = OMe, **140**

R^1 = H, R^2 = H, **141**
R^1 = OEt, R^2 = H, **142**
R^1, R^2 = OMe, **143**

R^1 = H, R^2 = H, **109**
R^1 = OEt, R^2 = H, **144**
R^1, R^2 = OMe, **145**

R^1 = H, R^2 = H, **109**
R^1 = OEt, R^2 = H, **144**
R^1, R^2 = OMe, **145**

Entry	Analyte (0.01 M (in 0.1 M *n*Bu_4NPF_6/DMF))	E^p (V *vs*. SCE)[a]	Literature E^p (V *vs.* SCE)
1	ferrocene	+0.46	+0.45[96]
2	**57b**	E^p_{red} = -2.45	E^p_{red} (PhBr)[b] = -2.44[36]
3	**57c**	E^p_{red} = -2.60	E^p_{red} (PhCl)[b] = -2.78[36]
4	**111**	E^{p1}_{red} = -1.56	-
		E^{p2}_{red} = < -2.50	
5	**139**	E^{p1}_{red} = -2.05	-
		E^{p2}_{red} = ≤ -2.50	
6	**140**	E^{p1}_{red} = -2.09	-
		E^{p2}_{red} = < -2.50	
7	biphenyl (**59**)[c]	-	E^p_{red} = -2.69[79]

All values quoted are in DMF. [a]Values are calibrated to Ferrocene as an external standard, run before and after a set of analytes to ensure consistency. [b]*n*Bu_4NBF_4 used as supporting electrolyte. [c]Et_4NI used as supporting electrolyte.

†The reactions in Scheme 27, the syntheses of compounds **137** and **140** and CV measurements of **57b**, **111** and **140** were carried out by Dr. Graeme Coulthard at the University of Strathclyde.

However, additive **137** was ineffective in C-H arylations with chloroarenes (see Scheme 27 and Experimental, Section 5.3.9.). Despite the reduction potentials of these dianions and chloroarenes being close in proximity, poor conversion is observed in the laboratory in all cases. The reduction potentials for biaryl radical anions should be sufficiently negative to expect reduction of chloroarenes [E^{p}_{red} (biphenyl/biphenyl$^{\bullet-}$) = -2.69 V *vs*. SCE in DMF].[79] Therefore, it is likely that the kinetics of the chloroarene reactions, associated with the loss of chloride ion from the chloroarene radical anion, constitutes the bottleneck.

2.2.5. Common Structural Features of Organic Electron Donors which Facilitate Coupling of Bromoarenes

Double deprotonation of **80** affords electron donor **109**, which can initiate transition metal-free C-H arylations with bromoarenes. When **phen** is used as an additive, dimerisation according to the previously outlined mechanism[44] affords dianion **64**, which is implicated as the electron donor initiator formed under Shi's conditions (see Chapter 1.2.). These reaction conditions similarly effect C-H arylations with bromoarenes. Electron donor initiators **64** and **109** share common features (Figure 21).

Firstly, both are very electron-rich by virtue of their nature as dianions. Secondly, both achieve aromaticity upon attaining electron neutrality, providing a powerful driving force for electron donation. Ultimately, this renders both **64** and **109** potent reductants [E^{p}_{red} = -1.94 V and E^{p}_{red} < -2.50 V *vs*. SCE, respectively] within range of bromoarenes [E^{p}_{red} (PhBr/PhBr$^{\bullet-}$) = -2.44 V *vs*. SCE].[36] In contrast, whilst *n*BuOH as an organic additive facilitates C-H arylation with iodoarenes, bromoarenes are out of scope. Under the reaction conditions, an electron donor initiator is formed, but this cannot be a dianion nor can it benefit from gaining aromaticity upon attaining electron neutrality.

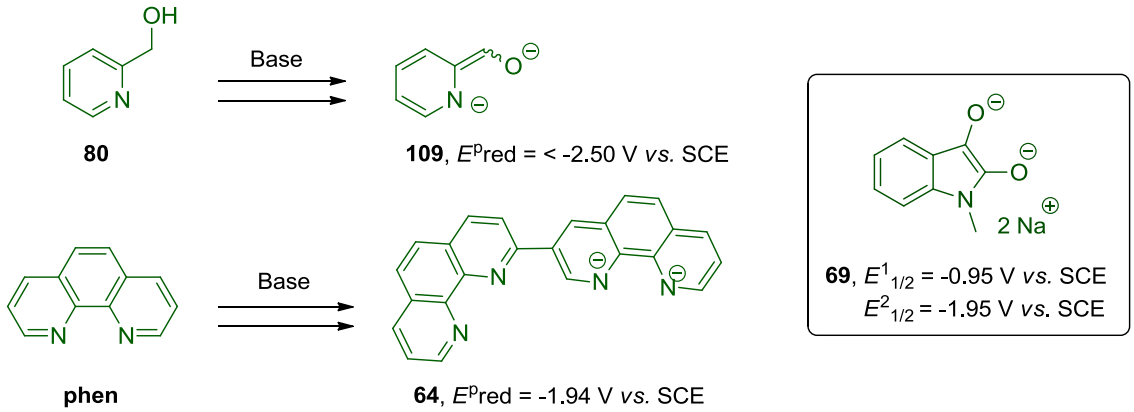

***Figure 21**: Comparing organic electron donors formed from 2-pyridinecarbinol and **phen**.*

Generating organic electron donors *in situ* is crucial to C-H arylation reactions. The very low concentration of electron donor initiator means that aryl radicals generated from haloarenes can enter the **BHAS** mechanism for C-H arylation instead of being reduced to aryl anions. In comparison, whilst pre-prepared organic electron donors [such as **69**, $E^1_{1/2}$ = -0.95 V, $E^2_{1/2}$ = -1.95 V *vs*. SCE in DMF][77] can effect reductive cleavage of haloarenes, **69** is present in stoichiometric concentration and therefore aryl radicals are rapidly reduced to aryl anions and dehalogenated products are the major products.

In summary, a selection of 2-pyridinecarbinol analogues were studied as additives in the transition metal-free C-H arylation with 2,6-dimethyliodobenene (**57a**). Structure-activity relationships derived from the study revealed that in the dominant mechanism of initiation, electron-deficient pyridinecarbinols are transformed into electron-rich electron donor initiators *via* double deprotonation. Comparison of 2-pyridinecarbinol with **phen** and other reported electron donors revealed the key to engaging bromoarenes; generation of organic electron donors which are dianions and gain aromaticity upon achieving electron neutrality.

2.3. The Role of potassium hydride in Transition Metal-free Reductive Dehalogenations

The work described in Chapter 2.3. was carried out as part of a collaborative project during a secondment to the University of Strathclyde, and includes contributions from Samuel Dalton for completeness of the story. Joshua Barham conducted the preliminary work; the reaction depicted in Scheme 28, the majority of reactions depicted in Table 4 and Table 7, and prepared polydeuterated materials **149**-d_{30} and **150**-d_{29} (Scheme 30). Samuel Dalton conducted the reactions depicted in Scheme 31 and Scheme 33 and the majority of reactions depicted in Table 5, Table 6 and Table 8. Computational studies were undertaken by Joshua Barham, ICP-OES samples were prepared by Samuel Dalton. Both Joshua Barham and Samuel Dalton contributed intellectually to the design and analysis of reactions.

2.3.1. Comparison of potassium *tert*-butoxide and potassium hydride in C-H Arylations Involving 1,10-phenanthroline as an Organic Additive and Control Reactions

The transition metal-free C-H arylation reaction of **57a** in the presence of **phen** additive was found to proceed with both KO*t*Bu and KH as a base (Table 1, Section 2.1.4.; reproduced here in Section 2.3.1., Table 4, entries 2 and 3 for comparison). Similar yields of biaryls **58** and **59** were observed in each case, in their signature 1 : ~3.5 ratio (**58** : **59**), which is determined by the relative rates of addition to, *vs.* HAT from, benzene. Interestingly, conversion of **57a** was significantly amplified by using KH instead of KO*t*Bu, but the yields of biaryl products were similar in each case (marginally lower, using KH as a base). Strikingly, whilst the additive-free control reaction using KO*t*Bu gives no reaction (Table 4, entry 1), an additive-free control reaction *using KH only* gave noticeable levels of biaryl products and only 15% returned starting material (Table 4, entry 4)! Furthermore, the ratio of **58** : **59**

was 1 : 8, suggesting a disturbance in the mechanisms available to the aryl radical (addition to, or HAT from, benzene). The corresponding bromoarene **57b** and chloroarene **57c** showed similar results (Table 4, entries 5 and 6), with poor recoveries of starting material. Interestingly, NaH gave no reaction of **57a** under the same conditions (Table 4, entry 7). Low yields of returned starting material (**57**) might be rationalised by dehalogenation, to afford the volatile *m*-xylene. This was difficult to quantify, directing attention to haloarenes which would afford non-volatile products.

***Table 4**: Coupling reactions of 2,6-dimethyliodobenzene with benzene in the presence and absence of **phen**. Comparison of KOtBu, KH and NaH.*

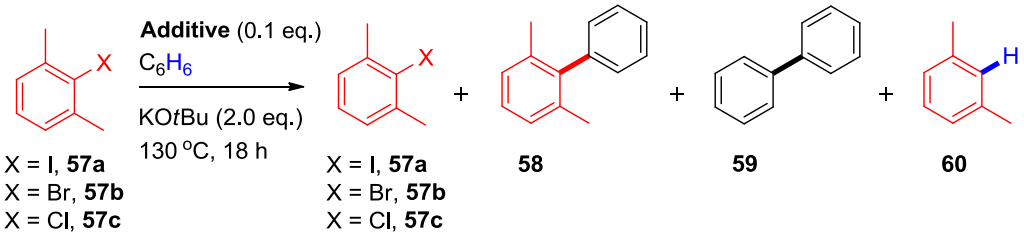

Entry	Additive/Base	57a[a] :	58[a] :	59[a] :	60[a]	Biaryl yield, mg[b] [recovered 57 (%)]
1	none/KO*t*Bu	1 :	< 0.01 :	< 0.01 :	< 0.01	< 0.5 [64][c]
2	phen/KO*t*Bu	1 :	0.12 :	0.41 :	0.15	15.5 [34][d]
3	phen/KH	1 :	5.32 :	21.0 :	15.9	13.0 [< 1][d]
4	none/KH	1 :	0.04 :	0.26 :	0.17	4.7 [15][e,f]
		1 :	0.02 :	0.20 :	0.15	3.8 [12]
5	none/KH	1 :	0.07 :	0.52 :	0.21	3.1 [3][g]
6	none/KH	1 :	0.02 :	0.14 :	0.20	1.2 [9][h]
7	none/NaH	1 :	< 0.01 :	< 0.01 :	< 0.01	-[e]

[a]2,6-Dimethyliodobenzene **57a** was used as substrate unless otherwise stated. Ratios determined by ^{1}H NMR of the reaction mixture at the end of the reaction, relative to the amount of **57a** which was arbitrarily set to 1 (see Experimental, Section 5.3.2., for example calculations). [b]Yield (mg) of combined biaryls (**58** and **59**), determined by 1,3,5-trimethoxybenzene (10 mol%) as an internal standard, yield (%) of returned **57** shown in [parenthesis], see Appendix for example calculations. [c]Reaction conducted by Dr. Graeme Coulthard at the University of Strathclyde. [d,e]The pair of reactions was conducted side-by-side. [f]The repeat reaction was conducted with a different commercial batch of KH. [g]2,6-Dimethylbromobenzene **57b** was used as substrate. [h]2,6-Dimethylchlorobenzene **57c** was used as substrate. ND = not determined.

2.3.2. POTASSIUM HYDRIDE-MEDIATED DEHALOGENATION OF 4-IODOBIPHENYL

Pierre reported the KH-mediated dehalogenation of iodobenzene in THF at rt.[88] The product is benzene which is troublesome to quantify due to its volatility. In order to validate the literature, 4-iodobiphenyl (**146**) was selected as a substrate which afforded a non-volatile product, biphenyl (**59**). Under the reported conditions, the reaction proceeded as stated and an 87% isolated yield of **59** resulted (Scheme 28 and Table 5, entry 1). Decreasing the equivalents of KH to 2.0 eq. gave **59** in 71% yield (Table 5, entry 2).

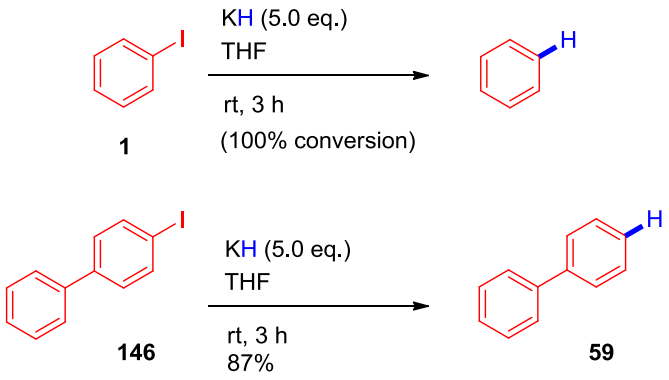

***Scheme 28**: Reductive dehalogenation of 4-iodobiphenyl mediated by KH.*

No D-incorporation was observed upon quenching the reaction with D_2O (Table 5, entry 3) or running the reaction in THF-d_8 and quenching with either D_2O or H_2O (Table 5, entries 4 and 5). This is strong evidence for incorporation of the H atom from KH. As with 2,6-dimethylhalobenzenes

(Table 4, entry 7), no reaction was observed with NaH as a base (Table 5, entry 6). No reaction occurred in C_6H_6 at rt, possibly due to inferior solubility of KH compared to reactions in THF.

***Table 5**: KH-mediated reductive dehalogenation of 4-iodobiphenyl under mild conditions.*

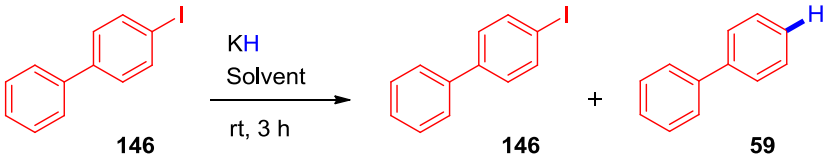

Entry	Base	Solvent	Quench	Yield		D-incorporation
				146, %[a]	59, %[a]	
1	KH (5.0 eq.)	THF	H_2O	ND	87[b]	N/A
2	KH (2.0 eq.)	THF	H_2O	< 1	71	N/A[c]
3	KH (2.0 eq.)	THF	D_2O	< 1	68	no[c,d]
4	KH (2.0 eq.)	THF-d_8	D_2O	9	62	no[c,d]
5	KH (2.0 eq.)	THF-d_8	H_2O	< 1	55	no[c,d]
6	NaH (2.0 eq.)	THF	H_2O	ND	ND	N/A[c,e]
7	KH (5.0 eq.)	C_6H_6	H_2O	ND	ND	N/A[c,e]

[a]Unless otherwise stated, yields (%) of **59** and returned **146** were determined by NMR spectroscopy using 1,3,5-trimethoxybenzene (10 mol%) as an internal standard (see Experimental, Section 5.4.3, for example calculations). [b]Isolated yield. [c]Reaction conducted by Samuel Dalton at the University of Strathclyde. [d]No D-incorporation detected by ^{2}H NMR spectroscopy or GCMS analysis of the reaction mixture. [e]No reaction occurred. N/A = not applicable. ND = not determined.

Under harsher conditions (130 ^{o}C, 18 h), reactions were observed in C_6H_6. In the presence of **phen** and KO*t*Bu, C-H arylation of benzene occurred to afford an 87% yield of terphenyl, **45**, and a 9% yield of **59**; thus a 10 : 1 ratio of **45** : **59** (Table 6, entry 1). Under additive-free conditions (KO*t*Bu only), a 7 : 1 ratio of **45** : **59** resulted (Table 6, entry 3) and a 1 : 1 mixture of regioisomeric by-products analogous those observed in Section 2.1.5., indicating formation of arynes under these conditions (see Appendix). Interestingly, using KH only gave a 1 : 3 ratio of **45** : **59** (Table 6, entry 4), suggesting dehalogenation as a competing pathway. That D-incorporation was not observed upon quenching with D_2O (Table 6, entry 5) but was observed for reactions in C_6D_6 (Table 6, entries 6 and 7) rules out anions and instead suggests a radical mechanism for the D-incorporation. Interestingly, using C_6D_6 as solvent gave a 1 : 1.2 ratio of **45** : **59**. Using NaH as a base gave no reaction (Table 6, entry 8). Neither sets of conditions in Table 5, nor Table 6, resulted in hydrogen evolution (11 mL is expected for an ideal gas at rt, 1 atm), consistent with Pierre's report.[88]

***Table 6**: KH-mediated reductive dehalogenation of 4-iodobiphenyl at high temperature.*

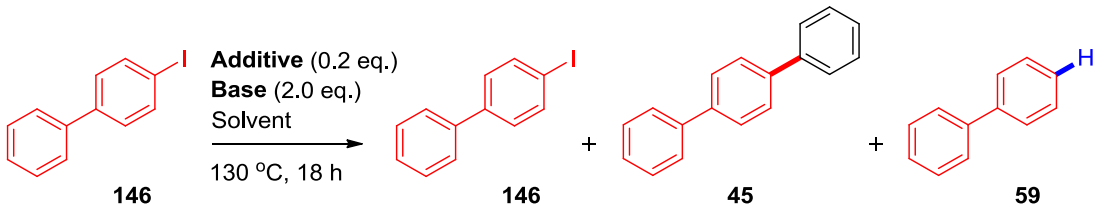

Entry	Additive /Base	Solvent /Quench	Yield 146, %[a]	Yield 45, %[a]	Yield 59, %[a]	D-incorporation
1	phen/KO*t*Bu	C_6H_6/H_2O	< 1	87	9	N/A[b]
2	phen/KO*t*Bu	C_6D_6/H_2O	< 1	79	4	ND[b]

Entry	Additive /Base	Solvent /Quench	Yield 146, %[a]	Yield 45, %[a]	Yield 59, %[a]	D-incorporation
3	none/KO*t*Bu[c]	C_6H_6/H_2O	7	76	11	N/A[b]
4	none/KH	C_6H_6/H_2O	3	16	54	no[b,d,e]
5	none/KH	C_6H_6/D_2O	4	24	58	no[b,e,f]
6	none/KH	C_6D_6/D_2O	34	15	18	yes[b,g]
7	none/KH	C_6D_6/H_2O	6	25	29	yes[b,g]
8	none/NaH	C_6H_6/H_2O	97	1	7	N/A[b]

[a]Unless otherwise stated, yields (%) of **45**, **59** and returned **146** were determined by NMR spectroscopy using 1,3,5-trimethoxybenzene (10 mol%) as an internal standard (see Experimental, Section 5.4.3, for example calculations). [b]Reaction conducted by Samuel Dalton at the University of Strathclyde. [c]Nucleophilic addition of *tert*-butoxide was observed to give a 1 : 1 ratio of regioisomeric by-products, in 6% combined yield, see Appendix for details. [d]Average of three replicates. [e]No D-incorporation detected by GCMS analysis of the reaction mixture. [f]Average of two replicates. [g]D-incorporated terphenyl (**45**-d_5) and biphenyl-d_1 (**59**-d_1) were detected by GCMS analysis of the reaction mixture but biphenyl-d_{10} (**59**-d_{10}) was not observed. N/A = not applicable. ND = not determined.

2.3.3. Potassium hydride-mediated Dehalogenation of 2,4,6-triisopropylbromobenzene

To investigate the KH-mediated dehalogenation further, 2,4,6-triisopropylbromobenzene (**147**) was employed as a hindered bromoarene which, upon forming the aryl radical, would be unable to couple to benzene (Table 7). Subjecting **147** to conditions **A** (Table 7, entry 1) gave a 9% yield of dehalogenated product (**148**), a 3% yield of **59** and 88% yield of returned **147** (when the reaction was conducted in C_6D_6, **148**-d_1 and biphenyl-d_{10} were detected, Table 7, entry 3. See Appendix for details). Pleasingly, no C-H arylation product was observed. Formation of biphenyl **59** is indicative of aryl

radicals undergoing HAT with benzene (see Scheme 12, Section 1.2.5.). Harsher conditions **B** (Table 7, entry 3) gave a 17% yield of dehalogenated product (**148**), a 9% yield of **59** and a 71% yield of returned **147**. Levels of product **148** were always higher than biphenyl (**59**), suggesting that formation of aryl radicals which abstract H atoms from benzene was not the only route to dehalogenation. Only traces of product **148** and biphenyl (**59**) were observed when NaH was employed under conditions **B**.

***Table 7**: Reactions of bromoarene **147** with potassium hydride.*

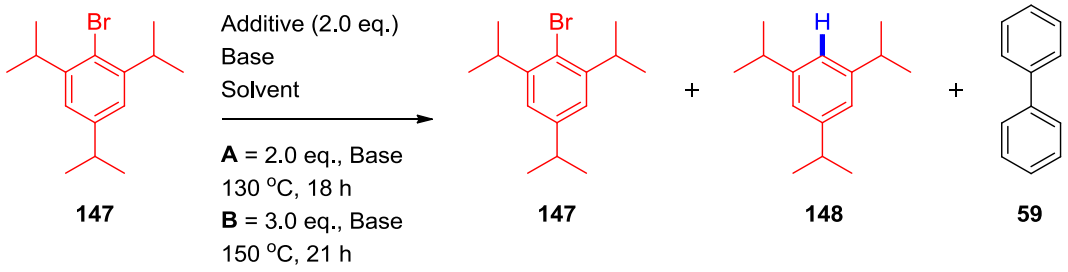

Entry	Base /Additive	Solvent /Quench	Yield 147, %[a]	Yield 148, %[a]	Yield 59, %[a]	D-incorporation
1	KH/none	C_6H_6/H_2O	88	9	3	N/A[b]
2	KH/none	C_6D_6/H_2O	65	1	ND	yes[c,d]
3	KH/none	C_6H_6/H_2O	71	17	9	N/A[e]
4	NaH/none	C_6H_6/H_2O	95	4	1	N/A[e]
5	$LiAlH_4$/KO*t*Bu	C_6H_6/H_2O	< 1	89	1	N/A[f,g]
6	$LiAlD_4$/KO*t*Bu	C_6H_6/H_2O	< 1	92	< 1	yes[f,g,h]
7	$LiAlH_4$	C_6H_6/H_2O	< 1	81	< 1	N/A

Unless otherwise stated, reactions were conducted using conditions **A**. [a]Yields (%) of **148**, **59** and returned **147** were determined by NMR spectroscopy using 1,3,5-trimethoxybenzene (10 mol%) as an internal standard (see Appendix for example calculations). [b]Average of

three repeats, one reaction was conducted by Samuel Dalton at the University of Strathclyde. [c]Reaction was conducted by Samuel Dalton at the University of Strathclyde. [d]D-incorporation (**148**-d_1) and **59**-d_{10} were detected by GCMS analysis of the reaction mixture but not by ^{2}H NMR. Under conditions **B**, both **148**-d_1 and **59**-d_{10} were observed by NMR, see Appendix. [e]Reaction conducted under conditions **B**. [f]The pair of reactions were carried out side-by-side. [g]Isolated yields. [h]D-incorporation was detected by ^{2}H NMR, ^{1}H NMR and HRMS of isolated **148**. N/A = not applicable. ND = not determined.

To confirm that KH was sourcing the hydrogen atom in product **148**, potassium deuteride (KD) would be the obvious choice. However, the cheapest quote retrieved for KD was £13,478.0/g and its preparation is non-trivial and was deemed too unsafe (passing deuterium gas over molten potassium at 300-350 ^{o}C) to pursue. Reflecting on the observations of Liu, who reported reductive cleavage of C-O bonds using a system of $LiAlH_4$ and KO*t*Bu (there, no other combination of metal hydrides or bases was superior),[97] it was postulated that KH might be generated *in situ*.

On that basis, $LiAlD_4$/KO*t*Bu (1 : 1) was compared side-by-side with $LiAlH_4$/KO*t*Bu (1 : 1) under conditions **A** (Table 7, entries 5 and 6), and D-incorporation was observed in **148**, demonstrating the incorporation of the H atom from a metal hydride in the dehalogenation mechanism. As a control reaction, it was found that $LiAlH_4$ effected reductive dehalogenation just as efficiently in the absence of KO*t*Bu (Table 7, entry 7), in line with Ashby and Beckwith's reports.[81,86,87] These reactions proceeded to yield **148** and **148**-d_1 as almost the sole products which were isolated in excellent (89 - 92%) yields.

Whilst it is possible that reactions mediated by KH and reactions mediated by $LiAlH_4$ proceed through a similar mechanism, there are dangers in drawing comparisons between $LiAlH_4$ and KH; their aggregation, surface properties and the nature of the metal hydride bond (covalent *vs*. ionic character) is likely to be rather different which could result in different dehalogenation mechanisms. Beckwith reported an ionic mechanism in $LiAlH_4$-mediated dehalogenations which dominated, depending on the reaction conditions.

2.3.4. POTASSIUM HYDRIDE-MEDIATED DEHALOGENATION OF 2,4,6-TRI-*tert*-BUTYL-BROMOBENZENE

To investigate the KH-mediated dehalogenation in the absence of intermolecular HAT as a possible mechanism, 2,4,6-tri-*tert*-butylbromobenzene (**149**) was employed as a very hindered bromoarene which, upon forming the aryl radical, is unable to undergo HAT with benzene (Table 8). Control reactions in the absence of base or using KO*t*Bu gave no reaction, as expected. Subjecting **149** to conditions **A** (Table 8, entry 3) gave a 28% yield of dehalogenated product (**150**) and a 57% yield of returned **149**. When the reaction was conducted in C_6D_6, reaction conversion suffered but D-incorporation was detected, see Table 8, entry 4). In the reactions of **149**, neither biphenyl (**59**) nor biphenyl-d_{10} (**59**-d_{10}) were ever observed, suggesting that these aryl radicals do not readily undergo HAT. However, comparisons between reactions in C_6H_6 *vs.* C_6D_6 and quenching with H_2O *vs*. D_2O revealed that any traces of D-incorporation must originate from the solvent (Table 8, entries 4, 5 and 6), consistent with results from other substrates, and suggesting that HAT must occur as a very minor pathway.

Overall, H-incorporated product **150** was the major product. Employing harsher conditions **B** only marginally increased the yield of product (**150**) but gave worse mass balance. Use of NaH gave no reaction (Table 8, entry 8), consistent with earlier results from other substrates. Strikingly, the combination of NaH and KO*t*Bu (which were ineffective additives separately) afforded full conversion of **149** to **150** and a 75% yield of **150** (Table 8, entry 9). The formation of KH *in situ* could be possible, but conversion is greater than KH only (Table 8, entry 9) therefore NaH and KO*t*Bu must exhibit some synergistic behaviour in the reaction mechanism. The term ‘complex base’ was coined by Caubere for a combination of bases which was more reactive than its individual components (for example, $NaNH_2$ and NaO*t*Bu).[98,99]

***Table 8**: Reactions of bromoarene **149** with potassium hydride.*

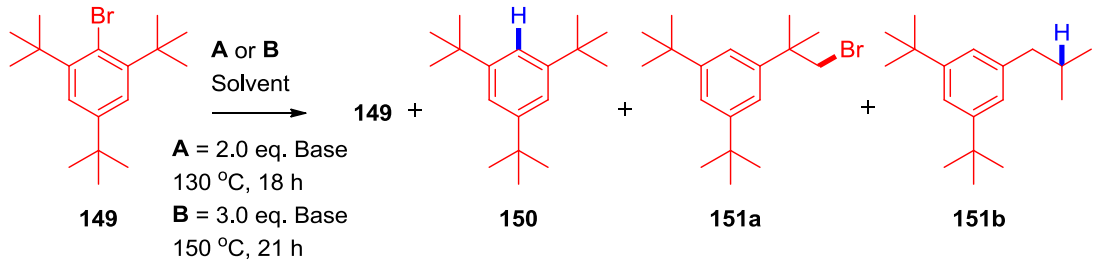

Entry	Base	Solvent /Quench	149, %[a]	150, %[a]	151a %[a]	151b %[a]	D-incorporation
1	none	C_6H_6/H_2O	ND	ND	ND	ND	N/A[b,c]
2	KO*t*Bu	C_6H_6/H_2O	ND	ND	ND	ND	N/A[b,c]
3	KH	C_6H_6/H_2O	57	28	6	6	N/A[d]
4	KH	C_6D_6/H_2O	94	11	9	1	yes[c,e]
5	KH	C_6D_6/D_2O	66	18	11	3	yes[c,e]
6	KH	C_6H_6/D_2O	85	11	4	2	no[c,f]
7	KH	C_6H_6/H_2O	29	31	1	13	N/A[c,g]
8	NaH	C_6H_6/H_2O	95	4	< 1	1	N/A[c,g]
9	KO*t*Bu / NaH (1 : 1)	C_6H_6/H_2O	< 1	75	< 1	10	N/A[c]

Unless otherwise stated, reactions were conducted using conditions **A**. [a]Yields (%) of **150**, **151** and returned **149** were determined by NMR spectroscopy using 1,3,5-trimethoxybenzene (10 mol%) as an internal standard (see Appendix for example calculations). [b]No reaction occurred. [c]Reaction was conducted by Samuel Dalton at the University of Strathclyde. [d]Average of seven repeats, five reactions were conducted by Samuel Dalton at the University of Strathclyde. [e]D-incorporation was detected by ^{2}H NMR and/or GCMS analysis of the reaction mixture. [f]Average of two repeats, no D-incorporation was detected by ^{2}H NMR or GCMS analysis of the reaction mixture. [g]Reaction conducted under conditions **B**. N/A = not applicable. ND = not determined.

An interesting observation was that of the rearranged bromide **151a** and the rearranged dehalogenated product **151b** as by-products, which identify a radical mechanism. Ingold reported that aryl radical **153** can partake in intramolecular 1,4-HAT with the *tert*-butyl group *via* quantum mechanical tunnelling.[100] The resulting alkyl radical (**154**) is known to dimerise to afford dimer **152** (Scheme 29).[100,101] In this and in similar reports, the initial aryl radical is generated at ambient or sub-ambient temperatures.[100–102] At high temperatures, neophyl rearrangement of the alkyl radical **154** to alkyl radical **155** is expected as demonstrated by Ingold.[103] Under conditions reported herein, although traces of dimer could be detected by GCMS,[†] the by-products observed were **151a** and **151b**. Bromide **151a** is proposed to arise from alkyl radical **154** abstracting a bromine atom.

One candidate bromine atom donor could be starting material **149** (thus propagating the reaction *via* halogen atom transfer). Alternatively, the mechanism which generated the aryl radical in the first place might yield a bromine atom donor which resides in close proximity to **154**. The latter seems more plausible given steric hinderance in a HAT reaction between **154** and **149**. Moreover, since benzene is present in excess it might be expected that **154** would undergo HAT with benzene, yet no biphenyl (**59**) is observed. Another observation is the difference in product distribution between substrates **147** and **149**, suggesting that their corresponding aryl radicals follow different mechanisms. Instead of a rearranged bromide in reactions of **147**, biphenyl (**59**) was the major by-product indicating that the aryl radical derived from **147** prefers to undergo intermolecular HAT rather than intramolecular HAT with the isopropyl group. The differences between transformations of **147** and **149** were investigated by computation.

[†]A peak was detected by GCMS of the crude reaction products which showes mass ions of 490 ([M^+]) and 287 ([M^+-$C_{15}H_{23}$]), consistent with dimer **156** but it was formed in too low amounts for isolation (see Appendix).

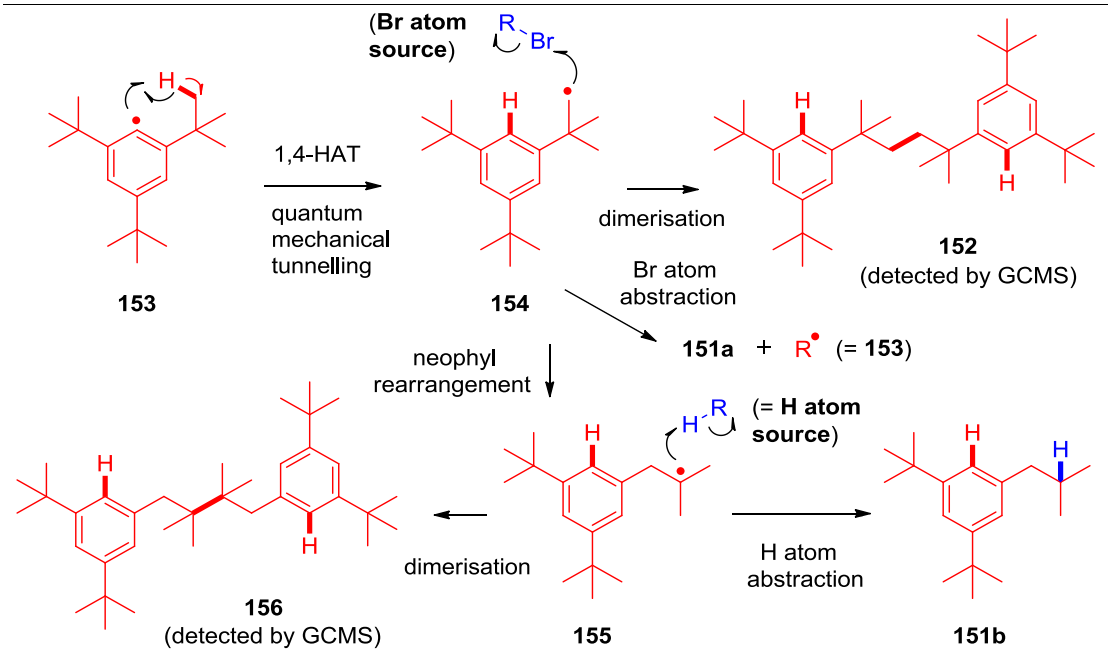

***Scheme 29**: Fates of alkyl radicals **154** and **155** rationalising the formation of products **151a** and **151b**.*

The barriers for electron transfer to **147** and **149** were assumed to be identical. The dissociation of $\mathbf{149}^{\bullet-}$ was found to be 13.8 kcal mol^{-1} more exergonic than the dissociation of $\mathbf{147}^{\bullet-}$ (Figure 22, left). For **147**, the minimised conformation sees the Br atom eclipsed by the two H atoms of the two *ortho*-isopropyl groups, whereas the minimised conformation of **149** has no choice but for the Br atom to be eclipsed by two CH_3 groups of the two *ortho-tert*-butyl groups. Therefore, release of strain is greater from dissociation of $\mathbf{149}^{\bullet-}$ than from dissociation of $\mathbf{147}^{\bullet-}$, in line with the enhanced conversion of **149** compared to **147**.

Computationally, 1,4-HAT of the aryl radical **153** derived from the *t*Bu substrate (**149**) to give the alkyl radical **154** is exergonic by -7.5 kcal mol^{-1} with a 15.3 kcal mol^{-1} barrier (relative to the starting aryl radical, see Figure 22, right). For the aryl radical derived from the *i*Pr substrate (**147**), 1,4-HAT is actually more exergonic (-9.8 kcal mol^{-1}) but with a slightly higher barrier of 17.2 kcal mol^{-1} (relative to the starting aryl radical). However, since quantum mechanical tunnelling occurs, these energy barriers for intramolecular 1,4-

HAT are not likely to be representative of the real situation. Attention was directed at the rotational barriers needed to reach the right conformation for intramolecular HAT/tunnelling. However, the barriers were similar, with *ca.* 3.9 kcal mol^{-1} for aryl radical **153** to attain the reactive conformation, and *ca.* 4.5 kcal mol^{-1} for the corresponding aryl radical derived from the *i*Pr substrate (**147**). These rotational barriers are upper limits (see Appendix).

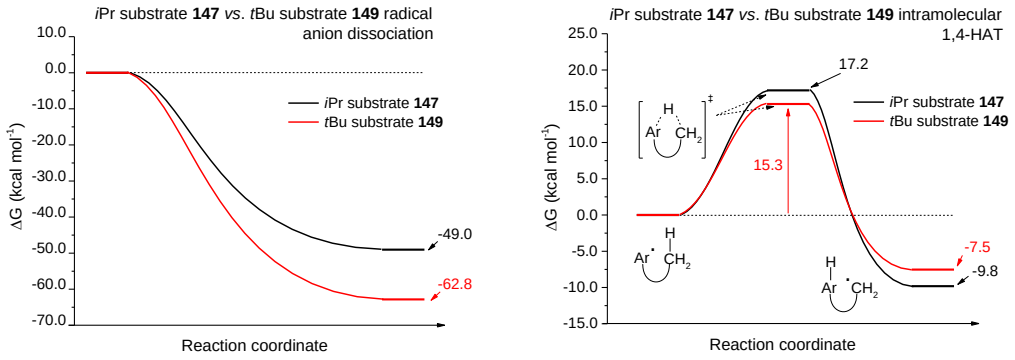

***Figure 22**: Left: Reaction free energy (ΔG) profile for dissociation of radical anions derived from **147** and **149**; DFT calculations used the M062X functional with a 6-311++G(d,p) basis set on all atoms except bromine, and a C-PCM implicit solvent model (benzene) as implemented in Gaussian09. Bromine was modelled using the MWB28 relativistic pseudo potential and associated basis set. Right: Reaction free energy (ΔG) profile for intramolecular 1,4-HAT comparing aryl radicals derived from **147** and **149**; DFT calculations used an unrestricted B3LYP functional with a 6-31+G(d,p) basis set on all atoms and C-PCM implicit solvent model (benzene) as implemented in Gaussian09.*

Neophyl rearrangement of **154** was exergonic by 10.7 kcal mol^{-1} (Figure 23, left) with a 13.8 kcal mol^{-1} barrier (relative to **154**). This is consistent with the expected stabilisation in transforming the more reactive 1^{o} radical **154** into the less reactive 3^{o} radical **155**. Finally, the transition state for intermolecular HAT between **153** and benzene was found to be 5.1 kcal mol^{-1} higher in energy than the corresponding transition state for the aryl radical derived

from **147** (Figure 23, right). This could account for the observation of biphenyl (**59**) in reactions of **147** and non-observation of biphenyl (**59**) in reactions of **149**. Further computation is needed to rationalise why the aryl radical derived from **147** does not form dimeric species; presumably it must not undergo intramolecular HAT/tunnelling. In order to unequivocally confirm the incorporation of hydride yet avoid the use of KD, a decision was made to synthesise perdeuterated substrate **149**-d_{29} and conduct a complementary experiment; reacting KH with perdeuterated substrate **149**-d_{29} in C_6D_6 (quenching with D_2O).

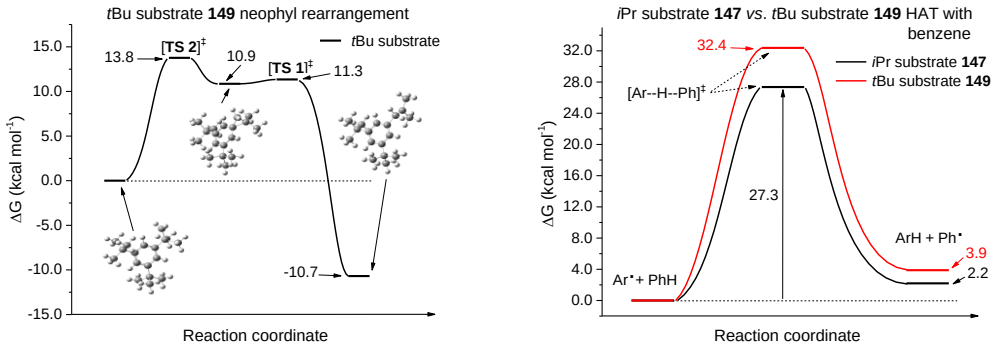

***Figure 23**: Left: Reaction free energy (ΔG) profile for neophyl rearrangement of alkyl radical **154**. Right: Reaction free energy (ΔG) profile for intermolecular HAT with benzene comparing aryl radicals derived from **147** and **149**. The level of theory employed for all calculations was identical to Figure 22, right.*

If aromatic H-incorporation were to occur, this must come from KH whereas if D-incorporation were to occur, intermolecular deuterium atom transfer (DAT) with solvent (shown in Scheme 12, Section 1.2.5.) or intramolecular DAT with the *tert*-butyl group (Scheme 29) must be responsible (or D_2O upon quenching, but this was deemed unlikely due to results with other bromoarene substrates). Perdeuterated substrate **149**-d_{29} was synthesised in two steps in 25% overall yield (Scheme 30), from C_6D_6 (£0.8/g) and *tert*-butylchloride-d_9 (£33.4/g) *via* a Friedel-Crafts alkylation and bromination of

150-d_{30}, with 98% aromatic D-incorporation and 95% aliphatic D-incorporation (the direct cost of **149**-d_{29} produced by this synthesis works out as £311.0/g compared to the £13,478.0/g for KD!).

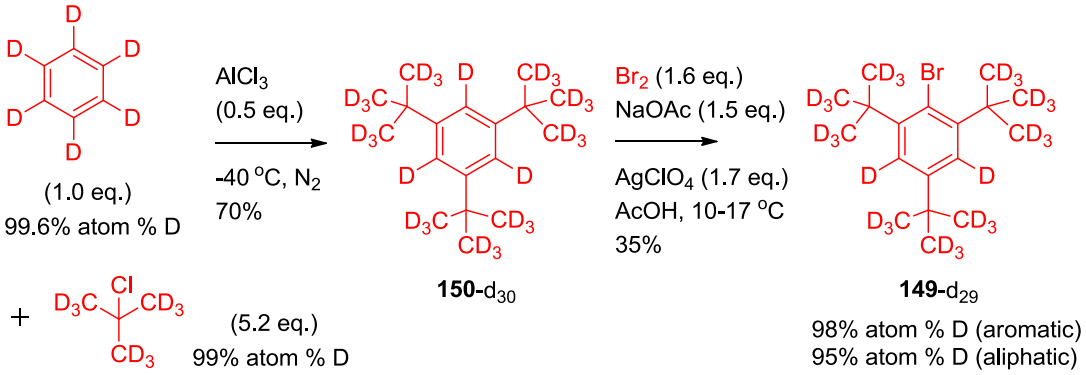

***Scheme 30**: Synthesis of perdeuterated bromoarene substrate **149**-d_{29}.*

Treating perdeuterated substrate **149**-d_{29} under the KH-mediated dehalogenation conditions (Scheme 31) gave a 65% yield of returned **149**-d_{29} and clear ^{1}H-incorporation into product (**150**-d_{29}) as deemed by a relative decrease in the aromatic ^{2}H in the ^{2}H NMR relative to the aliphatics (see Appendix for details). A 5% yield of **150**-d_{29} was estimated by ^{1}H NMR by comparison to 1,3,5-trimethoxybenzene as an internal standard (see Appendix). Traces of **150**-d_{30} were detectable by GCMS, possibly due to tunnelling followed by DAT between the alkyl radical and C_6D_6. One concern was that residual aliphatic H-incorporation in the *ortho-tert*-butyl groups could be selectively transferred to the aryl radical despite the statistical bias for exchange of deuterium; the difference in relative rates of HAT *vs*. DAT would be accentuated by quantum mechanical tunnelling.[103] However, even if the entirety of the H-incorporation in the *ortho*-aliphatics were to be transferred, this still could not amount to the increase in aromatic H-incorporation observed (see Appendix).

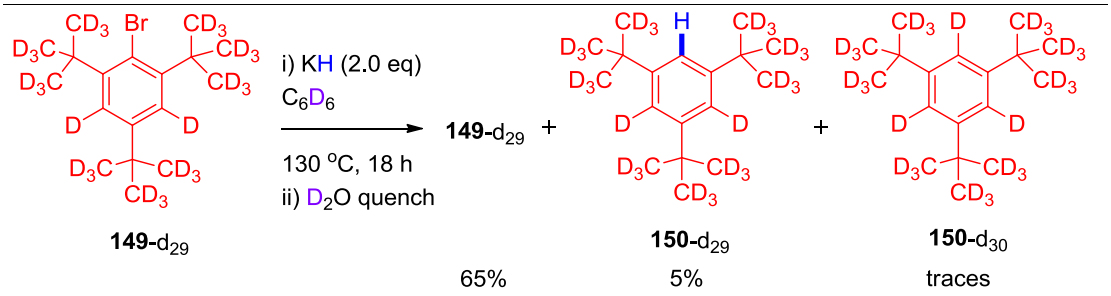

***Scheme 31**: Reaction of perdeuterated bromoarene **149**-d_{29} with potassium hydride. Results shown are an average of two replicates.*

2.3.5. Potassium hydride-mediated Dehalogenation of Bunnett-Creary Probes

Having established that a radical mechanism was in operation, and that H atoms were incorporated by hydride, it seemed logical to propose an $S_{RN}1$-type mechanism (Scheme 32). An initiation event (SET reduction) would generate aryl radical **158**, which could combine with hydride in an $S_{RN}1$ process, thereby generating radical anion **159**. In order to probe the intermediacy of radical anions, dihaloarenes **157a** and **157b** were employed (a Bunnett-Creary probe analogue,[4,32,37] but inert to benzyne formation). If radical anion **159** was an intermediate in the reaction mechanism, then it is expected to preferentially undergo intramolecular ET and dissociation to form radical **160** and bromide. This would be in line with C-H arylations with dihaloarene probes reported by Lei (who observed direct transformation into the di-arylated product)[4] and such behaviour is rationalised by intramolecular processes normally being faster than intermolecular processes (for example, ET to another molecule of haloarene). In the laboratory, this would manifest as conversion of **157a/b** straight to the double dehalogenated product (**161**). However, subjecting Bunnett-Creary probe **157a** to the usual KH-mediated dehalogenation reaction conditions afforded monodehalogenated product **162** in 9% yield and an 82% yield of returned **157a** (Scheme 33). No didehalogenated product (**150**) was observed.

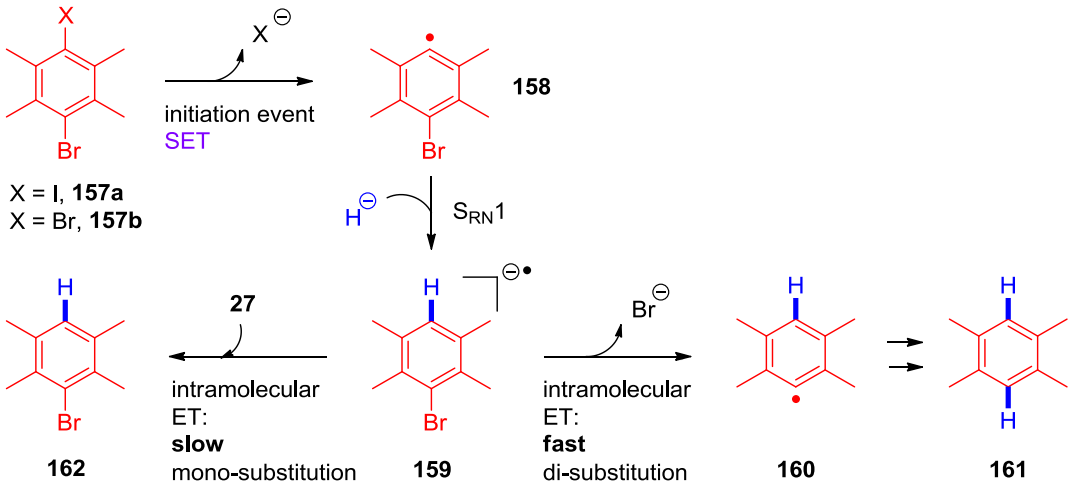

***Scheme 32**: Initially proposed $S_{RN}1$-type mechanism for KH-mediated dehalogenation and Bunnett-Creary probe analogues.*

A similar result was observed for probe **157b**; no didehalogenated product (**161**) was observed. These results suggest that the intermediacy of radical anions is unlikely (the possibility that intermolecular ET competes with intramolecular ET under these particular conditions cannot be ruled out).[47] However, it is appreciated that probes **157a** and **157b** contain 4x inductively donating alkyl groups and therefore could be significantly more electron-rich than other substrates. Interestingly, the absence of biphenyl (**59**) here indicated that HAT was not a favourable pathway. A question now arises over the nature of the transformation from haloarene to aryl radical in this KH-mediated dehalogenation.

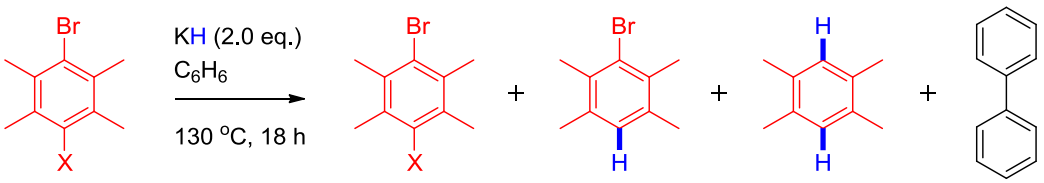

***Scheme 33**: KH-mediated dehalogenation of Bunnett-Creary probes.*

2.3.6. TRACE METAL ANALYSIS OF ALKALI METAL HYDRIDES AND POTASSIUM *tert*-BUTOXIDE

Substrate **57** is blocked to benzyne formation and has been termed an unambiguous reporter of single electron transfer.[44,58] By inference, this similarly applies to substrates **147** and **149**, which implicates potassium hydride as a single electron reductant! Caubère claimed that NaH can function as a single electron donor under certain conditions,[104] but NaH gives no reaction for any of the substrates tested herein. If potassium hydride acted as a single electron reductant, one might expect this to liberate hydrogen gas, yet hydrogen gas were not detected by Pierre and were not observed in studies disclosed herein. Evolution of trace hydrogen gas cannot be ruled out if potassium hydride donated a single electron as part of a radical chain initiation. Before making such a claim, it would be important to rule out the involvement of trace transition metals or trace elemental potassium. Therefore, ICP-OES was used to study KH, NaH and KO*t*Bu. The levels of transition metals in inorganic chemicals will always be non-zero, and are normally quoted in parts-per-million (ppm) or parts-per-billion (ppb). Table 9 shows the values obtained for a selection of transition metals under quantitative ICP-OES analysis, all were under the limits of quantification.

Table 9*: ICP-OES trace metal analysis of KOtBu, KH and NaH.*

Analyte	Blank[a]	KO*t*Bu	NaH	KH[b]
Na	LOQ (0.487)	4.618	1099.641	6.700
K	LOQ (0.636)	1417.485	2.220	1645.846
Al	LOQ (1.301)	LOQ	LOQ	LOQ
Ti	LOQ (0.106)	LOQ	LOQ	LOQ
Mn	LOQ (0.113)	LOQ	LOQ	LOQ

Analyte	Blank[a]	KO*t*Bu	NaH	KH[b]
Fe	LOQ (0.205)	LOQ	LOQ	LOQ
Co	LOQ (0.777)	LOQ	LOQ	LOQ
Ni	LOQ (0.506)	LOQ	LOQ	LOQ
Cu	LOQ (0.391)	LOQ	LOQ	LOQ
Zr	LOQ (0.292)	LOQ	LOQ	LOQ
Mo	LOQ (0.369)	LOQ	LOQ	LOQ
Ru	LOQ (1.464)	LOQ	LOQ	LOQ
Rh	LOQ (1.462)	LOQ	LOQ	LOQ
Pd	LOQ (0.363)	LOQ	LOQ	LOQ
Os	LOQ (1.107)	LOQ	LOQ	LOQ
Ir	LOQ (4.379)	LOQ	LOQ	LOQ
Pt	LOQ (2.867)	LOQ	LOQ	LOQ
Au	LOQ (1.444)	LOQ	LOQ	LOQ

Samples were prepared by Samuel Dalton at the University of Strathclyde and were analysed by a GSK in-house service. Values for a 5 mL sample in H_2O, in ppm (μg/g). To back-calculate to the levels present in the amount of solid used in the reaction, simply multiply values by 2.24. LOQ indicates that the analyte concentration (μg/g) is below the instrument's lowest limit of quantification. [a]In this column, the limits of quantification are given for each element in parenthesis. [b]Results are an average of three samples.

Results show that transition metals would have to be significantly active catalysts/initiators at sub-ppm levels to carry out the transformation. Whilst transition metal elements are below the limits of quantification, levels of potassium were similar in KH and KO*t*Bu. This, coupled with the

experimental observation that KO*t*Bu gives no reaction, is inconsistent with trace potassium metal in KH initiating the dehalogenation reaction *via* SET.

2.3.7. PROPOSED MECHANISMS FOR THE POTASSIUM HYDRIDE-MEDIATED DEHALOGENATION

Interpretation of the collective results in Chapter 2.3. allows some conclusions to be drawn. Firstly, a radical mechanism must be in operation as evidenced by intermolecular HAT to form biphenyl (**59**) and intramolecular HAT to ultimately form by-products **151a** and **151b**. Secondly, the main dehalogenation pathway involves incorporation of the H atom from hydride, as evidenced by H-incorporation in the reaction of 4-iodobiphenyl (**146**) in C_6D_6 (with a D_2O quench) and the reaction of perdeuterated substrate **149**-d_{29} in C_6D_6 (with a D_2O quench). Thirdly, the mechanism does not appear to proceed through radical anions as evidenced by monodehalogenation of **157a** and **157b**. The importance of the potassium cation is highlighted by the reactions of KH *vs.* non-reactions of NaH under the same conditions. The order of reactivity observed by Pierre (Ar-I > Ar-Br > Ar-Cl) and herein (Scheme 33) is inconsistent with an S_NAr-type mechanism. Formation of stable aryl anions can be ruled out by D_2O *vs.* H_2O quenching experiments. ICP-OES analysis revealed that participation of trace transition metals or elemental potassium is highly unlikely.

In the first proposed mechanism (Scheme 34), hydride anion (bound to the KH surface) engages in SET with the haloarene to generate (upon fragmentation) an aryl radical. The aryl radical can undergo HAT with, or addition to, C_6H_6 to give minor by-products. Alternatively, it could undergo radical-radical combination with the H atom still bound to the KH surface. The second proposed mechanism is an $S_{RN}1$-type mechanism (Scheme 35), where a cation-π interaction[105,106] between the haloarene and potassium cation promotes intermolecular SET to either that potassium cation or a second molecule of haloarene (in line with monodehalogenation of **157a** and

157b). Finally, concerted transformation of KH and haloarene to afford the aryl radical and HX radical anion is proposed (Scheme 36). If the first step were reversible, this would regenerate starting material in most substrates studied herein. However, aryl radical **153** could rearrange to alkyl radical **154** prior to retrieving the halogen atom (Scheme 29) thus rationalising the rearranged bromide **151a**. Alternatively, neophyl rearrangement could occur prior to incorporation of the H atom thus rationalising the rearranged dehalogneated product **151b**.

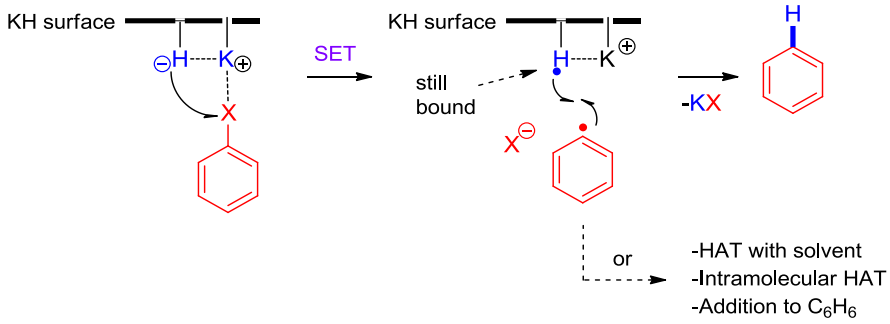

***Scheme 34**: Proposed mechanism 1: SET from hydride bound to the KH surface, then radical-radical combination.*

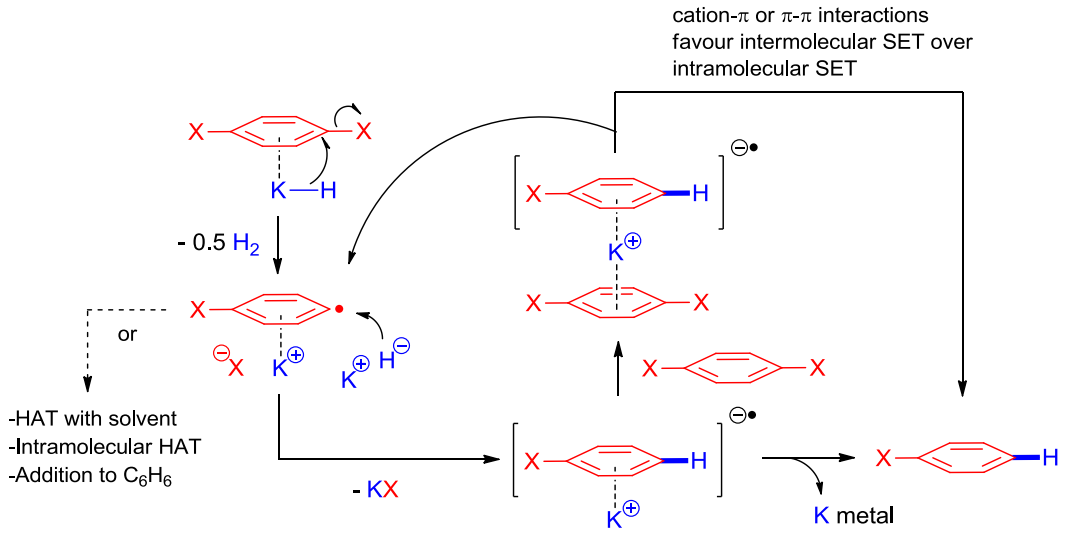

***Scheme 35**: Proposed mechanism 2: $S_{RN}1$-type mechanism whereby rapid intramolecular electron transfer is facilitated by cation-π or π-π interactions.*

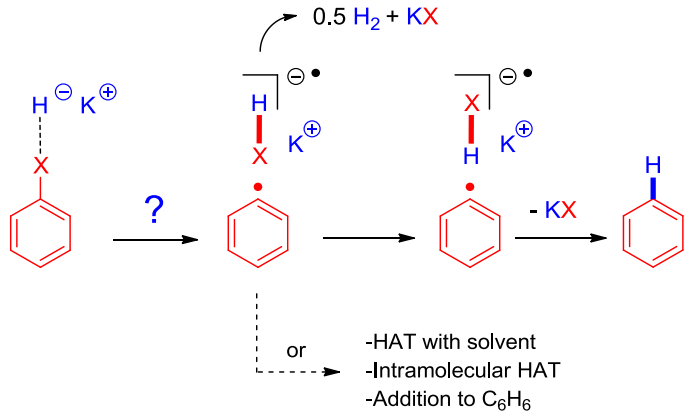

***Scheme 36**: Proposed mechanism 3: Concerted transformation to HX radical anion and aryl radical which abstracts a hydrogen atom from the HX radical anion.*

The results disclosed herein cannot rule out the concerted delivery of hydride/loss of KX proposed by Pierre[88] (Scheme 18, Section 1.3.2.) as the main mechanism for H-incorporation. However, under the conditions employed herein, aryl radicals are clearly responsible for by-products observed *which thus implicates KH as a single electron donor*.

3. CONCLUSIONS

Volume 2 of this Thesis presents novel mechanistic information toward the understanding of transition metal-free C-H arylation reactions and dehalogenations. In Chapter 2.1., the 'evidence' attributed to KO*t*Bu, or a complex of **phen**/KO*t*Bu, as the electron donor initiator in transition metal-free C-H arylations was critically examined and rationalised. It was concluded that to date, there is no evidence for KO*t*Bu donating single electrons to haloarenes in these transition metal-free C-H arylation reactions, consistent with this process being thermodynamically unfeasible according to redox potentials and computational results (Scheme 37). New mechanistic information instead supports the *in situ* formation or organic electron donors.

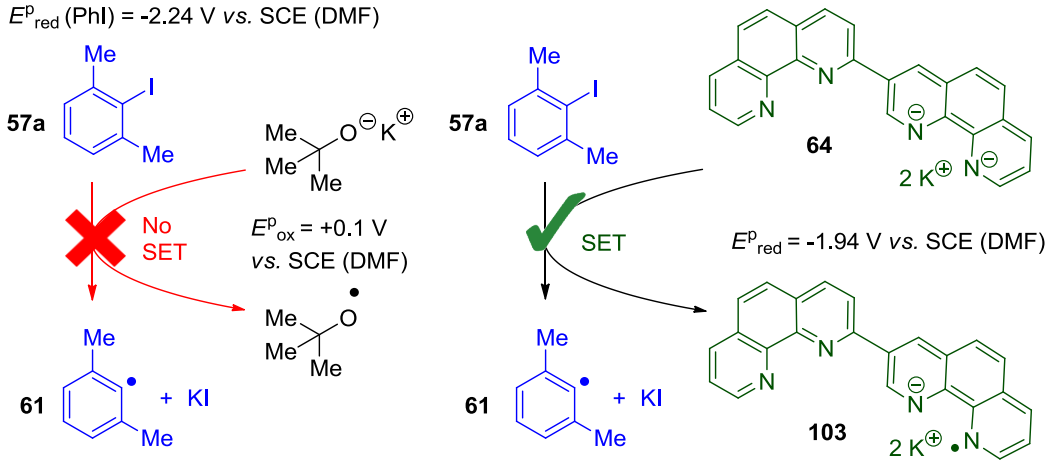

***Scheme 37**: Summary of work: Single electron transfer from organic electron donors, not KOtBu, is responsible for initiating transition metal-free C-H arylation reactions.*

Whilst iodoarenes are ubiquitous substrates in C-H arylations, bromoarenes are much less precedented. In order to elucidate the structural features of organic additives which allow successful C-H arylation with bromoarenes, 2-pyridinecarbinol and a range of derivatives were compared under the same

conditions. Structure-activity relationships revealed that electron-deficient pyridinecarbinols are transformed into electron donor initiators *via* double deprotonation (Scheme 38). Comparison of 2-pyridinecarbinol with **phen** revealed the key to engaging bromoarenes; generation of organic electron donors which are dianions and which gain aromaticity upon achieving electron neutrality. Finally, control reactions revealed a surprising result; KH-mediated dehalogenation of haloarenes. Mechanistic studies and computation uncovered a radical mechanism which incorporates the H atoms from the metal hydride, yet is unlikely to proceed *via* radical anion intermediates (Scheme 39).

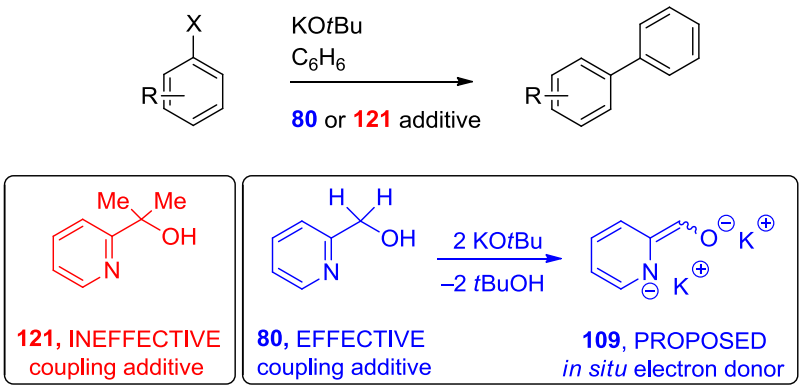

***Scheme 38**: Double deprotonation of pyridinols generates potent organic electron donor initiators for transition metal-free C-H arylation reactions with bromoarenes.*

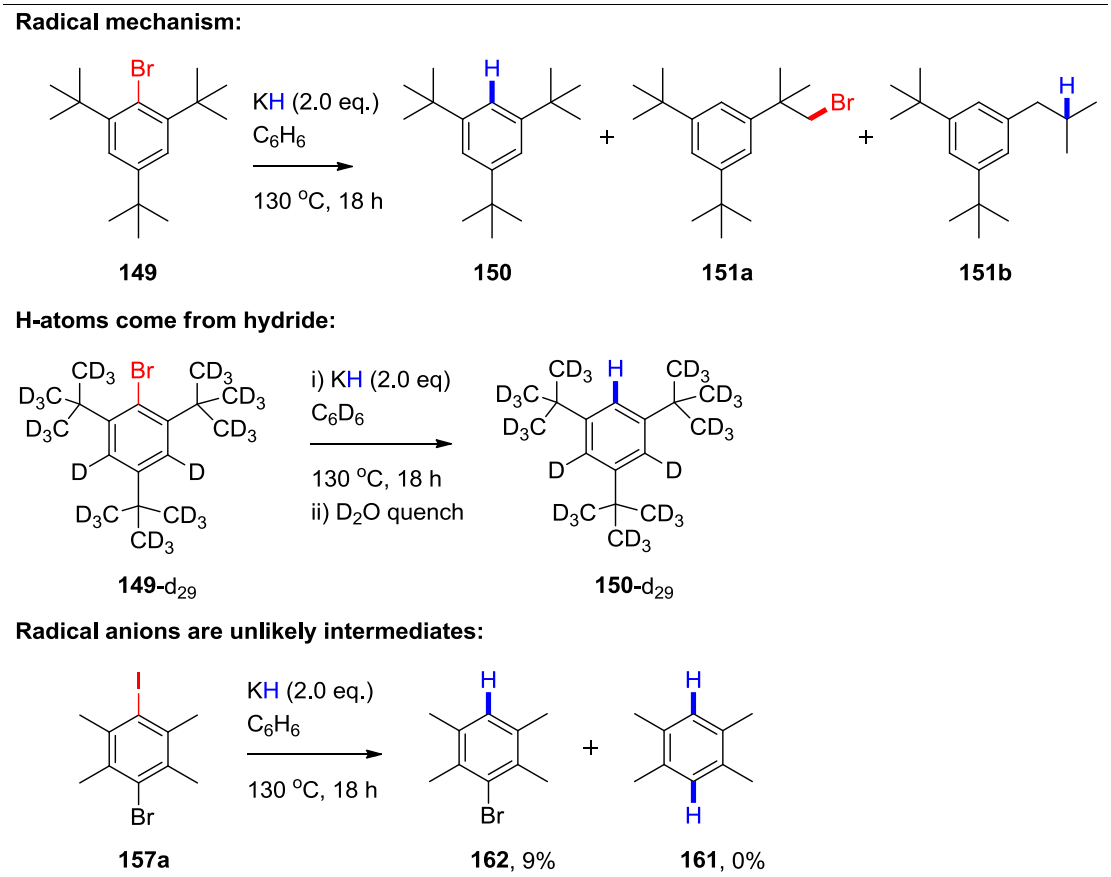

***Scheme 39**: Potassium hydride dehalogenates haloarenes via a radical mechanism, incorporating hydrogen atoms from hydride but not via the intermediacy of radical anions.*

4. Future Work

4.1. Achieving Transition Metal-free sp^2-sp^2 Cross-coupling Reactions

The KO*t*Bu/organic additive-mediated transition metal-free C-H arylation chemistry pioneered by Itami,[18] Shi[1] and Hayashi[3] is regiospecific with respect to the halogen-bearing carbon atom of the haloarene, due to the **BHAS** mechanism.[37,44,58,107] However, a fundamental limitation is the lack of selectivity on the arene coupling partner. Regioselectivity can be achieved *via* tethering the arene in an intramolecular C-H arylation reaction,[34] but the achievement of regioselectivity in intermolecular couplings would be a breakthrough in this field of research (Scheme 40).

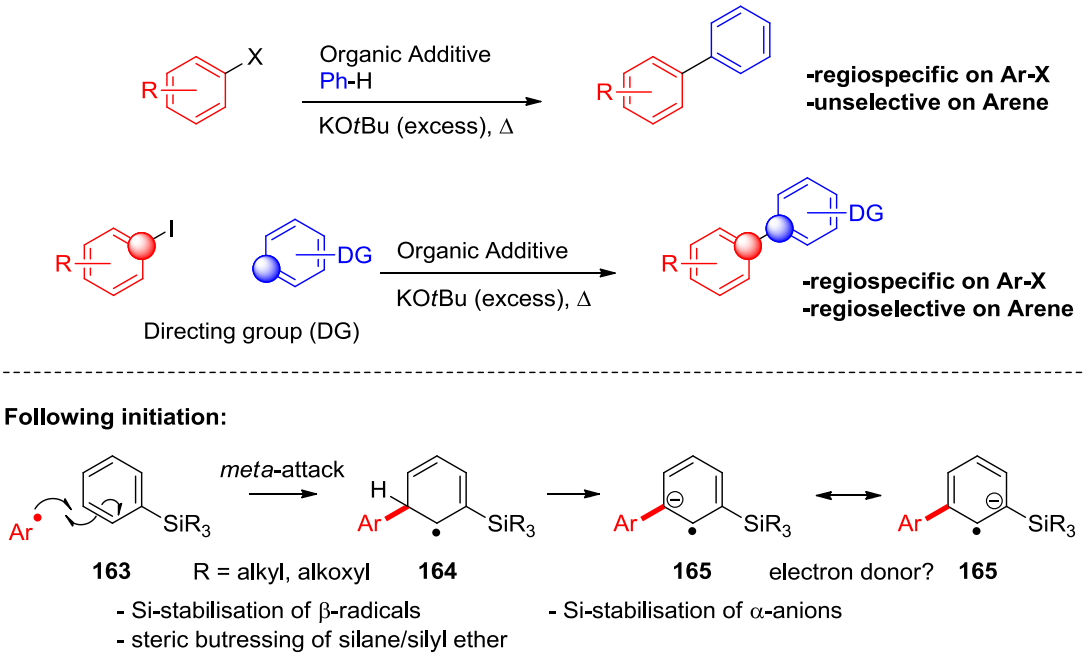

***Scheme 40**: Current scope of transition metal-free C-H arylations vs. potential for Cross-coupling reactions. Silane/silyl ether as proposed directing group for aryl radical addition.*

To achieve this, a directing group on the arene would be needed to direct the addition of the aryl radical (derived from the haloarene) in a regioselective manner. Silicon is known to stabilise radicals at the β-position,[108–110] which could work synegistically with a steric effect to direct a *meta*-selective addition of an aryl radical to aryl silane/aryl silyl ether **163**. Deprotonation of **164** would give radical anion **165** (stabilised by the α-silicon atom), thereby propagating the **BHAS** mechanism by donating an electron to the haloarene to regenerate the aryl radical.

4.2. Expanding the Scope and Application of Transition Metal-free C-H Arylations

Transition metal-free C-H arylation reactions are generally conducted at high temperature (T > 100 ^{o}C) for extended time (18 h) within sealed pressure tubes and must be prepared under an inert atmosphere (recently, progress was made when *N*-methylaniline was showcased as a robust initiator which allowed reactions of iodoarenes to be conducted under air and at lower temperatures of *ca*. 80 ^{o}C).[111] High reaction temperatures are presumably associated with the initiation step. Furthermore, chloroarenes still present challenges in these reactions. The combination of a very negative reduction potential [E^{p}_{red} (PhCl/PhCl$^{\bullet-}$) = -2.78 V *vs*. SCE],[36] together with the slow dissociation of the chloroarene radical anion, can mean that high loadings of additive are required to see even traces of product (for example, a 7% yield, see Scheme 27, Section 2.2.4.). Additives which form highly potent electron donors, or which can form electron donors more effectively, may allow milder temperatures to be used and chloroarenes to be engaged. One strategy might be to use additives predisposed to triple (or quadruple) deprotonation under the reaction conditions (Scheme 41), for example, **166** and **168** giving electron donors **167** and **169**.

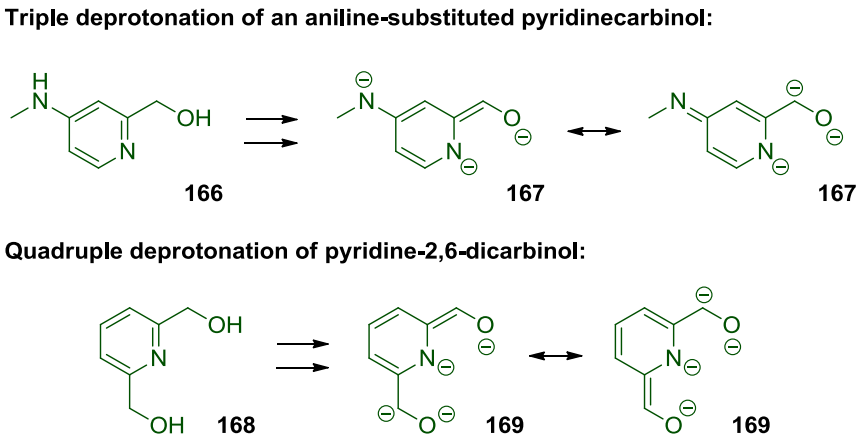

***Scheme 41**: Triple and quadruple deprotonation of pyridinecarbinol analogues to form trace amounts of highly potent organic electron donors.*

4.3. FURTHER INVESTIGATIONS OF THE KH-MEDIATED DEHALOGENATION REACTION MECHANISM

The work described herein has provided some clues as to the mechanism of the KH-mediated dehalogenation, but unanswered questions still remain. One observation was that reactions of the durene-based Bunnett-Creary probes **157a/b** gave no detectable levels of biphenyl (**59**), in contrast to reactions of the much more hindered 2,4,6-triisopropylbromobenzene (**147**). In addition, the aryl radical derived from 1,3-dimethylhalobenzenes **57** (radical **61**, Scheme 12, Section 1.2.5.) is certainly capable of HAT with benzene leading to formation of biphenyl (**59**). This raised concerns over how well the reactivity of the Bunnett-Creary probes **157a/b** represented the reactivity of other haloarenes. Compared to other haloarenes, the aryl radical derived from **157a/b** (radical **158**, Scheme 32, Section 2.3.5.) could be stabilised by the *para*-halogen. Moreover, the four electron-donating CH_3 substituents will render the aromatic system more electron-rich. Monohalogenated species **162** could be subjected to the KH-mediated dehalogenation conditions and the KO*t*Bu/**phen**-mediated C-H arylation conditions (see Table 1, entry 2, Section 2.1.4.) to confirm whether or not radical **160** (Scheme 32, Section 2.3.5.) can form biphenyl (**59**) *via* HAT with

benzene (Scheme 42). In addition, Bunnett-Creary probe **170** was identified which is a closer comparison to 2,4,6-tri-*tert*-butylbromobenzene (**149**).

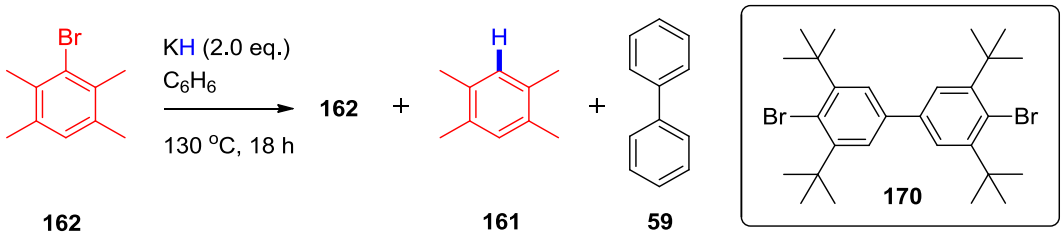

***Scheme 42**: Control reaction of monohalogenated species **162** to investigate formation of biphenyl **59**. Identification of **170** as a more representative Bunnett-Creary probe.*

A radical mechanism was confirmed through the observation of by-products **151a** and **151b**. Further evidence for a radical mechanism should derive from a radical cyclisation reaction of **171** (Scheme 43). Substrate **171** is based on the substrate used by Beckwith during studies of $LiAlH_4$ (see substrate **83**, Scheme 17, Section 1.3.1.), but is blocked to benzyne formation which could be envisaged under the reaction conditions. Following radical cyclisation, alkyl radical **172** should undergo coupling with hydride or HAT to generate **173**.

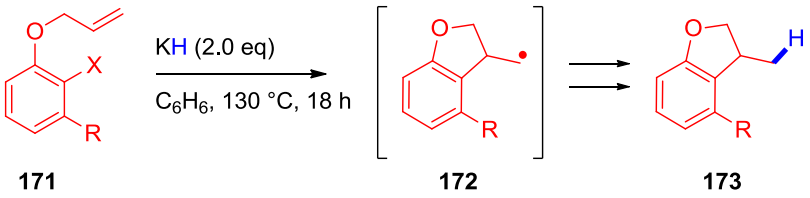

***Scheme 43**: Radical cyclisation of **171**, an aryl radical reporter substrate which is blocked to benzyne formation.*

Further computation is needed to complete the rationalisation of the different mechanistic pathways exhibited by substrates 2,4,6-triiso-propylbromobenzene (**147**) and 2,4,6-tri-*tert*-butylbromobenzene (**149**). Rather than ICP-OES, ICP-MS should be conducted which is a technique sensitive enough to quantify ppb (μg/kg) levels of transition metals. The

results obtained for KO*t*Bu as a control could be benchmarked against ICP-MS results obtained by Grubbs for KO*t*Bu (the sample preparation used herein was similar to that used by Grubbs, see Experimental, Section 5.4.10.).[112]

Finally, a very exciting result was that a 1 : 1 mixture of NaH and KO*t*Bu gave full conversion of 2,4,6-tri-*tert*-butylbromobenzene (**149**) and a 75% yield of 1,3,5-tri-*tert*-butylbenzene (**150**), where neither of these additives gave any conversion individually (Table 8, entries 2 and 8, Section 2.3.4.). Since the conversion is vastly different to KH-mediated reactions, the mechanism for the H atom incorporation could be different (a 10% yield of **151b** was observed, confirming that a radical mechanism has scope to operate). Control reactions using deuterated solvents, comparison of quenching with D_2O *vs*. H_2O and reaction of perdeutero substrate **149**-d_{29} would determine whether or not the H atoms are deriving from NaH. Further investigations would test the synthetic applications of these conditions, using challenging chloroarenes or toward other classes of reductive cleavage, for example, a non-photochemical reductive cleavage of 1,3-dithiane **94** (Scheme 44).

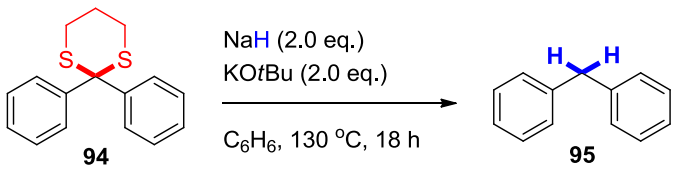

94 **95**

***Scheme 44**: A non-photochemical reductive cleavage of 1,3-dithianes mediated by a 1 : 1 NaH/KOtBu mixture.*

5. EXPERIMENTAL

5.1. GENERAL EXPERIMENTAL DETAILS

Unless specified otherwise, reactions were carried out in oven-dried ACE pressure tubes, having prepared and sealed reaction mixtures in an N_2-filled glovebox (Innovative Technology Inc., U.S.A.), or in flame-dried flasks connected to an argon Schlenk line using dry, degassed solvents. Heating was achieved through use of a silicone oil bath. Solvents (diethyl ether, tetrahydrofuran, dichloromethane, toluene and hexane) were dried by passage through an activated alumina column under argon with a Pure-Solv 400 solvent purification system by Innovative Technology Inc., U.S.A. In this Volume, reaction progress was monitored by thin-layer chromatography (TLC) or ^{1}H NMR analyses. Cryogenic conditions (-78 ^{o}C) were achieved using dry ice/acetone baths. Temperatures of 0 ^{o}C were obtained by means of an ice bath. 'Room temperature' (rt) indicates temperatures in the range of 20 - 25 ^{o}C.

For purposes of TLC, POLYGRAM SIL G/$_{UV254}$ silica plates were used, with UV light ($\lambda = 254$ nm) and phosphomolybdic acid stain used for visualisation. Purification was generally achieved by manual column chromatography using silica gel 60 Å (200 - 400 mesh). Reverse phase purification was carried out by Rita Tailor at GSK using an Agilent 1200 Prep HPLC system fitted with a Phenomenex kromasil C_{18} column and using a gradient of MeCN/H_2O. Unless otherwise stated, all GCMS were collected at the University of Strathclyde on an Agilent 5975C MSD system fitted with a 7890A GC device, using a Restek Rxi-5Sil MS column (30m x 0.25 mm x 0.25 μM) and helium as a carrier gas at 1 mL/min. In one instance (annotated by means of a footnote), GCMS was conducted at GSK on a Thermo Electron PolarisQ

system fitted with a Agilent HP-5ms column (30m x 0.25 mm x 3.0 μM) and helium as a carrier gas at 1 mL/min.

^{1}H and ^{13}C NMR data were collected using a Bruker Avance 400 Ultrashield instrument (400 MHz and 101 MHz for ^{1}H NMR and ^{13}C NMR, respectively). Data were manipulated using ACD/SpecManager version 12.5. Reference values for residual solvents were taken as δ = 7.27 ($CDCl_3$) for ^{1}H NMR; δ = 77.00 ppm ($CDCl_3$) for ^{13}C NMR. Multiplicities for coupled signals were denoted as: s = singlet, d = doublet, t = triplet, q = quartet, m = multiplet, br. = broad, apt. = apparent and dd = double doublet *etc.* Coupling constants (*J*) are given in Hz. Where appropriate, COSY, DEPT, HSQC and HMBC experiments were carried out to aid assignment. In this Volume, UV-visible absorption measurements were performed using a PerkinElmer Lambda 25 UV/VIS spectrophotometer. In this Volume, infrared data were collected using Shimadzu FT-IR Spectrophotometer (Model IRAffinity-1) with a MIRacle Single Reflection Horizontal ATR Accessory, as a thin film unless otherwise stated. High Resolution Mass spectral analyses were carried out at ESPRC National Mass Spectrometry Service Centre in Swansea on a LTQ Orbitrap XL instrument, using Atmospheric Pressure Chemical Ionisation (APCI), Chemical Ionisation (CI), Electron Impact Ionisation (EI), Electrospray Ionisation (ESI) or High Resolution Nano-Electrospray Ionisation (HNESP), and masses observed are accurate to within 5 ppm. All reagents were purchased from Sigma-Aldrich or Alfa Aesar and used as supplied or purified using standard techniques.[113] ICP analysis details are described in Section 5.4.10.

5.2. Experiments to Probe the Role of Potassium *tert*-Butoxide in Transition Metal-Free C-H Arylations with Haloarenes and in Reductive Cleavages

5.2.1. Preparation of Substrates

1-(2,4-Dinitrophenyl)propan-2-one (54b)

This compound was synthesised by Dr. Graeme Coulthard at the University of Strathclyde and is reproduced here for completeness:

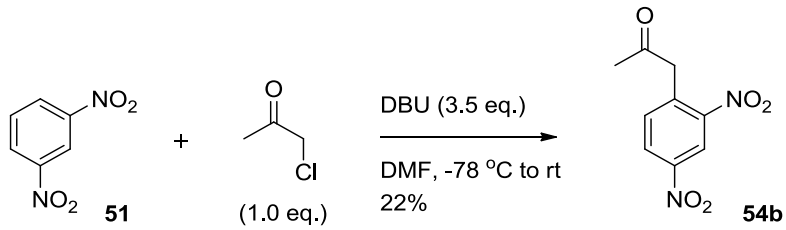

Prepared according to a modified literature procedure.[114] A solution of 1,3-dinitrobenzene **51** (1.68 g, 10.0 mmol) and chloroacetone (796.0 μL, 10.0 mmol, 1.0 eq.) in DMF (25 mL) was cooled to -78 °C. DBU (5.23 mL, 35.0 mmol, 3.5 eq.) was added dropwise. The reaction was allowed to warm to rt and stirred for 3.5 h, before addition of 1 M HCl (100 mL) and EtOAc (50 mL). The organic phase was washed with water (2 x 50 mL), dried (Na_2SO_4), filtered and concentrated to afford the crude product. Purification by column chromatography (DCM) gave **54b** as an orange oil (490.0 mg, 22%) which solidified on standing; m.p. 59 - 63 °C (lit. 61 - 63 °C[115]); ^{1}H NMR (400 MHz, $CDCl_3$) δ 8.97 (1H, d, *J* = 2.5 Hz, C*H*), 8.44 (1H, dd, *J* = 8.5, 2.5 Hz, C*H*), 7.51 (1H, d, *J* = 8.5 Hz, C*H*), 4.28 (2H, s, CH_2), 2.38 (3H, s, CH_3); HRMS (+Cl) *m/z* calculated for $C_9H_9N_2O_5$ [M+H$^+$] 225.0506; Found 225.0504. Data are consistent with the literature.[115]

2,3′-Bi(1,10-phenanthroline) (65)

This compound was synthesised by Dr. Graeme Coulthard at the University of Strathclyde and is reproduced here for completeness:

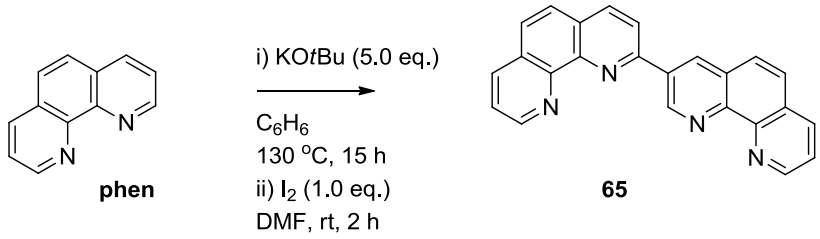

In a glovebox, 1,10-phenanthroline (180.0 mg, 1.00 mmol) was added to an oven-dried pressure tube. Anhydrous benzene (10 mL) and KO*t*Bu (561 mg, 5.00 mmol, 5.0 eq.) were added. The pressure tube was sealed, removed from the glovebox and stirred at 130 °C for 15 h. After cooling to rt, the pressure tube was returned to the glovebox and the blue/green precipitate was filtered and washed with benzene. The solids were transferred to an oven-dried pressure tube and DMF (8 mL) was added. Iodine (254.0 mg, 1.00 mmol) was added and the mixture stirred at rt for 2 h. The reaction was quenched by addition of water (150 mL) and the resulting light brown solids were filtered and washed with water (100 mL). Purification by column chromatography (10% MeOH/MeCN) gave **65** as a brown solid (83.0 mg, 23%); ^{1}H NMR (400 MHz, $CDCl_3$) δ 9.88 (1H, d, *J* = 2.1 Hz, C*H*), 9.49 (1H, d, *J* = 2.1 Hz, C*H*), 9.30 (1H, dd, *J* = 4.4, 1.8 Hz, C*H*), 9.25 (1H, dd, *J* = 4.4, 1.8 Hz, C*H*), 8.47 (1H, d, *J* = 8.3 Hz, C*H*), 8.38 (1H, d, *J* = 8.3 Hz, C*H*), 8.32 (2H, *apt.* td, *J* = 8.2, 1.6 Hz, C*H*), 8.08 (1H, d, *J* = 8.8 Hz, C*H*), 7.91 (1H, d, *J* = 8.8 Hz, C*H*), 7.88 (1H, d, *J* = 8.8 Hz, C*H*), 7.87 (1H, d, *J* = 8.8 Hz, C*H*), 7.69 (1H, dd, *J* = 8.0, 4.3 Hz, C*H*), 7.66 (1H, dd, *J* = 8.0, 4.3 Hz, C*H*); data are consistent with the literature.[44]

2,2-Diphenyl-1,3-dithiane (94)

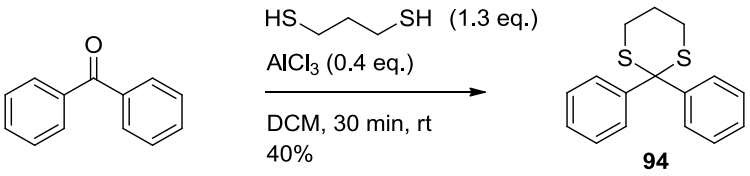

94

Prepared according to a literature procedure.[116] Benzophenone (0.94 g, 5.20 mmol) and 1,3-propanedithiol (0.69 mL, 6.76 mmol, 1.3 eq.) were added to an oven-dried pressure tube and dissolved in DCM (6 mL). $AlCl_3$ (0.26 g, 1.95 mmol, 0.4 eq.) was added and the pressure tube sealed and stirred for 30 min at rt. 2 M HCl (10 mL) was added, the organic layer separated and aqueous layer extracted with DCM (2 x 10 mL). The combined organic layers were dried (Na_2SO_4), filtered and concentrated *in vacuo* to yield a white solid, which was recrystallised (DCM/petroleum ether 40 - 60) to yield **94** as a white microcrystalline solid (571.0 mg, 40%); m.p. 100 - 102 ^oC (lit. 105 - 106 ^oC[116]); IR ν_{max} (neat) 3059 - 2891 (C-H), 1593 (Ar), 1481 (Ar), 1442, 1281 cm^{-1}; ^1H NMR (400 MHz, $CDCl_3$) δ 7.72 (4H, d, *J* = 7.6 Hz, C*H*), 7.36 (4H, t, *J* = 7.6 Hz, C*H*), 7.28 (2H, m, C*H*), 2.82 (4H, m, CH_2), 2.02 (2H, m, CH_2); ^{13}C NMR (101 MHz, $CDCl_3$) δ 142.6 (*C*), 129.3 (*C*H), 128.4 (*C*H), 127.5 (*C*H), 62.8 (*C*), 29.4 (*C*H_2), 24.5 (*C*H_2); HRMS (+ESI) *m/z* calculated for $C_{16}H_{17}S_2$ [$M+H^+$] 273.0766; Found 273.0768. Data are consistent with the literature.[116,117]

5.2.2. JANOVSKY TEST ADDUCTS: UV-VISIBLE SPECTROSCOPY INVESTIGATION

The starting point for the investigation of the Janovsky test was to reproduce the literature.[63] Accordingly, the UV-visible spectra of the following mixtures were recorded (see Figure 24):

1) A 1 : 1 acetone : H_2O mixture (trace not shown) which showed no absorption.
2) A 0.01 M aqueous solution of NaOH which, as expected, showed no absorption (Figure 24, black trace).

3) A 1 : 1 0.01 M 1,3-dinitrobenzene (**51**) in acetone : H_2O mixture which showed no absorption in the visible part of the spectrum (Figure 24, red trace).

4) A 1 : 1 0.01 M 1,3-dinitrobenzene (**51**) in acetone : 0.01 M NaOH mixture which showed an absorption at ~550 nm (Figure 24, green trace).

5) A re-run of mixture (4) after 2 mins. This showed an increase in intensity of the peak at ~550 nm (Figure 24, blue trace).

6) A re-run of mixture (5) after 2 further min. This showed a further increase in intensity of the peak at ~550 nm (Figure 24, light blue trace).

These results were in accordance with the literature[63] which suggested that the peak at 550 nm was due to adduct **53b**.

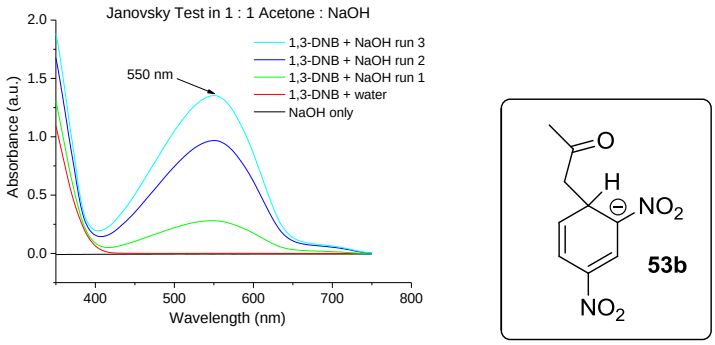

***Figure 24**: UV-visible spectroscopy of a Janovsky test reported in the literature[63] and structure of the corresponding Meisenheimer adduct.*

Next the UV-visible spectra of the following mixtures (see Figure 25, reproduced here from Figure 6, Section 2.1.1.) was investigated:

1) A THF blank which shows no absorption (trace not shown).

2) A 0.01 M solution of 1,3-dinitrobenzene (**51**) in THF showed no absorption in the 350-750 nm window (trace not shown).

3) A 1 : 1 0.01 M solution of ketone **54b** in THF : 0.01 M KO*t*Bu in THF mixture which appeared red in colour and showed an absorption at 490 nm (Figure 25, right, **A** and Figure 25, left, red trace).

4) A 1 : 1 : 1 0.01 M 1,3-dinitrobenzene (**51**) in THF : 0.01 M KO*t*Bu in THF : 0.01 M 1,10-phenanthroline in THF which appeared purple in colour and showed an absorption at 554 nm (Figure 25, right, **B** and Figure 25, left, green trace).
5) A 1 : 1 : 1 0.01 M 1,3-dinitrobenzene (**51**) in THF : 0.01 M KO*t*Bu in THF : 0.01 M acetone in THF which appeared purple in colour and showed an absorption at 552 nm (Figure 25, right, **C** and Figure 25, left, blue trace).
6) A 1 : 1 0.01 M 1,3-dinitrobenzene (**51**) in THF : 0.01 M KO*t*Bu in THF mixture which appeared purple in colour and showed an absorption at 558 nm (Figure 25, right, **D** and Figure 25, black trace).

In (5), it was found that the order of addition of acetone, KO*t*Bu, and 1,3-DNB made no difference to the outcome. In each case a peak at ~550 nm resulted and no peak at ~490 nm was seen.

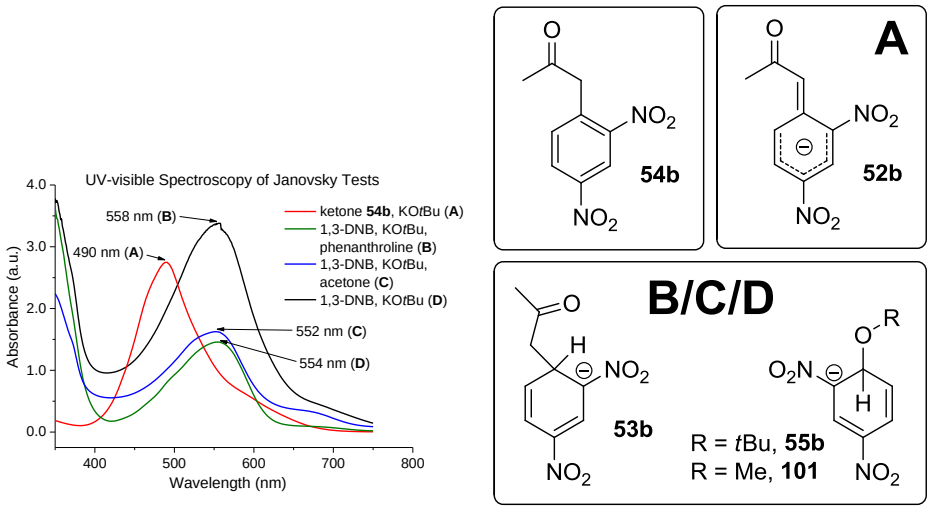

***Figure 25**: Left: UV-visible spectroscopy of Janovsky tests. Right: Meisenheimer adducts which UV-visible and NMR spectroscopy studies identified.*

Next, it was investigated how the UV-visible spectrum of the 1 : 1 1.0 mM 1,3-dinitrobenzene (**51**) in acetone : 1.0 mM NaOH mixture changed over time (Figure 26). The UV-visible spectrum of a freshly prepared sample was run every 2 minutes for 60 mins. The sample colours are shown in Figure 27,

left (developing over 20 min). The 30 UV-visible traces show an increase in the intensity of the peak at ~550 nm, but no peak at ~490 nm was detected which suggested that no transformation to the enolate **52b** (enolate of ketone **54b**) was occurring. The data for the 3 h and 24 h samples were collected by Dr. Graeme Coulthard and are reproduced here for completeness. After 3 h and after 24 h the UV-visible spectrum was measured again (Figure 26, right, black trace). The previously discernable peak at ~550 nm had flattened out and the sample had changed colour from purple to light brown (Figure 27, right). No peak to due enolate **52b** (at ~490 nm) was observed. A similar result was observed when the same sample was left for 3 days (Figure 26, right, red trace)

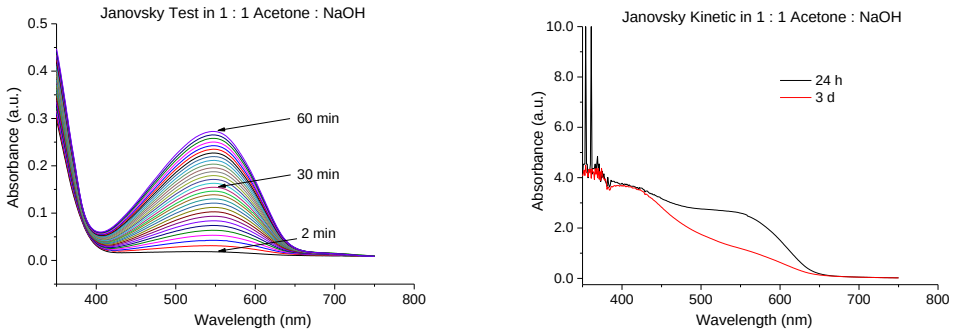

***Figure 26**: UV-visible spectroscopy of a Janovsky test reported in the literature[63] over time.*

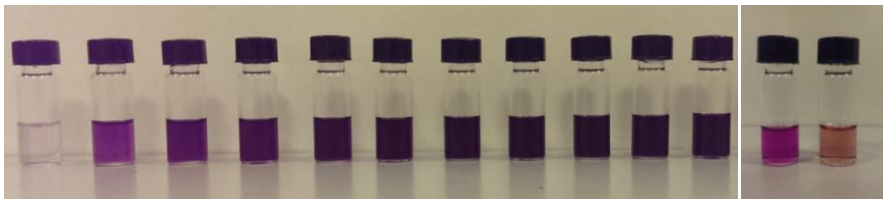

***Figure 27**: Left: Colour of Janovsky test samples over time (from left to right: 0 min to 20 min). Right: Colour of fresh Janovsky test sample (left) and of a sample aged for 24 h (right).*

Finally, it was investigated whether the same UV-visible absorption at ~550 nm resulted when a 1,3-dinitrobenzene (**51**) and acetone mixture was treated

with NaOH in THF as opposed to NaOH in water (in order to relate the traces shown in Figure 24, obtained using NaOH in water : acetone, to the blue trace shown in Figure 25, obtained using KO*t*Bu in THF : acetone). Since a 0.01 M solution of NaOH in THF could not be prepared due to solubility (as a direct comparison to a 0.01 M NaOH in H_2O), a 0.01 M solution of NaOH in 4 : 1 THF : H_2O was used as a surrogate. The following mixtures were prepared and their UV-visible spectra measured (Figure 28):

1) An 8 : 1 THF : H_2O blank which shows no absorption (trace not shown).
2) A 1 : 1 0.01 M 1,3-dinitrobenzene (**51**) in THF : 0.01 M NaOH (in 4 : 1 THF : H_2O solution, with 100.0 eq. acetone added) which showed an absorption at 550 nm (Figure 28, black trace), attributed to **53b**.
3) A 1 : 1 0.01 M ketone **54b** in THF : 0.01 M NaOH (in 4 : 1 THF : H_2O solution) which showed an intense absorption at 490 nm (Figure 28, red trace), attributed to **52b**.

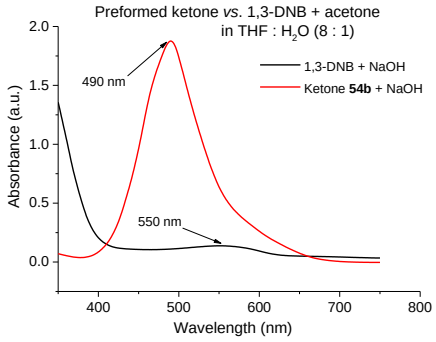

***Figure 28**: UV-visible spectra of 1,3-dinitrobenzene/acetone/NaOH in THF/H_2O and of ketone **54b**/NaOH in THF/H_2O.*

5.2.3. JANOVSKY TEST ADDUCTS: NMR SPECTROSCOPY INVESTIGATION

Initially Fyfe and Foster's procedure[64] was repeated; 1,3-dinitrobenzene (**51**) (16.8 mg, 0.10 mmol was dissolved in a 1 : 1 mixture of DMSO-d_6 and acetone. NaOMe (5.4 mg, 0.10 mmol) was added as a solid and an intense purple colour resulted. The resulting spectrum (Figure 7, Section 2.1.2.) identified adduct **53b** and was consistent with that obtained by Fyfe and Foster; ^{1}H NMR (600 MHz, 1 : 1 DMSO-d_6 : acetone) δ 8.34 (1H, d, *J* = 2.0 Hz, C*H*), 6.61 (1H, m, C*H*), 5.37 (1H, dd, *J* = 10.0, 5.0 Hz, C*H*), 4.21 (1H, dt, *J* = 8.7, 4.2 Hz, C*H*), 3.19 (3H, s, CH_3), 2.83 (1H, dd, *J* = 16.1, 3.5 Hz, CH_2), 2.44 (1H, dd, *J* = 16.1, 9.0 Hz, CH_2).†

Alternatively, when the above experiment was repeated using an identical amount of KO*t*Bu (11.2 mg, 0.10 mmol) in place of NaOMe an intense purple colour was observed and adduct **53b** was again detected by ^{1}H NMR. Subsequently, 1,3-dinitrobenzene (**51**) was reacted with either NaOMe or KO*t*Bu in DMSO-d_6 with acetone omitted and the reaction mixture sampled for ^{1}H NMR. The use of KO*t*Bu gave rise to (visually) the same intense purple colour but a complex mixture was observed by ^{1}H NMR.

Attempts to detect the alkoxide adduct **101** of NaOMe and 1,3-dinitrobenzene (**51**) in DMSO-d_6 were hampered by DMSO and water signals overlapping with signals from the adduct and key assignments could not be made. Therefore DMF-d_7 was selected as an appropriate alternative solvent. Firstly the detection of acetone adduct **53b** was sought when 1,3-dinitrobenzene (**51**) (16.8 mg, 0.10 mmol) was dissolved in a 1 : 1 mixture of DMF-d_7 and acetone.

NaOMe (5.4 mg, 0.10 mmol) was added as a solid and an intense purple colour resulted, as was the case when DMSO-d_6 was used. The following aromatic signals characteristic of the addition of acetone were observed (see Figure 9, Section 2.1.2.); ^{1}H NMR (400 MHz, 1 : 1 DMF-d_7 : acetone) δ 8.50

†The signal at δ 2.44 ppm intregrates of > 1 due to the overlapping acetone signal.

(1H, dd, *J* = 2.0, 0.5 Hz, C*H*), 6.75 - 6.68 (1H, m, C*H*), 5.44 (1H, dd, *J* = 10.3, 5.0 Hz, C*H*), 3.89 (1H, apt. q, *J* = 5.3 Hz, C*H*).

Subsequently, 1,3-dinitrobenzene (**51**) was reacted with NaOMe in DMF-d_7 with acetone omitted and the reaction mixture sampled for ^{1}H NMR (Figure 10, Section 2.1.2.). The sample was prepared as follows: 1,3-dinitrobenzene (**51**) (16.8 mg, 0.10 mmol) was dissolved in DMF-d_7. NaOMe (5.4 mg, 0.10 mmol) was added as a solid and an intense purple colour again resulted. This time the spectra showed the following set of signals; ^{1}H NMR (400 MHz, DMF-d_7) δ 8.65 (1H, dd, *J* = 2.1, 1.1 Hz, C*H*), 7.14 (1H, dd, *J* = 9.4, 2.1 Hz, C*H*), 5.65 - 5.50 (2H, m, C*H*), 3.03 (3H, s, CH_3).

The adduct obtained (Figure 10, Section 2.1.2.) was clearly different than with acetone present (Figure 9, Section 2.1.2.). The absence of a quartet at δ ~3.9 ppm and presence of an additional signal at δ 5.65 - 5.50 ppm was indicative of a proton adjacent to a heteroatom, suggesting the addition of methoxide ($^-$OMe).

5.2.4. INTERACTION OF POTASSIUM *tert*-BUTOXIDE AND 1,10-PHENANTHROLINE: NMR SPECTROSCOPY

The following two reactions were conducted and analysed by Dr. Graeme Coulthard at the University of Strathclyde, and are included for completeness.

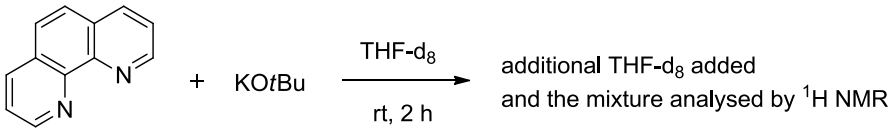

phen (1.0 eq.) (1.0 eq.)

An oven-dried pressure tube was taken into a glovebox and 1,10-phenanthroline (18.0 mg, 0.10 mmol) and KO*t*Bu (11.2 mg, 0.10 mmol) were added. THF-d_8 (267 µL) was added and the pressure tube sealed. The reaction mixture was then stirred at room temperature for 2 h.

The pressure tube was then opened and additional THF-d_8 added in order to give an appropriate volume for NMR (~0.7 mL) which was transferred to an NMR tube. No collapse of the aliphatic *tert*-butyl peak at δ 1.16 ppm was observed (see Figure 11, Section 2.1.3.).

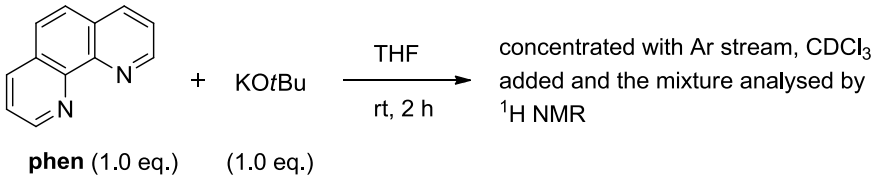

An oven-dried pressure tube was taken into a glovebox and 1,10-phenanthroline (18.0 mg, 0.10 mmol) and KO*t*Bu (11.2 mg, 0.10 mmol) were added. THF (267 µL) was added and the pressure tube sealed. The reaction mixture was then stirred at room temperature for 2 h. The pressure tube was then removed from the glovebox, opened, and the mixture concentrated with an argon stream. $CDCl_3$ (~0.5 mL) was added and the mixture analysed by ^{1}H NMR. Collapse of the aliphatic *tert*-butyl peak at δ 1.25 ppm was observed (see Figure 12, Section 2.1.3.), attributed to a reaction between KO*t*Bu and $CDCl_3$.

5.2.5. Initiation *via* Dimerisation of 1,10-phenanthroline to Generate an Electron Donor *in situ*

The experiments relating to data in Table 1 were carried out according to **General Procedure 1** (conditions **A**), see Chapter 5.3. for details.

5.2.6. Evidence of Aryne Formation Under Additive-free Conditions

The following reaction was conducted and data obtained by Florimond Cumine at the University of Strathclyde, and is included for completeness.

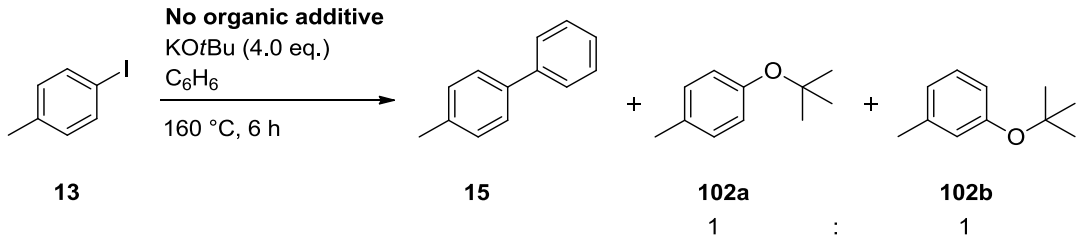

Inside a glovebox, 4-iodotoluene **13** (218.0 mg, 1.00 mmol) was dissolved in benzene (10 mL) in an oven-dried pressure tube. KO*t*Bu (449.0 mg, 4.00 mmol, 4.0 eq.) was added, the tube sealed, removed from the glovebox, and the reaction stirred at 160 ^{o}C for 6 h. After cooling to rt, the reaction was quenched with water (30 mL) and extracted with Et_2O (3 × 30 mL). The combined organic phases were dried (Na_2SO_4), filtered, and concentrated to give the crude material. Purification by column chromatography (hexane) gave **15** (45.0 mg, 27%) as a colourless solid (for data pertaining to **15**, see Section 5.3.5.) and an inseparable 1 : 1 mixture of **102a** : **102b** (65.0 mg, 40%) as a colourless oil; ^{1}H NMR (400 MHz, $CDCl_3$) δ 7.18 - 7.11 (1H, m, C*H*), 7.07 (2H, d, *J* = 8.5 Hz, C*H*), 6.92 - 6.87 (1H, m, C*H*), 6.89 (2H, d, *J* = 8.5 Hz, C*H*), 6.84 - 6.78 (1H, m, C*H*), 6.82 (1H, s, C*H*), 2.33 (3H, s, CH_3), 2.32 (3H, s, CH_3), 1.35 (9H, s, CH_3), 1.32 (9H, s, CH_3). These data are consistent with the literature.[118]

5.2.7. Cyclic Voltammetry of 1,10-phenanthroline Derivatives

For general experimental details pertaining to cyclic voltammetry, see Appendix. In this particular study, all solutions were prepared at 4.0 mM concentration (in 0.3 M *n*Bu_4NBF_4/DMF) using ferrocene as an external standard to ensure consistency throughout the study and whose peak height (*ca.* 2.5 x 10^{-6} A) corresponds to a one-electron oxidation. Anhydrous, degassed DMF was used throughout the study which was conducted within a glovebox under N_2 with 0.3 M *n*Bu_4NBF_4/DMF as the electrolyte.

The CV for 1,10-phenanthroline, at a scan rate of 50 mV s^{-1}, shows two reduction peaks at -2.05 V and -2.24 V *vs*. SCE and on the reverse scan, the

anodic peaks for both processes are observed (Figure 29, left, blue trace). The cathodic-anodic peak separation for the second reduction, $\Delta E^{p\text{-}p}$ obtained was 90 mV [close to the value obtained for ferrocene at the same scan rate (80 mV *cf.* 59 mV/n for an ideal one-electron transfer)],[119,120] indicating a high degree of reversibility (and so rapid kinetics) for the electron transfer processes. By comparison with ferrocene (Figure 29, right, red trace), both these processes again appear to be single-electron transfer steps, in accordance with the low $\Delta E^{p\text{-}p}$ values.

A scan rate dependence was carried out for 1,10-phenanthroline (Figure 30, left). Randles-Sevcik plots obtained for the two peak currents were linear (Figure 30, right), indicating no complications in the kinetics of electron transfer nor any chemical changes (for an introduction to scan rate dependence studies, the Randles-Sevcik equation and the calculation of diffusion coefficients, see Appendix). The diffusion coefficient D = 1.29 x 10^{-5} cm^2 s^{-1} was calculated for 1,10-phenanthroline in the DMF medium.

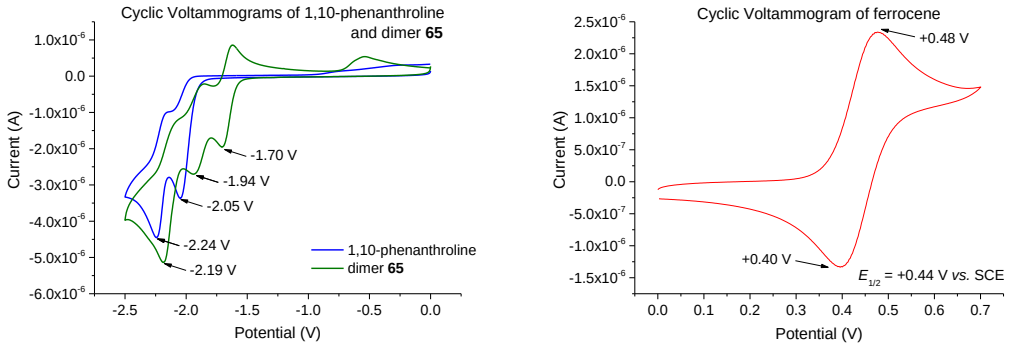

***Figure 29**: Left: Cyclic voltammograms of 1,10-phenanthroline and dimer **65**. Right: Cyclic voltammogram of ferrocene as an external standard (reproduced here from Figure 13).*

For dimer **65**, two one-electron transfer peaks (for the first reduction, $\Delta E^{p\text{-}p}$ obtained was 90 mV) were found at -1.70 V and -1.94 V *vs*. SCE, (Figure 29, left, green trace) corresponding to consecutive electron injections (Scheme

45). Both of these potentials are less negative than those observed for 1,10-phenanthroline, consistent with enhanced electron delocalisation in the dimer. A scan rate dependence was similarly carried out here (Figure 31, left) and the Randles-Sevcik plots (Figure 31, right) yielded a diffusion coefficient of D = 6.00 x 10^{-6} cm^2 s^{-1}, which is consistent with the larger size of dimer **65** and for the lower peak currents obtained here (compared to 1,10-phenanthroline). At more negative potentials, a third reduction process occurs giving a current peak at -2.19 V *vs.* SCE.

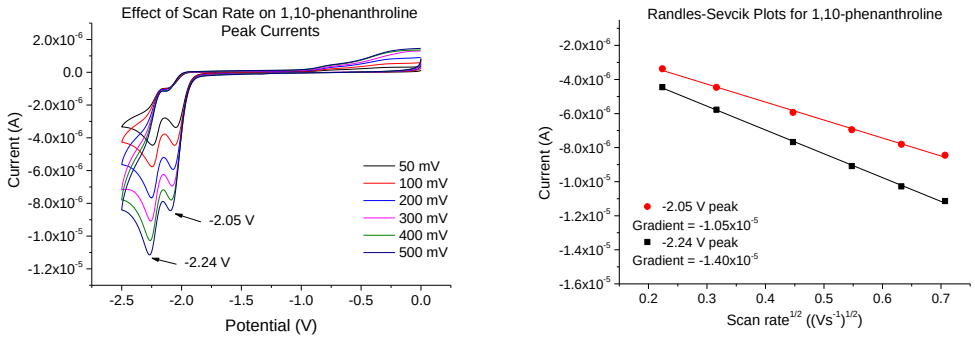

***Figure 30**: Left: Effect of scan rate on 1,10-phenanthroline peak currents. Right: Randles-Sevcik plots for peak currents showing, in both cases, a linear relationship.*

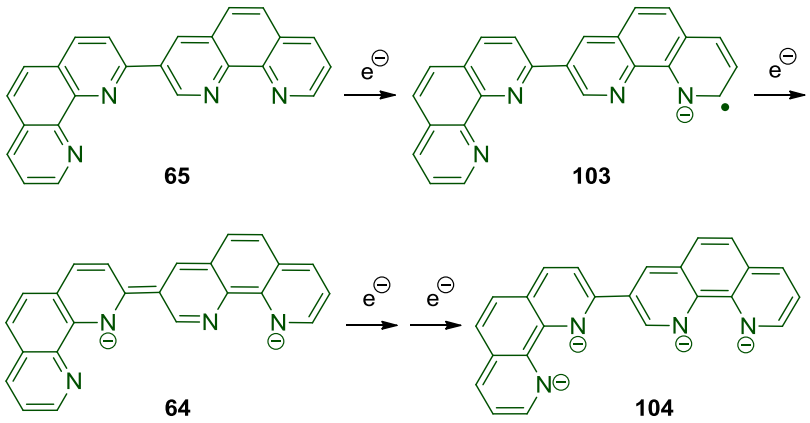

***Scheme 45**: Sequential transfer of single electrons to dimer **65**.*

Comparison with ferrocene indicates that this involves a two-electron reduction step. It is highly unlikely that two electrons are simultaneously transferred to the doubly-charged species **64** at the same applied potential. It is more probable here that the electron gained by species **64** leads to a species which is even more easily reduced (*i.e.* its reversible potential is more positive than for the first step and this triggers the gain of a fourth electron to the dimer) to give **104** (Scheme 45). Overall then, this last process appears as a two-electron transfer step.

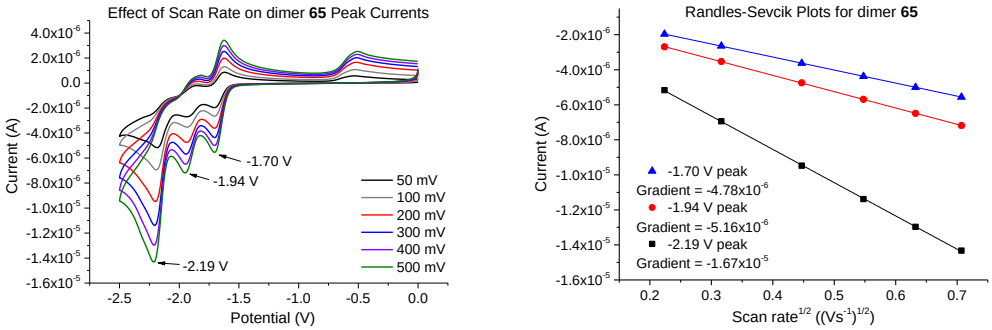

***Figure 31**: Left: Effect of scan rate on dimer **65** peak currents. Right: Randles-Sevcik plots for peak currents showing, in each case, a linear relationship.*

Normalised plots of $I / v^{1/2}$ *vs*. V were examined in order to determine whether the reduced products were involved in any chemical reaction prior to the reverse scan (Figure 32). The data show that this was not the case as the shape of the voltammograms remained unaltered over the scan rate range examined. It would have been expected from such plots that all the scans should have superimposed. They do superimpose, but not perfectly; this is due to the contribution of the charging of the electrical double layer[79,120] (see Appendix) which is not taken into account in the normalised plots.

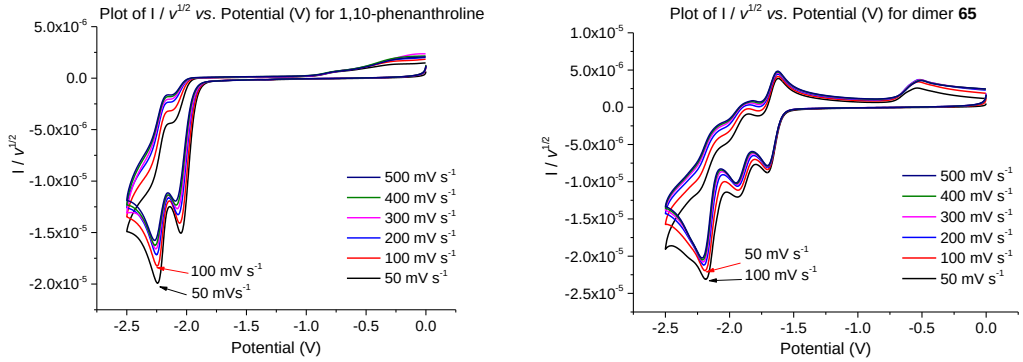

***Figure 32**: Normalised plots of I / $v^{1/2}$ vs. V for 1,10-phenanthroline and dimer **65**.*

5.2.8. EPR Spectroscopy Sample Preparation

The following samples were prepared by Dr. Eswararao Doni and analysed by Prof. John Walton at the University of St. Andrews. In a glovebox, an oven-dried pressure tube was charged with 1,10-phenanthroline (18.0 mg, 0.10 mmol), DMF (2 mL) and KO*t*Bu (44.9 mg, 0.40 mmol, 4.0 eq.). The tube was sealed and stirred at 100 ^{o}C for 2 h. After cooling to rt, the mixture was diluted with toluene (8 mL), providing a 0.01 M solution (w.r.t. 1,10-phenanthroline) which was sampled and analysed by EPR spectroscopy (Figure 33, left). The second derivative spectrum (Figure 33, right) shows that there is more than one radical species in solution.

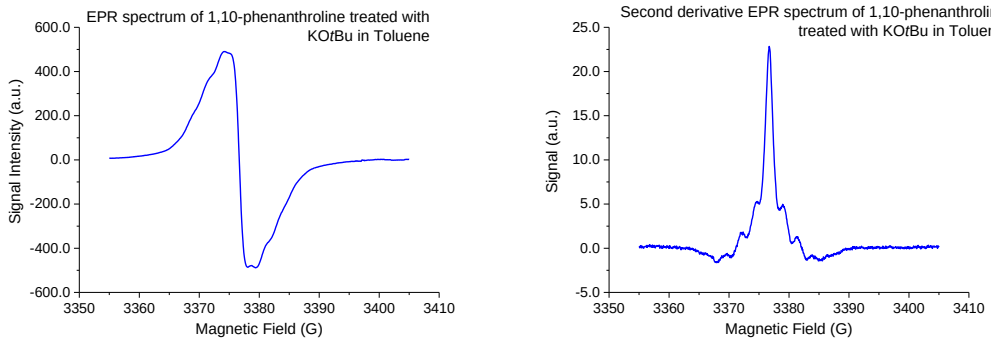

***Figure 33**: Left: EPR spectrum of 1,10-phenanthroline treated with KOtBu in Toluene. Right: Second derivative EPR spectrum.*

5.2.9. REDUCTIVE FRAGMENTATION OF DITHIANES: PHOTOCHEMICAL REACTIONS

Diphenylmethane (95)

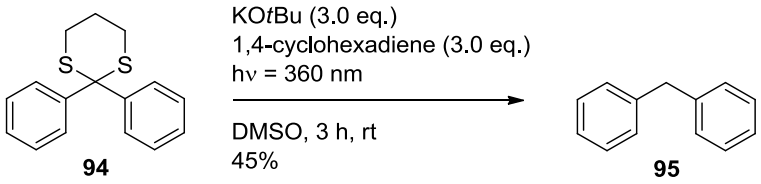

Prepared according to a literature procedure.[90] An flattened oven-dried glass vessel was equipped with a stirrer bar and KO*t*Bu (112 mg, 1.00 mmol, 3.0 eq.), 2,2-diphenyl-1,3-dithiane (**94**) (91.0 mg, 0.33 mmol), 1,4-cyclohexadiene (81.0 mg, 1.00 mmol, 3.0 eq.) and dry, degassed DMSO (3.3 mL) were added in a glovebox. The reaction mixture appeared dark red in colour. The flask was sealed and removed from the glovebox, then irradiated with 2x 100 W UV-light (365 nm) lamps at a distance of *ca.* 10 cm for 3 h at rt. The reaction mixture was removed from the light and quenched with MeI (0.05 mL, 0.83 mmol), which changed the colour from dark red to light yellow. Water (10 mL) was added and the mixture extracted with DCM (3 x 20 mL). The combined organics were dried (Na_2SO_4), filtered and concentrated *in vacuo* to yield a brown oil. ^{1}H NMR of the crude reaction mixture revealed a 50% yield of **95** by comparison with an added internal standard [1,3,5-trimethoxybenzene (5.6 mg, 33.0 μmol, 10 mol%)]. Column chromatography (hexane) gave **95** as a colourless residue (25.0 mg, 45%); ^{1}H NMR (400 MHz, $CDCl_3$) δ 7.31 (4H, apt. t, *J* = 7.5 Hz, C*H*), 7.24 - 7.20 (6H, m, C*H*), 4.01 (2H, s, CH_2); ^{13}C NMR (101 MHz, $CDCl_3$) δ 141.1 (*C*), 128.9 (*C*H), 128.4 (*C*H), 126.1 (*C*H), 41.9 (*C*H_2); Data are consistent with literature.[121]

Alternatively, the reaction was conducted using KH (40.1 mg, 1.00 mmol, 3.0 eq.) in place of KO*t*Bu. On completion of the addition of all reagents, the reaction mixture appeared dark red in colour. Gas evolution was allowed to cease before the flask was sealed and irradiated. ^{1}H NMR of the crude reaction mixture revealed a 16% yield of **95** by comparison with an added

internal standard [1,3,5-trimethoxybenzene (5.6 mg, 33.0 μmol, 10 mol%)]. Column chromatography (hexane) gave pure **95** as a colourless film (7.0 mg, 13%).

Alternatively, the reaction was conducted in the absence of base. No coloration was observed. ^{1}H NMR of the crude reaction mixture revealed a 69% yield of returned **94** by comparison with an added internal standard (5.6 mg, 33.0 μmol, 10 mol%) 1,3,5-trimethoxybenzene. No desired product **95** was detected.

5.2.10. Reductive Fragmentation of Dithianes: UV-visible Spectroscopy

The following samples were prepared and the UV-visible spectra of the resulting mixtures were measured (Figure 34):

1) 1.2 x 10^{-5} M dithiane **94** in DMSO (Figure 34, **A**, black trace)
2) 0.05 M KO*t*Bu in DMSO [UV-visible trace and appearance were the same as for (1)]
3) 1.2 x 10^{-5} M dithiane **94** / 0.05 M KO*t*Bu in DMSO (Figure 34, **B**, red trace)
4) 1.2 x 10^{-5} M dithiane **94** / 0.05 M KH in DMSO (Figure 34, **C**, blue trace)

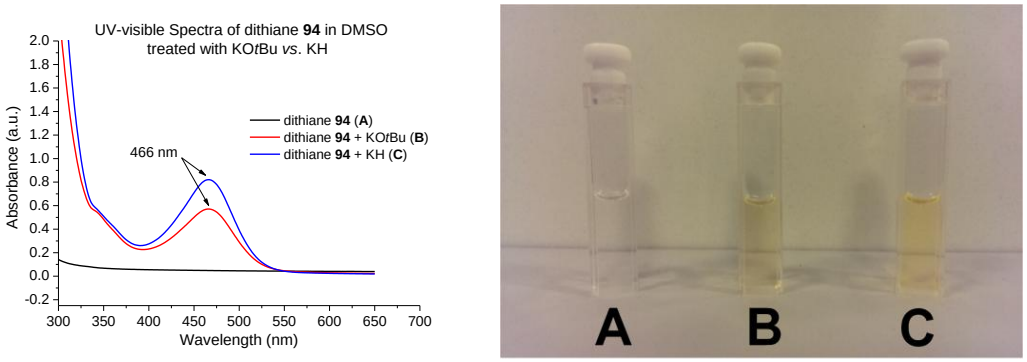

***Figure 34**: Left: UV-visible spectra of dithiane **94** in the presence of KOtBu vs. KH in DMSO. Right: Sample colours observed (reproduced here from Figure 15).*

The observation that the mixture of dithiane **94** and KH in DMSO gives rise to a yellow coloration and a UV-visible absorption at 466 nm in the same way as dithiane **94** and KO*t*Bu in DMSO suggested that the yellow colour and UV-visible absorption could be arising from a electron donor-acceptor (**EDA**) complex between the dithiane **94** and the dimsyl anion (resulting from the deprotonation of DMSO by either KO*t*Bu, or KH) and not an **EDA** complex between dithiane **94** and KO*t*Bu. Further evidence for this was obtained when the following samples were prepared and their colour observed and UV-visible spectra measured (Figure 35):

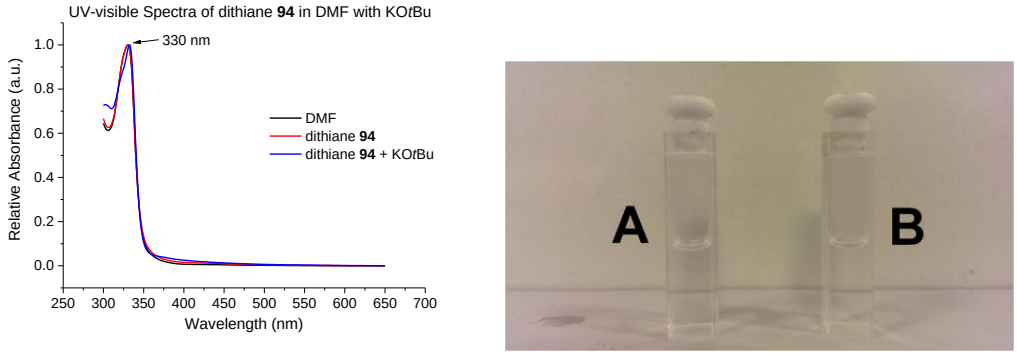

***Figure 35**: Left: UV-visible spectra of dithiane **84** in the presence of KOtBu in DMF. Right: Sample colours observed (reproduced here from Figure 16).*

1) DMF only (Figure 35, black trace).
2) 1.2×10^{-5} M dithiane **94** in DMF (Figure 35, **A**, red trace).
3) 1.2×10^{-5} M dithiane **94** / 0.05 M KO*t*Bu in DMF (Figure 35, **B**, blue trace).

In these cases no coloration was seen and no UV-visible absorption observed at 466 nm. This demonstrates that no **EDA** complex occurs between dithiane **94** and KO*t*Bu and that it is deprotonation of DMSO that leads to the dimsyl anion which forms an **EDA** complex with dithiane **94**.

5.3. Experiments to Probe the Function of 2-Pyridinecarbinol as an Additive in Transition Metal-free C-H Arylations with Bromoarenes

5.3.1. Preparation of Organic Additives for Transition Metal-free C-H Arylation Reactions

2-(Pyridin-2-yl)propan-2-ol (121)

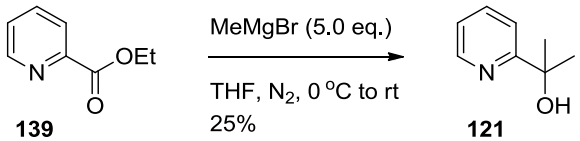

An oven-dried flask was charged with ethyl picolinate (**139**) (1.21 g, 8.0 mmol) and THF (80 mL). The flask was sealed inside a N_2-filled glovebox and stirred at 0 °C, before addition of MeMgBr (3.0 M in Et_2O) (13.3 mL, 40.0 mmol, 5.0 eq.) dropwise over 30 min at 0 °C. The reaction was allowed to warm to rt, before careful addition of sat. NH_4Cl (20 mL) to quench. The mixture was poured into a separatory funnel with Et_2O (30 mL), the layers separated and aqueous layer extracted with Et_2O (2 x 30 mL). The combined organic layers were dried (Na_2SO_4), filtered and concentrated *in vacuo* to yield a yellow oil, which was purified by column chromatography (5 - 12.5% Et_2O/hexane (1% Et_3N)) to yield **121** as a pale brown oil (278.0 mg, 25%); IR ν_{max} (neat) 3389 (O-H), 2974 - 2859 (Ar), 1591 (Ar), 1570 (Ar), 1476, 1462, 1431, 1370, 1290, 1275, 1236 cm^{-1}; ^1H NMR (400 MHz, $CDCl_3$) δ 8.52 (1H, d, *J* = 4.9 Hz, C*H*), 7.70 (1H, td, *J* = 7.7, 1.8 Hz, C*H*), 7.39 (1H, dt, *J* = 7.8, 1.0 Hz, C*H*), 7.28 (1H, ddd, *J* = 7.4, 4.9, 1.1 Hz, C*H*), 5.06 (1H, br. s, O*H*), 1.55 (6H, s, CH_3); ^{13}C NMR (101 MHz, $CDCl_3$) δ 166.0 (*C*), 147.4 (*C*H), 136.9 (*C*H), 121.8 (*C*H), 118.7 (*C*H), 71.7 (*C*), 30.7 (*C*H_3); HRMS (+ESI) *m/z* calculated for $C_8H_{12}NO$ [$M+H^+$] 138.0919; Found 138.0915. Data are consistent with literature.[122]

Benzaldehyde (**112**)

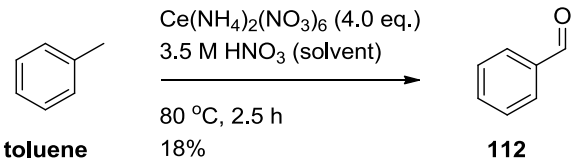

Prepared according to a literature procedure.[123] To a solution of toluene (1.25 g, 12.5 mmol) in 3.5 M HNO_3 (25 mL) was added $Ce(NH_4)_2(NO_3)_6$ (27.4 g, 50 mmol) in 3.5 M HNO_3 (100 mL). The reaction was stirred at 80 °C for 2.5 h (the orange solution turned yellow in colour at 80 °C), then cooled to rt. The crude product was extracted with $CHCl_3$ (3 x 50 mL) and the combined organics were washed with water until pH = 7. The organic layer was dried (Na_2SO_4), filtered and concentrated *in vacuo*. Purification by distillation gave benzaldehyde-h_6 (**112**) as a pale yellow oil (275 mg, 18%); ^{1}H NMR (400 MHz, $CDCl_3$) δ 10.04 (1H, s, C*H*O), 7.89 (2H, dd, *J* = 8.3, 1.3 Hz, C*H*), 7.65 (1H, td, *J* = 7.5, 1.4 Hz, C*H*), 7.55 (2H, t, *J* = 7.5 Hz, C*H*).

Benzaldehyde-d_6 (**112-d_6**)

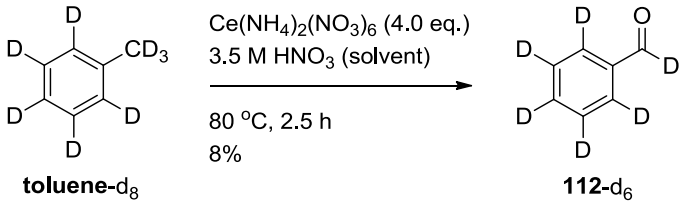

Toluene-d_8 was subjected to the preceding procedure to afford benzaldehyde-d_6 (**112**-d_6) as a pale yellow oil (111 mg, 8%); ^{2}H NMR (61 MHz, $CHCl_3$) δ 10.04 (1D, s, C*D*O), 7.91 (2D, br. s, C*D*), 7.66 (1D, br. s, C*D*), 7.56 (2D, br. s, C*D*); ^{13}C NMR (101 MHz, $CDCl_3$) δ 192.1 (t, *J* = 25.6 Hz, *C*DO), 136.2 (*C*), 133.9 (t, *J* = 24.9 Hz, *C*D), 129.3 (t, *J* = 24.9 Hz, *C*D), 128.5 (t, *J* = 24.4 Hz, *C*D); HRMS (+CI) *m/z* calculated for $C_7{}^1H_1{}^2H_6O$ [M+H$^+$] 113.0868 Found 113.0870.

2-Phenoxy-1-phenylethanol (**135**)

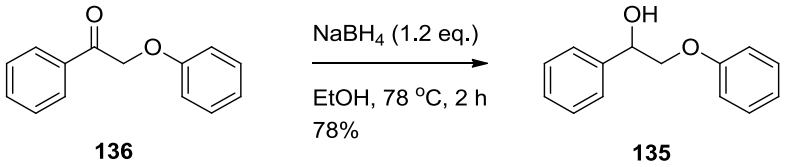

136 **135**

Prepared according to a literature procedure.[124] An oven-dried flask was charged with 2-phenoxy-1-phenylethanone (**136**) (91.0 mg, 0.42 mmol) and EtOH (6.5 mL). $NaBH_4$ (19.5 mg, 0.50 mmol) was added in one portion at rt. The flask was equipped with a reflux condenser and stirred at reflux (78 ^oC) for 2 h, before cooling to rt and pouring onto ice. Excess NH_4Cl was added (until pH = 5 - 6) and the reaction mixture stirred for 1 h. The crude product was extracted with Et_2O (3 x 20 mL) and the combined organics were washed with brine (30 mL), dried (Na_2SO_4), filtered and concentrated *in vacuo* loading onto celite. Column chromatography (40% EtOAc/hexane) gave 2-phenoxy-1-phenylethanol (**135**) as a white microcrystalline solid (70.0 mg, 78%); m.p. 50 - 52 ^oC (lit 48 - 50 ^oC[125]); IR ν_{max} (neat) 3298 (br., O-H), 3059 - 2873 (C-H), 1597 (Ar), 1583 (Ar), 1496 (Ar), 1452, 1388, 1344, 1334, 1290, 1238, 1195, 1170, 1151, 1097, 1078, 1066, 1043, 1026 cm^{-1}; ^1H NMR (400 MHz, $CDCl_3$) δ 7.47 (2H, d, *J* = 7.3 Hz, C*H*), 7.41 (2H, t, *J* = 7.2 Hz, C*H*), 7.38 - 7.28 (3H, m, C*H*), 6.99 (1H, t, *J* = 7.3, C*H*), 6.95 (2H, d, *J* = 8.1 Hz, C*H*), 5.14 (1H, dd, *J* = 8.8, 3.3 Hz, C*H*), 4.16 - 4.11 (1H, m, CH_2), 4.03 (1H, apt. t, *J* = 9.2 Hz, CH_2), 2.34 (1H, br. s, O*H*); ^{13}C NMR (101 MHz, $CDCl_3$) δ 158.4 (*C*), 139.6 (*C*), 129.6 (*C*H), 128.6 (*C*H), 128.2 (*C*H), 128.3 (*C*H), 121.3 (*C*H), 114.6 (*C*H), 73.3 (*C*H_2), 72.6 (*C*H); HRMS (+CI) *m/z* calculated for $C_{14}H_{18}O_2N$ [M+NH_4^+] 232.1333; Found 232.1332. Data are consistent with the literature.[125]

2-Phenoxy-1-phenylethanone (**136**)

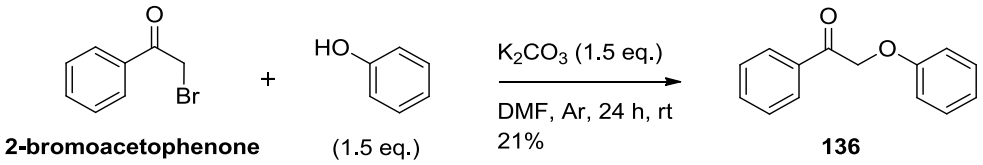

2-bromoacetophenone (1.5 eq.) **136**

Prepared according to a literature procedure.[126] An oven-dried flask was charged with K_2CO_3 (622.0 mg, 4.5 mmol), 2-bromoacetophenone (579.0 mg, 3.0 mmol), phenol (424.0 mg, 4.5 mmol) and DMF (10 mL) and was stirred at rt under Ar for 24 h. The reaction was quenched with water (30 mL) and extracted with Et_2O (3 x 30 mL). The combined organics were dried (Na_2SO_4), filtered and concentrated *in vacuo* to yield an off-white solid, which was recrystallised from DCM/hexane to yield **136** as a white microcrystalline solid (133.0 mg, 21%); m.p. 62 - 64 ^oC (lit. 60 - 61 ^oC[117]); IR ν_{max} (neat) 3064 - 2800 (C-H), 1705 (C=O), 1597 (Ar), 1581 (Ar), 1498 (Ar), 1479, 1448, 1431, 1384, 1302, 1290, 1247, 1224 cm^{-1}; ^1H NMR (400 MHz, $CDCl_3$) δ 8.02 (2H, dd, *J* = 8.3, 1.2 Hz, C*H*), 7.63 (1H, t, *J* = 7.4 Hz, C*H*), 7.51 (2H, apt. t, *J* = 7.8 Hz, C*H*), 7.30 (2H, dd, *J* = 8.8, 1.3 Hz, C*H*), 7.00 (1H, t, *J* = 7.3 Hz, C*H*), 6.97 (2H, dd, *J* = 8.8, 0.9 Hz, C*H*), 5.28 (2H, s, CH_2); ^{13}C NMR (101 MHz, $CDCl_3$) δ 194.6 (*C*=O), 158.0 (*C*), 134.6 (*C*), 133.8 (*C*H), 129.6 (*C*H), 128.8 (*C*H), 128.2 (*C*H), 121.7 (*C*H), 114.8 (*C*H), 70.9 (*C*H_2) HRMS (+ESI) *m/z* calculated for $C_{14}H_{13}O_2$ [M+H^+] 213.0910; Found 213.0909. Data are consistent with the literature.[125]

5.3.2. General Procedure 1: C-H Arylation with 2,6-Dimethylhalobenzenes to Measure Efficacy of Organic Additives in Initiation

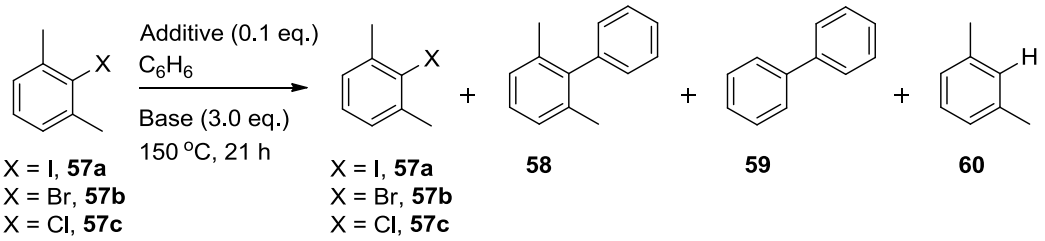

Two sets of conditions were used, Conditions **A** and Conditions **B**.

General Procedure 1 (conditions **A**): To an oven-dried pressure tube was added 2,6-dimethylhalobenzene **57** (0.5 mmol) and additive (0.05 mmol, 0.1 eq.). KO*t*Bu (112 mg, 1.0 mmol, 2.0 eq.) and benzene (5 mL) were added. The tube was sealed in a glovebox and stirred at 130 °C for 18 h. After cooling to rt, the reaction was quenched with water (50 mL) and extracted with Et_2O (3 x 50 mL). The combined organic layers were dried (Na_2SO_4), filtered and concentrated *in vacuo* to afford the crude product.

General Procedure 1 (conditions **B**): To an oven-dried pressure tube was added 2,6-dimethyliodobenzene **57a** (116 mg, 0.5 mmol) and additive (0.05 mmol, 0.1 eq.). KO*t*Bu (168 mg, 1.5 mmol, 3.0 eq.) and benzene (5 mL) were added. The tube was sealed in a glovebox and stirred at 150 °C for 21 h. Work up and purification was conducted as above for Conditions **A**. Purification by column chromatography (hexane) afforded an inseparable mixture of 2,6-dimethyl-1,1′-biphenyl (**58**) and biphenyl (**59**) (typically in a 1 : ~3.5 molar ratio by ^{1}H NMR) as a white microcrystalline solid (see Appendix for the ^{1}H NMR spectrum);

2,6-Dimethyl-1,1′-biphenyl (**58**): ^{1}H NMR (400 MHz, $CDCl_3$) δ 7.48 - 7.41 (2H, m, C*H*),† 7.39 - 7.33 (1H, m, C*H*),‡ 7.19 - 7.10 (5H, m, C*H*), 2.05 (6H, s, CH_3);

†,‡These signals of **58** and **59** superimposed in the ^{1}H NMR spectrum.

Biphenyl (**59**): ^{1}H NMR (400 MHz, $CDCl_3$) δ 7.64 - 7.59 (4H, m, C*H*), 7.46 (4H, apt. t, *J* = 7.5 Hz, C*H*),† 7.38 - 7.34 (2H, m, C*H*);‡ ^{1}H NMR data are consistent with the literature.[127]

Representative ^{1}H NMR spectra for crude reaction mixtures derived from 2,6-dimethyliodobenzene (**57a**) are shown on the following pages.

^{1}H NMR (400 MHz, $CHCl_3$) - 2-pyridinecarbinol (**80**) as an additive.

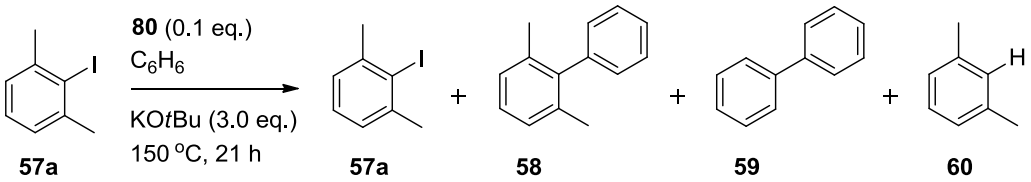

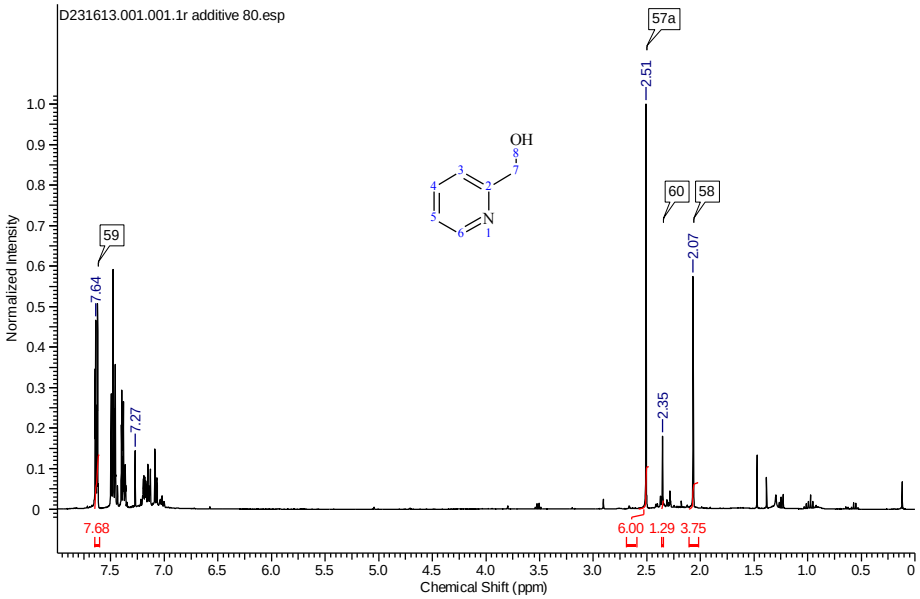

Ratio **57a** : **58** : **59** : **60** = 1 : 0.63 : 1.92 : 0.22

†,‡These signals of **58** and **59** superimposed in the ^{1}H NMR spectrum.

^{1}H NMR (400 MHz, $CHCl_3$) - 2-(pyridin-2-yl)propan-2-ol (**121**) as an additive.

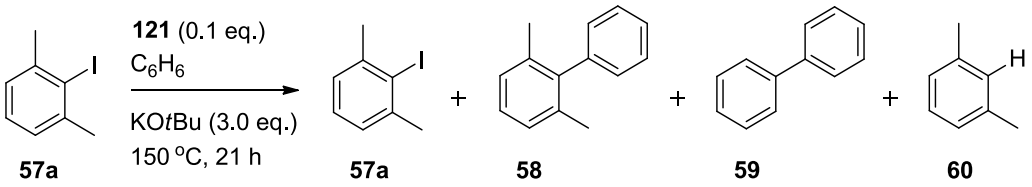

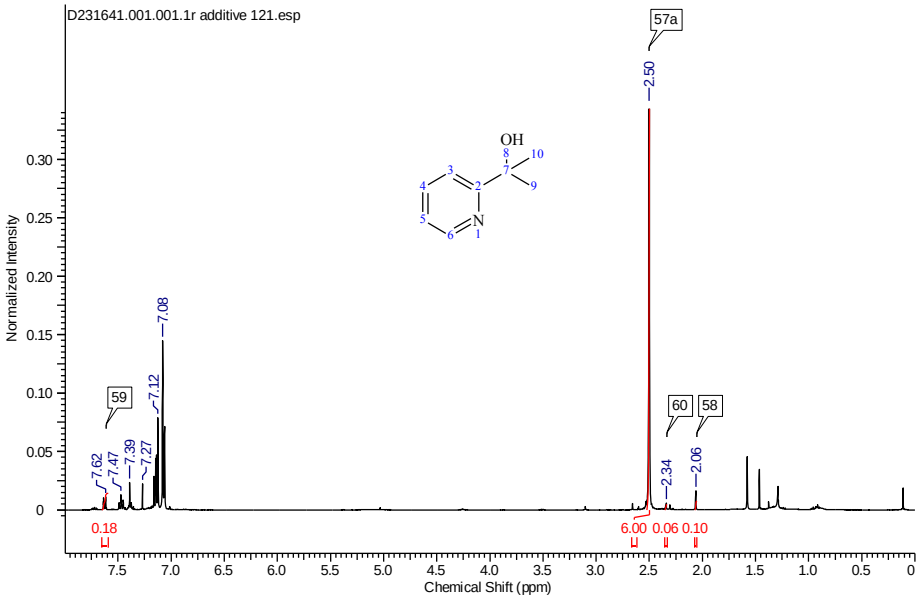

Ratio **57a** : **58** : **59** : **60** = 1 : 0.02 : 0.05 : 0.01

Alternatively, 1,3,5-trimethoxybenzene (8.4 mg, 0.05 mmol, 10 mol%) was added to the crude reaction mixture, the residue dissolved in $CDCl_3$ and combined yield of biaryls **58** and **59** determined by ^{1}H NMR (see Appendix for details).

5.3.3. TRANSESTERIFICATION OF ETHYL BENZOATE WITH POTASSIUM *tert*-BUTOXIDE

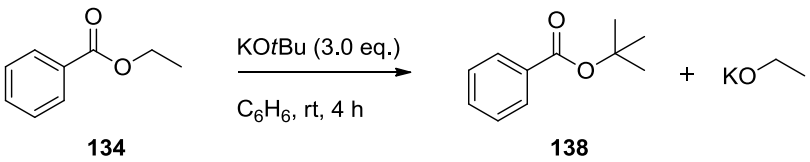

To an oven-dried pressure tube was added ethyl benzoate (**134**) (75.1 mg, 0.5 mmol). KO*t*Bu (168.0 mg, 1.5 mmol, 3.0 eq.) and benzene (5 mL) were added. The tube was sealed in a glovebox and stirred at rt for 4 h. A 1 mL sample of the cloudy white slurry was quenched with water (50 mL) and extracted with Et_2O (3 x 50 mL). The combined organic layers were dried (Na_2SO_4), filtered through a plug of silica gel and concentrated *in vacuo* to yield (**138**) as a colourless oil (8.0 mg, 11%);† IR ν_{max} (neat) 2976 - 2931 (C-H), 1710 (C=O), 1594 (Ar), 1450, 1367, 1313, 1288, 1253, 1165, 1112, 1068, 1026 cm^{-1}; ^1H NMR (400 MHz, $CDCl_3$) δ 7.99 (2H, d, *J* = 7.8 Hz, C*H*), 7.53 (1H, t, *J* = 8.0, C*H*), 7.42 (2H, t, *J* = 7.6 Hz, C*H*), 1.61 (9H, s, CH_3); ^{13}C NMR (101 MHz, $CDCl_3$) δ 165.8 (*C*), 132.4 (*C*H), 132.0 (*C*), 129.4 (*C*H), 128.2 (*C*H), 81.0 (*C*), 28.2 (*C*H_3). Data are consistent with the literature.[128]

5.3.4. POTASSIUM *tert*-BUTOXIDE-MEDIATED BENZYLIC DEUTERATION OF 2-PYRIDINECARBINOL IN THE PRESENCE OF D_2O

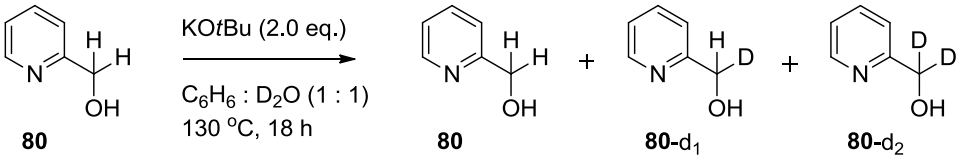

A pressure tube was charged with 2-pyridinecarbinol **80** (55.0 mg, 0.5 mmol) and KO*t*Bu (112.0 mg, 1.0 mmol, 2.0 eq.). Benzene (2.5 mL) and D_2O (2.5 mL) were added. The reaction was sealed, removed from the glovebox and stirred at 130 °C for 18 h. The reaction was quenched with H_2O (50 mL) and DCM (30 mL) was added. The layers were separated and aqueous extracted with DCM (2 x 30 mL). The combined organics were dried (Na_2SO_4), filtered and concentrated *in vacuo* to yield the crude product which was analysed by ^1H, ^2H and ^{13}C NMR. The reaction was conducted side-by-side with an equivalent reaction using H_2O (2.5 mL) for comparison. See Appendix for spectra.

†Product **138** was observed as the sole component in the crude ^1H NMR, but only a sample of product was isolated. Based on the 1 mL aliquot taken from the 5 mL reaction mixture, the yield is estimated as 55%.

5.3.5. 2-PYRIDINECARBINOL-MEDIATED C-H ARYLATION WITH *p*-BROMOTOLUENE UNDER LITERATURE CONDITIONS

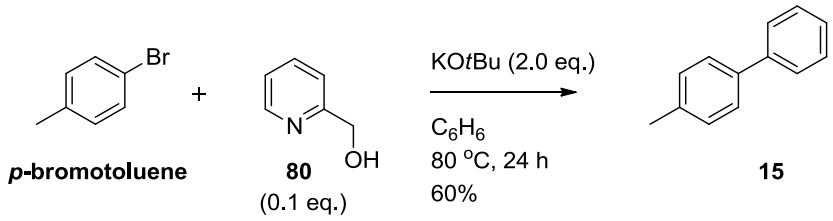

Prepared according to a literature procedure.[14] To an oven-dried pressure tube was added *p*-bromotoluene (0.5 mmol) and 2-pyridinecarbinol **80** (0.05 mmol, 0.1 eq.). KO*t*Bu (112 mg, 1.0 mmol, 2.0 eq.) and benzene (5 mL) were added. The tube was sealed in a glovebox and stirred at 80 °C for 24 h. After cooling to rt, the reaction was quenched with water (50 mL) and extracted with Et_2O (3 x 50 mL). The combined organic layers were dried (Na_2SO_4), filtered and concentrated *in vacuo*. Purification by column chromatography (hexane) afforded 4-methyl-1,1′-biphenyl (**15**) as a white microcrystalline solid (50.3 mg, 60%); m.p. 46 - 48 °C (lit. 46 - 48 °C[129]); IR ν_{max} (neat) 2958 - 2852 (C-H), 1458 (Ar), 1377 cm^{-1}; ^{1}H NMR (400 MHz, $CDCl_3$) δ 7.60 (2H, dd, *J* = 8.3, 1.3 Hz, C*H*), 7.52 (2H, d, *J* = 8.3 Hz, C*H*), 7.44 (2H, t, *J* = 7.5 Hz, C*H*), 7.34 (1H, t, *J* = 7.4, C*H*), 7.26 (2H, d, *J* = 8.0 Hz, C*H*), 2.41 (3H, s, CH_3); ^{13}C NMR (101 MHz, $CDCl_3$) δ 141.2 (*C*), 138.4 (*C*), 137.0 (*C*), 129.5 (*C*H), 128.7 (*C*H), 127.1 (*C*H), 127.0 (2 x *C*H), 21.1 (CH_3). Data are consistent with the literature.[129,130]

5.3.6. ^{1}H NMR COMPARISON OF PIVALOPHENONE AND ACETOPHENONE

Pivalophenone (**132**) and acetophenone were analysed by ^{1}H NMR spectroscopy. The aromatic protons *ortho*- to the ketone are significantly more shielded for pivalophenone (**132**) than acetophenone by ^{1}H NMR, which indicates deviation from co-planarity of the carbonyl group and the arene in the case of pivalophenone (**132**).

***Table 10**: [1]H NMR chemical shifts (ppm) of the aromatic protons comparing pivalophenone (**132**) and acetophenone in $CDCl_3$. Literature values given for reference.*

Ketone[a]	δ [H_{ortho}] (ppm)	δ [H_{meta}] (ppm)	δ [H_{para}] (ppm)
132[b]	7.71 - 7.68	7.42 - 7.38	7.48 - 7.44
132[131]	7.70 - 7.67	7.45 - 7.35	7.45 - 7.35
acetophenone[b]	7.96 - 7.93	7.46 - 7.42	7.56 - 7.52
acetophenone[132]	7.97	7.49 - 7.45	7.57

[a]Literature values are given with corresponding references. [b]Results from this study.

5.3.7. 2-Pyridinecarbinol-mediated C-H Arylation with *p*-chlorotoluene under Literature Conditions

The following three reactions were conducted by Dr. Graeme Coulthard at the University of Strathclyde, and are included for completeness.

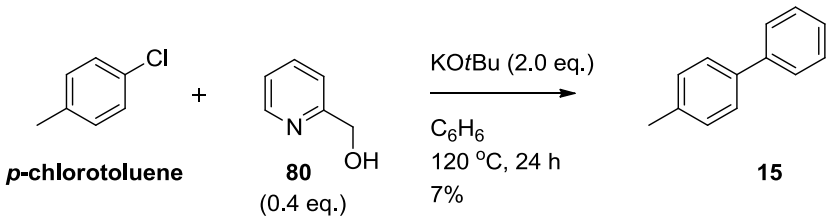

***p*-chlorotoluene** **80** (0.4 eq.) **15**

According to a modified literature procedure.[14] To an oven-dried pressure tube was added 4-chlorotoluene (116.0 mg, 1.0 mmol) and 2-pyridinecarbinol **80** (43.7 mg, 0.40 mmol). KO*t*Bu (224.4 mg, 2.0 mmol) and benzene (8 mL) were added. The tube was sealed in a glovebox and stirred at 120 °C for 24 h. After cooling to rt, the reaction was quenched with water (10 mL) and extracted with Et_2O (3 x 20 mL). The combined organic layers were dried (Na_2SO_4), filtered and concentrated *in vacuo*. 1,3,5-Trimethoxybenzene (16.8 mg, 0.10 mmol) was added to the crude reaction mixture (as an internal

standard for NMR calibration), the residue dissolved in $CDCl_3$ and yield of **15** determined as 7.0% by ^{1}H NMR. This is consistent with the literature which reports an 8% yield of **15** (determined by calibrated GC methods) under identical conditions.[14]

This reaction was conducted side-by-side with a blank reaction (carried out as above, but without additive **80**) which gave no detectable coupled product.

Alternatively, a reaction carried out at 80 °C for 24 h [using the above conditions, but with of additive **80** (0.1 eq.)] gave only a trace amount of coupled product.

5.3.8. Synthesis of (5-methoxypyridin-2-yl)methanol for use as an Additive in Couplings of Chloroarenes

The following two compounds were synthesised by Dr. Graeme Coulthard at the University of Strathclyde, and are included for completeness.

Methyl 5-methoxypyridine-2-carboxylate (140)

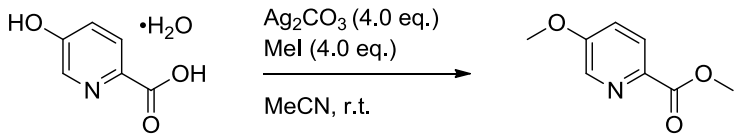

5-hydroxypyridine monohydrate **140**

Iodomethane (2.71 g, 1.19 mL, 19.1 mmol) was added to a suspension of 5-hydroxypyridine monohydrate (750.0 mg, 4.8 mmol), Ag_2CO_3 (5.27 g, 19.1 mmol) and MeCN (23 mL). The mixture was stirred at room temperature for 64 h before the solids were filtered and washed with EtOAc (3 x 20 mL). The filtrate was concentrated under reduced pressure to give the crude material. Purification by column chromatography (EtOAc) gave **140** as a yellow solid (482.0 mg, 60%); m.p. 64 - 66 °C (lit. 69 - 72 ^oC[133]); ^{1}H NMR (400 MHz, $CDCl_3$) δ 8.40 (1H, dd, *J* = 3.0, 0.5 Hz, C*H*), 8.12 (1H, dd, *J* = 8.6, 0.5 Hz, C*H*), 7.27 (1H, dd, 8.6, 3.0 Hz, C*H*), 3.99 (3H, s), 3.93 (3H, s); ^{13}C NMR (101

MHz, $CDCl_3$) δ 165.4 (*C*=O), 158.1 (*C*), 140.2 (*C*), 138.1 (*C*H), 126.4 (*C*H), 119.6 (*C*H), 55.7 (*C*H_3), 42.5 (*C*H_3). Data are consistent with the literature.[134]

(5-Methoxypyridin-2-yl)methanol (137)

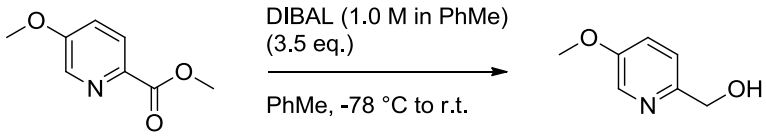

140 **137**

Methyl 5-methoxypyridine-2-carboxylate **140** (250.0 mg, 1.5 mmol) was added to an oven-dried flask under argon and dissolved in anhydrous toluene (14.9 mL). The solution was cooled to -78 °C, DIBAL (1.0 M in toluene) (5.2 mL, 5.2 mmol) was added dropwise by syringe, and the reaction was stirred at 0 °C for 1.5 h. The reaction was then quenched with sat. aq. potassium sodium tartrate (20 mL) and stirred at room temperature for 1 h. The mixture was extracted with EtOAc (3 x 20 mL). The combined organic phases were dried (Na_2SO_4), filtered, and concentrated *in vacuo*. Purification by column chromatography (EtOAc) gave **137** as a pale yellow oil, which solidified on standing to a pale yellow solid (126.0 mg, 61%); m.p. 46 - 48 °C; IR ν_{max} (neat) 3140 - 2837 (C-H), 1580 (Ar), 1489 (Ar), 1292 cm^{-1}; ^{1}H NMR (400 MHz, $CDCl_3$) δ 8.25 (1H, dd, *J* = 2.7, 0.9 Hz, C*H*), 7.23 (1H, dd, *J* = 8.5, 2.7 Hz, C*H*), 7.19 (1H, dd, *J* = 8.5, 0.9 Hz, C*H*), 4.71 (2H, s), 3.87 (3H, s), 3.45 (1H, br. s, O*H*); ^{13}C NMR (101 MHz, $CDCl_3$) δ 154.9 (*C*), 151.5 (*C*), 135.8 (*C*H), 121.7 (*C*H), 121.1 (*C*H), 64.1 (*C*H_2), 55.7 (*C*H_3). Data are consistent with the literature.[135,136] A melting point had not been reported for this compound in the literature.

5.3.9. (5-METHOXYPYRIDIN-2-YL)METHANOL-MEDIATED C-H ARYLATION WITH *p*-CHLOROTOLUENE UNDER LITERATURE CONDITIONS

The following two reactions were conducted by Dr. Graeme Coulthard at the University of Strathclyde, and are included for completeness.

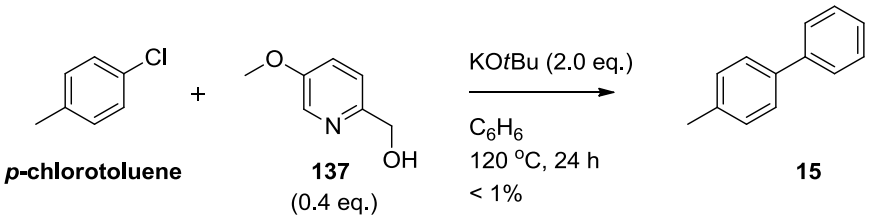

***p*-chlorotoluene** **137** (0.4 eq.) **15**

According to a modified literature procedure.[14] To an oven-dried pressure tube was added 4-chlorotoluene (116.0 mg, 1.0 mmol) and (5-methoxypyridin-2-yl)methanol **137** (55.7 mg, 0.4 mmol, 0.4 eq.). KO*t*Bu (224.4 mg, 2.0 mmol, 2.0 eq.) and benzene (8 mL) were added. The tube was sealed in a glovebox and stirred at 120 °C for 24 h. After cooling to rt, the reaction was quenched with water (10 mL) and extracted with Et_2O (3 x 20 mL). The combined organic layers were dried (Na_2SO_4), filtered and concentrated *in vacuo*. 1,3,5-Trimethoxybenzene (16.8 mg, 0.10 mmol, 10 mol%) was added to the crude reaction mixture, the residue dissolved in $CDCl_3$ and yield of **15** determined as 0.3% by ^{1}H NMR.

This reaction was conducted side-by-side with a blank reaction (carried out as above, but without (5-methoxypyridin-2-yl)methanol **137**) which gave no detectable coupled product.

5.3.10. CYCLIC VOLTAMMETRY INVESTIGATION OF PYRIDINOL-DERIVED DIANIONS

See Appendix for voltammograms. Cyclic voltammograms of **57b**, **111** and **140** were recorded by Dr. Graeme Coulthard at the University of Strathclyde.

The CV for 2-pyridinecarboxaldehyde (**111**), ethyl 2-picolinate (**139**) and methyl 5-methoxypyridine-2-carboxylate (**140**), 0.01 M in a solution of 0.1 M

nBu_4NPF_6 in DMF, at a scan rate of 50 mV s^{-1}, each show single-electron reduction peaks at -1.55, -2.04 and -2.14 V, respectively (Figure 36). The cathodic-anodic peak separation for each of these reductions, $\Delta E^{p\text{-}p}$ obtained was 100 mV (close to the value obtained for ferrocene at the same scan rate (90 mV *cf.* 59 mV/n for an ideal one-electron transfer), indicating a high degree of reversibility (and so rapid kinetics) for the electron transfer processes.

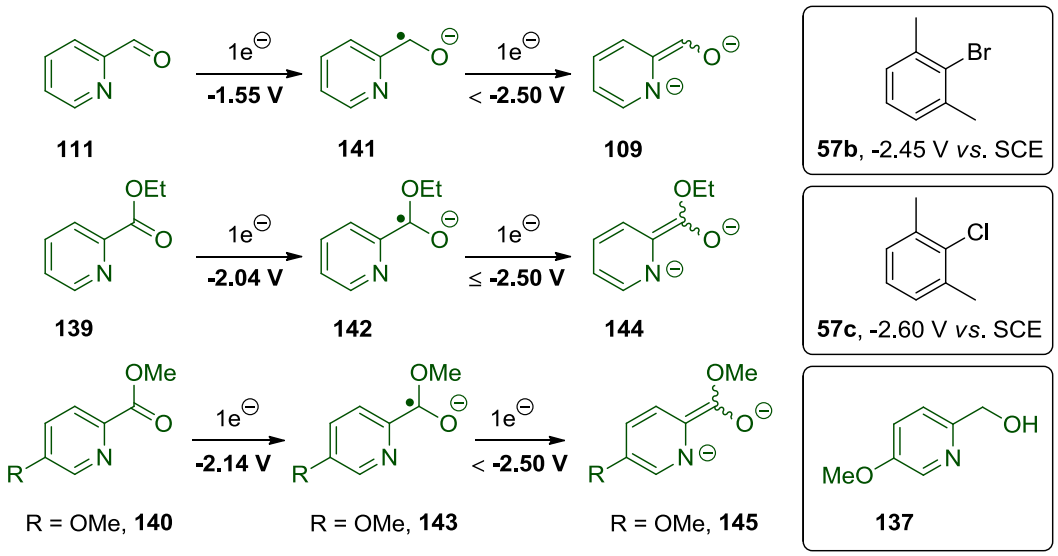

***Figure 36**: Sequential electron transfers to additives to characterise redox potentials of dianions.*

In the case of 2-pyridinecarboxaldehyde (**111**), the beginning of a second reduction is visible at a potential < -2.50 V *vs.* SCE. For ethyl 2-picolinate (**139**) the second event is more visible and a reduction peak can be observed at a potential ≤ -2.50 V *vs.* SCE. For methyl 5-methoxypyridine-2-carboxylate (**140**) the event is no longer visible and likely occurs at a potential more negative than < -2.50 V *vs.* SCE. This suggests feasible thermodynamics for the reduction of bromo- and chloroarenes (E^{p}_{red} (**57b**) = -2.45 V, E^{p}_{red} (PhBr)[36] = -2.44 V, E^{p}_{red} (**57c**) = -2.60 V, E^{p}_{red} (PhCl)[36] = -2.78 V, all *vs.* SCE in DMF) by these pyridinecarbinol-derived dianions. Dianion **145**, derived from reduction of methyl 5-methoxypyridine-2-carboxylate (**140**), appears to

be more reducing than dianion **109**, derived from reduction of 2-pyridinecarboxaldehyde (**111**). However, in reactions of chloroarenes, 2-pyridinecarbinol (**111**) appears to be a more effective (although ineffective overall) additive than (5-methoxypyridin-2-yl)methanol (**137**). This is rationalised by the additional alkoxy-substituent deactivating benzylic deprotonation in **137** by electron donation into the aromatic ring.

5.4. Experiments to Probe the Role of potassium hydride in Transition Metal-free Reductive Dehalogenations

5.4.1. General Procedure 2: Dehalogenation Procedure for 2,6-Dimethylhalobenzenes

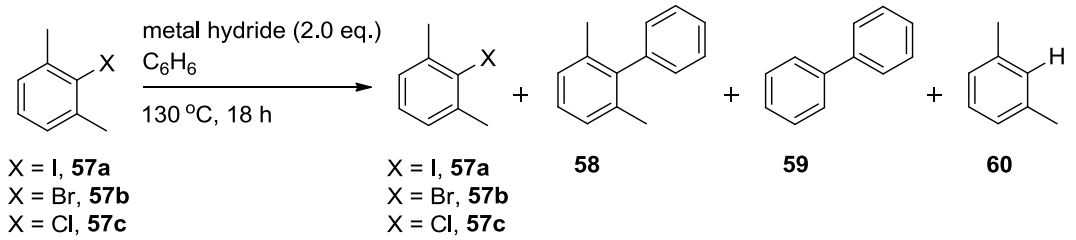

General Procedure 2: To an oven-dried pressure tube was added 2,6-dimethylhalobenzene **57** (0.5 mmol), KH (40 mg, 1.0 mmol) and benzene (5 mL). The tube was sealed in a glovebox and stirred at 130 ^{o}C for 18 h. After cooling to rt, the reaction was quenched carefully with water (50 mL) and extracted with Et_2O (3 x 50 mL). The combined organic layers were dried (Na_2SO_4), filtered and concentrated *in vacuo* to afford the crude product. 1,3,5-Trimethoxybenzene (8.4 mg, 0.05 mmol) was added to the crude reaction mixture, the residue dissolved in $CDCl_3$ and combined yield of biaryls **58** and **59** (and returned **57**) determined by ^{1}H NMR (see Appendix for example calculations).

5.4.2. DEHALOGENATION OF 4-IODOBIPHENYL UNDER LITERATURE CONDITIONS

Biphenyl (**59**)

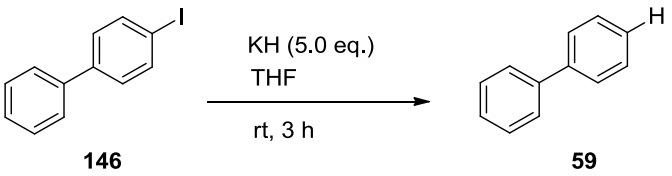

146 **59**

Prepared according to a literature procedure.[88] An oven-dried pressure tube was charged with KH (100.0 mg, 2.50 mmol) and THF (0.5 mL), before 4-iodobiphenyl (**146**) (140.0 mg, 0.50 mmol) was washed into the mixture with THF (0.5 mL). A purple colour was observed in the slurry after a few seconds. The tube was sealed in a glovebox and stirred for rt for 3 h (a red brown colour was observed), then quenched carefully with water (50 mL) and extracted with Et_2O (3 x 50 mL). The combined organic layers were dried (Na_2SO_4), filtered and concentrated *in vacuo* to yield a brown oil. Purification by column chromatography (hexane) gave **59** as a white microcrystalline solid (67.0 mg, 87%), m.p. 66 - 68 ^oC (lit. 67 - 69 ^oC);[137] IR ν_{max} (neat) 3034 (C-H), 1481 (Ar), 1429 cm^{-1}; ^1H NMR (400 MHz, $CDCl_3$) δ 7.64 - 7.59 (4H, m, C*H*), 7.46 (4H, apt t., *J* = 7.5 Hz, C*H*), 7.37 (2H, t, *J* = 7.4 Hz, C*H*); ^{13}C NMR (101 MHz, $CDCl_3$) δ 141.2 (*C*), 128.7 (*C*H), 127.2 (2 x *C*H). Data are consistent with the literature.[127,137] This result is shown in Table 5, entry 1, Section 2.3.2. The following reactions were conducted by Samuel Dalton at the University of Strathclyde.

Alternatively, the reaction was conducted with KH (2.0 eq.) and a 71% yield of **59** resulted by internal standard (Table 5, entry 2). The yields of **59** and **146** were determined by ^1H NMR, see Appendix for example calculations.

Alternatively, the reaction was conducted with KH (2.0 eq.) and the reaction quenched with D_2O. A 68% yield of **59** resulted by internal standard (Table 5, entry 3). No D-incorporation was observed by ^2H NMR and GCMS of the

reaction mixture.

Alternatively, the reaction was conducted with KH (2.0 eq.) in THF-d_8 and the reaction quenched with D_2O (Table 5, entry 4). This reaction was conducted on a 0.1 mmol scale of haloarene (**146**). No D-incorporation was observed by ^2H NMR and GCMS of the reaction mixture, see Appendix for examples of D-incorporation determination.

Alternatively, the reaction was conducted with KH (2.0 eq.) in THF-d_8 and the reaction quenched with H_2O (Table 5, entry 5). This reaction was conducted on a 0.1 mmol scale of haloarene (**146**). No D-incorporation was observed by ^2H NMR and GCMS of the reaction mixture.

Alternatively, the reaction was conducted with NaH (2.0 eq.) in place of KH (Table 5, entry 6). No reaction occurred.

Alternatively, the reaction was conducted with KH (2.0 eq.) in C_6H_6 (Table 5, entry 7). No reaction occurred.

5.4.3. General Procedure 3: Dehalogenation of 4-iodobiphenyl in benzene

The following reactions were conducted by Samuel Dalton at the University of Strathclyde.

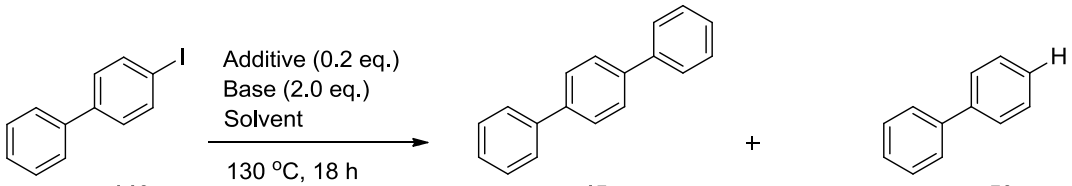

146 **45** **59**

General Procedure 3: To an oven-dried pressure tube was added 4-iodobiphenyl (0.50 mmol), KH (1.00 mmol, 2.0 eq.) and benzene (5 mL). The tube was sealed in a glovebox and stirred at 130 °C for 18 h. After cooling to rt, the reaction was quenched carefully with water (5 mL) under an Ar stream.

The mixture was diluted with water (45 mL) and extracted with Et_2O (3 x 25 mL). The combined organic layers were dried through a hydrophobic frit and concentrated *in vacuo*. 1,3,5-trimethoxybenzene (8.4 mg, 0.05 mmol) was added to the crude reaction mixture, the residue dissolved in $CDCl_3$ and yields of **45**, **59** and returned **146** determined by ^{1}H NMR (see Appendix for example calculations). A average of 3 replicates for this reaction gave the yields shown in Table 6, entry 1, Section 2.3.2.

Alternatively, **General Procedure 3** was conducted with KO*t*Bu (2.0 eq.) and 1,10-phenanthroline (0.2 eq.) in place of KH (Table 6, entry 1).

Alternatively, **General Procedure 3** was conducted in C_6D_6 with KO*t*Bu (2.0 eq.) and 1,10-phenanthroline (0.2 eq.) in place of KH, (Table 6, entry 2). This reaction was conducted on a 0.1 mmol scale of haloarene (**146**).

Alternatively, **General Procedure 3** was conducted with KO*t*Bu (2.0 eq.) in place of KH (Table 6, entry 3).

Alternatively, **General Procedure 3** was conducted and quenched with D_2O (Table 6, entry 5). No D-incorporation was observed by ^{2}H NMR and GCMS of the reaction mixture.

Alternatively, **General Procedure 3** was conducted in C_6D_6 and quenched with D_2O (Table 6, entry 6). This reaction was conducted on a 0.1 mmol scale of haloarene (**146**). D-incorporation was observed by ^{2}H NMR and GCMS of the reaction mixture.

Alternatively, **General Procedure 3** was conducted in C_6D_6 and quenched with H_2O (Table 6, entry 7). This reaction was conducted on a 0.1 mmol scale of haloarene (**146**). D-incorporation was observed by ^{2}H NMR and GCMS of the reaction mixture.

Alternatively, **General Procedure 3** was conducted using NaH (2.0 eq.) in place of KH. No reaction occurred (Table 6, entry 7).

5.4.4. GENERAL PROCEDURE 4: DEHALOGENATION PROCEDURE FOR 1,3,5-TRIISOPROPYLBROMOBENZENE

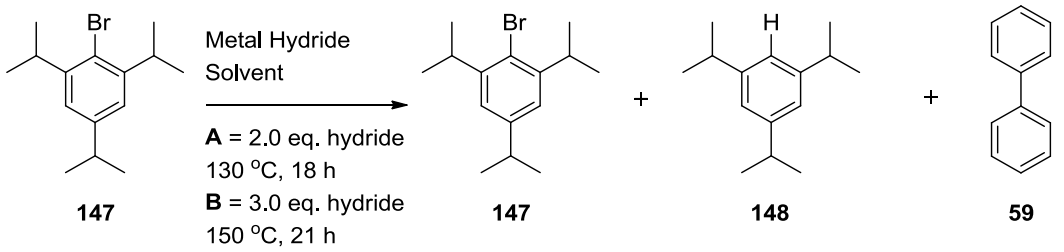

General Procedure 4 (conditions **A**): To an oven-dried pressure tube was added 1,3,5-triisopropylbromobenzene (0.50 mmol), KH (1.00 mmol, 2.0 eq.) and benzene (5 mL). The tube was sealed in a glovebox and stirred at 130 °C for 18 h (conditions **A**). After cooling to rt, the reaction was quenched carefully with water (50 mL) and extracted with Et_2O (3 x 50 mL). The combined organic layers were dried (Na_2SO_4), filtered and concentrated *in vacuo*. 1,3,5-Trimethoxybenzene (8.4 mg, 0.05 mmol) was added to the crude reaction mixture, the residue dissolved in $CDCl_3$ and yields of **148**, **59** and returned **147** determined by ^1H NMR (see Appendix for details). A average of 3 replicates for this reaction gave the yields shown in Table 7, entry 1, Section 2.3.3. One replicate was conducted by Samuel Dalton.

Alternatively, **General Procedure 4** (conditions **A**) was employed, using C_6D_6 as solvent (Table 7, 2). This reaction was conducted by Samuel Dalton on a 0.1 mmol scale of haloarene (**147**). D-incorporation was observed by GCMS of the reaction mixture but not by ^2H NMR (this reaction was also conducted by Joshua Barham at 150 °C for 21 h on a 0.5 mmol scale of **147**, clearly showing **148**-d_1 and **59**-d_{10}, see Appendix for spectra).

Alternatively, **General Procedure 4** (conditions **B**) was employed, using KH (1.50 mmol, 3.0 eq.) and the reaction was stirred at 150 °C for 21 h (Table 7, entry 3).

Alternatively, **General Procedure 4** (conditions **A**) was employed, using NaH

as the metal hydride (Table 7, entry 4). No reaction occurred.

Alternatively (Table 7, entry 5), according to a modified **General Procedure 4** (conditions **A**), an oven-dried pressure tube was charged with lithium aluminium hydride (1.10 mmol, 1.0 M in THF, 2.2 eq.) and the contents stirred at 100 ^{o}C under vacuum with vigorous stirring in a glovebox. After 1 h, the reaction was allowed to cool to rt before KO*t*Bu (112.0 mg, 1.0 mmol, 2.0 eq.), 1,3,5-triisopropylbromobenzene (141.6 mg, 0.50 mmol) and benzene (5 mL) were added. The tube was sealed in a glovebox and stirred at 130 ^{o}C for 18 h. Work up and purification by column chromatography (hexane) gave **148** as a colourless oil (91.0 mg, 89%);

1,3,5-Triisopropylbenzene (**148**)

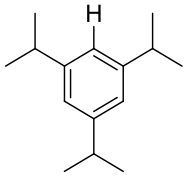

IR ν_{max} (neat) 2957 - 2868 (Ar), 1599 (Ar), 1466, 1381, 1362, 1314, 1248, 1188, 1096, 1070 cm^{-1}; ^{1}H NMR (400 MHz, $CDCl_3$) δ 6.98 (3H, s, C*H*), 2.94 (3H, sept, *J* = 7.0 Hz, C*H*), 1.33 (18H, d, *J* = 7.0 Hz, CH_3); ^{13}C NMR (101 MHz, $CDCl_3$) δ 148.7 (*C*), 122.1 (*C*H), 34.3 (*C*H), 24.1 (*C*H_3); HRMS (+ESI) *m/z* calculated for $C_{15}H_{24}$ [M^+] 204.1878 Found 204.1874. Data are consistent with the literature.[138]

Alternatively (Table 7, entry 7), the modified **General Procedure 4** (conditions **A**) employed lithium aluminium hydride (1.1 mmol, 1.0 M in THF, 2.2 eq.) only. Work up and addition of 1,3,5-trimethoxybenzene revealed a 81% yield of **148**. Alternatively (Table 7, entry 6), the modified **General Procedure 4** (conditions **A**) employed lithium aluminium deuteride (1.1 mmol, 1.0 M in THF, 2.2 eq.) and KO*t*Bu (112.0 mg, 1.00 mmol, 2.0 eq.). Work up and purification by column chromatography (hexane) gave **148**-d_1 as a colourless oil (94.0 mg, 92%);

1,3,5-Triisopropylbenzene (**148**-d_1)

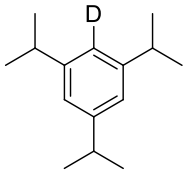

^{1}H NMR (400 MHz, $CDCl_3$) δ 6.96 (2.4H, s, C*H*),[†] 2.92 (3H, sept, *J* = 7.0 Hz, C*H*), 1.31 (18H, d, *J* = 7.0 Hz, CH_3); ^{2}H NMR (61 MHz, $CHCl_3$) δ 6.97 (s, Ar*D*), ^{13}C NMR[‡] (101 MHz, $CDCl_3$) δ 148.7 (*C*), 148.6 (*C*), 122.1 (*C*H), 34.3 (*C*H), 24.1 (*C*H_3); HRMS (+ESI) *m/z* calculated for $C_{15}{}^1H_{23}{}^2H_1$ [M^+] 205.1941 Found 205.1939.

5.4.5. General Procedure 5: Dehalogenation Procedure for 1,3,5-tri-*tert*-butylbromobenzene

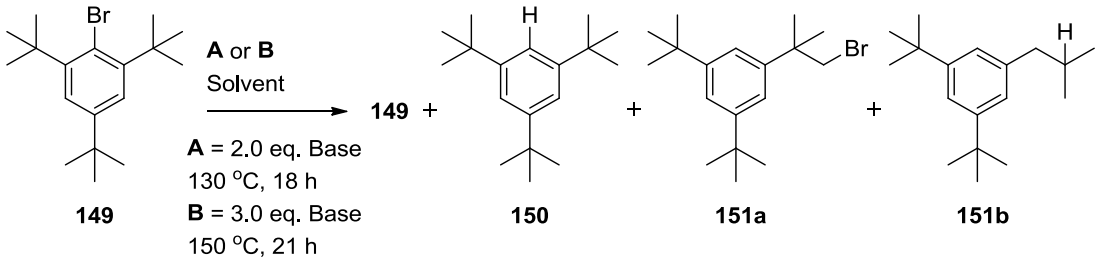

General Procedure 5 (conditions **A**): To an oven-dried pressure tube was added 1,3,5-tri-*tert*-butylbromobenzene (**149**) (0.50 mmol), KH (1.00 mmol, 2.0 eq.) and benzene (5 mL). The tube was sealed in a glovebox and stirred at 130 °C for 18 h (conditions **A**). After cooling to rt, the reaction was quenched carefully with water (50 mL) and extracted with Et_2O (3 x 50 mL). The combined organic layers were dried (Na_2SO_4), filtered and concentrated *in vacuo*. 1,3,5-Trimethoxybenzene (8.4 mg, 0.05 mmol) was added to the crude mixture, the residue dissolved in $CDCl_3$ and yields of **150**, **151a**, **151b** and returned **149** determined by ^{1}H NMR (see Appendix for details)

[†]Integration of the aromatic peak was lower than 3H, indicating deuteration. [‡]Coupling of the deuterium-bearing carbon was not observed. Two signals at δ ~149 ppm indicated two species (**148** and **148**-d_1).

A average of 7 replicates for this reaction gave the yields shown in Table 8, entry 3, Section 2.3.4. Five of these replicates and the following reactions were conducted by Samuel Dalton at the University of Strathclyde.

Alternatively, **General Procedure 5** (conditions **A**) was employed in the absence of metal hydride (Table 8, entry 1). No reaction occurred.

Alternatively, **General Procedure 5** (conditions **A**) was employed, using KO*t*Bu (2.0 eq.) in place of KH (Table 8, entry 2). No reaction occurred.

Alternatively, **General Procedure 5** (conditions **A**) was employed, using C_6D_6 as solvent and quenching with H_2O (Table 8, entry 4). This reaction was conducted on a 0.1 mmol scale of haloarene (**149**). D-incorporation was observed by ^2H NMR and GCMS of the reaction mixture, see Appendix for examples of D-incorporation determination.

Alternatively, **General Procedure 5** (conditions **A**) was employed, using C_6D_6 as solvent and quenching with D_2O (Table 8, entry 5). This reaction was conducted on a 0.1 mmol scale of haloarene (**149**). D-incorporation was observed by ^2H NMR and GCMS of the reaction mixture.

Alternatively, **General Procedure 5** (conditions **A**) was employed, using C_6H_6 as solvent and quenching with D_2O (Table 8, entry 6). No D-incorporation was observed by ^2H NMR and GCMS of the reaction mixture.

Alternatively, **General Procedure 5** (conditions **B**) was employed (Table 8, entry 7).

Alternatively, **General Procedure 5** (conditions **A**) was employed using NaH in place of KH (Table 8, entry 8). No reaction occurred.

Alternatively, **General Procedure 5** (conditions **A**) was employed using NaH (2.0 eq.) and KO*t*Bu (2.0 eq.) in place of KH (Table 8, entry 9). Product **150** was observed by ^1H NMR of the reaction mixture, in 75.3% yield by

comparison to 1,3,5-trimethoxybenzene (8.4 mg, 0.05 mmol, 10 mol%) as an internal standard. Product **151b** was observed in 10.0% yield.

1-(1-bromo-2-methylpropan-2-yl)-3,5-di-*tert*-butylbenzene (**151a**)

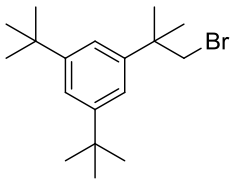

Three crude reaction mixtures from replicates of **General Procedure 5** were combined and purified by reverse phase chromatography (a gradient of 70 - 100% MeCN/H_2O)[†] to yield **151a** as an colourless gum (15.0 mg, 3%); IR ν_{max} (neat) 2961 - 2852 (Ar), 1597 (Ar), 1464 (Ar), 1363, 1248 cm^{-1}; ^1H NMR (400 MHz, $CDCl_3$) δ 7.32 (1H, t, *J* = 1.7 Hz, C*H*), 7.23 (2H, d, *J* = 1.7 Hz, C*H*), 3.59 (2H, s, CH_2), 1.49 (6H, s, CH_3), 1.34 (18H, s, CH_3); ^{13}C NMR (101 MHz, $CDCl_3$) δ 150.4 (*C*), 144.9 (*C*), 120.5 (*C*H), 120.0 (*C*H), 47.4 (*C*H_2), 39.4 (*C*), 35.0 (*C*), 31.5 (*C*H_3), 27.2 (*C*H_3); GCMS R_T = 11.30 min,[‡] (+EI) calculated for $C_{18}H_{29}{}^{79}Br$ [M^+] = 324.1; Found [M^+] = 323.9. The following fragment ions in the GCMS were detected, (+EI) calculated for $C_{17}H_{26}{}^{79}Br$ [M^+-CH_3] = 309.1; Found = 309.1; (+EI) calculated for $C_{17}H_{27}$ [M^+-CH_2Br] = 231.2; Found = 231.3; Data are consistent with the literature.[‡,101]

1,3-di-*tert*-butyl-5-isobutylbenzene (**151b**)

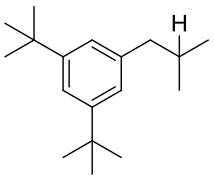

The purification on the previous page also gave **151b** as a colourless residue (3.3 mg, 1%); IR ν_{max} (neat) 2955 - 2868 (Ar), 1599 (Ar), 1465 (Ar), 1363, 1248 cm^{-1}; ^1H NMR (400 MHz, $CDCl_3$) δ 7.24 (1H, t, *J* = 1.7 Hz, C*H*), 6.98

[†]Purification was done by Rita Tailor at GSK. [‡]GCMS analysis performed at GlaxoSmithKline on the Polaris-Q.

(2H, d, *J* = 1.7 Hz, C*H*), 2.46 (2H, d, *J* = 7.0 Hz, CH_2), 1.91 - 1.80 (1H, m, C*H*), 1.33 (18H, s, CH_3), 0.92 (6H, d, *J* = 6.5 Hz, CH_3); ^{13}C NMR (101 MHz, $CDCl_3$) δ 150.2 (*C*), 140.6 (*C*), 123.3 (*C*H), 119.4 (C*H*), 46.0 (*C*H_2), 34.7 (*C*), 31.5 (*C*H_3), 30.3 (*C*H), 22.5 (*C*H_3); GCMS R_T = 9.32 min,† (+EI) calculated for $C_{18}H_{30}$ [M^+] = 246.2; Found [M^+] = 246.1. The following fragment ions in the GCMS were detected, (+EI) calculated for $C_{17}H_{27}$ [M^+-CH_3] = 231.2; Found = 231.3; (+EI) calculated for $C_{15}H_{23}$ [M^+-CH_2Br] = 203.2; Found = 203.4. Data are consistent with the literature.[139]

5,5'-(2,5-Dimethylhexane-2,5-diyl)bis(1,3-di-*tert*-butylbenzene) [**152**]

Dimer **152** was synthesised by Samuel Dalton at the University of Strathclyde.

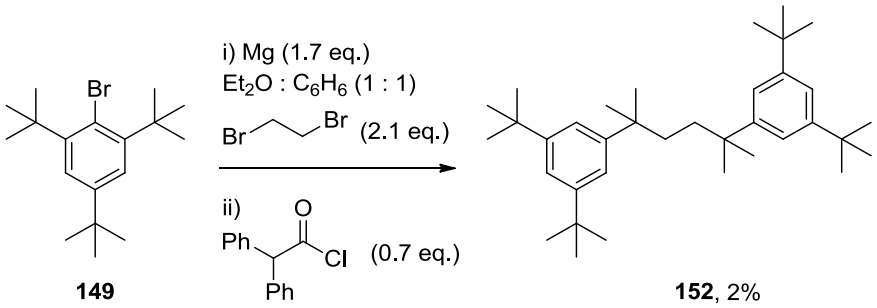

Prepared according to a literature procedure.[102] Anhydrous Et_2O (2.2 mL) was added to magnesium turnings (66.0 mg, 2.6 mmol) and the slurry stirred under Ar. 1,2-Dibromoethane (265.0 µL, 3.1 mmol) and 1-bromo-2,4,6-tri-*tert*-butylbenzene (500.0 mg, 1.5 mmol) in ether (6.5 mL) was then added dropwise over 30 min. Anhydrous toluene (9 mL) was then added, and the reaction heated at 40 °C until the magnesium turnings had dissolved. A solution of diphenylacetylchloride (248.0 mg, 1.1 mmol) in dry ether (2.2 mL) was then added dropwise over 30 min. After the addition, the reaction was poured into 0.1 M HCl (5 mL) and washed with 0.1 M aqueous K_2CO_3 (3 x 5 mL), and brine (2 x 5 mL). The organics were dried through a hydrophobic frit, and concentrated *in vacuo*. The product was then purified by flash

† GCMS analysis performed at GlaxoSmithKline on the Polaris-Q.

chromatography on silica gel (hexane) to afford dimer **152** as an off-white gum (11.0 mg, 1.5%); ^{1}H NMR (400 MHz, $CDCl_3$) δ 7.22 (2H, t, *J* = 1.5 Hz, C*H*), 7.14 (4H, d, *J* = 1.8 Hz, C*H*), 1.44 (4H, s, CH_2), 1.32 (36H, s, CH_3), 1.25 (12H, s, CH_3); ^{13}C NMR (101 MHz, $CDCl_3$) δ 149.7 (*C*), 148.7 (*C*), 120.0 (*C*H), 119.1 (*C*H), 39.0 (*C*), 37.6 (*C*H_2), 35.0 (*C*), 31.6 (*C*H_3), 29.0 (*C*H_3); GCMS R_T = 17.12 min (+EI) calculated for $C_{36}H_{58}$ [M^+] = 490.5; Found [M^+] = 490.6. Data are consistent with the literature.[102] The following fragment ion in the GCMS was detected, (+EI) calculated for $C_{17}H_{27}$ [M^+-$C_{19}H_{31}$] = 231.2; Found = 231.2.

5.4.6. Preparation of a Perdeuterated Bromoarene Substrate and Corresponding Perdeuterated Arene Product Authentic Marker

1,3,5-Tri-*tert*-butylbenzene-d_{30} (*150*-d_{30})

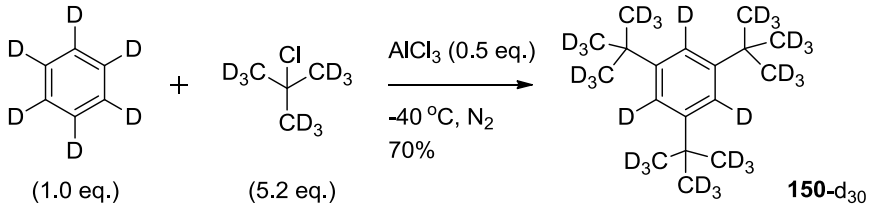

Prepared according to a modified literature procedure.[140] A reaction vessel was charged with benzene-d_6 (0.41 mL, 4.65 mmol) and *tert*-butylchloride-d_9 (3.08 mL, 5.2 eq.) and the system purged with N_2. The mixture was cooled below -40 °C and anhydrous $AlCl_3$ (0.335 g, 0.5 eq.) was added over 15 min to the mixture which was maintained at -40 °C for 35 min. The temperature was then slowly raised to -13 °C in 30 min (to address the evolution of DCl gas, the reaction vessel was attached to a NaOH scrubber). After 4 h, the reaction was terminated by addition of TBME (10 mL) and water (10 mL) and stirred overnight. The reaction mixture was poured into a separatory funnel with TBME (20 mL) and water (20 mL) and the layers were separated. The aqueous layer was extracted with TBME (2 x 20 mL). The combined organics were dried ($MgSO_4$), filtered and concentrated to dryness to give the crude

product, which was purified by reverse phase chromatography (a gradient of 70 - 100% MeCN/H_2O)[†] to yield ***150***-d_{30} as a colourless microcrystalline solid (874.6 mg, 70%); m.p. 54 - 57 ^oC; IR ν_{max} (neat) 2212 - 2046 (C-D), 1568 (Ar), 1377 cm^{-1}; ^1H NMR (400 MHz, $CDCl_3$) δ 7.27 (s, C*H*), 1.32 (s, CH_3); ^2H NMR (61 MHz, $CHCl_3$) δ 7.29 (3D, s, C*D*), 1.31 (27D, s, CD_3); ^{13}C NMR (101 MHz, $CDCl_3$)[‡] δ 149.8 (*C*), 119.2 (t, *J* = 23.0 Hz, *C*D), 34.3 (*C*), 30.5 (quintet, *J* = 19.2 Hz, *C*D_3); HRMS (+ESI) *m/z* calculated for $C_{18}{}^2H_{30}$ [M^+] 276.4231; Found 276.4227.

To quantify isotopic purity, a sample of ***150***-d_{30} (35.3 mg, 0.127 mmol) was mixed in a 1 : 1 molar ratio with 1,3,5-trimethoxybenzene (21.5 mg, 0.127 mmol) and the sample was analysed by ^1H NMR. The aliphatic region showed 99% D-incorporation. The aromatic region showed 97% D-incorporation (an overlapping $CDCl_3$ residual led to overestimation of the integration).

2-Bromo-1,3,5-tri-*tert*-butylbenzene-d_{29} (*149*-d_{29})

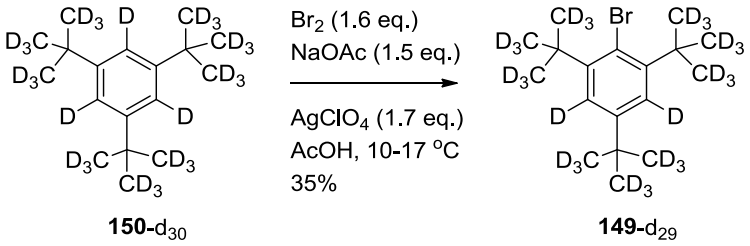

Prepared according to a modified literature procedure.[141] A solution of bromine (209.0 uL, 1.6 eq.) and anhydrous sodium acetate (311.0 mg, 1.5 eq.) in AcOH (4.10 mL) was added dropwise (over 60 min) to a vigorously stirred solution of 1,3,5-tri-*tert*-butylbenzene-d_{30} (**150**-d_{30}) (700.0 mg, 2.53 mmol) and silver perchlorate (866.0 mg, 1.7 eq.) in AcOH (20.2 mL) and 1,4-dioxane (4.10 mL). The temperature was maintained between 10 - 17 ^oC during the addition, then allowed to rise to rt and the reaction mixture stirred

[†]Purification was done by Rita Tailor at GSK. [‡]Signals were overlapping with partially H-incorporated **149**.

for 16 h. Residual bromine was reduced by addition of solid sodium sulfite (until the brown colour dissipated) and heptane (15 mL) was added to dissolve precipitated organic products. The reaction mixture was filtered through celite and filter residue washed heavily with heptane. The filtrate was washed with water (50 mL), layers separated and organic layer washed sequentially with water (2 x 15 mL), 5% NaOH (2 x 10 mL) and water (3 x 10 mL). The combined organic layers were dried ($MgSO_4$), filtered and concentrated to dryness to afford the crude product, which was purified by reverse phase chromatography (a gradient of 70 - 100% $MeCN/H_2O$)[†] to yield ***149***-d_{29} as a colourless microcrystalline solid (310.0 mg, 35%); m.p. 157 - 162 ^oC; IR ν_{max} (neat) 2212 - 2048 (C-D), 1344 cm^{-1}; ^1H NMR (400 MHz, $CDCl_3$) δ 7.27 (s, C*H*), 1.32 (s, CH_3); ^2H NMR (61 MHz, $CHCl_3$) δ 7.43 (2D, s, C*D*), 1.55 (18D, s, CD_3), 1.28 (9D, s, CD_3); ^{13}C NMR (101 MHz, $CDCl_3$)[‡] δ 148.5 (*C*), 148.3 (*C*), 123.4 (t, *J* = 24.0 Hz, *C*D), 121.6 (*C*), 37.6 (*C*), 34.2 (*C*), 30.0 (quintet, *J* = 19.3 Hz, *C*D_3), 29.9 (quintet, *J* = 21.4 Hz, *C*D_3); HRMS (+ESI) *m/z* calculated for $C_{18}{}^2H_{29}{}^{79}Br$ [M^+] 353.3273; Found 353.3268. To quantify isotopic purity, a sample of ***149***-d_{29} (4.5 mg, 12.7 umol) was mixed in a 1 : 1 molar ratio with 1,3,5-trimethoxybenzene (2.1 mg, 12.7 umol) and the sample analysed by ^1H NMR. The aliphatic region showed 95% D-incorporation. The aromatic region showed 98% D-incorporation.

5.4.7. Potassium hydride-mediated Dehalogenation of a Perdeuterated Bromoarene

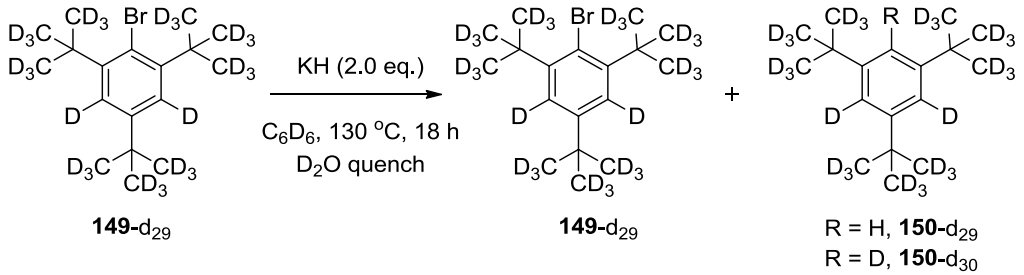

[†]Purification was done by Rita Tailor at GSK. [‡]Signals were overlapping with partially H-incorporated **149**.

An oven-dried pressure tube was charged with 2-bromo-1,3,5-tri-*tert*-butylbenzene-d_{29} (**149**-d_{29}) (35.0 mg, 0.10 mmol) and KH (8.0 mg, 0.20 mmol) in a glovebox. C_6D_6 (1 mL) was added and the tube sealed, removed from the glovebox and heated at 130 °C for 18 h. The reaction was then quenched carefully with D_2O (1 mL) under an Ar flow and in an ice bath. The reaction was stirred for 10 min and then diluted with H_2O (2 mL) and extracted to Et_2O (3 x 5 mL). The organics were dried through a hydrophobic frit and concentrated in vacuo. 1,3,5-Trimethoxybenzene (1.7 mg, 0.01 mmol) was added to the crude reaction mixture, the residue was then dissolved in $CDCl_3$ and analysed by ^1H NMR. The reaction mixture was also analysed by ^2H NMR in $CHCl_3$ (see Appendix for spectra and calculations of yields and change in the aromatic H-incorporation).

5.4.8. Preparation of Bunnett-Creary Probes to Probe for Radical Anion Intermediates

3-Bromo-1,2,4,5-tetramethylbenzene (162)

The following three compounds were synthesised by Samuel Dalton at the University of Strathclyde, and are included for completeness.

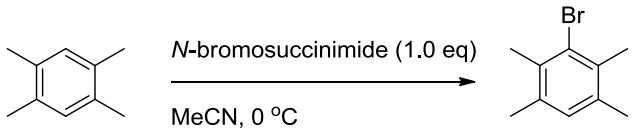

durene **162**

Prepared according to a literature procedure.[142] To a stirred solution of durene (0.67 g, 5.00 mmol) in MeCN (5 mL) at 0 °C was added a solution of *N*-bromosuccinimide (0.89 g, 5.00 mmol, 1.0 eq.) in MeCN (5 mL). The solution was allowed to warm to rt. After 22 h, the reaction was quenched with water (10 mL), and extracted with hexane (3 x 15 mL). The combined organics were dried through a hydrophobic frit and concentrated *in vacuo*. The residue was purified by column chromatography (hexane) to afford **162**

as a white microcrystalline solid (881.0 mg, 4.30 mmol, 86%); ^{1}H NMR (400 MHz, $CDCl_3$) δ 6.90 (1H, s, C*H*), 2.37 (6H, s, CH_3), 2.28 (6H, s, CH_3); ^{13}C NMR (101 MHz, $CDCl_3$) δ 134.7 (*C*), 133.9 (*C*), 130.3 (*C*H), 129.0 (*C*), 20.9 (*C*H_3), 20.2 (*C*H_3); HRMS (+EI) *m/z* calculated for $C_{10}H_{13}{}^{79}Br$ [M^+] 212.0201; Found 212.0205. ^{1}H and ^{13}C NMR data are consistent with the literature.[142] A melting point was not obtained.

1-Bromo-4-iodo-2,3,5,6-tetramethylbenzene (*157a*)

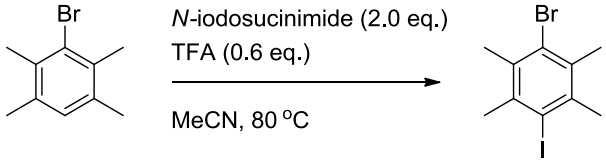

162 **157a**

N-iodosuccinimide (565.0 mg, 2.50 mmol) and 3-bromo-1,2,4,5-tetramethylbenzene (**162**) (530.0 mg, 2.50 mmol, 1.0 eq.) were stirred in MeCN (10 mL) at rt. Trifluoroacetic acid (57.0 µL, 0.75 mmol, 0.3 eq.) was added and the reaction stirred at 80 °C. After 16 h, further equivalents of *N*-iodosuccinimide (565.0 mg, 2.5 mmol) and TFA (57 µL, 0.75 mmol, 0.3 eq.) were added. After stirring at 80 °C for a further 2 h, the reaction was quenched by the addition of aqueous sodium thiosulfate (10 mL, 10% w/v), and extracted with DCM (3 x 15 mL). The combined organics were dried through a hydrophobic frit and concentrated *in vacuo*. The product was recrystallised twice from boiling IPA and filtered to afford ***157a*** as white needles (403.0 mg, 1.20 mmol, 48%);[†] m.p. 154 - 156 °C; IR ν_{max} (neat) 3002 - 2857, 1435, 1405, 1381, 1169, 979, 833 cm^{-1}; ^{1}H NMR (400 MHz, $CDCl_3$) δ 2.60 (6H, s, CH_3), 2.54 (6H, s, CH_3); ^{13}C NMR (101 MHz, $CDCl_3$) δ 138.5 (*C*), 134.3 (*C*), 129.7 (*C*), 110.4 (*C*), 28.9 (*C*H_3), 23.1 (*C*H_3); HRMS (+ASAP) *m/z* calculated for $C_{10}H_{12}{}^{79}BrI$ [M^+] 337.9167; Found 337.9161.

[†]An inseparable 1% impurity of dibromodurene (**157b**) was observed by ^{1}H NMR

1,4-Dibromo-2,3,5,6-tetramethylbenzene (157b)

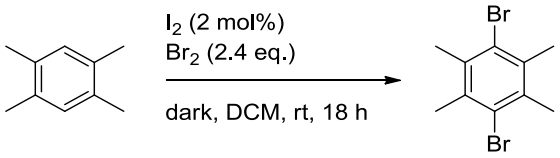

durene **157b**

Prepared according to the literature procedure.[143] To a three-necked flask fitted with a stirring bar, dropping funnel, and reflux condenser was added durene (5.00 g, 37.0 mmol), iodine (0.20 g, 0.80 mmol) and DCM (15 mL). The flask and dropping funnel were surrounded in foil, and the reaction conducted in the dark. To the dropping funnel was added DCM (8 mL) and bromine (5.00 mL, 90.0 mmol). The DCM/bromine solution was added dropwise in the dark and the reaction left stirred for 18 h at rt. The reaction was then quenched by careful addition of aq. sodium thiosulfate (50 mL, 10% w/v) and NaOH (2.0 M, 50 mL). The mixture was transferred to a separating funnel, diluted with a further 50 mL aq. sodium thiosulfate solution (50 mL, 10% w/v) and extracted with DCM (3 x 50 mL). The combined organics were dried through a hydrophobic frit and concentrated *in vacuo* to afford off-white needles, which were triturated with ice-cold DCM and filtered to afford **157b** as a white microcrystalline solid (8.3 g, 28.4 mmol, 77%); m.p. 186 - 190 ^{o}C (lit. 196 - 198 ^{o}C[144]); ^{1}H NMR (400 MHz, $CDCl_3$) δ 2.50 (12H s, CH_3); ^{13}C NMR (101 MHz, $CDCl_3$) δ 135.0 (*C*), 128.1 (*C*), 22.3 (*C*H_3); HRMS (+EI) *m/z* calculated for $C_{10}H_{12}Br_2$ [M^+] 291.9286, found 291.9239. ^{1}H and ^{13}C NMR data are consistent with the literature.[143] There is a discrepancy between the literature and observed melting point.

5.4.9. Potassium hydride-mediated Dehalogenation of Bunnett-Creary Probes to Probe for Radical Anion Intermediates

The following reactions were conducted by Samuel Dalton at the University of Strathclyde, and are included for completeness.

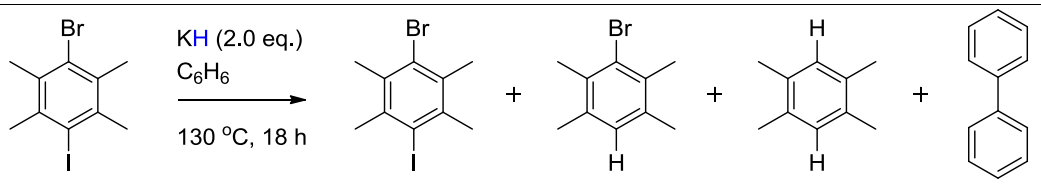

To an oven-dried pressure tube was added 1-bromo-4-iodo-2,3,5,6-tetramethylbenzene **157a** (169.0 mg, 0.50 mmol), KH (40.0 mg, 1.00 mmol, 2.0 eq.) and benzene (5 mL). The tube was sealed in a glovebox and heated at 130 °C for 18 h. After cooling to rt, the reaction was quenched carefully with water (50 mL) and extracted with Et_2O (3 x 50 mL). The combined organic layers were dried (hydrophobic frit), and concentrated *in vacuo*. 1,3,5-trimethoxybenzene (8.4 mg, 0.05 mmol, 10 mol%) was added, the residue dissolved in $CDCl_3$ and yields of **161**, **162** and returned **157a** determined by ^{1}H NMR (see Appendix for details, where calculations are exeplified for the reaction of **157b**). The yields are shown in Scheme 33, Section 2.3.5.

Alternatively, the reaction was conducted using **157b** (146.0 mg, 0.5 mmol) as a substrate in place of **157a**. The yields, determined by ^{1}H NMR as above (see Appendix for details), are shown in Scheme 33, Section 2.3.5.

5.4.10. ICP Analysis and Sample Preparation

ICP-OES analysis was conducted on a 0.45 mmol sample of KO*t*Bu (1 x 50.0 mg), KH (3 x 17.8 mg) and NaH (1 x 10.7 mg). Samples were prepared by Samuel Dalton at the University of Strathclyde and analysed using a GSK in-house service. All liquid transfers were carried out using eppendorf pipettes, all solid transfers were carried out using glass pipettes and vials. All pipettes, vials and 6x 50 mL Greiner culture tubes were pre-washed with 13% aq. nitric acid (a 1 : 4 mixture of Plasma Pure (69%) nitric acid : Milli Q water) and allowed to dry overnight under air. The 5x tubes were charged with the desired samples inside a glovebox (the 6th tube was used as a blank sample).

The tubes were sealed and removed from the glovebox, cooled to 0 ^{o}C and **carefully** digested with IPA under an Ar funnel (with the exception of the KO*t*Bu sample). After effervescence had ceased, all samples were diluted to 5 mL with Milli Q water. Then, 0.3 mL of 69% Plasma Pure (69%) nitric acid was added, all vials were sealed and heated at 75 ^{o}C for 36 h in a sand bath. Samples were analysed on an Varian 730 ICP-OES spectrometer, taking 200 μL aliquots and diluting with 2% v/v HCl in DMSO, values are back-calculated to the 5 mL aqueous samples. Results are displayed in Table 9, Section 2.3.6. The concentration of KH, NaH and KO*t*Bu in ICP samples here (0.1 M) in H_2O is *ca*. half the theoretical concentration of the reaction mixtures in benzene (0.2 M, assuming the inorganics had fully dissolved in benzene).

5.4.11. COMPUTATIONAL INVESTIGATIONS

All calculations were performed using Density Functional Theory (DFT)[145,146] using the Gaussian09 software package.[147] Unless otherwise stated, all minima (reactants, intermediates, products) and maxima (transition states) were optimised using the UB3LYP functional with a 6-31+G(d,p) basis set on all atoms,[148] paralleling a study on hydrogen atom abstraction from tertiary amines using the cumyloxyl radical.[149] Calculations of bromoarenes and bromoarene radical anions used a higher level of theory; the M062X functional[150,151] with a 6-311++G(d,p) basis set[152–156] on all atoms except bromine. Bromine was modelled using the MWB28 relativistic pseudo-potential and associated basis set.[157] Solvation was modelled implicitly using the Conductor-like Polarisable Continuum Model (C-PCM)[158,159] for benzene. Frequency calculations were performed on all optimised structures in order to characterise minima (zero imaginary frequencies) and maxima (single imaginary frequency). All profiles are plotted using the Gibbs free energy values. GaussView 5.0.9 was used for the visualisation of structures. Computational data are contained within the Appendix.

6. REFERENCES

(1) Sun, C.-L.; Li, H.; Yu, D.-G.; Yu, M.; Zhou, X.; Lu, X.-Y.; Huang, K.; Zheng, S.-F.; Li, B.-J.; Shi, Z.-J. *Nat. Chem.* **2010**, *2*, 1044–1049.

(2) Wertz, S.; Leifert, D.; Studer, A. *Org. Lett.* **2013**, *15*, 928–931.

(3) Shirakawa, E.; Itoh, K.; Higashino, T.; Hayashi, T. *J. Am. Chem. Soc.* **2010**, *132*, 15537–15539.

(4) Liu, W.; Cao, H.; Zhang, H.; Zhang, H.; Chung, K. H.; He, C.; Wang, H.; Kwong, F. Y.; Lei, A. *J. Am. Chem. Soc.* **2010**, *132*, 16737–16740.

(5) Rueping, M.; Leiendecker, M.; Das, A.; Poisson, T.; Bui, L. *Chem. Commun.* **2011**, *47*, 10629–10631.

(6) Shirakawa, E.; Zhang, X.; Hayashi, T. *Angew. Chem. Int. Ed.* **2011**, *50*, 4671–4674.

(7) Liu, W.; Li, L.; Li, C.-J. *Nat. Commun.* **2015**, *6*, 6526.

(8) Appukkuttan, P.; Dehaen, W.; Van der Eycken, E. *Eur. J. Org. Chem.* **2003**, 4713–4716.

(9) Manahan, S. E. *Environmental Science and Technology: A Sustainable Approach to Green Science and Technology*, 2nd ed.; CRC Press, 2006.

(10) Challener, C. *Chem. Ind.* **2013**, *77*, 20–23.

(11) Hunt, A. J.; Farmer, T. J.; Clark, J. H. *Elemental Recovery and Sustainability*; Royal Society of Chemistry: Cambridge, 2013.

(12) Umile, T. P. *Catalysis for Sustainability: Goals, Challenges, and Impacts*; CRC Press, 2015.

(13) Cuthbertson, J.; Gray, V. J.; Wilden, J. D. *Chem. Commun.* **2014**, *50*, 2575–2578.

(14) Wu, Y.; Choy, P. Y.; Kwong, F. Y. *Org. Biomol. Chem.* **2014**, *12*, 6820–6823.

(15) Tanimoro, K.; Ueno, M.; Takeda, K.; Kirihata, M.; Tanimori, S. *J. Org.*

Chem. **2012**, *77*, 7844–7849.

(16) De, S.; Ghosh, S.; Bhunia, S.; Sheikh, J. A.; Bisai, A. *Org. Lett.* **2012**, *14*, 4466–4469.

(17) Arvela, R. K.; Leadbeater, N. E.; Sangi, M. S.; Williams, V. A.; Granados, P.; Singer, R. D. *J. Org. Chem.* **2005**, *70*, 161–168.

(18) Yanagisawa, S.; Ueda, K.; Taniguchi, T.; Itami, K. *Org. Lett.* **2008**, *10*, 4673–4676.

(19) Cazin, C. S. J. *N-Heterocyclic Carbenes in Transition Metal Catalysis and Organocatalysis*; Springer: London, 2011.

(20) Akzinnay, S.; Bisaro, F.; Cazin, C. S. J. *Chem. Commun.* **2009**, 5752–5753.

(21) Ramanathan, A.; Jimenez, L. S. *Synthesis* **2010**, 217–220.

(22) Roush, W. R.; Kageyama, M. *Tetrahedron Lett.* **1985**, *26*, 4327–4330.

(23) Roush, W. R.; Kageyama, M.; Riva, R.; Brown, B. B.; Warmus, J. S.; Moriarty, K. J. *J. Org. Chem.* **1991**, *56*, 1192–1210.

(24) Dobbs, A. *J. Org. Chem.* **2001**, *66*, 638–641.

(25) Jang, D. O. *Synth. Commun.* **1997**, *27*, 1023–1027.

(26) Bailey, W. F.; Patricia, J. J. *J. Organomet. Chem.* **1988**, *352*, 1–46.

(27) Knochel, P.; Dohle, W.; Gommermann, N.; Kneisel, F. F.; Kopp, F.; Korn, T.; Sapountzis, I.; Vu, V. A. *Angew. Chem. Int. Ed.* **2003**, *42*, 4302–4320.

(28) Narayanam, J. M. R.; Tucker, J. W.; Stephenson, C. R. J. *J. Am. Chem. Soc.* **2009**, *131*, 8756–8757.

(29) Biajoli, A. F. P.; Schwalm, C. S.; Limberger, J.; Claudino, T. S.; Monteiro, A. L. *J. Braz. Chem. Soc.* **2014**, *25*, 2186–2214.

(30) Allwein, S. P.; Roemmele, R. C.; Haley Jr., J. J.; Mowrey, D. R.; Petrillo, D. E.; Reif, J. J.; Gingrich, D. E.; Bakale, R. P. *Org. Process Res. Dev.* **2012**, *16*, 148–155.

(31) Bajracharya, G. B.; Daugulis, O. *Org. Lett.* **2008**, *10*, 4625–4628.

(32) Bunnett, J.; Creary, X. *J. Org. Chem.* **1974**, *39*, 3611–3612.

(33) Andrieux, C. P.; Blocman, C.; Dumas-Bouchiat, J. M.; M'Halla, F.;

Savéant, J.-M. *J. Am. Chem. Soc.* **1980**, *102*, 3806–3813.

(34) Roman, D. S.; Takahashi, Y.; Charette, B. *Org. Lett.* **2011**, *13*, 3242–3245.

(35) Chami, Z.; Gareil, M.; Pinson, J.; Savéant, J.-M.; Thiébault, A. *J. Org. Chem.* **1991**, *56*, 586–595.

(36) Pause, L.; Robert, M.; Savéant, J.-M. *J. Am. Chem. Soc.* **1999**, *121*, 7158–7159.

(37) Studer, A.; Curran, D. P. *Angew. Chem. Int. Ed.* **2011**, *50*, 5018–5022.

(38) Pichette Drapeau, M.; Fabre, I.; Grimaud, L.; Ciofini, I.; Ollevier, T.; Taillefer, M. *Angew. Chem. Int. Ed.* **2015**, *54*, 10587–10591.

(39) Eberle, B.; Hübner, O.; Ziesak, A.; Kaifer, E.; Himmel, H. J. *Chem. Eur. J.* **2015**, *21*, 8578–8590.

(40) Patil, M. *J. Org. Chem.* **2016**, *81*, 632–639.

(41) Anderson, G. M.; Cameron, I.; Murphy, J. A.; Tuttle, T. *RSC Adv.* **2016**, *6*, 11335–11343.

(42) Murphy, J. A.; Zhou, S.-Z.; Thomson, D. W.; Schoenebeck, F.; Mahesh, M.; Park, S. R.; Tuttle, T.; Berlouis, L. E. A. *Angew. Chem. Int. Ed.* **2007**, *46*, 5178–5183.

(43) Nguyen, J. D.; D'Amato, E. M.; Narayanam, J. M. R.; Stephenson, C. R. J. *Nat. Chem.* **2012**, *4*, 854–859.

(44) Zhou, S.; Anderson, G. M.; Mondal, B.; Kranz, M.; Doni, E.; Ironmonger, V.; Tuttle, T.; Murphy, J. A. *Chem. Sci.* **2014**, *5*, 476–482.

(45) Ghosh, I.; Ghosh, T.; Bardagi, J. I.; König, B. *Science* **2014**, *346*, 725–728.

(46) De, S.; Mishra, S.; Kakde, B. N.; Dey, D.; Bisai, A. *J. Org. Chem.* **2013**, *78*, 7823–7844.

(47) Emery, K. J.; Tuttle, T.; Kennedy, A. R.; Murphy, J. A. *Tetrahedron* **2016**, *72*, 7875–7887.

(48) Liu, W.; Tian, F.; Wang, X.; Yu, H.; Bi, Y. *Chem. Commun.* **2013**, *49*, 2983–2985.

(49) Wu, Y.; Wong, S. M.; Mao, F.; Chan, T. L.; Kwong, F. Y. *Org. Lett.*

2012, *14*, 5306–5309.

(50) Sun, C.-L.; Gu, Y.-F.; Wang, B.; Shi, Z.-J. *Chem. Eur. J.* **2011**, *17*, 10844–10847.

(51) Dewanji, A.; Murarka, S.; Curran, D. P.; Studer, A. *Org. Lett.* **2013**, *15*, 6102–6105.

(52) Chen, W.-C.; Hsu, Y.-C.; Shih, W.-C.; Lee, C.-Y.; Chuang, W.-H.; Tsai, Y.-F.; Chen, P. P.-Y.; Ong, T.-G. *Chem. Commun.* **2012**, *48*, 6702–6704.

(53) Sharma, S.; Kumar, M.; Kumar, V.; Kumar, N. *Tetrahedron Lett.* **2013**, *54*, 4868– 4871.

(54) Zhao, H.; Shen, J.; Guo, J.; Ye, R.; Zeng, H. *Chem. Commun.* **2013**, *49*, 2323–2325.

(55) Yong, G.-P.; She, W.-L.; Zhang, Y.-M.; Li, Y.-Z. *Chem. Commun.* **2011**, *47*, 11766–11768.

(56) Ng, Y. S.; Chan, C. S.; Chan, K. S. *Tetrahedron Lett.* **2012**, *53*, 3911–3914.

(57) Qiu, Y.; Liu, Y.; Yang, K.; Hong, W.; Li, Z.; Wang, Z.; Yao, Z.; Jiang, S. *Org. Lett.* **2011**, *13*, 3556–3559.

(58) Zhou, S.; Doni, E.; Anderson, G. M.; Kane, R. G.; Macdougall, S. W.; Ironmonger, V. M.; Tuttle, T.; Murphy, J. A. *J. Am. Chem. Soc.* **2014**, *136*, 17818.

(59) Yi, H.; Jutand, A.; Lei, A. *Chem. Commun.* **2015**, *51*, 545–548.

(60) Gray, P.; Williams, A. *Chem. Rev.* **1959**, *59*, 239–328.

(61) DiRocco, D. A.; Dykstra, K.; Krska, S.; Vachal, P.; Conway, D. V; Tudge, M. *Angew. Chem. Int. Ed.* **2014**, *53*, 4802–4806.

(62) Doering, W. von E.; Hoffmann, A. K. *J. Am. Chem. Soc.* **1954**, *76*, 6162–6165.

(63) Pollitt, R. J.; Saunders, E. C. *J. Am. Chem. Soc.* **1965**, 4615–4628.

(64) Fyfe, C. A.; Foster, R. *Chem. Commun.* **1967**, 1219.

(65) Janovsky, J. V; Erb, L. *Ber.* **1886**, *19*, 2155.

(66) Bhakuni, B. S.; Kumar, A.; Balkrishna, S. J.; Sheikh, J. A.; Konar, S.;

Kumar, S. *Org. Lett.* **2012**, *14*, 2838–2841.

(67) Murphy, J. A. *J. Org. Chem.* **2014**, *79*, 3731–3746.

(68) Morita, Y.; Murata, T.; Yamochi, H.; Saito, G.; Nakasuji, K. *Synthetic. Met.* **2003**, *135-136*, 579–580.

(69) Lampard, C.; Murphy, J. A.; Lewis, N. *J. Chem. Soc., Chem. Commun.* **1993**, 295–297.

(70) Kizil, M.; Lampard, C.; Murphy, J. A. *Tetrahedron Lett.* **1996**, *37*, 2511–2514.

(71) Romańczyk, P. P.; Rotko, G.; Kurek, S. S. *Electrochem. Commun.* **2014**, *48*, 21–23.

(72) Hanson, S. S.; Doni, E.; Traboulsee, K. T.; Coulthard, G.; Murphy, J. A.; Dyker, C. A. *Angew. Chem. Int. Ed.* **2015**, *54*, 11236–11239.

(73) Burkholder, C.; Dolbier Jr., W. R.; Médebielle, M. *J. Org. Chem.* **1998**, *63*, 5385– 5394.

(74) Since, M.; Terme, T.; Vanelle, P. *Tetrahedron* **2009**, *65*, 6128–6134.

(75) Takechi, N.; Aït-Mohand, S.; Médebielle, M.; Dolbier Jr., W. R. *Tetrahedron Lett.* **2002**, *43*, 4317–4319.

(76) Garnier, J.; Kennedy, A. R.; Berlouis, L. E. A.; Turner, A. T.; Murphy, J. A. *Beilstein J. Org. Chem.* **2010**, *6*, No. 73.

(77) Sword, R.; O'Sullivan, S.; Murphy, J. A. *Aust. J. Chem.* **2013**, *66*, 314–322.

(78) Woodward, R. B.; Wendler, N. L.; Brutschy, F. J. *J. Am. Chem. Soc.* **1945**, *67*, 1425–1429.

(79) Grzeszczuk, M.; Smith, D. E. *J. Electroanal. Chem.* **1983**, *157*, 205–219.

(80) Beckwith, A. L. J.; Goh, S. H. *J. Chem. Soc., Chem. Commun.* **1983**, 907–907.

(81) Beckwith, A. L. J.; Goh, S. H. *J. Chem. Soc., Chem. Commun.* **1983**, 905–906.

(82) Eisch, J. J.; Burlinson, N. E. *J. Am. Chem. Soc.* **1976**, *98*, 753–761.

(83) Baird, M. S.; Bellus, D.; Chessum, N.; Couty, S.; Dzielendziak, A.;

Eilbracht, P. *Science of Synthesis: Houben-Weyl Methods of Molecular Transformations Vol. 48: Alkanes*; Georg Thieme Verlag, 2014.

(84) Trost, B. M.; Fleming, I.; Semmelhack, M. F. *Comprehensive Organic Synthesis: Additions to and substitutions at C-C[pi]-Bonds*; Pergamon, 1992.

(85) Jefford, C. W.; Kirkpatrick, D.; Delay, F. *J. Am. Chem. Soc.* **1971**, *94*, 8905–8907.

(86) Ashby, E. C.; DePriest, R. N.; Goel, A. B.; Wenderoth, B.; Pham, T. N. *J. Org. Chem.* **1984**, *49*, 3545–3556.

(87) Welder, C. O.; Ashby, E. C. *J. Org. Chem.* **1997**, *62*, 4829–4833.

(88) Pasquini, M. A.; Le Goaller, R.; Pierre, J. L. *Tetrahedron* **1979**, *36*, 3205–3208.

(89) Too, P. C.; Chan, G. H.; Tnay, Y. L.; Hirao, H.; Chiba, S. *Angew. Chem. Int. Ed.* **2016**, *55*, 3719–3723.

(90) Oksdath-Mansilla, G.; Argüello, J. E.; Peñéñory, A. B. *Tetrahedron Lett.* **2013**, *54*, 1515–1518.

(91) Buncel, E.; Menon, B. *J. Am. Chem. Soc.* **1977**, *99*, 4457–4461.

(92) Smith, M. B.; March, J. *March's Advanced Organic Chemistry: Reactions, Mechanisms and Structure*, 5th ed.; Wiley Interscience: New York, 2001.

(93) Brown, C. A. *J. Org. Chem.* **1974**, *39*, 3913–3918.

(94) Zhang, L.; Bi, X.; Guan, X.; Li, X.; Liu, Q.; Barry, B.-D.; Liao, P. *Angew. Chem. Int. Ed.* **2013**, *52*, 11303–11307.

(95) Vasin, V. A.; Razin, V. V. *Synlett* **2001**, *5*, 658–660.

(96) Connelly, N. G.; Geiger, W. E. *Chem. Rev.* **1996**, *96*, 877–910.

(97) Xu, H.; Yu, B.; Zhang, H.; Zhao, Y.; Yang, Z.; Xu, J.; Han, B.; Liu, Z. *Chem. Commun.* **2015**, *51*, 12212–12215.

(98) Caubère, P. *Acc. Chem. Res.* **1974**, *7*, 301–308.

(99) Coudert, G.; Ndebeka, G.; Caubère, P.; Raynal, S.; Lecolier, S.; Boileau, S. *J. Polym. Sci., Polym. Lett. Ed.* **1978**, *16*, 413–417.

(100) Brunton, G.; Gray, J. A.; Griller, D.; Barclay, L. R. C.; Ingold, K. U. *J.*

Am. Chem. Soc. **1978**, *100*, 4197–4200.

(101) Yoshifuji, M.; Shimura, K.; Toyota, K. *Bull. Chem. Soc. Jpn.* **1994**, *67*, 1980–1983.

(102) Frey, J.; Nugiel, D. A.; Rappoport, Z. *J. Org. Chem.* **1991**, *56*, 466–469.

(103) Brunton, G.; Griller, D.; Barclay, L. R. C.; Ingold, K. U. *J. Am. Chem. Soc.* **1976**, *98*, 6803–6811.

(104) Caubère, P. *Angew. Chem. Int. Ed.* **1983**, *22*, 599–613.

(105) Kumpf, R. A.; Dougherty, D. A. *Science* **1993**, *261*, 1708–1710.

(106) Davis, M. R.; Dougherty, D. A. *Phys. Chem. Chem. Phys.* **2015**, *17*, 29262–29270.

(107) Barham, J. P.; Coulthard, G.; Emery, K. J.; Doni, E.; Cumine, F.; Nocera, G.; John, M. P.; Berlouis, L. E. A.; McGuire, T.; Tuttle, T.; Murphy, J. A. *J. Am. Chem. Soc.* **2016**, *138*, 7402–7410.

(108) Yoon, U. C.; Mariano, P. S. *J. Photosci.* **2003**, *10*, 89–96.

(109) Ibrahim, M. R.; Jorgensen, W. L. *J. Am. Chem. Soc.* **1989**, *111*, 819–824.

(110) Cooper, B. E.; Owen, W. J. *J. Organomet. Chem* **1971**, *29*, 33–40.

(111) Yang, H.; Zhang, L.; Jiao, L. *Chem. Eur. J.* **2017**, *23*, 65–59.

(112) Toutov, A. A.; Liu, W.-B.; Betz, K. N.; Fedorov, A.; Stoltz, B. M.; Grubbs, R. H. *Nature* **2015**, *518*, 80–84.

(113) Perrin, D. D.; Armarego, L. F. *Purification of Laboratory Compounds*, 3rd Ed.; Pergamon Press, New York, 1992.

(114) Bujok, R.; Wróbel, Z.; Wojciechowski, K. *Synlett* **2012**, *23*, 1315–1320.

(115) Prüger, B.; Hofmeister, G. E.; Jacobsen, C. B.; Alberg, D. G.; Nielsen, M.; Jørgensen, K. A. *Chem. Eur. J.* **2010**, *16*, 3783–3790.

(116) Fuchs, C.; Edgar, M.; Elsegood, M. R. J.; Weaver, G. W. *RSC Adv.* **2013**, *3*, 21911.

(117) Hajipour, A. R.; Pourmousavi, S. A.; Ruoho, A. E. *Synth. Commun.* **2008**, *38*, 2548–2566.

(118) DeCosta, D. P.; Bennett, A.; Pincock, A. L.; Pincock, J. A.; Stefanova, R. *J. Org. Chem.* **2000**, *65*, 4162–4168.

(119) Rhile, I. J.; Markle, T. F.; Nagao, H.; DiPasquale, A. G.; Lam, O. P.; Lockwood, M. A.; Rotter, K.; Mayer, J. M. *J. Am. Chem. Soc.* **2006**, *128*, 6075–6088.

(120) Bard, A. J.; Faulkner, L. R. *Electrochemical Methods: Fundamentals and Applications*; John Wiley and Sons: New York, 2000.

(121) Peña-López, M.; Ayán-Varela, M.; Sarandeses, L. A.; Sestelo, J. P. *Chem. Eur. J.* **2010**, *16*, 9905–9909.

(122) Wong, Y.; Yang, Q.; Zhou, Z.; Lee, H. K.; Mak, T. C. W.; Ng, D. K. P. *New J. Chem.* **2001**, *25*, 353–357.

(123) Zhao, H. *J. Label. Compd. Radiopharm.* **2008**, *51*, 293–296.

(124) Galkin, M. V; Sawadjoon, S.; Rohde, V.; Dawange, M.; Samec, S. M. *ChemCatChem* **2014**, *6*, 179–184.

(125) Enthaler, S.; Spilker, B.; Erre, G.; Junge, K.; Tse, M. K.; Beller, M. *Tetrahedron* **2008**, *64*, 3867–3876.

(126) Huang, K.; Ortiz-Marciales, M.; Correa, W.; Pomales, E.; Lo, X. Y. *J. Org. Chem.* **2009**, *74*, 4195–4202.

(127) Pereira, R.; Cvengroš, J. *J. Organomet. Chem.* **2013**, *729*, 81–85.

(128) Jia, X.; Zhu, L.; Li, Q.; Li, J.; Li, D.; Li, S. *J. Chem. Res.* **2007**, 203–204.

(129) McCann, L. C.; Organ, M. G. *Angew. Chem. Int. Ed.* **2014**, *53*, 4386–4389.

(130) Saha, D.; Ghosh, R.; Dutta, R.; Mandal, A. K.; Sarkar, A. *J. Organomet. Chem.* **2015**, *776*, 89–97.

(131) Zhu, Y.; Zhao, B.; Shi, Y. *Org. Lett.* **2013**, *15*, 992–995.

(132) Walsh, K.; Sneddon, H. F.; Moody, C. J. *Org. Lett.* **2014**, *16*, 5224–5227.

(133) Deady, L. W.; Shanks, R. A.; Campbell, A. D.; Chooi, S. Y. *Aust. J. Chem.* **1971**, *24*, 385–392.

(134) Mikami, S.; Nakamura, S.; Ashizawa, T.; Sasaki, S.; Taniguchi, T.; Nomura, I.; Kawasaki, M. Nitrogenated heterocyclic compound. EP2848618A1, 2015.

(135) Hatanaka, M.; Takahashi, K.; Nakamura, S.; Mashino, T. *Bioorg. Med.*

Chem. **2005**, *13*, 6763–6770.

(136) Horwell, D. C.; Pritchard, M. C. Non-Peptide Bombesin Receptor Antagonists. US6194437B1, 2001.

(137) Kirai, N.; Yamamoto, Y. *Eur. J. Org. Chem.* **2009**, 1864–1867.

(138) Barker, G.; Webster, S.; Johnson, D. G.; Curley, R.; Andrews, M.; Young, P. C.; MacGregor, S. A.; Lee, A.-L. *J. Org. Chem.* **2015**, *80*, 9807–9816.

(139) Guthrie, R. D.; Hartmann, C.; Neill, R.; Nutter, D. E. *J. Org. Chem* **1987**, *52*, 736–740.

(140) Barclay, L. R. C.; Mercer, J. R.; Macaulay, P. J. *Can. J. Chem.* **1975**, *53*, 3171–3174.

(141) Myhre, P. C.; Owen, G. S.; James, L. L. *J. Am. Chem. Soc.* **1968**, *90*, 2115–2123.

(142) Zysman-Colman, E.; Arias, K.; Siegel, J. S. *Can. J. Chem.* **2009**, *87*, 440–447.

(143) Kularatne, R. S.; Sista, P.; Magurudeniya, H. D.; Hao, J.; Nguyen, H. Q.; Biewer, M. C.; Stefan, M. C. *J. Polym. Sci. A Polym. Chem.* **2015**, *53*, 1617–1622.

(144) Bose, A.; Mal, P. *Tetrahedron Lett.* **2014**, *55*, 2154–2156.

(145) Hohenberg, P.; Kohn, W. *Phys. Rev.* **1964**, *36*, 864–871.

(146) Kohn, W.; Sham, L. J. *Phys. Rev.* **1965**, *140*, 1133–1138.

(147) Frisch, M. J.; Trucks, G. W.; Schlegel, H. B.; Scuseria, G. E.; Robb, M. A.; Cheeseman, J. R.; Scalmani, G.; Barone, V.; Mennucci, B.; Petersson, G. A.; Nakatsuji, H.; Caricato, M.; Li, X.; Hratchian, H. P.; Izmaylov, A. F.; Bloino, J.; Zheng, G.; Sonnenberg, J. L.; Hada, M.; Ehara, M.; Toyota, K.; Fukada, R.; Hasegawa, J.; Ishida, M.; Nakajima, T.; Honda, Y.; Kitao, O.; Nakai, H.; Vreven, T.; Montgomery Jr, J. A.; Peralta, J. E.; Ogliaro, F.; Bearpark, M. J.; Heyd, J.; Brothers, E. N.; Kudin, K. N.; Staroverov, V. N. .; Kobayashi, R.; Normand, J.; Raghavachari, K.; Rendell, A. P.; Burant, J. C.; Iyengar, S. S.; Tomasi, J.; Cossi, M.; Rega, N.; Millam, N. J.; Klene, M.; Knox, J. E.; Cross, J.

B.; Bakken, V.; Adamo, C.; Jaramillo, J.; Gomperts, R.; Stratmann, R. E.; Yazyev, O.; Austin, A. J.; Cammi, R.; Pomelli, C.; Ochterski, J. W.; Martin, R. L.; Morokuma, K.; Zakrzewski, V. G.; Voth, G. A.; Salvador, P.; Dannenberg, J. J.; Dapprich, S.; Daniels, A. D.; Farkas, Ö.; Foresman, J. B.; Ortiz, J. V.; Cioslowski, J.; Fox, D. J. Wallingford, CT, USA 2009.

(148) Becke, A. D. *J. Chem. Phys.* **1993**, *98*, 5648–5652.

(149) Salamone, M.; Dilabio, G. A.; Bietti, M. *J. Org. Chem.* **2011**, *76*, 6264–6270.

(150) Zhao, Y.; Truhlar, D. G. *J. Chem. Phys.* **2006**, *125*, 194101/1–18.

(151) Zhao, Y.; Truhlar, D. G. *Acc. Chem. Res.* **2008**, *41*, 157–167.

(152) Krishnan, R.; Binkley, J. S.; Seeger, R.; Pople, J. A. *J. Chem. Phys.* **1980**, *72*, 650–654.

(153) Frisch, M. J.; Pople, J. A.; Binkley, J. S. *J. Chem. Phys.* **1984**, *80*, 3265–3269.

(154) McLean, A. D.; Chandler, G. S. *J. Chem. Phys.* **1980**, *72*, 5639–5648.

(155) Blandeau, J.-P.; McGrath, M. P.; Curtiss, L. A.; Radom, L. *J. Chem. Phys.* **1997**, *107*, 5016–5021.

(156) Clark, T.; Chandrasekhar, J.; Spitznagel, G. W.; Schleyer, P. V. R. *J. Comput. Chem.* **1983**, *4*, 294–301.

(157) Bergner, A.; Dolg, M.; Küchle, W.; Stoll, H.; Preuß, H. *Mol. Phys.* **1993**, *80*, 1431–1441.

(158) Barone, V.; Cossi, M. *J. Phys. Chem. A.* **1998**, *102*, 1995–2001.

(159) Cossi, M.; Rega, N.; Scalmani, G.; Barone, V. *J. Comput. Chem.* **2003**, *24*, 669–681.

APPENDIX: SINGLE ELECTRON TRANSFER IN ORGANIC SYNTHESIS TARGETED TOWARDS SUSTAINABLE MANUFACTURE

Joshua Philip Barham

A thesis presented in partial fulfilment of the requirements
for the degree of Doctor of Philosophy

Department of Pure and Applied Chemistry, University of Strathclyde

API Chemistry, GlaxoSmithKline

March 2017

TABLE OF CONTENTS

TABLE OF FIGURES

A1. CYCLIC VOLTAMMETRY

A1.1. PRINCIPLES OF REDOX POTENTIALS

Charge conservation dictates that an oxidation process must coincide with a corresponding reduction (and *vice versa*). Hence, redox processes consist of two half-reactions: a reduction (red-) and an oxidation (-ox). Associated with each half-reaction is a *redox potential* (*E*), measured in volts, which describes how easy or difficult it is to oxidise or reduce a redox-active species.[1] Comparing redox potentials allows the organic chemist to gauge the thermodynamic feasibility of a redox process. Redox potentials of each half-reaction are combined linearly to obtain ΔE, which is the potential difference of the cell and relates to the Gibbs free energy (ΔG) by equation 1:

$$\Delta G = -nF\Delta E = -nF[E(final) - E(initial)] \quad (1)$$

Where n is the integer number of electrons transferred and F is Faraday's constant (96,485 C mol^{-1}). Since n and F are positive, a given chemical reaction requires a positive ΔE to have favourable thermodynamics (a negative ΔG). Redox half-reactions are normally attributed with *standard redox potentials* (E^0) which are the equilibrium or reversible potentials for a given system. The values for E^0 are referenced against the standard hydrogen electrode (SHE).[†,2] The SHE is a platinised electrode dipped in an acidic solution with hydrogen gas bubbled over it. It is attributed a value of 0.00 V at 298 K in 1 M H^+ with 1.0 bar pressure of H_2. The interpretation of this value is that there is an equal probability of H_2 oxidising as there is a proton (H^+) being reduced. Large positive E^0 values indicate that the species involved are strong oxidising agents; it is very difficult to oxidise the corresponding species on the other side of the half-cell equilibrium reaction.

[†]The SHE is sometimes referred to as the Normal Hydrogen Electrode (NHE), this is outmoded terminology.

Conversely, large negative E^0 values mean species are strong reducing agents (note that here, 'positive' or 'negative' refers to *vs.* SHE). Convention represents half reactions as reductions.[†]

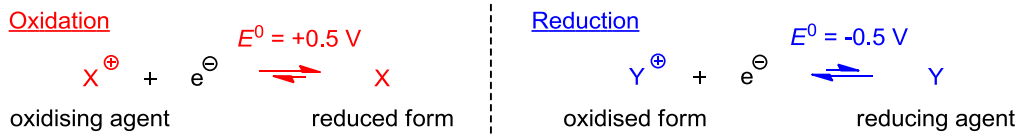

***Scheme A1**: Conceptual half reactions demonstrating E^0 for oxidising and reducing agents.*

Standard redox potentials (E^0) are determined under standard conditions (298 K, any dissolved species have concentrations of 1 M and any gaseous species have partial pressures of 1 atm), which are rarely used. The Nernst equation (equation 2) is used to calculate standard redox potentials (E^0) from redox potentials measured under non-standard conditions (E):

$$E = E^0 - \frac{RT}{nF} \ln Q \qquad (2)$$

Where R is the universal gas constant (8.314 J mol^{-1}) and Q is the reaction quotient; an equilibrium expression using initial concentrations:[‡]

$$Q = \frac{[red]}{[ox]} \qquad (3)$$

Since the SHE is not very conveinent to use, redox potentials are commonly quoted *vs.* another reference electrode, such as the saturated calomel electrode (SCE). The SCE is a mercury electrode with calomel ($HgCl_2$) immersed in saturated aqueous KCl. The relationship between the SCE and the SHE is known (SCE = +0.241 V *vs.* SHE).[3] Another common reference electrode is Ag/AgCl (a silver wire immersed in aqueous 3.0 M NaCl solution, saturated with AgCl). The relationship between the Ag/AgCl and the SHE is known (Ag/AgCl = +0.196 V *vs.* SHE),[3] therefore, 45 mV can be subtracted from $E_{1/2}$ *vs.* Ag/AgCl to convert values into $E_{1/2}$ *vs.* SCE. Redox potentials (E) can be easily measured by a technique known as cyclic voltammetry.

[†]Note that as an *equilibrium value*, the sign and value of E^0 is irrespective of how the half equation is drawn. [‡]The concept of 'activities' is appropriate here, see Bard and Faulkner.[1]

A1.2. PRINCIPLES OF CYCLIC VOLTAMMETRY

The chemical species under study is called the analyte,[1] and the process that occurs in simple electrode reactions is described in Figure A1 (left). When the voltage applied across a solution of analyte aligns with the redox potential of that analyte, electron transfer occurs. In the case of oxidation, a species (R) capable of donating an electron diffuses to the electrode (anode) surface, donates an electron and the product (O) diffuses away from the surface. As the electrode 'sweeps' across a range of potentials (assuming the electron transfer from the species (R) to the electrode is very fast) the current observed depends on the diffusion of fresh species (R) to the electrode. The current i that is measured is directly related to the 'flux' of redox species to the electrode, J, by equation 4:

$$i = nFAJ \tag{4}$$

Where n is the number of electrons transferred, F is Faraday's constant, A is the surface area of the electrode and J is the flux of redox species to the electrode. The flux is governed by Fick's law (equation 5), where D is the diffusion coefficient of the redox species, x is the distance from the electrode surface, $(dC/dx)_{x=0}$ is the concentration gradient at the electrode surface, C^* is the bulk concentration of the redox species and $C_{x=0}$ is the concentration at the electrode surface.

$$J = -D\left(\frac{dC}{dx}\right)_{x=0} \cong D\frac{(C^* - C_{x=0})}{\Delta x} \tag{5}$$

According to Fick's law, the greater the concentration gradient, the greater the flux (J) and (according to equation 4) the greater the current (i).[1] The cyclic voltammogram of ferrocene (Fc) is shown *vs.* SCE to exemplify this. For ferrocene, essentially no current flows as the potential sweeps between 0 → 0.25 V (*vs.* SCE). After 0.25 V, the redox reaction starts ($Fc \rightarrow Fc^+ + e^-$) and ferrocene donates an electron to the electrode. As the potential is increased beyond that point (0.25 → 0.48 V *vs.* SCE), the rate of Fc oxidation

increases, the concentration gradient at the electrode surface increases, and so the current increases. Eventually, all Fc at the electrode surface is consumed. The reaction can then only proceed by more Fc reaching the electrode from the bulk solution *via* diffusion.

The current peak thus indicates the point at which the reaction becomes limited by diffusion. A peak (i_p) in current arises because this is a non-steady state process and so, the current decays beyond the peak (0.48 → 0.70 V *vs.* SCE). This potential at the maximum current (i_p) in the oxidation (anodic) wave is the anodic peak potential, $E_{p,a}$.†

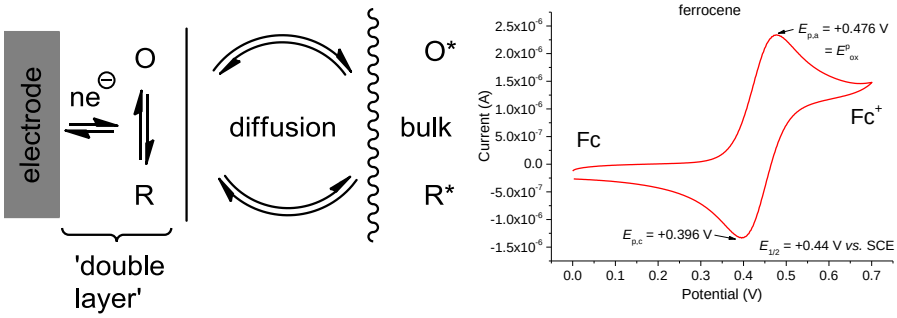

***Figure A1**: Left: Schematic for redox reactions occurring at an electrode surface. Right: Cyclic voltammogram of ferrocene (0.04 M in 0.3 M nBu_4NBF_4/DMF as solvent) vs. SCE.*

Linear sweep voltammetry sweeps across potentials until it reaches a preset value. However, cyclic voltammetry (CV) involves a reversal of potential at the electrode once the preset value is reached. For ferrocene, the oxidised species (Fc^+) is stable so as the potential sweeps back from +0.70 → 0 V the forward trace is mirrored as the electrode donates an electron to the Fc^+ at the electrode surface. The potential at the maximum current (i_p) in the cathodic wave is denoted by $E_{p,c}$. In the Thesis, this is referred to as the *reduction potential* E^p_{red}, when referring to the *reduction* of an analyte (for example, 1,10-phenanthroline).

†In the Thesis, this is referred to as the *oxidation potential* E^p_{ox}, when referring to the *oxidation* of an analyte (for example, DIPEA).

Note that E^{p}_{red} will *not* refer to the cathodic wave peak ($E_{p,c}$) following the *oxidation* of an analyte (for example, ferrocene, at +0.40 V as shown in Figure A1, right). The cyclic voltammogram shown by ferrocene (Figure A1, left) signifies a reversible one-electron electrochemical redox system. For reversible redox systems, the *half-wave potential*, $E_{1/2}$, is often quoted. This is the potential at which the current (i) is half the maximum current (i_p) for a given peak (cathiodic or aniodic are identical). It is given by equation 6:

$$E_{1/2} = (E_{p,a} + E_{p,c})/2. \quad (6)$$

However, many systems suffer irreversible oxidation or reduction. This can occur, for example, if the oxidised or reduced species undergoes chemical reaction, or the electron transfer results in a species unable to undergo further electron transfer. For such irreversible redox systems, only the oxidation (E^{p}_{ox}) or reduction (E^{p}_{red}) peak potential can be measured.[1]

It is appreciated that the terms E^{p}_{red} or E^{p}_{ox} may arise confusion, since electrochemical convention is to represent both as *reductions* [for example, E^{p}_{ox} (Fc/Fc^{+}) = +0.48 V *vs.* SCE in DMF, see Figure A1, right. As another example, E^{p}_{red} (**phen**/**phen**$^{\bullet-}$) = -2.05 V *vs*. SCE in DMF]. However, E^{p}_{red} or E^{p}_{ox} carry value in describing which half reactions are under discussion in redox reactions. In this Thesis, terms E^{p}_{red}, E^{p}_{ox} and $E_{1/2}$ are used in concert with the electrochemical convention as exemplified above. Redox potential values are reported together with the solvent and reference electrode employed for their measurement (typically, in MeCN and *vs*. SCE).

When making comparisons, peak potentials will be compared like-for-like (E^{p}_{ox} with E^{p}_{ox}), which have been obtained under identical conditions and scan rate, regardless of whether reversible or irreversible behavior is observed. For example, for the oxidation of DIPEA by $*[Ru(bpy)_3]^{2+}$, the oxidising power of $*[Ru(bpy)_3]^{2+}$ [E^{p}_{ox} ($*Ru^{II}/Ru^{I}$) = +0.83 V *vs*. SCE] is compared with the ease of oxidation of DIPEA [E^{p}_{ox} ($DIPEA^{\bullet+}$/DIPEA) = +0.85 V *vs*. SCE]. Note that $E_{1/2}$ ($*Ru^{II}/Ru^{I}$) = +0.78 V *vs*. SCE is *not* used. As

another example, for the reduction of bromobenzene by the radical anion of 1,10-phenanthroline (**phen**$^{\bullet-}$), the reducing power of **phen**$^{\bullet-}$ [E^{p}_{red} (**phen**/**phen**$^{\bullet-}$) = -2.05 V *vs*. SCE] is compared with the ease of reduction of bromobenzene [E^{p}_{red} (PhBr/PhBr$^{\bullet-}$) = -2.44 V *vs*. SCE].

A1.3. EXPERIMENTAL SETUP FOR CYCLIC VOLTAMMETRY

A three-electrode setup is typically used for CV (Figure A2). A source of potential is required which is measured by the voltmeter, whilst the ammeter measures the current of the circuit (these are encompassed by a device called a potentiostat). It is possible for analyte ions to migrate due to the electric field resulting from the applied potential difference. To ensure that the observed current depends on diffusion (concentration gradients), not migration (potential gradients), a large excess of a supporting electrolyte (for example, nBu$_4$NPF$_6$) is added. Therefore, it is the supporting electrolyte ions which will migrate to equalise potential gradients, not the analyte ions. Furthermore, the supporting electrolyte increases conductivity without interfering with the electrochemical reaction at the electrode/solution interface.[1] The working electrode (WE) consists of an inert metal (for example, gold or platinum) or a non-metal (glassy carbon). Similarly, the counter electrode (CE) (or auxiliary electrode) consists of an inert metal.

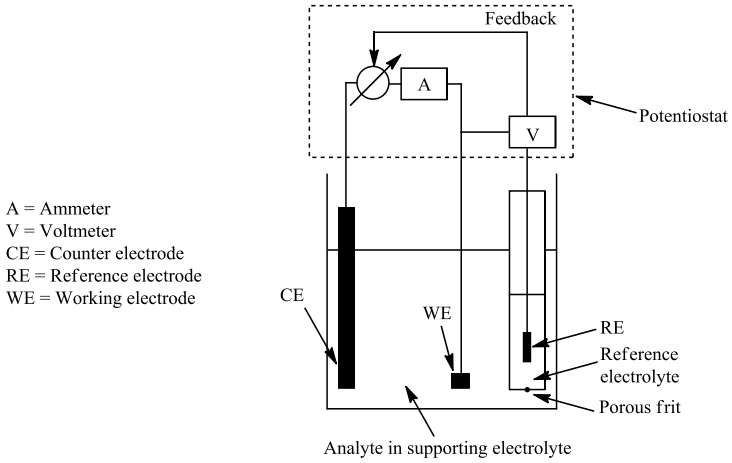

Figure A2: *Three-electrode experimental setup for cyclic voltammetry.*

Since it has a much larger surface area than the WE, the CE ensures that its own reaction is not limiting the reaction at the WE. Finally, the reference electrode (RE) functions as an unpolarisable half-cell reaction whose potential must remain constant, such that redox potentials can be referenced against it. The CE is present to ensure that the current does not flow through the RE and affect its potential. The SCE (= +0.241 V *vs.* SHE),[3] or Ag/AgCl (= +0.196 V *vs.* SHE and -0.045 V vs. SCE)[3] are commonly used as the RE.

The three-electrode setup leads to more precise control of the potential of the WE. However, there can be sources of inaccuracies in the measurement of the redox potentials of analytes. For example, the RE contains an aqueous electrolyte solution which is separated from the analyte solution (usually MeCN or DMF solutions) by a porous frit. The interface between the two liquid phases creates a liquid junction potential which will interfere with the diffusion of ions, causing the reference potential to deviate from the ideal value. Moreover, solubility of the analyte, solvent choice and salt (electrolyte) content of the analyte solution contribute to inaccurate measurements.[1] To account for these systematic errors, ferrocene ($E_{1/2}$ (Fc^+/Fc^+) = +0.45 V *vs.* SCE in DMF)[4] was employed as an external standard, which was always measured both before and after running any series of analytes.

A1.4. Summary of Definitions

E^0 is the standard redox potential, measured under standard conditions.

$E_{p,a}$ is the anodic peak potential.

$E_{p,c}$ is the cathodic peak potential.

E^p_{ox} is the oxidation peak potential (= $E_{p,a}$ herein, when referring to *oxidation* of an analyte).

E^p_{red} is the reduction peak potential (= $E_{p,c}$ herein, when referring to *reduction* of an analyte).

$E_{1/2}$ is the half-wave potential for a reversible process [=($E_{p,a}$ + $E_{p,c}$) / 2].

A1.5. Estimation of Redox Potentials of Photoexcited Species

It is impractical to directly measure the redox potentials of photoexcited states, which exhibit very short lifetimes [from microseconds (μs) to as short as picoseconds (ps)]. Here, the Gibbs free energy equation for photoinduced electron transfer (equation 7) is relevant.[5,6] This rearranges to treat the redox potentials of excited states (e.g. excited photocatalysts, *PC) by summing their ground state redox potentials and the excitation energy $E_{0,0}$.

$$\Delta G = -F\Delta E - w - E_{0,0} = -F\left[E_{1/2}(PC) + E_{0,0} - E_{1/2}(Quencher)\right] - w \qquad (7)$$

Where w is an electrostatic work term, accounting for the solvent-dependent energy difference due to the Coulombic impact of charge separation.† In the estimation of the Gibbs free energy change in the context of photoredox catalysis, w is ignored as the correction of w to ΔG is generally very small (<0.1 eV).‡,[6] On the basis of equation 7, the excited state redox potential can be defined [E(*PC) = E(PC) + $E_{0,0}$] and easily calculated. This is exemplified for $E_{1/2}$ (*Ru^{II}/Ru^{I}) of [*Ru(bpy)$_3$]$^{2+}$ in equation 8 (*vs*. SCE), using a literature

†Rehm and Weller are recognised for including this term in their equation for ΔG. ‡A value of ~0.06 eV was calculated for w in MeCN, see the reference provided.

value for $E_{0,0}$ = 2.13 eV.[7]

$$E_{1/2}(*Ru^{II}/Ru^{I}) = E_{1/2}(Ru^{II}/Ru^{I}) + E_{0,0} = -1.35\ V + 2.13\ eV = +0.78\ V \quad (8)$$

However, a given reductive quencher of $[*Ru(bpy)_3]^{2+}$ might display *irreversible* oxidation; an $E_{1/2}$ value cannot be measured for the reductive quencher and so an $E_{1/2}$ value is being compared with E^{p}_{ox} value. Here, it is more appropriate to compare E^{p}_{ox} ($*Ru^{II}/Ru^{I}$) of $[*Ru(bpy)_3]^{2+}$ with E^{p}_{ox} of the reductive quencher. To estimate E^{p}_{ox} ($*Ru^{II}/Ru^{I}$), the $E_{p,a}$ value (*vs*. SCE) used to calculate $E_{1/2}(Ru^{II}/Ru^{I})$ is taken:

$$E^{p}_{ox}(*Ru^{II}/Ru^{I}) = E^{p}_{ox}(Ru^{II}/Ru^{I}) + E_{0,0} = -1.30\ V + 2.13\ eV = +0.83\ V \quad (9)$$

This oxidation potential (E^{p}_{ox}) represents an upper boundary for the excited state, and is used to make comparisons with E^{p}_{ox} of reductive quenchers in this Thesis (the corresponding argument applies for comparing E^{p}_{red} of excited states with E^{p}_{red} of an oxidative quencher).

A1.6. Cyclic Voltammetry General Experimental

Ferrocene was purified by recrystallisation twice from hexane prior to use, nBu$_4$NPF$_6$ was used as supplied commercially. Unless otherwise stated, all solutions were prepared at 10.0 mM concentration (in 0.1 M nBu$_4$NPF$_6$/MeCN as solvent) using anhydrous, degassed MeCN. Unless otherwise stated, a default scan rate of 50 mV s^{-1} was used and potentials are given relative to the saturated calomel electrode (*vs.* SCE). Peak heights are given in amps (A). Ferrocene was used as an external standard, measured both before and after running any series of analytes, to ensure consistency. Measurements performed *vs*. Ag/AgCl were converted to *vs*. SCE by subtracting 45 mV. Two experimental setups were used for CV, one at the University of Strathclyde and one at GlaxoSmithKline. Voltammograms showed good consistency between the two setups (for example, ferrocene, DABCO, dextromethorphan and *trans*-1-phenyl-2-buten-1-one). In both setups, the anodic-cathodic peak separation for ferrocene $\Delta E^{p\text{-}p}$ obtained was

90-100 mV, (compare to 59 mV/n for an ideal one-electron transfer), indicating a high degree of reversibility (and so rapid kinetics) for the electron transfer process.

A1.6.1. UNIVERSITY OF STRATHCLYDE CV SETUP

Cyclic voltammetry was conducted using a three-electrode setup consisting of a platinum wire working electrode (d = 0.50 mm) and platinum gauge counter electrode. The reference electrode was either a saturated calomel electrode (SCE), or a Ag/AgCl electrode (containing 3.0 M NaCl saturated with AgCl). Electrochemical measurements were carried out in a glovebox under N_2 using an Autolab®/PGSTAT302N potentiostat.

A1.6.2. GLAXOSMITHKLINE CV SETUP

Cyclic voltammetry was conducted using a three-electrode setup consisting of a platinum wire working electrode (d = 1.50 mm) and platinum gauge counter electrode. The reference electrode was a Ag/AgCl electrode (containing 3.0 M NaCl saturated with AgCl). Electrochemical measurements were carried out in a bespoke glass cell using an CH Instruments/CHI1140C potentiostat.

A1.7. CYCLIC VOLTAMMOGRAMS FOR VOLUME 1: TERTIARY AMINES AND PHOTOCATALYSTS

The following voltammograms were recorded using the University of Strathclyde CV setup. $Ru(bpz)_3(PF_6)_2$ and $Ru(phen)_3Cl_2$ were analysed at 1.0 mM concentration. Here, the ferrocene peak height (*ca.* 6.0 x 10^{-6} A) corresponds to a one-electron oxidation. With the exception of tri-*p*-biphenylamine (sparingly soluble), $Ru(bpz)_3(PF_6)_2$ (1.0 mM) and $Ru(phen)_3Cl_2$ (1.0 mM), all oxidations of analytes† gave a similar peak height

†For the analysis of *N*-methylmorpholine only, a different working electrode was used which resulted in a higher peak current (x 10^{-5} A) but which was consistent with the ferrocene peak currents measured before and after *N*-methylmorpholine (7.87 x 10^{-5} A and 8.10 x 10^{-5} A, respectively).

(*ca.* 4.0 x 10^{-6} A to 7.0 x 10^{-6} A) to ferrocene, corresponding to a one-electron oxidation. All reductions of analytes gave a similar peak height (*ca.* -3.3 x 10^{-6} A to -8.0 x 10^{-6} A) to ferrocene, corresponding to a one-electron reduction. Under these conditions, Randles-Sevcik analysis was obtained for ferrocene, dextromethorphan (**73**) and DIPEA (see Chapter A1.9.). Representative voltammograms are given in Figure A3.

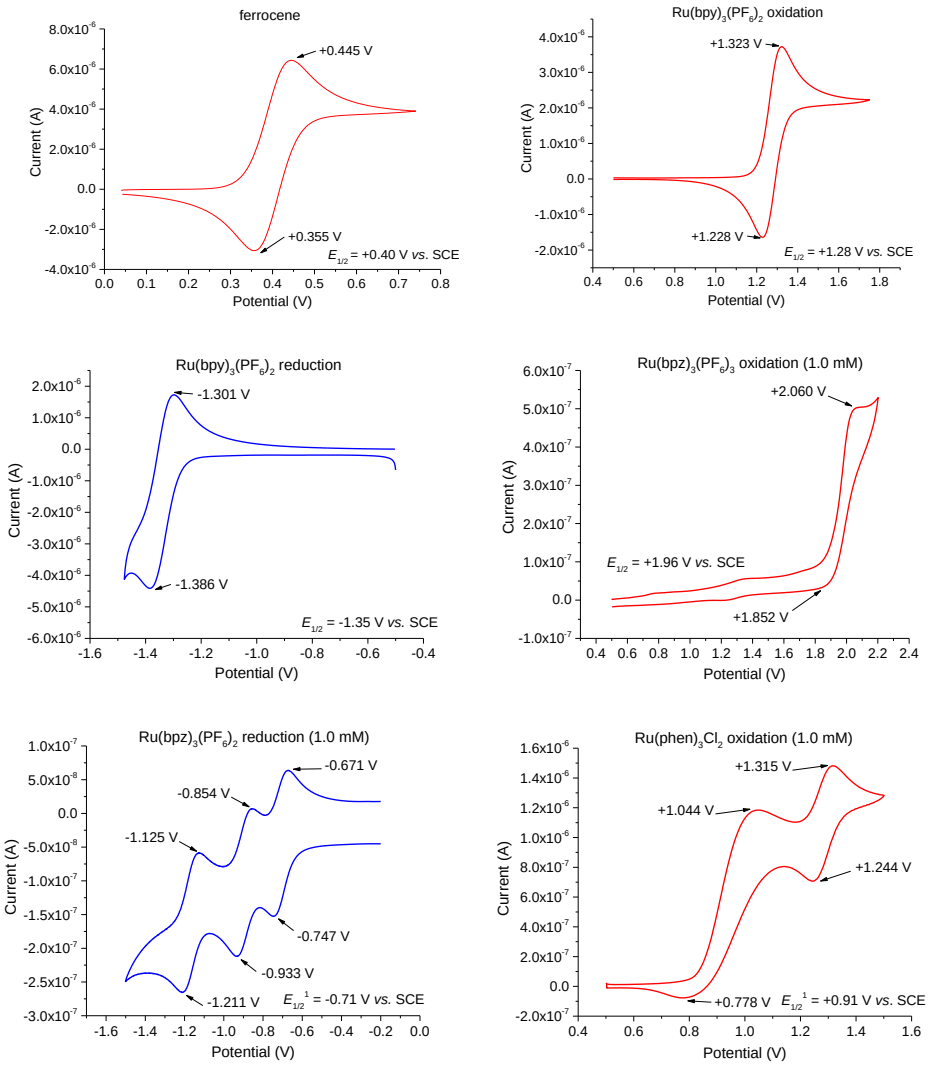

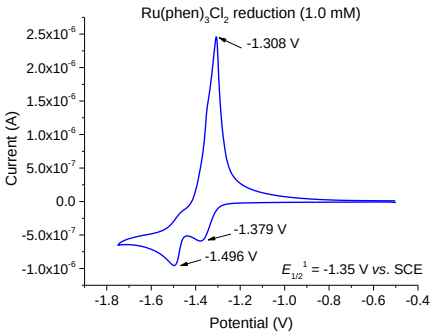
Ru(phen)3Cl2 reduction (1.0 mM)
-1.308 V
-1.379 V
-1.496 V
E1/2 1 = -1.35 V vs. SCE
Current (A)
Potential (V)

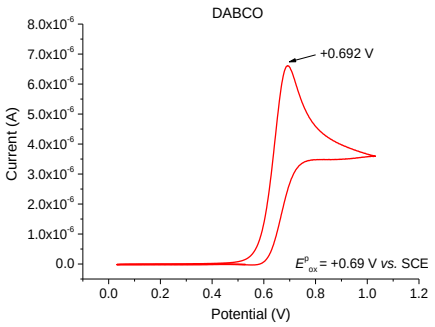
DABCO
+0.692 V
E°ox = +0.69 V vs. SCE
Current (A)
Potential (V)

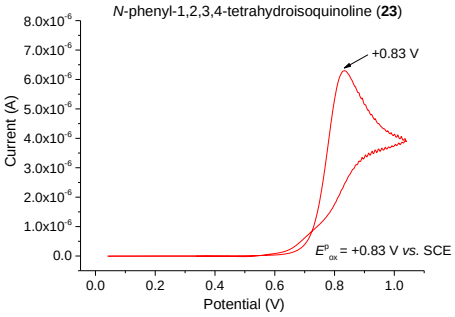
N-phenyl-1,2,3,4-tetrahydroisoquinoline (23)
+0.83 V
E°ox = +0.83 V vs. SCE
Current (A)
Potential (V)

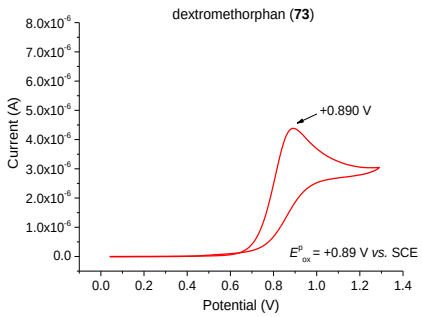
dextromethorphan (73)
+0.890 V
E°ox = +0.89 V vs. SCE
Current (A)
Potential (V)

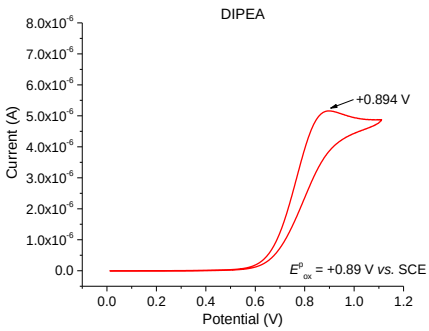
DIPEA
+0.894 V
E°ox = +0.89 V vs. SCE
Current (A)
Potential (V)

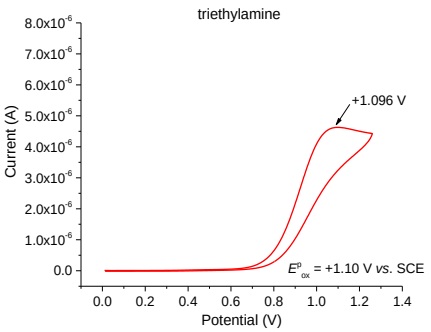
triethylamine
+1.096 V
E°ox = +1.10 V vs. SCE
Current (A)
Potential (V)

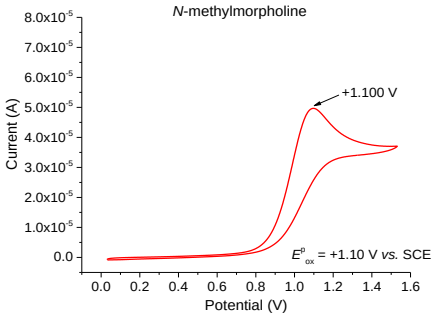
N-methylmorpholine
+1.100 V
E°ox = +1.10 V vs. SCE
Current (A)
Potential (V)

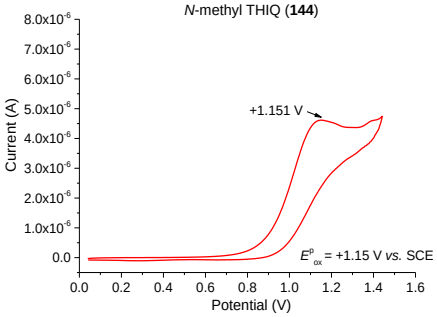
N-methyl THIQ (144)
+1.151 V
E°ox = +1.15 V vs. SCE
Current (A)
Potential (V)

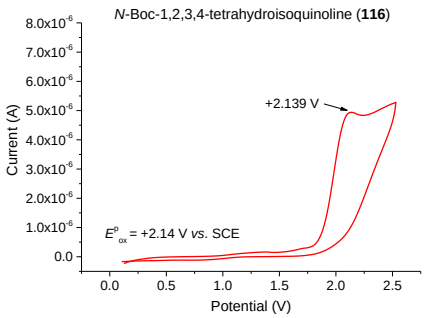
N-Boc-1,2,3,4-tetrahydroisoquinoline (**116**)
Current (A)
Potential (V)
+2.139 V
E^{o}_{ox} = +2.14 V *vs.* SCE

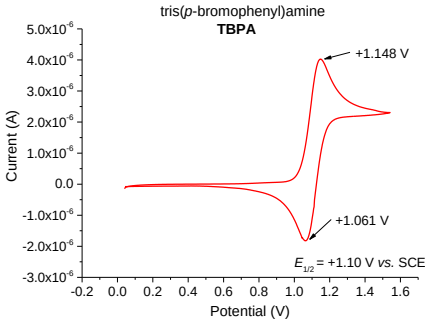
tris(*p*-bromophenyl)amine
TBPA
Current (A)
Potential (V)
+1.148 V
+1.061 V
$E_{1/2}$ = +1.10 V *vs.* SCE

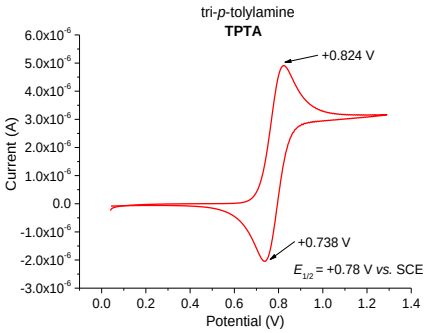
tri-*p*-tolylamine
TPTA
Current (A)
Potential (V)
+0.824 V
+0.738 V
$E_{1/2}$ = +0.78 V *vs.* SCE

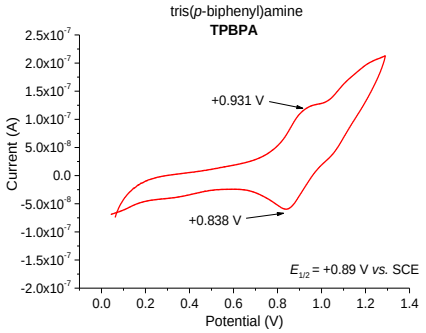
tris(*p*-biphenyl)amine
TPBPA
Current (A)
Potential (V)
+0.931 V
+0.838 V
$E_{1/2}$ = +0.89 V *vs.* SCE

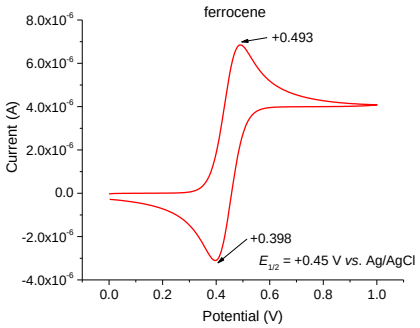
ferrocene
Current (A)
Potential (V)
+0.493
+0.398
$E_{1/2}$ = +0.45 V *vs.* Ag/AgCl

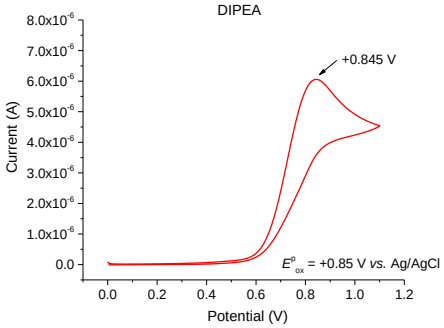
DIPEA
Current (A)
Potential (V)
+0.845 V
E^{o}_{ox} = +0.85 V *vs.* Ag/AgCl

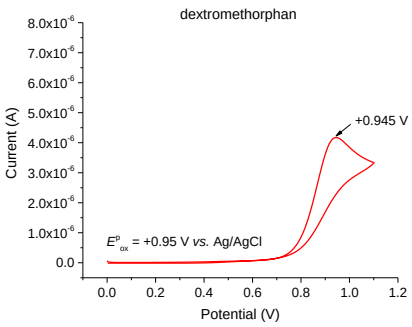
dextromethorphan
Current (A)
Potential (V)
+0.945 V
E^{o}_{ox} = +0.95 V *vs.* Ag/AgCl

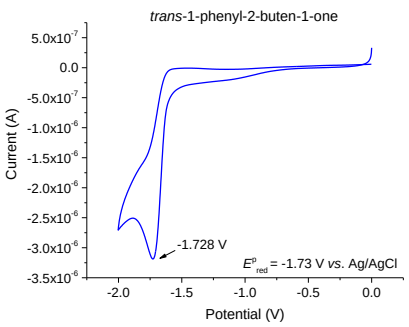
trans-1-phenyl-2-buten-1-one
Current (A)
Potential (V)
-1.728 V
E^{o}_{red} = -1.73 V *vs.* Ag/AgCl

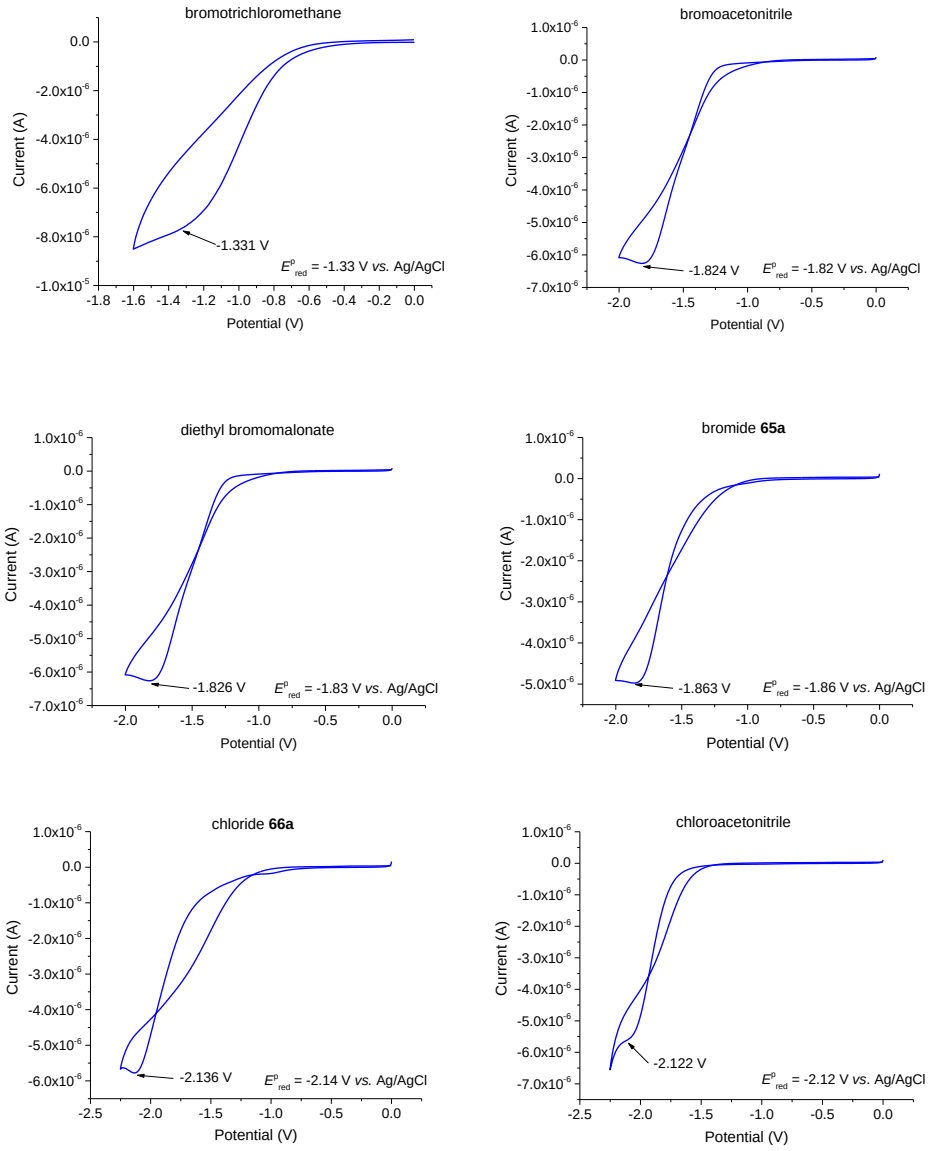

***Figure A3**: Cyclic voltammograms of analytes vs. SCE, or vs. Ag/AgCl, using the University of Strathclyde CV setup.*

The following voltammograms were recorded using the GlaxoSmithKline CV setup. All analytes were completely soluble in the electrolyte solution. Here, the ferrocene peak height (*ca.* 4.5 x 10^{-5} A) corresponds to a one-electron oxidation. All oxidations of other analytes gave a similar peak height *(ca.* 3.0 x 10^{-6} A to 5.0 x 10^{-6} A) to ferrocene, corresponding to a one-electron oxidation. With the exception of a 1 : 1 mixture of *trans*-1-phenyl-2-buten-1-one : $LiBF_4$, all reductions of analytes gave a similar peak height (*ca.* -2.3 x

10^{-6} A to -4.5 x 10^{-6} A) to ferrocene, corresponding to a one-electron reduction. Representative voltammograms are given below (Figure A4). All CV data are summarised in Table A1. Where possible, literature data is shown for comparison (and calibrated to ferrocene, if reported in the literature study). Literature redox potentials are quoted *vs*. SCE. As far as possible, literature redox potentials quoted have been obtained using identical CV conditions (298 K, 0.1 M nBu$_4$NPF$_6$ in degassed MeCN used as solvent) but variations occur in some cases, readers are referred to the literature referenced in Table A1 for details.

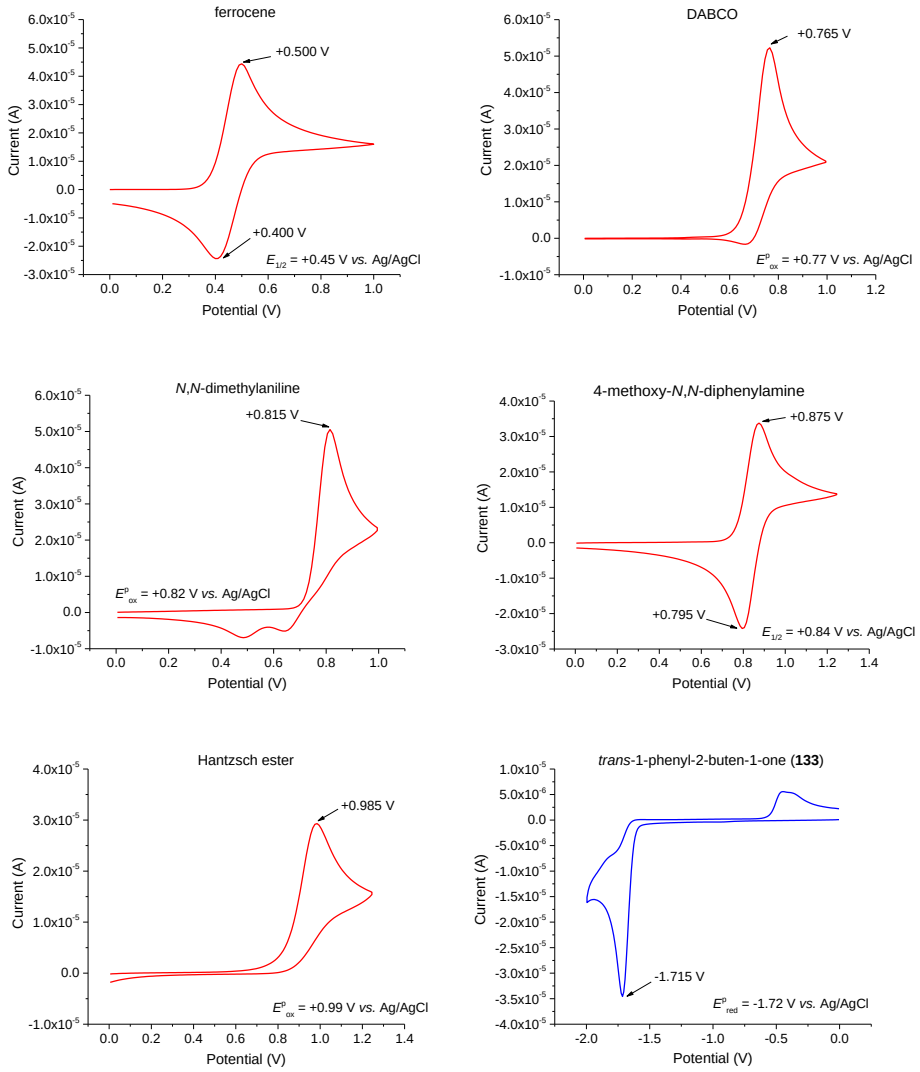

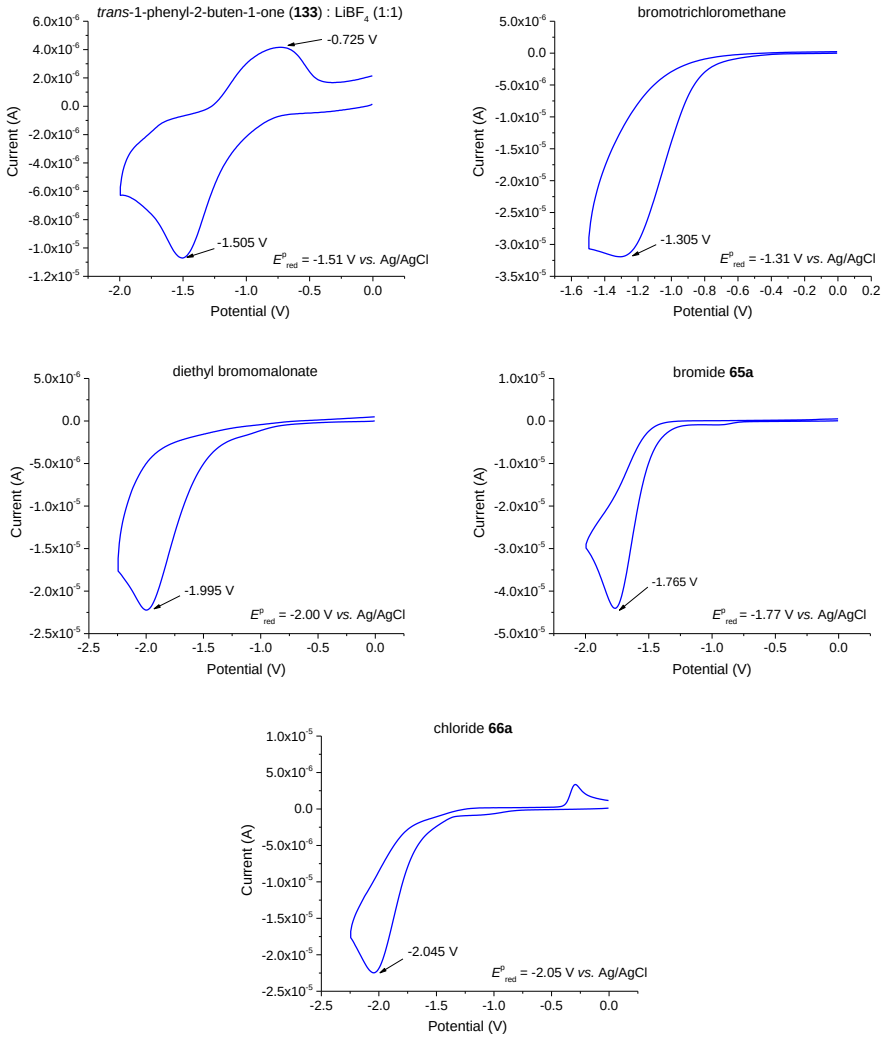

***Figure A4**: Cyclic voltammograms of analytes vs. Ag/AgCl using the GlaxoSmithKline CV setup.*

***Table A1**: Comparison of measured with literature potentials for Volume 1.*

Entry	Redox active species	$E_{1/2}$ (V *vs.* SCE)[a]	Literature $E_{1/2}$ (V *vs.* SCE)
1	Ferrocene	+0.40 (E^{p}_{ox} = +0.83)[b]	+0.40[4]
2	O_2 (1 atm)	-	-0.75[8], -0.58[9]
3	$[Ru(bpy)_3]^{2+}$ (reduction to Ru^{I})	-1.35 (E^{p1}_{red} = -1.39)	-1.35,[10] -1.33[7]
4	$*[Ru(bpy)_3]^{2+}$ (reduction to Ru^{I})	+0.78 (E^{p}_{ox} = +0.83)[c]	+0.78,[10] +0.77[7]

Entry	Redox active species	$E_{1/2}$ (V *vs*. SCE)[a]	Literature $E_{1/2}$ (V *vs.* SCE)
5	$[Ru(bpy)_3]^{2+}$ (oxidation to Ru^{III})	+1.28 (E^p_{ox} = +1.32)	+1.26,[10] +1.29[7]
6	$*[Ru(bpy)_3]^{2+}$ (oxidation to Ru^{III})	-0.85 (E^p_{red} = -0.90)[c]	-0.87,[10] -0.81[7]
7	$[Ru(bpz)_3]^{2+}$ (reduction to Ru^{I})	-0.71 (E^{p1}_{red} = -0.75)	-0.71,[11] -0.80[7]
8	$*[Ru(bpz)_3]^{2+}$ (reduction to Ru^{I})	+1.41 (E^p_{ox} = +1.45)[d]	+1.30,[12] +1.45[7]
9	$[Ru(bpz)_3]^{2+}$ (oxidation to Ru^{III})	+1.96 (E^p_{ox} = +2.06)	+1.95,[11] +1.86[7]
	$*[Ru(bpz)_3]^{2+}$ (oxidation to Ru^{III})	-0.16 (E^p_{red} = -0.27)[d]	-0.26,[13] -0.26[7]
10	$[Ru(phen)_3]^{2+}$ (reduction to Ru^{I})	-1.35 (E^{p1}_{red} = -1.38)	-1.36[14]
	$*[Ru(phen)_3]^{2+}$ (reduction to Ru^{I})	+0.81 (E^p_{ox} = +0.87)[e]	+0.82[14]
11	$[Ru(phen)_3]^{2+}$ (oxidation to Ru^{III})	+0.91 (E^{p1}_{ox} = +1.04), +1.28 (E^{p2}_{ox} = +1.32)	+1.26[14]
	$*[Ru(phen)_3]^{2+}$ (oxidation to Ru^{III})	-0.90 (E^p_{red} = -0.94)[e]	-0.87[14]
12	DABCO	E^p_{ox} = +0.69[b]	E^p_{ox} = +0.70[15]
13	*N*,*N*-dimethylaniline	E^p_{ox} = +0.78[f,g]	E^p_{ox} = +0.79[h,16], +0.79[17]
14	tri-*p*-tolylamine (**TPTA**)	+0.78 (E^p_{ox} = +0.82)	+0.78[18]
15	4-methoxyphenyl-*N*,*N*-diphenylamine	+0.79 (E^p_{ox} = +0.83)	-
16	*N*-phenyl-1,2,3,4-tetrahydroisoquinoline (**23**)	E^p_{ox} = +0.83	E^p_{ox} = +0.84[h,19] (in DMF), +0.83[8] (in $MeNO_2$)
17	DIPEA	E^p_{ox} = +0.85[b]	E^p_{ox} = +0.76[i,20]
18	tri-*p*-biphenylamine (**TPBPA**)	+0.89 (E^p_{ox} = +0.93)	
19	dextromethorphan (**73**)	E^p_{ox} = +0.90[b]	-
20	Hantzsch ester	E^p_{ox} = +0.95[f,g]	E^p_{ox} = +0.93,[h,21] +1.02[h,22]
21	triethylamine	E^p_{ox} = +1.10	E^p_{ox} = +1.05[15]
22	*N*-methylmorpholine	E^p_{ox} = +1.10	E^p_{ox} = +1.20[23]

Entry	Redox active species	$E_{1/2}$ (V *vs*. SCE)[a]	Literature $E_{1/2}$ (V *vs.* SCE)
23	*N*-methyl-1,2,3,4-tetrahydroisoquinoline (**114**)	E^{p}_{ox} = +1.15	E^{p}_{ox} (*N*-ethyl-1,2,3,4-tetrahydroisoquinoline) = +1.20[24]
24	tris(*p*-bromophenylamine) (**TBPA**)	+1.10 (E^{p}_{ox} = +1.15)	+1.07[18]
25	*N*-Boc-1,2,3,4-tetrahydroisoquinoline (**116**)	E^{p}_{ox} = +2.14	+2.09 (*N*-Boc piperidine)[25]
26	bromotrichloromethane	E^{p}_{red} = -1.36[b,g]	-
27	*trans*-1-phenyl-2-buten-1-one (**133**)	E^{p}_{red} = -1.77[b,g]	E^{p}_{red} = -1.26[j,26]
28	*trans*-1-phenyl-2-buten-1-one (**133**) : $LiBF_4$ (1:1)	E^{p}_{red} = -1.56[f,g]	-
29	bromide **65a**	E^{p}_{red} = -1.81[b,g]	-
30	diethyl bromomalonate	E^{p}_{red} = -1.96[b,g]	E^{p}_{red} = -0.62[j,27]
31	bromoacetonitrile	E^{p}_{red} = -1.86[g]	E^{p}_{red} = -1.58 (in DMF)[28]
32	chloride **66a**	E^{p}_{red} = -2.14[b,g]	-
33	chloroacetonitrile	E^{p}_{red} = -2.17[g]	E^{p}_{red} = -2.00 (in DMF),[28] -1.97[29]

[a]Values are calibrated to ferrocene as an external standard, run before and after a set of analytes to ensure consistency. Unless otherwise stated, all values are half-wave potentials ($E_{1/2}$) in MeCN *vs*. SCE and were obtained using the University of Strathclyde CV setup. [b]Average of two values (*vs.* SCE) obtained from two different CV setups. [c]Excited state redox potentials for $[Ru(bpy)_3]^{2+}$ calculated assuming $E_{0,0}$ = 2.13 eV as assumed in the literature.[7] [d]Excited state redox potentials for $[Ru(bpz)_3]^{2+}$ calculated assuming $E_{0,0}$ = 2.12 eV as assumed in the literature.[7] [e]Excited state redox potentials for $[Ru(phen)_3]^{2+}$ calculated assuming $E_{0,0}$ = 2.18 eV as assumed in the literature.[14] [f]Obtained using GlaxoSmithKline CV

setup. [g]Measured *vs*. Ag/AgCl and converted to *vs.* SCE by subtracting 45 mV. [h]In these papers, values are measured *vs*. an $Ag/AgNO_3$ reference electrode and converted to *vs*. SCE by addition of +0.29 V.[16,30] [i]In that paper, E^{p}_{ox} ($DABCO^{\bullet+}$/DABCO) = +0.57 V *vs*. SCE in MeCN was quoted.[20] The difference between the DIPEA and DABCO values reported therein is +0.19 V, which is consistent with the difference found between the DIPEA and DABCO values reported herein (+0.16 V). [j]There is a significant discrepancy between the values reported in the literature and those reported herein; confidence can be placed in values reported herein which are consistent between the two experimental setups.

A1.7. CYCLIC VOLTAMMETRY FOR VOLUME 2, CHAPTER 2.1.

The following voltammograms were recorded using the University of Strathclyde setup, where all solutions were prepared at 4.0 mM concentration (in 0.3 M nBu$_4$NBF$_4$/DMF) using anhydrous, degassed DMF. Here, the ferrocene peak height (*ca.* 2.5 x 10^{-6} A) corresponds to a one-electron oxidation. Randles-Sevcik analysis was carried out on 1,10-phenanthroline and dimer **65**, see Chapter A1.9. for details (see Volume 2, Experimental, Section 5.2.7. for voltammograms and discussion). Voltammograms are given below (Figure A5).

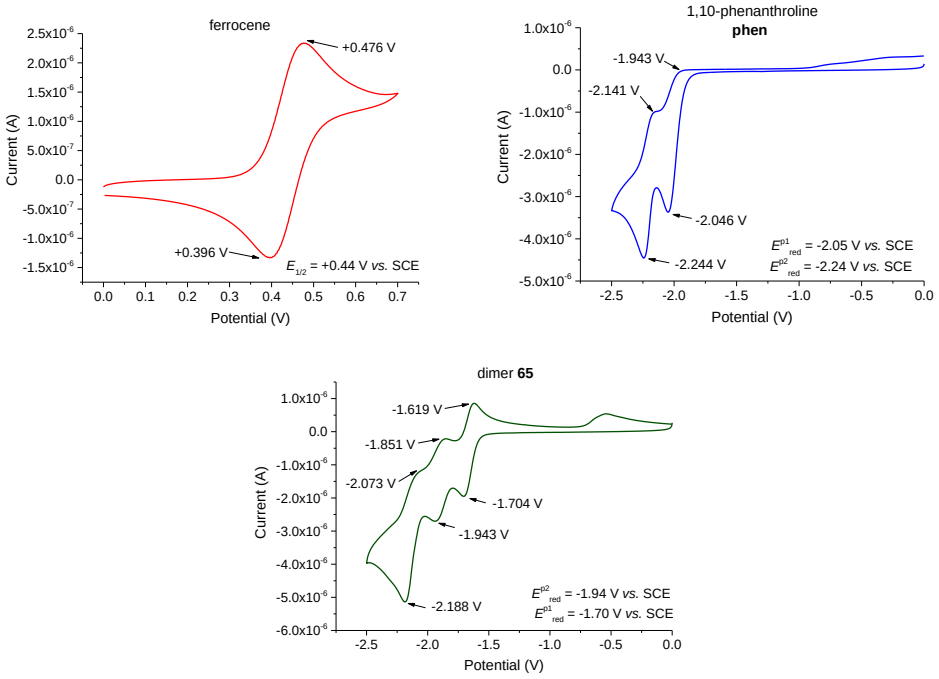

***Figure A5**: Cyclic voltammograms for Volume 2, Chapter 2.1.*

***Table A2**: Comparison of measured with literature potentials for Volume 2, Chapter 2.1.*

Entry	Analyte (0.04 M (in 0.3 M *n*Bu_4NBF_4/DMF))	$E_{1/2}$ (V *vs*. SCE)[a]	Literature $E_{1/2}$ (V *vs.* SCE)
1	ferrocene	+0.44 (E^{p}_{ox} = 0.48)	E^{p}_{ox} = 0.50[31]
2	**phen**	E^{p1}_{red} = -2.05	E^{p1}_{red} = -2.06[32]
		E^{p2}_{red} = -2.24	E^{p2}_{red} = -2.23[32]
3	dimer **65**	E^{p1}_{red} = -1.70	-
		E^{p2}_{red} = -1.94	-

[a]Values are calibrated to ferrocene as an external standard, run before and after a set of analytes to ensure consistency. Unless otherwise stated, values are half-wave potentials ($E_{1/2}$) in DMF *vs*. SCE and were obtained using the University of Strathclyde CV setup.

A1.8. Cyclic Voltammetry for Volume 2, Chapter 2.2.

The following voltammograms were recorded using the University of Strathclyde setup. All solutions were prepared at 0.01 M concentration (in 0.1 M *n*Bu_4NPF_6/DMF) using anhydrous, degassed DMF. Here, the ferrocene peak height (*ca.* 5.0 x 10^{-6} A) corresponds to one-electron oxidation. All samples were completely soluble in the electrolyte solution. With the exception of 2-chloro-1,3-dimethylbenzene (**57c**), all reductions gave a similar peak height (ca. 3.0 x 10^{-6} to 6.5 x 10^{-6} A) to ferrocene, corresponding to one-electron reduction. Voltammograms are given below (Figure A6).

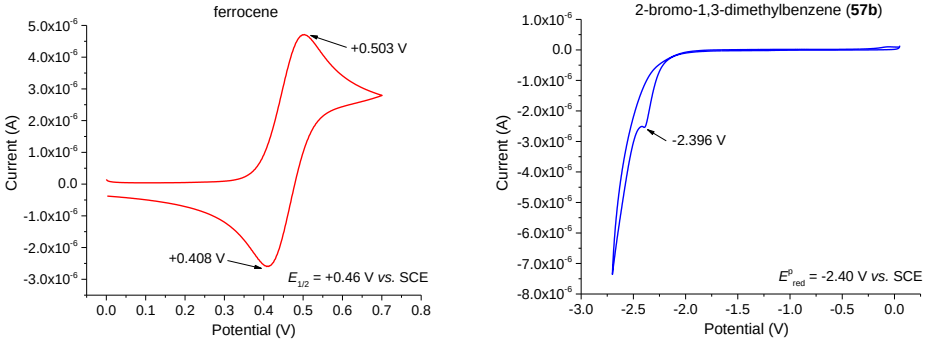

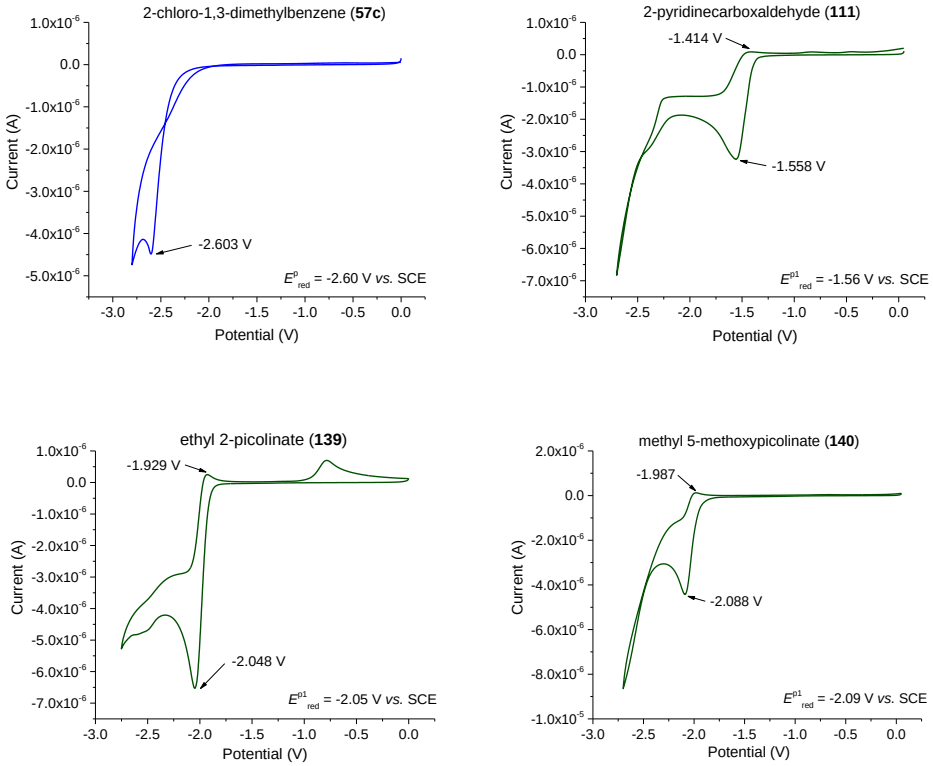

***Figure A6**: Cyclic voltammograpms for Volume 2, Chapter 2.2.*

***Table A3**: Comparison of measured with literature potentials for Volume 2, Chapter 2.2.*

Entry	Analyte (0.01 M (in 0.1 M *n*Bu_4NPF_6/DMF))	$E_{1/2}$ (V *vs.* SCE)[a]	Literature $E_{1/2}$ (V *vs.* SCE)
1	ferrocene	+0.46	+0.45[4]
2	2-bromo-1,3-dimethylbenzene (**57b**)	E^p_{red} = -2.45	E^p_{red} (bromobenzene) = -2.44[33]
3	2-chloro-1,3-dimethylbenzene (**57c**)	E^p_{red} = -2.60	E^p_{red} (chlorobenzene) = -2.78[33]
4	2-pyridinecarboxaldehyde (**111**)	E^{p1}_{red} = -1.56, E^{p2}_{red} = < -2.50	-
5	ethyl 2-picolinate (**139**)	E^{p1}_{red} = -2.05, E^{p2}_{red} = ≤ -2.50	-

Entry	Analyte (0.01 M (in 0.1 M nBu$_4$NPF$_6$/DMF))	$E_{1/2}$ (V *vs*. SCE)[a]	Literature $E_{1/2}$ (V *vs.* SCE)
6	methyl 5-methoxypicolinate (**140**)	E^{p1}_{red} = -2.09, E^{p2}_{red} = < -2.50	-

[a]Values are calibrated to ferrocene as an external standard, run before and after a set of analytes to ensure consistency. Unless otherwise stated, values are half-wave potentials ($E_{1/2}$) in DMF *vs*. SCE and were obtained using the University of Strathclyde CV setup.

A1.9. Randles-Sevcik Analysis and Calculation of Diffusion Coefficients

A1.9.1. Introduction and Randles-Sevcik Analysis of ferrocene as an Example

Whilst redox potentials provide thermodynamics information for a given redox process, they do not provide kinetic information. In organic electrosynthesis, the applied potential could be much greater than the redox potential of the organic substrate, yet poor conversion could result due to slow reaction kinetics. For example, a reaction was reported using a 6 V applied potential which took 1.5 h to complete,[34] despite the substrate half-wave potential being only $E_{1/2}$ = +0.90 V *vs*. Ag/AgCl (+0.71 V *vs*. SHE).[35]

One aspect is the kinetics of diffusion through the solution medium, characterised by the diffusion coefficient (D). This is obtained through a scan rate dependence study, using the Randles-Sevcik equation. The Randles-Sevcik equation (equation 10) predicts a linear dependance of peak current (i_p) on the square root of the scan rate ($v^{1/2}$).[1,36] Here, n is the number of electrons transferred, A is the area of the electrode, D is the diffusion coefficient and C_i is the concentration. Deviations from linearity indicate i) complications in the kinetics of electron transfer or, ii) chemical changes as a result of electron transfer in solution.[36]

$$i_p = (2.69 \times 10^5) n^{3/2} A D^{1/2} C_i v^{1/2} \quad (10)$$

This equation is in the form $y = mx$, such that a plot of i_p *vs.* $v^{1/2}$ will give:

$$m\,(gradient) = (2.69 \times 10^5) n^{3/2} A D^{1/2} C_i \quad (11)$$

If the WE area is known, rearrangement gives D, the diffusion coefficient:

$$D = \left(\frac{m}{(2.69 \times 10^5) n^{3/2} A C_i}\right)^2 \quad (12)$$

Alternatively, if D is known, rearrangement gives A, the WE surface area:

$$A = \frac{m}{(2.69 \times 10^5) n^{3/2} D^{1/2} C_i} \quad (13)$$

Which yields the WE diameter:

$$d = 2\sqrt{\frac{A}{\pi}} \quad (14)$$

A scan rate dependence study was conducted for ferrocene, in order to validate the CV setups. Unless otherwise stated, measurements were conducted using the same parameters outlined in the General Procedure (10.0 mM concentration of analyte in 0.1 M *n*Bu_4NPF_6/anhydrous, degassed MeCN as solvent), varying the scan rate between 50 mV s^{-1} and 500 mV s^{-1}. For the GlaxoSmithKline CV setup (Figure A7) and using the known WE diameter (d = 1.50 mm), D = 2.50 x 10^{-5} cm^2 s^{-1} is obtained for ferrocene, which is consistent with the literature (D = 2.30 x 10^{-5} cm^2 s^{-1})[37] where both values are measured in 0.1 M *n*Bu_4NPF_6/MeCN. Accordingly, using the literature diffusion coefficient,[37] the calculated WE diameter is d = 1.53 mm, which is consistent with the measured diameter (d = 1.50 mm).

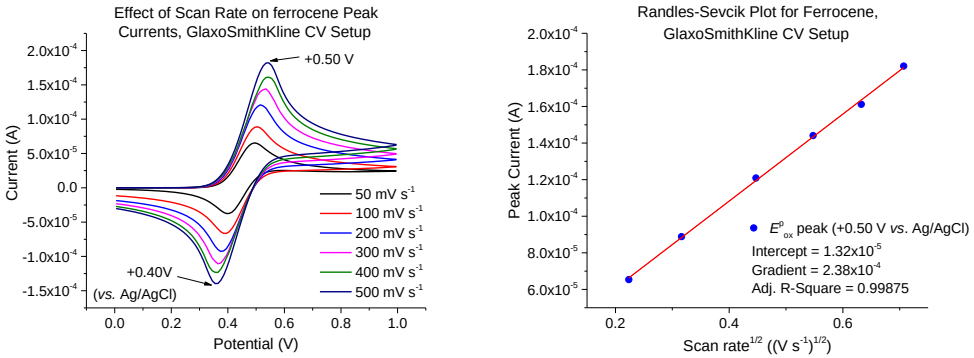

***Figure A7**: Left: Effect of scan rate on ferrocene peak currents for the GlaxoSmithKline CV setup. Right: Randles-Sevcik plot for ferrocene peak currents.*

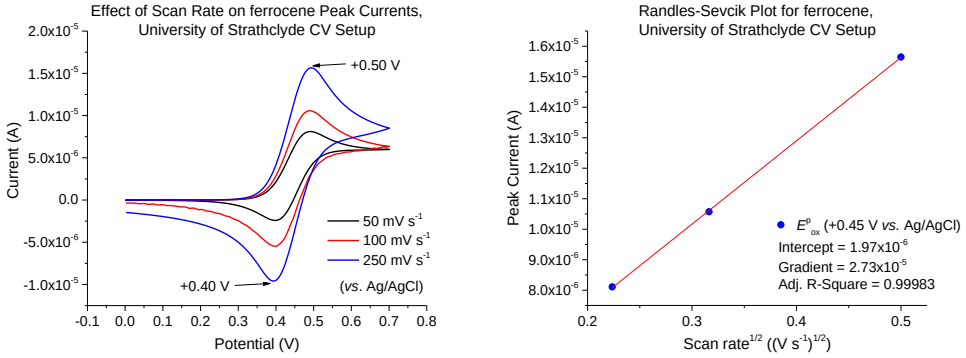

***Figure A8**: Left: Effect of scan rate on ferrocene peak currents for the University of Strathclyde CV setup. Right: Randles-Sevcik plot for ferrocene peak currents.*

For the University of Strathclyde CV setup (Figure A8) and using the known WE diameter (d = 0.50 mm), D = 2.68 x 10^{-5} cm^2 s^{-1} is obtained for ferrocene, which is consistent with the literature[37] where both values are measured in 0.1 M $n$$Bu_4NPF_6$/MeCN. Accordingly, using the literature diffusion coefficient,[37] the calculated WE diameter is d = 0.52 mm, which is consistent with the measured diameter (d = 0.50 mm). Normalised plots of I / $v^{1/2}$ *vs.* V were examined to determine whether the oxidised product (ferrocenium, Fc^+) was involved in any chemical reaction prior to the reverse scan (Figure A9). The data show that, as expected, this was not the case as the shape of the

voltammograms remained unaltered over the scan range examined. It would have been expected from such plots that all the scans should have superimposed but the contribution to the charging of the electrical double layer (depicted in Figure 1, left. The electrode/solution interface behaves essentially as a capacitor; a description of the electrical double layer and its consequences is beyond the scope of this Appendix, readers are referred to other texts)[1,38] is not taken into account in the normalised plots. Overall, these data show strong agreement with the literature data for ferrocene[37] and the measured WE diameters, thereby validating both experimental CV setups. Ultimately, calculations of analyte diffusion coefficients used the calculated WE diameters that were derived from the ferrocene literature diffusion coefficient[37] (1.53 mm and 0.52 mm for the GlaxoSmithKline and University of Strathclyde CV setups, respectively).

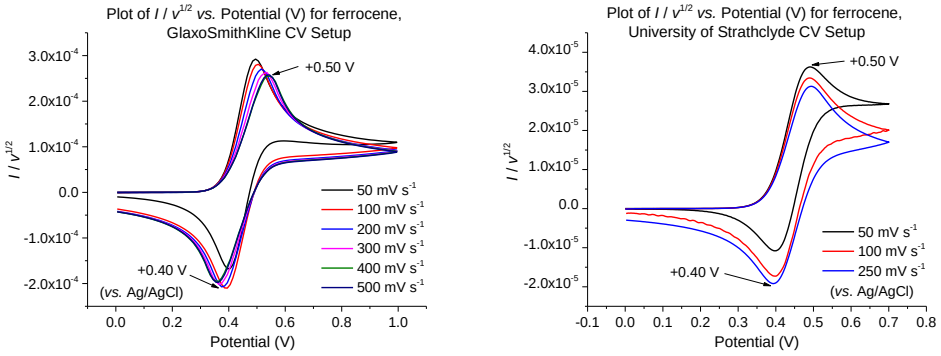

***Figure A9**: Left: Normalised I / $v^{1/2}$ vs. V plot for ferrocene, GlaxoSmithKline CV setup. Right: Normalised I / $v^{1/2}$ vs. V plot for ferrocene, University of Strathclyde CV setup.*

A1.9.2. RANDLES-SEVCIK ANALYSIS OF DEXTROMETHORPHAN AND DIPEA FOR VOLUME 1

Scan rate dependence analyses were performed on dextromethorphan and DIPEA using the University of Strathclyde CV setup, unless otherwise stated (Figures A10 and A11). Using a WE diameter of d = 0.52 mm (derived in Section A1.9.1.), the diffusion coefficients were D = 1.17 x 10^{-5} cm^2 s^{-1} for DIPEA and D = 6.20 x 10^{-6} cm^2 s^{-1} for dextromethorphan. These values were in good agreement with values obtained from the GlaxoSmithKline CV setup (Figure A12 for Randles-Sevcik plots); D = 1.41 x 10^{-5} cm^2 s^{-1} for DIPEA (here, [DIPEA] = 5.0 mM) and D = 7.40 x 10^{-6} cm^2 s^{-1} for dextromethorphan, using a WE diameter of d = 1.53 mm (derived in Section A1.9.1.).

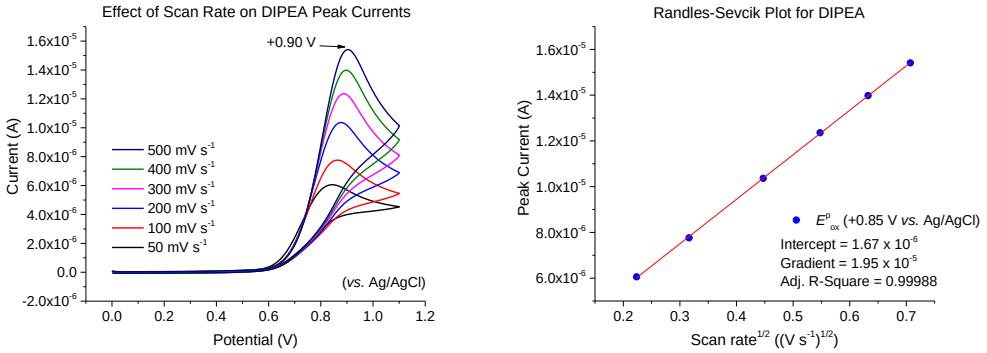

***Figure A10**: Left: Effect of scan rate on DIPEA peak currents. Right: Randles-Sevcik plot for DIPEA peak currents.*

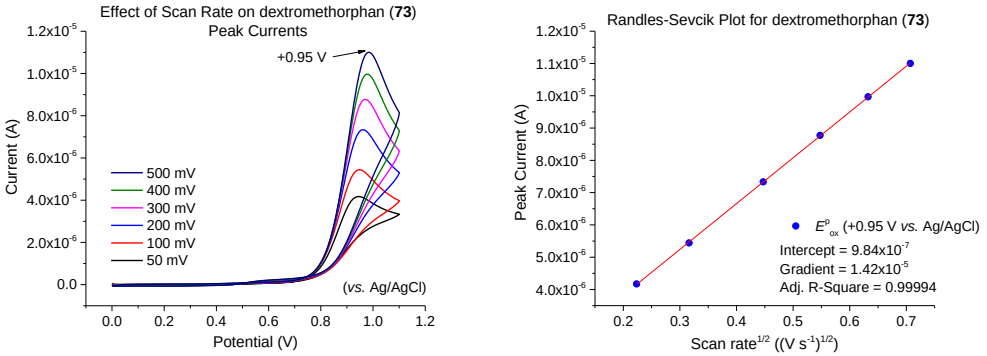

***Figure A11**: Left: Effect of scan rate on dextromethorphan peak currents. Right: Randles-Sevcik plot for dextromethorphan peak currents.*

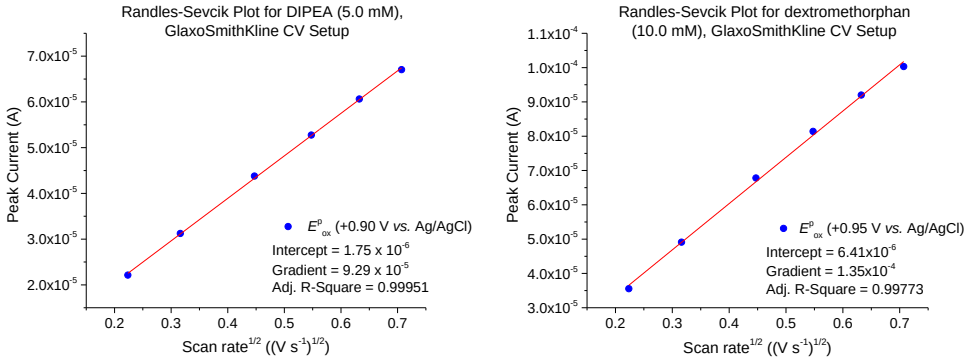

***Figure A12**: Left: Randles-Sevcik plot for dextromethorphan peak currents. Right: Randles-Sevcik plot for DIPEA peak currents. Obtained using the GlaxoSmithKline CV setup.*

A1.9.3. RANDLES-SEVCIK ANALYSIS OF 1,10-PHENANTHROLINE AND DIMER 65 FOR VOLUME 2

Randles-Sevcik analyses of 1,10-phenanthroline and dimer **65** were obtained using the University of Strathclyde CV setup, and are discussed in detail in Volume 2, Experimental, Section 5.2.7. Individual Randles-Sevcik plots are given below (Figures A13, A14 and A15).

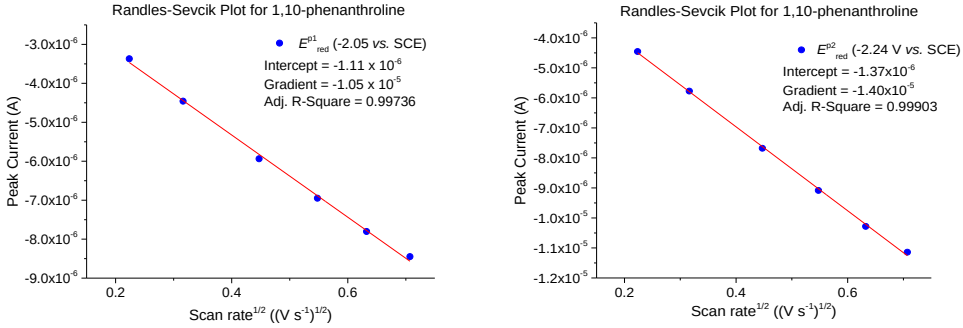

***Figure A13**: Left: Randles-Sevcik plot for 1,10-phenanthroline peak currents of the E^{p}_{red} = -2.05 V peak. Right: Randles-Sevcik plot for 1,10-phenanthroline peak currents of the E^{p}_{red} = -2.24 V peak. Obtained using the University of Strathclyde CV setup.*

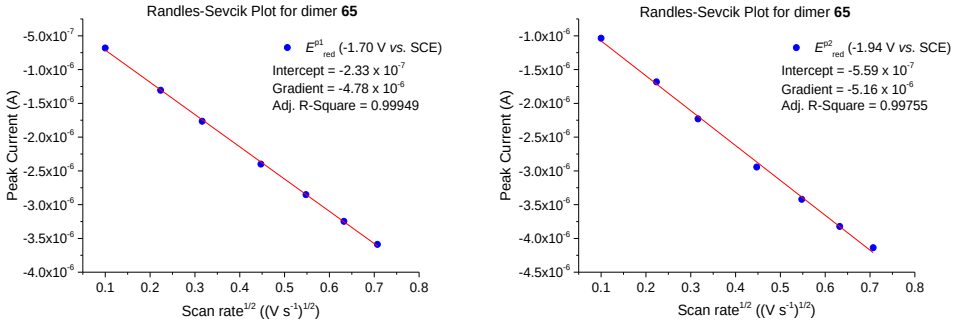

***Figure A14**: Left: Randles-Sevcik plot for dimer **65** peak currents of the E^{p1}_{red} = -1.70 V peak. Right: Randles-Sevcik plot for dimer **65** peak currents of the E^{p2}_{red} = -1.94 V peak. Obtained using the University of Strathclyde CV setup.*

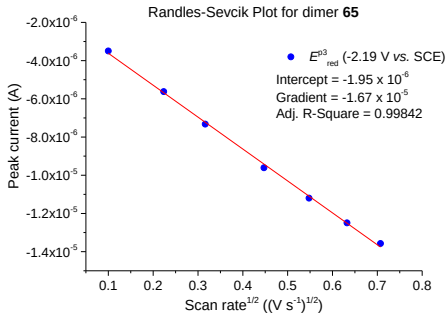

***Figure A15**: Randles-Sevcik plot for dimer **65** peak currents of the E^{p3}_{red} = -2.19 V peak.*

A2. Transmission Spectra of Light Sources

All light sources described in Volume 1 were characterised using an BWTek Exemplar LS CCD spectrometer, equipped with a fibre-optic cable. Raw data were acquired by BWTek BWSpec4 software. For transmission measurements of Vapourtec UV-150 light sources, the Exemplar LS spectrometer was attached to the Vapourtec UV-150 coil *via* fibre optic cable and transmission of light was recorded through the coil in the absence of solvent. Transmission spectra are shown in Figure A16:

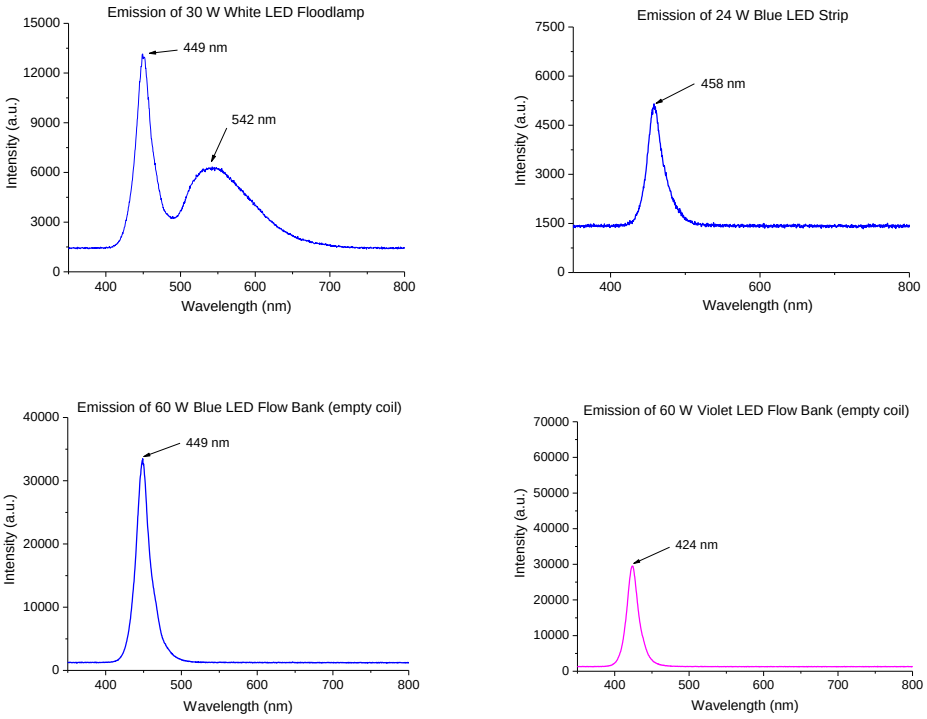

***Figure A16**: Transmission spectra of light sources employed in Volume 1.*

A3. Pictures of Vapourtec UV-150 Flow Reactor Assembly

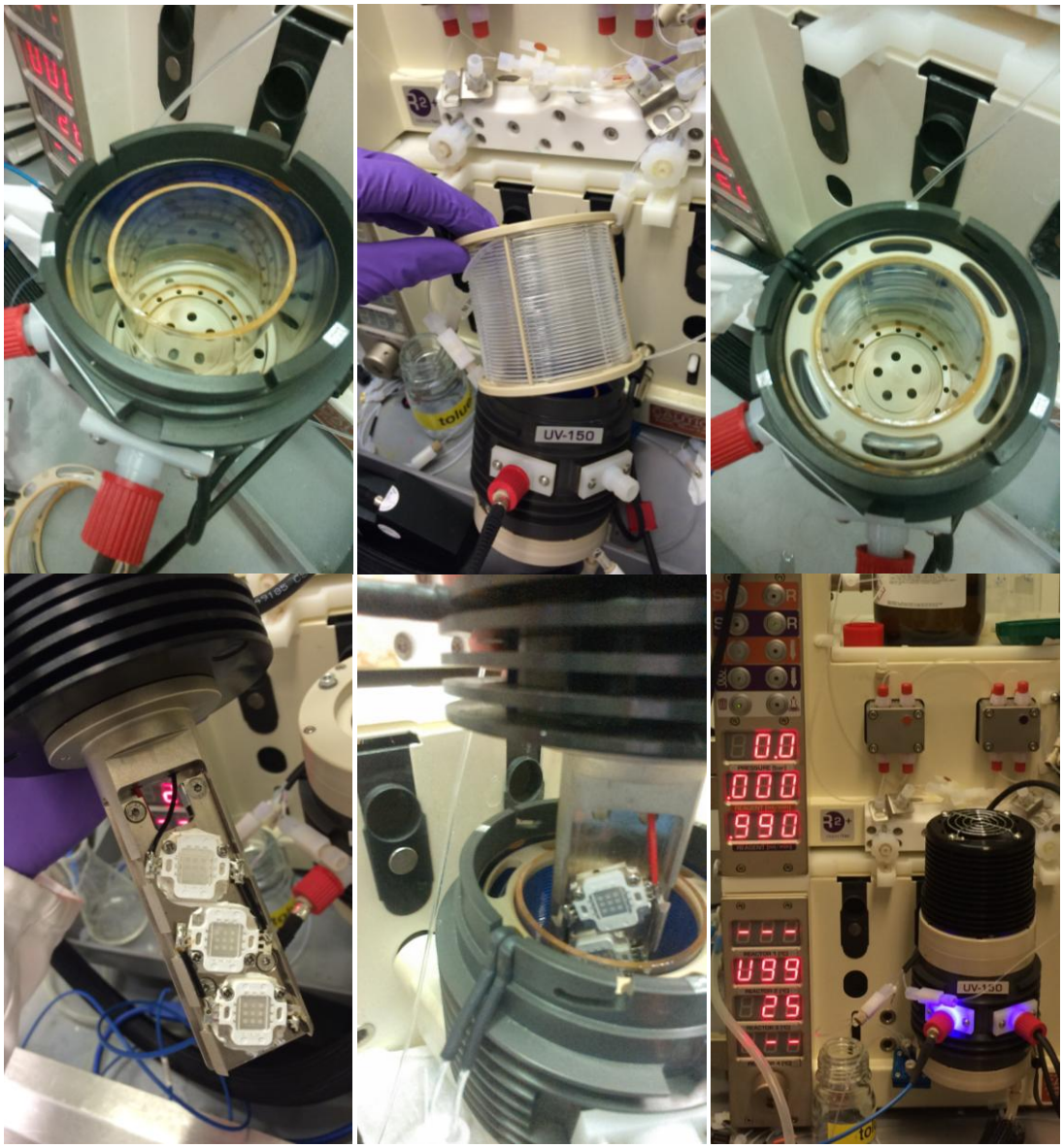

***Figure A17**: Top left: Vapourtec photochemical reactor mirrored cavity fitted with UV-visible transmission spectrometer and temperature probe. Top middle: 10 mL PTFE coil. Top right: 10 mL PTFE coil fitted inside mirrored cavity. Bottom left: LED bank. Bottom middle: LED bank fitted inside the 10 mL PTFE coil, inside the mirrored cavity. Bottom right: Fully assembled and operational Vapourtec UV-150 photochemical flow reactor.*

A4. QUANTUM YIELD DETERMINATION

In order to estimate the photochemical efficiency of the photocatalyst-free reaction shown below (Scheme A2, also see Volume 1, Table 6, entry 12, Section 2.1.6.), quantum yields (ϕ) at 449 nm were calculated by using the transmission spectrometer built in to the Vapourtec UV-150. The optical power (at 449 nm) emitted into the cavity ($P_{emitted}$) is calculated from the known radiant power output and efficiency of the LED at 449 nm, specified by Vapourtec Ltd. as 24 W, 40% efficiency (see Vapourtec UV-150 part number 50-1448).[39]

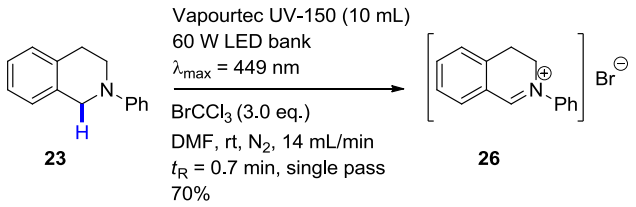

***Scheme A2**: Photoredox catalyst-free photochemical anaerobic iminium salt formation from N-phenyl THIQ (**23**) in flow.*

The photons amounting to this optical power pass through the fluoropolymer coil filled only with solvent, are reflected by the mirrored surface walls of the reactor and bounce around the cavity. Assuming that no photons are 'lost' from the mirrored cavity (it is 100% reflective) and in the absence of the reaction coil, the optical power emitted ($P_{emitted}$) can be assumed equal to the optical power contained within the cavity ($P_{no\ coil}$). Since: $\frac{power\ (P)}{area\ (A)} = intensity\ (I)$, this optical power (W) is directly proportional to the intensity (W/m^2) measured within the cavity ($P_{emitted} \approx P_{no\ coil} \propto I_{no\ coil}$). The intensity is then measured in the presence of the reaction coil filled with solvent only (I_{ref}), in order to relate $P_{emitted} \approx P_{no\ coil}$ (which is known) to P_{ref}

(Since $P_{ref} \propto I_{ref}$, then $\frac{I_{no\ coil}}{I_{ref}} = \frac{P_{no\ coil}}{P_{ref}}$, so $P_{ref} = P_{no\ coil}\frac{I_{ref}}{I_{no\ coil}}$). Here, P_{ref} is the power contained within the cavity containing a reaction coil filled with solvent only. Upon replacing the solvent in the coil with reaction mixture, the intensity is measured (I_{sample}). Since intensity and optical power in the mirrored cavity are decreased by the same factor ($P_{sample} = \frac{I_{ref}}{I_{sample}} P_{ref}$), the power contained within the cavity containing the coil filled with reaction mixture (P_{sample}) can be calculated. Thus, the optical power absorbed by the coil (P_{abs}) can be calculated ($P_{abs} = P_{ref} - P_{sample}$).

By knowing P_{abs}, the number of moles of photons absorbed per unit time can be calculated ($moles\ of\ photons\ absorbed/time = \frac{P_{abs}/h\nu}{N_A}$) and the product moles generated per unit time can be measured. The quantum yield at a given wavelength is:

$$\phi_\lambda = \frac{moles\ of\ product}{moles\ of\ photons\ absorbed} = \frac{moles\ of\ product/time}{moles\ of\ photons\ absorbed/time} \quad (15)$$

The approximation made here is that $P_{emitted} \approx P_{no\ coil}$, but inevitably, $P_{emitted} > P_{no\ coil}$ since the efficiency of photoinsulation of the cavity is unlikely to be 100%. Application of any correction factors which address the approximation $P_{emitted} \approx P_{no\ coil}$ would only serve to determine higher quantum yields and so a minimum threshold for the quantum yield can be calculated.

For the reaction shown in Scheme A2, a 9.91 x 10^{-2} M reaction mixture at a flow rate of 14 mL/min gave a 70% yield of product (a productivity of 9.71 x 10^{-4} mol/min = 0.97 mmol/min). The optical power transmitted into the cavity by the 449 nm LED is 24 W, corresponding to the intensity measured in the absence of the coil ($I_{no\ coil}$). Intensity was measured in the absence and presence of a DMF-filled coil, $\frac{I_{no\ coil}}{I_{ref}}$ = 1.75 (see Figure A18, left), and during the flow of reaction mixture of known concentration $\frac{I_{ref}}{I_{sample}}$ = 1.65 (see Figure A18, right). Similar ratios derive from use of the peak areas.

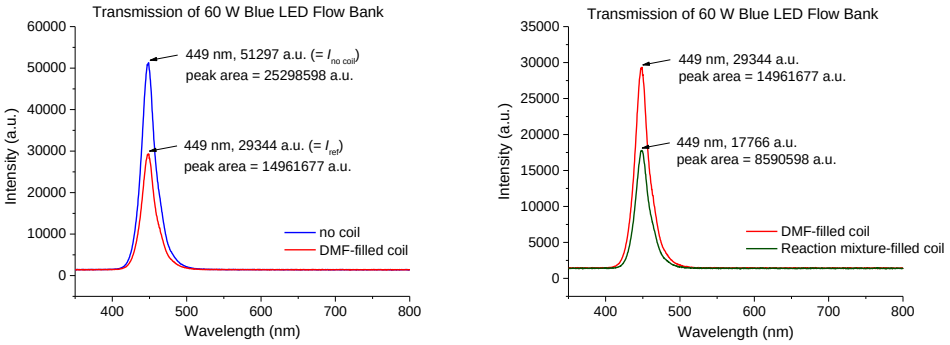

***Figure A18**: Transmission spectra used for quantum yield determination of a photochemical flow reaction.*

Since $P_{ref} = P_{no\ coil}\frac{I_{ref}}{I_{no\ coil}} = 24 \times \frac{1}{1.75} = 13.7$ W, then;

$P_{sample} = \frac{I_{ref}}{I_{sample}}P_{ref} = 13.7 \times \frac{1}{1.65} = 8.3$ W, therefore;

$P_{abs} = P_{ref} - P_{sample} = 13.7 - 8.3 = 5.4$ W.

The number of photons absorbed/time can now be calculated:

$moles\ of\ photons\ absorbed/min = \frac{P_{abs}/h\nu}{N_A} = \frac{5.4/(6.63 \times 10^{-34} \times 6.66 \times 10^{14})}{6.02 \times 10^{23}} \times 60 =$

1.22 x 10^{-3} mol/min = 1.22 mmol/min.

$$\phi_{450\ nm} = \frac{moles\ of\ product/time}{moles\ of\ photons\ absorbed/time} = \frac{0.97\ mmol/min}{1.22\ mmol/min} = 0.80$$

More accurate quantum yield values could be determined by actinometry,[40] but this was deemed unnecessary for the purposes of the investigation in Volume 1. Reactions with known quantum yields could be checked using the method described above to confirm the validity of the calculation method.

A5. ULTRAVIOLET-VISIBLE ABSORPTION SPECTRA

Two UV-visible spectrometers were used, one at the University of Strathclyde and one at GlaxoSmithKline. Apart from the spectra shown in Figure A19, all UV-visible spectra relevant to Volume 1 were collected using a Merck Pharo 100 Spectroquant spectrophotometer at GlaxoSmithKline. All samples were prepared at 1.0 x 10^{-5} M. All UV-visible spectra relevant to Volume 2 were collected using a PerkinElmer Lambda 25 UV/VIS spectrophotometer at the University of Strathclyde. UV-visible spectra showed good consistency between the two spectrometers (for example, $[Ru(bpy)_3]^{2+}$).

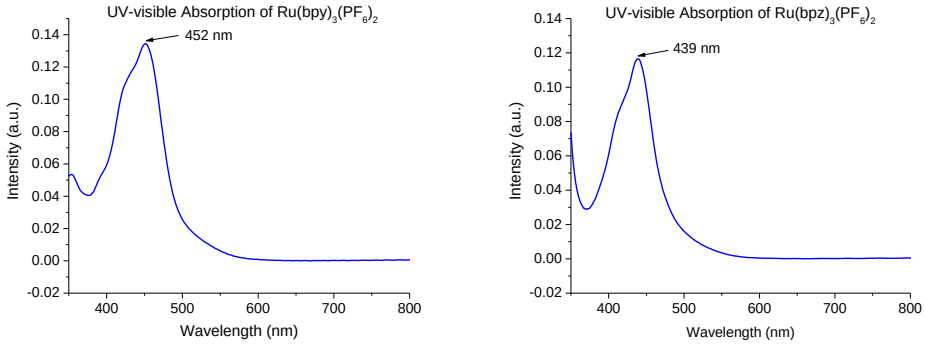

***Figure A19**: Left: UV-visible absorption spectra of $Ru(bpy)_3(PF_6)_2$ in MeCN. Right: UV-visible absorption spectra of $Ru(bpz)_3(PF_6)_2$ in MeCN. Obtained using the University of Strathclyde UV-visible spectrometer.*

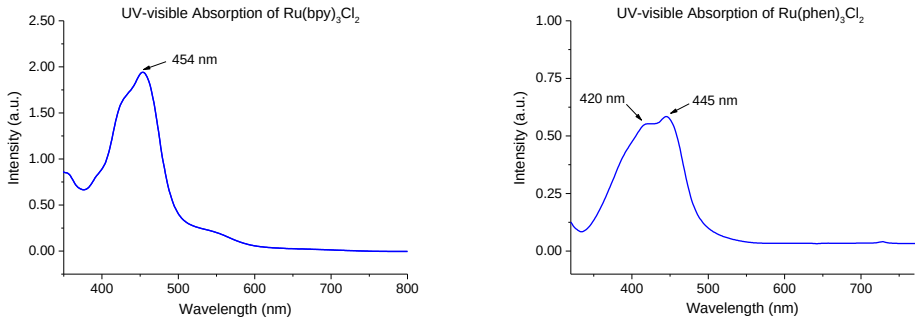

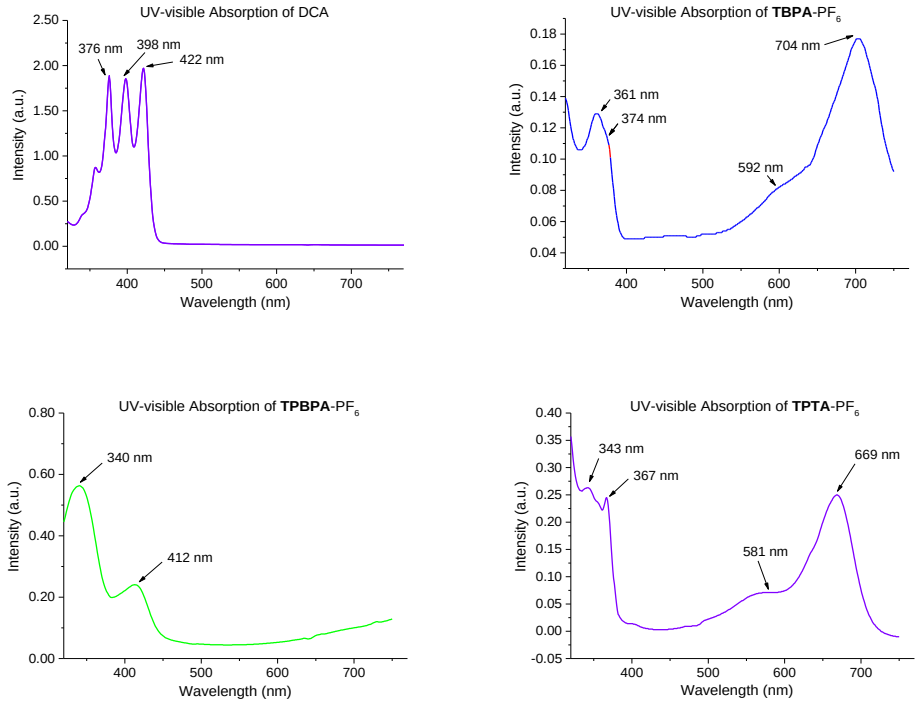

***Figure A20**: UV-visible absorption spectra of various photocatalysts and tri-para-substituted triarylaminium radical cation salts in MeCN. Obtained using the GlaxoSmithKline UV-visible spectrometer.*

A6. LUMINESCENCE QUENCHING

Derivations presented herein are based on (or arrive at) equations presented by Hoffman.[41]

A6.1. STEADY-STATE LUMINESCENCE QUENCHING EXPERIMENTS AND STERN-VOLMER PLOTS

The simplest view of quenching of an electronically excited species (S^*) is its irreversible bimolecular reaction with Q (quencher), governed by the second-order rate constant k_q (Scheme A3).[41] Generation of the excited species is governed by I_a (the rate at which light is absorbed by S) and η^* (the efficiency of population of S^* from the absorption of one photon at the excitation wavelength). Deactivation of S^* by radiative, or non-radiative means is governed by k_0 ($k_0 = k_{rd} + k_{nr} + k_{rx}$, where k_{rd}, k_{nr} and k_{rx} are the rate constants for deactivation by radiative, non-radiative and intramolecular reaction modes, respectively). The rate of change of $[S^*]$ can be set to zero according to the Steady-State Approximation (SSA) (equation 16).

$$S + h\nu \underset{k_0}{\overset{I_a\eta^*}{\Longleftrightarrow\!\Longrightarrow}} S^* + Q \xrightarrow{k_q} P$$

Scheme A3*: Simple bimolecular quenching model.*

$$\frac{d[S^*]}{dt} = I_a\eta^*[S][h\nu] - k_0[S^*] - k_q[S^*][Q] = 0 \text{ (SSA)} \quad (16)$$

Therefore: $[S^*] = I_a\eta^*[S][h\nu]/(k_0 + k_q[Q])$ (17)

The quantum yield for luminescence (ϕ_{lum}) is defined by:

$$\phi_{lum} = k_0[S^*]/I_a\eta[S][h\nu] \quad (18)$$

Combining the two equations above gives: $\phi_{lum} = k_0/(k_0 + k_q[Q])$ (19)

For $[Q] = 0, {\phi_{lum}}^0 = 1$. The fraction of luminescence quantum yield without quenching (${\phi_{lum}}^0$) over the luminescence quantum yield with quenching (ϕ_{lum}) is represented by the corresponding fraction of intensities (I^0/I) or, the Stern-Volmer equation (equation 20):

$${\phi_{lum}}^0/\phi_{lum} = I^0/I = (k_0 + k_q[Q])/k_0 = 1 + (k_q/k_0)[Q] = 1 + k_q\tau^0[Q] \quad (20)$$

where the lifetime $\tau^0 = 1/k_0$. It follows that the intensities (I) of a number of samples containing different $[Q]$ can be measured and a plot of $(I^0/I) - 1$ *vs*. $[Q]$ predicts a straight line with gradient $k_q\tau^0$.[41] If the lifetime (τ) is known, the quenching rate constant k_q can be calculated. Assuming quenching according to Scheme A3, the same Stern-Volmer equation can be derived by defining the lifetime (τ) of S^* in the presence of quencher Q as:

$$\tau = 1/(k_0 + k_q[Q]) \quad (21)$$

The corresponding Stern-Volmer equation results:

$$\tau^0/\tau = 1 + (k_q/k_0)[Q] = I^0/I \quad (22)$$

A6.2. Considerations for Luminescent Precursor Complexes under Steady-state

However, when considering the microscopic details of quenching, reversible diffusion of S^* and Q together to form $\{S^* - Q\}$ (a *precursor complex*) can occur governed by rate constants k_d and k_{-d}. Unimolecular deactivation of $\{S^* - Q\}$ is governed by rate constant k_{de} (Scheme A4).

$$S + h\nu \underset{k_0}{\Longleftarrow} \overset{I_a\eta^*}{\Longrightarrow} S^* + Q \underset{k_{-d}}{\Longleftarrow} \overset{k_d}{\Longrightarrow} \{S^* - Q\} \overset{k_{de}}{\longrightarrow} P$$

Scheme A4*: Reversible formation and irreversible deactivation of a precursor complex.*

In this case the quantum yield ϕ must express contributions of both S^* and $S^* - Q$ to luminescence. It can be defined by equation 23:

$$\phi = (k_0[S^*] + k_0\gamma[\{S^* - Q\}])/I_a\eta^*[S][h\nu] \quad (23)$$

where γ represents the ratios of intensity of emission at the selected wavelength and under the entire emission band for S^* and $\{S^* - Q\}$, respectively.[41]

Therefore: $\phi^0/\phi = I^0/I = \tau^0/\tau = \left[1 + \left(\frac{k_{de}k_d[Q]}{k_0(k_{-d}+k_{de})}\right)\right]/\left[1 + \gamma\left(\frac{k_d[Q]}{k_{-d}+k_{de}}\right)\right]$ (24)

The denominator in equation 24 will result in negative deviation from linearity. The plot reaches a plateau for $[Q] \to \infty$, $I^0/I = k_{de}/\gamma\, k_0$. If $\gamma = 0$ (no emission from $\{S^* - Q\}$), equation 24 reduces to equation 20 *via* equations 25 and 26.

$$I^0/I = 1 + (k_{de}k_d[Q]/k_0(k_{-d} + k_{de})) \quad (25)$$

$$k_q = k_d k_{de}/(k_{-d} + k_{de}) \quad (26)$$

A6.3. Advantages Presented by Time-resolved Lifetime Spectroscopy Techniques

Steady-state emission spectroscopy provides intensity information over a spectrum of wavelengths but cannot resolve whether or not the broad emission bands result from multiple emitters in the system. Time-resolved (lifetime) measurements can provide more detail around the physical mechanism of quenching (for example, precursor complexes, see Chapter A6.6) but only collect data at a specified wavelength. However, this specified wavelength can be easily changed to acquire information across a spectrum of wavelengths.

Steady-state emission spectroscopy is dependent on the concentration of the photocatalyst because the measured variable is emission intensity, dependent on $[S^*]$. This can lead to issues. Firstly, absolute intensity data is

generally irreproducible between sample sets and between spectrometers. Different spectrometers use different emission detectors, units of intensity and correction factors. Moreover, broad excitation sources and detector performance can vary with day-to-day use. Therefore, intensity ratios and correlations are needed to compare data. Secondly, Stern-Volmer plots require several samples at different concentrations to evaulate a single quencher, and the associated time investment for sample preparation and degassing.

Finally, for phosphorescence which is a 'spin-forbidden' process, measured intensities are fundamentally low. Experimental error (for example, fluctuations in the gas flow rate of the degasser setup) can influence the intensity and sometimes be even more pronounced than the influence of quenching, especially for poor quenchers. However, since τ is independent of $[S^*]$,† time-resolved lifetime measurements are comparable for a range of $[S]$ provided that *the same relative excess of quencher is employed*.

A6.4. Lifetime Measurements: Time-correlated Single Photon Counting

Lifetime measurements are achieved by Time-correlated Single Photon Counting (TCSPC) spectroscopy. TCSPC irradiates the sample with an ultrafast (nanosecond) excitation pulse such that the system is not allowed to reach steady-state. As soon as the pulse ends, the photon count decreases exponentially as luminescence occurs (Figure A21). The decay is fitted by HORIBA Scientific Decay Analysis Software (DAS6) with a mathematical function (for example, of the form: $A + Be^{(-k/T)}$ for a monoexponential decay) which calculates the lifetime of the excited state. To derive this behaviour mathematically, the model described in Scheme A4 will be used.

†This is generally true at the concentration regimes of photocatalyst typically employed in luminescence quenching studies (μM to mM). However, at high (mM to M) concentrations, photocatalyst-photocatalyst interactions such as collision and an assortment of energy transfer mechanisms will change the lifetime).

When luminescence measurements are performed under pulsed laser irradiation, the system cannot reach steady-state. Therefore, $\frac{d[S^*]}{dt} \neq 0$ and $\frac{d[\{S^*-Q\}]}{dt} \neq 0$; the concentrations of $[S^*]$ and $[\{S^* - Q\}]$ are time-dependent and are described by equations 27 and 28.[41]

$$\frac{d[S^*]}{dt} = k_{-d}[\{S^* - Q\}] - (k_0 + k_d[Q])[S^*] \quad (27)$$

$$\frac{d[\{S^*-Q\}]}{dt} = k_d[S^*][Q] - (k_{-d} + k_{de})[\{S^* - Q\}] \quad (28)$$

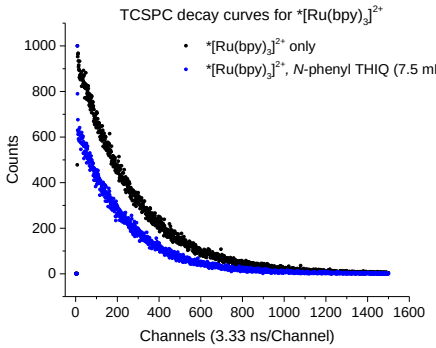

***Figure A21**: TCSPC decay curves of Ru(bpy)$_3^{2+}$ only, and with N-phenyl THIQ present following the excitation pulse.*

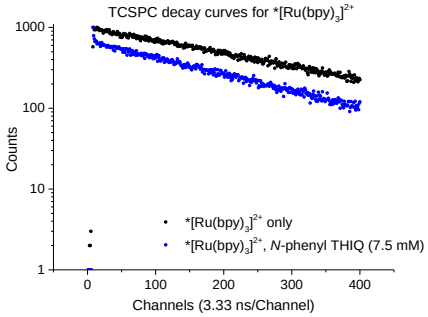

***Figure A22**: TCSPC decay curves of Ru(bpy)$_3^{2+}$ only, and with N-phenyl THIQ present following the excitation pulse (Log$_{10}$ scale used on the y axis).*

Since the system is irradiated with an ultrafast laser pulse, the initial conditions (equation 29) can be applied and used to solve coupled differential equations 27 and 28.

$[S^*] = [S^*]_0$ at $t = 0$ and $[S^* - Q] = 0$ at $t = 0$ (29)

To do this, the following labels will be used:

$[S^*] = y$ and $[S^*]_0 = y_0$ at $t = 0$

$[S^* - Q] = x$ and $[S^* - Q]_0 = x_0 = 0$ at $t = 0$

$\alpha = k_{-d}$

$\beta = k_{rd} + k_{nr} + k_{rx} + k_d[Q] = k_0 + k_d[Q]$

$\gamma = k_d[Q]$

$\omega = k_{-d} + k_{de}$

During the decay, equations 27 and 28 apply and can be written:

$$\frac{d[S^*]}{dt} = k_{-d}[\{S^* - Q\}] - (k_0 + k_d[Q])[S^*] = \frac{dy}{dt} = \alpha x - \beta y \quad (30)$$

$$\frac{d[\{S^* - Q\}]}{dt} = k_d[S^*][Q] - (k_{-d} + k_{de})[\{S^* - Q\}] = \frac{dx}{dt} = \gamma y - \omega x \quad (31)$$

Making x the subject of equation 30 gives equation 32:

$$x = \frac{1}{\alpha}\left(\frac{dy}{dt} + \beta y\right) \quad (32)$$

Substituting into equation 31 gives:

$$\frac{1}{\alpha}\frac{d}{dt}\left[\frac{dy}{dt} + \beta y\right] = \gamma y - \frac{\omega}{\alpha}\left[\frac{dy}{dt} + \beta y\right] \quad (33)$$

Multiplying both sides by α, collecting all terms and collecting all terms = 0 gives:

$$\frac{d^2y}{dt^2} + (\beta + \omega)\frac{dy}{dt} + y(\omega\beta - \alpha\gamma) = 0 \quad (34)$$

This is a second order differential equation to which the following auxiliary equation can be applied:

$$ax^2 + bx + c = 0 \quad (35)$$

The quadratic equation has two solutions (labelled m_1 and m_2) given by: $\frac{-b\pm\sqrt{b^2-4ac}}{2a}$, therefore:

$$m_1 = \frac{-(\beta+\omega)+\sqrt{(\beta+\omega)^2-4(\omega\beta-\alpha\gamma)}}{2} \quad (36)$$

$$m_2 = \frac{-(\beta+\omega)-\sqrt{(\beta+\omega)^2-4(\omega\beta-\alpha\gamma)}}{2} \quad (37)$$

Label the square root term = R:

$$R = (\beta+\omega)^2 - 4(\omega\beta-\alpha\gamma)$$

Expanding the labels gives:

$$R = (k_0 + k_{de} + k_{-d} + k_d[Q])^2 - 4[(k_{-d}+k_{de})(k_0+k_d[Q]) - k_{-d}k_d[Q] \quad (38)$$

Expanding the quadratic gives:

$$R = (k_0 + k_{de} + k_{-d} + k_d[Q])^2 - 4(k_0k_{-d} + k_0k_{de} + k_{de}k_d[Q]) \quad (39)$$

Equation 36 and equation 37 become equation 40 and equation 41, respectively:

$$m_1 = \frac{1}{2}(k_0 + k_{de} + k_{-d} + k_d[Q]) + \frac{1}{2}\sqrt{R} \quad (40)$$

$$m_2 = \frac{1}{2}(k_0 + k_{de} + k_{-d} + k_d[Q]) - \frac{1}{2}\sqrt{R} \quad (41)$$

Equations 39, 40 and 41 from this derivation are consistent with the equations stated in the literature (see equation 30 reported therein).[41]

The solution to the homogenous problem in equation 34 is given by:

$$y = Ae^{-(root1)t} + Be^{-(root2)t} = Ae^{-m_1t} + Be^{-m_2t} \quad (42)$$

Pre-exponentials A and B can be identified using the initial conditions. Equation 42 becomes equation 43:

$$y_0 = A + B \quad (43)$$

Equation 42 can be substituted into equation 30:

$$\frac{d}{dt}[Ae^{-m_1 t} + Be^{-m_2 t}] = \alpha x - \beta y \quad (44)$$

Differentiating and rearranging for y terms gives:

$$-m_1 Ae^{-m_1 t} - m_2 Be^{-m_2 t} - \alpha x = -\beta y \quad (45)$$

At $t = 0$: $y = y_0$, $x = x_0 = 0$ and $e^{-0} = 1$ therefore:

$$\beta y_0 = m_1 A + m_2 B \quad (46)$$

Equation 46 and equation 43 can now be solved as simultaneous equations to find A and B. Multiplication of equation 43 by m_1 gives:

$$m_1 y_0 = m_1 A + m_1 B \quad (47)$$

Subtracting equation 46 from equation 47 gives:

$$m_1 y_0 - \beta y_0 = m_1 B - m_2 B \quad (48)$$

Therefore, $B = y_0 \frac{(m_1 - \beta)}{m_1 - m_2}$ (49)

Similarly, multiplication of equation 43 by m_2 gives:

$$m_2 y_0 = m_2 A + m_2 B \quad (50)$$

Subtracting equation 52 from equation 48 gives:

$$\beta y_0 - m_2 y_0 = m_1 A - m_2 A \quad (51)$$

Therefore, $A = y_0 \frac{(\beta - m_2)}{m_1 - m_2}$ (52)

Substituting equation 49 and equation 52 into equation 42 gives:

$$y = y_0[\frac{(\beta - m_2)}{(m_1 - m_2)} e^{-m_1 t} + \frac{(m_1 - \beta)}{(m_1 - m_2)} e^{-m_2 t}] \quad (53)$$

Labelling the pre-exponentials as C_1 and C_2 and expanding the other labels gives:

$$[S^*] = [S^*]_0[C_1e^{-m_1t} + C_2e^{-m_2t}] \quad (54)$$

Equation 54 from this derivation is consistent with the equation stated in the literature (see equation 28 reported therein).[41]

An expression for x can now be derived by substituting equation 53 into equation 32:

$$x = \frac{y_0}{\alpha}\left[\left[C_1\frac{d}{dt}e^{-m_1t} + C_2\frac{d}{dt}e^{-m_2t}\right] + \beta(C_1e^{-m_1t} + C_2e^{-m_2t})\right] \quad (55)$$

Multiplication of both sides by α, division of both sides by y_0 and differentiation of the exponential terms gives:

$$\frac{\alpha x}{y_0} = -m_1C_1e^{-m_1t} - m_2C_2e^{-m_2t} + \beta C_1e^{-m_1t} + \beta C_2e^{-m_2t} \quad (56)$$

Collecting terms gives:

$$\frac{\alpha x}{y_0} = [(\beta - m_2)C_2]e^{-m_2t} - [(m_1 - \beta)C_1]e^{-m_1t} \quad (57)$$

Substituting in C_1 and C_2 gives:

$$\frac{\alpha x}{y_0} = \left[\frac{(\beta - m_2)(m_1 - \beta)}{(m_1 - m_2)}\right]e^{-m_2t} - \left[\frac{(\beta - m_2)(m_1 - \beta)}{(m_1 - m_2)}\right]e^{-m_1t} \quad (58)$$

Collecting terms gives:

$$x = y_0\left[\frac{(\beta - m_2)(m_1 - \beta)}{\alpha(m_1 - m_2)}\right][e^{-m_2t} - e^{-m_1t}] \quad (59)$$

Expanding the labels x, y_0, α and β gives:

$$[S^* - Q] = [S^*]_0\left[\frac{(k_0 + k_d[Q] - m_2)(m_1 - k_0 - k_d[Q])}{k_{-d}(m_1 - m_2)}\right][e^{-m_2t} - e^{-m_1t}] \quad (60)$$

Labelling the pre-exponential as C_3 gives:

$$[S^* - Q] = C_3[S^*]_0[e^{-m_2t} - e^{-m_1t}] \quad (61)$$

Equation 61 is consistent with an equation reported in a literature derivation (see equation 29 reported therein).[41]

However, if one wishes to measure samples every minute the number of photon counts in TCSPC has to be kept low (1000) and resolution suffers. Microsecond Multi-Channel Scaling (MCS) mode is more appropriate to measure quenching of the $^3MLCT_1$ state, because >10000 counts can be achieved per minute, albeit at the compromise of less time resolution. During the microsecond-range excitation pulse (between 500 and 2500 channels) the photon count peak reaches a steady-state (Figure A23).

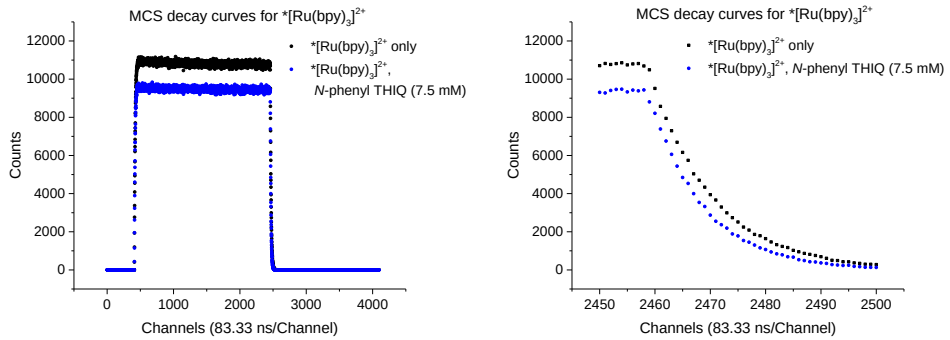

***Figure A23**: Left: MCS decay curves of excited state $Ru(bpy)_3^{2+}$ only and with N-phenyl THIQ (7.5 mM) following the excitation pulse. Right: Expanded decay curves.*

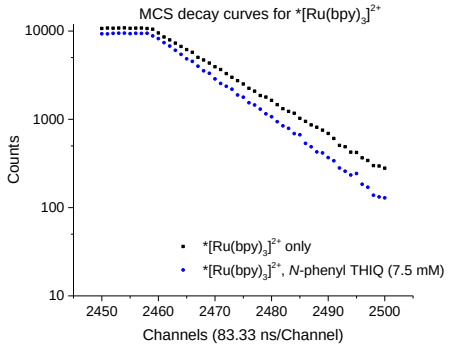

***Figure A24**: MCS decay curves of excited state $Ru(bpy)_3^{2+}$ only and with N-phenyl THIQ (7.5 mM) following the excitation pulse (Log_{10} scale used on the y axis).*

As soon as the pulse ends, the photon count decreases according to one or more exponential decay functions as luminescence occurs and the lifetime is obtained from the decay analysis software (DAS6). To model this mathematically, the model described in Scheme A4 will be used. Here, different initial conditions must be applied to solve equations 27 and 28, since the system is at steady state before the decay.

$[S^*] = [S^*]_0$ at $t = 0$ and $[S^* - Q] = [S^* - Q]_0 \neq 0$ at $t = 0$ (62)

$$\frac{d[S^*]}{dt} = k_{-d}[\{S^* - Q\}] - (k_0 + k_d[Q])[S^*] \quad (27)$$

$$\frac{d[\{S^* - Q\}]}{dt} = k_d[S^*][Q] - (k_{-d} + k_{de})[\{S^* - Q\}] \quad (28)$$

During the decay, equation 27 and equation 28 *still* apply. Therefore, equation 42 still applies since initial conditions are not applied until elucidation of the pre-exponentials A and B.

$$y = Ae^{-m_1 t} + Be^{-m_2 t} \quad (42)$$

As before in Chapter A6.4, at $t = 0$ equation 43 and equation 45 still apply:

$$y_0 = A + B \quad (43)$$

$$-m_1 Ae^{-m_1 t} - m_2 Be^{-m_2 t} - \alpha x = -\beta y \quad (45)$$

Initial conditions were described on the previous page. At $t = 0$, $y = y_0$, $x = x_0 \neq 0$ and $e^{-0} = 1$. Applying these initial conditions to equation 45 gives equation 63:

$$\beta y_0 = m_1 A + m_2 B + \alpha x_0 \quad (63)$$

As in Chapter A6.4., equation 47 and equation 50 are generated by multiplying equation 43 by m_1 or by m_2:

$$m_1 y_0 = m_1 A + m_1 B \quad (47)$$

$$m_2 y_0 = m_2 A + m_2 B \quad (50)$$

Subtracting equation 63 from equation 47 gives:

$$m_1 y_0 - \beta y_0 = m_1 B - m_2 B - \alpha x_0 \quad (64)$$

Therefore, $B = \frac{y_0(m_1-\beta)+\alpha x_0}{(m_1-m_2)}$ (65)

Subtracting equation 50 from equation 63 gives:

$$\beta y_0 - m_2 y_0 = \alpha x_0 + m_1 A - m_2 A \quad (66)$$

Therefore, $A = \frac{y_0(\beta-m_2)-\alpha x_0}{(m_1-m_2)}$ (67)

Substituting A and B in to equation 42 gives:

$$y = \frac{y_0(\beta-m_2)-\alpha x_0}{(m_1-m_2)}[e^{-m_1 t}] + \frac{y_0(m_1-\beta)+\alpha x_0}{(m_1-m_2)}[e^{-m_2 t}] \quad (68)$$

Substituting equation 68 into equation 30 gives:

$$\alpha x = \left[\frac{y_0(\beta-m_2)-\alpha x_0}{(m_1-m_2)}\right]\frac{d}{dt}[e^{-m_1 t}] + \left[\frac{y_0(m_1-\beta)+\alpha x_0}{(m_1-m_2)}\right]\frac{d}{dt}[e^{-m_2 t}] + \beta y \quad (69)$$

Differentiation gives:

$$\alpha x = -m_2\left[\frac{y_0(m_1-\beta)+\alpha x_0}{(m_1-m_2)}\right]e^{-m_2 t} - m_1\left[\frac{y_0(\beta-m_2)-\alpha x_0}{(m_1-m_2)}\right]e^{-m_1 t} + \beta\left[\frac{y_0(\beta-m_2)-\alpha x_0}{(m_1-m_2)}\right]e^{-m_1 t} + \beta\left[\frac{y_0(m_1-\beta)+\alpha x_0}{(m_1-m_2)}\right]e^{-m_2 t} + \beta\left[\frac{y_0(\beta-m_2)-\alpha x_0}{(m_1-m_2)}\right]e^{-m_1 t} + \beta\left[\frac{y_0(m_1-\beta)+\alpha x_0}{(m_1-m_2)}\right]e^{-m_2 t} \quad (70)$$

Collection of terms gives:

$$\alpha x = e^{-m_2 t}\left[\frac{\beta y_0(m_1-\beta)+\alpha\beta x_0-m_2 y_0(m_1-\beta)-m_2\alpha x_0}{(m_1-m_2)}\right] - e^{-m_1 t}\left[\frac{m_1 y_0(\beta-m_2)-m_1\alpha x_0-\beta y_0(\beta-m_2)+\alpha\beta x_0}{(m_1-m_2)}\right] \quad (71)$$

Rearranging for x gives equation 72 (see next page).

$$x = \left[\frac{-y_0\beta^2+(m_1y_0+m_2y_0+\alpha x_0)\beta-m_2(m_1y_0+\alpha x_0)}{\alpha(m_1-m_2)}\right]e^{-m_2t} - \left[\frac{-y_0\beta^2+(m_1y_0+m_2y_0+\alpha x_0)\beta-m_1(m_2y_0+\alpha x_0)}{\alpha(m_1-m_2)}\right]e^{-m_1t} \quad (72)$$

Applying the initial conditions to equation 30 gives:

$$\frac{dy}{dt} = \alpha x_0 - \beta y_0 = 0 \quad (73)$$

Therefore: $\alpha x_0 = \beta y_0$. Now, equation 72 is simplified to equation 74:

$$x = y_0\left[\frac{m_1(\beta-m_2)}{(m_1-m_2)}\right]e^{-m_2t} - y_0\left[\frac{m_2(\beta-m_1)}{(m_1-m_2)}\right]e^{-m_1t} \quad (74)$$

Labelling the pre-exponentials as C_3 and C_4 and expanding labels x, y and β gives:

$$[S^* - Q] = C_3[S^*]_0e^{-m_2t} - C_4[S^*]_0e^{-m_1t} \quad (75)$$

Given equation 73, equation 68 becomes:

$$y = y_0\left[\frac{-m_2}{(m_1-m_2)}\right]e^{-m_1t} + y_0\left[\frac{m_1}{(m_1-m_2)}\right]e^{-m_2t} \quad (76)$$

And labelling the pre-exponentials in equation 76 gives the corresponding 'y' expression: $[S^*] = C_1[S^*]_0e^{-m_1t} - C_2[S^*]_0e^{-m_2t}$ (77)

In most cases, m_1 (the faster decay component) can not be observed because it occurs within times too short relative to the resolution of the apparatus.[41] Therefore, the lifetime (τ' , measured by time-resolved luminescence quenching) is derived by:

$$\tau' = \frac{1}{m_2} \quad (78)$$

Equations 41 and 39 are reproduced here as a reminder:

$$m_2 = \frac{1}{2}(k_0 + k_{de} + k_{-d} + k_d[Q]) - \frac{1}{2}\sqrt{R} \quad (41)$$

$$R = (k_0 + k_{de} + k_{-d} + k_d[Q])^2 - 4(k_0k_{-d} + k_0k_{de} + k_{de}k_d[Q]) \quad (39)$$

A6.6. Comparison of Steady-state with Time-resolved Luminescence Quenching

The lifetime predicted by time-resolved methods was derived and given by equation 78:

$$\tau' = \frac{1}{m_2} \tag{78}$$

This contrasts to the lifetime predicted by the Stern-Volmer equation (τ) (see Chapter A6.1.), reproduced here as equation 21. Equation 22 shows the corresponding Stern-Volmer equation).

$$\tau = 1/(k_0 + k_q[Q]) \tag{21}$$

$$I^0/I = \tau^0/\tau = 1 + (k_q/k_0)[Q] \tag{22}$$

The assumption made in the Stern-Volmer is that the ratio of intensities I^0/I equals the ratio of lifetimes τ^0/τ, but this does not always hold (for example, if static quenching occurs).[42] Based on the discussion in Chapter A.3., it is proposed herein that directly measuring observed lifetimes is likely to be much more accurate than calculating them based on intensity measurements. Discussions of the comparison of measured τ' (time-resolved) and calculated τ (steady-state) are beyond the scope of this Thesis Appendix, the reader is directed to the following references.[43,44] Regardless of subtle differences between methods, both Stern-Volmer plots and time-resolved lifetime measurements can and have been successfully used to compare different excited state quenchers.

A6.6.1. Relationship Between Measured Lifetimes and Lifetimes Calculated by k_q.

There is generally good agreement between the measured lifetime τ' from time-resolved luminescence quenching and the lifetime τ calculated from the Stern-Volmer equation using k_q (equation 21) for a range of quenchers (Table A4 and Figure A25). For a literature example comparing k_q (measured

by Stern-Volmer plots) and k_q' (predicted by lifetimes measured by time-resolved methods), see the following reference.[45]

***Table A4**: Predicted vs. Measured τ for *[Ru(bpy)$_3$]$^{2+}$ in the Presence of Various Quenchers.*

Entry	Quencher	k_q[a]	[Q] /mM	τ (ns) measured	τ (ns)[b] calculated
1	-	-	-	977[c]	0.0
2	O_2	2.84 x 10^9	1.7	237[d]	189
3	O_2	2.84 x 10^9	8.1	112[d]	45
4	DIPEA	7.15 x 10^6	7.5	956[d]	928
5	DIPEA	7.15 x 10^6	37.5	733[e,f]	774
6	DIPEA	7.15 x 10^6	75.0	650[e,f]	641
7	*N*-phenyl THIQ	5.65 x 10^7	7.5	853	691
8	*N*-phenyl THIQ	5.65 x 10^7	75.0	205	190
8	4-methoxy-N-N-diphenylamine	3.48 x 10^8	7.5	269[e,f]	275
19	*N*,*N*-dimethylaniline	1.13 x 10^8	7.5	571[d,e]	534
110	DABCO	1.43 x 10^8	7.5	447	477
111	tri-*p*-tolylamine	5.57 x 10^8	7.5	228	192

The concentration of Ru(bpy)$_3$(PF$_6$)$_2$ was 10.0 μM. [a]Lifetimes are calibrated to *[Ru(bpy)$_3$]$^{2+}$ as an external standard, run before and after a set of samples to ensure consistency. For comparisons to literature lifetimes of *[Ru(bpy)$_3$]$^{2+}$ under Ar (τ^0), see Chapter A6.7. [b]Calculated by the Stern-Volmer equation. [c]Average of six samples. [d]Average of two samples. [e]Measurement was conducted by Katie Emery at the University of Strathclyde. [f]Average of three samples.

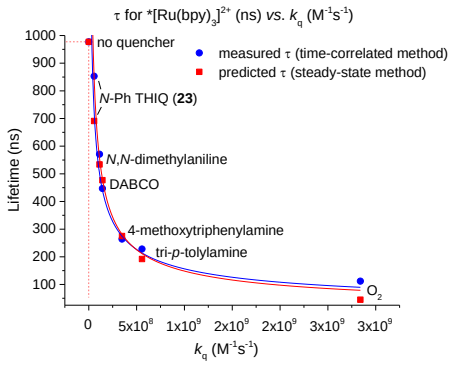

***Figure A25**: Blue: Relationship between k_q measured by Stern-Volmer plots vs. $\boldsymbol{\tau}'$ measured by time-resolved MCS for *Ru(bpy)$_3^{2+}$. Red: Relationship between k_q measured by Stern-Volmer plots vs. $\boldsymbol{\tau}$ calculated from the Stern-Volmer equation.*

A6.6.2. Evidence for a Precursor Complex Detected by MCS

MCS decay curves observed for samples containing $[Ru(bpy)_3]^{2+}$ only, $[Ru(bpz)_3]^{2+}$ only, and most added quencher combinations fitted well to one exponential. An indication of $\{S^* - Q\}$ was detected by TCSPC (Figure A22) for *N*-phenyl THIQ, but was not observed by MCS (Figure A24), which has lower time resolution. Thus, the contribution is small and the observed lifetime $\tau_{obs} \approx \tau_{[S^*]}$. However, dextromethorphan (**73**) quenched *$[Ru(bpz)_3]^{2+}$ so strongly that even the less time-resolved MCS decay curve could detect $\{S^* - Q\}$; two exponentials were required to fit the data (Figure A26). This is indicative of two lifetimes; for S^* and one for $\{S^* - Q\}$ as predicted by Scheme A4. The two decays coinciding meant that τ could not be determined accurately for S^* (or $\{S^* - Q\}$), but a weighted average of τ = 198 ns was determined for the decay. The ability to access such resolution demonstrates the power of time-resolved luminescence quenching spectroscopy. Upon inspection of Figure A26, the first exponential is not expected to contribute noticeably to the intensity, so may have gone unnoticed if steady-state methods (relying on an overall intensity measurement) had been employed.

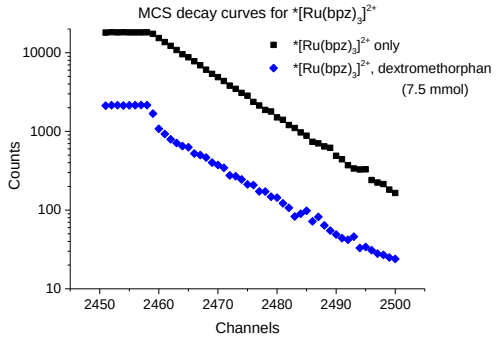

***Figure A26**: Decay curves of *[Ru(bpz)$_3$]$^{2+}$ only and with dextromethorphan (7.5 mM) following the excitation pulse (Log$_{10}$ scale used).*

A6.7. Optimisation of Degassing for Luminescence Quenching Experiments

When *[Ru(bpy)$_3$]$^{2+}$ was treated with different concentrations of *N*-phenyl THIQ in aerated MeCN, differences in I^0/I as a function of [*N*-phenyl THIQ] were not detectable due to the substantial extent to which the *[Ru(bpy)$_3$]$^{2+}$ was quenched by O_2 (Figure A27, left). Initially, degassing was achieved by placing open cuvettes inside the spectrometer and then purging the entire spectrometer with N_2 (the emission of *[Ru(bpy)$_3$]$^{2+}$ was measured every 30 s for 36 minutes, see Figure A27, right) but this approach was wasteful in N_2, was ineffective and was time-consuming.

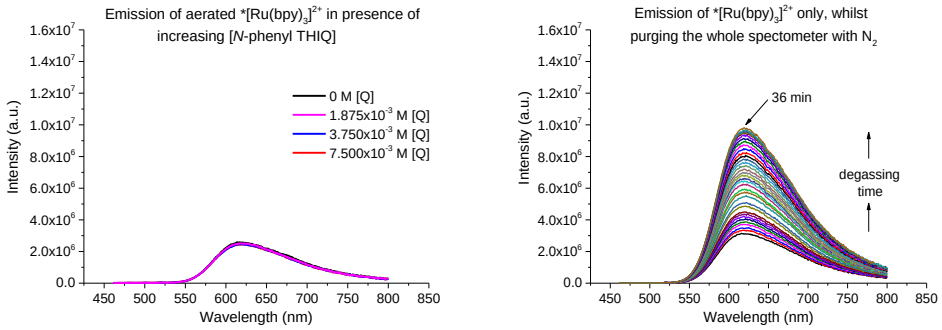

***Figure A27**: Left: Steady-state emission intensity of aerated samples of *[Ru(bpy)$_3$]$^{2+}$ with increasing concentrations of N-phenyl THIQ. Right: Steady-state emission intensity of *[Ru(bpy)$_3$]$^{2+}$ only whilst purging the spectrometer with N_2.*

Ultimately, Sample degassing was achieved by bubbling sealed cuvettes through a needle with Ar/N_2 for 5 min and then measuring immediately. After 5 min, τ reaches a steady constant value indicating degassing is complete (Figure A28, left). Differences in I^0/I as a function of [*N*-phenyl THIQ] could now be resolved (Figure A28, right). To account for any variations in the gas flow rate from the N_2/Ar cylinders during or between sets of experiments, samples containing $Ru(bpy)_3(PF_6)_2$ only were run at regular intervals and used to calibrate data accordingly. This method reproducibly gave lifetime values for $*[Ru(bpy)_3]^{2+}$ and $*[Ru(bpz)_3]^{2+}$ which were in good agreement with the literature (Table A5).

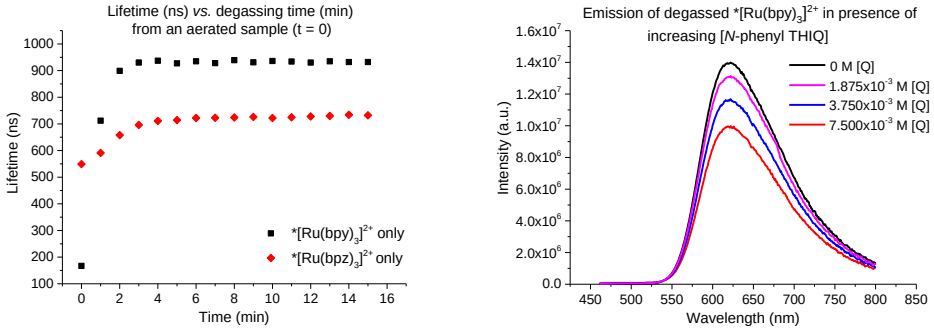

***Figure A28**: Left: TCSPC lifetimes of $*[Ru(bpy)_3]^{2+}$ and $*[Ru(bpz)_3]^{2+}$ bubbling the sample cuvette with N_2 over time, fully purged at 5 min. Right: Steady-state emission intensity of $*[Ru(bpy)_3]^{2+}$ with increasing concentrations of N-phenyl THIQ, bubbled for 5 min with N_2.*

***Table A5**: Lifetime measurements of $*[Ru(bpy)_3]^{2+}$, $*[Ru(bpz)_3]^{2+}$ and literature comparisons.*

Entry[a]	τ /ns[b]	Gas	Degassing method	Spectroscopy used
1[10]	1100[c]	n/a[d]	freeze/pump/thaw	TCSPC
2[46]	898[e]	Ar	prepared and run in glovebox	TCSPC
3[13]	(740)[c]	N_2	bubbling for 15 min	TCSPC

Entry[a]	τ /ns[b]	Gas	Degassing method	Spectroscopy used
4[47]	890[c]	N_2	bubbling for 15 min	TCSPC
5[f]	933[c,g], (705)[c,g]	N_2	bubbling for 5 min	TCSPC (MCS)
6[f]	977[c,h], (720)[c,g]	Ar	bubbling for 5 min	TCSPC (MCS)

[a]References to literature. [b]$[Ru(bpy)_3]^{2+}$ τ values not in parenthesis, $[Ru(bpz)_3]^{2+}$ τ values in parenthesis. [c]PF_6 salt. [d]Unspecified. [e]Cl salt. [f]This study. [g]Average of 3 measurements. [h]Average of 6 measurements.

A6.8. STERN VOLMER PLOTS FOR VOLUME 1, CHAPTER 2.2.

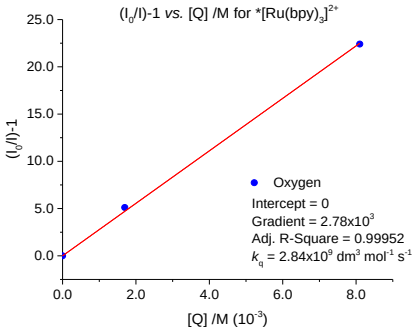

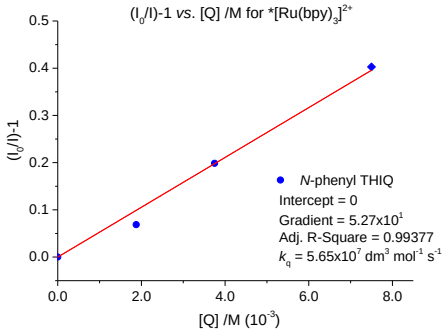

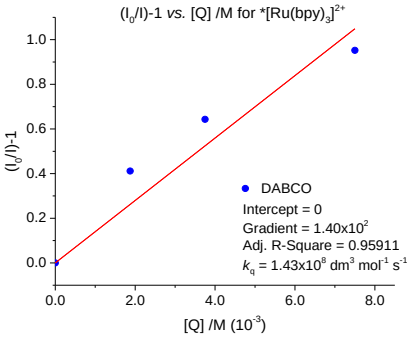

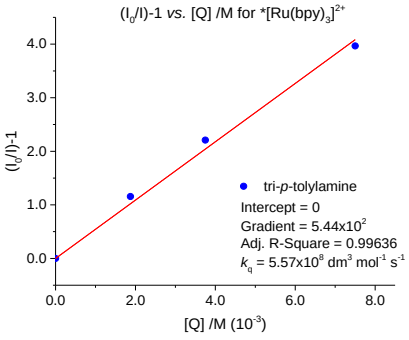

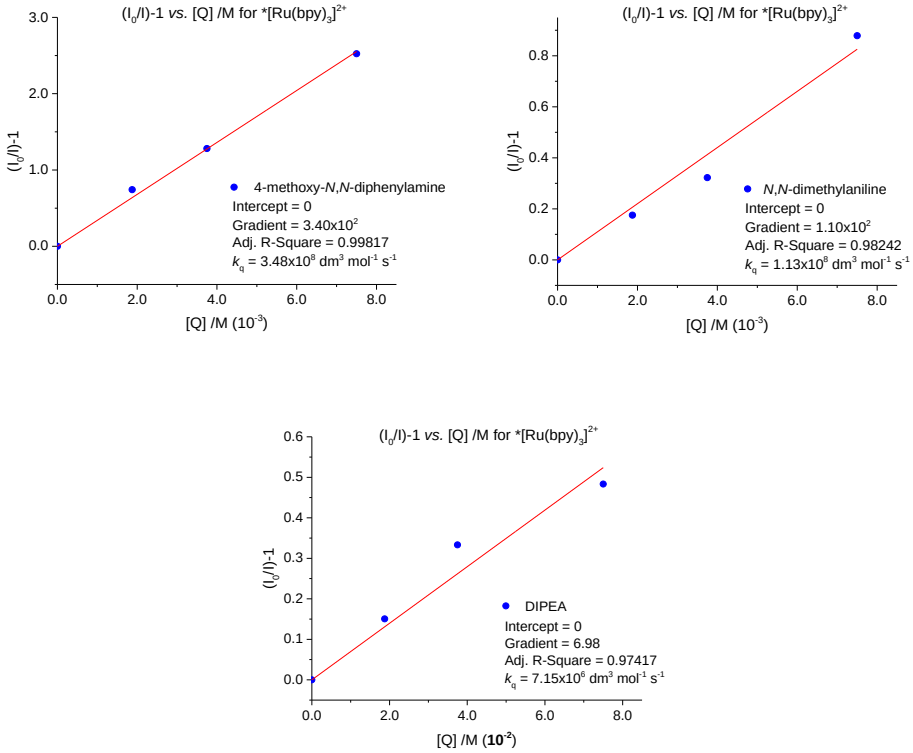

***Figure A29**: Stern-Volmer analysis of degassed samples of $Ru(bpy)_3^{2+}$ with increasing concentrations of various quenchers.*[†]

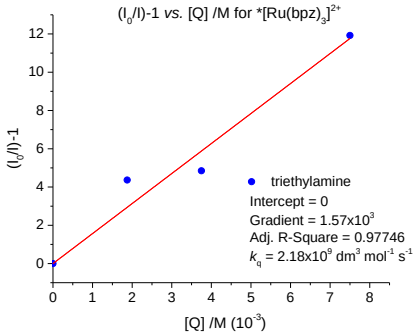

***Figure A30**: Stern-Volmer analysis of degassed samples of $Ru(bpz)_3^{2+}$ with increasing concentrations of triethylamine.*

[†]DABCO as a quencher appears to give a curved, rather than linear Stern-Volmer plot. This could be explained by formation of a precursor complex which emits, as described in Chapter A.6., equation 24.

A7. EPR SPECTRA

A7.1. EPR SPECTRA OF TRI-*para*-SUBSTITUTED TRIARYLAMINIUM SALTS FOR VOLUME 1, CHAPTER 2.3.

The EPR samples in both Chapters A7.1. and A7.2. were prepared by Joshua Barham and analysed by Prof. John Walton at the University of St. Andrews. See Volume 1, Experimental, Chapter 5.7.

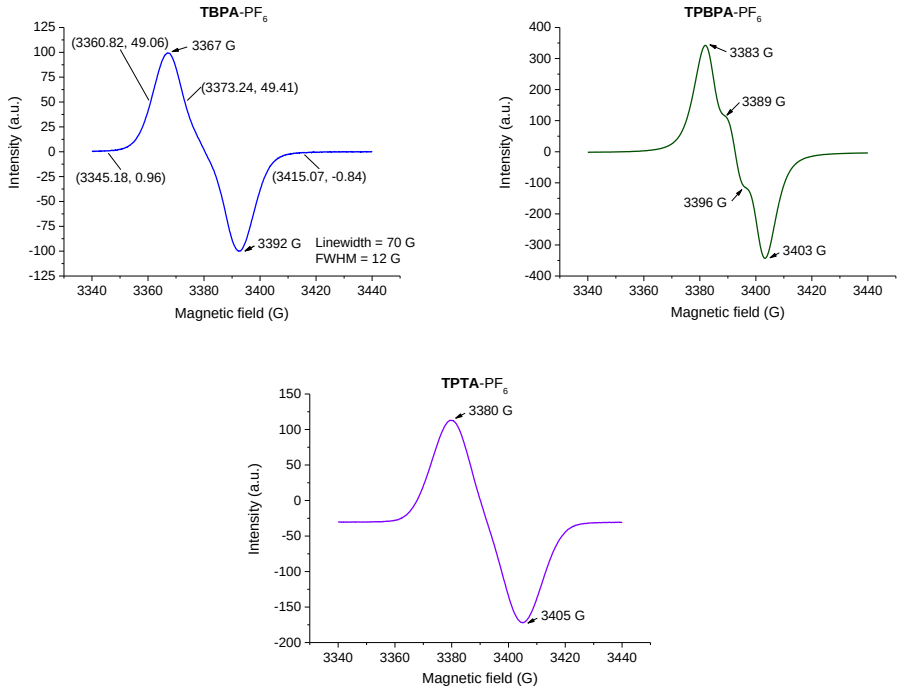

***Figure A31**: EPR spectra for tri-para-substituted triarylaminium radical cation salts.*

A7.2. Attempts to Detect DABCO Radical Cation by EPR Spectroscopy for Volume 1, Chapter 2.3.

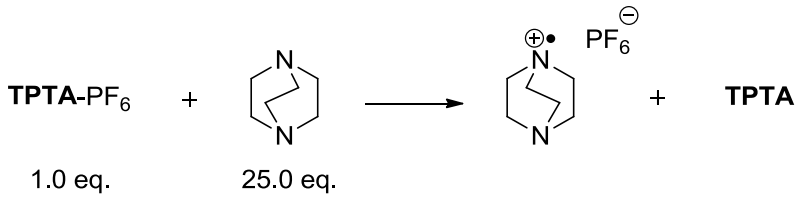

***Scheme A5**: Generation of DABCO radical cation from **TPTA**-PF_6.*

In order to measure EPR whilst **TPTA**-PF_6 and DABCO were mixed, a bespoke EPR sample tube (Figure A32) was prepared which could separate two solutions with a stopcock. This was filled inside a glovebox. In the bottom compartment (capillary tube) was placed a solution of DABCO in degassed MeCN (0.02 M, 25.0 eq.). In the top compartment was placed a solution of **TPTA**-PF_6 in degassed MeCN (8.0 x 10^{-3} M, 1.0 eq.). The bottom compartment of the tube (capillary tube, containing DABCO solution only) was placed inside the resonant cavity (cooled to -23 ^{o}C) and no signal was observed (Figure A33, right).

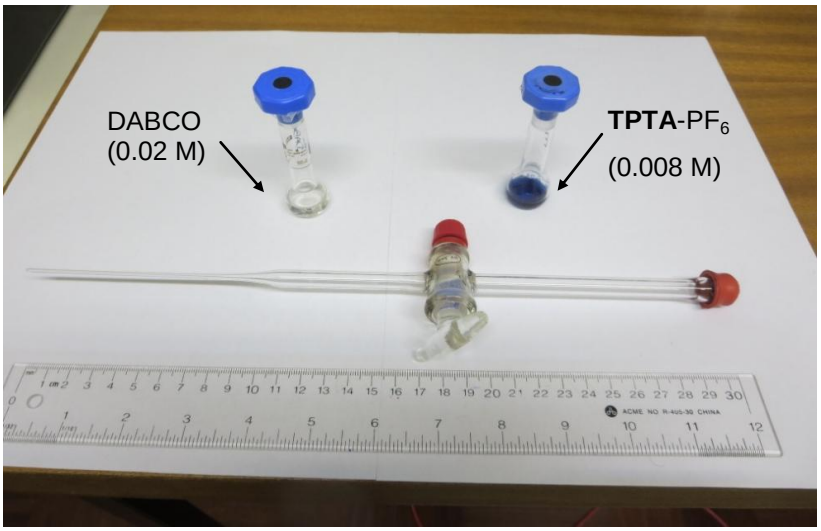

***Figure A32**. Bespoke EPR sample tube for mixing **TPTA**-PF_6 and DABCO within the EPR spectrometer.*

The **TPTA**-PF_6 solution (top compartment) was allowed to run slowly into the bottom compartment (capillary tube) whilst it was inside the resonant cavity, allowing mixing by diffusion. The dark blue solution of **TPTA**-PF_6 from the top compartment of the tube faded as it met the DABCO solution, however no signal was observed by EPR (Figure A34, left).

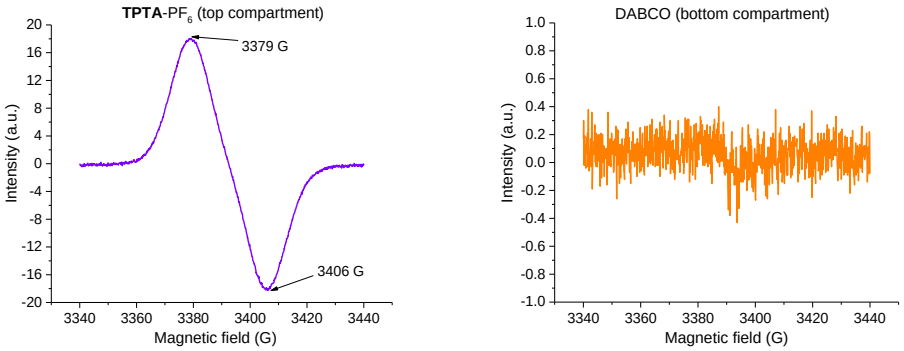

Figure A33. *EPR spectra of* ***TPTA****-PF_6 and DABCO prior to mixing.*

Repeating this process in a resonant cavity (cooled to -33 ^{o}C) with fresh solutions and rapidly mixing the solutions (after the DABCO solution was cooled to -33 ^{o}C) also gave no signal by EPR (Figure A34, right). If formation of DABCO/**TPTA**-PF_6-derived compounds ***196***, ***197*** and ***198*** (Figure A35) is rapid, this would preclude observation of DABCO radical cation.

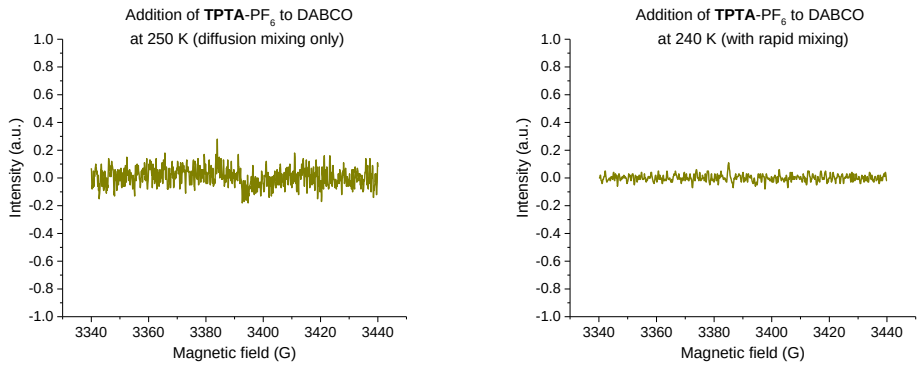

Figure A34. *EPR spectra of* ***TPTA****-PF_6 and DABCO upon mixing.*

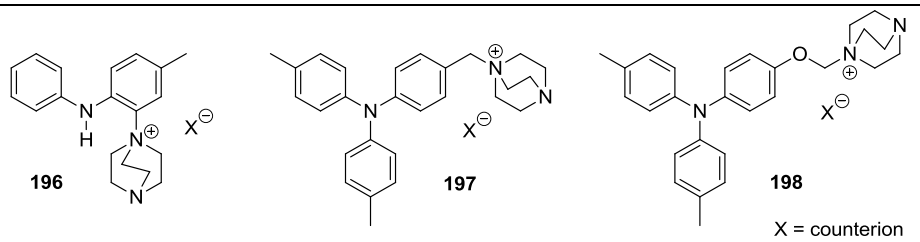

***Figure A35**: Products derived from treatment of **TPTA**-PF_6 with DABCO only.*

A8. YIELD DETERMINATIONS BY INTERNAL STANDARD

A8.1. EXAMPLE RELEVANT TO VOLUME 1, CHAPTER 2.1.

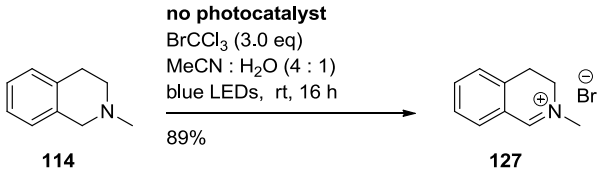

***Scheme A6**: Photogeneration of iminium salt **127** from N-methyl THIQ (**114**)*

^{1}H NMR (400 MHz, $CDCl_3$) - crude reaction mixture

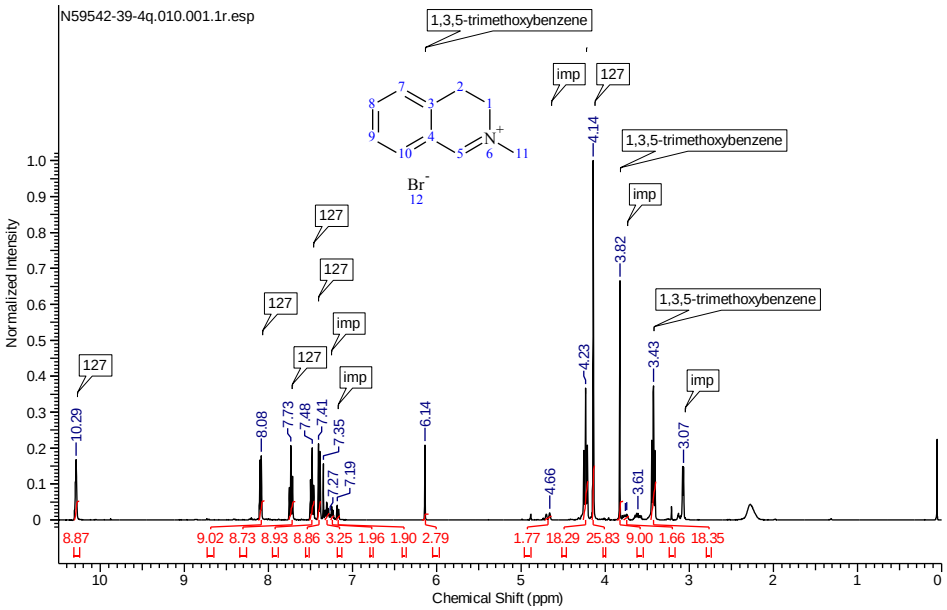

The ^{1}H NMR spectrum of the crude reaction mixture revealed **127** as the major component together with an unknown by-product. The integral of the aromatic signal of the internal standard (δ 3.82 ppm, 9H) was set to 9. The discernable ^{1}H NMR peaks of **127**, the triplet at δ 4.23 ppm (2H), the singlet at δ 4.14 ppm (3H) and the triplet at δ 3.43 ppm (2H), were used to determine the yield of **127** by the following calculation: [(18.28+25.82+18.34)/7] x 10 = 89.2%. The integration of the ^{1}H doublet at δ 4.66 ppm (assumed to be 2H;

identified as a CH_2 by HSQC NMR) was used to determine the yield of the unknown by-product by the following calculation: (1.77/2) x 10 = 8.6%.

A8.2. EXAMPLES RELEVANT TO VOLUME 1, CHAPTER 2.3.

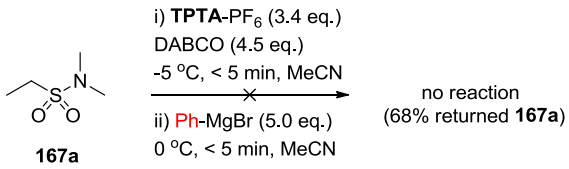

***Scheme A7**: Attempted N-C**H**$_3$ functionalisation of N,N-dimethyl-ethanesulfonamide. No reaction observed.*

^{1}H NMR (400 MHz, $CDCl_3$) - crude reaction mixture

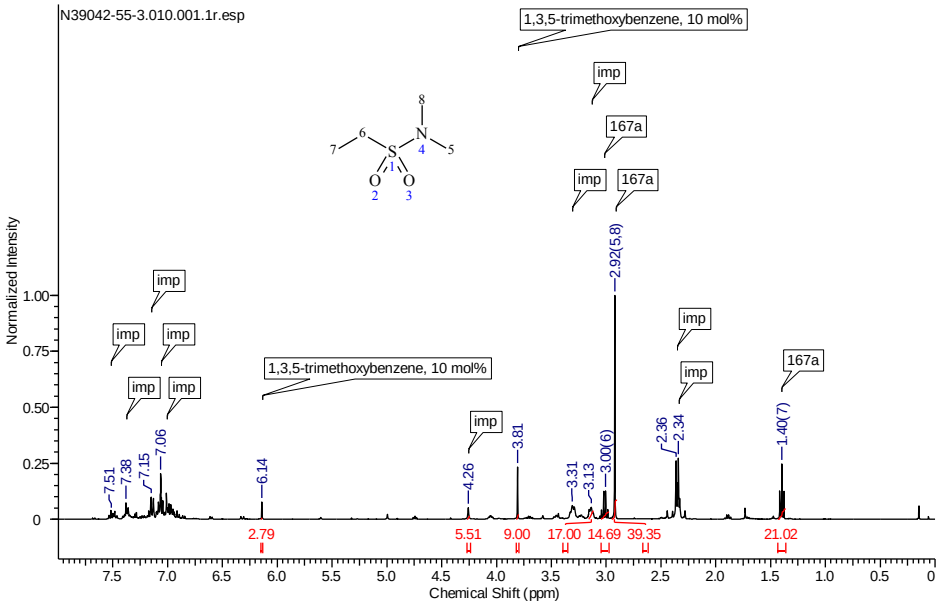

The ^{1}H NMR of the crude reaction mixture revealed **167a** (returned starting material) and no other identifiable **167a**-derived products. Other components (imp = impurity) presumably arise from background nucleophilic addition reactions of phenylmagnesium bromide with MeCN solvent, or are **TPTA**-PF_6-related (the peaks at δ 4.26, 3.31 and 3.13 ppm are common to other crude ^{1}H NMR spectra of reactions where the substrate was inert to *N*-C**H**$_3$ functionalisation. These peaks are attributable to compound **197**, which is detected in the LCMS of the reaction mixture). The integral of the aliphatic

signal of the internal standard (δ 3.81 ppm) was set to 9. The integrations of the discernable ^{1}H NMR peaks of **167a**, the quartet at δ 3.00 ppm (2H), the singlet at δ 2.92 ppm (6H) and the triplet at δ 1.40 ppm (3H), were used to determine the yield of **167a** by the following calculation: [(14.69 + 39.35 + 21.02)/11] x 10 = 68.2%.

^{1}H NMR (400 MHz, $CDCl_3$) - crude reaction mixture

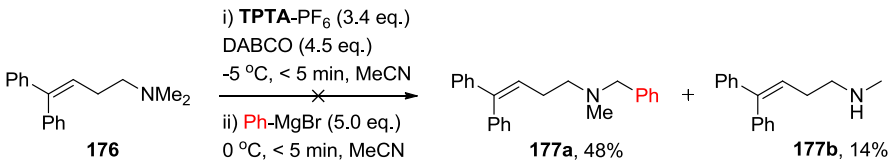

***Scheme A8**: N-C**H**$_3$ functionalisation of an α-amino radical reporter substrate. No radical cyclisation observed.*

^{1}H NMR (400 MHz, $CDCl_3$) - crude reaction mixture

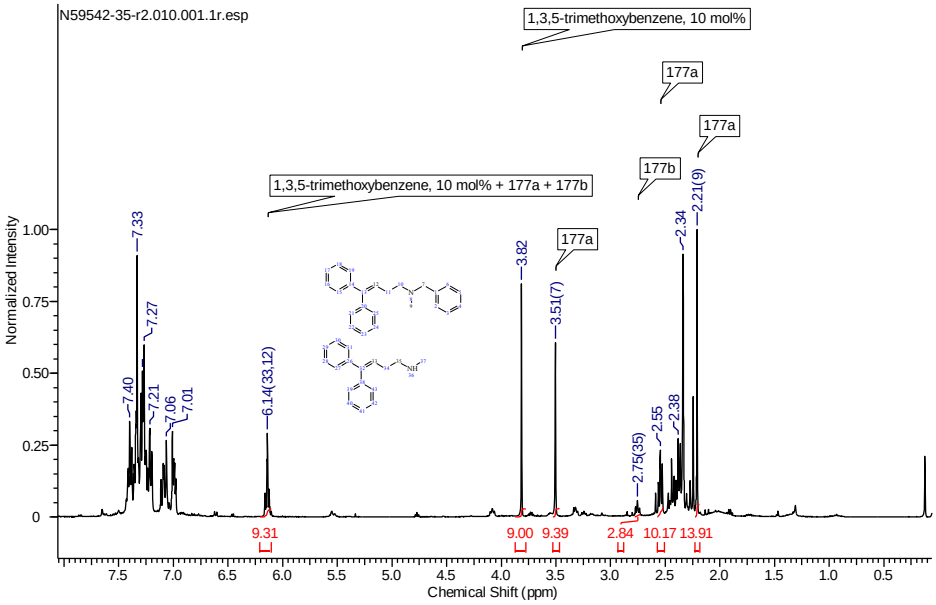

The ^{1}H NMR of the crude reaction mixture revealed **177a** as the major substrate(**176**)-derived component and **177b** as the minor substrate(**176**)-derived component. Other components (imp = impurity) presumably arise from background nucleophilic addition reactions of phenylmagnesium bromide with MeCN solvent, or are **TPTA**-PF_6-related. The integral of the

aliphatic signal of the internal standard (δ 3.82 ppm) was set to 9. The integrations of the discernable ^{1}H NMR peaks of **177a**, the singlet at δ 3.51 ppm (2H), the triplet at δ 2.55 ppm (2H) and the singlet at δ 2.21 ppm (3H), were used to determine the yield of **177a** by the following calculation: [(9.39 + 10.17 + 13.91)/7] x 10 = 47.8%. The integration of the ^{1}H triplet at δ 2.75 ppm (2H) was used to determine the yield of **177b** by the following calculation: (2.84/2) x 10 = 14.2%. Therefore, by this method the yield of **177a** was 48% and the yield of **177b** was 14%.

A8.3. EXAMPLES RELEVANT TO VOLUME 2, CHAPTER 2.1. AND CHAPTER 2.2.

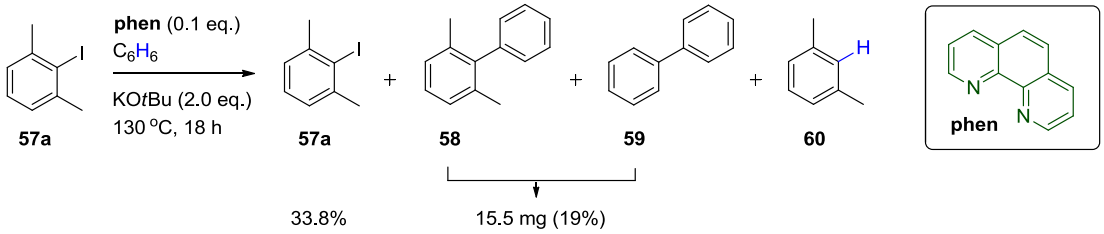

***Scheme A9**: KOtBu-mediated C-H arylation of **57a** using **phen** as an additive.*

^{1}H NMR (400 MHz) - 1,10-phenanthroline as an additive

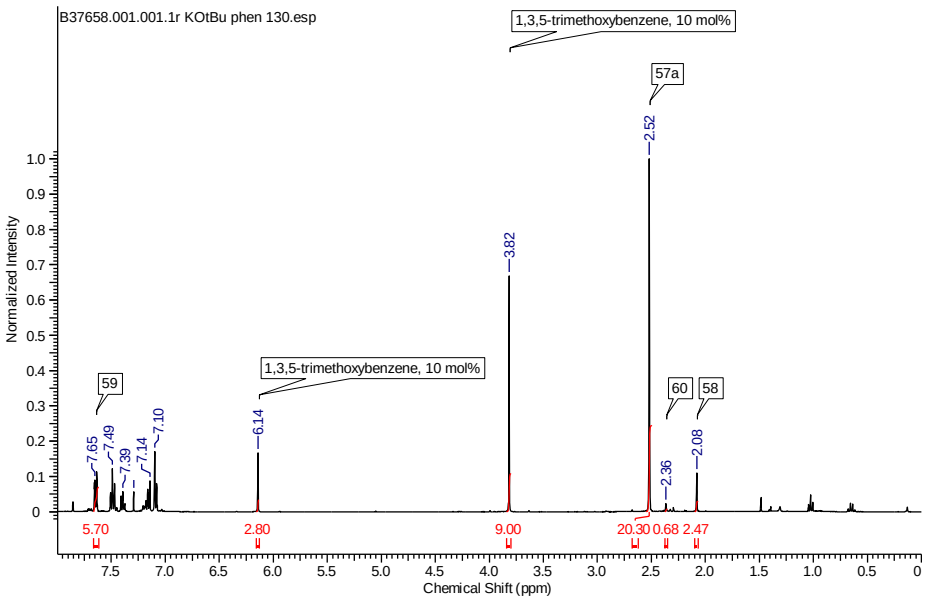

For the returned starting material **57a**, the integral of the methoxy signal of the internal standard (δ 3.82 ppm) was set to 9. The integration of the methyl signal of **57a** (δ 2.52 ppm, 6H) was measured and the following calculation gave the amount of **57a** present: (20.30/6) x 10 = 33.8%. The integration of the methyl signal of **58** (δ 2.08 ppm, 6H) was measured and the following calculation gave the amount of **58** present: (2.47/6) x 10 = 4.1%. To obtain the mass, the following calculation was used: (0.5 mmol x 0.041 x 182.26 mg/mmol) = 3.74 mg.

For biphenyl product **59**, the integral of the aromatic signal of the internal standard (δ 6.14 ppm) was set to 3. The integration of the aromatic signals of **59** (δ 7.66 - 7.61 ppm, 4H) was measured and the following calculation gave the amount of **59** present: (6.11/4) x 10 = 15.3%. To obtain the mass, the following calculation was used: (0.5 mmol x 0.153 x 154.21 mg/mmol) = 11.8 mg. Therefore, by this method the yield of returned starting material **57a** was 34% and mass of combined biaryls **58** and **59** was 15.5 mg.

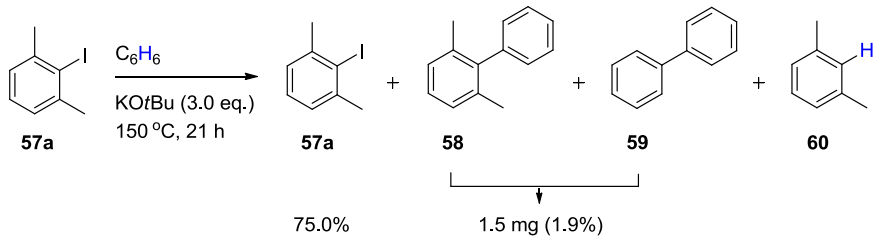

***Scheme A10**: KOtBu-mediated C-H arylation of **57a** in the absence of an organic additive.*

^{1}H NMR (400 MHz) - no additive, KO*t*Bu only

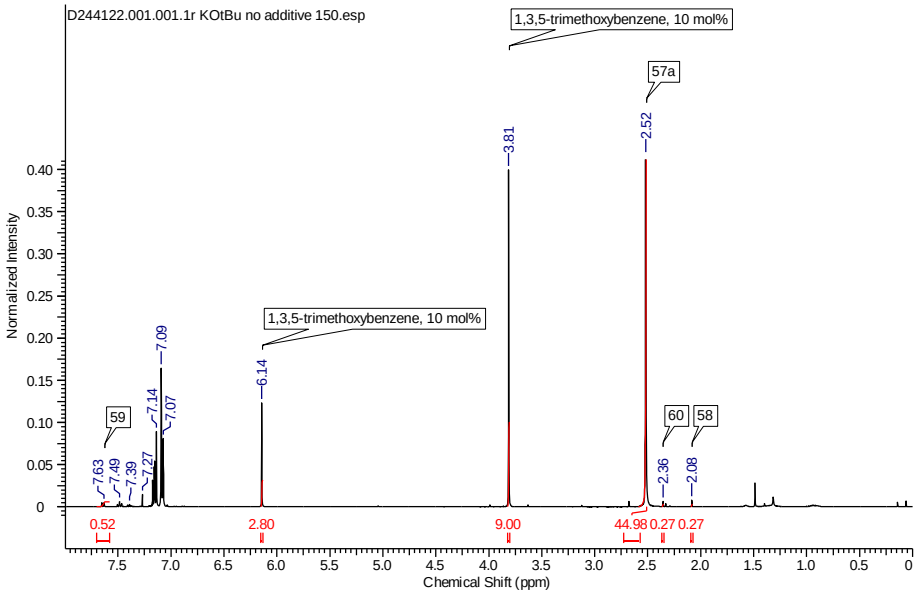

For the returned starting material **57a**, the methoxy signal of the internal standard (δ 3.82 ppm) was set to 9. The integration of the methyl signal of **57a** (δ 2.52 ppm, 6H) was measured and the following calculation gave the amount of **57a** present: (44.98/6) x 10 = 75.0%. The integration of the methyl signal of **58** (δ 2.08 ppm, 6H) was measured and the following calculation gave the amount of **58** present: (0.27/6) x 10 = 0.5%. To obtain the mass, the following calculation was used: (0.5 mmol x 0.005 x 182.26 mg/mmol) = 0.46 mg.

For biphenyl product **59**, the aromatic signal of the internal standard (δ 6.14 ppm) was set to 3. The integration of the aromatic signals of **59** (δ 7.66 - 7.61 ppm, 4H) was measured and the following calculation gave the amount of **59** present: (0.56/4) x 10 = 1.4%. To obtain the mass, the following calculation was used: (0.5 mmol x 0.014 x 154.21 mg/mmol) = 1.07 mg. Therefore, by this method the yield of returned starting material **57a** was 75% and yield of combined biaryls **58** and **59** was 1.5%.

A8.4. EXAMPLES RELEVANT TO VOLUME 2, CHAPTER 2.3.

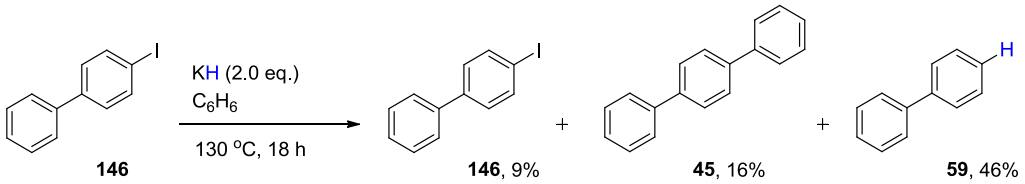

***Scheme A11**: KH-mediated dehalogenation of **146** in benzene solvent.*

^{1}H NMR (400 MHz, $CDCl_3$) - crude reaction mixture

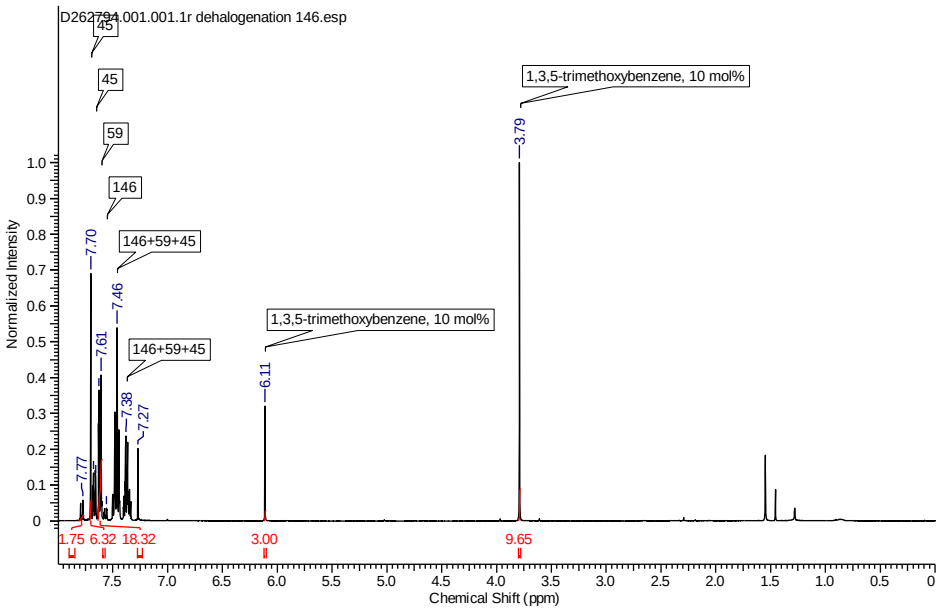

^{1}H NMR (400 MHz, $CDCl_3$) - crude reaction mixture expanded

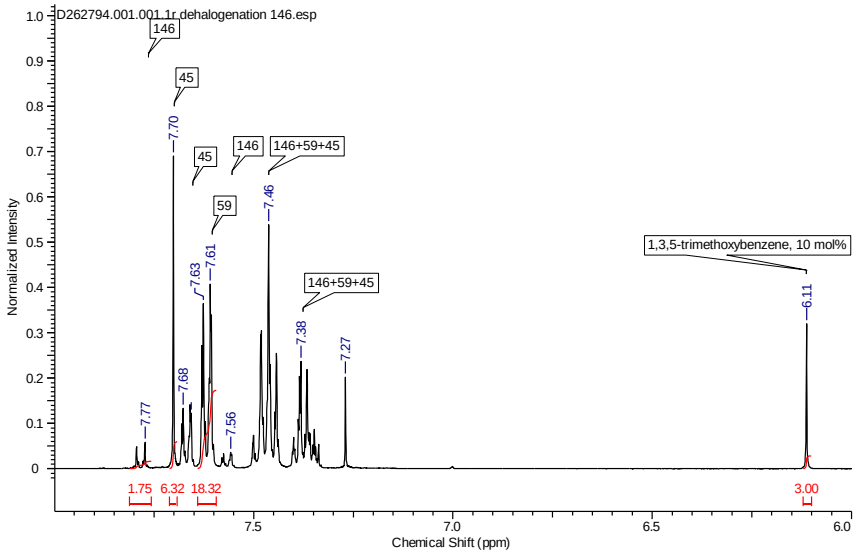

For the returned starting material **146**, the integral of the aromatic signal of the internal standard (δ 6.11 ppm) was set to 3. The integration of the discernable aromatic multiplet of **146** (δ 7.81 - 7.70 ppm, 2H) was taken and the following calculation gave the amount of **146** present: (1.75/2) x 10 = 8.8%. The integration of the discernable aromatic singlet of **45** (δ 7.70 ppm, 4H) was taken and the following calculation gave the amount of **45** present: (6.32/4) x 10 = 15.8%. The integration of the aromatic multiplet of **59** (δ 7.64 - 7.60 ppm, 4H) was taken and the following calculation gave the amount of **59** present: (18.32/4) x 10 = 45.8%. Therefore, by this method the yield of returned starting material **146** was 9%, the yield of terphenyl **45** was 16% and the yield of biphenyl **59** was 46%. An average of 3 replicates gave the yields shown in Volume 2, Table 6, entry 4, Section 2.3.2.

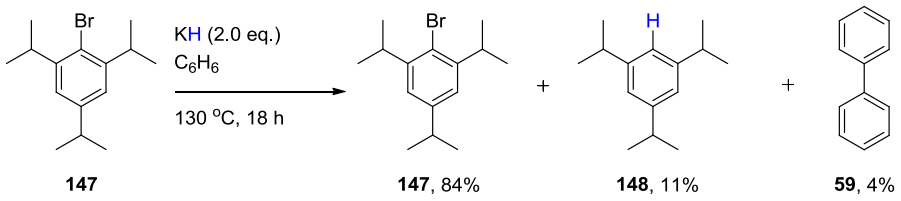

***Scheme A12**: KH-mediated dehalogenation of **147** in benzene solvent.*

^{1}H NMR (400 MHz, $CDCl_3$) - crude reaction mixture

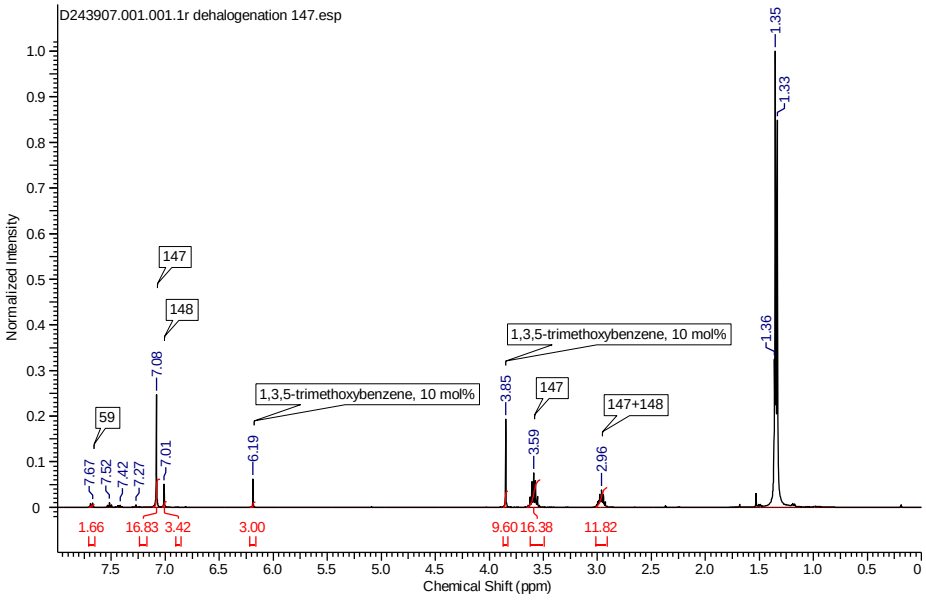

For the returned starting material **147**, the integral of the aromatic signal of the internal standard (δ 6.19 ppm) was set to 3. The integration of the aromatic signal of **148** (δ 7.08 ppm, 2H) was measured and the following calculation gave the amount of **148** present: (16.83/2) x 10 = 84.2%. The integration of the aromatic signal of **148** (δ 7.01 ppm, 3H) was measured and the following calculation gave the amount of **148** present: (3.42/3) x 10 = 11.4%. The integration of the aromatic signal of **59** (δ 7.71-7.65 ppm, 4H) was measured and the following calculation gave the amount of **59** present: (1.66/4) x 10 = 4.2%. Therefore, by this method the yield of returned starting material **147** was 84%, the yield of 1,3,5-triisopropylbenzene **148** was 11% and the yield of biphenyl **59** was 4%. An average of 3 replicates including this reaction gave the yields shown in Table 7, entry 1, Section 2.3.3.

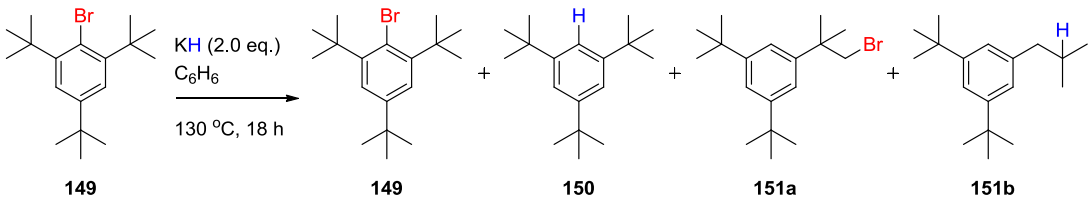

***Scheme A13**: KH-mediated dehalogenation of **149** in benzene solvent.*

^{1}H NMR (500 MHz, $CDCl_3$) - crude reaction mixture

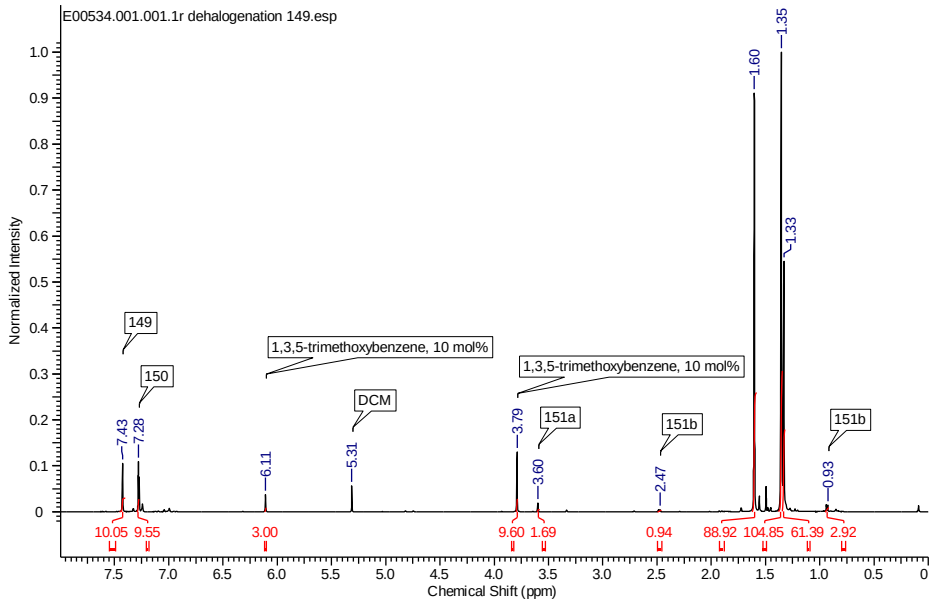

For the returned starting material **149**, the integral of the aromatic signal of the internal standard (δ 6.19 ppm) was set to 3. The integration of the aromatic signal of **149** (δ 7.43 ppm, 2H) was measured and the following calculation gave the amount of **149** present: (10.06/2) x 10 = 50.3%. The integration of the aromatic signal of **150** (δ 7.28 ppm, 3H) was measured and the following calculation gave the amount of **150** present: (9.55/3) x 10 = 31.8%. For bromide **151a**, the methoxy signal of the internal standard was set to 9. The integration of the benzylic CH_2 signal of **151a** (δ 3.60 ppm, 2H) was measured and the following calculation gave the amount of **151a** present: (1.58/2) x 10 = 7.9%. For rearranged dehalogenated product **151b**, the methoxy signal of the internal standard was set to 9. The integrations of the benzylic CH_2 signal (δ 2.47 ppm, 2H) and the isopropyl CH_3 signals (δ 0.93 ppm, 6H) of **151b** were measured and the following calculation gave the amount of **151b** present: ((0.88+2.72)/8) x 10 = 4.5%. Therefore, by this method the yield of returned starting material **149** was 50%, the yield of 1,3,5-tri-*tert*-propylbenzene **150** was 32%, the yield of bromide **151a** was 8% and the yield of rearranged dehalogenated product **151b** was 5%. An average of 7 replicates including for this reaction gave the yields shown in Table 8, entry 3, Section 2.3.4. Five of these replicates were conducted by Samuel Dalton at the University of Strathclyde.

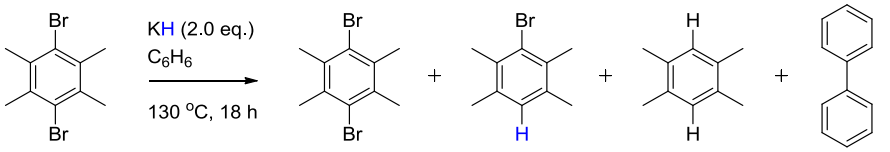

157b **157b**, 77% **162**, 8% **161**, < 1% **59**, < 1%

***Scheme A14**: KH-mediated dehalogenation of **157b** in benzene solvent.*

^{1}H NMR (400 MHz) - KH-mediated dehalogenation of **157b**

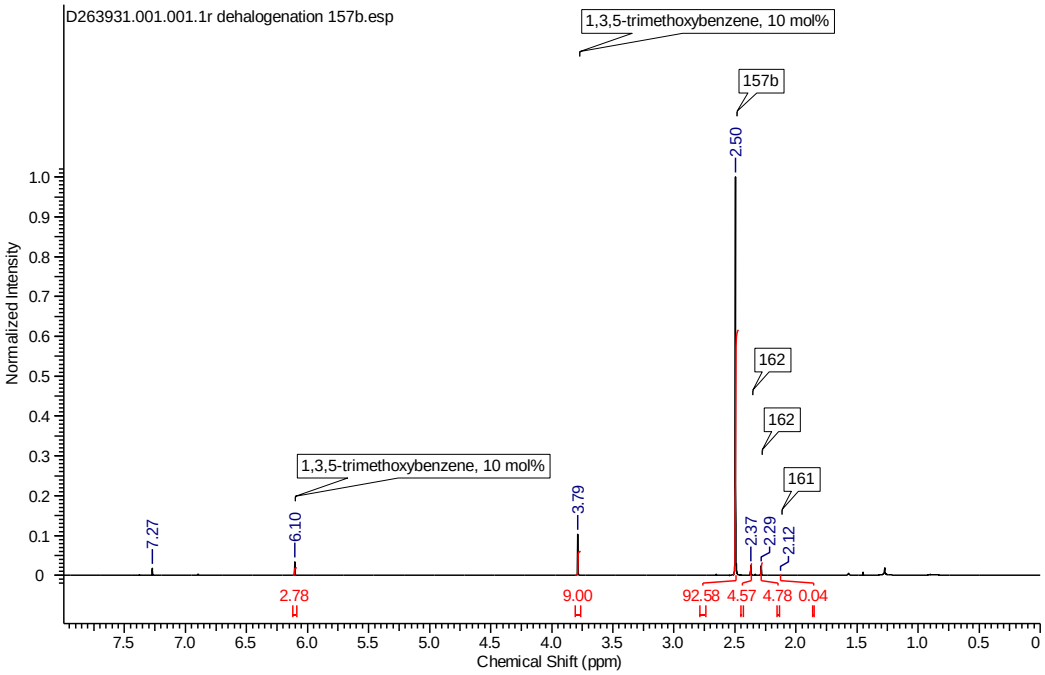

For the returned starting material **157b**, the integral of the aliphatic signal of the internal standard (δ 3.79 ppm) was set to 9. The integration of the aliphatic singlet of **157b** (δ 2.50 ppm, 12H) was taken and the following calculation gave the amount of **157b** present: (92.58/12) x 10 = 77.2%. The integrations of the aliphatic singlets of **162** (δ 2.37 ppm, 6H and δ 2.29 ppm, 6H) were taken and the following calculation gave the amount of **162** present: {[(4.57+4.78)/2]/6} x 10 = 7.8%. The aliphatic singlet of **161** in the baseline (δ 2.12 ppm, 12H) was taken and the following calculation gave the amount of **161** present: (0.04/12) x 10 = 0.5%. Therefore, by this method the yield of returned starting material **157b** was 77%, the yield of bromodurene (**162**) was 8% and the yield of durene (**161**) was <1%. This reaction was conducted by Samuel Dalton at the University of Strathclyde.

A9. KEY NMR SPECTRA AND CHROMATOGRAPH TRACES

A9.1. KEY SPECTRA PERTAINING TO VOLUME 1, CHAPTER 2.1.

A9.1.1. EXAMPLE HPLCS AND RESPONSE FACTORS FOR *N*-PHENYL THIQ FUNCTIONALISATION.

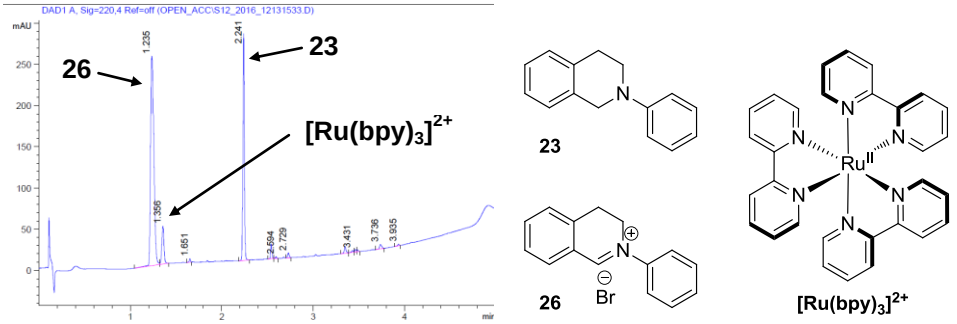

***Figure A36**: HPLC chromatogram for an equimolar mixture of **26** and **23**.*

The ratio of **26** : **23** is 2.07 : 1.00 by HPLC peak area (220 nm). This means that **26** absorbs 2.07x more strongly than **23** at 220 nm, and is used to correct the peak area ratios (220 nm) obtained from HPLC and LCMS analysis of reactions. The calculation is demonstrated below using the HPLC result in Volume 1, Table 1, entry 6 (16 h) as an example.

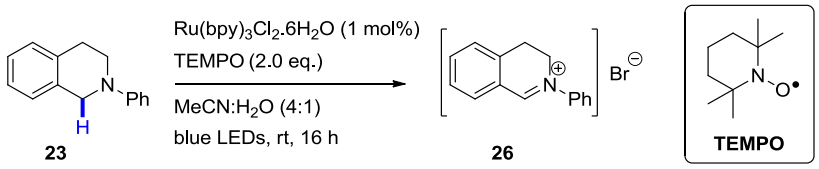

***Scheme A15**: Photogeneration of iminium salt **26** from N-phenyl THIQ (**23**) in the presence of $[Ru(bpy)_3]^{2+}$ as a photocatalyst and TEMPO as an oxidant.*

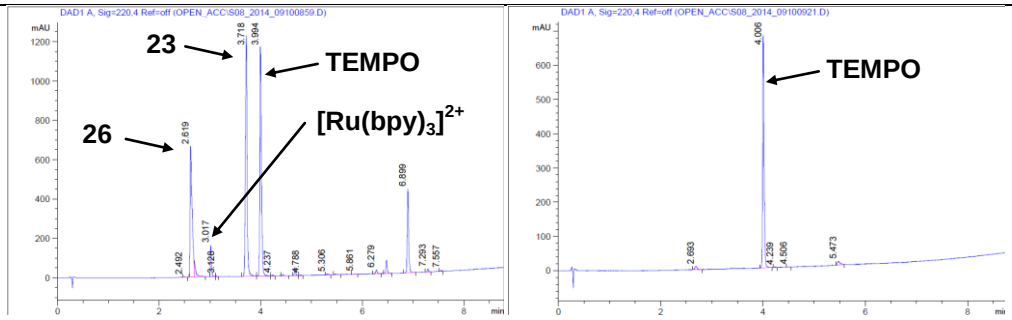

In this reaction, the ratio of **23** : **26** is 1.5 : 1. Since **26** absorbs 2.07x more strongly than **23** at 220 nm, the molar composition is 1.5 : (1/2.07) = 1.5 : 0.5 = 75 : 25.

A9.1.2. Full NMR Data for dextromethorphan 73, Detailing Characterisation

Assignment of the NMR spectra of semi-synthetic opioids is non-trivial, due to rigid fused ring system giving rise to a number of diastereotopic protons (16 for dextromethorphan, **73**), which have complex splitting patterns. The ^{1}H and ^{13}C NMR assignment of dextromethorphan (**73**) is given here.

^{1}H NMR (400 MHz, $CDCl_3$) - **73**

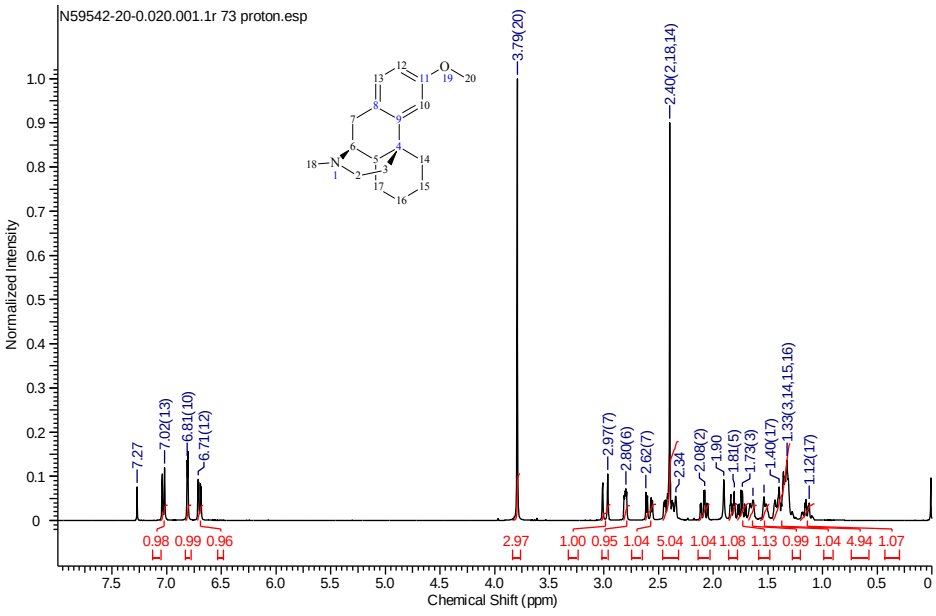

^{13}C NMR (101 MHz, $CDCl_3$) - **73**

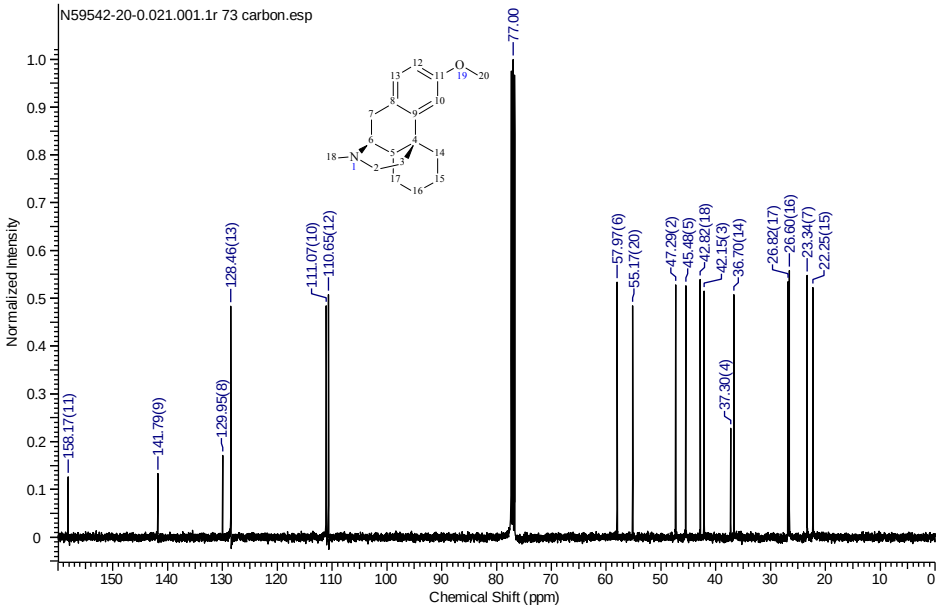

DEPT NMR (101 MHz, $CDCl_3$) - **73**

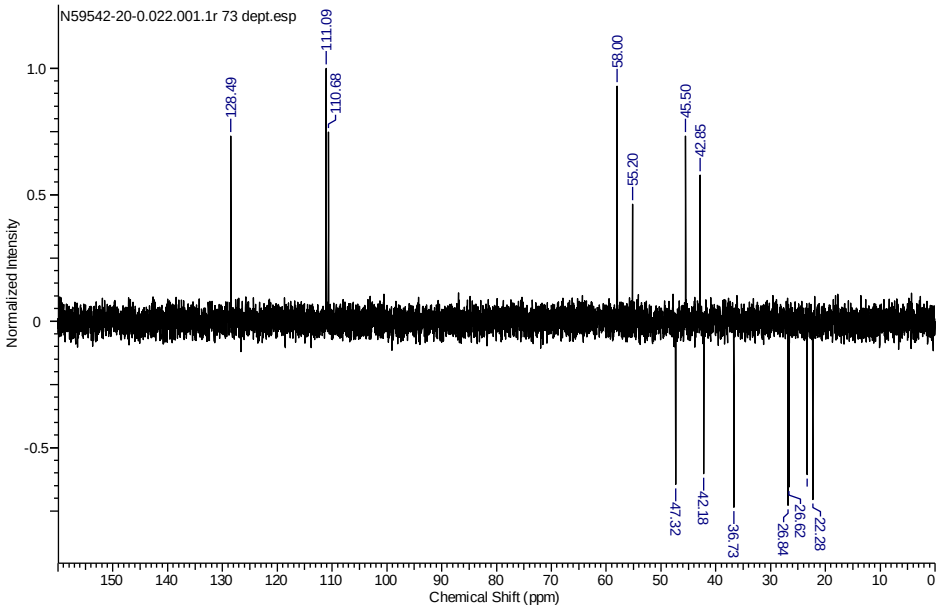

Here, *C*H and *C*H_3 environments are shown on the bottom phase, *C*H_2 environments are shown on the top phase.

COSY NMR ($CDCl_3$) - **73**

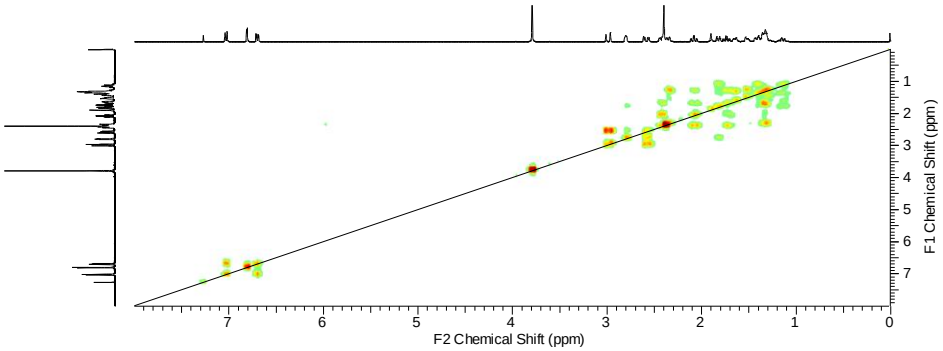

HSQC NMR ($CDCl_3$) - **73**

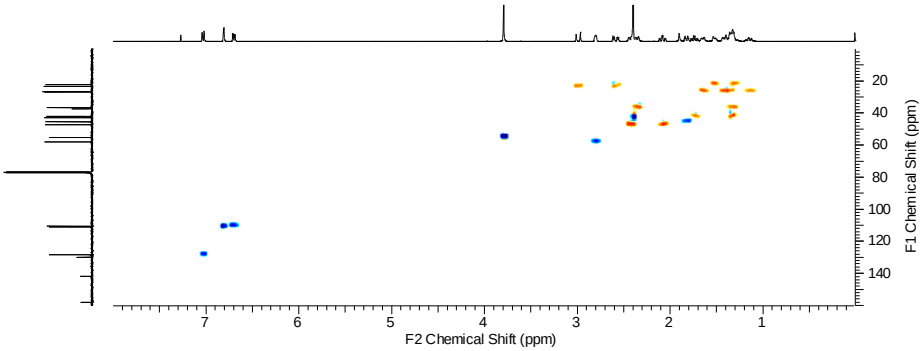

Here, *C*H and *C*H_3 environments are blue in colour, *C*H_2 environments are red in colour.

HMBC NMR ($CDCl_3$) - **73**

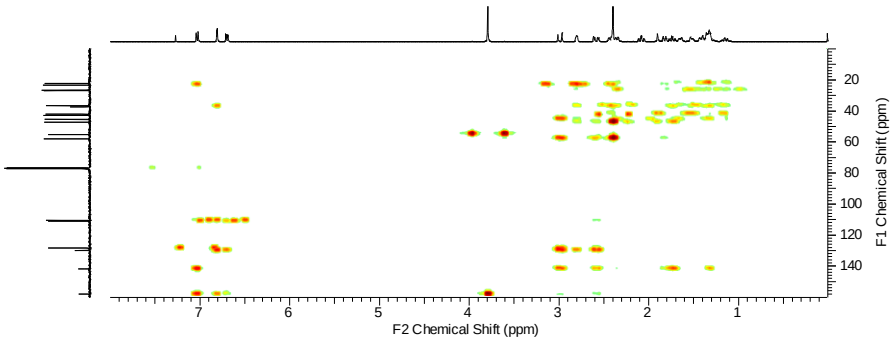

COSY: The ^{1}H double doublet at δ 2.80 ppm couples to 1) the ^{1}H doublet at δ 2.97 ppm (1H of the benzylic C*H*$_2$), 2) the ^{1}H double doublet at δ 2.62 ppm (1H of the benzylic C*H*$_2$) and 3) the doublet of triplets at δ 1.81 ppm (the ring junction *CH*). The ^{1}H triplet of doublets at δ 1.73 ppm (the C*H*$_2$ β- to both the

aromatic ring and the N atom) couples to the multiplet at δ 2.47 - 2.32 ppm and the triplet of doublets at 2.08 ppm (the C*H*$_2$ α- to the N atom). The ^{1}H doublet of triplets at δ 1.81 ppm (the ring junction *CH*) couples to the multiplets at δ 1.45 - 1.29 ppm and δ 1.21 - 1.07 ppm (the C*H*$_2$ neighbouring the ring junction CH). **HSQC:** The double doublet at δ 2.80 ppm couples to the ^{13}C peak at δ 58.0 ppm, and is a *C*H according to the phase (these peaks are assigned to the N*CH* β- to the aromatic ring). The double of triplets at δ 1.81 ppm couples to the ^{13}C peak at δ 45.5 ppm, which is a *C*H according to the phase. These peaks were assigned to the ring junction *CH*. **HMBC:** The ^{1}H doublet at δ 7.02 (the C*H meta*- to OMe) couples to the ^{13}C peak at δ 23.3 ppm (the benzylic *C*H$_2$). The ^{1}H doublet at δ 6.81 ppm (the C*H meta*- to OMe) couples to the ^{13}C peak at δ 37.3 ppm (the aliphatic *C*). The ^{1}H triplet of doublets at δ 1.73 ppm (the C*H*$_2$ β- to both the aromatic ring and the N atom) couples to the ^{13}C peak at δ 141.8 ppm (the quaternary *C meta*-to OMe).

A9.2. Key Spectra Pertaining to Volume 1, Chapter 2.3.

A9.2.1. Full NMR Data for Compound 201, Detailing Characterisation

^{1}H NMR (400 MHz, $CDCl_3$) – **201**

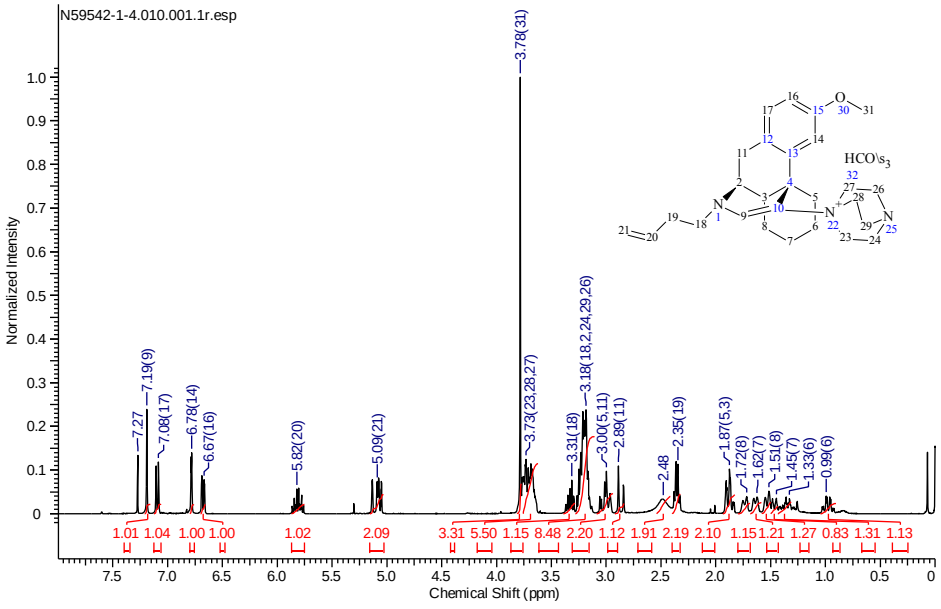

A broad ^{1}H singlet is observed at δ 2.48 ppm, tentatively assigned as the exchangable *H*CO_3^- proton. As an exchangable proton, the integration here is not reliable.

COSY NMR ($CDCl_3$) – **201**

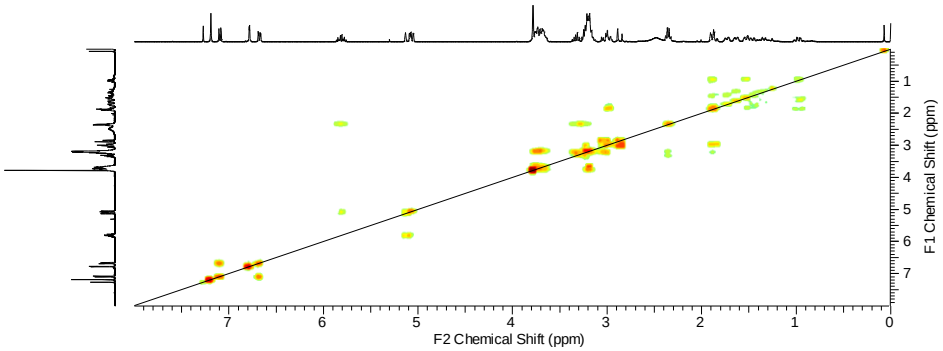

COSY: The ^{1}H multiplet at δ 5.87 – 5.76 ppm is coupling to the ^{1}H quartet at δ 2.35 ppm (the C*H*$_2$ β- to the nitrogen atom). The ^{1}H quartet at δ 2.35 ppm is coupling to the multiplet at δ 3.38 – 3.28 ppm (one of the C*H*$_2$ H-atoms α- to the nitrogen atom).

^{13}C NMR (101 MHz, $CDCl_3$) – **201**

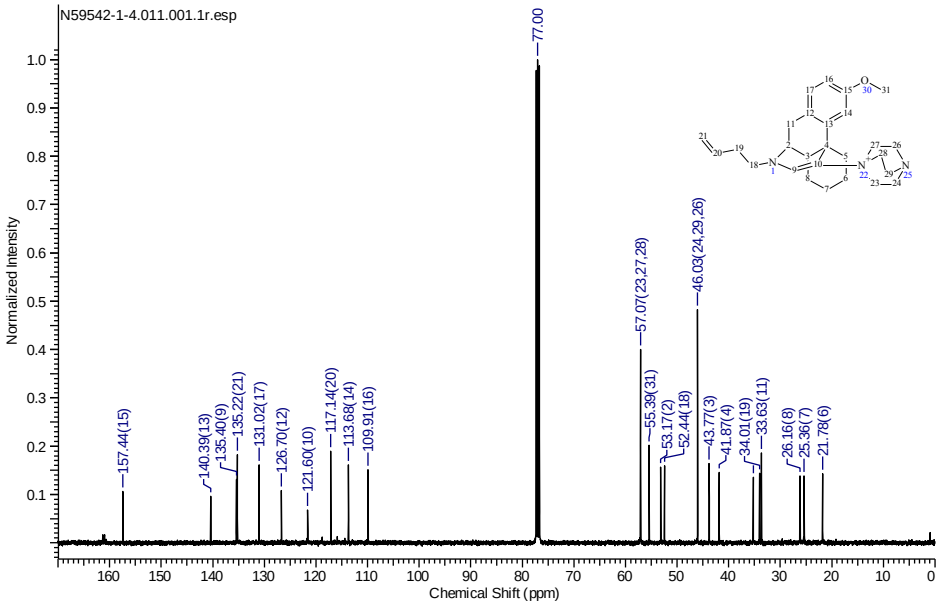

DEPT NMR (101 MHz, $CDCl_3$) – **201**

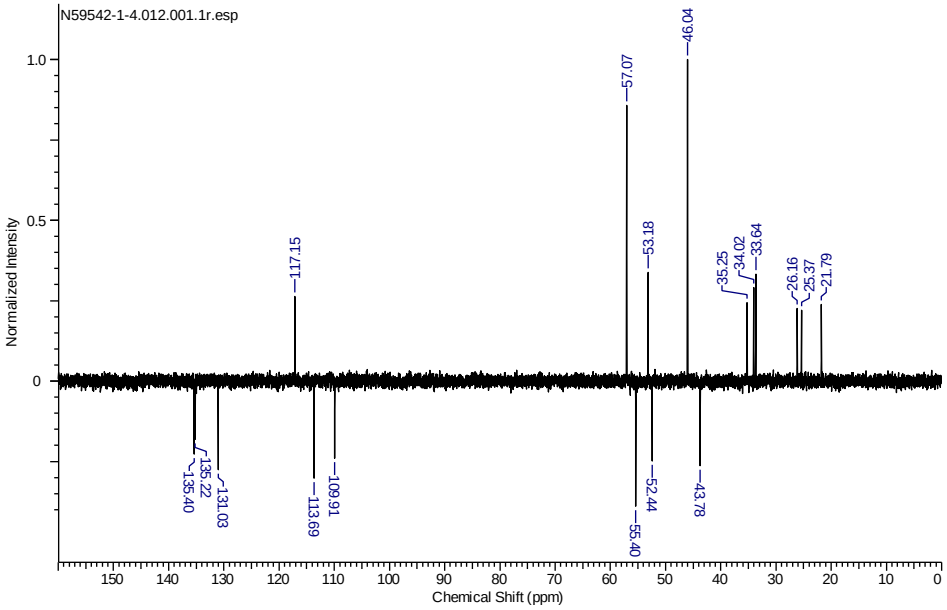

Here, *C*H_2 environments are shown on the top phase, *C*H and *C*H_3 environments are shown on the bottom phase.

HSQC NMR ($CDCl_3$) – **201**

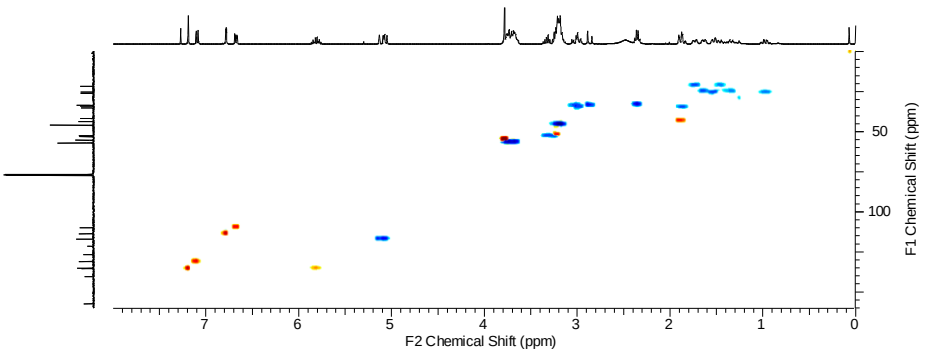

Here, *C*H and *C*H_3 environments are red in colour, *C*H_2 environments are blue in colour. **HSQC:** The deshielded singlet at δ 7.19 ppm is coupling to the ^{13}C peak at δ 135.4 ppm, which is a *C*H according to the phase. These peaks were assigned as the alkene *CH*. The ^{1}H multiplet at δ 3.38 – 3.28 (one of the C*H*$_2$ H atoms α- to the nitrogen atom) is coupling to the ^{13}C peak at δ 53.2 ppm, which is a *C*H_2 according to the phase. This was assigned as one of the α-amino C*H*$_2$ H atoms. The ^{1}H multiplet at δ 3.28 – 3.12 ppm contains

the other α-amino C*H*$_2$ H atom, six H atoms from the DABCO 3x equivalent C*H*$_2$ groups (furthest from the quarternary nitrogen atom) and the H atom from the α-amino C*H* group, according to the phase. The α-amino C*H* is coupling to the ^{13}C peak at δ 52.4 ppm. The broad ^{1}H singlet at δ 2.48 ppm is not coupling to a carbon, supporting its tentative assignment as the exchangable proton of *H*CO$_3^-$.

HMBC NMR ($CDCl_3$) – **201**

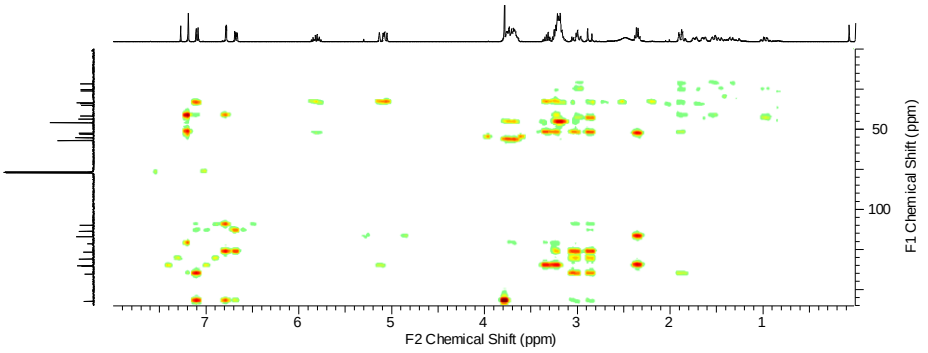

HMBC NMR ($CDCl_3$) – **201 expanded**

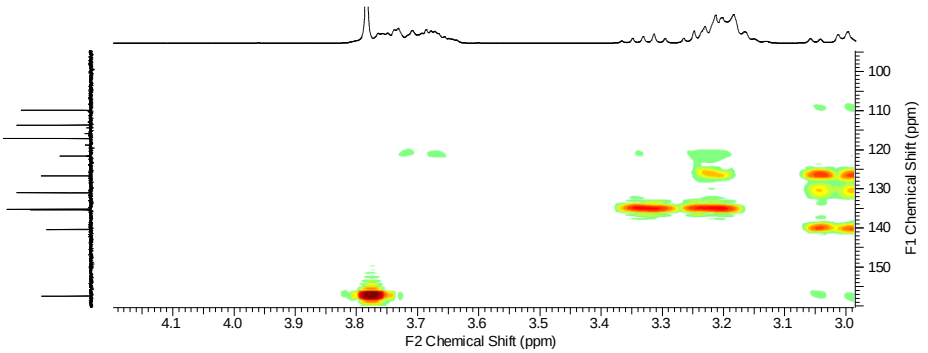

HMBC: Coupling is seen between the ^{1}H multiplet at δ 3.38 – 3.28 (one of the C*H*$_2$ H atoms α- to the nitrogen atom) and the ^{13}C peak at δ 135.4 ppm (the alkene *C*H). Coupling is seen between the ^{1}H singlet at δ 7.19 ppm (the alkene C*H*) and the ^{13}C peak at δ 52.4 ppm (the α-amino *C*H). A weak coupling is seen between the ^{1}H multiplet at δ 3.78 – 3.63 ppm (the 3x equivalent N$^+$-C*H*$_2$ groups of the DABCO fragment) and the ^{13}C peak at δ 121.6 ppm (the alkene quaternary *C*).

A9.2.2. Full NMR Data for Compound 198, Detailing Characterisation

^{1}H NMR (400 MHz, $CDCl_3$) – **198**

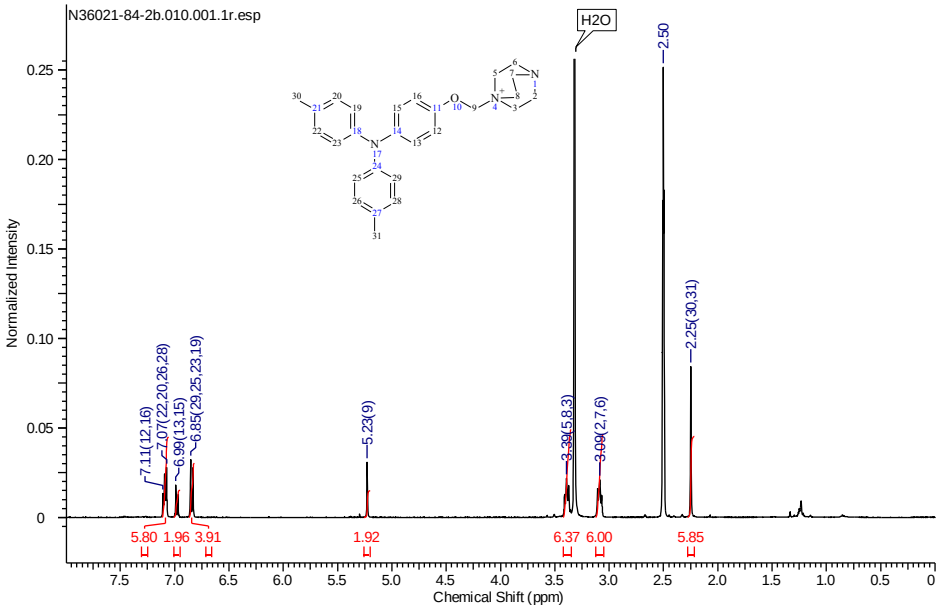

^{13}C NMR (400 MHz, $CDCl_3$) – **198**

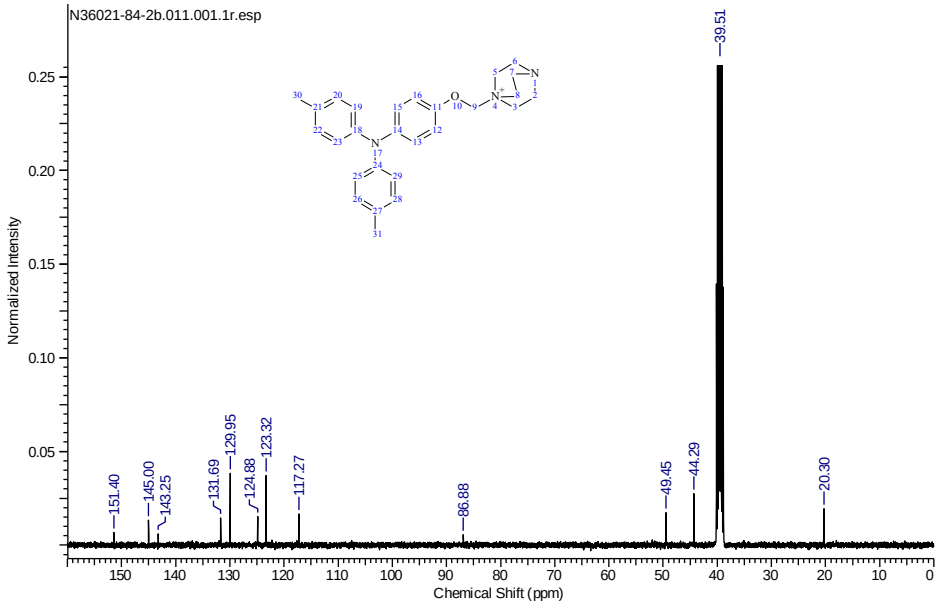

DEPT NMR (101 MHz, DMSO-d_6) – **198**

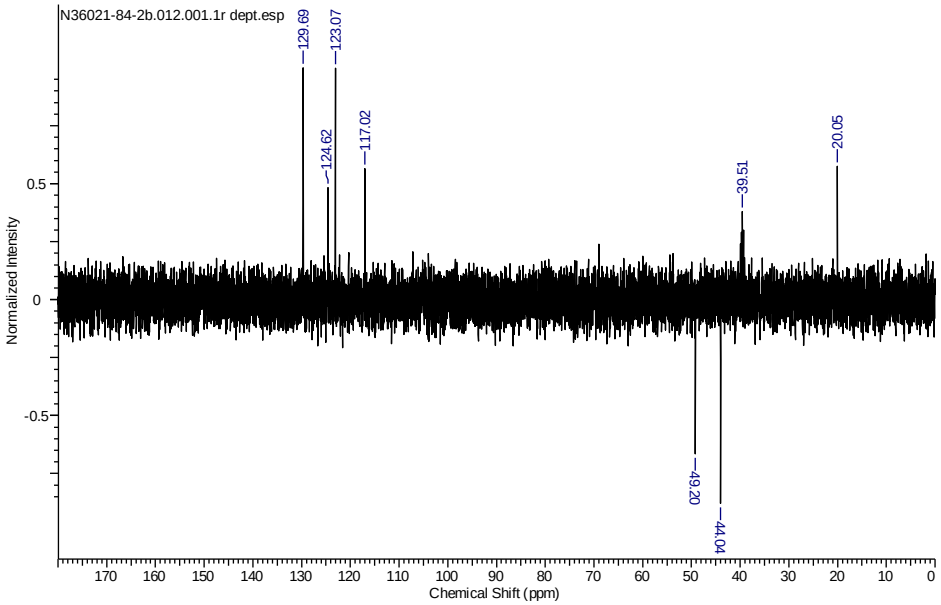

Here, *C*H and *C*H_3 environments are shown on the top phase, *C*H_2 environments are shown on the bottom phase.

COSY NMR (DMSO-d_6) – **198**

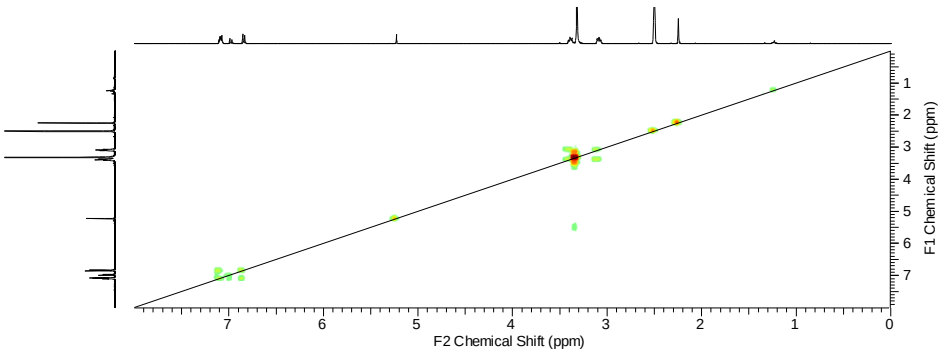

COSY: Coupling can be seen between the triplet at δ 3.39 ppm, 6H and the triplet at 3.09 ppm (6H).

HSQC NMR (DMSO-d_6) – **198**

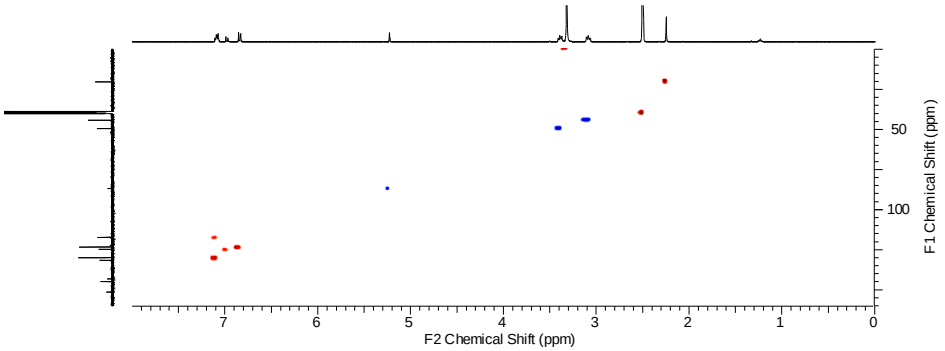

Here, *C*H and *C*H_3 environments are red in colour, *C*H_2 environments are blue in colour. **HSQC:** The deshielded singlet at δ 5.23 ppm is coupling to the ^{13}C at δ 86.8 ppm, which is a *C*H_2 according to the phase. This was tentatively assigned as N^+-*C*H_2-O.

HMBC NMR (DMSO-d_6) – **198**

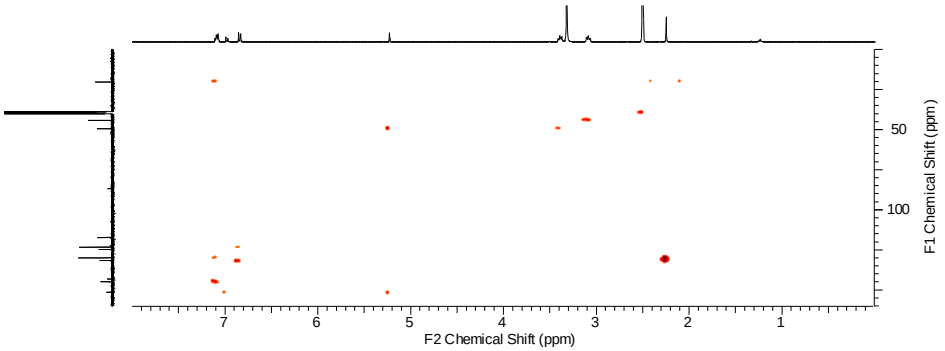

HMBC NMR (DMSO-d_6) – **198** expanded

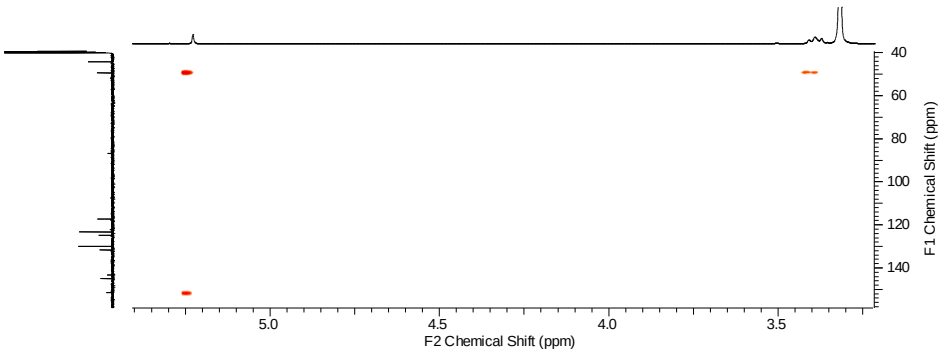

HMBC: Coupling is seen between the ^{1}H singlet at δ 5.23 ppm and both the ^{13}C at δ 49.5 ppm (the N^{+}-*C*H_2 of the DABCO fragment) and the ^{13}C at δ 151.4 ppm (a quaternary *C*). The observed couplings, together with the deshielding of this quarternary *C* is more consistent with the structural fragment ArOCH_2- than ArCH_2O-.

A9.2.3. DETERMINATION OF *N*-CH_3 *VS.* *N*-CH_2 REGIOSELECTIVITY BY ^{1}H NMR

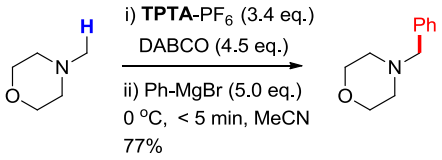

***Scheme A16**: N-C**H**$_3$-functionalisation of N-methylmorpholine.*

^{1}H NMR (400 MHz, $CDCl_3$) – crude reaction mixture

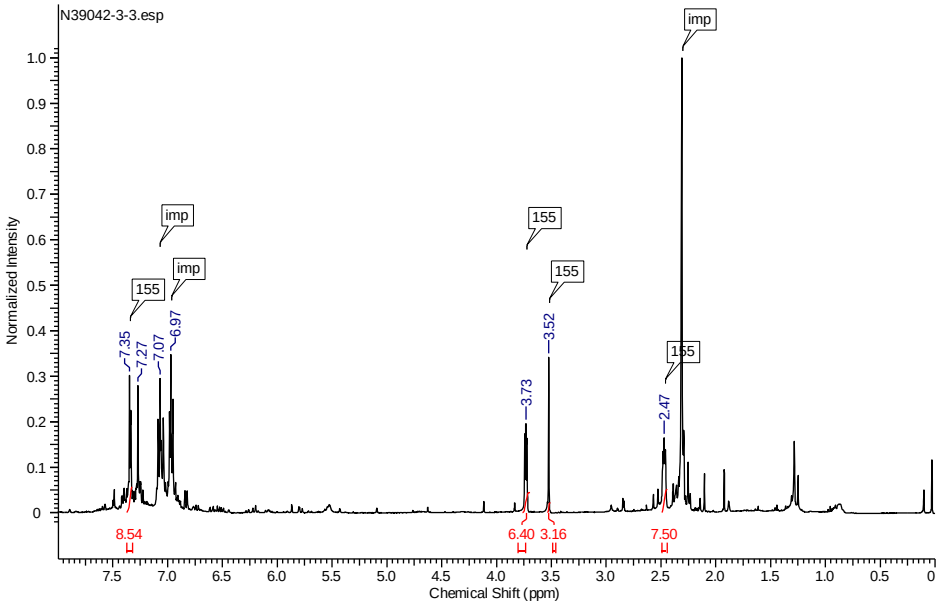

The ^{1}H NMR of the crude reaction mixture revealed **155** as the only significant substrate-derived component. Other detectable components (imp = impurity) arise from background nucleophilic addition reactions of phenylmagnesium bromide with MeCN solvent, or are **TPTA**-PF_6-related (tri-*p*-tolylamine is observed). The *N*-C**H**$_2$-functionalised product, 3-phenyl-*N*-methylmorpholine, is reported in the literature[48] with the following ^{1}H NMR

data; ^{1}H NMR (400 MHz, $CDCl_3$) δ 7.34 – 7.27 (5H, m, C*H*), 3.92 (1H, s, C*H*), 3.80 (1H, td, *J* = 11.5, 1.4 Hz, CH_2), 3.72 (1H, dd, *J* = 11.6, 3.3 Hz, CH_2), 3.41 (1H, t, *J* = 10.9 Hz, CH_2), 3.08 (1H, dd, *J* = 10.3, 3.1 Hz, CH_2), 2.85 (1H, t, *J* = 10.9 Hz, CH_2), 2.43 (1H, td, *J* = 11.7, 3.4 Hz, CH_2), 2.08 (3H, s, CH_3); these peaks are not detected in the crude reaction mixture ^{1}H NMR spectrum. For example, integrating the baseline where the δ 3.41 (1H) peak would appear estimates 0.02 integration units. Compared to the integration of the δ 3.52 (2H) peak of **155**, the ratio of *N*-C**H**$_3$: *N*-C**H**$_2$ functionalised product is deemed > 30 : 1.

^{1}H NMR (400 MHz, $CDCl_3$) – crude reaction mixture expanded

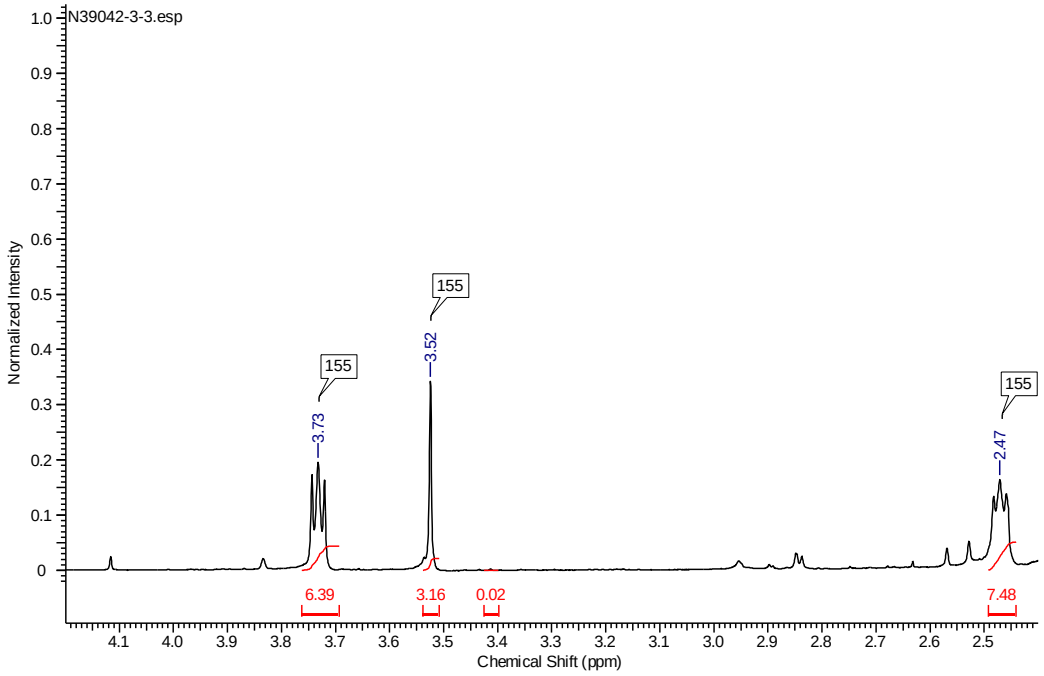

A9.2.4. CALIBRATION CURVE FOR PCA MODEL SOLVENT SCREEN

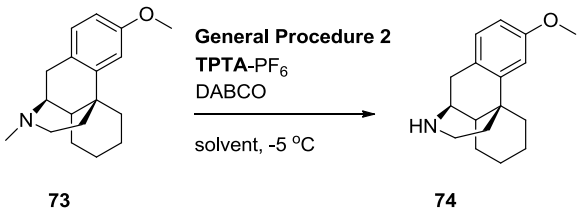

73 **74**

Scheme A17*: Determination of conversion for the optimisation of the* ***TPTA****-PF_6/DABCO-mediated oxidation reaction using the LCMS ratio of* ***73*** *:* ***74*** *as a response.*

When subjected to low pH LCMS or HPLC methods, **73** and **74** eluted at the same retention time in a single, well defined peak in the UV (220 nm) trace. Whilst **73** and **74** could be resolved by a high pH LCMS method, broadening of the peak associated with **74** was observed in the UV (220 nm) traces of crude reaction mixtures. This led to inaccuracies in integration of peak areas. For accurate determination of the conversion, the single, well defined peak of the low pH LCMS was used. The ratio of **73** : **74** by relative ionisation (total ion count) associated with that peak was directly proportional to the ratio of **73** : **74** by high pH LCMS peak areas (Figure A37, left), and the ratio of **73** : **74** by high pH LCMS peak areas was related to the relative molar composition (%) of **74** by means of a calibration curve (Figure A37, right). This method was used to determine conversion of **73** to **74** during the solvent screen (Volume 1, Experimental, Table 17, Section 5.20.3).

An equimolar ratio of **73** : **74** gave a 1.00 : 0.93 ratio of LCMS peak areas (220 nm), indicating that **73** and **74** had very similar relative response factors. This validates the comparison of LCMS (220 nm, high pH method) peak areas to determine conversion of **73** to **74**.

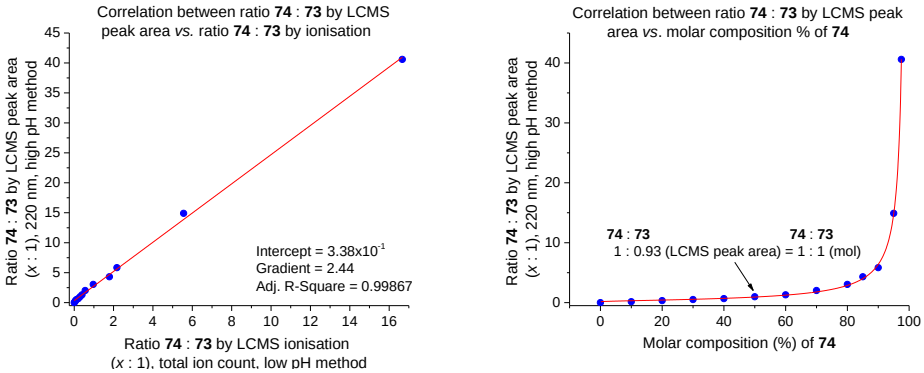

***Figure A37**: Left: Correlation between ratio **74** : **73** by LCMS peak area (220 nm, high pH method) vs. ratio **74** : **73** by ionisation (total ion count, low pH method). Right: Correlation between ratio **74** : **73** by LCMS peak area (220 nm, high pH method) vs. molar composition (%) of **74**.*

A9.3. KEY SPECTRA PERTAINING TO VOLUME 2, CHAPTER 2.1. AND CHAPTER 2.2.

A9.3.1. COMBINED BIARYLS ISOLATED FROM REACTIONS OF 2,6-DIMETHYLIODOBENZENE (57a)

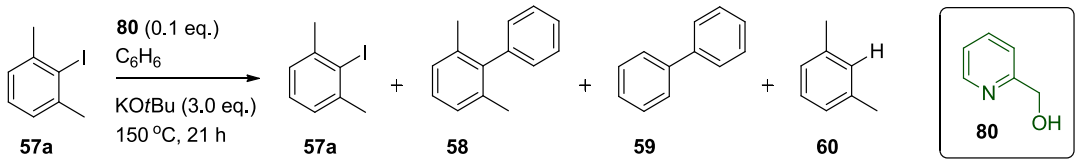

***Scheme A18**: KOtBu-mediated C-H arylation of 2,6-dimethyliodobenzene (**57a**) with benzene using 2-pyridinecarbinol (**80**) as an additive.*

^{1}H NMR (600 MHz, $CHCl_3$) – isolated inseparable biaryls **58** and **59**

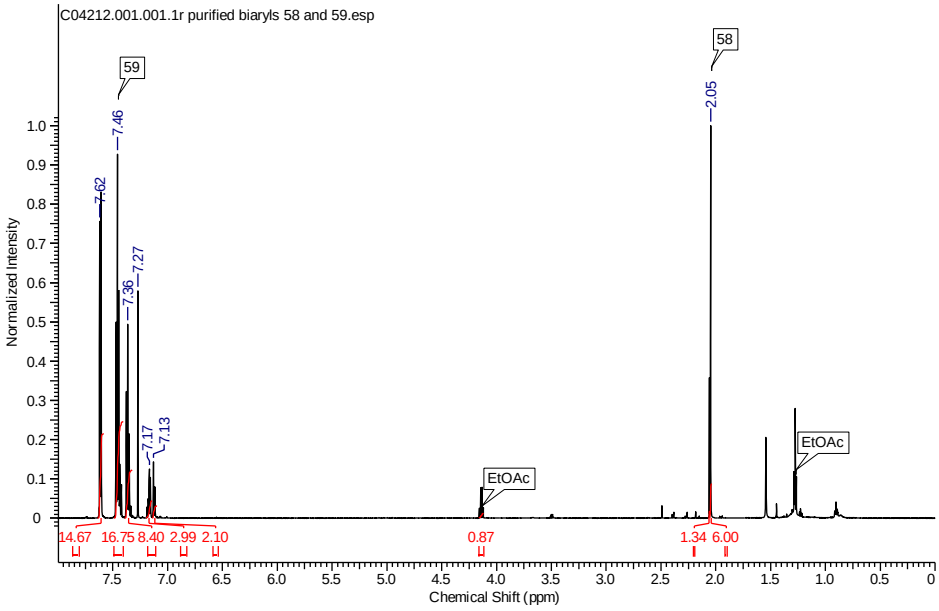

A9.3.2. KO*t*Bu-MEDIATED BENZYLIC DEUTERATION OF 2-PYRIDINECARBINOL FROM D_2O

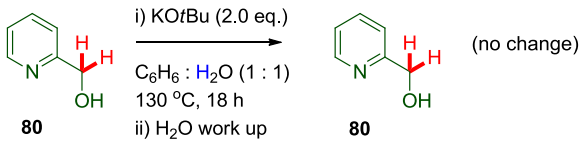

***Scheme A19**: Control reaction treating 2-pyridinecarbinol (**80**) under the reaction conditions in the absence of a haloarene and in the presence of H_2O.*

^{1}H NMR (400 MHz, $CDCl_3$) – crude reaction mixture, H_2O used in the reaction

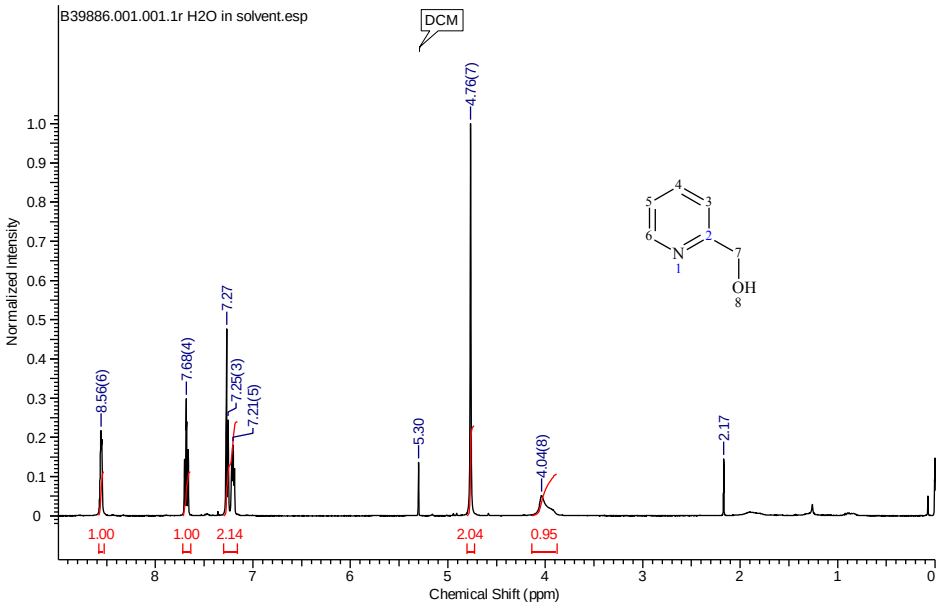

The ^{1}H NMR spectrum shows **80** as the sole component. The integration of an aliphatic 1H is 1.02x the integration of an aromatic 1H.

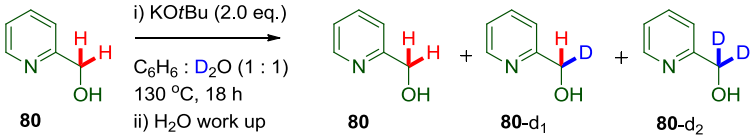

***Scheme A20**: Treating 2-pyridinecarbinol (**80**) under the reaction conditions in the absence of a haloarene and in the presence of D_2O.*

Relative to the aromatic H signals, the ^{1}H singlet at δ 4.77 ppm is almost half the integration shown in the previous spectrum, indicating D-incorporation at the benzylic C*H*$_2$. A characteristic ^{1}H triplet (*J* = 2.0 Hz) is observed at 4.75 ppm, assigned as the benzylic C*H* of **80**-d$_1$. By subtracting the integrations of 1H of **80** (0.53 integration units) and 1H of **80**-d$_1$ (1H = 0.37 integration units) from the ^{1}H doublet at δ 8.58 ppm, an estimation of the relative amount of **80**-d$_2$ can be estimated (1H = 0.10 integration units). This affords the following ratio; **80** : **80**-d$_1$: **80**-d$_2$ = 1.00 : 0.70 : 0.19. By ^{2}H NMR, the expected ratio of **80**-d$_1$: **80**-d$_2$ is 1.00 : 0.54. Two singlets are observed at δ 4.73 ppm and δ 4.77 ppm in a ratio of 1.00 : 0.64 by ^{2}H NMR, thus attributed to **80**-d$_1$ and **80**-d$_2$, respectively.

^{1}H NMR (400 MHz, $CDCl_3$) - crude reaction mixture, D_2O used in the reaction

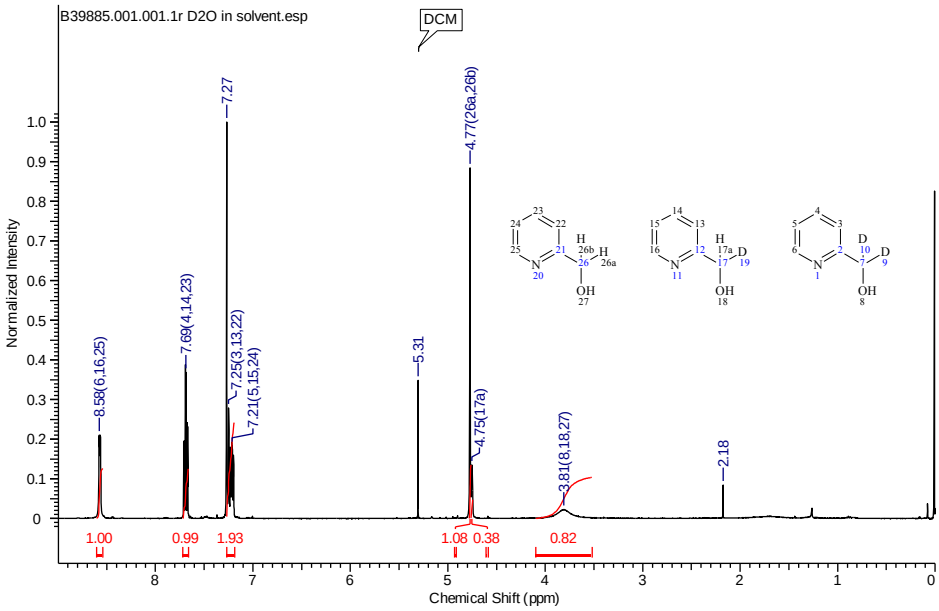

^{1}H NMR (400 MHz, $CDCl_3$) - crude reaction mixture expanded, D_2O used in the reaction

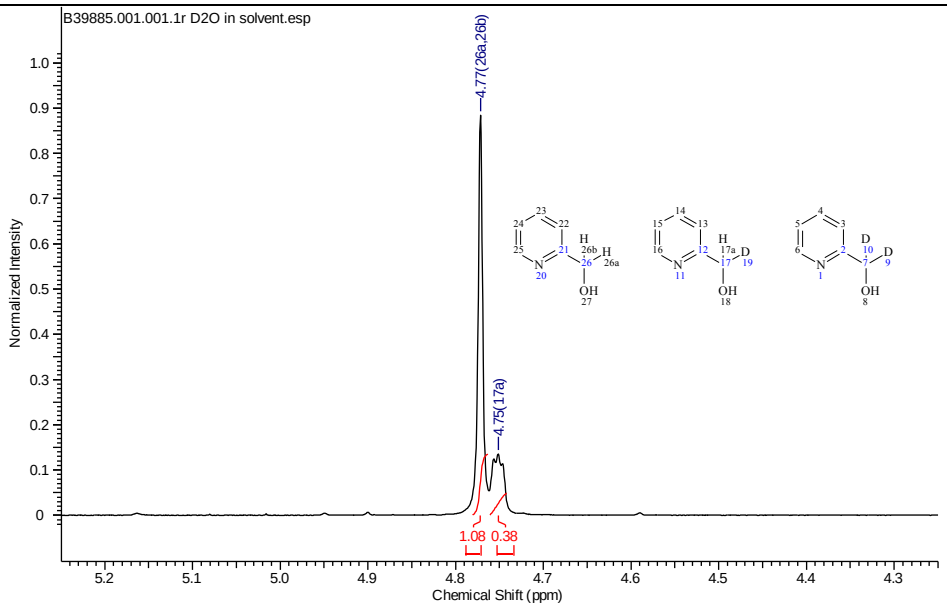

The ^{13}C NMR of the crude reaction mixture shows a characteristic ^{13}C triplet (J = 22.0 Hz) at δ 63.8 ppm, assigned as the benzylic *C*H of **80**-d_1. The benzylic *C* of **80**-d_2 could not be observed. Overall, these data conclusively show D-incorporation at the benzylic position of 2-pyridinecarbinol under the KO*t*Bu-mediated reaction conditions.

^{2}H NMR (61 MHz, $CHCl_3$) - crude reaction mixture. D_2O used in the reaction

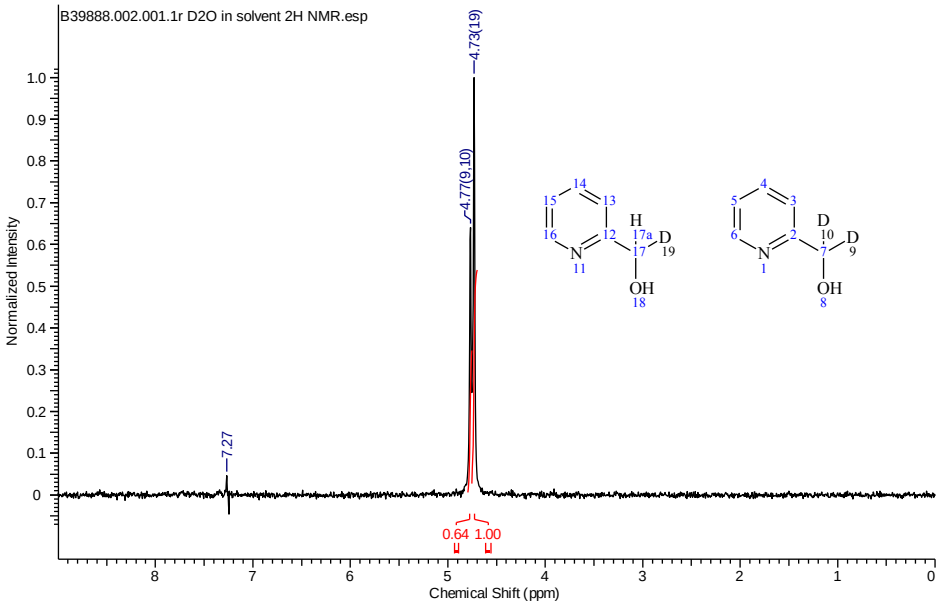

^{13}C NMR (101 MHz, $CDCl_3$) - crude reaction mixture. D_2O used in the reaction

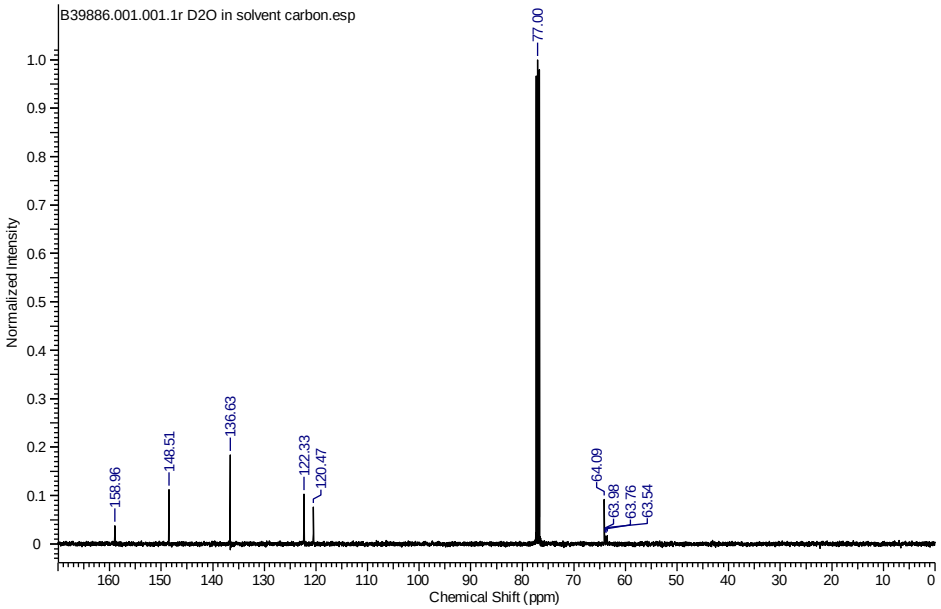

^{13}C NMR (101 MHz, $CDCl_3$) - crude reaction mixture expanded, D_2O used in the reaction

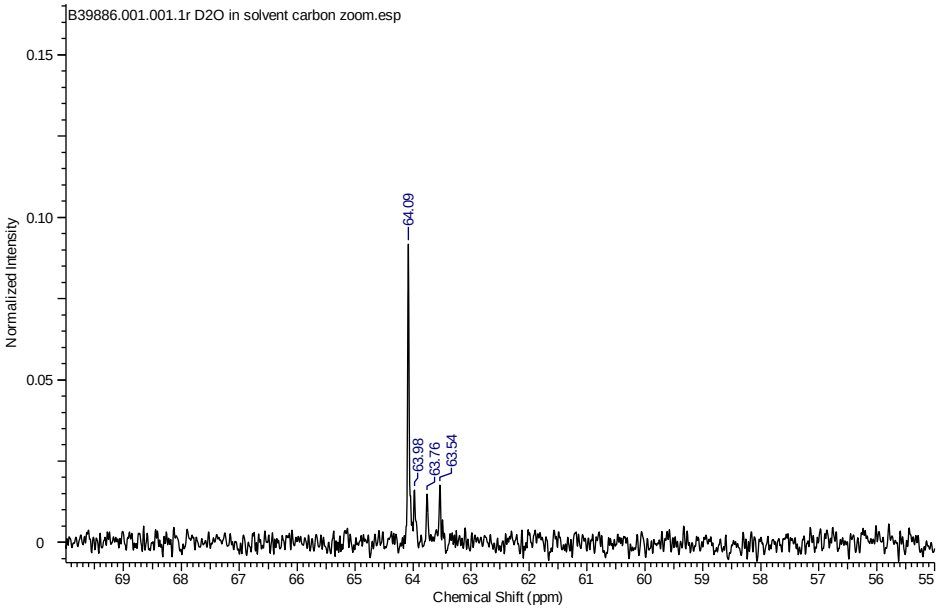

A9.3.3. ACETOPHENONE AND PIVALOPHENONE NMR COMPARISON

^{1}H NMR (400 MHz, $CDCl_3$) - acetophenone

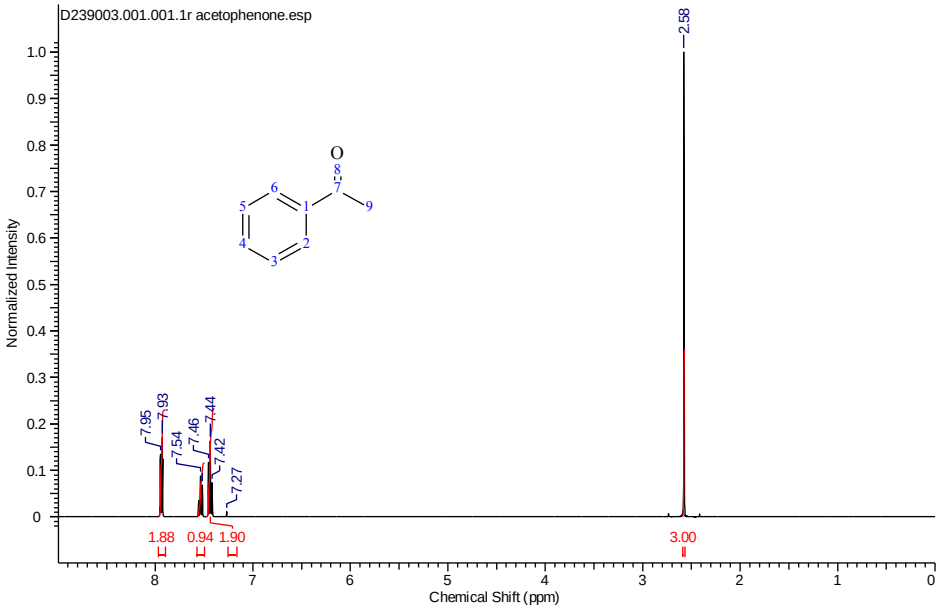

^{1}H NMR (400 MHz, $CDCl_3$) - pivalophenone (**122**)

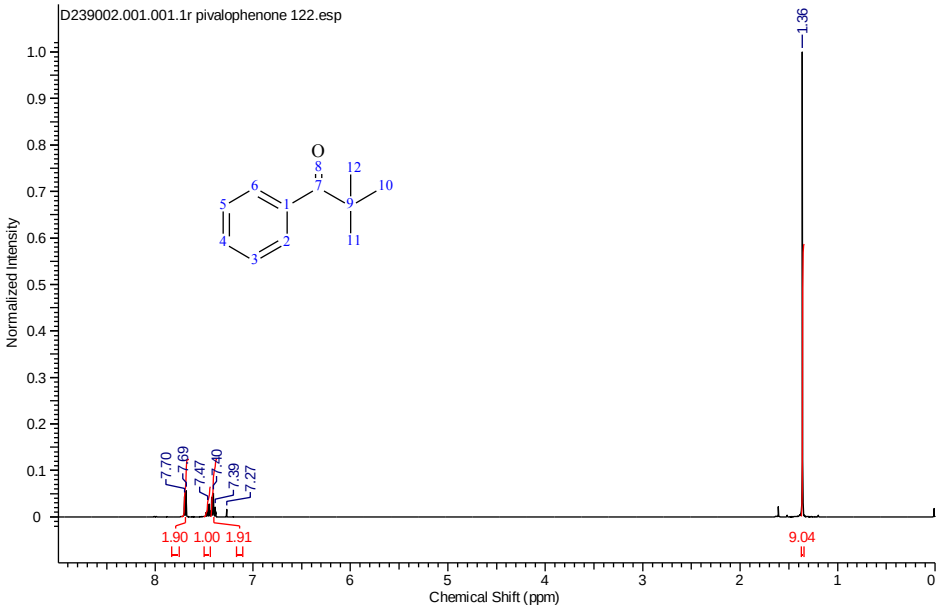

A9.3.4. TRANSESTERIFICATION OF ETHYL BENZOATE WITH KO*t*BU

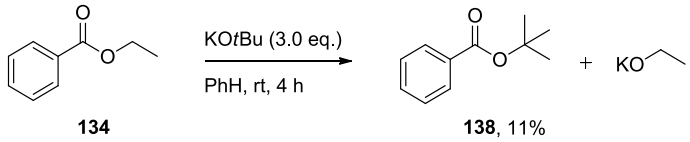

***Scheme A21**: Transesterication of ethyl benzoate with KOtBu.*

^{1}H NMR (400 MHz, $CDCl_3$) - crude product (**138**)

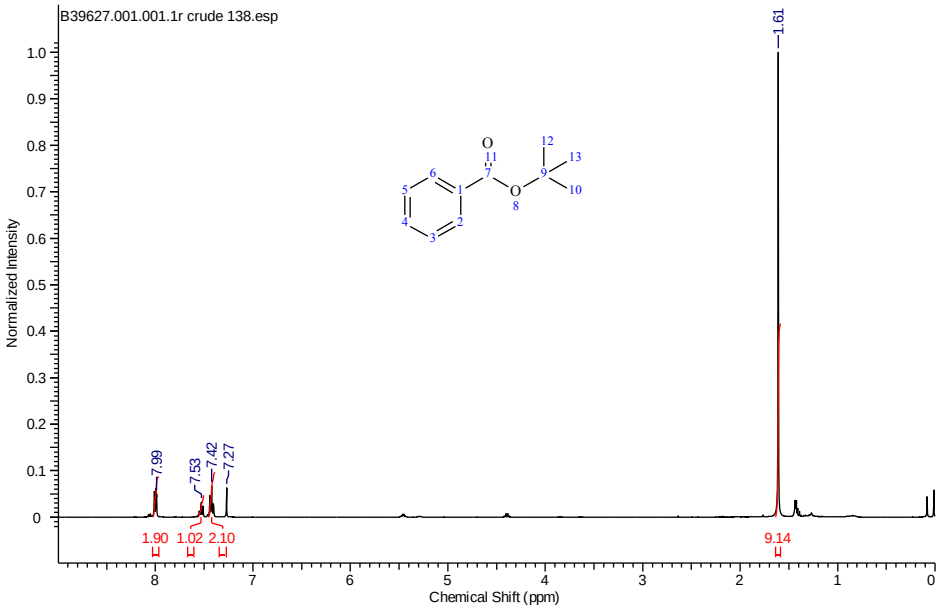

^{13}C NMR (100 MHz, $CDCl_3$) - crude product (**138**)

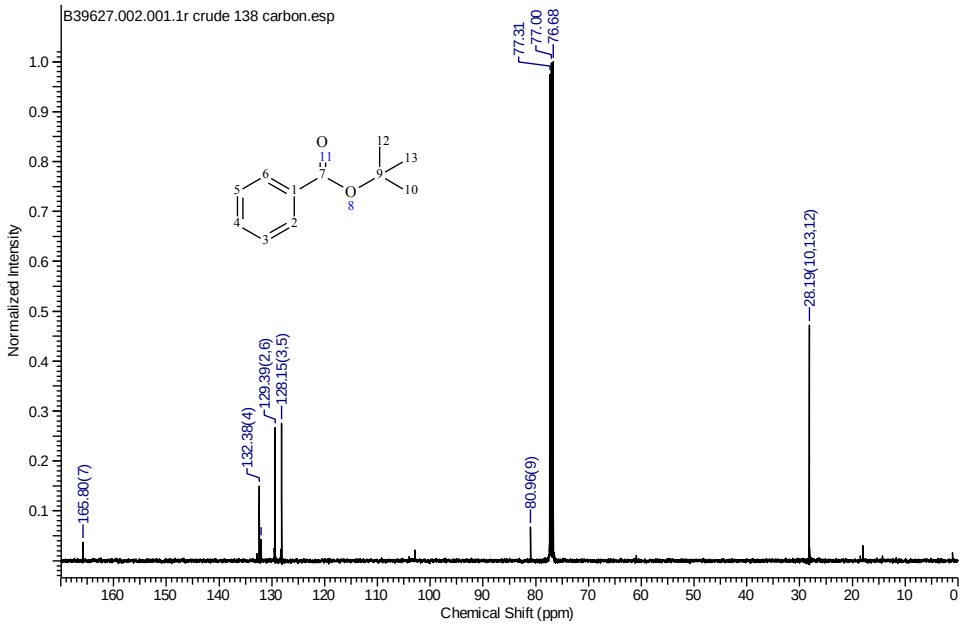

A9.4. KEY SPECTRA PERTAINING TO VOLUME 2, CHAPTER 2.1. AND CHAPTER 2.2.

A9.4.1. EVIDENCE OF BENZYNE FORMATION IN THE KO*t*BU-MEDIATED C-H ARYLATION OF 4-IODOBIPHENYL

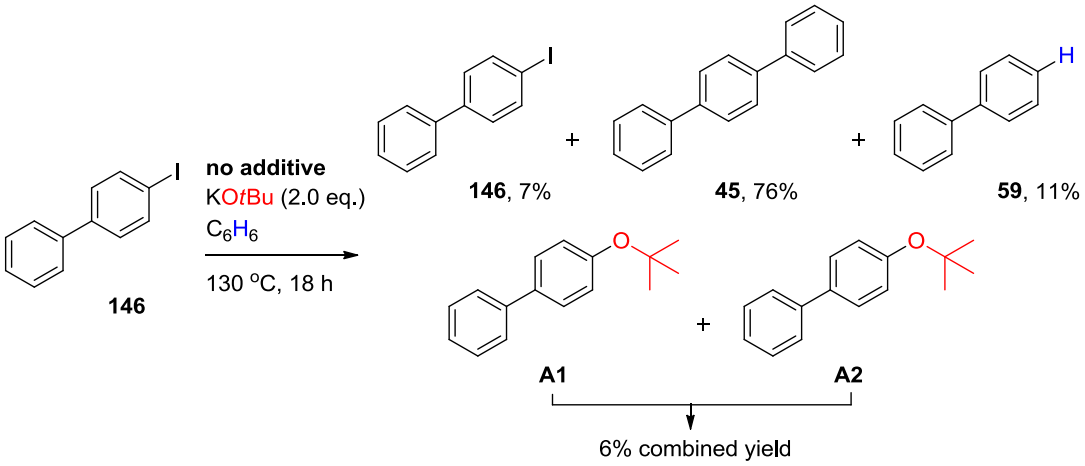

***Scheme A22**: Additive-free KOtBu-mediated C-H arylation of **146**.*

^{1}H NMR (400 MHz, $CDCl_3$) - crude reaction mixture

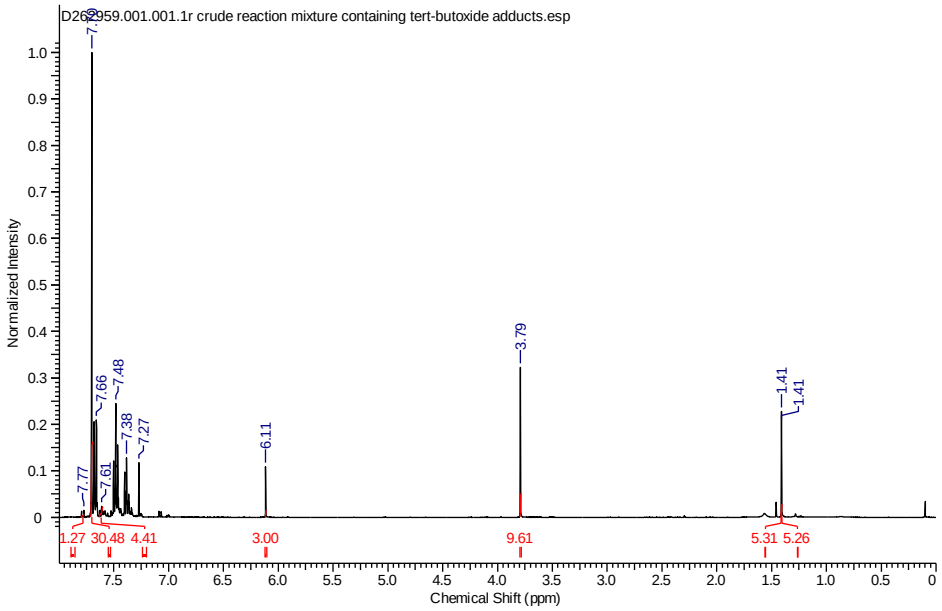

Yields of **146**, **45** and **59** were calculated as demonstrated in Chapter A8.4 and are shown in Volume 2, Section 2.3.2., Table 6, entry 3.

^{1}H NMR (400 MHz, $CDCl_3$) - crude reaction mixture expanded

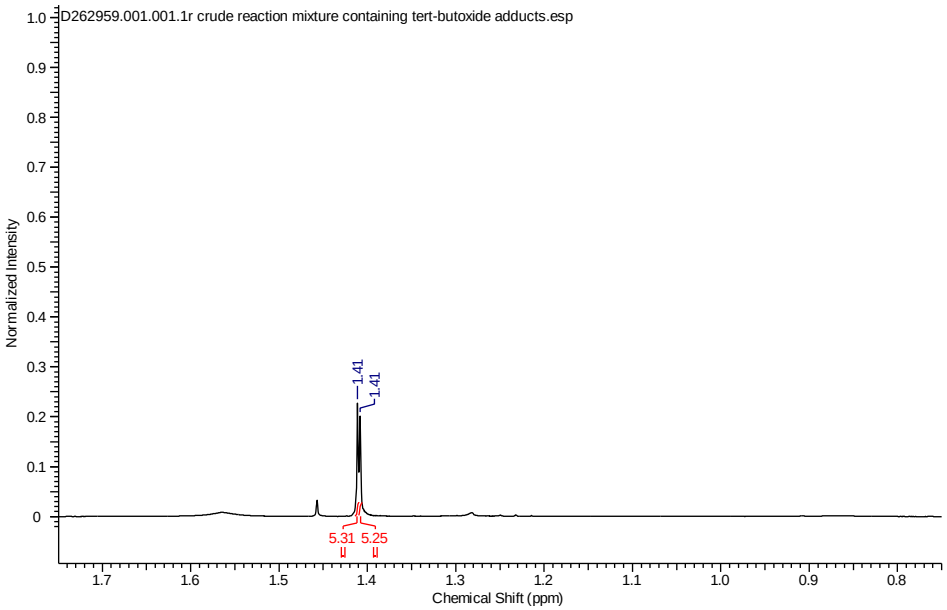

GCMS - **crude reaction mixture**, mass spectrum at 12.8 min.

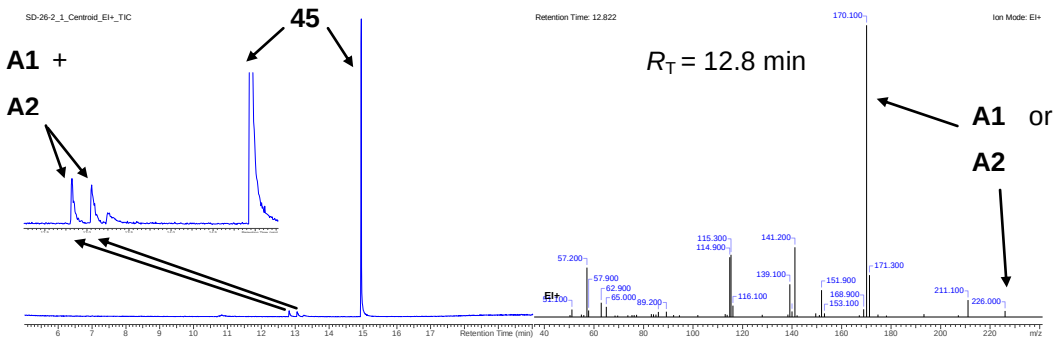

Two singlets were observed at δ 1.41 ppm. These were tentatively assigned to structures **A1** and **A2** above, which paralleled the outcome observed in Volume 2, Section 2.1.5. under similar reaction conditions (see Volume 1 Experimental, Section 5.2.6 for ^{1}H NMR data). The following calculation gave the combined yield of **A1** and **A2**: [(5.31+5.25)/18] x 10 = 5.9%. By GCMS, two new peaks were observed at R_T = 12.8 min and 13.1 min (the mass spectrum of both were identical, showing a weak parent ion $[M]^+$ = 226.0 and a strong fragment ion $[M\text{-}C(CH_3)_3]^+$ = 170.1). The reaction above was conducted by Samuel Dalton at the University of Strathclyde.

A9.4.2. DETERMINATION OF D-INCORPORATION IN KH-MEDIATED DEHALOGENATIONS

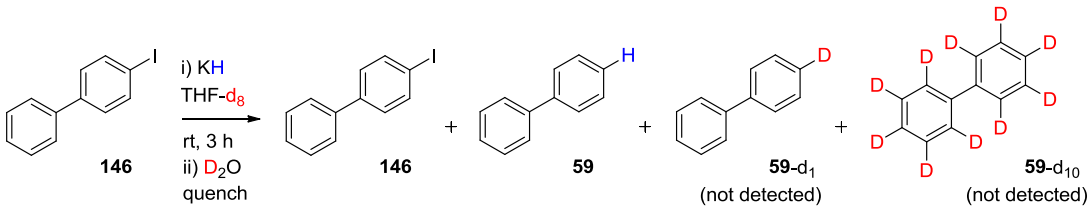

***Scheme A23**: KH-mediated dehalogenation of substrate **146** in THF-d_8 with D_2O quench.*

GCMS - **crude reaction mixture**.

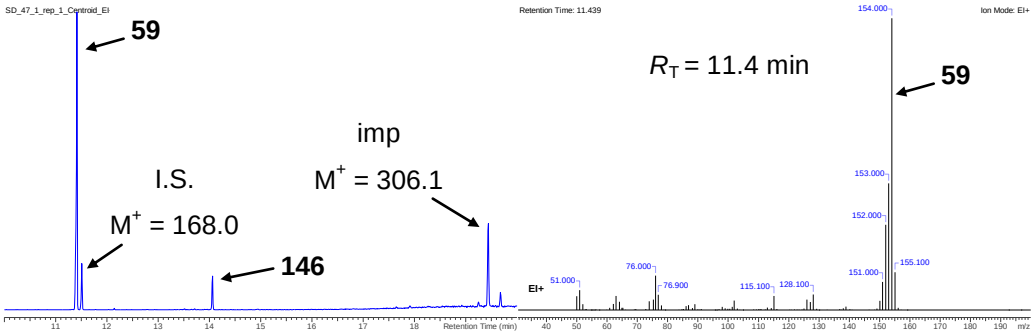

No significant **59**-d_1 could be observed (above its natural isotopic abundance) by GCMS. Furthermore, **59**-d_1 could not be detected by ^{2}H NMR (see next page). This result was summarised by 'D-incorporation = no' in Volume 2, Section 2.3.2., Table 5, entry 4.

^{2}H NMR (61 MHz, THF-h_8) - crude reaction mixture

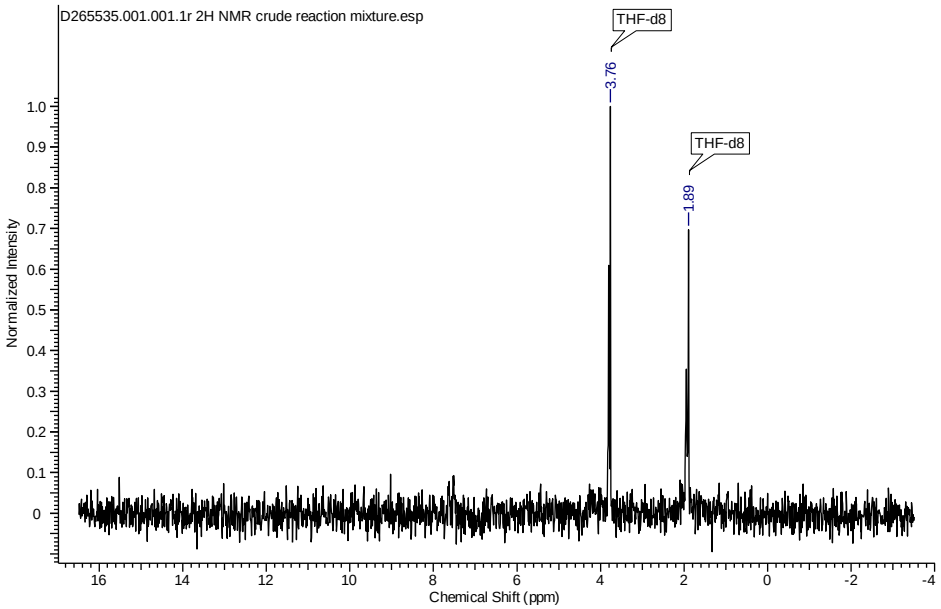

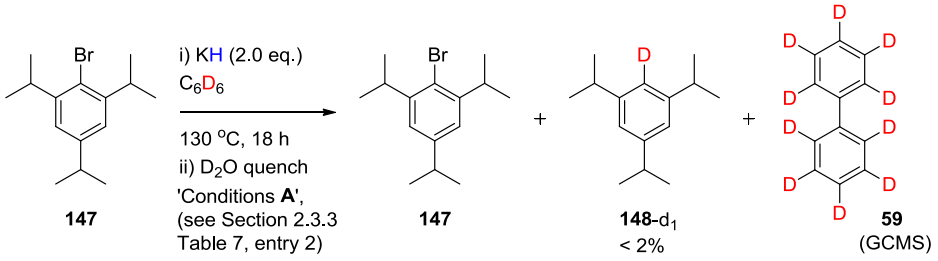

***Scheme A24**: KH-mediated dehalogenation of substrate **147** in C_6D_6 with D_2O quench.*

GCMS - **crude reaction mixture**.

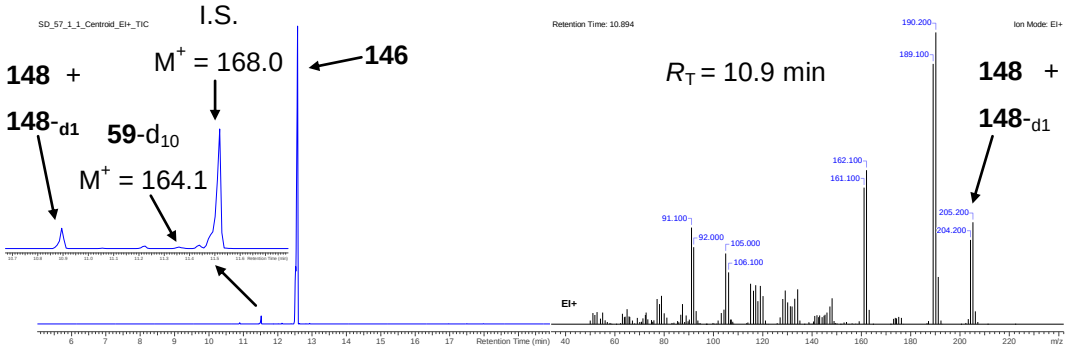

This result was summarised by 'D-incorporation = yes' in Volume 2, Section 2.3.3., Table 7, entry 2. This reaction was conducted by Samuel Dalton. Alternatively, the reaction was conducted as outlined in Scheme A25. ^{1}H NMR revealed D-incorporation into the aromatics of **148** (thus, **148**-d_1) and ^{2}H NMR of the crude reaction mixture clearly revealed **59**-d_{10} and **148**-d_1. This reaction was conducted by Joshua Barham.

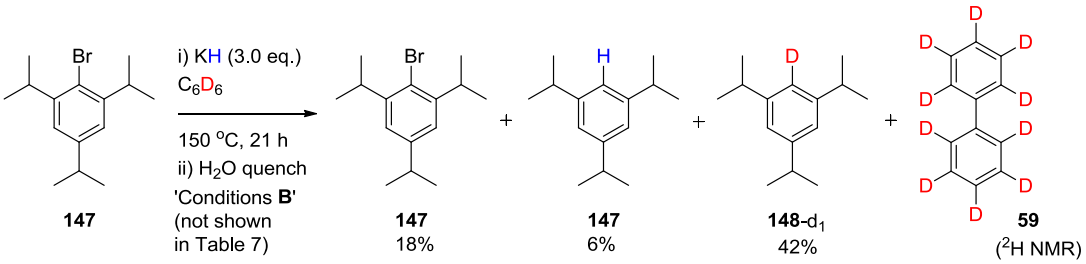

***Scheme A25**: KH-mediated dehalogenation of substrate **147** in C_6D_6 under harsher conditions with H_2O quench.*

^{1}H NMR (400 MHz, $CDCl_3$) - crude reaction mixture

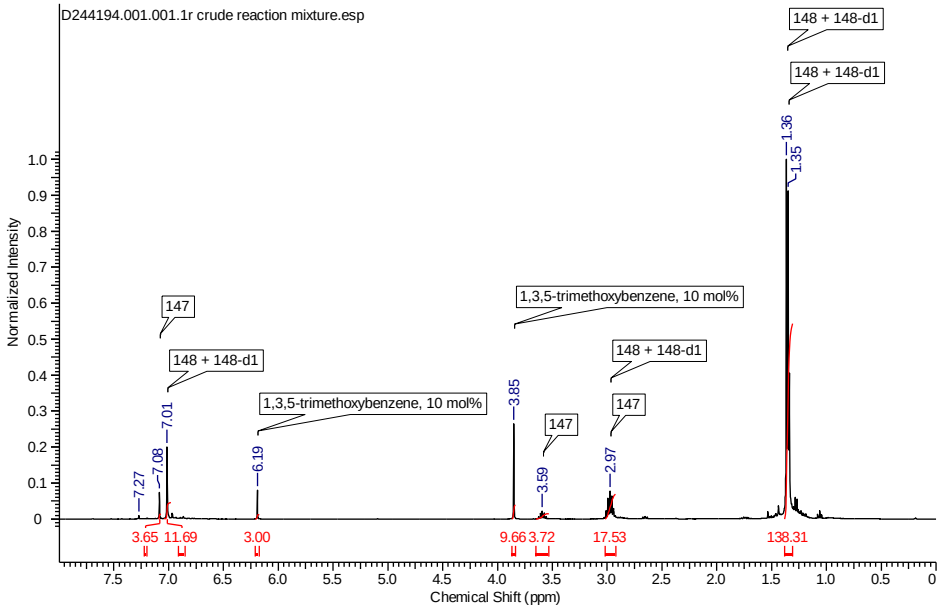

The yield of returned **147** was calculated as 18.3% as shown in Chapter A.8. For the combined yield of **148** + **148**-d_1, it is assumed that no D-incorporation occurred in the aliphatic region. Therefore, the contribution of **147** to the integral of the peak at δ 2.97 ppm, 1H from **147** and 3H from **148**) can be subtracted by the following calculation: 17.53 - (3.72/2) = 15.67 integration units (for the 3x aliphatic C*H* peaks of **148** + **148**-d_1). Correcting for the marginally different integrations of aliphatic : aromatic H (ratio aromatic H : aliphatic H = 1 : 1.07) provides 14.64 integration units for the peak at δ 2.97 ppm. The combined yield of **148** + **148**-d_1 is given by: [(14.64/3) x 10] = 48.8%. If 100% D-incorporation had occurred in the aromatics to give **148**-d_1, the peak at δ 7.01 ppm would give 9.76 integration units [(14.64/3) x 2 = 9.76]. Therefore, the yield of **148** is calculated by the following equation: 11.69 - 9.76 = 1.93; [(1.93/3) x 10] = 6.4%. The yield of **148**-d_1 is therefore: 48.8 - 6.4 = 42.4%. The crude ^{2}H NMR data [^{2}H NMR (61 MHz, $CHCl_3$) δ 10.04 (1D, s, C*D*O), 7.91 (2D, br. s, C*D*), 7.66 (1D, br. s, C*D*), 7.56 (2D, br. s, C*D*)] was consistent with the literature. Given the ratio of **148**-d_1 : **59**-d_{10} (1 : 0.26) by ^{2}H NMR, the yield of **59**-d_{10} can be estimated as 12.7%.

^{2}H NMR (61 MHz, $CHCl_3$) - crude reaction mixture

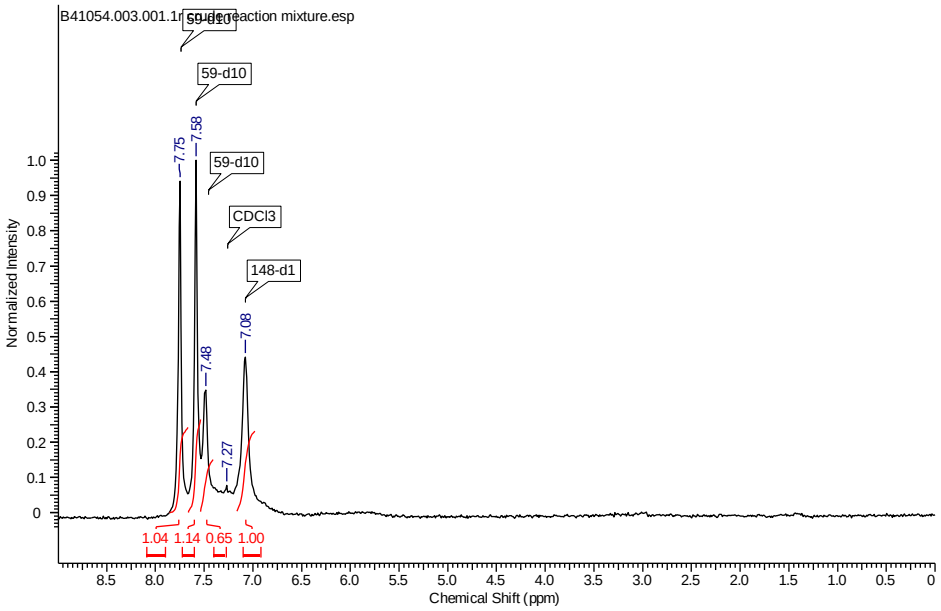

A9.4.3. D-INCORPORATION IN 1,3,5-TRIISOPROPYLBENZENE FROM LITHIUM ALUMINIUM DEUTERIDE

^{1}H NMR (400 MHz, $CDCl_3$) - crude reaction mixture, $LiAlD_4$/KO*t*Bu used in reaction.

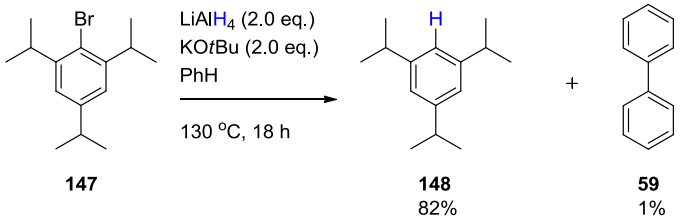

***Scheme A26**: LiAlH$_4$-mediated dehalogenation of **147** in the presence of KOtBu.*

^{1}H NMR (400 MHz, $CDCl_3$) - crude reaction mixture, $LiAlH_4$/KO*t*Bu used in reaction.

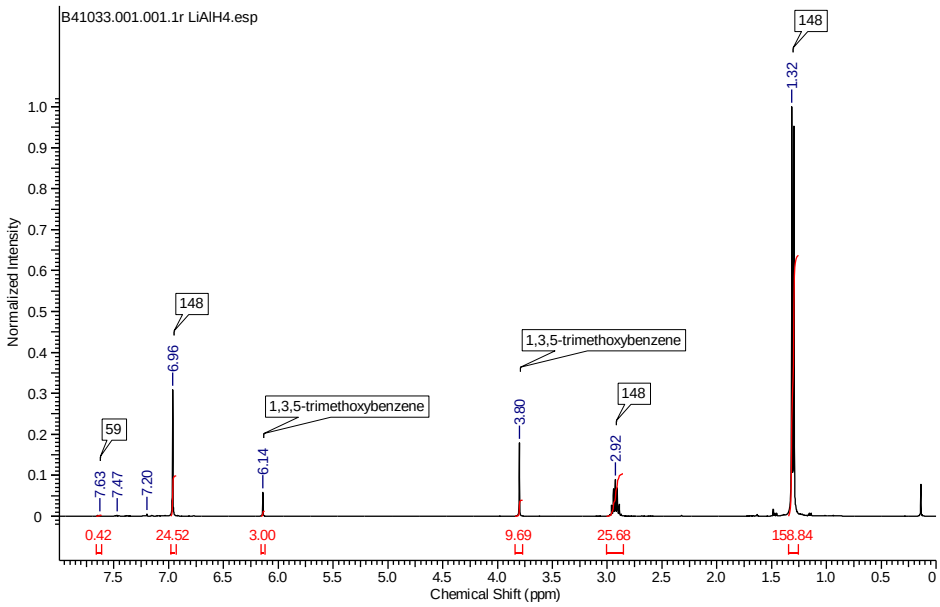

For the product **148**, the integral of the aromatic signal of the internal standard (δ 6.14 ppm) was set to 3. The integration of the aromatic signal of **148** (δ 6.96 ppm, 3H) was measured and the following calculation gave the amount of **148** present: (24.52/3) x 10 = 81.7%. For biphenyl product **59**, the integral of the aromatic signal of the internal standard (δ 6.14 ppm) was set to 3. The integration of the aromatic signals of **59** (δ 7.66 - 7.61 ppm, 4H) was measured and the following calculation gave the amount of **59** present: (0.42/4) x 10 = 1.1%. The integration of an aliphatic 1H is 1.05x the integration of an aromatic 1H. This reaction was now repeated with $LiAlD_4$ instead of $LiAlH_4$ (Scheme A27). No starting material was observed.

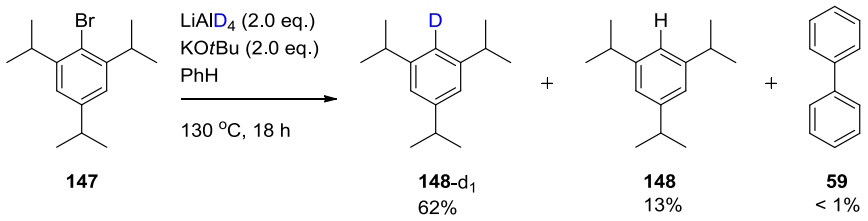

***Scheme A27**: LiAlD$_4$-mediated dehalogenation of **147** in the presence of KOtBu.*

^{1}H NMR (400 MHz, $CDCl_3$) - crude reaction mixture, $LiAlD_4$/KO*t*Bu used in reaction.

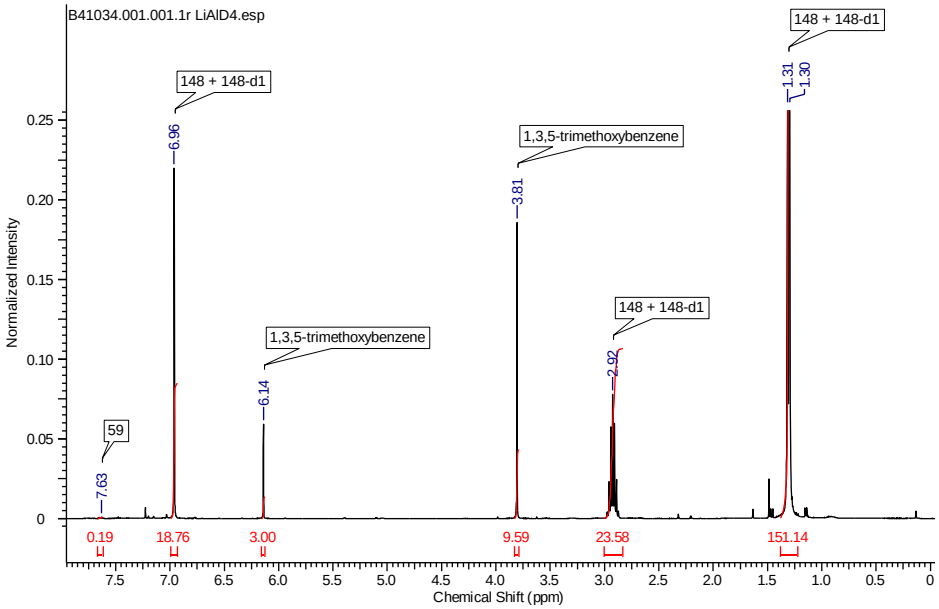

The integral of the aromatic signal of the internal standard (δ 6.14 ppm) was set to 3. The following calculations, based on the integration of the ^{1}H septet (δ 2.92 ppm, 3H), gave the amount of combined **148** + **148**-d_1 present: 23.58/1.05 = 22.46 units (the integration of an aliphatic 1H is 1.05x the integration of an aromatic 1H), (22.46/3) x 10 = 74.9%. Based on the integration of the ^{1}H septet (δ 2.92 ppm), the expected integration of the aromatic ^{1}H singlet (δ 6.96 ppm) is 22.46 units, if 100% H-incorporation had occurred to give exclusively **148**. If 100% D-incorporation had occurred to give exclusively **148**-d_1, the integration would be 14.97 units [(22.46/3) x 2 = 14.97]. The observed integration of the aromatic ^{1}H singlet is 18.76 units, therefore 18.76 - 14.97 = 3.79 units account for H-incorporation (**148** as the product). The following calculation gave the amount of **148** present: (3.79/3) x 10 = 12.6%. Therefore, the yield of **148**-d_1 was 62.3%. For biphenyl product **59**, the integral of the aromatic signal of the internal standard (δ 6.14 ppm) was set to 3. The integration of the aromatic signals of **59** (δ 7.66 - 7.61 ppm, 4H) was measured and the following calculation gave the amount of **59** present: (0.19/4) x 10 = 0.5%. Therefore, by this method the yield of **148** was

13%, the yield of **148**-d_1 was 62% and the yield of 59 was < 1%.

A9.4.4. DETERMINATION OF D-INCORPORATION IN 1,3,5-TRI-*tert*-BUTYLBENZENE-d_{29}

The ^{1}H NMR spectrum of purified **148**-d_{29} showed some traces of H-incorporation (see next page, spectrum prior to quantification). Quantification was determined by analysing an equimolar ratio of **149**-d_{29} and 1,3,5-trimethoxybenzene by ^{1}H NMR (here, the moles of **149**-d_{29} were approximated on the basis of the molecular weight of fully deuterated **149**-d_{29}). Whilst the aromatic H-incorporation peaks could be easily resolved, determining levels of aliphatic H-incorporation in **148**-d_{29} at such trace levels was challenging due to the low-lying H_2O residual in $CDCl_3$ and traces of grease/heptane which overlapped with the aliphatic signals of **148**-d_{29} (despite best efforts to remove these). Assuming minimal contribution of residual solvent signals [H_2O or grease/heptane (the peak at δ 0.91 ppm is very small)] to the integration of the aliphatics in the spectrum prior to quantification, the ratio of aromatic H : aliphatic (*ortho*-*tert*-butyl) H = 1 : 13.61. The ratio of aromatic H : aliphatic (*para*-*tert*-butyl) H = 1 : 4.31. These ratios are used subsequently.

^{1}H NMR (400 MHz, $CDCl_3$) - **148**-d_{29} residual H-incorporation (before quantification)

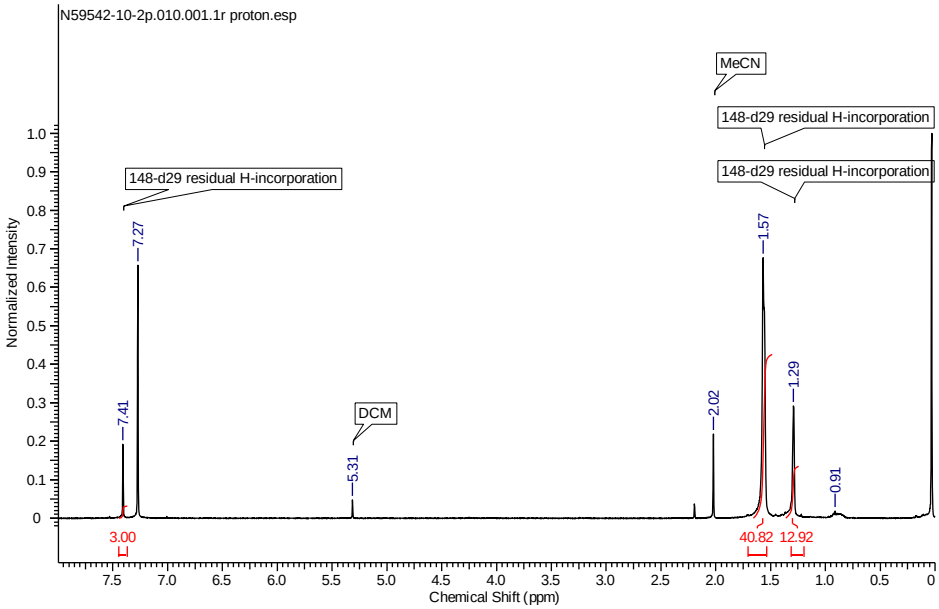

^{1}H NMR (400 MHz, $CDCl_3$) - **148**-d_{29} residual H-incorporation (after quantification)

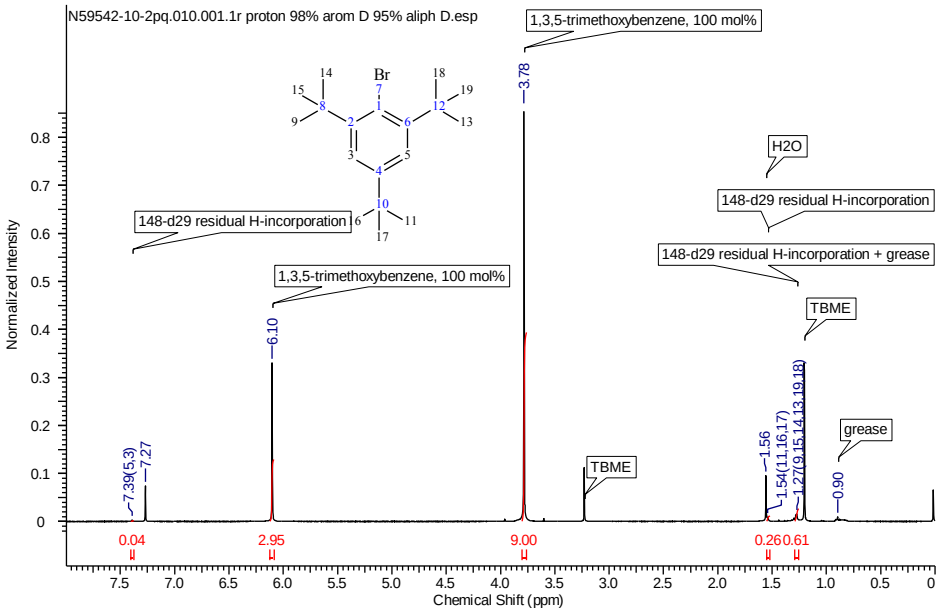

^{1}H NMR (400 MHz, $CDCl_3$) - **148**-d_{29} residual H-incorporation expanded

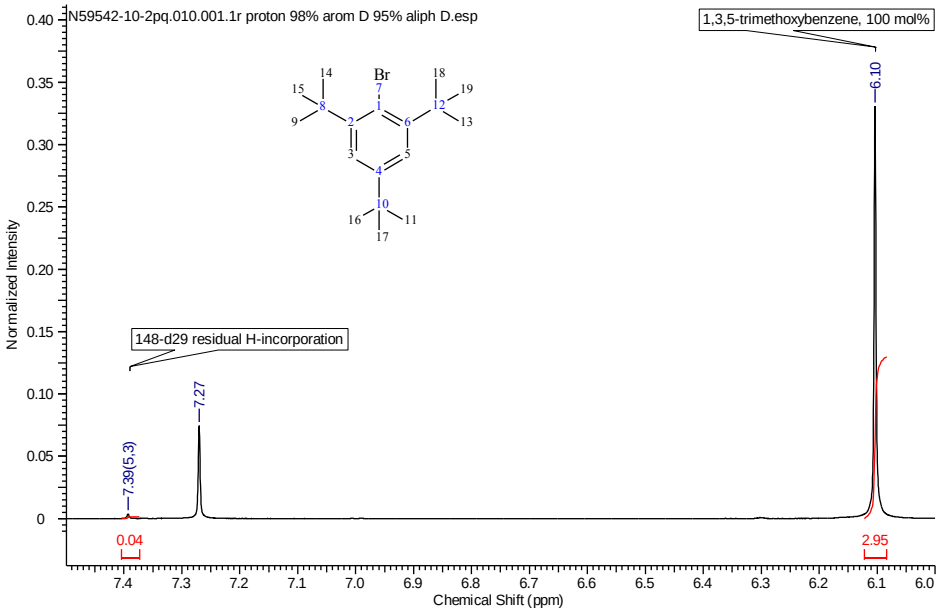

^{1}H NMR (400 MHz, $CDCl_3$) - **148**-d_{29} residual H-incorporation, expanded

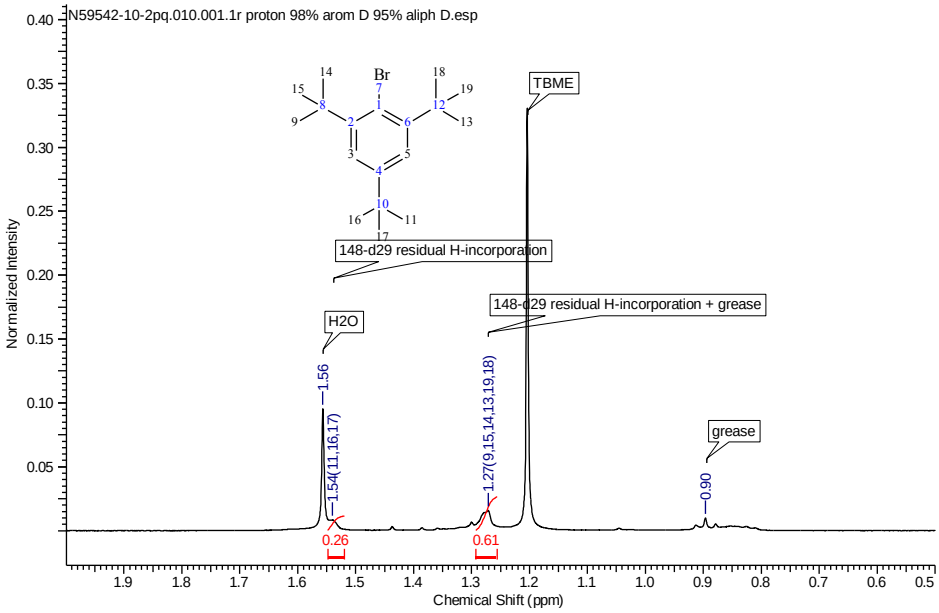

If 100% H-incorporation had occurred, the aromatic signal at δ 7.39 ppm should give 2.0 integration units. Therefore, the following calculation gave the aromatic H-incorporation: 0.04/2 x 100 = 2%.

Here, the aliphatic H-incorporation signals are overlapping with the H_2O residual in $CDCl_3$ and traces of grease. Based on the aromatic signal at δ

7.39 ppm and the ratios determined above, the aliphatic signal at δ 1.54 ppm has a calculated 0.54 integration units (0.04 x 13.61 = 0.54). This accords with the measured integration of the peak at δ 1.54 ppm, it appears that ~half of the peak integration is obscured by H_2O (0.26 x ~2 = 0.52 integration units). The following calculation gave the *ortho*-*tert*-butyl H-incorporation: (0.54 / 18) x 100 = 3%). The aliphatic signal at δ 1.27 ppm has a calculated 0.17 integration units (0.04 x 4.31 = 0.17). The following calculation gave the *para*-*tert*-butyl H-incorporation: (0.17 / 9) x 100 = 2%). Therefore, the overall aliphatic H-incorporation is calculated as 5%.

A9.4.5. H-INCORPORATION IN 1,3,5-TRI-*tert*-BUTYLBENZENE FROM POTASSIUM HYDRIDE

^{1}H NMR (400 MHz, $CDCl_3$) - **148** (fully H-incorporated authentic marker)

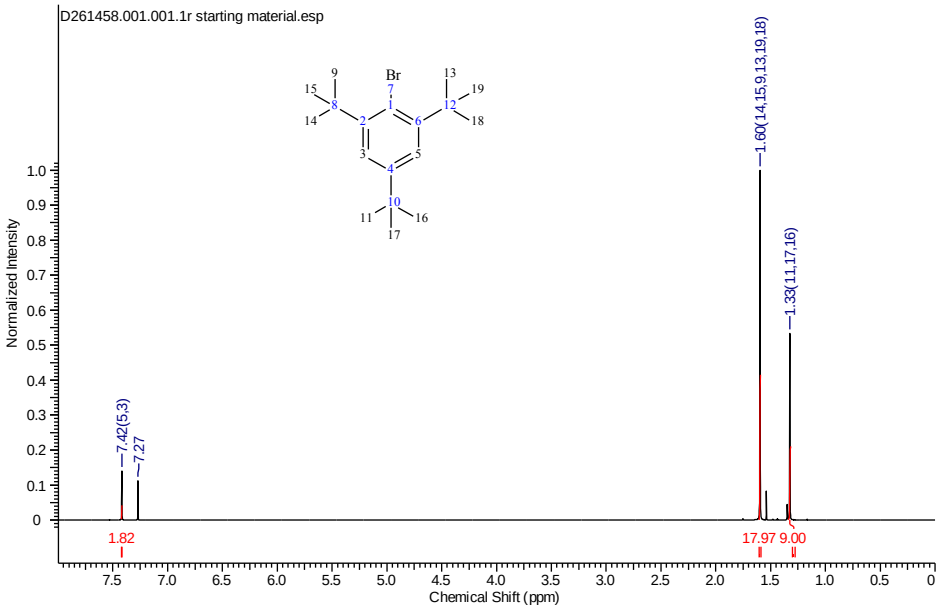

The integration of an aliphatic 1H is 1.10x the integration of an aromatic 1H. The perdeuterated analogue, **149**-d_{29}, was subjected to the KH-mediated dehalogenation conditions shown in Scheme A28.

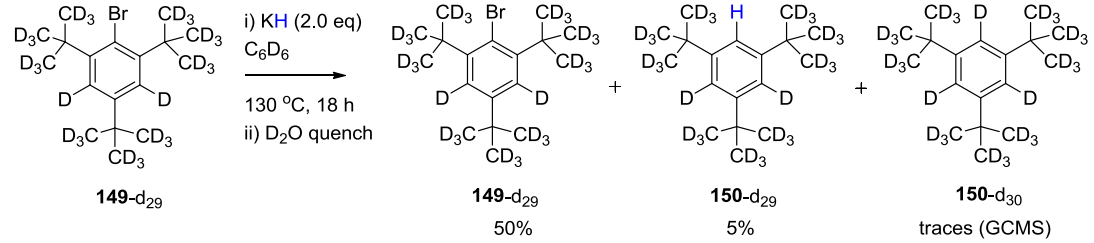

***Scheme A28**: Reaction of perdeuterated bromoarene **149**-d_{29} with potassium hydride.*

^{2}H NMR (61 MHz, THF-h_8) - crude reaction mixture

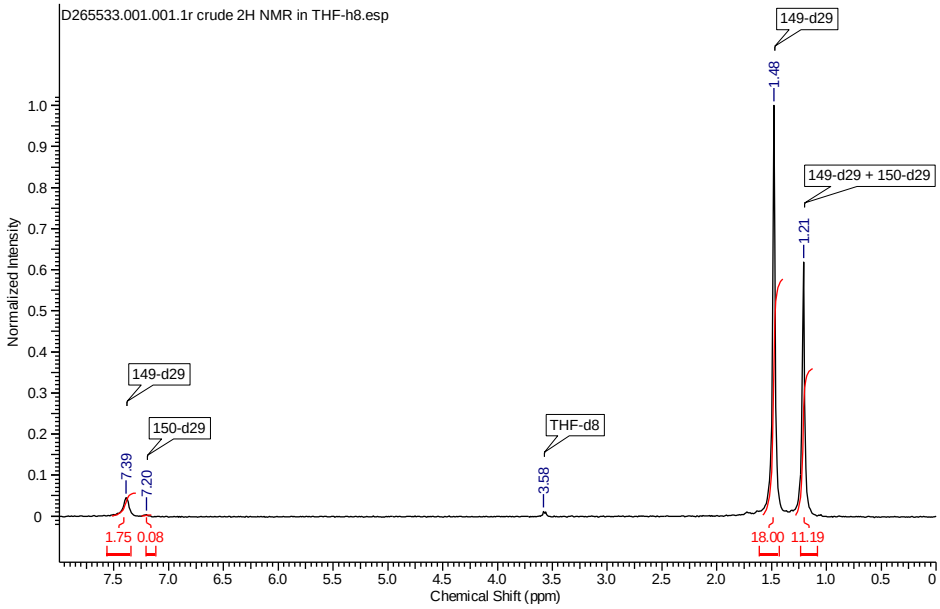

The ^{2}H NMR spectrum was obtained in THF-h_8 in order to avoid residual $CDCl_3$ (in $CHCl_3$ solvent). The relative amounts of **149**-d_{29} and **150** are reported by the aliphatic region. The contribution of **149**-d_{29} to the integration of the ^{2}H singlet at δ 1.21 ppm is 9 units. Therefore, 11.19 - 9.00 = 2.19 units account for the contribution of **150**. Assuming that H-incorporation has not occurred in the *tert*-butyl groups of **150** (2.19/27 = 0.08), then the ratio of **149**-d_{29} : **150** is 1.00 : 0.08. If **150**-d_{30} had been formed, the expected integration of the aromatic ^{2}H singlet at δ 7.20 ppm (3H) is 0.24 units (3 x 0.08). The observed integration of the ^{2}H singlet at δ 7.20 ppm is significantly short of this, providing strong evidence of aromatic H-incorporation (the inaccuracy of integrating such a baseline peak are likely to be large).

^{1}H NMR (400 MHz, $CDCl_3$) - crude reaction mixture

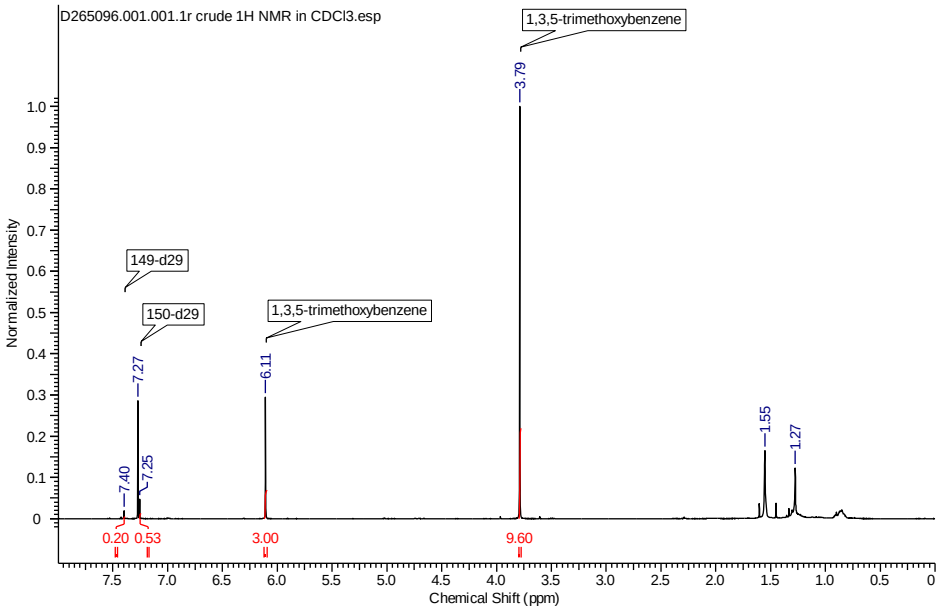

^{1}H NMR (400 MHz, $CDCl_3$) - crude reaction mixture expanded

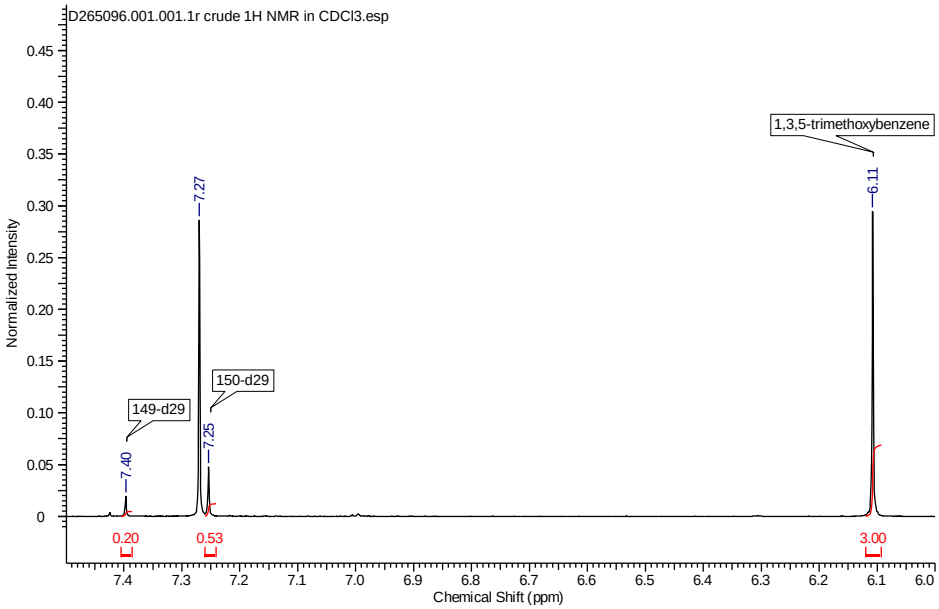

The aliphatics are obscured by H_2O and grease residuals (note that this spectrum only shows the traces of **149-**d_{29} and **150** which have H atoms). If the reaction had returned 100% starting material (**149**-d_{29}), with unchanged aromatic H-incorporation (2%), the expected integration of the ^{1}H singlet at δ 7.40 ppm (2H) is 0.40 units. The observed integration is 0.20 units, reporting

50.0% returned starting material (**149**-d_{29}).

Assuming that the baseline 2% aromatic H-incorporation present in the starting material (D-incorporation was 98% in the aromatics of **149**-d_{29}) is carried over to **150**, and using the ratio of **149**-d_{29} : **150** (1.00 : 0.08) derived from the ^{2}H NMR, the expected integration of the ^{1}H singlet at δ 7.25 ppm (3H) is 0.02 units (0.20 x 0.08 = 0.016). The observed integration is far greater than this, providing clear evidence for H-incorporation into the aromatics. Assuming that 1x aromatic H has been incorporated into each molecule of **150** formed (that **150**-d_{29} is the product, not **150**-d_{28} or **150**-d_{27}), the following calculation gave the amount of **150**-d_{29}: [(0.53 - 0.02)/1] x 10 = 5.1%.

Based on the ratio of **149**-d_{29} : **150** (1.00 : 0.08), even if the entire 3% baseline *ortho*-*tert*-butyl aliphatic H-incorporation in the starting material was transferred to the aromatics *via* HAT/tunnelling *this still could not account for the aromatic H-incorporation observed*. The expected integration of the ^{1}H aromatic at δ 7.25 ppm would be 0.24 units (based on the 1 : 13.61 aliphatic : aromatic area ratio in the ^{2}H NMR of **149**-d_{29}, the following calculation gives the expected baseline aliphatic H-incorporation: 0.016 x 13.61 = 0.22. Therefore, if this was completely transferred to the aromatics: 0.22 + 0.016 = 0.24 integration units). Therefore, H atoms must be incorporated from potassium hydride.

A replicate reaction returned **149**-d_{29} in 80.0% yield and gave **150**-d_{29} in 5.4% yield, giving the average yields shown in Volume 2, Section 2.3.4, Scheme 31, 63% for returned **149**-d_{29} and 5% for **150**-d_{29}. Both these reactions were carried out by Samuel Dalton at the University of Strathclyde.

A10. MISCELLANEOUS ITEMS

A10.1. PROPOSED MECHANISM FOR FORMATION OF DABCO-ENAMINE ADDUCTS

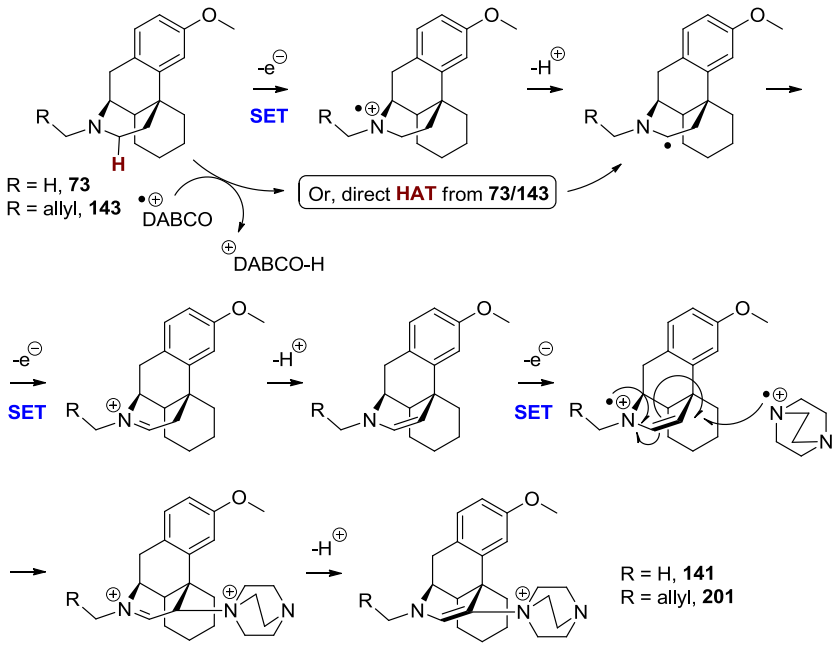

***Scheme A29**: Proposed mechanism for formation of DABCO-enamine adducts.*

A10.2. SELECTION OF REACTION CONDITIONS EMPLOYED TO OBSERVE DABCO-ADDUCT INTERMEDIATE 172 BY ^{1}H NMR

The use of **TPTA**-PF_6 as an oxidant made ^{1}H NMR studies of the reaction mixture in MeCN-d_3 challenging, due to partial solubility of tri-*p*-tolylamine in MeCN-d_3 leading to peaks which swamped substrate-related signals. Therefore, **TPBPA**-PF_6 was used, affording tri-*p*-biphenylamine which was sparingly soluble in MeCN-d_3 and leading to clear NMR spectra of the reaction mixture (See Volume 1, Experimental, Chapter 5.27). The use of **TPBPA**-PF_6 in place of **TPTA**-PF_6 led to increased formation of **141** (ratio **172** : **141** = 4 : 1 by ^{1}H NMR). This is consistent with direct *N*-oxidation of **73**

(Scheme A29) to its radical cation as the mechanistic pathway to **141**, which is consistent with the higher oxidation potential of **TPBPA**-PF_6 [E^p_{ox} (**TPBPA**$^{\bullet+}$/**TPBPA**) = +0.93 *vs.* SCE] compared to **TPTA**-PF_6 [E^p_{ox} (**TPTA**$^{\bullet+}$/**TPTA**) = +0.82 *vs.* SCE]. The reaction conditions are summarised in Scheme A30.

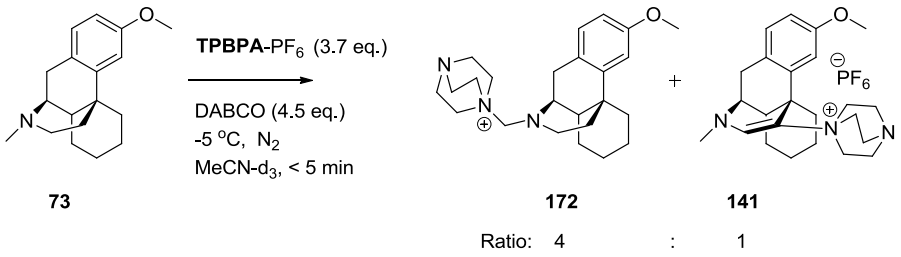

***Scheme A30**: Reaction conditions used resulting in the observation of DABCO-adduct intermediate **172**.*

A10.3. GCMS DETECTION OF DIMERS IN KH-MEDIATED DEHALOGENATION REACTIONS OF 2,4,6-TRI-*tert*-BUTYLBROMOBENZENE (149)

GCMS - **crude reaction mixture**.

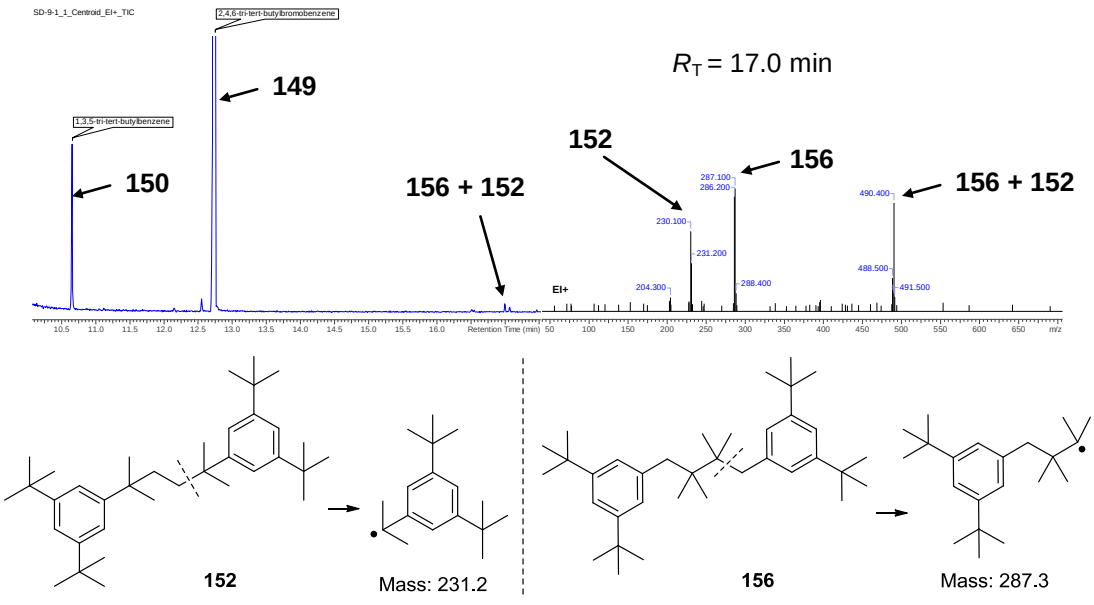

***Scheme A31**: GCMS evidence for dimers **152** and **156** in the KH-mediated dehalogenation reaction of 2,4,6-tri-tert-butylbromobenzene.*

A11. Computational Investigations for Volume 1, Chapter 2.3.

A11.1. Computational Methods

All calculations were performed using Density Functional Theory (DFT)[49,50] using the Gaussian09 software package.[51] All minima (reactants, intermediates, products) and maxima (transition states) were optimised using the UB3LYP functional with a 6-31+G(d,p) basis set on all atoms,[52] paralleling a study on hydrogen atom abstraction from tertiary amines using the cumyloxyl radical.[53] Solvation was modelled implicitly using the Conductor-like Polarisable Continuum Model (CPCM)[54,55] for a solvent of acetonitrile. Frequency calculations were performed on all optimised structures in order to characterise minima (zero imaginary frequencies) and maxima (single imaginary frequency). All profiles are plotted using the Gibbs free energy values. GaussView 5.0.9 was used for the visualisation of structures.

A11.2. Computational Reaction Energy Profiles

A11.2.1. HAT Reactions of *N*-methylmorpholine

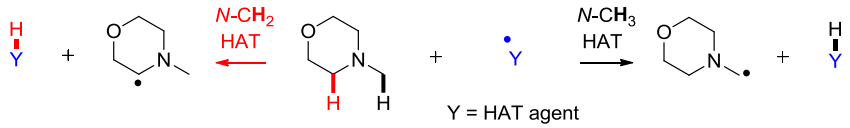

***Scheme A32**: N-C**H**$_3$ vs. N-C**H**$_2$ HAT reactions of N-methylmorpholine.*

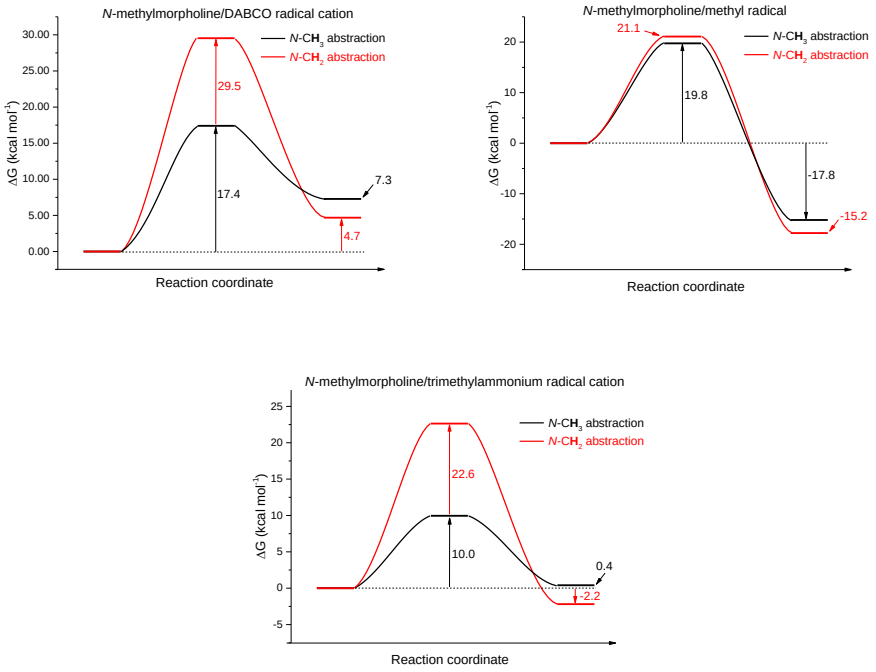

Figure A38: *Reaction profiles for N-C**H**$_3$ vs. N-C**H**$_2$ HAT from N-methylmorpholine.*

A11.2.2. HAT REACTIONS OF *N*-ETHYL-*N*-METHYLETHANAMINE

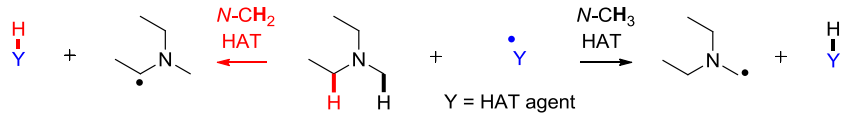

Scheme A33*: N-C**H**$_3$ vs. N-C**H**$_2$ HAT reactions of N-ethyl-N-methylethanamine.*

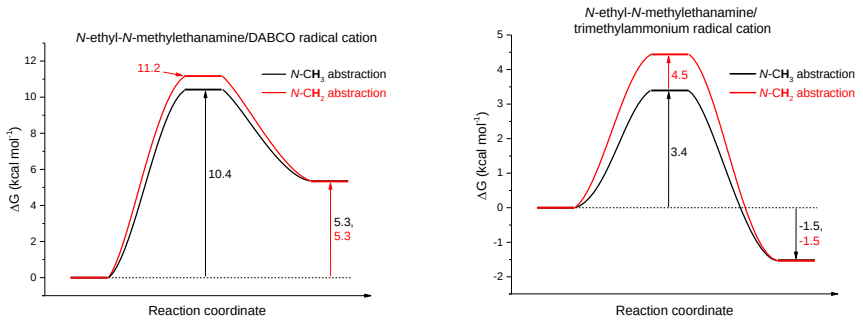

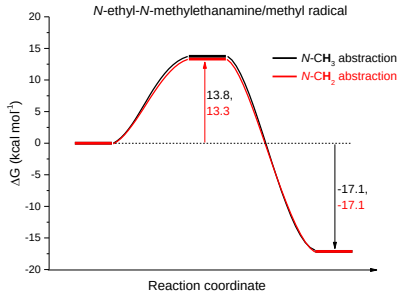

Figure A39: *Reaction profiles for N-C**H**$_3$ vs. N-C**H**$_2$ HAT from N-ethyl-N-methylethanamine.*

A11.2.3. HAT REACTIONS OF *N*-METHYL-*N*-OCTYLOCTAN-1-AMINE (160)

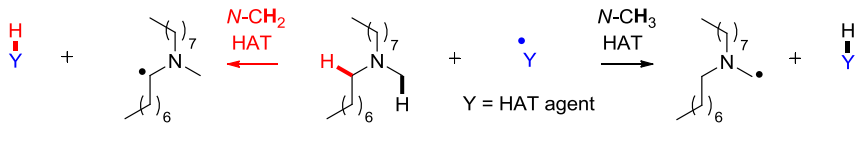

160

Scheme A34*: N-C**H**$_3$ vs. N-C**H**$_2$ HAT reactions of N-methyl-N-octyl-octanamine (**160**) with various HAT agents.*

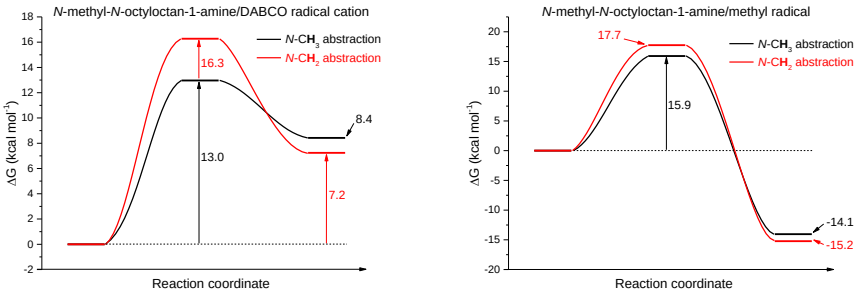

Figure A40: *Reaction profiles for N-C**H**$_3$ vs. N-C**H**$_2$ HAT from N-methyl-N-octyloctanamine (**160**) to various HAT agents.*

A11.2.4. HAT REACTIONS OF *N*-METHYL-1,2,3,4-TETRAHYDROISOQUINOLINE (114)

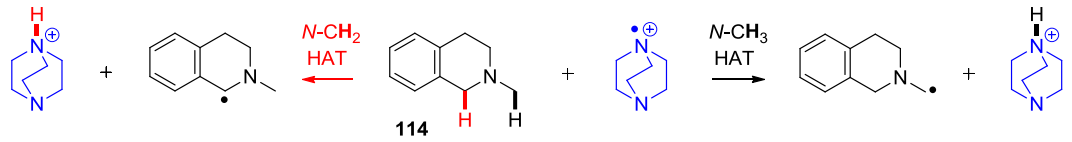

***Scheme A35**: N-C**H**$_3$ vs. N-C**H**$_2$ HAT reactions of N-methyl-1,2,3,4-tetrahydroisoquinoline (**114**) with DABCO radical cation.*

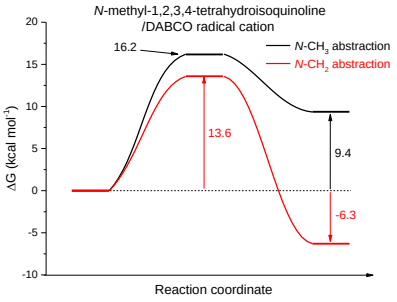

***Figure A41.** Reaction profiles for N-C**H**$_3$ vs. N-C**H**$_2$ HAT from N-methyl-1,2,3,4-tetrahydroisoquinoline (**114**) to DABCO radical cation.*

A11.2.5. HAT REACTIONS OF 6,7-DIMETHOXY-*N*-METHYL-1,2,3,4-TETRAHYDROISOQUINOLINE (115)

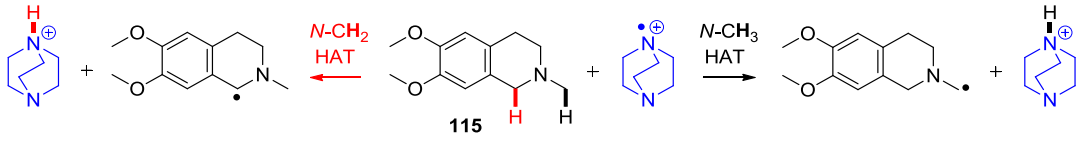

***Scheme A36**: N-C**H**$_3$ vs. N-C**H**$_2$ HAT reactions of 6,7-dimethoxy-N-methyl-1,2,3,4-tetrahydroisoquinoline (**115**) with DABCO radical cation.*

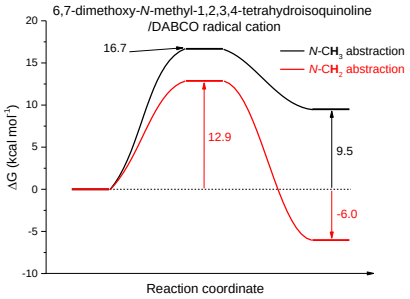

Figure A42. *Reaction profiles for N-C**H**$_3$ vs. N-C**H**$_2$ HAT from 6,7-dimethoxy-N-methyl-1,2,3,4-tetrahydroisoquinoline (**115**) to DABCO radical cation.*

A11.2.6. HAT REACTIONS OF DEXTROMETHORPHAN (73)

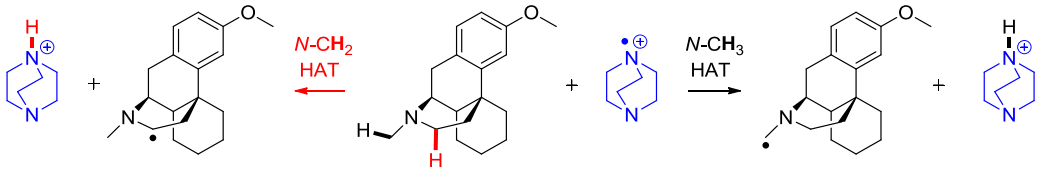

73

Scheme A37*: N-C**H**$_3$ vs. N-C**H**$_2$ HAT reactions of dextromethorphan (**73**) with DABCO radical cation.*

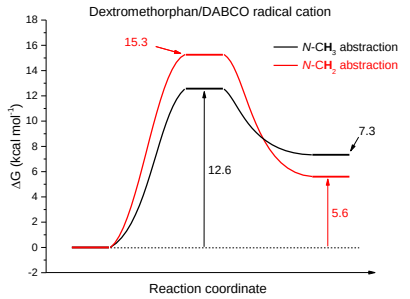

Figure A43. *Reaction profiles for N-C**H**$_3$ vs. N-C**H**$_2$ HAT from dextromethorphan (**73**) to DABCO radical cation.*

A11.2.7. HAT REACTION OF *N*,*N*-DIMETHYLDECANAMIDE (168a)

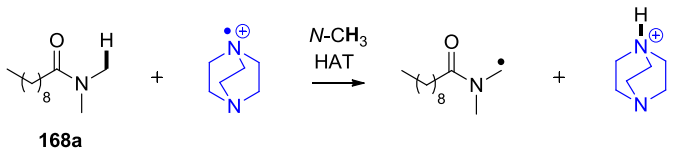

***Scheme A38**: N-C**H**$_3$ HAT reaction of N,N-dimethyldecanamide (**168a**) with DABCO radical cation.*

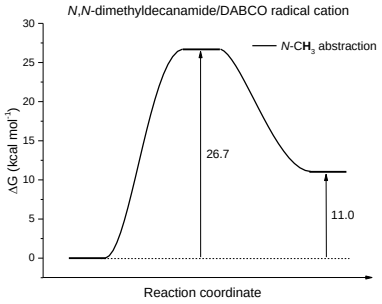

***Figure A44.** Reaction profile for N-C**H**$_3$ HAT from N,N-dimethyldecanamide (**168a**) to DABCO radical cation.*

A11.3. XYZ CO-ORDINATES FOR SUBSTRATE MOLECULES

***N*-Methylmorpholine**, solvent = MeCN

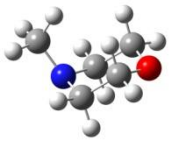

Charge = 0; Multiplicity = 1

18

-326.999258

C	-0.23866600	-1.20342100	-0.60832500
C	0.97263600	-1.18417200	0.32949100
C	0.97263900	1.18417100	0.32949100
C	-0.23866300	1.20342200	-0.60832500
H	0.66015200	-1.23234600	1.38401200
H	1.63379500	-2.03165400	0.12819400

H	0.12358100	-1.26885500	-1.64305100
H	-0.85114200	-2.09010700	-0.41222300
H	0.66015300	1.23234400	1.38401200
H	1.63380000	2.03165100	0.12819600
H	-0.85113600	2.09011000	-0.41222400
H	0.12358600	1.26885400	-1.64305000
O	1.75602200	-0.00000200	0.12140400
N	-1.07934300	0.00000200	-0.49742800
C	-1.96255900	0.00000100	0.67134200
H	-2.60471900	0.88583700	0.63406300
H	-2.60475300	-0.88581000	0.63403600
H	-1.44840900	-0.00002400	1.64675200

***N*-Ethyl-*N*-methylethanamine**, solvent = MeCN

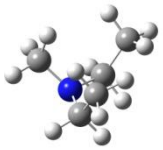

Charge = 0; Multiplicity = 1

19

-252.981813

C	-1.25236000	0.06991000	0.67738300
C	1.25222600	0.07006900	0.67749300
H	-1.14835100	0.66481200	1.59319000
H	-2.03429700	-0.67630100	0.87748200
H	2.03420100	-0.67602500	0.87789300
H	1.14797600	0.66514000	1.59316300
N	-0.00001200	-0.66662400	0.49310700
C	0.00009800	-1.60053300	-0.62415200
H	0.88656800	-2.24233900	-0.56170700
H	-0.88633300	-2.24240300	-0.56182800
H	0.00015000	-1.13018700	-1.62247200
C	1.75037600	0.98176700	-0.46225200
H	1.08421400	1.83126300	-0.63631600
H	2.73844800	1.37979300	-0.20231500
H	1.85442700	0.43163100	-1.40366000
C	-1.75034800	0.98179800	-0.46228000
H	-1.08429800	1.83147200	-0.63591000
H	-1.85398600	0.43187800	-1.40386000
H	-2.73858000	1.37956500	-0.20255600

***N*-Methyl-*N*-octyloctan-1-amine**, solvent = MeCN

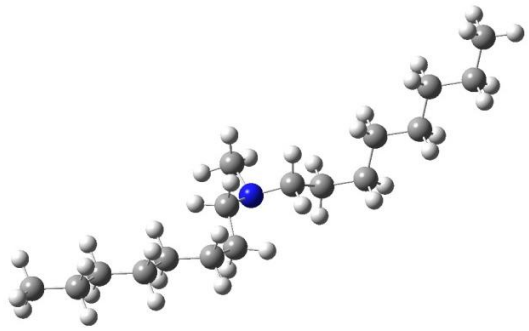

Charge = 0; Multiplicity = 1

55

-724.476552

C	-1.15144800	1.05674500	0.04190200
C	1.24481200	0.85091500	-0.35963800
H	-0.91122100	0.42028000	0.89976600
H	-1.48941200	0.38029300	-0.76692100
H	2.02410400	1.32385300	-0.96537700
H	1.00313300	-0.10995100	-0.85768500
C	1.80384600	0.57874900	1.04332400
H	1.00482400	0.20622200	1.69531600
H	2.14031100	1.53009900	1.47725800
C	-2.28697500	2.00088000	0.45809700
H	-1.89280300	2.68842900	1.21745700
H	-2.60301600	2.62020400	-0.39081000
C	2.95988600	-0.43677600	1.06668400
H	3.20733900	-0.65244000	2.11504200
H	2.61701100	-1.38800400	0.63393200
C	-3.51992800	1.27520000	1.02581400
H	-4.19890200	2.02926500	1.44681400
H	-3.21160200	0.63903000	1.86855700
C	4.23872400	0.01600700	0.34559100
H	4.03651400	0.16335800	-0.72386600
H	4.54560200	0.99667000	0.73870600
C	5.40047400	-0.97519400	0.49910100
H	5.61934800	-1.11186100	1.56831800
H	5.08696800	-1.96004000	0.12254600
C	6.68056400	-0.54219800	-0.22745100
H	6.46334600	-0.41190900	-1.29786600
H	6.99285900	0.44506500	0.14398200
C	7.84370700	-1.53029000	-0.06704300
H	7.53020500	-2.51812300	-0.43275200
H	8.06502500	-1.65592000	1.00205800

C	9.11619900	-1.09519400	-0.80327900
H	9.47448100	-0.12612200	-0.43515600
H	9.92495300	-1.82208800	-0.66879000
H	8.93429600	-0.99401800	-1.88005700
C	-4.30164800	0.42814400	0.00927800
H	-3.66844100	-0.38488800	-0.37000300
H	-4.55269600	1.05321500	-0.86050200
C	-5.59025100	-0.17314600	0.58667600
H	-6.23542700	0.63941700	0.95181700
H	-5.34205100	-0.78573400	1.46590900
C	-6.37410700	-1.02802700	-0.41810200
H	-5.73236000	-1.84665100	-0.77593100
H	-6.61470800	-0.41908000	-1.30207300
C	-7.67006200	-1.61856000	0.15321800
H	-7.43100300	-2.22494800	1.03805500
H	-8.31349200	-0.80098300	0.50712300
C	-8.44330000	-2.47472000	-0.85675200
H	-7.83747800	-3.32105400	-1.20252400
H	-9.36201800	-2.87986200	-0.41814800
H	-8.72580400	-1.88714900	-1.73867400
C	-0.07726600	2.37552900	-1.68466200
H	-0.28145400	1.63486300	-2.48263700
H	-0.90134000	3.09289000	-1.67337300
H	0.83515900	2.91861900	-1.94810000
N	0.08005600	1.75295400	-0.36828000

***N*-Methyl-1,2,3,4-tetrahydroisoquinoline**, solvent = MeCN

Charge = 0; Multiplicity = 1

24

-443.503320

C	-2.80026100	-1.04189100	0.01364600
C	-1.48429000	-1.50453400	0.05144000
C	-0.40265400	-0.61066200	0.02859600
C	-0.64799400	0.77160100	-0.03360300
C	-1.97542000	1.22802900	-0.07141200
C	-3.04754200	0.33495100	-0.04766500
H	-3.62579300	-1.74773000	0.02971200
H	-1.28979400	-2.57387600	0.09758700
H	-2.16540500	2.29806900	-0.11821900
H	-4.06744800	0.70792300	-0.07632000

N	2.01486600	-0.17513200	-0.33308700
C	3.36415600	-0.70234200	-0.14804800
H	4.09674000	0.01366600	-0.53223400
H	3.59993400	-0.90379700	0.91455300
H	3.47455000	-1.63941000	-0.70298000
C	0.50992700	1.74800000	-0.08292400
H	0.62147000	2.12403300	-1.10900800
H	0.29497700	2.61937900	0.54695100
C	1.82663100	1.10549300	0.35446700
H	2.66422300	1.76352300	0.10302100
H	1.83771900	0.96880900	1.45486000
C	1.01343500	-1.14519300	0.11279100
H	1.21330400	-1.45655900	1.16050700
H	1.10554000	-2.04882600	-0.50056000

6,7-dimethoxy-*N*-Methyl-1,2,3,4-tetrahydroisoquinoline, solvent = MeCN

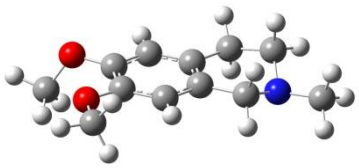

Charge = 0; Multiplicity = 1

32

-672.499773

C	1.64633100	0.59598000	0.14278800
C	0.38958600	1.19654300	0.04613800
C	-0.78556300	0.42525300	0.03729800
C	-0.71015800	-0.96917100	0.12688300
C	0.55777000	-1.56824600	0.21227900
C	1.72467400	-0.81393900	0.21861300
H	0.30644600	2.27626400	-0.01604000
H	0.64941700	-2.64934000	0.28248100
N	-3.21326800	0.23662600	-0.43477600
C	-4.49679400	0.93210900	-0.39549200
H	-5.28819600	0.26744900	-0.75441900
H	-4.76538900	1.27333800	0.62269900
H	-4.46203800	1.81007600	-1.04835600
C	-1.96981400	-1.81080800	0.10535800
H	-2.07637400	-2.28647100	-0.87915500
H	-1.89440000	-2.62301900	0.83822500
C	-3.21906900	-0.97538400	0.38932000
H	-4.11708200	-1.55432800	0.15213200
H	-3.27021700	-0.71948800	1.46705700
C	-2.12729900	1.12855500	-0.02464100
H	-2.34351400	1.57291000	0.97057000
H	-2.07698500	1.96397000	-0.73234400

O	2.94316900	-1.44825700	0.36902500
O	2.83367600	1.27319200	0.17807100
C	3.74007900	-1.52573400	-0.82627100
H	3.98260300	-0.52701000	-1.20152700
H	4.65788200	-2.04721600	-0.54900200
H	3.21312400	-2.09689600	-1.59974600
C	2.80249200	2.70063400	0.10776500
H	3.84332600	3.02119600	0.15398900
H	2.35566200	3.04117800	-0.83315600
H	2.25043300	3.12676200	0.95302900

Dextromethorphan, solvent = MeCN

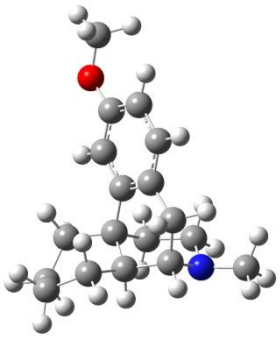

Charge = 0; Multiplicity = 1

45

-830.640934

C	2.23609300	2.82566300	-1.11776400
C	1.96590600	1.36373700	-1.57493200
C	1.97489800	0.42616300	-0.36079000
C	0.78427600	0.72696900	0.59135000
C	0.67959500	2.27412000	0.81763300
C	1.94234900	3.03402200	0.38539100
C	2.01642400	-1.07628300	-0.66132900
C	-0.53126400	0.15329000	0.03535000
C	-0.53642800	-0.91523400	-0.88761000
C	0.75063300	-1.50404200	-1.43280200
C	-1.76601900	-1.42979600	-1.31607500
H	-1.77286100	-2.25050300	-2.03032400
C	-2.98887900	-0.93536600	-0.85445100
C	-2.97796800	0.11040400	0.07615500
C	-1.75686000	0.63843000	0.51104400
H	2.88268000	-1.28478400	-1.30280400
H	3.27920500	3.09626700	-1.32067400
H	0.99778000	1.30279200	-2.08656000
H	-0.16023400	2.67171900	0.23667100
H	2.80040900	2.70942900	0.98689900
H	0.87641100	-1.18967500	-2.47873000

H	-3.91448100	-1.36859100	-1.21398000
H	-1.78906900	1.44312700	1.23873300
H	0.67341700	-2.59702800	-1.46669700
H	2.72213300	1.04706900	-2.30367500
H	1.61785100	3.51376800	-1.70708800
H	1.81523900	4.10282800	0.59412900
H	0.45253000	2.48422600	1.87018900
H	2.89472000	0.63198600	0.20006800
O	-4.10388800	0.68032000	0.61806200
C	-5.37859100	0.18378400	0.20729300
H	-6.11721000	0.77418700	0.75006300
H	-5.52746400	0.31519900	-0.87071200
H	-5.49559500	-0.87467700	0.46706900
C	1.10836600	-0.01774000	1.91615900
H	0.29527500	0.12050000	2.63907300
H	2.01315800	0.42615900	2.35215000
C	1.32913300	-1.51918400	1.69166200
H	0.35772400	-2.01263400	1.50164000
H	1.72918500	-1.96958200	2.60823500
N	2.28936900	-1.78539600	0.61162000
C	2.53596300	-3.21289000	0.45128900
H	3.27610900	-3.37477700	-0.33939000
H	2.94034000	-3.61937200	1.38492000
H	1.63250000	-3.79870400	0.19951700

***N*,*N*-dimethyldecanamide**, solvent = MeCN

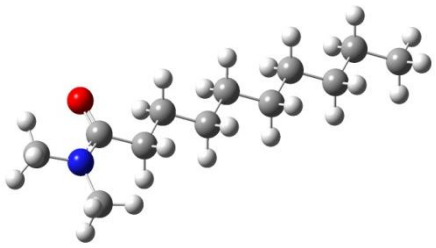

Charge = 0; Multiplicity = 1

39

-602.094738

N	-5.03167200	0.25979200	-0.04522700
C	-3.84903800	-0.42144200	-0.01968000
C	-6.29426800	-0.46846200	0.05153800
H	-6.98747700	-0.10792800	-0.71539500
H	-6.10978600	-1.53078200	-0.09378300
H	-6.75501500	-0.31416100	1.03581200
C	-5.15307900	1.71365100	0.03055100
H	-4.23605800	2.20852900	-0.28024900
H	-5.95670500	2.03960800	-0.63674000
H	-5.40120000	2.03613700	1.05033000

C	-2.55811400	0.39761900	-0.03785100
H	-2.55781500	1.07727400	0.82434800
H	-2.55543000	1.04094900	-0.92732900
C	-1.28931000	-0.45887400	-0.02044800
H	-1.29036200	-1.12881500	-0.88857000
H	-1.29836200	-1.10500900	0.86542000
C	-0.01100900	0.39008900	-0.02582000
H	-0.01406800	1.06011100	0.84626500
H	-0.00763900	1.04083100	-0.91237800
C	1.27299200	-0.45013000	-0.01186100
H	1.27781900	-1.11697200	-0.88633000
H	1.26733000	-1.10398100	0.87237000
C	2.55728700	0.38962900	-0.01013300
H	2.56201400	1.04541600	-0.89304600
H	2.55324100	1.05477500	0.86574700
C	3.84103200	-0.45115800	0.00077400
H	3.84578600	-1.11493000	-0.87618800
H	3.83514300	-1.10851600	0.88255700
C	5.12614900	0.38727800	0.00563600
H	5.13293300	1.04545400	-0.87569600
H	5.12282700	1.05058900	0.88312800
C	6.41023900	-0.45303300	0.01555800
H	6.41446500	-1.11521300	-0.86147800
H	6.40368000	-1.11093600	0.89580100
C	7.68887200	0.39315100	0.02141200
H	8.58569500	-0.23624400	0.02880300
H	7.74036100	1.03696100	-0.86496700
H	7.72907900	1.04164400	0.90496300
O	-3.81615900	-1.66415800	0.00939200

A11.4. XYZ CO-ORDINATES FOR HYDROGEN ATOM TRANSFER AGENTS

DABCO radical cation, solvent = MeCN

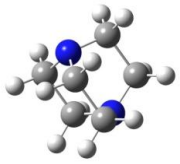

Charge = 1; Multiplicity = 2

20

-345.024735

C	-0.81842600	0.26817600	1.35285400
C	0.81831200	0.26793200	1.35297000
H	-1.17887900	1.24472900	1.67557500
H	-1.17869600	-0.51165200	2.02357600

H	1.17901100	1.24436700	1.67577100
H	1.17825600	-0.51202200	2.02371900
C	-0.81821600	1.03839600	-0.90853100
H	-1.17860200	0.83099800	-1.91601700
H	-1.17834800	2.00858800	-0.56707600
C	0.81861800	1.03820700	-0.90839300
H	1.17912700	0.83077900	-1.91582800
H	1.17892300	2.00829900	-0.56683300
C	0.81825400	-1.30612000	-0.44436200
H	1.17836100	-1.49823400	-1.45504800
H	1.17789000	-2.07455700	0.23995100
C	-0.81854000	-1.30592000	-0.44443300
H	-1.17860700	-1.49798600	-1.45514200
H	-1.17842900	-2.07423800	0.23988200
N	-1.23218100	-0.00005900	-0.00030800
N	1.23217800	-0.00038200	-0.00014300

Trimethylammonium radical cation, solvent = MeCN

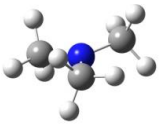

Charge = 1; Multiplicity = 2

13

-174.208285

N	0.00003500	0.00005700	0.00108300
C	-1.44407400	-0.08931500	-0.00000300
H	-1.75814300	-1.13092500	0.00779900
H	-1.83070700	0.43732800	0.88089700
H	-1.82782500	0.42233000	-0.89123300
C	0.64462900	1.29506800	-0.00022400
H	1.28962000	1.36688300	-0.88439000
H	-0.09980900	2.08852700	-0.00431500
H	1.28405800	1.37119800	0.88769000
C	0.79934700	-1.20579100	-0.00003200
H	0.53824300	-1.80280700	0.88202500
H	0.54615000	-1.79517900	-0.88978700
H	1.85875800	-0.95752700	0.00528000

Methyl radical, solvent = MeCN

Charge = 0; Multiplicity = 2

4

-39.837439

C	0.00000000	0.00000000	0.00029100
H	0.00000000	0.00000000	-1.08296000
H	0.00000000	0.93875300	0.54060800
H	0.00000000	-0.93875300	0.54060800

A11.5. XYZ CO-ORDINATES FOR RADICAL PRODUCTS FROM HAT

***N*-Methylmorpholine radical A**, solvent = MeCN

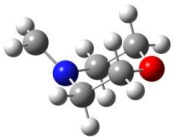

Charge = 0; Multiplicity = 2

17

-326.361859

C	0.28470900	-1.21442000	0.54002000
C	-0.98041200	-1.18448700	-0.32256200
C	-0.98040600	1.18448900	-0.32256200
C	0.28471500	1.21441800	0.54002100
H	-0.71018900	-1.22151000	-1.38880300
H	-1.63239300	-2.03076100	-0.09055900
H	-0.00077700	-1.27584300	1.59782600
H	0.89383900	-2.08958900	0.29728100
H	-0.71017900	1.22151000	-1.38880200
H	-1.63238200	2.03076800	-0.09056200
H	0.89384900	2.08958500	0.29728100
H	-0.00077100	1.27584200	1.59782700
O	-1.74355400	0.00000400	-0.06185200
N	1.08106100	-0.00000300	0.34338600
C	2.06923300	-0.00000200	-0.63468900
H	2.60648800	0.93337700	-0.77087100
H	2.60648100	-0.93338500	-0.77087700

***N*-Methylmorpholine radical B**, solvent = MeCN

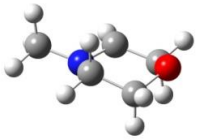

Charge = 0; Multiplicity = 2

17

-326.365996

C	0.27264300	-1.20967500	0.11821000
C	-1.20471300	-1.20159100	-0.12252000
C	-1.18133200	1.14404900	-0.23479900
C	0.29637000	1.20458600	0.14087500
H	-1.44506700	-1.29759900	-1.20138400
H	-1.68690000	-2.03103900	0.40078200
H	0.81461100	-2.14245800	-0.01118400
H	-1.29212500	1.10187200	-1.32972700
H	-1.70254400	2.02952100	0.13663900
H	0.77883100	2.02821000	-0.39610900
H	0.39469000	1.39842200	1.22276500
O	-1.81794100	0.00865500	0.35364700
N	0.96925100	-0.05056900	-0.20983000
C	2.40759000	-0.04750700	0.02707300
H	2.64803900	0.04312600	1.09901400
H	2.86384200	0.79241500	-0.50428500
H	2.84204200	-0.97689500	-0.34991600

***N*-Ethyl-*N*-methylethanamine radical A**, solvent = MeCN

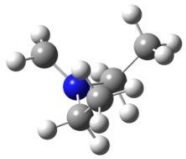

Charge = 0; Multiplicity = 2

18

-252.347489

C	-1.26289400	0.02089300	0.63763600
C	1.26339400	0.02023100	0.63718700
H	-1.12068600	0.56212600	1.57935100

H	-2.00197200	-0.76752100	0.82989200
H	2.00235700	-0.76860100	0.82812000
H	1.12214900	0.56067100	1.57950900
N	0.00002100	-0.63690700	0.30852300
C	-0.00042100	-1.66061000	-0.62100600
H	0.93420200	-2.19494800	-0.75986500
H	-0.93540800	-2.19437900	-0.75961400
C	1.81849500	0.97464400	-0.43231500
H	1.15573500	1.82940700	-0.59548900
H	2.79450200	1.35855500	-0.11446400
H	1.95036200	0.45400800	-1.38621000
C	-1.81858600	0.97451700	-0.43226700
H	-1.15552600	1.82874300	-0.59701700
H	-1.95173100	0.45297500	-1.38548900
H	-2.79406000	1.35926800	-0.11379800

***N*-Ethyl-*N*-methylethanamine radical B**, solvent = MeCN

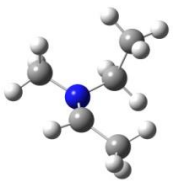

Charge = 0; Multiplicity = 2

18

-252.347513

C	1.16049500	-0.51060900	0.35461200
C	-0.76154900	0.64769600	-0.67800100
H	1.54581000	-1.47928100	0.66476000
H	-1.54104800	0.37720100	-1.39905100
H	-0.05113000	1.28804800	-1.20883100
N	-0.06937500	-0.59026100	-0.30205200
C	-0.94072100	-1.69187100	0.09345600
H	-1.74448200	-1.80539000	-0.63984400
H	-0.36357100	-2.62067900	0.11842300
H	-1.39418700	-1.54578000	1.08681700
C	-1.38526900	1.42714100	0.49097600
H	-0.62127200	1.72318700	1.21713000
H	-1.87178200	2.33424400	0.11601400
H	-2.14150400	0.83288100	1.01408500
C	2.15437600	0.54957200	-0.01518800
H	2.43595200	0.52369700	-1.08414200
H	1.79745100	1.56708000	0.18999500
H	3.07139200	0.40504800	0.56387500

***N*-Methyl-*N*-octyloctan-1-amine radical A**, solvent = MeCN

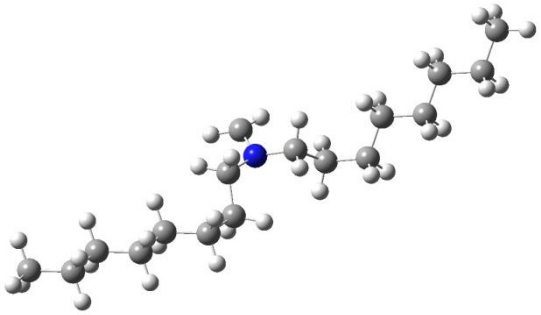

Charge = 0; Multiplicity = 2

54

-723.837325

C	1.18111100	0.69115300	0.11254800
C	-1.28764800	0.66217800	0.47601100
H	0.88636800	-0.26356500	-0.33316200
H	1.71061900	0.45782600	1.04951000
H	-2.02371400	1.26100100	1.01811800
H	-1.12881100	-0.25612200	1.06678100
C	-1.82613200	0.29823600	-0.91496900
H	-1.03322600	-0.19449800	-1.49108100
H	-2.07047500	1.22491000	-1.45135000
C	2.10972400	1.42505200	-0.86617000
H	1.52893600	1.67029900	-1.76424500
H	2.43032100	2.38040800	-0.43124200
C	-3.05519600	-0.62613700	-0.88325300
H	-3.28224600	-0.93094000	-1.91367500
H	-2.80046600	-1.54906200	-0.34211700
C	3.35021300	0.60990600	-1.27035500
H	3.84788900	1.13117300	-2.09916500
H	3.03068300	-0.36287200	-1.67211000
C	-4.31792700	-0.00728300	-0.26450000
H	-4.13625100	0.24549000	0.78887500
H	-4.54096100	0.94112200	-0.77508600
C	-5.54324100	-0.92771400	-0.34967700
H	-5.73531000	-1.17614300	-1.40376600
H	-5.31593100	-1.87921800	0.15289600
C	-6.81223600	-0.32310700	0.26547400
H	-6.62209100	-0.07771200	1.32070500
H	-7.03900900	0.62993300	-0.23469200
C	-8.03811900	-1.24195200	0.17564800
H	-7.81240400	-2.19445600	0.67501400
H	-8.22882800	-1.48652600	-0.87863200

C	-9.30152600	-0.63017200	0.79252600
H	-9.57049100	0.30793300	0.29215300
H	-10.15708000	-1.30958600	0.70921500
H	-9.15412100	-0.40815800	1.85636900
C	4.37560000	0.38525400	-0.14840100
H	3.91696300	-0.17828400	0.67517900
H	4.66743100	1.35945200	0.27070800
C	5.63234000	-0.35908400	-0.62011900
H	6.09905000	0.20462700	-1.44126500
H	5.33922800	-1.33092500	-1.04361100
C	6.66738300	-0.58437100	0.48965400
H	6.20170400	-1.14913200	1.31074600
H	6.96103900	0.38700900	0.91409200
C	7.92439900	-1.32784700	0.01825000
H	7.63155400	-2.29803100	-0.40697100
H	8.39158800	-0.76328300	-0.80079900
C	8.95229900	-1.55060700	1.13376200
H	8.52623900	-2.14538700	1.95077200
H	9.83692000	-2.07993900	0.76257400
H	9.28785700	-0.59663500	1.55810500
C	0.07120000	2.53851800	1.25805700
H	1.01042600	3.07938800	1.23413300
H	-0.83826300	3.08973500	1.47188900
N	-0.04408500	1.43829100	0.42546000

***N*-Methyl-*N*-octyloctan-1-amine radical B**, solvent = MeCN

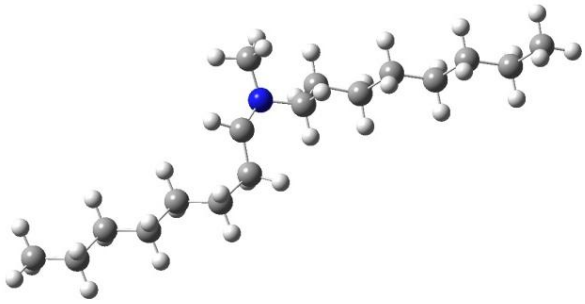

Charge = 0; Multiplicity = 2

54

-723.839212

C	1.11027100	0.66509600	0.05336800
C	-1.25817200	0.58066500	0.73183600
H	0.87028200	-0.32330800	-0.34428400
H	1.67213300	0.50607700	0.99005300
H	-2.07956100	1.17620200	1.12176500

C	-1.59904100	-0.69952500	0.01952700
H	-0.85238400	-1.47865300	0.23027000
H	-1.56863600	-0.55824400	-1.07815100
C	1.97826400	1.40083700	-0.97749000
H	1.36083100	1.59676500	-1.86326700
H	2.29152500	2.37846600	-0.59025300
C	-2.98515500	-1.25179200	0.40463400
H	-3.07248300	-2.27253400	0.00960000
H	-3.04582400	-1.33911000	1.49887100
C	3.23089200	0.61131200	-1.39807300
H	3.69268700	1.12962500	-2.24924000
H	2.92980100	-0.37834700	-1.77153600
C	-4.17278100	-0.42438700	-0.10881800
H	-4.12003200	0.59778800	0.28920800
H	-4.09695500	-0.33171200	-1.20227700
C	-5.53547800	-1.02989900	0.25442800
H	-5.59908800	-2.04965600	-0.15295300
H	-5.60594700	-1.13175100	1.34731700
C	-6.72812700	-0.20833900	-0.25266000
H	-6.66494100	0.81129600	0.15532100
H	-6.65936500	-0.10558100	-1.34566600
C	-8.09164200	-0.81114400	0.11115900
H	-8.15911800	-0.91729300	1.20290000
H	-8.15803300	-1.82812000	-0.30000000
C	-9.27678700	0.02056700	-0.39348600
H	-9.25510100	0.11713700	-1.48573700
H	-10.23344400	-0.43731900	-0.11838300
H	-9.25753200	1.03239500	0.02923400
C	4.28860900	0.43995900	-0.29685900
H	3.86883100	-0.13002800	0.54257000
H	4.55151300	1.42979900	0.10457400
C	5.56382900	-0.26176000	-0.78397900
H	5.99592300	0.31062800	-1.61789600
H	5.30037000	-1.24817100	-1.19303900
C	6.62337300	-0.43667700	0.31187600
H	6.19088300	-1.00916800	1.14563600
H	6.88680300	0.54950900	0.72179800
C	7.90053600	-1.13820600	-0.16934100
H	7.63830700	-2.12346500	-0.57960600
H	8.33539600	-0.56612400	-1.00080100
C	8.95049000	-1.30962800	0.93479800
H	8.55553200	-1.90628100	1.76595500
H	9.84771300	-1.81404300	0.55922400
H	9.25894600	-0.33871400	1.34089800
C	0.01578900	2.58996200	1.12016500
H	0.43254600	2.39887700	2.12395900
H	0.68387900	3.27491200	0.59460200
H	-0.95266400	3.08279900	1.23559900

N	-0.15314300	1.35330000	0.35960400

***N*-Methyl-1,2,3,4-tetrahydroisoquinoline radical A**, solvent = MeCN

Charge = 0; Multiplicity = 2

23

-442.862589

C	-2.77570900	-0.99115200	0.00638100
C	-1.47375000	-1.48681200	0.07864300
C	-0.36879700	-0.62194300	0.04928000
C	-0.57570100	0.76421600	-0.04997400
C	-1.89033700	1.25352100	-0.11911200
C	-2.98549700	0.38965100	-0.09301100
H	-3.61953900	-1.67472700	0.02680700
H	-1.30847700	-2.55910000	0.15667300
H	-2.05083200	2.32669400	-0.19248300
H	-3.99447800	0.78836200	-0.14698900
N	2.07370800	-0.24449100	-0.15913800
C	3.36297800	-0.73133300	-0.27763500
H	4.14418800	-0.00220400	-0.46358800
H	3.47162000	-1.73454100	-0.67647400
C	0.60480100	1.71285800	-0.10054900
H	0.78156000	2.02125800	-1.13975400
H	0.37927100	2.62486300	0.46397900
C	1.87855800	1.07122300	0.44860500
H	2.74925600	1.69044900	0.21974900
H	1.81810000	0.97462100	1.54674600
C	1.02546900	-1.20775200	0.16426900
H	1.17367500	-1.59566900	1.18979600
H	1.12761300	-2.06342900	-0.51187700

***N*-Methyl-1,2,3,4-tetrahydroisoquinoline radical B**, solvent = MeCN

Charge = 0; Multiplicity = 2

23

-442.887551

C	-2.76761600	-1.06008100	0.08681900
C	-1.46492000	-1.53144200	-0.00584900
C	-0.36362200	-0.62849300	-0.08218900
C	-0.63886900	0.77800600	-0.08602800
C	-1.95281900	1.22425100	0.01902500
C	-3.02700300	0.32283300	0.10858300
H	-3.59111400	-1.76688100	0.14825500
H	-1.27134200	-2.60158800	-0.01286300
H	-2.14830200	2.29490400	0.02330600
H	-4.04525400	0.69105000	0.18940200
N	2.05043400	-0.22868000	-0.17071300
C	3.37196400	-0.78184300	0.09684800
H	4.13873400	-0.10345900	-0.28691100
H	3.54456600	-0.93074100	1.17492000
H	3.47584400	-1.74496100	-0.40845400
C	0.53414000	1.71475300	-0.26452700
H	0.70071100	1.89939900	-1.33600400
H	0.33175800	2.68791400	0.19552700
C	1.81728500	1.12867700	0.33218500
H	2.68022900	1.74543900	0.06565000
H	1.74823100	1.10897100	1.43385800
C	0.97257400	-1.08883200	-0.16150700
H	1.19621700	-2.14626600	-0.25186400

6,7-dimethoxy-*N*-Methyl-1,2,3,4-tetrahydroisoquinoline radical A, solvent = MeCN

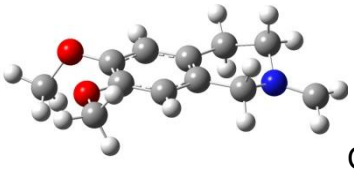

Charge = 0; Multiplicity = 2

31

-671.858818

C	-2.79073500	-0.94223500	0.17942500
C	-1.61993900	-1.21050100	0.89055600
C	-0.46218800	-0.43603400	0.70118500
C	-0.46910700	0.62777300	-0.20782400
C	-1.64894500	0.88746500	-0.92568800
C	-2.79602600	0.12398600	-0.75025700
H	-1.59343400	-2.02346200	1.60814400
H	-1.68664700	1.70807700	-1.63759500

N	1.96431000	-0.07804000	1.05375500
C	3.16941300	-0.45549400	1.61840900
H	4.04980500	0.09228900	1.30006900
H	3.27020300	-1.49777500	1.90259400
C	0.77331600	1.46609800	-0.42888500
H	1.27138900	1.15386100	-1.35679700
H	0.50050200	2.51986500	-0.55802100
C	1.75852400	1.33391700	0.73187400
H	2.72412900	1.77164000	0.46712500
H	1.38138600	1.87176300	1.61927600
C	0.76444600	-0.75862500	1.53275900
H	0.57315500	-0.48698800	2.58815300
H	0.95516900	-1.83713100	1.51617200
O	-3.94784700	0.46305200	-1.43286600
O	-3.96106400	-1.63398300	0.31607800
C	-4.29907800	-0.41921000	-2.51423000
H	-4.47992500	-1.43452000	-2.14931700
H	-5.21439400	-0.01679100	-2.95155700
H	-3.50519700	-0.43014400	-3.27028200
C	-4.00466300	-2.71743300	1.24781900
H	-5.01795000	-3.11503800	1.19083800
H	-3.28773000	-3.50068500	0.97729500
H	-3.80428200	-2.37024900	2.26760600

6,7-dimethoxy-*N*-Methyl-1,2,3,4-tetrahydroisoquinoline radical B, solvent = MeCN

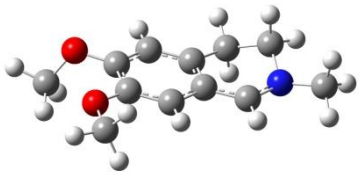

Charge = 0; Multiplicity = 2

31

-671.883576

C	-1.60749400	0.61892500	-0.12266600
C	-0.36573700	1.21730600	0.05211400
C	0.82756400	0.43403500	0.10165900
C	0.72383900	-0.98543100	-0.01165000
C	-0.53058500	-1.56259300	-0.18913900
C	-1.69623600	-0.79265500	-0.24644200
H	-0.28167600	2.29491900	0.13615300
H	-0.62855100	-2.64162000	-0.28447900
N	3.26933500	0.30799100	0.25186900
C	4.51955400	1.03209200	0.05980700
H	5.35566800	0.42043700	0.40945200

H	4.69018900	1.28504400	-0.99929600
H	4.50030400	1.95813900	0.63962900
C	1.98989000	-1.79784700	0.13200000
H	2.15102500	-2.05742000	1.18885600
H	1.91428200	-2.74288400	-0.41673000
C	3.20931100	-1.01899300	-0.36898900
H	4.13217300	-1.55288500	-0.12496100
H	3.16430900	-0.91302000	-1.46731100
C	2.09709900	1.03921400	0.26439500
H	2.19381500	2.10468900	0.44131600
O	-2.91120600	-1.40937000	-0.48909500
O	-2.79402900	1.30018300	-0.20244800
C	-3.75821900	-1.55442500	0.66380800
H	-4.01500500	-0.57802200	1.08653300
H	-4.66531500	-2.05537300	0.31963700
H	-3.26601600	-2.17085400	1.42573600
C	-2.76664400	2.72230700	-0.07604000
H	-2.17475700	3.18096200	-0.87652900
H	-3.80400000	3.04750800	-0.15896200
H	-2.36396500	3.02633800	0.89706900

Dextromethorphan radical A, solvent = MeCN

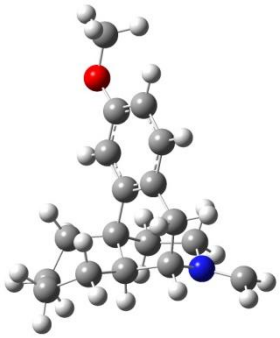

Charge = 0; Multiplicity = 2

44

-830.003445

C	2.30917500	2.75552100	-1.11412200
C	2.00524700	1.30187500	-1.57459100
C	1.98887200	0.36410500	-0.36085300
C	0.80113900	0.68641400	0.58729600
C	0.71901400	2.23645600	0.80257700
C	2.00114000	2.97165500	0.38512800
C	1.99266500	-1.13511200	-0.67362300
C	-0.52252400	0.12802300	0.03226300
C	-0.54609100	-0.93475000	-0.89743500
C	0.72885600	-1.54273100	-1.44968700
C	-1.78404300	-1.42892400	-1.32574700

H	-1.80437200	-2.24511400	-2.04473500
C	-2.99781800	-0.91838400	-0.85890500
C	-2.96936500	0.12152100	0.07809200
C	-1.73962900	0.62843700	0.51375900
H	2.86788600	-1.37261000	-1.28941600
H	3.36179500	2.99696800	-1.30346100
H	1.03666200	1.26379300	-2.08725800
H	-0.10559500	2.64283000	0.20627800
H	2.84520500	2.63178900	0.99791600
H	0.85714400	-1.23464900	-2.49682400
H	-3.93058700	-1.33502300	-1.21940400
H	-1.75812700	1.43019500	1.24511300
H	0.65213400	-2.63635600	-1.46287500
H	2.75504900	0.96819900	-2.30207400
H	1.71741600	3.45907400	-1.71199000
H	1.89162400	4.04274100	0.59119000
H	0.47961600	2.45637000	1.85014400
H	2.91207100	0.54937000	0.20217400
O	-4.08503000	0.70505500	0.62499200
C	-5.36822700	0.23174500	0.21231000
H	-6.09647900	0.82987000	0.76050700
H	-5.51609700	0.37368200	-0.86443200
H	-5.50144100	-0.82653800	0.46457300
C	1.11731700	-0.04971100	1.91829500
H	0.31341400	0.11421900	2.64544600
H	2.03486200	0.37727900	2.34360200
C	1.29237000	-1.55985600	1.71548000
H	0.30912800	-2.03350100	1.56595800
H	1.72658300	-2.00781400	2.61529000
N	2.18436900	-1.87595500	0.59171300
C	2.67164400	-3.16743100	0.51300100
H	2.80959600	-3.69609300	1.45063400
H	3.33371400	-3.39054700	-0.31770300

Dextromethorphan radical B, solvent = MeCN

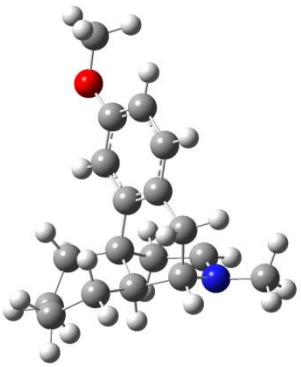

Charge = 0; Multiplicity = 2

44

-830.006206

C	2.38487600	2.73223400	-1.11789700
C	2.05849500	1.27922400	-1.56230000
C	1.99987300	0.36025800	-0.33567500
C	0.79856900	0.71913500	0.58262700
C	0.72316400	2.27330800	0.75420300
C	2.02703600	2.98534200	0.36486600
C	1.98304700	-1.14372500	-0.62781100
C	-0.52201000	0.15384000	0.03068700
C	-0.54589200	-0.92267900	-0.88300500
C	0.72989700	-1.52378000	-1.43619900
C	-1.78347700	-1.42645500	-1.30062100
H	-1.80388700	-2.25516900	-2.00520400
C	-2.99779100	-0.90942500	-0.84097800
C	-2.96897700	0.14876600	0.07482500
C	-1.73900700	0.66424000	0.50057000
H	2.86743100	-1.40597200	-1.22143400
H	3.45040300	2.94075800	-1.27131700
H	1.09731000	1.25535900	-2.08984100
H	-0.07699400	2.67088300	0.11941100
H	2.84438500	2.64733100	1.01386800
H	0.88319100	-1.17995000	-2.46873200
H	-3.93049400	-1.33424400	-1.19201200
H	-1.75732200	1.47871100	1.21793600
H	0.63351800	-2.61346400	-1.50068100
H	2.81240300	0.92054400	-2.27372000
H	1.83632600	3.43934900	-1.75174500
H	1.92483800	4.06197200	0.54445300
H	0.44970600	2.52169100	1.78718300
H	2.91440700	0.53834600	0.24470800
O	-4.08524600	0.74310200	0.61057300
C	-5.36780200	0.26143000	0.20663200
H	-6.09686400	0.87056800	0.74155200
H	-5.51484500	0.38078100	-0.87303400
H	-5.50142400	-0.79153000	0.48039900
C	1.09572600	0.01189600	1.93480000
H	0.25894700	0.14873800	2.63059600
H	1.96486800	0.52435800	2.39241200
C	1.35916700	-1.45486200	1.74738300
H	1.46183100	-2.08438100	2.62796800
N	2.12078400	-1.87140400	0.65279300
C	2.38490400	-3.29989900	0.54537100
H	3.15820000	-3.47418100	-0.20851200
H	2.74973000	-3.67427100	1.50646400
H	1.49201700	-3.88430600	0.27027900

***N*,*N*-dimethyldecanamide radical A**, solvent = MeCN

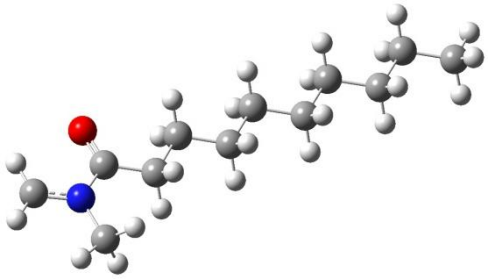

Charge = 0; Multiplicity = 2

38

-601.451357

N	-3.22478	-0.45984	0.00668
C	-2.73477	0.23312	1.20693
C	-2.73697	0.23467	-1.19357
H	-3.09204	-0.27085	-2.06722
H	-3.09682	1.24235	-1.19357
C	-2.73261	-1.84499	0.00534
H	-3.08747	-2.35044	0.87911
H	-3.08949	-2.34946	-0.86819
H	-1.66261	-1.84331	0.0041
C	-3.24584	-0.49444	2.46433
H	-2.58215	-1.29825	2.70581
H	-4.22481	-0.88399	2.27786
C	-3.30313	0.49554	3.64258
H	-4.03028	1.25307	3.43691
H	-2.34302	0.94912	3.77433
C	-3.69571	-0.25758	4.92722
H	-2.95962	-1.00381	5.14225
H	-4.64814	-0.72534	4.7895
C	-3.77689	0.73652	6.10057
H	-4.51703	1.47944	5.88805
H	-2.82601	1.20849	6.23462
C	-4.16139	-0.01792	7.38688
H	-5.11181	-0.49073	7.25249
H	-3.42073	-0.76016	7.59996
C	-4.24401	0.97641	8.55995
H	-4.98512	1.71828	8.34715
H	-3.29377	1.44969	8.69393
C	-4.6276	0.22183	9.84644
H	-5.57781	-0.2515	9.71243
H	-3.88645	-0.51999	10.05927
C	-4.71031	1.21618	11.01949
H	-5.45157	1.95792	10.80672

H	-3.76015	1.68962	11.1534
C	-5.0937	0.46157	12.30602
H	-5.15117	1.15244	13.12106
H	-6.04387	-0.01188	12.17211
H	-4.35245	-0.28017	12.51879
O	-3.18006	1.48637	1.20814

A11.6. XYZ CO-ORDINATES FOR PRODUCTS DERIVED FROM HAT AGENTS

Protonated DABCO, solvent = MeCN

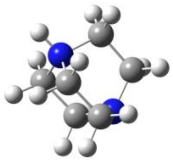

Charge = 1; Multiplicity = 1

21

-174.845030

C	0.74068400	0.65614700	1.27560100
C	-0.81578100	0.63599200	1.23623800
H	1.15653300	0.08677000	2.10776500
H	1.15687900	1.66412800	1.29152000
H	-1.20820400	0.08146100	2.09156800
H	-1.20792500	1.65429500	1.28411900
C	0.73731300	-1.43546800	-0.06978600
H	1.15311200	-1.87083700	-0.97935100
H	1.15226000	-1.95605500	0.79437100
C	-0.81855700	-1.38735300	-0.06839300
H	-1.21163200	-1.84984400	-0.97654800
H	-1.21268100	-1.93713600	0.78924700
C	-0.81573900	0.75456500	-1.16773300
H	-1.20913900	0.28779200	-2.07350500
H	-1.20690700	1.77297800	-1.11453700
C	0.74075700	0.77711500	-1.20586600
H	1.15574400	0.29059200	-2.08937800
H	1.15781200	1.78161900	-1.12435700
N	1.22438700	-0.00242200	-0.00019000
N	-1.30068600	0.00149400	0.00003900
H	2.24617200	-0.00525400	-0.00022700

Methane, solvent = MeCN

Charge = 0; Multiplicity = 1

5

-40.499049

C	0.00000000	0.00000000	0.00000000
H	0.63097900	0.63097900	0.63097900
H	-0.63097900	-0.63097900	0.63097900
H	-0.63097900	0.63097900	-0.63097900
H	0.63097900	-0.63097900	-0.63097900

Trimethylammonium cation, solvent = MeCN

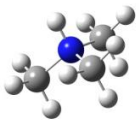

Charge = 1; Multiplicity = 1

14

-174.845030

C	1.43790200	0.02146100	-0.10397600
H	1.90862400	0.92192200	0.28883500
H	1.93498000	-0.86506300	0.28803600
H	1.46552200	0.02235700	-1.19335100
C	-0.73787100	1.23289000	-0.10338900
H	-1.75237900	1.18893300	0.29096200
H	-0.21892100	2.10768800	0.28618200
H	-0.75486500	1.25467000	-1.19276400
C	-0.70065400	-1.25434800	-0.10338600
H	-0.15600000	-2.11325100	0.28645100
H	-1.71608100	-1.24054300	0.29070500
H	-0.71654400	-1.27683600	-1.19276500
N	0.00094700	0.00000800	0.33604100
H	0.00277100	0.00005000	1.35992900

A11.7. XYZ Co-ordinates for Transition States of HAT Reactions

***N*-Methylmorpholine/DABCO radical cation - *N*-CH_3 abstraction transition state**, solvent = MeCN

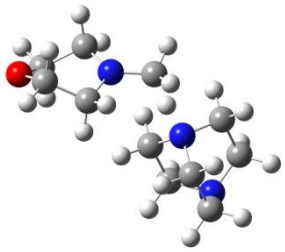

Charge = 1; Multiplicity = 2

38

-671.996262

C	1.28414600	1.13206800	-0.00592200
C	2.69534800	1.66667800	-0.41995700
H	0.53621700	1.29719900	-0.78512300
H	0.92648300	1.58816800	0.92018500
H	2.65893700	2.11229700	-1.41771600
H	3.03451300	2.43445600	0.28082400
C	1.84454200	-1.01269700	-1.02640600
H	1.86600300	-2.08823500	-0.83495300
H	1.10144700	-0.81394400	-1.80203900
C	3.25548700	-0.45166500	-1.40198100
H	3.99812000	-1.25408200	-1.40872100
H	3.23546500	-0.00101800	-2.39796200
C	3.74893600	-0.03204200	0.91026500
H	4.50299500	-0.82364400	0.89854200
H	4.07418300	0.73357100	1.61997500
C	2.35562200	-0.60874800	1.32522700
H	2.38682300	-1.68953600	1.48185000
H	1.96764800	-0.13837300	2.23183500
N	1.39253900	-0.33574300	0.22169800
N	3.68049900	0.57187500	-0.43143300
H	0.17574000	-0.82500100	0.57496100
C	-2.68360200	0.39927900	1.26172900
C	-3.24784700	1.44344600	0.30358000
C	-4.06490400	-0.48258900	-0.91391500
C	-2.60632100	-0.92300000	-0.84524200
H	-3.73057500	2.24114900	0.87331600
H	-2.43340500	1.88644100	-0.28544500
H	-3.47727700	0.00917000	1.91398000

H	-1.92001100	0.85308800	1.89920700
H	-4.43962200	-0.61495700	-1.93185700
H	-4.67050000	-1.10281700	-0.23978000
H	-2.00142100	-0.35995200	-1.56996600
H	-2.52556200	-1.98478200	-1.09519700
O	-4.24182300	0.90218800	-0.57777600
N	-2.09187700	-0.71055000	0.50837000
C	-0.98439900	-1.39587400	0.97674300
H	-0.89065900	-1.36455000	2.06437900
H	-0.89113500	-2.40036500	0.55674600

***N*-Methylmorpholine/DABCO radical cation - *N*-CH_2 abstraction transition state**, solvent = MeCN

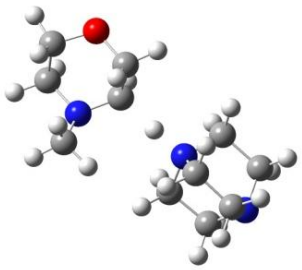

Charge = 1; Multiplicity = 2

38

-671.976916

C	-0.07359400	-0.02810400	-0.06116500
C	-0.10682600	0.13440400	1.49292400
H	0.94332800	0.00789800	-0.45685500
H	-0.67219800	0.72865200	-0.57270900
H	0.89736100	0.33632300	1.87442300
H	-0.75087300	0.97094000	1.77579200
C	0.19077100	-2.45101300	0.20201400
H	-0.26058000	-3.40698700	-0.07117400
H	1.18509100	-2.39624400	-0.24585200
C	0.22746700	-2.22955400	1.74915000
H	-0.12977600	-3.12266200	2.26818900
H	1.24965500	-2.03070200	2.08128300
C	-1.99770800	-1.33265000	1.67564400
H	-2.36330300	-2.24787900	2.14832600
H	-2.63019800	-0.50502700	2.00689000
C	-2.04782800	-1.46402300	0.11912200
H	-2.45670500	-2.42372600	-0.20318000
H	-2.62661300	-0.66366300	-0.34624400

N	-0.64690700	-1.36740300	-0.39789400
N	-0.61965400	-1.08832700	2.13212600
H	-0.67336500	-1.48564200	-1.64336500
C	-0.84611500	-1.50679300	-3.08740500
C	-1.06769300	-2.93232100	-3.60606700
C	-0.56211700	-2.04638500	-5.79736500
C	-0.21389000	-0.64902500	-5.19888800
H	-0.16334500	-3.54882800	-3.56132900
H	-1.89036700	-3.44087500	-3.10268500
H	-1.77439300	-0.94183100	-3.23116400
H	0.35451700	-2.63817400	-5.92054600
H	-1.04270800	-1.92522200	-6.77085600
H	0.58660200	-0.16957900	-5.76890700
H	-1.10276000	-0.01163600	-5.21710700
O	-1.49139500	-2.74882200	-4.97530800
N	0.18857900	-0.87585300	-3.80990400
C	1.56807300	-1.32359100	-3.61241400
H	2.24230600	-0.58217000	-4.04806900
H	1.78305200	-2.29554200	-4.07621200
H	1.77570100	-1.39796100	-2.54497600

***N*-Methylmorpholine/methyl radical - *N*-CH_3 abstraction transition state**, solvent = MeCN

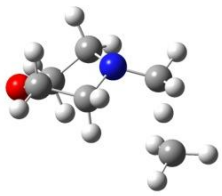

Charge = 0; Multiplicity = 2

22

-366.805222

H	-0.15309400	-0.16985700	0.36459500
C	0.16261100	0.08369100	3.29420300
C	1.68021200	0.20990300	3.40297700
C	1.21306300	2.57602500	3.25490800
C	0.48024100	2.14802300	1.99146800
H	2.06230400	-0.44876400	4.18837400
H	2.15406000	-0.07772000	2.45419800
H	-0.28752800	0.29519100	4.27367700
H	-0.09490300	-0.94732800	3.03347000
H	1.84160500	3.44736100	3.05145400

H	0.48588100	2.84942200	4.03254300
H	1.21568700	1.90850700	1.20388500
H	-0.12887500	2.98191200	1.62280800
O	2.08187300	1.54421600	3.75767500
N	-0.39066100	1.00280500	2.28073700
C	-0.99140600	0.40832900	1.13537200
H	-1.70184400	-0.37712900	1.40829800
H	-1.46758400	1.16115000	0.49871800
C	0.77479000	-0.87953100	-0.58005400
H	0.10511300	-1.30636200	-1.32673500
H	1.27514600	-1.61860000	0.04548900
H	1.43265700	-0.10048500	-0.96457800

***N*-Methylmorpholine/methyl radical - *N*-CH_2 abstraction transition state**, solvent = MeCN

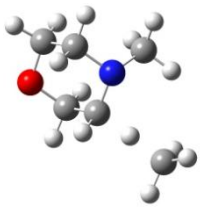

Charge = 0; Multiplicity = 2

22

-366.803080

H	0.06111200	0.02006900	0.18462400
C	-0.05101000	0.14011400	1.50463800
C	1.34098000	0.18562300	2.10676100
C	0.46833800	-0.75208200	4.11588000
C	-0.93234400	-0.82395300	3.49362200
H	1.92156200	-0.71789700	1.86998800
H	1.89867600	1.06019800	1.76214900
H	-0.56043900	1.10372500	1.62646200
H	1.00932900	-1.70084600	3.98116400
H	0.40443500	-0.54294100	5.18761400
H	-1.48556600	-1.67793200	3.90106100
H	-1.48201900	0.08972500	3.75295500
O	1.23441200	0.31761200	3.54235000
N	-0.89070400	-0.92754800	2.01964000
C	-0.54838300	-2.26991600	1.53478500
H	-1.26976000	-2.98482100	1.94249400
H	0.46077000	-2.62146700	1.80199400
H	-0.63075900	-2.28699700	0.44495700
C	0.15727200	-0.03675800	-1.19396900

H	0.91160900	-0.79647200	-1.39822600
H	-0.84306300	-0.30714400	-1.53202100
H	0.45966800	0.97026900	-1.48141300

***N*-Methylmorpholine/trimethylammonium radical cation - *N*-CH_3 abstraction transition state**, solvent = MeCN

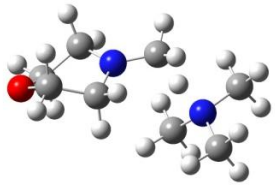

Charge = 1; Multiplicity = 2

31

-501.191670

C	0.05099500	-0.00519900	-0.04296800
H	0.07943400	0.02953000	1.04766500
H	1.07059500	-0.01029100	-0.43246400
C	-2.00696900	-1.33842200	0.08608500
H	-2.44477200	-2.29613200	-0.20100700
H	-1.95525200	-1.27549400	1.17437500
C	-0.62816400	-1.40575900	-1.94328000
H	-1.08126400	-2.36539100	-2.19967700
H	0.40373000	-1.38574100	-2.29828300
N	-0.64230500	-1.23739900	-0.47429600
H	0.06649200	-2.28774800	0.03377500
C	2.74874000	-2.69740000	1.71855200
C	2.93811500	-1.84310200	2.96784100
C	1.65548000	-3.58729600	4.05034800
C	0.66108200	-3.30612600	2.92847700
H	3.97814200	-1.51451000	3.03270000
H	2.29916000	-0.95159300	2.90963900
H	3.44281100	-3.54913000	1.72732500
H	2.96063800	-2.10336800	0.82545700
H	1.12540600	-3.63620600	5.00472200
H	2.14480900	-4.55504500	3.87717500
H	0.11179600	-2.37528400	3.12848000
H	-0.06836300	-4.11850700	2.86390700
O	2.65353100	-2.56270900	4.17558500
N	1.37325800	-3.20154300	1.65407000
C	0.72624700	-3.39526900	0.44637600
H	1.41366700	-3.57589500	-0.38256400
H	-0.08672600	-4.12269900	0.50791900

H	-2.63520800	-0.52543900	-0.29476600
H	-0.47513200	0.87916900	-0.41935700
H	-1.19295200	-0.59942200	-2.42436200

***N*-Methylmorpholine/trimethylammonium radical cation - *N*-CH_2 abstraction transition state**, solvent = MeCN

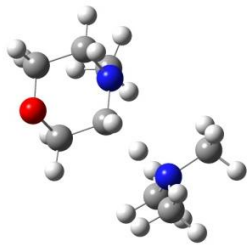

Charge = 1; Multiplicity = 2

31

-501.171472

C	0.01333400	-0.02962600	0.04501700
H	-0.01614000	-0.02506000	1.13545400
H	1.05105100	-0.02009500	-0.29176800
C	-2.03470800	-1.40095900	0.05473000
H	-2.45160500	-2.34549600	-0.29719800
H	-2.01798200	-1.39341000	1.14534000
C	-0.59809900	-1.34201500	-1.94195200
H	-1.03623900	-2.28787700	-2.26326000
H	0.44198800	-1.29026900	-2.26668700
N	-0.65002900	-1.25703800	-0.46004800
H	0.02714500	-2.22719100	-0.02968900
C	0.93943400	-3.29674100	0.32520300
C	0.26023900	-4.67207600	0.28333400
C	2.16076700	-5.47464400	1.54368400
C	2.73586700	-4.02983300	1.67930300
H	-0.44793100	-4.82281100	1.10533700
H	-0.22802600	-4.87182200	-0.67076800
H	1.68288800	-3.26065900	-0.47925600
H	1.57395900	-5.72607300	2.43707300
H	2.97816000	-6.19157900	1.43881100
H	3.24522100	-3.90236300	2.63833600
H	3.44123400	-3.83777700	0.86571700
O	1.35561200	-5.60855600	0.37489500
N	1.59781700	-3.11830500	1.55928700
C	0.80153500	-2.93490600	2.77331300
H	1.44242600	-2.51282500	3.55158200
H	0.37142400	-3.87036700	3.15488600

H	-0.01150700	-2.23727800	2.57380400
H	-1.16016600	-0.51203100	-2.37999000
H	-2.65225100	-0.57231400	-0.30447900
H	-0.50305900	0.85601900	-0.33628000

***N*-Ethyl-*N*-methylethanamine/DABCO radical cation - *N*-CH_3 abstraction transition state**, solvent = MeCN

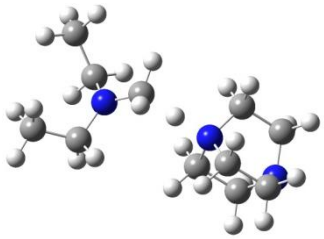

Charge = 1; Multiplicity = 2

39

-597.989942

C	-0.36032400	0.05998000	-0.15333400
C	0.44909800	0.13920700	2.24016100
H	0.72505000	0.04225700	-0.27996500
H	-0.74087000	0.92190000	-0.71323000
H	0.09640000	0.54362700	3.19154700
H	1.28990500	0.76160600	1.90803900
N	-0.64132300	0.27943500	1.27094100
C	-1.86727500	0.79659900	1.65941900
H	-2.12511200	0.57634600	2.69748600
H	-1.85683000	2.16825800	1.66006100
H	-2.67307900	0.58003600	0.95519700
C	0.91268500	-1.31042500	2.42113100
H	1.31026000	-1.72749900	1.49129800
H	1.71091100	-1.34002300	3.16930300
H	0.09044400	-1.94442800	2.76602600
C	-0.98134200	-1.23156700	-0.70047200
H	-0.58711900	-2.11185700	-0.18546700
H	-2.07000300	-1.22491000	-0.59227000
H	-0.74736000	-1.32094400	-1.76601300
C	-0.58488500	4.06785000	1.34304300
C	-0.68173800	5.62790100	1.39129200
H	0.13660500	3.67771300	2.06467700
H	-0.31520000	3.70227500	0.34945400
H	0.00739600	6.03216800	2.13769700
H	-0.41946800	6.05832300	0.42101900

C	-2.32031300	3.94686400	3.05484900
H	-3.28101200	3.48166100	3.28811600
H	-1.57275800	3.56830700	3.75601800
C	-2.40309000	5.50793100	3.06160500
H	-3.41484000	5.83764800	3.31292000
H	-1.71784500	5.92530900	3.80433900
C	-2.98884200	5.52618100	0.73284100
H	-3.99597000	5.86917300	0.98492600
H	-2.72383900	5.94454400	-0.24199100
C	-2.93532100	3.96444500	0.69290000
H	-3.89285200	3.51137900	0.96071700
H	-2.63533200	3.58530900	-0.28685400
N	-1.92298700	3.50806400	1.68696500
N	-2.04911200	6.05149400	1.73845800

***N*-Ethyl-*N*-methylethanamine/DABCO radical cation - *N*-CH_2 abstraction transition state**, solvent = MeCN

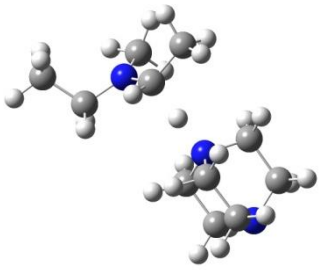

Charge = 1; Multiplicity = 2

39

-597.988751

C	-0.30924200	0.28849300	-0.06613800
C	0.28486200	0.08646400	2.32847100
H	0.77922000	0.37177000	-0.11319300
H	-0.72848800	1.20500600	-0.49852800
H	0.83112000	1.32471400	2.58188700
H	1.16753000	-0.41735700	1.92247100
N	-0.69603700	0.21585500	1.34766800
C	-2.06666700	0.58103500	1.68866100
H	-2.12286400	1.62144100	2.03659300
H	-2.69628400	0.47793800	0.80445200
H	-2.45912400	-0.07113500	2.47143400
C	-0.13489300	-0.43472200	3.69411900
H	-0.57926200	-1.43568700	3.61718400
H	0.74667500	-0.50983900	4.33610600
H	-0.85578900	0.21844500	4.19388600
C	-0.77419400	-0.93593200	-0.86262100

H	-0.32935000	-1.85109100	-0.46038800
H	-1.86315000	-1.04081200	-0.84267500
H	-0.46493700	-0.82942700	-1.90726900
C	1.16079100	3.44928200	1.74541700
C	1.87352000	4.80271900	2.06931600
H	1.54105500	2.99472300	0.82787000
H	0.07880000	3.56613200	1.65287400
H	2.61848500	5.03660000	1.30393300
H	1.14843900	5.62068900	2.09547800
C	2.89185600	2.28467300	3.01297500
H	3.04471900	1.55258700	3.80913400
H	3.25951500	1.85918100	2.07628100
C	3.56033100	3.65967600	3.33993700
H	4.06078600	3.62165500	4.31128400
H	4.30931000	3.91109100	2.58409900
C	1.55607700	4.42677700	4.41938300
H	2.06242500	4.40755600	5.38819800
H	0.81660400	5.23189300	4.44074600
C	0.86502100	3.05341700	4.13613700
H	1.05731200	2.32678200	4.92842500
H	-0.21562500	3.15292800	4.01130800
N	1.42326700	2.50265800	2.86771600
N	2.55008600	4.73186900	3.37568400

***N*-Ethyl-*N*-methylethanamine/methyl radical - *N*-CH_3 abstraction transition state**, solvent = MeCN

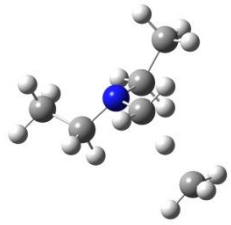

Charge = 0; Multiplicity = 2

23

-292.797335

C	-0.04304900	-0.05960400	0.14077300
C	-0.09988100	-0.09508900	2.59996600
H	1.02726700	-0.17062600	0.33127600
H	-0.82650800	-0.22905000	3.40742700
C	1.15357900	-0.91018400	2.92508000
H	1.93526500	-0.79439500	2.16799200
H	0.91197800	-1.97505000	3.00678000
C	-0.39821000	-0.85708700	-1.11551100
H	-0.21524200	-1.92586800	-0.96160200

H	-1.44332800	-0.72698900	-1.41175300
C	-2.16106600	-0.23114800	1.32967500
H	-2.64515700	-0.59635000	0.42138700
H	-2.66084000	-0.62617600	2.21852000
N	-0.75860500	-0.50139000	1.34812300
H	0.22387800	-0.51969700	-1.95129300
H	1.57139100	-0.57764100	3.88150300
H	-2.42846500	1.02395400	1.34471700
C	-2.82620500	2.46314400	1.37030000
H	-2.47911400	2.86882500	0.42015700
H	-3.91152100	2.42464900	1.46642300
H	-2.31748700	2.87451500	2.24200300
H	-0.22452500	1.01655400	-0.03410800
H	0.14673300	0.98157300	2.57405500

***N*-Ethyl-*N*-methylethanamine/methyl radical - *N*-CH_2 abstraction transition state**, solvent = MeCN

Charge = 0; Multiplicity = 2

23

-292.798047

C	0.09390400	-0.13035800	0.12085700
C	-0.00295800	-0.12486900	2.57644800
H	1.14836000	-0.33944500	0.31181200
H	-0.71028100	-0.26913100	3.39998800
C	1.30801000	-0.84394500	2.86090900
H	2.10446200	-0.57242500	2.16110900
H	1.17985800	-1.93328600	2.82294100
C	-0.34560300	-0.93639300	-1.10377500
H	-0.26477400	-2.01121200	-0.90966700
H	-1.37559800	-0.71843000	-1.40162700
C	-2.03975500	0.03927700	1.29459700
H	-2.08815400	1.14169700	1.24188200
H	-2.56044000	-0.36583300	0.42424100
H	-2.57639800	-0.28652600	2.18985900
N	-0.66291300	-0.45281500	1.34045500
H	0.29987400	-0.69248600	-1.95436900
H	1.65400400	-0.57853000	3.86518800
H	0.01883800	0.95098600	-0.09719300

C	0.60341300	2.57753500	2.78132600
H	0.79957300	2.69027400	3.84755100
H	1.48211200	2.70730300	2.14991600
H	-0.27981000	3.11168900	2.43221500
H	0.25183800	1.12555100	2.63912700

***N*-Ethyl-*N*-methylethanamine/trimethylammonium radical cation - *N*-CH_3 abstraction transition state**, solvent = MeCN

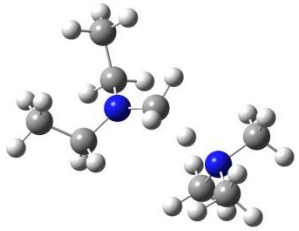

Charge = 1; Multiplicity = 2

32

-427.184688

C	0.01907900	0.00129100	0.01793300
C	-0.02020400	-0.01177200	2.54535500
H	1.08383900	-0.02520400	0.26284700
H	-0.15162600	0.88962900	-0.60084000
H	-0.67900800	0.34819000	3.33862500
H	0.87170000	0.62818800	2.54058000
N	-0.72492700	0.16827600	1.27292400
C	-2.01057300	0.68424700	1.24694600
H	-2.59988900	0.43134800	2.13066100
H	-2.01585200	2.05737400	1.29611500
H	-2.53395800	0.49770500	0.30723300
C	0.38148400	-1.46658000	2.81040700
H	1.07255300	-1.84105800	2.04968900
H	0.88591400	-1.52747800	3.77971900
H	-0.49767400	-2.11731200	2.83531300
C	-0.38052900	-1.25946200	-0.75887700
H	-0.18508100	-2.16417400	-0.17675600
H	-1.44116600	-1.24142400	-1.02646900
H	0.20130200	-1.31172600	-1.68448300
C	-0.76919600	3.95301400	1.42948300
H	-0.28229500	3.57366000	2.32962900
H	-0.19856000	3.64668600	0.55112100
C	-2.93910100	3.69949700	2.54850300
H	-3.91492200	3.21799600	2.46167000
H	-2.42257100	3.31462400	3.42967900

C	-2.82729100	3.79938800	0.09796100
H	-3.79815300	3.30281900	0.04922500
H	-2.22355800	3.49955500	-0.76045800
N	-2.13696600	3.39678300	1.34298500
H	-2.97445800	4.88480900	0.07763400
H	-3.07676000	4.78135300	2.65213300
H	-0.80637200	5.04714500	1.47201700

***N*-Ethyl-*N*-methylethanamine/trimethylammonium radical cation - *N*-CH_2 abstraction transition state**, solvent = MeCN

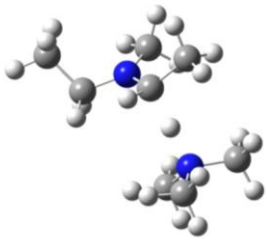

Charge = 1; Multiplicity = 2

32

-427.183000

C	0.01590400	-0.00065200	-0.00058700
C	0.01590700	0.02686600	2.47944400
H	1.08860300	-0.02721800	0.20545300
H	-0.18189600	0.89089600	-0.60766500
H	0.59808200	1.24645100	2.76938200
H	0.92063800	-0.57307000	2.34338300
N	-0.68293600	0.14077400	1.28064500
C	-2.07565100	0.57627200	1.26007700
H	-2.19496300	1.52503600	1.79540300
H	-2.39368500	0.71897700	0.22747800
H	-2.72784100	-0.16889700	1.72687800
C	-0.77374800	-0.34065800	3.72639500
H	-1.25476000	-1.32115200	3.61357300
H	-0.09498200	-0.39854100	4.58113500
H	-1.55104400	0.39080100	3.96482200
C	-0.40412800	-1.26299500	-0.76274300
H	-0.17906000	-2.16174900	-0.18062100
H	-1.47374800	-1.25644100	-0.99343800
H	0.14471400	-1.31537700	-1.70841300
C	1.29062400	3.18583100	1.82773600
H	1.85372900	2.62203100	1.08209400
H	0.28057500	3.37030300	1.45793200

C	2.56362800	2.04105100	3.58320100
H	2.46236100	1.42832700	4.48070800
H	3.09156000	1.47323500	2.81494800
C	0.40930200	3.09348100	4.11265300
H	0.34662100	2.46670500	5.00336400
H	-0.59406800	3.27235900	3.72259700
N	1.21880600	2.40444800	3.08256200
H	0.87047500	4.05162500	4.37663500
H	3.13568900	2.94402600	3.82308900
H	1.78960600	4.14434900	2.00766900

***N*-Methyl-*N*-octyloctan-1-amine/DABCO radical cation - *N*-CH_3 abstraction transition state**, solvent = MeCN

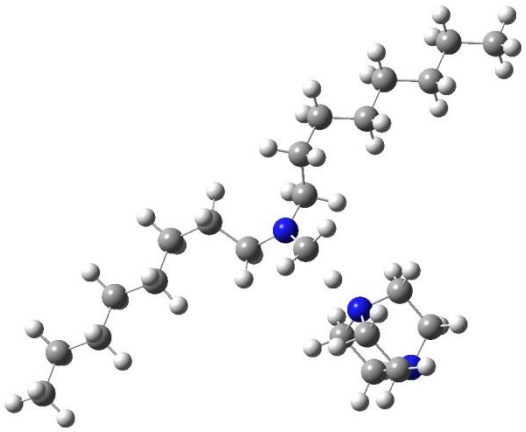

Charge = 1; Multiplicity = 2

75

-1069.480624

H	-0.19924800	0.04876000	0.06201000
C	1.95334200	0.52035200	0.74431700
C	2.88225900	0.43067200	1.99860200
H	2.31916100	-0.08845200	-0.08588900
H	1.83203300	1.54770800	0.39315000
H	3.73520000	-0.22350200	1.79835900
H	3.26895600	1.41928000	2.26042700
C	0.71071800	-1.40868700	1.58034600
H	-0.29843100	-1.76147600	1.80649900
H	1.10406600	-1.99629000	0.74744000
C	1.64725000	-1.45461000	2.83015500
H	1.11040400	-1.84539600	3.69883600
H	2.50549400	-2.10575800	2.64306000
C	0.99625200	0.77239700	3.44673200
H	0.47053800	0.37895300	4.32095500

H	1.37512400	1.76642600	3.69953200
C	0.03444800	0.84893600	2.21671300
H	-0.96242300	0.46475100	2.44545200
H	-0.06650100	1.86773900	1.83573000
N	0.60620600	0.00814500	1.12631300
N	2.14256400	-0.10554200	3.15474400
C	-1.79496400	2.27999900	-1.51951500
C	0.03756300	1.17978100	-2.86464800
H	-1.35048600	3.12856000	-2.04730500
H	-1.71010000	2.48273700	-0.44647800
H	0.69191000	0.31299100	-2.75261200
H	0.64295100	2.07754700	-2.68073300
C	-0.55173400	1.23520200	-4.28495400
H	-1.26027700	2.06947500	-4.34479900
H	-1.12440700	0.31709800	-4.46833500
C	-3.27464800	2.13286400	-1.91906400
H	-3.32703200	1.88701000	-2.98572000
H	-3.71542700	1.28663700	-1.37745600
C	0.51735600	1.41777800	-5.37562800
H	0.00030500	1.58277000	-6.32990600
H	1.08574400	2.33689100	-5.17378500
C	-4.10042500	3.40241700	-1.64836300
H	-5.09599800	3.25720700	-2.08774000
H	-3.65127300	4.24989800	-2.18571100
C	1.49090400	0.24052400	-5.53917600
H	2.06734700	0.09427800	-4.61571300
H	0.91584000	-0.68397200	-5.69410400
C	2.46952100	0.43047900	-6.70616800
H	1.90005600	0.56056500	-7.63786200
H	3.03176600	1.36381100	-6.55707000
C	3.45731100	-0.73158100	-6.87494300
H	4.02628100	-0.86162000	-5.94262100
H	2.89654700	-1.66585400	-7.02493100
C	4.43784300	-0.54069300	-8.03979400
H	4.99563300	0.39445400	-7.89162100
H	3.87037500	-0.41454500	-8.97231200
C	5.42549400	-1.70291800	-8.19746600
H	4.89876800	-2.64713900	-8.38130100
H	6.11065100	-1.53500100	-9.03576700
H	6.03097500	-1.83177600	-7.29217700
C	-4.26467200	3.76650300	-0.16469300
H	-3.28500000	3.97956700	0.28378100
H	-4.66929400	2.89851900	0.37602700
C	-5.18296100	4.97575300	0.05987700
H	-6.17265100	4.76287800	-0.36964800
H	-4.78652100	5.83846600	-0.49511100
C	-5.34373500	5.35701000	1.53744200
H	-4.35373500	5.57269700	1.96549200

H	-5.73692700	4.49367100	2.09413400
C	-6.26375700	6.56384200	1.76543400
H	-5.87257300	7.42584100	1.20728800
H	-7.25402300	6.34782100	1.34075300
C	-6.41443600	6.94043600	3.24407300
H	-5.44431100	7.19563800	3.68730500
H	-7.07659900	7.80396000	3.37166100
H	-6.83506700	6.10913900	3.82271400
C	-1.06816300	-0.02469700	-1.00550100
H	-2.02781200	-0.12344100	-0.49425800
H	-0.73758600	-0.94462400	-1.49247000
N	-0.98867600	1.09211700	-1.82319700

***N*-Methyl-*N*-octyloctan-1-amine/DABCO radical cation - *N*-CH_2 abstraction transition state**, solvent = MeCN

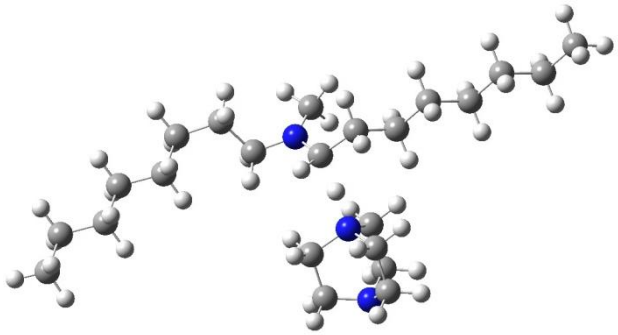

Charge = 1; Multiplicity = 2

75

-1069.475353

C	0.13762500	0.07594400	0.14237200
C	-0.01600200	0.39728700	2.59186800
H	1.19347200	0.15328300	0.40823300
H	-0.07514600	0.85767100	-0.59790500
H	0.61047800	1.63384300	2.72526900
H	0.89765800	-0.20515100	2.55701900
N	-0.65031200	0.34425500	1.35036800
C	-2.02930500	0.77703800	1.16104100
H	-2.11156400	1.87036900	1.21753300
H	-2.37431700	0.45693100	0.17763600
H	-2.68190900	0.33474000	1.91607000
C	-0.83803900	0.12448900	3.85696400
H	-1.52023900	-0.71495300	3.65699000
H	-0.12960600	-0.23981600	4.60983500
C	-0.16224900	-1.31046200	-0.45685300
H	0.06476400	-2.07662400	0.29550200
H	-1.23532800	-1.38307800	-0.66910800

C	0.47969100	3.96098400	2.66629100
C	1.37682500	5.23520100	2.78343300
H	-0.00483300	3.88614300	1.69020000
H	-0.29218100	3.92981800	3.43753800
H	1.31882900	5.82994600	1.86786500
H	1.04436900	5.86229900	3.61514900
C	2.38677900	2.73764400	1.76303400
H	2.98355200	1.83178300	1.89363400
H	1.87286000	2.68185000	0.80096500
C	3.25171800	4.03370200	1.88794500
H	4.30166200	3.77929800	2.05585900
H	3.19022100	4.62428500	0.96991900
C	2.88337300	4.08425400	4.25844800
H	3.93315200	3.82890200	4.42605800
H	2.55284400	4.71418100	5.08883300
C	2.01094000	2.79084700	4.17172300
H	2.60812100	1.88096300	4.26837700
H	1.23076300	2.77295100	4.93537900
N	1.34730900	2.75866000	2.83529300
N	2.78357700	4.86228500	3.01140700
C	0.62377000	-1.59594400	-1.74817300
H	0.22230300	-2.51644900	-2.19159100
H	0.42914200	-0.79640200	-2.47720100
C	2.13906100	-1.76163700	-1.55844900
H	2.57591900	-0.83420200	-1.16386100
H	2.32222100	-2.53608300	-0.79937600
C	2.87097400	-2.14030000	-2.85327200
H	2.44041200	-3.07010400	-3.25276800
H	2.68727900	-1.36609400	-3.61240500
C	4.38360900	-2.32153900	-2.67155000
H	4.56691200	-3.09636300	-1.91265100
H	4.81476900	-1.39225500	-2.27089300
C	5.11862000	-2.70023500	-3.96423100
H	4.68827400	-3.62851100	-4.36529600
H	4.93697200	-1.92594400	-4.72259400
C	6.62892300	-2.88110600	-3.77211700
H	6.84223000	-3.67122500	-3.04203900
H	7.12187300	-3.15384300	-4.71181300
H	7.09442600	-1.95764300	-3.40702700
C	-1.63416700	1.28726300	4.47828500
H	-2.30602900	1.74143800	3.74068800
H	-0.94033700	2.07820100	4.78863700
C	-2.45325400	0.84419100	5.69831100
H	-3.17177700	0.07144200	5.38980300
H	-1.78437500	0.36788500	6.42954700
C	-3.20642500	1.99608600	6.37714700
H	-3.87123100	2.47610700	5.64437800
H	-2.48508400	2.76574300	6.68790300

C	-4.03024900	1.55640100	7.59456500
H	-3.36679800	1.07054700	8.32503400
H	-4.75682600	0.79138900	7.28393900
C	-4.77546900	2.70886800	8.28127500
H	-5.43802200	3.19546600	7.55192300
H	-4.04934300	3.47265800	8.59257900
C	-5.59665600	2.26106000	9.49613300
H	-6.11606300	3.10605100	9.96151900
H	-6.35347400	1.52080600	9.20979100
H	-4.95590100	1.80224800	10.25880500

***N*-Methyl-*N*-octyloctan-1-amine/methyl radical - *N*-CH_3 abstraction transition state**, solvent = MeCN

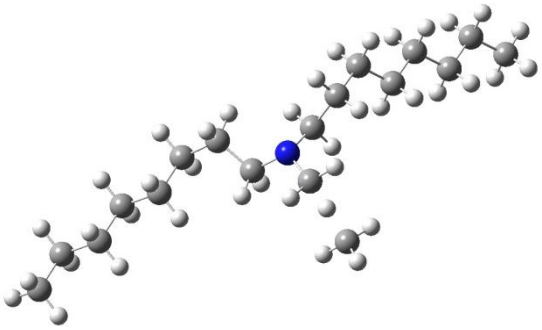

Charge = 0; Multiplicity = 2

59

-764.288617

H	0.00860400	0.67964000	0.41541100
C	0.04845500	1.01458200	3.28139300
C	2.25455800	0.87917600	2.19592100
H	0.65754800	0.69714900	4.13304300
H	-0.44302200	0.10811100	2.88809000
H	2.70208400	1.12169100	1.22776300
H	2.11073900	-0.21694100	2.20952800
C	3.21640000	1.29007800	3.31968900
H	2.71945000	1.16800900	4.28972800
H	3.43833200	2.36083500	3.21746400
C	-0.99594100	2.01836200	3.78827600
H	-0.46816800	2.93298300	4.08681200
H	-1.68031500	2.30109000	2.97840200
C	4.52794900	0.48677400	3.34157400
H	5.08460200	0.76233800	4.24754700
H	4.29610800	-0.58373400	3.44125100
C	-1.81961500	1.50146600	4.98102000
H	-2.40782500	2.33872500	5.38053200
H	-1.13711500	1.19746700	5.78824500

C	5.44049000	0.69672000	2.12327600
H	4.93417800	0.35655800	1.20985500
H	5.62231500	1.77368500	1.99167600
C	6.78585000	-0.03138800	2.24536300
H	7.30378600	0.31694600	3.15097400
H	6.60298800	-1.10614200	2.39128200
C	7.70451800	0.16339100	1.03177900
H	7.18899700	-0.18973400	0.12653200
H	7.88486000	1.23815400	0.88203800
C	9.05222300	-0.55937700	1.15710500
H	8.87290000	-1.63307000	1.30798100
H	9.56875200	-0.20538400	2.06016900
C	9.96254000	-0.36147600	-0.06079800
H	10.19047600	0.70009800	-0.21556600
H	10.91349100	-0.89225200	0.05952000
H	9.48545500	-0.73473400	-0.97509600
C	-2.77647700	0.34195100	4.66279900
H	-2.20993900	-0.52814100	4.30510800
H	-3.43842000	0.63944600	3.83613900
C	-3.62908700	-0.08030800	5.86702400
H	-4.19765800	0.78890900	6.22902200
H	-2.96552900	-0.37731900	6.69241200
C	-4.60154000	-1.22806900	5.56447300
H	-4.03524200	-2.09783600	5.20010000
H	-5.26871700	-0.93055900	4.74209000
C	-5.44910300	-1.65036500	6.77193200
H	-4.78293200	-1.95201700	7.59222300
H	-6.01214700	-0.78087200	7.13888300
C	-6.42307200	-2.79295900	6.46046600
H	-5.88691100	-3.68850600	6.12375000
H	-7.01185000	-3.06902400	7.34231600
H	-7.12435200	-2.50837200	5.66673400
C	0.34702900	1.77521300	0.98825900
H	-0.58523500	2.34033400	1.05824100
H	1.03415500	2.25036800	0.28246500
N	0.95655100	1.56902700	2.26354800
H	-0.67410100	-0.17909300	-1.31200200
H	-1.24179600	-0.95669300	0.24286800
H	0.48377500	-1.18737600	-0.31822400
C	-0.40314700	-0.55394100	-0.32475300

_N_-Methyl-_N_-octyloctan-1-amine/methyl radical - _N_-CH_2 abstraction transition state, solvent = MeCN

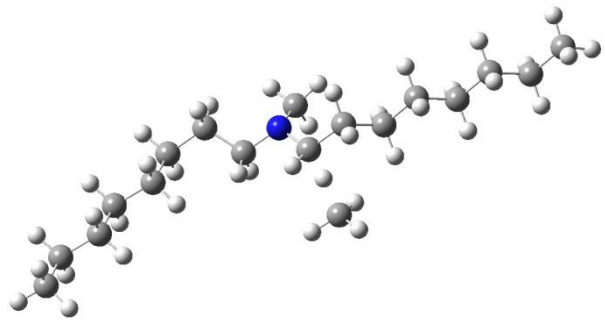

Charge = 0; Multiplicity = 2

59

-764.285706

C	0.00474800	-0.48658000	0.14649700
C	-0.08961300	-0.31764500	2.56985700
H	1.02955100	-0.75745000	0.41570500
H	0.03350000	0.56811400	-0.18600400
H	0.26264700	0.91055800	2.57589200
H	0.87899300	-0.82514700	2.52140900
N	-0.81254800	-0.62200800	1.36181800
C	-2.11754200	0.02695800	1.24527200
H	-2.03151000	1.12707500	1.19022800
H	-2.62880800	-0.32105300	0.34559400
H	-2.74691500	-0.22768600	2.10003300
C	-0.80499800	-0.62889000	3.89383600
H	-1.53344700	-1.43464500	3.72104500
H	-0.05916100	-1.04327800	4.58400500
C	-0.46243300	-1.37543000	-1.01464100
H	-0.45185400	-2.42260200	-0.68329800
H	-1.50196200	-1.13835900	-1.26926400
C	0.39401700	-1.22573400	-2.28527700
H	-0.09489100	-1.78098700	-3.09705300
H	0.39933900	-0.17161100	-2.59862000
C	1.84096000	-1.72456500	-2.15276200
H	2.37382000	-1.14010400	-1.39081300
H	1.82958400	-2.76336500	-1.79103700
C	2.63005400	-1.65627600	-3.46764700
H	2.11042400	-2.25089900	-4.23318900
H	2.63293100	-0.61943300	-3.83463000
C	4.07716300	-2.14983200	-3.33991200

H	4.07498500	-3.18692600	-2.97339300
H	4.59624600	-1.55551500	-2.57357500
C	4.87115500	-2.08138400	-4.65146200
H	4.35479400	-2.67664300	-5.41743900
H	4.87250700	-1.04543200	-5.01833300
C	6.31653400	-2.57364700	-4.51216500
H	6.34801100	-3.61843700	-4.18031600
H	6.85442000	-2.51007400	-5.46460400
H	6.86819300	-1.97543300	-3.77690000
C	-1.49873800	0.54679000	4.60645500
H	-2.22423800	1.02570700	3.93668700
H	-0.75021300	1.31368100	4.84252600
C	-2.20905800	0.12070300	5.89817600
H	-2.97508400	-0.63209700	5.66084800
H	-1.48657900	-0.37688800	6.56185200
C	-2.86268600	1.28782400	6.65029500
H	-3.58249100	1.78830100	5.98620000
H	-2.09440400	2.03743500	6.88987100
C	-3.57626800	0.86710500	7.94201800
H	-2.85853800	0.36203900	8.60514900
H	-4.34962100	0.12216200	7.70350400
C	-4.22081700	2.03692200	8.69768700
H	-4.93694700	2.54310200	8.03540500
H	-3.44753900	2.78006200	8.93754900
C	-4.93296800	1.60919900	9.98641700
H	-5.37768600	2.46773700	10.50185800
H	-5.73714100	0.89402000	9.77524400
H	-4.23529100	1.12752600	10.68217000
C	0.78324300	2.32746700	2.55703800
H	-0.10645100	2.95621600	2.55348600
H	1.37373600	2.38341100	1.64285900
H	1.37157900	2.39272300	3.47225700

***N*-Methyltetrahydroisoquinoline/DABCO radical cation - *N*-CH_3 abstraction transition state**, solvent = MeCN

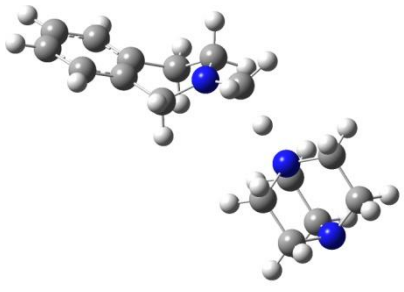

Charge = 1; Multiplicity = 2

-788.502275

C	-0.06369100	-1.27784000	1.60631600
C	-1.11434800	-1.83968900	2.61880700
H	-0.24419700	-1.62765500	0.58722600
H	0.95936900	-1.53970400	1.88641600
H	-1.83247300	-2.48653500	2.10763800
H	-0.62017800	-2.43081800	3.39460800
C	-1.54145300	0.62114100	1.19452000
H	-1.56490000	1.71289000	1.15784500
H	-1.71810700	0.23665400	0.18745600
C	-2.55576000	0.04269700	2.23368900
H	-3.10487100	0.85020000	2.72552000
H	-3.28272500	-0.60682500	1.73860000
C	-0.89738300	0.13563700	3.96795500
H	-1.45691500	0.93024100	4.46910300
H	-0.38687400	-0.45276000	4.73517800
C	0.13534000	0.74185000	2.96319600
H	0.07291800	1.83173800	2.91459000
H	1.16332200	0.46484900	3.20913800
N	-0.16906500	0.20866300	1.60448700
N	-1.85197000	-0.73963600	3.26478100
H	0.71912500	0.72489800	0.73646600
C	2.95228300	-0.34653100	-1.27065300
C	2.77105900	-1.34725000	-2.41790200
C	0.93911900	0.75237700	-2.36731400
H	3.66161000	-1.97874800	-2.47761900
H	1.92468100	-2.00898000	-2.18811400
H	3.90458400	0.18801900	-1.38839300
H	2.98092600	-0.86367000	-0.30646500
H	0.11125600	0.04382200	-2.20249500
H	0.50818500	1.75633400	-2.36547000
N	1.87284300	0.65222800	-1.23606700
C	1.62394700	1.35752800	-0.07095900
H	2.49791500	1.42908100	0.57992800
H	1.12549700	2.31484000	-0.24123800
C	1.61869500	0.45035500	-3.68279500
C	2.52421900	-0.62286600	-3.71837900
C	1.34577400	1.18023500	-4.84366000
C	3.15326300	-0.95222500	-4.92350400
C	1.96722100	0.83651700	-6.04863200
H	0.65030500	2.01475900	-4.80835600
C	2.87128700	-0.22973600	-6.08773200
H	3.86290000	-1.77507800	-4.95201000
H	1.75251700	1.40389400	-6.94928500
H	3.36134500	-0.49417100	-7.02019700

***N*-Methyltetrahydroisoquinoline/DABCO radical cation - *N*-CH_2 abstraction transition state**, solvent = MeCN

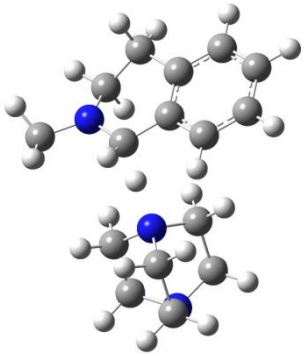

Charge = 1; Multiplicity = 2

44

-788.506403

C	1.23120200	-5.49480400	-2.89177400
C	2.56405500	-6.31620800	-2.98140300
H	1.22608000	-4.82794900	-2.02669600
H	0.35467800	-6.14476500	-2.83282300
H	3.21347500	-6.08409800	-2.13287100
H	2.35507500	-7.38936400	-2.96486600
C	2.25047700	-3.72055800	-4.20864800
H	2.11739000	-3.11593400	-5.10866600
H	2.21623500	-3.05884600	-3.34018000
C	3.57745300	-4.55501100	-4.25652100
H	4.13678100	-4.33199000	-5.16943800
H	4.21416400	-4.31200500	-3.40137000
C	2.42859100	-6.33961400	-5.37482100
H	2.97211100	-6.10639500	-6.29458800
H	2.23541000	-7.41579200	-5.35859300
C	1.08094300	-5.54069900	-5.31587300
H	0.94911100	-4.90894700	-6.19710400
H	0.21905400	-6.20669400	-5.23071500
N	1.10722900	-4.66427600	-4.11675000
N	3.28148500	-5.99663500	-4.22587100
H	-1.82822200	-3.90937400	-3.27407900
C	-1.28090200	-3.24296900	-3.94950400
C	-1.68856100	-0.73509200	-5.40916700
C	-1.51453100	-2.08650400	-6.10413400
H	-0.19214300	-3.88329100	-4.06265100
H	-2.75993500	-0.51014000	-5.32115200
H	-1.25299900	0.04702500	-6.03898900
H	-2.13730900	-2.14980200	-6.99819900
H	-0.46843000	-2.22688400	-6.41440800

C	-0.90493900	-1.93349900	-3.32770900
C	-1.05899300	-0.72407000	-4.03325700
C	-0.38523500	-1.91674600	-2.02186900
C	-0.68038300	0.47533100	-3.41688600
C	-0.01582400	-0.71569500	-1.41826200
H	-0.28127000	-2.84956400	-1.47370100
C	-0.15800000	0.48616900	-2.12144800
H	-0.80028600	1.40994400	-3.95898500
H	0.38005200	-0.71660800	-0.40730500
H	0.13364600	1.42600000	-1.66232500
N	-1.89652800	-3.17493000	-5.20347300
C	-2.56007800	-4.33909200	-5.76912100
H	-3.47244300	-4.02236300	-6.28331900
H	-1.91430900	-4.84635900	-6.49750100
H	-2.82060600	-5.03895300	-4.97417000

6,7-dimethoxy-*N*-Methyltetrahydroisoquinoline/DABCO radical cation - *N*-CH_3 abstraction transition state, solvent = MeCN

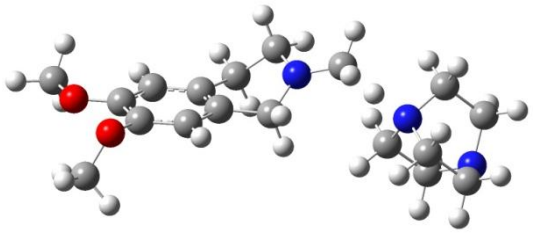

Charge = 1; Multiplicity = 2

52

-1017.497937

C	4.22386600	1.53044700	-0.21209400
C	5.52579800	1.60349900	0.65077400
H	4.38521100	1.88343800	-1.23343600
H	3.40408000	2.10400400	0.22679000
H	6.35035000	2.02146400	0.06684900
H	5.37205000	2.24353000	1.52388100
C	4.85955600	-0.71641900	-0.92541700
H	4.49259800	-1.74321600	-0.99422400
H	5.01220300	-0.33483900	-1.93779400
C	6.15133400	-0.60603900	-0.05191600
H	6.45908000	-1.59303200	0.30390400
H	6.97448300	-0.18530300	-0.63567000
C	4.82252400	-0.30693400	1.92545400
H	5.12921500	-1.29494400	2.27934500
H	4.66816500	0.33199400	2.79913800
C	3.50815200	-0.40959500	1.08395100

H	3.15887800	-1.44014700	0.98812200
H	2.70142800	0.19271700	1.50769300
N	3.79289300	0.10540300	-0.28540400
N	5.91429600	0.26070000	1.11595300
H	2.68387500	0.02218500	-1.03809500
C	0.03148900	-1.72824100	-1.05389500
C	-0.90493800	-1.88753900	0.14864300
C	-0.32305100	0.75709500	-0.61915500
H	-1.25556200	-2.92265000	0.18530000
H	-0.34022600	-1.70765800	1.07366100
H	-0.47385200	-2.07605600	-1.96549500
H	0.93509400	-2.33132800	-0.92566200
H	0.17173000	1.01196600	0.33183200
H	-0.25400300	1.64099200	-1.25918800
N	0.43448000	-0.32974400	-1.25877800
C	1.62486200	-0.04450700	-1.90557000
H	1.94495400	-0.83896600	-2.58319600
H	1.64558000	0.95018600	-2.35692300
C	-1.76441100	0.38232000	-0.36914800
C	-2.05948600	-0.92101100	0.04377900
C	-2.79810800	1.31783800	-0.49452800
C	-3.38444300	-1.28705100	0.31384400
C	-4.11499500	0.96786100	-0.20984000
H	-2.59622700	2.33497400	-0.81889500
C	-4.42065500	-0.35371200	0.19097200
H	-3.59869700	-2.30733200	0.61069700
O	-5.11417100	1.89810400	-0.40578800
O	-5.73838200	-0.62764600	0.41148500
C	-5.69806200	2.43589600	0.79577100
H	-6.45430900	3.15252300	0.47152200
H	-6.16731800	1.64719400	1.39066000
H	-4.93550800	2.95088500	1.39149300
C	-6.10240700	-1.95021600	0.81888100
H	-7.18558900	-1.93322500	0.93776100
H	-5.82881300	-2.68727200	0.05600800
H	-5.63227800	-2.21241700	1.77292300

6,7-dimethoxy-*N*-Methyltetrahydroisoquinoline/DABCO radical cation - *N*-CH_2 abstraction transition state, solvent = MeCN

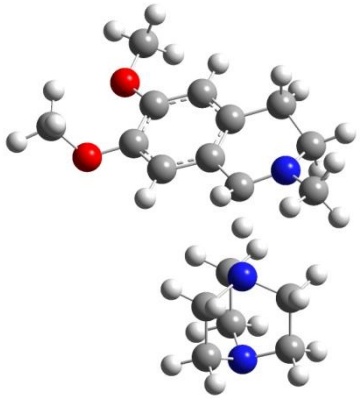

Charge = 1; Multiplicity = 2

52

-1017.504008

C	2.03869100	-3.95683700	-4.54060500
C	3.30089700	-4.79255500	-4.94678900
H	1.47038700	-3.62405100	-5.41233900
H	2.30603100	-3.07916000	-3.94828800
H	3.37530300	-4.87079400	-6.03499500
H	4.21207000	-4.31329100	-4.57837500
C	0.73258400	-6.00693300	-4.50083000
H	0.05398100	-6.59879500	-3.88235900
H	0.18855800	-5.65858500	-5.38162500
C	2.01520600	-6.81712100	-4.89555900
H	1.97219500	-7.82808400	-4.48090900
H	2.09570700	-6.90035400	-5.98290600
C	3.13779100	-6.06244100	-2.91603200
H	3.10270100	-7.07588200	-2.50671200
H	4.04371200	-5.57717600	-2.54255100
C	1.86585000	-5.25309200	-2.48814500
H	1.17708100	-5.85845900	-1.89365800
H	2.12859900	-4.36312200	-1.91191400
N	1.15218000	-4.81703000	-3.71593600
N	3.22288300	-6.15048600	-4.38331200
H	-1.12273300	-3.67652000	-1.87445100
C	-1.06894900	-3.34348500	-2.91676400
C	-2.46618300	-1.58342600	-4.79624000
C	-2.44912000	-3.10679400	-4.93298000
H	-0.07403400	-4.02968800	-3.31686500
H	-3.39252900	-1.27606000	-4.29231300
H	-2.48835500	-1.13792100	-5.79582700
H	-3.40427800	-3.47363200	-5.31381700
H	-1.66583700	-3.41942100	-5.64053000

C	-0.65096400	-1.91887700	-3.07705100
C	-1.27765900	-1.07593700	-4.00897700
C	0.39695700	-1.40882000	-2.28805100
C	-0.83910400	0.24747500	-4.15011400
C	0.82890900	-0.09737600	-2.42086500
H	0.88785900	-2.03275400	-1.54648200
C	0.21570700	0.74759500	-3.37883700
H	-1.33088000	0.88427900	-4.87663000
N	-2.20377800	-3.73681300	-3.63519700
C	-2.84019400	-5.01680900	-3.36417200
H	-3.92642600	-4.90437800	-3.43307100
H	-2.52776000	-5.77860500	-4.09057900
H	-2.57822600	-5.35342900	-2.36013600
O	0.71891000	2.00696500	-3.47967900
O	1.89725700	0.34061700	-1.66946900
C	0.13042800	2.90945600	-4.42350000
H	-0.92612700	3.08407600	-4.19412500
H	0.68591900	3.84140600	-4.32268400
H	0.23174000	2.53012600	-5.44586500
C	1.57045000	1.26039400	-0.60954400
H	2.51378000	1.50440100	-0.11879000
H	1.11407600	2.17096400	-1.00742800
H	0.89374000	0.78488200	0.10958200

Dextromethorphan/DABCO radical cation - *N*-CH_3 abstraction transition state, solvent = MeCN

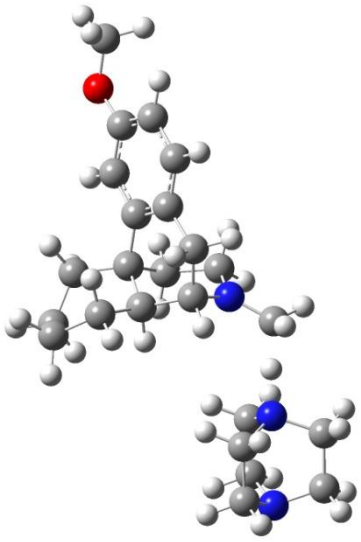

Charge = 1; Multiplicity = 2

65

-1175.645635

C	2.15117500	-0.62349900	-3.41866500
C	1.40622400	-1.63971300	-2.50828600

C	1.68187200	-1.31172100	-1.03529100
C	1.05093300	0.04707700	-0.62503100
C	1.35673700	1.11013200	-1.73456100
C	2.49401800	0.68814200	-2.67597200
C	1.25973000	-2.39111200	-0.03082300
C	-0.46340200	-0.08546600	-0.37736500
C	-1.06153500	-1.32967500	-0.08145300
C	-0.26072400	-2.61720600	-0.06480200
C	-2.43416200	-1.37233900	0.19064600
H	-2.89756700	-2.33018900	0.41595100
C	-3.23222300	-0.22632700	0.18994700
C	-2.63188400	1.00833200	-0.08658000
C	-1.26095700	1.06589700	-0.36301000
H	1.76173500	-3.33335900	-0.26774900
H	3.07488600	-1.07211200	-3.80227600
H	0.32782600	-1.59909500	-2.70124900
H	0.45880700	1.26409100	-2.34306500
H	3.42637600	0.57050100	-2.10979700
H	-0.48095200	-3.20297100	-0.96736100
H	-4.28995700	-0.30832700	0.40845100
H	-0.82980200	2.04108400	-0.56531900
H	-0.56008600	-3.24330800	0.78314700
H	1.72598700	-2.66310500	-2.73745400
H	1.52965700	-0.39633000	-4.29276800
H	2.68194600	1.48758800	-3.40159100
H	1.58618100	2.07726500	-1.27164300
H	2.76875300	-1.21065000	-0.92628200
O	-3.29617100	2.20715400	-0.10710000
C	-4.69772300	2.21208800	0.17378000
H	-5.01054200	3.25407000	0.10468800
H	-5.25138400	1.61525000	-0.55987900
H	-4.90102800	1.83578200	1.18278400
C	1.72921400	0.43017100	0.71783100
H	1.33417500	1.38043000	1.09343500
H	2.80370300	0.56690700	0.54449600
C	1.50767200	-0.63681700	1.79963100
H	0.47765100	-0.57438700	2.17693600
H	2.17532100	-0.46930400	2.64785100
N	1.73306200	-2.00592100	1.31545000
C	2.32908900	-2.94824100	2.13884800
H	3.69138300	-2.98819400	1.96053800
H	2.25300900	-2.71001200	3.20203900
H	2.04937300	-3.97685700	1.89999000
C	5.62025800	-1.73093300	1.90545300
C	7.17287800	-1.87841900	1.79207000
H	5.20022100	-1.15027100	1.08095100
H	5.31634400	-1.26633600	2.84649100
H	7.54626000	-1.33926400	0.91722400

H	7.66310800	-1.46601100	2.67814800
C	5.35757800	-3.74923900	0.55978100
H	4.87014400	-4.72708400	0.54363900
H	4.93653900	-3.13965800	-0.24315200
C	6.91367300	-3.86209000	0.46292300
H	7.21739000	-4.90807600	0.36729900
H	7.28393000	-3.32214400	-0.41280600
C	7.07910600	-4.03046000	2.85359500
H	7.38016500	-5.07729400	2.75848300
H	7.57372000	-3.61657300	3.73658500
C	5.52632800	-3.91568600	2.98959000
H	5.03390500	-4.89015400	2.94231800
H	5.22805600	-3.42231100	3.91779700
N	5.01899300	-3.09323300	1.85442300
N	7.55036900	-3.29704500	1.66540000

Dextromethorphan/DABCO radical cation - *N*-CH_2 abstraction transition state, solvent = MeCN

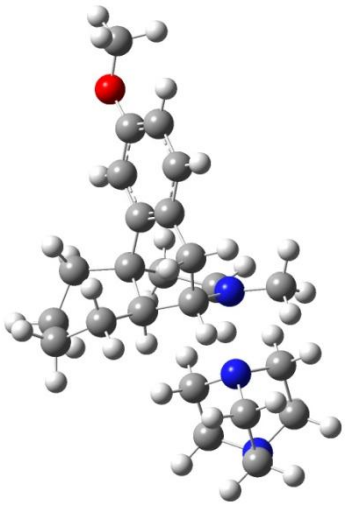

Charge = 1; Multiplicity = 2

65

-1175.641360

C	-0.23937200	2.36726300	3.13244200
C	0.43402300	2.19254600	1.74598800
C	0.84554900	0.72682100	1.55639700
C	-0.38983200	-0.20600600	1.43855400
C	-1.48641400	0.25202200	2.45691300
C	-0.90759800	1.06105400	3.62574000
C	1.77351700	0.44972500	0.37373500
C	-0.96321400	-0.22434300	0.00698600
C	-0.25685000	0.29159200	-1.10067300
C	1.11630100	0.90622800	-0.93779500
C	-0.84379300	0.22345600	-2.36983200

H	-0.29821400	0.61695500	-3.22446600
C	-2.10512300	-0.33748300	-2.58049400
C	-2.79788000	-0.86020000	-1.48105300
C	-2.22230700	-0.80062200	-0.20700500
H	2.72598100	0.98125400	0.50445800
H	0.50431100	2.69302900	3.86915200
H	-0.26367200	2.48671400	0.95336800
H	-2.22080500	0.87687700	1.93642900
H	-0.18084100	0.45129000	4.17703800
H	1.05727900	2.00179400	-0.91779900
H	-2.51955600	-0.36833200	-3.58079300
H	-2.78877000	-1.21619700	0.62055600
H	1.74824200	0.65952700	-1.79655300
H	1.30465600	2.85293400	1.65793600
H	-0.98790200	3.16567200	3.07123500
H	-1.70476000	1.29527000	4.34000900
H	-2.03391000	-0.62073100	2.83167300
H	1.39212600	0.43622600	2.46252300
O	-4.03506800	-1.44653200	-1.55106900
C	-4.67786900	-1.52607800	-2.82530800
H	-5.63407100	-2.01759300	-2.64513700
H	-4.85309300	-0.52841500	-3.24366200
H	-4.08801400	-2.12226000	-3.53075900
C	0.13690600	-1.61940000	1.79987800
H	-0.58278800	-2.38704500	1.49455000
H	0.20818400	-1.68644500	2.89232000
C	1.50329900	-1.94080200	1.16891700
H	1.55610300	-2.93667800	0.71778200
H	2.36442900	-2.18703700	2.21424900
N	2.07928200	-0.99523300	0.31777900
C	3.06755800	-1.42445600	-0.66527300
H	3.88912200	-0.70355900	-0.71165000
H	3.46952200	-2.39978900	-0.38887900
H	2.61862300	-1.50795100	-1.66260500
C	2.47221800	-2.54863400	4.53043200
C	3.47748500	-2.97401100	5.65004100
H	2.06788400	-1.54967600	4.70673600
H	1.64090700	-3.25104500	4.43634700
H	3.53300700	-2.20531800	6.42560800
H	3.15551300	-3.90667400	6.12105300
C	4.30447900	-1.52337200	3.28679100
H	4.80667500	-1.52165700	2.31685500
H	3.85786300	-0.53938500	3.44697700
C	5.27185000	-1.92529700	4.44786000
H	6.28624500	-2.07224800	4.06731300
H	5.30603800	-1.13970200	5.20747800
C	4.76997100	-4.24463000	4.07749400
H	5.77367400	-4.38474500	3.66706100

H	4.47354200	-5.17507200	4.56924900
C	3.75967900	-3.87857500	2.94295500
H	4.24108600	-3.84612100	1.96293400
H	2.92230300	-4.57866400	2.89353200
N	3.20098100	-2.52428500	3.22822200
N	4.82384900	-3.17425000	5.08827100

***N*,*N*-dimethyldecanamide/DABCO radical cation - *N*-CH_3 abstraction transition state**, solvent = MeCN

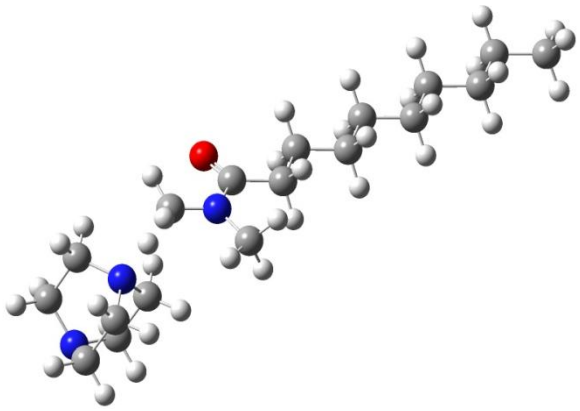

Charge = 1; Multiplicity = 2

59

-947.076962

N	-3.28250000	-2.46678500	2.49558600
C	-2.27889700	-1.48881200	2.36731900
C	-4.02725100	-2.52345600	3.67823800
H	-4.45782600	-3.50697900	3.86609900
H	-3.51308400	-2.07341800	4.52564300
H	-5.10072700	-1.77306500	3.59668100
C	-3.62225400	-3.37241000	1.38847900
H	-4.39802700	-4.05735800	1.72619600
H	-3.99752100	-2.81441300	0.52675000
H	-2.74876200	-3.95449000	1.08625600
C	-1.48816500	-1.48227600	1.07463200
H	-2.18687800	-1.36833400	0.23541700
H	-1.02905000	-2.47116000	0.94302600
C	-0.41419100	-0.39269500	1.02156300
H	0.26183900	-0.50752600	1.87712700
H	-0.88764800	0.59037800	1.13067300
C	0.39194600	-0.43814100	-0.28317300
H	-0.29064200	-0.33290000	-1.13871500
H	0.86261600	-1.42657600	-0.38499600
C	1.47333700	0.64729600	-0.36256600
H	2.14859100	0.54876700	0.49974900
H	1.00113500	1.63618100	-0.27164700

C	2.29651500	0.59697400	-1.65651400
H	2.77141600	-0.39110900	-1.74394300
H	1.62073300	0.68981200	-2.51925600
C	3.37513200	1.68507300	-1.74097800
H	4.04791400	1.59534600	-0.87548500
H	2.89948300	2.67326800	-1.65820200
C	4.20379600	1.63088300	-3.03123200
H	4.68213700	0.64376100	-3.11326300
H	3.53173400	1.71834400	-3.89769900
C	5.28056200	2.72067500	-3.11810400
H	5.95230300	2.63383900	-2.25264600
H	4.80280400	3.70701600	-3.03684800
C	6.10420900	2.65867800	-4.40986700
H	6.86437400	3.44720600	-4.43796500
H	6.61937100	1.69505200	-4.50383000
H	5.46476100	2.78020200	-5.29258800
O	-2.07475600	-0.70194600	3.28730300
C	-7.44543900	0.87210600	2.53878700
C	-6.12465300	0.01746800	2.52573300
H	-7.94711500	0.80205500	1.57068100
H	-7.21031500	1.92226300	2.72807500
H	-5.98120900	-0.49752900	1.57400800
H	-5.24268000	0.62502600	2.73662000
C	-8.69885200	-1.01234400	3.32397500
H	-9.39308900	-1.35620300	4.09449500
H	-9.20004900	-1.08182600	2.35551400
C	-7.40283800	-1.90257500	3.32727200
H	-7.43173800	-2.66269200	4.11019100
H	-7.23944100	-2.39256300	2.36563800
C	-6.38640200	-0.36152400	4.92371500
H	-6.43075800	-1.14676700	5.68107100
H	-5.49916500	0.24945000	5.10024200
C	-7.70174900	0.50038400	4.89241300
H	-8.39418300	0.15612400	5.66438800
H	-7.46761300	1.54997600	5.08549500
N	-8.35806800	0.39213000	3.58326200
N	-6.24541400	-1.00878600	3.59324400

A11.8. XYZ Co-ordinates for Intermediates, Reagents and Products Following HAT Reactions of *N*-methylmorpholine

_N_-Methylmorpholine DABCO _N_-CH_3 adduct, solvent = MeCN

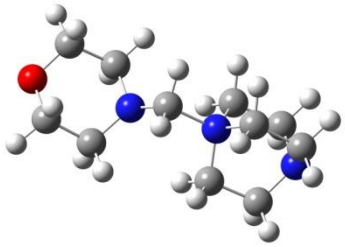

Charge = 1; Multiplicity = 1

37

-671.441848

C	2.17097500	-1.22463100	-0.40574900
C	3.58118000	-1.18227200	0.18635500
C	3.58142700	1.18206300	0.18643400
C	2.17124100	1.22475700	-0.40567200
H	3.53416200	-1.21455200	1.28607000
H	4.17345500	-2.03039600	-0.16703300
H	2.23930000	-1.32284200	-1.49715200
H	1.63361900	-2.09719800	-0.02640900
H	3.53436900	1.21428800	1.28615000
H	4.17385100	2.03011200	-0.16689300
H	1.63401800	2.09738000	-0.02623300
H	2.23959100	1.32300200	-1.49707000
O	4.27390100	-0.00014300	-0.22821300
N	1.42477200	0.00013200	-0.08473800
C	0.45714600	0.00019400	0.92491600
H	0.48955500	-0.89246500	1.55341000
H	0.48940600	0.89338000	1.55261200
C	-1.99062000	-0.00114200	1.55155500
C	-1.29486200	-1.22935400	-0.46477000
C	-1.29528000	1.23016800	-0.46328300
C	-3.45083000	0.00386400	1.00816800
H	-1.76952800	-0.89052900	2.14454900
H	-1.76550700	0.88355100	2.15001000
H	-0.58126900	-1.20324000	-1.28841000
H	-1.08551100	-2.09840300	0.16181200
C	-2.77442700	-1.19873900	-0.95307100
C	-2.77216400	1.19508000	-0.95922600

H	-0.57753000	1.20882300	-1.28344400
H	-1.09241400	2.09840400	0.16656000
H	-3.98827600	-0.87691000	1.36721800
H	-3.98089900	0.89107500	1.36231600
H	-2.81091800	-1.20103900	-2.04493000
H	-3.30605400	-2.08360000	-0.59507300
H	-2.80320400	1.18799400	-2.05123500
H	-3.30551900	2.08293400	-0.61136500
N	-1.03796500	-0.00002600	0.37732100
N	-3.46803800	0.00009900	-0.46168300

***N*-Methylmorpholine DABCO *N*-CH_2 adduct**, solvent = MeCN

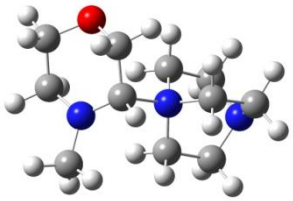

Charge = 1; Multiplicity = 1

37

-671.431040

C	-1.57880300	-1.24206600	-1.08966100
C	-3.17942500	-0.93597600	0.60835400
C	-2.59844400	0.41868600	0.99124400
H	-2.34050400	-1.13867900	-1.87642700
H	-0.83610100	-1.95863200	-1.43994100
H	-3.97008900	-0.81437000	-0.14599900
H	-3.59323900	-1.44457300	1.48120500
H	-3.41662900	1.11120300	1.20783800
H	-1.99491900	0.33581400	1.90572600
O	-2.15253300	-1.78796100	0.08637000
N	-1.81945400	0.97568400	-0.12206200
C	-1.88751700	2.42213700	-0.32138700
H	-1.43715800	2.98241200	0.50777600
H	-2.93503800	2.72966000	-0.41073000
H	-1.37347300	2.69597100	-1.24493100
C	-0.99542800	0.16182100	-0.88147000
H	-0.77117800	0.62201600	-1.84493800
C	1.07425600	1.37276900	0.16727100
C	1.50014100	-0.42849300	-1.42909700
C	0.73525900	-0.95223300	0.85144900
C	2.57808400	1.28123500	0.56620600
H	0.91367000	2.07692200	-0.64993200
H	0.44618300	1.65961800	1.00976500

H	1.11868800	-1.37311300	-1.81581600
H	1.42488200	0.32472800	-2.21580200
C	2.95782700	-0.57397800	-0.89630400
C	2.21498100	-0.94953900	1.34664700
H	0.42632700	-1.93382700	0.49576500
H	0.04425000	-0.63421000	1.63062700
H	3.18566600	1.89775600	-0.10098500
H	2.71655200	1.64979900	1.58558800
H	3.27262300	-1.61967100	-0.93370200
H	3.64169400	0.00723800	-1.51973200
H	2.61127200	-1.96801100	1.33962200
H	2.27113800	-0.57304100	2.37096500
N	0.60065000	0.01792100	-0.29955700
N	3.06024400	-0.10467800	0.49213200

***N*-Benzylmorpholine product from *N*-CH_3 functionalisation**, solvent = MeCN

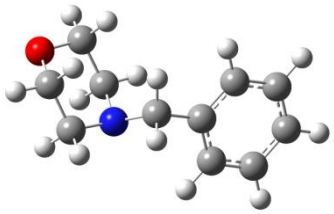

Charge = 0; Multiplicity = 1

28

-557.993026

C	1.27597800	-0.39245300	-1.14255300
C	2.30073300	-1.39318500	-0.60050700
C	3.32068300	0.30388300	0.69848700
C	2.31381000	1.33211100	0.17390000
H	1.91577500	-1.91401200	0.28956700
H	2.54634000	-2.14363400	-1.35724600
H	1.65358700	0.01680400	-2.08875700
H	0.33006300	-0.90037000	-1.35557400
H	2.97582300	-0.14233500	1.64427800
H	4.29595900	0.76763700	0.87205500
H	2.13385000	2.10361100	0.93052200
H	2.74811600	1.82309600	-0.70726400
O	3.53222600	-0.73491700	-0.26824300
N	1.02915200	0.73850700	-0.23057600
C	-1.29887700	0.18401900	0.45551800
C	-2.00146300	1.16453800	-0.26331300
C	-1.95925200	-1.00713200	0.78443400

C	-3.32993000	0.95864600	-0.64156500
H	-1.49912400	2.09122900	-0.52654800
C	-3.29154100	-1.21854400	0.40864200
H	-1.42821400	-1.77720000	1.33891100
C	-3.98063900	-0.23562700	-0.30612400
H	-3.85997500	1.72952100	-1.19421100
H	-3.78549500	-2.14974300	0.67163300
H	-5.01413000	-0.39579500	-0.59975200
C	0.13409700	0.42684200	0.89633500
H	0.15870900	1.29693000	1.56359600
H	0.46526100	-0.43454900	1.49923900

***N*-Methyl-1-phenylmorpholine product from *N*-CH_2 functionalisation**, solvent = MeCN

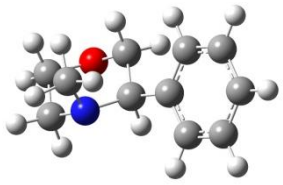

Charge = 0; Multiplicity = 1

28

-557.989904

C	1.24956700	-1.39271200	-0.24572100
C	3.31095500	-0.24754700	0.03047200
C	2.61543000	1.09280900	-0.21646800
H	1.20673900	-1.66256300	0.81930700
H	0.81078800	-2.20817900	-0.82715100
H	3.36132300	-0.47994500	1.10492800
H	4.32965700	-0.23763300	-0.36717400
H	3.11870700	1.88820800	0.34408600
H	2.69302600	1.33447100	-1.28471400
O	2.62124000	-1.30399900	-0.65323500
N	1.18728800	1.08233000	0.14363100
C	0.95609000	1.18033300	1.58933700
H	1.44969200	2.08515100	1.95698900
H	1.33048500	0.32983800	2.18178100
H	-0.11459700	1.27690800	1.78362800
C	0.52488500	-0.06535300	-0.53165500
H	0.66969700	0.12204700	-1.60499300
C	-0.97623700	-0.09234200	-0.28532500
C	-1.59622100	-1.00525700	0.58044100
C	-1.78382700	0.83765500	-0.96096200

C	-2.98372400	-0.98853100	0.76667700
H	-1.00626900	-1.73773200	1.12201800
C	-3.16744400	0.86175000	-0.77486500
H	-1.31906300	1.54782100	-1.64015100
C	-3.77379000	-0.05473200	0.09208400
H	-3.44297900	-1.70565700	1.44114800
H	-3.77199600	1.58878500	-1.30978400
H	-4.85025000	-0.04228200	0.23646000

Phenylmagnesium chloride, solvent = MeCN

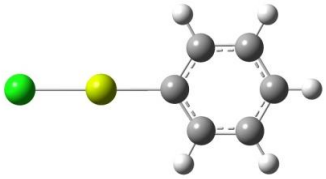

Charge = 0; Multiplicity = 1

13

-892.013525

C	3.42939200	-0.00032600	-0.00028400
C	2.72139400	1.20650400	-0.00016900
C	1.31896400	1.19635500	0.00020600
C	0.56372700	0.00035400	0.00044100
C	1.31830900	-1.19612700	0.00011900
C	2.72080100	-1.20683900	-0.00013300
H	4.51651600	-0.00059400	-0.00038700
H	3.26010500	2.15196100	-0.00034600
H	0.80662500	2.15858400	0.00048900
H	0.80560300	-2.15813800	0.00037500
H	3.25918600	-2.15248200	-0.00005900
Mg	-1.55880200	0.00015800	0.00016300
Cl	-3.90458400	-0.00004500	-0.00018300

Magnesium chloride cation, solvent = MeCN

Charge = 1; Multiplicity = 1

2

-660.297657

Mg	0.00000000	0.00000000	-1.34791000
Cl	0.00000000	0.00000000	0.95146600

A12. COMPUTATIONAL INVESTIGATIONS FOR VOLUME 2, CHAPTER 2.3.

A12.1. COMPUTATIONAL METHODS

All calculations were performed using Density Functional Theory (DFT)[49,50] using the Gaussian09 software package.[51] Unless otherwise stated, all minima (reactants, intermediates, products) and maxima (transition states) were optimised using the UB3LYP functional with a 6-31+G(d,p) basis set on all atoms,[52] paralleling a study on hydrogen atom abstraction from tertiary amines using the cumyloxyl radical.[53] Calculations of bromoarenes and bromoarene radical anions used a higher level of theory; the M062X functional[56,57] with a 6-311++G(d,p) basis set[58–62] on all atoms except bromine. Bromine was modelled using the MWB28 relativistic pseudo-potential and associated basis set.[63] Solvation was modelled implicitly using the Conductor-like Polarisable Continuum Model (C-PCM)[54,55] for benzene. Frequency calculations were performed on all optimised structures in order to characterise minima (zero imaginary frequencies) and maxima (single imaginary frequency). All profiles are plotted using the Gibbs free energy values. GaussView 5.0.9 was used for the visualisation of structures.

A12.2. INVESTIGATION OF THE DISSOCIATION OF BROMOARENE RADICAL ANIONS

Using the minimised structures of 2,4,6-tri-*tert*-butylbromobenzene (**149**) and 2,4,6-triisopropylbromobenzene (**147**) as inputs, computational optimisation of the corresponding radical anions (**149**$^{\bullet-}$ and **147**$^{\bullet-}$) was attempted. However, dissociation to the aryl radical and halide resulted in both cases (Figures A45 and A46). Therefore, the energy of the first computed geometry read from the optimisation was defined as zero. The difference between this and the energy of the final geometry (once the calculation had converged) was used to represent ΔG in Figure A47.

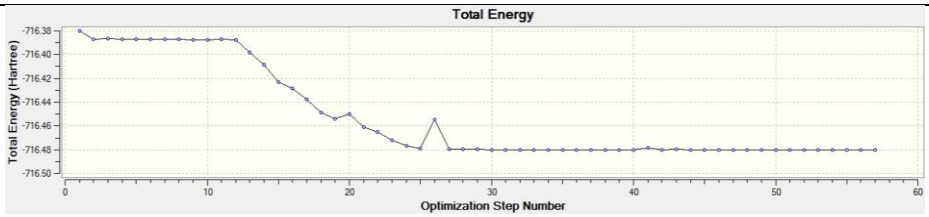

***Figure A45**: Total energies of intermediate geometries upon optimisation of 2,4,6-tri-tert-butylbromobenzene radical anion.*

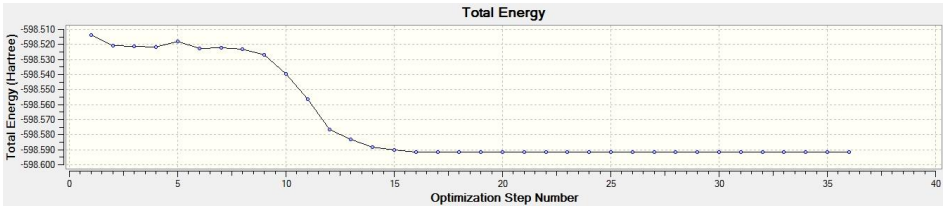

***Figure A46**: Total energies of intermediate geometries upon optimisation of 2,4,6-triisopropylbromobenzene radical anion.*

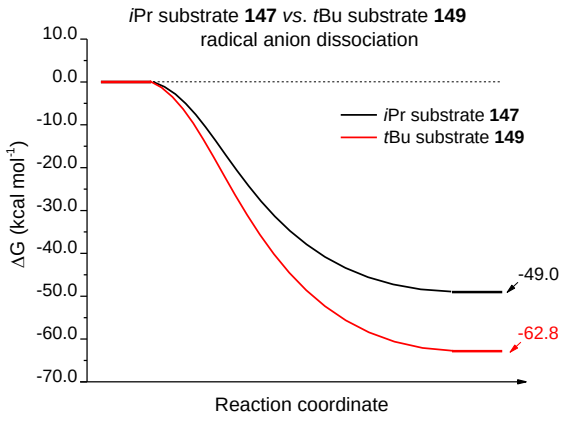

***Figure A47**: Reaction free energy (ΔG) profile for dissociation of radical anions derived from **147** and **149**; density functional theory (DFT) calculations used the M062X functional with a 6-311++G(d,p) basis set on all atoms except bromine. Bromine was modelled using the MWB28 relativistic pseudo potential and associated basis set.*

A12.3. XYZ-Co-ordinates Relating to the Investigation of the Dissociation of Bromoarene Radical Anions

2,4,6-Tri-*tert*-butylbromobenzene, solvent = benzene

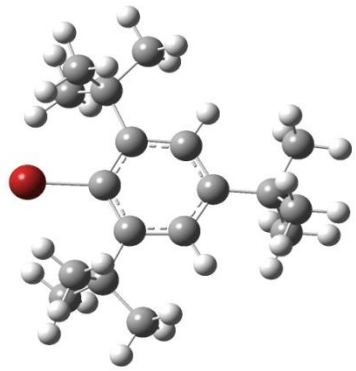

Charge = 0; Multiplicity = 1

48

-716.001987

C	-0.76413800	-0.00909300	0.00000200
C	-0.13599200	1.25341600	0.00000200
C	1.27054000	1.24457700	0.00000200
C	2.02357000	0.07792000	0.00000100
C	-0.05689900	-1.23571400	0.00000100
H	1.78950800	2.18412200	0.00000200
C	3.55758800	0.07941600	0.00000000
C	-0.84839600	2.63430400	0.00000100
C	-0.68428100	-2.65644700	0.00000000
C	4.06892800	-0.65135600	1.25888400
H	5.16044400	-0.65111200	1.26957400
H	3.71311400	-0.15193100	2.16114200
H	3.73007500	-1.68733200	1.28446500
C	4.06892900	-0.65139200	-1.25886300
H	3.71310900	-0.15199600	-2.16113500
H	5.16044500	-0.65114200	-1.26955500
H	3.73008200	-1.68737100	-1.28441100
C	-1.51570700	-2.90104700	-1.28057500
H	-1.87513200	-3.93186800	-1.27762600
H	-2.37405500	-2.24528400	-1.36646500
H	-0.88517000	-2.76377700	-2.16091000
C	-1.51570700	-2.90104700	1.28057500
H	-1.87512500	-3.93187100	1.27763100
H	-0.88517400	-2.76376800	2.16091100
H	-2.37406100	-2.24529100	1.36646100
C	-1.69256900	2.83026800	1.28026500
H	-2.51258700	2.12711400	1.36630300

H	-1.05556100	2.72935400	2.16084800
H	-2.10980400	3.83906200	1.27727100
C	0.16952500	3.79837700	-0.00000200
H	0.80134400	3.78934800	-0.88877800
H	-0.38924600	4.73410800	-0.00000400
H	0.80134600	3.78935300	0.88877200
C	0.40027400	-3.75746800	0.00000000
H	1.03052800	-3.71236200	-0.88894400
H	1.03053100	-3.71236100	0.88894200
H	-0.10287300	-4.72433300	0.00000100
C	4.13763200	1.50227300	-0.00002100
H	3.83097800	2.05936800	0.88680600
H	5.22668700	1.44297500	-0.00002800
H	3.83096500	2.05934500	-0.88685900
C	-1.69256800	2.83025900	-1.28026700
H	-2.10979000	3.83905800	-1.27728900
H	-1.05556000	2.72932300	-2.16084800
H	-2.51259300	2.12711400	-1.36629400
C	1.33962100	-1.13640800	0.00000000
H	1.92349000	-2.04009500	-0.00000200
Br	-2.74680000	-0.07150800	0.00000000

2,4,6-Tri-*tert*-butylbromobenzene radical anion (undissociated), solvent = benzene

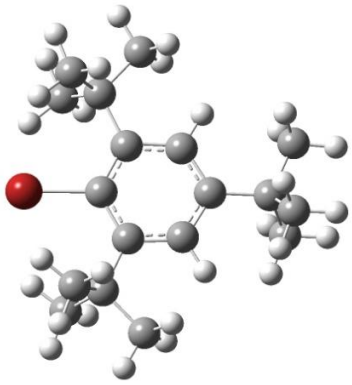

Charge = -1; Multiplicity = 2

48

-716.380200 (uncorrected, read from optimisation curve)

C	-0.76413800	-0.00909300	0.00000200
C	-0.13599200	1.25341600	0.00000200
C	1.27054000	1.24457700	0.00000200
C	2.02357000	0.07792000	0.00000100
C	-0.05689900	-1.23571400	0.00000100
H	1.78950800	2.18412200	0.00000200
C	3.55758800	0.07941600	0.00000000
C	-0.84839600	2.63430400	0.00000100
C	-0.68428100	-2.65644700	0.00000000

C	4.06892800	-0.65135600	1.25888400
H	5.16044400	-0.65111200	1.26957400
H	3.71311400	-0.15193100	2.16114200
H	3.73007500	-1.68733200	1.28446500
C	4.06892900	-0.65139200	-1.25886300
H	3.71310900	-0.15199600	-2.16113500
H	5.16044500	-0.65114200	-1.26955500
H	3.73008200	-1.68737100	-1.28441100
C	-1.51570700	-2.90104700	-1.28057500
H	-1.87513200	-3.93186800	-1.27762600
H	-2.37405500	-2.24528400	-1.36646500
H	-0.88517000	-2.76377700	-2.16091000
C	-1.51570700	-2.90104700	1.28057500
H	-1.87512500	-3.93187100	1.27763100
H	-0.88517400	-2.76376800	2.16091100
H	-2.37406100	-2.24529100	1.36646100
C	-1.69256900	2.83026800	1.28026500
H	-2.51258700	2.12711400	1.36630300
H	-1.05556100	2.72935400	2.16084800
H	-2.10980400	3.83906200	1.27727100
C	0.16952500	3.79837700	-0.00000200
H	0.80134400	3.78934800	-0.88877800
H	-0.38924600	4.73410800	-0.00000400
H	0.80134600	3.78935300	0.88877200
C	0.40027400	-3.75746800	0.00000000
H	1.03052800	-3.71236200	-0.88894400
H	1.03053100	-3.71236100	0.88894200
H	-0.10287300	-4.72433300	0.00000100
C	4.13763200	1.50227300	-0.00002100
H	3.83097800	2.05936800	0.88680600
H	5.22668700	1.44297500	-0.00002800
H	3.83096500	2.05934500	-0.88685900
C	-1.69256800	2.83025900	-1.28026700
H	-2.10979000	3.83905800	-1.27728900
H	-1.05556000	2.72932300	-2.16084800
H	-2.51259300	2.12711400	-1.36629400
C	1.33962100	-1.13640800	0.00000000
H	1.92349000	-2.04009500	-0.00000200
Br	-2.74680000	-0.07150800	0.00000000

2,4,6-Tri-*tert*-butylbromobenzene radical anion (dissociated), solvent = benzene

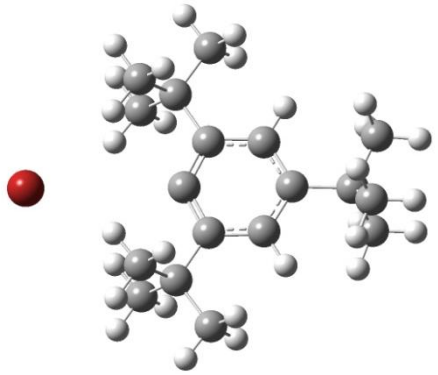

Charge = -1; Multiplicity = 2

48

-716.480302 (uncorrected, read from optimisation curve)

C	-0.21703700	0.01185700	0.00058600
C	0.38998400	1.25194600	0.00040300
C	1.79834000	1.24045000	-0.00003000
C	2.52024400	0.04085700	-0.00017000
C	0.41646200	-1.22039100	0.00044100
H	2.32616900	2.18121000	-0.00019100
C	4.05696800	0.01029800	-0.00061100
C	-0.45536900	2.52693300	0.00065700
C	-0.40490600	-2.51024000	0.00066400
C	4.55794800	-0.72883300	1.25748000
H	5.64999900	-0.75315500	1.26710900
H	4.21311400	-0.21955900	2.15868100
H	4.19347400	-1.75572600	1.28570000
C	4.55723600	-0.72938900	-1.25863900
H	4.21179300	-0.22060200	-2.15988600
H	5.64928500	-0.75358200	-1.26893300
H	4.19288800	-1.75634600	-1.28615600
C	-1.30224100	-2.52369400	-1.25320300
H	-1.90703600	-3.43330800	-1.26645800
H	-1.97677200	-1.66683700	-1.24300500
H	-0.69461400	-2.49323400	-2.16020300
C	-1.30214800	-2.52338900	1.25459900
H	-1.90692500	-3.43301100	1.26810600
H	-0.69447800	-2.49270600	2.16156100
H	-1.97669500	-1.66654500	1.24424900
C	-1.35296200	2.52337600	1.25440100
H	-2.01080700	1.65365500	1.24378300
H	-0.74491300	2.50390900	2.16142300
H	-1.97488600	3.42142400	1.26799500
C	0.41143300	3.79332800	0.00111200
H	1.04624900	3.84223500	-0.88616500

H	-0.23830500	4.66987700	0.00146000
H	1.04631700	3.84154100	0.88837800
C	0.48581600	-3.75980100	0.00078700
H	1.12125700	-3.79632100	-0.88666800
H	1.12163300	-3.79585400	0.88799400
H	-0.14695800	-4.64868700	0.00113800
C	4.66952700	1.41981800	-0.00110900
H	4.37288900	1.98318600	0.88499500
H	5.75772800	1.33673600	-0.00162400
H	4.37200400	1.98291100	-0.88709500
C	-1.35273400	2.52414300	-1.25324800
H	-1.97442900	3.42235600	-1.26654200
H	-0.74454600	2.50493800	-2.16018400
H	-2.01080800	1.65459900	-1.24313800
C	1.81794600	-1.17654200	0.00005500
H	2.37351700	-2.10417500	-0.00005300
Br	-4.24037700	-0.02952300	-0.00089500

2,4,6-Triisopropylbromobenzene, solvent = benzene

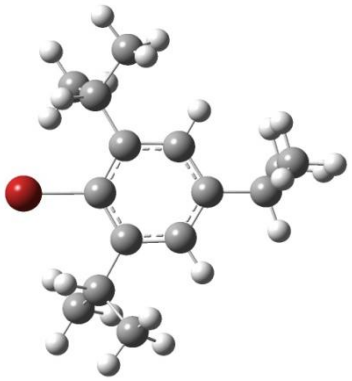

Charge = 0; Multiplicity = 1

39

-598.220402

C	-1.57063600	0.77324200	-0.05379100
C	-0.22088200	1.13240200	-0.12985400
C	0.71234500	0.08644000	-0.15028700
C	0.35737900	-1.26631300	-0.12139400
C	-1.98286300	-0.56023200	-0.00640900
H	-2.31602800	1.55654300	-0.03476900
C	1.38335100	-2.38988800	-0.11785400
H	2.22654100	-2.06774800	-0.73009200
C	0.18770800	2.59849500	-0.13903900
H	1.08054700	2.68694600	-0.75950900
C	-3.45749500	-0.91297700	0.08086800
H	-3.52850200	-2.00354900	0.12058700
C	1.89401800	-2.62677200	1.31569000

H	2.66690700	-3.39650700	1.31998400
H	2.31055600	-1.71601000	1.74378900
H	1.07103800	-2.96084600	1.95062500
C	0.85723700	-3.70080400	-0.71573200
H	0.40667500	-3.54107500	-1.69552200
H	1.68351700	-4.40295200	-0.82767900
H	0.11628200	-4.16949300	-0.06647300
C	-4.22216400	-0.43272200	-1.16288700
H	-5.26785200	-0.73850100	-1.10778800
H	-4.19211100	0.65613200	-1.23580300
H	-3.78742000	-0.84593000	-2.07287200
C	-4.09276200	-0.34983500	1.36213200
H	-5.13272800	-0.66884300	1.44217400
H	-3.55589700	-0.69104600	2.24720900
H	-4.07489000	0.74153400	1.35349600
C	-0.87816300	3.52669100	-0.73435900
H	-1.22016900	3.17129800	-1.70654000
H	-1.74311100	3.61863000	-0.07563000
H	-0.45722000	4.52425100	-0.86138400
C	0.54861300	3.05050400	1.28815600
H	1.33237300	2.42667600	1.71567700
H	0.89462000	4.08497300	1.28160600
H	-0.33247900	2.98565600	1.92978700
C	-1.01142300	-1.55791700	-0.04631300
H	-1.32714600	-2.59190600	-0.02137400
Br	2.63202600	0.54628200	-0.22637300

2,4,6-Triisopropylbromobenzene radical anion (undissociated), solvent = benzene

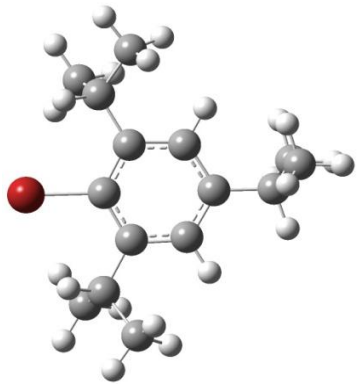

Charge = -1; Multiplicity = 2

39

-598.513597 (uncorrected, read from optimisation curve)

C	-1.57063600	0.77324200	-0.05379100
C	-0.22088200	1.13240200	-0.12985400
C	0.71234500	0.08644000	-0.15028700

C	0.35737900	-1.26631300	-0.12139400
C	-1.98286300	-0.56023200	-0.00640900
H	-2.31602800	1.55654200	-0.03476900
C	1.38335200	-2.38988800	-0.11785400
H	2.22654200	-2.06774700	-0.73009200
C	0.18770700	2.59849500	-0.13903900
H	1.08054600	2.68694600	-0.75950900
C	-3.45749500	-0.91297800	0.08086800
H	-3.52850100	-2.00355000	0.12058700
C	1.89401900	-2.62677100	1.31569000
H	2.66690800	-3.39650600	1.31998400
H	2.31055700	-1.71600900	1.74378900
H	1.07103900	-2.96084600	1.95062500
C	0.85723800	-3.70080400	-0.71573200
H	0.40667600	-3.54107500	-1.69552200
H	1.68351800	-4.40295100	-0.82767900
H	0.11628300	-4.16949300	-0.06647300
C	-4.22216400	-0.43272300	-1.16288700
H	-5.26785200	-0.73850200	-1.10778800
H	-4.19211100	0.65613100	-1.23580300
H	-3.78742000	-0.84593100	-2.07287200
C	-4.09276200	-0.34983600	1.36213200
H	-5.13272800	-0.66884400	1.44217400
H	-3.55589700	-0.69104700	2.24720900
H	-4.07489000	0.74153300	1.35349600
C	-0.87816400	3.52669100	-0.73435900
H	-1.22017000	3.17129800	-1.70654000
H	-1.74311200	3.61863000	-0.07563000
H	-0.45722100	4.52425100	-0.86138400
C	0.54861200	3.05050400	1.28815600
H	1.33237200	2.42667600	1.71567700
H	0.89461900	4.08497300	1.28160600
H	-0.33248000	2.98565600	1.92978700
C	-1.01142300	-1.55791700	-0.04631300
H	-1.32714500	-2.59190600	-0.02137400
Br	2.63202600	0.54628300	-0.22637300

2,4,6-Triisopropylbromobenzene radical anion (dissociated), solvent = benzene

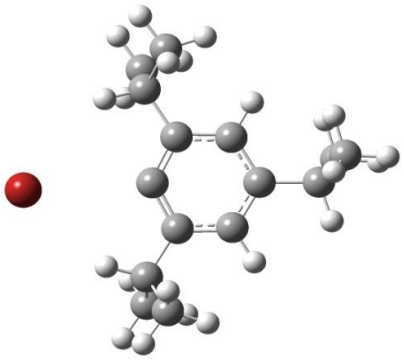

Charge = -1; Multiplicity = 2

39

-598.591737 (uncorrected, read from optimisation curve)

C	-1.80162100	0.92244600	-0.05772800
C	-0.43693100	1.12221100	-0.31583900
C	0.33817300	-0.01980300	-0.42301000
C	-0.10940300	-1.31912900	-0.28115200
C	-2.33289500	-0.36825700	0.08618300
H	-2.45636600	1.78230200	0.03638700
C	0.84663100	-2.49599300	-0.35669800
H	1.80327800	-2.09683200	-0.69869200
C	0.18055900	2.50513400	-0.42592500
H	1.19687800	2.36522900	-0.79981200
C	-3.81640900	-0.56422300	0.36001300
H	-3.98919400	-1.64075400	0.45147800
C	1.06270000	-3.09821800	1.04076600
H	1.78240100	-3.91757600	0.99553900
H	1.44571300	-2.34097000	1.72424000
H	0.12191800	-3.48601000	1.44020000
C	0.36745400	-3.56490200	-1.34892100
H	0.21173400	-3.13570800	-2.33916500
H	1.10827700	-4.36211600	-1.43080900
H	-0.57254000	-4.01269600	-1.01845600
C	-4.67583000	-0.04637800	-0.80448500
H	-5.73385100	-0.23987600	-0.61783600
H	-4.54344700	1.03044400	-0.92718500
H	-4.39243600	-0.52983300	-1.73951600
C	-4.24125300	0.09436300	1.68193900
H	-5.29292000	-0.10972100	1.89197900
H	-3.64089200	-0.27914400	2.51145300
H	-4.11011500	1.17686500	1.63052100
C	-0.58858200	3.40731100	-1.40088000
H	-0.67043000	2.94143800	-2.38331100

H	-1.59735900	3.61016700	-1.03426300
H	-0.07575100	4.36393900	-1.51321000
C	0.27892700	3.15433500	0.96414600
H	0.87363200	2.53111500	1.63143800
H	0.75177900	4.13572000	0.89461000
H	-0.71664300	3.27944900	1.39772300
C	-1.48291700	-1.47462500	-0.02390000
H	-1.89708100	-2.46989400	0.09893000
Br	3.68176500	0.33939500	0.21802000

A12.4. INVESTIGATION OF INTRAMOLECULAR HAT FOR 2,4,6-TRIALKYL-SUBSTITUTED BENZENE RADICALS

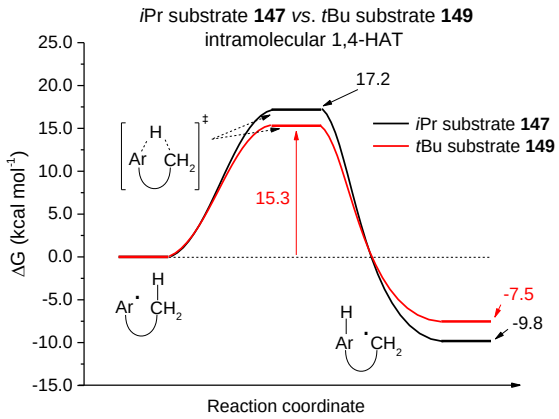

***Figure A48**: Reaction free energy (ΔG) profile for intramolecular 1,4-HAT comparing aryl radicals derived from **147** and **149**; DFT calculations used an unrestricted B3LYP functional with a 6-31+G(d,p) basis set on all atoms.*

2,4,6-Tri-*tert*-butylbenzene aryl radical, solvent = benzene

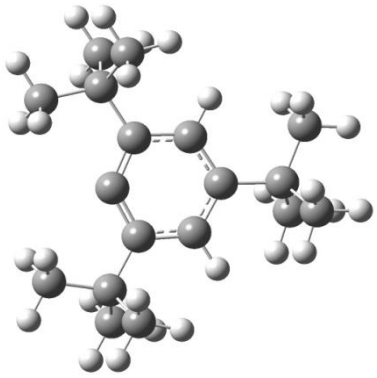

Charge = 0; Multiplicity = 2

-703.017459

C	-0.40681900	1.33829000	-0.00001400
C	0.95928800	1.02137300	0.00005600
C	1.32866000	-0.33653600	0.00012900
C	0.37971100	-1.37600200	0.00017300
C	-0.93694900	-0.95174400	0.00009600
C	-1.41004100	0.34384500	0.00002500
H	-0.71692100	2.37731600	-0.00012200
H	2.38332300	-0.59845100	0.00016100
C	0.78888500	-2.85827600	0.00001800
C	2.05852200	2.10538000	0.00000900
C	-2.90564200	0.70044300	-0.00001100
C	1.62819300	-3.16825100	1.26155100
H	1.91652200	-4.22597300	1.27335100
H	2.54520400	-2.57142300	1.29539200
H	1.05670700	-2.96110100	2.17287400
C	-0.45927800	-3.76175300	0.00037300
H	-1.07879100	-3.58406200	-0.88493400
H	-0.16017200	-4.81586300	0.00013600
H	-1.07814500	-3.58427100	0.88617600
C	-3.24442300	1.52809400	-1.26200100
H	-4.31168700	1.77869700	-1.27444600
H	-2.68036400	2.46566100	-1.29556700
H	-3.01646000	0.96413200	-2.17303500
C	-3.24437000	1.52857400	1.26171600
H	-4.31163000	1.77918800	1.27405300
H	-3.01638700	0.96490900	2.17291800
H	-2.68029900	2.46614400	1.29491500
C	1.47948300	3.53411300	-0.00052000
H	0.86813300	3.72717800	-0.88858100
H	0.86805300	3.72782700	0.88734200
H	2.29979500	4.25975600	-0.00074100
C	2.94124300	1.94916000	1.26270200
H	3.42734500	0.96954700	1.30169500
H	3.72751700	2.71308200	1.27278300
H	2.34368600	2.06427100	2.17380200
C	-3.76537800	-0.57820800	0.00028600
H	-3.56678900	-1.19112900	-0.88519900
H	-3.56669300	-1.19076200	0.88600300
H	-4.82928500	-0.31585600	0.00028900
C	1.62731600	-3.16798900	-1.26221300
H	2.54407800	-2.57080500	-1.29668600
H	1.91598100	-4.22561900	-1.27424800
H	1.05503300	-2.96097200	-2.17305400
C	2.94183900	1.94850800	-1.26219300
H	3.72809600	2.71244700	-1.27229400
H	3.42800500	0.96889400	-1.30043100

H	2.34471100	2.06311200	-2.17363100

2,4,6-Tri-*tert*-butylbenzene intramolecular HAT transition state, solvent = benzene

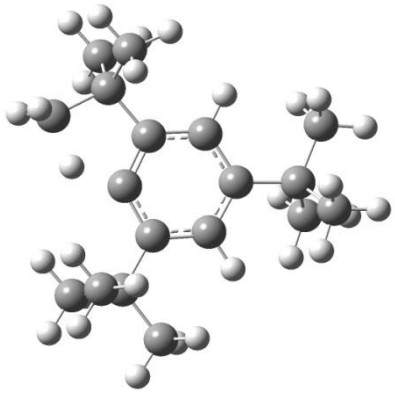

Charge = 0; Multiplicity = 2

47

-702.993063

C	-0.84149400	1.07812800	0.00007600
C	0.48246300	1.48173100	0.00012000
C	1.48633500	0.50298400	0.00009800
C	1.14017700	-0.85575200	0.00006000
C	-1.26468100	-0.25165100	0.00001400
H	-1.39780500	2.35360000	0.00019500
H	2.52814700	0.80571000	0.00010900
C	2.19909000	-1.97843500	0.00001200
C	0.65531200	3.00826000	0.00008500
C	-2.75994200	-0.61211500	-0.00001600
C	2.02458900	-2.85855800	1.26230600
H	2.77303000	-3.65967900	1.27279700
H	2.15079100	-2.26358900	2.17365100
H	1.03567600	-3.32539900	1.30047200
C	2.02493900	-2.85805100	-1.26268300
H	2.15145600	-2.26272400	-2.17375100
H	2.77333500	-3.65921400	-1.27326500
H	1.03600300	-3.32480600	-1.30133100
C	-3.42350100	-0.00683400	-1.26039600
H	-4.49714300	-0.22859100	-1.26939200
H	-3.30084900	1.08018000	-1.28971800
H	-2.98211000	-0.42136600	-2.17356600
C	-3.42342400	-0.00731600	1.26063800
H	-4.49708100	-0.22901000	1.26957800
H	-2.98203000	-0.42225800	2.17362000
H	-3.30070300	1.07967800	1.29041000
C	1.41255100	3.47684700	1.26142200
H	2.42380100	3.05591700	1.29335600

H	1.50214400	4.56930700	1.27371800
H	0.88900500	3.16597900	2.17188800
C	-3.00382000	-2.13257700	-0.00030200
H	-2.57984500	-2.61410700	-0.88822000
H	-2.57994300	-2.61443100	0.88748800
H	-4.08108800	-2.33068500	-0.00039400
C	3.63917600	-1.42817700	0.00033500
H	3.84378400	-0.82035200	0.88823500
H	4.34884900	-2.26236400	0.00035300
H	3.84410600	-0.82013100	-0.88734000
C	1.41144000	3.47677700	-1.26195000
H	1.50113200	4.56923000	-1.27432400
H	2.42261000	3.05573200	-1.29482600
H	0.88701200	3.16596600	-2.17192900
C	-0.22989600	-1.20239400	0.00001500
H	-0.49349500	-2.25428000	-0.00003000
C	-0.79733100	3.53890400	0.00066000
H	-1.12371800	4.05143500	0.90762600
H	-1.12401500	4.05262800	-0.90552100

2,4,6-Tri-*tert*-butylbenzene alkyl radical, solvent = benzene

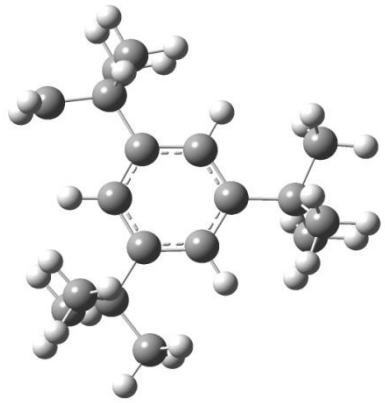

Charge = 0; Multiplicity = 2

47

-703.029453

C	-1.01746200	0.97204100	0.00000600
C	0.30753900	1.40789900	-0.00002300
C	1.32907400	0.43894300	-0.00004700
C	1.04571300	-0.92893300	-0.00003300
C	-1.35347100	-0.39620700	0.00002900
H	-1.80733600	1.71598200	-0.00001600
H	2.36078000	0.76914600	-0.00007800
C	2.14864000	-2.00760600	-0.00000600
C	0.67204100	2.91693100	-0.00000200
C	-2.83849200	-0.81331100	0.00000000
C	2.00697000	-2.89341600	1.26240900

H	2.78318400	-3.66761300	1.27118900
H	2.11384000	-2.29456500	2.17369300
H	1.03507800	-3.39457400	1.30193300
C	2.00707700	-2.89347200	-1.26239100
H	2.11396400	-2.29465800	-2.17369700
H	2.78334100	-3.66761800	-1.27109100
H	1.03522900	-3.39470800	-1.30196200
C	-3.53446600	-0.24732100	-1.26242300
H	-4.59350500	-0.53098700	-1.27117800
H	-3.48116300	0.84490100	-1.30174300
H	-3.06966500	-0.63965000	-2.17373700
C	-3.53467800	-0.24705000	1.26217700
H	-4.59370400	-0.53076200	1.27082600
H	-3.07000900	-0.63914200	2.17366100
H	-3.48145100	0.84518300	1.30126600
C	1.50732600	3.24253000	1.26642700
H	2.42696300	2.65102100	1.30426300
H	1.78522900	4.30221900	1.27437400
H	0.93287900	3.03181100	2.17490500
C	-3.02288600	-2.34331900	0.00016700
H	-2.58086700	-2.80843200	-0.88758800
H	-2.58082100	-2.80822600	0.88800700
H	-4.09163000	-2.58299500	0.00020900
C	3.56659400	-1.40336100	0.00002100
H	3.74871700	-0.78837100	0.88791100
H	4.30733500	-2.21016500	-0.00009800
H	3.74863900	-0.78815700	-0.88773800
C	1.50678000	3.24278300	-1.26668300
H	1.78461800	4.30249000	-1.27456400
H	2.42645500	2.65136400	-1.30501200
H	0.93199400	3.03218500	-2.17497700
C	-0.30802900	-1.32268500	0.00001600
H	-0.53835500	-2.38096500	0.00006300
C	-0.54922900	3.79517500	0.00038000
H	-1.03201300	4.07829800	0.93141300
H	-1.03196700	4.07926200	-0.93038000

2,4,6-Triisopropylbenzene aryl radical, solvent = benzene

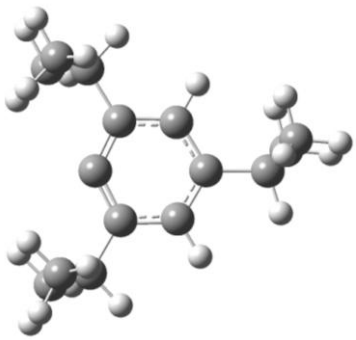

Charge = 0; Multiplicity = 2

38

-585.154768

C	1.12114300	0.84488200	0.00001000
C	1.49194800	-0.50984800	0.00000100
C	0.48459700	-1.48494100	-0.00001500
C	-0.88534600	-1.14660900	-0.00007300
C	-1.14521300	0.20950800	-0.00008100
C	-0.22926900	1.24602400	-0.00003300
H	1.88804100	1.61741600	0.00006100
H	0.76167400	-2.53840700	0.00000600
C	-1.97324400	-2.21134200	-0.00005400
H	-1.46743600	-3.18565400	-0.00028100
C	2.95945000	-0.92591500	0.00003000
H	2.97842300	-2.02356100	0.00018300
C	-0.62923000	2.71498900	-0.00002200
H	0.29957300	3.30015000	-0.00011900
C	-2.84182800	-2.12981400	1.26937600
H	-3.58721300	-2.93314800	1.27794500
H	-2.23240000	-2.21941000	2.17476200
H	-3.37339400	-1.17241300	1.31418100
C	-2.84227900	-2.12946600	-1.26915000
H	-2.23317200	-2.21881700	-2.17477600
H	-3.58766200	-2.93280000	-1.27766100
H	-3.37387100	-1.17205800	-1.31351300
C	-1.42017700	3.08354100	1.26932700
H	-1.65800800	4.15333100	1.27787500
H	-2.36242600	2.52563100	1.31402700
H	-0.84903500	2.85319700	2.17481000
C	-1.42042200	3.08349600	-1.26923800
H	-1.65826400	4.15328200	-1.27777700
H	-0.84944400	2.85312100	-2.17481500
H	-2.36267000	2.52557000	-1.31373600
C	3.69462400	-0.45427200	-1.26987000
H	3.19557100	-0.81698700	-2.17460300
H	3.73327500	0.63973800	-1.32344600
H	4.72599000	-0.82500700	-1.27673800
C	3.69475800	-0.45393000	1.26970200
H	3.19583200	-0.81642300	2.17459800
H	4.72612900	-0.82465300	1.27653100
H	3.73341600	0.64009500	1.32302600

2,4,6-Triisopropylbenzene intramolecular HAT transition state, solvent = benzene

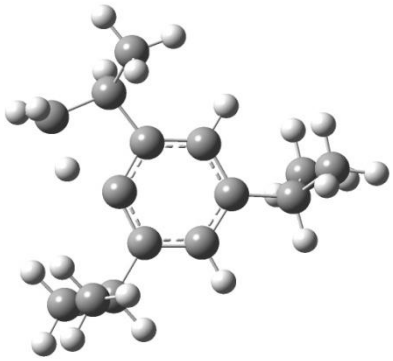

Charge = 0; Multiplicity = 2

38

-585.127381

C	1.34552900	0.26225900	0.03112400
C	1.00308400	-1.09979700	-0.02013100
C	-0.35586800	-1.46046800	-0.02229300
C	-1.39664800	-0.51235400	0.02165700
C	0.33781800	1.23089500	0.07842500
H	2.39178800	0.56158300	0.03106900
H	-0.61629200	-2.51759200	-0.06065000
C	-2.85742300	-0.93873700	0.01255800
H	-2.87260200	-2.03583300	-0.02760400
C	2.07660000	-2.18201600	-0.07489200
H	1.55483700	-3.14748700	-0.10467700
C	0.48714300	2.75090100	0.13358300
H	0.99048300	3.09220600	-0.78182100
C	-3.58348400	-0.50614100	1.30076000
H	-4.61859500	-0.86641200	1.29849900
H	-3.08513800	-0.90478700	2.19069800
H	-3.60581700	0.58599700	1.38810000
C	-3.59248600	-0.41343800	-1.23558400
H	-3.10115600	-0.74694800	-2.15572000
H	-4.62815800	-0.77176900	-1.25190700
H	-3.61363400	0.68217000	-1.24320800
C	1.31621400	3.23294900	1.33687300
H	1.40427300	4.32499700	1.33586300
H	0.84517900	2.92888600	2.27878200
H	2.32822700	2.81427000	1.31585100
C	2.93207500	-2.08293700	-1.35337100
H	2.30726200	-2.11870300	-2.25201700
H	3.50279400	-1.14755200	-1.37844300
H	3.64788500	-2.91151100	-1.40196400
C	2.96581700	-2.17860400	1.18387300
H	2.36555900	-2.28598800	2.09348700

H	3.68423700	-3.00563400	1.14938300
H	3.53493200	-1.24554900	1.26543700
C	-0.98952800	0.81667700	0.07134200
H	-1.55603500	2.09233700	0.11741500
C	-0.95877100	3.28057300	0.14957200
H	-1.28149800	3.76066900	1.07581900
H	-1.29188300	3.82328600	-0.73633500

2,4,6-Triisopropylbenzene alkyl radical, solvent = benzene

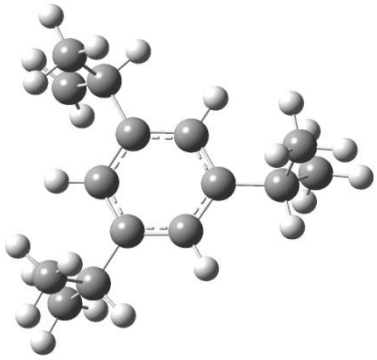

Charge = 0; Multiplicity = 2

38

-585.170418

C	1.14702600	0.81526800	-0.07262000
C	1.46383400	-0.55024800	-0.01053400
C	0.40963100	-1.47202700	0.02955200
C	-0.93337300	-1.06640800	0.00815000
C	-0.18121200	1.25691300	-0.09648400
H	1.94555800	1.55330900	-0.10646400
H	0.63882300	-2.53520500	0.07628100
C	-2.05060400	-2.10277300	0.05372600
H	-1.56861100	-3.08864800	0.08846600
C	2.91054200	-1.03012100	0.00989700
H	2.88175900	-2.12653100	0.05952700
C	-0.50153200	2.74973800	-0.13902300
H	0.45765000	3.26909900	-0.32054900
C	-2.91148700	-1.96702500	1.32535200
H	-3.66143400	-2.76516900	1.36856700
H	-2.29602500	-2.02825300	2.22909600
H	-3.44292700	-1.00868200	1.34527600
C	-2.92888500	-2.06398700	-1.21206300
H	-2.32627900	-2.19474900	-2.11706700
H	-3.67894800	-2.86261400	-1.18330400
H	-3.46083600	-1.10970600	-1.29760700
C	-1.02423500	3.26044400	1.22395000
H	-1.20104900	4.34118600	1.18616900
H	-1.96699700	2.77010100	1.48854100

H	-0.29978600	3.05873100	2.01921100
C	3.66489500	-0.64740700	-1.27876900
H	3.15060100	-1.02816300	-2.16742500
H	3.75097100	0.44044500	-1.38095600
H	4.67919800	-1.06256000	-1.26744100
C	3.66651800	-0.53275400	1.25775900
H	3.15447000	-0.83365900	2.17780900
H	4.68172600	-0.94510700	1.28159500
H	3.75020600	0.55999300	1.26205300
C	-1.21056000	0.30536800	-0.05640500
H	-2.24196600	0.64876600	-0.08134000
C	-1.43621500	3.10687500	-1.25419500
H	-2.05954300	3.99399900	-1.18661500
H	-1.39262400	2.58227200	-2.20358500

The barriers associated with rotation of the aryl radicals derived from 2,4,6-tri-*tert*-butylbenzene (**149**) and 2,4,6-triisopropylbenzene (**147**), to achieve the correct conformation for intramolecular HAT, were investigated. A relaxed coordinate scan (the geometry of the entire molecule was optimised at each step of the rotation) was performed across the dihedral angle of interest, using 72 steps and 5^{o} increments (360^{o} rotation). The difference between the geometry corresponding to the minimised aryl radical and the maxima was taken as ΔG for the rotation, representing an upper limit on the rotational barrier. For the aryl radical derived from 2,4,6-tri-*tert*-butylbenzene (**149**), the minimised geometry saw one of the CH_3 groups of the *tert*-butyl group eclipsed with the aryl radical. Therefore, only a rotation of the CH_3 group is needed to achieve the conformation for intramolecular HAT (Figure A49).

2,4,6-Tri-*tert*-butylbenzene aryl radical, solvent = benzene

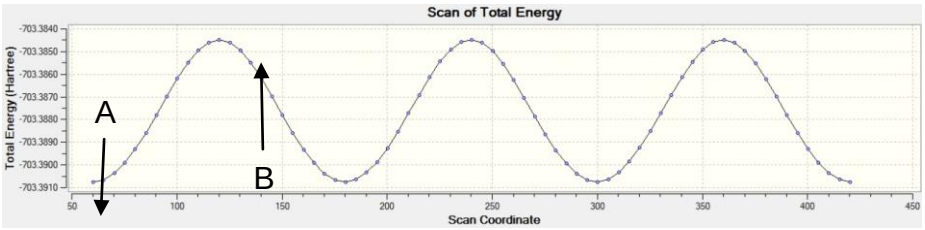

***Figure A49**: Relaxed co-ordinate scan of the rotation of the CH_3 group of **149**.*

2,4,6-Tri-*tert*-butylbenzene aryl radical, **geometry A**: solvent = benzene

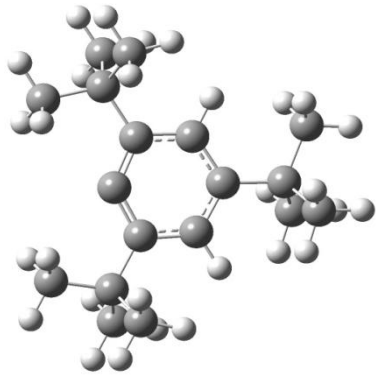

Charge = 0; Multiplicity = 2

47

-703.390755 (uncorrected, read from optimisation curve)

2,4,6-Tri-*tert*-butylbenzene aryl radical, **geometry B**: solvent = benzene

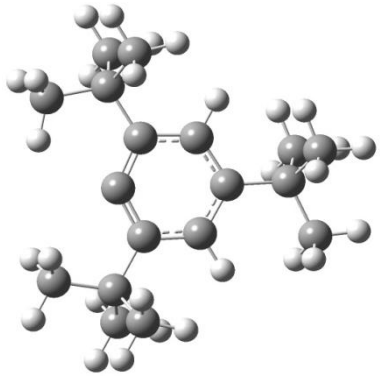

Charge = 0; Multiplicity = 2

47

-703.384474 (uncorrected, read from optimisation curve)

Therefore, the rotational energy barrier upper limit ΔG_{rot} = 3.9 kcal mol^{-1}.

For the aryl radical derived from 2,4,6-triisopropylbenzene (**147**), two rotations are needed to achieve the conformation for intramolecular HAT. Firstly, the isopropyl group needs to rotate until a CH_3 group is eclipsed with the aryl radical (Figure A50).

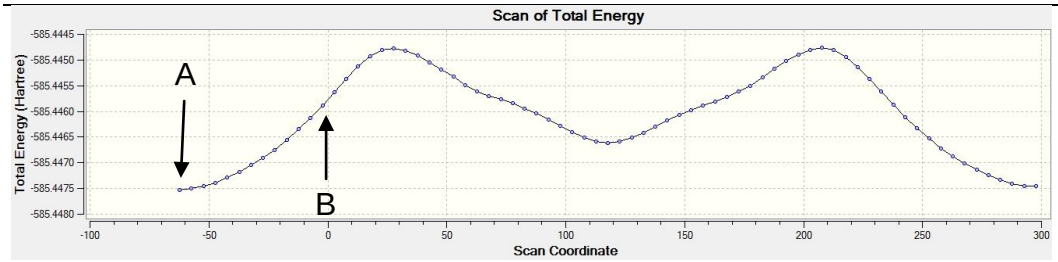

***Figure A50**: Relaxed co-ordinate scan of the rotation of the isopropyl group of **150**.*

2,4,6-Triisopropylbenzene aryl radical, **geometry A**: solvent = benzene

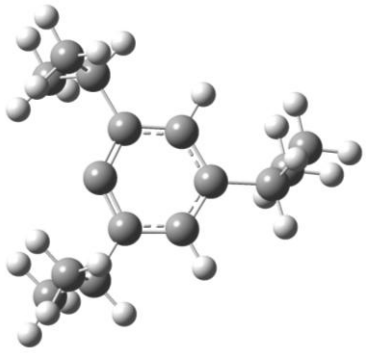

Charge = 0; Multiplicity = 2

38

-585.447535 (uncorrected, read from optimisation curve)

2,4,6-Triisopropylbenzene aryl radical, **geometry B**: solvent = benzene

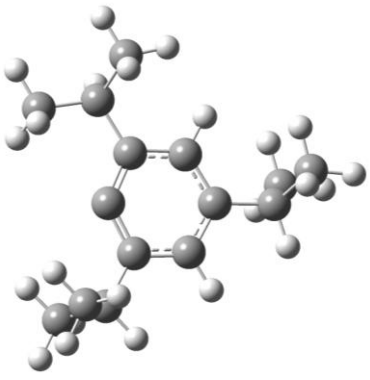

Charge = 0; Multiplicity = 2

38

-585.445625 (uncorrected, read from optimisation curve)

The rotational energy barrier for rotation of the isopropyl group is ΔG_{rot} = 1.2 kcal mol^{-1}. Secondly, the CH_3 group of the isopropyl group (now eclipsing the aryl radical) needs to rotate in order to achieve the conformation for intramolecular HAT (Figure A51).

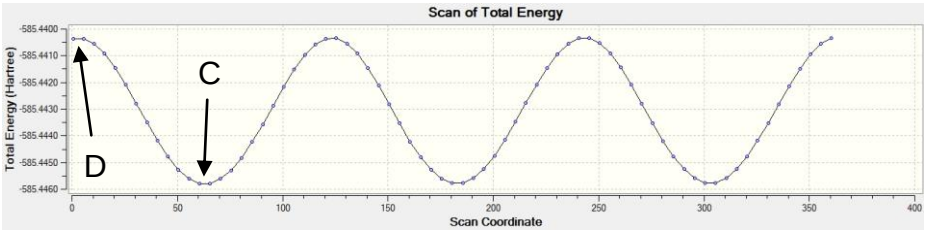

Figure A51*: Relaxed co-ordinate scan of the rotation of the CH_3 group of* ***150*** *following rotation of the isopropyl group.*

2,4,6-Triisopropylbenzene aryl radical, **geometry C**: solvent = benzene

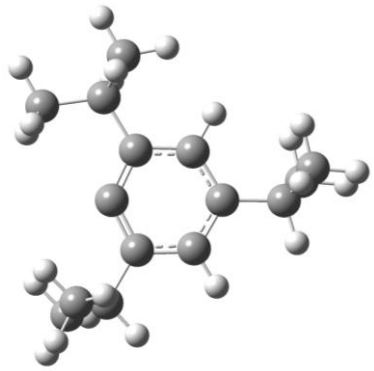

Charge = 0; Multiplicity = 2

38

-585.445785 (uncorrected, read from optimisation curve)

2,4,6-Triisopropylbenzene aryl radical, **geometry D**: solvent = benzene

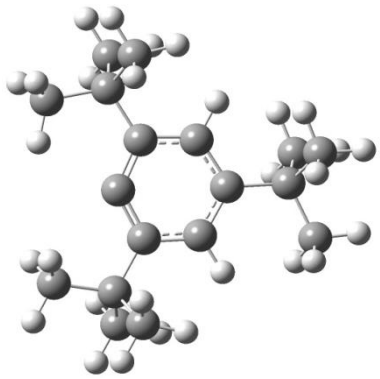

Charge = 0; Multiplicity = 2

47

-585.440360 (uncorrected, read from optimisation curve)

The rotational energy barrier for rotation of the CH_3 group is ΔG_{rot} = 3.4 kcal mol^{-1}. Therefore, the sum of rotational energy barriers (upper limits) for the isopropyl rotation and CH_3 rotation is ΔG_{rot} = 4.6 kcal mol^{-1}.

A12.5. INVESTIGATION OF THE NEOPHYL REARRANGEMENT OF THE 2,4,6-TRI-*tert*-BUTYLBENZENE RADICAL

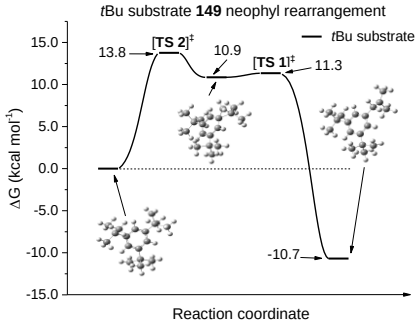

***Figure A52**: Reaction free energy (ΔG) profile for neophyl rearrangment of the alkyl radical derived from intramolecular 1,4-HAT of the aryl radical derived from **149**.*

2,4,6-Tri-*tert*-butylbenzene alkyl radical neophyl rearrangement TS 1, solvent = benzene

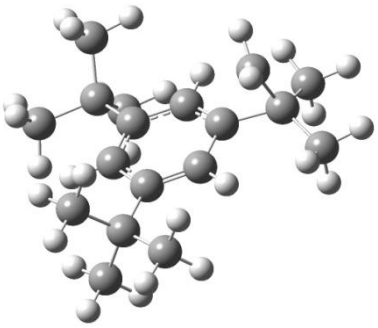

Charge = 0; Multiplicity = 2

47

-703.007510

C -1.03897500 0.95711300 -0.00169900

C	0.32337100	1.42908700	0.04926500
C	1.35283700	0.41067000	0.00265200
C	1.05362700	-0.93880400	0.02452000
C	-1.35827800	-0.39760900	0.02648300
H	-1.83786000	1.68740900	-0.03376900
H	2.38495500	0.73007800	-0.02730400
C	2.14794900	-2.02704600	0.00623300
C	0.66379700	2.91165600	-0.11894500
C	-2.84414100	-0.82564800	0.01160900
C	2.03218300	-2.89466600	1.28384900
H	2.80211400	-3.67528600	1.28300400
H	2.16819500	-2.28415900	2.18351300
H	1.05764500	-3.38675800	1.35631900
C	1.96512800	-2.92820000	-1.23974500
H	2.05270900	-2.34204200	-2.16134800
H	2.73424100	-3.70938600	-1.25923300
H	0.98851300	-3.42140800	-1.24747900
C	-3.52453600	-0.29964200	-1.27583400
H	-4.57896400	-0.59998700	-1.29851700
H	-3.48690700	0.79207500	-1.33968400
H	-3.03600100	-0.70530300	-2.16873300
C	-3.56665300	-0.23556000	1.24730500
H	-4.62153800	-0.53494400	1.25071400
H	-3.10843000	-0.59419300	2.17572400
H	-3.53008300	0.85809100	1.25630000
C	2.03082400	3.25379200	-0.71287900
H	2.06120900	3.02139200	-1.78352600
H	2.21888800	4.32631100	-0.59087300
H	2.85192200	2.72440700	-0.22483400
C	-3.01913300	-2.35687700	0.04758400
H	-2.56088600	-2.84154100	-0.82113300
H	-2.58819600	-2.79646200	0.95352100
H	-4.08655500	-2.60250900	0.03718900
C	3.57146300	-1.43812000	-0.03967200
H	3.78443600	-0.81536200	0.83592500
H	4.30369900	-2.25263700	-0.05116500
H	3.73460500	-0.83456800	-0.93906400
C	-0.42034000	3.81449900	-0.70877800
H	-0.12194400	4.86210800	-0.59051900
H	-0.55414500	3.61635800	-1.77837700
H	-1.38779900	3.69676700	-0.21592300
C	-0.30972400	-1.33693400	0.05507400
H	-0.54164000	-2.39329800	0.07625300
C	0.61292200	2.67870700	1.34762800
H	1.52138700	2.48229100	1.90653300
H	-0.28915500	2.89688700	1.90869300

2,4,6-Tri-*tert*-butylbenzene alkyl radical neophyl rearrangement intermediate, solvent = benzene

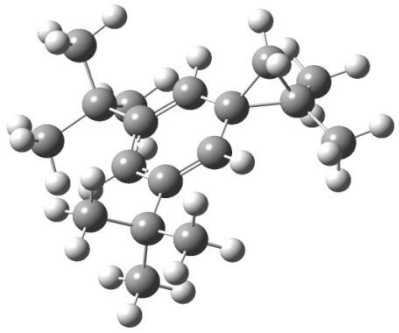

Charge = 0; Multiplicity = 2

47

-703.012145

C	-1.26372500	0.65682700	0.36795100
C	-0.07549100	1.51522300	0.48058100
C	1.21182800	0.80720600	0.37010300
C	1.29583900	-0.53236900	0.07901400
C	-1.18652600	-0.69219100	0.07005900
H	-2.23271200	1.11408300	0.53311300
H	2.11271900	1.38352400	0.53402100
C	2.64554300	-1.26950500	-0.05169300
C	-0.16409300	3.01729300	-0.06716800
C	-2.48843600	-1.51988600	-0.05281300
C	2.71455200	-2.41637300	0.98635000
H	3.66964700	-2.94796500	0.90085400
H	2.63379500	-2.02407500	2.00621900
H	1.91295900	-3.14742500	0.84396000
C	2.77192800	-1.86273000	-1.47649500
H	2.73852400	-1.07053900	-2.23274300
H	3.72463600	-2.39498300	-1.58285800
H	1.96818000	-2.57161300	-1.69728500
C	-3.37808100	-0.92915200	-1.17344300
H	-4.29998200	-1.51396800	-1.27630900
H	-3.66112100	0.10685900	-0.96394900
H	-2.85561500	-0.94586500	-2.13641600
C	-3.26069600	-1.47373600	1.28812100
H	-4.18396300	-2.06116000	1.21675500
H	-2.65538300	-1.88914400	2.10147900
H	-3.53605200	-0.45110800	1.56348200
C	1.06509800	3.61968200	-0.72946000
H	1.16491800	3.27669200	-1.76615700
H	0.96840800	4.71289700	-0.74837700
H	1.99332100	3.38489200	-0.20477100
C	-2.22005900	-2.99999300	-0.39316300

H	-1.69976200	-3.11187800	-1.35053600
H	-1.62548600	-3.49649500	0.38105900
H	-3.17302200	-3.53443500	-0.47079300
C	3.85406800	-0.34323200	0.18588300
H	3.84499600	0.08939300	1.19223500
H	4.78092900	-0.91770700	0.08191700
H	3.89020200	0.47607500	-0.54025300
C	-1.45668100	3.46955600	-0.72800100
H	-1.49408200	4.56639900	-0.73995500
H	-1.51288600	3.12329200	-1.76678300
H	-2.34941000	3.11972400	-0.20593900
C	0.08962400	-1.27938300	-0.09828800
H	0.16212300	-2.33049000	-0.34138600
C	-0.14909400	2.76180900	1.39987400
H	0.75263500	2.99465400	1.96255700
H	-1.07211500	2.88608900	1.96238800

2,4,6-Tri-*tert*-butylbenzene alkyl radical neophyl rearrangement TS 2, solvent = benzene

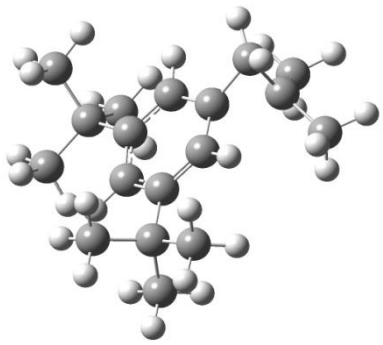

Charge = 0; Multiplicity = 2

47

-703.011378

C	-1.26446300	0.70954400	0.60137700
C	-0.08476300	1.53508800	0.76121000
C	1.19341100	0.85772100	0.61626600
C	1.28289200	-0.44445100	0.16891900
C	-1.19132100	-0.60209400	0.14766400
H	-2.22875800	1.14532700	0.84026600
H	2.08924200	1.41201200	0.86623000
C	2.63499200	-1.16315300	-0.02333000
C	-0.16824600	3.14424200	0.02162800
C	-2.49293700	-1.41755200	-0.03348300
C	2.69790100	-2.40917800	0.89360400
H	3.65264800	-2.93158300	0.76000000
H	2.61189900	-2.12164200	1.94740700
H	1.89508800	-3.11899900	0.67267000
C	2.77528900	-1.60948700	-1.49957200

H	2.74804500	-0.74540400	-2.17280300
H	3.72961100	-2.12819200	-1.64984500
H	1.97411500	-2.29240100	-1.79761100
C	-3.42907500	-0.69701200	-1.03384500
H	-4.35654200	-1.26702400	-1.16548300
H	-3.69957300	0.30545900	-0.68897900
H	-2.94989100	-0.59675900	-2.01411800
C	-3.21295800	-1.55008600	1.33101800
H	-4.13635800	-2.13099000	1.21939000
H	-2.57540400	-2.06163700	2.06063300
H	-3.47996200	-0.57330800	1.74597700
C	1.08049600	3.65517400	-0.65715400
H	1.17533500	3.26152400	-1.67636100
H	1.03137400	4.75163100	-0.73403800
H	1.99382600	3.40810100	-0.11219000
C	-2.23197100	-2.83878800	-0.57161900
H	-1.74099200	-2.82096800	-1.55070900
H	-1.61244400	-3.42839600	0.11237600
H	-3.18543300	-3.36502900	-0.68974500
C	3.84007400	-0.26372100	0.31567100
H	3.82739700	0.05964200	1.36219200
H	4.76899900	-0.82153500	0.15458600
H	3.87596700	0.62806700	-0.31943900
C	-1.45457600	3.51024100	-0.67971800
H	-1.54477400	4.60566400	-0.72987000
H	-1.47296000	3.13464800	-1.70977800
H	-2.34136400	3.13349600	-0.16624600
C	0.08094500	-1.15997500	-0.09993500
H	0.15349200	-2.17685800	-0.46136300
C	-0.16659500	2.86860900	1.48008700
H	0.72068200	3.15433900	2.04571400
H	-1.09073500	3.05173800	2.02902400

2,4,6-Tri-*tert*-butylbenzene alkyl radical neophyl rearrangement alkyl radical, solvent = benzene

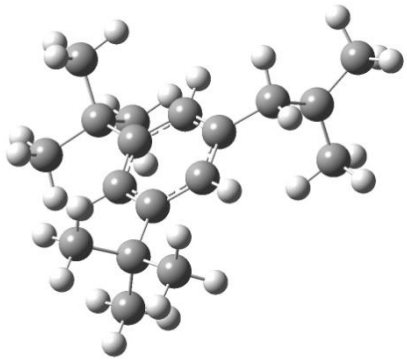

Charge = 0; Multiplicity = 2

47

-703.046484

C	-0.98181500	0.73381300	-0.41864800
C	-1.09471600	-0.64838000	-0.58568300
C	0.04963000	-1.44584700	-0.43817500
C	1.29578100	-0.88663200	-0.12888500
C	0.24646400	1.34141800	-0.10700600
H	-1.87570100	1.34108200	-0.53440900
H	-0.05292600	-2.51732000	-0.57224300
C	2.57235400	-1.73635100	0.03655900
C	0.32015800	2.87291900	0.06068700
C	3.63911500	-1.27502700	-0.98685200
H	4.55313200	-1.87026700	-0.87606700
H	3.27493200	-1.39827100	-2.01277600
H	3.90758500	-0.22314200	-0.84988200
C	3.13140300	-1.55801800	1.46965200
H	2.40085500	-1.88544000	2.21762600
H	4.04162700	-2.15540400	1.59881000
H	3.38342100	-0.51433800	1.68083700
C	-0.63878200	3.31646500	1.19271600
H	-0.59858500	4.40470200	1.31925000
H	-1.67640400	3.04356300	0.97814700
H	-0.35948900	2.85278800	2.14528900
C	-0.10311300	3.55606900	-1.26307900
H	-0.05986900	4.64671400	-1.15886800
H	0.56421900	3.26603700	-2.08221700
H	-1.12427000	3.28810200	-1.55064700
C	1.73725900	3.36338900	0.41735300
H	2.09134400	2.93868300	1.36294600
H	2.46442300	3.11687300	-0.36385300
H	1.72857500	4.45302500	0.52769800
C	2.31355000	-3.23881600	-0.19113100
H	1.94241500	-3.44047800	-1.20176600
H	3.24965500	-3.79353800	-0.06602800
H	1.59167600	-3.64316100	0.52657900
C	1.36533800	0.50987600	0.03327000
H	2.32343800	0.95441600	0.27363700
C	-2.44130100	-1.26821200	-0.93014900
H	-2.28021500	-2.33740100	-1.16559700
H	-2.81672600	-0.81835700	-1.85925800
C	-3.50355900	-1.13877400	0.13387300
C	-3.19292900	-1.57476500	1.53318800
H	-3.27843300	-2.67308200	1.64042700
H	-2.17443400	-1.30691800	1.83266300
H	-3.89175000	-1.13677500	2.25577000
C	-4.93829600	-1.12311900	-0.29804000
H	-5.31102300	-2.14178300	-0.51851300
H	-5.59141700	-0.71810300	0.48435000

H	-5.08530200	-0.53225000	-1.20980600

A12.6. Investigation of the Intermolecular HAT from Benzene to 2,4,6-trialkyl-substituted benzene Radicals

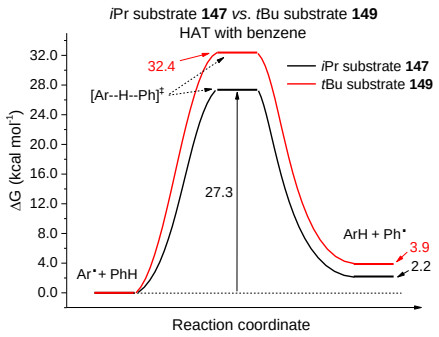

***Figure A53**: Reaction free energy (ΔG) profile for intermolecular HAT with benzene comparing aryl radicals derived from **147** and **149**.*

Benzene, solvent = benzene

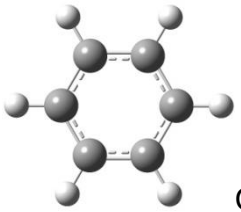

Charge = 0; Multiplicity = 1

12

-232.197011

C	-0.97621700	-1.00226400	0.00000200
C	0.38001800	-1.34643100	0.00007300
C	1.35614200	-0.34427300	-0.00006200
C	0.97613200	1.00234700	0.00000700
C	-0.37990500	1.34646100	0.00006500
C	-1.35617100	0.34416200	-0.00006100
H	-1.73391500	-1.78052200	-0.00006200
H	0.67487200	-2.39185000	0.00007900
H	2.40895200	-0.61140700	-0.00013900
H	1.73402400	1.78040900	0.00001200
H	-0.67500500	2.39180400	0.00001400
H	-2.40892200	0.61155700	-0.00005000

2,4,6-Tri-*tert*-butylbenzene aryl radical intermolecular HAT with benzene transition state, solvent = benzene

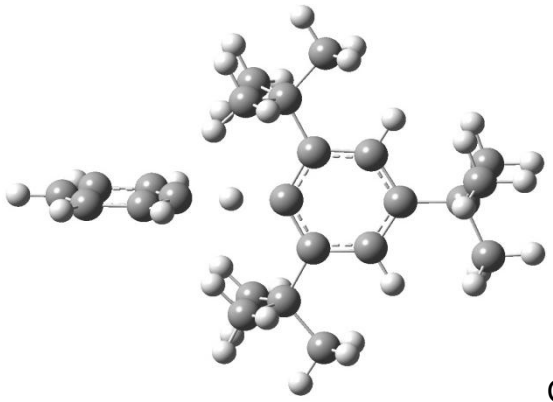

Charge = 0; Multiplicity = 2

59

-935.162869

C	-0.45480700	1.34543000	0.00331200
C	0.89470300	0.98895300	0.00772500
C	1.20351200	-0.37671700	-0.01256700
C	0.22433100	-1.38381600	-0.03431600
C	-1.11914200	-0.95706900	-0.03434200
C	-1.49718700	0.39631900	-0.01818200
H	-0.71404800	2.39301600	0.01670500
H	2.24571000	-0.66676000	-0.01168000
C	0.66147900	-2.87125100	-0.05825200
C	2.03146600	2.03128400	0.03168500
C	-2.96806800	0.88848200	-0.02374300
C	2.19738300	-3.03729800	-0.06450700
H	2.43619200	-4.10577700	-0.08472300
H	2.66121100	-2.58200100	-0.94595700
H	2.66493300	-2.61526900	0.83140100
C	0.13720100	-3.59962800	1.20164300
H	-0.95059800	-3.58923000	1.26034000
H	0.46034000	-4.64751500	1.19134900
H	0.53410500	-3.13223200	2.10996200
C	-3.68755300	0.39579500	-1.30131500
H	-4.72276800	0.75732200	-1.31266600
H	-3.18604900	0.77805000	-2.19764400
H	-3.71559900	-0.69141300	-1.36398300
C	-3.07820900	2.42967800	-0.01513200
H	-4.13766000	2.70668200	-0.02340500
H	-2.63163300	2.87381200	0.88073700
H	-2.61447500	2.88464200	-0.89675300
C	1.50414900	3.47965900	0.05823200
H	0.90395000	3.71264900	-0.82786900
H	0.89545600	3.67654500	0.94730000

H	2.34967600	4.17557200	0.07631800
C	2.90418600	1.81696800	1.29284000
H	3.35369600	0.81944100	1.31271900
H	3.71837400	2.55072900	1.32048700
H	2.30878100	1.93554000	2.20491500
C	-3.70306100	0.38004800	1.23878400
H	-3.73381400	-0.70787300	1.28639900
H	-3.21122700	0.74921200	2.14588700
H	-4.73770100	0.74345500	1.24314600
C	0.13154600	-3.55901400	-1.33847700
H	0.52327100	-3.06170400	-2.23306800
H	0.45582000	-4.60623600	-1.36396700
H	-0.95653600	-3.54808400	-1.39130500
C	2.91221700	1.86558200	-1.23125600
H	3.72586600	2.60038500	-1.22577900
H	3.36224400	0.86959200	-1.28589100
H	2.32231600	2.01833800	-2.14180800
C	-5.08767900	-4.78583600	-0.04881100
C	-4.58014300	-4.30612100	1.16303600
C	-3.57131500	-3.33237400	1.16683400
C	-3.08687900	-2.85479700	-0.04710700
C	-3.58044700	-3.32066400	-1.26188700
C	-4.58925900	-4.29451000	-1.25976200
H	-5.86936300	-5.53993600	-0.04949200
H	-4.96580600	-4.68604100	2.10543000
H	-3.17946600	-2.96213000	2.11061700
H	-2.09766300	-1.90092200	-0.04471100
H	-3.19592200	-2.94149700	-2.20513000
H	-4.98206600	-4.66533700	-2.20282500

Phenyl radical, solvent = benzene

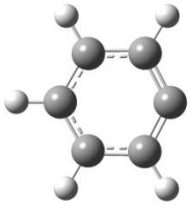

Charge = 0; Multiplicity = 2

11

-231.522274

C	1.22903200	-0.77349700	-0.00000900
C	1.21618400	0.63344100	0.00001500
C	0.00000700	1.32625200	-0.00000400
C	-1.21619400	0.63341900	-0.00000600
C	-1.22903900	-0.77348200	0.00001700
C	0.00000800	-1.39958900	-0.00000700

H	2.16511600	-1.32441400	-0.00001400
H	2.15653500	1.17869700	0.00001300
H	-0.00002200	2.41218500	-0.00001200
H	-2.15652000	1.17871900	-0.00002000
H	-2.16509400	-1.32445100	-0.00000100

2,4,6-Tri-*tert*-butylbenzene, solvent = benzene

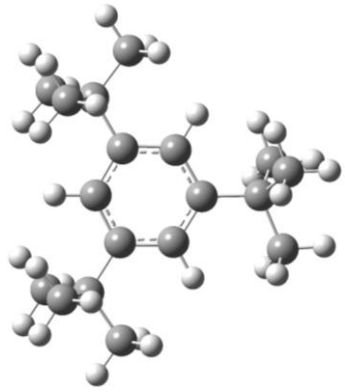

Charge = 0; Multiplicity = 1

48

-703.685990

C	-1.01950800	-0.94050400	-0.00000200
C	0.31743100	-1.35592600	-0.00000900
C	1.31008500	-0.36206300	-0.00000800
C	1.00221400	1.00433700	0.00002000
C	-1.38018300	0.41791900	0.00000800
H	-1.80512300	-1.68589200	-0.00000800
H	2.35279400	-0.66432400	-0.00001900
C	2.14093200	2.04602300	0.00000200
C	0.72465900	-2.84449200	0.00000000
C	-2.87364300	0.80686500	0.00000000
C	1.61653700	3.49578400	0.00015800
H	2.46345200	4.19029800	0.00011700
H	1.01230900	3.71194900	-0.88745800
H	1.01249100	3.71182400	0.88792800
C	3.01780900	1.85529400	1.26206500
H	3.46699200	0.85812200	1.29881600
H	3.83216400	2.58937700	1.27370000
H	2.42524100	1.99060500	2.17367100
C	-3.55981100	0.22830200	1.26217200
H	-4.62387700	0.49251500	1.27073600
H	-3.48667800	-0.86277400	1.30189800
H	-3.10252000	0.62907900	2.17361200
C	-3.55966700	0.22873500	-1.26245100
H	-4.62372400	0.49298400	-1.27107000
H	-3.10224300	0.62979700	-2.17369900

H	-3.48655900	-0.86232900	-1.30251800
C	-0.49244400	-3.79026200	-0.00010100
H	-1.11828600	-3.64985500	0.88770500
H	-1.11815700	-3.64982200	-0.88799200
H	-0.14720000	-4.82964200	-0.00009100
C	1.56797300	-3.15102900	-1.26218500
H	2.47839500	-2.54541600	-1.30116000
H	1.86773200	-4.20565600	-1.27157300
H	0.99322800	-2.95285600	-2.17369200
C	-3.08828200	2.33324100	0.00025500
H	-2.65585500	2.80706400	0.88811300
H	-2.65568700	2.80738900	-0.88734800
H	-4.16163700	2.55135900	0.00019100
C	3.01758900	1.85549800	-1.26224600
H	2.42486700	1.99097000	-2.17372700
H	3.83195600	2.58956900	-1.27389900
H	3.46674500	0.85832300	-1.29923700
C	1.56778900	-3.15104000	1.26230500
H	1.86756600	-4.20566200	1.27172100
H	2.47818900	-2.54540400	1.30142200
H	0.99290300	-2.95289200	2.17372900
C	-0.35397700	1.37169900	0.00003000
H	-0.61249200	2.42101600	0.00004800

2,4,6-Triisopropylbenzene aryl radical intermolecular HAT with benzene transition state, solvent = benzene

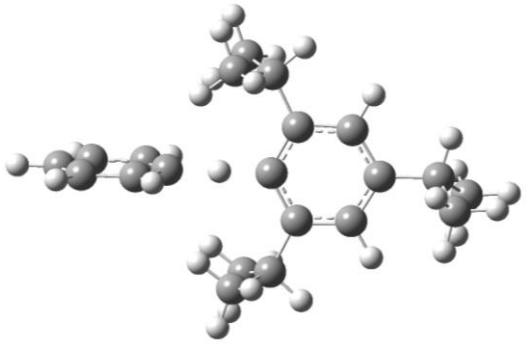

Charge = 0; Multiplicity = 2

50

-817.308150

C	-0.47533000	1.34516500	-0.00910100
C	0.87995000	0.99496100	0.00970600
C	1.20247800	-0.36472300	-0.00058800
C	0.22266800	-1.37568900	-0.02934600
C	-1.11628100	-0.96510000	-0.04837000
C	-1.50114100	0.38413800	-0.03826800
H	-0.75877100	2.39570100	-0.00128000

H	2.25076500	-0.65889600	0.01423400
C	0.70259100	-2.82744400	-0.03544800
C	1.97740000	2.05241100	0.04153200
C	-2.94468300	0.88839400	-0.05517400
C	0.32529100	-3.58090300	-1.32505300
H	0.79363300	-4.57205900	-1.33234500
H	-0.75516900	-3.72256700	-1.40739200
H	0.66766100	-3.03828400	-2.21283100
C	-3.73906000	0.47950000	1.19979000
H	-4.72246600	0.96399800	1.19711100
H	-3.90045700	-0.60058100	1.24056500
H	-3.21539200	0.78167500	2.11316400
C	-3.69651400	0.51863300	-1.34793700
H	-4.67927000	1.00413900	-1.36338800
H	-3.14246800	0.84783400	-2.23364700
H	-3.85670600	-0.55950000	-1.42685700
C	1.95677800	2.94368600	-1.21563600
H	2.03514400	2.34377000	-2.12840900
H	1.02999700	3.52562200	-1.27464500
H	2.79413300	3.65057600	-1.19881000
C	1.91844600	2.90646400	1.32325700
H	1.96809800	2.27987800	2.21998100
H	2.75639900	3.61221000	1.35302600
H	0.99064900	3.48788000	1.37074200
C	0.27463300	-3.60670700	1.22266800
H	-0.80841700	-3.74778900	1.25994300
H	0.74107600	-4.59878300	1.22786000
H	0.58262200	-3.08301500	2.13407900
C	-5.02689700	-4.80612400	-0.19793200
C	-4.50167000	-4.29561500	-1.38988800
C	-3.50199300	-3.31291300	-1.35324600
C	-3.04807800	-2.86080900	-0.11862900
C	-3.55731300	-3.35554800	1.07738600
C	-4.55687900	-4.33818600	1.03386500
H	-5.80123000	-5.56719400	-0.22894900
H	-4.86675700	-4.65905100	-2.34690300
H	-3.09315500	-2.91573900	-2.27872900
H	-2.07846700	-1.90849500	-0.08048200
H	-3.19162400	-2.99154800	2.03405500
H	-4.96491700	-4.73465200	1.95990800
H	1.79845100	-2.77386100	-0.01311700
H	-2.87264800	1.98327800	-0.03717900
H	2.93547500	1.51624200	0.04824000

2,4,6-Triisopropylbenzene, solvent = benzene

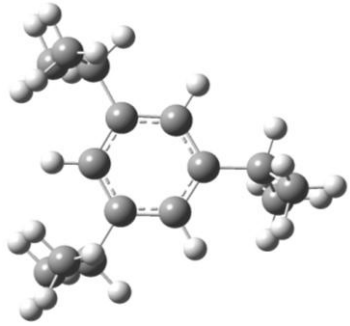

Charge = 0; Multiplicity = 1

39

-585.825993

C	-1.20147200	-0.23810800	0.00009900
C	-0.87816200	1.12515000	0.00012500
C	0.47738100	1.48672700	0.00007800
C	1.49887500	0.52838000	-0.00000200
C	-0.20691900	-1.22812900	0.00001200
H	-2.24661300	-0.53763000	0.00015000
H	0.74247600	2.54262600	0.00010100
C	2.96121900	0.95861900	-0.00003000
H	2.97016800	2.05653400	-0.00019600
C	-1.96035400	2.19942600	0.00011200
H	-1.44552700	3.16919500	0.00037700
C	-0.56592800	-2.71034200	-0.00004600
H	0.38030900	-3.26711200	-0.00013800
C	3.70077300	0.49269600	1.26960600
H	4.72924800	0.87153300	1.27603000
H	3.19939300	0.85149400	2.17464900
H	3.74780600	-0.60095600	1.32301300
C	3.70083300	0.49233100	-1.26950500
H	3.19945600	0.85083600	-2.17466500
H	4.72929100	0.87121000	-1.27601000
H	3.74792100	-0.60133300	-1.32258500
C	-1.33938700	-3.11813900	-1.26957200
H	-1.52150100	-4.19893300	-1.27808500
H	-2.31227300	-2.61601500	-1.32071200
H	-0.78020900	-2.85945800	-2.17492800
C	-1.33923900	-3.11828400	1.26951300
H	-1.52132400	-4.19908400	1.27792700
H	-0.77997500	-2.85968900	2.17484100
H	-2.31213300	-2.61619100	1.32081100
C	-2.83208600	2.14200800	-1.26970500
H	-2.22002800	2.21790500	-2.17461900
H	-3.39519400	1.20330300	-1.32298800
H	-3.55526400	2.96556400	-1.27670200

C	-2.83270800	2.14163900	1.26946100
H	-2.22111000	2.21721000	2.17471300
H	-3.55582900	2.96524600	1.27635500
H	-3.39593400	1.20297400	1.32218100
C	1.13520100	-0.82686200	-0.00004300
H	1.90868700	-1.59190600	-0.00012300

A13. REFERENCES

(1) Bard, A. J.; Faulkner, L. R. *Electrochemical Methods: Fundamentals and Applications*; John Wiley and Sons: New York, 2000.

(2) Ramette, R. W. *J. Chem. Educ.* **1987**, *64*, 885.

(3) Pocaznoi, D.; Calmet, A.; Etcheverry, L.; Erable, B.; Bergel, A. *Energy Environ. Sci.* **2012**, *5*, 9645–9652.

(4) Connelly, N. G.; Geiger, W. E. *Chem. Rev.* **1996**, *96*, 877–910.

(5) König, B.; Hari, D. P. *Org. Lett.* **2011**, *13*, 3852–3855.

(6) Romero, N. A.; Nicewicz, D. A. *Chem. Rev.* **2016**, *116*, 10075–10166.

(7) Prier, C. K.; Rankic, D. A.; MacMillan, D. W. C. *Chem. Rev.* **2013**, *113*, 5322–5363.

(8) Bartling, H.; Eisenhofer, A.; König, B.; Gschwind, R. M. *J. Am. Chem. Soc.* **2016**, *138*, 11860–11871.

(9) Blanc, S.; Pigot, T.; Cugnet, C.; Brown, R.; Lacombe, S. *Phys. Chem. Chem. Phys.* **2010**, *12*, 11280–11290.

(10) Juris, A.; Balzani, V. *Helv. Chim. Acta* **1981**, *64*, 2175–2182.

(11) Gonzales-Velasco, J.; Rubinstein, I.; Crutchley, R. J.; Lever, A. B. P.; Bard, A. J. *Inorg. Chem.* **1982**, *22*, 822–825.

(12) Silverman, R. B.; Hoffman, S. J.; Catus III, W. B. *J. Am. Chem. Soc.* **1980**, *102*, 7128–7129.

(13) Haga, M.-A.; Dodsworth, E. S.; Eryavec, G.; Seymour, P.; Lever, A. B. P. *Inorg. Chem.* **1985**, *24*, 1901–1906.

(14) Kalyanasundaram, K. *Coord. Chem. Rev.* **1982**, *46*, 159–244.

(15) Satpati, A. K.; Nath, S.; Kumbhakar, M.; Maity, D. K.; Senthilkumar, S.; Pal, H. *J. Mol. Struct.* **2008**, *878*, 84–94.

(16) Fukuzumi, S.; Yuasa, J.; Satoh, N.; Suenobu, T. *J. Am. Chem. Soc.* **2004**, *126*, 7585–7594.

(17) Burget, D.; Jacques, P.; Vauthey, E.; Suppan, P.; Haselbach, E. *J. Chem. Soc. Faraday Trans.* **1994**, *90*, 2481–2487.

(18) Rhile, I. J.; Markle, T. F.; Nagao, H.; DiPasquale, A. G.; Lam, O. P.; Lockwood, M. A.; Rotter, K.; Mayer, J. M. *J. Am. Chem. Soc.* **2006**, *128*, 6075–6088.

(19) Chow, P.-K.; To, P.-T.; Low, K.-H.; Che, C.-M. *Chem. - An Asian J.* **2014**, *9*, 534–545.

(20) Hub, W.; Schneider, S.; Dörr, F.; Oxman, J. D.; Lewis, F. D. *J. Am. Chem. Soc.* **1984**, *106*, 701–708.

(21) Stradins, J.; Baumane, L.; Kalnins, A.; Uldrikis, J.; Bisenieks, E.; Poikans, J.; Duburs, G. *Chem. Heterocycl. Compd.* **2000**, *36*, 1177–1184.

(22) Ozols, Y.; Vigante, B.; Baumane, L.; Mishnev, A.; Turovskis, I.; Duburs, G.; Stradyn, Y. *Chem. Heterocycl. Compd.* **1998**, *34*, 1166–1173.

(23) Tajima, T.; Fuchigami, T. *Angew. Chem. Int. Ed.* **2005**, *44*, 4760–4763.

(24) Pandey, G.; Rani, K. S.; Lakshmaiah, G. *Tetrahedron Lett.* **1992**, *33*, 5107–5110.

(25) Tajima, T.; Nakajima, A. *J. Am. Chem. Soc.* **2008**, *130*, 10496–10497.

(26) Roh, Y.; Jang, H.-Y.; Lynch, V.; Bauld, N. L.; Krische, M. J. *Org. Lett.* **2002**, *4*, 611–613.

(27) Roth, H. G.; Romero, N. A.; Nicewicz, D. A. *Synlett* **2016**, *27*, 714–723.

(28) Cardinale, A.; Isse, A. A.; Gennaro, A.; Robert, M.; Savéant, J.-M. *J. Am. Chem. Soc.* **2002**, *124*, 13533–13539.

(29) Isse, A. A.; Gottardello, S.; Durante, C.; Gennaro, A. *Phys. Chem. Chem. Phys.* **2008**, *10*, 2409–2416.

(30) Nakanishi, I.; Ohkubo, K.; Ogawa, Y.; Matsumoto, K.; Ozawa, T.; Fukuzumi, S. *Org. Biomol. Chem.* **2016**, *14*, 7956–7961.

(31) Desbois, M.-H.; Guillin, J.; Mariot, J.-P.; Varret, F.; Astruca, D. *J. Chem. Soc., Chem. Commun.* **1985**, 447–449.

(32) Yi, H.; Jutand, A.; Lei, A. *Chem. Commun.* **2015**, *51*, 545–548.

(33) Pause, L.; Robert, M.; Savéant, J.-M. *J. Am. Chem. Soc.* **1999**, *121*, 7158–7159.

(34) Mihelcic, J.; Moeller, K. D. *J. Am. Chem. Soc.* **2003**, *125*, 36–37.

(35) Horn, E. J.; Rosen, B. R.; Baran, P. S. *ACS Cent. Sci.* **2016**, *2*, 302–

308.

(36) Ozkan, S. A.; Kauffmann, J.-M.; Zuman, P. *Electroanalysis in Biomedical and Pharmaceutical Sciences: Voltammetry, Amperometry, Biosensors, Applications (Monographs in Electrochemistry)*; Springer, 2015.

(37) Silvester, D. S.; Broder, T. L.; Aldous, L.; Hardacre, C.; Crossley, A.; Compton, R. G. *Analyst* **2007**, *132*, 196–198.

(38) Grzeszczuk, M.; Smith, D. E. *J. Electroanal. Chem.* **1983**, *157*, 205–219.

(39) Vapourtec Photochemical UV-150 reactor - light-sources https://www.vapourtec.com/products/flow-reactors/photochemistry-uv-150-photochemical-light-sources/ (accessed Jan 20, 2017).

(40) Cismesia, M. A.; Yoon, T. P. *Chem. Sci.* **2015**, *6*, 5426–5434.

(41) Hoffman, M. Z.; Bolletta, F.; Moggi, L.; Hug, G. *J. Phys. Chem. Ref. Data* **1989**, *18*, 219–544.

(42) Keizer, J. *J. Am. Chem. Soc.* **1983**, *105*, 1494–1498.

(43) Laws, W. R.; Contino, P. B. *Methods Enzym.* **1992**, *210*, 448–463.

(44) Castanho, M. A. R. B.; Prieto, M. J. E. *Biochim. Biophys. Acta* **1998**, *1373*, 1–16.

(45) Melavanki, R. M.; Patil, N. R.; Patil, H. D.; Kusanur, R. A.; Kadadevaramath, J. S. *Indian J. Pure Appl. Phys.* **2011**, *49*, 748–753.

(46) Lombard, J.; Boulaouche, R.; Amilan Jose, D.; Chauvin, J.; Collomb, M.-N.; Deronzier, A. *Inorg. Chim. Acta* **2010**, *363*, 234–242.

(47) Nakamaru, K. *Bull. Chem. Soc. Jpn.* **1982**, *55*, 2697–2705.

(48) Armstrong, A.; Pullin, R. D. C.; Jenner, C. R.; Foo, K.; White, A. J. P.; Scutt, J. N. *Tetrahedron Asymmetry* **2014**, *25*, 74–86.

(49) Hohenberg, P.; Kohn, W. *Phys. Rev.* **1964**, *36*, 864–871.

(50) Kohn, W.; Sham, L. J. *Phys. Rev.* **1965**, *140*, 1133–1138.

(51) Frisch, M. J.; Trucks, G. W.; Schlegel, H. B.; Scuseria, G. E.; Robb, M. A.; Cheeseman, J. R.; Scalmani, G.; Barone, V.; Mennucci, B.; Petersson, G. A.; Nakatsuji, H.; Caricato, M.; Li, X.; Hratchian, H. P.; Izmaylov, A. F.; Bloino, J.; Zheng, G.; Sonnenberg, J. L.; Hada, M.;

Ehara, M.; Toyota, K.; Fukada, R.; Hasegawa, J.; Ishida, M.; Nakajima, T.; Honda, Y.; Kitao, O.; Nakai, H.; Vreven, T.; Montgomery Jr, J. A.; Peralta, J. E.; Ogliaro, F.; Bearpark, M. J.; Heyd, J.; Brothers, E. N.; Kudin, K. N.; Staroverov, V. N. .; Kobayashi, R.; Normand, J.; Raghavachari, K.; Rendell, A. P.; Burant, J. C.; Iyengar, S. S.; Tomasi, J.; Cossi, M.; Rega, N.; Millam, N. J.; Klene, M.; Knox, J. E.; Cross, J. B.; Bakken, V.; Adamo, C.; Jaramillo, J.; Gomperts, R.; Stratmann, R. E.; Yazyev, O.; Austin, A. J.; Cammi, R.; Pomelli, C.; Ochterski, J. W.; Martin, R. L.; Morokuma, K.; Zakrzewski, V. G.; Voth, G. A.; Salvador, P.; Dannenberg, J. J.; Dapprich, S.; Daniels, A. D.; Farkas, Ö.; Foresman, J. B.; Ortiz, J. V.; Cioslowski, J.; Fox, D. J. Wallingford, CT, USA 2009.

(52) Becke, A. D. *J. Chem. Phys.* **1993**, *98*, 5648–5652.

(53) Salamone, M.; Dilabio, G. A.; Bietti, M. *J. Org. Chem.* **2011**, *76*, 6264–6270.

(54) Barone, V.; Cossi, M. *J. Phys. Chem. A.* **1998**, *102*, 1995–2001.

(55) Cossi, M.; Rega, N.; Scalmani, G.; Barone, V. *J. Comput. Chem.* **2003**, *24*, 669–681.

(56) Zhao, Y.; Truhlar, D. G. *J. Chem. Phys.* **2006**, *125*, 194101/1–18.

(57) Zhao, Y.; Truhlar, D. G. *Acc. Chem. Res.* **2008**, *41*, 157–167.

(58) Krishnan, R.; Binkley, J. S.; Seeger, R.; Pople, J. A. *J. Chem. Phys.* **1980**, *72*, 650–654.

(59) Frisch, M. J.; Pople, J. A.; Binkley, J. S. *J. Chem. Phys.* **1984**, *80*, 3265–3269.

(60) McLean, A. D.; Chandler, G. S. *J. Chem. Phys.* **1980**, *72*, 5639–5648.

(61) Blandeau, J.-P.; McGrath, M. P.; Curtiss, L. A.; Radom, L. *J. Chem. Phys.* **1997**, *107*, 5016–5021.

(62) Clark, T.; Chandrasekhar, J.; Spitznagel, G. W.; Schleyer, P. V. R. *J. Comput. Chem.* **1983**, *4*, 294–301.

(63) Bergner, A.; Dolg, M.; Küchle, W.; Stoll, H.; Preuß, H. *Mol. Phys.* **1993**, *80*, 1431–1441.